PROCEEDINGS
OF THE
WEDNESDAY SLIDE
CONFERENCE 2024-2025

JOINT PATHOLOGY CENTER
VETERINARY PATHOLOGY SERVICE
SILVER SPRING, MD 20910

On behalf of the Joint Pathology Center, I would like to extend our sincere thanks to all the contributors who submitted cases to the 2024-2025 Wednesday Slide Conference. We reviewed many excellent cases in conference this year and we were pleased to highlight submissions from Asia, Oceania, Europe, South America, and North America. Veterinary pathology truly is a global discipline.

Throughout this conference year, the following veterinary pathologists shared their time and expertise by moderating for Wednesday Slide Conference: Jeremy Bearss, Bruce Williams, Daniel Bland, Janice Gray, Michael Eckhaus, Taryn Donovan, Kelsey Fiddes, Rebecca Smedley, John Cullen, Corrie Brown, Charles Bradley, Elise LaDouceur, Anna Travis, Tony Alves, Sherri Daye, Tom Cecere, Maggie Highland, Lauren Peiffer, Erica Barkei, Karen Terio, Enrico Radaelli, Patricia Pesavento, Francisco Uzal, Brian Murphy, and Jey Koehler. We thank them for taking time out of their busy schedules to join us in discussions that were informative and often highly entertaining!

The success of this conference owes much to the hard work of our civilian staff behind the scenes. I would like to personally thank Dr. Bruce Williams for his steadfast support of the WSC program and website troubleshooting; Ms. Rachel Terry for her help in compiling and distributing conference results; Ms. Kenenya Gathers for accessioning and organizing cases; and Ms. Stacey Tamer for providing special and immunohistochemical stain support.

I have sought to present each contributor's case with minimal edits for clarity and organization of content, to include the many wonderful images and tables submitted. For JPC comments, I focused heavily on slide features and interpretation as well as adding recent literature of interest. I hope you will find these useful. Some of the most interesting cases of these conferences were where we differed in interpretation from the contributor – these discussions are well worth a glance for the learning issues they raise.

Finally, I would also like to thank my wife Yuki Nishida for her patience and support during the past year (and for her insights on tanuki nomenclature – see Case 2, Conference 17). To all of my fellow residents, thank you for your enthusiasm and ideas in exploring these cases together this past year.

James Gaffney, DVM
2024-2025 WSC Coordinator

Case	Species	Tissue	Lesion/condition	Page
Conference 1 - August 14, 2024				
1	Horse (foal)	Liver	Equine herpesvirus-1 hepatitis	
2	Horse	Haired skin	Dermatophytic mycetoma	
3	Horse	Guttural pouch	Guttural pouch mycosis	
4	Horse	Nasal vestibule	Nasal amyloidosis	
Conference 2 - August 21, 2024				
1	Cat (adult)	Intestine	GI lymphoma (EATL)	
2	Dog	Cranial mediastinal mass	Branchial cyst carcinoma	
3	Cat (juvenile)	Lymph node, spleen, liver	FALPS (Feline Autoimmune Lymphoproliferative Syndrome)	
4	Cat	Intestine	Sclerosing encapsulating peritonitis	
Conference 3 - August 28, 2024				
1	Guinea pig	Heart	Rhabdomyomatosis (glycogenosis)	
2	Minipig	Kidney	Thrombocytopenic purpura syndrome	
3	Rhesus macaque	Heart	Chagas disease (*T. cruzi*)	
4	Rhesus macaque	Mouth (hard palate)	Amelanotic oral melanoma	
Conference 4 - September 4, 2024				
1	Pig	Haired skin	Greasy pig disease	
2	File-eared tree frog	Eye	Lipid keratopathy	
3	Dog	Brain	Canine adenovirus-1 brainstem vasculitis	
4	Crested gecko	Liver	Verminous hepatitis (*Strongyloides*)	
Conference 5 - September 11, 2024				
1	Common woolly monkey	Testis, intestine	Polyarteritis nodosa	
2	Common marmoset	Kidney	Nephroblastoma	
3	Brahman heifer	Skeletal muscle	Monensin toxicity	
4	Rhesus macaque	Brain	SV40 leukoencephalomalacia and meningioangiomatosis	
Conference 6 - September 18, 2024				
0b2	Rat	Kidney, adrenal gland	Hematopoietic sarcoma	

Case	Species	Tissue	Lesion/condition	Page
2	Mouse	Abdominal mass (seminal vesicle)	Teratoma	
3	Rhesus macaque	Ovary, uterus, vertebral body	Metastatic adenocarcinoma	
4	African green monkey	Brain	Granulomatous encephalitis (*Schistosoma*)	
Conference 7 - October 2, 2024				
1	Dog	Lung	Pulmonary adenocarcinoma	
2	Dog	Lung	Bronchointerstitial pneumonia (Distemper, *Toxoplasma*)	
3	Dog	Heart	Atherosclerosis, myocardial fibrosis	
4	Domestic shorthair cat	Lung	Plexiform arteriopathy, interstitial pneumonia (FIP)	
Conference 8 - October 9, 2024				
1	Dog	Haired skin	Ischemic dermatopathy	
2	Dog	Haired skin	Demodicosis and dermal mucinosis	
3	Icelandic pony	Preputial skin	Equine sarcoidosis	
4	Mouse	Haired skin	Ulcerative dermatitis (primary follicular dystrophy)	
Conference 9 – October 16, 2024				
1	Colobus monkey	Liver, lung	Necrotizing hepatitis and pneumonia (*Entamoeba*)	
2	Dog	Lung	Fibrinous and organizing pneumonia and heart failure	
3	Drill	Eye	Hydatid cyst	
4	Rhesus macaque	Uterus	Endometritis	
Conference 10 – October 23, 2024				
1	Sheep	Liver	Hepatocellular carcinoma (clear cell variant)	
2	Dog	Testis	Mixed germ cell tumor	
3	Dog	Adrenal gland	Phaeochromocytoma and adrenal cortical adenoma	
4	Dog	Spleen, liver	Poorly melanized malignant melanoma	
Conference 11 – October 30, 2024				
1	Dog	Heart	*Hepatozoon* myocarditis	
2	Dog	Esophagus	Oomycete esophagitis and pyogranulomas	
3	Mouse	Lung	*Chlamydia muridarum* pneumonia	

Case	Species	Tissue	Lesion/condition	Page
4	Dog	Brain	Granulomatous meningoencephalitis (Coccidiomycosis)	
Conference 12 – November 6, 2025				
1	American shorthair cat	Liver	Ductal plate malformation	
2	European shorthair cat	Liver	Chronic sinusoidal outflow disruption	
3	Texel sheep	Liver, kidney	Copper toxicity	
4	Nevisian donkey	Liver	Cholangiocellular carcinoma	
Conference 13 - December 4, 2024				
1	Lion	Oral cavity	Squamous cell carcinoma	
2	Sprague-Dawley rat	Sternum	Myeloid leukemia	
3	Giant Pacific octopus	Renal appendage	Nephritis and dicyemids (endosymbiont)	
4	Dog	Ovary	Ovarian adenoma, dysgerminoma, granulosa cell tumor, and ovarian cysts	
Conference 14 – December 11, 2024				
1	Limousine bull	Esophagus	Epiglottitis (*Besnoitia*)	
2	Oberhasli goat	Brain	Cache Valley virus	
3	Pig	Lung	HPAI pneumonia (experimental)	
4	Brangus calf	Lung	*Salmonella* Dublin pneumonia	
Conference 15 - January 8, 2025				
1	White Leghorn chicken	Head (entire)	Infectious coryza (*Avibacterium paragallinarum*)	
2	Swiss Large White pig	Rib	PCV-3 associated bone fracture	
3	Pig	Intestine	Intestinal salmonellosis	
4	Domestic white turkey	Gastrocnemius	Turkey arthritis reovirus	
Conference 16 - January 15, 2025				
1	Collared finchbill	Brain	Cerebral clostridiosis	
2	Texel lamb	Esophagus	Bluetongue virus	
3	Dog	Stomach	Fungal gastritis (*Scedosporium*)	
4	Sheep	Intestine (cecum)	Johne's Disease	
Conference 17 – January 22, 2025				
1	Rhesus macaque	Liver	*Enterocytozoon* cholangiohepatitis and *M. avium* hepatitis	

Case	Species	Tissue	Lesion/condition	Page
2	Ezo (Hokkaido) raccoon dog	Eye	HPAI conjunctivitis	
3	Angus heifer	Skin	Bovine herpesvirus-2 dermatitis (pseudolumpy skin disease)	
4	C.B-17 *scid* mouse	Hind limb	*Borrelia* tenosynovitis (experimental)	
Conference 18 – January 29, 2025				
1	Rock dove	Cloaca	Toxoplasmosis and circovirus (cloacitis and lymphoid depletion)	
2	Cockatiel	Bone	Mycobacterial osteomyelitis	
3	Elegant crested tinamou	Ventriculus	Ventricular amyloidosis *Macrorhabdus* ventriculitis	
4	Blue-fronted Amazon parrot	Bone / Spinal cord	*Aspergillus* osteitis and meningomyelitis	
Conference 19 – February 5, 2025				
1	Green anaconda	Lung	*Ophidiomyces* pneumonia	
2	Bearded dragon	Stomach	Neuroendocrine carcinoma	
3	Great blue heron	Ventriculus, proventriculus	*Eustrongylides* and *Tetrameres* (serositis and glandular ectasia)	
4	Budgerigar	Kidney	Renal adenocarcinoma	
Conference 20 – February 12, 2025				
1	Cherry shrimp	Whole body	Cladogoniasis	
2	Betta fish	Whole body	Mycobacteriosis, trematodes, and xenomas	
3	Cockatiel	Spinal cord	Lafora disease	
4	Humpback whale	Brain	Cetacean morbillivirus	
Conference 21 – March 26, 2025				
1	Sprague-Dawley rat	Kidney	Pyelonephritis and chronic progressive nephropathy	
2	Sprague-Dawley rat	Ear/skin	Zymbal's gland tumor	
3	Standard fancy rat	Lung	Mycoplasmal pneumonia	
4	NSG experimental mouse	Lung, esophagus	Graft vs host disease	
Conference 22 – April 2, 2025				
1	Lowland sheep	Placenta	Listerial placentitis	

Case	Species	Tissue	Lesion/condition	Page
2	Texel lamb	Liver	Leptospirosis	
3	Merino cross sheep	Kidney	Oxalate nephrosis	
4	Toggenburg goat	Brain, Lung	Caprine arthritis encephalitis virus	
Conference 23 – April 19, 2025				
1	White-faced saki monkey	Tibia	Fibrous osteodystrophy	
2	European shorthair cat	Bone (humerus)	Simple bone cyst (pseudocyst)	
3	Domestic rabbit	Oral cavity	Ameloblastoma	
4	Giant schnauzer dog	Maxilla	Oral papillary squamous cell carcinoma	
Conference 24 – April 24, 2025				
1	Commercial crossbred pig	Heart	Encephalomyocarditis virus pancarditis	
2	Standardbred horse	Liver, Kidney	Equine viral arteritis pneumonia	
3	Bulldog	Lung	Canine herpesvirus-1 hepatitis and nephritis	
4	Angus calf	Brain	Bovine herpesvirus-5 meningoencephalitis	
Conference 25 – April 28, 2025				
1	Jersey cow	Brain	*Naegleria fowleri* meningoencephalitis	
2	Sitatunga	Brain	*Parelaphostrongylus tenuis* meningoencephalitis	
3	Domestic shorthair cat	Brain	Feline hippocampal and piriform necrosis	
4	North American beaver	Brain	*Baylisascaris* meningoencephalitis	

Joint Pathology Center
Veterinary Pathology Services

WEDNESDAY SLIDE CONFERENCE 2024-2025

Conference #1 — 14 August 2024

CASE I:

Signalment:
Aborted thoroughbred equine foetus (*Equus caballus*).

History:
A late gestation aborted thoroughbred foetus was submitted for postmortem examination. No placenta was submitted. According to the submitted clinical history, the mare had been vaccinated for equine herpesvirus and had no history of previous abortions.

Gross Pathology:
The equine foetus was presented dead, in a fair state of preservation. Fetal weight was 40 kg and body length 110 cm (estimated gestational age between 300 and 330 days). No placenta was available for examination. There were no gross lesions on external examination. Examination of the thoracic cavity revealed diffusely firm and rubbery lung lobes (non-aerated). No other lesions present.

Microscopic Description:
Liver: Within the hepatic parenchyma are multifocal, random areas of hepatocellular necrosis characterised by sinusoidal disruption, accumulation of karyorrhectic cellular debris, hepatocyte hypereosinophilia, cellular swelling, nuclear pyknosis and rare mixed inflammatory cells. Hepatocytes in adjacent areas frequently contain 2-4 um, pale eosinophilic intranuclear inclusions that displace the nuclear chromatin to the periphery.

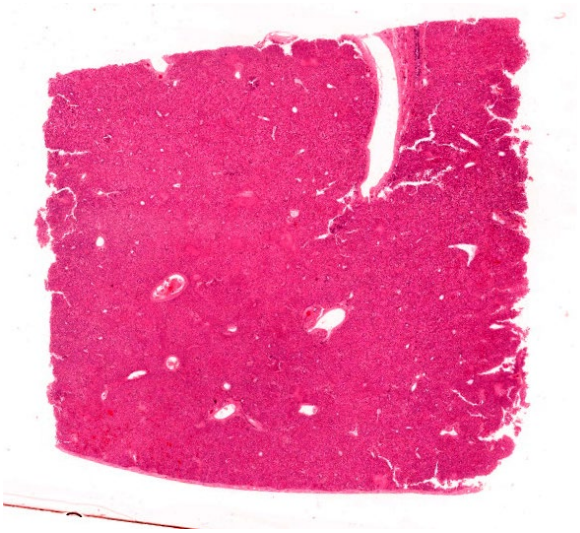

Figure 1-1. Liver, foal. One section of liver is submitted for examination. (HE, 5X)

Hepatic sinusoids are mildly congested. Periportal areas are moderately expanded by oedema and moderate numbers of lymphocytes, plasma cells and macrophages. Occasionally, small to medium calibre blood vessel walls are expanded by oedema, and necrosis of endothelial cells, characterised by pyknosis, cellular swelling, karyorrhexis and karyolysis.

Contributor's Morphologic Diagnosis:
Liver: Hepatocellular necrosis, acute, multifocal, random, with hepatocellular intranuclear inclusion bodies.

Contributor's Comment:
Equine herpesvirus type-1 (EHV-1) and equine herpesvirus type-4 (EHV-4) are important ubiquitous pathogens of all breeds of horses and other equids worldwide. In general,

EHV-1 strains are associated with respiratory disease, abortion, and paresis/paralysis, whereas EHV-4 strains are predominantly associated with respiratory disease.[2-4] In New Zealand, and similar to the rest of the world, most cases of equine herpesviral abortions are due to EHV-1. Equine herpesvirus type-1 (EHV-1) is a large, enveloped, DNA virus that is classified within the family *Alphaherpesviridae* in the order *Herpesvirales.* The virus is spread via multiple routes, including fomites, fetuses and placentas from EHV-1 induced abortions, and particularly by horse-horse contact and contamination. Horses shed EHV-1 in their respiratory secretions for up to three weeks post-infection.[3] Once infection is established, subclinical latency in the trigeminal ganglion occurs, and helps viral transmission between horses, which may or may not be associated with signs of illness.[3,5]

In clinically ill animals, following exposure, the virus replicates in a restricted plaque wise manner in the epithelial cells lining the upper respiratory tract,[5,6] including the pharynx, nasal turbinates, soft palate, and tracheal epithelium.[4] Entrance into epithelial cells is established either via direct fusion with the plasma membrane, or by endocytosis and fusion with an endosomal membrane.[3] After infecting the respiratory tract, the virus crosses the basement membrane via infected leukocytes ($CD172^+$ cells and T/B lymphocytes).[5] Once through the basement membrane, these infected leukocytes, penetrate connective tissues and enter the bloodstream and draining lymph nodes within 24-48 hours post infection.[4,6] Thus, viraemia via infected leukocytes disseminates the virus around the body, resulting in pyrexia and lymphadenomegaly.[5] Once in the circulation, EHV-1 can travel around the body and establish infection in target organs, including the pregnant uterus or the central nervous system.[3,5] This is established via strong adherence of EHV-1 infected leukocytes to endothelial cells, which subsequently results in an inflammatory environment that recruits additional monocytes to the endothelium.[5] The resulting inflammatory cascade may promote further endothelial cell infection, via increased expression of adhesion molecules (selectins secondary to release of IL-2 and TNF-alpha) on endothelial cells and stronger adherence of infected leukocytes.[7] After adherence, the virus replicates in the endothelial cells of the uterus, allantochorion, and umbilical vein.[8] The resulting vasculitis and thrombosis, damages the placenta and disrupts blood supply, leading to abortion[6]. This has been demonstrated in experimentally infected animals, where a lymphocytic vasculitis, focal thrombosis, and infarction of the microcotyledons results in abortion.[8] Abortion typically occurs, after 2-12 weeks in late gestation, and the incubation period varies widely from 9-120 days. [4,8] Interestingly, most cases result in no obvious uterine lesions, however in the presented case a severe metritis was diagnosed in the mare. However, it has been reported that there are no long term effects on reproductive performance in affected mares.[2]

As previously mentioned, viral latency can also develop, this occurs after replication in the respiratory epithelium. The virus enters nerve endings of the peripheral nervous system, including the trigeminal ganglia, and sympathetic and parasympathetic neurons that innervate the respiratory epithelium.[5] Here it travels via retrograde transport to the sensory and autonomic peripheral ganglia.[5] Along with this, it has been demonstrated to establish latency in the circulating T lymphocytes. Under stress, reactivation of EHV-1 replication occurs and particles spread from these infected T lymphocytes or trigeminal neurons through anterograde transport to the respiratory epithelium.[5]

Gross foetal lesions described in the literature include icterus, splenomegaly, perirenal oedema, pulmonary oedema or haemorrhage,

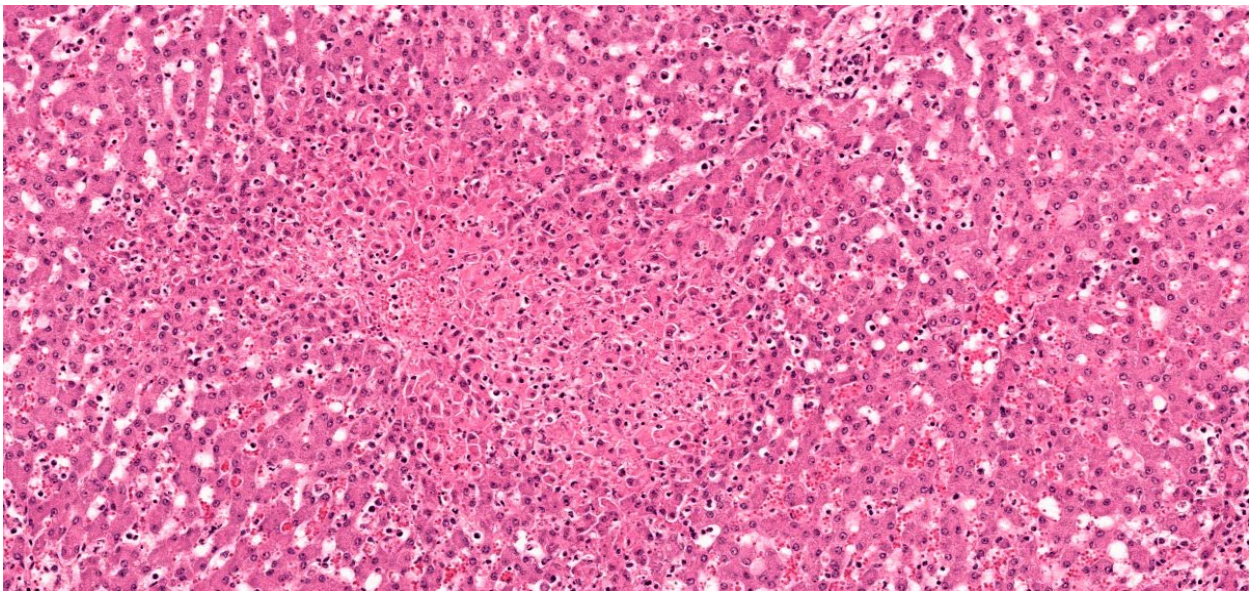

Figure 1-2. Liver, foal Areas of coagulative necrosis are scattered throughout the section. (HE, 144X)

and pale miliary foci on the surface of the liver.[8,9] In the present case, no gross lesions were present in the foetus, and a definitive cause for the abortion was not established during gross postmortem examination.

Confirmation of EHV-1 infection can be done via a number of ways, including immunohistochemistry of frozen or paraffin embedded tissues, and PCR for direct and rapid detection in frozen or paraffin embedded tissues.[8] Additionally, histological lesions, if present, can be used to support a diagnosis of EHV-1. Respiratory lesions include uniform pulmonary interlobular septal oedema and infiltration with mononuclear inflammatory cells, with fibrinous alveolar exudation and necrosis of bronchial and alveolar epithelial cells.[7] Hepatic lesions are not as common, but include focal necrosis, oedema, and leukocytes in the necrotic foci and portal triads. The acidophilic inclusion bodies in the nuclei of hepatic parenchymal cells surrounding these necrotic foci are specific for EHV.[6,7]

Preventative measures include management strategies and vaccination of breeding mares. Separating animals into groups or maintaining a closed herd can be an effective strategy. Quarantine of any new arrivals onto the farm for a minimum of 30 days is also highly recommended[4] as is investigation into the horses vaccination status, health certificate and negative tests results. All equipment used for new arrivals should be separate or disinfected and cleaned thoroughly if shared around the property.[4] Any personal involved in handling said animals, should also clean their bodies, boots and clothing thoroughly before handling other animals. Vaccines currently used include, inert or live vaccines. Current guidelines are to vaccinate foals over 3-5 months of age, with a booster within 4-6 weeks, along with vaccination every 3-6 months to enhance immunity.[4] Pregnant mares should also be vaccinated at the fifth, seventh, and ninth months of pregnancy.[4]

Contributing Institution:
Massey University
School of Veterinary Science
Private Bag 11 222
Palmerston North 4442
New Zealand

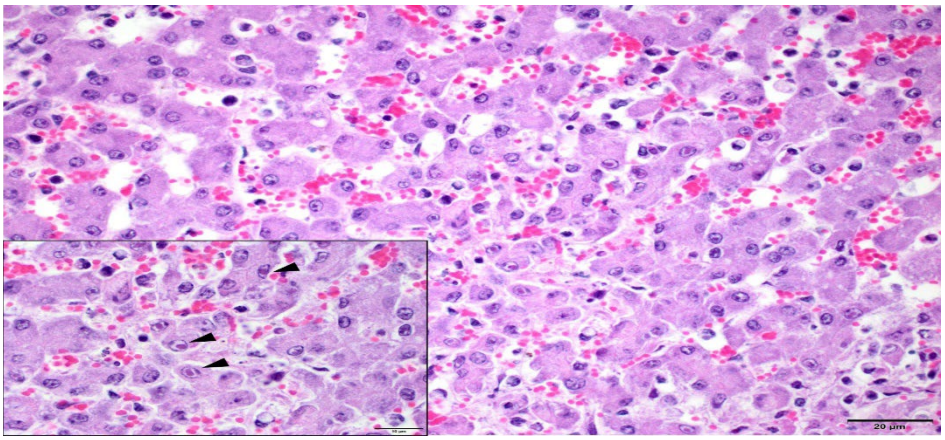

Figure 1-3. Liver, foal. At the edges of areas of necrosis, hepatocellular nuclei contain prominent viral inclusions. (HE, 400X) (*Photo courtesy of:* Massey University, School of Veterinary Science, Palmerston North 4442, New Zealand)

JPC Diagnosis:
Liver: Hepatitis, necrotizing, subacute, multifocal, random, moderate, with hetpacellular intranuclear viral inclusions.

JPC Comment:
This week's session was led by Colonel Sherri Daye, Director of JPC Veterinary Pathology (and all-around equine enthusiast). The cases for the first conference of WSC 2024-2025 were entirely an 'equine affaire' with 4 classic entities that have been seen in the conference before. This first particular case is diagnostically rewarding with multifocal, random areas of necrosis within the liver that provide a solid hint at the underlying pathogenesis. Likewise, intranuclear viral inclusions within hepatocytes are characteristic (figure 1-3) and help refine differentials for this case. Conference participants remarked at the distribution of necrosis in this case – there was a brief discussion of whether coagulative necrosis secondary to viral ischemic effects was a significant feature of this case. Ultimately, the group felt that endothelial cells lacked obvious viral inclusions and that the lesions were not predominately vasocentric and lacked significant thrombi. Additionally, the group slightly differed from the contributor in chronicity, noting that most cases of abortion take an extended period of time to develop given the cell-to-cell spread of alphaherpesviruses.[1] Moreover, a similar case of EHV in a neonatal horse was reviewed in a previous WSC (Conference 7, Case 3, 2015-2016) with extensive regions of hemorrhage and lytic necrosis within the lung, liver, and adrenal gland that reflects the expected distribution of lesions in animals that may be infected late in term and/or survive to parturition with EHV. Absent confirmation of the diagnosis via PCR and/or IHC of tissue in this case, we are left to favor EHV-1 over EHV-4.

The case contributor provides a nice overview of equine herpesviruses with emphasis on their role in equine abortion. Prevention of EHV-associated disease remains paramount; current consensus recommendations were recently updated by the ACVIM[6] and include vaccination in conjunction with a robust biosecurity program. To date, vaccination alone is not sufficient to prevent spread of EHV nor does it ameliorate clinical signs in sick horses. That stated, the ability of vaccines to prevent the development of viremia, at least in some animals, can serve to avoid devastating sequalae such as abortion or myeloencephalopathy.[6]

There are a number of other potential causes for abortion and stillbirth in foals. Bacterial causes include beta-hemolytic streptococci, *E. coli*, *Pseudomonas aeruginosa*, *Staphylococ-*

cus aureus, *Klebsiella pneumoniae*, and *Actinobacillus equuli* among others.[1, 7] Infection may occur as a consequence of mare bacteremia or, more commonly, via ascending infection through the cervix. Fungal causes are typically attributed to *Aspergillus* spp., though other organisms may occasionally be isolated.[1,7] Rarely, equine viral arteritis has been isolated in abortion cases.[1,7] Non-infectious causes such as umbilical cord torsion and congenital malformation also remain common. Definitive cause of abortion and stillbirths remains elusive in many cases with only 29.2% of all submissions to a California diagnostic lab having a certain etiology identified.[1]

Finally, EHV-1 and EHV-4 should be distinguished from EHV-2 and EHV-5 which are both gamma herpesviruses that do not cause abortion, but are isolated both from healthy horses and those with equine multinodular pulmonary fibrosis (EMPF; EHV-5) and respiratory illness (EHV-2). There are multiple examples of EHV-5 in previous WSC proceedings. EHV-3 is associated with equine coital exanthema, and rarely, subclinical respiratory infections in yearling horses.[7]

References:

1. Cantón GJ, Navarro MA, Asin J, et al. Equine abortion and stillbirth in California: a review of 1,774 cases received at a diagnostic laboratory, 1990-2022. *J Vet Diagn Invest.* 2023 Mar;35(2):153-162.
2. Dunowska M. A review of equid herpesvirus 1 for the veterinary practitioner. Part A: clinical presentation, diagnosis, and treatment. *New Zeal Vet J.* 2014;62: 171-178.
3. Dunowska M. A review of equid herpesvirus 1 for the veterinary practitioner. Part B: pathogenesis and epidemiology. *New Zeal Vet J*. 2014;62: 179-188.
4. Khusro A, Aarti C, Rivas-Caceres RR, Barbabosa-Pliego A. Equine herpesvirus-1 infection in horses: Recent updates on its pathogenicity, vaccination, and preventive management strategies. *J Equine Vet Sci.* 2020;87: 102923.
5. Laval K, Poelaert KCK, Van Cleemput J, et al. The pathogenesis and immune evasive mechanisms of equine herpesvirus type 1. *Front Microbiol*. 2021;12: 662686.
6. Lunn DP, Burgess BA, Dorman DC, et al. Updated ACVIM consensus statement on equine herpesvirus-1. *J Vet Intern Med*. 2024 May-Jun;38(3):1290-1299.
7. Schlafer DH, Foster RA. Chapter 4: Female genital system. ln: Maxie MG ed. *Jubb, Kennedy, and Palmer's Pathology of Domestic Animals*. Vol 3. 6th ed. Missouri, USA: Elsevier; 2016:358-464.
8. Smith KC. Herpesviral abortion in domestic animals. *Vet J*. 1997;153: 253-268.
9. Smith KC, Blunden AS, Whitewell KE, Dunn KA, Wales AD. A survey of equine abortion, stillbirth and neonatal death in the UK from 1988 to 1997. *Equine Vet. J.* 2003;35: 496-501.
10. Van Maanen C. Equine herpes virus 1 and 4 infections: an update. *Vet Q*. 2002;24: 57-78.

CASE II:

Signalment:
8-year-old, male castrated, Arabian horse (*Equus ferus caballus*).

History:
This is a mass surgically removed from the left thorax.

Gross Pathology:
N/A

Microscopic Description:
Subcutis (mass from the left thorax): Expanding the deep dermis and extending to the subcutis are numerous multifocal to coalescing pyogranulomas. The pyogranulomas are com

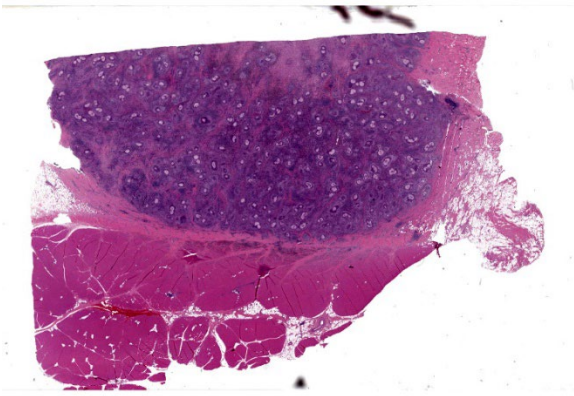

Figure 2-1. Panniculus and subcutis, horse. The subcutis is effaced by an inflammatory nodule which extends into the underlying skeletal muscle. (HE, 5X)

posed of intact and necrotic neutrophils surrounded by epithelioid macrophages, occasional multinucleated giant cells with up to 20 nuclei, fewer lymphocytes and plasma cells. In the center of the pyogranulomas are irregular pools of lightly eosinophilic amorphous material forming grain or granular structures measuring up to 500 um that contain countless tight clusters of polymorphic, refractile, fungal hyphae with frequent bulbous dilations. Surrounding the pyogranulomas are variably thick bands composed of fibroblasts and collagen (fibrosis). Multifocally, the surrounding dermis and subcutis are infiltrated by moderate numbers of lymphocytes and plasma cells, and rare macrophages and neutrophils.

PAS and GMS stains highlight the approximate 2-5 um, polymorphic, fungal hyphae with frequent and bulbous dilatations up to 30 um, consistent with dermatophytic pseudomycetoma.

Contributor's Morphologic Diagnosis:
Subcutis (mass from the left thorax): Multifocal to coalescing, marked, chronic, pyogranulomas with numerous intralesional fungal hyphae (pseudomycetoma).

Contributor's Comment:
A pseudomycetoma represents a subcutaneous infection with either bacteria or dermatophytes present in the tissue as granules or grains.[7] Dermatophytic pseudomycetoma in horses is a rare form of dermatophytosis with colonization beyond the superficial layers of the skin to the live tissues of the deep dermis and subcutis. The lesions are thought to form following the rupture of an infected hair follicle that results in a granulomatous or pyogranulomatous reaction around the dermatophyte hyphae.[8]

The most common cause of dermatophytosis in horses is *Trichophyton equinum*, with less frequent infection by *T. mentagrophytes, T. verrucosum, Microsporum equinum,* and *M. gypseum*.[10] Dermatophytosis is a common and contagious fungal infection of equine skin affecting horses of all ages, and young animals in crowded environments, and those in hot and humid climates may be over represented.[9,10] Infection rarely invades beyond the superficial layers of the skin in healthy animals.[9] Although the health status of this horse is unknown, it can be speculated that an immunocompromised state may have predisposed it to the deeper infection and subsequent psudeomycetoma formation. Pseudomycetomas, while rare, are documented in other domestic

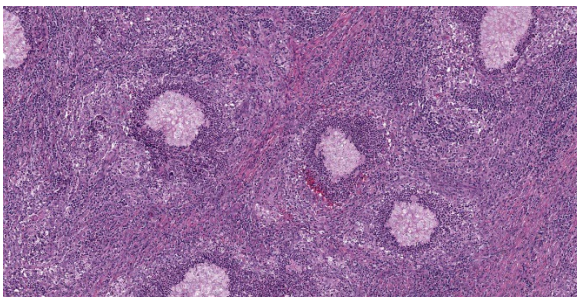

Figure 2-2. Panniculus and subcutis, horse: The nodule is composed of coalescing pyogranulomas centered on aggregates of poorly staining fungal hyphae. (HE, 86X)

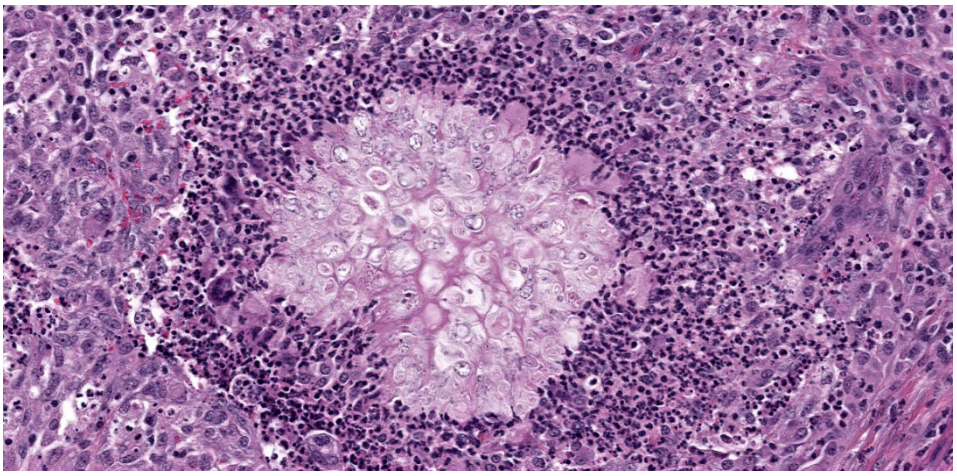

Figure 2-3. Panniculus and subcutis, horse. High magnification of an aggregate of fungal hyphae. Bulbous dilations are numerous within this aggregate. Fungal hyphae are surrounded by numerous neutrophils which are in turn surrounded by a layer of robust epithelioid macrophages and rare multinucleated foreign body-type macrophages. (HE 380X)

pecies, with a predisposition for Persian cats and Yorkshire terriers with *Microsporum canis* as the most common etiologic agent.[8] Given the predominance in Persian cats over other domestic feline species, a genetic deficit in immunity has been a proposed cause.[6]

With standard hematoxylin and eosin staining, grain or granule-like structures composed of fungal hyphae that are embedded in an amorphous eosinophilic matrix presumed to be antigen-antibody complexes[5] are seen to be surrounded by granulomatous or pyogranulomatous inflammation with multinucleate giant cells, and variable lymphoplasmacytic inflammation that are separated by varying degrees of fibrosis. Differential diagnoses include causes of true mycetomas including actinomycetes (actinomycetoma) or fungi (eumyoctic mycetoma).[2]

Contributing Institution:
University of Illinois at Urbana-Champaign, Veterinary Diagnostic Laboratory

http://vetmed.illinois.edu/vet-resources/veterinary-diagnostic-laboratory/

JPC Diagnosis:
Panniculus and underlying skeletal muscle: Pyogranulomas, multiple with numerous fungal hyphae, Splendore-Hoeppli material, and marked panniculular fibrosis.

JPC Comment:
This second case is striking from subgross, with identification of the lesion distribution hardly a diagnostic quandary (Figure 2-1). Although special stains were not necessary to arrive at the diagnosis for this case, we found that the methenamine silver (GMS) and periodic acid-Schiff (PAS) stains highlighted fungal elements nicely (Figure 2-4, Figure 2-5). Significant features include the presence of septate hyphae, chain-like pseudohyphae, and large (12um) pseudogranules.[10] Conference participants remarked that the H&E features were convincing for a fungal etiology, but exact speciation was not possible without additional ancillary diagnostics such as PCR or fungal culture. We differed from the contributor therefore in this case by omitting the mycetoma/pseudomycetoma distinction from the morphologic diagnosis. As a final treat for conference participants, Dr. Bruce Williams reminded the group that PAS is pronounced 'per-eye-OD-ik acid – Schiff' as the name of the reagent that we use 'periodically' for cases has decidedly different pronunciation that is easy to confuse.

As pointed out by the contributor, the location of these fungal pyogranulomas in the deep dermis with extension into the pectoral muscle is unusual for this entity however. Mycetoma

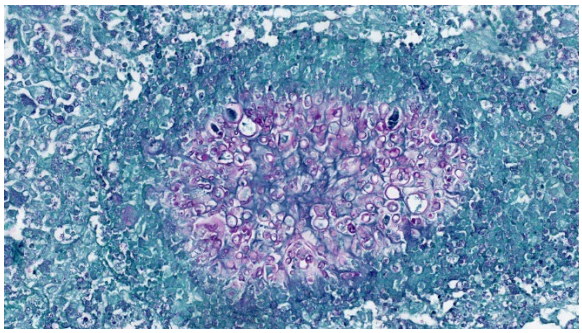

Figure 2-4. Panniculus and subcutis, horse. Fungal hyphae stain positively with periodic-acid Schiff stain. (PAS, 400X)

should be distinguished from pseudomycetoma by several key features. Mycetomas are fibrotic inflammatory nodules with draining fistulous tracts, and tissue grains of fungal aggregates with fewer hyphal elements surrounded by minimal amounts of Splendore-Hoeppli material and more cement material.[5] In contrast, pseudomycetomas are typically multifocal, may lack overt skin changes, are associated with dermatophytes, and typically have more abundant fungal hyphae and Splendore-Hoeppli material present histologically than true mycetomas do.[5] The abundant fungal hyphae, multifocal distribution of lesions, and abundant amorphous eosinophilic material (Splendore-Hoeppli) in this case is most consistent with dermatophytic pseudomycetoma, absent other confirmatory diagnostics. Wider distribution of lesions, to include regional draining lymph nodes, is an occasional finding.[1,5]

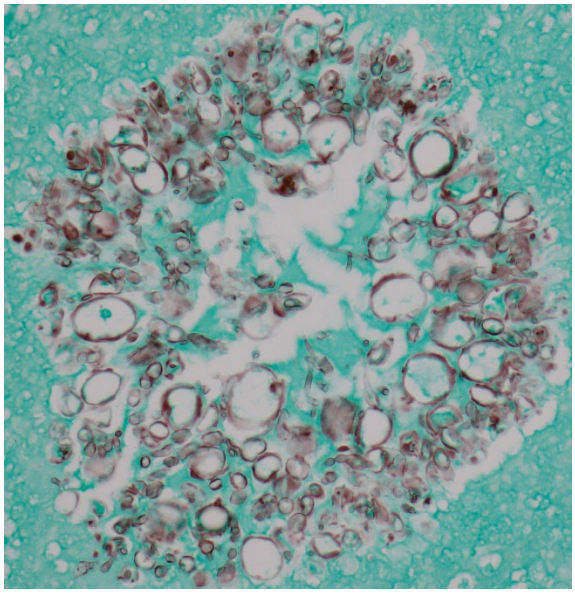

Figure 2-5. Panniculus and subcutis, horse. The cell wall of the fungal hyphae stain positively with a silver stain. (GMS, 400X)

Dermatophytic pseudomycetoma has been rarely reported in the cat[1,3,5] and has been previously covered in WSC (see Conference 11, Case 2, 2019-2020 and Conference 11, Case 3, 2008-2009). Persian, and to a lesser extent, Himalayan cats appear to have a predilection that may be explained by a longer hair coat and/or increased susceptibility to dermatophytes secondary to variation in the calprotectin gene which encodes an antimicrobial peptide.[1] Dermatophytic pseudomycetoma in shorthair cats has also been described, to include a recent case report from Korea.[3] Pseudomycetomas have also been described in the ferret[4], though case reports in the horse are sparse in the literature.

References:

1. Barrs VR, Bęczkowski PM, Talbot JJ, et al. Invasive fungal infections and oomycoses in cats: 1. Diagnostic approach. *Journal of Feline Medicine and Surgery*. 2024;26(1).
2. Cafarchia C, Figueredo L, Otranto D. Fungal diseases of horses. *Veterinary Microbiology*. 2013;167: 215-234.
3. Cho J, Park C, Park J, Yoon JS. Case report: Dermatophytic pseudomycetoma in a domestic Korean short hair cat treated with intralesional injection of amphotericin B and oral terbinafine administration. *Front Vet Sci*. 2024 Jun 13;11:1402691.
4. Giner J, Bailey J, Juan-Salles C, Joiner K, Martinez-Romero EG, Oster S. Dermatophytic pseudomycetomas in two ferrets. *Vet Derm* 2018: 29:452-e154.
5. Gross TL, Ihreke PJ, Walder EJ, Affolter VK. *Skin Diseases of the Dog and Cat*

Clinical and Histopathologic Diagnosis. 2nd ed. Ames, IA: Blackwell Publishing; 2005: 288-291.
6. Hargis AM, Ginn P, The integument. Ln: McGavin MD, Zachary JF eds. *Pathologic Basis of Veterinary Disease.* 6th ed. St. Louis, MO:Mosby Elsevier; 2017: 1079-1144.
7. Maudlin EA, Peter-Kenney J. Integumentary. ln: Maxie MG ed. *Jubb, Kennedy, and Palmer's Pathology of Domestic Animals*. Vol. 1. 6th ed. Philadelphia, PA: Elsevier Saunders. 2016: 649-653.
8. Nardoni S Franceschi A & Mancianti F. Identification of *Microsporum canis* from dermatophytic pseudomycetoma in paraffin-embedded veterinary specimens using a common PCR protocol. *Mycoses.* 2007;50(3): 215-217.
9. Pilsworth R, Knottenbelt D. Common Equine Skin Diseases. Equine Veterinary Journal Ltd, Newmarket, Suffolk, UK; 2006: 52-53.
10. Scott, DW, Miller WH. *Equine Dermatology.* 2nd ed. St. Louis, MO: WB Saunders Co; 2011: 161-163, 171-201.

CASE III:

Signalment:
7 years of age, female, Selle Français, *Equus caballus*, Horse.

History:
The mare was initially presented to the referral clinic due to symptoms of chronic, recurrent diarrhea and intermittent exercise intolerance. General clinical examination revealed no abnormalities, with the exception of an enlarged, non-painful, retropharyngeal lymph node on the left side. Hematology, basic blood chemistry, and parasitological examination were normal. The horse was sent home after oral treatment with prednisolone (Equisolon®).

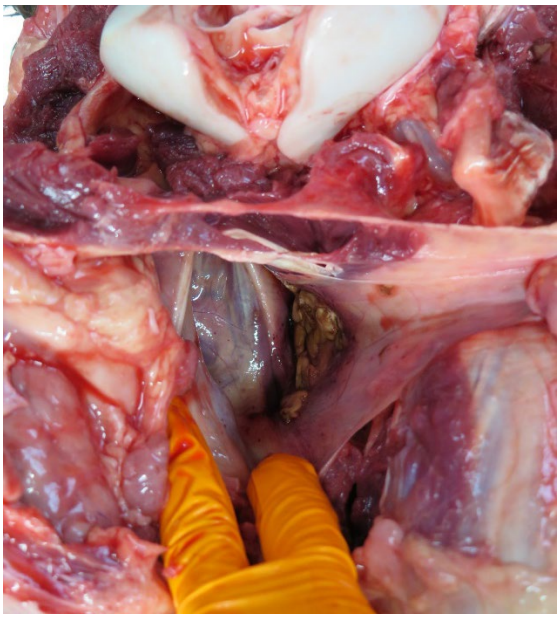

Figure 3-1. Guttural pouch, horse. The right guttural pouch was filled with clotted blood and contained a sharply delineated slightly raised irregular white plaque ca. 6 cm in diameter (suggestive of mycosis) at the level of the medial wall. (*Photo courtesy of:* Department of Pathology, Microbiology and Avian Diseases, Faculty of Veterinary Medicine, University of Ghent, Salisburylaan 133, 9820 Merelbeke, BELGIUM, veterinaire.pathologie@ugent.be, + 32 9 264 77 41, https://www.ugent.be/di/di05/nl).

1 month later the horse suffered from severe, acute, right-sided epistaxis and was re-admitted to the clinic and hospitalized. Endoscopy of the upper airways revealed the presence of large amounts of blood in pharynx and trachea, as well as a large blood clot filling the lumen of the right guttural pouch. The left guttural pouch was evaluated as normal.

Surgery under general anesthesia was performed with fluoroscopy-guided placement of 7 intra-arterial coils in carotid and maxillary arteries. During recovery excitation and epistaxis developed. An emergency ligation of the right-sided a. carotis communis was attempted but proved ineffective. The horse was subsequently euthanized.

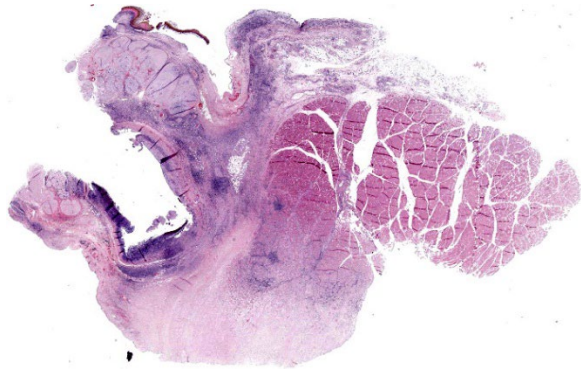

Figure 3-2. Guttural pouch, horse. An excellent section from the guttural pouch is submitted for examination. The internal carotid artery is at left, and the guttural pouch proper is at top center. (HE, 4X)

Gross Pathology:
The right guttural pouch was filled with clotted blood and contained a sharply delineated slightly raised irregular white plaque ca. 6 cm in diameter (suggestive of mycosis) at the level of the medial wall, with several smaller blood clots adherent to this area. Which, when removed, revealed a focal depression in the wall and a frayed transmural defect of a large thick-walled blood vessel (a. carotis interna).
The left side guttural pouch did not contain any blood but a smaller, ca. 4 cm diameter, pale plaque was found adherent to the wall.
Other significant gross findings included pale oral mucosae, blood exuding from both nostrils, and hemorrhagic contents of stomach and duodenum.

Microscopic Description:
Guttural pouch, part of large vessel wall, associated nerves and muscle.
The endothelium of the large artery is multifocally eroded and replaced by a layer of fibrin, admixed with erythrocytes (hemorrhage), eosinophilic necrotic cell and nuclear debris, and few partially degenerate neutrophils (arteritis).

At the level of the eroded surface and penetrating deeper into the tunica media and connective tissues a moderate amount of ca. 5-8µm long deeply basophilic structures with parallel walls can be found, sometimes seen to be dichotomously branching, and often endospore-forming (fungal hyphae). The severity of the arteritis and presence of hyphae is dependent on the level of tissue section.

Smaller vessels show hyalinization of the wall and contain mixed nuclear dust and a dense infiltration of neutrophils (thrombosis and vasculitis).

Multifocal areas of coagulative necrosis surround and infiltrate muscle fibers and nerve fibers deep in the tissue, along with the presence of occasional fungal hyphae.

Contributor's Morphologic Diagnosis:
Mycotic air sacculitis, chronic, severe, erosive, necrotizing, with fungal hyphae, obliterating necrosuppurative arteritis, multifocal vascular thromboses, and local necrotizing fungal myositis and neuritis.

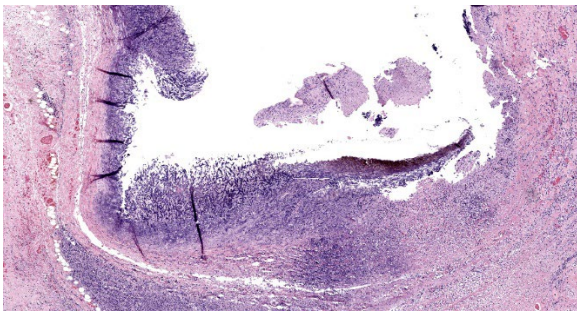

Figure 3-3. Internal carotid artery, horse. There is segmental loss of the endothelium and necrosis of the underlying arterial wall with growth of fungal hyphae into the lumen. (HE, 39X)

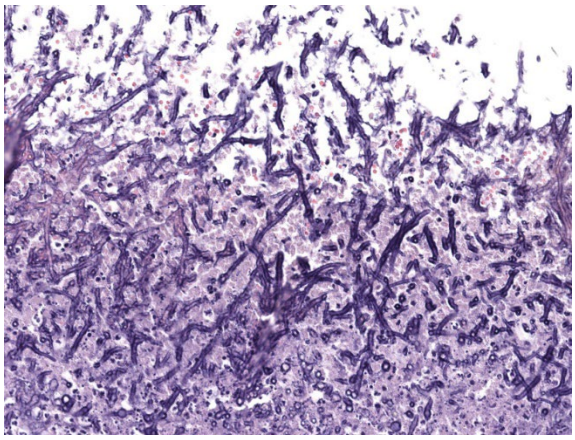

Figure 3-4. Internal carotid artery, horse. Higher magnification of septate, dichotomously branching, 4-6um fungal hyphae within the internal carotid artery. (HE, 240X)

Contributor's Comment:
The equine guttural pouches are a somewhat unique bilaterally symmetrical anatomical structure which can be interpreted as a local diverticulum of the inner auditory tube or Eustachian tube in which several important structures can be found.[10] It is longitudinally divided into two communicating compartments, lateral and medial, by the stylohyoid bone. Their functionality has been a topic of discussion for many decades or even centuries, but Ninomiya & Kuwano confirmed them to play a role as an effective countercurrent heat exchanger cooling arterial blood flowing towards the brain.[10]

Equine guttural pouch mycosis is a rare but potentially highly morbid and possibly fatal disease, most often caused by *Aspergillus* spp. in temperate climates, which are fairly ubiquitous opportunistic pathogens present in upper airways of healthy equids as well as in their immediate surroundings.[3,4,5,6,8]

There appears to be no predilection in regard to breed, sex, age, or left versus right side air sacs.[3] The fungal hyphae, especially of *A. fumigatus*, are typically angiotropic/angioinvasive and therefore often form infiltrative mycotic plaques associated with the large blood vessels lying closely beneath the guttural pouch surfaces.[1,8,5]

It can be considered challenging to diagnose, in part due to the wide spectrum of possible clinical signs, but also due to the high risks associated with confirmation of the pathogen in situ.[7,11] In this particular case, based on the history, gross lesions, and microscopic findings, infection with *Aspergillus spp*. was found to be most likely, though the presence of other non-pigmented hyphae producing fungi cannot be excluded.[4]

Contributing Institution:
Department of Pathology, Microbiology and Avian Diseases
Faculty of Veterinary Medicine, University of Ghent
Salisburylaan 133, 9820 Merelbeke, BELGIUM
https://www.ugent.be/di/di05/nl

JPC Diagnosis:
Guttural pouch: Eustachitis and arteritis, necrotizing, chronic, diffuse, severe, with numerous fungal hyphae, fibrin thrombi, and infarction of skeletal muscle and nerves.

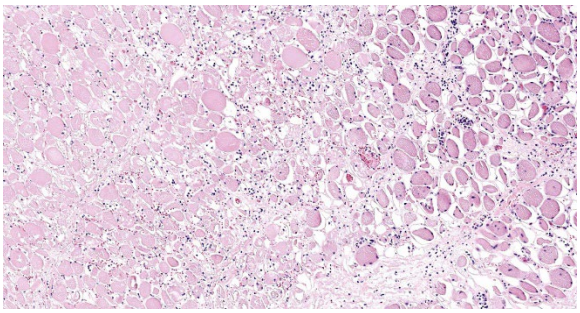

Figure 3-5. Guttural pouch horse. Infarcted skeletal muscle (at left) adjacent to the inflamed internal carotid artery. Viable muscle and inflammatory cells are present at right.) (HE, 75X)

JPC Comment:
The exact tissue identification for Case 3 is subtle, though the presence of a large blood

vessel next to nerves, deeper muscle and a thin layer of squamous epithelium is suggestive of the equine guttural pouch (Figure 1-1). That stated, the magnificent fungal arteritis that the contributor has shared with us quickly pares down the differential list. Like the previous case, fungal elements are also a major diagnostic feature though the distribution and tissue response is quite different from Case 2. GMS and PAS stains were less remarkable for this case, though this may simply reflect luck and plane of section for the slides we selected. Conference participants felt that the features on H&E were highly suggestive of *Aspergillus*, though they did remark on the pigmentation present along the guttural pouch mucosa and whether this might be related to another fungal species instead (Figure 3-7).

As the contributor notes, guttural pouch mycosis is often caused by *Aspergillus* species and the large fungal mats along the surface of and expanding into large blood vessels is a helpful diagnostic feature.[2] While hemorrhage and epistaxis are common clinical manifestations of guttural pouch mycosis, they are not the only significant ones to consider. Marked guttural pouch inflammation can extend into adjacent structures to include the vagosympathetic trunk, bones , middle ear, brain, or

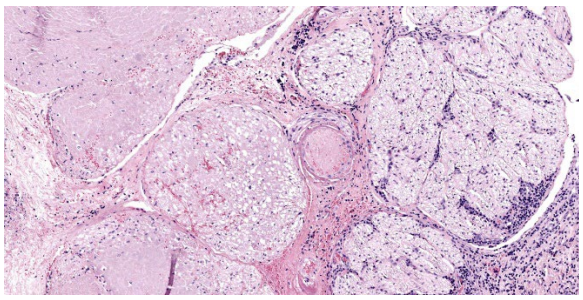

Figure 3-6. Guttural pouch horse. There is infarction (left) of bundles of nerves, with multifocal inflammation and hemorrhage. A thrombosed arteriole is present in the center of this field. (HE, 175X)

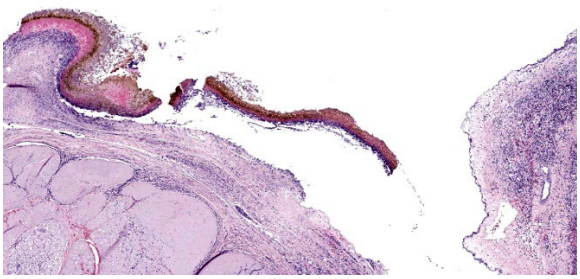

Figure 3-7. Guttural pouch, horse. A large mat of fungal hyphae extends along the ulcerated surface of the guttural pouch as well. (HE, 39X)

joints.[2] Dysphagia, Horner's syndrome, and laryngeal hemiparesis have all been reported secondary to guttural pouch mycosis.[2] Although the animal in the present case did not have reported neurologic deficits at the time of euthanasia, there is marked necrotizing arteritis that spills over to adjacent skeletal muscle (myositis) and nerves (neuritis) quite spectacularly. For a similar case from the WSC archives, see Conference 21, Case 2, 2012-2013.

Other diseases of the guttural pouch to consider include guttural pouch tympany, guttural pouch empyema, temporohyoid osteoarthropathy, and neoplasia.[2,11] Tympany is uncommon and is seen in young horses secondary to congenital conformational abnormalities or inflammation that leads to retention of air and expansion of the guttural pouch. Empyema is seen secondary to respiratory infection, most commonly *Streptococcus equi*, and purulent nasal discharge (not hemorrhage) is the typical finding. Neoplasia of the guttural pouch is rare, but squamous cell carcinoma has been reported.[2] Temporohyoid osteoarthropathy reflects remodeling of either/both the stylohyoid bone and petrous temporal bone; this may occur secondary to otitis media, respiratory infection, or degenerative conditions.[11] Diagnostic imaging, to include, radiography, endoscopy, and computed tomography are helpful at distinguishing these diseases amid a complex anatomical landscape. [11]

References:

1. Brandão ISL, Oliveira-Moraes H, Souza Motta CM, Oliveira NTD, Magalhães O. Elastin increases biofilm and extracellular matrix production of *Aspergillus fumigatus*. *Brazilian Journal of Microbiology*. 2018; 49: 675–682.
2. Caswell JL, Williams KJ. Respiratory System. In: Maxie MG, ed. *Jubb, Kennedy & Palmer's Pathology of Domestic Animals*. Vol 2. 6th ed. St. Louis, MO: Elsevier; 2016:480-481.
3. Dobesova O, Schwarz B, Velde K, Jahn P, Zert Z, Bezdekova B. Guttural pouch mycosis in horses: a retrospective study of 28 cases. *Veterinary Record*. 2012; 171: 561-561.
4. Guarner J, Brandt ME. Histopathologic diagnosis of fungal infections in the 21st century. *Clinical Microbiology Reviews*. 2011; 24: 247-280.
5. Kipar A, Frese K. Hypoglossal neuritis with associated lingual hemiplegia secondary to guttural pouch mycosis. *Veterinary Pathology*. 1993; 30: 574-576.
6. Lepage OM, Perron MF, Cadoré JL. The mystery of fungal infection in the guttural pouches. *The Veterinary Journal*. 2004; 168: 60-64.
7. Lepage OM. Challenges associated with the diagnosis and management of guttural pouch epistaxis in equids. *Equine Veterinary Education*. 2016; 28: 372-378.
8. Ludwig A, Gatineau S, Reynaud MC, Cadoré JL, Bourdoiseau G. Fungal isolation and identification in 21 cases of guttural pouch mycosis in horses (1998–2002). *The Veterinary Journal*. 2005; 169: 457-461.
9. Nadkarni T, Goel A. Aspergilloma of the brain: an overview. *Journal of Postgraduate Medicine*. 2005; 51: 37-41.
10. Ninomiya H, Kuwano A. Microvasculature of the Guttural Pouch Mucosa and Relationship With the Internal Carotid Artery in Horses. *Journal of Equine Veterinary Science*. 2019; 74: 84-89.
11. Pollock PJ. Diagnosis and management of guttural pouch mycosis. *Equine Veterinary Education*. 2007; 19: 522-527.
12. Thomas-Cancian A, Ségard-Weisse E, Drumond B, Cadoré J-L. Diagnostic Imaging of Diseases Affecting the Guttural Pouch. *Veterinary Sciences*. 2023; 10(8):525.

CASE IV:

Signalment:
9-year-old, gelding, warmblood, horse, Equus caballus.

History:
This horse presented with a 1-year history of a bleeding rostral nasal mass.

Gross Pathology:
N/A

Microscopic Description:
Slide A: Examined are three sections of the nasal vestibule lined by a multifocally eroded stratified squamous epithelium that has numerous individualized neutrophils percolating throughout (neutrophilic exocytosis). The ves

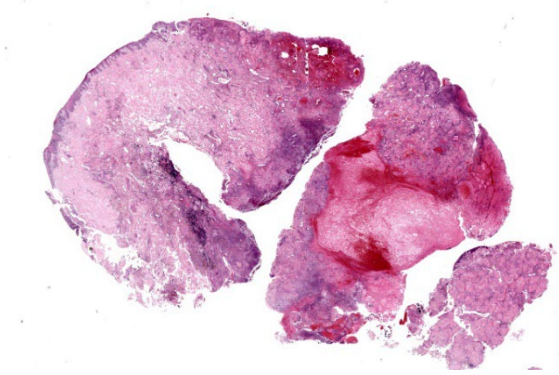

Figure 4-1. Nasal mucosa, horse. Multiple hemorrhagic and ulcerated fragments of nasal mucosa and underlying lamina propria are submitted. (HE, 5X).

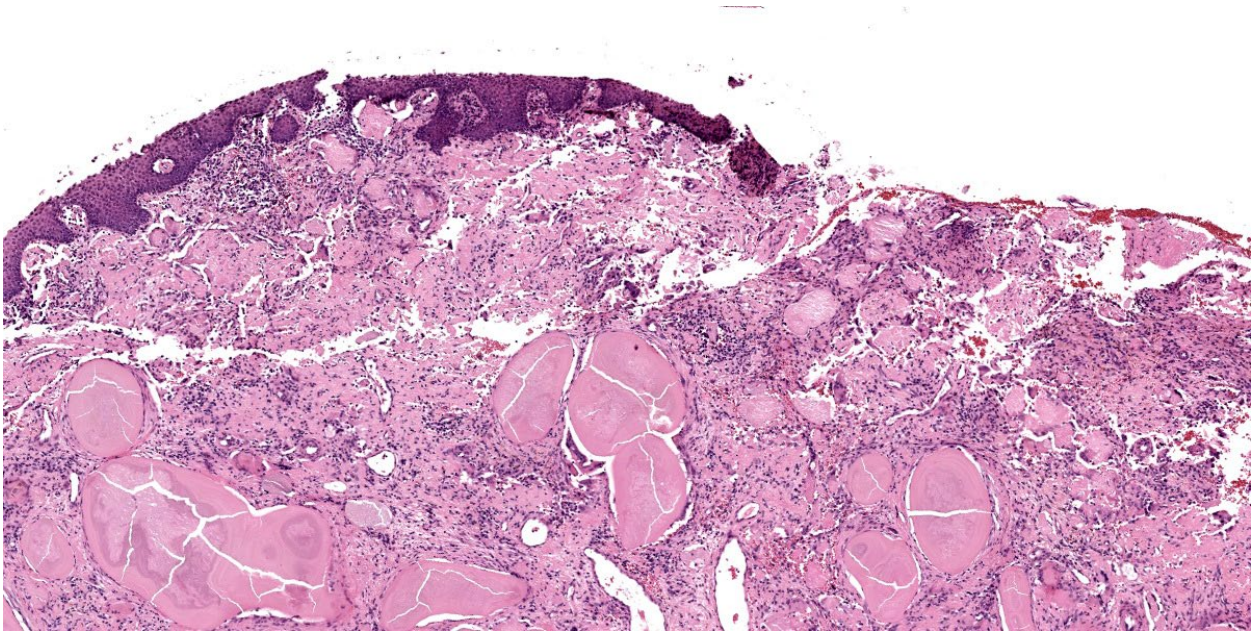

Figure 4-2. Nasal mucosa, horse. There is segmental ulceration of the nasal mucosa. Within the underlying lamina propria, there are aggregates of amyloid. (HE, 60X).

tibular lamina propria is markedly expanded by numerous, large, multinodular deposits of pale eosinophilic, amorphous, smudgy, extracellular material (amyloid). Associated with this amyloid deposition are thick anastomosing bands of fibrous connective tissue that are punctuated by plump reactive fibroblasts and branching small-caliber vessels lined by plump endothelium (granulation tissue). Numerous neutrophils, lymphocytes, plasma cells, macrophages, and multinucleated giant cells percolate throughout this granulation tissue and are interspersed between amyloid deposits. The vestibular lamina propria is additionally expanded by large pools of brightly eosinophilic amorphous to fibrillar material (necrosis) admixed with numerous extravasated red blood cells (hemorrhage), degenerate leukocytes, and hemosiderin and hematoidin-laden macrophages.

Congo red: The pale eosinophilic, amorphous extracellular material stains orange-red (congophilic) and exhibits apple-green birefringence under polarized light.

Contributor's Morphologic Diagnosis:
Nasal vestibule: Severe, chronic, locally extensive amyloidosis with neutrophilic and histiocytic nasal vestibulitis, granulation tissue, epithelial erosion, multifocal necrosis, and chronic-active hemorrhage.

Contributor's Comment:
Equine nasal amyloidosis is an uncommon manifestation of local amyloidosis. Its most common presentation is a single or multiple, often ulcerated, mass-like lesions in the rostral nasal cavity or nasal vestibule; however, amyloidosis can occur in any portion of the nasal cavity and can present as diffuse swelling and not a discrete mass.[1,5-8,12] Concurrent cutaneous, conjunctival, and/or corneal amyloidosis has also been documented.[5,12] Clinical signs often include epistaxis and larger masses may lead to respiratory difficulty and exercise intolerance.[1,5-8] Grossly, the masses caused by amyloidosis can be soft to firm, are often ulcerated, and can have a smooth to waxy appearance.[5-8] Histologic findings are similar amongst all described cases with the presence

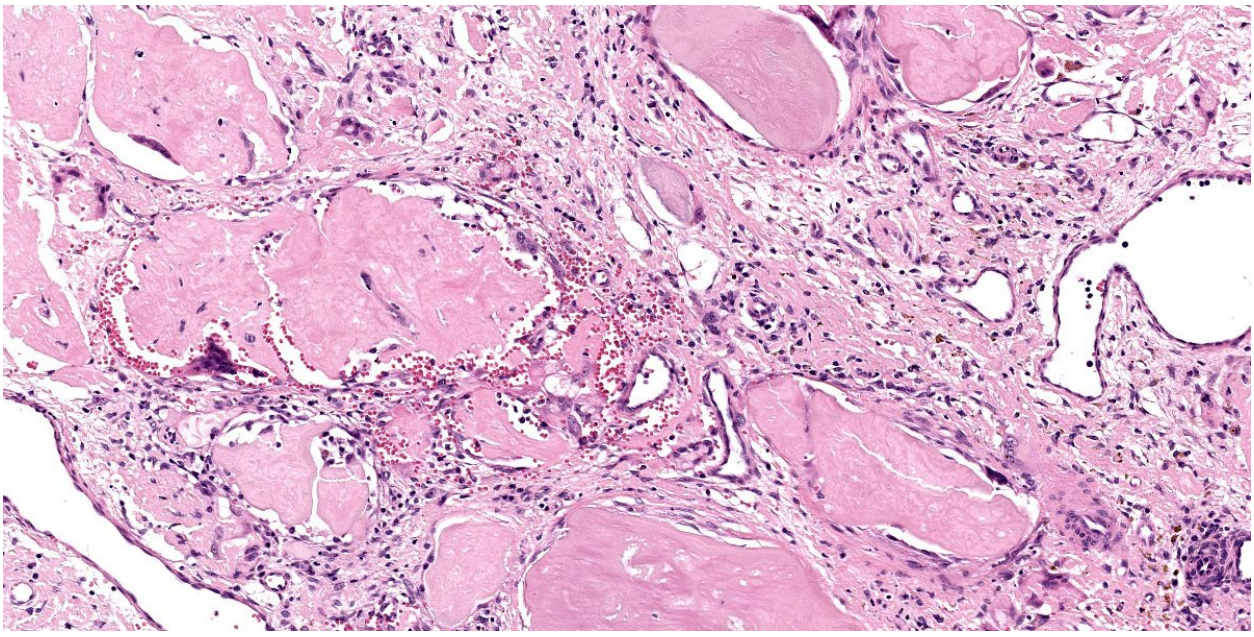

Figure 4-3. Nasal mucosa, horse. High magnification of aggregates of amyloid, which is surrounded by macrophages and foreign body macrophages. (HE, 157X)

of eosinophilic, amorphous material, often associated with granulation tissue, hemorrhage, lymphoplasmacytic histiocytic inflammation, multinucleated giant cells, and occasionally mineralization. The histopathologic findings in this case were similar to those in previous reports.

Amyloid is an extracellular, hyalinized, proteinaceous material composed of polypeptides arranged in beta-pleated sheets forming fibrillar proteins.[4] Due to the conformation of amyloid, it is resistant to degradation leading to accumulation within tissues. Thirty different types of types of amyloid fibril proteins have been discovered, but only nine have been studied in domestic animals and only two, amyloid light chain (AL) and amyloid A (AA), have been described in horses.[1,2,9] Equine nasal amyloidosis is caused by accumulation of the amyloid light chain (AL) type.[1]

Diagnosis of amyloid is commonly achieved through histochemical staining of with Congo Red, which results in orange to red coloration that exhibits apple-green birefringence when observed under polarizing light.[4] Additionally, amyloid light chain (AL) and amyloid A (AA) can be differentiated using a pre-treatment with potassium permanganate. Amyloid A (AA), when pre-treated with potassium permanganate will lose its affinity for Congo red and subsequently lacks the typical birefringent properties.[10]

Differentials on gross examination include fungal granuloma, ethmoid hematoma, habronemiasis, sarcoids/soft tissue sarcomas, and maxillary dental tumors that extend into the nasal cavity; however, all of these differentials can be differentiated histologically by the absence of amyloid.

Contributing Institution:
Department of Population Medicine and Diagnostic Sciences, Section of Anatomic Pathology, Cornell University College of Veterinary Medicine, Ithaca, New York

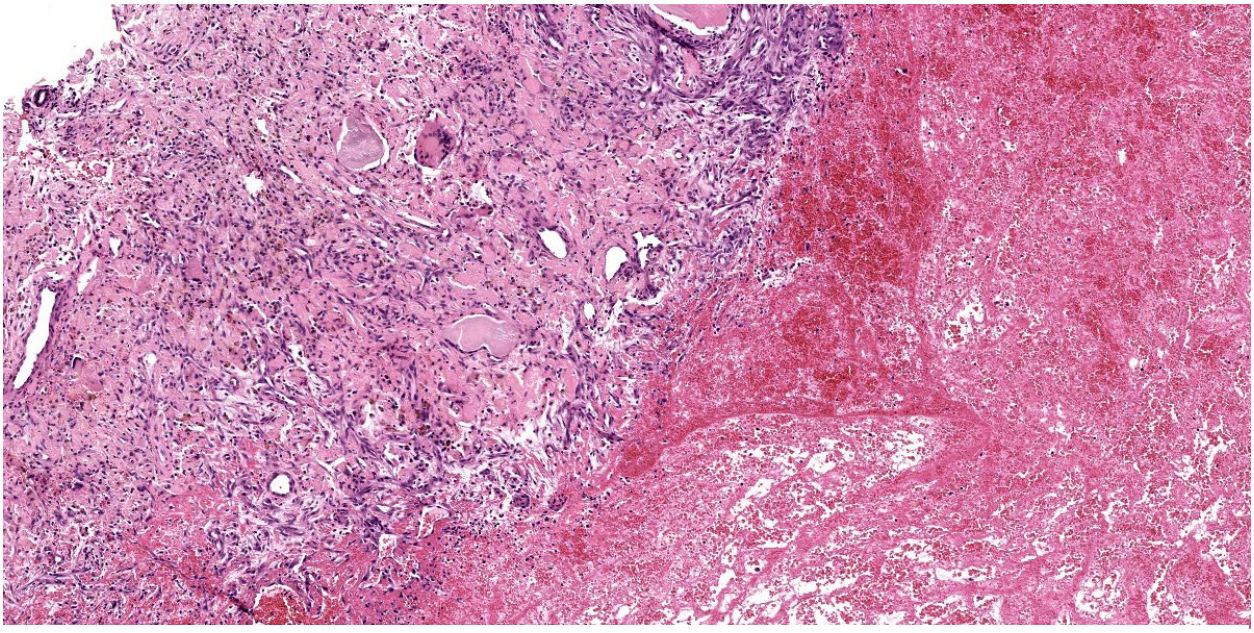

Figure 4-4. Nasal mucosa, horse. In some fragments, amyloid is enmeshed in hemorrhagic granulation tissue. (HE, 78X)

JPC Diagnosis:
Nasal muscosa: Amyloidosis, multifocal, severe, with fibrin thrombi, chronic hemmorrhage, and ulceration.

JPC Comment:
Conference 1 concludes with a relatively straightforward case. The thick squamous epithelial layer that lacks underlying hair follicles helps to place the tissue as the nostril (specifically within the nasal vestibule). The contributor provides a nice description of the features of this case and reviews the salient points of equine amyloidosis as well. The diagnosis of amyloidosis was readily confirmed as the eosinophilic extracellular material was strongly congophilic and sharply birefringent under polarized light. There was discussion among conference participants about the degree of hemorrhage and fibrin present in this case. The major takeaway was that these changes were the direct result of amyloid being deposited within the walls of blood vessels.

This case is an example of immunoglobulin-derived (AL) amyloidosis which is rare in animals though relatively common in humans.[11] Other reported causes of primary amyloidosis include immune dyscrasias such as extramedullary plasmacytomas and multiple myeloma where overproduction of immunoglobulin light chains (or fragments) by plasma cells coalesce to form insoluble fibrils.[1,11] One case of systemic AL amyloidosis secondary to multiple myeloma in a horse has been described to date.[3] In contrast, secondary (reactive; AA) amyloidosis is more common in veterinary species and familial forms of AA amyloidosis have also been described. Reactive amyloidosis occurs secondary to chronic inflammatory stimulus and production of serum amyloid A protein, or less commonly, due to nonimmunocyte dyscrasia or idiopathic causes.[11] Renal and/or hepatic involvement with deposition of extracellular amyloid A protein disrupts normal function and eventually may cause organ failure; others tissues may similarly be affected.[11] This is seen in both domestic animals as well as captive wildlife species such as flamingos and cheetahs among many

others. Familial forms of AA amyloidosis occur in Shar Pei dogs and Abyssinian cats, though other breeds have also been identified.[11]

Amyloidosis has been a frequent feature in slide conferences over the years, though horses are not as well represented as the dog in this regard. Ocular amyloid secondary to recurrent uveitis ('moon blindness') was covered in Conference 7, Case 3, 2018-2019 and represents AA amyloid. Cutaneous amyloidosis in the horse represents a localized AL amyloidosis that is distinct from the nasal form.

References:

1. Caswell JL, Williams KJ. Respiratory System. In: Maxie MG, ed. *Jubb, Kennedy & Palmer's Pathology of Domestic Animals*. Vol 2. 6th ed. St. Louis, MO: Elsevier; 2016:483.
2. Johnson KH, Westermark P, Sletten K, O'brien TD. Amyloid proteins and amyloidosis in domestic animals. Amyloid. 1996 Jan 1; 3(4):270-89.
3. Kim DY, Taylor HW, Eades SC, Cho DY. Systemic AL amyloidosis associated with multiple myeloma in a horse. *Vet Pathol*. 2005 Jan;42(1):81-4.
4. Kumar V, Abbas AK, Aster JC. Diseases of the Immune System. Kumar V, Abbas AK, Aster JC, eds. In: *Robbins and Cotran Pathologic Basis of Disease.* 10th ed. Philadelphia, PA: Elsevier Saunders; 2021:259-264.
5. Mould JR, Munroe GA, Eckersall PD, Conner JG, McNeil PE. Conjunctival and nasal amyloidosis in a horse. *Equine Veterinary Journal*. 1990 Sep;22(S10):8-11.
6. Nappert G, Vrins A, Doré M, Morin M, Beauregard M. Nasal amyloidosis in two quarter horses. *The Canadian Veterinary Journal*. 1988 Oct;29(10):834.
7. Portela R, Dantas A, Melo D, Marinho J, Neto P, Riet-Correa F. Nasal Amyloidosis in a Horse. *Brazilian Journal of Veterinary Pathology*. 2012; 5: 86-88.
8. Shaw DP, Gunson DE, Evans LH. Nasal amyloidosis in four horses. *Veterinary Pathology*. 1987 Mar;24(2):183-5.
9. Sipe JD, Benson MD, Buxbaum JN, et al. Amyloid fibril protein nomenclature: 2012 recommendations from the Nomenclature Committee of the International Society of Amyloidosis. *Amyloid*. 2012;19(4):167-70.
10. Van Rijswijk MH, van Heusden CW. The potassium permanganate method. A reliable method for differentiating amyloid AA from other forms of amyloid in routine laboratory practice. *Am J Pathol*. 1979;97(1):43-58.
11. Woldemeskel M. A concise review of amyloidosis in animals. *Vet Med Int.* 2012;2012:427296.
12. Østevik L, Gunnes G, de Souza GA, Wien TN, Sørby R. Nasal and ocular amyloidosis in a 15-year-old horse. Acta Vet Scand. 2014 Aug 27;56(1): 50.

Joint Pathology Center
Veterinary Pathology Services

WEDNESDAY SLIDE CONFERENCE 2024-2025

Conference #2 — 21 August 2024

CASE I:

Signalment:
15 years, castrated male, domestic shorthair cat, *Felis catus,* feline.

History:
1-2 days' retching, vomiting, diarrhea.

Gross Pathology:
The surgeon noted that the intestinal wall was subjectively thickened and the mesenteric lymph nodes were prominent.

Microscopic Description:
Five specimens, per submitter quadrate liver lobe, stomach, jejunum, mesenteric lymph node, and cecum, are bisected and embedded en toto in blocks 1-5, respectively. The major lesions are in the jejunal specimen (submitted slide 3), which has diffuse heavy mucosal infiltration by neoplastic lymphocytes with extension into the submucosa and multifocally along the vasculature into and through the tunica muscularis. A few lymphoid follicles with normal polarity remain in the submucosa. In the mucosa, epitheliotropism is prominent (indicating a T-lymphocyte population) with individual, clusters, and plaques of lymphocytes within the villous epithelium. The neoplastic cells are mostly small to intermediate-sized lymphocytes with a small nucleolus, 0 to 2 mitotic figures per 400x field, and scanty cytoplasm.

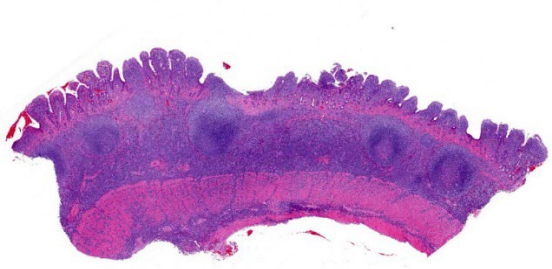

Figure 1-1. Jejunum, cat. A section of jejunum with markedly blunted villi and a transumural round cell neoplasm is submitted for examination. There are prominent germinal centers scattered along the submucosa. (HE, 22X)

The following description is from slides that were not submitted: Similar neoplastic lymphocytes are found focally in the cecal mucosa and submucosa, but the epitheliotropism is not so obvious in the cecum, and submucosal lymphoid tissue has more organized follicles. The lymph node has only focal expansion of the paracortex by monomorphic small lymphocytes. Only a few sinusoidal clusters of neoplastic lymphocytes are in the liver. Otherwise, the liver has variable centrilobular congestion and degeneration that might account for the dark blotches noted at surgery. The sections of stomach are unremarkable.

Contributor's Morphologic Diagnosis:
Epitheliotropic T-cell lymphoma, jejunum.

Contributor's Comment:
Despite the reportedly short duration of clinical signs, the histologic findings are typical of feline enteropathy-associated T-cell lymphoma. This alimentary small cell lymphoma

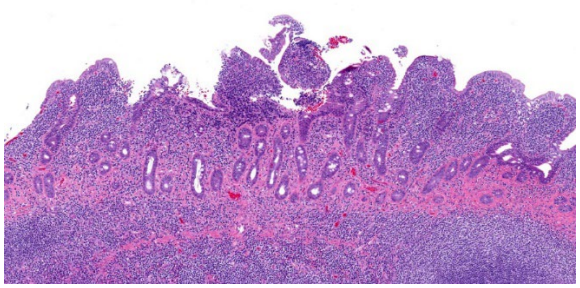

Figure 1-2. Jejunum cat. There is marked blunting and fusion of villi and loss of crypts within the infiltrated sections of jejunum. (HE, 101X)

can be difficult to distinguish from inflammatory bowel disease; indeed, there may be a continuum from chronic inflammation to lymphoma.[2,3,6] However, in this case, the clusters and plaques of lymphocytes within the villous epithelium plus the extension into the submucosa and tunica muscularis left little doubt that this is a neoplasm of T lymphocytes.[2,5] Therefore, neither PCR testing for antigen receptor gene rearrangement (PARR) clonality nor immunohistochemical (IHC) phenotyping with T-lymphocyte and B-lymphocyte markers was performed.

Alimentary lymphoma has become the most common form of feline lymphoma and seems to be increasing in prevalence. Most feline small intestinal lymphomas are composed of small cells and confined to the mucosa similar to the human WHO enteropathy-associated T-cell lymphoma type II.[5,8] However, neoplastic lymphocytes extended through the submucosa into the tunica muscularis in this case, making it a transmural T-cell lymphoma (like WHO enteropathy-associated T-cell lymphoma type I). Small cell feline transmural T-cell lymphomas exist, but most are of large granular lymphocyte type.[5] Importantly, transmural T-cell lymphomas have shorter median survival than that of mucosal T-cell lymphomas, but this could reflect the size of the neoplastic cells rather than the depth of invasion.[5]

Duodenal endoscopy is commonly used to assess cats with chronic enteropathy because it is a minimally invasive technique,[1,6] but distinction of transmural lymphoma from mucosal lymphoma requires examination of full-thickness intestinal sections. A lymphoma diagnosed in endoscopic duodenal biopsy specimens would by default be classified as mucosal.[5] In addition, because the jejunum is the most common location of feline intestinal lymphoma, the diagnosis could be missed in a duodenal specimen.[1,5]

The histologic distinction of lymphoma from inflammatory bowel disease, particularly in endoscopic specimens, is greatly facilitated by IHC and PARR.[5,7] In fact, Sabattini et al. reported that for endoscopic duodenal specimens only the diagnosis of lymphoma based on clonality correlated with decreased survival.[7] Nevertheless, clonality results can be mixed, leading authors of a literature review[6] to propose that feline intestinal small cell lymphoma may more closely resemble human indolent digestive T-cell lymphoproliferative disease than enteropathy-associated T-cell lymphoma. In a study of gastric or duodenal endoscopic biopsy specimens of clinically normal adult cats, histologic, IHC, and clonality test results were consistent with small cell lymphoma in 12 of 20 cats.[3] Thus, the authors concluded that the standard criteria for diagnosing chronic enteropathy in cats may need modification.[3]

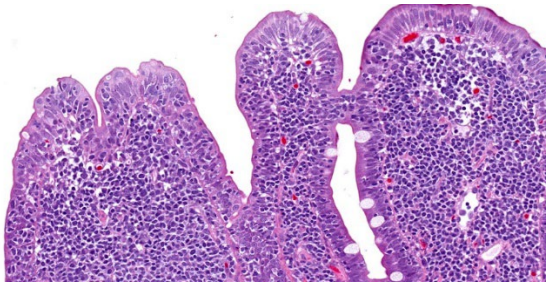

Figure 1-3. Jejunum, cat. Within the mucosa, neoplastic lymphocytes expand the lamina propria and infiltrate and aggregate within the overlying mucosal epithelium. (HE, 144X)

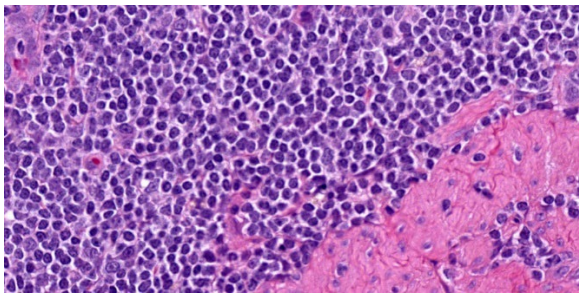

Figure 1-4. Jejunum, cat. High magnification of neoplastic lymphocytes infiltrating the tunica muscularis (HE,700X)

Contributing Institution:
Purdue University
Animal Disease Diagnostic Laboratory: http://www.addl.purdue.edu/

Department of Comparative Pathobiology: https://vet.purdue.edu/cpb/

JPC Diagnosis:
Small intestine: Lymphoma, intermediate to large cell, transmural.

JPC Comment:
This week's moderator was the one and only Dr. Bruce Williams who combined his twin loves of unusual pathology and cats to assemble a conference that featured a good amount of both aspects. The first case is a classic enteropathy-associated T-cell lymphoma (EATL) which the contributor nicely describes and generated substantial discussion among conference participants (see below). We performed IHC for CD3, CD20, PAX5, and MUM1 which were diffusely reactive with strong cytomembranous immunoreactivity for CD3 (T-cell marker) in the cells of interest, confirming the diagnosis of T-cell lymphoma (figures 1-5, 1-6). We agree with the contributor that the extension of neoplastic lymphocytes through the submucosa into the tunica muscularis bests fits with an EATL type I interpretation. Interestingly, this case featured large lymphoid follicles that were strongly immunoreactive for CD20 and PAX5 (highlighting B cells) with fewer plasma cells (staining with MUM1) and B cells scattered within the lamina propria. We remarked on a similar finding in Conference 20, Case 4, 2014-2015 – this too probably represents a nexus of chronic intestinal inflammation that has transformed into lymphoma. However, the contribution of a leaky gut (and associated antigen pouring through an incomplete barrier) due to neoplastic lymphocytes disrupting and effacing the enteric mucosa should not be overlooked either in this case.

While the case seemed straightforward, conference participants pointed out several factors that could make this entity more difficult to describe definitively. Foremost, the size of the neoplastic lymphocytes was a point of contention, with some conference participants agreeing with the contributor's description of small to intermediate size while others favored an intermediate to large distribution. Ultimately, the group felt that intermediate to large cells accurately reflected the neoplastic cells based on the more open chromatin pattern and large prominent nucleolus of these cells ('centrocyte-like'). Dr. Williams entertained (and ultimately discarded) the possibility that these cells could reflect a large granular lymphoma (LGL) which is another high-grade large cell T-cell neoplasm, though this diagnosis is often better made on cytology which was not available for this case. Another confounder we considered were the normal population of small lymphocytes within the

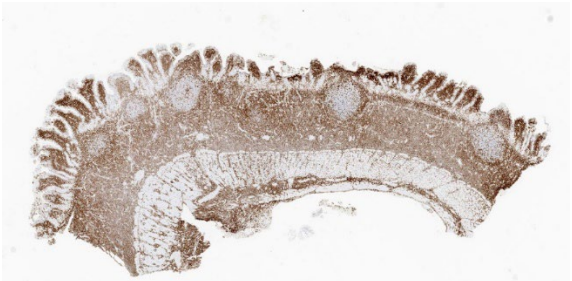

Figure 1-5. Jejunum, cat. Neoplastic cells stain strongly for CD3, indicating a T-cell origin. (anti-CD3, 22X)

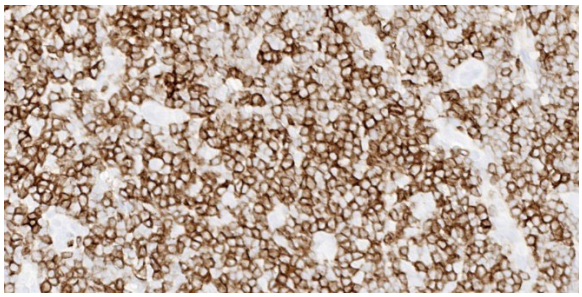

Figure 1-6. Jejunum, cat. Neoplastic cells demonstrate strong membranous immunopositivity for CD3. (anti-CD3, 459X)

lamina propria – we focused on the submucosa first and later identified these same cells within the mucosa in making our determination. Participants were also focused on the intraepithelial nests and plaques of lymphocytes which is more classically associated with EATL type 2. There was also spirited discussion of the putative grade of this neoplasm as mitotic figures were rare (1 per 40x hpf) for some participants while others felt that the mitotic rate was at least intermediate (2 per 40x hpf). EATL type 1 tends to fit better with a more high-grade lymphoma which gave us pause. Ultimately, we resolved these points by focusing on the distinction between transmural and mucosal-associated lymphoma and leaving the EATL types aside which is a convention now shared by the ACVIM as discussed in the next section.[4]

Since the submission of case materials to the WSC several years ago, the ACVIM has published new guidance for distinguishing low-grade neoplastic (i.e. EATL type 2) from inflammatory lymphocytic chronic enteropathies in cats.[4] Distinguishing these entities is challenging given the overlap in features. Clinical signs are largely identical for both conditions and current laboratory tests lack appropriate specificity and sensitivity to screen individual cats accurately, though they can help to pare down the differential list (e.g. rule out pancreatitis).[4] Diagnostic imaging is a helpful adjunct for characterizing abnormalities of the intestine and adjacent lymph nodes as well as identifying appropriate regions for biopsy. Histopathology remains the gold standard for diagnosis, though the decision of endoscopic or laparoscopic biopsy, the number of samples to take, and the exact locations to sample remains an active area of discussion among clinicians.[1,4] From a pathologist's perspective, the ideal samples should be cut parallel to the lamina propria of the intestine, facilitating examination of the mucosa and any underlying tissue layers if present.[1,4]

Ancillary diagnostics tests help support the diagnosis of neoplastic or inflammatory enteropathy, but do not make the distinction in a vacuum. The use of IHCs such as CD3, CD20, PAX5, BLA36, CD79a, Granzyme B, CD56, Ki-67 and MAC387/IBA1 is helpful to confirm or refute H&E impressions.[1] In this particular case, the monomorphic population of lymphocytes with transmural infiltration is highly suggestive of EATL on H&E alone before any antibodies are applied. In contrast, mild to moderate cases of lymphoplasmacytic enteritis also feature intraepithelial lymphocytes and increased numbers of lymphocytes within the lamina propria that are similar in appearance to plaques and nests found in emerging EATL.[1] In many cases, the use of PARR could help resolve this debate, though for a subset of cases small biopsy samples with little DNA and/or patchy lesions with few

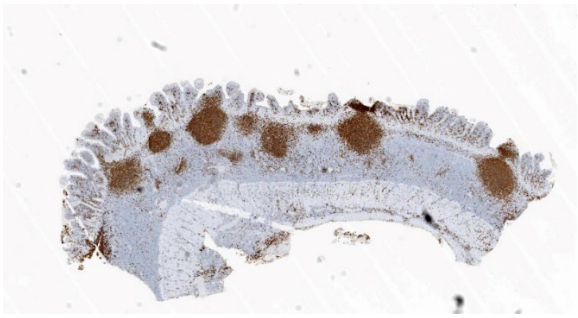

Figure 1-7. Jejunum cat. Neoplastic cells are immunonegative for CD20, a B-cell marker, but lymphocytes within germinal centers provide a positive internal control. (anti-CD20, 22X)

T- and/or B-cells present could yield frustrating results.[1] Therefore, clonality should never be considered in a vacuum. It's fair to say that if one enjoys the certainty or confident conclusions often found in WSC proceedings, reading feline intestinal biopsies probably isn't the place to find it.

References:

1. Freiche V, Paulin MV, Cordonnier N, et al. Histopathologic, phenotypic, and molecular criteria to discriminate low-grade intestinal T-cell lymphoma in cats from lymphoplasmacytic enteritis. J Vet Intern Med. 2021;35(6):2673-2684
2. Kiupel M, Smedly RC, Pfent C, Xie Y, Xue Y, Wise AG, DeVaul JM, Maes RK. Diagnostic algorithm to differentiate lymphoma from inflammation in feline small intestinal biopsy samples. *Vet Pathol*. 2011;48(1):212-222.
3. Marsilio S, Ackermann MR, Lidbury JA, et al. Results of histopathology, immunohistochemistry, and molecular clonality testing of small intestinal biopsy specimens from clinically healthy client-owned cats. *J Vet Intern Med*. 2019;33:551-558.
4. Marsilio S, Marsilio S, Freiche V, Johnson E, Leo C, Langerak AW, Peters I, Ackermann MR. ACVIM consensus statement guidelines on diagnosing and distinguishing low-grade neoplastic from inflammatory lymphocytic chronic enteropathies in cats. *J Vet Intern Med*. 2023 May-Jun;37(3):794-816.
5. Moore PF, Rodriguez-Bertos A, Kass PH. Feline gastrointestinal lymphoma: mucosal architecture, immunophenotype, and molecular clonality. *Vet Pathol*. 2012;49(4):658-668.
6. Paulin MV, Couronné L, Beguin J, et al. Feline low-grade alimentary lymphoma: an emerging entity and a potential animal model for human disease. *BMC Vet Res*. 2018;14:306-324.
7. Sabattini S, Bottero E, Turba ME, et al. Differentiating feline inflammatory bowel disease from alimentary lymphoma in duodenal endoscopic biopsies. *J Small Anim Pract*.2016;57:396-401.
8. Valli VEOT, Kiupel M, Bienzle D, Wood RD. Hematopoietic System. In: Maxie MG, ed. Jubb, Kennedy & Palmer's Pathology of Domestic Animals. Vol 3. 6th ed. St. Louis, MO: Elsevier; 2016:230-232.

CASE II:

Signalment:

12.9 year-old FS Yorkshire terrier dog (*Canis lupus familiaris*)

History:

The dog has a history of tracheal collapse and coughing. Over the previous 6 months, the owner noted increased respiratory effort and restlessness. Thoracic radiographs indicated a soft tissue opacity in the cranial thorax along with mild cardiomegaly and a mild, diffuse bronchointerstitial pattern in the lungs. An echocardiogram indicated myxomatous mitral valve degeneration and second-degree AV block, as well as confirming a lobulated structure in the cranial mediastinum. Bloodwork was unremarkable. The mass was removed and submitted for histopathology.

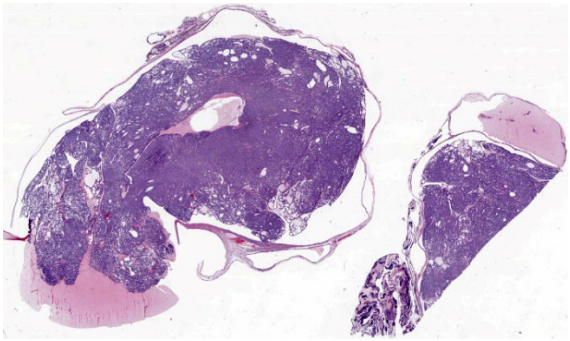

Figure 2-1. Mediastinum, dog. Two sections of a mass ferom the cranial mediastinum is submitted for examination. (HE, 24X)

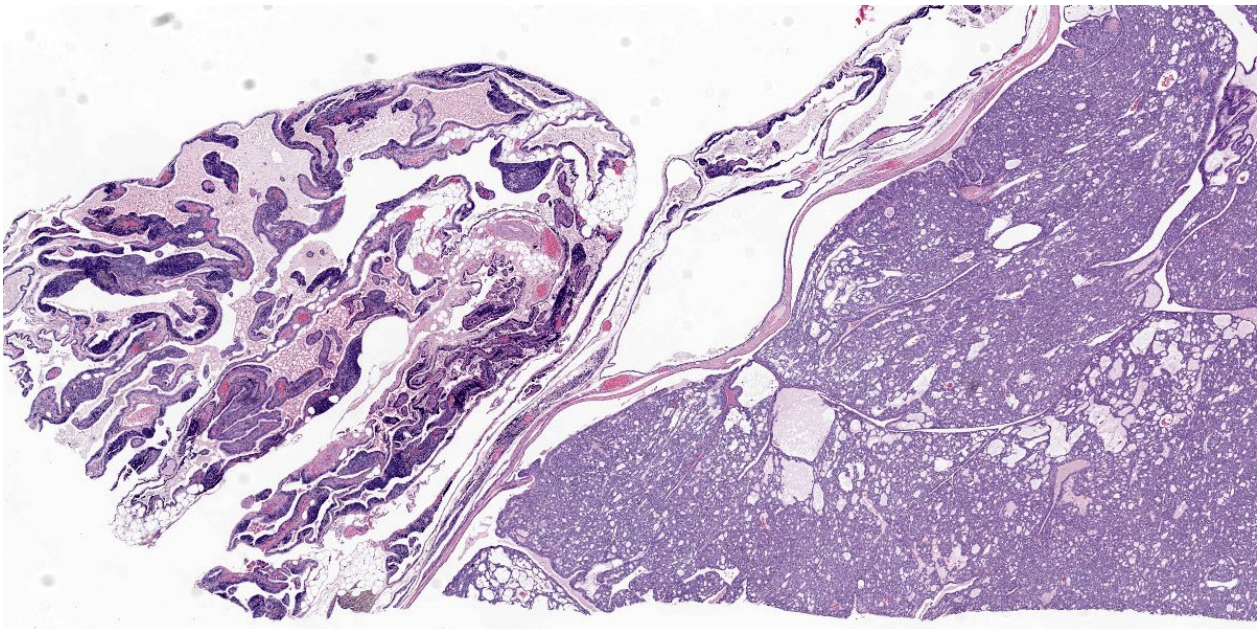

Figure 2-2. Thymus, dog. The neoplasm arises from the wall of a large, multilocular branchial cyst within the thymic remnant. (HE, 24X)

Gross Pathology:
The mass received measured 3.9 x 2.8 x 1.6 cm and was mottled tan to dark purple, multinodular, and semi-firm to firm.

Microscopic Description:
There is minimal residual thymic tissue present, with only minimal lymphoid cells present. There are several, variably sized cysts, containing eosinophilic or clear space and which are lined by ciliated cuboidal epithelium. Within the lumen of several large cysts, with retained cyst lining epithelium, there are mass effects, produced by proliferations of similar epithelial cells to form solid islands, sheets, rare tubules and ducts, some of which contain eosinophilic fluid. The neoplastic cells have moderate amounts of lightly vacuolated cytoplasm, round to ovoid vesicular nuclei, with small to no nucleoli. There is moderate anisokaryosis and anisocytosis. Mitoses are 2 per 10 high power fields (400x).

Contributor's Morphologic Diagnosis:
Cranial mediastinal mass: Branchial cysts with transformation to branchial carcinoma

Contributor's Comment:
Branchial cysts arise from remnants of pharyngeal (branchial) pouches, which are a series of 4 to 5 bilateral embryonic endodermal evaginations that project laterally between the pharyngeal arches. The pharyngeal pouches and clefts contribute to the formation of the thymus (from the third pharyngeal pouch), parathyroid gland, pharyngeal tonsils, and middle and external ear.[7] Epithelia migrate caudally from the submandibular region, down the neck, and into the cranial mediastinum during development, occasionally leaving remnants at points along this tract that can develop into cysts.[5]

Cervical and mediastinal branchial cysts have been reported in dogs, but there are few reports of thymic branchial cysts in veterinary medicine[2,5] and even fewer reports of neoplastic transformation.[5,8] Some of these

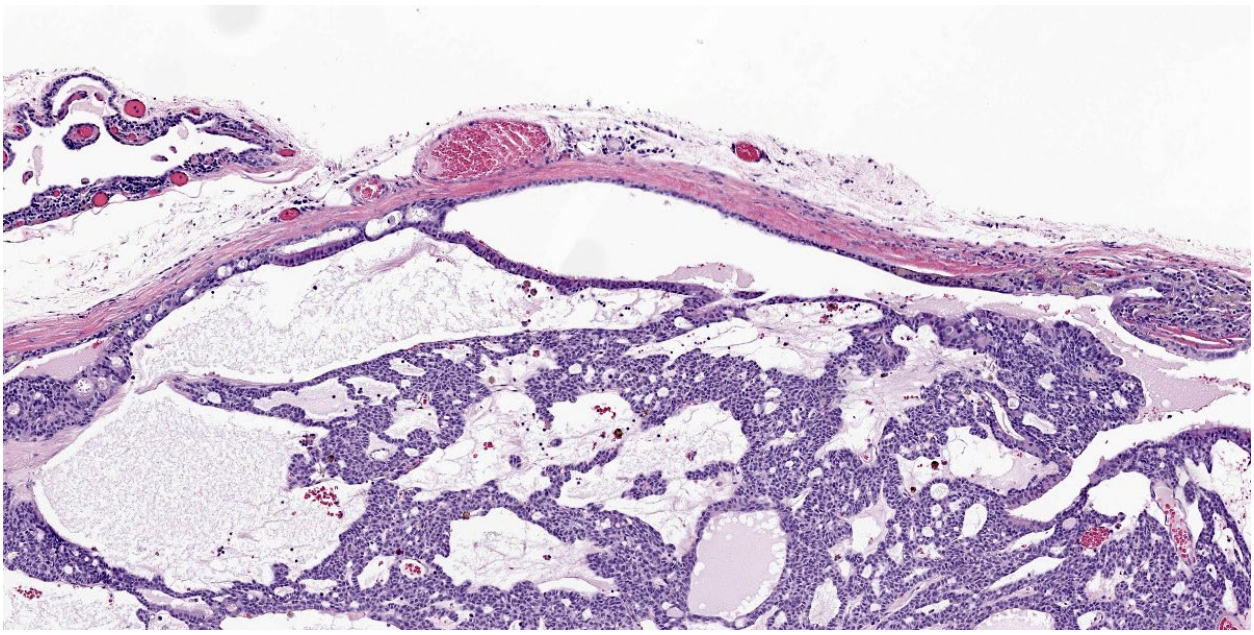

Figure 2-3. Thymus, dog. A multicystic neoplasm arises from the wall of the branchial cyst. Thymic remnant. (HE, 67X)

thymic cysts may be attributed to cystic proliferation of thymic reticular cells rather than remnants from the third pharyngeal pouch. Branchial cysts are distinguished by the presence of variably squamous to ciliated lining epithelial cells with no external opening.[9] Thymic branchial cysts are typically benign and more common in older dogs, but can become space-occupying, leading to cranial vena cava syndrome and pleural effusion.[5] In a report of a dog with malignant transformation of a thymic branchial cyst to a carcinoma, pulmonary metastases were present as well.[4]

In humans, suspected malignant transformation of cervical branchial cysts has been reported with a variety of terms, including branchiogenic carcinoma, branchioma or malignant branchioma. The nomenclature and origin of these masses remains under debate. It has been suggested that these masses are metastases to the cyst from an unrecognized primary tumor, most commonly oropharyngeal carcinomas such as tonsillar carcinoma.[3] Overall, these tumors are considered exceptionally rare in humans.[1]

Differential diagnoses for a cranial mediastinal mass in dogs include thymoma, thymic lymphoma, thymic carcinoma, thymofibrolipoma, chemodectoma, ectopic thyroid tumor, schwannoma, thymic hyperplasia, abscess, or granuloma. Given its rarity and a lack of definitive immunohistochemical markers, branchial cyst carcinomas should be considered a diagnosis of exclusion.

Contributing Institution:
University of Wisconsin-Madison
School of Veterinary Medicine
Department of Pathobiology
2015 Linden Dr
Madison WI 53703
https://www.vetmed.wisc.edu/departments/pathobiological-sciences/

JPC Diagnosis:
Thymic remnant: Branchial carcinoma arising in branchial cyst.

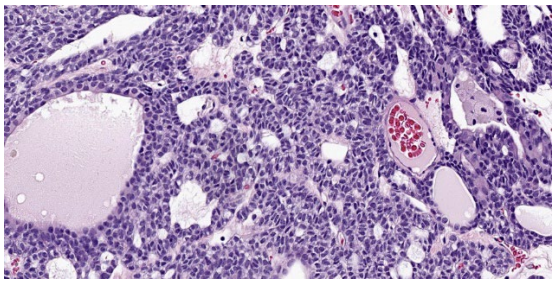

Figure 2-4. Thymus, dog. Neoplastic cells are columnar and are arranged in anastmosing cords, often lining cystic spaces. (HE, 305X)

JPC Comment:

This particular case is somewhat challenging to recognize the salient features and arrive at an exact diagnosis. The large cystic spaces, the small numbers of lymphocytes, and ciliated cuboidal epithelium are all helpful to note, especially starting from the position shown in figure 2-2. Ciliated epithelium (figure 2-5) is commonly seen in respiratory and reproductive epithelium, though the other two facets don't quite fit with those interpretations. Cilia are also a component of branchial pouch epithelia[8,9] – together with the CD3 positive lymphocytes, the tissue in section most resembles a cyst of branchial pouch origin which is located within the thymic remnant of an older dog. That said, the eosinophilic fluid in the background could easily be mistaken for thyroidal colloid at first glance as well. Conference participants as a whole thought that the tissue was ovarian and that the cystic fluid partially resembled Call-Exner bodies of a granulosa cell tumor (figure 2-4) and explained the ciliated epithelium as part of the oviduct. Though these interpretatoins were not ultimately correct, they were good ruleouts for an exquisitely unusual entity. Although branchial cysts have been reported in veterinary medicine, malignant transformation is rare[4,7] In this case, Dr. Williams felt that there was supporting evidence of transformation of the cyst lining itself into a discrete neoplasm (figure 2-3) within the section presented.

An important differential in this case is multiple thymic cyst and thymic origin neoplasia though we also considered the possibility of a neuroendocrine or thyroid tumor too. The animal in this case reportedly had a mass within the cranial thorax which was localized to the mediastinum via echocardiography. In addition to CD3, we also ran IHCs for pancytokeratin, TTF-1, chromogranin, and synaptophysin. Pancytokeratin was diffusely and strongly cytomembranously immunoreactive while chromogranin, synaptophysin were diffusely negative which was consistent with a cystic epithelial tumor. TTF-1 was not immunoreactive in the cells of interest, which excluded a thyroid tumor. Likewise, the malignant neoplastic cells the contributor describes lack squamous differentiation and a high (>10) mitotic rate that is associated with thymic carcinomas.[9] For these reasons, we favor a branchial cyst carcinoma arising in a thymic remnant for this case. Lastly, branchial cyst remnants were previously (briefly) covered in Conference 7, Case 2, 2017-2018 – we suspect it may be some time before we see this entity again.

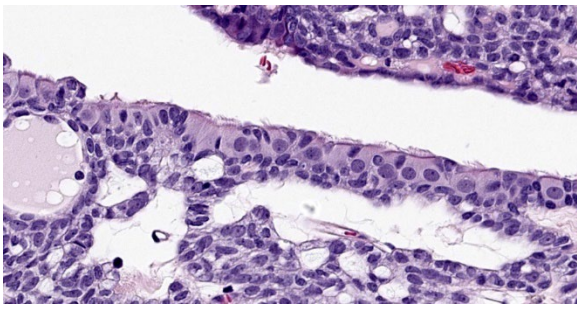

Figure 2-5. Thymus, dog. Cilia are evident on neoplastic cells lining large cystic spaces (HE, 400X)

References:

1. Bradley PT, Bradley PJ. Branchial cleft cyst carcinoma: fact or fiction? *Curr Opin Otolaryngol Head Neck Surg*. 2013;21:118-123
2. Day MJ. Review of thymic pathology in 30 cats and 36 dogs. *J Small Anim Pract.* 1997;38:393-403.
3. Jereczek-Fossa BA, Casadio C, Jassem J, et al. Branchiogenic carcinoma – conceptual or true clinic-pathological entity? *Cancer Treat Rev*. 2005;31:106-114.
4. Levien AS, Summers BA, Szladovits B, Benigni L, Baines, SJ. Transformation of a thymic branchial cyst to a carcinoma with pulmonary metastasis in a dog. *J Small Anim Pract*. 2010;51: 604-608.
5. Nelson LL, Coelho JC, Mietelka K, Langohr IM. Pharyngeal pouch and cleft remnants in the dog and cat: a case series and review. *J Am Anim Hosp Assoc*. 2012;48:105-112.
6. Rosol TJ, Gröne A. Endocrine Glands In: Maxie MG, ed. *Jubb Kennedy and Palmer's Pathology of Domestic Animals*. 6th ed. Elsevier; 2016:310.
7. Sano Y, Seki K, Miyoshi K, Sakai T, Kadosawa T, Matsuda K. Mediastinal basaloid carcinoma arising from thymic cysts in two dogs. *J Vet Med Sci*. 2021;83(5): 876-880.
8. Uzal FA, Plattner BL, Hostetter JM. Alimentary System. In: Maxie MG, ed. *Jubb, Kennedy & Palmer's Pathology of Domestic Animals*. Vol 2. 6th ed. St. Louis, MO: Elsevier; 2016:22.
9. Valli VEOT, Kiupel M, Bienzle D, Wood RD. Hematopoietic System. In: Maxie MG, ed. *Jubb, Kennedy & Palmer's Pathology of Domestic Animals*. Vol 3. 6th ed. St. Louis, MO: Elsevier; 2016:151-157.

Figure 3-1. Cervical lymph nodes, kitten. There is marked enlargement of cervical lymph nodes. (*Photo courtesy of:* Massey University, School of Veterinary Science , Palmerston North, New Zealand).

CASE III:

Signalment:
Fourteen-week-old, female, British shorthair cat (*Felis catus*).

History:
This kitten was one of two in a litter of four British shorthair (BSH) kittens that developed multicentric lymphadenopathy involving all peripheral lymph nodes at 6 weeks of age. Over the following weeks, the lymphadenopathy rapidly progressed to marked but non-painful enlargement of multiple nodes with progressive abdominal distension and lethargy (Figures 1 and 2). Both kittens showed mild regenerative anemia, and blood smears from this kitten showed gross auto-agglutination. Both kittens received immunosuppressive doses of corticosteroids (2.2mg/kg prednisone *per os* sid) for the 2 weeks prior to euthanasia,

Figure 3-2. Cervical and mandibular lymph nodes, kitten. There is marked enlargement of mandibular and cervical lymph nodes. (*Photo courtesy of:* Massey University, School of Veterinary Science , Palmerston North, New Zealand).

but no significant clinical improvement was observed and they were euthanized at 12 and 14 weeks respectively.

Gross Pathology:

On necropsy examination, all identifiable peripheral and visceral lymph nodes showed very marked enlargement (Figures 3 and 4) with effacement of corticomedullary architecture when incised (Figure 5). Mild diffuse hepatic enlargement and moderate diffuse splenic enlargement were also present.

Laboratory Results:

Blood was negative for the presence of both FeLV antigen and FIV antibody (Snap® Combo FeLV Ag/FIV Ab Test Kit) and was negative on direct Coombs' testing. Immunocytochemistry to assess CD3, CD4 and CD8 expression performed on fine needle aspirates from multiple lymph nodes indicated a CD3+/CD4/CD8- immunophenotype for the majority of cells. Results of molecular clonality PCR amplification of antigen receptor rearrangements (PARR) of both the T-cell receptor gamma (*TCRG*) and immunoglobulin heavy chain (*IGH*) loci on genomic DNA extracted from FFPE lymph node tissue was consistent with a polyclonal and non-neoplastic T-cell proliferation. DNA extracted from fresh-frozen kidney and tested by PCR revealed homozygous Fas-ligand gene (FASLG) variants associated with feline autoimmune lymphoproliferative syndrome (FALPS).

Microscopic Description:

Lymph nodes: There is marked expansion of the cortex and medulla of both nodes by a population of round cells consistent with lymphocytes, which effaces or markedly distorts nodal architecture and follicular remnants and expands subcapsular sinuses (Figure 6). Lymphocytes are intermediate to large in size, have generally distinct borders with a scant to moderate amount of eosinophilic cytoplasm, large round nuclei with clumped chromatin and one to two prominent nucleoli. The nuclear diameter of lymphocytes is typically equal to the diameter of approximately 1.5-2 regional erythrocytes. Mitotic figures average 8-10 per 400x high power fields. In some areas, low to

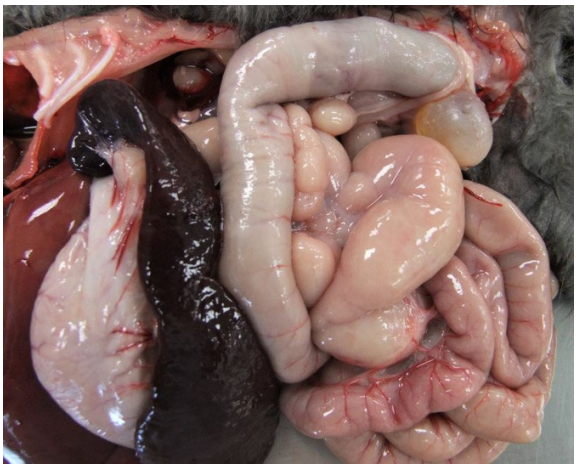

Figure 3-3. Abdominal lymph nodes, kitten. There is marked enlargement of abdominal lymph nodes. (*Photo courtesy of:* Massey University, School of Veterinary Science , Palmerston North, New Zealand)

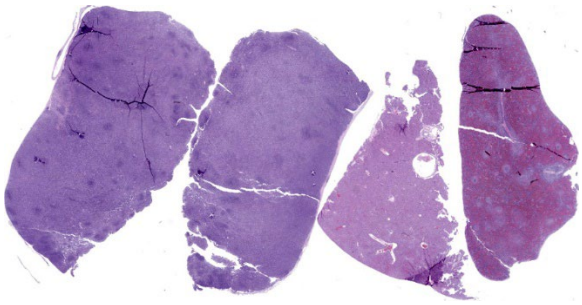

Figure 3-4. Multiple tissues, kitten. Two sections of lymph node, and one of sliver and spleen are submitted for examination. At this magnification, the architecture of the lymh node is lost. (HE, 6X)

moderate numbers of small lymphocytes, plasma cells, macrophages and rare neutrophils are also admixed with the lymphocyte population (Figure 7).

Spleen: There is moderate multifocal expansion of the splenic white pulp by a population of lymphocytes similar to those present and described within the lymph nodes.

Liver: There is mild multifocal expansion of periportal areas and more variably, hepatic sinusoids, by a population of cells including both small and large lymphocytes, plasma cells (including Mott cells), and macrophages. Multifocal areas of scattered extramedullary hematopoiesis are present throughout the section and low numbers of Kupffer cells contain intracytoplasmic erythrocytes.

Immunohistochemistry for CD3 and CD20 performed on sections of lymph nodes and spleen confirmed a predominantly CD3+/CD20- cell population consistent with T cells within both tissues (Figure 8), while variable numbers of CD3-/CD20+ B-cells were also present within follicular remnants and subscapular sinuses of some nodes. This staining pattern is consistent with a T-cell proliferation.

Contributor's Morphologic Diagnosis:
Lymph nodes, spleen and liver: T-cell lymphoid hyperplasia, severe, diffuse
Liver: Pericholangitis and perivasculitis, mild, multifocal, lymphoplasmacytic with erythrophagocytosis and extramedullary hematopoiesis

Contributor's Comment:
This case illustrates typical features of feline autoimmune lymphoproliferative syndrome (FALPS), an unusual autosomal recessive lymphoproliferative disease first seen in multiple related British shorthair kittens in Australia in the 1990s and in New Zealand from 2008.[2] Kittens affected by FALPS appear normal at birth but show failure to thrive, lethargy, regenerative anemia, abdominal distension and generalized lymphadenopathy from 6-10 weeks of age. The disease progresses quickly, has no known effective treatment, and affected kittens usually die or require euthanasia shortly after diagnosis. The disease is easily misdiagnosed as lymphoma, as gross pathology, routine histology and immunohistochemistry results all suggest a diagnosis of a neoplastic (T-cell) proliferation in multiple lymph nodes, spleen and other organs. However, PCR molecular clonality assays (PARR) confirm a polyclonal and non-neoplastic T-cell proliferation within affected nodes indicative of a hyperplastic process and inconsistent with lymphoma.

The genetic basis for FALPS has recently been identified as a monogenic autosomal recessive mutation in the Fas-ligand gene (*FASLG*).[3] Both the *FAS* and *FASLG* genes code for proteins critical in normal cell apoptosis. The mutation in kittens with FALPS involves the insertion of an adenine base in exon 3 of *FASLG*, causing a frameshift mutation and insertion of a premature stop codon, predicted to produce a truncated Fas ligand protein that is unlikely to initiate effective lymphocyte apop-

tosis. Kittens homozygous for the *FASLG* variant allele develop FALPS while heterozygotes are carriers of the defect but phenotypically normal. Genetic testing (buccal swabs or blood) is currently available through Massey University (New Zealand) and Langford Vets (United Kingdom). Recent studies show a relatively high frequency of the variant *FASLG* allele in BSH cats in New Zealand, with 22% of healthy BSH cats from three breeding catteries identified as carriers of the *FASLG* variant.[1] The disease is not currently reported outside Australasia, but as breeding BSH cats from New Zealand and Australia are often exported, it is possible that FALPS may also be seen in BSH and BSH-cross cats in other countries.

The disease in BSH cats is analogous to the inherited disease autoimmune lymphoproliferative syndrome (ALPS) in people.[8] The majority of people with ALPS have inherited *FAS* gene mutations causing defective lymphocyte apoptosis, non-neoplastic lymphoproliferation and variable autoimmunity, although mutations in both *FASLG* and *caspase 10* genes can also cause the disease. In people, most ALPS cases have autosomal dominant inheritance, but the genotype often shows incomplete penetrance with a variable phenotype. Feline autoimmune lymphoproliferative syndrome appears similar to a rare autosomal recessive ALPS variant in people with homozygous *FASLG* mutations which causes a severe and often fatal form of the disease ("ALPS-FASLG") in children.[6] The feline disease also shows similarities to the autosomal recessive "gld" mouse model for ALPS, where mice with homozygous *FASLG* mutations develop severe lymphoproliferative disease early in life.[7]

As this case illustrates, the main gross and histological differential diagnosis for FALPS is multicentric lymphoma, and early cases of FALPS were misdiagnosed as this. Cytology

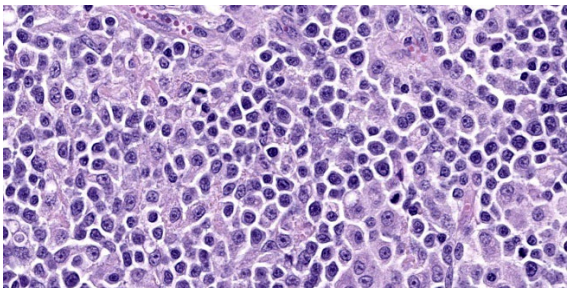

Figure 3-5. Lymph node, kitten. Nodal architecture is effaced by a proliferation of large lymphocytes with a single prominent nucleoli. (HE, 607X)

(not shown here) and histology of multiple enlarged lymph nodes in this kitten reveal a monomorphic population of large lymphocytes with a high mitotic rate. Lymphocytes efface or markedly distort normal nodal architecture and fill subcapsular sinuses. These features are strongly suggestive of a neoplastic lymphoid proliferation. In most FALPS cases, as here, low numbers of randomly distributed plasma cells, macrophages and neutrophils also present in some node sections, while other cases show less complete effacement and more obvious retention of cortical architecture. Similar but less dramatic lymphoproliferation is also consistently seen within the spleen (as in this case), and more variably within the liver and gastrointestinal tract in kittens with FALPS. The majority of lymphocytes within lymph nodes and spleen typically show a CD3+ immunophenotype (consistent with T-cells), also suggesting (T-cell) lymphoma. Immunocytochemistry shows these lymphocytes to be an unusual population of "double negative T-cells" (CD3+/CD4-/CD8-), also similar to those seen in people with ALPS.[8] Mild erythrophagocytosis and extramedullary hematopoiesis, possibly secondary to hemolytic anemia, are also seen in the liver in this case; in other FALPS cases these histological features are more marked. The milder erythrophagocytosis and extramedullary hematopoiesis in this case may be related to this kitten's corticosteroid treatment prior to euthanasia; corticosteroids are the first-line of

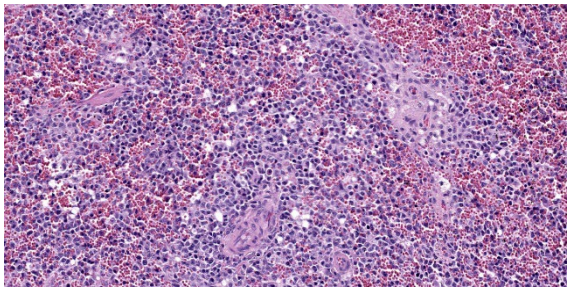

Figure 3-6. Spleen, kitten. Similar large lymphocytes efface the red pulp of the spleen. (HE, 240X)

therapy in people to reduce the autoimmune manifestations of ALPS, including anemia.[10]

Despite microscopic features suggesting T-cell lymphoma in this kitten, PARR testing of lymph node samples showed a polyclonal non-neoplastic T-cell proliferation within lymph nodes and other lymphoid tissues, as is characteristic in FALPS-affected kittens. Subsequent genetic testing also confirmed the presence of the homozygous *FASLG* mutations now known to be associated with FALPS.[3] Lymphoma should also be considered an unusual diagnosis in such a young kitten (FALPS-affected kittens are usually less than 5 months of age), particularly where multiple related or sibling kittens are affected by the disease. Although lymphoma has been reported in kittens as young as 9 weeks of age following experimental FeLV infection at birth,[4] lymphoma in kittens under 6 months of age following natural infection appears very rare. FALPS should therefore be considered as a potential differential diagnosis in any BSH or BSH-cross kitten under 5 months of age with enlargement of multiple peripheral lymph nodes, especially where multiple related animals are affected by disease.

Contributing Institution:
Massey University
School of Veterinary Science
Private Bag 11 222
Palmerston North 4442
New Zealand

JPC Diagnosis:
Lymph nodes, spleen: Atypical lymphoid proliferation, diffuse, severe.

Liver: Extramedullary hematopoiesis, multifocal, mild to moderate.

JPC Comment:
In case you thought we lost our minds (we haven't, but thanks for asking!) and put the same entity within the same conference as a separate case, you can be at ease. While this entity may look like lymphoma at first glance, the contributor provides an excellent slide description and summary of FALPS and highlights how a good history and ancillary diagnostics are needed to recognize this entity and spot the differences. That the animal in this case was only 14 weeks old is important – we actually put this detail on the Conference Worksheet to help push participants away from lymphoma and open the door to thinking about other possible diagnoses. Although some conference participants listed FALPS as their associated condition for this case, other rule outs considered were myeloma and FELV-associated lymphoma though the expected time course of these neoplasms do not fit the age of the animal in this case well. The atypical lymphocyte morphology in this case is similar to the lymphocyte morphology in Case 1 with regards to size and chromatin patterns – that these cells were noted in the red and white pulp of the spleen and lymph node led some participants to still favor lymphoma for this case. Although subtle, the low to moderate numbers of inflammatory cells in the background are not an expected feature of lymphoma the same way that they were in the intestine in Case 1. Notably, there are plasma cells and even numerous Mott cells that multiple conference participants pointed out. We ran IHCs for CD3,

CD20, PAX5, MUM1, and IBA1. Lymphocytes did not label with B-cell markers (PAX-5 and CD20) consistent with the contributor's assessment of CD3 reactivity for these cells of interest. IBA1 was not particularly helpful in this case as it labeled the normal existing population of histiocytes within the spleen, liver, and lymph nodes quite well. These findings altogether highlight the validity of PARR to distinguish FALPS from lymphoma as noted by the contributor.

The present entity circles back to general pathology and apoptosis rather nicely. In the extrinsic pathway of apoptosis, plasma membrane receptors (so called 'death receptors') respond to changes in the extracellular environment by trimerizing in response to ligand presentation.[3,5,9] Examples of death receptors include members of the tumor necrosis factor superfamily (e.g.TNFR1) and FS-7-associated surface antigen (FasR) among others.[5] After the ligand-receptor binding interaction, propagation of this signal continues within the cell via continues via associated death domain proteins (FADD/TRADD) which complex with pro caspase-8 to form a death induced signaling complex (DISC).[5,9] The net effect of this interaction is that the death domain protein serves to activate caspase 8 at an appropriate time and initiate a death cascade via downstream 'executioner' caspases with caspase 3 being the most significant. These caspases cleave nuclear and cytoplasmic proteins, leading to disintegration of the nucleus and disruption of the cytoskeleton during apoptosis.[5] Connecting these details back to the case at hand, Fas ligand is normally expressed on a variety of cells including T-lymphocytes – FasL therefore acts as brake of sorts on an excessive immune response. As the contributor points out, a frameshift mutation in the Fas-ligand gene would be expected to disrupt FasL

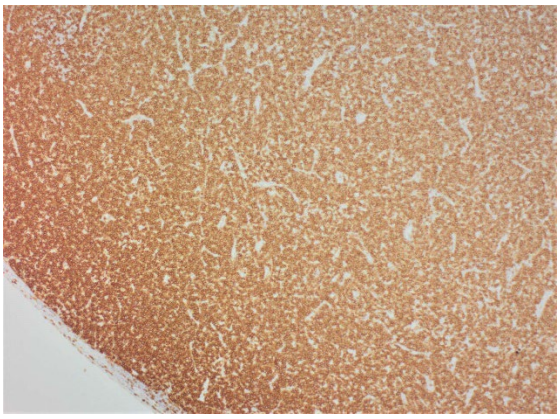

Figure 3-7. Lymph node kitten: Neoplastic cells stain demonstrate strong diffuse cytoplasmic immunoreactivity for CD-3, a T-cell marker.) (anti-CD3, 400X). (*Photo courtesy of:* Massey University, School of Veterinary Science , Palmerston North, New Zealand).

and FasR interaction and lead to a non-neoplastic accumulation of lymphocytes due to lack of downstream caspase activity and lack of apoptosis. Conference participants remarked about the presence of tingible body macrophages within lymphoid follicles in this case despite this mutation and felt that alternate death receptors in the TNF superfamily might still be active and allow some lymphocytes to be sufficiently phosphorylated to activate downstream caspases.

Finally, testing for this rare condition has expanded in recent years. In Europe, commercially available testing for FALPS is included with genetic screening for polycystic kidney disease and progressive retinal atrophy in British Short/Longhair cats via Laboklin. As the popularity of British Shorthair cats increases in the United States, demand for such testing may also follow.

References:

1. Aberdein D, Munday JS, Dittmer KE, Heathcott RW, Lyons LA: Frequency of a FAS ligand gene variant associated with inherited feline autoimmune lymphoproliferative syndrome in British

shorthair cats in New Zealand. *New Zealand Veterinary Journal*. 2017:1-5.
2. Aberdein D, Munday JS, Fairley RA, Vernau W, Thompson KG: A novel and likely inherited lymphoproliferative disease in British shorthair kittens. *Veterinary Pathology*. 2015:52(6):1176-1182.
3. Aberdein D, Munday JS, Gandolfi B, Dittmer KE, Malik R, Garrick DJ, et al.: A FAS-ligand variant associated with autoimmune lymphoproliferative syndrome in cats. *Mamm Genome*. 2017:28(1-2):47-55.
4. Hoover EA, Perryman LE, Kociba GJ: Early lesions in cats inoculated with feline leukemia virus. *Cancer Res*. 1973:33(1):145-152.
5. Miller MA, Lyle LT, Zachary JF. Mechanisms and Morphology of Cellular Injury, Adaptation, and Death. In: Zachary JF, ed. *Pathologic Basis of Veterinary Disease*. 7th ed. St. Louis, MO: Elsevier; 2022:28-29.
6. Nabhani S, Honscheid A, Oommen PT, Fleckenstein B, Schaper J, Kuhlen M, et al.: A novel homozygous Fas ligand mutation leads to early protein truncation, abrogation of death receptor and reverse signaling and a severe form of the autoimmune lymphoproliferative syndrome. *Clinical Immunology*. 2014:155(2):231-237.
7. Nagata S, Suda T: Fas and Fas ligand: lpr and gld mutations. *Immunol Today*. 1995:16(1):39-43.
8. Oliveira JB, Bleesing JJ, Dianzani U, Fleisher TA, Jaffe ES, Lenardo MJ, et al. Revised diagnostic criteria and classification for the autoimmune lymphoproliferative syndrome (ALPS): report from the 2009 NIH International Workshop. *Blood*. 2010:116(14):e35-40.
9. Santagostino SF, Assenmacher C-A, Tarrant JC, Adedeji AO, Radaelli E. Mechanisms of Regulated Cell Death: Current Perspectives. *Veterinary Pathology*. 2021;58(4):596-623.
10. Worth A, Thrasher AJ, Gaspar HB: Autoimmune lymphoproliferative syndrome: molecular basis of disease and clinical phenotype. *British Journal of Haematology*. 2006:133(2):124-140.

CASE IV:

Signalment:
Cat (*Felis vulgaris*) – 5 months – female castrated

History:
Presented with clinical complaints of vomiting and lethargy. Huge amount of fluid in peritoneal cavity (ascites). No abnormalities found on echocardiac examination and blood examination. Laparascopy performed: suspicion of encapsulating peritoneal sclerosis. Died at night.

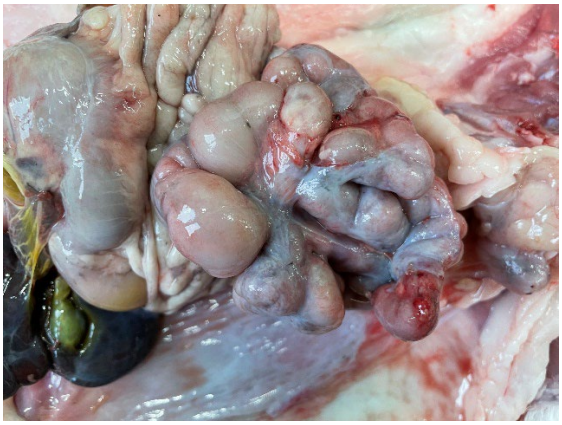

Figure 4-1. Abdominal viscera, cat. The peritoneum is diffusely thickened, resulting in an opaque appearance. There is a fibrous adhesion between multiple dilated loops of intestine. (*Photo courtesy of:* Department of Pathobiology, Pharmacology and Zoological Medicine, Faculty of Veterinary Medicine, University of Ghent, Salisburylaan 133, 9820 Merelbeke, Belgium https://www.ugent.be/di/di05/nl)

Figure 4-2. Abdominal viscera, cat: The thickened peritoneum is visible over the liver capsule. (*Photo courtesy of:* Department of Pathobiology, Pharmacology and Zoological Medicine, Faculty of Veterinary Medicine, University of Ghent, Salisburylaan 133, 9820 Merelbeke, Belgium https://www.ugent.be/di/di05/nl)

Gross Pathology:
Most peritoneal organs show an abnormal morphology and are surrounded by a thick, glistening, white layer of peritoneum (figure 1 peritoneal organs *in situ* and figure 2 peritoneal organs removed from body).

- Small intestines are severely attached to each other. Duodenum shows a normal wall thickness but is moderately dilated. Jejunum shows a very tortuous appearance (figures 3 and 4), with a diffusely moderately to severely thickened intestinal wall and a moderate amount of yellow, granular content. The rest of the small intestine does not contain any content.
- Large intestine proximally shows the same appearance as the jejunum, more distally it has a normal appearance and contains a moderate amount of normally formed brown feces. Mucosa of all the intestinal segments is normal. There is no obvious mesentery visible.
- Liver is small with ventrally enlarged rounded edges (figure 5). It has a diffuse dark red black color with multifocal sharply delineated linear grey strikes (fibrosis, figure 6).
- Spleen is severely shrunken with absence of the normal architecture (figure 7). It is surrounded by a thick layer of connective tissue and fat (figure 8).

Laboratory Results:
Blood examination normal.

Microscopic Description:
Transections of multiple intestinal segments are present. All intestines are clustered together and surrounded by a diffusely severely thickened peritoneal layer, on top of their normal thin peritoneum. The thickened peritoneal layer contains large amounts of linearly arranged collagen fibers. The connective tissue differs in maturity dependent on the location. Multifocal areas have a more mature appearance with accumulation of amorphous eosinophilic material, interspersed with small amounts of spindloid fibroblasts and densely packed connective tissue fibers, while other areas have a less mature appearance with a higher cellularity of more plump fibroblasts, a loose collagenous stroma, and moderate amounts of

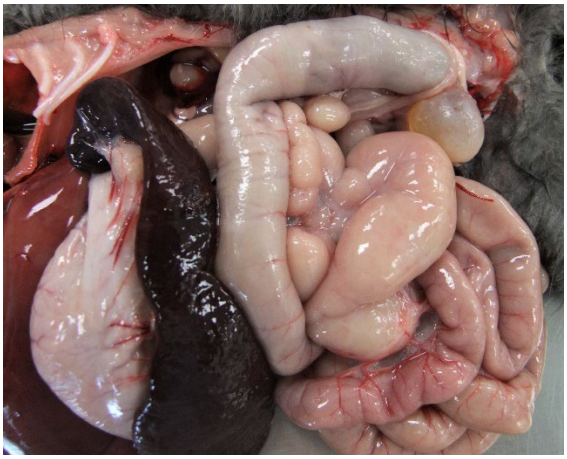

Figure 4-3. Intestine, cat. Multiple contiguous loops of intestine are submitted for examination. (HE, 6X)

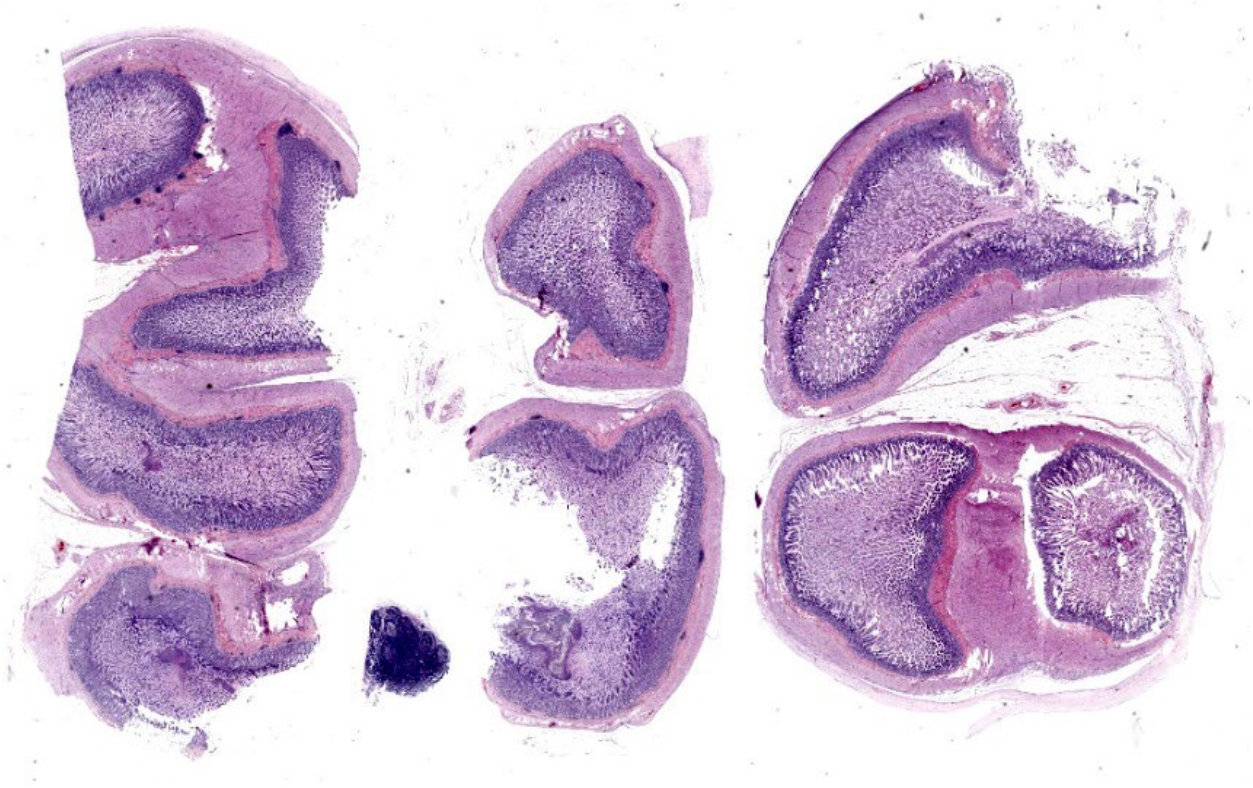

Figure 4-4. Intestine, cat. Loops of intestine are surrounded by variably dense bands of fibrous connective tissue (arrows) (HE, 6X)

small tortuous blood vessels lined by plump endothelial cells (granulation tissue). Multifocal there are areas with diffuse linear translucency between the connective tissue fibers (edema). The inner part of the peritoneum shows multifocal mild mixed inflammation, mainly containing neutrophils and lymphocytes, and a mild to moderate amount of small tortuous blood vessels with plump endothelial cells. Mild to moderate lymphoplasmacytic inflammation is also seen in the tunica muscularis, tunica submucosa and the lamina propria of the tunica mucosa.

Trichrome Masson stain performed: severely thickened peritoneum

Contributor's Morphologic Diagnosis:
Diffuse severe chronic encapsulating peritoneal sclerosis of the intestines.

Contributor's Comment:
Sclerosing encapsulating peritonitis (SEP), also known as 'encapsulating peritoneal sclerosis', is a very rare disease described in humans as well as in animals. Up until 2022, it is described in only 13 canine cases[10] and 2 feline cases.[6,8] It is characterized by a chronic, diffuse, fibrocollagenous thickening of parietal and visceral peritoneum with secondary encapsulation of abdominal organs, mostly small intestines.[1-11,13] In human medicine, it is classified into 4 different types depending on the extent of involved abdominal organs;[2,4,7] type 1 involves small intestines partially, type 2 involves small intestines completely, type 3 involves small intestines and other organs, such as stomach, cecum, colon, liver and/or ovaries, and type 4 involves the entire peritoneal cavity.

Etiopathogenesis remains incompletely understood.[1,2,7] SEP can be divided in primary,

idiopathic forms and secondary forms, which can be caused by lots of different underlying disorders that cause chronic low-grade inflammation of the peritoneum.[1,2,8] In human medicine, peritoneal dialysis is the most common one, while other possible causes are infectious peritonitis, administration of certain medications and intra-abdominal surgery.[2-11,13]

SEP can give a wide variety of vague symptoms in humans, such as intermittent and recurrent, moderate to severe abdominal pain, caused by intestinal obstruction and necrosis.[1,2,3,7,9,11,13] This is mostly in combination with a malnourished appearance, abdominal distention, palpable abdominal mass, nausea and vomiting.[4,6,7,9,11,13]. Common clinical symptoms in canine cases are also vague, and can include vomiting, diarrhea, soft feces, anorexia, depression or lethargy, enlarged abdomen and abdominal pain.[1,3,5,6,10] Chronic cases can show moderate to severe low body condition and low muscle score,[3,5,6] combined with symptoms specific for the underlying etiology.[6] Cats show similar symptoms as seen in dogs: anorexia, intermittent vomiting, rare diarrhea, weight loss, abdominal distention and sensitivity are all described.[6,7]

SEP in humans and animals gives a very typical gross thick collagenous encapsulation of the small intestines with secondary adhesions between the intestinal loops, giving them a very tortuous and mass-like appearance in the central abdomen.[1-3,5-7,9-11,13] Depending on the type of the disease, other organs can be additionally involved, such as stomach, cecum, colon, liver or ovaries.[2,7-9] In humans, an important consequence of SEP is intestinal obstruction with necrosis,[1,2,4,6,13] something that is not described in dogs and cats.[1,5,6] An explanation for this lies in the very active fibrinolytic system of these species.

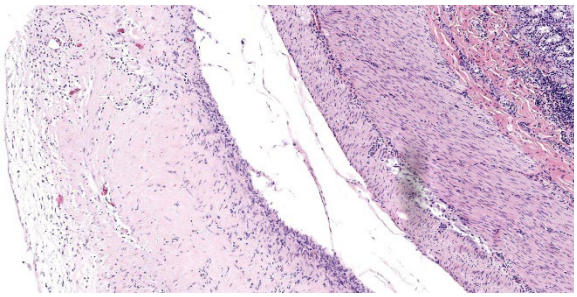

Figure 4-5. Intestine, cat. In some areas, the fibrous tissue is immature, resembling granulation tissue. (HE, 97X)

Ascites is seen typically in dogs, while it is not common in humans.[1,3,5,6,10,11,13]

SEP causes very characteristic histopathological lesions: visceral and parietal peritoneum have an uneven, diffusely, moderately to severely thickened appearance.[1,2,5-11,13] Different layers can be seen in the thickened peritoneum of animals. The deepest layer show mature collagenous connective tissue with densely packed collagen fibers, while the more superficial layers are built up of granulation tissue, characterized by loose collagenous stroma with presence of numerous fibroblasts, mixed with abundant, small, tortuous blood vessels lined by plump endothelium (neovascularization), and a mild mucinous deposition.[5,6,8,11] Both in humans and animals, mild to moderate, mostly mononuclear, inflammation can be seen in the thickened peritoneum.[4-6,8-11,13]

Diagnosis of SEP remains difficult due to its vague clinical symptoms, therefore in most of the cases, there is need for a combination of history, pre-existing predisposing factors, clinical symptoms and abdominal imaging before SEP will be suspected.[7] For definitive diagnosis, surgery with histopathology is necessary.

Treatment is not easy, and both surgery, medicinal therapy, nutritional support and treat-

ment of underlying disorders are used. Surgery mostly consists of adhesiolysis with ablation of the fibrous capsule and intestinal adhesions.[1,2,6,9,13] It is very important to realize the dangers of these surgeries, and complicated and fatal results are not uncommon.[1,2,4] Most commonly used medicines are corticosteroids, which work anti-inflammatory and immunosuppressive, and tamoxifen, which has an anti-fibrotic function.[3,4,7-9,11,13]

Contributing Institution:
Department of Pathobiology, Pharmacology and Zoological Medicine
Faculty of Veterinary Medicine, University of Ghent
Salisburylaan 133, 9820 Merelbeke, Belgium
+3292647741 -
Veterinaire.pathologie@ugent.be
https://www.ugent.be/di/di05/nl

JPC Diagnosis:
Visceral peritoneum, small intestine: Fibrosis, diffuse, moderate with adhesions and scant granulation tissue.

JPC Comment:
Conference 2 concludes with a case of yet another rare entity in a cat. While we suspect some readers may not know of this particular disease, we are confident that a good description of histologic features gets one pretty close (and the search engine of choice does the rest). The large bundles of immature collagen and granulation tissue that encircle the serosal tunic (figures 4-4 and 4-5) and extend between loops of intestine is bizarre yet distinct. For this case, we ran IHCs for desmin and smooth muscle actin (SMA) to delineate fibrosis from muscle as well as special stains (Masson's trichrome, Movat's pentachrome) to highlight tissue architecture overall. Both desmin and SMA are strongly cytoplasmically immunoreactive within the multiple (thick and thin) layers of

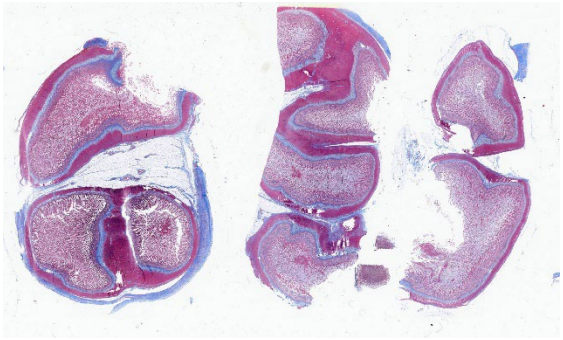

Figure 4-6. Intestine, cat. A Masson's trichrome demonstrates a sheath of fibrous connective tissue encircling multiple loops of bowel. (Masson's trichrome, 6X)

smooth muscle that surrounds each loop of intestine, but the chromatic stains are particularly helpful for appreciating the degree of fibrosis and adhesions between adjacent loops of bowel that are not simply a function of cut of the microtome (figures 4-7 and 4-8). Granulation tissue in particular was largely immature collagen (non-polarizing) with fewer small caliber blood vessels, though this aspect may not be consistent between all cases of SEP. Dr. Williams emphasized that the submucosa of this cat, while fairly thick, was likely normal and it was easy to be fooled unless reading feline intestinal biopsies on a consistent basis.

A recent case report from Japan describes a rare successful treatment of SEP in a cat.[12] In that particular case, clinical findings were somewhat similar to the ones described by the contributor, though the cat in conference was only 5 months old at the time of presentation vice being a mature adult as the cat in Japan was. As such, our case may reflect a primary idiopathic cause rather than a chronic inflammatory one. Notably, the cat from Japan also lacked ascites and was intestinally obstructed at the time of presentation. The treatment described for the Japanese cat included multiple surgical adhesiolyses along with tapering courses of prednisolone. During

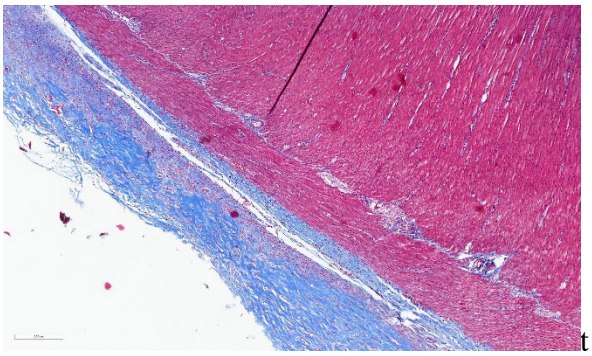 t

Figure 4-7. Intestine cat. Higher magnification of the trichrome-stained fibrous connective tissue expanding the visceral peritoneum. (HE, 100X)

surgery, placement of a hyaluronate-carboxymethylcellulose membrane around the intestine was intended to prevent recurrence of adhesions. The authors reported that the cat was symptom-free over 3 years after the second surgery. Possible factors that they considered included prevention of fibrin deposition both chemically (via anti-inflammatory doses of steroids) and physically through the use of a bioresorbable barrier.[12] From a general pathology perspective, this multipronged attempt to thwart conversion of fibrin to collagen by decreasing synthesis and avenues for cross-linking was successful in this case but may prove challenging in severe and/or advanced cases of SEP.

References:

1. Adamama-Moraitou LL, Prassinos NN, Patsikas MN, Psychas V, Tsioli B, Rallis TS. Sclerosing encapsulating peritonitis in a dog with leishmaniasis. *JSAP*. 2004;45:117-121.
2. Alshomimi S, Hassan A, Faisal Z, Mohammed A, Dandan OA, Alsaid HS. Sclerosing Encapsulating Carcinomatous Peritonitis: A Case Report. *Saudi J Med Med*. 2021;9:63-6.
3. Barnes K. Vet Med Today: What Is Your Diagnosis? *JAVMA*. 2015;247(1): 43-45
4. Danford CJ, Lin SC, Smith MP, Wolf JL. Encapsulating peritoneal sclerosis. *World J Gastroenterol*. 2018;24(28):3101-3111.
5. Etchepareborde E, Heimann M, Cohen-Solal A, Hamaide A. Use of tamoxifen in a German shepherd dog with sclerosing encapsulating peritonitis. *J Small Anim Pract*. 2010;51:649-53.
6. Hardie EM, Rottman JB, Levy JK. Sclerosing Encapsulating Peritonitis in Four Dogs and a Cat. *Vet Surg*. 1994;23:107-114.
7. Machado NO. Sclerosing Encapsulating Peritonitis: Review. *Sultan Qaboos University Med J*. 2016;16(2): 142–151.
8. Sonck L, Chiers K, Ducatelle R, Van Brantegem L. Encapsulating peritoneal sclerosis in a young cat. *Vet Rec Case Rep*. 2018;6:1-4.
9. Tannoury JN, Abboud BN. Idiopathic sclerosing encapsulating peritonitis: Abdominal cocoon. *World J Gastroenterol*. 2021;18(17):1999-2004.
10. Tsukada Y, Park YT, Mitsui I, Murakami M, Tsukamoto A. Sclerosing encapsulating peritonitis in a dog with pancreatic ductal adenocarcinoma. *BMC Veterinary Research*. 2022;18:383-391.
11. Veiga-Parga T, Hecht S, Craig L. Imaging Diagnosis: Sclerosis encapsulating peritonitis in a dog. *Vet Radiol Ultrasound*. 2015;56(6):65–69.
12. Yokoyama N, Kinoshita R, Ohta H, Okada K, Shimbo G, Sasaoka K, Nagata N, et al. Successful treatment of sclerosing encapsulating peritonitis in a cat using bioresorbable hyaluronate-carboxymethylcellulose membrane after surgical adhesiolysis and long-term prednisolone. *JFMS Open Rep*. 2023 Nov 24;9(2):20551169231209917.
13. Zhang Z, Zhang M, Li L. Sclerosing encapsulating peritonitis: three case reports and review of the literature. *J Int Med Res*. 2020;48(8):1-6.

Joint Pathology Center
Veterinary Pathology Services

WEDNESDAY SLIDE CONFERENCE 2024-2025

Conference #3 28 August 2024

CASE I:

Signalment:
2-3 month old, intact male guinea pigs (*Cavia porcellus*)

History:
These guinea pigs were from a control group on study at a contract research organization. A nodule was found in the heart during post-life processing. No clinical signs were noted prior to euthanasia.

Gross Pathology:
A poorly-demarcated, tan nodule expands the right or left ventricular free wall or the interventricular septum of the heart.

Microscopic Description:
The subendocardial muscle is regionally effaced by expansile, well-circumscribed foci of atypical cardiac myocytes that are arranged in bundles and streams. Atypical cardiac myocytes are plump polygonal and have distinct cell borders. These cells are markedly distended by clear vacuoles, pale eosinophilic granular material, and acidophilic bodies. Nuclei are round; have finely to coarsely stippled chromatin; frequently contain a single prominent nucleolus; and are occasionally surrounded by radiating, linear sarcoplasmic processes (spider cells). The surrounding cardiac myofibers are minimally compressed. Small numbers of mixed mononuclear cells multifocally infiltrate the normal cardiac muscle.

Figure 1-1. Heart, guinea pig. A longitudinal and a transverse section of the ventricles is submitted. (HE, 5X)

Contributor's Morphologic Diagnosis:
Heart: Severe regional cardiac myofiber vacuolar degeneration and glycogen accumulation.

Condition: Cardiac rhabdomyomatosis

Contributor's Comment:
The pathogenesis of this condition is still debated, though it is considered an incidental finding. Common features across veterinary species include the presence of PAS-positive material (interpreted as glycogen) within sarcoplasmic vacuoles and the formation of spider cells, which represent an artifact of glycogen loss during histologic processing.[4-10] Some sources attribute this condition to a defect in glycogen storage or metabolism.[3,9] An association with hypovitaminosis C

Cardiac Rhabdomyomatosis/Rhabdomyoma Cross-Species Comparison of Histochemical and IHC staining characteristics									
Species	Diagnosis	PAS	PTAH	Desmin	Myo-globin	SMA	Vimentin	PGP 9.5	NSE
Guinea pig (*Cavia porcellus*)	Cardiac rhabdomyomatosis	+	+	+	+	Variable			
Pig (*Sus scrofa*)	Cardiac rhabdomyoma	+	+	+			+	+	+
Canid (*Canis familiaris*)	Cardiac rhabdomyoma	+	+	+	+	-	-		
Bearded harbor seal *(Erignathus barbatus)*	Cardiac pukinjeoma	+	+					+	+
Fallow deer (*Dama dama*)	Cardiac rhabdomyoma	+	+	+			+		

(scurvy) has been suggested in guinea pigs, but is not well-established.[9]

Recent veterinary literature indicates that in swine, the abnormal myocytes contain ultrastructural and immunohistochemical features of both postnatal cardiac myocytes and Purkinje cells. These characteristics, in conjunction with the age predilection for juvenile animals, support the contention that this may represent a congenital dysplasia or a tumor arising from a pluripotent embryonic cell.[3,12] In humans, cardiac rhabdomyomas represent the most common primary pediatric cardiac neoplasm and, interestingly, are often associated with tuberous sclerosis complex.[5]

Contributing Institution:
Pathology Department
Charles River Laboratories – Mattawan

www.crl.com

JPC Diagnosis:
Heart, myocardium: Glycogenosis, multifocal, moderate.

JPC Comment:
This week's moderator was Major Daniel Bland, Chief of Histology (Veterinary Pathology) at the Walter Reed Army Institute of Research (WRAIR) and his cases were anything but mundane. This first entity is a classic in the guinea pig, though as the contributor also notes there are occasional case reports in other species as well. Recently, there was a short report of this condition in Göttingen Minipigs as well.[1] Tissue identification and lesion recognition was relatively simple for this case, so we focused on better characterizing the plump, atypical cardiac myocytes that the contributor so nicely describes/ Similar to the table provided, we ran IHCs and special stains for Periodic-Acid Schiff (with and without diastase), muscle specific actin, desmin, GFAP, IBA1, NSE, synaptophysin, and chromogranin. These atypical myocytes were

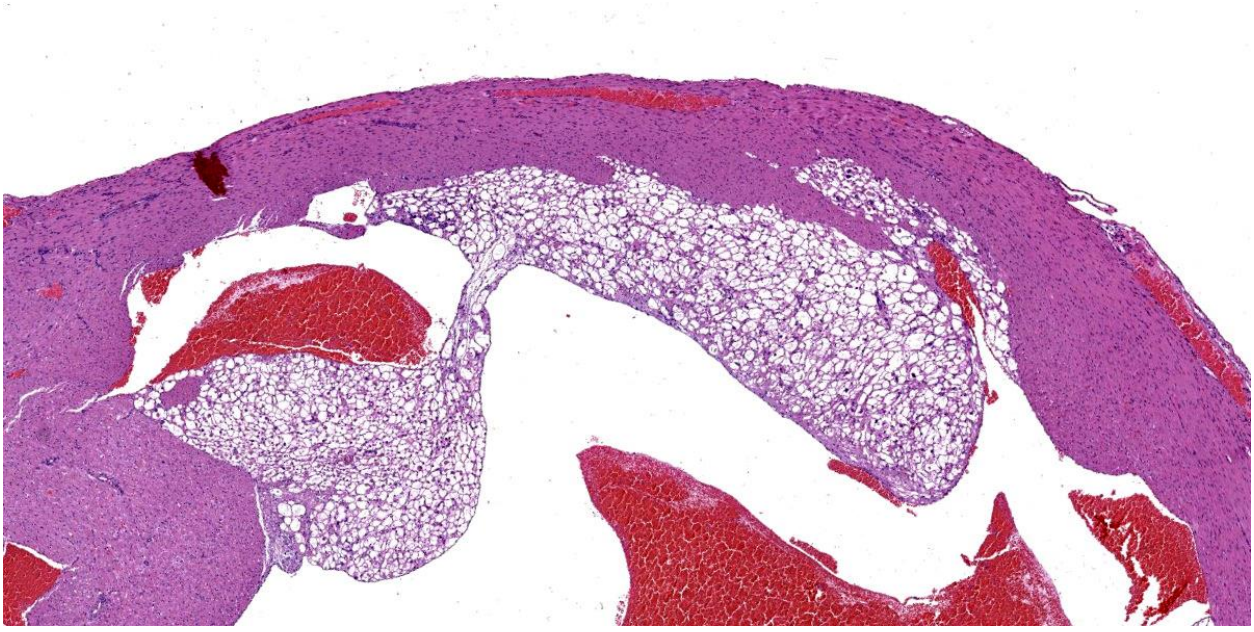

Figure 1-2. Heart, guinea pig. A focally extensive area of swollen cardiomyocytes is present within the right ventricle subjacent to the endocardium. (HE, 36X)

strongly PAS-positive within the cytoplasm, though this staining intensity was greatly diminished by treatment with diastase, consistent with interpretation of these vacuoles as containing glycogen. Compared with normal cardiac myocytes, these atypical myocytes also had minimal cytoplasmic immunoreactivity for desmin and muscle specific actin. Chromogranin and synaptophysin were immunonegative.

Conference participants had a few interesting takeaways from this case. Foremost, there was the observation that the PAS section following diastase treatment was quite washed out. As Dr. Bruce Williams reminded participants, cells with increased glycogen content include hepatocytes, neurons, and cardiac/skeletal myocytes – it is hardly a surprise then that the staining profile of these cells should change with this glycogen content also being digested. Participants also debated how to best describe this condition, with the consensus falling on a moderate severity given the limited ancillary changes within the heart (i.e. degeneration and necrosis of adjacent myocytes).

There are several other lesions to be aware of in the heart of guinea pigs which were not present in this case. These include rare mineralization of cardiac myocytes which may be accompanied by fibrosis and minimal mononuclear cell infiltration; alone this is typically subclinical.[9] Additionally, the underlying cause for myocardial protein aggregates in pet guinea pigs has been described,[11] with accumulation of these alpha B crystallin (a small heat shock chaperone protein) being most common in the right ventricular free wall, though they may also be found within papillary muscles within the left and right ventricles of the heart as well.

References:

1. Feller LE, Sargeant A, Ehrhart EJ, Balmer B, Nelson K, Lamoureux J. Cardiac Rhabdomyoma in Four Göttingen Minipigs. *Toxicol Pathol*. 2023 Jan;51(1-2):61-66.
2. Holley D, et al. Diagnosis and management of fetal cardiac tumors; a multicenter

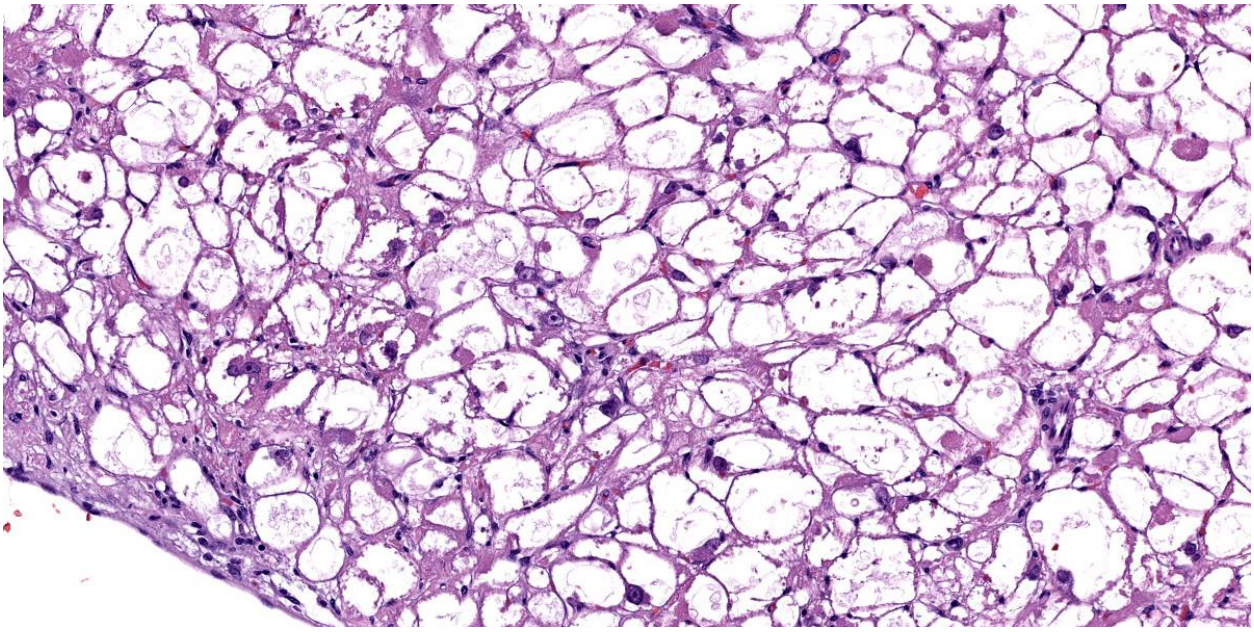

Figure 1-3. Heart, guinea pig. Cardiomyocytes are markedly expanded by glycogen forming "spider cells" (HE, 228X)

experience and review of published re ports. *J Am Coll Cardiol*, p. 516-520, 1995.

3. Jacobsen B, et al. Proposing the term purkinjeoma: Protein Gene Product 9.5 Expression in 2 Porcine Cardiac Rhabdomyoma Indicates Possible Purkinje Fiber Cell Origin. *Vet Pathol.* 2010;47(4):738-740.
4. Kizawa KK, et al. Cardiac rhabdomyoma in a Beagle dog. *Journal of Toxicologic Pathology*. 2002; 15(1):69-72.
5. Kobayashi TT, et al. A Cardiac rhabdomyoma in a guinea pig. *Journal of Toxicologic Pathology*. 2010;23(2):107-110.
6. Kolly C, et al. Cardiac rhabdomyoma in a juvenile fallow deer (Dama dama). *Journal of Wildlife Diseases*. 2004;40(3):603-606.
7. Krafsur G, et al. Histomorphologic and immunohistochemical characterization of a Cardiac Purkinjeoma in a Bearded Seal (Erignathus barbatus). *Case Reports in Veterinary Medicine*. 2014.
8. Pereira PA, et al. Cardiac rhabdomyoma in a slaughtered pig. *Cienc. Rural, Santa Maria.* 2018; 48(10):e20180460.
9. Percy DH, Griffey SM, and Barthold SW. *Pathology of Laboratory Rodents and Rabbits*. Ames, Iowa: Blackwell Pub, 2016, 241-242.
10. Radi ZA, Metz Z. Canine cardiac rhabdomyoma. *Toxicologic Pathology*. 2009;37(3):348-350.
11. Southard T, Kelly K, Armien AG. Myocardial protein aggregates in pet guinea pigs. *Vet Pathol*. 2022 Jan;59(1):157-163.
12. Tanimoto T, Ohtsuki Y. The pathogenesis of so-called cardiac rhabdomyoma in swine: a histological, immunohistochemical and ultrastructural study. *Virchows Archiv*. 1995;47(2):213-221.

CASE II:

Signalment:
Adult, male, Göttingen minipig, *Sus scrofa domesticus*

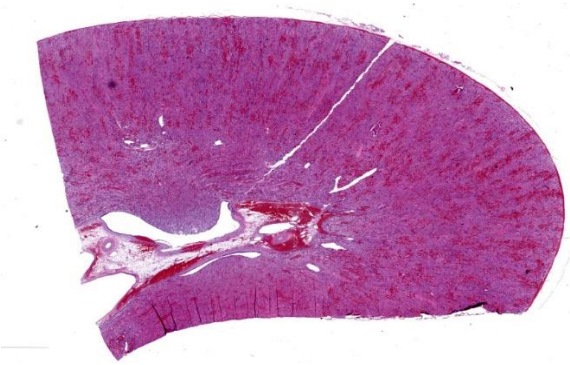

Figure 2-1. Kidney, Gottingen minipig. One section of kidney is submitted for examination. At subgross magnification, multifocal hemorrhage is present throughout the section. (HE, 4X)

History:
This source animal had an acute history of decreased activity, decreased appetite, and generalized orange-pink skin discoloration prior to initial test article administration. It was subsequently discovered laterally recumbent with an intermittent, abnormal breathing pattern. Bloodwork was collected immediately prior to euthanasia.

Gross Pathology:
There were no significant gross lesions.

Microscopic Description:
In the kidneys, renal tubules in the cortex and extending into the medulla are diffusely, mildly to moderately dilated and filled with eosinophilic proteinaceous fluid or erythrocytes. Epithelial cells lining effected tubules are multifocally flattened with basophilic cytoplasm and frequently contain hypereosinophilic, globular, cytoplasmic material. There are few scattered clusters of necrotic tubules within the cortex, characterized by hypereosinophilia, loss of differential staining, and nuclear pyknosis of the tubular epithelium. Occasionally, Bowman's spaces are dilated and filled with similar eosinophilic fluid and hypereosinophilic globular material which moderately compresses glomerular tufts. There is moderate, multifocal expansion of the renal interstitium and peri-pelvic adipose tissue by abundant hemorrhage which surrounds and separates renal tubules and adipocytes.

Contributor's Morphologic Diagnosis:
Kidney: Renal tubular hemorrhage and proteinosis, diffuse, acute, severe, with rare tubular degeneration and necrosis and diffuse interstitial hemorrhage

Contributor's Comment:
Histologic lesions are compatible with hemorrhagic syndrome in Göttingen minipigs, also known as thrombocytopenic purpura syndrome (TP). Hemorrhagic syndrome has been previously described in Göttingen minipigs with thrombocytopenia as the underlying cause.[1] Currently, the mechanism of the thrombocytopenia associated with hemorrhagic syndrome is unknown, but is thought to be secondary to an immune complex-associated disorder, specifically a type II-mediated thrombocytopenia and/or a type III-mediated vasculitis/glomerulonephritis.[1,7] Animals between 7 weeks and 1 year have been reported as affected with no apparent hereditary etiology.[1,6]

Clinically, pigs suffering from hemorrhagic syndrome are typically anemic and severely thrombocytopenic ($\leq$ 20,000/µl).[1,6] Depending on the severity of the disease and the organs affected, additional bloodwork abnormalities such as increased liver or renal values may be present, as in this case. Macroscopically, widespread hemorrhage is a key feature in hemorrhagic syndrome, including petechial to ecchymotic hemorrhages or hematomas most commonly observed in the skin, heart, urinary bladder, and kidney.[7] While there were no discrete hemorrhages observed macroscopically in this case, the generalized orange to pink skin discoloration and hyperbilirubinemia suggest that there was significant hemolysis in this animal.

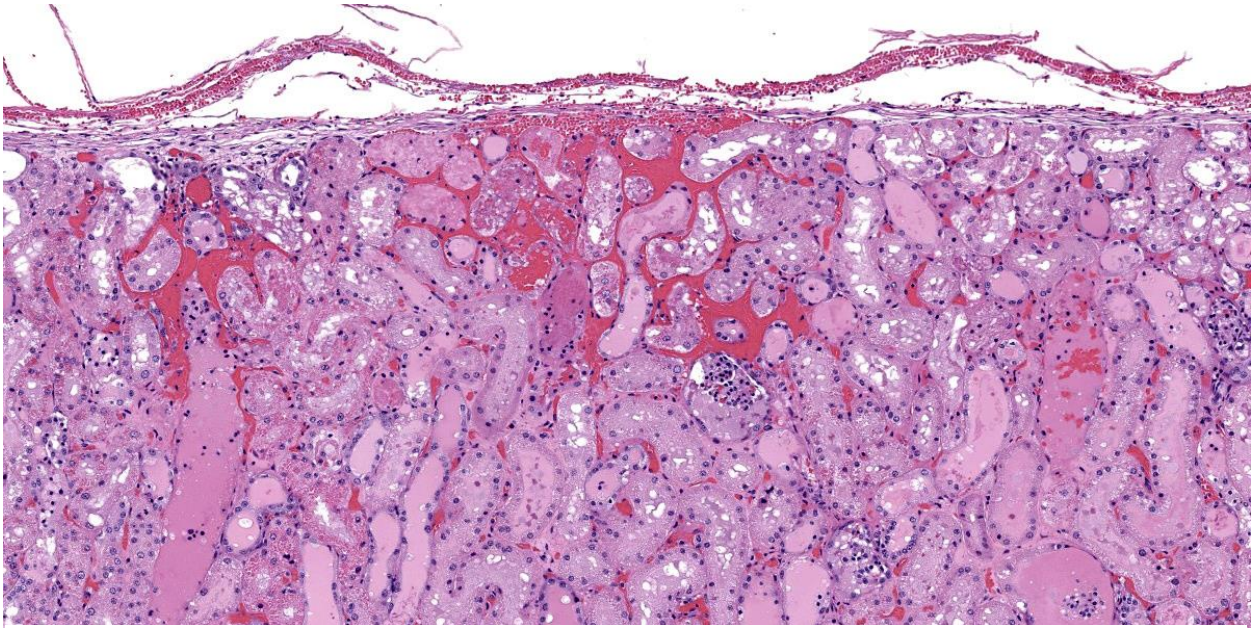

Figure 2-2. Kidney, Gottingen minipig: In this subcapsular field, there is multifocal acute hemorrhage, with tubular epithelial degeneration and necrosis. (HE, 294X)

Microscopically, lesions of hemorrhagic syndrome consist of multifocal interstitial to mucosal hemorrhages in multiple organs including but not limited to the skin, kidney, bladder, intestine, pancreas, lymph nodes, lungs, and skeletal musculature.[1,7] In the kidneys, membranoproliferative glomerulonephritis is a common feature, characterized by thickening of glomerular basement membranes and an increase in the number of mesangial cells within glomerular tufts.[1,6] Degenerative and proliferative vascular lesions affecting small to medium-sized muscular arteries and arterioles have also been reported in cases of hemorrhagic syndrome.[6] Previously described vascular lesions range from endothelial cell hypertrophy and smooth muscle cell vacuolation to proliferation of the tunica intima, necrosis and thickening of the tunica media, and disruption of the internal elastic membrane.[6] These lesions can also be accompanied by lymphohistiocytic to neutrophilic periarteritis.[6] Vascular lesions are most commonly observed in the heart and renal pelvis, but can found in other affected tissues.[6]

Based on the rapid progression of clinical signs, lack of significant gross lesions and microscopic evidence of hemorrhage in the kidney, this case is considered to represent a peracute presentation of hemorrhagic syndrome in the Göttingen minipig. Certain histologic lesions typically observed in TP, such as hemorrhages in multiple organs and appreciable membranoproliferative changes in the kidney, were not present in this case, but may have developed later in the course of disease had this animal not been euthanized. The hypereosinophilic, globular material observed in the cytoplasm and lumen of renal tubules has been previously reported in cases of hemorrhagic syndrome and, in those cases, was confirmed to be IgG, IgM or C1q with immunohistochemistry, supporting an immune-mediated cause for the disease.[1]

Some differentials to consider for hemorrhagic syndrome in Göttingen minipigs include other hemorrhagic disorders such as neo-natal alloimmune thrombocytopenia and von Willebrand disease (VWD). Neonatal alloimmune thrombocytopenia occurs in piglets

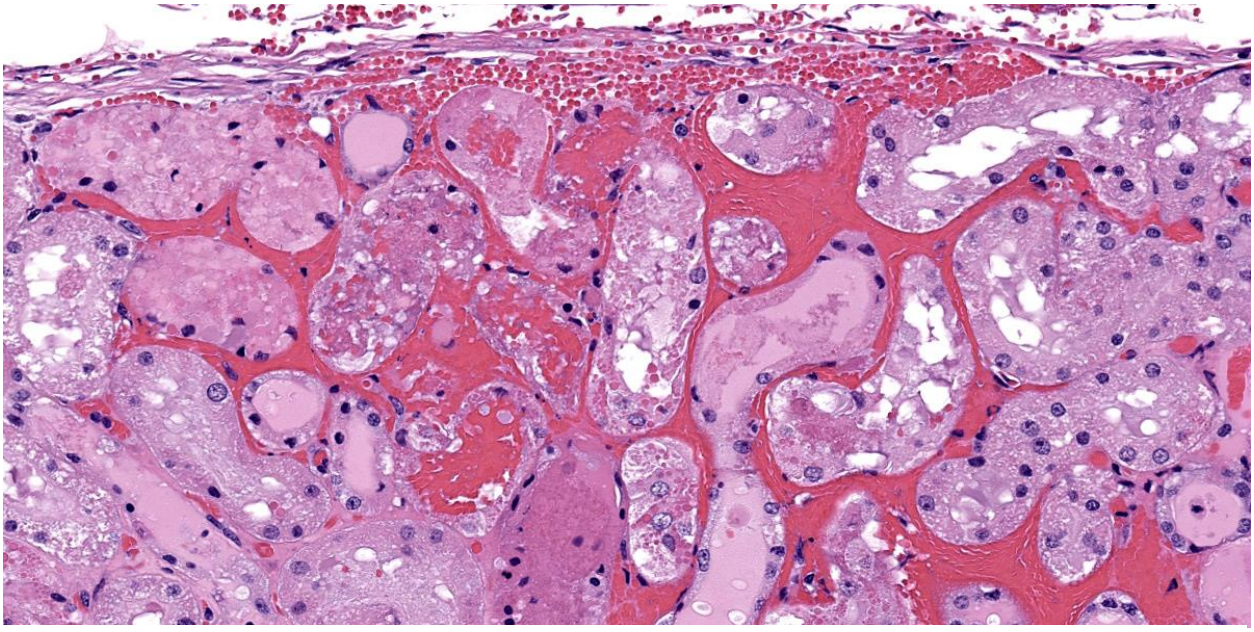

Figure 2-3. Kidney, Gottingen minipig. Higher magnification of the field in Fig. 2-2, with tubular degeneration and necrosis (HE, 294X).

less than a week old and is associated with immune-mediated platelet destruction by alloantibodies produced in sow colostrum against fetal platelet antigens inherited from the boar.[2] Von Willebrand disease is a dominant recessive, hereditary bleeding disorder caused by a mutation in von Willebrand factor.[5] Type 3 VWD, the most severe form of the disease in which there is a near total absence of von Willebrand factor, has been previously reported in farm pigs and causes severe mucocutaneous and periarticular hemorrhage that can be fatal if not treated.[5] While petechial to ecchymotic hemorrhages can occur virtually anywhere with hemorrhagic syndrome and may present similar to VWD grossly, VWD does not commonly cause visceral hemorrhages and has not been reported to cause membranoproliferative changes in the kidney.

Contributing Institution:
Charles River Laboratories, Mattawan, MI
www.crl.com

JPC Diagnosis:
Kidney: Hemorrhage, acute, multifocal to coalescing, marked with tubular degeneration, necrosis, regeneration, and proteinosis.

JPC Comment:
Case 2 ratchets up the pathology seasoning nicely, with our case discussion being particularly spicy. In this case, the widespread hemorrhage within the renal interstitium is an obvious feature, though the tubular changes should not be overlooked (Figures 2-2, 2-3, and 2-4). As this animal was euthanized and quickly necropsied, the cellular preservation of this section is excellent which negates the frustration of reading through autolytic changes. We agreed with the contributor that the hemorrhage noted fits with an acute interpretation of this lesion, though some participants quibbled that a true 'peracute' lesion would have no supporting histologic features as the animal would succumb too quickly. This however was the easy part of the case discussion.

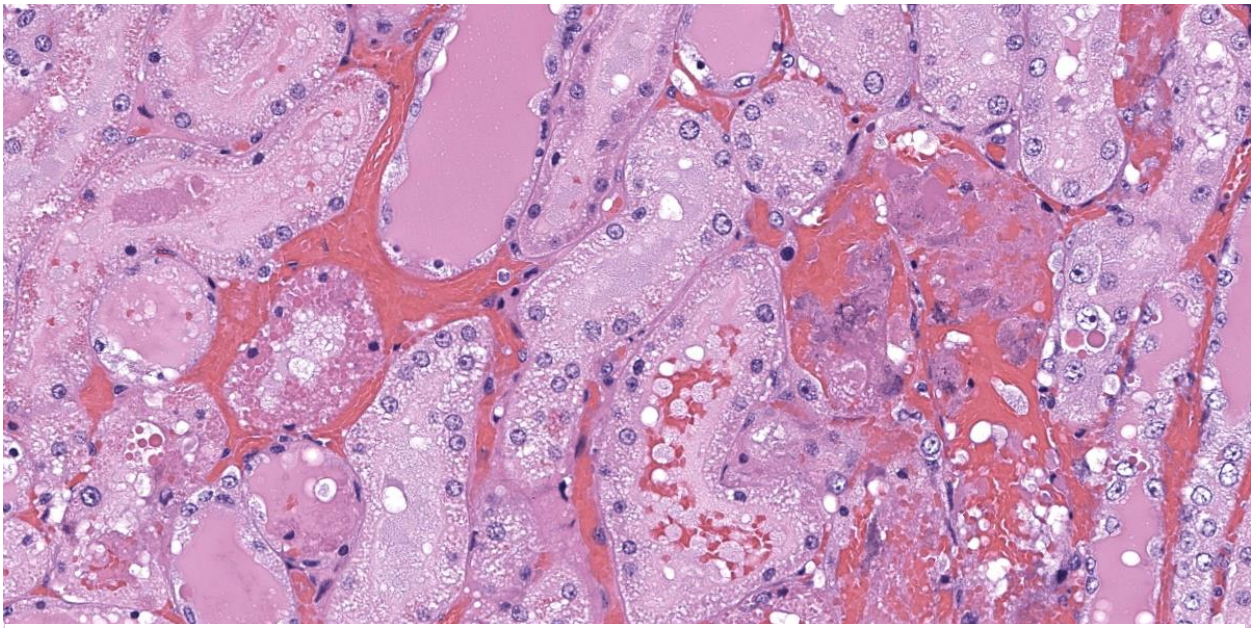

Figure 2-4. Kidney, Gottingen minipig. More tubular degeneration and necrosis within tubules. Numerous tubules contain abundant luminal protein. (HE, 314X)

Interestingly, a number of conference participants also raised the question of whether there could be underlying chronic changes in this case which we catalog in detail. Participants felt strongly that thrombocytopenic purpura syndrome would likely have some supporting chronic changes given the pathogenesis the contributor describes. We last saw this entity in Conference 3 in 2023-2024, though there are some key differences to note. In last year's case, we reviewed multiple sections from the ear that featured arteriosclerosis with modest arteritis and periarteritis, including thrombi in section. In this case, there are some small- and medium-caliber blood vessels near the renal pelvis/hilus (figure 2-1) that have medial hypertrophy of the tunica media ('onion-skinning') with endothelial hypertrophy. Additionally, some participants noted rare foci of basophilic renal tubular cells that were stacked and had mitotic figures (interpreted as regeneration) which would support a chronic interpretation of this lesion. Within the collecting ducts, there are also multiple granular casts present which points towards a longer time course in this case as well. We looked carefully for ancillary changes that would align with this interpretation and ran both PAS and JMS (Jones Methenamine Silver) to highlight the glomerular basement membrane as well as a Movat's pentachrome to examine the wall of blood vessels. We agree with the contributor that there were no glomerular changes in this case to include thickening of the basement membrane, discontinuity or deposits within the membrane, or any glomerular synechiae in any of the sections examined. Movat's stain did show discontinuity of both the inner and outer elastic lamina in select vessels which was not readily apparent on H&E section. Nonetheless, we struggled to find a good example of vasculitis on our section as the lack of vascular change (vascular necrosis and/or surrounding inflammation) or obvious fibrin thrombi made it difficult to pin down the exact connection to the large degree of hemorrhage and subsequent tubular change in this animal. This could be related to thrombocytopenia, though we did wonder about the nature of the perimortem blood sample clotting and its relation to this case too. With these features in

mind, we cautiously approached the morphological diagnosis for this case, and focused only on the features that we felt we had solid support for histologically. We thank the contributor for submitting this case as it prompted a fruitful discussion here at the JPC.

There are a number of potential rule outs for acute tubular injury and hemorrhage in swine. These include porcine circovirus (dermatitis and nephropathy syndrome), porcine respiratory and reproductive syndrome virus, classical swine fever, African swine fever, septicemia, and anticoagulant rodenticide ingestion.[3] For Göttingen minipigs, background renal lesions are fairly limited and mild, and did not confound interpretation of this case.[4]

References:

1. Carrasco L, et al. Immune complex-associated thrombocytopenic purpura syndrome in sexually mature Göttingen minipigs. *J Comp Pathol*. 2003 Jan;128(1):25-32.
2. Forster LM. Neonatal alloimmune thrombocytopenia, purpura, and anemia in 6 neonatal piglets. *Can Vet J*. 2007 Aug;48(8):855-7.
3. Imai DM, Cornish J, Nordhausen R, Ellis J, MacLachlan NJ. Renal tubular necrosis and interstitial hemorrhage ("turkey-egg kidney") in a circovirus-infected Yorkshire cross pig. *J Vet Diagn Invest*. 2006 Sep;18(5):496-9.
4. Jeppesen G, Skydsgaard M. Spontaneous background pathology in Göttingen minipigs. *Toxicol Pathol*. 2015 Feb;43(2):257-66.
5. Lehner S, et al. A 12.3-kb Duplication Within the VWF Gene in Pigs Affected by Von Willebrand Disease Type 3. *G3 (Bethesda)*. 2018 Feb 2;8(2):577-585.
6. Maratea KA, Snyder PW, Stevenson GW. Vascular lesions in nine Göttingen minipigs with thrombocytopenic purpura syndrome. *Vet Pathol*. 2006 Jul;43(4):447-54.
7. Skydsgaard M, et al. International Harmonization of Nomenclature and Diagnostic Criteria (INHAND): Nonproliferative and Proliferative Lesions of the Minipig. *Toxicol Pathol*. 2021 Jan;49(1):110-228.

CASE III:

Signalment:
17-year-old, intact female, rhesus macaque, *Macaca mulatta*, Non-human primate (NHP)

History:
This NHP was part of several animals who lived in a research colony in Texas for several years prior to being transported to Maryland. The animal had recently become very unthrifty with a very poor body condition. Due to a worsening condition, humane euthanasia was elected.

Gross Pathology:
The heart was diffusely enlarged up to 1.5 times the normal size and bilaterally the ventricular free walls were thin and flabby. The pericardium contained approximately 75 mL of serosanguineous fluid. In the left ventricle, there were multiple white nodules adhered to the endocardium. The serosal surfaces of the small and large intestines were reddened. The liver had a diffuse cobblestone appearance. The gallbladder was markedly enlarged up to three times normal. The splenic capsule had a diffusely nodular appearance. The right adrenal gland had a single, tan, 2 mm nodular lesion in the cortex. There was approximately 50 mL of serosanguineous fluid in the thorax and 50 mL of similar fluid in the abdomen.

Laboratory Results:
Biochemistry profiles showed chronically elevated liver and kidney values with low protein. Exact values were unavailable. PCR testing on formalin-fixed cardiac tissue was positive for *Trypanosoma cruzi*.

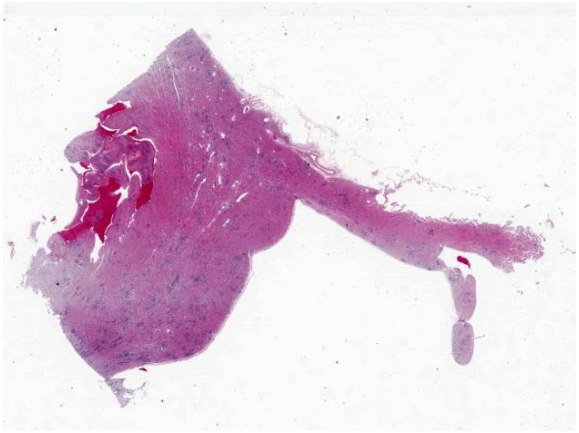

Figure 3-1. Heart, macaque. One section of heart including the base of the left and right ventricle and the interventricular septum is submitted for examination (HE, 5X)

Microscopic Description:
Diffusely and transmurally affecting approximately 60% of the section, large numbers of inflammatory cells composed of macrophages, lymphocytes, plasma cells, and neutrophils with fibroblasts surround, infiltrate, and replace cardiomyocytes. Cardiomyocytes adjacent to these inflammatory cells are often degenerate characterized by swollen, pale and vacuolated sarcoplasm or are necrotic characterized by hypereosinophilic sarcoplasm with loss of cross striations, and fragmentation of the nucleus with cellular and karyorrhectic debris. Multifocally within cardiomyocytes are numerous pseudocysts measuring up to 40 um x 90 um which contain a plethora of 2-4 um protozoal amastigotes with a basophilic nucleus and kinetoplast. Fibrin, hemorrhage, and edema is also present in these inflammatory regions. Present within the left ventricular lumen are multiple enmeshed clots adhered to the papillary muscles composed of fibrin, hemorrhage, edema, and similar inflammatory cells.

Contributor's Morphologic Diagnosis:
Heart: Panmyocarditis, histiocytic and lymphoplasmacytic, chronic, diffuse, severe, with myocardial degeneration, necrosis, and loss, and intramyocytic protozoal amastigotes, rhesus macaque, non-human primate.

Contributor's Comment:
The histopathologic findings and PCR test results are diagnostic for cardiac trypanosomiasis caused by *Trypanosoma cruzi*. *T. cruzi* is the causative agent for Chagas disease, otherwise known as American trypanosomiasis. Trypanosomes are hemoflagellate protozoans known to infect humans and a variety of domestic and wild animals throughout North and South America. In the southern United States, opossums, raccoons, and armadillos serve as the primary reservoir hosts.[1,3,5,7]

T. cruzi is most commonly spread through stercorarian transmission when its vector, the triatomine bug (also called the reduviid or kissing bug), defecates or urinates trypomastigotes of *T. cruzi* at the site of a recent blood feeding. Trypomastigotes from the feces or urine enter the wound and disseminate hematogenously to cardiomyocytes. Trypomastigotes invade cardiomyocytes where they develop within the sarcoplasm into amastigotes within a pseudocyst. After replication, the amastigotes mature into trypomastigotes, rupture the host cell, and re-enter systemic circulation. This infective form is then ingested by a triatomine bug during a blood feeding where it transforms into an epimastigote in the insect's gut and replicates through binary fission while awaiting the cycle to begin anew.[1,3,5,7,8] While the heart is the primary organ affected, amastigotes have also been identified in several other organs.[3] In this case, a pseudocyst was also identified in the diaphragm. Additional documented forms of transmission include oral ingestion of the vector or contaminated feces, transplacental and transmammary transmission, blood transfusions, and organ transplantation.[1,5,8]

Classic clinical and pathologic findings follow a pattern of cardiac disease. In the acute phase,

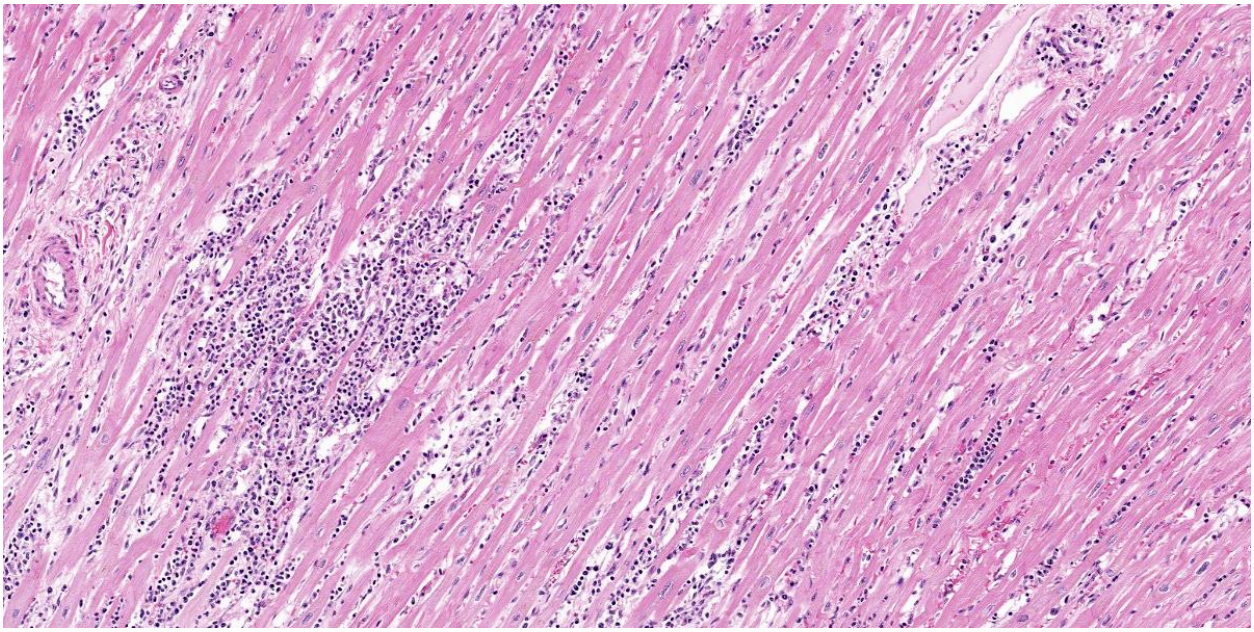

Figure 3-2. Heart, macaque. Multifocally throughout the section, there are large aggregates of macrophages, lymphocytes, and plasma cells with surround, separate and replace cardiomyocytes. (HE, 118X)

cardiac arrhythmias, sudden collapse, or even death, weak pulses, and signs of respiratory distress can all be expected. Animals that survive the acute phase can anticipate developing chronic heart disease. Cardiac dilatation is common as are more frequent cardiac arrhythmias and clinical signs consistent with unilateral or bilateral heart failure.[3]

Cytology of blood smears during the acute phase can be used to identify trypomastigotes present in the systemic circulation. In the chronic phase when parasitemia is lower, a thick-film buffy coat smear should be used to increase the concentration of the organisms. Lymph node aspirates and cytologic analysis of abdominal effusion has also been documented to identify *T. cruzi*. Serologic and molecular testing has also been useful in premortem diagnosis.[5]

Post-mortem findings will vary depending on if the animal died during the acute or chronic phase of infection. Lesions from death during the acute phase include a pale myocardium with hemorrhages in the subendocardial and subepicardial surfaces. Right-sided heart lesions are often more severe than the left side. Generalized lymphadenopathy has also been reported. Chronically infected animals often present with generalized cardiomegaly with thinning of the ventricular free walls and a serosanguineous fluid in the pericardial, pleural, and abdominal cavities. Microscopic findings include multifocal to diffuse histiocytic to lymphoplasmacytic myocarditis with varying stages of cardiomyocyte degeneration and necrosis with fibrosis. The presence of intracardiomyocytic amastigotes is a very helpful but can be difficult to find especially in chronic cases.[1,5]

A recent study documenting the histologic findings of *T. cruzi* in domestic cats documented lymphoplasmacytic myocarditis with fibrosis in 42.1% of seropositive cats compared to 28.6% of seronegative cats. In the same study, PCR for *T. cruzi* was performed on a variety of tissues from seropositive and seronegative cats. PCR-positive tissues included heart, biceps femoris muscle, sciatic nerve, esophagus, and mesentery.[8] Although

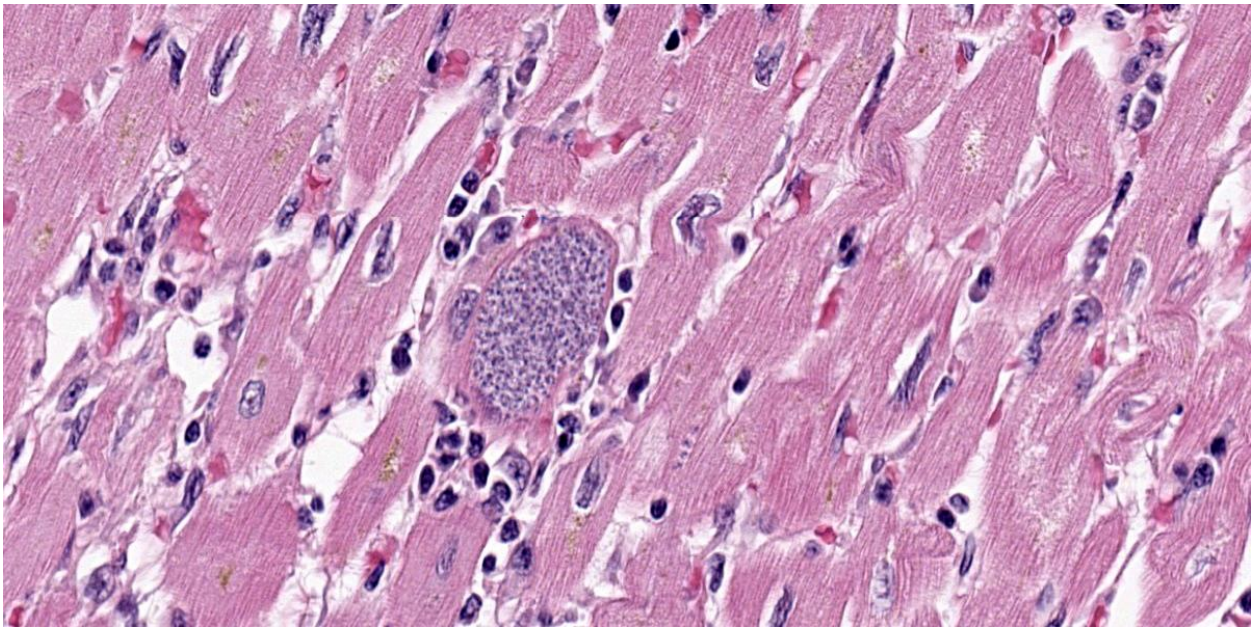

Figure 3-3. Heart, macaque. Occasionally cardiomyocytes contain a large cytoplasmic pseudocyst containing numerous 2-3um round trypanosomal amastigotes with a central nucleus and poorly discernable kinetoplasts. (HE, 727X)

CNS disease is considered an uncommon manifestation of *T. cruzi* infection in non-human mammals, disseminated trypanosomiasis with central nervous system (CNS) involvement was recently reported in four dogs, with CNS involvement confirmed by quantitative PCR. Lymphohistiocytic myocarditis and histiocytic meningoencephalitis with rare to numerous intralesional and intracellular amastigotes were reported in all 4 dogs, while gross lesions within the CNS were observed in 2/4 dogs.[3]

Contributing Institution:
Walter Reed Army Institute of Research; Department of Pathology;
https://www.wrair.army.mil/

JPC Diagnosis:
Heart: Pancarditis, lymphoplasmacytic and histiocytic, chronic, multifocal to coalescing, marked, with fibrosis and numerous intrmyocytic amastogotes.

JPC Comment:
At first glance, this section of heart is nondescript save for the random, coalescing regions of basophilia (Figure 3-1) that represent the inflammatory cells in the myocardium that the contributor describes. On higher magnification however, there are a plethora of changes occurring in this case that provide some zest to the pathology palate. To wit, we ran special stains (Giemsa, PTAH, Masson's trichrome) for this case and they did not disappoint. The degree of fibrosis in this case is not surprising given the loss of cardiac myocytes secondary to both rupture of amastigote-laden cells and the marked inflammatory response (figures 3-2 and 3-3), though cardiac fibrosis can also be a background lesion in aged macaques. In this case, trypanosomal amastigotes were obvious on H&E, though they were also highlighted metachromatically by Giemsa with the kinetoplasts being a sharp red against the medium blue background. We also ran a modified

Gram stain (Brown-Brenn, Brown-Hopps) and fungal stains (GMS, PAS Light Green) which did not identify any concurrent infections in this animal. Although tinctorially similar to the myofibers, there are also two fibrin thrombi nestled within the ventricle as the contributor points out. Conference participants overall liked the quality of this slide and the descriptive features as they felt they were rewarding to discuss.

Natural infection of non-human primates with Chagas disease has been described in the veterinary literature previously. [2,4,6] Given the preponderance of primate facilities in Texas similar to where the animal in this case originated, discussion of trypanosomiasis and its impacts on medical research remains relevant. A similar case of trypanosomal myocarditis in a rhesus macaque was previously covered in Conference 17, Case 2, 2013-2014.

Finally, another important rule out for this case is leishmaniasis which appears nearly identically to trypanosomes histologically. In theory, the orientation of the kinetoplast (parallel to the nucleus for trypanosomes, perpendicular for *Leishmania*) might help to discriminate these entities, though PCR is preferable if available. The advancing range of reduviid bugs has implications on animal and human health that are not lost on us at the JPC. Given that the Department of Defense's Military Working Dog Program is anchored in San Antonio, Texas[6], we see several cases of canine trypanosomiasis each year when such cases were rarer previously. Given worldwide deployment of Military Working Dogs, discerning *T. cruzi* infection against other agents remains an important task.

References:

1. Boes KM, Durham AC. Bone marrow, blood cells, and the lymphoid/lymphatic system. In: McGavin MD, Zachary JF, eds. *Pathologic Basis of Veterinary Disease*. 7th ed. St. Louis, MO: Elsevier; 2022:834.
2. Hodo CL, Wilkerson GK, Birkner EC, Gray SB, Hamer SA. Trypanosoma cruzi Transmission Among Captive Nonhuman Primates, Wildlife, and Vectors. *Ecohealth*. 2018 Jun;15(2):426-436.
3. Landsgaard K, et al. Protozoal meningoencephalitis and myelitis in 4 dogs associated with *Trypanosoma cruzi* infection. *Vet Pathol*. 2023;60(2):199-202.
4. Rovirosa--Hernández MJ, López-Monteon A, García-Orduña F, et al. Natural infection with Trypanosoma cruzi in three species of non-human primates in southeastern Mexico: A contribution to reservoir knowledge. *Acta Tropica*. 2021;213:105754.
5. Snowden KF, Kjos SA. American trypanosomiasis. In: Greene CE, ed. *Infectious Diseases of the Dog and Cat*. 4th ed. St. Louis, MO: Elsevier-Saunders; 2012:722-30.
6. Tarleton R, Saunders A, Lococo B, et al. The Unfortunate Abundance of Trypanosoma cruzi in Naturally Infected Dogs and Monkeys Provides Unique Opportunities to Advance Solutions for Chagas Disease. *Zoonoses*. 2024;4(10).
7. Valli VEO, Kiupel M, Bienzle D. Hematopoietic system. In: Maxie MG, ed. *Jubb, Kennedy, and Palmer's Pathology of Domestic Animals*. Vol 3. 6th ed. Philadelphia, PA: Saunders Elsevier; 2016:121-124.
8. Zecca IB, et al. Prevalence of *Trypanosoma cruzi* infection and associated histologic findings in domestic cats (*Felis catus*). *Vet Parasitol*. 2020;278:109014.

Figure 4-1. Oral cavity, rhesus macaque. A 4 x 2 cm mass extends from the caudal aspect of the hard palate into the soft palate and pharynx (arrow). The mass was soft with an irregular surface that was mottled light and dark gray. (*Photo courtesy of:* NIH, 9000 Rockville Pike, Building 28A, Room 117, Bethesda, MD 20892)

CASE IV:

Signalment:
18 year-old, male, rhesus macaque, Macaca mulatta

History:
During a physical examination, a mass was found at the back of the mouth and was biopsied. A week later, based on the biopsy result, the monkey was euthanized.

Gross Pathology:
A 4 x 2 cm mass extended from the caudal aspect of the hard palate into the soft palate and pharynx. The mass was soft with an irregular surface that was mottled light and dark gray. The draining lymph nodes appeared to be enlarged. Photo of fixed tissue: arrows delineate the extension of the mass from the ulcerated hard palate into the pharynx.

The liver was markedly enlarged and diffusely pink and had a white texture on cut section. Along the apical margins of the liver were white well demarcated firm foci that also were waxy in texture. Lungs, heart, spleen, kidneys and GI were grossly normal.

Microscopic Description:
Moderately pleomorphic neoplastic cells expanded the submucosa and extended to the cut edges of the sections. The cells were round to oval to stellate and ranged in size from 15-50um. Nuclei were round to oval and had prominent nucleoli. Cells had abundant wispy cytoplasm with small vesicles and a few had faint brown pigment granules. Mitoses averaged 2/HPF although some fields had as many as 5 mitotic figures. Some of the mitoses had an unusual appearance. In addition, hyphae consistent with candida and bacterial cocci were present in ulcerated areas [not present in all slides]

Submandibular lymph nodes were largely effaced by similar cells. A section of lung had microscopic metastasis.

Liver: The liver had severe amyloidosis with tumorous deposits at the apical margins. Heart, spleen, kidney and salivary glands were normal.

Special stains:
Fontana-Masson: biopsy, tumor, and lymph node had scattered positive cells.
Giemsa: (-)

Immunohistochemistry**:**
S-100, SOX-10, Melan A, PNL, HM45: (+)
Cytokeratin AE1/AE3: (-)

TEM: One percent of the tumor cells were positive for melanin and `contained 1 to 50 granules. All four stages of melanin granules were present with stages 3 and 4 predominating. The enclosed image shows all four stages.

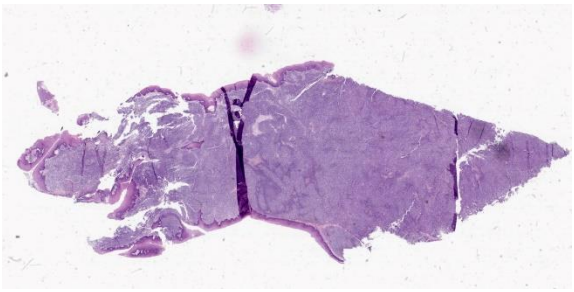

Figure 4-2. Oral cavity, rhesus macaque. A superficial section of the mass is submitted for examination. Neoplastic cells efface the lamina propria and extend to the overlying mucosal epithelium. (HE, 9X)

Contributor's Morphologic Diagnosis:
Amelanotic melanoma

Contributor's Comment:
Melanocytes arise from neural crest cells and reside not only in the basal cells of the epidermis and hair follicles, but also the eyes and meninges. Melanin synthesis occurs in melanosomes, lysosome-like organelles in melanocytes. Two major melanin pigments synthesized are pheomelanin (red/yellow in color) and eumelanin (brown/black). Both pigments arise from L-tyrosine which, when acted upon by tyrosinase, leads to DOPA (dihydroxyphenylalanine) formation. Production of DOPA from L-tyrosine is the rate limiting step in melanogenesis.[3] Oxidation and polymerization of DOPA leads to the formation of pheomelanin. Further enzymatic action by tyrosinases produces eumelanin. The percentage of eumelanin and pheomelanin determines the color of the skin/hair.[3,5]
Packaging of melanin into melanosomes occurs in four identifiable stages as seen by electron microscopy. Early melanosome stages I and II do not contain melanin but fibers formed during these stages give melanosomes their ovoid shape. Deposition of melanin begins in stage III and completely fills the melanosome in stage IV melanosomes.[5] Once formed, melanosomes are transferred to keratinocytes and are moved into the supranuclear area to form melanin caps which protect nuclei against UV damage. Melanin degrades as keratinocytes undergo squamous maturation.[3,5]

Melanoma is called the "great imitator" as the cells can have epithelioid, spindloid, clear, signet ring–like, myxoid, desmoplastic, rhabdoid, ballooning, and plasmacytoid forms.[7,9,10] Additional features of melanoma include high mitotic rate, unusual morphology of mitotic figures and the presence of junctional change by neoplastic cells.[6,12]

Some common stains used for diagnosis are Fontana-Masson which stains melanin granules brown in tumors that have little pigmentation. Bleach clears melanin in deeply pigmented tumors to examine the morphology of the cells. Giemsa is another stain to rule out mast cell tumors

Since melanomas, and other pigmented masses, may express more than one marker and immunohistochemistry can stain more than one cell type, including non-neoplastic cells, "cocktails" of markers are used to make diagnoses, identify micrometastases in sentinel lymph nodes, determine prognosis, and develop treatment strategies.[2,3,7] Specific markers include:

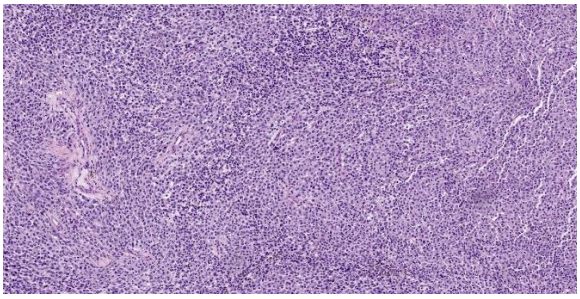

Figure 4-3. Oral cavity, rhesus macaque. Neoplastic round cells are arranged in sheets (HE, 91X)

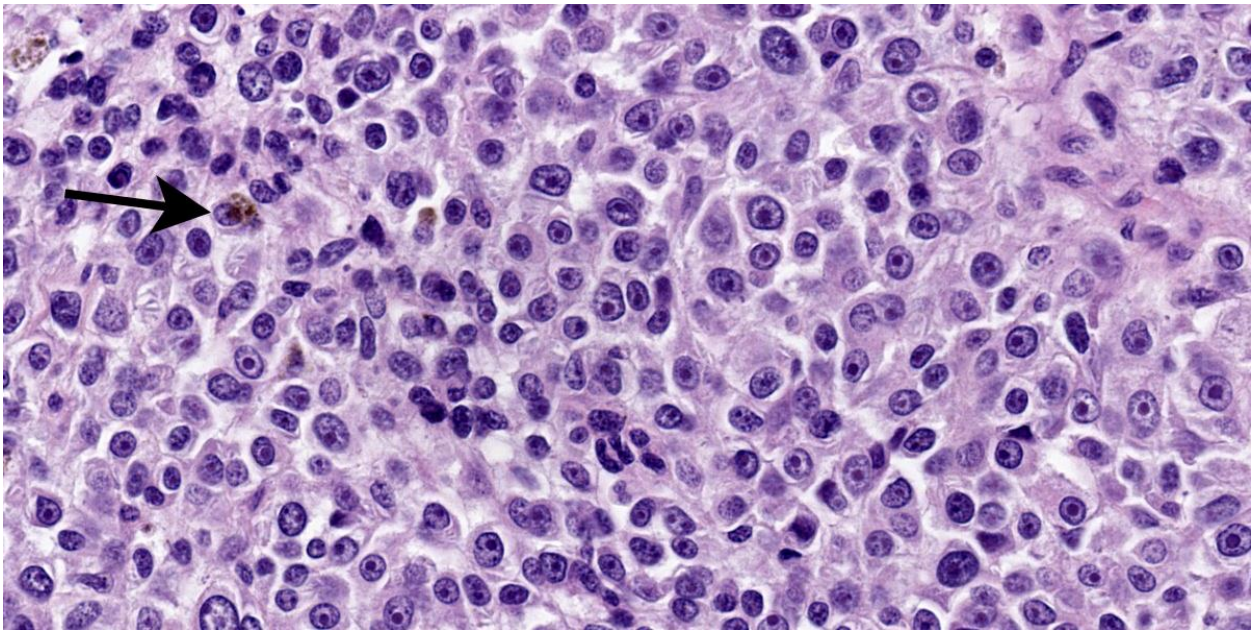

Figure 4-4. Oral cavity, rhesus macaque. Neoplastic cells have round nuclei with prominent nucleoli and few cells contain cytoplasmic melanin (arrow). (HE, 581X)

Cytokeratin: expressed in epithelial origin tumors.

S-100: is expressed in all subtypes of melanoma and identifies cells derived from the neural crest.[7] S-100 may also be expressed in other tumors.

Melan-A: (aka melanoma-associated antigen recognized by T cells) plays an important role in the formation of stage II melanosomes which have structural proteins.[2,7]

MITF: (microphthalmia-associated transcription factor) is the central regulator of melanogenesis. It is essential for melanocyte development and regulates genes for melanogenesis, cell survival, and differentiation.[3,7] MITF stain is sensitive but not specific. It is used as part of a cocktail because the staining pattern is nuclear and most other stains are cytoplasmic.[3,7]

HMB-45: (human melanoma black) is associated with the structural organization of melanosomes and with the fibrillar matrix and the maturation in stages I to II melanocytes.[7]

SOX10: (sry-related HMg-box gene10) is a nuclear transcription factor that regulates the differentiation of neural crest progenitor cells into melanoblasts and melanocytes.[3,7]

A pigmented, perioral melanoma with metastases to the lymph nodes, lung, liver, and kidney has been reported in a mountain gorilla.[4] Oral melanoma has not been reported in macaques and reports of melanoma involving other sites are rare. There is one report of melanoma in the choroid with no metastases in a cynomolgus macaque[1] and one report of cutaneous melanoma with metastases to local lymph nodes, also in a cynomolgus macaque.[8]

In humans, melanoma can be separated into three categories based on the amount of sun exposure: high cumulative sun damage, low cumulative sun damage and sun protected. Sun protected areas are further divided into acral (i.e. palms of the hands, soles of the feet, and the nails), mucosal/genital, uveal and CNS. The type and number of mutations can vary based on the location of the primary tumor.[2,13]

Figure 4-5. Oral cavity, rhesus macaque. Neoplastic melanocytes demonstrate multiple stages of melanosomes, ranging from Stage 1 (lightest) to Stage 4 (darkest). (TEM, 5000k)

While the incidence of cutaneous melanoma has increased over the last 50 years, the incidence of mucosal melanoma has remained fairly constant.[2,13] Mucosal membrane melanomas are rare and are more aggressive with a less favorable outcome compared to cutaneous melanomas. The low survival rate is due to lack of clinical signs and the likelihood that melanoma has already spread to local lymph nodes at the time of diagnosis.[2,9,12] In addition to local lymph nodes, melanoma tends to metastasize to the lungs and liver.[2,13]

Malignant melanoma has been reported to develop in a variety of mammalian and nonmammalian species including dog, rabbit[14], shark, parrot, pig and monkey.[2,13] In the dog, malignant melanoma is the most common oral tumor[9], is locally aggressive and tends to metastasize to local lymph nodes and lung.[9,10] Breeds that are more likely to develop oral melanoma are Poodle, Golden and Labrador retrievers, Rottweilers and Yorkshire terriers.[9]

Some aspects of canine oral melanoma are similar to humans. In both, the etiology is unknown, clinical course is aggressive and definitive treatment for oral melanoma is lacking.[2,9] The appearance of the neoplastic cells is variable and combinations of immunohistochemistry markers are used to diagnose the subtype of melanoma more definitively.[7,9] For example, a cocktail of Melan-A, PNL2, TRP-1(tyrosinase related protein-1), and TRP-2 (tyrosinase related protein-2) has been found to be useful in the diagnosis of amelanotic melanoma in dogs.[10]

Treatment may include surgical excision, radiotherapy, and chemotherapy but none have been particularly effective as the behavior of oral melanoma differs from that of cutaneous

melanoma.[2,9] Immunotherapy with checkpoint inhibitors that allow T-cells to become activated against tumor cells has been successful in treating cutaneous melanoma in man, but less so for oral melanoma.[2] In dogs, the potential of identifying checkpoint inhibitors and developing immunotherapy is being explored.[9,11]

Contributing Institution:
NIH
9000 Rockville Pike
Building 28A, Room 117
Bethesda, MD 20892

JPC Diagnosis:
Oral cavity: Melanoma.
Oral mucosa: Stomatitis, ulcerative, focally extensive, marked with numerous yeast, pseudohyphae, hyphae, and cocci.

JPC Comment:
We repeated the same list of IHC and special stains outlined by the contributor and got nearly identical results. In particular, neoplastic cells were strongly and diffusely immunoreactive for PNL2, Melan-A Red, and SOX10, though they did not react with HMB-45 which may reflect a difference in lab assay performance. With our Fontana-Masson stain applied, approximately 5-10% of neoplastic cells have intracytoplasmic black granules (melanin) which is also evident on H&E to a lesser extent (figure 4-4). Conference participants felt that these results were consistent with the diagnosis of a melanoma but felt that there were enough granules evident on H&E alone to forgo the 'amelanotic' label. The exact cutline for having little melanin present may vary per pathologist and many hypopigmented lesions probably fall into the amelanotic camp. At the JPC, we typically withhold the qualifier of 'amelanotic' for cases that have no discernable melanin on H&E. To our knowledge, published reports of oral melanoma in the non-human primate remain rare in line with what the contributor notes.

The inclusion of electron microscopy in this case workup is a welcome addition (figure 4-5). Recognizing melanosomes on EM is helpful as they characteristically have an oblong shape that Dr. Bruce Williams swears looks like a watermelon (or perhaps a football) in second of the four phases of melanin synthesis that contributor highlights.

In addition, conference participants honed in on a second aspect of this case that the contributor may have curtailed given the lengthy write up on melanoma they provided. In the bottom left (approximately 8 o'clock on figure 4-2), the oral mucosa is ulcerated, edematous, and has several small blood vessels with clear indications of vasculitis. Immediately adjacent, there are numerous fungal mats that contain yeast, pseudohyphae, and hyphae as well as colonies of cocci. Participants felt that these changes were consistent with ulcerative stomatitis secondary to *Candida*. In the history provided for this case, there was no mention of immunosuppression (i.e. SHIV infection) or antibiotic use though both of these are reasonable differentials for this lesion alone. After careful discussion, we added a second morphologic diagnosis for this case (a rarity for neoplasms) as we felt that this process was not directly connected to the melanoma in this case given the lack of junctional activity and condition of the remaining portion of the oral mucosa. Lastly, tissue ID for this case was aided by the presence of plant material (food) in section, though other similar tissues with stratified epithelium in a primate include the vagina and sex skin.

References:

1. Albert DM, Dubielzig RR, Li Y, et al. Choroidal Melanoma Occurring in a Non-human Primate. *Arch Ophthalmol*. 2009;127(8):1080–1082.
2. Dika E, Lambertini M, Pellegrini C, et al.. Cutaneous and Mucosal Melanomas of Uncommon Sites: Where Do We Stand Now? *J Clin Med*. 2021 Jan 28;10(3):478.
3. D'Mello SA, Finlay GJ, Baguley BC, Askarian-Amiri ME. Signaling Pathways in Melanogenesis. *Int J Mol Sci*. 2016 Jul 15;17(7):1144.
4. Kambale Syaluha E, Zimmerman D, Ramer J, et al. Metastatic perioral melanoma in a wild mountain gorilla (Gorilla beringei beringei). *J Med Primatol*. 2021 Jun;50(3):197-200.
5. Lambert MW, Maddukuri S, Karanfilian KM, Elias ML, Lambert WC. The physiology of melanin deposition in health and disease. *Clin Dermatol*. 2019 Sep-Oct;37(5):402-417.
6. Mauldin EA, Peters-Kennedy J. Integumentary System. In: Maxie MG, ed. *Jubb, Kennedy & Palmer's Pathology of Domestic Animals*. Vol 1. 6th ed. St. Louis, MO: Elsevier; 2016:720-722.
7. Ordóñez, NG. Value of melanocytic-associated immunohistochemical markers in the diagnosis of malignant melanoma: a review and update. *Hum Pathol*. 2014 Feb;45(2):191-205.
8. Pellegrini G, Bienvenu JG, Meehan JT, et al. Cutaneous melanoma with metastasis in a cynomolgus monkey (Macaca fascicularis). *J Med Primatol*. 2009 Dec;38(6):444-7.
9. Prouteau A, André C. Canine Melanomas as Models for Human Melanomas: Clinical, Histological, and Genetic Comparison. *Genes (Basel)*. 2019 Jun 30;10(7):501.
10. Smedley RC, Lamoureux J, Sledge DG, Kiupel M. Immunohistochemical diagnosis of canine oral amelanotic melanocytic neoplasms. *Vet Pathol.* 2011 Jan;48(1):32-40.
11. Stevenson VB, Perry SN, Todd M, Huckle WR, LeRoith T. PD-1, PD-L1, and PD-L2 Gene Expression and Tumor Infiltrating Lymphocytes in Canine Melanoma. *Vet Pathol*. 2021 Jul;58(4):692-698.
12. Thomas NE, Kricker A, Waxweiler WT, et al. Comparison of Clinicopathologic Features and Survival of Histopathologically Amelanotic and Pigmented Melanomas: A Population-Based Study. *JAMA Dermatol*. 2014;150(12):1306–1314.
13. Van der Weyden L, Brenn T, Patton EE, Wood GA, Adams DJ. Spontaneously occurring melanoma in animals and their relevance to human melanoma. *J Pathol*. 2020;252(1):4-21.
14. Zerfas PM, Brinster LR, Starost MF, Burkholder TH, Raffeld M, Eckhaus MA. Amelanotic melanoma in a New Zealand White Rabbit (Oryctolagus cuniculus). *Vet Pathol*. 2010 Sep;47(5):977-81.

Joint Pathology Center
Veterinary Pathology Services

WEDNESDAY SLIDE CONFERENCE 2024-2025

Conference #4 04 September 2024

CASE I:

Signalment:
4.5 month old, 27 kg neutered male pig (*Sus scrofa domesticus*).

History:
This pig arrived from a facility that had an outbreak of *Staphylococcus hyicus*, with several animals arriving with small lesions on the pinna, or developing lesions after arrival. Lesions progressed the longer the animals were housed in our facility.

Gross Pathology:
There is multifocal, regionally extensive erosion, erythema, and crusting affecting the head, pinna, the lateral left leg, and the lateral rump. There is moderate exudation and hypotrichosis in affected areas, with mild lichenification and fissures in the most severely affected regions.

Laboratory Results:
Gram stains show numerous colonies of gram positive cocci and gram negative bacilli within crusts, and extending into follicles.

Microscopic Description:
Haired skin, pinna and unspecified site: Affecting approximately 90% of the section, there is marked parakeratotic hyperkeratosis, with multifocal intracorneal pustules composed of necrotic cellular debris, necrotic neutrophils, and often individual to colonies of 1

Figure 1-1. Haired skin, pig. There is multifocal to coalescing areas of erythema and crusting on the face, neck and pinna. (*Photo courtesy of:* Walter Reed Army Institute of Research, Department of Pathology, https://www.wrair.army.mil/)

um diameter basophilic cocci. There is multifocal elevation of the necrotic debris, forming a serocellular crust. There is multifocal ulceration, with necrosis of both the epidermis and subjacent dermis. Within the hyperplastic stratum corneum are also multifocal lakes of serum, transmigrating neutrophils, and degenerating and necrotic keratinocytes. Subjacent to the stratum corneum, there is marked acanthosis, with prominent intercellular and intracellular edema, and deep anastomosing rete ridges extending to the mid dermis. Follicles are multifocally dilated with luminal neutrophilic debris admixed with cocci adherent to the inner follicular epithelium. Within the dermis, there are perivascular to superficial histi

Figure 1-2. Haired skin, pig. There is multifocal to coalescing areas of erythema and crusting on the lateral left leg (left images) and lateral rump (images at right). (*Photo courtesy of:* Walter Reed Army Institute of Research, Department of Pathology, https://www.wrair.army.mil/)

ocytic and eosinophilic infiltrates, fewer lymphocytes and plasma cells, and mildly increased white space between bundles of collagen (edema). Multifocal lymphatics are ectatic, and apocrine glands are ectatic with attenuated epithelium.

Brown and Brenn stain: There are individual and colonies of gram positive cocci within the serocellular crusts, stratum corneum, and adherent to luminal follicular epithelium. There are also gram negative bacilli admixed with gram positive cocci.

Contributor's Morphologic Diagnosis:

1. Haired skin, multiple locations including ear: Epidermitis, exudative and proliferative, diffuse, severe, with intracorneal pustules, rare ulceration, mild chronic active superficial dermatitis, and intracorneal cocci, breed not specified, swine.
2. (Not submitted) Lymph nodes, multiple: No significant findings.

Contributor's Comment:

Exudative epidermitis, or "greasy-pig disease", primarily affects 5-35 day old piglets and is caused by *Staphylococcus hyicus*. The condition is also known as impetigo contagiosa suis, and seborrhea oleosa, and is occasionally caused by *Staphylococcus chromogenes* or *Staphylococcus sciuri*.[6] While this disease can have high morbidity and variable mortality, this is considered an important disease due to economic loss.[6] The bacterium is considered a commensal organism that survives on the skin and within hair follicles, most often not causing disease. However, with compromise to immune function from environmental stressors like overcrowding, transport, poor husbandry, an individual animal's susceptibility to this disease may increase.[8] If not strictly required, it is currently thought that damage to the epidermis from fighting, abrasions from housing, ectoparasitism, or concurrent vesicular disease allows entry of *S. hyicus* for colonization.[2]

The disease is classically categorized into three different presentations. In the acute form, lesions around the eyes, snout, chin, and ears appear rapidly, then spread to the medial aspect of the legs, thorax, abdomen, and coronets. As the stratum corneum of affected regions peels away, moist underlying epidermis and dermis are replaced by greasy, dark brown exudate. In the subacute form, the progression of disease is slower, resulting in thick, wrinkled skin that eventually shows a generalized furrowed appearance. The chronic form affects older piglets, with milder disease, usu-

Figure 1-3. Haired skin, pig. Two sections of haired skin are submitted for examination. At this magnification, there is mild diffuse hyperkeratosis and crusting which at the section of bottom, are often detached as a result of processing. (HE, 5X)

ally erythema and waxy brown crusts confined to the head and ears. Older piglets often survive the disease but may have stunted growth.[6]

The most important virulence factors identified to date include a number of exfoliative toxins, *ExhA*, *ExhB*, *ExhC*, *ExhD*, *SHETA*, and *SHETB*. The *Exh* family toxins digest desmoglein-1 in the epidermis, affecting the effectiveness of desmosomes.[6] There are also a number of fibronectin-binding proteins on the surface of the bacteria that allow for adhesion to fibronectin in collagen, fibrin, and heparan sulfate proteoglycans found in the skin. Once the bacteria are established in the dermis, the infection often spreads to hair follicles, causing suppurative dermatitis with sebaceous gland hyperplasia and increased secretion (i.e. the "greasy" aspect of the disease).[7]

Lesions usually progress to exudative dermatitis starting in the groin, axillae, caudal auricular, and traumatized areas. Haired areas are more often affected, but lesions may also arise on the tongue and oral mucosa.[2] While not specific for the disease, a number of histologic features would support the diagnosis, such as subcorneal vesicular to pustular dermatitis, purulent luminal folliculitis, variable acanthosis with elongated rete ridges, intracellular edema of the stratum spinosum, and orthokeratotic and parakeratotic crusts with lakes of serum, accumulations of neutrophils, debris, and colonies of gram-positive cocci.[6]

The virulence and antibiotic resistance of *S. hyicus* continues to change as a function of its environment. A comparison of isolates from Brazilian swine herds in the 1980's and 2012 highlights significant shifts of *ExhA* and *ExhB* expression, as well as different antibiotic resistance profiles.[7] As antimicrobial peptides are investigated to combat increasing antibiotic resistance to macrolides, B-lactams, tetracycline, sulfonamides, and streptomycin, some compounds such as lactoferricin (Lfcin)

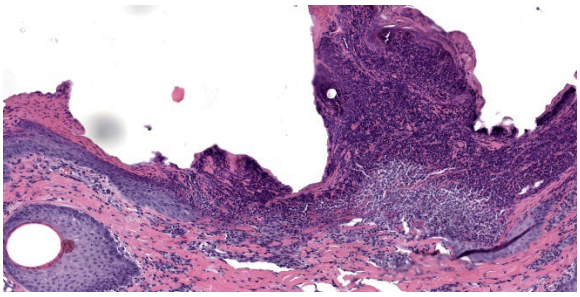

Figure 1-4. Haired skin, pig. Two sections of haired skin are submitted for examination. At this magnification, there is mild diffuse hyperkeratosis and crusting which at the section of bottom, are often detached as a result of processing. (HE, 5x)

have recently shown effectiveness in treating *S. hyicus* in a mouse model. Lfcin disrupts the bacterial cell wall and was effective in reducing both the bacterial load and levels of proinflammatory cytokines TNF-a, IL-6, and IL-1B.[4] Other biologics with efficacy have been recently investigated as well, such as the insect defensin DLP4 from *Hermetia illucens* (black soldier fly),[5] fungal defensin NZL from *Pseudoplectania nigrella*,[3] and *Siphoviridae*-like bacteriophages.[9]

Contributing Institution:
Walter Reed Army Institute of Research
Department of Pathology
https://www.wrair.army.mil/

JPC Diagnosis:
Haired skin: Epidermitis and folliculitis, suppurative, subacute, diffuse, severe, with multifocal ulceration, pustules, and intracorneal cocci.

JPC Comment:
The moderator for this week's conference was Major Kelsey Fiddes who serves as the Chief of Resident Training at the JPC. Each year, conference 4 is the annual rite of passage for our new first-year residents, presenting their first WSC case. This first case is a classic entity that we have covered in WSC before (Case 1, Conference 9, 2008-2009 and

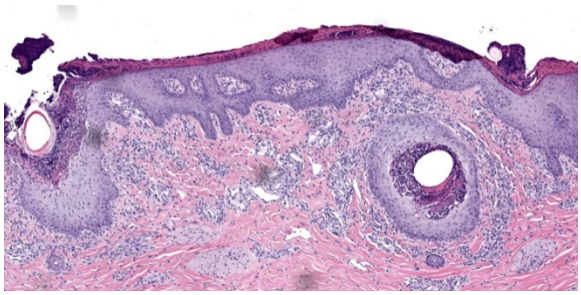

Figure 1-5. Haired, skin, pig. The hyperkeratosis and pustule formation extends down into the follicular ostia. (HE, 99X)

Case 3, Conference 8, 2009-2010) and the supplied section supplied is diagnostically rewarding.

As the contributor notes, the sebaceous gland hyperplasia elicited by *S. hyicus* may be the most visually obvious clue of this disease grossly, but there are several histologic features that should not be overlooked (Figures 1-4 and 1-5). In particular, the changes within the follicular infundibulum spanning the lumen and wall led us to include folliculitis with our morphologic diagnosis. In addition, the morphologic diagnosis focuses on epidermal changes, as the underlying dermis lacks significant changes. Gram stains (not particularly necessary in this case) highlight cocci within the serocellular crusts, stratum corneum, and adherent to luminal follicular epithelium similar to what the contributor reports.

As the contributor summarizes, the exfoliative toxins of *S. hyicus* play an important role in the pathogenesis of this disease. Other staphylococci such as *S. aureus* also produce serine protease exfoliative toxins;[1] these have been associated with human cases of bullous impetigo and staphylococcal "scalded skin syndrome"[6] which bear some similarity to exudative epidermitis of pigs. Microscopic lesions may be seen in other tissues due to exfoliative toxins. Renal lesions, including degeneration and/or exfoliation of the tubular epithelium, are a common sequela and do not require concurrent bacteremia. In cases of bacteremia, purulent pyelonephritis is a common finding[6] though it should be distinguished from other potential causes (e.g. *Actinobacillus)* that have a different pathogenesis.

References:

1. Bukowski M, Wladyka B, Dubin G. Exfoliative Toxins of Staphylococcus aureus. *Toxins*. 2010; 2(5):1148-1165.
2. Helke KL, Ezell PC, Duran-Struuck R, Swindle MM. Biology and Diseases of Swine. In: Fox JG, et al. eds. *Laboratory Animal Medicine*. 3rd ed. San Diego, CA: Elsevier. 2015:742-743.
3. Lui H, Yang N, Teng D, et al. Design and pharmacodynamics of recombinant fungus defensin NZL with improved activity against *Staphylococcus hyicus in vitro* and *in vivo*. *Int. J. Mol. Sci*. 2021; 22:5435.
4. Liu H, Yang N, Teng D, et al. Fatty acid modified-antimicrobial peptide analogues with potent antimicrobial activity and topical therapeutic efficacy against *Staphylococcus hyicus*. *Applied Microbiology and Biotechnology*. 2021; 105: 5845–5859.
5. Ma X, Yang N, Mao R, et al. The pharmacodynamics study of insect defensin DLP4 against toxigenic *Staphylococcus hyicus* ACCC 61734 *in vitro* and *vivo*. *Front Cell Infect Microbiol*. 2021; 11:638598.
6. Mauldin EA, Peters-Kennedy J. Integumentary System. In: Maxie MG, ed. *Jubb, Kennedy, and Palmer's Pathology of Domestic Animals*, Vol 3. 6th ed. Philadelphia, PA: Saunders Elsevier; 2016:630-632.
7. Moreno AM, Moreno LZ, Poor AP, et al. Antimicrobial resistance profile of *Staphylococcus hyicus* strains isolated from Brazilian swine herds. *Antibiotics*. 2022; 11(2):205.

8. Stanton JB, Zachary JF. Mechanisms of Microbial Infections. In: McGavin MD, Zachary JF, eds. *Pathologic Basis of Veterinary Disease*. 6th ed. St. Louis, MO: Elsevier; 2017:235.
9. Tetens J, Sprotte S, Thimm G, et al. First molecular characterization of *Siphoviridae*-like bacteriophages infecting *Staphylococcus h*yicus in a case of exudative epidermitis. *Front. Microbiol*. 2021; 12:653501.

CASE II:

Signalment:
Adult, female, file-eared tree frog (*Polypedates otilophus*)

History:
A captive, adult, female file-eared tree frog (*Polypedates otilophus*) was found dead.

Gross Pathology:
Approximately 70% of the left cornea and 80% of the right cornea contains white, multifocal to coalescing, irregularly marginated, and opaque material.

Figure 2-1. Eye, tree frog. Approximately 80% of the cornea is expanded by a dense opaque white material (lipid). (Wildlife Conservation Society, Zoological Health Program; https://oneworldonehealth.wcs.org, www.wcs.org)

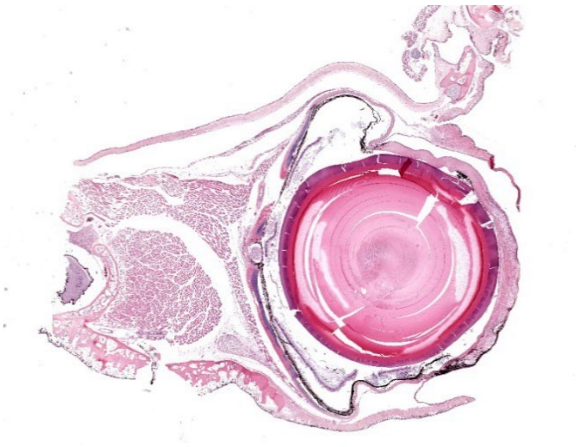

Figure 2-2. Eye, tree frog. One section of eye with attached lids is submitted for examination. At subgross magnification, the cornea is markedly expanded by clear space and at the ventral aspect, abundant pigment. (HE, 5X)

Microscopic Description:
Diffusely expanding the corneal stroma, extending to the limbus, and mildly elevating the overlying corneal epithelium are hundreds of coalescing, clear, acicular clefts (cholesterol clefts), interspersed with fewer individual lymphocytes and histiocytes. Histocytes are occasionally expanded by small to moderate amounts of intracytoplasmic finely vacuolated and clear material (lipid), with an eccentrically displaced nucleus. The corneal stroma occasionally contains small-caliber blood vessels (neovascularization) interspersed with inflammation and rare individual extravasated erythrocytes. The corneal epithelium is multifocally thickened up to 5 cells thick (epithelial hyperplasia), attenuated, and rarely absent. An adjacent nerve within the section is infiltrated by small numbers of scattered lymphocytes and rare individual histiocytes.

Contributor's Morphologic Diagnosis:
Eye, Keratitis, xanthomatous, chronic, diffuse, severe, with cholesterol clefts and neovascularization.

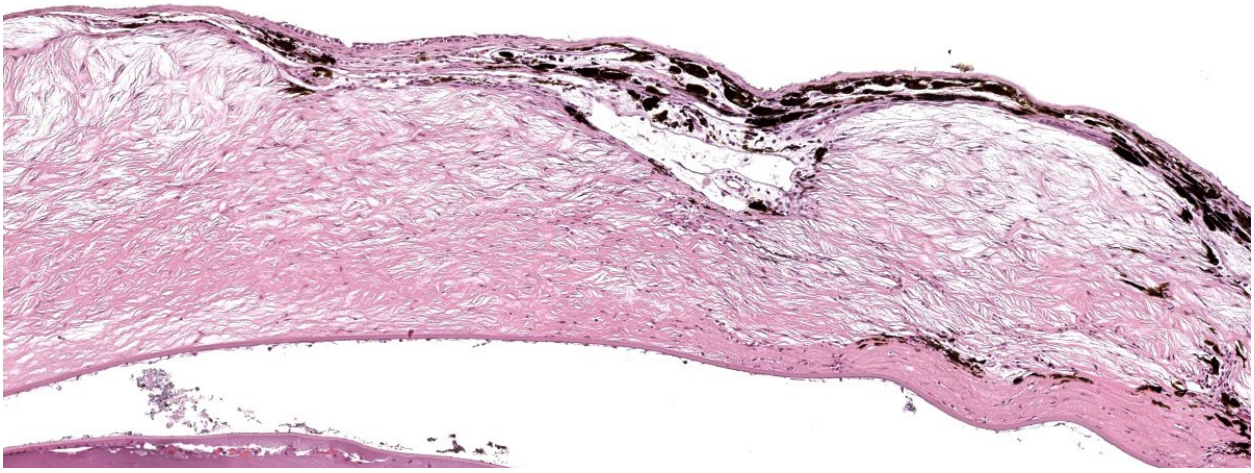

Figure 2-3. Eye, tree frog. The corneal stroma is expanded by innumerable clear acicular clefts (lipid). The overlying epithelium is infiltrated by large numbers of melanin-containing macrophages which occasionally infiltrate the underlying corneal stroma. (HE, 106X)

Contributor's Comment:
Bilateral corneal opacities noted at gross necropsy in this captive, adult, female file-eared tree frog (*Polypedates otilophus*) correlated to microscopic evidence of severe corneal lipid deposition. Given the species affected and the apparent absence of underlying ocular pathology, a diagnosis of lipid keratopathy was favored.

Corneal lipid deposition, also referred to as lipid keratopathy or corneal lipidosis, is a commonly encountered ocular disorder of captive amphibians.[2] While initially reported in Cuban tree frogs, lipid keratopathy has since been identified in multiple anuran species.[1,2,5,6] The disease presents clinically as a circumferential accumulation of white infiltrative material extending across the cornea over the course of weeks to months.[6] Lesions begin as small white foci at the corneal limbus and as disease advances can extend centrally to involve up to one-half of the corneal circumference.[5,6] Vision may become compromised in severe disease, affecting thermoregulation and ability to detect food.[8] In this case, the frog remained in good body condition, suggesting it was still able to find food despite the presence of corneal lesions.

Corneal lipid deposition is typically bilateral, and the corneal surface may become raised, thickened, and irregular from lipid deposition, grossly appearing as white plaques or nodules.[3,8,9] Early lesions are characterized histologically as small numbers of cholesterol clefts and foamy macrophages within the corneal stroma. As disease progresses, lipid accumulation can become associated with variable degrees of inflammation, neovascularization, and fibrosis.[4] Underlying ocular disease is typically not identified within affected cases.[6] Special stains including oil red O and Sudan black B can be used to highlight lipid within the corneal stroma.[6]

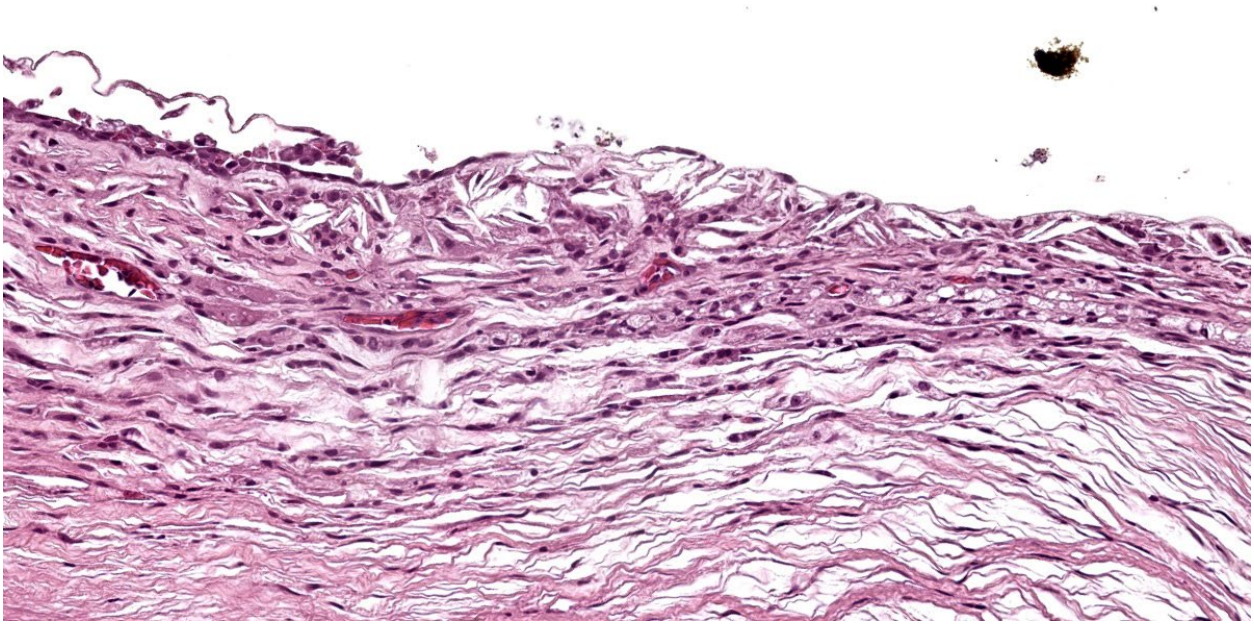

Figure 2-4. Eye, tree frog. In areas in which the corneal epithelium is ulcerated, there is vascularization of the underlying lipid-laden stroma with infiltration of low numbers of granulocytes. (HE, 240X)

The inciting cause for corneal lipid deposition in captive anurans is suspected to be nutritional and associated with variations in diet lipid composition. In one experimental study, corneal lipid deposition was found to be more prevalent in frogs fed high-cholesterol diets.[6] Furthermore, captive frogs fed both normal and high-cholesterol diets were found to have a higher serum total cholesterol than wild frogs, suggesting there may be an association with diets in captivity and disease development. Some reports also identify an increased prevalence of corneal lipid deposition in female anurans.[2,5]

In some species of amphibians, corneal lipid deposition has been reported in conjunction with disseminated xanthomatosis.[1] Xanthomas are non-neoplastic masses comprised of cholesterol and associated granulomatous inflammation, which form via extravasation of lipids.[10] Xanthomas have been reported in a wide range of taxa, can occur in multiple tissues, and can be associated with elevations in serum cholesterol.[5] Anurans diagnosed with xanthomatosis have been reported to have associated lesions involving the cornea, central nervous system, peripheral nerves, multiple visceral organs, and periarticular and digital soft tissues.[2,4] In this case, a xanthoma was identified in the choroid plexus.

Contributing Institution:
Wildlife Conservation Society, Zoological Health Program
https://oneworldonehealth.wcs.org
www.wcs.org

JPC Diagnosis:
Eye, cornea: Lipidosis, chronic, focally extensive, severe, with multifocal ulceration, vascularization, and pigmentation.

JPC Comment:
This second case is descriptively simple which admittedly is a rarity for many of the eyeballs we cover in conference. The numerous clear acicular clefts within the cornea is an obvious feature of this case which nicely correlate to the submitted gross image.. The migration of pigmented epithelial cells from the limbus is

both a response to ulceration and an adaptive response to chronic irritation. Conference participants looked carefully through this section, but found little else of note. Changes in other parts of the globe were largely ascribed to autolysis, although a focal area of hyperplasia of the retinal pigmented epithelium suggests an area of antemortem retinal detachment. Although hemorrhage was not a feature corneal neovascularization in this case, it has been documented in this entity in other frog species.[3]

Although lipid keratopathy is an important differential in this species, there are other differentials for corneal opacity (or 'white eye' in general) across species that merit brief discussion.[7] Corneal dystrophy may be acquired or inherited and reflects abnormal lipid metabolism of corneal endothelial cells, stromal, cells, or epithelial cells (keratocytes). Affected animals may not have an underlying serum lipid abnormality; this has been described in dogs (among others, beagles, Siberian huskies, and collies) and rabbits (New Zealand White). Familial hyperlipidemia as a cause of lipid deposition is well known in Schnauzers and Watanabe rabbits. Other potential rule outs include hypopyon, and rarely, anterior staphyloma. Finally, corneal granulation tissue and/or mineralization secondary to inflammation and hypercalcemia should also be considered.

References:

1. Carpenter JL, Bachrach A Jr, Albert DM, Vainisi SJ, Goldstein MA. Xanthomatous keratitis, disseminated xanthomatosis, and atherosclerosis in Cuban tree frogs. *Vet Pathol.* 1986; 23(3):337-339.
2. Holmberg BJ. Ophthalmology of exotic pets. In: Maggs DJ, Miller PE, Ofri R, eds. *Slatter's Fundamentals of Veterinary Ophthalmology.* 4th ed. St. Louis, MO, USA: Elsevier; 2008: 427-441.
3. Moore BA, Gjeltema J. Once in a blue moon: Lipid keratopathy and intrastromal hemorrhage in a Mission golden-eyed tree frog (Trachycephalus resinifictrix). *Vet Ophthalmol*. 2019 Nov;22(6):933-936.
4. Pessier AP. Amphibia. In: Terio KA, McAloose D, St. Leger J, eds. *Pathology of Wildlife and Zoo Animals*. 1st ed. London, UK: Elsevier; 2018:921-951.
5. Russell WC, Edwards DL, Stair EL, Hubner DC. Corneal lipidosis, disseminated xanthomatosis, and hypercholesterolemia in Cuban tree frogs (*Osteopilus septentrionalis*). *J Zoo Wildl Med*. 1990; 21(1):99-104.
6. Shilton CM, Smith DA, Crawshaw GJ, et al. Corneal lipid deposition in Cuban tree frogs (*Osteopilus septentrionalis*) and its relationship to serum lipids: an experimental study. *J Zoo Wildl Med*. 2001; 32(3):305-319.
7. Wilcock BP, Njaa BL. Special Senses. In: Maxie MG, ed. *Jubb, Kennedy & Palmer's Pathology of Domestic Animals*. Vol 1. 6th ed. St. Louis, MO: Elsevier; 2016:407-508.
8. Williams DL, Whitaker BR. The amphibian eye: a clinical review. *J Zoo Wildl Med*. 1994; 25(1):18-28.
9. Wright K. Cholesterol, corneal lipidosis, and xanthomatosis in amphibians. *Vet Clin North Am Exot Anim Pract*. 2003;6(1):155-67.
10. Zak A, Zeman M, Slaby A, Vecka M. Xanthomas: clinical and pathophysiological relations. *Biomed Pap Med Fac Univ Palacky Olomouc Czech Repub*. 2014; 158(2):181-188.

CASE III:

Signalment:

7-months-old, male, pit bull terrier, *Canis lupus familiaris*, canine.

Figure 3-1. Brainstem, dog. One section of brainstem at the level of the pons is submitted for examination. (HE, 5X)

History:
The dog was taken into the animal shelter as a stray. It was found dead in the kennel the next morning.

Gross Pathology:
The dog was in good body condition with mild postmortem decomposition. The lungs were congested, heavy, and wet. The liver and spleen were congested.

Laboratory Results:
The affected blood vessels in the brainstem contained intact and degenerate endothelial cells that were positive for canine adenovirus using immunohistochemistry.

Microscopic Description:
There are multifocal hemorrhages in the neuropil of the brainstem. The capillaries and venules are dilated. The affected capillaries and venules are often lined by swollen endothelial cells and karyorrhectic endothelial cells. Multifocally, there are intranuclear inclusion bodies in the vascular endothelial cells. In a few areas, the tunicae media of the blood vessels are expanded by brightly eosinophilic, homogenous to beaded material admixed with scattered pyknotic and karyorrhectic debris (fibrinoid necrosis) and infiltrated by lymphocytes, and macrophages(vasculitis).

Contributor's Morphologic Diagnosis:
Brainstem – Vasculitis with endothelial cell necrosis, intranuclear inclusion bodies in endothelial cells, and perivascular hemorrhage; etiology, canine adenovirus - 1

Contributor's Comment:
Infectious canine hepatitis (ICH) is an uncommon disease of dogs that is caused by canine adenovirus-1 (CAV-1).[2-7] CAV-1 is a non-enveloped, icosahedral, double-stranded DNA virus.[6,7] CAV-1 can infect and cause disease in domestic dogs, wild canids, skunks, and bears.[2-7] In domestic dogs, ICH is uncommon due to the routine vaccination of dogs, but ICH can be seen in unvaccinated dogs.[2-7] ICH is typically seen in young dogs less than 1 to 2-years-old, but any dog not vaccinated for canine adenovirus can develop ICH. CAV-1 is antigenically related to canine adenovirus-2, which causes respiratory disease in dogs.
CAV-1 is secreted in the saliva, urine, and feces of infected dogs.[2,-7] Transmission to a naïve dog is by oronasal exposure from dog-to-dog contact or from the contaminated environment. After oronasal exposure, CAV-1 infects the tonsils causing tonsillitis. The virus will then spread to the regional lymph nodes and then to the blood causing viremia 4 – 9 days after exposure, which corresponds to the incubation period of ICH. Viremia of CAV-1 results in dissemination to the hepatocytes, endothelial cells, and mesothelial cells. Disease caused by CAV-1 can be divided into three syndromes.[4,6,7] Peracute disease that occurs within a brief illness that ranges from 3 – 48 hours and is characterized by circulatory collapse and death. Acute ICH is characterized by fever, depression, anorexia, vomiting, diarrhea, petechiae on the mucus membranes, pale mucus membranes, and mild icterus. Acute ICH can be fatal. The last syndrome of ICH is a mild chronic disease where the infected dog has partially immunity and may recover or die weeks to months later due to chronic liver disease.

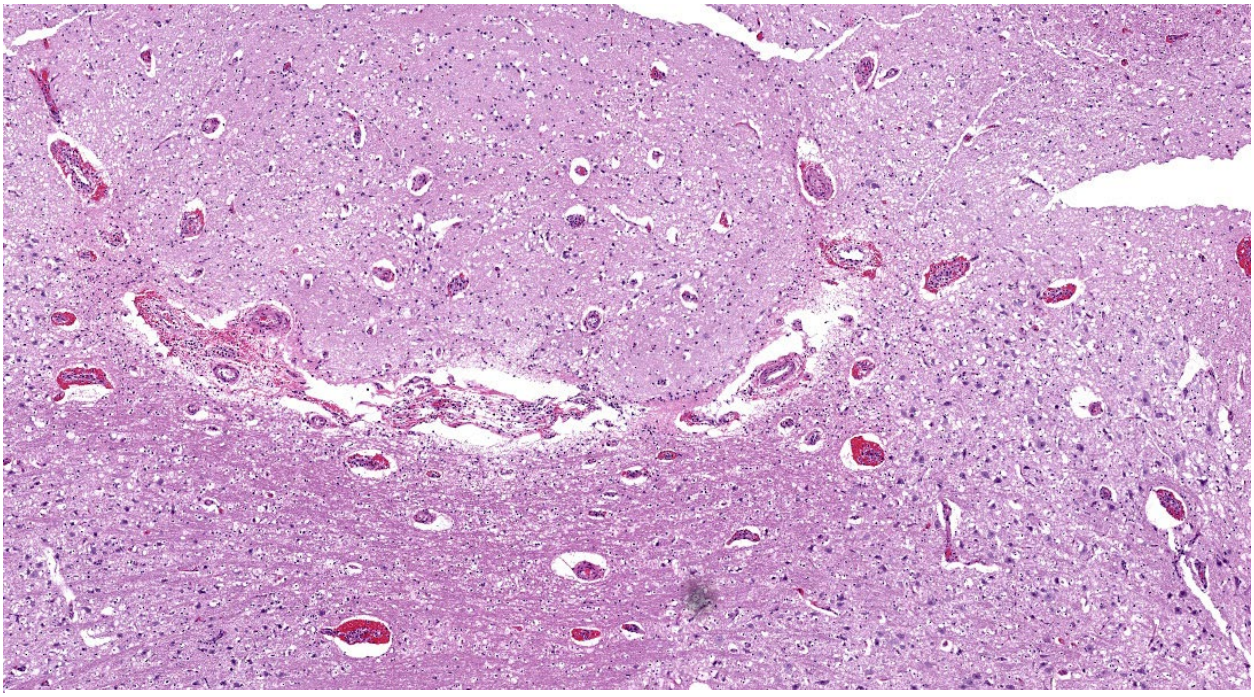

Figure 3-2. Brainstem, dog. Venules within the brainstem exhibit mural hemorrhage and extramural hemorrhage and edema. throughout the section. (HE, 44X)

CAV-1 infection of its target cells corresponds to the lesions seen grossly.[2-7] There can be enlargement and reddening of the tonsils and lymph nodes in the area. Petechiae on serosal surfaces and clear fluid in the peritoneal and surfaces can occur. The liver can be swollen, turgid, and friable with fine yellow mottling to a distinct accentuated reticular pattern. There can be fibrin on the surface of the liver. The gallbladder can be variably edematous, and gallbladder edema is considered to be pathognomonic of ICH. Icterus is mild when present. There can be hemorrhagic infarcts in the renal cortex as well as hemorrhages in the lungs. Hemorrhage and necrosis can occur at the metaphysis of long bones. The brainstem and midbrain can have hemorrhages in a small percentage of cases.[1-7] The late development of corneal edema due to a type III hypersensitivity reaction corresponding to increasing neutralizing antibodies can occur with ICH.[2,3,4,6,7]

The microscopic lesions of ICH in the liver are of centrilobular necrosis with intranuclear inclusion bodies in hepatocytes adjacent to the necrotic foci.[2-7] The necrotic foci contain small numbers of infiltrating leukocytes mainly neutrophils heterophils. The microscopic lesions in the other organs are the result of the endothelial cell injury secondary to infection with CAV-1. CAV-1 infection of endothelial cells in the renal glomeruli can cause glomerulonephritis, and infection of renal tubules cells can result in virus shedding in the urine. Pulmonary hemorrhages are secondary to vascular damage in the lung. Corneal edema is secondary to the immune response to CAV-1 infection of the corneal endothelium. When brain lesions due occur, there tend to occur in the brainstem and midbrain and consist of hemorrhages secondary to endothelial damage.[1,-7] Widespread endothelial damage can result in disseminated intravascular coagulopathy, which can also result in widespread

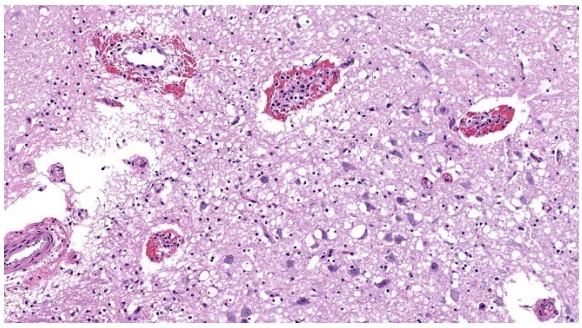

Figure 3-3. Brainstem, dog. Higher magnification of affected vessels. The extensive edema in the perivascular space has extended into the adjacent neuroparenchyma, resulting in spongiosis. (HE, 99X)

petechiae in serosal surface and multiple organs and death of the dog.[2-7]

Contributing Institution:
New Mexico Department of Agriculture Veterinary Diagnostic Services

https://nmdeptag.nmsu.edu/labs/veterinary-diagnostic-services.html

JPC Diagnosis:
Pons: Vasculitis, necrotizing, acute, diffuse, moderate, with rare neuronal necrosis, mild gliosis, and endothelial intranuclear viral inclusions.

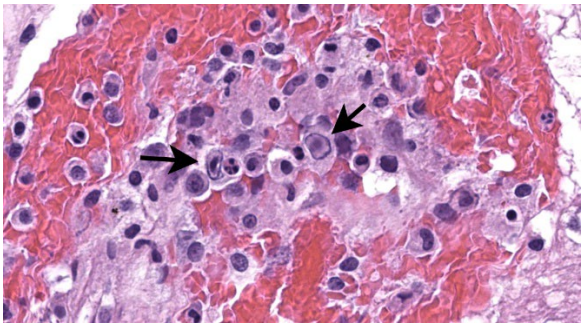

Figure 3-4. Brainstem, dog. Endothelial cells occasionally contain a large basophilic viral inclusion surrounded by a halo (arrow). (HE, 650X)

JPC Comment:
The contributor provides a succinct summary of CAV-1 and ICH. Connecting the dots to the present case, this section features diffuse vascular mural and transmural hemorrhage and edema attributable to endothelial intranuclear adenoviral inclusions. IHC for adenovirus performed by the contributor strongly and specifically labeled these endothelial cells, confirming the diagnosis. Conference participants felt that there was also microglial activation resulting from early parenchymal inflammation . These microglial cells were nicely highlighted by IBA1 (ionized calcium-binding adapter molecule 1) immunostain, which highlights dendritic cells, macrophages, and in the neuroparenchyma, microglia. Early characterization of this protein was performed in rat brain microglia.[9] In our experience, IBA1 has generally worked well across species and expression seems to be reasonably conserved.

Neurologic manifestation of CAV-1 is rare in domestic canines[1,5]; the animal in this case was reportedly a stray with an unknown vaccination history.

References:

1. Caudell D, Confer AW, Fulton RW, Better A, Saliki JT, Fent GM, Ritchey JR. Diagnosis of infectious canine hepatitis virus (CAV-1) in puppies with encephalopathy. *J Vet Diagn Invest*. 2005;17:58-61.
2. Cullen JM and Stalker MJ. Liver and biliary system. In: Maxie GM, ed. *Jubb Kennedy, and Palmer's Pathology of Domestic Animals*. 6th ed. vol 2. Elsevier; 2016.
3. De Jonge B, Van Brantegem L, Chiers K. Infectious canine hepatitis, not only in the textbook: a brief review and three case reports. *Vlaams Diergeneeskd Tijdschr*. 2020;89: 284-291.
4. Green CE. Infectious canine hepatitis and canine acidophil cell hepatitis. In: Greene CE, ed. *Infectious Diseases of the Dog and Cat*. 4th ed. Elsevier; 2012.

5. Hornsey SJ, Philibert H, Godson DL, Snead ECR. Canine adenovirus type 1 causing neurological signs in a 5-week-old puppy. *BMC Vet Res*. 2019 Nov 21;15(1):418.
6. Knowles DP. Adenoviridae. In: MacLachlan NJ and Dubovi EJ, eds. *Fenner's Veterinary Virology*. 4th ed. Elsevier; 2011.
7. Sykes JE. Infectious canine hepatitis. In: Sykes JE, ed. *Canine and Feline Infectious Diseases*. 1st ed. Elsevier; 2014.
8. Van Wettere AJ and Brown DL. Hepatobiliary system and exocrine pancreas. In: Zachary JF, ed. *Pathologic Basis of Veterinary Disease*. Elsevier; 2022.
9. Ito D, Imai Y, Ohsawa K, et al. Microglia-specific localisation of a novel calcium binding protein, Iba1. *Molecular Brain Research* 1998; 57(1): 1-9.

CASE IV:

Signalment:
8 years old, female, *Correlophus ciliatus* (formerly *Rhacodactylus ciliatus*), crested gecko

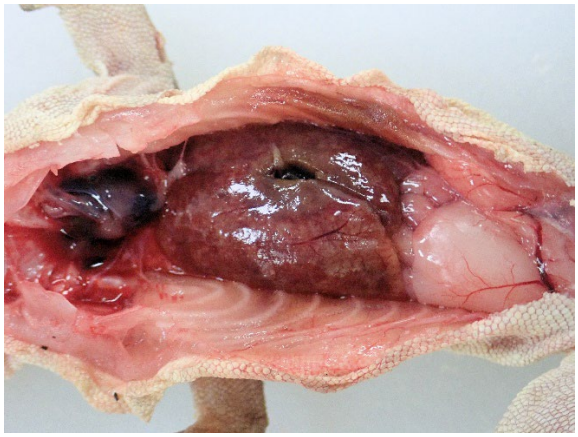

Figure 4-1. Liver, gecko. The liver was markedly enlarged, pale, firm and contained numerous coalescing variably sized tan foci (*Photo courtesy of:* New Mexico Department of Agriculture Veterinary Diagnostic Services, www.nmda.nmsu.edu/vds)

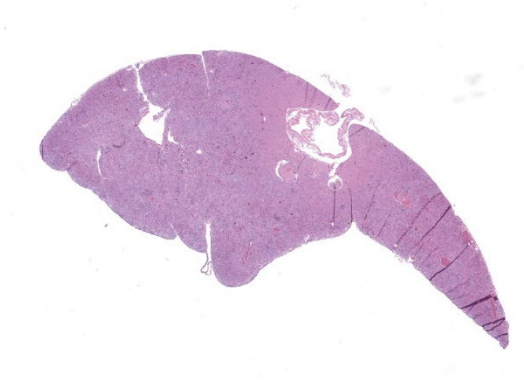

Figure 4-2. Liver, gecko. One section of liver is submitted for examination. (HE, 6X)

History:
The gecko was lethargic and sitting on the floor of the terrarium for prolonged periods instead of its normal climbing activity on the terrarium's vegetation. The owner noticed cutaneous ulcers on the gecko, which the owner treated topically. The gecko was found dead two days after clinical signs started.

Gross Pathology:
The carcass presented for postmortem examination was an 8 years old, 31.5 grams, female, crested gecko. The gecko was slightly underweight (normal weight of an adult female crested gecko is 35-55 grams) with moderate amounts of fat in the coelomic fat pads. The subcutis and organs were dry and tacky suggesting dehydration. The liver was markedly enlarged, pale, firm and contained numerous coalescing variably sized tan foci (Figure 1).

Microscopic Description:
The liver contained numerous small adult and larval rhabditid nematodes that were often surrounded by variably sized coalescing foci of necrosis admixed with macrophages, multinucleated giant cells, lymphocytes, and granulocytes. A few nematodes were fragmented and mineralized. The musculature of the nematodes was indistinguishable due to their small size. The nematodes had a rhabditiform esophagus with a corpus, isthmus and bulb (Figure

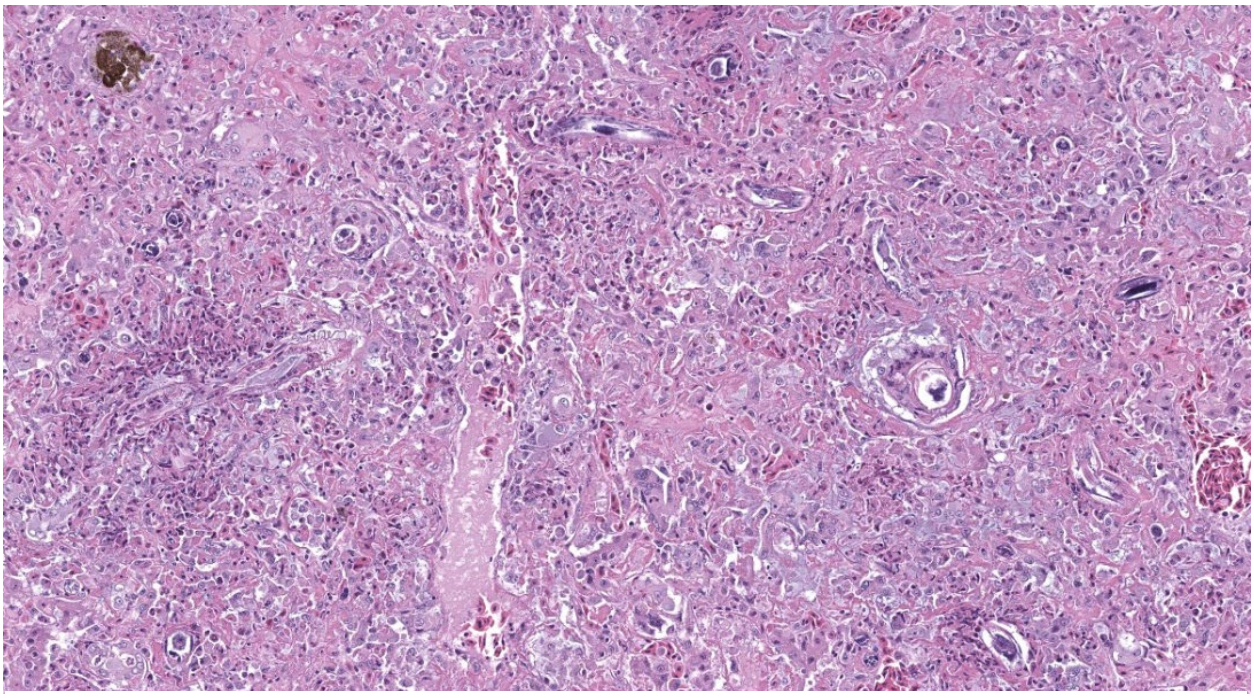

Figure 4-3. Liver, gecko. There is diffuse loss of normal plate architecture. Plate architecture is distorted by profound inflammation, moderate fibrosis, and numerous migrating rhabditoid adults, larvae, and rare eggs. (HE, 114X)

2). They had a single intestine and a paired genital tract (Figure 3). The genital tract contained large uninucleate ova as well as multinucleated ova (Figure 4). There were rare free multinucleated ova within the hepatic parenchyma (Figure 5). There was bile duct hyperplasia in the portal areas that were within the affected foci. The capsule was multifocally mineralized. In addition to the liver, rhabditid nematodes could be seen intravascular and within the parenchyma of the kidney (Figure 6), lung (Figure 7), brain (Figure 8), intestine, spleen, pancreas and ovary. These organs were not submitted.

Contributor's Morphologic Diagnosis:
Liver: Hepatitis, necrotizing, granulocytic and granulomatous, multifocal to coalescing with intralesional adult and larval rhabditid nematodes most consistent with *Strongyloides* species.

Contributor's Comment:
Endoparasitism is a frequent disorder of reptiles.[2,18] They are host to a large number of parasites including protozoa, trematodes, cestodes, nematodes, acanthocephalans, and pentastomes.[2,7,11,12,18] The most common two genera of rhabditiform nematodes to infect reptiles are *Rhabdias* and *Strongyloides* .[12,18] *Rhabdias* species are pulmonary parasites of anurans and reptiles.[1,12, 18] *Entomelas* species are rhabditid parasites of the lungs of some species of lizards.[18] *Strongyloides* are intestinal parasites of a large number of vertebrate species including mammals, birds, reptiles and amphibians.[1,12,14,16,17] *Rhabdias* species can be identified histopathologically by their intestine that has pigmented intestinal cells, vacuolated lateral chords, and females can have larvated ova in their paired uteri.[5] *Strongyloides* species also have a paired genital tract, do not have pigmented intestinal cells, and most species lay uninucleate ova that develop in the tissue or intestine.[5] The ova of

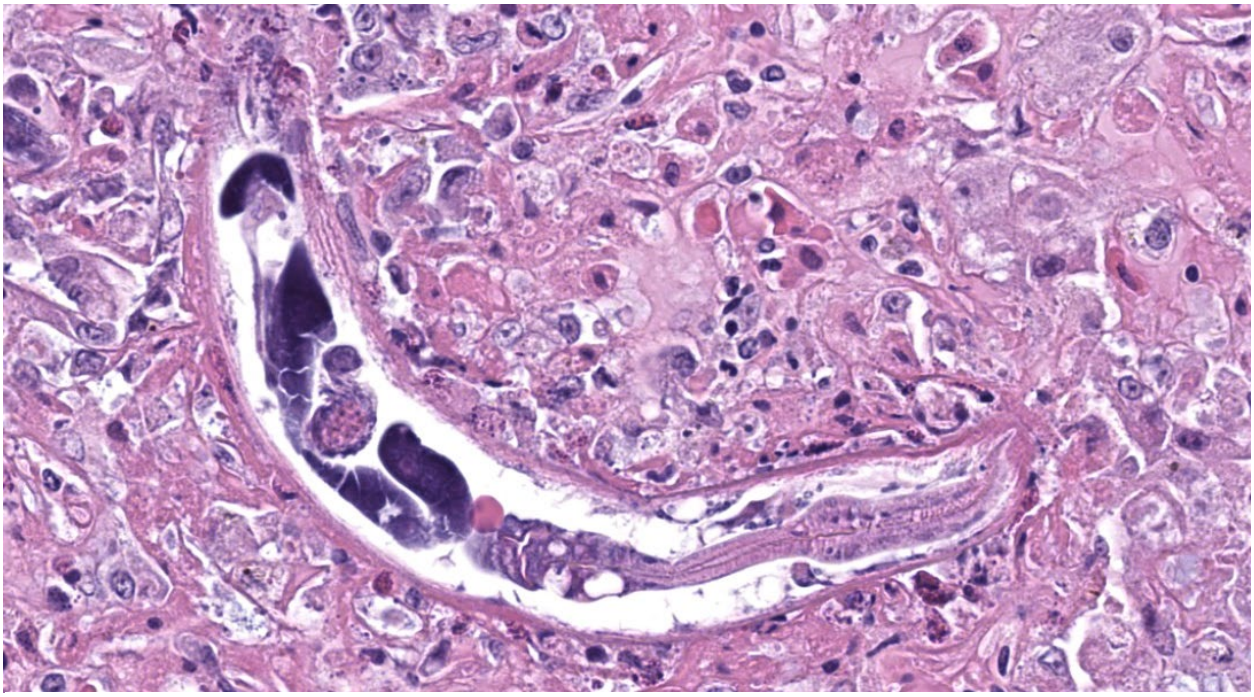

Figure 4-4. Liver, gecko. Tangential section of an adult rhabditoid nematode with esophagus with prominent corpus and bulb and a more distal triradiate esophagus and multiple sections of a deeply basophilic uterus. (HE, 572X)

Rhabdias species and *Strongyloides* species are embryonated in the feces of the host, and it is common to find free first stage rhabditiform larvae in the feces of infected hosts.[12,18] The embryonated ova and larvae of both species in the feces of the host are morphologically similar and difficult to impossible to distinguish from one another.[12,18]

As stated previously, *Rhabdias* species are lung parasites of anurans and reptiles.[1,9,12] The third stage larvae of *Rhabdias* species infect the host percutaneously or orally.[9] Oral infection mediated by eating infected prey is most likely important in reptiles with dry and scaly skin. After penetration into the connective tissue, the parasites molt into fourth stage larvae and enter the body cavity. The worms migrate to and enter the lungs as adult where they feed on the host's blood. The parasitic worms are female with some species reproducing by parthenogenesis or some species are hermaphrodites.[1] *Rhabdias* species ova can be laid by the female or the embryonated ova can develop within the body cavity of the female worm being release when she dies (matricidal endotoky). *Rhabdias* ova passed in the feces can develop by heterogony (first stage larvae molt twice to form third stage larvae of both sexes to become adults, mate and produce ova) or homogony (first stage larvae molt twice to become filariform third stage larvae that infect the host and mature into parthenogenetic females). Infected animals can exhibit respiratory distress, which can be severe.[12,18]

The intestinal parasite *Strongyloides* species can infect numerous vertebrate hosts.[1,14,16,17] The genus has been best studied in mammals. There appears to be some degree of host specificity with the different *Strongyloides* species, but some species like *S. stercoralis* can infect multiple mammalian species and have the potential to be zoonotic particularly between dogs and nonhuman primates and humans.[10,14] However, molecular techniques

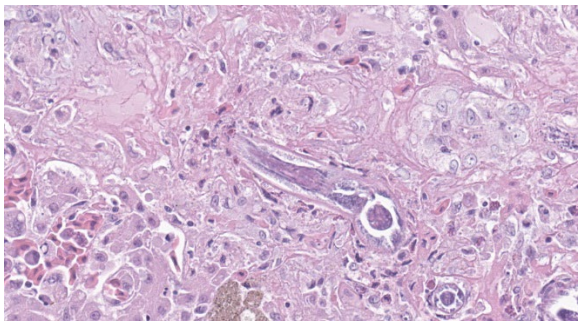

Figure 4-5. Liver, gecko. A single larva demonstrates the typical rhabditoid esophagus as well, with corpus, isthmus, and bulb. (HE, 600X) (*Photo courtesy of:* New Mexico Department of Agriculture Veterinary Diagnostic Services, www.nmda.nmsu.edu/vds)

have demonstrated that there are differences between the human and dog strains of *S. stercoralis* raising the question of whether the dog strains of *S. stercoralis* are truly zoonotic.[10,14]

The life cycle of *Strongyloides* species is similar to that of *Rhabdias* with one major difference; some *Strongyloides* species (particularly *S. stercoralis*, *S. fuelleborni*, and *S. fuelleborni kellyi* in humans) have the potential to autoinfect the host that can lead to infections that last decades.[8,10,13,15,16,17,19] The parasitic form of *Strongyloides* are parthenogenetic females. The female nematodes mostly live burrowed in the mucosa of the small intestine with some exceptions notably *S. tumefaciens* and occasionally *S. stercoralis* where the females live in nodules in the colon of cats.[14,19] The ova laid by the females embryonate in the mucosa and lumen of the small intestine and are passed in the feces as embryonated eggs or first stage rhabditiform larvae. The first stage rhabditiform larvae in the environment will molt twice to become third stage filariform larvae. The filariform larvae can then either penetrate the skin or mucosa of the mouth to infect the host or molt two more times to form adult free-living male and female worms. The adult free-living male and female worms can mate and their female offspring will molt to the infective filariform larvae to percutaneously or orally infect the host. Once inside the host, the filariform larvae can migrate to the small intestine or enter the vasculature where they migrate through the heart to the lungs. The filariform larvae in the lungs are coughed up and swallowed to reach the small intestine. When in the small intestine, the filariform larvae will mature into adult females. In autoinfection, the first stage rhabditiform larvae will molt twice in the large intestine to the infective third stage filariform larvae. The filariform larvae will penetrate the intestinal mucosa or perianal skin and migrate to the small intestine, which in some cases occurs through random organs. Humans and animals are initially exposed to infective filariform larvae of *Strongyloides* in a contaminated environment particularly in endemic areas.[17] The environment (water, foodstuffs, soil, and unwashed body parts) is contaminated by feces from an infected human or animal.[17] In addition, insects can mechanically carry ova of *Strongyloides*.[17]

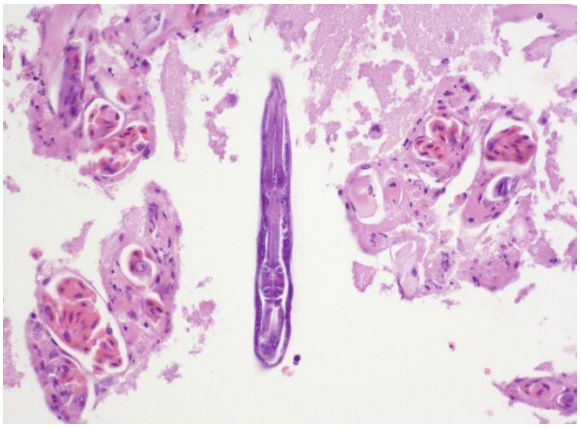

Figure 4-6. Liver, gecko. A single isolated larva demonstrates the typical rhabditoid esophagus as well, with corpus, isthmus, and bulb. (HE, 600X) (*Photo courtesy of:* New Mexico Department of Agriculture Veterinary Diagnostic Services, www.nmda.nmsu.edu/vds)

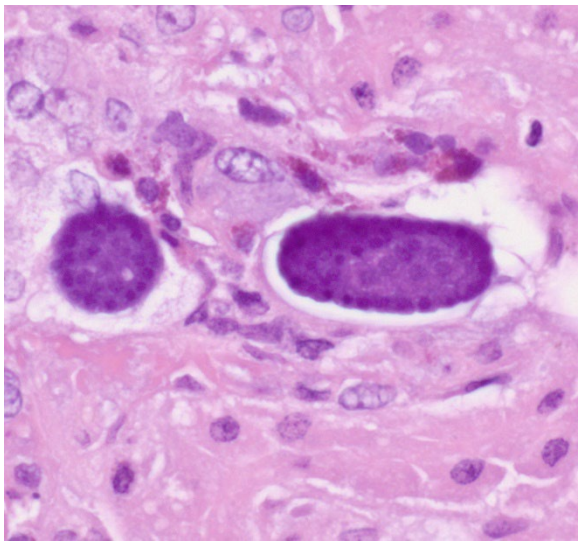

Figure 4-7. Liver, gecko. There are rhabditid eggs free within the parenchyma. (HE, 600X) (*Photo courtesy of:* New Mexico Department of Agriculture Veterinary Diagnostic Services, www.nmda.nmsu.edu/vds)

Clinical disease caused by *Strongyloides* species is typically mild and self-limiting.[13,14,15,16,19] It usually consists of diarrhea and respiratory disease that is most prevalent in individuals when they are initially exposed to the parasites. Naïve individuals exposed to infective filariform larvae can also develop dermatitis due to the parasites migrating through the skin. In domestic animals, disease caused by *Strongyloides* typically occurs in neonatal animals. In reptiles, particularly snakes, disease caused by *Strongyloides* can manifest as diarrhea, anorexia, weight loss and lethargy.[12,18] There are, however, cases of severe disease caused by *Strongyloides* species that have been described in humans and rarely dogs.[3,4,7,8,13,15,16] Severe disease caused by *Strongyloides* has been divided into two syndromes termed hyperinfection syndrome and disseminated disease, but some consider the syndromes to be the same.[8,13,15,16] Hyperinfection syndrome can occur in any infected individual, but is most often seen in immunocompromised individuals. Disseminated disease occurs in immunocompromised individuals. Both of these syndromes are often fatal. Hyperinfection syndrome is defined as a severe infection with *Strongyloides* nematodes in the normal locations of the parasites: the skin, the intestine, and the lungs. The time of completion of the life cycle of *Strongyloides* in hyperinfections is shortened. Disseminated strongyloidiasis occurs when *Strongyloides* parasites are found in organs outside of the normal life cycle (i.e., organs other than the skin, intestine or lungs). The gecko in this case most likely had disseminated strongyloidiasis.

Contributing Institution:
New Mexico Department of Agriculture Veterinary Diagnostic Services

www.nmda.nmsu.edu/vds

JPC Diagnosis:
Liver: Hepatitis, necrotizing and granulomatous, chronic, diffuse, marked, with intraparenchymal rhabditoid adults, larvae, and eggs.

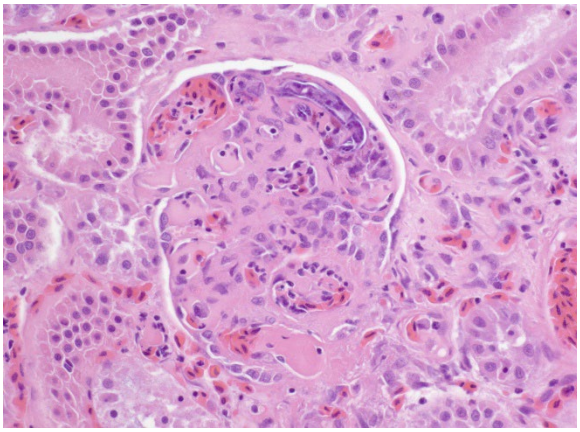

Figure 4-8. Kidney, gecko. A rhabditid larva is present within a renal glomerulus. (HE, 600X) (*Photo courtesy of:* New Mexico Department of Agriculture Veterinary Diagnostic Services, www.nmda.nmsu.edu/vds)

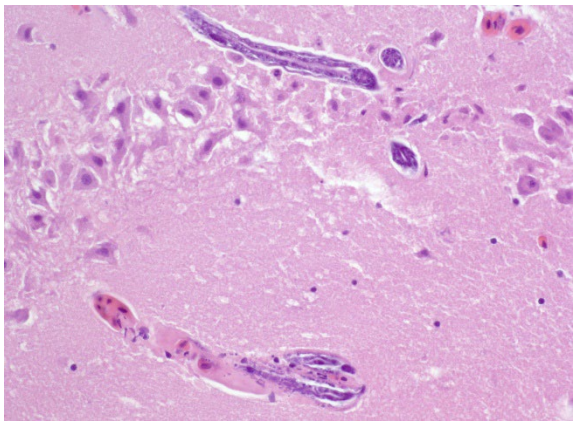

Figure 4-9. Brain, gecko. Rhabditid larva are present within the neuroparenchyma. (HE, 600X) (*Photo courtesy of:* New Mexico Department of Agriculture Veterinary Diagnostic Services, www.nmda.nmsu.edu/vds)

JPC Comment:

This conference concludes with a wonderful parasite case. We previously showed this slide to Dr. Chris Gardiner who confirmed the features of this nematode in histologic section and remarked that he had never seen a case like this one in over 50 years as a parasitologist! The presence of *Strongyloides* within the liver is unusual as they are typically encountered within the epithelial layer of the enteron, or less commonly, within the mucosa of the urinary bladder or the skin and lungs as the contributor notes.

Conference participants were able to appreciate most of the major features of adult and larval rhabditid nematodes. Careful examination of the slide is required to identify the few eggs scattered within the parenchyma.

Finally, we commend the contributor for their exhaustive discussion of *Strongyloides*. We have little to add on save for mentioning a recent *Veterinary Pathology* article concerning proliferative strongyloidiasis in a colony of colubrid snakes.[6] The histologic features of *Strongyloides* in these snakes was similar to the conference case, aberrant migration to the reproductive, respiratory and upper alimentary tracts, as well as the eye.[6] These findings in this paper highlight the utility of speciating the *Strongyloides* via molecular techniques to characterize novel species in the face of unexpected tissue distribution.

References:

1. Anderson RC. Nematode transmission patterns. *J Parasitol*. 1988;74(1):30-45.
2. Benson KG. Reptilian gastrointestinal diseases. *Semin Avian Exot Pet Med*. 1999;8(2):90-91.
3. Cervone M, Giannelli A, Otranto D, Perrucci. *Strongyloides stercoralis* hyperinfection in an immunosuppressed dog from France. *Revue Vétérinaire Clinique*. 2016;51(2):55-59.
4. Dillard KJ, Saari SAM, Marjukka A. *Strongyloides stercoralis* infection in a Finnish kennel. *Acta Vet Scand*. 2007;49,37.
5. Gardiner CH, Poynton SL. Rhabditoids. In: *An Atlas of Metazoan Parasites in Animal Tissues*. Armed Forces Institute of Pathology; 2006.
6. Graham EA, Los Kamp EW, Thompson NM, et al. Proliferative strongyloidiasis in a colony of colubrid snakes. *Veterinary Pathology.* 2024;61(1):109-118.
7. Graham JA, Sato M, Moore AR, *et al*. Disseminated *Strongyloids stercoralis* infection in a dog following long-term treatment with budesonide. *J Am Vet Med Assoc*. 2015;254(8):974-978.
8. Ippen R, Zwart P. Infectious and parasitic diseases of captive reptiles and amphibians with special emphasis on husbandry practices which prevent or promote diseases. *Rev Sci Tech Off Int Epiz*. 1996;15(1):43-54.
9. Kassalik M, Mönkemüller K. *Strongyloides stercoralis* hyperinfection syndrome and disseminated disease. *Gastroenterol Hepatol*. 2011;7(11): 766-768.

10. Langford GJ, Janovy Jr. J. Comparative life cycles and life histories of North American *Rhabdias* spp. (Nematoda: Rhabdiasidae): lungworms from snakes and anurans. *J Parasitol*. 2009;95(5):1145-1155.
11. Page W, Judd JA, Bradbury RS. The unique life cycle of *Strongyloides stercoralis* and implications for public health action. *Trop Med Infect Dis*. 2018; 3(2), 53;
12. Ratai AV, Lindtner-Knific R, Vlahović K, *et al*. Parasites in pet reptiles. *Acta Vet Scand*. 2011;53,33.
13. Šlapeta J, Modrý D, Johnson R. Reptile parasitology in health and disease. In: Doneley B, Monks D, Johnson R, Carmel B, eds. *Reptile Medicine and Surgery in Clinical Practice*. 1st ed. John Wiley & Sons Ltd.; 2018.
14. Tefé-Silva C, Machado ER, Faccioli LH, Ramos SG. Hyperinfection syndrome in strongyloidiasis. In: Rodriquez-Morales AJ, ed. *Current Topics in Tropical Medicine*. InTech; 2019.
15. Thamsborg SM, Ketzis J, Horii Y, Matthews JB. *Strongyloides* spp. infections of veterinary importance. *Parasitol*. 2017;144:274-284.
16. Vasquez-Rios G, Pineda-Reyes R, Pineda-Reyes J, *et al*. *Strongyloides stercoralis* hyperinfection syndrome: a deeper understanding of a neglected disease. *J Parasit Dis*. 2019;43(2):167-175.
17. Viney ME, Lok JB. *Strongyloides* spp. In: *WormBook*. 1-15; doi:10.1895/wormbook.1.141.1.
18. White MAF, Whiley H, Ross KE. A review of *Strongyloides* spp. environmental sources worldwide. *Pathogens*. 2019;8,91; doi:10.3390/pathogens803009.
19. Wilson SC, Carpenter JW. Endoparasitic diseases of reptiles. *Semin Avian Exot Pet Med*. 1996;5(2):64-74.
20. Wulcan JM, Dennis MM, Ketzis JK, *et al*. *Strongyloides* spp. in cats: a review of the literature and the first report of zoonotic *Strongyloides stercoralis* in colonic epithelial nodular hyperplasia in cats. *Parasit Vectors*. 2019;12,349.

Joint Pathology Center
Veterinary Pathology Services

WEDNESDAY SLIDE CONFERENCE 2024-2025

Conference #5 — 11 September 2024

CASE I:

Signalment:
Six years-old male common woolly monkey (*Lagothrix lagotricha*).

History:
The animal was housed at the BH-ZOO (Belo Horizonte, Brazil) and developed acute lethargy, with hypoglycemia, apathy, and hypothermia. Ultrasound examination demonstrated abundant fluid in the abdominal cavity. The animal was treated with therapeutic dos-es of ceftriaxone, dexamethasone, and mor-phine, but did not respond to treatment and died two days later.

Gross Pathology:
There was abundant yellow fibrinous exudate in the peritoneal cavity, with multifocal to coalescent hemorrhage on the serosa. Gastric and intestinal serosae had multiple red, firms, nodules ranging from 0.1 to 0.2 cm in diameter. The gastric mucosa had multifocal ulcerations with approximately 0.2 cm in diameter. There were multiple areas of fibrinous adhesion between intestinal loops, associated with a necrotic area in the jejunum. The intestinal mucosa had moderate multifocal hemorrhage. There were also multifocal hemorrhages on the mucosa of the urinary bladder. Thoracic cavity and pericardial sac had moderate amounts of translucent fluid with a small amount of fibrin. The lungs had a smooth shiny red surface, with atelectasis in left and right cranial lobes.

Figure 1-1. Abdominal viscera, woolly monkey. There is abundant yellow fibrinous exudate in the peritoneal cavity, with multifocal to coalescent hemorrhage on the serosa, (*Photo courtesy of:* Departamento de Clínica e Cirurgia Veterinária, Escola de Veterinária, Universidade Federal de Minas Gerais, Av. Presidente Antônio Carlos, 6627 – CEP 30161-970, Belo Horizonte, MG, Brazil. www.vet.ufmg.br)

Laboratory Results:
Swabs of peritoneal cavity were plated on Muller-Hinton agar (Difco, USA) supplemented with 5% equine blood, mannitol salt agar (Kasvi, Brazil), and MacConkey agar (Kasvi, Brazil), followed by aerobic incubation at 37ºC for 48 h. Colonies were subjected to matrix-assisted laser desorp-tion/ionization time-of-flight (MALDI-TOF, Bruker Daltonics) mass spectrometry with results compatible with E. coli. The E. coli isolate was positive for several virulence fac-tors encoding genes: fimH, focG, papC, papG, sfaS, cnf1, usp, hlyA, iutA, and traT. No other bacteria were isolated.

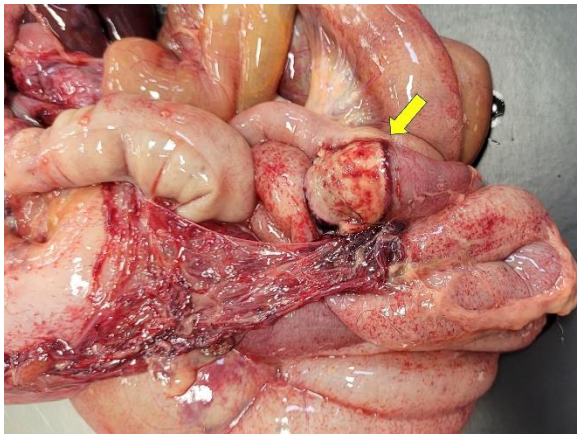

Figure 1-2. Abdominal viscera, woolly monkey. There are multiple areas of fibrinous adhesion between intestinal loops, associated with a necrotic area in the jejunum (*Photo courtesy of:* Departamento de Clínica e Cirurgia Veterinária, Escola de Veterinária, Universidade Federal de Minas Gerais, Av. Presidente Antônio Carlos, 6627 – CEP 30161-970, Belo Horizonte, MG, Brazil. www.vet.ufmg.br)

Samples of liver and spleen tested negative for yellow fever virus and dengue virus infections by RT-qPCR.

Microscopic Description:

Large intestine: submucosa was expanded with small to medium sized arteries exhibiting variable degrees of inflammation, characterized by infiltration of the tunica adventitia and media with small to moderate numbers of lymphocytes, histiocytes, neutrophils, and some plasma cells. Some of the affected vessels had proliferation of fusi-form cells with a small amount of extracellular mucinous matrix within the intima and marked accumulation of collagen in the tunica media and adventitia. Picrosirius red stained sections examined under polarized light demonstrated predominantly reddish birefringent mature type I collagen. Macrophages rich in intracytoplasmic brown pigment (suggestive of hemosiderin) were observed adjacent some of these vessels. In some sections there was marked arterial fibrinoid necrosis affecting the tunica media, often associated with thrombosis. Distribution of arterial lesions was random and segmental. The muscular layer adjacent to the areas of vascular lesion had moderate myocyte hypotrophy. Serosa had a diffuse and moderate inflammatory infiltrate, composed mainly by neutrophils, and the mesothelial cells were diffusely hypertrophic with deposition of moderate amount of fibrin at the serosa associated with neutrophils and histiocytes (peritonitis). Additionally, it was observed a moderate focally extensive area of hemorrhage at the mucosa.

Testis: similar vascular changes were observed in the testis. In addition, seminiferous tubules were marked degenerate with vacuolated Sertoli cells, thickened basal membrane and some sclerotic tubules. Diffusely, there was moderate interstitial infiltrate composed mainly by lymphocytes, histiocytes and plasma cells.

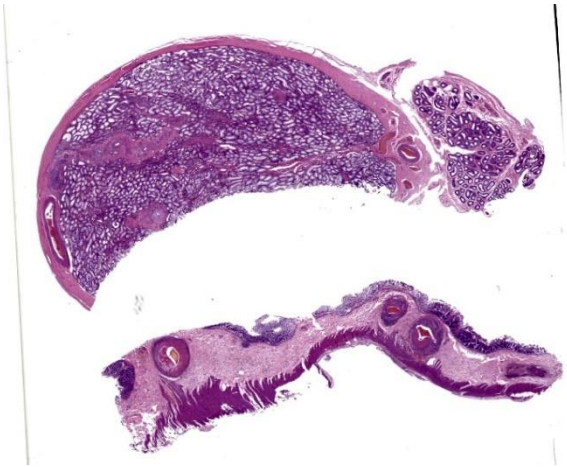

Figure 1-3. Testis and colon, woolly monkey. One section of testis (top) and colon (bottom) are submitted for examination. At this magnification, enlarged arterioles are visible within the submucosa. (HE, 6X)

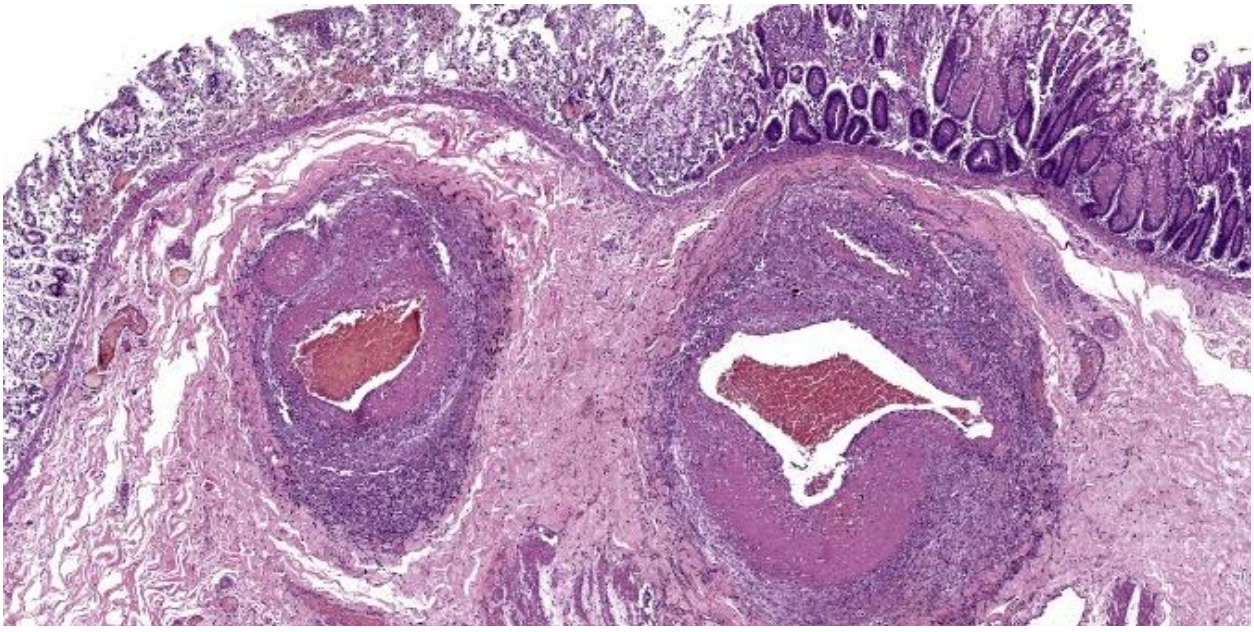

Figure 1-4. Colon, woolly monkey. The mural architecture of colonic submucosal arterials is effaced by abundant eosinophilic protein, loss of smooth muscle, and marked adventitial inflammation. (HE, 43X)

Vascular lesions were observed also at the kidneys, small intestines and stomach. At the small intestine, vascular lesions were associated with multiple focally extensive areas of transmural necrosis. Other lesions included diffuse fibrinous peritonitis, characterized by large amounts of eosinophilic fibrinous exudate with numerous neutrophils, Gram-positive and Gram-negative coccobacilli, and a few vegetal fibers. Mild pulmonary edema was also noted.

Contributor's Morphologic Diagnoses:
Large intestine: arteritis, necrotizing and proliferative, diffuse, severe with fibrinoid necrosis, thrombosis, and fibrinous peritonitis.

Testis: 1) arteritis, necrotizing and proliferative, diffuse, severe with fibrinoid necrosis and thrombosis. 2) orchitis, lymphoplasmacytic, diffuse, moderate with tubular degeneration, diffuse, moderate.

Contributor's Comment:
Vascular lesions in this common woolly monkey were consistent with polyarteritis nodosa (PAN) affecting small to medium sized arteries in the kidney, testis, stomach, small, and large intestines. This is the first reported case of PAN in this neotropical primate species. PAN is a progressive, degenerative, inflammatory, and necrotizing disease that most commonly affects small to large arteries of the mesentery, pancreas, kidney, testis, intes-tine, and heart, as described in humans,[6,14] cynomolgus macaques, rhesus monkey, owl monkey, and pigs.[2,8,9,16] The diverse types of vascular lesions suggest that the damage is polyphasic, i.e. it occurs intermittently.[6] Alt-hough the pathogenesis of PAN is not com-pletely clear, it is considered a type III hyper-sensitivity reaction caused by deposition of antigen/antibody complexes in small arteries followed by complement activation.[9]

PAN is a systemic necrotizing vasculitis, which affects predominantly medium size arteries. It has been described in humans, oc-

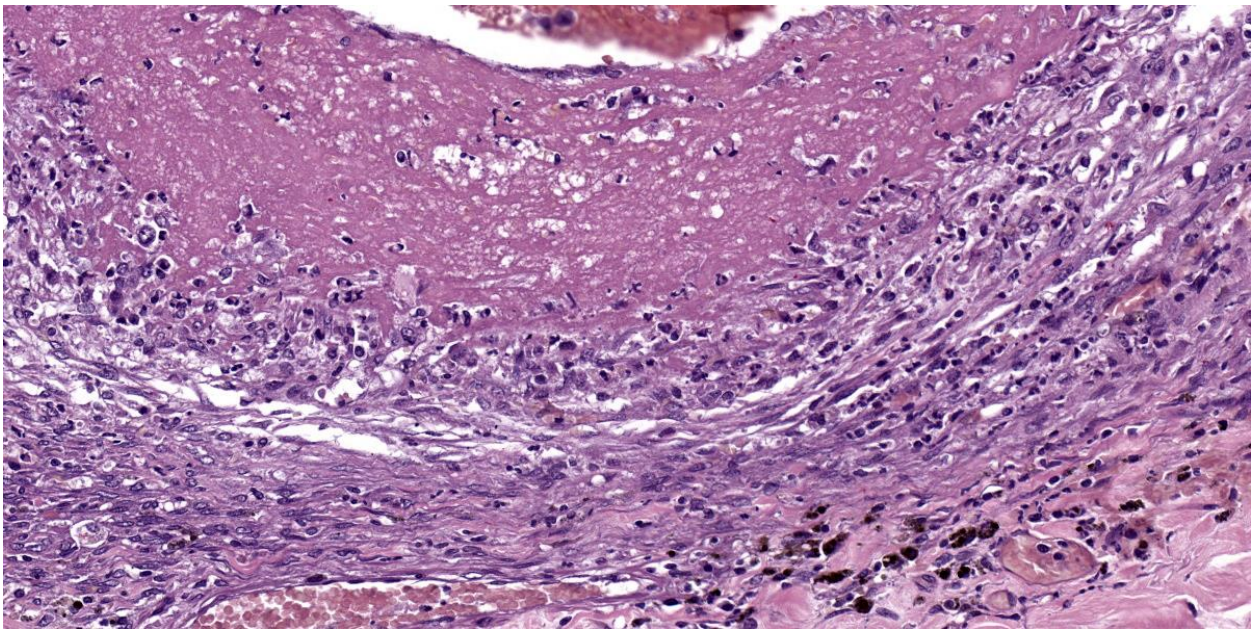

Figure 1-5. Colon, woolly monkey. The wall of an affected arteriole with the lumen at top. The media is markedly expanded by protein with necrosis and loss of smooth muscle, and marked inflammation, fibrosis, and proliferation of small vessels within the adventitia. The adjacent submucosa contains moderate numbers of siderophages. (HE, 334X)

curring more often in young adults. Small arteries may also be involved, but there is no involvement of smaller vessels, including arterioles, capillaries, and venules.[6] In animals, PAN has been reported in sheep,[15] dogs,[21] cats,[18] pigs,[12] and rats.[10] Among non-human primates, the disease has been described in cynomolgus monkey (*Macaca fasciculres*),[2,17] rhesus monkey (*Macaca mulatta*),[9] and owl monkey (*Aotus* sp.).[8]

In this case, PAN lesions were associated with transmural intestinal necrosis that resulted in peritonitis. PAN often results in narrowing of the vascular lumen due to vasculitis, with secondary gastrointestinal ulcerations or erosions due to ischemia.[1] Intestinal perforation or necrosis caused by PAN resulting in acute peritonitis has been reported in humans.[11]

Pathogenic *E. coli* was isolated from the peritoneal cavity in this case. *E. coli* is a major cause of extra-intestinal infections including meningitis, bacteremia, pyelonephritis, cystitis, prostatitis, metritis, and peritonitis.[7,20] However, it is also a member of the intestinal microbiota in mammals.[19] Extra-intestinal pathogenic *E. coli* and commensal *E. coli* typically differ in virulence factors.[7,20] In this case, the *E. coli* isolate was positive for several virulence factors encoding genes: *fimH, focG, papC, papG, sfaS, cnf1, usp, hlyA, iutA,* and *traT*.

In conclusion, this is a case of PAN associated with transmural intestinal necrosis and lethal septic peritonitis in a common woolly monkey, which has been recently published.[3] Therefore, PAN must be considered for the differential diagnosis of inflammatory, necrotizing and/or proliferative multi-systemic segmental arterial lesions in neotropical primates.

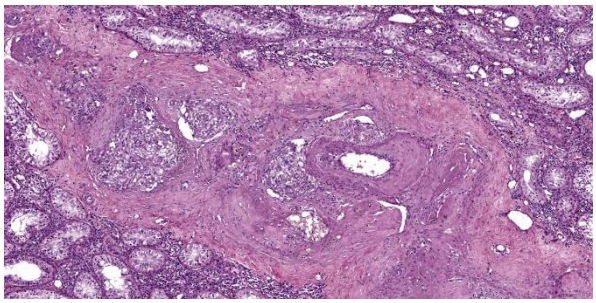

Figure 1-6. Testis, woolly monkey. Similar changes are present within the arterioles of the testis. There is atrophy of the seminiferous tubules and mild lympoplasmacytic orchitis. (HE, 75X)

Contributing Institution:
Departamento de Clínica e Cirurgia Veterinária, Escola de Veterinária, Universidade Federal de Minas Gerais, Av. Presidente Antônio Carlos, 6627 – CEP 30161-970, Belo Horizonte, MG, Brazil. www.vet.ufmg.br

JPC Diagnoses:
Colon and testis: Arteritis, proliferative, necrotizing, fibronous, chronic, multifocal, severe.

Testis: Orchitis, lymphoplasmacytic, chronic, multifocal, mild.

Colon: Serositis, fibrinous, subacute, diffuse, moderate.

JPC Comment:
This week's conference was moderated by Major Janas Gray, presently at the US Army Medical Research Institute of Chemical Defense (USAMRICD) in Aberdeen, Maryland. This first case is a terrific example of polyarteritis (periarteritis) nodosa (PAN). Alt-hough we have covered PAN in laboratory species before (most recently Conference 1, Case, 2018-2019 in a rat) we have also seen similar lesions in a cat (Conference 12, Case 4, 2022-2023), so this entity should be considered as a differential in any case of systemic necrotizing vasculitis. In particular, the sections of intestine and testis from this monkey feature robust infiltration of the adventitia and outer media by inflammatory cells (Figures 1-3 and 1-4).

This case is unusual in the degree of secondary changes present in which generated lengthy discussion. Conference participants largely agreed with the contributor's interpretation of the case but differed on how to best interpret the testis. Given that the arteritis was only multifocal, diffuse tubular changes were harder to support. In section, participants noted few spermatids within the epididymis as well as spermatogonia and spermatocytes within the seminiferous tubules, and coupled with the finding that this young in-dividual was entering the phase of sexual ma-turity reported in this species[15] led some participants to conclude that the testis was immature rather than senescent.

Another consideration for vascular lesions in the woolly monkey is idiopathic (essential) hypertension.[4,5] Microscopic features of this entity include hyaline arteriosclerosis with intramural deposition of amorphous, brightly eosinophilic material and hyperplastic arteriosclerosis with smooth muscle proliferation of the tunica intima and media. Small muscular arteries and arterioles are classically involved and the kidney is the principal organ, though changes in other arteries have been described. A recent case series looking at similar lesions in pygmy marmosets[4] identified a small number of non-renal, non cardio-pulmonary in the inner retina, stomach, spleen, and cerebrum. In the present case, the intact inner elastic lamina and lack of overt hyalinization are against this particular interpretation.

As a final aside for this case, PAN has been reported as a sequalae to human COVID-19 vaccination in line with the type III hypersensitivity reaction and resulting anti-gen/antibody complex pathogenesis the con-tributor lays out. Although PAN in humans has been

associated previously with hepatitis B vaccination, the production of viral protein through mRNA vaccines may inadvertently drive T-lymphocyte autoreactivity and resulting complement activation and cytokine cascade.[13]

References:

1. Agard C, Mouthon L, Mahr A, et al. Microscopic polyangiitis and polyarteritis nodosa: how and when do they start? *Arthritis Rheum*. 2003;49:709-715.
2. Albassam MA, Lillie LE, Smith GS. Asymptomatic polyarteritis in a cynomolgus monkey. *Lab Anim Sci.*1993;43:628-629.
3. Carvalho TP, Oliveira Santos D, Oliveira AR, et al. Polyarteritis nodosa in a captive common wooly monkey (*Lagothrix lagotricha*) associated with intestinal necrosis, peritonitis, and sepsis. *J Med Primatol*. 2023;52:197-200.
4. Cooley AJ, Savage A, Snowdon CT. Vascular, cardiac, and renal lesions attributed to primary systemic hypertension in western pygmy marmosets (*Cebuella pygmaea*). *Vet Pathol.* 2022; 59(2): 358-370.
5. Giddens WE, Combs CA, Smith OA, et al. Spontaneous hypertension and its sequelae in woolly monkeys (Lagothrix lagotricha). *Lab Anim Sci.* 1987;37(6):750–756.
6. Guillevin L. Polyarteritis nodosa and microscopic polyangiitis. In: Ball GV, ed. *Vasculitis.* Bridges; 2012:34-52.
7. Johnson JR, Stell AL. Extended virulence genotypes of *Escherichia coli* strains from patients with urosepsis in relation to phylogeny and host compromise. *J Infect Dis.* 2000;181:261-272.
8. Joint Pathology Center. Veterinary pathology service. In: Wednesday Slide Conference Proceedings. 2012- 2013; Conf 4, Case III, Accessed http://www.ask-jpc.org/wsco/wsc_show-case4.php?id=YzZnSjlnRzBk-TytDcE5QWm5EbUZCUT09 (Accessed 6 July 2022); 2012.
9. Joint Pathology Center. Veterinary pathology service. In: Wednesday Slide Conference Proceedings. 2016-2017; Conf 3, Case III http://www.ask-jpc.org/wsco/wsc_show-case4.php?id=SXgweHNQbEpUS2JU-UmhNcDlHelNYdz09 (Accessed 6 July 2022); 2016.
10. Lepherd ML, Schlafer DH, De Matos R, et al. Pathology in pratice. Polyarteritis nodosa. *J Am Vet Med Assoc.* 2013;243:1399-1401.
11. Levine SM, Hellmann DB, Stone JH. Gastrointestinal involvement in polyarteritis nodosa (1986-2000): presentation and outcomes in 24 patients. *Am J Med*. 2002;112:386-391.
12. Liu CH, Chiang YH, Chu RM, et al. High incidence of polyarteritis nodosa in the brains of culled sows. *J Vet Med Sci.* 2005;67:125-127.
13. Makiyama A, Abe Y, Furusawa H, Kogami M, Ando T, Tada K, Onimaru M, Ishizu A, Yamaji K, Tamura N. Polyarteritis nodosa diagnosed in a young male after COVID-19 vaccine: A case report. *Mod Rheumatol Case Rep*. 2023 Dec 29;8(1):125-132.
14. Mitchell RN, Halushka MK. Blood Vessels. Kumar V, Abbas AK, Fausto N, eds. In: *Robins and Cotran Pathologic Basis of Disease*. Elsevier, 2015;509-510.
15. Pereira T. H d. S., Mayor, P., Evangelista, J. S. A. M., Lima, A. K. F., de Andrade, R. d. S., & Monteiro, F. O. B. (2024). Reproductive physiology with emphasis on endometrial cycles of woolly and uakari monkeys—A literature review. *American Journal of Primatology*, 86, e23585.
16. Pesavento PA, Dange RB, Ferreras MC, et al. Systemic necrotizing vasculitis in sheep is associated with ovine herpesvirus 2. *Vet Pathol.* 2019;56:87-92.

17. Porter BF, Frost P, Hubbard GB. Polyarteritis nodosa in cynomolgus macaque (*Macaca fascicularis*). *Vet Pathol.* 2003;40:570-573.
18. Salvadori C, Vezzosi T, Marchetti V, et al. Polyarteritis nodosa in a cat with involvement of the central and peripheral nervous system. *J Comp Pathol.* 2019;167:6-11.
19. Selander RK, Levin BR. Genetic diversity and structure in *Escherichia coli* populations. *Science*. 1980;210:545-547.
20. Siqueira AK, Ribeiro MG, Leite DS, et al. Virulence factors in *Escherichia coli* strains isolated from urinary tract infection and pyometra cases and from feces of healthy dogs. *Res Vet Sci*. 2009;86:206-210.
21. Snyder PW, Kazacos EA, Scott-Moncrieff JC, et al. Pathologic Features of naturally occurring juvenile polyarteritis in beagle dog. *Vet Pathol.* 1995;32:337-345.

CASE II:

Signalment:
1-year-old, female Common Marmoset (*Callithrix jacchus*)

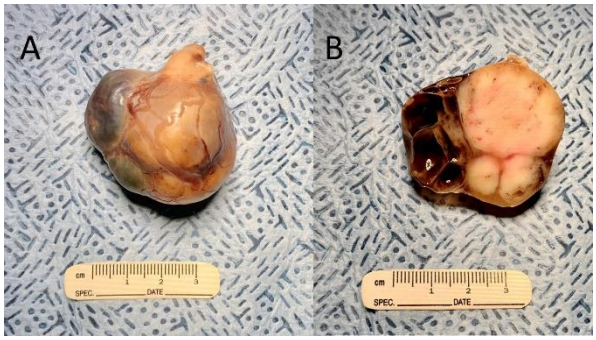

Figure 2-1. Kidney, common marmoset. A large white-tam multilobular mass is present within the kidney (intact left, cut section right) (*Photo courtesy of: Division of Laboratory Animal Resources, University of Pittsburgh. http://www.dlar.pitt.edu/)*

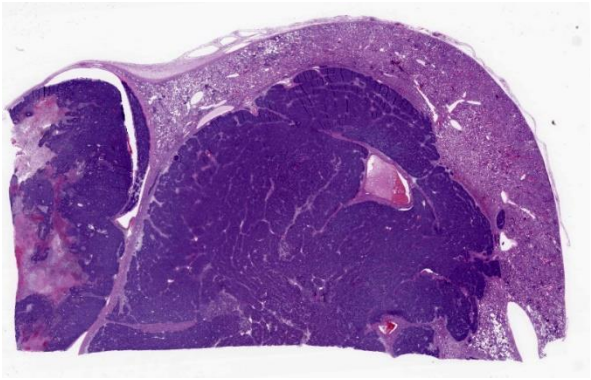

Figure 2-2. Kidney, common marmoset. Approximately 80% of the section of kidney is effaced by a neoplasm. (HE, 5X)

History:
Animal was thought to be pregnant, but ultrasound revealed a large (~5cm diameter, cystic, abdominal mass in the area of the left kidney.

Gross Pathology:
The multilobular abdominal mass enveloped the entire left kidney. On cut section, portions were white-tan and first while others were cystic and filled with yellow-brown fluid.

Microscopic Description:
Kidney: Within the cortex, compressing and effacing adjacent renal parenchyma and extending to cut borders is a mostly encapsulated, well-demarcated, lobulated, and expansile neoplasm. The neoplasm is composed of a disorganized mixture of three distinct cell populations: epithelial, mesenchymal and blastemal. In all sections, the blastemal population is the primary component and consists of polygonal cells arranged in nests sometimes separated by connective tissue. These neoplastic cells have indistinct cell borders, a small amount of eosinophilic cytoplasm and a high nuclear to cytoplasmic ratio. Nuclei are round to oval with vacuolated chromatin and indistinct nucleoli. The mitotic rate is 1 per 40x field. In some sections, these cells cant be seen within blood vessels at the periphery of

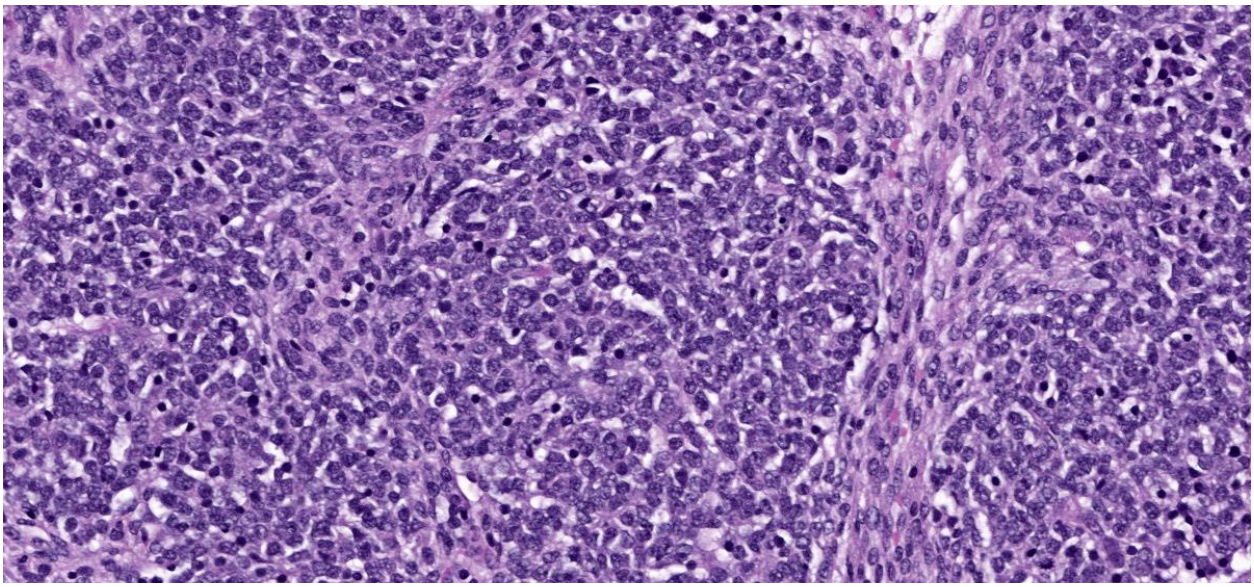

Figure 2-3. Kidney, common marmoset. The predominant cell type is a small polygonal to spindle blastemal cells which occasionally elongate forming bands of mesenchymal cells which course through the neoplasm. (HE, 315X)

the neoplasm. The epithelial population is composed of cuboidal to columnar cells arranged in irregular and often infolded tubules. Occasionally, these tubules project tufts into lumina (primitive glomeruli). These neoplastic cells have variably distinct cell borders, a moderate amount of eosinophilic fibrillar cytoplasm, round to oval nuclei, loosely clumped chromatin, and rarely contain a distinct nucleolus. The mitotic rate is 0-1 per 40x field. The mesenchymal component often blends with the other two components, and generally consists of spindle cells present within a loose, myxoid, extracellular matrix (embryonal mesenchyme). Spindle cells are stellate to spindle with indistinct cell borders, a scant amount of eosinophilic fibrillar cytoplasm, oval to elongate nuclei with finely stippled chromatin and indistinct nucleoli. The mitotic rate is <1 per 40x field. In some sections, spindle cells differentiate along the lines of cardiomyocytes characterized by elongated cells with one to several round centrally located nucleus/nuclei with vesicular chromatin and eosinophilic, crossed-striated cytoplasm containing occasional intercalated discs. Cystic areas are present in some sections of the neoplasm and are lined by attenuated epithelial cells.

Necrosis and hemorrhage are present multifocally within the neoplasm and adjacent kidney. The kidney also contains tubular atrophy and foci of mixed inflammatory cells.

Contributor's Morphologic Diagnoses:
Kidney: Nephroblastoma, Common Marmoset

Contributor's Comment:
Often called Wilms' tumor, nephroblastoma is the most common primary renal neoplasm in children, swine, chicken, and fish, the second most common primary renal tumor in cats, and the third most common in dogs.[3,10] Nephroblastoma is commonly reported in rats, and can be experimentally induced by prenatal exposure to the carcinogen N-ethylnitrosourea (ENU).[13]

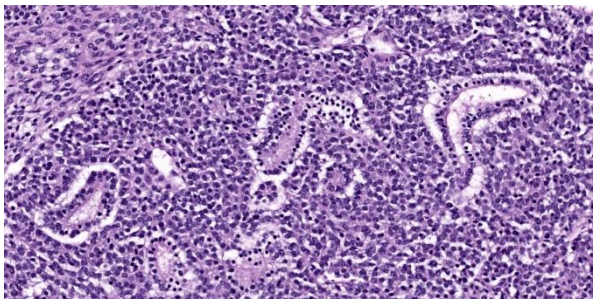

Figure 2-4. Kidney, common marmoset. Occasionally, palisading blastemal cells differentiate into tubules. (HE, 293X)

In nonhuman primates, primary neoplasms of the kidney have been reported infrequently as spontaneous cases and in association with exposure to radiation, chemical carcinogens, and parasites.[7] The most commonly described renal neoplasms in nonhuman primates include carcinomas and adenomas.[7] Only a few reports exist of nephroblastomas in Old World and New World monkeys including a report of nephroblastoma in a black-tufted marmoset[4] and a single report describing a malignant nephroblastoma in a common marmoset.[13] Interestingly, this case had similar features to that case report, including cystic areas and evidence of malignancy.

Nephroblastomas are true embryonal tumors that arise in primitive nephrogenic blastema and foci of renal dysplasia.[3] The etiology and pathogenesis of nephroblastoma has still not been fully clarified. In children, the neoplasm is frequently associated with congenital abnormalities or syndromes, including cryptorchism, hemihypertrophy, hypospadias, and sporadic aniridia. Two loci on chromosome 11, locus 11p13 (WT1 gene) and locus 11p15 (WT2 gene), have been implicated in the genesis of Wilms' tumors in children with developmental disorders. An abnormal WT1 gene is present in patients with WAGR syndrome (Wilms' tumor, aniridia, genitourinary abnormalities, mental retardation) or Denys-Drash syndrome (Wilms' tumor, progressive glomerulonephritis, male pseudohermaphroditism). A mutated WT2 gene can be observed in patients with Beckwith-Wiedemann syndrome or hemihypertrophy. However, the genetics of Wilms' tumor appear to be multifactorial and probably include further chromosomal abnormalities. Familial Wilms' tumor is rare and occurs in about 1% of cases and is not associated with mutations in chromosome 11.[1,8,13]

Contributing Institution:
Division of Laboratory Animal Resource
University of Pittsburgh
S1040 Thomas E. Starzl Biomedical Science Tower
200 Lothrop Street
Pittsburgh, PA 15261
http://www.dlar.pitt.edu/

JPC Diagnosis:
Kidney:Nephroblastoma.

Kidney: Nephritis, interstitial and lymphoplasmacytic, chronic, multifocal, mild with proteinosis.

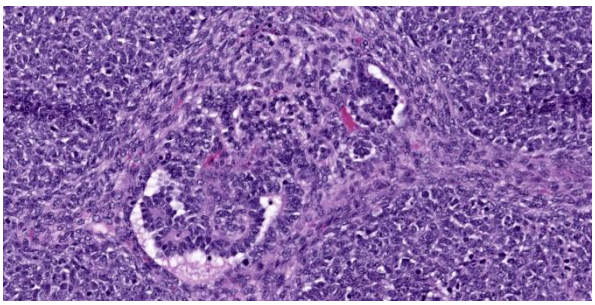

Figure 2-5. Kidney, common marmoset. Rarely, epitelial cells protrude into tubular lumina, recapitulating primitive glomeruli. (HE, 300X)

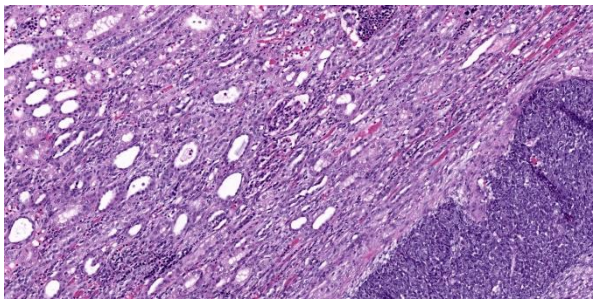

Figure 2-6. Kidney, common marmoset. At the periphery of the neoplasm, glomeruli and tubules are compressed with interstititial fibrosis. (HE, 139X)

JPC Comment:
Nephroblastoma remains a fan-favorite submission to the WSC and this case is a good example that clearly delineates the three components to describe (blastemal, mesenchymal, and epithelial) that are outlined in Figures 2-3, 2-4, and 2-5. In this case, the predominance of the blastemal cells with only rare tubular and glomerular differentiation was helpful, as trainees often have difficulty identifying blastemaConfirmatory IHCs for this case (WT1, CD56, pancytokeratin, vimentin, desmin) were not needed to arrive at the diagnosis.

Conference participants devoted a significant portion of the discussion to changes in the adjacent kidney. Participants noted occasional glomerular hypercellularity, synechiae, proteinosis, fibrosis, casts, and interstitial nephritis – we added a second morphologic diagnosis for the features we felt were best represented and not related to the neoplasm.

The constellation of glomerular changes and interstitial nephritis in this species suggests two potential concurrent pathologies. Spontaneous (chronic) progressive glomerulonephropathy (CPG) has been described previously in common marmosets[2,6,12] as has "marmoset wasting syndrome" (MWS).[9,11] Both CPG and MWS are common in this species (*Callithrix jacchus*) and can occur at any age. Additionally, both CPG and MWS cause chronic interstitial nephritis with predominantly lymphocytes and plasma cells and proteinosis as observed in this case. Low grade CPG can have subtle changes to the glomeruli, namely either hypercellularity or sclerosis of the mesangium. These changes are often absent in MWS however. In this case, we considered the possibility of low grade CPG given mildly hypercellular glomeruli with rare synechiae. In advanced cases of CPG, glomerular changes are marked and this condition can be more easily differentiated from MWS. Additionally, in cases of MWS, lymphoplasmacytic enteritis is invariably present. The presence or absence of enteric lesions was not mentioned in the clinical history, and MWS cannot be excluded as cause for the renal lesions in this case.

Finally, an important ruleout for this neoplasm is teratoma as the three cell types may be interpreted as primordial germ layers, particularly in cases where well-differentiated tissue (hair, cartilage, neural tissue, etc) is not included within the teratoma itself (see Conference 10, Case 1, 2023-2024).

References:

1. Al-Hussain T, Ali A, Akhtar M. Wilms tumor: an update. *Adv Anat Pathol*. 2014 May;21(3):166-73.
2. Brack M, Rothe H. Chronic Tubulointerstitial Nephritis and Wasting Disease in Marmosets (*Callithrix jacchus*). *Veterinary Pathology*. 1981;18(6_suppl):45-54.
3. Cianciolo RE, Mohr FC. The urinary system. In: Maxie MG, ed. *Jubb, Kennedy, and Palmer's Pathology of Domestic Animals*. Vol. 2, 6th ed. St. Louis, MO: Elsevier Limited; 2016:446-447.
4. Ferreira Junior J.A., Rissi D.R., Elias M.A., Leonardo A.S., Nascimento K.A.,Macêdo J.T.S.A. & Pedroso P.M.O. Nephroblastoma in a black-tufted marmoset (*Callithrix penicillata*). *Pesquisa Veterinária Brasileira*. 2018. 38(11):2155-2158.

5. Goens SD, Moore CM, Brasky KM, Frost PA, Leland MM, Hubbard GB. Nephroblastomatosis and nephroblastoma in nonhuman primates. *J Med Primatol*. 2005 Aug;34(4):165-70.
6. Isobe K, Adachi K, Hayashi S, et al. Spontaneous Glomerular and Tubulointerstitial Lesions in Common Marmosets (*Callithrix jacchus*). *Veterinary Pathology*. 2012;49(5):839-845.
7. Jones SR, Casey HW. Primary renal tumors in nonhuman primates. *Vet Pathol*. 1981 Apr;18(Suppl 6):89-104.
8. Lowe LH, Isuani BH, Heller RM, Stein SM, Johnson JE, Navarro OM, Hernanz-Schulman M. Pediatric renal masses: Wilms tumor and beyond. *Radiographics*. 2000 Nov-Dec;20(6):1585-603.
9. Ludlage E, Mansfield K. Clinical care and diseases of the common marmoset (*Callithrix jacchus*). Comp Med. 2003 Aug;53(4):369-82.
10. Meuten DJ, Mansfield K. Clinical care and diseases of the common marmoset (*Callithrix jacchus*). Comp Med. 2003 Aug;53(4):369-82.
11. Olstad KJ, Bleyer M. Other noninfectious conditions (inflammatory/degenerative/proliferative, immune-mediated/idiopathic/unknown in nonhuman primates. In: *Atlas of Diagnostic Pathology in Nonhuman Primates*. Kondova-Perseng I, Mansfield KG, Miller AD, editors. 211-228.
12. Yamada N, Sato J, Kanno T, Wako Y, Tsuchitani M. Morphological Study of Progressive Glomerulonephropathy in Common Marmosets (*Callithrix jacchus*). *Toxicologic Pathology*. 2013;41(8):1106-1115.
13. Zoller M, Matz-Rensing K, Fabrion A, Kaup F. Malignant nephroblastoma in a common marmoset (*Callithrix jacchus*). *Vet Pathol*. 2008:45:80-84.

CASE III:

Signalment:
7-month old, 141 kg, weaned, female, Brahman calf

History:
The calf was from the Beef Research Unit at the University of Florida (UF) composed of 237 weaned calves ranging from 6 to 8 months of age. The herd had experienced three deaths subsequent to a recent introduction of a post-weaning feed supplement to the animals. The affected calves presented with lethargy, weakness, incoordination, tachycardia, and recumbency. Clinical examination of this particular calf revealed a history of lateral recumbency and weakness within the last 24 hours, moderate dehydration, tachycardia (130 bpm), dyspnea, and ruminal hypomotility (1 weak contraction/min). The animal remained in lateral recumbency and died spontaneously within 24 hours of examination. The calf was submitted to the UF Veterinary Diagnostic Laboratories for necropsy.

Gross Pathology:
The animal was in good postmortem condition and good nutritional condition, with symmetrical muscling and appropriate subcutaneous and visceral adipose stores. Several muscle groups in the left and right thighs, especially the semimembranosus and semitendinosus muscles, contained multiple, multifocal to coalescing, ill-defined, pale tan streaks. Some skeletal muscle groups exhibited large, pale tan areas of discoloration. The superficial muscle fibers appeared more affected than the deeper ones. The pericardial sac contained mild to moderate amounts of a watery, translucent, yellow-tinged fluid. The epicardial surface of the left ventricle wall had multiple, 1-2 mm, round, flat, dark red foci. The myocardium of the left and right ventricles and interventricular septum contained multiple, multifocal to coalescing, ill-defined, pale tan streaks. The left and right cranial lung lobes

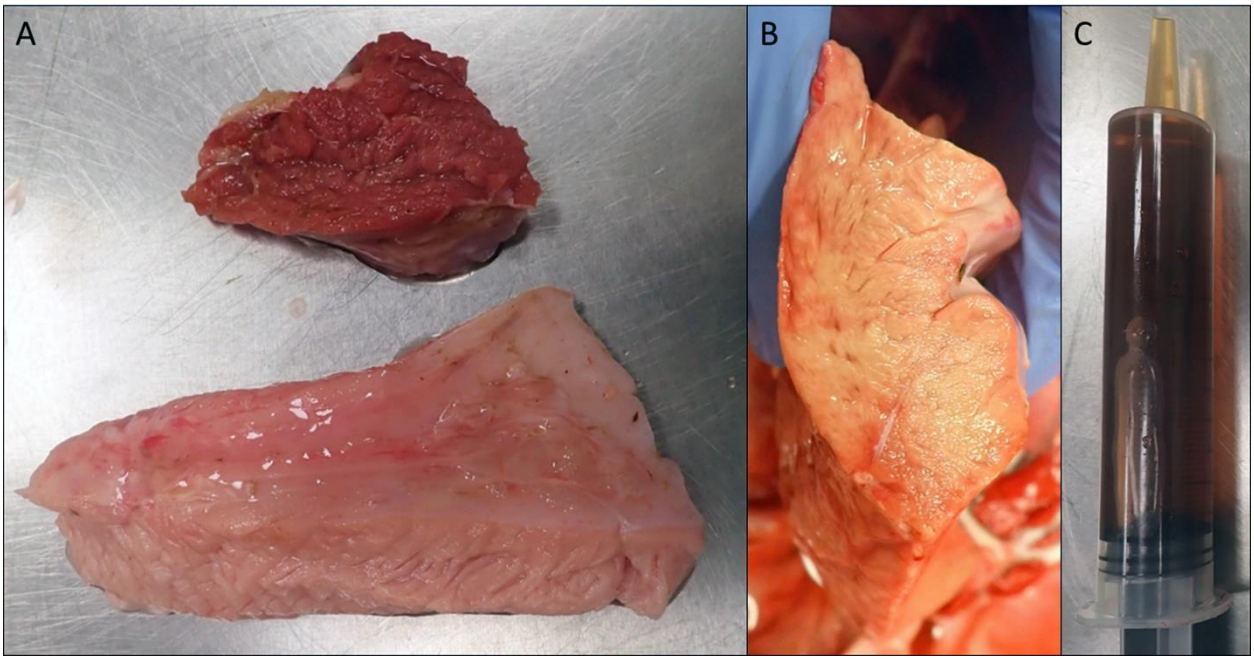

Figure 3-1. Skeletal muscle, calf. A) Some muscle groups in the thighs, especially the semimembranosus and semitendinosus muscles, exhibited large, pale tan areas of discoloration. Normal skeletal muscle at top. B) The myocardium contains multiple, ill-defined, pale tan areas of discoloration. C) Urine was dark brown. (*Photo courtesy of:* University of Florida, College of Veterinary Medicine, Department of Comparative, Diagnostic, and Population Medicine, Gainesville, Florida, USA. https://cdpm.vetmed.ufl.edu/)

had a gelatinous consistency and were mottled dark red to purple. On cut section, those lung lobes oozed a watery, translucent, red-tinged fluid. Samples of all lung lobes floated when placed in formalin. A prominent reticular pattern was observed throughout the liver lobes. The urinary bladder was distended by and filled with moderate amounts of a watery, translucent, brown-tinged fluid. No additional significant gross findings were observed in the remainder of the carcass.

Laboratory Results:

Pertinent laboratory results are indicated below.

Serum chemistry results: Creatine Kinase: 343,240 U/L; Aspartate aminotransferase: 2,335 U/L (ref: 48-139 U/L); Alkaline phosphatase: 181 U/L (ref: 30-69 U/L); Total bilirubin: 0.8 mg/dL (ref: ≤ 0.3 mg/dL); Sodium: 135.9 mEq/L (ref: 140-148 mEq/L); Calcium: 8.6 mg/dL (ref: 9.3-10.8 mEq/L); Chloride: 89.1 mEq/L (ref: 101-113 mEq/L).

Toxicology*: The levels of Monensin detected in two random samples of the feed supplement were 573 ppm and 856 ppm (Recommended label range: 11-33 ppm).

Vitamin E analysis**: The level of vitamin E detected in the submitted liver sample was 61.85 ug/g (Reference range: 7-40 ug/g)

Selenium analysis**: The level of selenium detected in the submitted liver sample was 1.31 ug/g (Reference range: 1.1-5.9 ug/g).

*Toxicology performed at the Iowa State University Veterinary Diagnostic Laboratory, Ames, Iowa

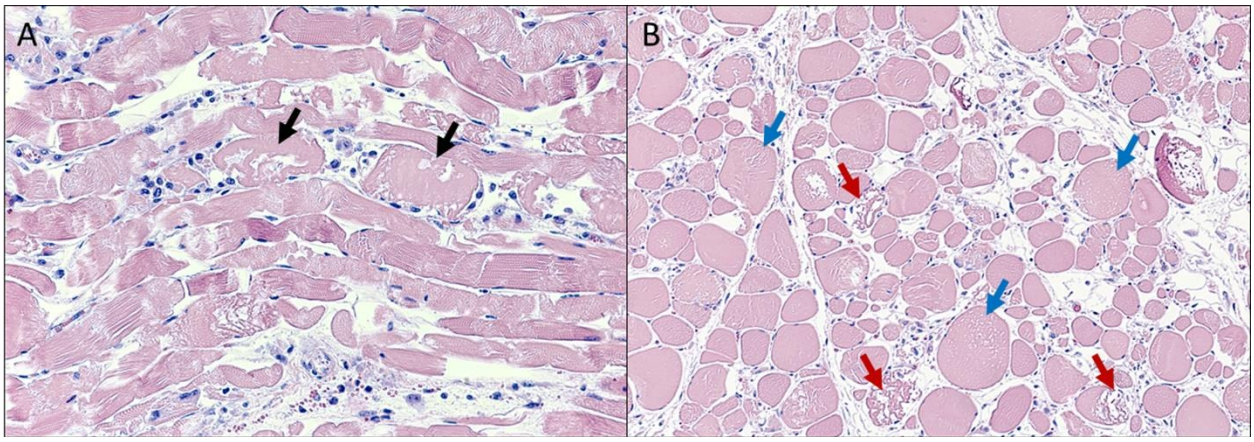

Figure 3-2. Skeletal muscle, calf. A) In longitudinal section, myofibers exhibit a hyalinized, vacuolated to fragmented sarcoplasm with loss of myofibrillar striations (black arrows). The interstitium is expanded by variable numbers of macrophages and plump, activated satellite cells (HE, 200x). B) In cross-section, myofibers were either moderately enlarged with vacuolated sarcoplasm (blue arrows) or shrunken with fragmented sarcoplasm (red arrows). Expanding the endomysium and less frequently the epimysium were small to moderate numbers of macrophages and plump satellite cells (*Photo courtesy of:* University of Florida, College of Veterinary Medicine, Department of Comparative, Diagnostic, and Population Medicine, Gainesville, Florida, USA. https://cdpm.vetmed.ufl.edu/)

**Nutrient analysis performed at the Michigan State University Veterinary Diagnostic Laboratory, Lansing, Michigan

Microscopic Description:

Skeletal muscle: Scattered throughout the musculature, myofibers are mild to moderately enlarged and have a hyalinized, often fragmented, homogeneous, eosinophilic sarcoplasm with loss of myofibrillar striations. In longitudinal sections, the myofibrils are often separated by longitudinal, empty spaces and occasionally lose their regular parallel pattern. In cross-sections, many myofibers contain variably sized, round to ovoid, empty vacuoles within the sarcoplasm. Some myofibers are shrunken, have a highly fragmented sarcoplasm, and are intermixed with pyknotic nuclei and karyorrhectic debris. Throughout the musculature, often between degenerate to necrotic myofibers are low to moderate numbers of macrophages and plump spindled cells (presumptive satellite cells).

Heart (tissue not included on the slide): The most prominent change was the presence of dense aggregates of plump, spindled cells and macrophages, replacing areas of cardiomyocyte loss. Multiple regions contain individual to small groups of cardiac myofibers with a mildly attenuated to mildly enlarged, mildly hyalinized, homogeneous, bright eosinophilic to amphophilic sarcoplasm with loss of myofibrillar striations. Often the sarcoplasm of affected myofibers is vacuolated. Occasional myofibers are hypereosinophilic with a pyknotic nucleus. Occasionally between myofibers are linear accumulations of an amphophilic granular material admixed with scant to mild amounts of karyorrhectic debris. In the interstitium, often associated with these areas and bordering myocardial vessels, are multiple, often linear, moderate density aggregates of plump spindled to stellate cells, fibroblastic cells, and macrophages. Occasionally these plump spindled cells have a large prominent nucleus with condensed, linear, deep basophilic chromatin (Anichkov cells).

Contributor's Morphologic Diagnoses:

1. Myofiber degeneration and necrosis, acute, multifocal to coalescing, marked, skeletal muscle.
2. Myocardial degeneration and necrosis, acute to subacute, multifocal, moderate, heart (tissue not included on the slide).

Contributor's Comment:

The major histopathologic changes in this calf involved several skeletal muscle groups and the myocardium, explaining clinical evidence of lethargy, weakness, and lateral recumbency noted on physical examination. Moreover, the histologic changes in the skeletal and cardiac musculatures confirm myodegeneration and myonecrosis. The widespread, synchronous muscle necrosis identified is consistent with a multifocal monophasic pattern of necrosis, suggesting a toxic myopathy or metabolic disorder[3]. Differential diagnoses for myodegeneration and myonecrosis in cattle typically include ionophore toxicosis, ingestion of myotoxic plants (e.g., *Senna* spp.), and nutritional myopathy.[1-3,7,9,13] The high serum levels of creatine phosphokinase, hepatic function dyscrasias, and hyponatremia and hypocalcemia are consistent with muscle necrosis, liver damage, and ionophore-induced influx of sodium and calcium into the cells, respectively. Pulmonary edema, pericardial effusion, and centrilobular necrosis are presumably sequelae to cardiac decompensation. A definitive cause for the cerebral vacuolar change is uncertain but may be related to tissue hypoxia/ischemia associated with cardiac failure.

In this calf, the multifocal monophasic pattern of myonecrosis, history of a newly introduced feed supplement, acute onset of clinical signs, serum chemistry abnormalities, and myocardial involvement would support the diagnosis of ionophore toxicosis.[3,4,6,13] Ultimately, this diagnosis was confirmed with the detection of toxic levels of monensin in the feed. The moderately increased levels of vitamin E in the liver and normal hepatic concentration of selenium would reduce the likelihood of nutritional myopathy as the cause of death in these calves. Furthermore, the feed and gastro-intestinal tract lacked plant parts suggestive of *Senna* spp.

Ionophore is the generic term to describe any lipid-soluble molecule that facilitates the transport of positively-charged ions across biologic membranes.[10] Monensin, lasalocid, and salinomycin are typical ionophores of veterinary clinical significance.[4,6,11,13]. Monensin is produced by the fermentation of *Streptomyces cinnamonensis*.[4,6,13] This ionophore is primarily used in veterinary medicine as an anticoccidial drug in poultry and for growth promotion and production efficiency in cattle.[4,6] Its three-dimensional (3-D) structure resembles a doughnut with the cation-binding site at the area of the doughnut hole.[10] This 3-D conformation confers some degree of selectivity for sodium and potassium to monensin.[10] The mechanism of action of monensin involves several sodium-hydrogen and potassium-hydrogen exchanges to move sodium ions into the cells and potassium ions out of the cells.[4,6,10,13]

Excessive ingestion of monensin can be toxic to several animal species. However, the susceptibility to monensin toxicosis, estimated by calculating the LD50, varies considerably among species.[3,10,14] For instance, the estimated LD50 in horses, cattle, and poultry are 2-3 mg/kg, 50-80 mg/kg, and 90-200 mg/kg, respectively, explaining why horses are very susceptible, and poultry are quite resistant to monensin toxicosis.[3,13] The pathogenesis of the disease is directly associated with the mechanism of action of monensin.[3,4,6,10,13] Long-standing, monensin-mediated accumulation of sodium into the cells, particularly myocytes and cardiomyocytes, leads to secondary water accumulation within the cytoplasm and organelles, which in turn induces

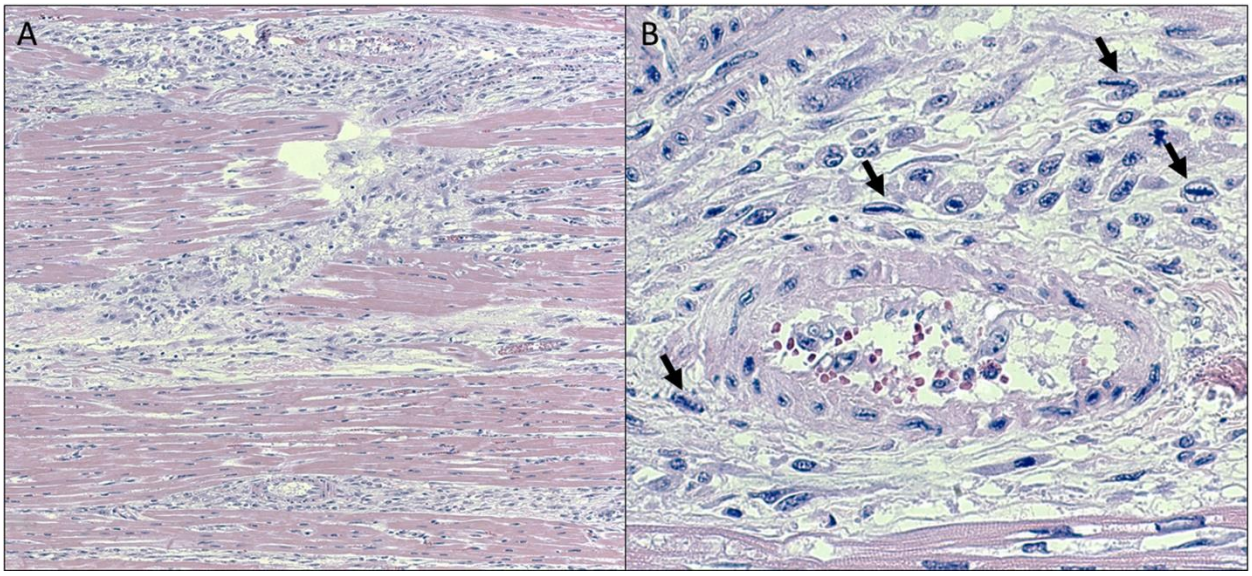

Figure 3-3. Heart, calf. A) Expanding the perimysium and replacing areas of cardiomyocyte loss are dense aggregates composed of plump spindled to stellate cells, fibroblasts, and macrophages (HE, 200x). B) These plump spindled cells (black arrows) had large prominent nuclei with condensed, linear, deep basophilic chromatin (Anichkov cells or caterpillar cells) (HE, 400x). (*Photo courtesy of:* University of Florida, College of Veterinary Medicine, Department of Comparative, Diagnostic, and Population Medicine, Gainesville, Florida, USA. https://cdpm.vetmed.ufl.edu/)

cell swelling and rupture of membranes, ultimately culminating with irreversible cell injury and cell necrosis.[3,4,6,10,13] In some instances, the toxic effects of Monensin may be potentiated with certain drugs.[1,10] Cattle ingesting nontoxic levels of Monensin in feed contaminated with macrolide antibiotic residue may still develop monensin toxicosis, presumably due to delayed hepatic clearance of monensin, resulting in accumulation and subsequent toxicity.[1]

Monensin toxicosis often is associated with feed-mixing errors that result in excess levels being added to the feed or access to feed sources destined for another species.[4,6,13,14] Grossly, several muscle groups and the myocardium have variably sized, pale tan areas of discoloration, representing areas of multifocal monophasic myonecrosis histologically.[3,4] Monensin poisoning may affect animals of all age groups.[3,4,6,13] However, heavier and stronger animals are typically the first ones to perish because of the dominant behavior allowing them to ingest more of the contaminated feed. Definitive diagnosis involves the detection of toxic levels of monensin in the suspected diet and sometimes in the ruminal content.[4,6,13] The suspected feed is the preferable sample for toxicology as the concentration of monensin in the ruminal content may be lower than that of the feed ingested due to absorption and/or ruminal breakdown[4].

Cattle may accidentally ingest *Senna* spp. when grazing or consuming feed contaminated with the plant.[5,8,12,13] Although *Senna* spp. poisoning typically causes multifocal monophasic necrosis, a similar pattern of necrosis to that induced by ionophore toxicosis,[3] absence of this toxic plant in the feedlot pen and beans and/or seeds in the feed and ruminal content would disfavor *Senna* spp. poisoning. Moreover, cattle grazing forage in soils deficient in selenium and/or being offered feed with low vitamin E content may develop nu-

tritional myopathy.[3,7] This condition commonly affects young animals, up to 6 months of age, ingesting poor-quality feed.[3] Since the calf, in this case, was in a similar age group and with myodegeneration and myonecrosis, selenium/vitamin E deficiencies were considered possible differentials. However, the typical multifocal polyphasic necrosis encountered with nutritional myopathies was not seen in this case,[3] decreasing the likelihood of nutritional myopathy. The moderately elevated levels of vitamin E and normal concentration of selenium in the submitted liver sample excludes selenium and vitamin E deficiencies as the cause of myodegeneration and myonecrosis in this calf.

Interestingly, all affected animals in the herd involved lighter animals, which is not usually the case in diet-related toxic causes where dominant animals may be exposed to a higher toxin dose. However, the animals in this herd were offered feed according to the average daily intake for the group based on the average herd weight. Therefore, by potentially receiving a higher dosage of monensin for their individual weight, it is possible these lighter animals were more susceptible to toxicosis. Deaths were not observed in the herd after discontinuing the monensin-supplemented feed.

Contributing Institution:
University of Florida, College of Veterinary Medicine, Department of Comparative, Diagnostic, and Population Medicine, Gainesville, Florida, USA.
https://cdpm.vetmed.ufl.edu/

JPC Diagnoses:
Skeletal muscle, myofibers: Degeneration and necrosis, monophasic, multifocal, moderate.

JPC Comment:
This case is a good example of a monophasic myonecrosis supported by ancillary diagnostics and a comprehensive writeup from the contributor. The lesions in the submitted slides are significantly less profound than the ones photographed by the contributor, but is consistent with "real-world" lesions in many cases of ionophore toxicosis.

Conference participants offered a number of interesting causes for this case including ionophores, vitamin E / selenium deficiency (white muscle disease), trauma (e.g. downer cow, capture myopathy) and glycogenosis type II. In downer cattle, massive focal necrosis of skeletal muscle is the result of ischemia driven by marked pressure i.e. the weight of the body is sufficient to collapse both venous and arterial blood flow.[3] The section examined lacked vascular changes and significant edema that would be anticipated as part of a reperfusion syndrome however. Given that Pompe's disease (type II glycogenosis; a lysosomal storage disease) has been described in Brahman cattle as a cause of skeletal muscle dysfunction[8,11], it does merit consideration in this case. However, the underlying cause is an autosomal recessive gene defect in acid maltase (acid α-glucosidase) with the net effect being the inability to breakdown glycogen within lysosomes during normal cellular metabolism. As such, major effects are noted in glycogen-rich, glucose-dependent tissues such as the heart and CNS with cardiac dysfunction and failure being the ultimate cause of death. The major histologic feature of Pompe's disease is marked vacuolation of skeletal myocytes, cardiac myocytes, and neurons of the PNS/CNS with vacuolization representing glycogen within lysosomes than can be confirmed via periodic acid-Schiff (PAS) with diastase treatment.[8] This is not the predominant microscopic feature in this case.

References:
1. Basaraba RJ, Oehme FW, Vorhies MW, Stokka GL. Toxicosis in cattle from concurrent feeding of monensin and dried distiller's grains contaminated with

macrolide antibiotics. *Journal of Veterinary Diagnostic Investigation*, 11(1), 79-86, 1999.
2. Blanchard PC, Galey FD, Ross F, Landgraf WW, Meyer H, Spiro N. Lasalocid toxicosis in dairy calves. *Journal of Veterinary Diagnostic Investigation*, 5(2), 300-302, 1993.
3. Cooper BJ, Valentine BA. Muscle and Tendon. In: Maxie, MG. *Jubb, Kennedy, and Palmer's Pathology of Domestic Animals*. Vol 1, 6th ed. St. Louis, Missouri; Elsevier; 2016:180-182, 208, 212-216, 218-220.
4. Ensley S. Ionophore Use and Toxicosis in Cattle. *Veterinary Clinics of North America: Food Animal Practice*, 36(3), 641-652, 2020.
5. Furlan FH, Zanata C, Damasceno ES, et al. Toxic myopathy and acute hepatic necrosis in cattle caused by ingestion of *Senna obtusifolia* (sicklepod; coffee senna) in Brazil. *Toxicon*, 92, 24-30, 2014.
6. Hall JO, Ionophore use and toxicosis in cattle. *Veterinary Clinics of North America: Food Animal Practice*, 16(3), 497-509, 2000.
7. Kennedy S, Rice DA, Davidson WB. Experimental myopathy in vitamin E- and selenium-depleted calves with and without added dietary polyunsaturated fatty acids as a model for nutritional degenerative myopathy in ruminant cattle. *Research in Veterinary Science*, 43(3), 384-394, 1987.
8. Lyons RE, Johnston DJ, McGowan MR, Laing A, Robinson B, Owen H, Hill BD, Burns BM. E7 (1057ΔTA) mutation of the acidic α-glucosidase gene causes Pompe's disease in Droughtmaster cattle. *Aust Vet J*. 2017 May;95(5):138-142.
9. Nicholson SS. Southeastern plants toxic to ruminants. *Veterinary Clinics of North America: Food Animal Practice*, 27(2), 447-458, 2011.
10. Novilla MN, McClary D, Laudert SC. Ionophores. In: *Reproductive and Developmental Toxicology*, 2nd Edition. Elsevier; 2017. pp. 503-517.
11. Reichmann K, Twist J, Thistlethwaite E. (1993), Clinical, diagnostic and biochemical features of generalised glycogenosis type II in Brahman cattle. *Australian Veterinary Journal*, 70: 405-408.
12. Rissi DR, Barros CSL. Pathology in Practice. *Journal of the American Veterinary Medical Association*, 250(1), 51-53, 2017.
13. Roder JD. Ionophore toxicity and tolerance. *Veterinary Clinics of North America: Food Animal Practice*, 27(2), 305-314, 2011.
14. Silva AWO, Mendonça MFF, Freitas MD, Filho ALR, Silva RDG, Leal PV, Pimentel LA, Peixoto TC. Accidental monensin poisoning in buffaloes in Bahia, Brazil. *Pesquisa Veterinaria Brasileira*, 42:e06937, 1-9, 2022.

Figure 4-1. Cerebrum, rhesus macaque. One section of cerebrum is submitted for examination. at subgross magnification, there are extensive areas of cavitation within the subcortical white matter. (HE, 5X)

CASE IV:

Signalment:
58 month-old, female rhesus macaque (*Macaca mulatta*)

History:
A female rhesus macaque was infected intrarectally with simian-human immunodeficiency virus [SHIV]. The monkey was on treatment for chronic diarrhea. Twenty eight months after infection, the animal developed acute epistaxis, ataxia, and a left-sided head tilt. The monkey was humanely euthanized due to worsening neurologic deficits.

Gross Pathology:
The monkey was in lean body condition with adequate hydration. The right axillary lymph node and spleen were mildly enlarged. No lesions were present in the heart, lungs, liver, kidneys, gastrointestinal or reproductive tract.

Although epistaxis was not noted grossly, there was blood on the swab collected for bacterial culture.

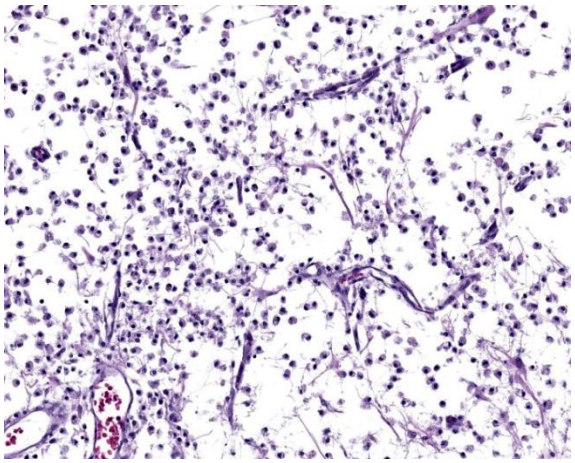

Figure 4-2. Cerebrum, rhesus macaque. Areas of cavitation contain gliovascular strands and numerous Gitter cells. (HE, 49X)

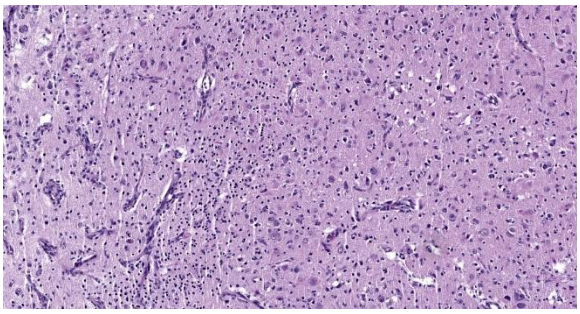

Figure 4-3. Cerebrum, rhesus macaque. Adjacent to areas of necrosis, there is marked gliosis with numerous gemistocytic astrocytes and vessels are prominent due to endothelial hypertrophy. (HE, 122X)

Laboratory Results:
Nasal culture: *Bordetella bronchiseptica*

No pathogens were noted by fecal bacterial culture. PCR results were negative for *Enterocytozoon bieneusi* and *Cryptosporidium parvum* of the liver, *Mycobacterium* sp. of the mesenteric lymph node and *Helicobacter* sp. of the stomach.

Microscopic Description:
Cerebrum: Within white matter, there is multifocal, severe parenchymal loss/cavitation with numerous central Gitter cells. Around the edges of the cavities there is marked gliosis. Oligodendrocytes are markedly enlarged, up to 5x normal, and contain variably-sized, basophilic – ground glass inclusions. Reactive(gemistocytic) astrocytes are markedly pleomorphic, bizarrely shaped, bi- or trinucleated and contain large, basophilic - ground glass inclusions. Similar astrocytes are present in the superficial cortex. Numerous vessels with markedly hypertrophic endothelial cells extend from the meninges and are present around and within the areas of cavitation. Few neutrophils and lymphocytes are present around some vessels. In the meninges, few lymphocytes, plasma cells and macrophages are present.

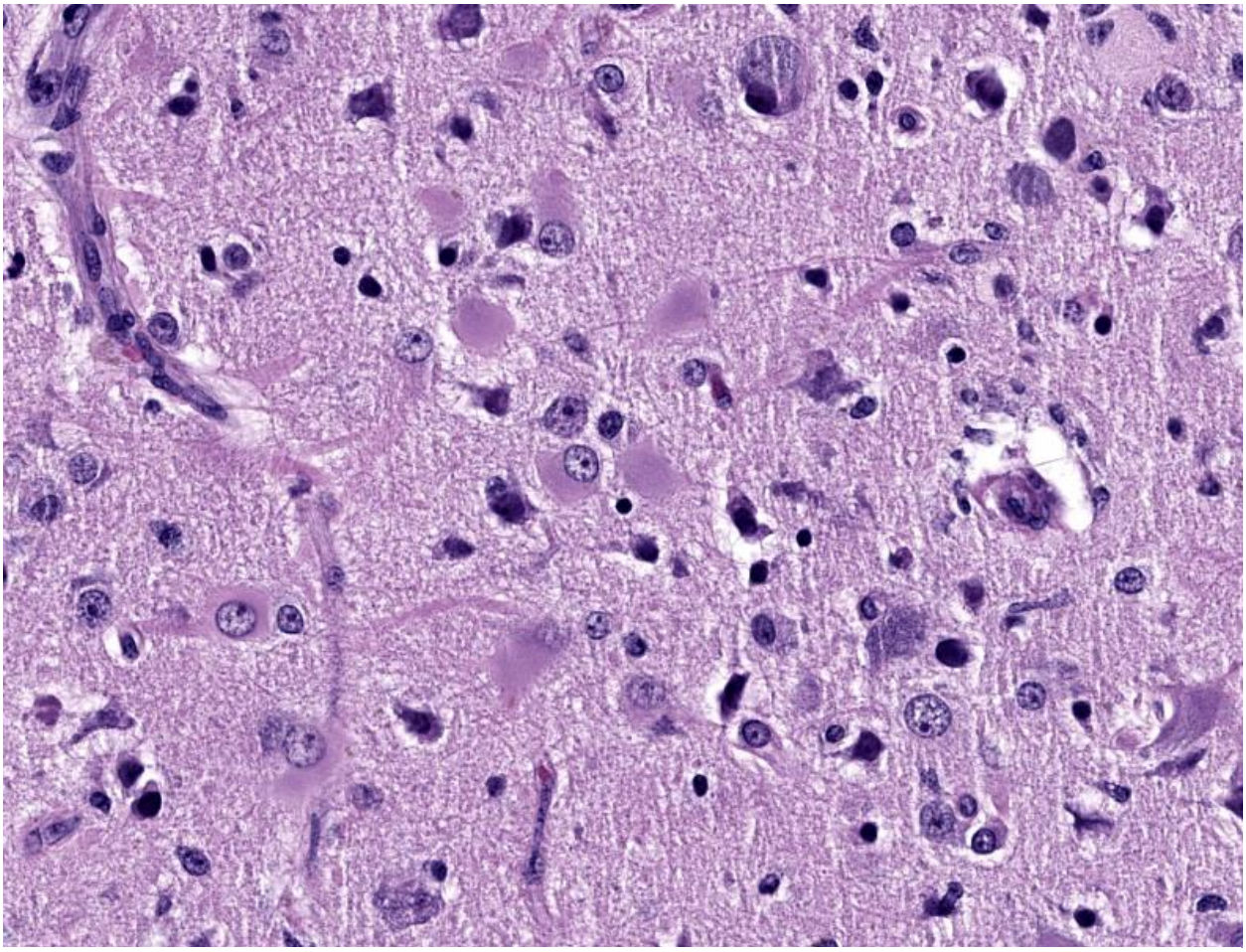

Figure 4-4. Cerebrum, rhesus macaque. High magnification of gemistocytic astrocytes in areas of gliosis. (HE, 122X)

PCR: SV40 was not detected on formalin fixed brain.

EM: Within the nucleus of oligodendrocytes, there are numerous, tightly packed, 40-45 nm viral particles arranged in paracrystalline arrays.

Contributor's Morphologic Diagnosis:
Cerebrum: Leukoencephalomalacia, severe with oligodendrocytic and astrocytic intranuclear inclusions and marked vascular hyperplasia.

Condition: Progressive multifocal leukoencephalopathy

Contributor's Comment:
SV40, Simian vacuolating virus 40, is a non-enveloped, 40 - 45nm, double stranded, circular, DNA virus of the polyomavirus family.[6,9,11] Transcription of the early regions of the viral genome produces large tumor antigen (LTag) and small tumor antigen (STag) proteins. Transcription of the late regions produces capsid proteins VP1, VP2, and VP3 and agnoprotein.[5,9,10]

Viral infection begins with VP1, VP2 and VP3 receptor mediated endocytosis.[9] Once in the nucleus, viral LTag stimulates host cell DNA synthesis and induces the cell to enter into S-phase and begin DNA synthesis. Small tumor antigen (STag) is not necessary for viral replication, but it enhances efficiency of viral replication by stimulating cells to move from G0/G1 to S phase.[10] Agnoprotein regulates viral proliferation.[5]

In addition to its capacity to cause lytic infection, SV40 LTag can cause malignant transformation by binding to and inactivating tumor suppressor proteins, retinoblastoma (pRb), p53, p107 and p130.[10] SV40 can cause tumors in vitro, or when the virus is injected into rodents or non-native hosts.[6,10,11]

SV40 is endemic in Rhesus macaques and is spread by exposure to bodily fluids such as urine or respiratory droplets. SV40 infection causes inapparent infection or mild respiratory disease or cystitis. After a period of viremia and viruria, the virus then settles in the kidneys and remains latent in immunocompetent animals.[6,11] In SIV (+) animals, virus may be found in kidney, brain, lungs and mononuclear cells.[6] Clinical disease occurs after immunosuppression due to SIV/SHIV infection, treatments with immunomodulatory medications or antirejection drugs given after experimental organ transplantation.[11-13] Clinical signs may be nonspecific, or due to other opportunistic infections, and include anorexia, diarrhea, anemia, and tissue wasting. Neurologic signs may include head tilt, ataxia, and blindness.[8] At necropsy, multifocal malacia may be visible at the junction of grey and white matter and subependymal grey matter of the cerebrum.[13]

In the CNS, two types of lesions may be found. The first resembles the changes seen in progressive multifocal leukoencephalopathy (PML) in humans. Demyelination due to infection and destruction of oligodendrocytes are found multifocally in white matter, especially at the junction with gray matter. Changes also may be found in subependymal grey matter.[6,11] Around foci of demyelination, remaining oligodendrocytes are enlarged and may contain basophilic – ground glass intranuclear inclusions. Gemistocytic astrocytes have a bizarre appearance and also may have inclusions. Numerous Gitter cells contain myelin debris.[6,11,13] The second type of lesion is meningoencephalitis of the superficial grey matter with little demyelination. In this form, inflammation expands the meninges and extends along vessels into the grey matter. More astrocytes than oligodendrocytes are affected although both cell types can have intranuclear inclusions. Vessels in affected areas have hypertrophic endothelial cells.[11,13] Both PML lesions and meningoencephalitis may be present in the same animal.[11]

In addition to the microscopic lesions in the CNS, there may be changes in the kidneys and lungs. In the kidneys, often at the corticomedullary junction, enlarged and vacuolated tubular or necrotic epithelial cells containing intranuclear inclusions along with tubulointerstitial nephritis may be present. In the lungs, there may be interstitial pneumonia with intranuclear inclusions in hypertrophic type 2 pneumocytes.[6,11-13] On electron microscopy, 45nm particles are arranged in paracrystalline arrays within the nucleus.[6]

Macaques, African green monkeys, baboons, chimpanzees, marmosets and squirrel monkeys, can be infected by polyoma virus.[11,13] Polyomaviruses in other species include:

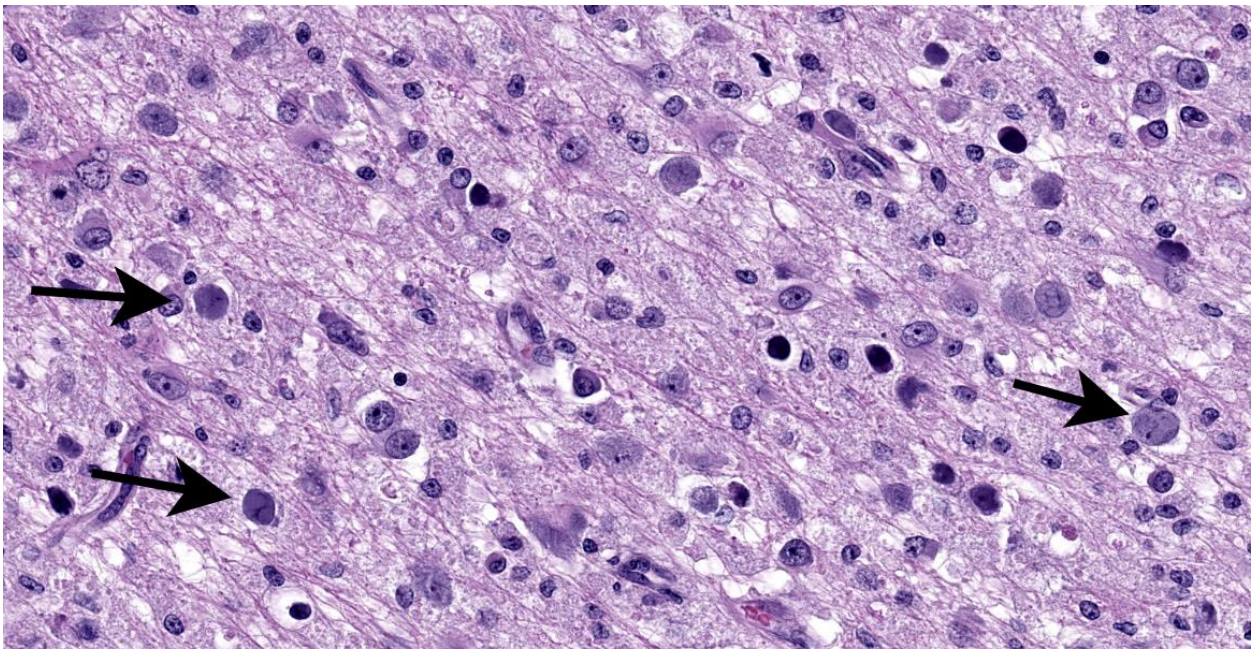

Figure 4-5. Cerebrum, rhesus macaque. Glial cells contain large amphophilic intranuclear viral inclusions (arrows). (HE, 715X)

Raccoons**:** Racoon polyomavirus: malignant peripheral nerve sheath tumors and olfactory sarcomas.[4]

Cattle: BoPy-V1, or Epsilon Polyomavirus bovis: severe tubulointerstitial nephritis with tubular epithelial cell necrosis has been reported in a fetus. However, infection in older cattle and humans has not been found to cause clinical disease.[5]

Budgerigars: Avian polyomavirus: Budgerigar fledgling disease, presents with hepatitis, ascites, and hydropericardium.[7]

Geese: Goose hemorrhagic polyoma virus: Hemorrhagic nephritis and enteritis disease, goslings die acutely with hemorrhagic nephritis and subcutaneous edema.[7]

In man, BK and JC polyomaviruses are widely spread and have a 70%-75% homology with SV40.[9,11] Most people are infected with BK and/or JC viruses in childhood and 70-90% of people are seropositive by the time they reach adulthood.[6,9,11,12] Reactivation of either virus by HIV infection, treatment with immunomodulatory drugs or immunosuppression following kidney/organ/bone marrow transplantation can lead to CNS or renal disease.[6,9] Reactivation of BK polyomavirus in kidney transplant recipients leads to nephropathy/nephritis, hemorrhagic cystitis and urethral stenosis and may lead to graft failure.[9,11,12] Reactivation of JC polyomavirus leads to progressive multifocal leukoencephalopathy characterized by demyelination with intranuclear inclusions in the oligodendrocytes. Effective treatment of HIV by antiviral medications has led to a drop of PML seen in individuals with AIDS.[9]

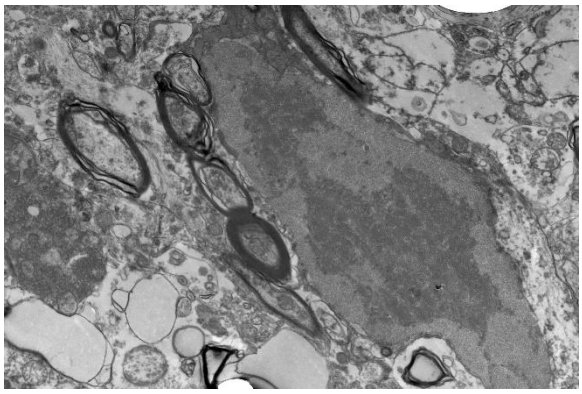

Figure 4-6. Cerebrum, rhesus macaque. Electron micrograph of a viral intranuclear inclusion in an oligodendroglial cell. (TEM, 3000X) (*Photo courtesy of:* National Institutes of Health, 9000 Rockville Pike, Bethesda, MD 20892)

Laboratory diagnosis, except for urine cytology, is based on detecting SV40 LTag, to include via PCR in CSF, urine, or sera.[3,9] Immunohistochemistry or in situ hybridization using an anti-SV40 LTag antibody can detect polyoma virus in renal or brain biopsies.[9] In urine samples, decoy cells, epithelial cells with intranuclear inclusions, and cytoplasmic fragmentation, may be used as a screening tool but inclusions due to CMV and adenovirus may look similar.[3] Progression of PML can be monitored by MRI.[1]

Polio vaccines that had been grown on rhesus kidney cell cultures and given to people from 1955 to 1963 were found to have been contaminated by SV40.[11] Due to the capacity of SV40 virus to induce malignant transformation in cell culture and cause tumors in rodents, there has been controversy over whether there has been an increased rate of cancer in people who received the contaminated vaccine. Studies have had conflicting results due to different methodologies, cross reactivity with BK and JC viruses and common seropositivity for SV40.[10,11]

Twelve new human polyoma viruses have been identified since 2007. Of the 12 new viruses, integrated BK virus has been found rarely in urological cancers. In addition, 80% of Merkel cell carcinomas, an aggressive form of skin cancer, have integrated Merkel cell polyomavirus. It may be that with newer, more sophisticated gene sequencing techniques, the association of polyomavirus and cancer may become clearer.[10]

Contributing Institution:
Matthew Starost, DVM, PhD.
National Institutes of Health
9000 Rockville Pike
Building 28A
Room 111
Bethesda, MD 20892
starostm@ors.od.nih.gov

JPC Diagnosis:
Cerebrum: Leukoencephalomalacia, multifocal to coalescing, with marked gliosis, gemistocytic astrocytosis, and glial intranuclear viral inclusions.

Cerebrum: Meningioangiomatosis, focally extensive, severe.

JPC Comment:
The contributor provides a detailed summary of SV40 that accompanies an equally impressive slide submission for this final case. We have covered SV40 leukoencephalomalacia in a rhesus macaque before (Conference 13, Case 3, 2015-2016) though this case presents outstanding histologic changes. The degree of loss of white matter (cavitation), the vascular changes, and the increased cellularity (basophilia) of the neuropil make this case almost diagnostic at subgross magnification (Figure 4-1). As the contributor notes, both oligodendro

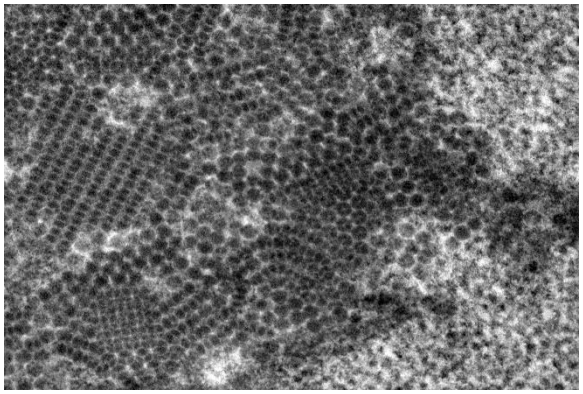

Figure 4-7. Cerebrum, rhesus macaque. Electron micrograph of a viral intranuclear inclusion in an oligodendroglial cells which demonstrates numerous icosahedral virions in paracrystalline array. (TEM, 30,000X) (*Photo courtesy of:* National Institutes of Health, 9000 Rockville Pike, Bethesda, MD 20892)

cytes and astrocytes contain characteristic intranuclear inclusions (Figure 4-5) that explain the pathogenesis of this lesion. A Luxol fast blue and modified Bielschowsky silver stain highlighted the severe loss of myelinated axons in this case. Though not particularly required at this point in lesion development, these stains may be helpful for less dramatic cases.

Conference participants were intrigued about the profound vascular changes within the cortical gray matter overlying the cavitated areas. We consulted with Dr. Andrew Miller (Cornell University) about this atypical meningovascular proliferation and ultimately decided to add a second morphologic diagnosis for this case. We excerpt his excellent commentary in part below:

"…There are 3 primary considerations for the vascular changes noted in this case. Foremost, the vasoproliferative lesion emanates from the meninges and invades into the neuroparenchyma around penetrating blood vessels and there are clearly two different cell populations present. There is one that is more spindled and likely derived from meningothelial cells and the other is blood vessels lined by reactive endothelial cells. This pattern is typical for meningioangiomatosis, though it is unlikely to be directly related to SV40 infection but instead a consequence of the profound necrosis of the underlying neuroparenchyma.

Additionally, the animal in this case was SHIV(+) and proliferative arteriopathy remains an uncommon concurrent lesion that can also been seen in SIV infection.[2] This proliferative arteriopathy can occur in a variety of organs including kidney, lung, and meningeal blood vessels where it can be associated with CNS infarction. The pathogenesis of this retroviral-associated arteriopathy is poorly understood; however, it is an important finding in a minority of SIV- and SHIV-infected macaques. That stated, these lesions are never as large or plaque-like as the area of interest in this case and typically present with single to small groups of vessels with asymmetric medial thickening, luminal narrowing, and variable thrombosis and mononuclear inflammation.[2]

Lastly, vasculitis and proliferative vascular lesions can also be associated with cytomegalovirus in immunosuppressed macaques though the large, intranuclear inclusions typical of those cases were absent in this case.[14] The lesions of this macaque do not fit the expected presentation of either retroviral-associated arteriopathy or cytomegalovirus-associated vasculitis."

References:

1. Cortese I, Reich DS, Nath A. Progressive multifocal leukoencephalopathy and the spectrum of JC virus-related disease. *Nat Rev Neurol*. 2021 Jan;17(1):37-51.
2. Chalifoux LV, Simon MA, Pauley DR, MacKey JJ, Wyand MS, Ringler DJ. Arteriopathy in macaques infected with simian immunodeficiency virus. *Lab Invest*. 1992 Sep;67(3):338-49.
3. Geetha V, Rao L, Monappa V, Susmitha M, Prabhu R. Decoy cells in urine cytology: A useful clue to post-transplant polyoma virus infection. *J Cytol*. 2012 Apr;29(2):133-4.
4. Giannitti F, Higgins RJ, Pesavento PA et al. Temporal and geographic clustering of polyomavirus-associated olfactory tumors in 10 free-ranging raccoons (Procyon lotor). *Vet Pathol*. 2014 Jul;51(4):832-45.
5. Giannitti F, da Silva Silveira C, Bullock H et al. Bovine Polyomavirus-1 (Epsilonpolyomavirus bovis): An Emerging Fetal Pathogen of Cattle That Causes Renal Lesions Resembling Polyomavirus-Associated Nephropathy of Humans. *Viruses*. 2022 Sep 14;14(9):2042.
6. Horvath CJ, Simon MA, Bergsagel DJ et al. Simian virus 40-induced disease in rhesus monkeys with simian acquired immunodeficiency syndrome. *Am J Pathol*. 1992 Jun;140(6):1431-40.
7. Johne R, Müller H. Polyomaviruses of birds: etiologic agents of inflammatory diseases in a tumor virus family. *J Virol*. 2007 Nov;81(21):11554-9.
8. Lednicky JA, Arrington AS, Stewart AR et al. Natural isolates of simian virus 40 from immunocompromised monkeys display extensive genetic heterogeneity: new implications for polyomavirus disease. *J Virol*. 1998 May;72(5):3980-90.
9. Pinto M, Pinto M, Dobson S. BK and JC virus: a review. *J Infect*. 2014 Jan;68 Suppl 1:S2-
10. Shuda, Masahiro. In: P.Boffetta and P.Hainaut, eds. Polyomaviruses in Human Cancer. *Encyclopedia of Cancer*. Vol 3, 3rd ed. Elsevier; 2019:266-27.
11. Simon MA. Polyomaviruses of nonhuman primates: implications for research. *Comp Med*. 2008 Feb;58(1):51-6.
12. Song M, Mulvihill MS, Williams KD, Collins BH, Kirk AD. Fatal SV40-associated pneumonia and nephropathy following renal allotransplantation in rhesus macaque. J *Med Primatol*. 2018 Feb;47(1):81-84.
13. Wachtman L, Mansfield K. In: C. Abee, K. Mansfield, S. Tardif, T. Morris, eds. Viral Diseases of Nonhuman Primates. *Nonhuman Primates in Biomedical Research*. Vol 2, 2nd ed. Academic Press; 2012: 25-33.
14. Yanai T, Lackner AA, Sakai H, Masegi T, Simon MA. Systemic arteriopathy in SIV-infected rhesus macaques (Macaca mulatta). *J Med Primatol*. 2006 Apr;35(2):106-12.

Joint Pathology Center
Veterinary Pathology Services

WEDNESDAY SLIDE CONFERENCE 2024-2025

Conference #6 — 18 September 2024

CASE I:

Signalment:
12.5 month old R672C heterozygous rat (Sprague-Dawley background)

History:
This R672C heterozygous rat was reported for bilateral hindlimb weakness. On exam, the rat was bright, alert, responsive, groomed, and had a BCS of 4/5. He was active and able to move around the cage using the fore limbs but dragged the hind limbs, which had severe proprioceptive deficits (right more severe than left). The withdrawal reflex was present but diminished in both hind limbs. The tail was also limp, and the rat was unable to freely move its tail (the tail dropped after picking it up and letting it go). There is no experimental history for this rat. The phenotype may include limb contracture, although the research group has not observed this phenotype.

Gross Pathology:
The rat is in fair postmortem condition and has a body condition score of 5/5 with substantial subcutaneous and visceral adipose stores. Within the abdomen, the spleen is markedly enlarged. There is a 5 mm x 1 mm green area on the serosal surface of the spleen that does not extend into the parenchyma. The kidneys have bilateral multifocal to coalescing green-tan foci, ranging in size from ~1mm to 5mm. Some of the foci are slightly raised; on cut section, they extend into the renal cortex and are semi-firm. The left and right renal cortex and medulla are moderately diffusely dark red in

Figure 1-1. Kidney, rat. The kidneys have bilateral slightly raised tan to green nodules extending into the cortex. (*Photo courtesy of:* University of Washington Veterinary Diagnostic Lab and Comparative Pathology Program, Department of Comparative Medicine, The Comparative Pathology Program (CPP) | Department of Comparative Medicine (washington.edu)

color with minimal corticomedullary distinction. The liver is mildly increased in size and is mottled red pink. There is a 1.5 cm x 1 cm green tubular soft tissue structure at the level of the ventral left lateral liver lobe. There is mild segmental reddening of the small intestine. Upon removal of the gastrointestinal tract, there are multiple 3-5 mm green soft tissue semi-firm structures within the visceral adipose tissue.

The vertebral column is removed from the level of the third lumbar vertebrae to the third sacral vertebrae. On cross section, within the vertebral canal, there is brown-green caseous material surrounding the spinal cord. Within

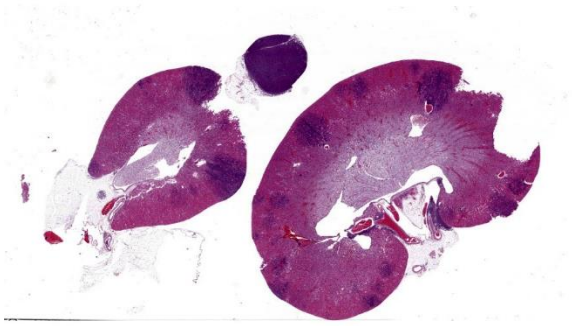

Figure 1-2. Kidney, adrenal gland, rat. The adrenal gland is diffusely effaced, and the renal cortex is multifocally infiltrated by a round cell neoplasm. (HE, 4X)

the bone marrow of the femur, there is green caseous material that exudes on cut section.

The lungs are mottled light red to pink. The heart is mildly enlarged. Within the mediastinum, there are multiple, 5mm-7mm green soft tissue structures. Within the ventral neck, structures of the same appearance are observed, approximately at the level of the cervical lymph nodes. There are no other significant findings.

Laboratory Results:
Mediastinal mass culture: No growth on initial plate media. Leuconostoc pseudomesenteroides from enrichment broth only – presume contaminant.

Microscopic Description:
Kidney: Expanding the interstitium and separating the tubules, there is an unencapsulated and infiltrative neoplasm characterized by sheets of round cells with mild to moderate cytoplasm in a scant preexisting fibrovascular stroma. Nuclei are circular to ovoid and occasionally reniform, with a single distinct nucleolus. In some cells, there is an eccentric nucleus with eosinophilic cytoplasm. Cell borders are generally distinct. There is moderate anisocytosis and anisokaryosis. Mitoses are frequent. Many tubular epithelial cells contain intracytoplasmic eosinophilic droplets of varying size, up to 20 microns in diameter. The adrenal gland is effaced by similar neoplastic cells.

The round cell neoplasm also affects the following organs: bone marrow, head (Harderian gland, nasal cavity, salivary gland), meninges, lung, liver, kidney, lymph node, pancreas, spleen, submucosa of the bladder, fat, epaxial skeletal muscle, and nerve roots

Contributor's Morphologic Diagnoses:
1. Multiorgan hematopoietic neoplasm.
2. Renal tubular epithelium: Intracytoplasmic hyaline droplets.

Contributor's Comment:
The neoplasm in this rat is most consistent with a hematopoietic neoplasm. Hematopoietic neoplasms reported in rats include lymphoma, granulocytic leukemia (myeloid sarcoma), and histiocytic sarcoma.[2] Hematopoietic neoplasms in general are much less common in the rat compared to the mouse.[2] In one report, lymphoma had an approximately 1.5% incidence in the Sprague Dawley rat, of which large granular lymphocyte lymphoma (or mononuclear leukemia) was most common, and granulocytic leukemia had a 0.1-0.3% incidence.[2] Granulocytic leukemia more often involves in the kidney in the rat in addition to other organs such as the liver, spleen and bone marrow, and cells with ring shaped nuclei or large, blastic cells may be seen. [2,3] Histiocytic sarcoma is the most common nonlymphoid hematopoietic neoplasm reported in the rat and is recognized as an age related neoplasm in the Sprague Dawley and other strains of rat.[2, 5] This neoplasm has been reported to have an incidence of approximately 1% in Sprague Dawley rats, usually affects rats over 12 months of age, and most commonly affects the lung and liver.[2,3] Other authors have

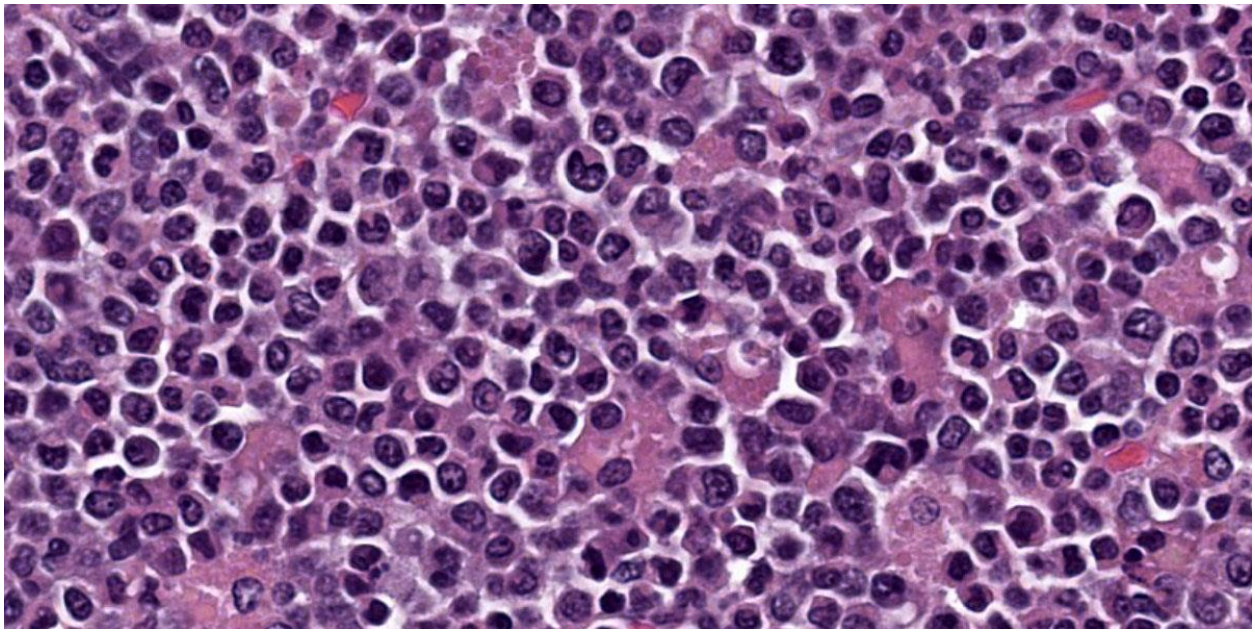

Figure 1-3. Adrenal gland, rat. Neoplastic rounds cells have a round to indented nucleus and there is a high mitotic count. (HE, 900X)

described the neoplasm affecting hematopoietic organs including bone marrow, spleen and lymph nodes in the rat.[5] Histiocytic sarcoma arises from histiocytes although the exact origin of the histiocytic cells remains uncertain.[3] These cells arise from the mononuclear-phagocyte system lineage, and include promonocytes, monocytes, tissue histiocytes, and macrophages.[3] Histologically, the neoplasm may have a granulomatous or sarcomatous appearance or present as sheets of round cells, and multinucleated giant cells are frequently observed.[4] This neoplasm does not have a granulomatous or sarcomatous appearance, and multinucleated giant cells are not observed in the present case.

In the rodent, histiocytic sarcoma and occasionally other hematopoietic neoplasms may be associated with intracytoplasmic round eosinophilic droplets containing lysozyme in the tubular epithelial cells.[3] In one study, 74 of 77 Sprague Dawley rats with
histiocytic sarcoma had renal hyaline droplet accumulation.[3] The presence of this feature in rodents with histiocytic sarcoma appears to correlate with tumor burden and is likely associated with overproduction of endogenous protein by the neoplastic cells.[3] Other differentials for eosinophilic droplets within the proximal tubular epithelium of the rat include α-2u globulin nephropathy.[3] In the mouse and rat, chronic progressive nephropathy and other neoplasms may also be associated with hyaline droplet formation.[1]

Immunohistochemistry is helpful to confirm the diagnosis of hematopoietic neoplasms. Macrophages may require a panel of antibodies for diagnosis due to varying phenotypes in different tissue environments.[6] Common antibodies used in the diagnosis of histiocytic sarcoma in the rat include CD68 (ED-1) and lysozyme, among others.[5,6] Lysozyme is also reported in the diagnosis of granulocytic leukemia, in addition to myeloperoxidase (MPO).[6] Antibodies useful in the diagnosis of lymphoma in the rat have also been reported.[6] None of these antibodies,

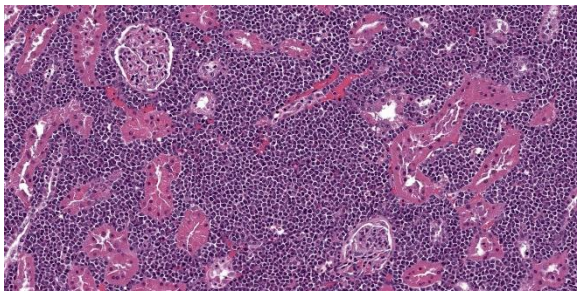

Figure 1-4. Kidney, rat. Similar neoplastic cells infiltrate the renal cortex. (HE, 190X)

unfortunately, are optimized in our laboratory for the rat.

Contributing Institution:
University of Washington Veterinary Diagnostic Lab and Comparative Pathology Program

Department of Comparative Medicine

The Comparative Pathology Program (CPP) | Department of Comparative Medicine (washington.edu)

JPC Diagnoses:
1. Kidney and lymph node: Hematopoietic sarcoma.
2. Renal tubular epithelium: Intracytoplasmic hyaline droplets.

JPC Comment:
This week's moderator was Dr. Michael Eckhaus from the National Institutes of Health who provided a lab-animal centric conference for participants.

In this first case, conference participants debated the exact origin of neoplastic cells, as the reniform nuclei may be seen in neoplasms of both histiocytic and granulocytic origin. To better characterize these neoplastic cells, we ran typical round cell immmunomarkers (IBA1, CD3, CD20, PAX5, MUM1, and lysozyme), all of which were negative. Unfortunately CD34 and myeloperoxidase, markers that should stain cells of myeloid origin were immunonegative as well. The gross description of the greenish nodules (figure 1-1) hints at a granulocytic (myeloid) leukemia origin, but we were unable to confirm their identity with more objective means. Based on the HE appearance, we ultimately agreed with the contributor on the morphologic diagnosis.

This case is also a nice example of hyaline droplets in the kidney of a rat (figure 1-5). While most participants recognized the hyaline droplets and associated them with a diagnosis of histiocytic sarcoma in this case, the droplets (and neoplastic cells) did not stain for lysozyme. Alpha-2u globulin nephropathy is another consideration for these droplets, though this animal did not have any history of chemical exposure. In Alpha-2u globulin nephropathy, hyaline droplets represent secondary lysosomes containing alpha-2u-globulin bound to a variety of chemicals and/or their metabolites with the complex being resistant to proteolytic degradation which promotes accumulation within the cytoplasm.[7] Hyaline droplets are also a normal finding in male rats, albeit at a low background level far less than that seen in this case.

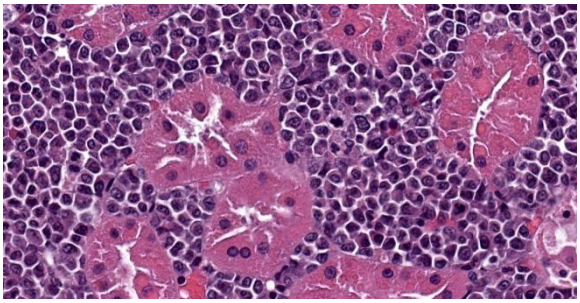

Figure 1-5. Kidney, rat. Proximal convoluted tubular epithelium contains numerous intracytoplasmic protein droplets. (HE, 900X)

References:

1. Decker JH, Dochterman LW, Niquette AL, et al. Association of Renal Tubular Hyaline Droplets with Lymphoma in CD-1 Mice. *Toxicol Pathol*. 2012; 40: 651-655.
2. Frith CH. Morphologic Classification and Incidence of Hematopoietic Neoplasms in the Sprague-Dawley Rat. *Toxicol Pathol.* 1998; 16: 451-457.
3. Frith CH, Ward JM, and Chandra M. The morphology, immunohistochemistry, and incidence of hematopoietic neoplasms in mice and rats. *Toxicol Pathol*. 1993; 21:206-218.
4. Hard GC and Snowden RT. Hyaline Droplet Accumulation in Rodent Kidney Proximal Tubules: An Association with Histiocytic Sarcoma. *Toxicol Pathol*. 1991; 19: 88-97.
5. Ogasawara H, Mitsumori K, Onodera, H et al. Spontaneous Histiocytic Sarcoma with Possible Origin from the Bone Marrow and Lymph Node in Donryu and F-344 Rats. *Toxicol Pathol*. 1993; 21: 63-70.
6. Rehg JE, Bush D, and Ward JM. The Utility of Immunohistochemistry for the Identification of Hematopoietic and Lymphoid Cells in Normal Tissues and Interpretation of Proliferative and Inflammatory Lesions of Mice and Rats. *Toxicol Pathol*. 2012; 40: 345-374.
7. Swenberg JA, Short B, Borghoff S, Strasser J, Charbonneau M. The comparative pathobiology of alpha 2u-globulin nephropathy. *Toxicol Appl Pharmacol*. 1989 Jan;97(1):35-46.

CASE II:

Signalment:

12-week-old male ABCA4 -/- mouse.

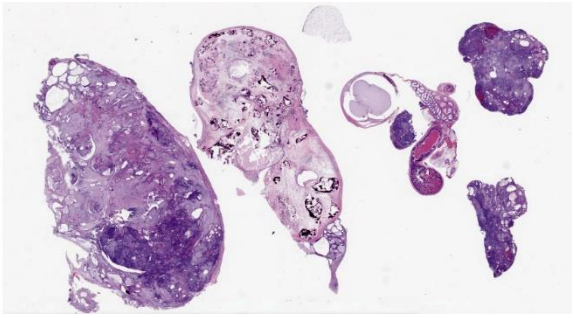

Figure 2-1. Caudal abdominal mass, mouse. Multiple sections of a caudal abdominal mass adjacent to the seminal vesicles is submitted for examination. (HE, 5X)

History:

A 12-week-old male ABCA4 -/- mouse was presented for routine necropsy; no associated clinical signs were reported.

All procedures performed on animals were in accordance with regulations and established guidelines and were reviewed and approved by an Institutional Animal Care and Use Committee or through an ethical review process.

Gross Pathology:

Expanding the abdominal cavity and displacing abdominal organs were multiple variably sized irregular masses. The masses were pale tan and smooth.

Microscopic Description:

Mass: Loosely associated with the seminal vesicle is a well-demarcated, unencapsulated, multinodular neoplastic mass. The densely cellular to cystic neoplasm is composed of variably differentiated neoplastic cells from three, depending on the section, germ cell layers and multiple tissue types. Ectodermal tissue includes neural tissue, including neurons and glial cells, surrounded by neuropil, and multifocal nests and cysts of squamous epithelium with variable keratinization. In addition, fusiform cells arranged in rosettes, suggestive of neuroendocrine origin, are scattered

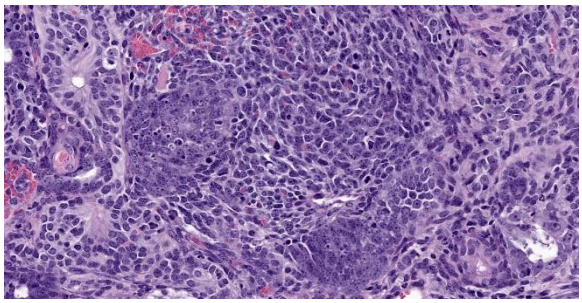

Figure 2-2. Caudal abdominal mass, mouse. Scattered throughout the mass is a population of poorly differentiated pluripotent cells. (HE, 350X)

throughout the mass. Endodermal tissue includes multifocal variably sized tubules lined by cuboidal to columnar epithelial cells. Columnar epithelial cells are often pseudostratified and have apical cilia (respiratory epithelium); goblet cells are interspersed. Mesodermal tissue includes multifocal bundles of smooth muscle, multifocal foci of osteocytes embedded in eosinophilic osteoid and depending on the section, foci of calcified bone, adipose tissue, and rare aggregates of chondrocytes embedded in chondroid matrix (consistent with cartilage). On average, there are less than 1 mitotic figures per high power field.

Contributor's Morphologic Diagnosis:
Abdominal mass, teratoma.

Contributor's Comment:
Although uncommon in domestic animals, teratomas have been reported in a wide variety of veterinary species. In domestic animals teratomas of the testis have been occasionally reported in foals[7], while in laboratory animals, teratomas have been reported in mice, rats, ferrets, and non-human primates.[3,4,8,13] In certain inbred mouse strains, notably 129 mice and its substrains, teratomas have been recognized in the veterinary literature as spontaneous neoplasms since 1954.[4,12] In the 129-mouse strain, a *ter* mutation is responsible for the increase in teratoma incidence.[4]

Thought to arise from multipotent germ cells, teratomas have been reported in multiple tissues including brain, adrenal glands, gonads, uterus.[2,4,10,13] In the nervous system, suprasellar germ cell tumors, like teratomas are most commonly identified on midline.[2] The presence of tissue derived from more than one germinal layer, ectoderm, endoderm, and/or mesoderm, is a requirement for a teratoma diagnosis.[1,7,11] The presence of two or more germinal layers is a result of the initial somatic differentiation of germ cells, giving rise to a variety of tissues that can be present in these tumors.[11] In females, ovarian teratomas are considered parthenogenic tumors, as they are thought to arise from a single germ cell, which has undergone an initial round of meiotic division, but not a second.[11]

Macroscopically, teratomas can be solid and/or cystic, and occasionally contain obvious hair, bone, or teeth.[7,11] Histologically, numerous tissue types have been reported to be components of teratomas, and these various tissue elements can be either mature or immature.[6] In this case, nervous tissues, squamous epithelium, respiratory epithelium, adipose

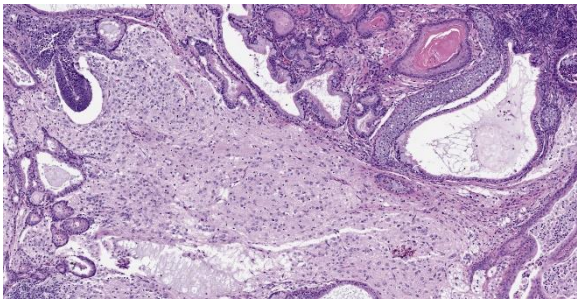

Figure 2-3. Caudal abdominal mass, mouse. Ectodermal tissue in this field includes well-differentiated neuropil with abundant glia, cysts of keratinizing epithelial cells, and cysts lined by ependymal cells. Mesenchymal tissues include well-differentiated cartilage, and several cysts lined by ciliated respiratory epithelium. (HE, 90X).

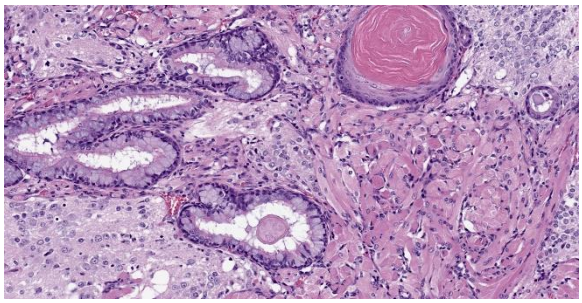

Figure 2-4. Caudal abdominal mass, mouse. Endodermal tissue in this field includes numerous cysts lined by enterocytes and goblet cells adjacent to disorganized bundles of smooth muscle (mesodermal). (HE, 90X)

tissue, smooth muscle, bone, and cartilage were all present. Nervous tissue, adipose tissue, and respiratory epithelium are commonly found in teratomas.[7]

Benign teratomas are characterized by well differentiated tissue, with no significant hemorrhage or necrosis.[5] Benign teratomas do not invade surrounding tissue and do not metastasize, while malignant teratomas have evidence of local invasion and/or metastasize.[4,5] At gross necropsy of this ABCA4-/- mouse, multiple masses were scattered throughout the abdomen, consistent with carcinomatosis and malignant behavior. Although standard histologic evaluation of teratomas is likely sufficient for diagnosis, immunohistochemistry can be employed to highlight the different tissue types.

Contributing Institution:
Pfizer Research and Development
455 Eastern Point Rd.,
Groton, CT 06340
www.pfizer.com

JPC Diagnosis:
Caudal abdominal mass: Teratoma

JPC Comment:
Teratomas are a regular submission to the WSC (Conference 1, Case 4, 2023-2024 and Conference 16, Case 2, 2020-2021). Case 2 is a classic teratoma with a wide array of recognizable tissues from multiple germ cell layers (figures 2-3 through 2-5. Although not needed for this case, histo- and immunohistochemical stains can assist in the recognition of certain tissues. In this case, cartilage is nicely outlined by an Alcian blue pH 1.0 while PAS highlights mucus within goblet cells and basement membranes adjacent to epithelial tissues. Conference participants noted ancillary features such as an inflammatory exudate (sans bacteria) within the cysts lined by respiratory epithelium (however, we refrained from diagnosis any type of pneumonia in this case). There was brief discussion of the potential behavior of this teratoma based on its morphology; participants agreed that the morphology appeared more "benign" than the history provided by the contributor. Other recent WSC submissions have featured more clear examples of malignant behavior with invasion of adjacent issues

Case reports of teratomas have recently been published in cats and in birds.[9,14] Extragonadal teratomas are unusual in domestic animals; two recent feline cases dealt with oropharyngeal teratomas.[14] Similar to human congenital oropharyngeal teratomas, affected cats were young and had masses near the sphenoid bone consistent with an origin from Rathke's

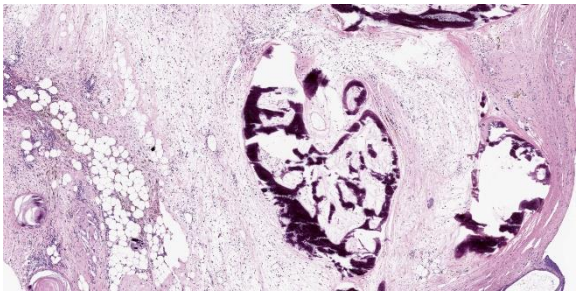

Figure 2-5. Caudal abdominal mass, mouse: Mesodermal tissue in this field includes bone and fat. (HE, 90X).

pouch. In contrast, a coelomic teratoma was described in a 26 year-old eclectus parrot. [9] Despite the mass being well-differentiated, the large size was sufficient to induce increased respiratory effort, lethargy, regurgitation, and adhesions to multiple organs. Although the mass was successfully resected, the bird decompensated and died after surgery.[9] This is an effective reminder that benign neoplasms can still have significant effects on morbidity and mortality.

References:

1. Agnew DW, MacLachlan NJ. Tumors of the Genital Systems. In: Meuten DJ, ed. *Tumors in Domestic Animals, 5th ed*. 2017; Ames, IA, John Wiley & Sons, Inc., p. 689-722.
2. Cantile C, Youssef S. Nervous System, In: Maxie MG, ed. *Jubb Kennedy and Palmer's Pathology of Domestic Animals, 6th ed*. 2016; St. Louis MO, Elsevier Press, vol 1, p. 404.
3. Cline JM, Wood CE, Vidal JD, et al. Selected Background Findings in Interpretation of Common Lesions in the Female Reproductive System in Macaques. *J Toxicol Pathol* 2008; 142S-163S.
4. Creasy D, Bube A, de Rijk E, et al. Proliferative and Nonproliferative Lesions of the Rat and Mouse Male Reproductive System, *J Toxicol Pathol* 2012; 40: 40S-121S.
5. Dixon D, Alison R, Bac U, et al. Nonproliferative and Proliferative Lesions of the Rat and Mouse Female Reproductive System. *J Toxicol Pathol* 2014; 27 (3 & 4 Supplemental):1S-107S.
6. Epstein JI, Lotan TL. The Lower Urinary Tract and Male Genital System. In: Kumar V et al. ed. *Robbins and Cotran Pathologic Basis of Disease.* 9th ed. 2015; Philadelphia, PA, Elsevier Saunders. p. 959-990.
7. Foster RA. Male Genital System, In: Maxie MG, ed. *Jubb Kennedy and Palmer's Pathology of Domestic Animals, 6th ed*. 2016; St. Louis MO, Elsevier Press, vol 3, p. 465-510.
8. Kirejczyk S, Pinelli C, Gonzalez O, et al. Urogenital Lesions in Nonhuman Primates at Two National Primate Research Centers. *Vet Pathol*. 2021 January; 58(1): 147-160.
9. Mayer CC, Richard JN, Lin CM, Conrado FO, Hahn S, Graham JE, Bercier M. Intracoelomic Teratoma in an Eclectus Parrot (Eclectus roratus). *J Avian Med* Surg. 2021 Jul;35(2):217-226.
10. Ogata K, Masahiko K, Miyata K et al. Well-Differentiated Teratoma in a Mouse Uterus. *J Toxicol Pathol* 2011; 39: 901-904.
11. Schlafer DH and Foster RA. Female Genital System, In: Maxie MG, ed. *Jubb Kennedy and Palmer's Pathology of Domestic Animals, 6th ed*. 2016; St. Louis MO, Elsevier Press, vol 3, p. 359-464.
12. Stevens LC and Little CC. Spontaneous Testicular Teratomas in and Inbred Strain of Mice. *Proc Natl Acad Sci USA.* 1954 Nov; 40(11): 1080-1087.
13. Williams BH, Yantis LD, Craig SL, et al. Adrenal Teratoma in Four Domestic Ferrets (*Mustela purorius furo*). *Vet Pathol* 2001; 38: 328-331.
14. Yuzbasioglu-Ozturk G, Gulcubuk A, Ozturk-Gurgen H, Demirutku A, Akcasiz ZN, Ozkul S. An unusual case of oropharyngeal mature teratoma in a kitten. *Iran J Vet Res*. 2023;24(4):365-368.

CASE III:

Signalment:

23.5 year old female rhesus macaque (*Macaca mulatta*).

History:

This monkey had acute, bilateral hind limb paralysis with intact patellar reflexes and an otherwise normal neurologic exam and was euthanized due to welfare concerns. Two years

Figure 3-1. Ovaries and uterus, rhesus macaque. The left ovary (top) is expanded by a 4.5 x 4 x 4 cm mottled tan to red encapsulated mass. The uterus (middle), and right ovary (bottom). (*Photo courtesy of:* Wake Forest School of Medicine, Department of Pathology, Section on Comparative Medicine,www.wakehealth.edu).

prior to euthanasia an adenocarcinoma was excised from the cecum.

Gross Pathology:
A 4.5 x 4 x 4 cm, 34.68 g tan to red firm mass and effaced the left ovary. On sectioned surface the neoplasm was mottled tan to pink with small, scattered areas of central hemorrhage and necrosis. The L1-L2 intervertebral disc had small hemorrhages and was friable.

Microscopic Description:
(The submitted slide includes portions of the ovarian tumor, oviduct, uterus, and ventral segment of the vertebral body.) Left ovary: An encapsulated epithelial neoplasm expands and effaces the entire ovary. The neoplastic cells are arranged in streams, nests and acini on a dense, highly cellular fibrovascular stroma. The cells are closely-spaced, and vary from columnar where forming acini, to spindle-shaped when in streams and along the capsule margin. They have eosinophilic cytoplasm and central nuclei with finely-stippled chromatin and single prominent nucleoli. Many cells are multinucleated, with up to four nuclei. Mitotic figures average 1 per 40x field, with rare bizarre forms. The capsule is invaded by neoplastic cells forming single-file rows. Central necrosis is prominent, and many neutrophils and lymphocytes are scattered throughout. Small rafts of neoplastic cells are present within the adhered myometrium, and in the lumina of uterine vessels.

Vertebra – L2: (ventral aspect of the vertebral body): Approximately 70% of the marrow cavity is effaced by neoplastic cells similar to those described for the ovary, interspersed with pale eosinophilic necrotic cellular debris and blood. Neoplastic acini invade into and through the vetebral cortical bone. The neo-

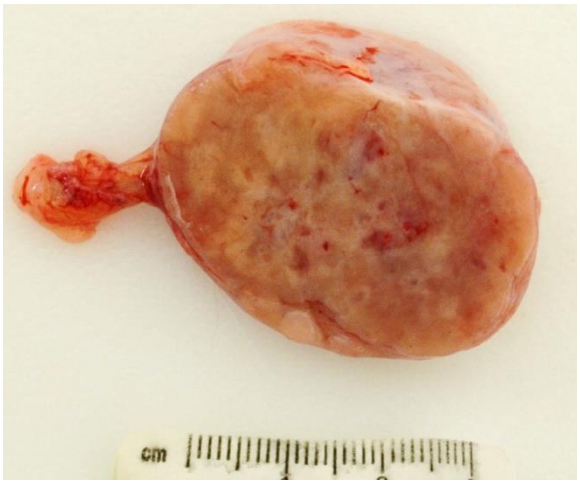

Figure 3-2. Ovary, rhesus macaque. On sectioned surface, the left ovarian neoplasm is mottled tan to red with small scattered areas of central necrosis and hemorrhage, and is contained by a thin fibrous capsule *Photo courtesy of:* Wake Forest School of Medicine, Department of Pathology, Section on Comparative Medicine,www.wakehealth.edu).

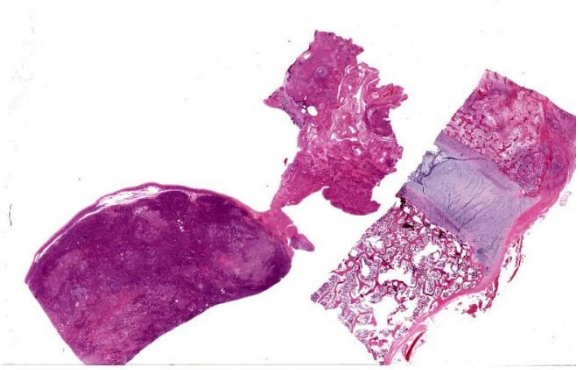

Figure 3-3. Ovary, uterus, vertebra, rhesus macaque. Sections of three organs are submitted for examination. The normal ovarian architecture (bottom left) is effaced by a neoplasm. (HE 4X)

plastic stroma is less pronounced than that in the ovarian lesion. The remaining bony trabeculae have empty lacunae and are unattended by osteoclasts or osteoblasts (necrosis).

Contributor's Morphologic Diagnosis:
Ovarian carcinoma with vertebral and uterine metastases.

Contributor's Comment:
In this case, subsequent histopathologic exam revealed a similar smaller neoplasm to that described above in the contralateral ovary. Ovarian carcinoma is a rarely reported neoplasm in this species,[7] and domestic animals in general.[5] In humans, metastases from the ovary to bone is rare, and in one survey of 1,481 cases of stage IV ovarian carcinoma, only 32 (3.2%) had bone metastases.[1] Bilateral carcinomas are reported in approximately 25% of humans with ovarian cancer,[6] and are relatively common in dogs as well.[5] The dense mesenchymal component of the primary tumor in this case was striking and the morphology did not fit into the common subtypes of ovarian carcinomas described in domestic animals and humans, IE: papillary, cystic, serous, endometrioid, clear cell or mucinous.[5]

In humans, differentiating primary ovarian carcinoma from metastatic intestinal carcinoma often proves challenging, as the ovaries are common metastatic sites. Metastatic intestinal carcinomas often histologically mimic ovarian carcinomas in humans, and while identifying the typical features of metastatic neoplasms may prove useful, none are considered highly specific.[3] Considering the history of intestinal adenocarcinoma in this animal, ruling-out intestinal adenocarcinoma was salient in this case. At necropsy, the entire intestinal tract was closely examined for evidence of recurrence but no gross or histologic intestinal neoplastic lesions were discovered.

Historically, the immunohistochemical (IHC) panel used to differentiate primary ovarian carcinoma from metastatic intestinal carcinoma included cytokeratin-7, cytokeratin-20, carcinoembryonic antigen (CEA) and cancer antigen-125, summarized in Table 1.[3] However, more recent studies have shown that tumors with a mucinous subtype further complicate diagnostics.[4] The contributors determined

Table 1:

Antibodies	Primary ovarian carcinoma	Metastatic intestinal carcinoma	Primary ovarian carcinoma (mucinous)
CK 7	+	-/+	+/-
CK 20	-	+	-/+
CEA	-	+	-/+
CA 125	+	-/+	+/-

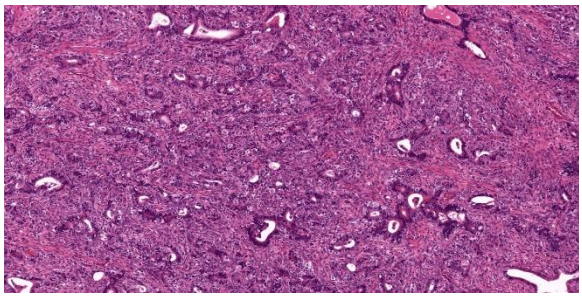

Figure 3-4. Ovary, rhesus macaque. Ovarian architecture is effaced by an epithelial neoplasm in which the neoplastic cells form well-defined tubules and acini on a moderately dense fibrous stroma. (HE, 110X)

that this his particular neoplasm was not mucinous.

Unfortunately the COVID-19 global pandemic precluded the completion of an IHC panel for this case prior to the Wednesday Slide Conference submission deadline, but will be performed at some stage and the results will be submitted.

Contributing Institution:
Wake Forest School of Medicine
Department of Pathology, Section on Comparative Medicine
Medical Center Boulevard, Winston-Salem, NC 27157
www.wakehealth.edu

JPC Diagnoses:
1. Ovary, uterus: Adenocarcinoma.
2. Vertebral body: Metastatic adenocarcinoma.

JPC Comment:
Dr. Eckhaus noted that in his experience, primary ovarian neoplasms are very rare in non-human primates – in his review of nearly 20,000 cases across almost 40 years at the NIH, he noted 4 total cases of ovarian neoplasia that were all benign (three adenomas and one granulosa cell tumor).

Tissue identification proved to be a bit of a problem for participants, as no normal ovarian tissue was present on the slide, and the orientation of the uterus is somewhat problematic. Intestinal adenocarcinoma, a very common malignancy in rhesus macaques, was favored by many participants given the formation of tubules and acini within the mass. This proved to be an important rule out for this case given this animal's previous history (which participants were not privy to before the case discussion). We completed the immunohistochemical panel suggested by the contributor in Table 1 with the exception of CA 125 which was not available in our lab. Neoplastic cells demonstrate strong cytoplasmic immunopositivity for AE1/AE3, consistent with an epithelial neoplasm. CEA, CK 7, and CK 20 were all immunonegative, which likely excludes a metastatic intestinal carcinoma. Other potential differentials that we considered are a fimbrial (oviductal) adenocarcinoma and uterine adenocarcinoma given the proximity of these neoplastic cells to the uterus (figure 3-6). Ultimately, as ovary cannot be identified as a primary site on the submitted HE, we prefer a morphologic diagnosis of carcinoma within the ovary to ovarian carcinoma in this case. (We do believe that the contributors correctly identified ovary at necropsy; it is simply the difficult of making this identification on the

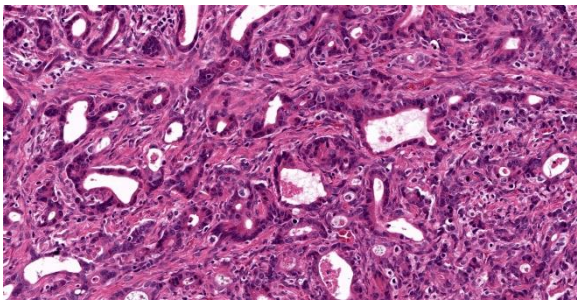

Figure 3-5. Ovary, rhesus macaque. High magnification of neoplastic cells. (HE, 292X)

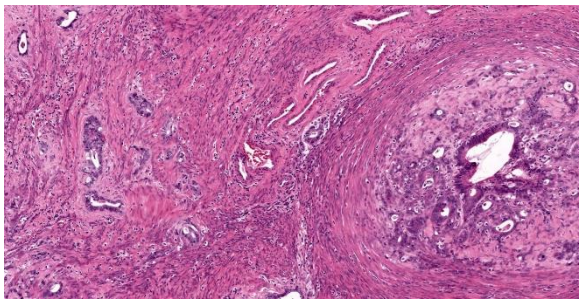

Figure 3-6. Uterus, rhesus macaque. Neoplastic cells infiltrated the mural smooth muscle of the uterus. (HE, 110X)

submitted HE slides which makes us reticent to go "all-in" on this histologic diagnosis as well. Conference participants found the dramatic vertebral changes easier to interpret for this case (figure 3-7).

Although ovarian epithelial neoplasms are rare in NHPs, they are common in human females.[8] Metastases to bone are rarely reported in humans, with a prevalence of approximately 1% in a large cohort study of over 32,000 ovarian carcinoma patients.[8] The frequency of ovarian neoplasms is companion animals is likely adversely impacted by the common practice of ovariohysterectomy, although malignant epithelial tumors do occur in female dogs. In a recent retrospective, 4 out of 18 dogs with malignant ovarian tumors had metastasis to regional lymph nodes, the lung, and/or the brain – bone is not a common site for metastasis in the dog, either.[2]

References:

1. Deng K, Yang C, Tan Q, et al. Sites of distant metastases and overall survival in ovarian cancer: A study of 1481 patients. *Gynecol Oncol*. 2018;150**:** 460-465.
2. Goto S, Iwasaki R, Sakai H, Mori T. A retrospective analysis on the outcome of 18 dogs with malignant ovarian tumours. *Vet Comp Onco*l. 2021; 19: 442–450.
3. Kir G, Gurbuz A, Karateke A, Kir M. Clinicopathologic and immunohistochemical profile of ovarian metastases from colorectal carcinoma. *World J Gastrointest Surg*. 2010;2**:** 109-116.
4. Lin X, Lindner JL, Silverman JF, Liu Y. Intestinal type and endocervical-like ovarian mucinous neoplasms are immunophenotypically distinct entities. *Appl Immunohistochem Mol Morphol*. 2008;16**:** 453-458.
5. Meuten DJ. *Tumors in domestic animals*, Fifth edition. ed. pp. viii, 989 pages. Ames, Iowa: Wiley/Blackwell; 2017.
6. Micci F, Haugom L, Ahlquist T, et al. Tumor spreading to the contralateral ovary in bilateral ovarian carcinoma is a late event in clonal evolution. *J Oncol*. 2010;2010**:** 646340.
7. Simmons HA, Mattison JA. The incidence of spontaneous neoplasia in two populations of captive rhesus macaques (Macaca mulatta). *Antioxid Redox Signal*. 2011;14**:** 221-227.
8. Zhang C, Guo X, Peltzer K, et al. The prevalence, associated factors for bone metastases development and prognosis in newly diagnosed ovarian cancer: a large population based real-world study. *J Cancer*. 2019 Jun 2;10(14):3133-3139.

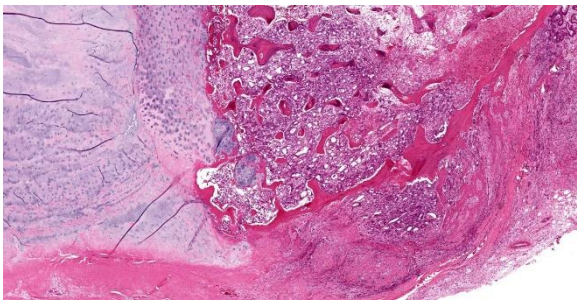

Figure 3-7. Vertebra, rhesus macaque. There is a metastatic focus within the vertebral body, resulting in loss of both trabecular and lamellar bone and resulting in a focus of periosteal new bone growth over the neoplasm. (HE, 27X)

CASE IV:

Signalment:
Adult, male African Green monkey (Chlorocebus sabeus).

History:
An adult male African green monkey had been wild caught on St. Kitts and arrived in quarantine in Maryland in November 2023 with limited clinical history prior available to September 2023.

He had four physical exams during September and October 2023 at the holding/shipping facility on St. Kitts which were unremarkable. He had received four doses of ivermectin and two doses of Drontal plus at the holding facility.

During the initial quarantine examination in November, he was noted to have mild bradycardia and a superficial injury on his distal tail. His appetite was reduced for biscuits, but he was interested in some fruit. On the technician recheck several days later he was noted to fall off his perch when stimulated. During the veterinary cage-side exam, he was bright, alert, and responsive. His head consistently tilted to the right during the exam. When gently stimulated he readily got off the perch and immediately circled to the right 1-2 times. This circling was repeatable and consistent to the right. No ataxia or nystagmus was appreciated. He was started on cerenia and appetite monitoring. A behavior consult was unremarkable. His reduced appetite continued through weekend. He was noted to have a possible right sided-tongue deviation on December 2nd but otherwise clinical signs remained relatively static (R sided head tilt w/right sided circling). Endoparasitology was positive for *Schistosoma mansoni* ova by fecal floatation exam on December 4th. Euthanasia was elected due to poor prognosis, and he was submitted for necropsy two days later.

Figure 4-1. Cerebrum, African green monkey. One section of cerebrum is submitted for examination. at subgross magnification, there is multifocal hypercellularity within the meninges and Virchow-Robin's spaces. (HE, 5X)

Gross Pathology:
A male African Green monkey was submitted following euthanasia with a history of a positive finding of *Schistosoma mansoni* on recent fecal endoparasite examination. The monkey was well-hydrated, well-muscled and contained adequate body fat. On examination of the chest cavity, there were mild adhesions between the left caudal lung lobe and the thoracic wall. The lung lobes were congested with no evidence of pneumonia and these lobes floated in formalin. The heart, kidneys, liver, gallbladder, spleen, pancreas and lymph nodes appeared normal. The stomach contained a moderate amount of ingesta and formed content was present in the colon. No abnormalities were noted involving the mesentery or mesenteric lymph nodes. The urinary bladder and testes appeared normal. The brain appeared grossly normal.

Laboratory Results:
Endoparasitology was performed and was positive for *Schistosoma mansoni* ova and Entamoeba sp.

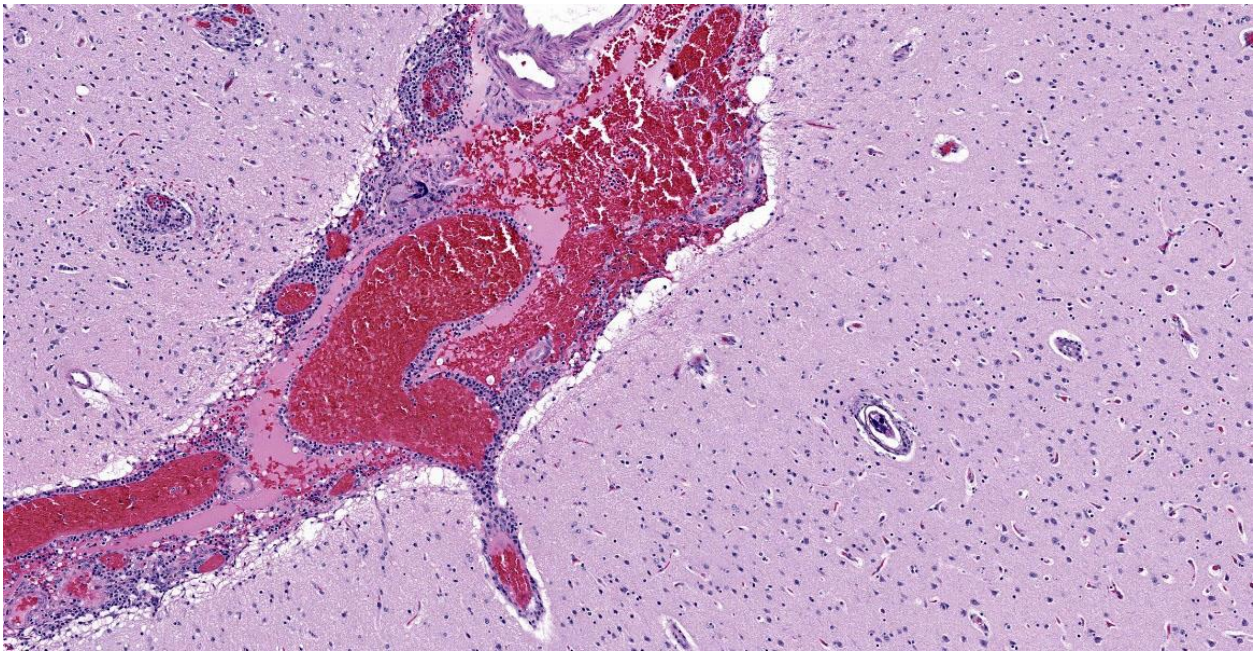

Figure 4-2. Cerebrum, African green monkey. Meninges and Virchow-Robins spaces are expanded by numerous macrophages, lymphocytes and plasma cells as well as hemorrhage. Within the parenchyma, there are scattered microgranulomas which are centered on schistosome eggs. (HE, 83X)

Microscopic Description:
Histopathology revealed multiple small granulomas throughout the hepatic parenchyma containing Schistosoma ova. A solitary granuloma containing a Schistosoma ova was noted in one of several lung sections. Mild nonuppurative pulmonary perivasculitis was present. Examination of sections of cerebrum, cerebellum, medulla and spinal cord revealed meningoencephalitis with multiple granulomas containing Schistosoma ova in the cerebrum, cerebellum and medulla. Sections of the middle/inner ears appeared normal. No other histologic lesions were noted.

Contributor's Morphologic Diagnosis:
Cerebrum: encephalitis, granulomatous, multifocal containing *Schistosoma mansoni* ova.

Contributor's Comment:
Schistosomiasis (also known as bilharziasis) is named after Theodor Bilharz, a German surgeon who discovered *S. haematobium* in 1851.

Schistosomiasis is a major problem worldwide with over 230 million people infected and approximately 200,000 deaths annually. It has been reported in over 52 countries primarily affecting the Eastern Mediterranean, South American, Africa, and the Caribbean.[11] The cause is a blood borne trematode, *Schistosoma sp*. with three primary species – *S. mansoni*, *S. japonicum* and *S. haematobium*. Laboratory identification commonly relies on identification of parasitic eggs in fecal material. The morphology of the eggs is characteristic for each species with *S. mansoni* having a distinct lateral spine.

The life cycle of *Schistosoma mansoni* is complex and indirect, requiring infection of an intermediate freshwater *Biomphalaria* snail.

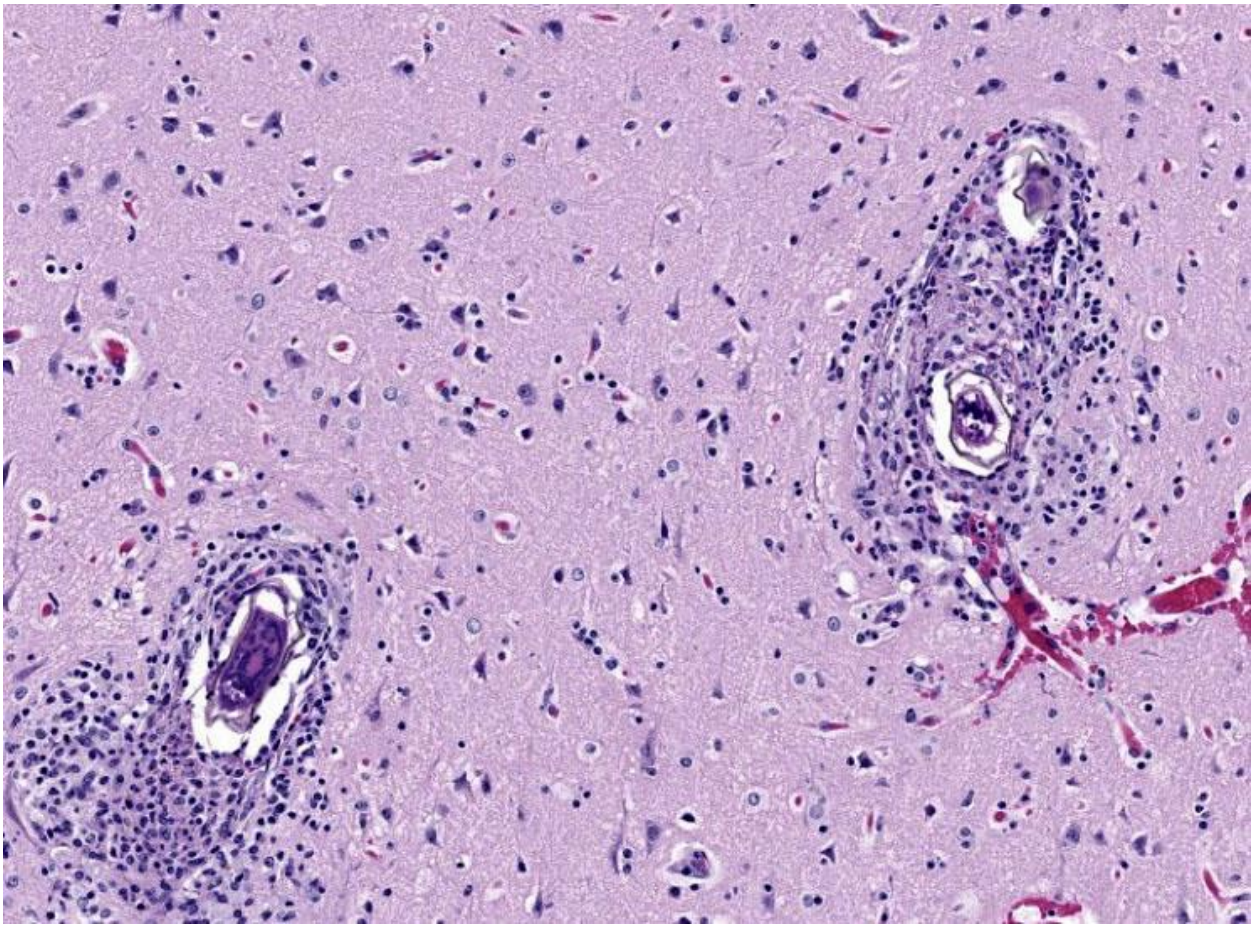

Figure 4-3. Cerebrum, African green monkey. Higher magnification of microgranulomas containing schistosome eggs. Eggs are surrounded by a yellow-brine hyaline shell and often contain a miracidium. (HE, 151X)

Cercariae are released after 4-6 weeks from infected snails and may survive up to 72 hours.

Cercariae attach to the skin of definitive hosts and penetrate the skin to enter dermal vessels, ultimately reaching the pulmonary and hepatic vasculature with maturation to adults in mesenteric veins. Male and female adults maintain a copulatory union in the mesenteric vessels. Ova travel to the lumen of the intestinal tract, are shed in feces, and hatch to free swimming cercariae which can survive up to 3 weeks before infecting appropriate snails to complete the life cycle.[11]

Schistosomiasis is a significant zoonotic disease. While humans are the definitive host, other vertebrate animals may play a significant role with the ability to transmit the agent within the environment. Wild rodents, domesticated animals, and nonhuman primates can serve as additional hosts for this infection.[2] Nonhuman primates including African green monkeys, patas monkeys, chimpanzees, and baboons have become infected with *Schistosoma mansoni* in a number of different African and Caribbean countries.[5] In 2019, an African green monkey from St. Kitts tested positive on fecal examination for *S. mansoni*. This was the first positive report in an African green monkey on St. Kitts after the island was declared negative for the presence of *S. mansoni* during the preceding 50 years.[6]

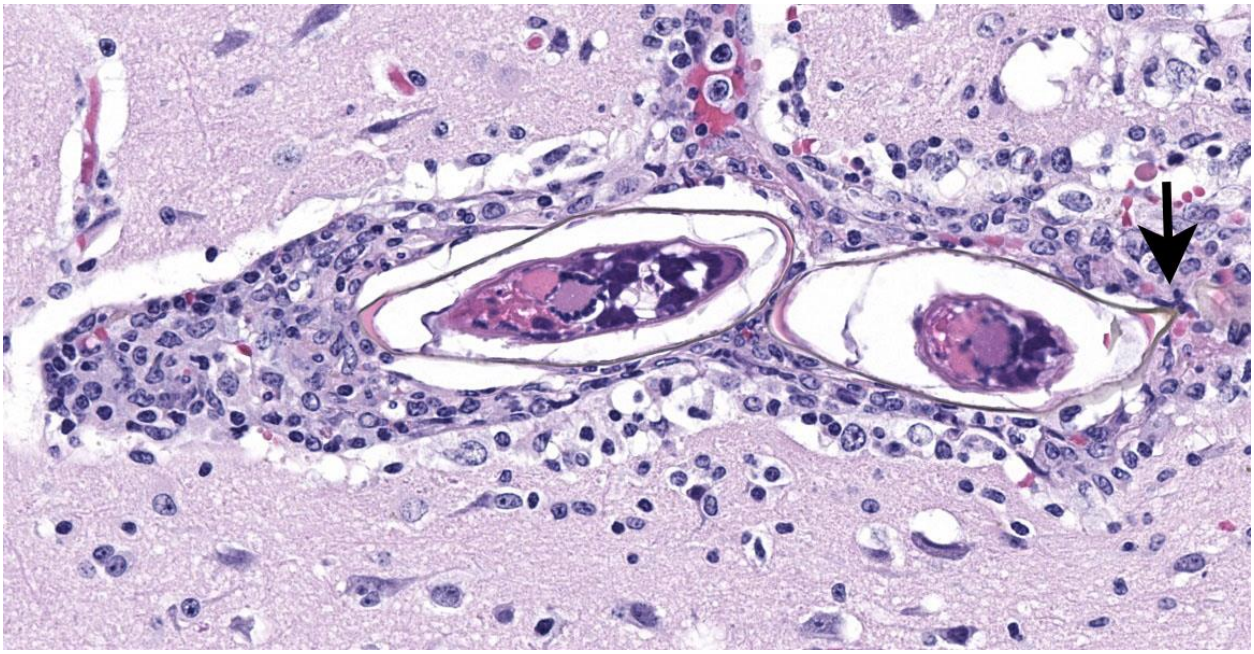

Figure 4-4. Cerebrum, African green monkey. High magnification of schistosome eggs. A lateral spine is present on one (arrow).

Diagnosis of *Schistosoma mansoni* relies primarily on endoparasitologic examination of fecal matter for shed ova. Due to possible discontinuous and insufficient shedding of ova

fecal examination should be conducted analyzing several samples collected on alternate days. PCR analyses for *Schistosoma* ITS-2 DNA sequence can be employed and indirect serologic assays are also available. Clinical findings may include fever, hepatosplenomegaly, eosinophilia and possibly CNS

signs.[8] The treatment of choice for schistosomiasis is praziquantel which targets adult parasites. The drug induces paralysis of the adult parasites which detach from vessel walls allowing the ability of host's immune responses to target the parasites. Additional drug therapies and several vaccines are currently in development.[8]

Morbidity is primarily due to the significant antigenicity of the circulating ova which may reach a variety of organs/tissues including the liver, spleen, lung, intestinal tract, testes, epididymis, prostate, uterus, eye, brain and spinal cord.[4] The inflammatory cell reaction in schistosomiasis is principally due to the intense granulomatous reaction to the dispersed ova. Ova become surrounded by T and B lymphocytes, epithelioid macrophages, foreign body type giant cells, eosinophils, and limited numbers of neutrophils. Chronic infection results in the development of fibrosis with collagen deposition (1). Numbers of studies of the granulomas have identified various lymphocytic subsets including B cells, Th17 cells and Treg cells, as well as various cytokines, chemokines and vascular endothelial factor.[3]

Neurologic involvement of *Schistosoma mansoni* infection can affect both the brain and spinal cord. The development of CNS signs depends on the relative numbers of ova within the brain and spinal cord and the severity of the accompanying inflammatory cell reaction. Clinical signs may include ataxia, nystagmus, visual impairment, and seizures. Vascular embolization of individual eggs is the most common mode for CNS involvement.[7]

Contributing Institution:
Diagnostic and Research Services Branch, Division of Veterinary Resources, National Institutes of Health, Bethesda, Maryland

JPC Diagnosis:
Cerebrum: Meningoencephalitis, granulomatous and eosinophilic, multifocal to coalescing, moderate with perivascular schistosome eggs.

JPC Comment:
The final case of this conference features a short description and an interesting backstory. Dr. Eckhaus actually submitted this case and was intently interested in the development of this lesion given the lack of overt pathology at necropsy. From subgross (figure 4-1), perivascular basophilia is indicative of the inflammatory response elicited by circulating schistosome ova within and extending from blood vessels (figure 4-2). Recognizing that these granulomas are centered on blood vessels and the lack of other life stages in section (larva or adult) is helpful for ruling out other metazoan parasites as the cause of the meningoencephalitis in this case. We were able to speciate the schistosome as *S. mansoni* by the distinct lateral spine (figure 4-4, arrow) which *S. japonicum* and *S. haematobium* lack. Conference participants briefly reviewed other sections of this case provided by Dr. Eckhaus, but were unable to identify adult schistosomes in section. As this animal was dewormed with praziquantel multiple times before developing overt clinical disease, it is likely that deworming likely removed adult trematodes from the vessels, but had no effect on the eggs already present within the bloodstream or perivascular tissues.

Finally, we elaborate further on the connection between granulomas and the life cycle of *Schistosoma*.[9,10] The ova of *S. mansoni* are metabolically active and highly antigenic, a combination that allows them to recruit inflammatory cells as a means to migrate from blood vessels into the lumen of the gut for excretion.[9,10] The ova secretes factors to potentiate attachment to the endothelium as well as bias the immune response of the host towards a Type 2 (Th2) response with marked increases in IL-4, -5, and -13.[9,10] Interestingly, these same proteins can also upregulate cellular adhesion molecules such as ICAM-1 on endothelial cells and increase recruitment of inflammatory cells to the nascent granuloma. The exact mechanism of movement through the extracellular milieu is unclear, though the role of M2 macrophages and matrix metalloprotease activity is likely.[9] Fibrosis induced by the M2 phenotype may also partially protect ova from eosinophils and basophils.[10] In addition, ova also have the ability to increase plasminogen activation which serves to clear fibrin and fibronectin alike. Likewise, how exactly the ova 'eggs-its'[9] out of this granuloma to enter the gut lumen has not been described, though interactions between the ova, gut microbiome, and macrophages are a possibility. Interestingly, humans and mice models with T-cell deficiencies shed fewer ova in their feces, highlighting the role of Th2 polarity in the life cycle of this parasite.

Finally, the timing of this immune relationship is key as immature ova do not recruit inflammatory cells and evade (initially) granuloma formation.[10] Additionally, schistosome ova only undergo development within the host. Together, this may be adaptive in that it ensures viable, developed miracidia are ready to be released to continue the life cycle.

References:

1. Carvalho OA. Mansonic neuroschistosomiasis. *Arq Neuropsiquiatr*. 2013 Sep;71(9B):714-6.
2. Modena CM, dos Santos Lima W, Coelho PM. Wild and domesticated animals as

reservoirs of Schistosomiasis mansoni in Brazil. *Acta Trop*. 2008 Nov-Dec;108(2-3):242-4.
3. Giorgio S, Gallo-Francisco PH, Roque GAS, Flóro E, Silva M, Granlulomas in parasitic diseases: the good and the bad. *Parasitol Res*. 2020 Oct;119(10):3165-3180.
4. Gryseels B. Schistosomiasis. *Infectious Disease Clinics of North America*; June 2012, 383-397.
5. Kebede T, Bech N, Allienne JF, Olivier R, Erko B, Boissier. Genetic evidence for the role of non-human primates as reservoir hosts for human schistosomiasis._*J.PLoS Negl Trop Dis*. 2020 Sep 8;14.
6. Ketzis JK, Lejeune M, Branford I, Beierschmitt A, Willingham AL. Identification of *Schistosoma mansoni* Infection in a Nonhuman Primate from St. Kitts More than 50 Years after Interruption of Human Transmission. *Trop Med Hyg*. 2020;103(6):2278-2281.
7. Llanwarne F, Helmby H. Granuloma formation and tissue pathology in Schistosoma japonicum versus Schistosoma mansoni infections. Parasite Immunol. 2021 Feb;43(2):e12778.
8. Ponzo E, Midiri A, Manno A, Pastorello M, Biondo C, Mancuso G. Insights into the epidemiology, pathogenesis, and differential diagnosis of schistosomiasis. Eur J Microbiol Immunol (Bp). 2024 Mar 18;14(2):86-96.
9. Schwartz C, Fallon PG. Schistosoma "Eggs-Iting" the Host: Granuloma Formation and Egg Excretion. *Front Immunol*. 2018 Oct 29;9:2492.
10. Takaki KK, Rinaldi G, Berriman M, Pagán AJ, Ramakrishnan L. Schistosoma mansoni Eggs Modulate the Timing of Granuloma Formation to Promote Transmission. *Cell Host Microbe*. 2021 Jan 13;29(1):58-67.
11. Verjee MA. Schistosomiasis: still a cause of significant morbidity and mortality. Res *Rep Trop Med*. 2019;10:153–63.

Joint Pathology Center
Veterinary Pathology Services

WEDNESDAY SLIDE CONFERENCE 2024-2025

Conference #7 02 October 2024

CASE I:

Signalment:
8-year-old, male castrated, 20.3 kilograms crossbreed dog (*Canis lupus familiaris)*

History:
The dog was rescued by a local animal shelter and presented to Ross University Veterinary Clinic for panting. All vitals and hematologic and serum chemical analysis results were within the reference range. Two weeks later, the dog was presented again for evaluation of difficulty breathing, non-productive cough, and inappetence. On physical examination of the most recent consultation, the dog was depressed with a lowered head carriage and showed signs of dyspnea and abdominal breathing. Auscultation revealed muffled heart sounds. The veterinarian discussed the possibility of a late-stage tumor and suggested euthanasia if the condition deteriorated due to quality-of-life concerns. The patient presented again five days later with worsened respiratory distress and recurrence of pleural effusion. Euthanasia was elected.

Gross Pathology:
Abdominal ultrasonography revealed splenomegaly with abnormal echogenicity. Thoracic radiographs showed pleural effusion, loss of silhouette sign, and nodular interstitial pattern of the lungs. Thoracocentesis drained out approximately 1.15 litters of serosanguineous fluid from each side. On thoracic radiographs, after thoracocentesis, a persistent opacity was noted in the left caudal lung field. On skeleton radiographs, marked thickening and deformity of long bones with periosteal new bone formation was noted on distal bones of both front and hindlimbs, including the humerus, radius, carpus, tibia, ulna, metatarsal, and metacarpal bones.

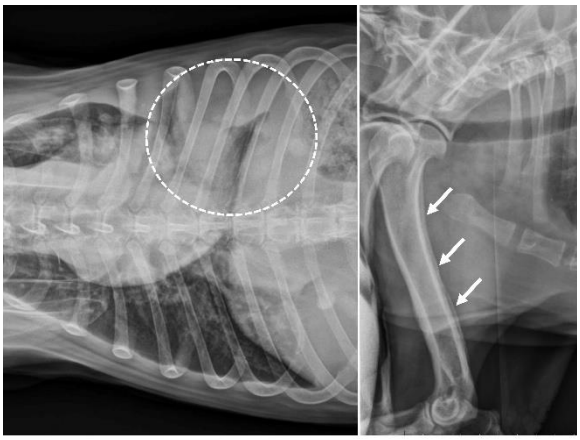

Figure 1-1. Survey radiographs, dog. Thoracic radiographs showed pleural effusion, loss of silhouette sign, and nodular interstitial pattern of the lungs. Thickening and deformity of long bones with periosteal new bone formation was noted on bones of the appendicular skeletal, including the humerus (arrows). (*Photo courtesy of:* Ross University School of Veterinary Medicine, St. Kitts, West Indies www.veterinary.rossu.edu).

On autopsy, approximately 90% of the left caudal lung lobe was infiltrated by a raised, moderately firm, irregularly shaped tan-white mass, 10-cm in largest diameter, with areas of hemorrhage, necrosis, and mucus on cross-sections. The rest of the lung lobes contained multifocal white raised nodules up to 1 cm in

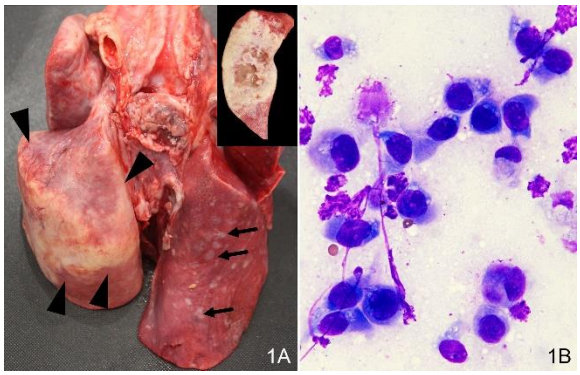

Figure 1-2. Lung, dog. A) Approximately 90% of the left caudal lung lobe is infiltrated by a raised, moderately firm, irregularly shaped tan-white mass, 10-cm in largest diameter. The rest of the lung lobes contained multifocal white raised nodules up to 1 cm in diameter. B) Cytologic demonstrates numerous pleomorphic polygonal cells admixed with fewer neutrophils. (*Photo courtesy of:* Ross University School of Veterinary Medicine, St. Kitts, West Indies, www.veterinary.rossu.edu).

diameter. The costal, mediastinal, and diaphragmatic pleura contained foci of white fibrotic plaques and adhesions to the pericardium. The pericardium was diffusely thickened with multiple coalescing white raised nodules. The distal esophagus near the cardia was thickened and had a 7-cm-diameter cystic lesion containing yellow viscous fluid. The spleen was attached to the omentum and contained a 2.5 cm round nodule near the attachment site. The caudal pole of the left kidney contained multiple raised grey to brown nodules extending to the renal cortex and appeared to be cystic on cross sections.

Laboratory Results:

In the past four months before the last consultation, serial hematologic and serum chemistry analysis during routine checkups showed a combination of mild mature neutrophilia (13.44 X 10^3 neutrophils/µL; reference interval, 3.00 X 10^3 to 12.00 X 10^3 neutrophils/µL), mild non-regenerative anemia, and mild hyperglobulinemia (5.6 g/dL; reference interval, 2.3 to 5.2 g/dL). On serologic qualitative test (Snap 4Dx Plus test, IDEXX laboratories Inc), the dog tested negative for heartworm disease, ehrlichiosis, Lyme disease, and anaplasmosis.

Table 1: Immunochemistry panel (lungs)

Marker	Results
Cytokeratin	80-90% positivity
Thyroid transcription factor 1	60-75% positivity
Napsin A	40% positivity

Microscopic Description:

Lungs: focally and extensively effacing the pulmonary parenchyma is a nonencapsulated, non-demarcated infiltrative neoplasm forming islands, tubules, and acinar structures and loss of polarity with intraluminal papillary projections, supported by a prominent fibrovascular stroma, admixed with areas of necrosis and inflammation characterized by a moderate to high number of viable and degenerate neutrophils, lymphocytes and plasma cells with the

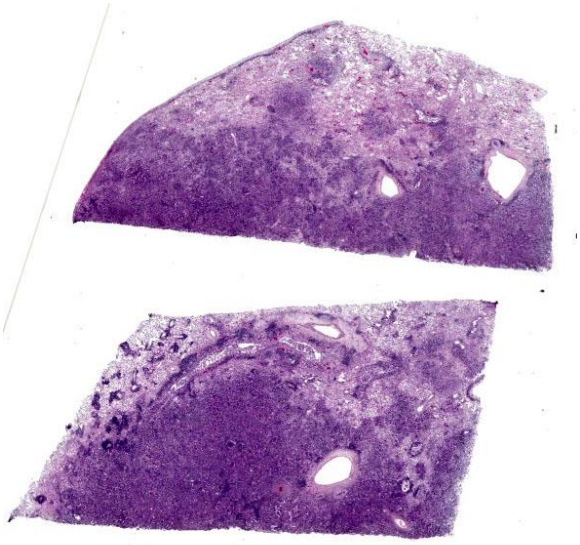

Figure 1-3. Lung, dog. Two sections of lung are submitted for examination. Effacing approximately 66% of the pulmonary architecture is vaguely nodular, unencapsulated, poorly demarcated neoplasm. (HE, 4X)

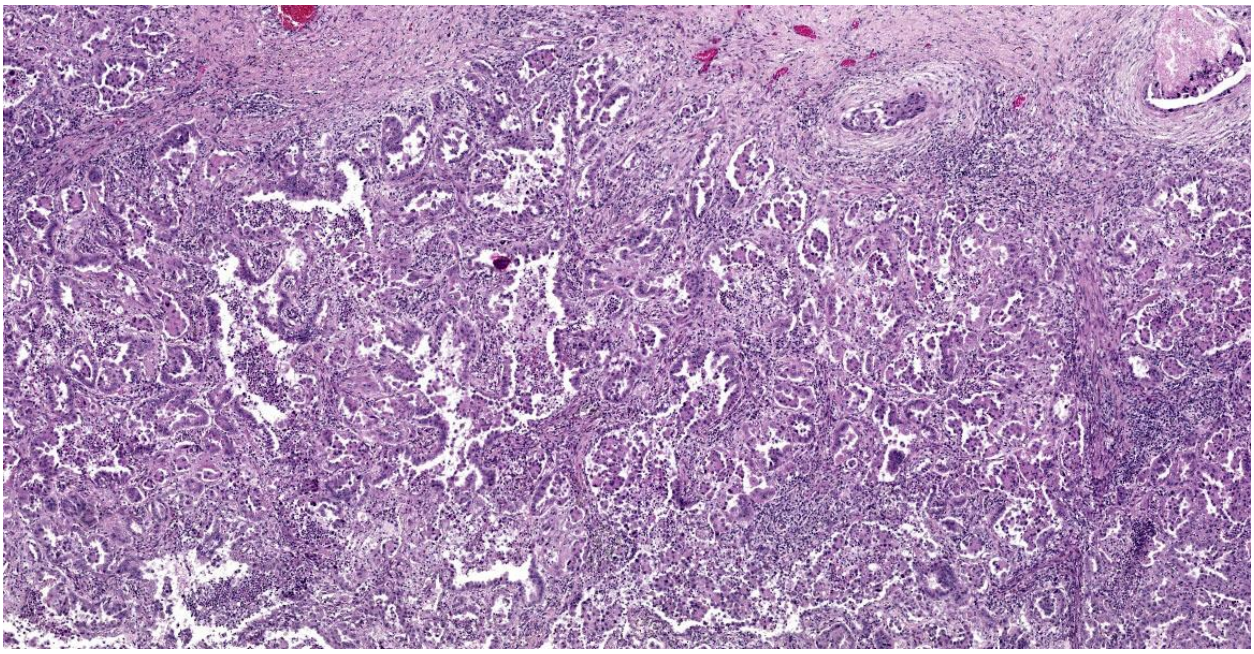

Figure 1-4. Lung, dog. Alveoli, bronchioles, and vessels contain neoplastic cells. (HE, 58X)

odd apoptotic cell. The neoplastic cells are pleomorphic (columnar to polyhedral) and lined the remnant of pulmonary airways with round to oval and basal nuclei. Moderate to high anisocytosis, anisokaryosis, often karyomegaly, and multinucleation with up to three nuclei are noted in the cell population. The cytoplasm of these cells is eosinophilic, finely granular to vacuolated. Mitotic count is 14 per 2.37 mm^2 with atypical mitotic figures. Satellite neoplastic cell clusters are seen in the airways (mostly bronchioles), and lymphovascular invasion is also present. Adjacent to the neoplasm, inside alveolar spaces, there are many foamy macrophages. Diffusely the pleura is expanded by a moderate amount of fibrovascular tissue.

Contributor's Morphologic Diagnosis:
Pulmonary adenocarcinoma, acinar and papillary type.

Contributor's Comment:
Respiratory distress in dogs can be associated with a variety of conditions, including congestive heart failure, upper airway obstruction, and pulmonary tumors. A multimodal approach is often required to investigate the cause of a dyspneic dog. Besides clinical history and physical examination, thoracic radiographs are considered the most important diagnostic test for pets with lung disease because imaging studies can provide a wealth of information on the presence, location, and intensity of the abnormality to guide differential diagnosis and diagnostic plans.[1] Though fine-needle aspiration of the pulmonary parenchyma can be viewed as a relatively invasive technique, it is inexpensive and safe and its result turnaround period is fast and should be considered when evaluating animals with a nodular lung pattern noted on imaging studies.

Primary lung tumors are relatively uncommon in domestic animals. However, pulmonary adenocarcinoma is the most commonly diagnosed primary pulmonary tumor in dogs.[4,6] The most frequent clinical sign associated with pulmonary carcinoma in dogs was coughing (52%), followed by dyspnea (24%), lethargy (18%), and weight loss (12%).[5] How

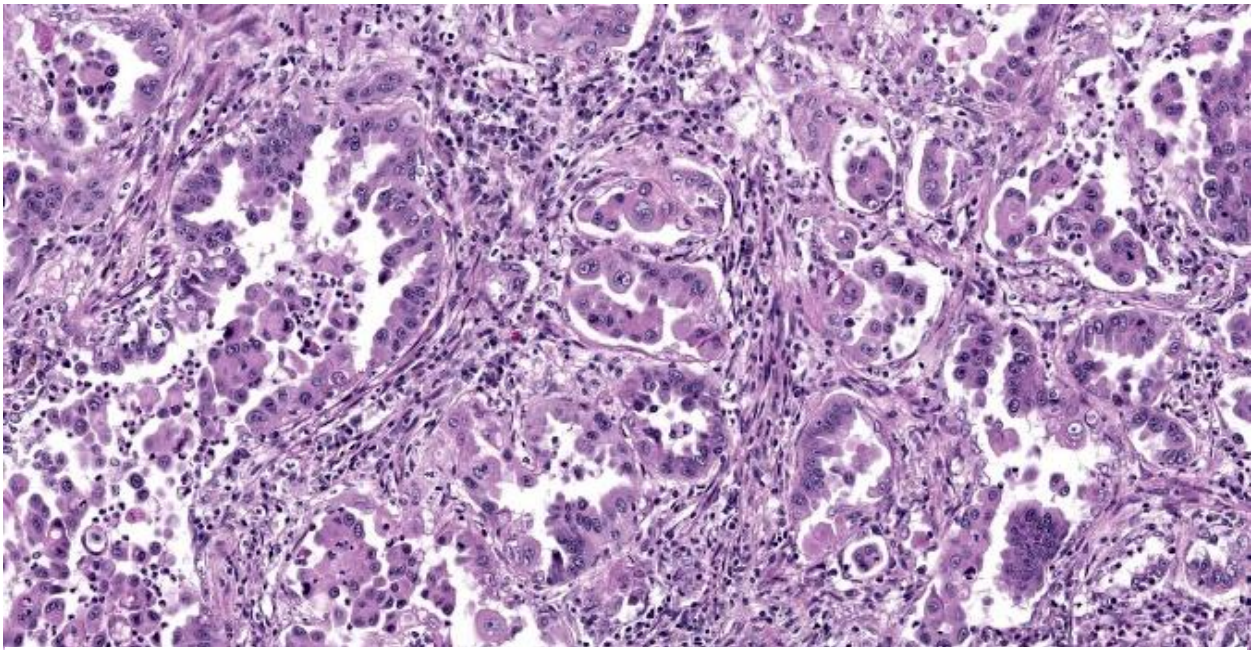

Figure 1-5. Lung, dog. Alveoli and airways are lined by pleomorphic columnar epithelial cells which form papillary projections. There are numerous viable and degenerate neutrophils admixed with cellular debris within some airway lumina that contain neoplastic cells, and numerous lymphocytes and plasma cells within the fibrotic stroma of the neoplasm. (HE, 222X)

ever, in the same survey, 25% of the pulmonary carcinoma cases were incidental findings with no evident clinical signs of respiratory disease before diagnosis.

The lung is also a frequent site for tumor metastasis, and it can sometimes be difficult to differentiate primary pulmonary neoplasms from metastatic neoplasms originating from another location. Immunohistochemistry on thyroid transcription factor-1 (TTF-1) and Napsin A are recommended to confirm the diagnosis of primary pulmonary neoplasia.[7] In the present case, within the lungs, the pulmonary adenocarcinoma had spread through bronchial invasion and re-aspiration with intra-airway seeding in other lobes and lymphovascular invasion The neoplasm also disseminated to the pericardium and esophageal serosa, most likely through direct extension. The fibrous pleuritis was thought to be from the rubbing effects of the neoplasm between the pulmonary and parietal pleura. The hypertrophic osteopathy demonstrated by the thickening of cortical bones is a common paraneoplastic syndrome associated with thoracic space-occupying lesions,[6] of which the exact mechanism is still unknown. The combination of hyperglycemia and mild mature neutrophilia supports that the patient was under stress and, in combination with the mild nonregenerative anemia, likely represented a result of chronic disease, such as cancer.

Contributing Institution:
Department of Biomedical Sciences
Ross University School of Veterinary Medicine, St. Kitts, West Indies
www.veterinary.rossu.edu

JPC Diagnosis:
Lung: Pulmonary adenocarcinoma.

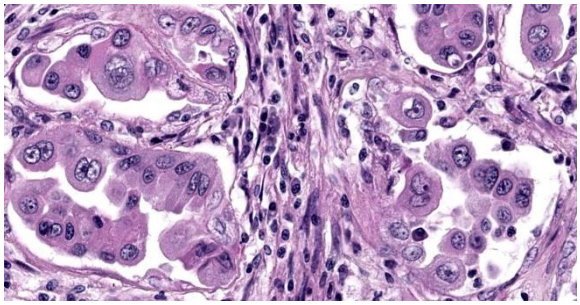

Figure 1-6. Lung, dog. High magnification of pleomorphic neoplastic cells. (HE, 554X)

JPC Comment:
This week's moderator was Dr. Taryn Donovan who is the head of Anatomic Pathology at the Animal Medical Center (AMC) in New York City. The conference cases had a decidedly cardiopulmonary emphasis with the first case being an opportunity to revisit the nomenclature of pulmonary neoplasms. Conference participants noted that the exact pattern of this adenocarcinoma was difficult to pin down with examples of papillary, acinar, and lepidic patterns all within the same neoplasm though this distribution was hardly uniform (figures 1-4 and 1-5). Dr. Donovan emphasized that morphology has diagnostic significance in the human literature[3] though data (and relative importance) is still being weighed in domestic animals. In particular, lepidic patterns (growth along a pre-existing alveolus) may be important if it is the only or predominant pattern as the lack of disruption of the existing pulmonary architecture may include some benign diagnoses such as bronchioalveolar hyperplasia and less aggressive neoplasms (*in situ* and minimally invasive carcinomas) that carry a better prognosis.[3]

Conversely, patterns that disrupt existing pulmonary architecture (e.g. papillary) are far more likely to be associated with an invasive neoplasm and poorer prognosis. Although not conducted for this case, a Verhoeff-Van Gieson stain for elastic fibers may help to illustrate this concept as papillary patterns will lack elastin fibers. Conference participants also discussed micropapillary patterns which are noted to confer the worst prognosis though this nomenclature has not caught on in the veterinary literature. Dr. Donovan described this pattern as 'florettes' with clustering of small numbers of neoplastic cells within alveolar spaces that lacked the more robust stalk of supporting stroma of a true papillary pattern (figure 1-6). Participants also noted evidence of lymphovascular invasion in section with neoplastic cells within a lymphoid vessel, though distinguishing this from an acinar pattern with surrounding myofibroblastic stroma (and an adjacent micropapillary focus) prompted some careful second looks among the group. Dr. Donovan noted 50% of canine and 38% of feline cases in a recent literature meta-review noted a papillary pattern as the predominant morphology of primary pulmonary tumors among the articles[4] reviewed.

As the contributor notes, delineating the origin of pulmonary masses requires consideration of both primary and metastatic neoplasia. We ran IHCs for AE1/3, TTF-1, CK7, Napsin A, vimentin, and P40. Our results mirrored the contributor's (figure 1-7). Neoplastic cells were also modestly immunoreactive for CK7, but not for P40 (marker for squamous differentiation). Altogether, these findings confirm the diagnosis of a primary lung adenocarcinoma. One interesting feature of this case was that select neoplastic cells also expressed vimentin, consistent perhaps with a change in phenotype i.e. epithelial to mesenchymal transition (EMT)[2], though this can also be a feature of poorly differentiated carcinomas as well. EMT of type II pneumocytes is coordinated via cytokines in response to disruption of normal lung architecture – in neoplasia, this also is associated with increased ability of transitioning cells to invade.[2]

Lastly, this case features ancillary diagnostics that are worth a quick look. The contributor

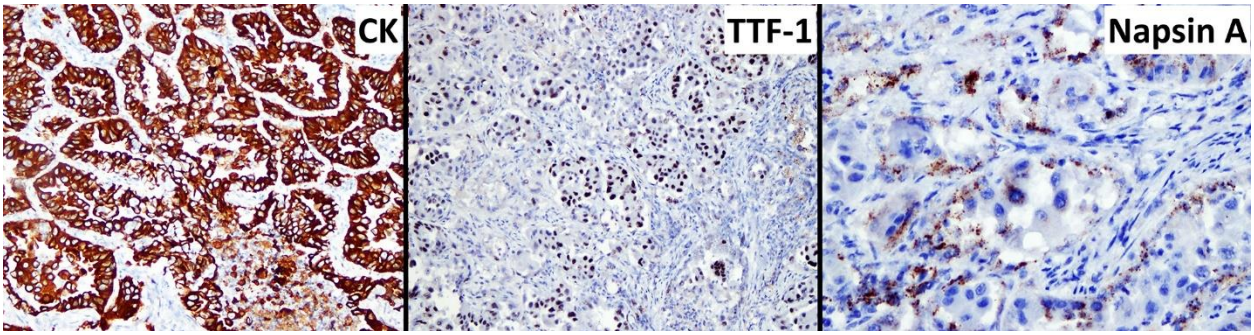

Figure 1-7. Lung, dog. Neoplastic cells demonstrate strong immunopositivity for cytokeratin, and scattered immunopositivity for thyroid transcription factor-1 and napsin A. (*Photo courtesy of:* Ross University School of Veterinary Medicine, St. Kitts, West Indies, www.veterinary.rossu.edu)

provides a solid example of hypertrophic osteopathy (figure 1-1) and representative cytology of a lung aspirate (figure 1-2) that tie this case together.

References:

1. Cohn LA. Diseases of the Pulmonary Parenchyma In: Ettinger SJ, Cote E,Feldman EC, eds. *Textbook of Veterinary Internal Medicine* 8ed: Elsevier Health Sciences 2016.
2. Kobayashi K, Takemura RD, Miyamae J et al. Phenotypic and molecular characterization of novel pulmonary adenocarcinoma cell lines established from a dog. *Nature Sci Rep 13*, 16823 (2023).
3. Kuhn E, Morbini P, Cancellieri A, Damiani S, Cavazza A, Comin CE. Adenocarcinoma classification: patterns and prognosis. *Pathologica*. 2018;110(1):5-11.
4. McPhetridge JB, Scharf VF, Regier PJ, et al. Distribution of histopathologic types of primary pulmonary neoplasia in dogs and outcome of affected dogs: 340 cases (2010-2019). *J Am Vet Med Assoc* 2021;260:234-243.
5. Ogilvie GK, Haschek WM, Withrow SJ, et al. Classification of primary lung tumors in dogs: 210 cases (1975-1985). *Journal of the American Veterinary Medical Association* 1989;195:106-108.
6. Wilson DW. Tumors of the respiratory tract In: Meuten DJ, ed. *Tumors in domestic animals*. Ames Iowa, USA: Wiley Blackwell, 2017;467-498.
7. Ye J, Findeis-Hosey JJ, Yang Q, et al. Combination of napsin A and TTF-1 immunohistochemistry helps in differentiating primary lung adenocarcinoma from metastatic carcinoma in the lung. *Appl Immunohistochem Mol Morphol* 2011;19:313-317.

CASE II:

Signalment:
4-month-old, intact male mixed breed dog (*Canis lupus familiaris*).

History:
This animal had severe upper respiratory signs with green nasal discharge, severe conjunctivitis, lethargy, loss of appetite and dehydration.

Gross Pathology:
Examined is a 5.75 kg, juvenile (4-months-old) intact male mixed breed dog in good postmortem condition. A moderate amount of thin red-tinged transparent fluid exudes from the nasal and oral cavities. There is some mild frond-like proliferation of the skin on the dorsal nasal planum. The nasal turbinates are mostly reddened. There is negative pressure and approximately 125 mL of semi-

Figure 2-1. Lung, dog. The lungs fail to collapse, are diffusely dark red to purple, firm and contain innumerable pinpoint white nodules. (*Photo courtesy of:* University of Illinois at Urbana-Champaign, Veterinary Diagnostic Laboratory, http://vetmed.illinois.edu/vet-resources/veterinary-diagnostic-laboratory/)

translucent to slightly cloudy, thin, red-tinged fluid within the pleural cavity. The lungs fail to collapse, are diffusely dark red to purple, firm and contain innumerable pinpoint, firm, white nodules scattered throughout all lung lobes. A few sections float in formalin while a few sections sink. The tracheobronchial lymph nodes are subjectively enlarged and are diffusely dark red. The stomach contains a small amount of watery, tan fluid and the rugal folds are prominent. The intestinal tract contains a scant amount of tan watery ingesta. The colon is empty. The serosal surfaces of the intestinal tract have a subtle ground glass appearance.

Laboratory Results:

1. Aerobic culture (lungs): Escherichia coli (moderate growth), Staphylococcus pseudintermedius (moderate growth)
2. Canine Adenovirus (CAdV) 1 and 2 PCR (lung): Negative
3. Canine Distemper Virus (CDV) PCR (lung): Positive
4. Canine Herpesvirus 1 PCR (lung): Negative
5. Influenza A PCR (lung): Negative

Microscopic Description:

Lung: Multifocally and randomly scattered throughout the parenchyma are numerous loosely nodular aggregates of amorphous to granular eosinophilic debris (necrosis) that replaces the normal architecture. Areas of necrosis are characterized by accumulations of small basophilic granules (karyorrhectic debris), eosinophilic ghosts of necrotic round cells, extravasated erythrocytes (hemorrhage), abundant hypereosinophilic granular to fibrillar material (fibrin), and low numbers of degenerate macrophages. The adjacent alveolar spaces are often filled by plump and foamy macrophages, low numbers of neutrophils, and occasional sloughed degenerate epithelial cells mixed with hemorrhage, eosinophilic wispy material (edema) and fibrin. Scattered throughout examined sections and distending the cytoplasm of macrophages, alveolar epithelial cells or occasionally free within the tissues adjacent to disrupted macrophages are occasional to few, variably sized dense clusters of protozoal organisms. Organisms are round to fusiform, 2-4 µm in diameter and contain a small, central basophilic nuclear body. Rarely, viable and sloughed alveolar and bronchiolar epithelial

Figure 2-2. Lung, dog. A single section of lung is submitted for examination. Airways and alveoli are diffusely filled with a cellular exudate. (HE, 4X)

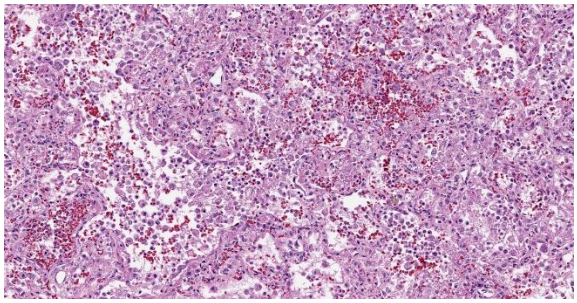

Figure 2-3. Lung, dog. The exudate filling all air spaces is primarily macrophages with fewer neutrophils, abundant polymerized fibrin, and cellular debris. (HE, 187X)

cells contain small, eosinophilic intranuclear or intracytoplasmic viral inclusion bodies. Few bronchioles contain variable numbers of degenerate neutrophils and macrophages mixed with necrotic debris. The respiratory epithelium lining these bronchioles is often hypocellular and remaining epithelial cells are flattened (attenuated) or angular with moth-eaten cytoplasm and pyknotic nuclei (necrosis).

Immunohistochemical (IHC) staining of organisms in the lungs with an antibody targeting *Toxoplasma spp.* is performed. Numerous intracytoplasmic discrete clusters and scattered individual 2-4 µm diameter protozoal organisms exhibit positive immunostaining.

Other histopathology findings that are not included in the provided slide include:

- Hyperkeratosis of the nasal planum
- Lymphoplasmacytic conjunctivitis with rare viral inclusion bodies
- Toxoplasma organisms in the bone marrow, thyroid gland, and spleen
- Splenic lymphocytolysis
- Viral inclusions in mononuclear cells of mesenteric lymph node

Contributor's Morphologic Diagnosis:
Lungs: Severe, multifocal to coalescing, necrotizing bronchointerstitial pneumonia with intranuclear and intracytoplasmic viral inclusion bodies and intracytoplasmic protozoal organisms consistent with *Toxoplasma spp.*

Contributor's Comment:
Canine distemper virus (CDV) is caused by a Morbillivirus (family Paramyxoviridae)[2] and has been shown to infect a wide variety of carnivores, including members of Canidae (domestic and wild dogs), Mustelidae (ferrets, mink), wild members of Felidae, raccoons[6] and skunks.[1] In addition to many terrestrial carnivores, some species of seals are also susceptible,[2] including Caspian seals.[8] In dogs, virus is transmitted through infected bodily tissues,[12] particularly respiratory secretions.[2] Within the upper respiratory tract, virus is phagocytosed by mucosal lymphocytes and macrophages, which travel to the tonsils and local lymph nodes. Here, the virus continues to replicate, infecting more lymphocytes and macrophages which then spread systemically.[12] Within 2-5 days of exposure, the virus has spread throughout the body and can be found in various lymphoid tissues including bone marrow, thymus, and intestinal lymphoid tissues.[2] Once within lymphoid tissues, the virus can then spread to and infect epithelial and mesenchymal (pantropic) cells throughout the body, particularly within the respiratory, nervous and alimentary systems.[12]

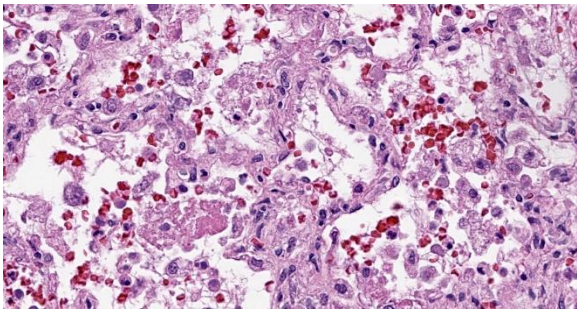

Figure 2-4. Lung, dog. High magnification of alveolar septa and lumina demonstrating the luminal exudate and the expansion of alveolar septa by inflammatory cells, edema, and hyperplastic type II pneumocytes. (HE, 554X)

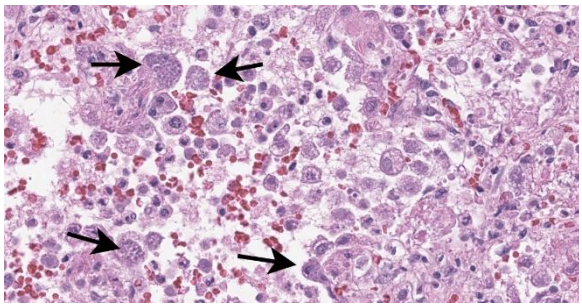

Figure 2-5. Lung, dog. Numerous cell types, including airway epithelium, alveolar macrophages, and Type II pneumocytes contain a large cytoplasmic cyst with numerous 2-3um round zoites consistent with *Toxoplasma gondii* (arrows). (HE, 554X)

Within the respiratory tract, viral infection leads to death of pneumocytes, bronchiolar epithelium and macrophages, leading to impaired oxygen exchange, removal of debris and potential infectious organisms and decreased phagocytic and antigen-presenting ability by macrophages.[12] Grossly, lesions of the respiratory tract include mucopurulent exudate within the nasopharynx as well as bronchointerstitial pneumonia characterized by patchy to diffuse red-tan, rubbery lesions,[2] both of which are seen in this case. Histologically, mild suppurative inflammation within bronchioles as well as necrosis, attenuation of bronchiolar epithelium and intracytoplasmic (rarely, intranuclear outside of the nervous system) inclusion bodies may be observed.[2]

An important potential consequence of CDV infection is immune suppression and increased susceptibility to co-infections.[2] Infection of and consequential cell death of lymphocytes and macrophages leads to lymphoid depletion of the thymus, lymph nodes, tonsils and various mucosal-associated lymphoid tissues. Various secondary infections have been documented in dogs including bacterial (*Bordetella*, *Rhodococcus equi*), viral (adenovirus), fungal (*Pneumocystis*, *Cryptosporidium*), and protozoal (*Toxoplasma*, *Sarcocystis*, *Neospora*).[2,4,9,10] Immune suppression and secondary infections also play an important role in CDV infections in many other species with co-infections of *Sarcocystis* and *Toxoplasma* reported in raccoons and skunks,[1,5,7] and *Toxoplasma* in mink, ferrets, and gray foxes.[7]

Toxoplasma gondii is an obligate intracellular coccidian protozoal organism[9] that utilizes felid species as its definitive hosts but can likely cause disease in any mammal.[11] Sexual reproduction only occurs within the feline gastrointestinal tract and infectious oocysts are released into the environment in feces. Transmission to other species occurs through ingestion of infected feces within the environment.[11] In most immunocompetent hosts, *Toxoplasma* does not cause clinical disease, but with immune suppression particularly in young hosts, can lead to systemic toxoplasmosis. Dissemination of infectious tachyzoites occurs in various immune cells (lymphocytes, macrophages, granulocytes) or freely within the blood.[11] Within the lungs, *Toxoplasma* infection is typically characterized grossly by small, white foci scattered throughout the parenchyma.[2] Histologically, multifocal necrotizing interstitial pneumonia with histiocytic and neutrophilic infiltrates and Type II pneumocyte hyperplasia may be observed.[6]

Contributing Institution:
University of Illinois at Urbana-Champaign, Veterinary Diagnostic Laboratory
http://vetmed.illinois.edu/vet-resources/veterinary-diagnostic-laboratory/

JPC Diagnosis:
Lungs: Pneumonia, bronchointerstitial, fibrinonecrotizing and histiocytic, chronic, diffuse, severe with intranuclear and intracytoplasmic viral inclusions, and intracellular and extracellular protozoa.

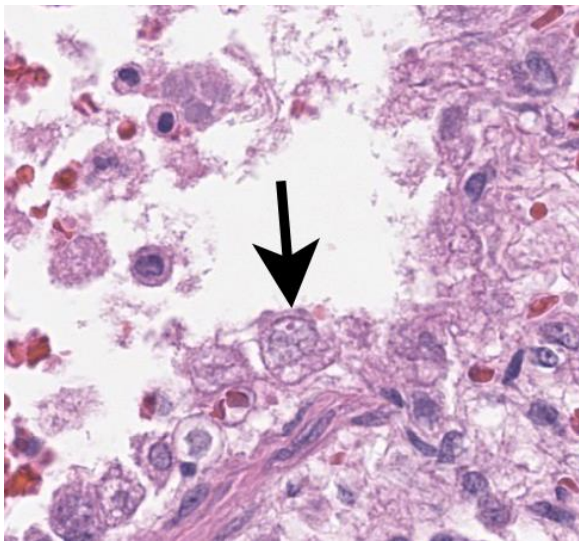

Figure 2-6. Lung, dog. Rarely, remnant airway epithelial cells (arrow) and alveolar macrophages contain one or more small 2-4um irregularly round eosinophilic cytoplasmic inclusions. (HE, 713X)

JPC Comment:
This second case is a wonderful example of an interstitial pneumonia that is generous enough to have two separate entities present at the same time (figures 2-3 and 2-4)! We performed modified Gram stains (Brown-Brenn, Brown-Hopps) that confirmed the bacterial culture results for this case, particularly within the larger airways that contained necrotic debris and neutrophilic inflammation. Though this was a minor feature for this case, it fits with the overall immunosuppression related to canine morbillivirus that the contributor nicely outlines. Both Giemsa and PAS stains highlighted intrahistiocytic and intraalveolar cysts of *Toxoplasma*, though these were also readily apparent on H&E alone (figure 2-5). The presence of viral particles within select alveolar and bronchiolar epithelial cells was subtle (figure 2-6), though conference participants noted convincing intranuclear and intracytoplasmic inclusions. Conference participants also discussed whether there were viral syncytial cells present but were not confident that these could be distinguished from multinucleated giant cell macrophages. One takeaway from this case is that necrotizing pneumonias where *Toxoplasma* is suspected should prompt a careful search for an inciting cause for immunosuppression with canine morbillivirus having recognizable features in section. There are several major risk factors for canine toxoplasmosis. As the contributor notes, primary disease is associated with immunosuppression.[3] Seroprevalence estimates from around the world vary, though national estimates vary from 7.9% to 42.8% of dogs.[3] Cohabitation of dogs with cats (the definitive host) is associated with greater seroprevalence as is outdoor housing of dogs and coprophagy habits. With these data in mind, exposure of dogs to *Toxoplasma* is a likely event in many environments though immunocompetent animals are typically subclinically infected and do not exhibit signs. The role of vaccination and the possibility of diminished maternal immunoglobulins from poor transfer or lack thereof is worth noting for this case, though the history for this animal is sparse.

References:
1. Burcham GN, Ramos-Vara JA, Vemulapalli R. Systemic Sarcocystosis in a Striped Skunk (Mephitis mephitis). *Veterinary Pathology*. 2010;47(3):560-564.
2. Caswell JL, Williams KJ. Respiratory System. ln: Maxie MG ed. *Jubb, Kennedy, and Palmer's Pathology of Domestic Animals*. Vol. 2. 6th ed. Philadelphia, PA: Elsevier Saunders. 2016: 574-576, 590.
3. Dini FM, Stancampiano L, Poglayen G. et al. Risk factors for Toxoplasma gondii infection in dogs: a serological survey. *Acta Vet Scand*. 2024;66(14).
4. Headley, SA, Oliveira TES, Pereira AHT, Moreira JR, et al. Canine morbillivirus (canine distemper virus) with concomitant canine adenovirus, canine parvovirus-2, and Neospora caninum in puppies: a retrospective

immunohistochemical study. *Nature Scientific Reports.*
5. Kubiski SV, Sisó S, Church ME, Cartoceti AN, Barr B, Pesavento PA. Unusual Necrotizing Encephalitis in Raccoons and Skunks Concurrently Infected with Canine Distemper Virus and Sarcocystis sp. *Veterinary Pathology*. 2016;53(3):674-676.
6. Lopez A. Respiratory System, Mediastinum and Pleurae. Ln: McGavin MD, Zachary JF eds. *Pathologic Basis of Veterinary Disease*. 5th ed. St. Louis, MO: Mosby Elsevier; 2012: 524-527.
7. Moller T, Nielsen SW. Toxoplasmosis in Distemper-Susceptible Carnivora. *Pathologia veterinaria*. 1964; 1(3): 189-203.
8. Namroodi S, Shirazi AS, Khaleghi SR, N. Mills J, Kheirabady V. Frequency of exposure of endangered Caspian seals to Canine distemper virus, Leptospira interrogans, and Toxoplasma gondii. PLoSONE. 2018;13(4).
9. Portilho FVR, Paes AC, Megid J, Hataka A, et al. Rhodococcus equip VAPN type causing pneumonia in a dog coinfected with canine morbillivirus (distemper virus) and *Toxoplasma gondii*. *Microbial Pathogenesis*. 2019; 129: 112-117.
10. Postma GC, Dellarupe A, Streitenberger N, Bratanich A, et al. Canine distemper virus, atypical Toxoplasma gondii, and Neospora caninum co-infection, in a dog with neurological signs from Argentina. *Brazilian Journal of Veterinary Pathology*. 2019; 12(3): 101-105.
11. Uzal FA, Plattner BL, Hostetter JM. Alimentary System. ln: Maxie MG ed. *Jubb, Kennedy, and Palmer's Pathology of Domestic Animals*. Vol. 2. 6th ed. Philadelphia, PA: Elsevier Saunders. 2016: 236-237.
12. Zachary JF. Mechanisms of Microbial Infections. Ln: McGavin MD, Zachary JF eds. *Pathologic Basis of Veterinary Disease*. 5th ed. St. Louis, MO: Mosby Elsevier; 2012: 226-227.

Figure 3-1. Heart, dog. Coronary blood vessels visible on the epicardium are thickened and yellow. (*Photo courtesy of:* Department of Biomedical Sciences and Pathobiology, Virginia Maryland College of Veterinary Medicine, https://vetmed.vt.edu/departments/biomedical-sciences-and-pathobiology.html)

CASE III:

Signalment:
A 13-year-old, neutered male, German Shepherd dog (*canis familiaris*)

History:
The patient had a history of hip dysplasia clinically diagnosed when the animal was 7-years-old and a fully excised mast cell tumor when this dog was 10-years-old. This animal always had good body condition. Animal was found dead without premonitory signs.

Gross Pathology:
The body had good post mortem preservation and good nutritional status, with ample deposits of adipose tissue in the subcutis and body cavities. There were large amounts of fibrin and alimentary contents in the abdominal cavity. In the gastric wall, a focal perforated transmural ulcer was identified in the fundic area. The lungs were red and wet. The myocardium was slightly pale and the

Figure 3-2. Heart, dog. Sections from the right (top) and left ventricles are submitted for examination. In both sections, the walls of coronary arteries and smaller arterioles are markedly thickened. (HE, 5X)

coronary blood vessels visible on the epicardium were thickened with a yellow, irregular plaque-like lesions. No significant findings in other internal organs.

Microscopic Description:
Heart, right and left ventricle: The most significant findings were identified in large and medium size arteries located in all layers of the heart. They all exhibit severe atheromatosis, characterized by the presence of numerous cholesterol clefts and foamy macrophages within the sub intima and/or in the adventitia of the vessels. In these areas, there are variable amounts of fibrin within the sub intima (fibrinoid necrosis) and also attached to the endothelial surface (thrombosis), and extensive hemorrhages and numerous hemosiderin laden macrophages. Some vessels are completely occluded with this inflammatory reaction. In the myocardium, multifocal areas of interstitial fibrosis are noted. In the sample collected from the right ventricle, there are numerous adipocytes tracking along the vessels in the myocardium (likely as a reflection of body condition).

Contributor's Morphologic Diagnosis:
Heart: Atherosclerosis, severe, multifocal, with foamy macrophages, cholesterol clefts and multifocal mild myocardial fibrosis.

Contributor's Comment:
Multiple vessels in different organs (including the stomach, kidney, brain, lung, liver and small intestine) displayed atherosclerosis. This vascular lesion probably predisposed to an area of gastric ischemia/hypoxia, with consequent necrosis and rupture of the stomach. The cause for atherosclerosis in this patient could not be elucidated, due to the absence of antemortem blood studies. No significant gross or histologic findings were identified in the thyroid gland, adrenal gland, or pancreas.

Atherosclerosis is defined as a focal or multifocal thickening of the arterial walls due to the deposition of lipids, forming plaques.[6,7] This condition has been associated with hyperlipidemia, which is defined as an elevation of plasma concentration of triglycerides and/or cholesterol. Hyperlipidemia can be physiologic or pathologic. Physiologic hyperlipidemia is frequently observed after meals (post prandial). Pathologic hyperlipidemia is associated with cholestasis, high fat diets, drug administration, nephrotic syndrome,

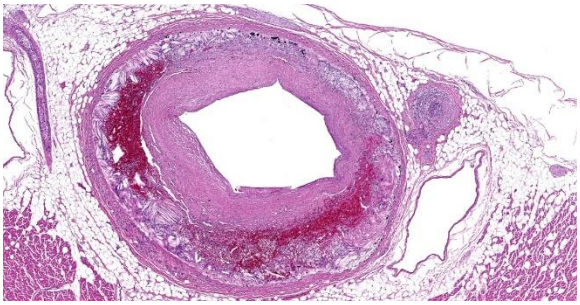

Figure 3-3. Heart, dog. There is marked intimal hyperplasia and the tunica media is markedly expanded by acicular cholesterol clefts admixed with large numbers of foamy macrophages, hemorrhage, and mineral. (HE, 34X)

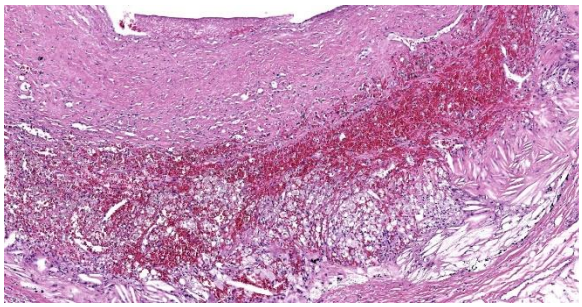

Figure 3-4. Heart, dog. Higher magnification of the arterial wall. (HE, 103X)

lymphoma or endocrinopathies, such as hypothyroidism, hyperadrenocorticism and diabetes mellitus.[5,9,11]

In domestic species, rabbits, chickens and pigs ae considered "atherosensitive", whereas dogs, cats, ruminants and rats are considered "atheroresistant".[9] In dogs, atherosclerosis is almost always present in association with hypothyroidism or diabetes mellitus, although canine hypertension and obesity has also been associated with this condition. Spontaneous atherosclerosis has also been described but is considered extremely rare.[5]

The pathogenesis of atherosclerosis is not completely nor well understood.[2] Dogs with hypothyroidism have increased very low-density lipoproteins (VLDL), low density lipoproteins (LDL) and high-density lipoproteins (HDL). Dogs with diabetes mellitus have increased VLDL and HDL, and dogs with hyperadrenocorticism have increased LDL.[1] As a result of hyperlipidemia, endothelial injury/dysfunction may occur.[9] Endothelial cell dysfunction is defined as non-adaptive alteration in functional phenotype, which are fundamental in the regulation of hemostasis and thrombosis, local vascular tone, redox balance and inflammatory reaction. This dysfunction allows focal permeating, trapping and physicochemical modifications of circulating lipoprotein particles in the subendothelial space.[10] This sequence of events leads to platelet adhesion, monocyte adhesion and infiltration, and insudation of lipid, as extracellular lipid or as intracellular lipid in "foam cells". In addition, multiple growth factors and chemokines are generated by activated macrophages and endothelial cells, which activate smooth muscle cells and their precursors to promote their proliferation and synthesis of extracellular matrix in the intimal compartment. In one individual, numerous atherosclerotic plaques can coexist, and each has their own pathobiological evolution.[4,9]

The histopathologic lesion of atherosclerosis in dogs differs from the human counterpart, as the lesion in dogs has been described to begin in the middle and outer layers of the media and is much more frequent in small muscular arteries. The deposition of lipids in the internal layers of the media can promote disruption of the internal elastic lamina and involvement of the intima. In humans, atherosclerosis is primarily present in the intima and may extend to the tunica media and adventitia.[9] Veins are not affected. Reports of immunohistochemical analysis of the atheromatous plaques in dogs conclude that lipids in the lesions contained low density lipoproteins, so they have similar features to human atherosclerotic lesions.[6]

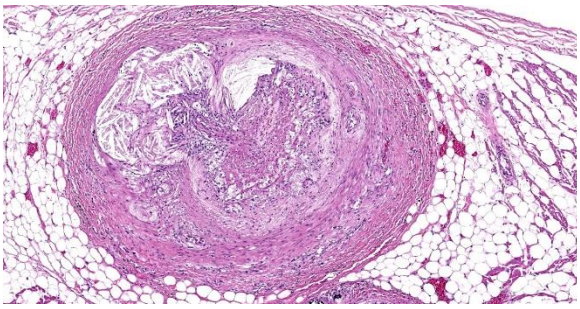

Figure 3-5. Heart, dog. In some vessels, the lumen is seriously compromised by aggregates of cholesterol clefts and macrophages. (HE, 103X)

Grossly, the lesions are identified as multifocal, sometimes confluent, yellow brown nodules in arterial walls in different organs. The heart, kidney and brain are usually more severely involved.[9] Miniature Schnauzers (particularly females) and Shetland sheepdogs are predisposed to primary hyperlipidemia and are considered to be breeds with high risk for developing atherosclerosis.[8]

Atherosclerosis can be confirmed by histopathology. Nevertheless, because of invasiveness of sampling, the use of diagnostic imaging (CT scanner) may be used to assess the antemortem presence of calcified atheromatous plaques and degree of damage. This technique is useful in animals without evidence of metastatic calcification or endocrinopathy.[7]

Contributing Institution:
Department of Biomedical Sciences and Pathobiology
Virginia Maryland College of Veterinary Medicine
205 Duck Pond Drive
Blacksburg, VA 24061.
https://vetmed.vt.edu/departments/biomedical-sciences-and-pathobiology.html

JPC Diagnosis:
Heart: Atherosclerosis, chronic, diffuse, severe with multifocal cardiomyocyte loss and fibrosis.

JPC Comment:
The contributor provides a detailed look at atherosclerosis that accompanies a great gross photo (figure 3-1) and a nice histology slide as well. The changes within muscular arteries are superb and are conveniently laid out both in cross-section and longitudinal section with a constellation of changes to appreciate (figures 3-2, 3-3, 3-4). Conference participants were also interested in the infil

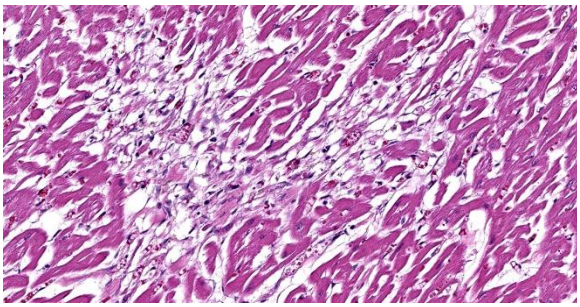

Figure 3-6. Heart, dog. There are scattered areas of myofiber loss, atrophy, and replacement fibrosis.

tration of adipocytes within the right ventricle and discussed the ultimate genesis. While arrhythmogenic right ventricular cardiomyopathy (ARVC) is a good differential for this case due to the concurrent fibrous and fatty appearance of this section, myocytes lack active degeneration/necrosis that would be expected with ARVC. Instead, another potential explanation for these changes is ischemic injury to myocytes with loss and fibrosis – the infiltration of adipocytes in a generously apportioned *(syn*: extremely well-fed) reflects a race to see which entity will fill the empty space up first.

We ran Movat's and Masson's chromatic stains to characterize vascular and perivascular changes in this case. There is narrowing to complete occlusion of the vascular lumina (figure 3-5) with marked disruption of the tunica intima to include a focal area with fibrin and hemorrhage that may represent a true rupture of the coronary artery. Recently, a similar case of atherosclerosis was reported in a dog that lacked a history of endocrinopathy with distribution of lesions centered solely on the abdominal aorta and renal vasculature.[3] The only clinical signs attributable in that presentation however were a history of hindlimb paresis and elevated renal values; primary cardiac lesions were absent grossly and histologically. Lastly, the distribution of lesions in this case (primarily subintimal) should be contrasted with atherosclerosis in

birds where the lesions occur primarily within the intima as stiff plaques. For an example of recent WSC, refer to Conference 6, Case 1, 2023-2024 for a contrasting case in a saker falcon.

References:

1. Barrie J, Watson TDG, Stear MJ et al. Plasma cholesterol and lipoprotein concentrations in the dog: The effects of age, breed, gender, and endocrine disease. *J Sm Anim Pract*. 1993; 34: 507-512.
2. Boynosky NA, Stokking L. Atherosclerosis associated with vasculopathic lesions in a golden retriever with hypercholesterolemia. *Can Vet J*. 2014; 55: 484-488.
3. Gimbrone MA Jr, García-Cardeña G. Endothelial Cell Dysfunction and the Pathobiology of Atherosclerosis. *Circ Res*. 2016; 118: 620-636.
4. González-Domínguez, A, Tormo JR, Herrería-Bustillo, VJ. Aortic thrombosis and acute kidney injury due to atherosclerosis in a dog. *JAVMA*. 2024; 262(8):1-4.
5. Hess RS, Kass PH, Van Winkle TJ. Association between diabetes mellitus, hypothyroidism or hyperadrenocorticism, and atherosclerosis in dogs. *J Vet Intern Med*. 2003; 17: 489-494.
6. Kagawa Y, Hirayama K, Uchida E et al. Systemic atherosclerosis in dogs: histopathological and immunohistochemical studies of atherosclerotic lesions. *J Comp Pathol*. 1998; 118: 195-206.
7. Lee E, Kim HW, Bae H, et al. Radiography and CT features of atherosclerosis in two miniature Schnauzer dogs. *J Vet Sci*. 2020; 21: e89.
8. Mori N, Lee P, Muranaka S, et al. Predisposition for primary hyperlipidemia in miniature Schnauzers and Shetland sheepdogs as compared to other canine breeds. *Res Vet Sci*. 2010; 88: 394-399.
9. Robinson WF, Robinson NA. Cardiovascular System. In: Maxie MG, ed. Jubb, Kennedy & Palmer's Pathology of Domestic Animals. Vol 3. 6th ed. St. Louis, MO: Elsevier; 2016:1-101.
10. Simionescu N, Vasile E, Lupu F, et al. Prelesional events in atherogenesis. Accumulation of extracellular cholesterol-rich liposomes in the arterial intima and cardiac valves of the hyperlipidemic rabbit. *Am J Pathol*. 1986; 123: 109-25.
11. Watson TDG, Barrie J. Lipoprotein metabolism and hyperlipidaemia in the dog and cat: A review. *J Sm Anim Pract*. 1993; 34: 479-487.

CASE IV:

Signalment:
1-year-old, spayed female, domestic shorthair cat (*Felis catus*)

History:
This patient presented to the Cardiology Service for evaluation of a heart murmur. An angiogram diagnosed a large, bidirectional patent ductus arteriosus (PDA). On subsequent recheck echocardiograms, shunting transitioned between left-to-right and bidirectional, as well as showed progressive right ventricular hypertrophy. Abdominal ultrasound showed development of mild ascites. At final presentation, this patient developed marked abdominal effusion and abdominocenteses with fluid analysis revealed a high-protein, exudative effusion. Euthanasia was elected due to progressive vomiting and anorexia.

Gross Pathology:
Examination of the lungs is after formalin fixation. The visceral pleura is multifocally expanded by dozens of sharply demarcated, pinpoint to 0.4 cm in diameter, hemispheric, white-tan nodules. On section, the lungs contain dozens of poorly demarcated, firm, tan areas. Lung lobes sections float in formalin.

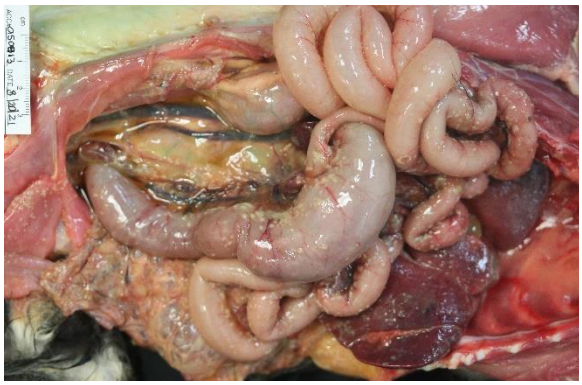

Figure 4-1. Abdominal viscera, cat. There are numerous tan-yellow nodules over the abdominal surfaces which range from pinpoint to 1 cm x 0.6 cm x 0.6 cm. (*Photo courtesy of:* Schwarzman Animal Medical Center, http://www.amcny.org/)

Extrapulmonary lesions include myriads of multifocal to coalescing, hemispheric, tan-yellow nodules over the peritoneum, omentum, serosa, splenic capsule, hepatic surface, renal capsules, and renal cortices, which range from pinpoint to 1 cm x 0.6 cm x 0.6 cm. Nodules often track along mesenteric and renal subcapsular veins. The mesenteric, hepatic, pancreaticoduodenal, and colonic lymph nodes are moderately to severely enlarged and the cut surfaces contain dozens of coalescing, poorly demarcated, tan-yellow regions. Within the abdominal cavity is approximately 80 mL of a viscous, mildly turbid, yellow fluid mixed with dozens of gelatinous, semi-translucent, yellow strands that are loosely adhered to the viscera (fibrin). The serosae are rough and dull and hepatic and splenic capsules are multifocally cloudy and dull.

Laboratory Results:
Albumin: 1.9 g/dL (reference 2.6 - 3.9 g/dL)
Globulin: 6.2 g/dL (reference 3.0 - 5.9 g/dL)
Albumin: Globulin Ratio: 0.3
Abdominal effusion: Fluid analysis: high-protein (greater than 4.0 g/dL), exudative effusion
Abdominal Fluid - Feline Coronavirus Real-PCR: Positive (Biotype FECV)

Microscopic Description:
Lungs: The submitted sections of lung show multiple overlapping pathologic processes. The pleura is multifocally elevated and expanded by an acellular, fibrillar, eosinophilic material (fibrin) mixed with karyorrhectic debris (necrosis) and moderate to large numbers of lymphocytes, plasma cells, macrophages, and neutrophils. Inflammation infiltrates and expands the subjacent alveolar septa, which are frequently lined by hyperplastic type II pneumocytes. Expanding and infiltrating the remaining alveolar septa are moderate numbers of macrophages, lymphocytes, plasma cells, and neutrophils with rare type II pneumocyte hyperplasia. Filling the alveolar spaces is variable pale eosinophilic (seroproteinaceous) fluid, extracellular bacteria (mixed morphologies), increased intra-alveolar macrophages, and intra-alveolar protein. Small to medium-sized pulmonary arteries/arterioles display multiple pathologic changes. The tunica intima and subintima are partially to circumferentially expanded by a homogenous, eosinophilic matrix (fibrosis). The tunica media is multifocally expanded by fibrosis and/or increased numbers of hypertrophied smooth muscles cells (muscular hypertrophy) that cause compression/obliteration of the vascular lumens. Vascular lumens are commonly bridged and filled by plexiform lesions characterized by sieve-like masses comprised of a core of an extracellular matrix, smooth muscle cells, and stromal cells lined by quiescent and hypertrophied endothelial cells. When longitudinally sectioned, plexiform lesions are prominent at branch points. Variable expansion of the tunica adventitia is by either concentric dense or loose onion-skin fibrosis. Multiple blood vessels are moderately to severely distended by sac-like dilations (highlighted by Masson's Trichrome stain). Intermittent blood vessels are cuffed by mild to moderate numbers of lymphocytes, plasma cells, macro-

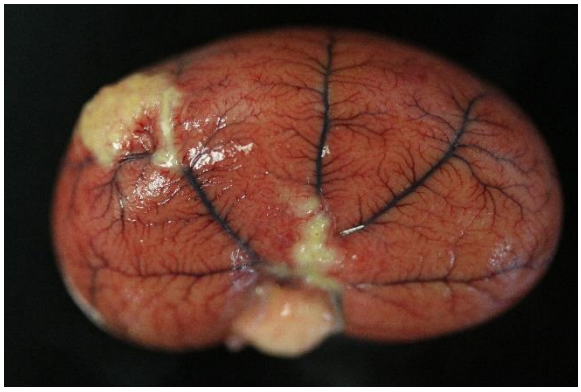

Figure 4-2. Kidney, cat: Nodules track along the renal subcapsular vein. (*Photo courtesy of:* Schwarzman Animal Medical Center, http://www.amcny.org/)

phages, and neutrophils. Separating the perivascular adventitia and tissues are clear spaces and an acellular, pale eosinophilic fluid (edema). There is multifocal, mild to moderate vascular congestion. Occasional macrophages contain morphologically separate intrahistiocytic pigments and foreign material (carbon, silica, hemosiderin, and/or lipofuscin).

Immunohistochemical stain for **FIPV** (Animal Health Diagnostic Center/Cornell University) revealed strong cytoplasmic immunoreactivity of macrophages within pleural granulomas.

Contributor's Morphologic Diagnosis:
Lungs:

1) Pulmonary arteriopathy, chronic, multifocal, severe with multifocal, mild to moderate, intimal, subintimal, medial, and adventitial fibrosis; moderate to marked medial hypertrophy; multifocal plexiform lesions; and multifocal, moderate to marked vascular dilation
2) Pleuritis and interstitial pneumonia, fibrinonecrotizing, histiocytic, lymphoplasmacytic, neutrophilic, chronic, multifocal to coalescing, moderate with regional type II pneumocyte hyperplasia
3) Interstitial pneumonia, histiocytic, lymphoplasmacytic, neutrophilic, chronic, diffuse, moderate with multifocal type II pneumocyte hyperplasia, alveolar histiocytosis, and minimal intra-alveolar protein
4) Edema, diffuse, mild to moderate

Contributor's Comment:
Microscopic examination in this case revealed two distinct pathologic processes consistent with concurrent feline infectious peritonitis virus (FIPV) infection and plexogenic pulmonary arteriopathy. Additional findings consistent with FIPV infection included high-protein abdominal effusion, multiorgan and body cavity inflammatory nodules, fibrinonecrotizing phlebitis, and pleocellular lymphadenitis. Immunohistochemistry confirmed FIPV within lesions. In this patient, systemic-to-pulmonary shunting through the PDA resulted in the prominent plexiform arteriopathy.

Coronaviruses infect a wide-range of wild and domestic species, where they are associated with respiratory, reproductive, gastrointestinal, and systemic diseases.[1,7,8,11-14,17] Virions are enveloped and contain large (80-220 nm), positive-sense, single-stranded RNA genome.[7,8,11,14,17] Viral proteins include 3-4 structural proteins (spike glycoprotein (S), transmembrane glycoproteins (M and E), nucleoprotein (N), and inconstant hemagglutinin (HE)) and non-structural accessory proteins.[7,8,11,17] Club-shaped spike glycoproteins (S) form a characteristic radiating crown-appearance on ultrastructure. [7,8,11] These spike proteins mediate receptor binding and fusion at the plasma membrane or endosomes facilitating viral entry.[7,8,11,14] Thus, the host range and cell tropism is predominantly determined by the spike (S) protein.[7,8,11,14] In addition, spike proteins participate in induction antibody and cell-mediated responses.[8] Coronaviruses exhibit a high mutation rate due to

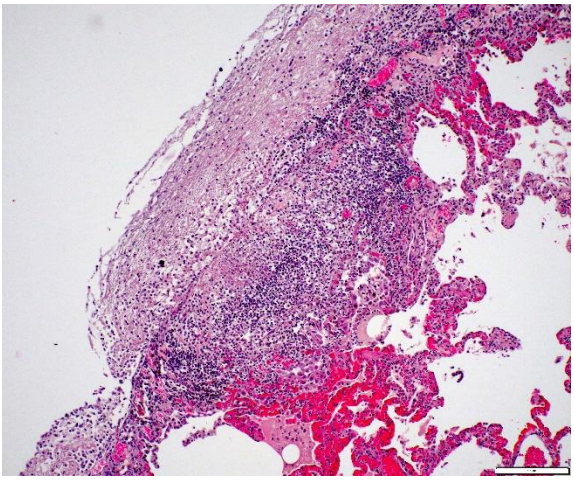

Figure 4-3. Lung, cat. Inflammation infiltrates and expands the subjacent alveolar septa, which are frequently lined by hyperplastic type II pneumocytes. (HE, 200X) (*Photo courtesy of:* Schwarzman Animal Medical Center, http://www.amcny.org/)

RNA-polymerase transcription errors and genetic recombination between related coronavirus during coinfections.[8,11,13,14] Feline coronaviruses (FCoVs) belongs to the family Coronaviridae within the alphacoronavirus genus.[7,8,11,17] Other important alphacoronaviruses in veterinary medicine include canine coronavirus, TGE virus of swine, porcine epidemic diarrhea virus (PEDV), porcine respiratory coronavirus, alpaca respiratory coronavirus, and ferret and mink coronaviruses.[7,11] There are two main circulating serotypes of feline coronaviruses (FCoVs): the predominant serotype I and rare serotype II.[7,8,11,13,14,17] Infection with serotype II is initiated through binding of the host aminopeptidase N receptor but the receptor for serotype I remains unknown.[7,8,11,13,17] A potential other host receptor, dendritic cell-specific ICAM (DC-ICAM), has been suggested for both serotypes.[7,8,13]

Feline coronaviruses (FCoV) include two separate biotypes: feline enteric coronavirus (FECV) and feline infectious peritonitis virus (FIPV).[1,7,8,11,12] FECV infects and replicates in the intestinal epithelium and is generally associated with a self-limiting, mild gastroenteritis.[1,8,11-13] A severe catarrhal and hemorrhagic enteritis can be seen in juveniles.[7,8] The main mode of transmission for FECV is fecal-oral but transmission can occur via direct contact (saliva, grooming behavior), respiratory droplets, and maternal shedding.[1,8,11,17,18] Meanwhile, FIPV infects and replicates in monocytes/macrophages and is associated with a severe, multisystemic immunoinflammatory disease.[1,7,8,11,13] The amount of replicating virus shed in FIPV-positive cats is extremely low with diminished replication in the enterocytes, therefore capacity for horizontal transmission is unlikely.[8,14] Feline infectious peritonitis (FIP) is an invariably fatal disease of both domestic and wild felids.[1,6-8,11-13,15,16] Outbreaks are related to environmental (crowding, concurrent infections, long-term exposure to shedders), virus, and host (individual immune response) factors.[8,13]The prevailing thought is that FIPV results from a mutated feline enteric coronavirus (in vivo mutation transition/internal mutation theory). [1,6-8,10-18] A single mutation has not been identified, rather multiple mutations associated with the 3C accessory gene and fusion and binding domains of the spike (S) protein are common in virulent biotypes.[1,7,8,11,13,14,17] Significant mutations in the FECV genome facilitates switching to FIPV by imparting tropism for macrophages, as well as productive and sustained replication in macrophages.[1,6-8,10-18] Acquired virulence factors allow for dissemination via leukocyte trafficking.[1,7,8,12-14,17] An alternative, less prominent theory states that FIP infections are due to distinct circulating avirulent and virulent strains, which may be the case in rare outbreaks.[8,14,16] FIP typically occurs in young or geriatric cats, with multi-cat environments, stress, and immunosuppression known risk factors.[7, 8,11,12,16] Increased incidence is reported in Abyssinians, Bengals, Birmans, Himalayans, Ragdolls, and Rex breeds.[7,8,11]

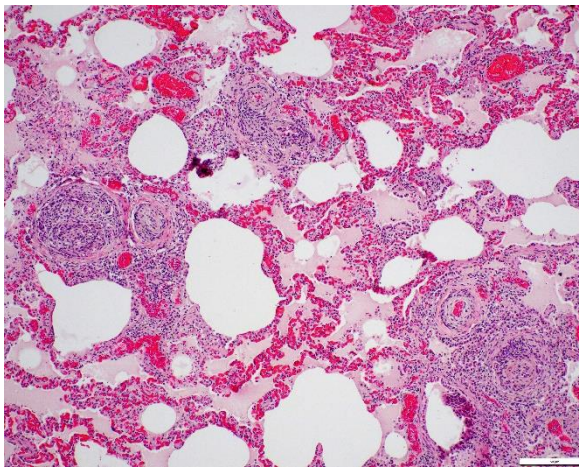

Figure 4-4. Lung, cat. Vascular lumens are commonly filled by plexiform lesions characterized by sieve-like masses comprised of a core of an extracellular matrix, smooth muscle cells, and stromal cells lined by quiescent and hypertrophied endothelial cells (HE, 100X) (*Photo courtesy of:* Schwarzman Animal Medical Center,http://www.amcny.org/)

Individual immune-responses play an essential role in FIPV disease progression.[7,8,13,14] Protective immunity is considered cell-mediated.[8,14] Severe disease is linked to a strong humeral response that is ineffective in virus elimination and simultaneous weak cell-mediated response.[1,7,8,11-14,17] Depletion and reduced cytotoxicity of NK cells coupled with decreased regulatory T-cells (Tregs) are seen in FIP cats.[8,14] In FIP infections a robust antibody response increases the severity of the disease, a phenomenon known as antibody dependent enhancement. [7,8,12-14,17,18] Classic FIP manifestations are "wet"/effusive and "dry"/pyogranulomatous forms, but a combination of the two is common.[1,7,8,11-14,16] The individual animal's immune response is thought to direct the spectrum of pathology.[1,7,8,11-14,16] With a vigorous cell-mediated response FIP lesions do not develop, while in patients who lack a cell-mediated response and have a strong humoral response the "wet"/effusion form develops.[1,8,12-14,17] The "dry"/pyogranulomatous form is associated with an intermediate response. [1,7,8,14,17] Typical gross pathology seen in the "wet" form is a fibrinous polyserositis with a viscous, high-protein, yellow exudative effusion with variable parenchymal involvement.[1,7,8,11,12, 14,16,17] With the "dry" form distinct granulomas/pyogranulomas throughout the body cavities and viscera are seen, which classically track along blood vessels and are not accompanied by effusion.[1,7,8,11,12,14,16,17] Commonly affected organs include the omentum, serosa, peritoneum, kidney, brain, and eye.[7,8,18] With brain involvement, meningeal plaques, intraventricular protein and fibrin-rich exudate, hydrocephalus, and cerebellar herniation can be seen. [7,12] Ocular manifestations include conjunctivitis, high-protein fluid in the anterior and posterior chambers, keratic precipitates, and retinal detachment.[7,10] Microscopic changes include characteristic vasculocentric, pyogranulomatous to pleocellular inflammation with overt phlebitis and variable vascular necrosis that preferentially involves small to medium size veins.[1,7,8,11,12,14,16,17] A similar progressive multisystemic inflammatory disease has been described in ferrets with coronavirus infection, which has been denoted as ferret systemic coronavirus.[6,7,11,12,15, 18]

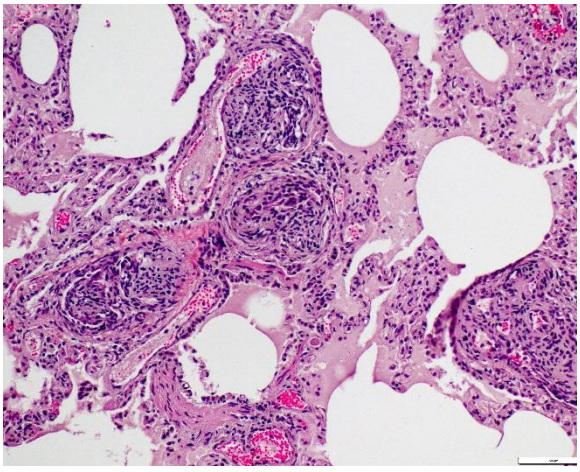

Figure 4-5. Lung, cat. Higher magnification of plexiform lesions. (HE, 400X) (*Photo courtesy of:* Schwarzman Animal Medical Center, http://www.amcny.org/)

Activation of FIP viral-infected macrophages contribute to the characteristic histopathologic changes, perivascular lesion distribution, and vascular damage with resulting vascular leakage.[7,8,11,16,17] Activated tissue macrophages secrete proinflammatory cytokines (TNFα, IL1β, IL6, IFNγ, GM-CSF and G-CSF), matrix enzymes (MMP9), and leukocyte adhesion molecules, as well as upregulation of surface integrins (CD18, CD11a, and CD49d) that lead to leukocyte chemotaxis, induce differentiation and proliferation of additional monocytes and neutrophils, intensify the inflammatory reaction, increase vascular permeability, and exacerbate tissue damage.[7, 8,11,13,14,16,17] Compliment activation accelerates chemotaxis and leukocyte adhesion.[16,17] Increased VEGF transcription and levels in infected cats further increase vascular permiability.[8,14] Both immune-mediated type III and type IV hypersensitivity reactions are hypothesized to play a role in the vascular lesions and perivascular inflammation.[7, 14] Antigen-antibody immune complexes and antibody-complement complexes deposit in vessel walls and perivascular tissues where they initiate tissue damage and recruit inflammatory cells.[7,8,12-14,16,17] Hyperstimulation of T-cells and macrophages, via type IV delayed hypersensitivity, cause perivascular tissues.[7,12,17]

Clinical signs associated with FIPV tend to be vague, non-specific, and depends on varying organ involvement.[1,7,11,12,16] FECV and FIPV cannot be distinguished serologically or morphologically making antemortem diagnosis of FIP challenging and therefore clinical signs and antemortem diagnostics need to be evaluated in concert using a diagnostic algorithm.[8,14] Bloodwork changes associated with FIP include lymphopenia, regenerative anemia, hypoproteinemia due to hypergammaglobulinemia, and biochemical changes associated with specific organ involvement.[8] FIP

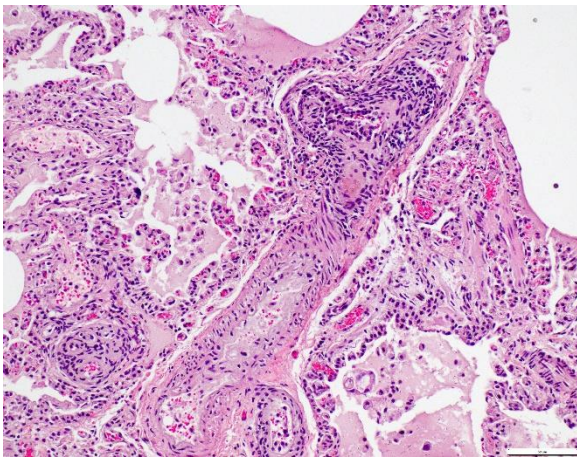

Figure 4-6. Lung, cat. When longitudinally sectioned, plexiform lesions are prominent at branch points. (HE,400X) (*Photo courtesy of:* Schwarzman Animal Medical Center, http://www.amcny.org/)

effusions typically have a high protein content (> 35g/L) with concurrent low cellularity (< 3500 nucleated cells/ml).[8] A serum albumin: globulin (A:G) ratio <0.8 is highly suggestive of FIP infection; meanwhile, an effusion A:G ratio <0.4 has a high positive predictive value for FIP.[8] Acute phase proteins, including alpha1 acid glycoprotein (AGP), are elevated with FIP.[8] Higher titers (≥1:1600) for FCoV-specific antibodies in the blood and effusion are more indicative of FIP.[8] RT-PCR can detect virus in feces, blood, and effusions but cannot differentiate between the two biotypes.[8] Immunohistochemistry allows for confirmation of coronavirus antigen within lesions on biopsy or postmortem samples, as in this case.[11]

The prominent vascular changes in this patient are characteristic for plexogenic pulmonary arteriopathy, a set of morphologic changes associated with pulmonary arterial hypertension (PAH). Causes of pulmonary hypertension include idiopathic (primary) PAH, systemic-to-pulmonary vascular shunts (including patent ductus arteriosus), chronic pulmonary thromboembolic disease, disor-

ders of pulmonary blood vessels (e.g., heartworm disease, pulmonary veno-occlusive disease, pulmonary vasculitis), hypoxic vasoconstriction, chronic interstitial lung disease, or pulmonary venous hypertension due to left-sided heart failure.[3] In the submitted case, PAH-associated lesions were associated with a known risk factor or condition (i.e., reported PDA).[3,19] Altered vascular tone is believed to be the result of imbalanced vasodilatory (e.g., prostacyclin, NO and cGMP) and vasoconstricting (e.g., endothelin, thromboxane A2, and serotonin) molecules.[3] Other implicated vasoactive molecules include TGFβ, BMP-2, FGF, and platelet-derived growth factor.[3] PAH results in endothelial injury/degeneration, vasculitis, fibrinoid vascular necrosis, smooth muscle proliferation, and "onion skin" perivascular fibrosis.[3,5,19] Thus, the vascular remodeling seen with PAH is considered the result rather than cause of hypertension; however, narrowed vascular lumens can exacerbate pulmonary hypertension.[3,5,19] Right ventricular pressure overload secondary to increased vascular resistance leads to right ventricular eccentric hypertrophy and ultimately right-sided congestive heart failure.[2,19]

PAH-associated histopathology represents a spectrum of both constrictive (medial and intimal remodeling) and complex (plexiform and dilative); these include endothelial hypertrophy, intimal, medial, and adventitial fibrosis, muscularization of small arterioles, vasculitis, thrombosis, plexiform lesions, and adventitial edema.[2-4,19] In humans, lesions are separated into grade I (muscular hypertrophy), grade 2 (intimal proliferation), grade 3 (concentric laminar intimal fibrosis), grade 4 (necrotizing vasculitis), grade 5 (plexiform lesions), and grade 6 (dilation and angiomatoid lesions) changes.[4] Higher grade lesions are typically associated with higher pulmonary artery pressures, although they do not represent a sequential disease progression

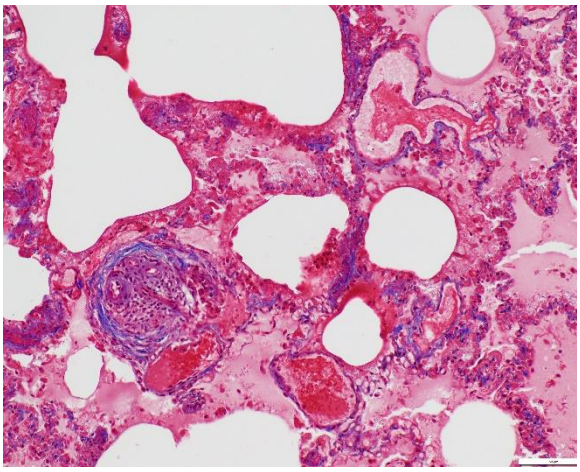

Figure 4-7. Lung, cat. Multiple blood vessels are moderately to severely distended by sac-like dilations (highlighted by Masson's trichrome stain) (Masson's trichrome, 400X) (*Photo courtesy of:* Schwarzman Animal Medical Center, http://www.amcny.org/)

and all grades can develop independently or concurrently.[4, 19] As in this case, characteristic plexiform lesions are characterized by vascular lumens filled by web-like proliferations formed by a core of smooth muscle cells and/or collagenous stroma lined by endothelial cells, which eventually lead to irreversible obliteration of the arterial lumens.[2-5,19] Lesion distribution is to the small muscular arteries and arterioles particularly at the branching points.[2-5,19] Dilation and angiomatoid lesions tend to occur at the artery/arteriole distal to the lesion suggesting impaired blood flow in their development.[2-5] Secondary pulmonary hemorrhages can be seen.[4] Plexiform lesions are dynamic structures involving the cross-talk between quiescent endothelial cells, apoptosis-resistant myofibroblasts, smooth muscle cells, and undifferentiated cells at the lesion's core.[2,5] Jet lesions at mouth of branch vessel and necrotizing arteritis may contribute to lesions.[5] Plexiform lesions are thought to be chronic attempts to repair injured vessels and likely represent cellular, recanalized thrombi secondary to vascular damage.[3-5]

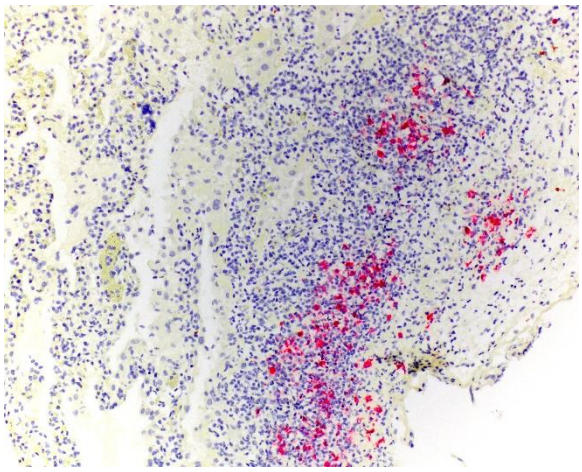

Figure 4-8. Lung, cat. Macrophages within the pleural granulomas stain strongly for feline coronavirus antigen. (anti-FIPV,400X) (*Photo courtesy of:* Schwarzman Animal Medical Center, http://www.amcny.org/)

Contributing Institution:
Schwarzman Animal Medical Center
510 E. 62nd Street
New York, NY 10065
http://www.amcny.org/

JPC Diagnosis:
1. Lung: Pneumonia, interstitial, lymphohistiocytic and neutrophilic, chronic, diffuse, moderate, with multifocal fibrinonecrotizing pleuritis.
2. Lung, small arterioles: Plexiform (plexogenic) arteriopathy, chronic, multifocal, severe with marked intimal hyperplasia and medial hypertrophy, fibrinoid necrosis, thrombosis, and recanalization.

JPC Comment:
The final case of this conference is quite complex with a plethora of features to put together to arrive at a final understanding of the case. Conference participants did not have access to the gross photos from this case (figures 4-1 and 4-2) beforehand, though they are highly suggestive of FIP and assist with interpretation of microscopic changes. The interstitial pneumonia and pleuritis are expected microscopic correlates (figures 4-3 and 4-4), though the vascular features are initially puzzling as the pulmonary veins lack overt phlebitis in the sections available while smaller pulmonary arteries have features reflecting hypertension (figures 4-5 and 4-6) which is not associated with FIP. Conference participants struggled to nail down how to best capture this feature as the arterial response to hypertension (plexiform) is not as commonly described perivascular concentric lamellated fibrosis ('onion skin'). Readers that are interested in exploring the genesis of this lesion in detail would greatly benefit from reviewing the excellent summary by Carman et al.[2]

Briefly, plexiform-type vascular changes arise from nonspecific medial and adventitial thickening of the pulmonary artery with extension of smooth muscle to small non-muscular arteries.[2] Subsequent complex remodeling driven by dysfunctional,[5] hyperproliferative, and apoptosis-resistant pulmonary endothelial cells leads to aberrant signaling between smooth muscle cells and fibroblasts with the result being progressive obliteration of the lumen of the vessel by laminar, stalk-like, or complete aneurysm-like projections of endothelial cells overlying a core of smooth muscle and/or collagenous stroma.[2] HIF-2α and VEGF signaling likely play a role and models of disease have focused on hypoxia as an inciting event in the development of this lesion though other concurrent factors are likely needed to induced complex lesions.[2,5] Interestingly, animals with experimentally treated with inhibition of VEGFR and hypoxic conditions that were later returned to normoxia developed large-scale plexiform pulmonary lesions. The interplay of ineffective endothelial apoptosis, strong impetus for angiogenesis, and aberrant cytokines and growth factors derived from a 'misguided' endothelial cell ringleader[5] is a solid hypothesis though this phenomenon remains incompletely understood.

References:

1. Andre NM, Miller AD, and Whittaker. Feline infectious peritonitis virus-associated rhinitis in a cat. *Journal of Feline Medicine and Surgery Open Reports*. 2020; 1-6.
2. Carman BL, Predescu DN, Machado R, et al. Plexiform Arteriopathy in Rodent Models of Pulmonary Arterial Hypertension. *The American Journal of Pathology*. 2019; 189(6): 1133-1144.
3. Caswell JL and Williams KJ. Respiratory System. In: Maxie MG, ed. *Jubb, Kennedy and Palmer's Pathology of Domestic Animals*. Vol 2. 6th ed. Philadelphia, PA: Elsevier Saunders; 2016: 492.
4. Churg A and Wright JL. Pulmonary Hypertension. In: Leslie KO and Wick MR, eds. *Practical Pulmonary Pathology*. 3rd ed. Philadelphia, PA: Elsevier; 2018: 404-407.
5. Fishman AP. Changing Concepts of the Pulmonary Plexiform Lesion. *Physiol Res*. 2000; 49: 485-492.
6. Garner MM, Ramsell K, Morera N, et al. Clinicopathologic Features of a Systemic Coronavirus-Associated Disease Resembling Feline Infectious Peritonitis in the Domestic Ferret (*Mustela putorius*). *Vet Pathol*. 2008; 45: 236-246.
7. Haake C, Cook S, Pusterla N, et al. Coronavirus Infectious in Companion Animal: Virology, Epidemiology, Clinical and Pathologic Features. *Viruses*. 2020; 12:1023-1043.
8. Kipar A and Meli ML. Feline Infectious Peritonitis: Still an Enigma? *Veterinary Pathology*. 2014; 51(2): 505-526.
9. Koharto A, Toba M, Alzoubi A, et al. Formation of Plexiform Lesions in Experimental Severe Pulmonary Arterial Hypertension. *Circulation*. 2010; 121: 2747-2754.
10. Labelle P. The Eye. In: Zachary JF and McGavin MD, eds. *Pathologic Basis of Veterinary Disease*. 7th eds. St Louis, MO: Elsevier. 2022; 1432.
11. Maclachlan NJ and Dubovi EJ. Coronavirus. In: Maclachlan NJ and Dubovi EJ, eds. *Frenner's Veterinary Virology*. 5th eds. Elsevier. 2017: 435-449.
12. Miller AD and Porter BF. Nervous System. In: Zachary JF and McGavin MD, eds. *Pathologic Basis of Veterinary Disease*. 7th eds. St Louis, MO: Elsevier. 2022; 982-983.
13. Palttrinieri S, Giordano A, Stranieri A, et al. Feline infectious peritonitis (FIP) and coronavirus disease 19 (COVID-19): Are they similar? *Transbound Emerg Dis*. 2021; 68: 1786-1799.
14. Pedersen NC. An update on feline infectious peritonitis: Virology and immunopathogenesis. *The Veterinary Journal*. 2014; 201: 123-132.
15. Shigemoto J, Muraoka Y, Wise AG, et al. Two cases of systemic coronavirus-associated disease resembling feline infectious peritonitis in domestic ferrets in Japan. *Journal of Exotic Pet Medicine*. 2014; 23: 196-200.
16. Spagnoli ST and Gelberg HB. Alimentary System and the Peritoneum, Omentum, Mesentery, and Peritoneal. In: Zachary JF and McGavin MD, eds. *Pathologic Basis of Veterinary Disease*. 7th eds. St Louis, MO: Elsevier. 2022; 485.
17. Stanton JB and Zachary JF. Mechanisms of Microbial Infections. In: Zachary JF and McGavin MD, eds. *Pathologic Basis of Veterinary Disease*. 7th eds. St Louis, MO: Elsevier. 2022; 263-264.
18. Sula MJM and Lane LV. The Urinary System. In: Zachary JF and McGavin MD, eds. *Pathologic Basis of Veterinary Disease*. 7th eds. St Louis, MO: Elsevier. 2022; 755-756.
19. Zabka TS, Campbell FE, and Wilson DW. Pulmonary Arteriopathy and Idiopathic Pulmonary Arterial Hypertension. *Vet Pathol*. 2006; 43: 510-522.

Joint Pathology Center
Veterinary Pathology Services

WEDNESDAY SLIDE CONFERENCE 2024-2025

Conference #8 09 October 2024

CASE I:

Signalment:
8-month-old, intact female, Pembroke Welsh Corgi, *Canis lupus familiaris*, canine.

History:
This patient presented with non-pruritic, erythematous, ulcerated, crusty skin lesions affecting the nose, muzzle, periocular tissue OU, ear pinna AU, and multiple nail beds of all four feet. Lesions started a month ago.

Gross Pathology:

Three punch biopsies of haired skin from multiple anatomic locations (forehead, muzzle, digit 4 of right hindfoot) were submitted for evaluation, with no overt gross findings.

Laboratory Results:
Aerobic bacterial culture – trace numbers of *Bacillus cereus, Staphylococcus equorum, Rummeliibacillus sp.*, and *Cellulolosimicrobium cellulans*

Fungal culture – absence of growth

Microscopic Description:
Haired skin (forehead, muzzle, digit 4 of right hindfoot): Multiple sections of haired skin are examined in which similar features are observed in all samples. Extending from the mid to deep dermis, and sharply demarcated from adjacent normal tissue in some

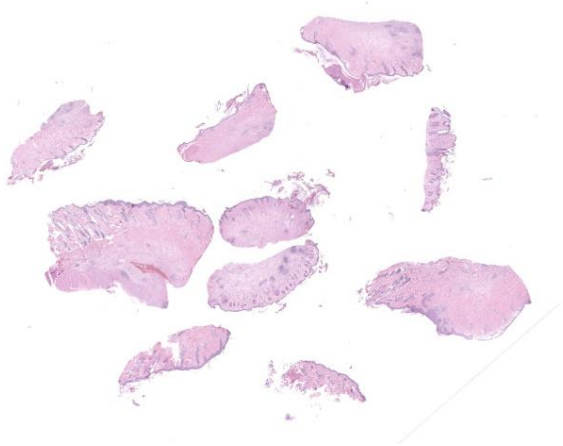

Figure 1-1. Haired skin, dog. Multiple sections of haired skin are submitted for examination. (HE, 4X)

sections, collagen fibers are regionally disorganized and pale to hypereosinophilic with variable loss of distinct bundle architecture. Medium to small caliber dermal vessels are distorted, characterized by pale, hyalinized eosinophilic tunics with loss of distinct separation of layers. Affecting other vessels, are circumferential perivascular cuffs of lymphocytes and plasma cells with fewer neutrophils and macrophages, which extend into the adjacent dermal stroma. Remaining pericytes and/or smooth muscle nuclei are frequently enlarged and prominent. Occasional aggregates of lymphocytes and histocytes are embedded in the dermis. Occasional clusters of lymphocytes and macrophages are also observed in the skeletal muscle layer, with separation, attenuation, and atrophy of affected fibers. Dermal nerve fibers have shrunken ax

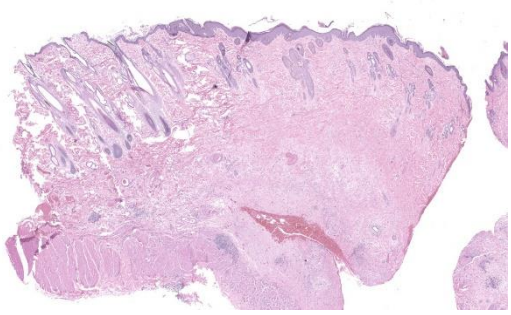

Figure 1-2. Haired skin, dog. In the right half of the section, beneath the hyperplastic epithelium, follicles are atrophic, and dermal collagen is poorly staining. There are cellular infiltrates surrounding deep dermal vessels and infiltrating the panniculus carnosus. (HE, 21X)

ons in decreased quantity, and rare lymphocytes and macrophages are embedded within affected fibers. Superficial to the affected dermis, multiple hair follicles are atrophied with a prominent fibrous root sheath. The overlying epidermis is hyperplastic, covered by segments of compact orthokeratotic to parakeratotic keratin that sometimes distend follicular ostia. Occasional serocellular crusts are also present.

Contributor's Morphologic Diagnosis:
Haired skin (forehead, muzzle, digit 4 of right hindfoot): Vasculitis with ischemic dermatopathy, regionally extensive, severe

Contributor's Comment:
Based on the clinical history, signalment, and histopathologic findings, a diagnosis of ischemic dermatopathy was warranted in this case. Ischemic dermatopathies (ID) refer to a group of cutaneous diseases that involve inflammation of the skin, vessels, and sometimes muscle or subcutaneous tissue, derived from a variety of causes. These conditions have been reported in humans[7] and dogs.[1,4,6,7,9,10] There are 5 main subtypes reported in dogs which include: 1) familial dermatomyositis (DM), 2) juvenile onset ischemic dermatopathy (dermatomyositis-like disease), 3) localized post-rabies vaccine panniculitis, 4) generalized vaccine-induced ischemic dermatopathy, and 5) generalized idiopathic ischemic dermatopathy.[4,6,10] Although the pathogenesis is incompletely elucidated for these diseases, the generally accepted premise is that of a cell-poor vasculitis, leading to decreased oxygen perfusion of the tissue, and subsequent ischemic change.[1,4,9]

Across the various subgroups of ischemic dermatopathies, clinical, gross, and histopathologic features are often similar. Clinically overall, anatomic locations most susceptible for mechanical trauma (i.e., bony protuberances), or distal extremities (i.e., phalanges) are preferentially affected.[4] Gross lesions include alopecia, scab formation, variation in pigmentation (hyper- or hypo-), and thinning of the skin.[4,8] Histopathologic lesions consist of follicular atrophy, hyperkeratosis, smudgy and indistinct collagen fibers, interface dermatitis and/or clefting at the epidermal basement membrane.[6,8] Diagnosing a specific subtype can sometimes be challenging, which requires a thorough clinical history and signalment, coupled with gross and histopathologic features. The use of electromyography or muscle physiology studies have also been useful in some cases.[1,3]

Familial Dermatomyositis (FDM) and juvenile onset ischemic dermatopathy (dermatomyositis-like or DM-like) have several identical clinicopathological features. They both occur in young dogs. Most commonly, lesions originate on the muzzle, periorbital and perioral tissues, dorsum of the distal phalanges and sometimes footpads,[4,8] but additionally the tips and folds of the pinnae, tip of the tail, and claw folds can also be affected.[4] Muscle changes and clinical abnormalities

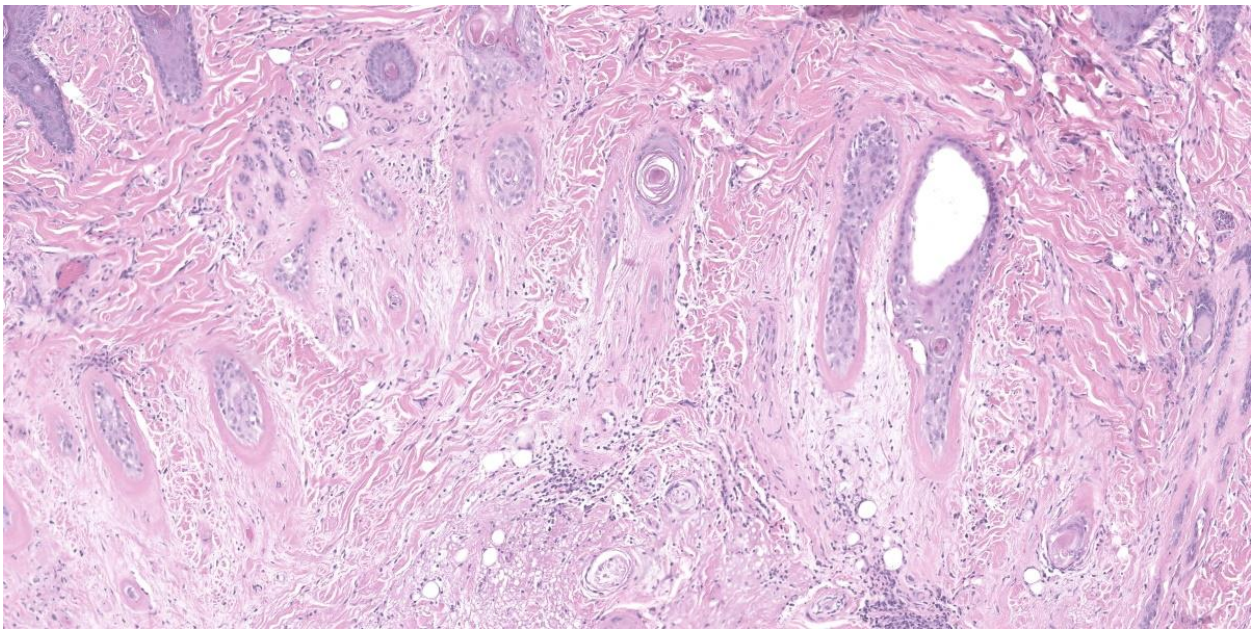

Figure 1-3. Haired skin, dog. Hair follicles are atrophic and surrounded by smudgy, diminished collagen fibers.

can be subtle but are often detected with histopathologic evaluation and/or electromyographic studies.[3] When present, atrophy can be most apparent affecting the temporal and masseter muscles.[4] Megaesophagus, growth retardation, and infertility are also reported findings.[4] FDM was first described in Collies,[5] with later reports in Shetland sheepdogs, Portuguese water dogs, and Belgian Tervuren dogs[3,4,6,10] whereas DM-like disease occurs sporadically in breeds without a scientifically proved genetic or familial component.[2,10]

Localized post-rabies panniculitis typically occurs 1 to 3 months after vaccine administration,[6] and initially, there is focal alopecia at the affected site that can progress to hyperpigmentation.[6] The neck and shoulder region in the vicinity of the scapulae, are primarily affected.[4]. Deposition of rabies viral antigens into the wall of vessels is suspected as the inciting stimulus.[4] Breeds predisposed to this condition include Toy and Miniature Poodles and Bichon Frises,[4,6] but there are reports also involving Yorkshire terriers and Chihuahuas.[8] The most characteristic histopathologic findings are lymphocytic perivascular inflammation and vasculitis,[11] coupled with other previously described features of ID. This condition can become more widespread and severe in some adult dogs, with the development of fever, lethargy, depression, and/or elevation in liver enzymes (generalized vaccine-induced ischemic dermatopathy).[4,6]

Generalized vaccine or idiopathic ischemic dermatopathy are identical clinicopathologically, and the presence of alopecia over a previous rabies vaccination site can assist in differentiating the two subtypes.[9] Generalized idiopathic ischemic dermatopathy is a diagnosis of exclusion.

For this case, the top three subtype differentials included: dermatomyositis-like disease, generalized idiopathic ischemic dermatopathy, and generalized vaccine-induced dermatopathy.

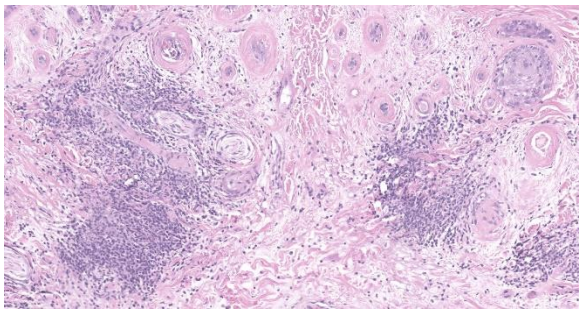

Figure 1-4. Haired skin, dog: In the deep dermis, vessel walls are thickened and vessels are surrounded by low to moderate numbers of lymphocytes, histiocytes and plasma cells. Vessels walls lack detail and are brightly eosinophilic (vasculitis). (HE, 158X)

Contributing Institution:
250 McElroy Hall

Department of Veterinary Pathobiology

College of Veterinary Medicine

Oklahoma State University

Stillwater, OK 74078 USA

https://vetmed.okstate.edu/veterinary-pathobiology/index.html

JPC Diagnosis:
Haired skin, dermis: Vasculitis, lymphohistiocytic, multifocal, moderate with regionally extensive adnexal atrophy, rare thrombi, and cell poor interface dermatitis.

JPC Comment:
This week's moderator was Dr. Charles Bradley, Associate Professor of Anatomic Pathology at the University of Pennsylvania. A perennial visitor to the WSC, Dr. Bradley emphasized cutaneous patterns of skin disease with participants. The first case is a good example of an interface dermatitis, albeit a cell-poor one. Case features are best observed first from low magnification with disruption of dermal collagen, loss of adnexal structures, and vasocentric lesions being helpful pickups that point at the underlying pathogenesis. Key histologic features on high magnification include disruption of the dermal-epidermal basement membrane, rare thrombi, and mild vasculitis. Although not strictly necessary for this case, PAS highlighted the basement membrane nicely and Movat's pentachrome highlighted select vessels.

Dr. Bradley also covered ancillary changes in section with conference participants. These included vacuolation of basal keratinocytes (likely a mild processing artifact) and focal parakeratosis which was attributable to tissue response to injury. In the superficial dermis, there was also granulation tissue present suggestive of previous ulceration and re-epithelization of the epidermis, perhaps from a previous episode of diminished blood flow. Likewise, the mild myositis in this case is likely a bystander lesion rather than a primary dermatomyositis – in Dr. Bradley's experience, muscle changes are rare to absent in histologic section in dermatomyositis (DM). Finally, it is also important to rule out other processes in the skin with ischemic changes such as reactive histiocytosis.

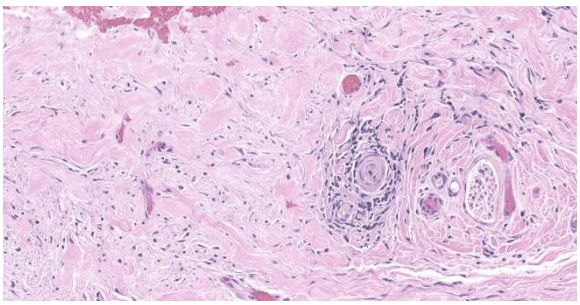

Figure 1-5. Haired skin, dog. Higher magnification of an affected vessel. Dermal collagen fibers are often markedly decreased in diameter, giving it a "smudgy" appearance (HE, 275X)

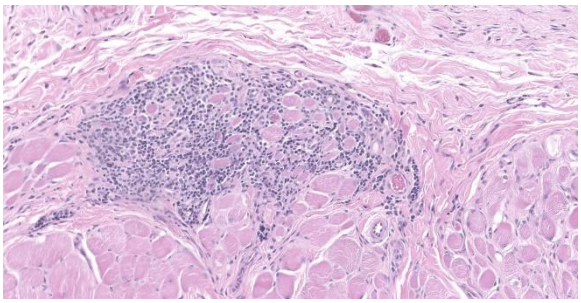

Figure 1-6. Haired skin, dog. The panniculus carnosus is occasionally infiltrated by inflammatory cells and in these areas, muscle fibers demonstrate evidence of degeneration and atrophy. (HE, 240X)

The clinical history of a young animal is helpful in this case and is suggestive of a vaccine-associated event. Histologically however, this is not distinguishable from DM. In addition, the location of the hyperpigmented alopecic skin ('poodle patch') may or may not be close to the site of vaccination, reflecting the systemic nature of this vasculitis. Deeper punch biopsies that sample the vaccine site may identify lymphohistiocytic aggregates within the subcutis that may contain vaccine adjuvant though. Dr. Bradley also touched on the role of anti-IL-31 therapy in dermatology cases, to include the use of oclacitinib and lokivetmab in modulating immune-related conditions. Apoquel, Cytopoint, and similar emerging therapies have been tried for a variety of canine skin conditions with reasonable success as an adjunct to more conventional drugs such as glucocorticoids.[8]

References:

1. Backel KA, Bradley CW, Cain CL, Morris DO et al. Canine ischaemic dermatopathy: a retrospective study of 177 cases (2005 – 2016). *Veterinary Dermatology*. 2019; 30: 403-e122.
2. Bresciani F, Zagnoli L, Fracassi F, Bianchi E, et al. Dermatomyositis-like disease in a Rottweiler. *Veterinary Dermatology*. 2014; 25; 229-e62.
3. Ferguson EA, Cerundolo R, Lloyd DH, et al. Dermatomyositis in five Shetland sheepdogs in the United Kingdom. *Veterinary Record*. 2000; 146, 214 – 217.
4. Gross TL, Ihrke, PJ, Walder EJ, Affolter VK. *Skin Diseases of the Dog and Cat: Clinical and Histopathologic Diagnosis*, 2nd ed., Blackwell Publishing. 2005; 49 – 52, 538 – 541.
5. Hargis AM, Hegreberg GA, Prieur DJ, Moore MP. Familial Canine Dermatomyositis. *American Journal of Pathology*. 1984; 116: 234 – 244
6. Ihrke PJ. Ischemic Skin Disease in the Dog. *31st World Small Animal Veterinary Association World Congress Proceedings*. 2006.
7. Kovacs SO, Kovacs SC. Dermatomyositis. *Journal of the American Academy of Dermatology*. 1998; 39(6), 899 – 920.
8. Levy BJ, Linder KE, Olivry T. The role of oclacitinib in the management of ischaemic dermatopathy in four dogs. *Vet Dermatol*. 2019; 30: 201-e63.
9. Morris DO. Ischemic Dermatopathies. V*eterinary Clinics of North America: Small Animal Practice*. 2013; 43, 99 – 111.
10. Romero C, Garcia G, Sheinberg G, et al. Three cases of Canine Dermatomyositis-like disease. *Acta Scientiae Veterinariae*. 2018; 46 (Suppl 1): 276.
11. Vitale CB, Gross, TL, Magro CM. Vaccine-induced ischemic dermatopathy in the dog. *Veterinary Dermatology*. 1999; 10, 131-142.

CASE II:

Signalment:
5 month old, intact female, Shar Pei, *Canis familiaris*, Dog.

History:
Limited history available. Alopecia and dermatitis, has been on cephalexin. epresentative samples submitted from face and legs.

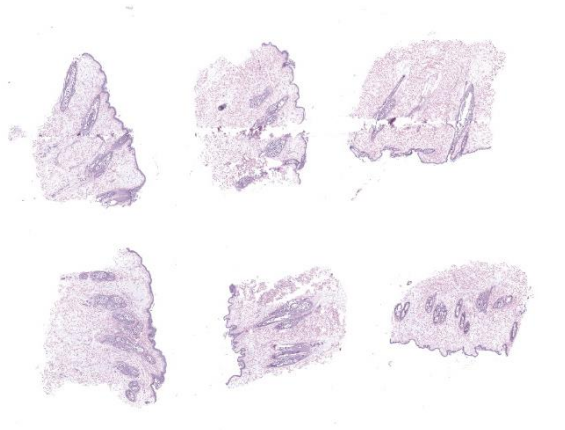

Figure 2-1. Haired skin, dog: Six punch biopsies are submitted for examination. (HE, 5X)

Gross Pathology:
3 haired skin punch biopsy specimens, 5-6mm diameter, ranging from 3-4mm deep

Microscopic Description:
Haired skin: All 3 punch biopsy samples are similar.

Diffusely, hair follicle lumina are moderately distended and filled with multiple longitudinal, transverse, and tangential sections of arthropods. These arthropods are elongate, up to 40µm diameter and 200µm in length; have a thin, eosinophilic, chitinous exoskeleton; short, jointed appendages; a hemocoel; striated musculature; digestive tract; and male or female reproductive tracts. There is minimal perifollicular as well as perivascular inflammation consisting of low numbers of lymphocytes, plasma cells, and eosinophils.

Dermal collagen fibers are diffusely fragmented and widely separated by abundant clear space and wispy, fibrillar, beaded, basophilic to amphophilic mucin. There are low numbers of histiocytes and lymphocytes scattered within the mucinous matrix.

There is clumping of melanin pigment within the follicular bulb matrix epithelium and to a lesser extent within the non-matrical follicular epithelium and follicular lumina.

Contributor's Morphologic Diagnosis:
1. Haired skin: Follicular ectasia, moderate, diffuse, with mild lymphoplasmacytic and eosinophilic perifolliculitis and numerous follicular intraluminal *Demodex canis* mites

2. Haired skin: Dermal mucinosis, diffuse, marked

3. Haired skin, hair follicles: Matrical epithelial, follicular epithelial, and intraluminal melanin clumping

Contributor's Comment:
This case represents three entities: juvenile-onset demodicosis, dermal mucinosis (a feature of "normal" skin in Shar Pei dogs), and color dilution.

Canine demodectic mange, also termed follicular mange or red mange, is one of the most common skin diseases of dogs.[6-10] It is a noncontagious disease that occurs when commensal *Demodex* mites are allowed to proliferate resulting in overpopulation.[1,5,6,9] Canine demodicosis is most commonly caused by *D. canis*, but *D. injai* can also cause disease.[1,5,8,9] *D. canis* is approximately 300µm in length, while *D. injai*, the "long-bodied mite", is 334-368µm in length.[8] Predisposing factors to *Demodex* overpopulation in its host include multiple causes of host immunosuppression.[1,6,8,9] Canine demodicosis can be either localized or generalized.[1,5,8,9] Localized disease is mild and typically self-limiting with spontaneous resolution, whereas generalized disease may spontaneously resolve but can continue into adulthood if inadequately treated, and may be fatal.[5,8] Canine demodicosis can also be either juvenile-onset or adult-onset.[1,5,8] Disease is considered adult-onset if disease onset occurs at 4 years of age or older,[8] although differentiation between these may be difficult.[1] Generalized demodicosis is typically a juvenile-onset disease.[4,8] Juvenile-onset demodicosis is thought to be

due to a genetically mediated immunodeficiency resulting in decreased T-cell function.[4,6,8,9] A recent study into the molecular pathogenesis of canine demodicosis found evidence that disease is associated with *Demodex*-induced host immune tolerance.[6] Studies into this immune tolerance identified host cellular endoplasmic reticulum stress which in turn results in the accumulation of unfolded proteins (i.e., unfolded protein response) which regulates signaling pathways involved in Toll-like receptors (especially TLR2) and promotion of M2-phenotype immunosuppressive macrophages.[7] Disease relapse, recurrence, or persistence is uncommon.[1]

Excessive accumulation of dermal mucin is termed cutaneous mucinosis.[2,5,8,10] This condition is abnormal and rare in most dogs.[5,8] In shar pei dogs, however, cutaneous mucinosis is due to a genetic mutation and is considered a normal feature which leads to their distinctive thick, wrinkled skin.[5,8,9] The mucinous material in the shar pei dermis has been identified as hyaluronan (or hyaluronic acid [HA]).[2,10] A study found that HA is produced in shar pei dermal fibroblasts in greater quantities than in control cells.[10] Shar pei cutaneous mucinosis has further been linked to increased mRNA expression of the HAS2 isoform of hyaluronan synthase (HAS), resulting in increased transcription of HAS2 by dermal fibroblasts.[2,9,10] The authors of that study suggest using the term "hereditary cutaneous hyaluronosis (HCH)" for the shar pei specific version of cutaneous mucinosis.[2] Diffuse canine cutaneous mucinosis has also been associated with hypothyroidism; this is rarely reported but clinically and histologically striking.[5,8,9] Cutaneous mucinosis is termed "myxedema" when associated with hypothyroidism.[5,8,9] Increased focal areas of dermal mucin have been reported in association with numerous inflammatory and neoplastic processes, such as mast cell tumor, severe pyoderma, and eosinophilic diseases.[5,8,9] A specific example of a cause of focal mucinosis in dogs is infection with the trombidioid mite *Stralensia cynotis* which causes characteristic mucinosis of the perifollicular dermis and pseudoepitheliomatous hyperplasia of the follicular epithelium (see WSC Conference 2, Case 4, 2018-2019).[8,9]

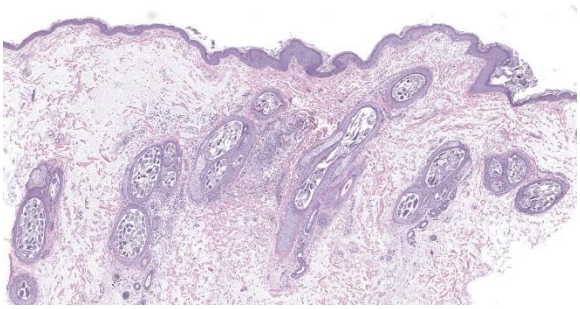

Figure 2-2. Haired skin, dog. Hair follicles are markedly expanded by numerous mites. Collagen fibers are diffusely and widely separated by abundant mucin. The overlying epidermis is mildly hyperplastic. (HE, 44X)

Color dilution has been reported in many species as well as in many breeds of dogs.[3,8,9] The condition in dogs is inherited as an autosomal recessive trait and is due to abnormalities in melanin transfer and storage.[3,5,8,9] In affected dogs, the coat color is pale, manifesting as blue, fawn, etc. This dilute color appearance is due to clumping of large melanin granules within hair follicles and characteristically within the epidermis.[5,8,9] There is preliminary evidence that the genetic cause of color dilution in dogs is an autosomal recessive mutation in the melanophilin gene (MLPH).[3,9] In dogs, the condition of color dilution may be associated with alopecia (i.e., color dilution alopecia), but is not always associated with alopecia.[5,8,9] Color dilution alopecia should only be diagnosed if histologic findings of both color dilution (clumped melanin) and follicular dysplasia/distortion are present.[5,9]

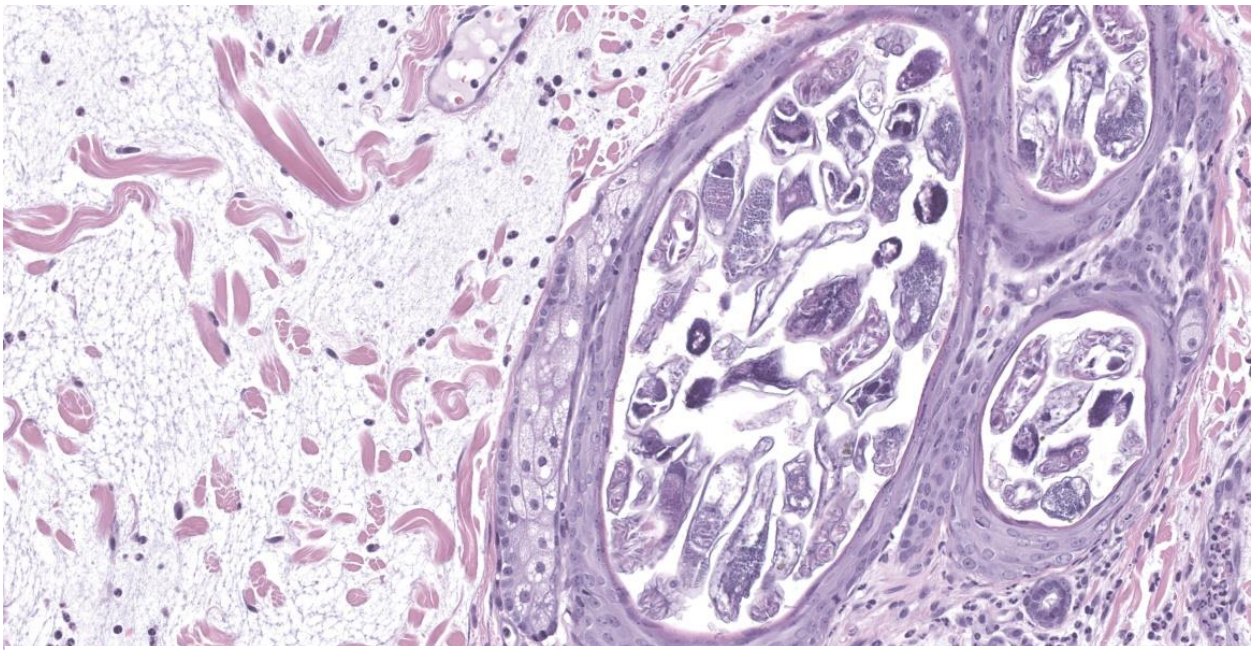

Figure 2-3. Haired skin, dog. Higher magnification of mite-laden hair follicles and adjacent mucinous dermis. Mites have chitinous exoskeletons, jointed appendages, striated muscles, a hemocoel, and nervous and reproductive tracts. (HE, 248X)

Contributing Institution:
Tri-Service Research Laboratory

4141 Petroleum Dr

San Antonio, TX 78234

JPC Diagnosis:
1. Haired skin: Follicular ectasia, moderate, diffuse, with mild lymphoplasmacytic and eosinophilic perifolliculitis and numerous follicular intraluminal adult *Demodex* mites.
2. Haired skin, dermis: Mucinosis, diffuse, moderate.

JPC Comment:
Case 2 has several entities for participants to consider. *Demodex* mites and dermal mucinosis are abundantly present in these sections. These findings together are interesting and should prompt consideration of immunosuppression such as Cushing's disease or severe hypothyroidism (myxedema) though the breed of this dog (Shar Pei) is an important detail as the contributor notes. Though these look similar histologically, the clinical presentation sorts these two camps out quickly. Other considerations for mite presence include long-term immunomodulatory drugs for control of allergic skin disease. In section, there are multiple examples of jointed appendages (figure #) and skeletal muscle that help to distinguish that hair follicle lumina are distended with many *Demodex* that the contributor nicely describes. Although not needed to distinguish the myxomatous dermis in this case, an Alcian blue pH 2.5 does highlight mucin nicely. One feature not present in this case is epidermal hyperplasia which is a secondary change due to the animal scratching (owing to mural folliculitis, rupture, and periadnexal mite fragments). Conference participants compared *Demodex* species across dogs and cats with *D. cati* being similarly follicularly-focused like *D. canis* while *D. gatoi* is found in the stratum corneum and is directly transferable between cats. The profound sebaceous hyperplasia induced by *D. injai* residing within sebaceous

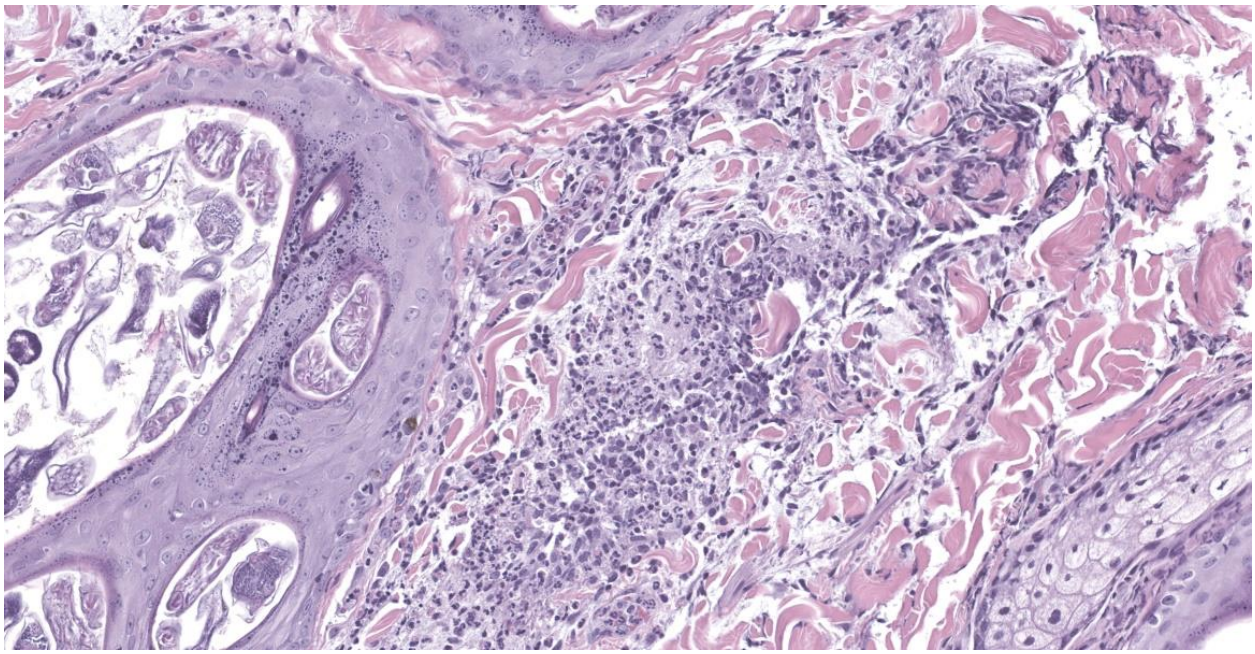

Figure 2-4. Haired skin, dog. Adjacent to ectatic follicles, there are variable amounts of mixed inflammation, including numerous lymphocytes, histiocytes, plasma cells, and eosinophils. (HE, 248X)

and ducts while lacking other epidermal changes explains the markedly greasy phenotype noted clinically.

The color dilution noted by the contributor prompted an interesting discussion among the group. Notably, many of the approved Shar Pei breed standard coats include dilute variants. As such, this could be a normal observation. We did not observe melanin clumping within epidermal melanocytes or the hair shaft in large quantity, though the hair bulb clumping is evident and worth describing. Though not in these section, distortion and fracture of the hair shaft is a helpful corroborating feature for color dilution alopecia.

Finally, Dr. Bradley touched on the role of inflammation in demodicosis. Although *Demodex* may be an incidental finding during routine skin biopsy, this case is clearly in excess of a single mite within a single follicle. Nonetheless, conference participants noted the overall muted inflammatory response in this case. Demodex is thought to play a role in the development of human rosacea in a two-fold manner. Foremost, proliferation of the mite activates TLR2 on inflammatory cells which upregulates production of cathelicidin (LL-37 peptide) which has both antimicrobial and proangiogenic effects.[4] Activation of endothelial cells by LL-37 increases in conjunction with UVB damage from sunlight, which then promotes increased production of VEGF which has both proangiogenic and immunosuppressive effects on immune cells.[4] In excess, VEGF binding causes loss of lymphocyte function and essential T cell exhaustion.[4] Secondly, Demodex also express a surface glycan Thomsen-Nouveau Antigen (Tn Ag) which is recognized by the dendritic cell galactose-type lectin receptor. Once bound to this receptor, Tn Ag induces production of IL-10 and recruitment of regulatory T-cells that further tamp down inflammation and allow *Demodex* to evade a committed host response and proliferate further.[4] These factors together hint at the interplay of

VEGF, LL-37, and IL-10 in a complex feedback loop for which the flushed face, papules, and telangiectasia are only a hint of the sinister scheme occurring at the molecular level.

References:

1. Bowden DG, Outerbridge CA, Kissel MB, Baron JN, White SD. Canine demodicosis: a retrospective study of a veterinary hospital population in California, USA (2000-2016). *Vet Dermatol*. 2018;29(1):19-e10.
2. Docampo MJ, Zanna G, Fondevila D, et al. Increased HAS2-driven hyaluronic acid synthesis in shar-pei dogs with hereditary cutaneous hyaluronosis (mucinosis). *Vet Dermatol*. 2011;22(6):535-545.
3. Dr ögemüller C, Philipp U, Haase B, Günzel-Apel AR, Leeb T. A noncoding melanophilin gene (MLPH) SNP at the splice donor of exon 1 represents a candidate causal mutation for coat color dilution in dogs. *J Hered*. 2007;98(5):468-473.
4. Forton FMN. The Pathogenic Role of Demodex Mites in Rosacea: A Potential Therapeutic Target Already in Erythematotelangiectatic Rosacea?. *Dermatol Ther (Heidelb)*. 2020;(10):1229–1253.
5. Gross TL, Ihrke PJ, Walder EJ, Affolter VK. *Skin diseases of the dog and cat*. 2nd ed. Oxford, UK:Blackwell Science; 2005:222-225, 380-383, 442-449, 482-483, 518-521, 526.
6. Kelly PA, Browne J, Peters S, et al. Gene expression analysis of Canine Demodicosis; A milieu promoting immune tolerance. *Vet Parasitol*. 2023;319:109954.
7. Kelly PA, McHugo GP, Scaife C, et al. Unveiling the Role of Endoplasmic Reticulum Stress Pathways in Canine Demodicosis. *Parasite Immunol*. 2024;46(4):e13033.
8. Mauldin EA, Peters-Kennedy J. Integumentary system. In: Maxie MG, ed. *Jubb, Kennedy, and Palmer's Pathology of Domestic Animals*. Vol 1. 6th ed. Philadelphia, PA: Elsevier Saunders; 2016: 557, 678-682, 683.
9. Welle MM, Linder KE. The integument. In: Zachary JF, ed. *Pathologic Basis of Veterinary Disease*. 7th ed., St. Louis, MO; Elsevier; 2022:1120, 1134, 1135, 1142.e1, 1149.e3, 1179-1181, 1182.e1, 1233.
10. Zanna G, Docampo MJ, Fondevila D, Bardagí M, Bassols A, Ferrer L. Hereditary cutaneous mucinosis in shar pei dogs is associated with increased hyaluronan synthase-2 mRNA transcription by cultured dermal fibroblasts. *Vet Dermatol*. 2009;20(5-6):377-382.

CASE III:

Signalment:

Horse (*Equus caballus*), Iceland pony, adult, male neutered.

History:

The horse has had penile lesions with multifocal mucosal thickenings and swelling for years.

Gross Pathology:

The penis was severely reddened and oedematous, the mucosa exhibited multifocal nodular thickenings and superficial yellow deposits. At the apex of the caecum, the mesentery of the large intestine and in the omentum there were multiple solid beige nodules about 1 to 3 cm in diameter.

Microscopic Description:

Penis/prepuce: The subepithelial connective tissue (submucosa) is severely expanded by a multifocal to coalescent, variable densely cellular inflammatory infiltrate consisting of high numbers of macrophages and lymphocytes, fewer numbers of plasma cells, and multinucleated giant cells (predominantly Langhans type). Lymphocytes often accompany the mucosa or surround deeper blood

Figure 3-1. Penis and prepuce, pony. The penis was reddened and edematous, the mucosa exhibited multifocal nodular thickenings and superficial yellow deposits (left and center). Similar changes were seen in the prepuce (right). (*Photo courtesy of:* Department of Veterinary Pathology, Freie Universität Berlin, http://www.vetmed.fu-berlin.de/en/einrichtungen/institute/we12/index.html).

vessels (perivascular cuffing). Cells frequently form merging granulomas characterized by nodules with abundant central partially epithelioid macrophages and few degenerate neutrophils, surrounded by lymphocytes, plasma cells, and multiple multinucleated giant cells admixed with plump, reactive fibroblasts and small amounts of loose collagenous connective tissue (fibrosis). The overlying mucosa is thickened, forming irregular rete ridges (hyperplasia) and infiltrated by neutrophils, partially forming serocellular crusts. In some areas, the mucosa is lost (ulceration) and the submucosa expanded by increased numbers of small caliber vessels, accompanied by activated fibroblasts admixed with loose collagenous connective tissue (granulation tissue).

<u>Additional special stains were used for histology:</u>

Ziehl-Neelsen stain for acid fast bacteria: negative

PAS reaction: negative

Contributor's Morphologic Diagnosis:
Penis/prepuce: Balanoposthitis, severe, chronic-active, multifocal to coalescing, granulomatous with epithelial hyperplasia, partial ulceration, granulation tissue formation, lymphocytic vasculitis and numerous multinucleated giant cells.

Lymph node: Lymphadenitis, mild, multifocal, chronic-active, granulomatous with numerous multinucleated giant cells.

Contributor's Comment:
The pathological findings are characterized by a systemic granulomatous inflammation without indications of a specific cause as no particular pathogen related lesions were present. The picture is therefore consistent with Equine idiopathic systemic granulomatous disease (ISGD), also referred to as "Equine sarcoidosis", "Equine generalized granulomatous disease", "Equine systemic granulomatous disease", "Equine histiocytic disease" or "Equine histiocytic dermatitis."[7]

The etiology of ISGD is unknown, though it has similarities to human sarcoidosis which is presumed to be a multifactorial disease due to

Figure 3-2. Cecum, pony. The penis was reddened and edematous, the mucosa exhibited multifocal nodular thickenings and superficial yellow deposits (left and center). Similar changes were seen in the prepuce (right). (*Photo courtesy of:* Department of Veterinary Pathology, Freie Universität Berlin, http://www.vetmed.fu-berlin.de/en/einrichtungen/institute/we12/index.html)

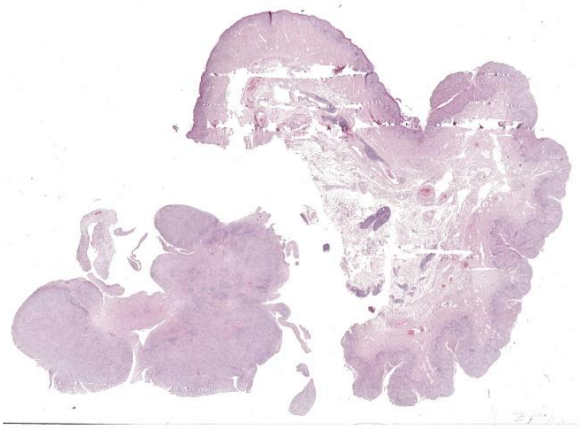

Figure 3-3. Penile mucosa and cecum, pony. A section of penis and one of cecum (left) is submitted tor examination.The mucosal epithelium is markedly hyperplastic, and there is a dense inflammatory infiltrate within the submucosa. (HE, 5X)

an abnormal host response to antigens.[5] Etiological investigations failed to identify specific agents. Similar lesions were documented after ingestion of *Vincia villosa* ('hairy vetch') by horses and more likely cattle, but not all by ISGD affected horses had been exposed to it.[9]

Clinical onset is variable. Cutaneous lesions in ISGD may present as an exfoliative dermatitis or less commonly, as a nodular lesions.[5,6] Additionally, internal organs are often involved in the course of a generalized disease with the lung, liver, gastrointestinal tract, spleen, kidney, bones, and central nervous system being affected in decreasing frequency. Although lymph nodes are often involved, a peripheral lymphadenopathy is mostly absent. In the case presented here, regional lymph nodes were enlarged and histopathology revealed multifocal sometimes nodular infiltrates by macrophages and giant cells were detectable. In generalized disease, most horses develop a wasting syndrome.[6,7] Diagnosis is primarily done by exclusion of infectious diseases (like dermatophilosis, dermatophytosis), autoimmune diseases (like pemphigus foliaceus, systemic lupus erythematosus), allergic reactions (like cutaneous adverse drug reaction, contact dermatitis), miscellaneous conditions (like seborrhea, multisystemic eosinophilic epitheliotropic disease), neoplasia (like epitheliotropic lymphoma), and toxins (like hairy vetch).[5] Characteristic pathohistological findings are so called sarcoidal granulomas affecting the skin or internal organs. Multinucleated histiocytic giant cells are typical and numerous.

Contributing Institution:

Department of Veterinary Pathology, Freie Universität Berlin

http://www.vetmed.fu-berlin.de/en/einrichtungen/institute/we12/index.html

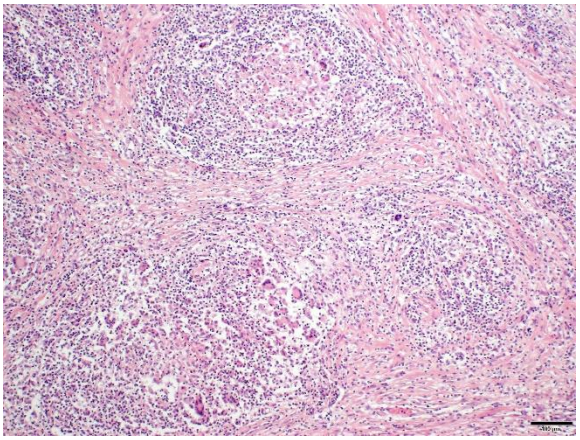

Figure 3-4. Penile mucosa, pony. The submucosa is expanded by coalescing, poorly formed granulomas. (*Photo courtesy of:* Department of Veterinary Pathology, Freie Universität Berlin, http://www.vetmed.fu-berlin.de/en/einrichtungen/institute/we12/index.html) (HE, 100X)

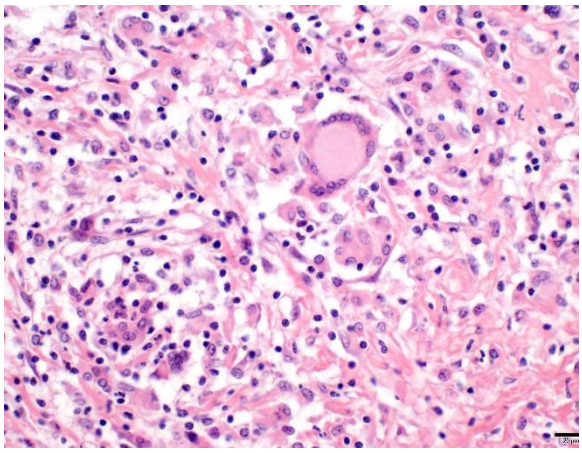

Figure 3-5. Penile mucosa, pony. Submucosal granulomas contain moderate foreign body and Langhans's type multinucleated giant cell macrophages admixed with numerous epithelioid macrophages and fewer lymphocytes and plasma cells. (*Photo courtesy of:* Department of Veterinary Pathology, Freie Universität Berlin, http://www.vetmed.fu-berlin.de/en/einrichtungen/institute/we12/index.html) (HE, 400X)

JPC Diagnosis:
Mucous membrane, penis: Balanoposthitis, lymphohistiocytic, chronic, diffuse, moderate with marked epidermal hyperplasia and ulceration and lymphocytic perivasculitis.

Fibrovascular tissue (presumed peritoneum): Peritonitis, granulomatous, chronic, diffuse, severe.

JPC Comment:
Case 3 was challenging for participants in that the exact location sampled is not obvious from the slide alone. The presence of large, multinucleated giant cell macrophages was a helpful feature that led participants to consider equine sarcoidosis for this case. Because sarcoidosis is a diagnosis of exclusion, excluding other causes of granulomatous inflammation (e.g. fungal, mycobacterial, pythiosis, foreign body reaction, *Actinobacillus*) must be performed. In addition to the acid-fast stain performed by the contributor, we performed modified Gram stains (Brown-Brenn, Brown-Hopps), GMS, and PAS Light Green which were negative for organisms. IHC for IBA1, CD3, and CD20 were also helpful is establishing the distribution of these inflammatory cells and excluding T-cell rich B-cell lymphoma as a possibility as well. Previously, equid gammaherpesvirus 2 was implicated as a potential cause of this condition,[3] which is a reasonable connection given that lymphohistiocytic inflammation is associated with gammaherpesviruses across species (e.g. malignant catarrhal fever). That stated, EHV-2 has not been a consistent finding in all cases of sarcoidosis and it is possible that the development of granulomatous inflammation may be the result of any number of antigens.[8]

Understanding of sarcoidosis is largely extended from human medicine, to include the entity name itself. Patients with sarcoidosis appear to have increased genetic susceptibility, to include variance in MHC class II genes[1] such as HLA-DRB1 that is associated with acute sarcoidosis and Löfgren syndrome. M1 macrophages are activated by a highly polarized T helper 1 (Th1) cytokine milieu including IFN-γ and TNF-α which correlate with the Langhans multinucleated giant cells seen in our case. Interestingly, not all of these macrophages may be classically activated. Cytokine studies of sarcoidosis patients have identified macrophages with increased IL-13 expression (i.e. M2 macrophages) that may play a role in later stages of the disease.[2] Additionally, M2 macrophages also form multinucleated giant cells (foreign body type), which were also observed in the present case.

As a final point, equine sarcoid should not be confused with sarcoidosis as they are entirely separate from one another. The term 'sarcoid' denotes a raised plaque or nodule in the skin (literally, sarcoma-like) which can be a feature of sarcoidosis, though other cutaneous

presentations can include crusting and scaling.[8] Equine sarcoids differ histologically from sarcoidosis in that they have increased density of dermal fibroblasts which form interlacing bundles and whorls within the dermis.[4] Bovine papillomavirus type 1 and type 2 are associated with the development of equine sarcoids[4] though the association of viruses in the development of sarcoidosis, if any, is uncertain.

References:

1. Chen ES, Moller DR. Sarcoidosis--scientific progress and clinical challenges. Nat Rev Rheumatol. 2011 Jul 12;7(8):457-67.
2. Locke LW, Crouser ED, White P, Julian MW, Caceres EG, Papp AC, Le VT, Sadee W, Schlesinger LS. IL-13-regulated Macrophage Polarization during Granuloma Formation in an In Vitro Human Sarcoidosis Model. Am J Respir Cell Mol Biol. 2019 Jan;60(1):84-95.
3. Nolte LC, Rosiak M, Baechlein C, Baumgärtner W, Allnoch L. Equine Idiopathic Systemic Granulomatous Disease With Manifestation in the Cerebellum Associated With Equid Gammaherpesvirus 2. Journal of Equine Veterinary Science. 2020; (94):103225.
4. Ogłuszka M, Starzyński RR, Pierzchała M, Otrocka-Domagała I, Raś A. Equine Sarcoids—Causes, Molecular Changes, and Clinicopathologic Features: A Review. *Veterinary Pathology*. 2021;58(3):472-482.
5. Scott DW, Miller WH: Chapter 15 - Miscellaneous Skin Diseases. *In*: Equine Dermatology, eds. Scott DW, Miller WH, pp. 647-697. W.B. Saunders, Saint Louis, 2003
6. Stannard AA. Immunologic diseases. *Veterinary Dermatology* 11: 163-178, 2000
7. Van Oldruitenborgh-Oosterbaan MMS, Grinwis GCM: Equine sarcoidosis: clinical signs, diagnosis, treatment and outcome of 22 cases. *Veterinary Dermatology* 24: 218-e248, 2013
8. Wimmer-Scherr CM & Schwarz, B.C. (2024) A narrative literature review of equine sarcoidosis. Equine Veterinary Education, 00, 1–8.
9. Woods LW, Johnson B, Hietala SK, Galey FD, Gillen D: Systemic granulomatous-disease in a horse grazing pasture containing Vetch (Vicia sp). *Journal of Veterinary Diagnostic Investigation* 4: 356-360, 1992

CASE IV:

Signalment:
10-week-old, female, C57BL/6 mice (*Mus musculus*)

History:
Mice arrived from vendor with no abnormalities observed upon entrance. Lab members shaved animals to prepare for subcutaneous tumor injection 2-week post-arrival and noted abnormal skin (bumpy, thick with patchy fur growth). No other health concerns. Lab stated this condition has only been observed with mice from this vendor. Three mice were submitted for skin histopathology.

Gross Pathology:
All mice from this cohort had skin lesions consisting of patchy alopecia and irregular/bumpy skin foci in the dorsal flank area with extension to the limbs and (rarely) abdomen.

Microscopic Description:
Haired skin: Three skin sections from different mice in the cohort are examined. In all sections, there are focal ulcers and erosions. Multifocally, longitudinal follicle sections show hair shafts with twist severely in the infundibulum and/or disintegrating of hair in the superficial dermis and as it emerges on the surface. Rarely, hair shafts can be seen

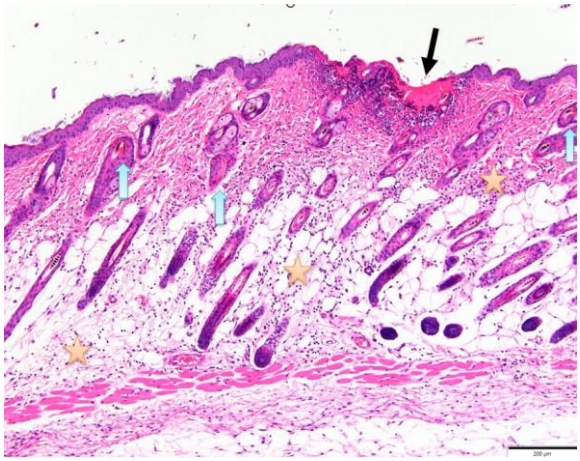

Figure 4-1. Haired skin, mouse. There is a focal ulcer (black arrow), several intrafollicular twisted, bent, and fragmented hair shafts (blue arrow), and diffuse chronic dermatitis (stars) in this section. (HE, 100X) (*Photo courtesy of:* Division of Laboratory Animal Resources, University of Pittsburgh, http://www.dlar.pitt.edu/)

penetrating the follicle wall with fragments free in the dermis and hypodermal fat layer surrounded by a mixed inflammatory cell infiltrate consisting of neutrophils, macrophages, rare multinucleated giant cells, and occasional lymphocytes forming a foreign body granuloma (trichogranuloma). Other areas have a more diffuse chronic lymphoplasmacytic infiltrate in the dermis and hypodermal fat. The overlying epidermis exhibits mild to moderate acanthosis, hypergranulosis, and orthokeratotic hyperkeratosis. Resolved ulcers often contain underlying superficial dermal granulation tissue proliferation, fibroplasia, and increased connective tissue.

Contributor's Morphologic Diagnosis:
Haired skin: Dermatitis, chronic, hyperplastic, ulcerative, with hair shaft twisting, fragmentation, trichogranuloma formation, and superficial dermal scarring.

Contributor's Comment:
Mice of the strain C57BL/6 and those on a C57BL/6 background develop ulcerative dermatitis (UD), a disease of unknown etiology that leads to significant morbidity.[4,10] In this entity, ulcerations present on the dorsal scapulae, torso, shoulder, and face from pruritis-induced self-trauma, and may be single or multifocal in distribution.[1,4,10] A recent large-scale studies in mice reveal that chronic ulcerative dermatitis is still the primary non-tumoral cause of euthanasia in both sexes (39.1% in males and 35.4% in females).[2] In the case of these mice, the lesions did not fit the typical clinical, gross, or histopathology lesions characteristic of UD. Specifically, no pruritis was noted in any of the cohort clinically, and lesions were initially noted when fur was removed. Histopathologically, small ulcerations were noted, however, the changes to the hair follicles, shafts, and secondary inflammation of the dermis were the most characteristic findings.

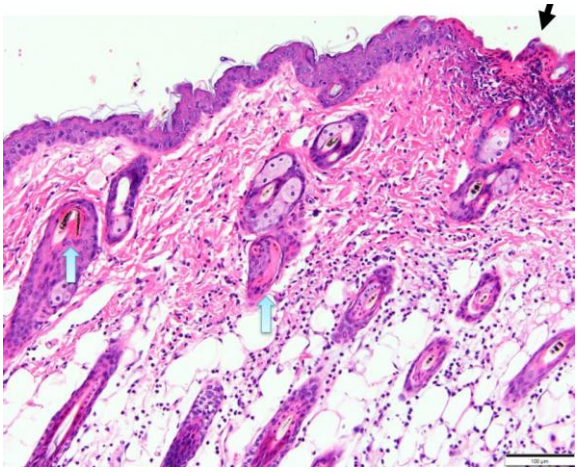

Figure 4-2. Haired skin, mouse. Higher magnification of the field in image 4-2 with twisted hair shafts (blue arrows) with surrounding chronic dermal infiltrates and a surface ulcer (black arrow). (HE, 100X) (*Photo courtesy of:* Division of Laboratory Animal Resources, University of Pittsburgh, http://www.dlar.pitt.edu/)

Many of the scarring alopecias in humans and other species, are based on primary sebaceous gland pathological features.[7] Although sebaceous gland loss can be seen in some areas with chronic scarring in these mice, the primary lesions are centered on the follicles. An entity was characterized in 2011 in C57BL/6J mouse substrains describing a primary follicular dystrophy (PFD) which leads to trichogranulomas, chronic scarring of the dermis, and alopecia.[8] The changes in the primary follicles include fragmentation and twisting of the hair shaft as we saw in these mice. In 2017, a large scale screening study of knockout mice revealed sporadic trichogranulomas are common in mutant mice, however, these are not consistently seen in all mice of a specific line. PFD was noted at a much lower frequency.[9] Although the etiology of PFD remains unclear, C57BL/6J mice were found to have defects in vitamin A metabolism.[9] The skin takes up circulating retinol and can either store it in the form of retinyl esters or metabolize it to retinoic acid.[5,8] Two enzymes are present in the skin that can oxidize retinol to retinal. These include the medium chain alcohol dehydrogenase type 4 (ADH4) and the short chain dehydrogenase/reductases epithelial retinol dehydrogenase (DHRS9).[3,8] DHRS9 is microsomal and can oxidize both free and CRBP-bound retinol.[3,8] Upregulation of DHRS9 in C57BL/6J and C57BL/6Tac but not C57BL/6NCr or C57BL/6Crl mice provides a potential explanation for why the first two strains have a much higher frequency of dorsal skin alopecia.[8]

The histologic lesions seen in mice with primary follicular dystrophy resemble the human disease currently termed central centrifugal cicatrical alopecia (CCCA).[8] Premature desquamation of the inner root sheath occurs in CCCA leading to marked thinning of the outer root sheaths with reactive perifollicular inflammation, and eventually entry of the hair fiber into the dermis with resulting destructive chronic granulomatous inflammation.[6,8,9] Although this entity does not have all features of CCCA in people, the degenerative features of the inner root sheath in PFD mirror those changes in CCCA.[8]

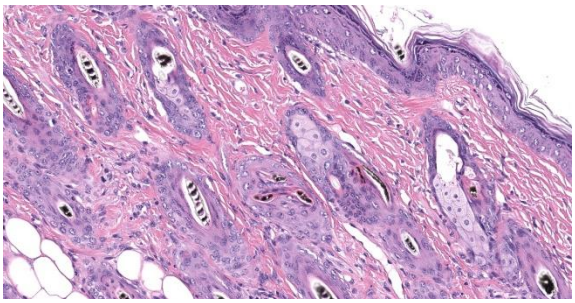

Figure 4-3. Haired skin, mouse. Hair shafts are twisted, fragmented, and poorly formed. (HE, 255X)

Contributing Institution:
Division of Laboratory Animal Resources
University of Pittsburgh
S1040 Thomas E. Starzl Biomedical Science Tower
200 Lothrop Street
Pittsburgh, PA 15261
http://www.dlar.pitt.edu/

JPC Diagnosis:
Haired skin: Follicular dysplasia, multifocal, moderate with ulcerative dermatitis, trichogranulomas, and superficial fibrosis.

JPC Comment:
The final case of this conference proved tricky for participants. Although these sections of skin featured dermatitis that was ulcerative, the cause was follicular dysplasia with ulcerative dermatitis developing similarly to the CCCA that the contributor describes. From low magnification, the twisting of hair shafts and abnormal orientation of hair follicles relative to the epidermis (figure #) are key details. Under higher magnification, dystrophic hairs are hypereosinophilic

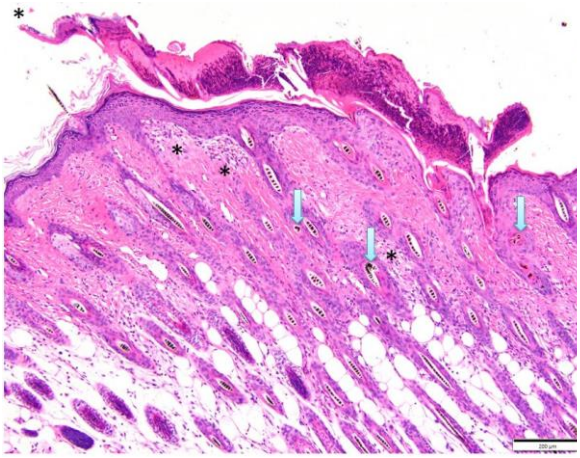

Figure 4-4. Haired skin, mouse. In addition to twisted and fragmented hair shafts (arrows), this section shows a large surface crust, underlying epithelial hyperplasia, and superficial dermal fibrosis and fibroplasia (*)(HE, 100X) (*Photo courtesy of:* Division of Laboratory Animal Resources, University of Pittsburgh, http://www.dlar.pitt.edu/)

due to poor cuticle maturation as well. Although subtle, these sections of skin also have increased space (widening) between abnormal hair follicles as well. In contrast, UD is characterized by marked lymphohistiocytic and neutrophilic inflammation of the dermis, epidermis, and deeper tissues (adipose, muscle, nerves) that can progress to fibrosis in chronic cases.[2] The overlying epidermis is also often hyperplastic. These features of UD are notably absent in this case however. Other causes of ulcerative skin disease and alopecia in mice include barbering, feeder/waterer-associated dermatitis, ectoparasites (e.g. *Myobia musculi*), self-trauma, fighting, and chemotherapy agents. Primary deficiencies of genes associated with hair development as was likely in this case should also be considered.

Lastly, conference participants discussed some of the unique features of mouse skin. Mice lack apocrine glands and rete ridge formation. They also have synchronized hair cycles such that growth occurs in waves (i.e. adjacent follicles in section are in the same phase) though overall mice tend to be anagen-heavy. In this case, there is disruption of this synchronization of hair development due to alopecia and inflammation.

References:

1. Andrews AG, Dysko RC, Spilman SC, Kunkel RG, Brammer DW, Johnson KJ. 1994. Immune complex vasculitis with secondary ulcerative dermatitis in aged C57BL/6NNia mice. Vet Pathol 31:293–300.
2. Elies L, Guillaume E, Gorieu M, Neves P, Schorsch F. Historical Control Data of Spontaneous Pathological Findings in C57BL/6J Mice Used in 18-Month Dietary Carcinogenicity Assays. Toxicologic Pathology. 2024 May 17:01926233241248658.
3. Haselbeck RJ, Ang HL, Duester G. Class IV alcohol/retinol dehydrogenase localization in epidermal basal layer: potential site of retinoic acid synthesis during skin development. Dev Dyn. 1997 Apr;208(4):447-53.
4. Kastenmayer RJ, Fain MA, Perdue KA. A retrospective study of idiopathic ulcerative dermatitis in mice with a C57BL/6 background. *J Am Assoc Lab Anim Sci*. 2006 Nov;45(6):8-12.
5. Roos TC, Jugert FK, Merk HF, Bickers DR. Retinoid metabolism in the skin. *Pharmacol Rev*. 1998 Jun;50(2):315-33.
6. Sperling LC. Scarring alopecia and the dermatopathologist. *J Cutan Pathol*. 2001 Aug;28(7):333-42.
7. Stenn KS, Sundberg JP, Sperling LC. Hair Follicle Biology, the Sebaceous Gland, and Scarring Alopecias. *Arch Dermatol.* 1999;135(8):973–974.
8. Sundberg JP, Taylor D, Lorch G, Miller J, Silva KA, Sundberg BA, Roopenian D, Sperling L, Ong D, King LE, Everts H. Primary follicular dystrophy with scarring dermatitis in C57BL/6 mouse substrains

resembles central centrifugal cicatricial alopecia in humans. *Vet Pathol*. 2011 Mar;48(2):513-24.
9. Sundberg JP, Dadras SS, Silva KA, Kennedy VE, Garland G, Murray SA, Sundberg BA, Schofield PN, Pratt CH. Systematic screening for skin, hair, and nail abnormalities in a large-scale knockout mouse program. *PLoS One*. 2017 Jul 10;12(7):e0180682.
10. Williams LK, Csaki LS, Cantor RM, Reue K, Lawson GW. Ulcerative dermatitis in C57BL/6 mice exhibits an oxidative stress response consistent with normal wound healing. *Comp Med*. 2012 Jun;62(3):166-71.

Joint Pathology Center
Veterinary Pathology Services

WEDNESDAY SLIDE CONFERENCE 2024-2025

Conference #9 — 16 October 2024

CASE I:

Signalment:
7-year-old female black and white colobus monkey (*Colobus guereza*).

History:
The animal was housed at a UK zoo collection as part of a colobus/patas monkey exhibit. It presented subdued and with reduced appetite; after a short period of clinical improvement the animal was found unable to move and was euthanized based on a poor prognosis. Previous appropriate fecal testing at a specialized laboratory was repeatedly positive for *Entamoeba species* for a period of 8 months prior to death. A male in the same group had also died in the past 5 months.

Gross Pathology:
The animal presented in poor body condition with no subcutaneous fat and widespread serous fat atrophy. Approximately 750ml of orange-yellow fluid were present in the abdominal cavity. The glandular portion of the stomach had a circular, 2cm diameter, slightly depressed, ulcer with a thin white and red halo (hyperemia). The liver showed a focal capsular adhesion to the gastric serosa. Cut surfaces displayed a diffusely enhanced lobular pattern and exhibited multifocal, dark yellow, 5mm to 5cm, nodular foci randomly distributed throughout the parenchyma. The right cranial lung lobe exhibited a focal, 4cm, mottled yellow-white and red nodule, with heterogeneously necrotic and mucopurulent

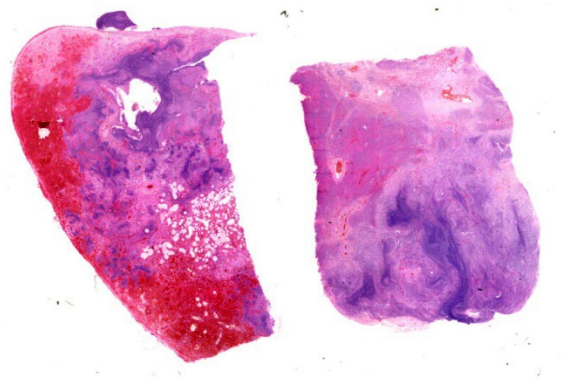

Figure 1-1. Lung and liver, colobus monkey. Much, if not all, of the subgross architecture of the sections of lung (left) and liver (right) is effaced by extensive areas of necrosis, hemorrhage, and abundant, often lamellated cellular debris. (HE, 4X)

cut surfaces. The middle right lung lobe was mottled red to dark-red and firm (consolidated). The left lung lobe had patchy areas of congestion. Remaining organs and body cavities were unremarkable on macroscopic examination.

Laboratory Results:
Clinical Pathology:

Liver, impression smear: Accumulations of degenerate neutrophils and vacuolated macrophages, including large central aggregations of densely cellular basophilic necrotic debris. Red blood cells and occasional multinucleated cells were present around the periphery of aggregates. A few normal hepatocytes were seen, with blue cytoplasm containing occasional dark blue/black granules

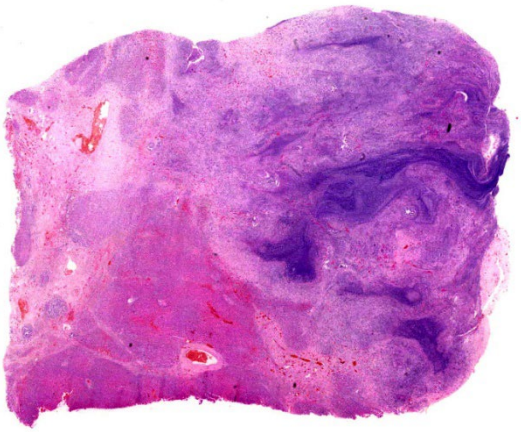

Figure 1-2. Liver, colobus monkey. 50% of the liver is effaced by large areas of necrosis. At the periphery of the necrosis, there is prominent fibrosis throughout the remainder of the section. (HE, 7X)

(presumed hemosiderin). Mixed populations of bacteria were present amongst the cellular debris. Some areas had more abundant populations of spindle cells (presumptive fibroblasts).

Right lung, impression smear: Mixed populations of inflammatory cells including small numbers of degenerate neutrophils, abundant macrophages, and occasional multinucleated cells. Macrophages had vacuolated cytoplasm, sometimes with intracytoplasmic granular debris. Red blood cells were intermingled with inflammatory populations.

Immunohistochemistry:

IHC for *E. histolytica*: Positive (carried out at the Institute for Veterinary Pathology, University of Liverpool, following standard operating procedures).

Microscopic Description:

Liver: Randomly to bridging, approximately 80% of the examined section is completely effaced by multifocal to coalescent areas containing abundant amphophilic and basophilic amorphous debris (lytic necrosis) admixed with cytoclastic inflammatory cells, small numbers of viable and non-viable neutrophils, and moderate numbers of circular to oval, 15-20µm, unicellular protozoa with a pale eosinophilic cytoplasm with large phagocytic vacuoles and a pale small amphophilic eccentric basophilic round to oval nucleus (amoebic trophozoites). Areas of necrosis are intermingled and rimmed by numerous macrophages, neutrophils (viable and non-viable) and occasional multinucleated giant cells (Foreign body giant cell type) admixed with moderate deposition of reactive fibroblasts and mature collagen fibers (fibrosis). Interlacing and incorporating between the immature granulation and fibrotic tissue, there are myriad of irregular proliferated biliary ductules (biliary hyperplasia or ductular reaction). The adjacent parenchyma is composed of widely separated hepatic cords with small, irregular hepatocytes (atrophy).

Lung: Multifocal to coalescing, affecting approximately 75% of the section, there is severe pyogranulomatous and necrotizing inflammation accompanied by large empty ar-

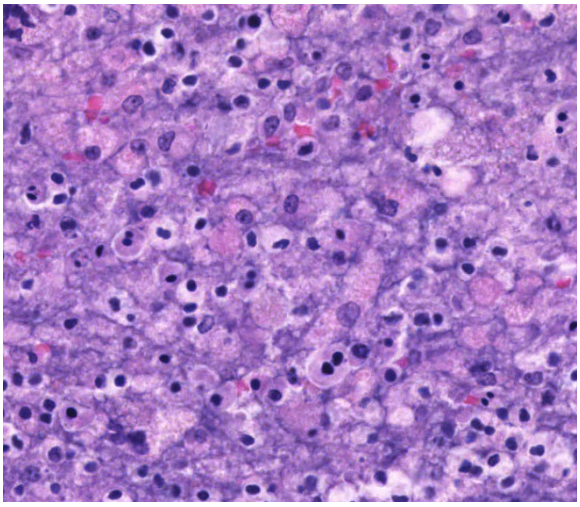

Figure 1-3. Liver, colobus monkey. There are numerous amebae within the areas of lytic necrosis. Amebae are round with prominent nuclei and abundant eosinophilic granular cytoplasm. (HE, 567X).

eas (cavitation of alveolar parenchyma) and dilated bronchi (bronchiectasis). Filling and expanding bronchi and bronchioles and effacing the adjacent pulmonary parenchyma, there are large numbers of amphophilic karyorrhectic and cellular debris (lytic necrosis), eosinophilic fibrillary beaded material (fibrin), viable and degenerated neutrophils, macrophages and extravasated erythrocytes (hemorrhage) admixed with orange/yellow hemoglobin breakdown pigments. Within the necrotic areas there are numerous circular or oval, 15-20µm, unicellular protozoa with a pale eosinophilic cytoplasm with large phagocytic vacuoles and pale small amphophilic eccentric round to oval nucleus (amoebic trophozoites). The necrotic areas are surrounded by abundant viable and degenerate neutrophils, macrophages (mostly epithelioid) and multinucleated giant cells (Langhans and foreign body type). Focally, there is a large thrombus filling a pulmonary vessel which is attached to the necrotic endothelium and composed of neutrophils, necrotic debris and fibrin. Multifocally, surrounding areas of inflammation, alveolar septa are expanded or effaced by increased collagen (fibrosis) and hypertrophic fibroblasts with perpendicularly arranged small blood vessels (granulation tissue). Adjacent septa are irregularly lined by cuboidal epithelium (pneumocyte type II hyperplasia). Less affected alveolar spaces are filled with a large amount of hemorrhage, occasionally admixed with fibrin, inflammatory debris and necrotic material. Multifocally, there are few discrete areas of pulmonary over inflation.

Contributor's Morphologic Diagnosis:
1. Hepatitis, necrotizing, pyogranulomatous, fibrosing, with abundant intralesional protozoal (amoebic) trophozoites consistent with *Entamoeba* spp., and bile duct hyperplasia, severe, multifocal to coalescent, random to bridging), chronic-active; liver.

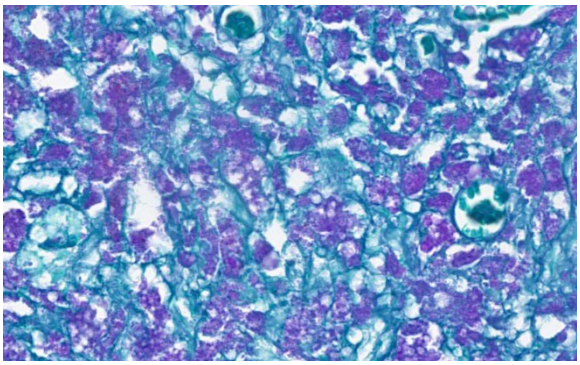

Figure 1-4. Liver, colobus monkey. A PAS stain demonstrates the amebae within areas of lytic necrosis. (PAS w/ malachite green, 200X)

2. Pneumonia, necrotizing, pyogranulomatous, with bronchiectasis, fibrin thrombus, and intralesional protozoal (amoebic) trophozoites consistent with *Entamoeba* spp., severe, multifocal to coalescent, chronic-active; lung.

Contributor's Comment:
Lesions in this case were consistent with chronic-active hepatic and pulmonary amebiasis. Other concomitant lesions in this case included ulcerative amebic gastritis, ascites, and emaciation. Unicellular protozoal organisms whose morphology were consistent with *Entamoeba* spp. were observed within the necrotic areas in the liver, lung, and stomach. Immunohistochemistry for *Entamoeba histolytica* was positive, further confirming the histopathological diagnosis.

E. histolytica is a protozoan parasite reported worldwide to occur in humans and a wide range of New and Old World monkeys, as well as apes.[8] Several species have been described which differ in their location in the host and nonhuman primate (NHP) species affected including *E. histolytica, E. dispar, E. moshkovskii, E. polecki, E. nutalli, E. chattoni, E. coli, E. hartmanni, E. ecuadoriensis and E. bangladeshi*.[8] In the United Kingdom, one study suggests a notable prevalence of

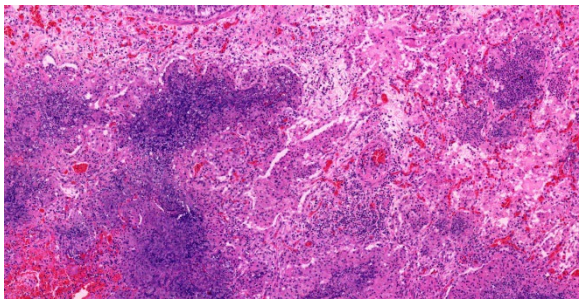

Figure 1-5. Lung, colobus monkey. There are numerous areas of lytic necrosis and alveolar exudate throughout the lung. (HE, 87X)

Entamoeba infection in NHPs with three main species circulating in the zoo's environment, namely *E. histolytica*, *E. dispar* and *E. polecki* ST4.[6]

Included under the *E. histolytica* species complex are *E. histolytica, E. dispar* and *E. moshkovskii.* They have different virulence capabilities, but are morphologically indistinguishable.[7] *E. histolytica* is the most commonly recognized zoonotic agent and can cause both intra- and extraintestinal disease.[1,8] There is a zoonotic risk for humans in close contact with primates.[6] The pathogenicity is determined by multiple virulence factors such as ubiquitin and adhesive surface lectins and is further depend on strain, host species, nutritional status, gastrointestinal (GI) microflora, environmental factors.[1,2,8] The essential steps leading to tissue damage are the adhesion of the organism to the hosts' protective mucus by lectin followed by enzymatic mucus breakdown and lectin-mediated adherence to host epithelium. Damage to mucosal epithelium is mediated by the release of cysteine proteases that attract inflammatory cells.

Usually, clinical signs are unspecific and NHPs show lethargy, weakness apathy, dehydration, anorexia, vomiting, rectal prolapse and severe catarrhal or hemorrhagic diarrhea.[1,8]

Fatal amebiasis with abscess formation particularly in the liver and more infrequently in the lung and the brain is reported in humans, colobus monkeys (*Colobus guereza*; *Colobus abyssinicus*), douc langurs (*Pygathrix nemaeus*), dusky leaf monkeys (*Presbytis obscurus*), chimpanzees (*Pan troglodytes*), baboons (*Papio* spp.), orangutans (*Pongo pygmaeus*), and spider monkeys (*Ateles* spp.).[1,6,8,9] Concurrent amebic gastritis is predominantly seen in leaf-eating primates (colobus monkey, silver-leafed monkey) and other gastric fermenting folivores such as langurs and proboscis and relates to higher stomach pH that is conducive to survival of ameba.[1,9]

The encystment of the infective forms appears to take place in the small intestine and the infection is established in the lumen of the large intestine. Infections are often transient and self-limiting. Under certain circumstances however, *E. histolytica* may invade the intestinal wall and cause colitis and consecutive amebic hepatitis by spread via the portal vein.[9] Hematogenous and/or lymphatic invasion of other organs (brain, lung) is rare and reported to be nearly always associated with liver abscesses.[8]

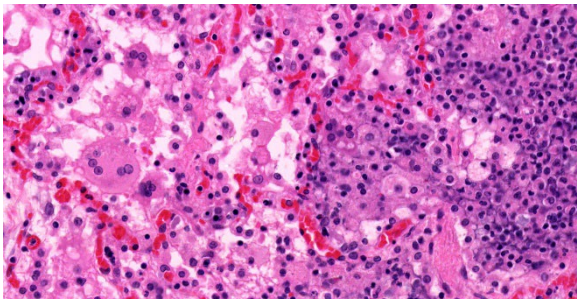

Figure 1-6. Lung, colobus monkey. Ameba are present within areas of necrosis. There are scattered multinucleated foreign body type giant cells within the alveoli as well. (HE, 443X)

Microscopically, amebae are surrounded by a clear halo with extensive pseudopodia and possess a nucleus with a dark karyosome. The cytoplasm appears foamy and they frequently phagocytize erythrocytes, which makes them difficult to distinguish from activated macrophages. The periodic acid-Schiff reaction highlights intracytoplasmic glycogen granules within amebae. Trichrome and Giemsa stains can also be utilized to emphasize amoebic trophozoites. On direct smears, Lugol's iodine can be used to aid the diagnosis of trophozoites, due to the presence of intracytoplasmic glycogen (starch).

Contributing Institution:
International Zoo Veterinary Group, Station House, Parkwood Street, Keighley, BD21 4NQ, UK. Website: www.izvg.co.uk

JPC Diagnosis:
1. Liver: Hepatitis, necrotizing, chronic-active, multifocal to coalescing, severe, with numerous amebic trophozoites.
2. Lung: Pneumonia, interstitial, necro-hemorrhagic, chronic-active, diffuse, severe, with pleural granulation tissue and numerous amebic trophozoites.

JPC Comment:
This week's moderator was Dr. Jeremy Bearss, previous chairman of the department and current research pathologist with the National Institute of Allergy and Infectious Diseases. This week's cases were chosen as they are all excellent "descriptive cases".

The profoundly necrotizing nature of these lesions was evident from low magnification, although more careful observation was required to pick up evidence of chronicity including type II pneumocyte hyperplasia, fibrosis, and subpleural granulation tissue within the lung and nodular regeneration and biliary hyperplasia within the liver. Although amebae were recognizable in large numbers

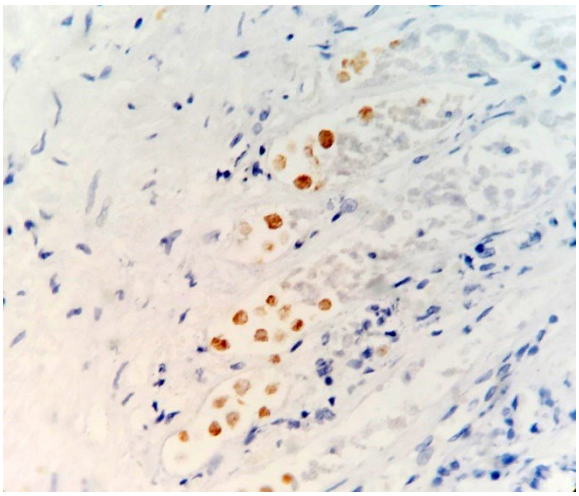

Figure 1-7. Stomach, colobus monkey. Ameba within the gastric ulcer are positive for an immunostain for *Entamoeba histolytica*. (anti *Entamoeba histolytica*, 400X) (*Photo courtesy of*: International Zoo Veterinary Group, Station House, Parkwood Street, Keighley, BD21 4NQ, UK. Website: www.izvg.co.uk)

on H&E, both PAS and GMS stains were helpful in highlighting them, and are consoiderations for cases in whichch their numbers are reduced.

As the contributor notes, diet plays a role in the pathogenesis of this entity in leaf-eating primates. Colobine monkeys have a large simple stomach with four compartments, which provide dedicated space for increased fermentation.[3] The relative increase in pH in this portion of the stomach is conducive to the survival of ameba. The gastric ulcers noted in the clinical history are the portal of entry of *Entamoeba* into the portal system with dissemination to liver and lungs. Dr. Kali Holder (Smithsonian conservation pathologist) was among conference attendees and noted that similar *Entamoeba* lesions can be seen in kangaroos and wallabies given their similar diet and compartmented stomach structure.

Finally, the role of *Entamoeba* as both a zo-

onosis and anthrozoonosis is worth considering. Transmission of *Entamoeba* from captive non-human primates to caretakers was previously described.[5] *E. nuttalli* is pathogenic in animals, though its role in human disease is unclear. Nonetheless, caretakers that did not care for NHPs lacked the presence of *E. nuttalli* in fecal specimens, consistent with transmission of the agent within the zoo environment. Conversely, potential transmission of *E. histolytica* from humans to chimpanzees and baboons in the Gombe region of Tanzania has also been detailed.[4]

References:

1. Calle P, Joslin J. Chapter 37 - New World and Old World monkeys. In: Miller R, Fowler M, eds. *Fowler's Zoo and Wild Animal Medicine, Volume 8*. St. Louis, Missouri: Elsevier Inc.; 2015:301–335.
2. Crisóstomo-Vázquez MDP, Jiménez-Cardoso E, Arroyave-Hernández C. Entamoeba histolytica sequences and their relationship with experimental liver abscesses in hamsters. *Parasitol Res*. 2006;98:94–98.
3. Davies G, Oates J. *Colobine Monkeys: Their Ecology, Behaviour and Evolution*. New York, Cambridge University Press, 1994, pp. 205-284.
4. Deere JR, Parsons MB, Lonsdorf EV, et al. Entamoeba histolytica infection in humans, chimpanzees and baboons in the Greater Gombe Ecosystem, Tanzania. *Parasitology*. 2019;146(9):1116-1122.
5. Levecke B, Dorny P, Vercammen F, et al. Transmission of Entamoeba nuttalli and Trichuris trichiura from Nonhuman Primates to Humans. *Emerging Infectious Diseases*. 2015;21(10):1871-1872.
6. Regan CS, Yon L, Hossain M, Elsheikha HM. Prevalence of Entamoeba species in captive primates in zoological gardens in the UK. *PeerJ*. 2014;DOI 10.7717/peerj.492.
7. Sargeaunt P, Williams JE, Jones DM. Electrophoretic Isoenzyme Patterns of Entamoeba histolytica and Entamoeba chattoni in a Primate Survey. *J Protozool*. 1982;29:136–139.
8. Strait K, Else J, Eberhard M. Parasitic diseases of nonhuman primates. In: Abee CR, Mansfield K, Tardif S, Morris T, eds. *Nonhuman Primates in Biomedical Research: Diseases, Vol.2*. London: Elsevier Inc.; 2012:197–297.
9. Ulrich R, Böer M, Herder V, et al. Epizootic fatal amebiasis in an outdoor group of Old World monkeys. *J Med Primatol*. 2010;39:160–165.

CASE II:

Signalment:
13 year old, castrated male, Yorkshire terrier, *Canis familiaris*, Dog

History:
History of inflammatory bowel disease treated with prednisone. Presented on 17 January 2024 for evaluation of dyspnea and hyporexia. Had multiple episodes of vomiting without response to an increased prednisone dose. He was hospitalized on supplemental O2. Exam revealed a grade 4/6 heart

Figure 2-1. Lung, dog. Two sections of lung are submitted for examination. There are several foci of hypercellularity in subpleural areas.. (HE, 5X)

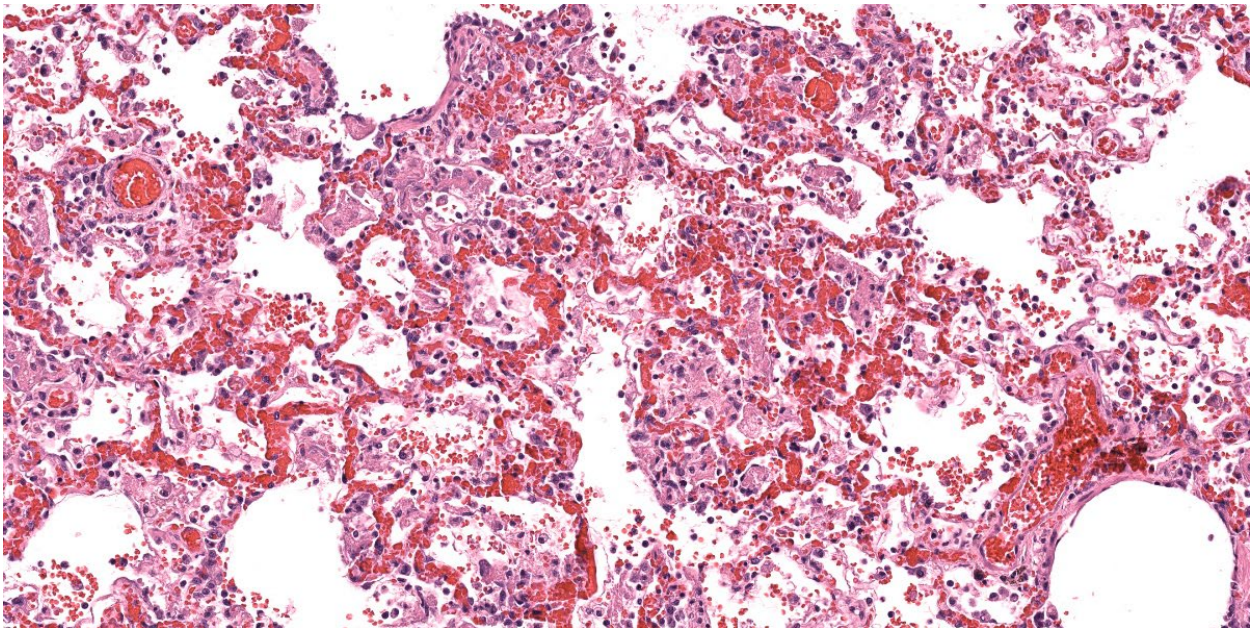

Figure 2-2. Lung, dog. in one section, in a patchy distribution, there are extensive areas in which alveolar septa are congested with intraseptal edema. There is exudation of fibrin into the alveoli, where it has polymerized and is admixed with hemorrhage, alveolar macrophages and neutrophils. (HE, 381X)

murmur, he was preemptively treated with Vetmedin/Lasix. Radiographs showed evidence of pneumonia. Echocardiogram revealed evidence of mitral and tricuspid valve degeneration with regurgitation, with no left atrial enlargement and no evidence of congestive heart failure. Patient was transitioned to room air on 18 January 2024 and he did well. On the morning of 19 January 2024, patient acutely decompensated and CPR was performed. CPR was successful but patient was euthanized.

Gross Pathology:
Heavy body condition, BCS 7/9, and distended abdomen. Lungs were diffusely wet and heavy, red fluid in the thoracic cavity. The right ventricle was large and dilated, and there were nodular proliferations on the right and left AV valves. No significant findings in the abdominal cavity.

Microscopic Description:
Lungs: Alveolar septa are diffusely thickened by variable combinations and concentrations of fibrin, histiocytes, fewer lymphocytes, edema, and congested alveolar capillaries. Multifocally affecting approximately 40% of the examined tissue, alveolar septa are lined by lamellae of polymerized eosinophilic hyaline material (hyaline membranes), and in these areas type I pneumocytes are often lost or necrotic with nuclear pyknosis or karyorrhexis. Diffusely, alveolar spaces contain variable combinations and concentrations of hemorrhage, edema fluid, variably polymerized fibrin, and increased numbers of foamy alveolar macrophages that occasionally contain phagocytosed erythrocytes and rarely contain hints of cytoplasmic hemosiderin. The perivascular tissue surrounding larger vessels is expanded by edema. The adventitia of small and medium veins multifocally is minimally to mildly expanded by increased fibrous connective tissue. Focally extensively affecting approximately 5% of the examined

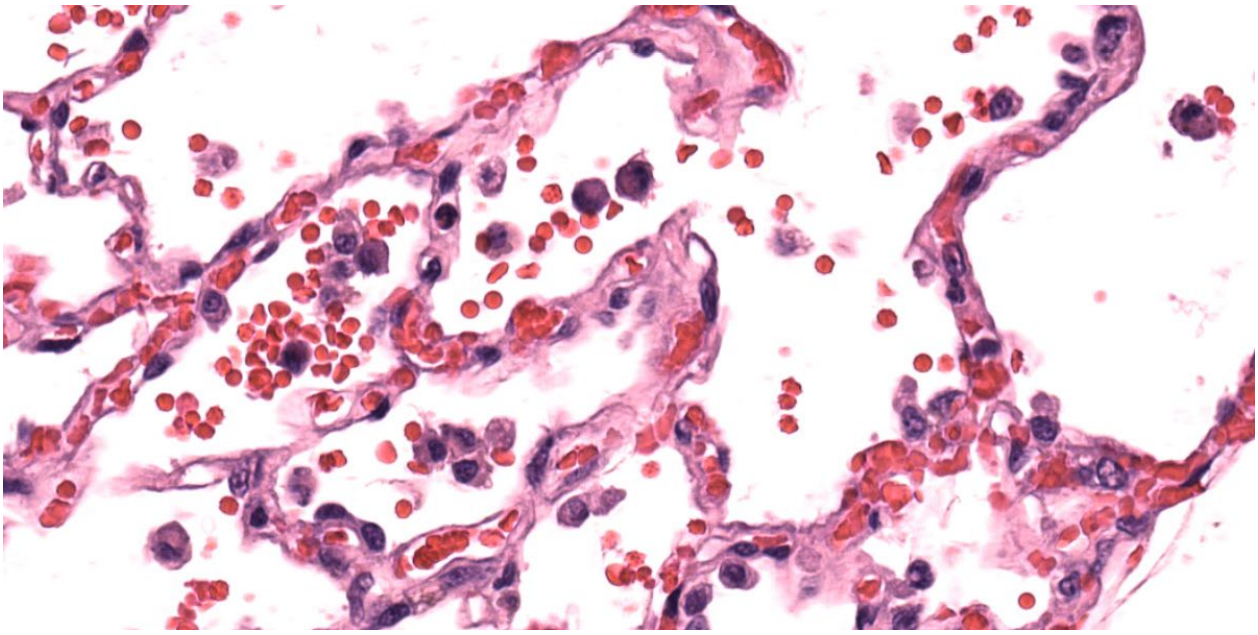

Figure 2-3. Lung, dog. Throughout the section, alveolar spaces contain clusters of macrophages which contain intracytoplasmic brown granular pigment (iron), know as "heart failure cells". (HE, 248X)

tissue, adjacent to a bronchus and pulmonary vein, alveoli are filled and expanded by extracellular and intrahistiocytic amorphous, homogeneous, amphophilic, anisotropic, aggregates of hyaline material that vary in size from 5-300 in diameter. The material is multifocally surrounded by granulomatous inflammation composed of foamy macrophages, multinucleate giant cells, and few lymphocytes and plasma cells. At the tip of the margin of one tissue section, there is a focal area of moderate to marked alveolar septal expansion by fibrosis. In this area, there is marked type II pneumocyte hyperplasia, and alveoli contain high numbers of entrapped foamy alveolar macrophages.

The intra-alveolar, hyaline, amphophilic material is strongly PAS-positive.

Not submitted for WSC, the liver had evidence of chronic passive congestion to include central vein adventitial fibrosis, centrilobular congestion, and centrilobular hepatocyte atrophy.

Contributor's Morphologic Diagnosis:

1. Lung: Pneumonia, interstitial, acute, necrotizing, multifocal to coalescing, moderate, with hyaline membrane formation
2. Lung: Congestion, diffuse, moderate, with increased alveolar macrophages and perivascular edema
3. Lung: Pneumonia, granulomatous, focal, mild, with intraalveolar, extracellular and intrahistiocytic, amphophilic, homogeneous, hyaline material

Contributor's Comment:

This case represents three pulmonary entities: acute respiratory distress syndrome, chronic passive congestion, and pulmonary hyalinosis.

Acute respiratory distress syndrome (ARDS) is the clinical manifestation of diffuse alveolar damage (DAD).[4,5,7] DAD is due to injury to type I pneumocytes and/or alveolar capillary endothelium which results in serum leakage into alveoli, with subsequent pulmonary edema and polymerization of fibrin into characteristic hyaline membranes lining alveolar

septa, and eventually type II pneumocyte hyperplasia and interstitial fibrosis.[5,7] The pathophysiology of ARDS/DAD is beautifully illustrated in *Robbins and Cotran Pathologic Basis of Disease* 10th Ed. Figure 15.3.[5] ARDS has garnered widespread attention in recent years because the pathogenesis of COVID-19-induced pneumonia is similar.[7] Clinically, animals affected with ARDS have acute-onset dyspnea, tachypnea, variable coughing, and lethargy that is often fatal within 3 days.[4] The key histologic feature of this condition is the formation of hyaline membranes; these are variably thick, eosinophilic membranes lining alveolar septa, which physiologically prevent gas diffusion leading to respiratory distress.[4] Histologically there is also often necrosis or attenuation of terminal bronchiolar epithelium.[4,7] DAD may be due to direct or indirect damage, such as the result of multiple organ dysfunction syndrome.[4,7] Notable causes of diffuse alveolar damage include smoke inhalation, oxygen toxicity, inhalation of toxic gases (ammonia, phosgene, ozone, etc.), toxin ingestion (paraquat, 3-methylindole, perilla mint, etc.), near drowning, strangulation, septicemia, shock, massive trauma, and chronic left sided heart failure, although many cases are idiopathic.[4,5,7]

In humans, congestive left-sided heart failure with subsequent pulmonary congestion often results in accumulation of so-called "heart failure cells" within alveoli.[6] These "heart failure cells", also termed siderophages, are simply hemosiderin-laden alveolar macrophages that have phagocytosed red blood cells.[4,6,7] In veterinary medicine (with the exception of non-human primates), it is rare to see classic "heart failure cells" associated with chronic heart failure; however, the number of non-hemosiderin-laden alveolar macrophages is often increased secondary to chronic pulmonary edema.[4] Additionally of note, hemosiderin-laden alveolar macrophages can be present in conditions other

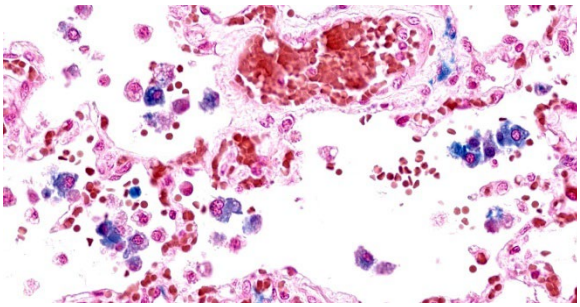

Figure 2-4. Lung, dog. A Perl's stain for iron demonstrates numerous iron pigment in the "heart failure cells". (Perl's iron, 400X)

than heart failure, such as pulmonary hemorrhage.[4] Pulmonary sequelae to chronic left-sided heart failure are pulmonary edema, increased alveolar macrophages, and pulmonary vein remodeling.[4,7] The pulmonary vein remodeling may simply consist of subtly increased adventitial collagen of small to medium-sized pulmonary veins.[4]

Pulmonary hyalinosis is an uncommon, idiopathic condition in older dogs that is due to an uncharacterized alveolar-filling disorder.[7,8] Alveolar-filling disorders are characterized by accumulations of abnormal material in alveoli, and include alveolar histiocytosis, endogenous lipid pneumonia, alveolar proteinosis, alveolar phospholipidosis, alveolar microlithiasis, and pulmonary hyalinosis.[7,8] Pulmonary hyalinosis is considered an incidental finding.[4,7,8] The material within alveolar lumina is characteristically amphophilic, amorphous or lamellar, birefringent, and strongly PAS-positive.[4,7,8] This condition was relatively recently reported in 6 captive sugar gliders.[8] This condition was also recently highlighted in the JPC Wednesday Slide Conference (see Conference 5, Case 4, 2022-2023).

Contributing Institution:
Tri-Service Research Laboratory

4141 Petroleum Dr

San Antonio, TX 78234

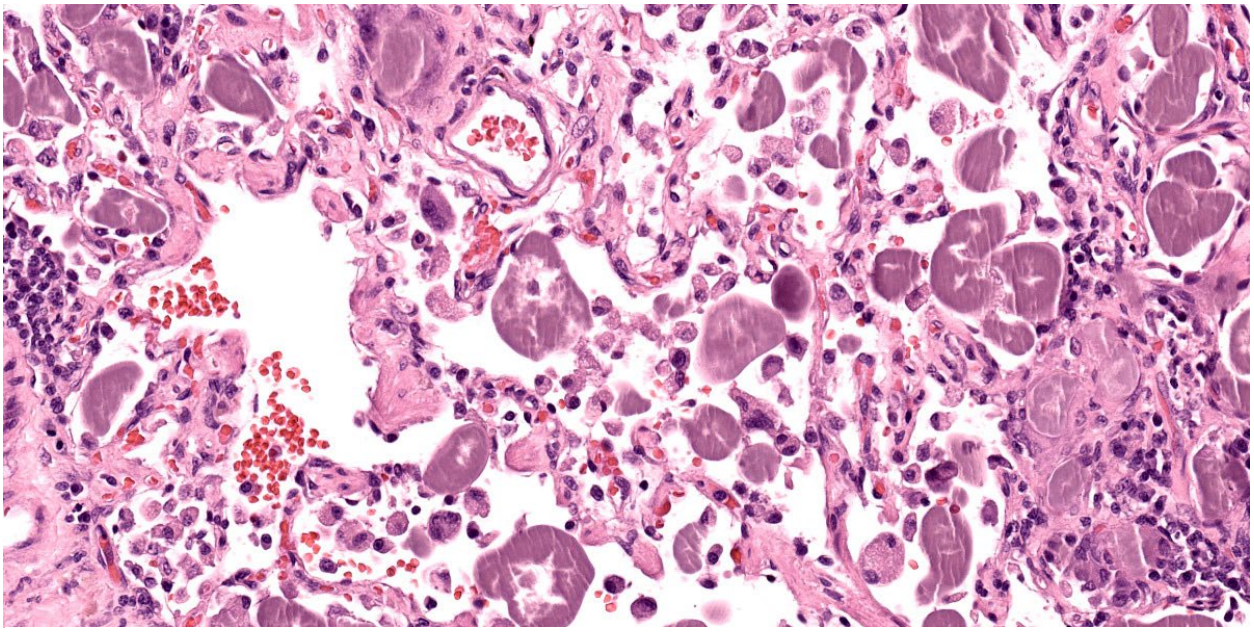

Figure 2-5. Lung, dog. Multifocally, there are foci of pulmonary hyalinosis with abundant amphophilic protein within alveoli. (HE, 390X)

JPC Diagnosis:

1. Lung: Pneumonia, interstitial and organizing, necrotizing and fibrinous, subacute, multifocal, moderate with type II pneumocyte hyperplasia.
2. Lung: Congestion, chronic, diffuse, mild to moderate with alveolar siderophages and edema.
3. Lung: Pneumonia, interstitial, granulomatous, chronic, multifocal, moderate, with abundant hyaline material.
4. Lung: Pneumonitis, lymphocytic, chronic, focal, marked (subpleural alveolar proteinosis).

JPC Comment:
Case 2 showcases multiple entities occurring simultaneously in the lung of an aged dog. Conference participants collectively were able to spot five distinct processes, which reinforces the value of complete slide examination. We did not add a morphologic diagnosis for anthracosilicosis in this case, as it is a common and incidental finding in aged animals, and of a relatively minor degree in this case. Likewise, the pulmonary hyalinosis in this case was not likely significant in the death of this animal. We added a separate morphologic diagnosis for the subpleural alveolar proteinosis, which is a common incidental finding in older dogs, but is worth noting.

The group differed from the contributor in their interpretation of hyaline membranes in this case. Participants noted that the polymerized fibrin filled the alveoli as "fibrin ball"[1,3] as opposed to a hyaline membrane, which is typically adherent to the basement membrane itself and visually lines the affected septa.. Likewise, the concurrent type II pneumocyte hyperplasia in this case and increased number of myofibroblasts highlighted by a smooth muscle actin IHC was consistent with at least a subacute course of disease in this animal. Dr Bearss noted that he has seen this phenotype in monkeys utilized for Nipah virus research and drew parallels from his experience

Acute fibrinous and organizing pneumonias

(AFOP) are a distinct entity in human medicine[1,2,3] that represent an acute to subacute phenotype of severe lung injury. With this slower onset, the mix of plasma protein, surfactant, fibrin, and cellular debris characteristic of a classic acute hyaline membrane is infiltrated by inflammatory cells and embedded myofibroblasts and forms a distinct "fibrin ball" in the alveolus. Likewise, this 'slow burn' also provides time for pneumocyte hyperplasia that prevents direct adhesion of material to the basement membrane. In time, this plug of material may also trap inhaled air and lead to secondary emphysema and/or bronchiectasis.[1,3]. Whether or not left-sided heart failure in conjunction with oxygen therapy (and generation of radical oxygen species) was sufficient to damage the endothelium and/or type I pneumocytes was not resolved in the conference discussion. Herein we use 'fibrinous' and 'organizing' to capture the nature and distribution of this material and introduce this term to a wider audience.

Finally, conference participants touched on the heart failure aspect of this case. Hemosiderin-laden macrophages were a more subtle pickup in this case absent the history, though some participants also noted erythrophagocytosis which was another confirmation of chronic congestion and stasis of pulmonary blood flow. Alveolar macrophages stained strongly with Perl's Prussian blue, confirming the presence of iron.

References:

1. Al-Khouzaie TH, Dawamneh MF, Hazmi AM. Acute fibrinous and organizing pneumonia. *Ann Saudi Med*. 2013 May-Jun;33(3):301-3.
2. Baque-Juston M, Pellegrin A, Leroy S, Marquette CH, Padovani B. Organizing pneumonia: what is it? A conceptual approach and pictorial review. *Diagn Interv Imaging*. 2014 Sep;95(9):771-7.
3. Bharti JN, Satyendra BT, Shekhawat RS, Gorchiya A. Acute Fibrinous and Organizing Pneumonia—A Rare Lung Pathology. *The American Journal of Forensic Medicine and Pathology* 43(1):p e1-e3, March 2022.
4. Caswell JL, Williams KJ. Respiratory System. In: Maxie MG, ed. *Jubb, Kennedy, and Palmer's Pathology of Domestic Animals*. Vol 2. 6th ed. St. Louis, MO: Elsevier; 2016: 485, 489, 493, 509-511, 514, 517, 518, 519.
5. Husain AN. The lung. In: Kumar V, Abbas AK, Fausto N, Aster JC, eds. *Robbins and Cotran Pathologic Basis of Disease*. 10th ed. Philadelphia, PA: Elsevier; 2021:676-678.
6. Kumar V, Abbas AK, Aster JC, eds. *Robbins and Cotran Pathologic Basis of Disease*. 10th ed. Philadelphia, PA: Elsevier; 2021:118.
7. López A, Martinson SA. Respiratory System, Thoracic Cavities, Mediastinum, and Pleurae. In: Zachary JF, ed. *Pathologic Basis of Veterinary Disease*. 7th ed. St. Louis, MO: Elsevier; 2022:571, 574-575, 577-578, 588, 638.
8. Sokol SA, Agnew DW, Lewis AD, Southard TL, Miller AD. Pulmonary hyalinosis in captive sugar gliders (Petaurus breviceps). *J Vet Diagn Invest*. 2017;29(5):691-695.

CASE III:

Signalment:
3.5 year-old, intact female, Drill, *Mandrillus leucophaeus*, non-human primate.

History:
The animal was kept in a zoo with access to indoor- and outdoor facilities. It was presented to the veterinarian due to a mass in the anterior chamber of the left eye. The left eye was removed and submitted for further inves

Figure 3-1. Eye, drill. Inspection of the left eye revealed a yellowish brown, and immovable mass filling the nasoventral part of the left anterior eye chamber (*Photo courtesy of:* Institute of Veterinary Pathology at the Centre for Clinical Veterinary Medicine, Ludwig-Maximilians-Universität München https://www.patho.vetmed.uni-muenchen.de)

tigation to the Institute of Veterinary Pathology at the Ludwig-Maximilians-Universität in Munich, Germany.

Gross Pathology:
In situ-inspection of the left eye revealed a yellowish brown, and immovable mass filling the nasoventral part of the left anterior eye chamber. After removal of the eye and 24 hours of fixation with modified Davidson solution, the mass was further examined and trimmed. The mass measured ca. 1 cm x 0.8 cm x 0.3 cm and was confined to the iris and ciliary body. On cut section, the surface of the iris and ciliary body appeared solid to cystic. The lens was mildly displaced.

Laboratory Results:
Echinococcus multilocularis - PCR (lung, liver, eye): positive.

Echinococcus multilocularis – Immunohistochemistry (eye): positive.

Microscopic Description:
Left eye: The stroma of the iris and ciliary body is focally extensively expanded by a multiloculated hydatid cyst accompanied by marked inflammatory cell infiltration and necrosis. In particular, the iridociliary stroma is partly effaced by multiple intact or collapsed cystic spaces of different sizes (ranging from 15 to 1500 µm in diameter) surrounded by a 10-15 µm thin hyaline acellular laminated cyst wall (laminated layer). The inner part of the cyst wall is often lined by a monolayer of cuboidal cells (germinal layer). The cystic spaces are either optically empty or simply contain finely granular amphophilic material (non-fertile hydatid cyst). The cyst walls are surrounded by numerous multinucleated giant cells with up to 60 nuclei that are irregularly distributed within the cytoplasm (foreign-body giant cells), intermingled with large numbers of macrophages, lymphocytes, and plasma cells, and lower numbers of eosinophilic granulocytes. Intralesionally, there are multiple areas consisting of small cyst wall fragments and cellular debris characterized by loss of cellular detail, hypereosinophilia, and shrinked and fragmented nuclei (necrosis). The expanded iris adheres to the cornea (anterior synechia) and the associated part of the iridocorneal angle is closed.

Moderate to large numbers of plasma cells, lymphocytes, and macrophages are infiltrating the remaining portions of the iridociliary stroma, the trabecular meshwork, as well as the immediately surrounding portions of the choroidea, sclera, and cornea.

Additionally, ocular adnexa including the conjunctiva show multifocal infiltration of

Figure 3-2. Eye, drill. Marked expansion of iris and ciliary body. The mass is partly solid, and partly cystic, displacing adjacent structures including the lens. Scale bar = 1 cm. (*Photo courtesy of:* Institute of Veterinary Pathology at the Centre for Clinical Veterinary Medicine, Ludwig-Maximilians-Universität München https://www.patho.vetmed.uni-muenchen.de)

low to moderate numbers of lymphocytes and plasma cells.

Contributor's Morphologic Diagnosis:
Left eye: Hydatid cyst, multiloculated, non-fertile, iridociliary, with marked chronic granulomatous and eosinophilic anterior uveitis with stromal necrosis, anterior synechia, and mild to moderate chronic lymphoplasmacytic scleritis and conjunctivitis.

Contributor's Comment:
Echinococcus multilocularis (EM) belongs to the phylum *Platyhelminthes*, class *Cestoda* (tapeworms), and subclass *Eucestoda*. Within the order *Cyclophyllidea* it is further subordinated to the family *Taeniidae*. The larval stage of EM is the causative agent of alveolar echinococcosis (AE), a parasitic zoonotic disease of great medical and veterinary importance distributed in the northern hemisphere.[2,8]

The parasite's life cycle usually involves various species of wild rodents, such as *Arvicolinae and Cricetinae*, and the lagomorph pika (*Ochotona curzoniae)* on the Tibetian plateau of China as intermediate hosts. Depending on the epidemiological setting, wild or domestic canid and felid species such as red or arctic foxes, jackals, wolves, dogs, and cats serve as the parasite's definitive hosts.[2,3,7,8] Moreover, dogs can simultaneously act as definitive and intermediate hosts.[2]

The definitive host harbors the egg-producing adult form of EM (tapeworm) within the intestine and eggs or the egg containing last segment of the worm (gravid proglottid) are shed via feces. The infective eggs are dispersed in the environment, where they can survive approximately 1 year in a suitable, moist environment at lower temperatures, but they are sensitive to desiccation and high temperatures.[3] Once the eggs are ingested by the intermediate host, they hatch in the small intestine. The hexacanth larva (oncosphere) is released and penetrates the gut wall. It then passes through the portal and lymphatic vessels, eventually reaching various organs in the intermediate host's body.[8,11] Within the affected organs of the intermediate host, the oncosphere develops into a metacestode, which is a larval stage characterized by multilocular vesiculated cyst formation. This disease is called 'alveolar echinococcosis' due to the appearance of these cysts.[1]

These cysts have an outer laminated layer and an inner germinal layer, and in case of fertile cysts, the germinal layer produces brood capsules containing protoscoleces.[4] The life cycle is completed when the definitive host consumes the organs of the intermediate host that contain fertile metacestodes. Within the intestine, the protoscoleces develop into adults. The prepatent period between ingestion of protoscoleces and the production of eggs by the matured tapeworm

Figure 3-3. Eye, drill. Midline section through globe. There is cystic space-occupying mass within the uvea and choroid at the base of the iris root and ciliary body. (HE, 5X)

typically ranges from 4 to 7 weeks.[8]

Aberrant intermediate host animals and humans can also become infected with the metacestode stage by accidental ingestion of oncosphere-containing eggs.[3] However, aberrant intermediate host animals do not play a role in the transmission cycle and include horses, cattle, domestic and wild pigs, nutria (*Myocastor coypus*), and several species of nonhuman primates (NHP).[3,11] Infection with EM metacestodes is reported from a variety of NHP, including gorilla (*Gorilla gorilla*), orangutan (*Pongo pygmaeus*), rhesus monkey (*Macaca mulatta*), cynomolgus monkey (*Macaca fascicularis*), lion-tailed macaque (*Macaca silenus*),[1,9] Japanese monkeys (*Macaca fuscata*),[5] and ring-tailed lemur (*Lemur catta*).[6] After a large outbreak in a German breeding enclosure with three different affected NHP species, cynomolgus monkeys were considered to be at higher risk, and therefore, presumably are more susceptible to infection than other NHP species. However, it is important to note that NHP in zoological gardens and institutional colonies, particularly in endemic regions, are at risk of becoming infected with EM.[9]

AE is of increasing concern globally due to the geographical spread of EM, its increasing prevalence in animals from endemic areas, the absence of a vaccine, and the lack of active control measures to prevent the infection.[2]

Once the aberrant intermediate host is infected, the metacestode infiltration and proliferation progress silently (in humans, over the course of 5 to 15 years), causing AE, a chronic and complex disease with a devasting clinical condition and high fatality rate if left untreated.[2,8]

AE primarily affects the liver in intermediate hosts as well as aberrant intermediate hosts and behaves like an infiltrative and eventually metastasizing tumor with further infiltration of tissues close to the liver or dissemination via blood and lymphatic vessels.[2,8,11] Less frequently than the liver are lungs, brain, bones, or any other organ of the (aberrant) intermediate host affected.[9,11] Immune suppression exacerbates disease progression.[2,8]

In the present case, a full body necropsy was carried out after the evaluation of the eye, and a subsequent histological examination of further organs failed to identify any additional diseases or evidence of immunosuppression. However, besides the earlier diagnosed intraocular invasion, multiple organs were affected by larval infection, including both common and less common tissues including liver, kidneys, lungs, heart, lymph nodes, skeletal muscles, and brain. The laminated layer of the cysts displayed consistently positive PAS-reactivity. In addition, none of the cysts in this animal contained brood capsules with protoscoleces (non-fertile cysts). In general, fertility of EM cysts is common in susceptible hosts, where it is reached within

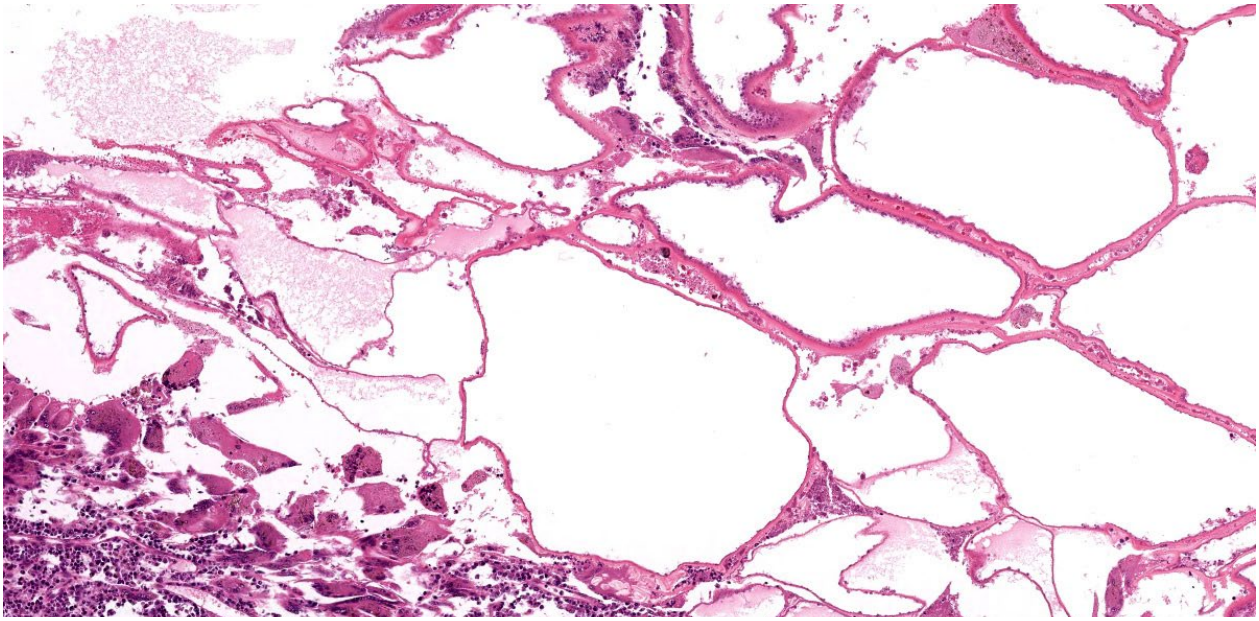

Figure 3-4. Eye, drill. The uveal mass consists of a microcyst of *E. multilocularis* embedded in granulomatous inflammation. The cysts are devoid of protoscoleces, indicating an infertile microcyst. There are numerous multinucleated foreign body-type macrophages at bottom left. (HE, 99X)

2–4 months. But it is far rarer (<20%) in resistant hosts, such as humans, or most domestic animals[8]. Aside from the absent brood capsules and protoscoleces, typical calcareous corpuscles were also not seen in the present case. These corpuscles can be very helpful for identification purposes in histological sections and appear as basophilic to clear ovals with a concentric ringed appearance, but they may "dissolve" in fixation or histological processing.[4]

In human as well as veterinary medicine, the gold standard for AE diagnosis is the identification of parasite structures/genome in samples obtained invasively. Imaging techniques demonstrate characteristic features of the lesions, while serology is complementary.[2,3]

In 2020, an international consensus on terminology to be used in the field of echinococcosis was published. To harmonize echinococcosis terminology on sound scientific and linguistic grounds, the World Association of Echinococcosis launched a Formal Consensus process. The main achievements of this process were: (1) an update of the current nomenclature of *Echinococcus* spp.; (2) an agreement on three names of diseases due to *Echinococcus* spp.: Cystic Echinococcosis, Alveolar Echinococcosis, and Neotropical Echinococcosis, and the exclusion of all other names; (3) an agreement on the restricted use of the adjective "hydatid" to refer to the cyst and fluid due to *E. granulosus sensu lato*; and (4) an agreement on a standardized description of the surgical operations for CE, according to the "Approach, cyst Opening, Resection, and Completeness" (AORC) framework. In addition, 95 "approved" and 60 "rejected" terms were listed.[10] In detail, the term "hydatid" (as noun and as adjective) as well as the term "cyst" should be restricted (by usage, not strictly by definition) to the metacestode of *E. granulosus sensu lato* causing cystic echinococcosis. It should not be used for the metacestode of *E. multilocu-*

laris. This consensus was processed and published in order to avoid confusion between human diseases caused by the various species of *Echinococcus*. "Hydatid" should further not be used to designate anything relating to AE or neotropical echinococcoses caused by *E. vogeli* or *E. oligarthra*. Among all the specialists working in the field of echinococcosis, such as in experimental models, veterinary pathologists are also asked to use the term (echinococcal) "microcyst" in AE lesion instead of the term "hydatid cyst."[10]

Further parasites that can be found incidentally in the animal eye:[12]

- *Echinococcus* in nonhuman primates
- *Cysticercus* in swines
- Microfilariae of *Elaeophora schneideri* in elks causing occlusive vasculitis with multifocal ischemic chorioretinitis and optic neuritis in elks
- fortuitous localization of larvae of *Toxocara canis* or other ascarids, *Angiostrongylus vasorum* and *Dirofilaria immitis* in canine species, associated with uveitis
- Larvae of *Onchocerca cervicalis* and adults of *Setaria* spp. in horses
- Fly larvae in various species causing ophthalmomyasis due to intraocular migration
- Larvae of *Diplostomum spathaceum* in fishes
-

The lens fluke (*Diplostomum spathaceum*) is the only known specific intraocular parasite. This parasite is primarily found in the eye lenses of fishes. After penetrating the fish's skin, the *Diplostomum* larvae migrate to the lens of the eye with remarkable speed and specificity. The presence of numerous larvae within the lens can lead to the development of cataracts. These larvae are ingested by fish-eating birds, which completes the life cycle of the parasite.[12]

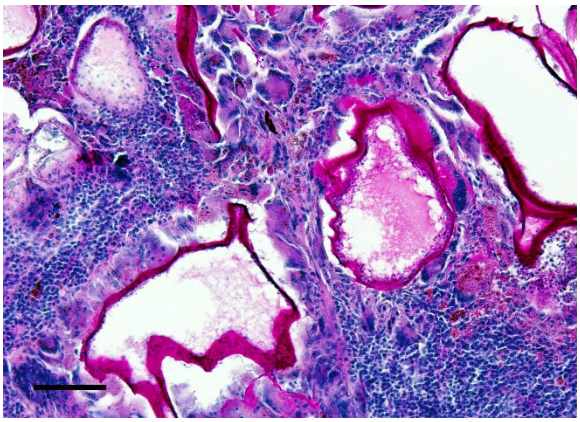

Figure 3-5. Eye, drill. A periodic acid-Schiff stain highlights the hyaline wall of the microcyst. (PAS, 200X) (*Photo courtesy of:* Institute of Veterinary Pathology at the Centre for Clinical Veterinary Medicine, Ludwig-Maximilians-Universität München, https://www.patho.vetmed.uni-muenchen.de)

Contributing Institution:

Institute of Veterinary Pathology at the Centre for Clinical Veterinary Medicine

Ludwig-Maximilians-Universität München
Veterinärstrasse 13

D-80539 Munich, Germany

https://www.patho.vetmed.uni-muenchen.de

JPC Diagnosis:
Eye: Panuveitis, granulomatous, focally extensive, severe, with anterior synechiae, lymphohistiocytic conjunctivitis, and hydatid cyst.

JPC Comment:
The contributor provides a detailed writeup on *Echinococcus* that accompanies great gross photos and an interesting histologic presentation.

Conference participants discussed ancillary changes within the eye which included clo-

sure of the iridocorneal angle and mild corneal edema beyond the other changes the contributor notes. Though there was a mild amount of fibrin lining the contralateral iridocorneal angle, this animal likely did not have sufficient deficit in aqueous humor drainage to cause glaucoma – comparison to the optic nerve, retina, and Descemet's membrane were helpful checks in this case to confirm that histologically. The lack of calcareous corpuscles or protoscoleces in histologic section of this infertile microcyst frustrated some conference participants, though recognition of the thick cyst wall (largely host derived) and germinal lining epithelium were key features. As the contributor hints at, the long duration of this infection in a resistant host makes identifying these features important as they may be the only specific ones that point to *Echinococcus* in these diagnostic cases. For comparison to a more acute infection in a Barbary ape, see VSPO D-P28A for examples of all representative organism features.

This case highlights the potential confusing nomenclature that arises with the shift (and adoption) of new terms to describe entities. Adoption of 'microcyst' and alveolar echinococcosis stymied some of the participants who felt that the morphologic diagnosis should retain the historical term as this change enters veterinary literature and awareness. In solidarity with the contributor, we kept the term hydatid cyst for this conference, but invite readers to explore the reference by Vuitton et al[10] that the contributor helpfully provides.

References:

1. Bacciarini L, Gottstein B, Pagan O, Rehmann P, Gröne A. Hepatic alveolar echinococcosis in cynomolgus monkeys (Macaca fascicularis). *Vet Pathol*. 2004;41:229-234.
2. Casulli A, Barth TFE, Tamarozzi F. Echinococcus multilocularis. *Trends Parasitol*. 2019;35:738-739.
3. Eckert J, Deplazes P. Biological, epidemiological, and clinical aspects of echinococcosis, a zoonosis of increasing concern. *Clin Microbiol Rev*. 2004;17:107-135.
4. Gardiner CH, Poynton SL. Morphological characteristics of cestodes in tissue section. In: *An Atlas of Metazoan Parasites in Animal Tissues*. Washington, DC: Armed Forces Institute of Pathology, American Registry of Pathology; 2006:50-55.
5. Kishimoto M, Yamada K, Yamano K, et al. Significance of imaging features of alveolar echinococcosis in studies on nonhuman primates. *Am J Trop Med Hyg*. 2009;81:540-544.
6. Kondo H, Wada Y, Bando G, Kosuge M, Yagi K, Oku Y. Alveolar hydatidosis in a gorilla and a ring-tailed lemur in Japan. *J Vet Med Sci*. 1996;58:447-449.
7. Oksanen A, Siles-Lucas M, Karamon J, et al. The geographical distribution and prevalence of Echinococcus multilocularis in animals in the European Union and adjacent countries: a systematic review and meta-analysis. *Parasit Vectors*. 2016;9: 519.
8. Tamarozzi F, Brunetti E, Vuitton D. Echinococcosis. In: Fabrizio B, ed. *Helminth Infections and their Impact on Global Public Health*. 2nd ed. Cham: Springer; 2022:257-312.
9. Tappe D, Brehm K, Frosch M, et al. Echinococcus multilocularis infection of several Old World monkey species in a breeding enclosure. *Am J Trop Med Hyg*. 2007;77:504-506.
10. Vuitton DA, McManus DP, Rogan MT, et al. International consensus on terminology to be used in the field of echinococcoses. *Parasite*. 2020;27:41.
11. Wen H, Vuitton L, Tuxun T, et al. Echinococcosis: Advances in the 21st

Century. *Clin Microbiol Rev*. 2019;32.
12. Wilcock BP, Njaa BL. Special Senses. In: Maxie MG, ed. *Jubb, Kennedy & Palmer's Pathology of Domestic Animals.: Volume 1*. 6th ed. St. Louis, Missouri: Elsevier; 2016:407-508.e402.

CASE IV:

Signalment:
11-year-old, female, rhesus macaque, Macaca mulatta, nonhuman primate

History:
This macaque has a history of seven liveborn infants by vaginal delivery and recently delivered a large, liveborn male infant with a body weight of 590 g the day prior to presenting for poor maternal care, a retained placenta and suspected endometritis. On physical examination, the placenta was necrotic with an associated purulent exudate and was manually removed. Samples were submitted for aerobic and anaerobic culture. Supportive and therapeutic care was provided. One week after presentation, the uterus was enlarged on palpation and peritonitis was observed on ultrasound examination. She was referred to surgery for exploratory laparotomy. Peritonitis and multiple uterine ruptures were observed. A hysterectomy was performed.

Figure 4-1. Uterus, rhesus macaque. The uterine body contains three areas of rupture with ragged margins and a fibrinopurulent exudate (*Photo courtesy of:* Oregon National Primate Research Center, https://www.ohsu.edu/onprc)

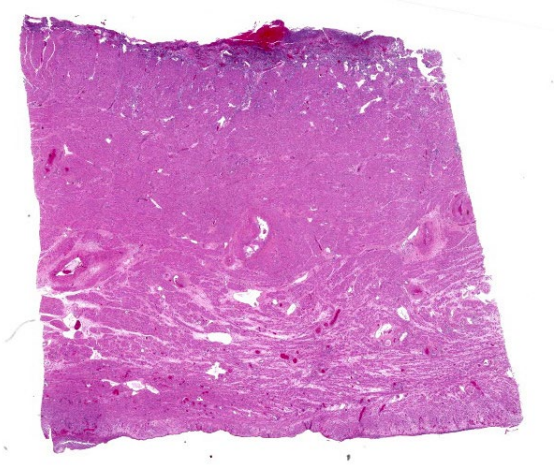

Figure 4-2. Uterus, rhesus macaque. One transmural section of uterus is presented for examination. (HE, 5X)

Gross Pathology:
The uterus is enlarged and the integrity of the uterine fundus and the dorsal aspect of the uterine body is disrupted by three transmural, necrotizing uterine ruptures with ragged margins and a fibrinopurulent exudate.
The placental fragments were not submitted for gross or microscopic examination

Laboratory Results:
Aerobic culture of placental fragments yielded a mixed bacterial population at initial presentation - beta-hemolytic Streptococcus (3+), alpha-hemolytic Streptococcus (not Streptococcus pneumoniae, 2+), Proteus (1+), Staphylococcus aureus (1+), and Staphylococcus epidermidis (1+)
Anaerobic culture of placental fragments at initial presentation yielded gram-positive bacillus (not Listeria, 2+), gram-negative bacillus (2+), and gram-positive coccus (3+)
Cytologic examination of the peritoneal fluid one week following initial presentation

CBC

Reference Intervals	WBC 4,200-13,600	Neuts 2,380-9610	Bands	Lys 1,130-3,770	Monos 190-920	Eos 600-1,100	Bas 20-100	HCT 32.9-41.8	HGB 10.7-13.8	MCV 65.6-76.4	MCHC 31.7 – 33.7	Platelets 119,000-471,000
CBC Results Presentation	7,500	2,400	41%	1,725	225	75	0	34.6	11.3	75	32.8	327,000
CBC Results 12 days later	21,000	13,230	9%	4,620	1,050	210	0	21.6	7.1	74	33	510,000

Serum chemistry

Reference Intervals	TP 6-7.9	ALB 3.3-4.7	ALKP 114-482	ALT 18.9-94.2	AST 18-58	GGT 35-72	TBIL 0-0.4	GLU 45-93	BUN 10-27	CREA 0.6-1.0	K 2.9-4.6	Na 136-153	Cl 102-115	Mg 1.6-2.5	P 4.1-7.8
Result 12 days after presentation	5.3	1.9	171	92	149	17	0.25	56	14.6	0.5	4.7	132	101	1.6	4.7

showed gram-negative bacilli within macrophages and neutrophils.
Aerobic culture of the peritoneal cavity one week after initial presentation yielded Streptococcus, nonhemolytic (4+)
Anaerobic culture of the peritoneal cavity one week after initial presentation yielded gram-positive coccus (3+), gram-negative bacillus (3+) and gram-positive bacillus (1+)

Microscopic Description:
The microarchitecture of the endometrium exhibiting variable stromal decidualization is effaced and overlain by an inflammatory infiltrate composed of myriad degenerate neutrophils, macrophages often laden with brown pigment and fewer lymphocytes admixed with karyorrhectic cellular debris, fibrin, hemorrhage and edema. Endothelial hypertrophy is prominent and there is diffuse congestion. Rare intravascular fibrin thrombi are present. The myofibers of the myometrium immediately subjacent to the endometrium exhibit multifocal, single cell necrosis and multifocally throughout the myometrium there is increased vacuolation of the myofibers. The myometrial interstitium is moderately expanded by fibrous connective tissue and an inflammatory infiltrate composed largely of lymphocytes and plasma cells with few neutrophils surrounds the vasculature. Foci of trophoblastic transformation are present multifocally in the myometrium. The serosa is expanded by degenerate neutrophils, macrophages, fibrin, hemorrhage and karyorrhectic cellular debris. A mixed bacterial population is present within the endometrium and the serosa.

Contributor's Morphologic Diagnosis:
Uterus: Endometritis, necrotizing, fibrinous, exudative, neutrophilic, histiocytic, lymphocytic, chronic-active, diffuse, severe with serositis, rhesus macaque, Macaca mulatta, nonhuman primate.
Myometrium: Vacuolation, myofibers, generally midsection of the uterus, multifocally extensive, moderate with mild perivascular lymphocytic and plasmacytic infiltrates and moderate interstitial fibrosis.
Oviduct (tissue not submitted): Mesosalpingitis, necrotizing, fibrinous, exudative, neutrophilic, histiocytic, lymphocytic, chronic-active, multifocal, moderate.

Contributor's Comment:
Placental retention, an obstetrical complication may occur with uterine atony or with the placenta accreta spectrum characterized by abnormal adherence of the placenta to the placental bed of the uterus.[11] Both entities result in impaired separation and thus release of the placenta. Cervical closure prior to the expulsion of the placenta also results in retained

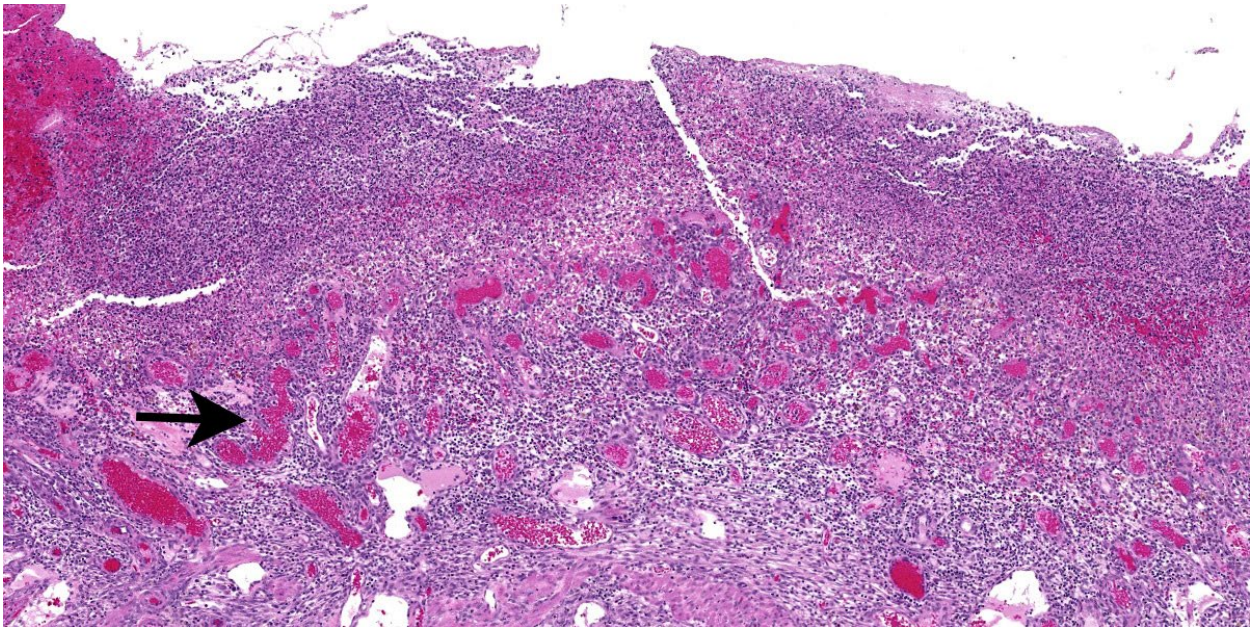

Figure 4-3. Uterus, rhesus macaque. The luminal surface contains decidua infiltrated by large numbers of neutrophils. Spiral arteries may be seen in the deep part of the decidua (arrow). (HE, 5X)

placenta.[11] Clinically, the cervix was open in this case. Placenta accreta, increta or percreta may lead to uterine rupture and were not observed on microscopic examination of the submitted tissues. There was no history of uterine trauma or cesarean section that would increase the risk of uterine rupture. In addition to the chronic-active inflammation, this macaque also had moderate interstitial fibrosis in the myometrium and vacuolation of myofibers which may have hampered effective contractions in expelling the infant and placenta. A retained placenta and uterine rupture with resulting hemorrhage would account for the laboratory findings of a normocytic, normochromic anemia and hypoproteinemia and hypoalbuminemia noted 12 days after clinical presentation. The inflammation present in the uterus and abdominal cavity most likely contributed to the depressed albumin levels as albumin is a negative acute phase reactant and also accounted for the remarkable degenerative left shift of 41% in the leukogram at presentation. The pathogenesis in this case of placental retention, endometritis and multiple uterine ruptures followed by peritonitis was considered to be a prolonged, difficult labor involving a large infant, consequent placental retention due to inadequate myometrial contractions and a subsequent, ascending infection through the vagina and open cervix.[6]

Retained placenta is not an uncommon finding in the breeding colony of rhesus macaques at the Oregon National Primate Research Center. A brief review of the scientific literature revealed a relatively low number of documented cases in nonhuman primates including baboons (*Papio spp.),*[1] cynomolgus macaques (*Macaca fascicularis*),[1,10] rhesus macaques (Macaca mulatta),[1] pigtailed macaques (*Macaca nemestrina*),[12,13] a bonobo (*Pan paniscus*),[7] a golden lion tamarin (*Leontopithecus rosalia*)[4] and a chimpanzee (*Pan troglodytes*).[5] Retained placentas in humans range from 1 – 3% of vaginal deliveries.[11]

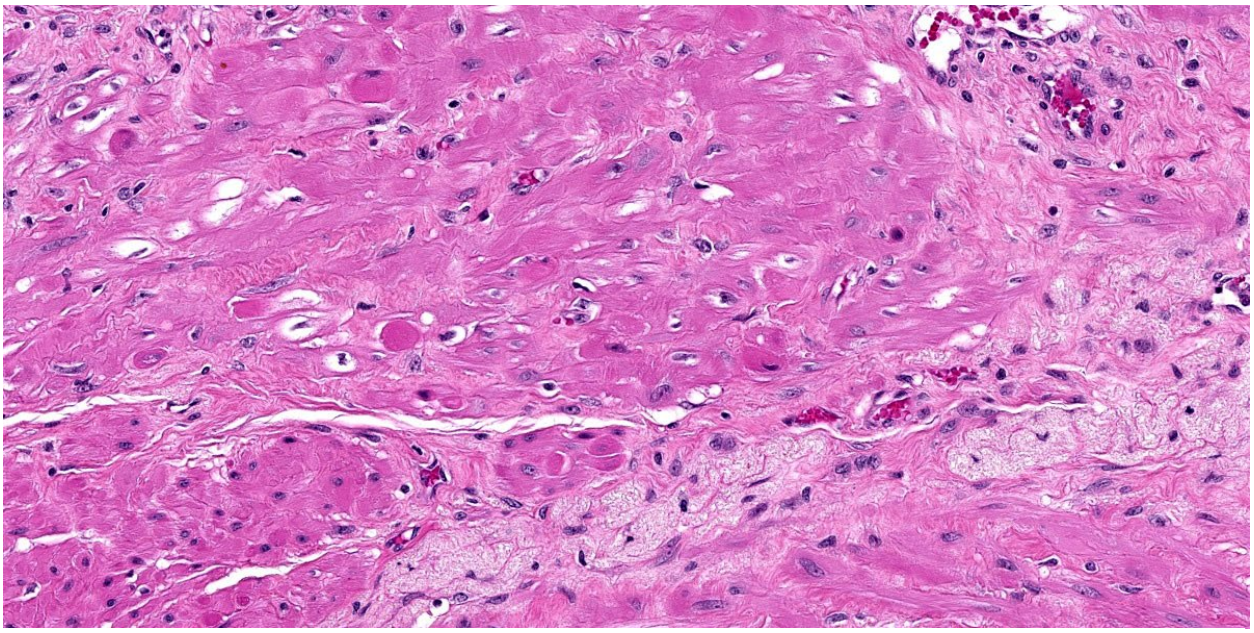

Figure 4-4. Uterus, rhesus macaque. There is scattered degeneration of smooth muscle within the uterine wall. (HE, 259X)

Contributing Institution:
Pathology Services Unit
Division of Animal Resources and Research Support
Oregon National Primate Research Center
505 NW 185th Avenue
Beaverton, OR 97006
https://www.ohsu.edu/onprc

JPC Diagnosis:
Uterus: Endometritis, necrohemorrhagic and suppurative, diffuse, marked with endometrial decidual change, multifocal myometrial degeneration necrosis, and fibrinosuppurative serositis.

JPC Comment:
The final case of this conference provided a challenge as tissue identification was not immediately obvious, though the large amount of irregularly arranged smooth muscle was a helpful feature for recognizing the uterus.

Likewise, participants were not aware of the history of this animal before conference, and considered whether the presence of small-caliber blood vessels and loose endometrial stroma could be evidence of granulation tissue secondary to endometritis. In fact, this was actually retained decidua, representing a transient but important part of the maternal uterine connection to the developing fetus and placenta. Similar to granulation tissue, the decidua is modified endometrium composed of large stromal cells and new blood vessels.[6] The decidua is formed as part of the menstrual cycle and persists with the establishment of pregnancy. Following parturition, the decidua is shed with the placenta, typically within 24 hours.[6] In normal uterine involution, this is represented histologically as regional foci of hemorrhage, inflammatory cells, and necrosis. In this animal however, the placenta was not immediately shed and the degree of inflammation and hemorrhage within the endometrium is entirely in excess. Some participants also noted endometrial spiral arteries in long section which should have also regressed post-partum as another indication of placental retention in this case. Partic

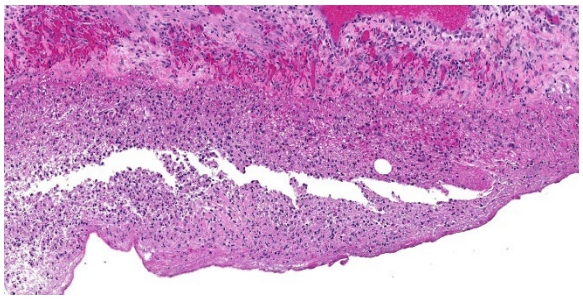

Figure 4-5. Uterus, rhesus macaque. Although the rent in the uterine wall is not evident in the submitted section, there is a fibrinosuppurative exudate expanding the mucosa, and hemorrhagic granulation tissue within the deepest layer of the myometrium above. (HE, 127X)

ipants did not feel confident that they recognized trophoblasts or syncytial trophoblasts amid the large amount of necrotic debris or embedded deeper within the uterine wall, however.

The degree of uterine myometrial degeneration and fibrosis may represent the cause of uterine rupture in this case. The history of difficult delivery in this animal may be correlated to decreased contractility and ability to expel a large fetus, with the resulting increase in uterine pressure from labor stretching this tissue even further and weakening it. Conference participants surmised that seven previous deliveries may have contributed to these myometrial changes, but that the retained placenta *per se* was not the initiating cause. The changes in this case were probably consistent with a placental accreta which is defined by an abnormally strong connection to the endometrium by trophoblasts. In contrast, placental increta represent invasion of trophoblasts into the myometrium with placental percreta extending through the uterus entirely and attaching to other viscera such as the urinary bladder.

Finally, this conference concluded with a discussion of resources for considering placental pathology given the large variation between species and even among non-human primates. We have listed these in the references[2,3,8] as a courtesy for our readers.

References:

1. Bauer C and Harrison T. Retrospective Analysis of the Incidence of Retained Placenta in 3 Large Colonies of NHP. *Comp Med*. 2016; 66(2):143–149.
2. Benirschke, Kurt. Comparative Placentation. UC San Diego. 2012. <http://placentation.ucsd.edu/index.html>.
3. Bowen R. Placental Structure and Classification. Colorado State University. 2011. <https://vivo.colostate.edu/hbooks/pathphys/reprod/placenta/structure.html>.
4. Bronson E, Deem SL, Sanchez C, Murray S. Placental Retention in a Golden Lion Tamarin (Leontopithecus rosalia). J. Zoo Wildl. Med. 2005;36(4):716-718.
5. Calle PP and Stringfellow C. Clinical Challenge: Case 2. *J. Zoo Wildl. Med*. 1991; 22(1):143-145.
6. Cline JM, Brignolo L, Ford EW. Urogenital System/Genital System Female/Placental Disorders. In: Abee CR, Mansfield K, Tardif S, Morris T, eds. *Nonhuman Primates in Biomedical Research: Diseases*. 2nd ed. New York, NY: Elsevier: 2012;522 and 532-533.
7. Halbwax M, Mahamba CR, Ngalula AM, Andre C. Placental retention in a bonobo (Pan paniscus). *J Med Primatol*. 2009;38:171-174.
8. Laurent L, Parast M, Mestan K .Comparative Placentation. UC San Diego. 2024. <https://perinataldiscovery.ucsd.edu/comparative-placentation/species-index/index.html>.
9. Mori M, Bogdan A, Balassa T, Csabai T, Szekeres-Bartho J. The decidua-the maternal bed embracing the embryo-maintains the pregnancy. *Semin Immunopathol*. 2016 Nov;38(6):635-649.
10. Naiken S, Griffiths MA, Edouard L, Pa-

dayatchy N. Factors Influencing Reproduction in Captive-Bred Cynomolgus Monkeys (Macaca fascicularis) From Mauritius. *Am. J. Primatol*. 2015;77:1290–1298.
11. Perlman NC and Carusi DA. Retained placenta after vaginal delivery: risk factors and management. *Int. J. Women's Health*. 2019;11:527-534.
12. Ruch TC. Diseases of the Endocrine, Reproductive and Urinary Systems/Reproductive System. In: Ruch TC ed. *Disease of Laboratory Primates*. Philadelphia, PA: W.B. Saunders Company: 1959;457.
13. Stockinger DE, Torrence AE, Hukkanen RR, Vogel KW, Hotchkiss CE, Ha JC. Risk Factors for Dystocia in Pigtailed Macaques (Macaca nemestrina). *Comp Med*. 2011;61(2):170-175.

Joint Pathology Center
Veterinary Pathology Services

WEDNESDAY SLIDE CONFERENCE 2024-2025

Conference #10 — 23 October 2024

CASE I:

Signalment:
Mature ewe, *Ovis aries*, ovine.

History:
The cadaver and viscera of a mature ewe underwent routine meat inspection by an abattoir veterinarian who noted an emaciated cadaver, abnormal kidneys and liver. The liver was donated to the Department of Veterinary Medicine, University of Cambridge, for veterinary public health teaching and was passed to the anatomic pathology service for further investigation.

Figure 1-1. Liver, sheep. The liver is expanded by multifocal to coalescing, well-demarcated, cream nodules that are unencapsulated and infiltrative. (*Photo courtesy of:* The Queen's Veterinary School Hospital, University of Cambridge. https://www.vet.cam.ac.uk)

Gross Pathology:
The liver is expanded by multifocal to coalescing, well-demarcated, cream nodules that are unencapsulated and infiltrative. The nodules are up to 25 mm diameter.

Microscopic Description:
Liver: Apparent sub-grossly within the hepatic parenchyma forming multifocal to coalescing nodular masses is an unencapsulated moderately densely cellular neoplasm that is infiltrative, with small neoplastic nodules infiltrating the surrounding hepatic parenchyma. The neoplastic cells are arranged in sheets supported by a moderately fine collagenous stroma with blood vessels. The neoplastic cells are polygonal and moderately sized, with clearly demarcated cellular boundaries and a moderate amount of cytoplasm that is clear, or exhibits either globular eosinophilic deposits, or fine fibrillar eosinophilic strands, that are PAS-positive. The nuclei are round and generally centrally placed within the cells, with lightly stippled chromatin and frequently a single prominent basophilic nucleolus. There is one mitosis per ten high power fields (per 2.37 mm^2). There is a moderate degree of anisocytosis and anisokaryosis. There are small foci of necrosis and haemorrhage, comprising less than 5% of the total area of neoplasm in the section examined, and scattered rare neoplastic cells exhibit apoptosis, characterised by shrunken brightly eosinophilic cytoplasm and nuclear pyknosis.

The hepatic parenchyma immediately adjacent to the neoplastic nodules is multifocally

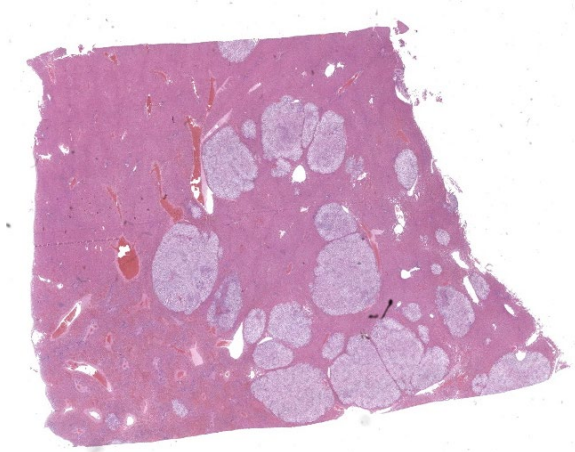

Figure 1-2. Liver, sheep. A multinodular neoplasm is present within the submitted section of liver. (HE, 4X)

compressed. Small numbers of lymphocytes and rarer plasma cells are present multifocally within portal areas, and portal areas also exhibit mild fibrosis multifocally. Deposits of clumped golden-brown granular pigment (haemosiderin) are present multifocally in hepatic Kupffer cells.

Bile duct epithelium exhibits strong positive cytoplasmic immunohistochemical reactivity to cytokeratin 19 (positive internal control tissue). The neoplastic cells do not exhibit positive staining with cytokeratin 19.

Contributor's Morphologic Diagnosis:
Liver: Hepatocellular carcinoma, clear cell variant.

Contributor's Comment:
In this case, a diagnosis of the clear cell variant of hepatocellular carcinoma was made on the basis of the histologic cellular arrangement and morphology. The diagnosis was supported by the macroscopic appearance of the lesion as unencapsulated and infiltrative nodular masses.

Hepatocellular carcinomas have a widely variable histologic appearance due to different cellular arrangements, likely reflecting the degree of differentiation of the neoplastic hepatocytes.[6] Four major histologic variants are described, namely trabecular, pseudoglandular, scirrhous, and solid. As the name suggests, in trabecular hepatocellular carcinomas, the predominant cellular arrangement has a resemblance to normal hepatic trabeculae, although the plates of cells may vary considerably in width, with trabeculae frequently composed of 5-10 cells thickness of neoplastic hepatocytes. In other foci the trabeculae may be quite thin, and this level of variability is a feature that may be helpful in the distinction between well-differentiated trabecular hepatocellular carcinoma and hepatocellular adenoma. In the latter, the trabeculae would be anticipated to be of uniform thickness.[6] In neoplasms exhibiting the pseudoglandular pattern, the neoplastic hepatocytes form rudimentary acini, whereas in the scirrhous form there is dense connective tissue, and aggregates of neoplastic hepatocytes are infiltrated by ductular epithelium.[6] As the name suggests, solid hepatocellular carcinomas are formed by solid sheets of neoplastic hepatocytes. In some variants of this sub-type, the neoplastic hepatocytes exhibit prominent cytoplasmic vacuolation and are described as clear cell hepatocellular carcinomas, as in this case.[6]

Clear cell hepatocellular carcinomas, or hepatocellular carcinomas that exhibit a partial clear cell pattern, have been described in a number of species including dogs,[14] captive fennec foxes,[13] and sheep.[1] It has previously been suggested that the clear cell pattern may be associated with cytoplasmic PAS-positivity and glycogen deposition[1] and PAS-positive cytoplasmic deposits are observed in the case described here.

In cases of hepatocellular carcinoma requiring immunohistochemical diagnostic confirmation, Hep Par-1 can be used to positively identify normal and neoplastic hepatocytes.[6,16] In human medicine, arginase-1 has

been suggested to be a more sensitive and specific marker of hepatocellular differentiation than Hep Par-1 and immunohistochemical staining with arginase-1 may therefore also be of diagnostic utility in veterinary pathology.[4] Normal and neoplastic biliary epithelial cells express cytokeratin 7 and 19, and epithelial membrane antigen. These immunohistochemical staining characteristics can be utilised to distinguish hepatocellular carcinoma from cholangiocellular neoplasms in many cases although some poorly differentiated canine hepatocellular carcinomas may downregulate Hep Par-1 expression and exhibit some cytokeratin 19 immunoreactivity.[6] In our case, cytokeratin 19 was utilised for additional educational confirmation that the neoplastic cells were not of biliary origin.

Fallen stock collection centres, abattoirs and meat packing plants all provide the opportunity to study the prevalence of neoplasms arising in sheep.[1,2,12] Hepatocellular carcinomas appear to be more frequent than cholangiocellular neoplasms and occur in lambs as well as adult animals.[1,2] Extramedullary haematopoiesis has been described as a feature of hepatic tumors in lambs aged less than six months.[1,2] Although considered to be rare in domestic species, hepatoblastomas, believed to arise from hepatic stem/progenitor cells, have also been described in lambs.[5,6] As in other species, the ovine liver is also a site for tumor metastases, lymphoma, and mast cell neoplasms.[8,10,11]

Metastasis has previously been reported in cases of ovine hepatocellular carcinoma.[1] Due to the nature of the abattoir case material described here, a full post mortem examination was not conducted and the presence or absence of metastatic spread to the draining lymph nodes or other viscera could not be determined. The renal lesions were not examined microscopically but the kidneys did not display macroscopic evidence of neoplastic infiltration.

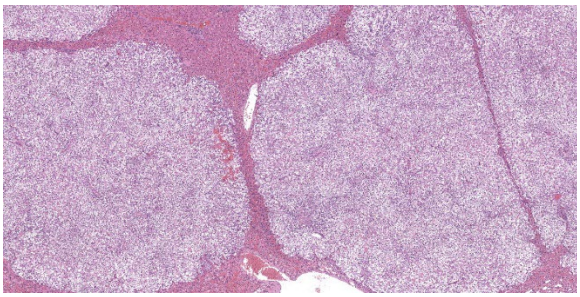

Figure 1-3. Liver sheep. Neoplastic hepatocytes have lost normal sinusoidal architecture and are arranged in sheets. (HE, 44X)

Contributing Institution:
Department of Veterinary Medicine, The Queen's Veterinary School Hospital, University of Cambridge.

Cambridge CB3 0ES, UK.

https://www.vet.cam.ac.uk

JPC Diagnosis:
Liver: Hepatocellular carcinoma, clear cell variant

JPC Comment:
This week's moderator was Dr. Rebecca Smedley of Michigan State University who led participants through a neoplasia-centric conference. This first case was recently published in the *Journal of Comparative Pathology*[9] and we were glad to explore it further.

From subgross, the contrast between neoplastic hepatocytes laden with glycogen (confirmed via PAS) and normal hepatocytes is stark. Several conference participants also noted hyaline inclusions within the cytoplasm of clear cell hepatocytes that were reminiscent of Mallory bodies.[3,7] Mallory bodies (syn. Mallory-Denk Bodies) have been previously noted within hepatocytes of humans (and in some lab animal models) and are composed of a mix of misfolded proteins such as keratins 8 and 18, ubiquitin, and heat shock proteins.[3,7] Associated conditions include alcohol-related steatohepatitis (fatty

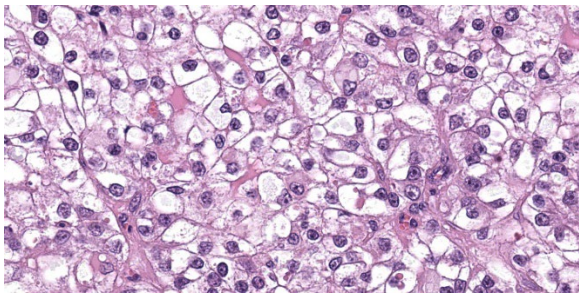

Figure 1-4. Liver sheep. High magnification of neoplastic hepatocytes with cleared eosinophilic cytoplasm. (HE, 627X)

liver disease), copper hepatopathy, and hepatic neoplasms. In human cases of hepatocellular carcinoma, Mallory-Denk bodies are noted in 20-30% of cases, though these should be distinguished from hyaline bodies which are histologically similar, but lack keratin.[7] IHC for P62 and other protein constituents (keratin) can aid in determination. Both elements represent hepatocellular dysfunction and aberrant protein folding.

Given the age (and of course, species) of this animal, we performed a reticulin and copper (rhodanine) stain, which were both negative. Copper-associated hepatopathy may be an inciting cause of HCC in the dog. Additionally, we tried a CK19 and CK7 to characterize hepatocyte and biliary changes as poorly differentiated neoplastic hepatocytes may gain CK19 expression and lose CK7 expression (and may be portend a worsened prognosis), but the stains did not show abnormalities along these lines. .

Finally, Dr. Smedley discussed the potential utility of glypican-3 with the group. As Glypican-3 labels neoplastic hepatocytes but not normal or hyperplastic foci,[15] it would be an invaluable tool in sorting through edge cases where suspect neoplasms also contain rare portal tracts which are typically a distinguishing feature of hepatic hyperplasia. In conjunction with P-glycoprotein or arginase-1 where expression is decreased in neoplastic cells compared with normal hepatocytes, glypican-3 may prove a useful diagnostic tool.

References:

1. Anderson LJ, Sandison AT. Tumors of the liver in cattle, sheep and pigs. *Cancer* 1968;21:289-301.
2. Bundza A, Greig AS, Dukes TW. Primary Hepatocellular Tumors in Animals Killed at Meat Packing Plants: Report of 11 cases. *Can Vet J* 1984;25:82-85.
3. Chelliah, Adeline R, Radhi, Jasim M., Hepatocellular Carcinoma with Prominent Intracytoplasmic Inclusions: A Report of Two Cases, Case Reports in Hepatology, 2016, 2032714.
4. Choi WT, Kakar S. Immunohistochemistry in the Diagnosis of Hepatocellular Carcinoma. *Gastroenterol Clin North Am* 2017;46:311-325.
5. Cotchin E. Spontaneous tumours in young animals. *Proc R Soc Med* 1975;68:653-655.
6. Cullen JM. Tumors of the liver and gallbladder. In: Meuten DM, ed. *Tumors in domestic animals*. 5th ed. John Wiley & Sons, Inc.; 2017.
7. Denk H, Abuja, P.M. & Zatloukal, K. Mallory-Denk bodies and hepatocellular senescence: a causal relationship?. *Virchows Arch* 484, 637–644 (2024).
8. Doige CE. Omasal squamous cell carcinoma in a ewe. *Can J Comp Med* 1983;47:382-384.
9. Hughes K, Radakovic M, Gorman F, Malinowska B, Cullen JM. Immunohistochemical characterization of clear cell variant of hepatocellular carcinoma in a sheep. J Comp Pathol. 2023 Jul;204:47-50.
10. Johnstone AC. Two cases of hepatic mastocytoma in sheep. *Vet Pathol* 1972;9:159-163.
11. Johnstone AC, Manktelow BW. The pathology of spontaneously occurring malignant lymphoma in sheep. *Vet Pathol*

1978;15:301-312.
12. Lovatt FM, Strugnell BW. An observational study involving ewe postmortem examination at a fallen stock collection centre to inform flock health interventions. *Vet Rec* 2013;172:504.
13. Monahan CF, Garner MM, Kiupel M. Hepatocellular Neoplasms in Captive Fennec Foxes (*Vulpes zerda*). *J Zoo Wildl Med* 2018;49:996-1001.
14. Patnaik AK, Hurvitz AI, Lieberman PH, Johnson GF. Canine hepatocellular carcinoma. *Vet Pathol* 1981;18:427-438.
15. Shih TC, Wang L, Wang HC, Wan YY. Glypican-3: A molecular marker for the detection and treatment of hepatocellular carcinoma☆. Liver Res. 2020 Dec;4(4):168-172.
16. Zhang W, Wang Q, Jiang YX, et al. Simultaneous double primary clear cell carcinomas of liver and kidney: a case report and review of literature. *Int J Clin Exp Pathol* 2015;8:995-999.

CASE II:

Signalment:
11 year old, male, Australian shepherd dog, *Canis lupus familiaris*

History:
The dog's owner noted asymmetry of the testes with enlargement of the left testis within a short period of time. After clinical examination, neoplasia of one testis was suspected, and the left testis was removed, and submitted for histopathologic examination. Signs of hormonal imbalance or feminization as well as other clinical symptoms were not observed.

Gross Pathology:
Testis with epididymis (5 x 4 x 3.5 cm) and funiculus spermaticus, testis consisting of approximately 90% neoplastic tissue with a small margin of normal tissue, centrally

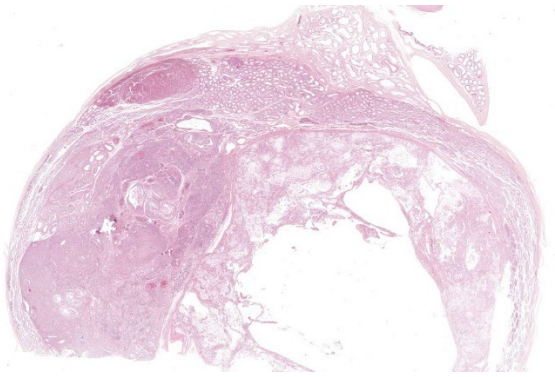

Figure 2-1. Testis, dog. One section of a testis with multiple neoplasms is submitted for examination. (HE, 5X).

cystic, multiple confluent whitish and yellowish-brown nodules.

Microscopic Description:
Testis: Infiltrating and compressing the testicular parenchyma and extending to one cut edge is a 2 x 1.5 cm large neoplastic proliferation composed of different cells and components. The first cell population consists of polygonal cells with often distinct cell borders, a moderate amount of eosinophilic, granular, or vacuolated cytoplasm (ranging from finely vacuolated to large vacuoles with compression of cytoplasm), and a round nucleus with finely stippled chromatin and an often prominent magenta nucleolus (interstitial cells). There is moderate anisocytosis and anisokaryosis. The mitotic rate is less than 1 per 2.37 mm^2 (10 HPF). These cells form both a 0.5 x 0.3 cm, compact, densely cellular, well-demarcated, partly encapsulated nodule composed of densely packed cords and nest of cells in a fine fibrovascular stroma and a 2 x 1.5 cm moderately cellular, well-demarcated, encapsulated nodule composed of packets and nests of cells with large vacuoles and a central clear space. The second cell population consists of large round cells with distinct cell borders, often a large amount of eosinophilic granular cytoplasm, and large, round, vesicular nuclei with coarse chromatin and 1-2 prominent, magenta nucleoli (germ cells).

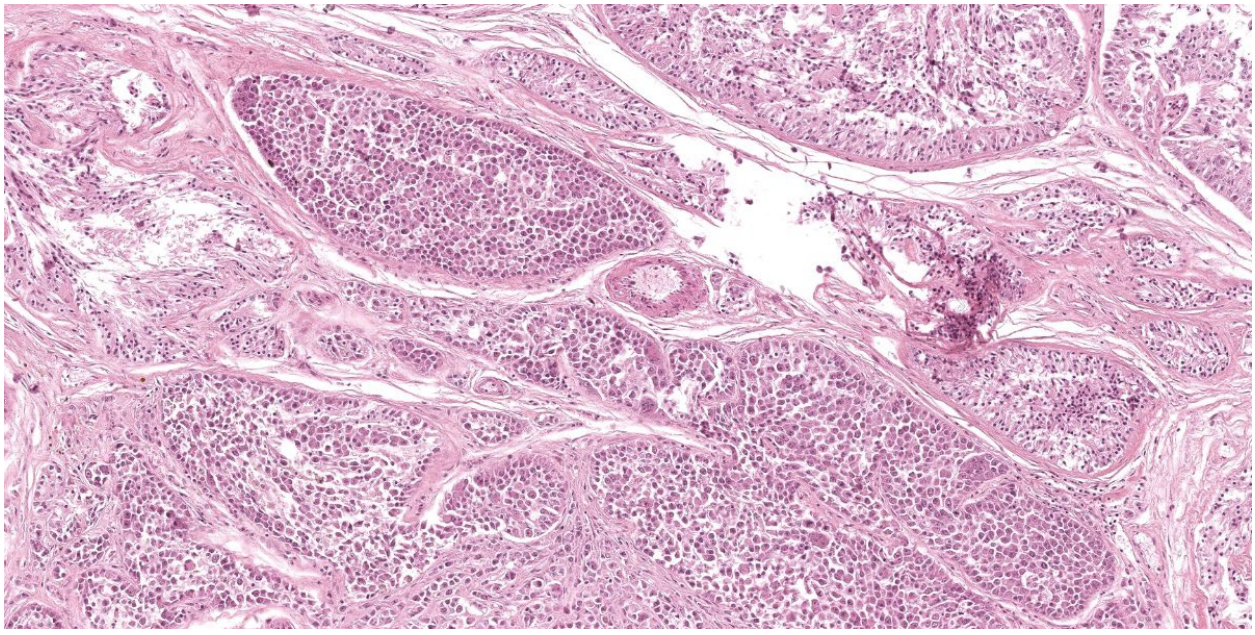

Figure 2-2. Testis, dog. An intratubular neoplasm is present with a mixture of columnar and polygonal cells. (HE, 107X)

There is moderate anisocytosis and anioskaryosis with frequent multinucleated cells, occasionally forming giant cells with up to 8 nuclei. Some macronuclei are visible. The mitotic rate averages 1-3 mitoses per 0.237 mm^2 (1 HPF). These cells are either infiltrate the lumina of the seminiferous tubules, replacing Sertoli and spermatogenic cells, or are intermingled with the third cell population within a 1.5 x 1 cm, moderately cellular, well-demarcated, partly encapsulated, partly infiltrative nodule composed of large nests, packets, and tubules of neoplastic cells, separated and surrounded by bands of fibrous connective tissue. The cells of the second population can sometimes be found within thin walled vessels (vascular invasion). The third population of neoplastic cells is polygonal to columnar with indistinct cell borders , a moderate amount of eosinophilic granular cytoplasm and an oval nucleus with coarsely stippled chromatin and a magenta nucleolus. Palisading of the cells perpendicular to the basement membrane of the seminiferous tubules is frequently noted. The population exhibits mild to moderate anisocytosis and anisokaryosis. The number of mitoses is less than 1 per 2.37 mm^2 (10 HPF). Interspersed within the neoplastic cells are few lymphocytes and plasma cells as well as aggregates of hemosiderin-laden macrophages.

A few seminiferous tubules show remnants of spermatogenesis. Epididymis and Ductus deferens contains single macrophages and no spermatids.

Contributor's Morphologic Diagnosis:
Testis:

1. Interstitial cell tumor in two localizations
2. Seminoma, intratubular multiple and diffuse
3. Mixed germ cell sex-cord stromal tumor (seminoma and Sertoli cell tumor)
4. Atrophy of residual seminiferous tubules

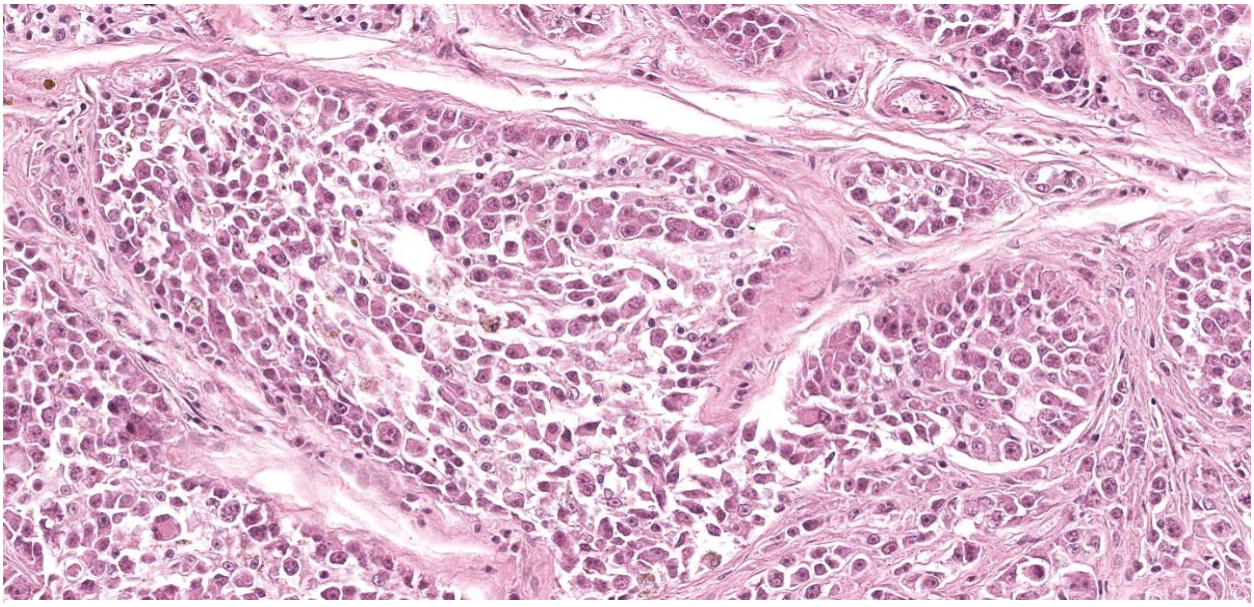

Figure 2-3. Testis, dog. Columnar cells palisade along the basement membrane, while polygonal cells fill the lumen. Nuclear and cytoplasmic features are similar in both populations. (HE, 288X)

Contributor's Comment:

In intact older male dogs, testicular tumors are one of the most common tumors. The cause for that is unknown. Seminoma, Sertoli cell tumors and Leydig cell tumors are found regularly.[1-3] Less common are mixed germ cell sex-cord stromal tumors of the testis,[5] embryonal carcinoma, or teratomas. Adenomas or adenocarcinomas of the rete testis are very rare. Secondary testicular tumors (metastases) are extremely rare.

In dogs, cryptorchism is an important predisposing factor for primary testicular tumors. Several types of neoplasms can be found in one testis,[1,2] so careful examination and lamellation of the testes is obligatory in preparation for histopathology.

The biologic behavior of testicular neoplasms in dogs is often benign, and metastases are rare, with a higher risk in seminomas and Sertoli cell tumors.[3] Leydig cell tumors are considered benign in dogs. Recently, however, two dogs with metastatic Leydig cell tumors have been described. Both cases were found to have a high mitotic count and high Ki-67 index.[4] Unfortunately, there are no other obvious cytologic or histopathologic signs of malignancy in testicular neoplasms in dogs. In malignant cases, distant metastases may be suspected in regional lymph nodes or along the spermatic cord.[1,2]

In the case presented, all three cell types of the common tumor types of canine testicular neoplasms are found, and the examiner must describe the characteristics of the tumor cells and the additional findings in the remaining non-neoplastic tissue. Testicular neoplasms in general and this case in particular are thus very good practice cases for veterinary pathology residents.

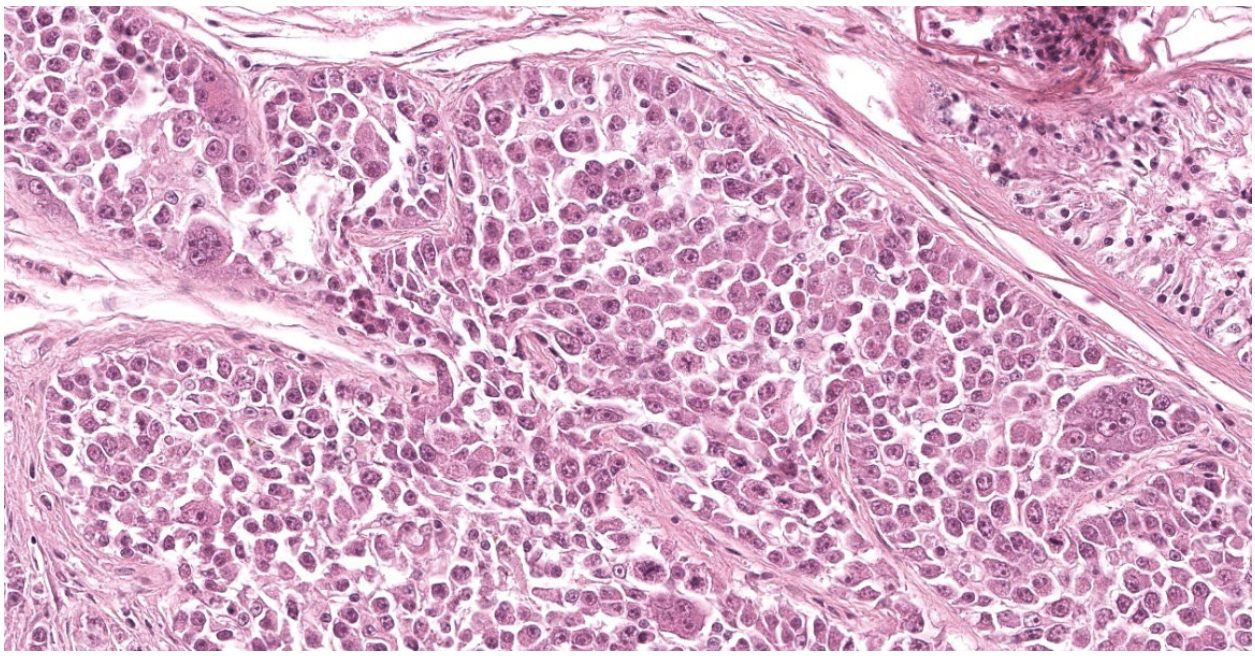

Figure 2-4. Testis, dog. Multinucleated forms are present in both the columnar and polygonal populations. (HE, 286)

Contributing Institution:
Institut fuer Veterinaer-Pathologie, Justus-Liebig-Universitaet Giessen

Frankfurter Str. 96, 35392 Giessen, Germany

http://www.uni-giessen.de/cms/fbz/fb10/institute_klinikum/institute/pathologie

JPC Diagnosis:

1. Testis: Mixed germ cell sex-cord stromal tumor
2. Testis, seminiferous tubules: Atrophy, diffuse, moderate, with aspermatogenesis

JPC Comment:

Case 2 presents an interesting diagnostic challenge in that there are 4 potential separate neoplasms in this neoplasm. Our morphologic diagnoses differed from that of the contributor only academically, in that we were unable to fully resolve what was an individual neoplasm versus a component of the larger mixed germ cell sex-cord stromal tumor. Herein. we simply covered all tumor entities under a single banner of mixed germ cell sex-cord stromal tumor. In addition, and with less spirited discussion, conference participants described degenerative changes to the remaining seminiferous tubules, degeneration of spermatids, and lack of sperm within the epididymis as we.. .

We performed a full workup for this case in conjunction with Dr. Smedley. Within this section of testis, there were 3 separate, distinct morphologies that participants described. Foremost, there was a seminoma-distinct portion that had intratubular round to polygonal cells with radiating chromatin and occasional multinucleation. Second, there was an interstitial (Leydig) cell-distinct portion that was unencapsulated with markedly eosinophilic polygonal cells with vacuolated cytoplasm. Finally, there was an encapsulated, expansile portion that had polygonal cells forming fibrous trabeculae

with palisading that represented an overlap of mrophologies of both Sertoli (sustentacular cells) and seminoma.

Conference participants discussed the nomenclature for this case carefully. Seminomas are a testicular germ cell tumor. Conversely, sex-cord stromal tumors represent neoplasms that exhibit features of either (or both) Sertoli cells and Leydig cells. In cases where seminoma (germ cell) and one or more stromal tumor features are overlapping, a diagnosis of mixed germ cell sex-cord stromal tumor is fitting. In some cases, it may be appropriate to diagnosis multiple discrete tumors within one testis when they are clearly distinct. Conference participants opined that the interstitial cell tumor-distinct population was smaller, separated by normal seminiferous tubules, and was morphologically the most distinct. It is possible that this was a separate tumor that arose earlier that was overshadowed by the emergence of the rapidly growing mixed tumor the contributor describes clinically.

Dr. Smedley emphasized that HE diagnoses alone could be misleading for approximately 20% of canine testicular tumors and that IHC was helpful for resolving exact cell type. We performed IHCs for CD117 (C-kit), desmin,

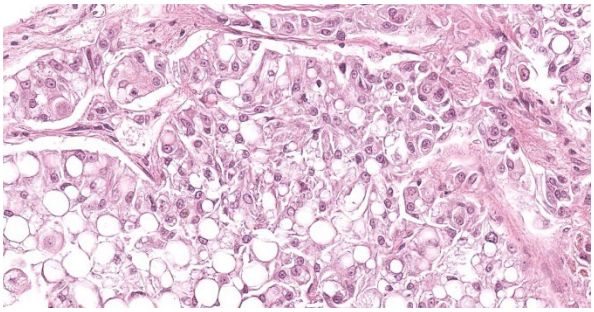

Figure 2-5. Testis, dog. Regionally, neoplastic cells often contain large intracytoplasmic lipid vacuoles. (HE, 381X)

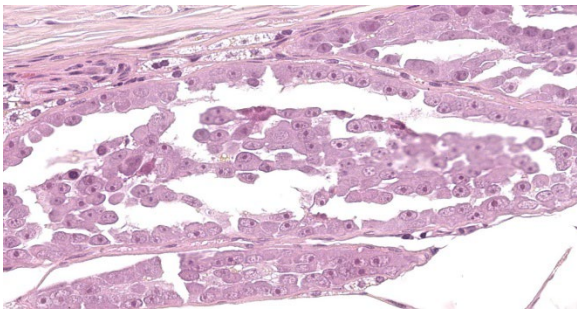

Figure 2-6. Testis dog. A conventional seminoma is present in this section. (HE, 580X)

vimentin, inhibin, LH, Melan-A, and NSE to characterize these neoplasms. Desmin outlined individual seminiferous tubules nicely while interstitial cell tumors were strongly and diffusely reactive for inhibin. GATA-4 is a transcription factor expressed in sex-cord cells, but not germ cells.[6] Dr. Smedley performed this IHC in her laboratory and noted moderate nuclear immunoreactivity within Sertoli cells and select Leydig cells. These patterns confirmed our H&E expectations of this case.

References:

1. Agnew DW, MacLachlan NJ. Tumors of the genital system. In: Meuten DJ, ed. *Tumors in domestic animals*. 5th ed. Ames, IA: Wiley Blackwell; 2017:706-713.
2. Foster RA. Male genital system. In: Maxie MG, ed. *Jubb, Kennedy, and Palmer's Pathology of Domestic Animals*. 6th ed. Philadelphia, PA: Elsevier; 2016; vol. 3:492-497.
3. Kennedy PC, Cullen JM, Edwards JF, Goldschmidt MH, Larsen S, Munson L, Nielsen S. *Histological classification of tumors the genital system of domestic animals*. WHO, Washington, DC: Armed Forces Institute of Pathology; 1998,second series, vol. 4.
4. Kudo T, Kamiie J, Aihara N, Doi M, Sumi A, Omachi T, Shirota K. Malignant

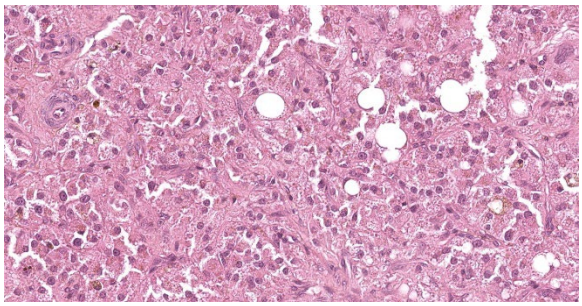

Figure 2-7. Testis, dog. A conventional interstitial cell tumor is present in this section as well. (HE, 363X)

Leydig cell tumor in dogs: two cases and a review of the literature. *J Vet Diagn Invest*. 2019;31(4):557-561.

5. Patnaik AK, Mostofi FK. A clinicopathologic, histologic, and immunohistochemical study of mixed germ cell-stromal tumors of the testis in 16 dogs. *Vet Pathol*. 1993;30:287-295.
6. Ramos-Vara JA, Miller MA. Immunohistochemical evaluation of GATA-4 in canine testicular tumors. *Vet Pathol*. 2009 Sep;46(5):893-6.
7. Reineking W, Seehusen F, Lehmbecker A, Wohlsein P. Predominance of granular cell tumours among testicular tumours of rabbits (Oryctolagus cuniculi dom.). *J Comp Pathol*. 2019;173:24-29.

CASE III:

Signalment:
12-year-old, intact female, dog (*Canis lupus familiaris*)

History:
The dog was submitted to a local veterinary clinic for computed tomography examination. Imaging revealed a tumor of the right adrenal gland measuring 2.5 x 2 cm adjacent to the caudal caval vein. There was no evidence for an intracaval infiltration or a thrombosis of the caval vein but infiltration of the phrenicoabdominal vein was detected. Both ovaries showed multiple cysts. The pre-surgical blood work showed a mildly decreased amount of lymphocytes (0.82, range: 1.05 – 5.1 M/l). Low-dose dexamethasone suppression test revealed inadequately suppressed cortisol secretion with plasma cortisol concentrations of 3.5 µg/dl after three hours, and 3.7 µg/dl after 8 hours of dexamethasone administration, respectively. During surgery, the right adrenal gland including the phrenicoabdominal vein and both ovaries were removed and submitted for histological examination.

Laboratory Results:
The adrenal sample was immunostained using the ABC method with commercially available antibodies specific for chromogranin A, synaptophysin and Melan A. The larger of the two proliferations stained positive for Melan A, the smaller one stained positive for chromogranin A and synaptophysin. The intravascularly detected cellular aggregate also stained positive for Melan A.

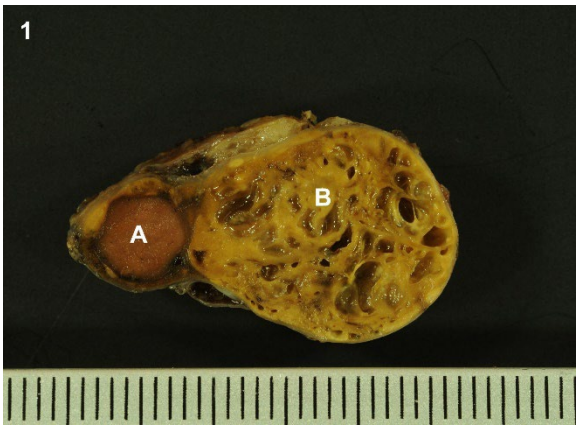

Figure 3-1. Adrenal gland, dog. Two discrete neoplasms are present within the adrenal gland. (*Photo courtesy of:* University of Veterinary Medicine, Hannover , http://www.tiho-hannover.de/kliniken-institute/institute/institut-fuer-pathologie/)

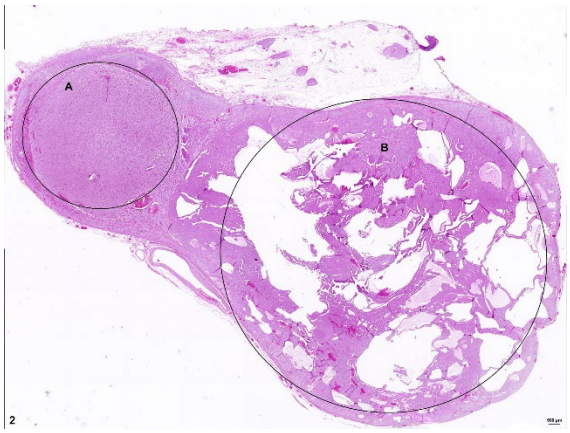

Figure 3-2. Adrenal gland, dog. Both nodules are clearly circumscribed, expansile and separated from each other by normal adrenal tissue (HE, 4X) (*Photo courtesy of:* University of Veterinary Medicine, Hannover , http://www.tiho-hannover.de/kliniken-institute/institute/institut-fuer-pathologie/)

Microscopic Description:
Histologically, two separate neoplastic proliferations are found in the adrenal gland. Both nodules are clearly circumscribed, expansile and separated from each other by normal adrenal tissue (Fig. 2). The larger, more cortically located proliferation measures approximately 1.4 cm in diameter. The nodular, moderately cell-rich, incompletely encapsulated, focally infiltrative mass is characterized by a predominantly solid growth pattern consisting of trabeculae of variable width, partly separated by optically empty or blood-filled spaces (dilated sinusoids). Polygonal, neoplastic cells measure approximately 15 µm in diameter (Fig. 3). The cells show distinct cellular borders and contain a moderate amount of a homogenous eosinophilic, partly highly vacuolated cytoplasm. The centrally located round nucleus displays a moderate amount of heterochromatin and one basophilic nucleolus. There is mild anisocytosis and -karyosis. Mitotic figures are not evident. The cells are accompanied by a scant fibrovascular stroma. Focally, a large aggregate of these tumor cells is present in a blood vessel (*angiosis carcinomatosa*) (Fig. 4).

The smaller nodule, located within the medullary area of adrenal gland measures approximately 0.5 cm in diameter. The well demarcated encapsulated neoplastic mass shows predominantly expansile growth of small polygonal cells measuring approximately 10-12 µm in diameter. Cells are arranged in small lobules and packages separated by thin, fibrous septa (neuroendocrine packaging; Fig. 5). Neoplastic cells are characterized by distinct cell borders, a moderate amount of fine granular, brightly eosinophilic cytoplasm, and a slightly eccentrically located, round, moderately heterochromatin-rich nucleus with up to one distinct nucleolus. There is a moderate anisocytosis and –karyosis. Multifocally, cells measuring up to 30 µm in size with karyomegaly are present. Up to 2 mitotic figures are found per high power field (400x).

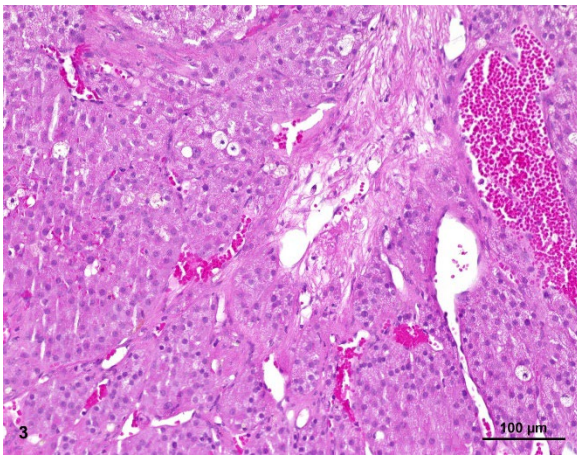

Figure 3-3. Adrenal gland, dog. The larger cortical nodule is composed of trabeculae of heavily vacuolated polygonal adrenocortical cells. (HE, 200X) (*Photo courtesy of:* University of Veterinary Medicine, Hannover , http://www.tiho-hannover.de/kliniken-institute/institute/institut-fuer-pathologie/)

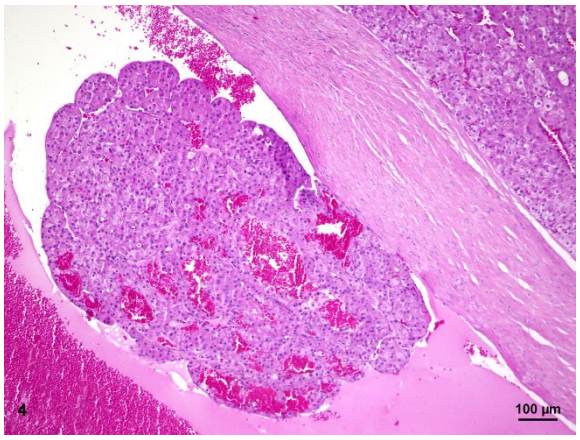

Figure 3-4. Adrenal gland, dog. A cluster of neoplastic cells from the larger nodules is present within a vessel. (HE, 400X) (*Photo courtesy of:* University of Veterinary Medicine, Hannover , http://www.tiho-hannover.de/kliniken-institute/institute/institut-fuer-pathologie/)

Contributor's Morphologic Diagnosis:

Adrenal gland: adrenocortical carcinoma with *angiosis carcinomatosa* and pheochromocytoma, canine.

Contributor's Comment:

The submitted case represents an unusual double lesion of the adrenal gland consisting of concurrent emergence of an adrenocortical carcinoma and a pheochromocytoma. Interestingly, when the dog was first presented to the clinicians, the animal did not show any obvious clinical signs of an altered adrenal function indicating a functional cortical or medullary neoplasia (excessive cortisol and/or catecholamine secretion).

Adrenocortical carcinomas occur in cattle, cats and elderly dogs and are also infrequently described in other species.[12,13] They tend to be larger than adenomas and bilateral occurrence is observed more frequently.[10,12,13] Affecting the zona fasciculata as well as the zona reticularis,[2] they often exhibit an infiltrative growth pattern into the adjacent tissue including the caudal caval vein, where large tumor-cell aggregations can form.[5,12,13]

Adrenocortical tumors can be found in 10-20% of dogs with Cushing syndrome,[6] and severe atrophy of the contralateral adrenal gland occurs in functional neoplasms due to a negative endocrine feedback loop.[12,13] It is estimated that most of the occurring adrenocortical tumors in dogs (up to 80%) are adrenocortical carcinomas.[4] Common sites for metastases are liver and lung.[12,13] The functional variants (endocrinologically active) of adrenocortical tumors usually secrete a massive amount of cortisol causing hyperadrenocorticism.[2,6,11] Clinical signs associated with functional adrenocortical tumors are polydipsia and polyuria, pendulous abdomen, polyphagia, muscle weakness, hypokalemia, hypertension, atrophic dermatosis with thin skin and hair loss as well as bilateral, symmetrical hypotrichosis or alopecia, hyperpigmentation scaling, comedones, and calcinosis cutis.[4,9,10,11,14]

Neoplastic cells of adrenocortical tumors typically show a specific immunoreactivity with antibodies targeting Melan-A, α-inhibin, vimentin, neuron specific enolase. Expression of synaptophysin may be variable.[5,12,13] The larger proliferation in the presented case as well as the intravascularly located neoplastic cells stained immunopositive for Melan-A which proves the presence of an adrenal cortical carcinoma.

Pheochromocytomas represent the most common tumor of the adrenal medulla and mostly occur in older dogs with no gender or breed predisposition. They can also be found in cattle and horses,[12,13] and are described in humans too.[1,3,8] They represent catecholamine-secreting tumors of the neuroectoderm-derived, chromaffin cells of the adrenal medulla or sympathetic ganglia, also termed sympathetic paragangliomas. They are composed of epinephrine-secreting

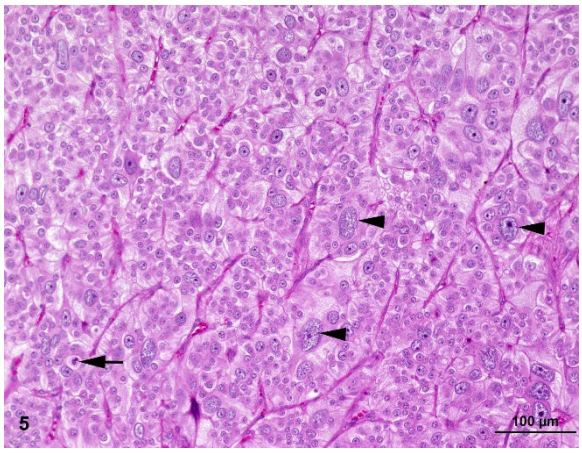

Figure 3-5. Adrenal gland, dog. There is nuclear gigantism (arrows) and occasional mitoses within the second, smaller, medullary neoplasm. (HE, 400X) (*Photo courtesy of:* University of Veterinary Medicine, Hannover , http://www.tiho-hannover.de/kliniken-institute/institute/institut-fuer-pathologie/)

cells, norepinephrine-secreting cells or both and occur mostly unilaterally and vary greatly in size.[1,3,7,12,15] These tumors often go along with clinical signs such as tachycardia, edema, panting, cardiac hypertrophy, hypertension, anorexia, lethargy, ascites, polyuria and polydipsia as well as diarrhea and vomiting resulting from excessive secretion of catecholamine.[3,7,12,13,15] In severe cases, the term 'pheochromocytoma crisis' is used to describe a serious complication characterized by obtundation, shock, disseminated intravascular coagulation, seizures, rhabdomyolysis and acute renal failure.[1] Malignancy of these tumors is assumed when invasion of the adrenal capsule and/or the caudal vena cava and the aorta or the surrounding tissue with potential metastases in distant organs is present.[1,5,12,13,15] Common sites for metastasis are adjacent lymph nodes, kidney, liver, spleen, lung and bone.[1,3,15] The pheochromocytoma of the presented case does not clearly show capsular invasion and/or an infiltrative growth pattern. However, especially the increased mitotic rate as well as the marked amount of pleomorphic cells can be interpreted as indications of a possible precancerous transformation.

During necropsy, a pheochromocytoma may present itself as a large mass occupying the entire adrenal gland, which is partly surrounded by a thin, compressed rim of adrenal cortex, sometimes forming small nodules.[15] Small pheochromocytomas remain confined to the adrenal medulla and are well encapsulated. The tissue shows light brown to yellow-red coloring emerging from hemorrhage and necrosis.

Immunohistological expression of chromogranin A and synaptophysin can be used to confirm the diagnosis.[1,5,12,13] In this case, the neoplasm stained immunopositive for chromogranin A and synaptophysin which confirms a pheochromocytoma in this case.

Contributing Institution:
Department of Pathology, University of Veterinary Medicine, Hannover, Buenteweg 17, 30559 Hannover, Germany.

http://www.tiho-hannover.de/kliniken-institute/institute/institut-fuer-pathologie/

JPC Diagnosis:

1. Adrenal gland, cortex: Adrenocortical adenoma
2. Adrenal gland, medulla: Pheochromocytoma.

JPC Comment:
This third case is another 'two-fer' case that the contributor has skillfully presented.

We agree with the contributor that the smaller neoplasm best represents a pheochromocytoma, although we differed from the contributor on the malignancy of the larger adrenocortical neoplasm Conference participants were somewhat split, with the lack of

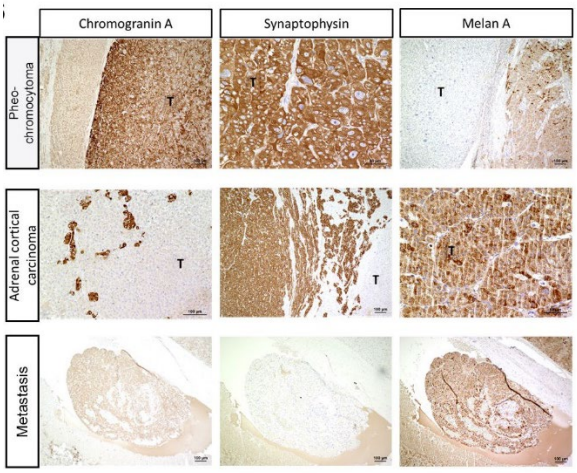

Figure 3-6. Adrenal gland, dog. Immunostaining of the two adrenal neoplasms and the intravascular cluster of neoplastic cells. (*Photo courtesy of:* University of Veterinary Medicine, Hannover , http://www.tiho-hannover.de/kliniken-institute/institute/institut-fuer-pathologie/)

nuclear atypia and well-demarcated nature of this neoplasm as helpful features supportive of an adenoma interpretation. Conference discussion also focused on whether lymphovascular invasion was present. We carefully reviewed the contributor's supplied image and the accompanying feature of the case slide of a large cluster of adrenocortical cells within the lumen of a blood vessel. In line with Meuten et al,[9] we felt that this was more likely to be pseudo-vascular invasion due to tissue sectioning and/or processing.

We performed a number of IHCs for this case to support these diagnoses with one surprise. Chromogranin and synaptophysin are both neuroendocrine markers that label pheochromocytomas, but are not specific *per se* as they do label other neuroendocrine and ganglion cell tumors. Dr Smedley graciously ran a met-enkephalin IHC at MSU for this case as both normal and neoplastic chromaffin cells of the adrenal medulla should react strongly. In this case, both chromogranin and synaptophysin were strongly and diffusely immunoreactive within this smaller neoplasm as well as highlighting the remnant portion of the adrenal medulla. Curiously, met-enkephalin labeled the adrenal medulla, but *not* the neoplasm, an odd finding which was new to Dr. Smedley (we do not have this immunomarker available to us at the JPC). . Although we report this neoplasm as being consistent with a pheochromocytoma, we cannot exclude the remote possibility of a metastasis of a neuroendocrine tumor to the adrenal gland. Curiously, the nuclear features of the pheochromocytooma displayed greater atypia and mitotic rate than is typical for pheochromocytomas.

References:

1. Barthez PY, Marks SL, Woo J, et al. Pheochromocytoma in dogs: 61 cases (1984-1995). *J Vet Intern Med*. 1997;11:272–278.
2. Bielinska M, Parviainen H, Kiiveri S, et al. Review paper: origin and molecular pathology of adrenocortical neoplasms. *Vet Pathol*. 2009;46:194–210.
3. Gilson SD, Withrow SJ, Wheeler SL, et al. Pheochromocytoma in 50 dogs. *J Vet Intern Med.* 1994;8: 228–232.
4. Goiska-Zygner O, Lechowski R, Wojciech Z. Functioning unilateral adrenocortical carcinoma in a dog. *Can Vet J*. 2012;53:623–625.
5. Kiupel M. Histological Classification of Tumors of the Endocrine System of Domestic Animals, vol. 12. Washington, DC: Armed Forces Institute of Pathology; 2008:44–47.
6. Labelle P, Kyles AE, Farver TB, et al. Indicators of malignancy of canine adrenocortical tumors: histopathology and proliferation index. *Vet Pathol.* 2004;41:490–497.
7. Machida T, Machida N. Invasion of pheochromocytoma from the caudal vena cava to the right ventricular cavity in a dog. Case Rep Vet Med. 2020; Feb

11;2020:5382687.doi: 10.1155/2020/5382687.
8. Mauldin EA, Peters-Kennedy J. Integumentary system In: Maxie G, ed. *Jubb, Kennedy and Palmer`s Pathology of Domestic Animals*. 6th ed. Vol. 1. St. Louis: Elsevier, 2016:509–736.
9. Meuten DJ, Moore FM, Donovan TA et al. International Guidelines for Veterinary Tumor Pathology: A Call to Action. Vet Pathol. 2021 Sep;58(5):766-794.
10. Nabeta R, Osada H, Ogawa M, et al. Clinical and pathological features and outcome of bilateral incidental adrenocortical carcinomas in a dog. *J Vet Med Sci.* 2017;79: 1489–1493.
11. Reusch CE, Feldman EC. Canine hyperadrenocorticism due to adrenocortical neoplasia. Pretreatment evaluation of 41 dogs. *J Vet Intern Med.* 1991;5: 3–10.
12. Rosol T, Gröne A. Endocrine Glands. In: Maxie G, ed. *Jubb, Kennedy and Palmer`s Pathology of Domestic Animals*. 6th ed. Vol. 3. St. Louis: Elsevier, 2016:326–428.
13. Rosol TJ, Meuten. Tumors of the endocrine glands. In: Meuten DJ, ed., Tumors in Domestic Animals: 6th ed., Iowa: Wiley & Sons; 2016:766–833.
14. Taylor J, Lee M, Nicholson M, et al. Functional ectopic adrenal carcinoma. *Can Vet J.* 2014; 55:845–848.
15. Zini E, Nolli S, Ferri F, et al. Pheochromocytoma in dogs undergoing adrenalectomy. *Vet Pathol.* 2019;56:358–368.

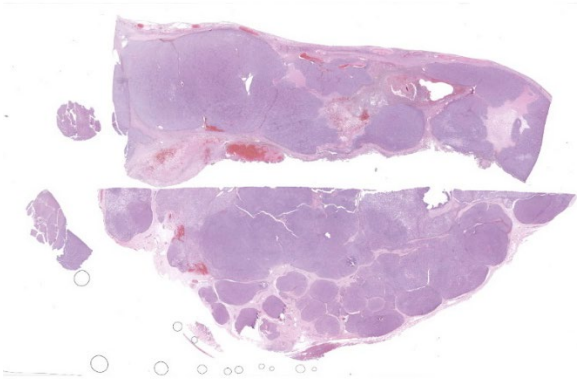

Figure 4-1. Spleen, dog. Two sections of spleen are submitted for examination, and both are effaced by a nodular neoplasm. (HE, 5X)

CASE IV:

Signalment:
3-year-old female canine, Pit Bull mix

History:
Prior to an ovariohysterectomy, the patient was reported to have a 4-month history of unexplained weight loss. Preoperative examination revealed a large intra-abdominal mass suspected to be associated with the spleen or liver and a subcutaneous perivulvar mass. An enlarged, cavitated spleen, a small mass noted on liver, and perivulvar subcutaneous mass were submitted for histopathology.

Gross Pathology:
Approximately 80% of splenic parenchyma was severely enlarged with multiple white to tan, irregular, soft coalescing nodules and necrotic cavitated areas. The liver had a focal, less than 0.5cm in diameter, tan irregular nodule. The perivulvar subcutis mass was tubular, tan, and soft and approximately 4-5cm in diameter.

Laboratory Results:
Cytology identified a spindloid neoplastic population with microvesiculated cytoplasm

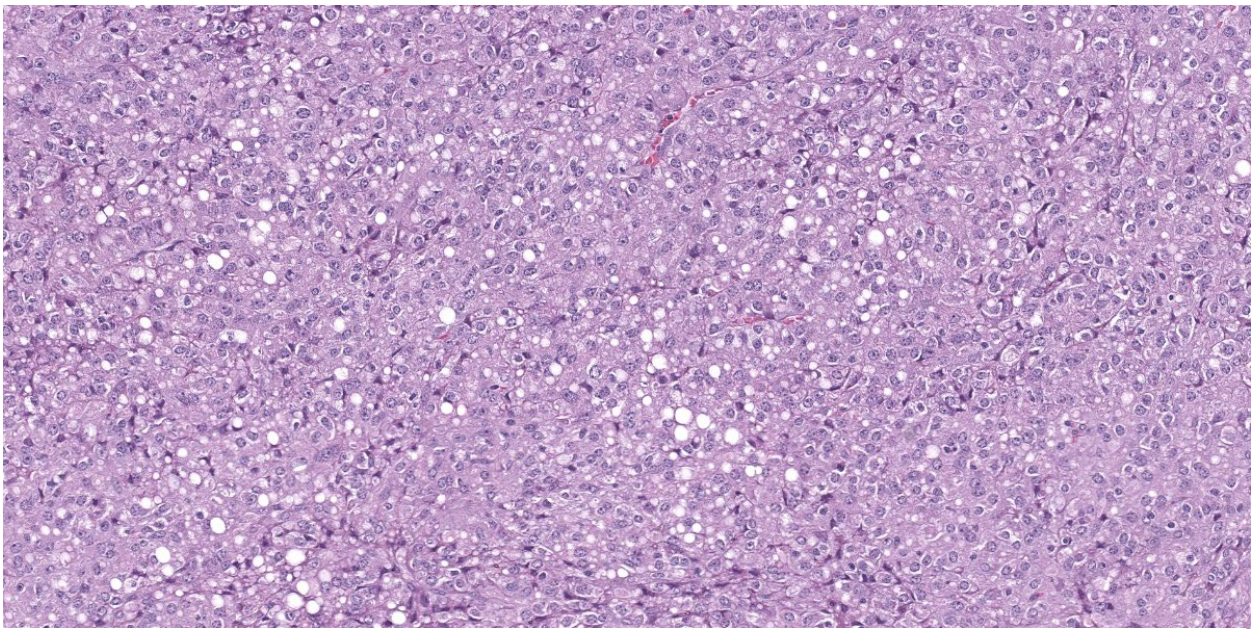

Figure 4-2. Spleen, dog. The neoplasm is composed of sheets of vacuolated spindled to polygonal cells. (HE, 259X)

in both the perivulvar subcutaneous mass and rare to occasionally in the splenic mass. These microvesiculated neoplastic cells were reminiscent of liposarcoma, but an epithelioid neoplasm could not be excluded.

Microscopic Description:
Splenic mass: Splenic parenchyma is expanded and replaced by multifocal to coalescing, poorly demarcated nodules of a moderately cellular neoplasm composed of pleomorphic cells arranged in nests and bundles separated by fine to moderate fibrovascular stroma. Neoplastic cells have indistinct cellular borders, moderate amounts of amphophilic cytoplasm that frequently contain variably sized clear discrete vacuoles (lipid), with one round to ovoid nuclei, with coarse chromatin and 1-3 discrete nucleoli. There is moderate anisocytosis and anisokaryosis with 5 mitotic figures in 10 high power fields ($2.37mm^2$). There are multifocal areas of necrosis with fibrin and hemorrhage, multinucleated giant cells, macrophages with intracytoplasmic dark brown pigment or yellow granular pigment (heme). Remaining spleen is congested with increased plasma cells.

Hepatic mass, incisional biopsy. Replacing approximately 50% of section is an unencapsulated, moderately well demarcated, moderately cellular neoplasm of similar neoplastic cells as described in spleen. Sometimes, there are intracytoplasmic pink globules within cytoplasm of neoplastic cells.

Perivulvar subcutaneous mass: Mass is composed of multiple coalescing nodules of previously described neoplastic cells in spleen separated by moderate amounts of mature collagen interrupted by macrophages laden with brown globular pigment (hemosiderin), lymphocytes, plasma cells, and mineral. There is electrocautery artifact along periphery.

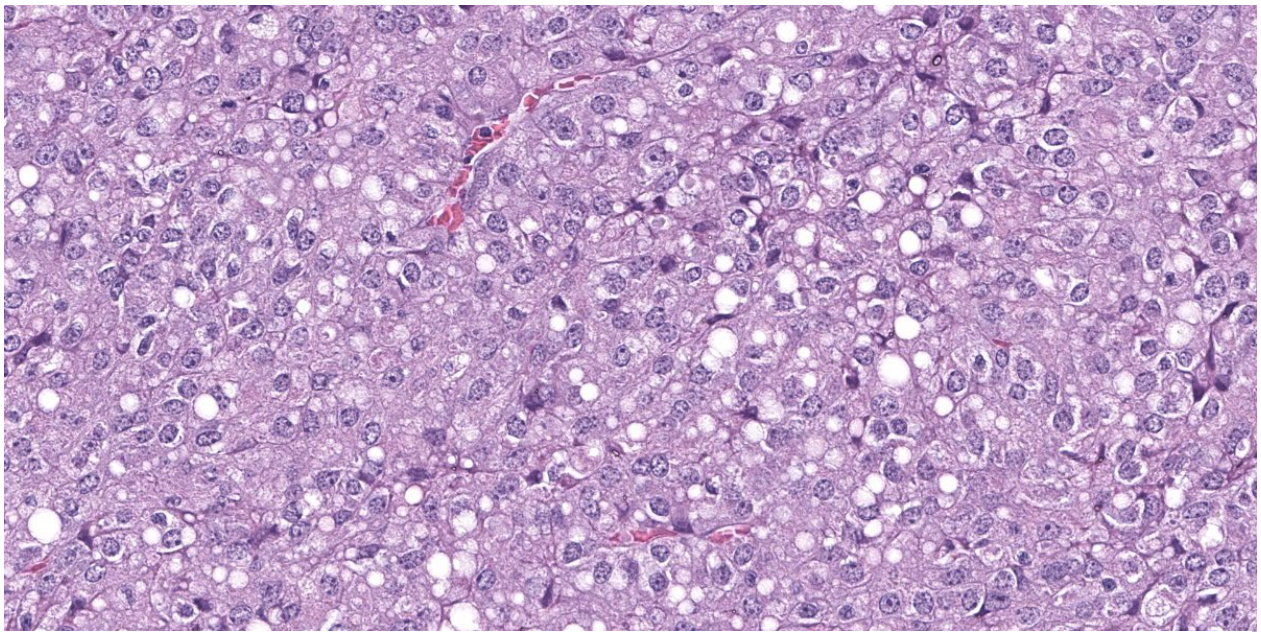

Figure 4-3. Spleen, dog. High magnification of neoplastic cells. Neoplastic cells contain discrete cytoplasmic vacuoles which often coalesce into a single vacuole. (HE, 381X)

Immunohistochemistry/Special Stains:
Hepatic, perivular, and splenic masses are examined and have the same results as below.

1. Cytokeratin: Neoplastic cells do not stain positively.
2. Vimentin: Neoplastic cells have positive cytoplasmic staining.
3. Melan-A: Neoplastic cells exhibit weak cytoplasmic staining which are occasionally stained strongly in cytoplasm. No membranous staining is seen in the neoplastic cells.
4. PNL-2: Approximately 10% of neoplastic cells exhibit cytoplasmic, occasionally membranous staining.
5. CD18: Neoplastic cells do not stain positively.
6. S-100: Neoplastic cells do not stain positively.
7. Synaptophysin: Neoplastic cells do not stain positively.
8. Chromogranin A: The cytoplasm of neoplastic cells diffusely are stained weakly which are considered negative.
9. Oil Red O: Neoplastic cells and vacuoles have positive intracytoplasmic staining.

Contributor's Morphologic Diagnosis:
Spleen: liposarcoma with metastasis to perivulvar subcutis and liver

Contributor's Comment:
Liposarcoma is an uncommon mesenchymal tumor originating from lipoblasts and lipocytes. More commonly, liposarcomas are a subtype of soft tissue sarcomas associated with the skin and subcutaneous tissues. Typically, locally invasive with low metastatic rates, liposarcomas in humans are classified by the World Health Organization into four histological subtypes: well differentiated liposarcoma/atypical lipomatous tumor, dedifferentiated liposarcoma, myxoid/round

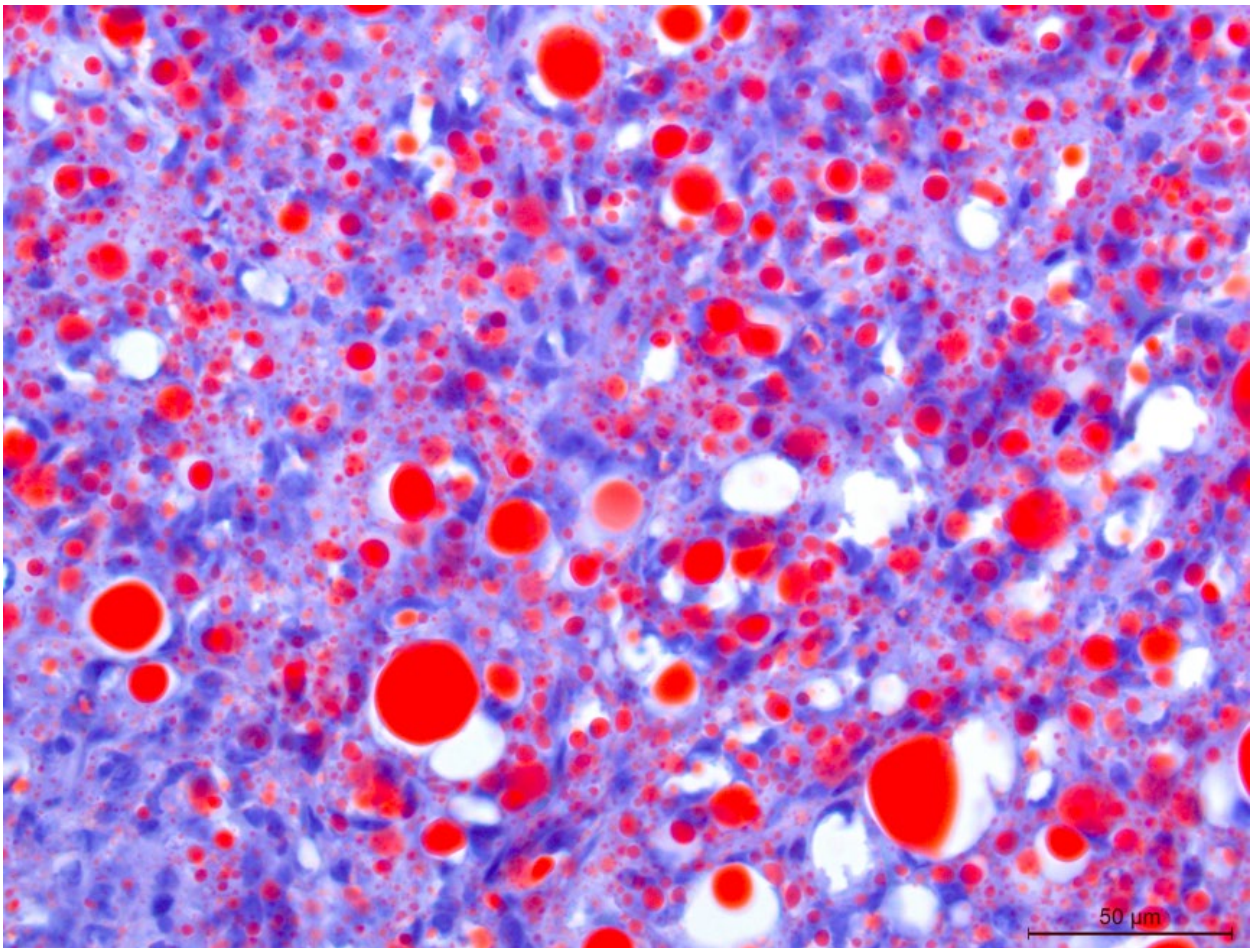

Figure 4-4. Spleen, dog. Cytoplasmic vacuoles stain strongly positive for Oil Red O.(Oil red 0, 400X) (Photo courtesy of: Midwestern University, Glendale, AZ https://clinics.midwestern.edu/animal-health-institute/diagnostic-pathology-center)

cell liposarcoma, and pleomorphic liposarcoma.[1] In domestic animals, there are three subtypes of liposarcomas: well-differentiated, pleomorphic, and myxoid.[4] In well differentiated liposarcomas, the majority of neoplastic cells have intracytoplasmic clear vacuoles.[4] Dedifferentiated liposarcomas arise in association with well differentiated liposarcomas and can have morphologic overlap with pleomorphic liposarcomas that may be multinucleated and irregular with a few to rare neoplastic cells containing intracytoplasmic lipid vacuoles. [4] Myxoid liposarcomas are distinguished by an abundant myxomatous matrix.[4]

Visceral liposarcomas associated with the spleen are a subtype of non-angiomatous non-lymphomatous mesenchymal neoplasm with higher metastatic potential.[3] Non-angiomatous non-lymphomatous mesenchymal neoplasms constitute 23-34% of primary splenic neoplasms and include fibrosarcoma, leiomyosarcoma, undifferentiated sarcoma, and liposarcoma.[2] A study analyzing the outcome of 32 cases of splenic stromal sarcomas in dogs, identified that a mitotic count exceeding 9 mitoses per 10 high power fields ($2.37mm^2$) to be a significant predictor of metastasis.[2] While liver metastases have been reported with splenic liposarcoma, metastases

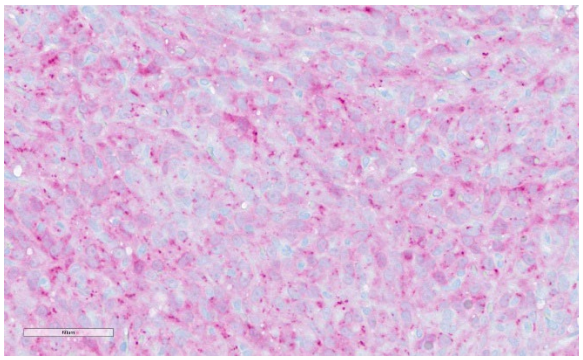

Figure 4-5. Spleen, dog. Neoplastic cells regionally demonstrate strong cytoplasmic immunopositivity for Melan A. (Melan A, 400X)

to subcutis have not been reported.[5]

In this case, given the similarity between neoplastic cells in the liver, subcutis, spleen, and the significantly larger neoplastic mass within spleen, it is favored that the splenic liposarcoma metastasized to both the liver and subcutis. Alternatively, it is possible the subcutaneous liposarcoma and spleen occurred independently. Metastases of sarcomas to subcutaneous tissues is extremely rare in all species. A retrospective study performed in human medicine found less than 0.25% of patients with sarcomas had cutaneous metastases.[10] Leiomyosarcomas were documented to be the most common mesenchymal tumor to metastasize to the skin.[10]

Generally, splenic sarcomas require additional immunohistochemistry or special stains for a definitive diagnosis. Specifically, particularly with a pleomorphic subtype of liposarcoma, Oil Red O is an invaluable stain for lipid within neoplastic cells.[9] Oil Red O is typically performed on frozen tissue sections, though there is a protocol for staining formalin fixed sections. Another lipid stain performed on frozen tissue is Sudan black.[9] Other immunohistochemical stains that may aid in favor of liposarcoma include S-100 and perilipin.[8] In human liposarcomas, immunohistochemical markers include MDM2 (murine double minute 2) and CDK4 (cyclin dependent kinase 4) that have also been used in subtype classification.[5]

Initially, this case was tentatively diagnosed as a melanoma given the positive immunoreactivity to Melan-A. However, given the predominantly negative immunoreactivity to PNL2, this diagnosis was seemingly refuted. In general, PNL2 is more sensitive than Melan-A with less cross reactivity to nonmelanocytic neoplasms.[6]

Contributing Institution:
https://clinics.midwestern.edu/animal-health-institute/diagnostic-pathology-center

JPC Diagnosis:
Spleen (per contributor) and liver: Malignant neoplasm

JPC Comment:
The final case for this conference is a story *within* a story! When we first received this case, we considered the contributor's diagnosis of liposarcoma based on both the gross and H&E features which were certainly suggestive. Although we ultimately reached a different final diagnosis in conference, the case was chosen as liposarcoma is not a common WSC submission.

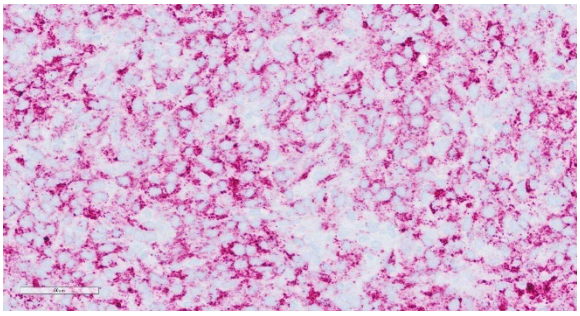

Figure 4-6. Spleen, dog. Neoplastic cells regionally demonstrate strong cytoplasmic immunopositivity for PNL2. (PNL2, 400X)

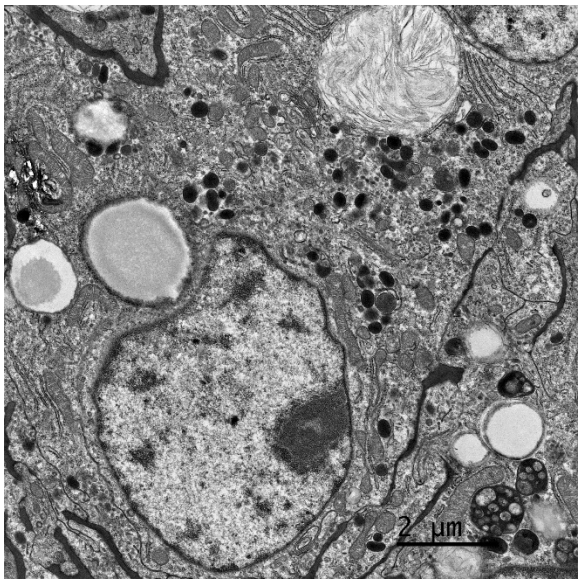

Figure 4-7. Spleen, dog. Ultrastructurally, neoplastic cells contain lipid droplets and clustered melanosomes in their cytoplasm. (Photo courtesy of: Midwestern University, Glendale, AZ https://clinics.midwestern.edu/animal-health-institute/diagnostic-pathology-center)

In prepping this case for conference, we noted that neoplastic cells were reactive for both Melan-A and PNL2 in our lab which did not fit with a liposarcoma. By chance, the contributor also consulted with Dr. Smedley on this case who repeated a melanocytic cocktail (Melan-A, PNL2, TRP-1, TRP-2) and performed a SOX10. The cocktail did label a proportion of cells (and we were cautioned by Dr. Smedley that these particular stains usually only stain a portion of the neoplastic cells. The SOX-10 was negative (which is unusual for melanomas, but the positive cells on the melanoma cocktail was de facie evidence that the tumor was indeed a melanoma.) As a result of these finding the contributor submitted this case to a third institution for transmission electronic microscopy where rare melanosomes within neoplastic cells. Given that Dr. Smedley, a renowned authority of canine melanoma) was on the WSC schedule this year, we knew that we couldn't pass up an opportunity to revisit this case and the superficially conflicting results.

Dr. Smedley focused on differentiating this case from a poorly differentiated sarcoma. Oil Red O in this case highlighted lipid-rich portions of the neoplasm. Lipid within neoplastic cells was also noted on EM. While seemingly an odd finding, the "balloon cell" subtype of melanoma may contain lipid, glycogen, resulting in the cleared swollen cytoplasm that gives this tumor its name. . Lastly, conference participants also considered sebaceous carcinoma as another rule out for lipid-rich tumors.

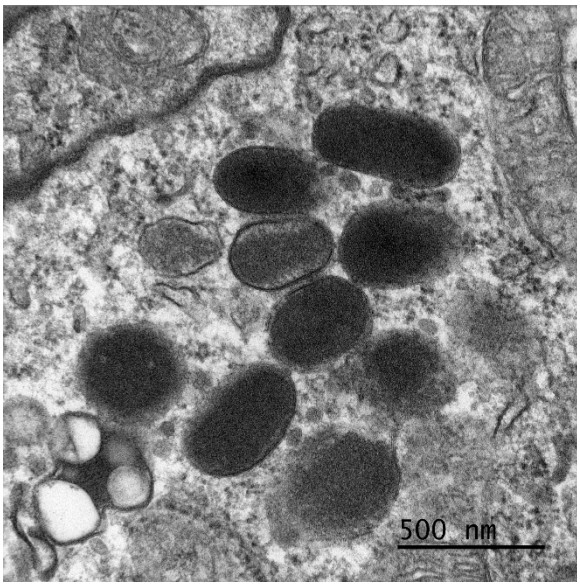

Figure 4-8. Spleen, dog. Higher magnification of melanosomes within the cytoplasm. (Photo courtesy of: Midwestern University, Glendale, AZ https://clinics.midwestern.edu/animal-health-institute/diagnostic-pathology-center)

References:

1. Amer KM, Congiusta DV, Thomson JE et al. Epidemiology and survival of liposarcoma and its subtypes: A dual database analysis. *J Clin Orthop Trauma*. 2020 Jul;11(Suppl 4):S479-S484.
2. Ferrari R, Marconato L, Boracchi P et al. Splenic stromal sarcomas in dogs: Outcome and clinicopathological prognostic factors in 32 cases. *Vet Comp Oncol*. 2024 Mar;22(1):12-21.
3. Gower KL, Liptak JM, Culp WT, Bravo L, Powers B, Withrow SJ. Splenic liposarcoma in dogs: 13 cases (2002-2012). *J Am Vet Med Assoc*. 2015 Dec 15;247(12):1404-7.
4. Meuten DJ, Hendrick M. Mesenchymal Tumors of the Skin and Soft Tissues. In: Meuten DJ, ed: *Tumors in Domestic Animals.* 5th edition. Ames, IO: John Wiley & Sons, Inc. 2017; 640.
5. Nishikawa G, Minamiguchi S, Hata H et al. Dedifferentiated liposarcoma involving the spleen and splenic hilum: a report of a case with a rare growth pattern. *Int Surg*. 2015 Jan;100(1):128-32.
6. Ramos-Vara JA, Miller MA. Immunohistochemical identification of canine melanocytic neoplasms with antibodies to melanocytic antigen PNL2 and tyrosinase: comparison with Melan A. *Vet Pathol*. 2011 Mar;48(2):443-50.
7. Saik JE, Diters RW, Wortman JA. Metastasis of a well-differentiated liposarcoma in a dog and a note on nomenclature of fatty tumours. *J Comp Pathol*. 1987 May;97(3):369-73.
8. Straub BK, Witzel HR, Pawella LM et al. Perilipin 1 Expression Differentiates Liposarcoma from Other Types of Soft Tissue Sarcoma. *Am J Pathol*. 2019 Aug;189(8):1547-1558.
9. Tracy RE, Walia P. A method to fix lipids for staining fat embolism in paraffin sections. *Histopathology*. 2002 Jul;41(1):75-9.
10. Wang WL, Bones-Valentin RA, Prieto VG et al. Sarcoma metastases to the skin. *Cancer*. 2012;118: 2900-2904.

Joint Pathology Center
Veterinary Pathology Services

WEDNESDAY SLIDE CONFERENCE 2024-2025

Conference #11 30 October 2024

CASE I:

Signalment:
A 4 year old intact Male Beagle dog (*Canis familiaris*).

History:
Presented for a 9 day history of hyporexia and regurgitation. Previous history of being treated for hepatozoonosis in April 2023 with relapse in May 2023. Radiographs revealed bilateral femoral periosteal bone reaction. Abdominal ultrasound found free fluid (which was frank blood determined via abdominocentesis) and multiple cavitated lesions in spleen and liver. An abdominal exploratory laparotomy was performed which found a ruptured splenic mass as well as two additional masses within the liver. Humane euthanasia was elected given uncertain prognosis and the remains were submitted for necropsy.

Gross Pathology:
Arising from the base of the heart immediately adjacent to the aorta are two ovoid, green to dark brown, smooth and firm nodules measuring 2 cm x 1 cm x 1 cm.

Within the abdominal cavity is approximately 32 mL of red, opaque, watery fluid. All lymph nodes are mildly to moderately enlarged, reaching up to 2 cm diameter with the abdominal lymph nodes most severely affected.

Figure 1-1. Heart, dog. Multiple sections of heart and lymph node are submitted for examination. (HE, 5X)

Laboratory Results:
Hepatozoon spp. RealPCR: Negative

Microscopic Description:
Heart: Examined are four sections. Multifocally infiltrating between and separating cardiomyocyte fibers are discrete, occasionally encapsulated, aggregates of predominantly lymphocytes and plasma cells with scattered macrophages and fibroblasts. Within several of these aggregates are reactive histiocytes containing spherical eosinophilic and intracytoplasmic round protozoan merozoites approximately 4-6µm in diameter and often displacing the host cell nuclei. Randomly distributed throughout the right, left, and interventricular septal walls are variably- sized multilamellar mucopolysaccharide rich cysts (Onion skin cysts, meronts) up to 200 µm in diameter. Occasionally within these maturing meronts are variable stages of merozoite development containing greater than 50, 2-3µm

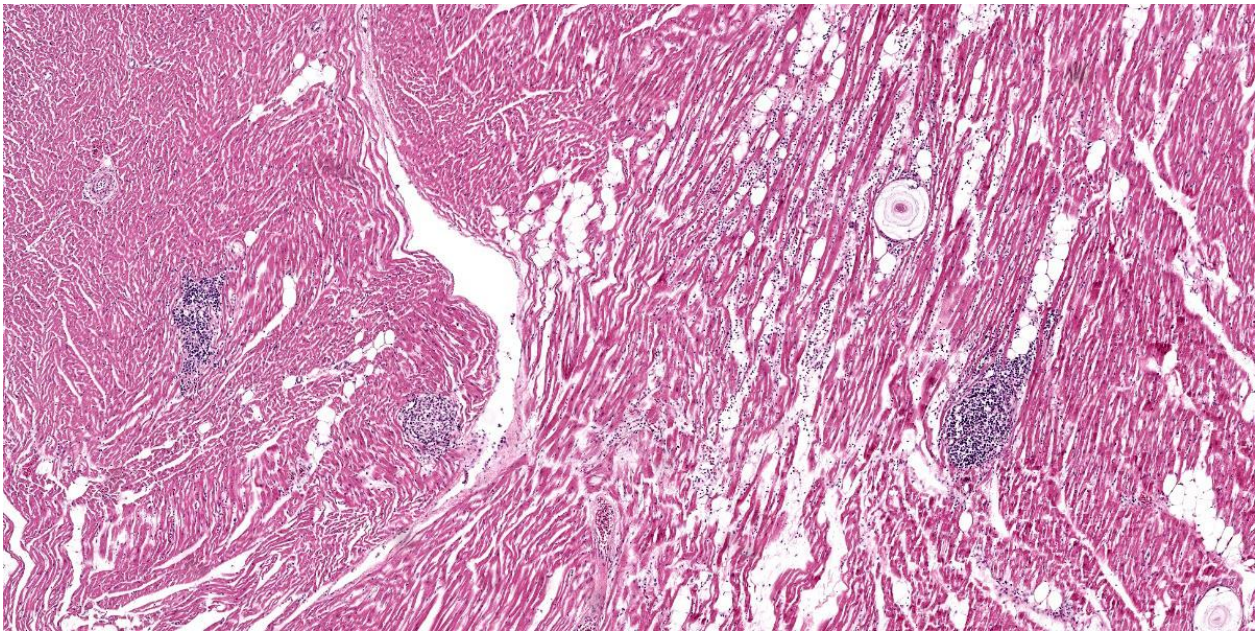

Figure 1-2. Heart, dog. There are multiple foci of hypercellularity within the myocardium as well as a single "onion-skin" cyst of *Hepatozoon americanum*. (HE, 47X)

in diameter merozoites. These meronts frequently enmesh neighboring fibrocytes and are often surrounded by rings of leukocytes. Lymphocytes and plasma cells infiltrate between the adjacent

Contributor's Morphologic Diagnosis:
Whole Body (Spleen, Lymph nodes, Heart, Blood vessels, Skeletal muscle): Chronic, multifocal lymphoplasmacytic and histiocytic inflammation with intralesional encysted protozoa (consistent with *Hepatozoon* sp.)

Contributor's Comment:
The patient's reported progressive decline was considered multifactorial, likely owing to a combination of systemic hepatozoonosis and ruptured splenic hemangiosarcoma (not captured in the provided slide). The patient's hemoabdomen noted during the abdominal exploration surgery was subsequent to the ruptured splenic hemangiosarcoma as well as several ruptured hematomas along the hepatic parenchyma. These hepatic hematomas are presumed sequela to robust, hepatozoonosis-mediated hepatitis and hepatic necrosis with pronounced hepatic parenchymal loss.

Hepatozoon is a protozoan classified among the apicomplexan phylum, primarily affecting the canine species (intermediate host) in the southeastern and central United States with several species variants noted in Latin America, Africa, Asia, and Europe.[1-9] Two primary species reported to infect domestic canids include *Hepatozoon americanum* and *Hepatozoon canis* while in felids *Hepatozoon felis*, *Hepatozoon silvestris*, and *Hepatozoon canis* are the primary species.[1] Hepatozoonosis has additionally been documented in rodent, racoon, kiwis, opossums, and wild canids.[1] Transmission of *Hepatozoon* spp. is via ingestion of arthropod vectors (direct host) with several tick species (e.g. *Rhipicephalus, Amblyomma*, and *Ixodes* spp.) being well-documented.[1-9] These ticks harbor the oocyst stage and upon ingestion release sporozoites into the host blood stream with subsequent deposition and infiltration in the spleen, bone marrow, lymph nodes, and ma

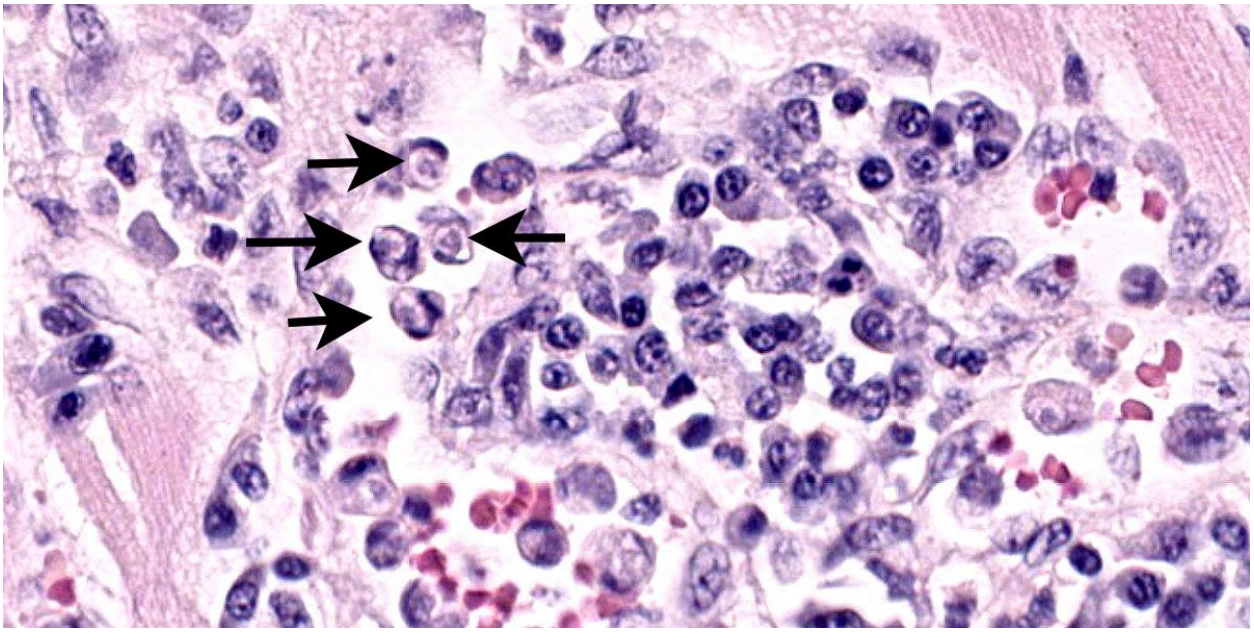

Figure 1-3. Heart, dog. Foci of hypercellularity contain moderate numbers of lymphocyte, plasma cells, and histiocytes. Within the cytoplasm of several histiocytes, there is a single protozoal meront (arrows). (HE, 1024X)

jor viscera where they encyst and form meronts.[1-9] Merozoites begin to safely develop in these seemingly innocuous meronts and are released in mass upon complete maturation, thus inciting an aggressive (typically pyogranulomatous) host response.[3] The true genius of this organism shines through, as these young merozoites safely hijack the recruited macrophages and neutrophils, escape the granuloma, and begin to undergo their final maturation into gamonts. Fully developed gamonts once again exit the leukocyte and reenter host blood circulation to be once again consumed by another tick during a hematogenous meal and perpetuate its life cycle.[1-9]

The typical gross presentation is primarily restricted to skeletal and cardiac muscle manifesting as a nonspecific myositis and muscle wasting (as evidenced in this case) but can additionally involve major organs such as bone marrow, liver, lungs, and the kidneys. A striking but less frequently observed gross finding is periosteal proliferation of the long bones, which was not observed in this case.[2,5]

On microscopic examination, the diagnostic lesion is multiple encysted approximately 250µm in diameter meronts[2] containing merozoites at varying stages of development enmeshed in a multilayered mucopolysaccharide and fibroblast-rich capsule (onion-skin cyst).[3] In systemic infection, leukocytes (macrophage, neutrophil, and monocytes) can be observed with intracytoplasmic merozoites approximately 4-6µm in diameter often displacing the host nuclei.[1,3,4] On cytologic smear intracytoplasmic gamonts can be rarely observed in monocytes.[1]

This case is an important reminder of the limitations of PCR as a confirmatory or definitive diagnostic tool. Despite both historic Hepatozoonosis and impressive multisystemic disease, the antemortem real time PCR was negative at the time of submission. A false negative PCR indicates that Hepatozoon DNA was not detected in the specific sample submission or may suggest that the numbers of detectable organisms is below the limit of

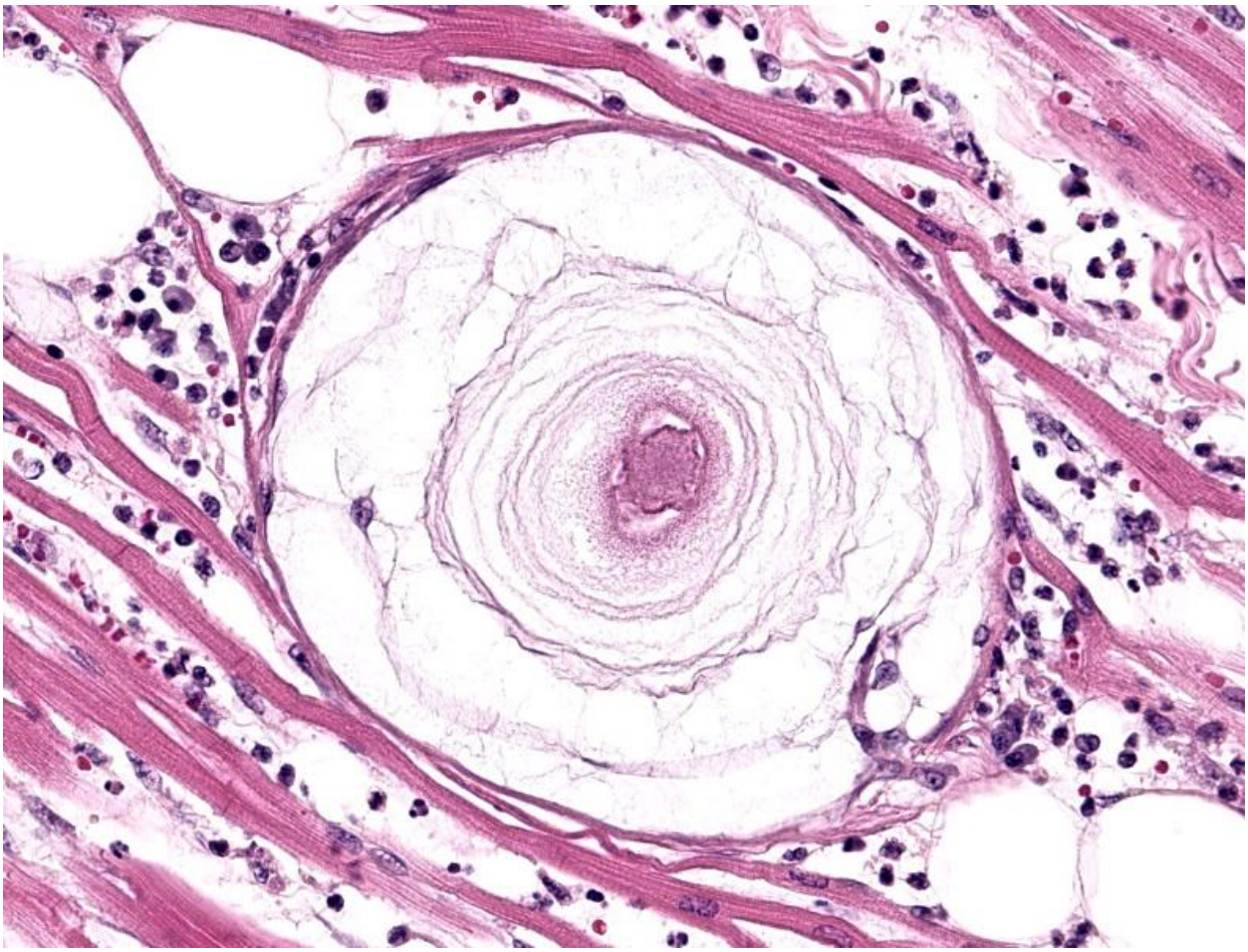

Figure 1-4. Heart, dog. High magnification of characteristic "onion-skin" cyst with multiple lamellations of mucopolysaccharide with a central host cell nucleus. There are low numbers of lymphocytes, histiocytes, and plasma cells within the interstitium. (HE, 381X)

detection (i.e. decreased numbers of organisms following treatment, a chronic carrier state, or the occurrence of new strain variations). When possible, PCR should be utilized in conjunction with corroborating tests such as cytologic blood smears, fine needle aspirates of hematopoietic and lymphoid tissue, and indirect fluorescent antibody (IFA). Muscle biopsy and/or necropsy remain the gold standard for definitive diagnosis.[1]

Contributing Institution:
North Carolina State University College of Veterinary Medicine

https://cvm.ncsu.edu/php/

JPC Diagnosis:

1. Heart: Myocarditis, histiocytic and lymphoplasmacytic, multifocal, moderate with intracellular apicomplexan meronts.
2. Lymph node: Sinus histiocytosis, diffuse, mild with apicomplexan meronts.

JPC Comment:
This week's moderator was Dr. Tony Alves, former JPC Veterinary Pathology Director and current pathologist at the National Institute of Allergy and Infectious Diseases (NIH/NIAID). Given his role within the NIAID Infectious Disease Pathogenesis Section, the theme for this conference was hardly surprising for participants.

This first case was relatively straightforward for residents (who, as WSC tradition provides, were not provided case history). From subgross magnification,, the large meronts (apicomplexan cysts) and inflammatory foci are scattered among the multiple tissues provided, underscoring that these changes contributed to the decline of this animal. The size and lamellation of these meronts along with the concurrent inflammation and hypertrophic osteopathy are highly suggestive of *H. americanum* over *H. canis*.[1,2] In the latter case, meronts are smaller and rarely incite significant inflammation. Conference participants discussed the cell of origin infected by sporozoites on the slide and concluded that cardiac myocytes and histiocytes (particularly within the lymph node) were most likely in this case. Stains for PAS, PAS-Alcian Blue, and Giemsa all reliably stained the cyst wall, mucinous material, and/or merozoites for this case.

Dr. Alves noted several ancillary features in this case, which might be overlooked at first glance, that hint at a wider clinical story.. Within the heart, there is a solitary arteriole with amorphous eosinophilic material that expands the tunica media and compresses the lumen, consistent with either hyalinosis (an aging change) or amyloidosis given the concurrent inflammation in section. Additionally, there were few megakaryocytes present within the lymph node, suggestive of extramedullary hematopoiesis in response to anemia from hemoabdomen.

Conference participants discussed several ruleouts for tissue cysts. *Trypanosoma cruzi* and *Sarcocystis* spp. both form discrete tissue cysts. In contrast to *Hepatozoon* (particularly *H. americanum*) these cysts lack lamellation (*Sarcocystis and Trypanosoma*); size and shape is variable and may appear similar. Distribution to cardiac myocytes is common among all 3 species, though distribution to other tissues (e.g. lymph node) may be a distinguishing diagnostic feature absent IHC. Additionally, smaller tissue cysts to consider are *Toxoplasma* and *Neospora*. We recently *covered T. cruzi* in WSC 2024-2025 (Conference 3, Case 3). For another example of *H. americanum* from the WSC archives, see Case 2, Conference 18, 2015-2016.

References:

1. Baneth G, Allen K. Hepatozoonosis of Dogs and Cats. *Veterinary Clinics of North America*. 2022; 52(6):1341-1358.
2. Craig LE, Dittmer KE, Thompson KG. Bones and Joints. In: Maxie MG, ed. *Jubb, Kennedy and Palmer's Pathology of Domestic Animals*. Vol 1. 6th ed. Louis, MO: Elsevier; 2016: 94
3. Cummings CA, Panciera RJ, Kocan KM, Mathew JS, Ewing SA. Characterization of stages of Hepatozoon americanum and parasitized canine host cells. *Vet Pathol*. 2005;42(6):788-796.
4. Ewing SA, Panciera RJ. American canine hepatozoonosis. *Clinical Microbiology Reviews*. 2003; 16(4):688-97.
5. Panciera RJ, Mathew JS, Ewing SA, Cummings CA, Drost WT, Kocan AA. Skeletal Lesions of Canine Hepatozoonosis Caused by Hepatozoon americanum. *Veterinary Pathology*. 2000;37(3):225-230.
6. Parkins ND, Stokes JV, Gavron NA, Frankovich AN, Varela-Stokes, JV. Scarcity of Hepatozoon americanum in Gulf Coast tick vectors and potential for cultivating the protozoan. *Vet Parasitol*. 2020
7. Potter TM, Macintire DK. Hepatozoon americanum: an emerging disease in the south-central/southeastern United States. *Journal of Veterinary Emergency and Critical Care*. 2010; 20:70-76.
8. Valli VEO, Kiupel M, Bienzle D. Hematopoietic system. In: Maxie MG, ed. *Jubb, Kennedy, and Palmer's Pathology of Domestic Animals*. 6th ed. Vol 3. St.

Louis, MO: Elsevier; 2016:109-111.
9. Van Vleet JF, Valentine BA. Muscle and tendons. Hepatozoonosis. In Maxie MG, ed. *Jubb, Kennedy and Palmer's Pathology of Domestic Animals*. 6th ed. Vol 1. Elsevier Saunders; 2007: 240.

CASE II:

Signalment:
1.2-year-old, intact female, German shepherd canine.

History:
This dog was adopted recently from a rescue in Texas. She had a history of a persistent, productive cough that worsened over time. She presented to the UWVC Small Animal Internal Medicine Service for a possible megaesophagus work up. The owner also reported occasional hemoptysis at home and hyporexia. Computed Tomography (CT) revealed a cranial mediastinal mass. Over time, her symptoms worsened and she returned to the hospital due to increased respiratory effort. Thoracic radiographs revealed aspiration pneumonia, atelectasis and confirmed the previously diagnosed static cranial mediastinal mass, which was associated with a segmental megaesophagus and compression of the trachea and primary bronchi. An endotracheal wash performed and showed neutrophilic and eosinophilic inflammation with no bacterial growth. A fine needle aspirate was taken from the mediastinal mass and showed evidence of neutrophilic and eosinophilic inflammation with rare linear material that was suggestive of fungal hyphae. Heartworm and blastomycosis antigen testing and coccidiosis titers were all negative. This dog continued to decline and euthanasia was elected.

Gross Pathology:
A locally extensive portion of the esophagus, beginning from midway down the neck and extending to the diaphragm, is markedly thickened, nodular and firm. In this region, the wall of the esophagus is massively expanded, up to 1.5 cm, by abundant firm, tan, fibrous material interspersed with well demarcated pockets of friable reddened tissue with a green tinge (see Figure 1). This change extends beyond the wall of the esophagus to incorporate the adjacent enlarged cranial mediastinal and tracheobronchial lymph nodes, the trachea and the adjacent dorsal portions of the lungs (see Figure 2). The luminal diameter of the trachea is significantly reduced. Within the most severely affected areas, the trachea is almost completely effaced by this process and the tracheal lumen has a significantly distorted and reduced diameter. The mucosal surface of the esophagus is friable and multifocally covered by plaques of stringy friable material (fibrin). Multifocally, there are variably sized areas where the mucosal epithelium is absent (ulcer), including a locally extensive 2.5 x 2 cm region.

Figure 2-1. Esophagus, dog. Gross photograph of esophagus with epiglottis (white arrow). The esophagus is markedly thickened and firm and there are locally extensive regions of ulceration. (*Photo courtesy of:* University of Wisconsin School of Veterinary Medicine, Department of Pathobiological Sciences, https://www.vetmed.wisc.edu/departments/pathobiological-sciences/)

Laboratory Results:
A panfungal PCR with sequencing identified *Cladosporium* species.

Figure 2-2. Esophagus, dog. Gross photograph of esophagus with trachea (white arrow). The process occurring in the esophagus extends to completely encapsulate the trachea, significantly reducing the luminal diameter. (*Photo courtesy of:* University of Wisconsin School of Veterinary Medicine, Department of Pathobiological Sciences, https://www.vetmed.wisc.edu/departments/pathobiological-sciences/)

Microscopic Description:
Esophagus (per submitter): Severely expanding and effacing up to 90% of the submucosa are multifocal to coalescing pyogranulomas composed of a central region of amorphous eosinophilic material (necrosis) admixed with cellular and karyorrhectic debris, surrounded by a ring of intact and fragmented neutrophils, epithelioid macrophages and fewer multinucleated giant cells, and further surrounded by a thin rim of lymphocytes and plasma cells (see Figure 3). Within the central areas of necrosis and rarely within the cytoplasm of multinucleated macrophages are many poorly staining, 7 to 10 µm hyphal organisms with thin non-parallel walls, irregular branching, infrequent septation, and rare bulbous dilations up to 15 µm in diameter (see Figure 4). The hyphal organisms are prominent and exhibit strong dark black staining with a Grocott's Methenamine Silver (GMS) stain (see figure 6) and lack melanin (confirmed with a Fontana Masson's stain). Intersecting between granulomas and further expanding the submucosa are abundant multifocal to coalescing regions of fibrosis and to a much lesser extent hemorrhage, with a few associated macrophages laden with variably sized, golden-brown, intracytoplasmic pigment (hemosiderin). A few granulomas are centered on or extend to adjacent small to medium caliber blood vessels. Affected vessels are often lined by a few necrotic endothelial cells that are occasionally sloughed into the lumen with the tunica intima partially replaced by variable amounts of fibrin and infiltrated by minimal numbers of similar inflammatory cells (fibrinoid necrosis; vasculitis). Within the adventitia, medium to large caliber vessels are frequently surrounded by moderate to large amounts of perivascular fibrosis.

Contributor's Morphologic Diagnosis:
Esophagus: Severe chronic multifocal to coalescing and pyogranulomatous esophagitis with intralesional hyphal organisms

Contributor's Comment:

Given the microscopic features, gross lesions, and morphology of the hyphal organisms, an infection with *Pythium* sp. or *Lagenidium* sp. is considered the cause of disease in this animal despite the results of PCR and sequencing, which identified *Cladosporium* sp. from the formalin fixed tissue. In particular, the microscopic features of this fungus are not consistent with this result and we do not believe that *Cladosporium* species are the source of infection in this animal.

Morphological features consistent with this case and *Pythium/Lagenidium* spp. include non-parallel walls, infrequent septa and irregular branching.[3,5] A few bulbous dilatations within hyphal structures were noted in examined sections which is more consistent with *Cladosporium* sp. as well as the irregular branching and infrequent septa; however, other morphological characteristics of *Cladosporium* sp. include thicker non-parallel walls and apparent pigmentation, which

were not evident.[11] In addition, *Cladosporium* sp. frequently exhibits pigmentation, seen either in routine H&E staining or with the aid of a Fontana Masson's stain, which was not seen in this case. Based on the morphological characteristics, we suspect the hyphal structures are likely *Pythium* sp. or *Lagenidium* sp. regardless of PCR results.

Despite the few morphological similarities shared between *Pythium/Lagenidium* spp. and true fungi, *Pythium* and *Lagenidium* spp. are oomycetes (water molds), not fungal organisms. Key differences between oomycetes and fungal organisms include the lack of chitin within oomycete cell walls and the absence of ergosterol within oomycete cytoplasmic membranes. Additionally, oomycetes undergo sexual reproduction via oogamy.[3]

Oomycetes are typically found in warm stagnant water with *Pythium* sp. having been reported in multiple continents, including North and South America, southern parts of Asia, and Australia. Conversely, *Lagenidium* sp. has only been reported in southern regions of North America.[2-4] Infection with oomycetes are rare in Wisconsin though this dog's recent travel history from Texas was suspect. In dogs, *Pythium insidiosum* and *Lagenidium giganteum* are the most common etiologic agents of pythiosis and lagenidiosis, respectively.[4,13] The life cycle of *Pythium insidiosum* first involves colonization of plants by *Pythium insidiosum* hyphae which then develop into zooporangia, eventually forming zoopores which mechanically break through the vesicle wall and are released into the stagnant water in which the plant resides.[4,8] Zoopores are considered the infective stage and target damaged skin via direct contact or gastrointestinal mucosa if ingested through chemotaxis and its biflagellate motility.[4,8] The zoospores encyst and form hyphal structures similar to the first life stage previously described. Exoantigens cause a T-helper 2 (Th2)-mediated immune response resulting in recruitment of eosinophils which then degranulate resulting in tissue damage.[1,3,4,5,8] With time, the tissue damage will induce more pyogranulomatous inflammation as seen in this case.[3-5] Little is known about the life cycle and pathogenesis of *Lagenidium* sp., though it is likely similar to *Pythium* sp..[4] Some studies have shown that the life cycle and pathogenesis of *Lagenidium* sp. may involve mosquitoes.[13]

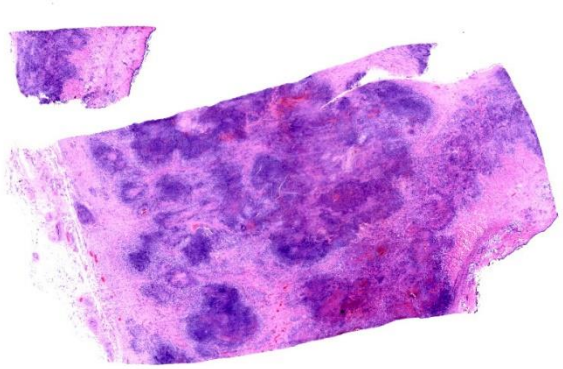

Figure 2-3. Esophagus, dog. Two sections of the esophagus are submitted for examination. The wall is markedly expanded by coalescing areas of inflammation and necrosis. (HE, 4X)

Pythium/Lagenidium sp. have been reported in dogs, cats and humans.[4,11] In addition, *Pythium* sp. have been well-documented in horses and sporadically diagnosed in cattle, sheep, a Californian nestling white-faced ibis, bears, camels, and large cats (i.e. tigers and jaguars).[1,3] In dogs and cats, *Pythium* sp. can cause cutaneous and more frequently, gastrointestinal tract lesions. Infections affecting horses and other documented species are typically limited to the cutis and subcutis.[3,8] In contrast to *Pythium* sp., there are currently no reports documenting gastrointestinal lesions caused by *Lagenidium* sp.. However, *Lagenidium* sp. can cause cutaneous lesions and affect other tissues such as great vessels, sublumbar and inguinal lymph nodes, lung, pulmonary hilus, and cranial mediastinum.[4]

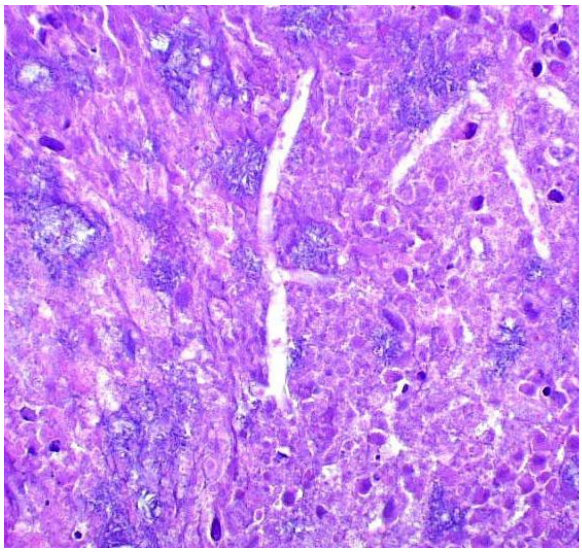

Figure 2-4. Esophagus, dog. Within areas of necrosis, poorly staining hyphal structures exhibit irregular branching and frequently non-parallel walls (HE, 400X) (*Photo courtesy of:* University of Wisconsin School of Veterinary Medicine, Department of Pathobiological Sciences, https://www.vetmed.wisc.edu/departments/pathobiological-sciences/)

When possible, wide surgical excision and various antimicrobial agents and immunotherapeutic drugs have exhibited successful treatment in various species infected with *Pythium*/*Lagenidium* spp.[3,4] Early detection of disease increases the probability of successful treatment; however, in many cases, there fails to be early detection and fatality occurs regularly.[3,4] In addition, local recurrence is common and may occur at the surgical excision site or in a regional lymph node.[4]

Contributing Institution:
University of Wisconsin

School of Veterinary Medicine

Department of Pathobiological Sciences

2015 Linden Drive Madison, WI 53706

https://www.vetmed.wisc.edu/departments/pathobiological-sciences/

JPC Diagnosis:

Esophagus: Esophagitis, necrotizing and pyogranulomatous, chronic-active, multifocal to coalescing, severe, with numerous intrahistiocytic and extracellular hyphae.

JPC Comment:

This second case featured a tricky tissue identification for participants given the marked inflammation, and in this case, features of a somewhat "hidden" organiam were more readily recognized. The nature of the distal esophagus transitioning from a stratified squamous epithelium to columnar epithelium gave some members pause, though this is actually a normal histologic feature[6] and not transitional epithelium (i.e. the urinary bladder).

Dr. Alves emphasized the chronic-active nature of this case. In section, there was a spectrum of inflammatory changes including coalescing areas of necrosis and discrete granulomas as well as maturing granulation tissue and fibrosis. These changes were largely within the serosal tunia, but did expand into the muscularis and submucosa, resulting in degeneration and necrosis of skeletal muscle and loss of esophageal glands in this particular section. GMS and PAS both outlined organisms well in section.

Conference participants then discussed the morphologic findings of the fungal hyphae in this case. We agree with the contributor that the major histologic features of the hyphae are consistent with *Pythium/Lagenidium* sp. and not with *Cladosporium*. Several conference participants raised the possibility of *Conidiobolus/Basidiobolus* sp. as another differential diagnosis. Associated hyphae are typically larger than oomycetes[8] (approximately 5-12 µm and 6-20µm respectively) though have the same irregular branching and rare septations present.[8] Though rare, gastrointestinal basidiobolomyocsis has been rec

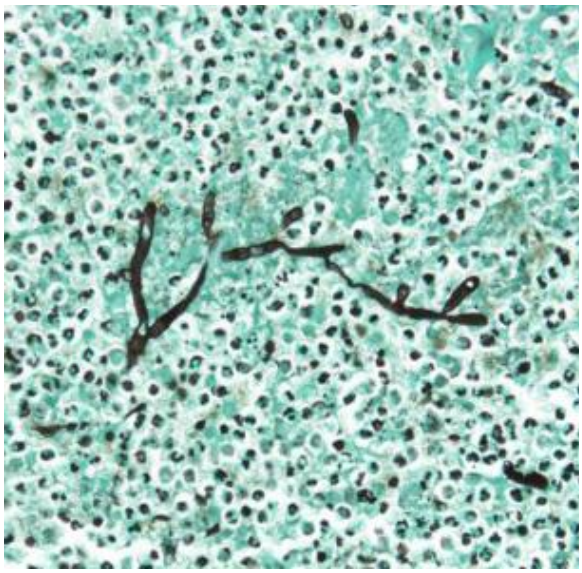

Figure 2-5. Esophagus, dog. Fungal hyphae exhibit strong positivity that highlight the non-parallel walls, infrequent septations and irregular branching (GMS, 200X). (*Photo courtesy of:* University of Wisconsin School of Veterinary Medicine, Department of Pathobiological Sciences, https://www.vetmed.wisc.edu/departments/pathobiological-sciences/)

orded both in the human[11] and veterinary[7] literature. In contrast, *Conidiobolus* is typically associated with respiratory disease in mammals.[7] In histologic section, *Basidiobolus* would be expected to elicit a strong Th2-response similar to what the contributor describes for this case. However, the chronicity of the lesion may also influence whether it is primarily eosinophilic. In this case, the degree of fibrosis and formed granulomas overshadowed eosinophils.

References:

1. Chitasombat MN, Larbcharoensub N, Chindamporn A, Krajaejun T. Clinicopathological features and outcomes of pythiosis. *Int J Infect Dis*. 2018;71:33-41.
2. Chitasombat MN, Jongkhajornpong P, Lekhanont K, Krajaejun T. Recent update in diagnosis and treatment of human pythiosis. *Peer J*. 2020 Feb 20;8:e8555.
3. Gaastra W, Lipman LJ, De Cock AW, Exel TK, Pegge RB, Scheurwater J, Vilela R, Mendoza L. Pythium insidiosum: an overview. *Vet Microbiol*. 2010;146(1-2):1-16.
4. Grooters AM, Pythiosis, lagenidiosis, and zygomycosis in small animals. *Vet Clin Small Anim*. 2003;33:695-720.
5. Grooters AM, Hodgin EC, Bauer RW, Detrisac CJ, Znajda NR, Thomas RC. Clinicopathologic Findings Associated with *Lagenidium* sp. Infection in 6 Dogs: Initial Description of an Emerging Oomycosis. *Vet Intern Med*. 2003;17:637-646.
6. Mann CV, Shorter RG. Structure of the canine esophagus and its sphincters. *Journal of Surgical Research*. 1964 April; 4(4):160-163.
7. Marclay M, Langohr IM, Gaschen FP, et al. Colorectal basidiobolomycosis in a dog. *J Vet Intern Med*. 2020; 34: 2091–2095.
8. Mendoza L, Hernandez F, Ajello L. Life cycle of the human and animal oomycete pathogen Pythium insidiosum. *J Clin Microbiol*. 1993 Nov;31(11):2967-73.
9. Rodrigues Hoffmann A, Ramos MG, Walker RT, Stranahan LW. Hyphae, pseudohyphae, yeasts, spherules, spores, and more: A review on the morphology and pathology of fungal and oomycete infections in the skin of domestic animals. Veterinary Pathology. 2023;60(6):812-828.
10. Romero A, Garcia J, Balestie S, Malfatto F, Vicentino A, Sallis ES, Schild AL, Dutra F. Equine pythiosis in the estern welands of Uruguay. *Pesq Vet Bras*. 2019;39(7):469-475.
11. Velázquez-Jiménez Y, Hernández-Castro R, Romero-Romero L, Salas-Garrido CG, Martínez-Chavarría LC. Feline Phaeohyphomycotic Cerebellitis Caused by *Cladosporium cladosporioides*-complex: Case Report and Review of Literature. *J*

Comp Path. 2019;170:78-85.
12. Vikram HR, Smilack JD, Leighton JA, Crowell MD, De Petris G. Emergence of gastrointestinal basidiobolomycosis in the United States, with a review of worldwide cases. Clin Infect Dis. 2012 Jun;54(12):1685-91.
13. Vilela R, Taylor JW, Walker ED, Mendoza L. *Lagenidium giganteum* Pathogenicity in Mammals. *Emerg Infect Dis*. 2015;21(2):290-297.

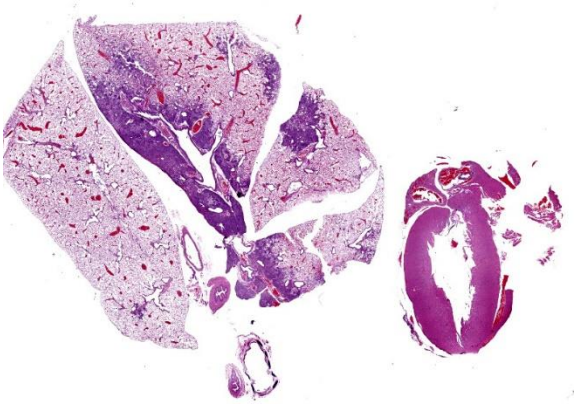

Figure 3-1. Lung, mouse. Approximately 25% of the lung is consolidated by inflammation. A section of heat is submitted as well. (HE, 5X)

CASE III:

Signalment:
6-month-old, female intact, NOD.Cg-*Prkdc*^{scid} *Il2rg*^{tm1Wjl}/SzJ (NSG) mouse (*Mus musculus*). This mouse strain has the *Prkdc* and interleukin 2 receptor *(Il2rg)* mutations, which results in phenotype that lacks numerous immune components including T cells, B cells, natural killer cells, and have deficient signaling for 6 cytokines (IL-2, IL-4, IL-7, IL-9, IL-15, and IL-21). [8]

History:
The mouse was part of experiment in which a NSG mouse shedding *Chlamydia muridarum* was cohoused with four naïve NSG mice. The mouse was lethargic, lost weight, and had a hunched posture and an increased respiratory effort.

Gross Pathology:

The right cranial, middle, and accessory pulmonary lobes were diffusely pale pink to white and atelectatic.

Laboratory Results:
CBC with manual differential showed leukocytosis characterized by mild to moderate neutrophilia and mild monocytosis.

Aerobic and anaerobic cultures of the lung were both negative.

IHC for Chlamydia MOPM-1 showed strong and specific detection of Chlamydia antigen in bronchiolar and alveolar epithelial cells and areas of inflammation.

qPCR for Cm 23S rRNA: Positive in lung

Microscopic Description:
Lung (right and left pulmonary lobes): Affecting approximately 40-45% of the airways in the right pulmonary lobes, there are multifocal to coalescing dense areas of leukocytic cell infiltration mixed with proteinaceous exudate and necrotic cellular debris. Multifocally, alveolar spaces are collapsed and filled with numerous neutrophils and degenerate neutrophils admixed with foamy macrophages, edema, fibrin, karyorrhectic debris and fewer linear clear acicular clefts (cholesterol clefts), and hemorrhage. Alveolar septa are lined by elongated epithelial cells and attenuated necrotic alveolar wall admixed with alveolar macrophages and vacuolated cells containing numerous round basophilic organisms measuring approximately 0.5 to 1.0µm in diameter (Chlamydia elementary and reticular bodies). The adjacent bronchioles are

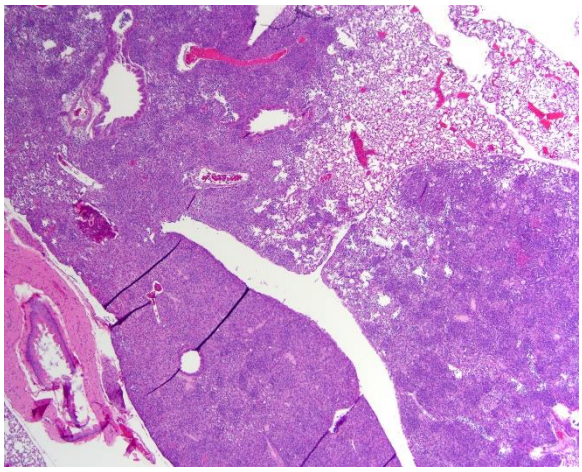

Figure 3-2. Lung, mouse. Areas of pneumonia affect both airways and interstitium (HE, 100X). (*Photo courtesy of*: Laboratory of Comparative Pathology; Memorial Sloan Kettering Cancer Center, Weill Cornell Medicine, Hospital for Special Surgery, and The Rockefeller University https://www.mskcc.org/research/ski/core-facilities/comparative-medicine-pathology-0)

filled by moderate amounts of proteinaceous fluid admixed with neutrophils, karyorrhectic debris, pyknotic cells, and fibrin. The bronchiolar epithelium is segmentally effaced by areas of necrosis and proteinaceous exudate and often contains degenerate bronchiolar epithelial cells with intracytoplasmic vacuoles filled with Chlamydia elementary and reticular bodies (Chlamydia inclusions). Blood vessels are congested and lined by plump endothelial cells with tethered neutrophils. The left pulmonary lobe is multifocally affected by small clusters of neutrophils and foamy macrophages admixed with edema and hemorrhage, predominantly affecting alveoli. Chlamydia inclusions are occasionally noted in the left pulmonary lobe and often observed in the adjacent extrapulmonary bronchi.

Contributor's Morphologic Diagnosis:

Lung: Bronchointerstitial pneumonia histiocytic and neutrophilic, chronic, multifocal to coalescing, moderate to severe, with edema, fibrin, necrotic debris, alveolar histiocytosis, numerous intracytoplasmic Chlamydia inclusions.

Bronchi, tracheal bifurcation: Multifocal intraepithelial Chlamydia inclusions.

Contributor's Comment:

Chlamydia muridarum (Cm) was recently reported as prevalent in research mouse colonies, affecting between 14% and 33% of non-commercial institutions.[5] Cm infections in mice were initially described in the 1930s and 1940s when this bacterium was discovered by accident while inoculating mice with various viruses by transferring lung homogenates.[4,7] In 2021, our group detected Cm inclusions associated with peribronchiolar lymphocytic and plasmocytic aggregates in immunocompetent GEM mouse strains.[4] The case presented in this submission was part of an investigation to evaluate the impact of Cm infection in severely immunocompromised mice (NSG) after cohousing with Cm shedding, naturally infected immunocompetent mice and/or their soiled bedding for 4 weeks.[9] All 19 NSG mice developed pulmonary lesions consistent with bronchointerstitial pneumonia and/or bronchiolitis with numerous intraepithelial Chlamydia inclusions bronchioles and alveoli.[9] Since 2021, our laboratory has reported that Cm infections can be associated with spontaneous clinical disease and pulmonary and/or urogenital pathology in NSG mice and in two genetically engineered mouse (GEM) strains, *Il12rb2* knockout and *STAT1* knockout mice, with impaired interferon-γ signaling and Th1 $CD4^+$ T cell responses.[4,9] As a result of these investigations, testing for Cm has been added to routine health surveillance testing panels in immunocompromised mouse colonies in our institution and commercial breeding colonies in other institutions in the U.S.

Chlamydiae are gram-negative obligate intracellular bacteria with an extensive host range at the genus level, but high host specificity at the species level.[3,7] Cm is the only natural chlamydial pathogen of mice and has been classically used to model the sexually transmitted *Chlamydia trachomatis* infection of humans.[3] Cm exhibits a biphasic life cycle involving a nonreplicating and infectious 'elementary body' and a replicating and noninfectious 'reticulate body.[3,7] Elementary bodies enter the host mucosal epithelial cells and incorporate into a membrane-bound compartment, termed an inclusion body. These elementary bodies then differentiate into reticular bodies. The reticular bodies replicate within the inclusions before reverting into elementary bodies, as which they can then be released and infect nearby cells.[3,7] Natural transmission is via the fecal-oral route, and the gastrointestinal tract is often the natural site of colonization.[14,15] It is thought that pulmonary lesions and colonization can also be acquired through aspiration of inhalation of the organism.[5,9]

The diagnosis of Cm infection in laboratory mice can be confirmed by Cm MOMP-1 IHC and/or qPCR or ISH using Cm-specific primers and probes, respectively.[9] The bronchointerstitial pneumonia and numerous intralesional CI inclusions are characteristic microscopic changes seen in spontaneous and/or experimental Cm infections in NSG mice.[5,9] Cm inclusions are rarely noted in infected lungs from immunocompetent mice[5] and requires the use of ancillary tests for confirmation. Differential diagnoses in immunodeficient mice include bronchopneumonia associated with *Mycoplasma pulmonis* or *Filobacterium rodentium* ("CAR bacillus") and primary viral infections with Sendai virus or Pneumonia Virus of Mice (PVM), granulomatous interstitial pneumonia associated with *Pneumocystis murina*, and bronchopneumonia associated with other opportunistic bacterial agents.[1,10]

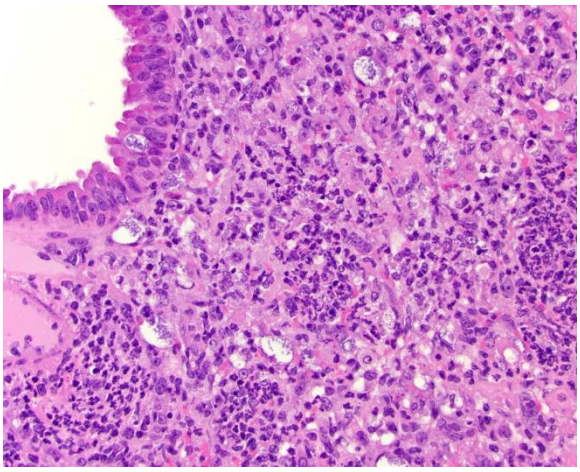

Figure 3-3. Lung, mouse. Peribronchiolar and alveolar spaces are infiltrated by numerous histiocytes and neutrophils admixed with fibrin, edema, karyorrhectic debris, and chlamydial inclusions. (HE, 400X). (*Photo courtesy of*: Laboratory of Comparative Pathology; Memorial Sloan Kettering Cancer Center, Weill Cornell Medicine, Hospital for Special Surgery, and The Rockefeller University https://www.mskcc.org/research/ski/core-facilities/comparative-medicine-pathology-0)

The bronchointerstitial pneumonia and bronchiolitis seen in Cm infected NSG mice shared similarities with pulmonary lesions seen in the acute phase of Cm infection in previous studies using BALB/c and *Tlr2* knockout mice following intranasal challenge.[2,12] Pulmonary lesions in *Il12rb2* knockout and *STAT1* knockout mice naturally infected with Cm are characterized by lymphoplasmacytic and histiocytic inflammation in bronchioles and peribronchiolar and perivascular spaces.[4] Cm inclusions are seen in bronchiolar epithelial cells, but these inclusions are less abundant than the inclusions seen from NSG-infected lungs.[4,9] The severity of the pulmonary lesions seen in NSG mice is likely exacerbated by the absence of CD4+ T and NK cells in this mouse strain.[9] These immune cells are important producers of interferon-gamma (IFN-γ), which is an essential effector cytokine involved in the reso-

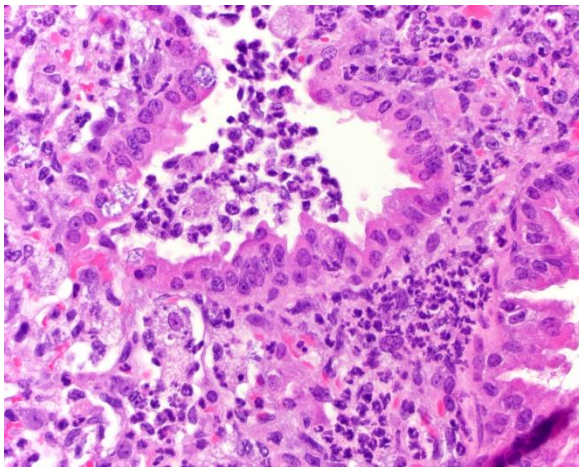

Figure 3-4. Lung, mouse. Histiocytic and neutrophilic bronchointerstitial pneumonia with intracytoplasmic chlamydial inclusions in bronchiolar epithelial cells (HE, 400X). (*Photo courtesy of*: Laboratory of Comparative Pathology; Memorial Sloan Kettering Cancer Center, Weill Cornell Medicine, Hospital for Special Surgery, and The Rockefeller University https://www.mskcc.org/research/ski/core-facilities/comparative-medicine-pathology-0)

lution of Cm infections in experimental models of murine chlamydiosis.[13]

Cm has shown a tropism for mucosal epithelial cells, which serves as a niche for intracellular survival, spread from cell to cell, and immune modulation.[3,6] Cm inclusions in NSG mice were observed in epithelial cells from the nasopharynx, nasal cavity, trachea, eustachian tube, bronchi/bronchioles, oviducts, uterus, and small and large intestines.[9] Among these tissues Cm extensively colonized the small and large intestinal epithelium, without eliciting histopathological changes in the mucosa.[9] Given that NSG mice do not have functional adaptive immune system,[8] Cm likely establishes long-lasting colonization in the intestines and persistent shedding of elementary bodies in feces.

Contributing Institution:
Laboratory of Comparative Pathology; Memorial Sloan Kettering Cancer Center, Weill Cornell Medicine, Hospital for Special Surgery, and The Rockefeller University

417 E. 68th St., ZRC-940

New York, NY 10065

https://www.mskcc.org/research/ski/core-facilities/comparative-medicine-pathology-0

JPC Diagnosis:
Lung: Pneumonia, bronchointerstitial, necrotizing, neutrophilic and histiocytic, subacute, multifocal to coalescing, marked, with numerous intraepithelial bacterial inclusions.

JPC Comment:
This case was recently published in *Veterinary Pathology*[11] and the submitted slides are just as good in person as they are "on paper". The contributor provides a great summary of the paper in their comments, but we invite readers to read it in its entirety in conjunction with this case.

The distribution of *Chlamydia* in this case is generous and the lack of IFN-γ in these mice allowed conference participants to appreciate inclusion bodies readily on H&E, though they stained strongly with PAS as well. Dr. Alves also performed ISH for Chlamydial RNA using a *C. trachomatis* probe which cross-reacted and labeled Cm-infected cells strongly. Additionally, alveolar macrophages (labeled with a F4/80 IHC marker) were assessed, though we did not see actual Chlamydial inclusion bodies within macrophages. Macrophage replication is a feature of *C. trachomatis* infection but was not observed here.

Conference participants also touched on several ancillary changes. In less affected regions of lung, there were numerous alveolar macrophages which was interpreted as alveo-

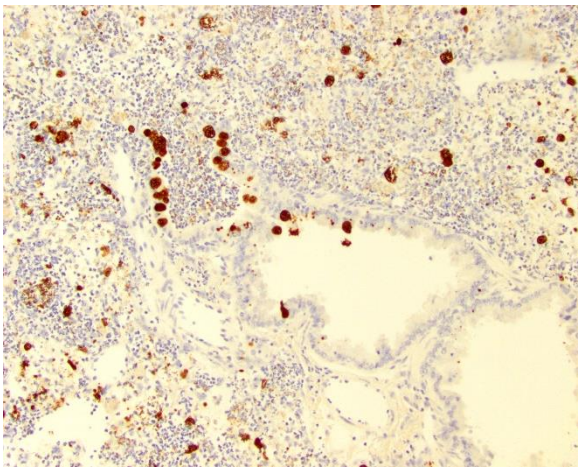

Figure 3-5. Lung, mouse. Chlamydia antigen in inclusions within bronchiolar epithelial cells and scattered in alveolar spaces. Immunohistochemistry (IHC) for Chlamydia major outer membrane protein antigen (MOMP-1). (HE, 400X). (*Photo courtesy of*: Laboratory of Comparative Pathology; Memorial Sloan Kettering Cancer Center, Weill Cornell Medicine, Hospital for Special Surgery, and The Rockefeller University https://www.mskcc.org/research/ski/core-facilities/comparative-medicine-pathology-0)

lar histiocytosis. This is a common background finding in knockout mice. Additionally, the large neutrophilic response in an animal lacking other tools to respond to a pathogen is not surprising – participants noted good examples of leukocyte margination in blood vessels. Though there was also a focus on inflammatory cells along the pericardium, these were interpreted as mast cells as they notably lacked PAS-staining or ISH probe labeling.

There were some indications of chronicity in section. Notably, there is a large, mature thrombus in a pulmonary vein. Additionally, the bronchiolar epithelium is markedly hyperplastic whereas in unaffected sections the epithelium is quite thin. The accumulation of cholesterol crystals is also suggestive of significant loss and accumulation of cell membrane components. In line with the contributor's purported infection timeline[11] we believe that the time course of these changes is at least subacute.

References:

1. Barthold SWP, D.H.; Griffey, S.M. Chapter 1: Mouse In: Barthold SWP, D.H.; Griffey, S.M., ed. *Pathology of Laboratory Rodents*. Fourth ed.: Wiley-Blackwell; 2016:14-81.
2. Beckett EL, Phipps S, Starkey MR, Horvat JC, Beagley KW, Foster PS, Hansbro PM. TLR2, but not TLR4, is required for effective host defence against Chlamydia respiratory tract infection in early life. *PLoS One*. 2012;7**:** e39460.
3. Elwell C, Mirrashidi K, Engel J. Chlamydia cell biology and pathogenesis. *Nat Rev Microbiol*. 2016;14**:** 385-400.
4. Mishkin N, Miranda IC, Carrasco SE, et al. *Chlamydia muridarum* Associated Pulmonary and Urogenital Disease and Pathology in a Colony of Enzootically Infected Il12rb2 Deficient and Stat1 Knockout Mice. *Comp Med*. 2024;74**:** 121-129.
5. Mishkin N, Ricart Arbona RJ, Carrasco SE, et al. Reemergence of the Murine Bacterial Pathogen *Chlamydia muridarum* in Research Mouse Colonies. *Comp Med*. 2022;72**:** 230-242.
6. Perry LL, Hughes S. Chlamydial colonization of multiple mucosae following infection by any mucosal route. *Infect Immun*. 1999;67**:** 3686-3689.
7. Rank RG. Chlamydial diseases. In: Fox JGD, M.T.; Quimby, F.W.; Barthold, S.W.; Newcomer, C.E.; Smith, A.I. , ed. *The mouse in biomedical research*. Burlington (MA): Elsevier; 2007:326-344.
8. Shultz LD, Lyons BL, Burzenski LM, et al. Human lymphoid and myeloid cell development in NOD/LtSz-scid IL2R gamma null mice engrafted with mobilized human hemopoietic stem cells. *J Immunol*. 2005;174**:** 6477-6489.

9. St Jean SC, Ricart Arbona RJ, Mishkin N, et al. *Chlamydia muridarum* infection causes bronchointerstitial pneumonia in NOD.Cg-Prkdc(scid)Il2rg(tm1Wjl)/SzJ (NSG) mice. *Vet Pathol*. 2024;61**:** 145-156.
10. Stair MI, Carrasco SE, Annamalai D, et al. The Epidemiology of Invasive, Multipleantibiotic-resistant *Klebsiella pneumoniae* Infection in a Breeding Colony of Immunocompromised NSG Mice. *Comp Med*. 2022;72**:** 220-229.
11. St Jean SC, Ricart Arbona RJ, Mishkin N, et al. Chlamydia muridarum infection causes bronchointerstitial pneumonia in NOD.Cg-PrkdcscidIl2rgtm1Wjl/SzJ (NSG) mice. *Veterinary Pathology*. 2024;61(1):145-156.
12. Virok DP, Raffai T, Kokai D, et al. Indoleamine 2,3-Dioxygenase Activity in *Chlamydia muridarum* and *Chlamydia pneumoniae* Infected Mouse Lung Tissues. *Front Cell Infect Microbiol*. 2019;9**:** 192.
13. Winner H, Friesenhahn A, Wang Y, Stanbury N, Wang J, He C, Zhong G. Regulation of chlamydial colonization by IFNgamma delivered via distinct cells. *Trends Microbiol*. 2023;31**:** 270-279.
14. Yeruva L, Spencer N, Bowlin AK, Wang Y, Rank RG. Chlamydial infection of the gastrointestinal tract: a reservoir for persistent infection. *Pathog Dis*. 2013;68**:** 88-95.
15. Zhong G. Chlamydia overcomes multiple gastrointestinal barriers to achieve long-lasting colonization. *Trends Microbiol*. 2021;29**:** 1004-1012.

CASE IV:

Signalment:
4-year-old, spayed female, Terrier mixed dog (*Canis familiaris*).

Figure 4-1. Myelencephalon, dog. A 0.7 x 0.4 x 0.3 cm, well-demarcated, expansile, white to tan and firm mass effaces the right-side of caudal cerebellar peduncle and the overlying cerebellar cortex. (*Photo courtesy of:* Midwestern University, College of Veterinary Medicine Diagnostic Pathology Center, Glendale, AZ 85308 https://clinics.midwestern.edu/animal-health-institute/diagnostic-pathology-center)

History:
This dog was presented for diarrhea, swollen paw, an increase respiratory, and a brain tumor. The dog had a long history of neurologic signs, facial tremors, ataxia, eye nystagmus, and myotonic like chomping of jaw. TPLO was done in 2023. CT was performed on 02/2024 and revealed a contrast enhancing mass at the right brainstem cerebral region. Valley Fever titers were negative. The patient was on Prednisone, Gabapentin, Diazepam, and Fluconazole. Patient showed continued deterioration including poor ability to open mouth. Euthanasia was elected.

Gross Pathology:
On thoracic examination, there is no pleural effusion. The left lung lobes are pink to dark red and mottle. The lung lobes are soft, aerated, and slightly wet. The distal 1/3 of the trachea and the mainstem bronchi contain a

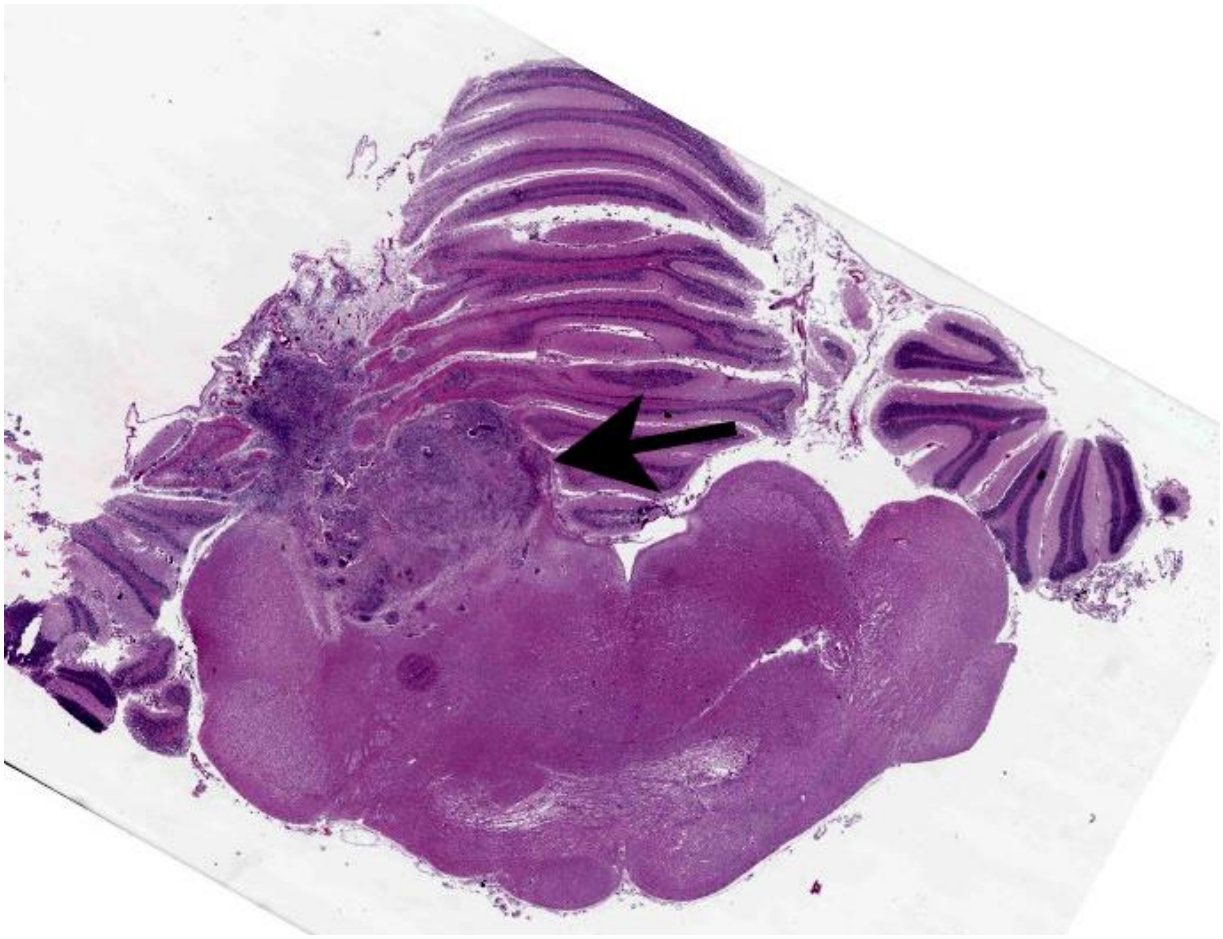

Figure 4-2. Myelencephalon, dog. Subgross magnification of the inflammatory nodule (arrow).

small amount of white froth. There is no pericardial effusion. The heart is unremarkable.

On abdominal examination, the liver is slightly swollen and congested, and weighs 1.36 kg (5% of the patient's body weight). The spleen, pancreas, and GI tract is unremarkable.

On examination of the head and bran, a 0.7 x 0.4 x 0.3 cm, well-demarcated, expansile, white to tan and firm mass effaces the right-side of caudal cerebellar peduncle and the overlying cerebellar cortex.

Clinical pathology:

Two cytospin preparations from the submitted CSF are reviewed. A 90-cell differential

reveals 31 (34%) non-degenerate neutrophils, 52 (58%) small mononuclear cells, 6 (7%) large mononuclear cells, and 1 (1%) eosinophils. The small mononuclear cells are consistent with small to intermediate sized lymphocytes and have occasional single prominent nucleoli. The lightly basophilic protein background contains many erythrocytes and few polychromatophils. No infectious agents or overt evidence of neoplasia is observed.

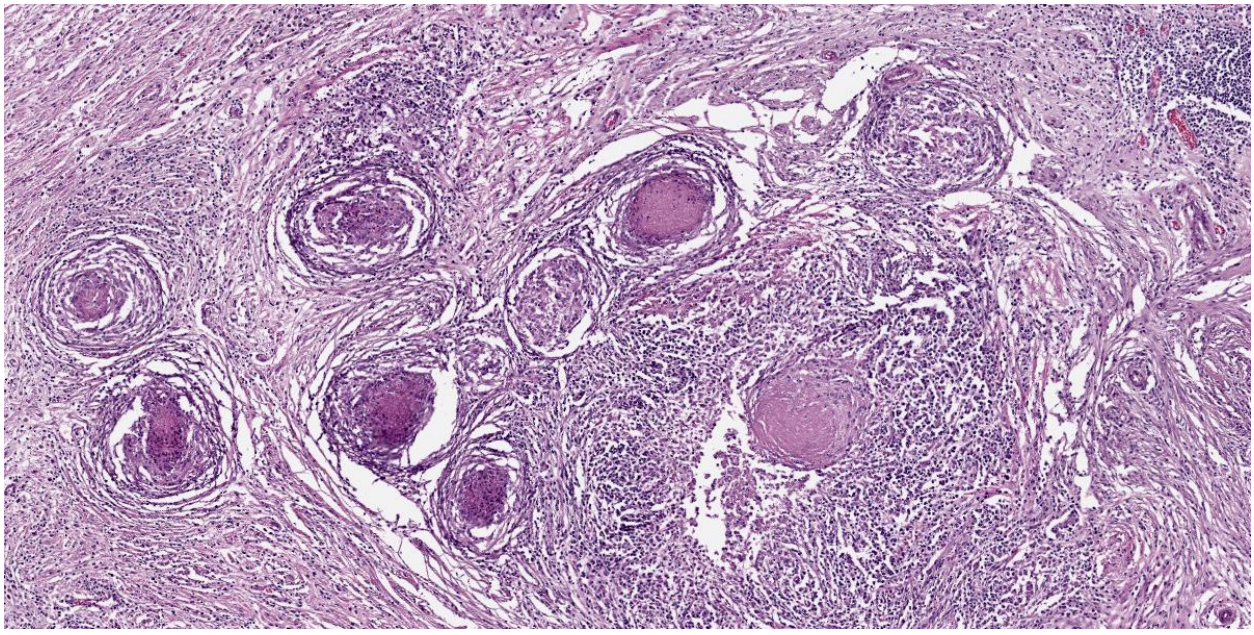

Figure 4-3. Myelencephalon, dog: Numerous granulomas are scattered throughout the inflammatory nodule and surrounding by abundttn fibrous connective tissue extending from the overlying meninges. (*Photo courtesy of:* Midwestern University, College of Veterinary Medicine Diagnostic Pathology Center, Glendale, AZ 85308

and effacing the right caudal cerebellar peduncle, right caudal vestibular nucleus and the overlying cerebellar cortical neuroparenchyma are multifocal to coalescing areas of extensive granulomatous inflammation, characterized by central necrosis and large numbers of epithelioid macrophages, which are surrounded by moderate numbers of lymphocytes, plasma cells, and thin band of fibrous connective tissue. The center of granulomas contain small to large amount of eosinophilic cellular debris, karyorrhectic and pyknotic debris, and degenerate leukocytes that occasionally surround a single, 20-30 um in diameter fungal spherule that has a smooth 4um thick, double contoured, hyaline wall containing multiple granular to flocculent, basophilic structures (endospores), consistent with *Coccidioides* spp. The affected and surrounding neuroparenchyma and meninges to moderate amount of clear space (edema).

Contributor's Morphologic Diagnosis:
Brain, cerebellum and brainstem: Meningoencephalitis, granulomatous, locally extensive, severe, chronic with intralesional fungal spherules (consistent with *Coccidioides* sp.)

Contributor's Comment:
Coccidiomycosis is commonly known as "Valley fever (VF)" and is endemic to human and animals in the southwestern USA (Arizona, California, New Mexico, Nevada) and

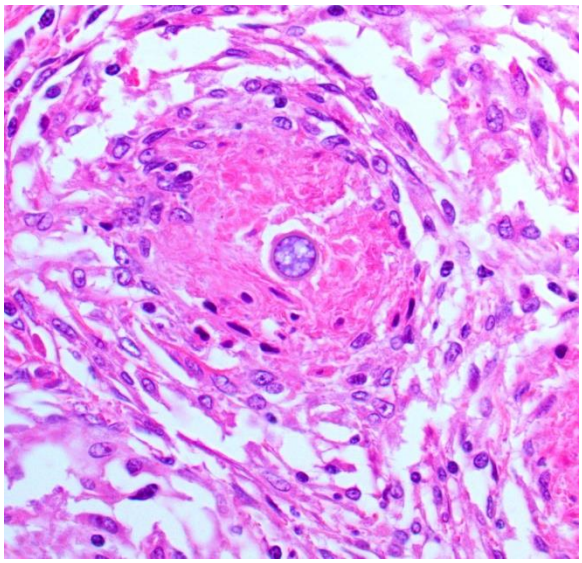

Figure 4-4. Myelencephalon, dog. Granulomas are centered on one or more endosporulating yeasts consistent with *Coccidioides* sp. (*Photo courtesy of:* Midwestern University, College of Veterinary Medicine Diagnostic Pathology Center, Glendale, AZ 85308 https://clinics.midwestern.edu/animal-health-institute/diagnostic-pathology-center)

northern Mexico.[3,7,12] Additional areas are Utah, Eastern Washington, Oregon, Central and South Americas.[14,15] Coccidiomycosis is caused by soil-dwelling, saprophytic, dimorphic fungi, *Coccidioides*. *Coccidioides* was originally described as one species *C. immitis*, but more recently, genetic analysis has defined two separated species with relative distinct geographical distribution. *C. immitis* is largely found in California and Eastern Washington State.[3,15] All cases in Arizona, Texas and Central and South America are *C. posadasii*. There have been no distinct differences in the phenotypical behavior of *C. immitis* and *C. posadasii*.[3,18] *Coccidioides* requires animal nutrients for growth and their distribution which is largely restricted to areas of human or animal habitation, such as small rodent burrows.[3,18] Animal carcasses may serve as a medium for the growth of *Coccidioides* in the soil.[6]

Coccidioides spp. grow in soil as a mycelium. Mycelia septate and produce spores known as arthroconidia which are fragile and become airborne with minimal soil disturbance. The infection is almost always through the inhalation of arthroconidia, rarely cutaneous inoculation, which transform into spherules that subsequently divide into endospores. With spherules lysis, the endospores are released and become spherules which result in exponential propagation in affected organs.[3,6,12]

In humans, 60% of infections are asymptomatic with the remaining 40% having respiratory illnesses. Approximately 1% of total infections are disseminated.[12] In dogs, infection most commonly results in self-limiting respiratory tract disease, but disease can be more severe in some dogs which can result in systemic disease.[14,15] Large breed, young adult dogs are most at risk. Risk factors are increased for outdoor dogs (roaming areas more than 1 acre) and walking in the desert.[4] Boxers, Pointers, Australian Shepherds, Beagles, and Scottish Terriers showed an increased risk of infections as well.[11]

Disseminated coccidioidomycosis includes cutaneous, osseous, cardiac, ocular, and nervous abnormalities along with other signs of systemic illness.[5,9,11] In dogs, CNS involvement typically involves the cerebrum with intracranial lesions often showing focally, or less commonly, as multifocal distinct granulomatous inflammation. Conversely, in human CNS infection, inflammation is more diffuse.[2,13,17] Diffuse, bilateral, symmetric lesions of the caudate nuclei and frontal lobes are less common form in dogs, and the median age of intracranial coccidioidomycosis is 7 years.[13] The time between infections and evidence of disseminated disease ranges from weeks to several years, and a history respiratory signs might not be present.[8,16] Antibody detection is the most sensitive method for VF

diagnosis, but it can be falsely negative in approximately 5-10% of cases.[17] Therefore, coccidioidomycosis should be considered as a potential cause for chronic illness, respiratory signs, lameness, lymphadenopathy, and nonhealing cutaneous lesions, neurological and cardiac illness within endemic regions.

Coccidioidomycosis occurs less frequently in cats, but their presentation and laboratory abnormalities are similar to dogs including respiratory illness, neutrophilia, monocytosis and hyperglobulinemia. However, cats at diagnosis are typically significantly ill and 60% of cats have disseminated infection, most commonly to the skin, in the endemic regions.[1,10]

Contributing Institution:
Midwestern University, College of Veterinary Medicine

Diagnostic Pathology Center

5725 West Utopia Rd.

Glendale, AZ 85308

https://clinics.midwestern.edu/animal-health-institute/diagnostic-pathology-center

JPC Diagnosis:
Cerebellum and brainstem: Meningoencephalitis, granulomatous, chronic, focally extensive, severe, with intra-and extracellular fungal spherules.

JPC Comment:
The contributor provides a nice writeup on coccidiomycosis that prompts some interesting questions for this case. The lesion in this case was focal and unilateral, and extended from the leptomeninges through the cerebellar peduncle and into the brainstem.

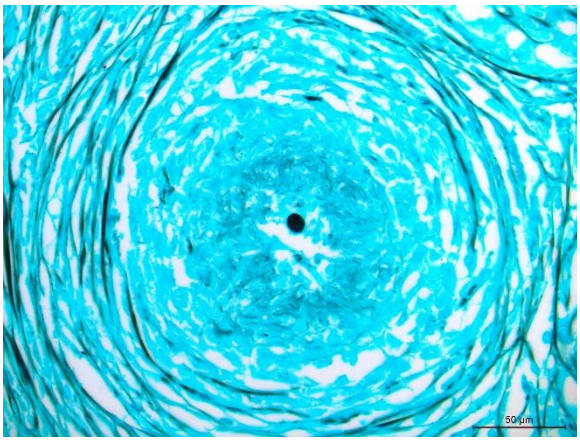

Figure 4-5. Myelencephalon, dog. A silver stain darkly stains the yeast's capsule. (Gomori's methenamine silver, 400X) (*Photo courtesy of:* Midwestern University, College of Veterinary Medicine Diagnostic Pathology Center, Glendale, AZ 85308 https://clinics.midwestern.edu/animal-health-institute/diagnostic-pathology-center)

That this animal reportedly had neurologic deficits attributable to cranial nerve V (motor) and VII deficits aligns with the relative location of these nuclei and the lesion within the brainstem – the focally extensive necrosis of the cerebellum and its role in smoothing motor output likely also played a role, to include the observed nystagmus.

Although the granulomas within the brainstem were an obvious feature on H&E, there were few organisms in histologic section. Even with a GMS or PAS Light Green Stain applied, we noted only 2 granulomas that had an intact spherule. This aligns with the longer clinical course reported by the contributor. Likewise, the lack of free infectious agent (either sequestered in a granuloma and/or low in total number) may have led to a paucity of antigen such that it was below the limit of detection for PCR in this case.

The changes in this case are a classic Th1-response. Participants were quite familiar with Th1 granulomas, though the origin of fibrosis

within the brain was less immediately apparent. With chronic antigen stimulation (such as failing to clear *Coccidioides*), there is predilection for Type-1 macrophages and CD4+ Th1 lymphocytes who in turn produce IFN-γ. IFN-γ is crucial for classical macrophage activation, though this phenotype is notably antifibrotic with cellular arginine being converted to citrulline by nitric oxide synthase 2 which enhances microbicidal activity. In Th2 responses, profibrotic alternatively activated macrophages instead convert arginine to ornithine and eventually proline (a collagen precursor). While the normal brain parenchyma lacks fibroblasts to create fibrous tissue, there are two potential sources to strategically acquire them. In this case, the extension of inflammation through to the meninges (and associated meningeal fibroblasts) is the most likely explanation. Alternatively, differentiation of perivascular fibroblasts (from pericytes) is another possibility that may explain some of the fibrosis deeper in tissue section.[7] The disruption of the blood-CNS barrier may also play a role.[7]

References:

1. Arbona N, Butkiewicz CD, Keyes M, et al. Clinical features of cats diagnosed with coccidioidomycosis in Arizona, 2004-2018. *J Feline Med Surg*. 2020 22(2):129-137.
2. Bentley RT, Heng HG, Thompson C, et al. Magnetic resonance imaging features and outcome for solitary central nervous system Coccidioides granulomas I 11 dogs and cats. *Vet Radiol Ultrasound*. 2015 56(5):520-530.
3. Brown J, Benedict K, Park BJ, et al. Coccidioidomycosis: epidemiology. *Clin Epidemiol*. 2013 25(5):185-197.
4. Butkiewicz CD, Shubitz LF, Dial SM. Risk factors associated with Coccidioides infection in dogs. *J Am Vet Med Assoc*. 2005;226(11):1851-1854.
5. Davidson AP, Shubitz AF, Alcott CJ, et al. Selected Clinical Features of Coccidioidomycosis in Dogs, *Medical Mycology*, 2019, S67–S75.
6. Del Rocio Reyes-Montes M, Ameyali Perez-Huitron M, Luis Ocana-Monroy J, et al. The habitat of *Coccidioides* spp. and the role of animals as reservoirs and disseminators in nature. *BMC Infectious Diseases*. 2016;16:550.
7. Fehlberg CR, Lee JK. Fibrosis in the central nervous system: from the meninges to the vasculature. Cell Tissue Res. 2022 Mar;387(3):351-360.
8. Galgiani JN, Ampel NM, Blair JE, et al. Infectious Diseases Society of America (IDSA) Clinical Practice Guideline for the Treatment of Coccidioidomycosis. *Clin Infect Dis*. 2016 15;63(6):e112-146.
9. Graupmann-Kuzma A, Valentine BA, Shubitz LF, et al. Coccidioidomycosis in dogs and cats: a review. *J Am Vet Med Assoc*. 2008;44(5):226-235.
10. Greene RT, Troy GC. Coccidioidomycosis in 48 cats: a retrospective study (1984-1993). *J Vet Intern Med*. 1995, 9(2):86-91.
11. Johnson LR, et al., Clinical, clinicopathologic, and radiographic findings in dogs with coccidioidomycosis: 24 cases (1995-2000). *J Am Vet Med Assoc*, 2003. 222(4):461-466.
12. Johnson RH, Sharma R, Kuran R, et al. Coccidioidomycosis: a review. *J Investig Med*. 2021, 69(2):316-323.
13. Kelley AJ, Stainback LB, Knowles KE, et al. Clinical characteristics, magnetic resonance imaging features, treatment, and outcome for presumed intracranial coccidioidomycosis in 45 dogs (2009-2019). *J Vet Intern Med*. 2021, 35(5):2222-2231.
14. Lockhart SR, McCotter OZ, Chiller TM. Emerging Fungal Infections in the Pacific Northwest: The Unrecognized Burden and Geographic Range of *Cryptococcus gattii* and *Coccidioides immitis*. *Microbiol Spectr*. 2016. 4(3).
15. Meisner J, Clifford WR, Wohrle RD, et al.

Soil and climactic predictors of canine coccidioidomycosis seroprevalence in Washington State: An ecological cross-sectional study. *Transbound Emerg Dis*. 2019. 66(5):2134-2142.
16. Shubitz LF, Butkiewicz CD, Dial SM, et al. Incidence of Coccidioides infection among dogs residing in a region in which the organism is endemic. *J Am Vet Med Assoc*. 2005;226(11):1846-1850.
17. Spoor E, Stainback L, Plummer S, et al. A novel form of intracranial coccidioidomycosis is present in dogs and exhibits characteristic clinical and magnetic resonance imaging findings. *Vet Radiol Ultrasound*. 2019. 60(1):47-55.
18. Taylor JW, Barker BM. The endozoan, small mammal reservoir hypothesis and the life cycle of Coccidioides species. *Med Mycol*. 2019, 1(57):S16-S20.

Joint Pathology Center
Veterinary Pathology Services

WEDNESDAY SLIDE CONFERENCE 2024-2025

Conference #12 06 November 2024

CASE I:

Signalment:
5-month-old, female intact, Domestic Shorthair, *Felis catus*, cat.

History:
The patient presented to the referring veterinarian at 3 months of age for a 1 month history of abdominal distention which worsened post-prandially. Approximately 45 mL of yellow fluid was removed from the abdomen at this time. The patient was then referred to Colorado State University Veterinary Teaching Hospital for further work up: serum biochemistry demonstrated elevated liver enzymes and hyperbilirubinemia. Abdominal ultrasound showed severe intrahepatic biliary tract dilatation with no identifiable gallbladder, and 300 mL of a similar abdominal fluid was removed. Top differentials included a ductal plate malformation or other congenital malformations. The patient continued to decline despite medical management (Ursodiol and Spironolactone) and was humanely euthanized 1 month later.

Gross Pathology:
On postmortem examination, there was moderate icterus and musculature atrophy. There was approximately 1300 mL of serous, yellow-green fluid in the abdominal cavity. The liver was yellow-to-green tinged and markedly enlarged with distorted, rounded lobes. There was serosal thickening with adhesions

Figure 1-1. Presentation, kitten. 1300 cc of fluid were present in the abdomen at autopsy. (*Photo courtesy of:* Colorado State University Veterinary Diagnostic Laboratory, https://vetmedbiosci.colostate.edu/vdl/)

from the liver to the diaphragm and stomach and there was no identifiable gall bladder. On cut section, the yellow to green discoloration was present throughout the parenchyma and there were numerous, tortuous, markedly dilated bile ducts filled with dark green fluid. The left lobe of the pancreas was edematous, nodular and irregular and markedly decreased in size with adhesions to the stomach. The spleen was very small, rounded and adhered to the stomach. The mesentery of the greater curvature of the stomach had prominent, slightly tortuous vasculature and was expanded by green-tinged edema.

Laboratory Results:
Chemistry:

Phosphorus	7.0 mg/dL	(3.0 - 6.0)
Total Protein	6.2 g/dL	(6.3 - 8.0)
CK	828 IU/L	(60 – 350)

T-Bilirubin	1.6 mg/dL	(0.0 - 0.1)
ALP	392 IU/L	(10 – 80)
ALT	893 IU/L	(30 – 140)
AST	275 IU/L	(15 – 45)
GGT	22 IU/L	(0 - 0.5)
Sodium	154 mEQ/L	(149 – 157)
Potassium	6.12 mEQ/L	(3.7 - 5.4)
Chloride	116.6 mEQ/L	(115 – 125)
Bicarb	16.3 mEQ/L	(13 – 22)
Anion Gap	27 mmol/L	(16 – 26)
Calc Osmolality	317 mOsm/Kg	
Lipemia	20	(0 – 50)
Hemolysis	99	(0 – 50)
Icterus	2	(0 – 1)

Urinalysis:

U-Protein/Create	0.54 Ratio	(0.0-0.19)
Urine Protein	2+	
Urine Bilirubin	1+	
Urine pH	6	

Abdominal Fluid Analysis & Cytology:

Fluid Color	Yellow
Fluid Clarity	Cloudy
NCC Fld	700#/uL
RBC Fld	<10000 #/uL
Fluid PCV	0
Refr Protein Est	3.0 g/dL
Neutrophils #	399 #/uL
Neutrophils %	57%
Large Mononuclear #	287 #/uL
Large Mononuclear %	41%
Lymphocytes #	14 #/uL
Lymphocytes %	2%

Microscopic Description:
The liver capsule is thickened by variably mature fibrous to myxomatous connective tissue up to 0.6 mm thick with few regularly spaced vessels. Within the adjacent hepatic parenchyma, there are markedly dilated biliary profiles with thickened fibrous capsules. Cystic biliary spaces are lined by elongated and branching villi of biliary epithelium. Within the lumen there is a homogenous basophilic to amphophilic occasionally wispy to vacuolated material. Portal regions are diffusely surrounded by fibrous stroma which bridges between portal regions and entraps islands of

Figure 1-2. Liver, kitten. The liver was yellow-to-green tinged and markedly enlarged with distorted, rounded lobes. (*Photo courtesy of:* Colorado State University Veterinary Diagnostic Laboratory, https://vetmed-biosci.colostate.edu/vdl/)

hepatocytes. Associated with portal tracts and fibrosis, there are abundant torturous biliary profiles with oval cell hyperplasia and arteriolar reduplication. Portal veins are often small and there is variable lymphatic dilation. Mild infiltrates of neutrophils with fewer lymphocytes, plasma cells and Kupffer cells dissect portal regions. There is increased connective tissue surrounding central veins and multifocal mild sinusoidal dilation.

Masson's Trichrome Histochemistry:

Liver: Trichrome staining demonstrates marked fibrosis surrounding dilated biliary profiles, often entrapping islands of hepatocytes. There is a finer collagen network bridging remaining portal regions and surrounding central veins.

Cytokeratin 19 Immunohistochemistry:

Liver: There is moderate to strong immunoreactivity to cytokeratin 19 throughout cystic bile ducts and proliferative biliary epithelium within portal regions and extending between lobules. Occasionally, individual oval to

Figure 1-3. Liver, kitten. On cut section, intrahepatic bile ducts are markedly ectatic and tortuous. (*Photo courtesy of:* Colorado State University Veterinary Diagnostic Laboratory, https://vetmedbiosci.colostate.edu/vdl/)

spindloid cytokeratin 19-positive cells directly oppose periportal hepatocytes.

Contributor's Morphologic Diagnosis:
Liver: Chronic marked bridging fibrosis with ductular reaction, arteriolar reduplication, portal vein hypoplasia and marked cystic dilation of bile ducts (Caroli's disease); moderate central vein fibrosis.

Contributor's Comment:
Physical exam, ultrasound, gross and histologic findings in this case are most suggestive of Caroli malformation/disease, which is a ductal plate malformation (DPM) characterized by congenital hepatic fibrosis and cystic bile ducts.[1]

DPMs are a group of developmental biliary disorders rarely reported in veterinary species.[1] In normal development, hepatoblasts are bipotent, capable of differentiating into biliary epithelium or periportal hepatocytes.

The fate of hepatoblasts is largely dependent on transcription factors. Hepatoblasts that give rise to biliary epithelium undergo tubulogenesis, forming a double layer of cuboidal cells surrounding a rudimentary portal vein. This coordinated series of events is orchestrated by TGF-β, Notch, and Wnt signaling pathways, forming the embryonic ductal plate.[7] Hepatoblasts that do not undergo tubulogenesis either involute or differentiate into periportal hepatocytes.[1,5-7]

Malformations within the ductal plate arise when hepatoblasts do not undergo tubulogenesis and also fail to involute, resulting in persistent embryonic bile ducts. It is important to note that DPM encompasses a continuum of phenotypes which reflect the level at which the developing biliary tree is affected.[1] This spectrum includes Caroli malformation (presented in this case), biliary hamartomas (also referred to as von Meyenburg complexes), congenital hepatic fibrosis (CHF), and polycystic liver disease (PCLD).[1,5] In cases of Caroli malformation, disruption occurs at the level of segmental bile ducts (first branch of the hepatic duct), leading to large dilated/cystic persistent ducts.

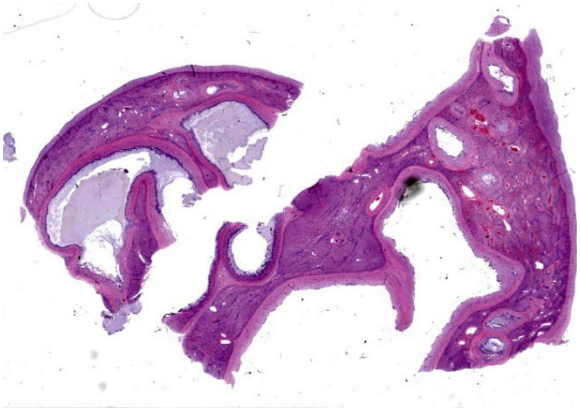

Figure 1-4. Liver, kitten. There is bridging portal fibrosis entrapping markedly ectatic bile ducts (which measure up to 6mm in diameter). (HE, 5X)

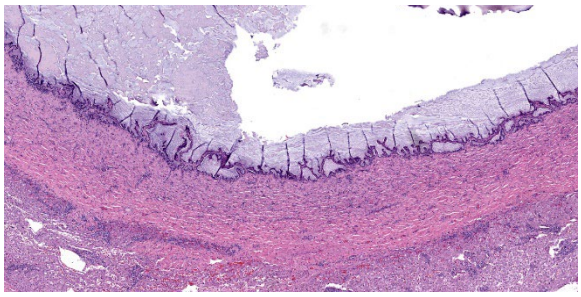

Figure 1-5. Liver, kitten. Ectatic bile ducts are lined by hyperplastic epithelium and have a thick 1mm fibrous capsule. (HE, 44X)

Few cases of DPMs have been reported in cats, including Caroli malformation with a portosystemic shunt,[6] congenital hepatic fibrosis[8] (see WSC 2019-2020, Conference 7, Case 1), bile duct hamartomas (see WSC 2021-2022, Conference 1, Case 4), and polycystic liver disease (often in combination with adult polycystic kidney disease).[3,4] One retrospective study characterized clinical findings in 30 boxer dogs diagnosed with DPMs.[5] In this study, the most common clinical feature was increased liver enzymes (n=28/30), followed by gastrointestinal signs (n=16/30), poor body condition (n=14/30), abdominal effusion (n=9/30), and hepatic encephalopathies (n=2/30); however, these changes are not unique to DPMs which can challenge clinical diagnoses. Such data is currently lacking in cats.

Gallbladder atresia has also been reported in dogs with DPMs.[5] In the presented case, the gall bladder was not identified with gross or histologic examination.

In cases of congenital hepatic fibrosis (CHF), histopathologic findings include bridging hepatic fibrosis, numerous irregular bile duct profiles, diminished or absent portal veins, and arteriolar reduplication. These histologic findings in addition to large, tortuous and cystic biliary ducts are termed Caroli malformation. DPMs lack nodular regeneration, cirrhosis, and cholangitis. Cytokeratin 19 (CK19) is expressed in hepatoblast precursor cells and committed biliary epithelium and can be used as a marker to confirm cellular histogenesis in these cases.[1,5]

Differential diagnoses include primary portal vein hypoplasia (PVHP), obstructive biliary disease, and lobular dissecting hepatic fibrosis (dogs only).

Primary portal vein hypoplasia (PVHP): In DPMs, intrahepatic presinusoid hypertension may redirect portal flow away from the liver, resulting in an acquired portosystemic shunt. Therefore, decreased/absent portal veins with arteriolar reduplication can overlap between DPMs and PVHPs; however, cases of a PVHP often lack marked biliary hyperplasia, biliary ectasia, and periportal fibrosis.[1,2]

Obstructive biliary disease: Similar to DPMs, obstructive biliary disease includes bile duct dilation and tortuosity; however, peribiliary fibrosis does not bridge portal regions, and the presence of periductal edema with inflammation are unique to obstructive biliary disease.[5]

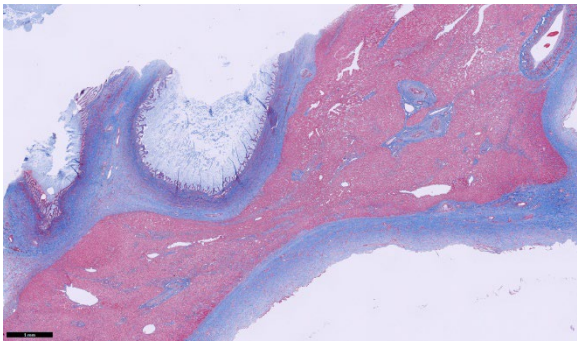

Figure 1-6. Liver, kitten. A Masson's trichrome demonstrates the thickened capsule, fibrotic walls of ectatic bile ducts, and bridging portal fibrosis. (Masson's trichrome, 40X) (*Photo courtesy of:* Colorado State University Veterinary Diagnostic Laboratory, https://vetmedbiosci.colostate.edu/vdl/)

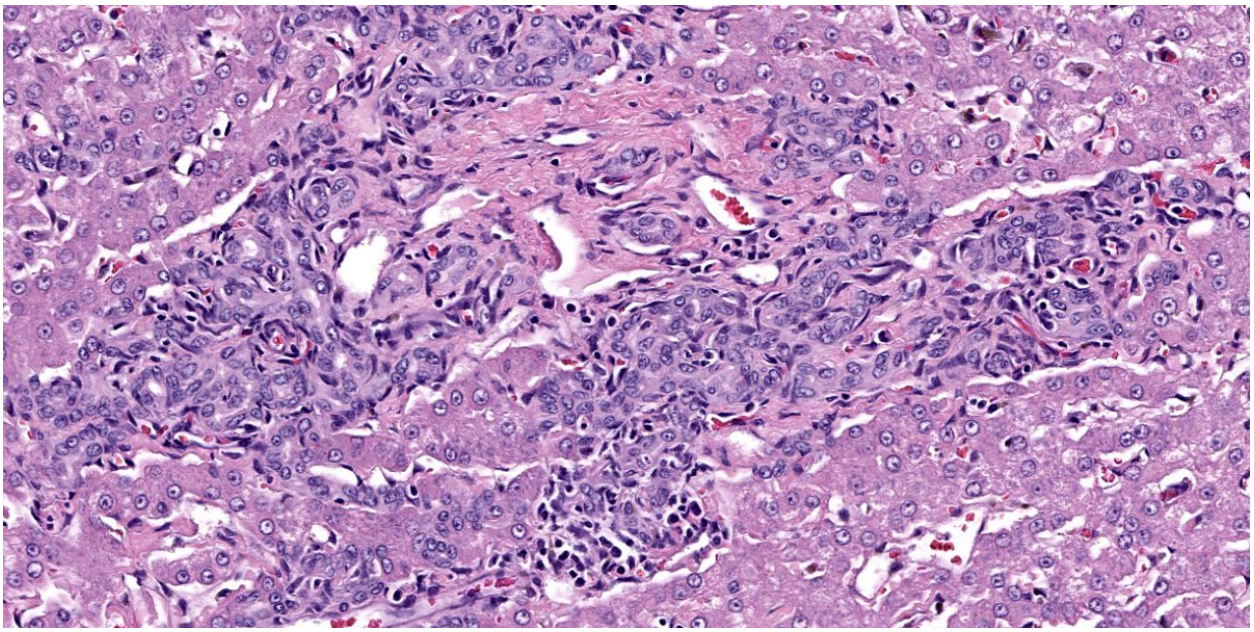

Figure 1-7. Liver, kitten. There is marked biliary hyperplasia in areas of portal fibrosis. Portal areas contain numerous arteriolar profiles, but few discernable portal veins. (HE, 300X)

Lobular dissecting hepatic fibrosis: Lobular dissecting hepatic fibrosis is often accompanied by nodular regeneration and cirrhosis, both of which are not features of DPMs.[1,2]

Contributing Institution:
Colorado State University Veterinary Diagnostic Laboratory

https://vetmedbiosci.colostate.edu/vdl/

JPC Diagnosis:
Liver: Ductal plate malformation.

JPC Comment:
This week's moderator was the renowned Dr. John Cullen who led participants through a liver-centric conference with 4 cases that emphasized careful review of the slide and taking a 'census' of liver features along the way.

The contributor provides an excellent summary of ductal plate malformations in this first case. Dr. Cullen ultimately agreed that the features presented were likely consistent with Caroli's disease, though there were several important additional criteria to consider. Foremost, there was no evidence of obstruction and/or inflammation as an inciting cause for dilatation of the bile ducts which is an important rule out – this can be complicated as ascending infection often accompanies distension of the duct. That this cat was young (5 months) likely limited inflammation. In addition, as Caroli's disease affects the large ducts specifically. . Figure 1-3 is supportive on its own for Caroli's disease. Careful dissection of the entire liver with a good gross description is therefore advisable. Though a lack of a gallbladder is associated with DPMs resembling Caroli's disease in dogs, gallbladder agenesis has been rarely reported in this condition in cats.

Though the abnormal proliferation of biliary ductules in the fibrotic portal areas was an obvious feature of this case, the absence of portal vein profiles was a bit more subtle. Dr.

Cullen emphasized reviewing multiple portal tracts as part of his census and specifically locating the portal vein, hepatic artery, bile duct, and lymphatics and comparing both larger tracts and smaller tracts for features. The latter is important for considering the branch level of primary portal vein hypoplasia as only secondary branches may be hypoplastic. Additionally, the marked dilatation of bile ducts was a helpful feature for this case, though the diagnosis of DPM writ large does not require this if there is modest dilation concurrent with portal vein hypoplasia.

Finally, there are several ancillary features of this slide worth capturing. The thick hepatic capsule likely represents stretching of the liver and increased mechanical response. The marked dilatation of bile ducts increases interstitial pressure which in turn allowed for leakage of fibrinogen in lymph and eventual conversion to the mature collagen seen in section. The degree of fibrosis present with Masson's trichrome is notable (figure 1-6) as well, and indicates (in a very non-specific vernacular), impaired "cross-talk" between epithelial and mesenchymal tissues during intrahepatic biliary tree development. Material within the ductular lumen stained with Alcian blue (i.e. containing mucus), though ductular epithelial secretions are variable and include other constituents as well.

References:

1. Cullen JM, Stalker MJ. Liver and biliary system. In: Maxie MG, ed. *Jubb, Kennedy, and Palmer's Pathology of Domestic Animals*. 6th ed. Vol 2. Philadephia, PA: Elsevier; 2016:264-267.
2. Cullen JM. Summary of the World Small Animal Veterinary Association standardization committee guide to classification of liver disease in dogs and cats. *Vet Clin North Am Small Anim Pract*. 2009 May;39(3):395-418.
3. Hirose N, Uchida K, Kanemoto H, et al. A retrospective histopathological survey on canine and feline liver diseases at the University of Tokyo between 2006 and 2012. *J Vet Med Sci*. 2014; 76: 1015–1020.
4. King EM, Pappano M, Lorbach SK, Green EM, Parker VJ, Schreeg ME. Severe polycystic liver disease in a cat. *Journal of Feline Medicine and Surgery Open Reports*. 2023;9(2).
5. Pillai S, Center SA, McDonough SP, et al. Ductal Plate Malformation in the Liver of Boxer Dogs: Clinical and Histological Features. *Vet Pathol*. 2016 May;53(3):602-13.
6. Roberts ML, Rine S, Lam A. Caroli's-type ductal plate malformation and a portosystemic shunt in a 4-month-old kitten. *JFMS Open Rep*. 2018 Nov 20;4(2):2055116918812329.
7. Wills ES, Roepman R, Drenth JP. Polycystic liver disease: ductal plate malformation and the primary cilium. *Trends Mol Med*. 2014; 20:261–270.
8. Zandyliet MM, Szatmári V, van den Ingh T, Rothuizen J. Acquired portosystemic shunting in 2 cats secondary to congenital hepatic fibrosis. *J Vet Intern Med*. 2005 Sep-Oct;19(5):765-7.

CASE II:

Signalment:
10-year-old, male neutered domestic cat, feline (*Felis silvester catus*).

History:
This animal was referred to the veterinary clinic for weakness and abnormal vocalizations. At the clinical examination, severe paleness of the external mucosae, asthenia and peritoneal blood effusion were detected. Complete blood count and clinical chemistry

Figure 2-1. Liver, cat. At subgross magnification, there is a retiform pattern of pallor in centrilobular areas. (HE, 5X)

showed severe anemia and increased liver enzymes. On ultrasound examination the liver appeared moderately enlarged in size, with a coarse granular texture and slightly rounded margins. Liver biopsies were performed during laparotomy for histological examination.

Gross Pathology:
At laparoscopy, it was referred that the liver appeared enlarged and on the surface there were multifocal dark-red lesions continuously draining blood (consistent with hemorrhages).

Laboratory Results:
Complete blood count revealed many abnormal values, including WBC 19,30 x10^3/ul , Reference Intervals (RI) 5,00-11,00); RBC 4,65 x10^6/ul (RI 5,00-10,00); MCH 17,80 pg (RI 12,50-17,50); MCHC 36,90 g/dl (RI 29,00-36,00); RDW 22,70 % (RI 13,00-17,00); HCT 22,50 % (RI 24,00-45,00); lymphocytes 8,40 % (RI 20,00-55,00); monocytes 5,10 % (RI 1,00-4,00); eosinophils 17,50 % (RI 0,00-12,00); MPV 10,00 fl (RI 12,00-17,00). Clinical chemistry showed creatine kinase 928,50 U/l (RI < 250,00); AST 94 U/l (RI 0 – 57); cholesterol 251,90 mg/dl (RI 56 – 241,00), glucose 34,27 mg/dl (RI 61 – 155,00); BUN 12 mg/dl (RI 13 – 31); iron 76,77 ug/dL (RI 110,00 - 169,00).

Microscopic Description:
Liver: approximately 70% of the liver parenchyma is affected by multifocal to coalescing areas of moderate to marked sinusoidal dilatation of variable dimensions, irregular in shape and randomly distributed. Occasionally in these areas, loss of endothelial demarcation is evident. Admixed with the dilated sinusoids and lacunae there are extravascular erythrocytes (hemorrhages), meshwork of eosinophilic, amorphous and fibrillar material (fibrin and necrotic debris), few cytoplasmic and nuclear fragments of hepatocytes (hepatocytes necrosis and loss) and rare neutrophils characterized by variable pyknosis, karyolysis and karyorrhexis. In unaffected areas the hepatocellular cords are irregularly distributed and there is loss of lobular architecture. Immediately adjacent to these areas the hepatocytes show mild to moderate atrophy. In the rest of the section, the hepatocyte cords show irregular radial organization and mild thickening (2-3 layers) and hepatocytes are diffusely characterized by large cytoplasm containing mild to moderate amounts of optically empty microvacuoles (vacuolar degeneration with mild steatosis). The hepatocytes show frequent binucleation and occasional mitoses (hyperplasia). Furthermore, multifocally the blood lacunae extend to the subsurface and here the hepatic capsule is covered by a small amount of fibrin mixed with scant extravascular erythrocytes. Small hemorrhages are evident diffusely in the subcapsular-capsular tissue. In addition, multifocally there is a mild hyperplasia of the lining mesothelium which is occasionally is distributed over two layers.

Contributor's Morphologic Diagnosis:
Liver: Sinusoidal lacunae (blood-filled), multifocal to coalescing and random, moderate with heptacellular necrosis, loss, and atrophy with multifocal mild fibrinous perihepatitis, hemorrhage, and multifocal mild mesothelial hyperplasia.

Contributor's Comment:

This case represents an unusual lesion that was not matching any specific entity. One

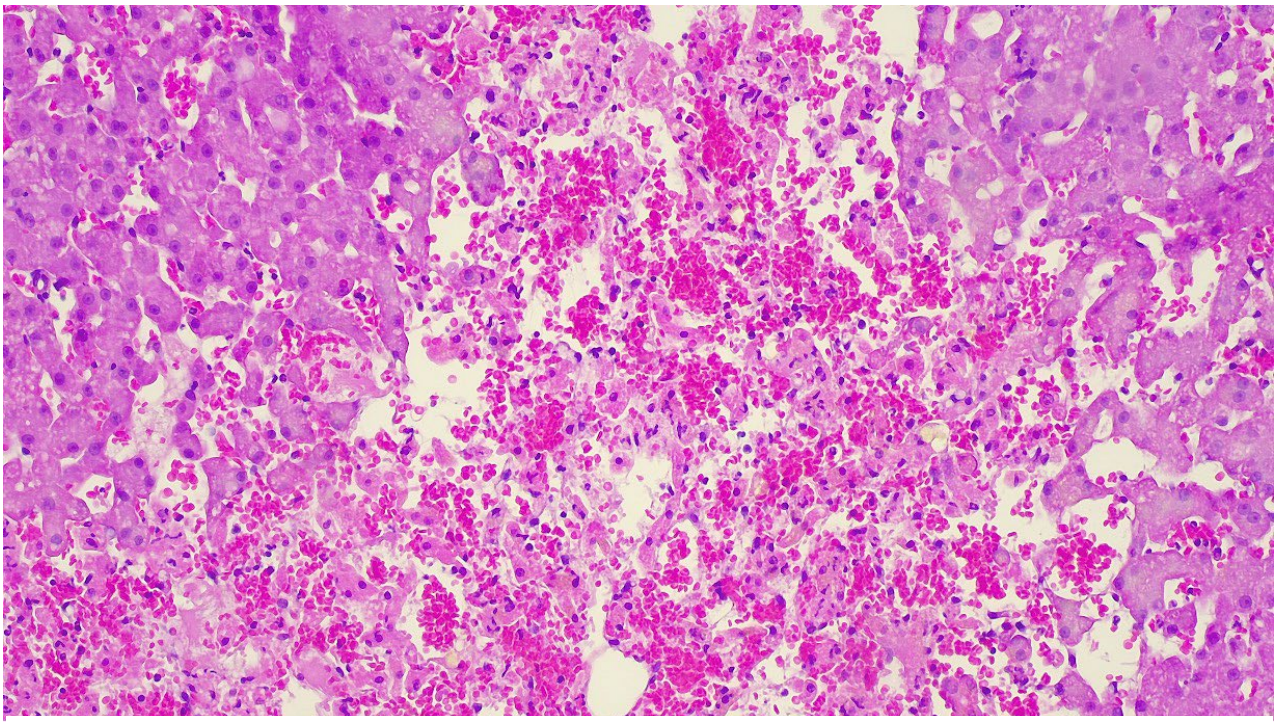

Figure 2-2. Liver, cat. Within dilated sinusoids, there is abundant hemorrhage, fibrin and necrotic debris, few cytoplasmic and nuclear fragments of hepatocytes (hepatocyte necrosis and loss) and viable and necrotic neutrophils (HE, 200X) (*Photo courtesy of:* Department of Comparative Biomedicine and Food Science, Viale dell'Università 15, 35020, Legnaro (PD), Italy; https://www.bca.unipd.it/)

disease that was discussed as possible part of the diagnosis was hepatis peliosis which is what this case was submitted as.

Hepatis peliosis is an uncommon condition of the liver characterized by the presence of numerous blood-filled cystic spaces. These cystic spaces may be lined by endothelial cells (phlebectatic form), therefore indicating sinusoidal dilatation associated also with reticulin alterations.[6] Conversely, in the parenchymal form the cystic spaces are formed by necrosis of the hepatocytes and endothelial lining that can therefore be absent multifocally.[6] In both cases, grossly, the lesions are characterized by multifocal dark-red areas, va
sc

perficial severe bleeding is usually not described.

In our case, a parenchymal form was considered as more suitable because of the detected necrosis.

Usually, hepatis peliosis is not associated with clinical alterations linked to liver dysfunction, whereas in our case an increase in liver enzymes and anemia were observed. For this reason, a primary necrotizing hepatitis with unusual and marked cystic sinusoidal dilation could not be ruled out as a diagnosis.

Hepatis peliosis has been reported in cattle,[11] dogs,[8,12] and cats.[3] Its pathogenesis is still unknown. In human medicine, this lesion is as-

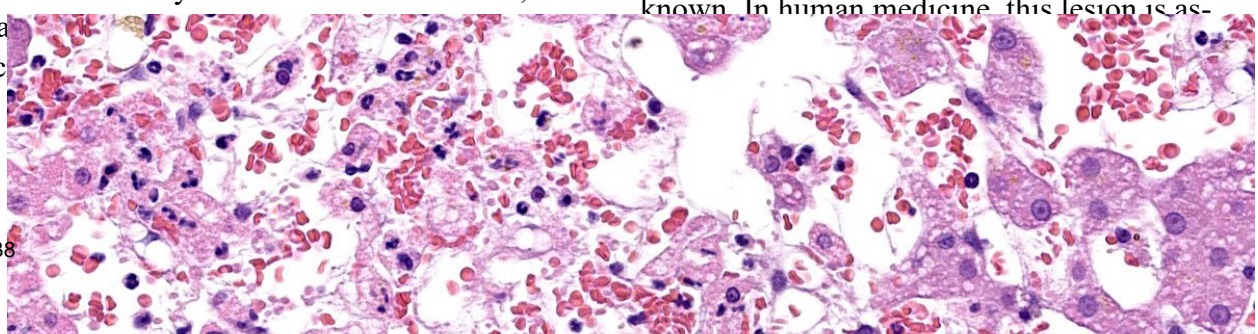

infections such as *Bartonella henselae* and *B. quintana.*[1] In humans and lab animals, increases in vascular endothelial growth factor (VEGF) have been implicated in lesion development.[14] In addition, *B. henselae* infection notably leads to activation of hypoxia-inducible factor-1 (HIF-1) which can induce a pro-angiogenic response in the host via VEGF and IL-8.[10] In dogs, hepatis peliosis has been described in one case following diphacinone[2] intoxication and in another case with *B. henselae* infection.[9] In cats, this condition is relatively common in elderly subjects (particularly the phlebectatic form) and it seems that there is not a clear association with *B. henselae* infection.[4] In cattle, a specific form of hepatis peliosis has been described in animals poisoned by *Pimelea* plants.[13]

In conclusion, this is an unusual case in which both necrosis and marked dilation of blood spaces (hepatis peliosis-like lesions) were detected. No additional analysis for infectious diseases or toxins were conducted for this case.

Contributing Institution:
Department of Comparative Biomedicine and Food Science, Viale

dell'Università 15, 35020, Legnaro (PD), Italy; https://www.bca.unipd.it/

JPC Diagnosis:
Liver: Sinusoidal dilation and hemorrhage, centrilobular, diffuse, severe, with hepatocellular atrophy and necrosis and multiple subcapsular hematomas.

JPC Comment:
We thank the contributor for submitting this interesting case. Many conference participants weren't initially sure what to make of the presentation, with the centrilobular to midzonal distribution of the necrosis leading some to consider a toxicant. We agree that hepatis peliosis is a excellent differential for this case; however, under the careful eye (and

immense expertise) of Dr. Cullen, we were able to arrive at a slightly different diagnosis however.

As the contributor notes, the diagnosis of hepatis peliosis involves disruption of the reticulin framework. Such changes were notably absent on our reticulin stain. In addition, Masson's trichrome highlighted centrilobular fibrosis which was suggestive of a more chronic lesion. Moreover, hepatis peliosis changes should reflect a random distribution, whereas the distribution of necrosis in the submitted sections was repeatable and specific in this case. For these reasons, we do not favor the contributor's diagnosis and prefer a diagnosis of chronic sinusoidal outflow issues (i.e. dilation and congestion).[15,16]

An important ruleout for centrilobular necrosis is hypertension secondary to chronic passive congestion (right-sided heart failure), veno-occlusive disease, or thrombosis of the vena cava (e.g. Budd-Chiari syndrome).[15,16] Though the contributor did not report cardiac lesions in this cat, the hypereosinophilia noted on bloodwork is an interesting (if nonspecific) finding that could hint a *Dirofilaria* infection – heartworm has been described in cats in northern Italy.[7] Thrombosis of the vena cava and veno-occlusive disease are both rare in cats.[5] Mechanistically, the progression of hepatocyte loss to fibrosis accentuates portal hypertension (and hypoxia) with subsequent atrophy and necrosis of remaining hepatocytes. An interesting ancillary feature of this case was numerous erythrocytes within the space of Disse. Conference participants felt that this likely reflected both endothelial damage and increased sinusoidal pressure. Erythrocyte extravasation may be encountered in cases with and without impairment of venous outflow however.[15]

Lastly, we briefly discussed the idea of a toxin in this case. There are several features that do not fit with acute intoxication, however. Histologically, atrophy, congestion, and fibrosis are not consistent with a single intoxicating event despite the presence of hepatocyte necrosis. The low AST on this cat's bloodwork also argues against this. Absent the other clinical data and history in this cat, a chronic intoxication with an acute disruption could present in this manner.

References:

1. Ahsan N, Holman MJ, Riley TR et al. Peliosis hepatis due to Bartonella henselae in transplantation: a hemato-hepato-renal syndrome. *Transplantation*. 1998;65(7):1000-1003.
2. Beal MW, Doherty AM, Curcio K. Peliosis hepatis and hemoperitoneum in a dog with diphacinone intoxication. *Journal of Veterinary Emergency and Critical Care*. 2008;18(4):388-392.
3. Brown PJ, Henderson JP, Galloway P, O'Dair H, & Wyatt JM. Peliosis hepatis and telangiectasis in 18 cats. *Journal of Small Animal Practice*. 1994;35(2):73-77.
4. Buchmann AU, Kempf VAJ, Kershaw O, Gruber AD. Peliosis hepatis in cats is not associated with Bartonella henselae infections. *Veterinary Pathology*. 2010;47(1):163-166.
5. Cave TA, Martineau H, Dickie A, Thompson H, Argyle DJ. Idiopathic hepatic veno-occlusive disease causing Budd-Chiari-like syndrome in a cat. *J Small Anim Pract*. 2002 Sep;43(9):411-5.
6. Cullen JM, Stalker MJ. Liver and Biliary System. In: Maxie MG, ed. *Jubb, Kennedy & Palmer's Pathology of Domestic Animals*. Vol 2. 6th ed. St. Louis, MO: Elsevier; 2016:258-352.
7. Grillini M, et al. Evidence of Dirofilaria immitis in Felids in North-Eastern Italy.

Pathogens. 2022;11(10):1216.
8. Inoue S, Matsunuma N, Ono K, Hayashi T, Takahashi R, Goto N, Fujiwara K. Five cases of canine peliosis hepatis. *Nihon Juigaku Zasshi* (*(The Japanese Journal of Veterinary Science)*. 1988 Apr;50(2):565-7.
9. Kitchell BE, Fan TM, Kordick D et al. Peliosis hepatis in a dog infected with Bartonella henselae. *Journal of the American Veterinary Medical Association*. 2000;216(4):519-523.
10. Kempf VA, Lebiedziejewski M, Alitalo K et al. Activation of hypoxia-inducible factor-1 in bacillary angiomatosis: evidence for a role of hypoxia-inducible factor-1 in bacterial infections. *Circulation*. 2005;111(8):1054-1062.
11. Onda H, Kaneda Y, Ito Y, Wakabayashi T. Peliosis hepatis: a specific lesion in the bovine liver. *Acta Patholigica Japonica 1982; 32*(6), 1053-1058.
12. Sapierzyński R. Peliosis hepatis-like lesion in a pekingese dog. A case report. *Polish Journal of Veterinary Sciences*. 2007;10(1):43-46.
13. Seawright AA. Phlebectatic peliosis hepatis in Australian cattle. *Veterinary and Human Toxicology*. 1984;26(3):208-213.
14. Wong AK, Alfert M, Castrillon DH et al. Excessive tumor-elaborated VEGF and its neutralization define a lethal paraneoplastic syndrome. *Proceedings of the National Academy of Sciences*. 2001;98(13):7481-7486.
15. Kakar S, Kamath PS, Burgart LJ. Sinusoidal dilatation and congestion in liver biopsy: is it always due to venous outflow impairment? Arch Pathol Lab Med. 2004 Aug;128(8):901-4.
16. Kakar S, Batts KP, Poterucha JJ, Burgart LJ. Histologic changes mimicking biliary disease in liver biopsies with venous outflow impairment. Mod Pathol. 2004 Jul;17(7):874-8.

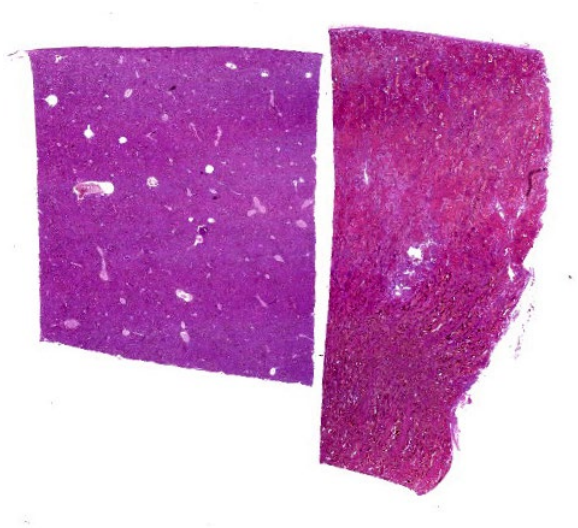

Figure 3-1. Liver and kidney, sheep. Sections from these tissues are submitted for examination. (HE, 5X)

CASE III:

Signalment:
Adult pregnant Texel sheep (*Ovis aries*).

History:
12 of ~1,500 sheep exhibited acute depression, red urine (hemoglobinuria), yellow discoloration of the conjunctiva (jaundice), and died over a 10-month period. The sheep grazed on red clover and annual ryegrass, had access to foxtail millet and oat hay, and were supplemented with soybean meal, molasses, and slow-release urea. The flock was administered a multivalent vaccine to prevent clostridial diseases, as well as anthelmintic drugs.

Gross Pathology:
The subcutaneous tissue and the abdominal and pericardial fat were slightly icteric, and the carcass had a brownish hue (presumably due to methemoglobinemia). Bilaterally, the renal parenchyma involving both the cortex and medulla showed a diffuse dark red to black discoloration (hemoglobinuric nephrosis). The urinary bladder contained ~3 mL of dark red urine (hemoglobinuria). The liver

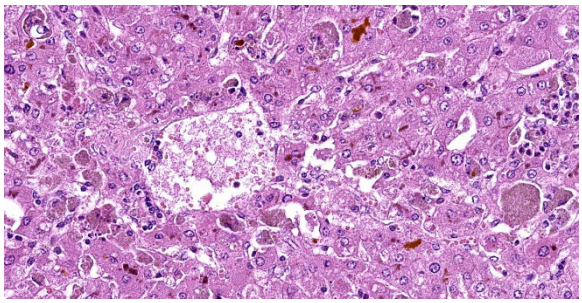

Figure 3-2. Liver, sheep. There is diffuse necrosis of centrilobular hepatocytes. There is marked canalicular cholestasis as well.

was diffusely tan. Additional changes included mild ecchymoses in the serosa of the small and large intestine, abundant pink stable froth in the lumen of the trachea, extra and intrapulmonary bronchi with diffuse pulmonary edema, and free dark, red-tinged fluid in the abdominal and thoracic cavities and pericardial sac (mild hydroperitoneum, hydrothorax and hydropericardium). Incidentally, there were multiple, white, spherical to ovoid, 7-9 mm in diameter, solid nodules in the esophageal muscular layer morphologically resembling *Sarcocystis gigantea* cysts, and a few adult nematodes compatible with *Trichuris* sp. in the lumen of the colon.

Laboratory Results:

No laboratory tests were performed before autopsy. Aerobic and microaerobic bacterial cultures from lung, liver, kidney, urine, and colon were unremarkable. PCR, qPCR and direct fluorescent antibody test for *Leptospira* spp. from liver, kidney, and urine were all negative. A heavy metal screen was performed in samples of liver and kidney with the following results:

Analyte	Liver	
	Result	Reference range
Lead	ND	<1
Manganese	1.8	2-4.4
Iron	400	30-300
Mercury	ND	<1
Arsenic	ND	<4
Molybdenum	ND	<6
Zinc	57	30-75
Copper	867	25-100*
Cadmium	ND	<2

Analyte	Kidney	
	Result	Reference range
Lead	ND	<1
Manganese	1.2	0.8-2.5
Iron	800	30-200
Mercury	ND	<1
Arsenic	ND	<1
Molybdenum	ND	<2
Zinc	43	20-40
Copper	207	4-5.5*
Cadmium	ND	<4

ND: not detected. All values are expressed in ppm on a wet-weight basis. *>250 ppm in liver and >15 ppm in kidney is consistent with copper toxicity.

Microscopic Description:

Liver: hepatocytes throughout centrilobular and midzonal areas exhibit swelling, poorly defined cell boundaries, and vesicular nuclei (degeneration) or have shrunken hypereosinophilic cytoplasm with angular borders and pyknotic nucleus or karyorrhexis (necrosis). Occasionally, necrotic hepatocytes are surrounded by aggregates of neutrophils, macrophages and extravasated erythrocytes. Hepatic cords are distorted, and hepatocyte orientation is altered, especially around the centrilobular regions. Scattered in the parenchyma many hepatocytes and Kupffer cells contain cytoplasmic, finely granular, brownish to gray material (interpreted as copper). Multifocally, a golden to orange amorphous

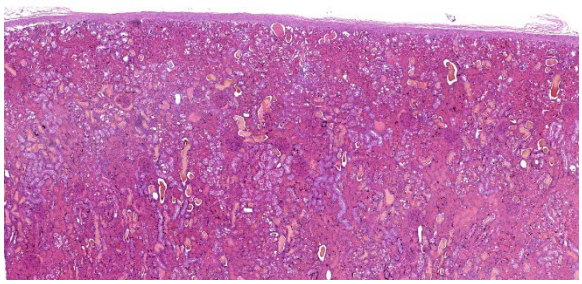

Figure 3-3. Kidney, sheep. Normal tubular architecture is altered with tubular lumina filled with protein and hemorrhage. (HE, 33X)

pigment plugs the canaliculi (cholestasis). Portal regions are multifocally infiltrated by moderate numbers of pigment-laden macrophages and fewer lymphocytes.

Kidney: diffusely, cortical and medullary tubules, and glomerular filtration spaces are ectatic, and contain eosinophilic proteinic material/droplets and hyaline casts (consistent with hemoglobin). Cortical tubular epithelial cells exhibit a wide variety of changes including foamy cytoplasm, tumefaction, nuclear swelling (degeneration), attenuation, or hypereosinophilic cytoplasm with pyknosis (necrosis) frequently involving entire segments of the tubules (tubulorrhexis). Multifocally necrotic epithelial cells slough into the tubular lumen. Intracytoplasmic, coarse, granular, brown to black pigment (consistent with iron/hemosiderin) is widely distributed throughout the epithelium of the proximal tubules.

Contributor's Morphologic Diagnosis:
1. Liver: Hepatocellular degeneration and necrosis, centrilobular to midzonal, acute, severe, diffuse, with intracytoplasmic granular material (consistent with copper) in Kupffer cells and hepatocytes, canalicular cholestasis, moderate, multifocal, neutrophilic and histiocytic hepatitis and portal hepatitis.

2. Kidney: Nephrosis (cortical tubular necrosis), acute, severe, diffuse with intratubular hyaline proteinic casts (consistent with hemoglobinuria) and intracytoplasmic brown to black pigment (consistent with iron/hemosiderin) in proximal tubular epithelial cells.

Contributor's Comment:
The diagnosis of copper poisoning was based on macroscopic and histologic pathological findings which clearly indicated an acute hemolytic crisis coupled with markedly elevated copper concentrations in the kidney and liver. Considering the severity and extension of the lesions, death was attributed to renal and potential hepatic failure.

Copper is a heavy metal and an essential microelement. It acts on cells in different biochemical processes such as respiration, catecholamine biosynthesis, iron metabolism by copper-dependent enzymes, elastin and collagen formation, and melanin production.[12]

Chronic copper poisoning is frequent in sheep, and it has been reported in most sheep rearing regions all over the world.[9] It may occur with daily intakes of 3.5 mg of copper/kg when grazing pastures that contain 15-20 ppm of copper (dry matter).[5] Sheep are particularly susceptible to this condition because they are not able to increase copper biliary excretion as intake increases.[7] Additionally, the protein that aids in the transport of copper in plasma (ceruloplasmin) possess a long half-life in sheep, thus increasing the time this mineral remains in the bloodstream.[4] Although all ovine breeds are susceptible to copper poisoning, Texel sheep (as in this case) are among the most vulnerable.[9]

Chronic copper toxicosis is usually the result of an excessive copper intake for a prolonged

period of time, often associated with contamination of water sources, pasture, or rations.[1] Additionally, secondary factors such as low molybdenum, iron, or sulphate levels in the diet can increase copper absorption and accumulation in the liver. In this case, ingestion of red clover (*Trifolium pratense*) could have predisposed this animal to retain excessive copper as clover can have elevated copper:molybdenum ratios.[5,10] Although molybdenum was not detected in liver and kidney of this sheep, the diet was not tested for molybdenum as would have been required to assess molybdenum intake.

Other factors including the ingestion of hepatotoxic plants such as those containing pyrrolizidine alkaloids (e.g. *Senecio* spp.) can induce copper release from damaged hepatocytes, resulting in increased blood levels of copper and risk of hemolytic crisis.[1,5] To the best of our knowledge, the sheep in this flock were not exposed to hepatotoxic plants. Stress resulting from starvation, vigorous exercise, transportation, handling, and/or adverse weather conditions could elicit the hemolytic crisis typical of copper poisoning.[5]

When toxic quantities of copper are released into the bloodstream, intravascular hemolysis occurs due to a reduction of the antioxidant capacity of erythrocytes and lipid peroxidation of their cell membrane. The resulting hemoglobinemia ultimately leads to hypoxia and hemoglobinuric nephrosis.[6,14]

Carcasses usually exhibit diffuse yellow discoloration (jaundice) of the subcutaneous tissue, fat and mucosae.[1,13] The liver can be enlarged and diffusely ochre/orange due to bile retention.[1,5] The spleen is often enlarged, dark and soft.[1,5] A black or dark red discoloration is present in the kidneys (colloquially referred to as gunmetal kidneys).[5,13] The

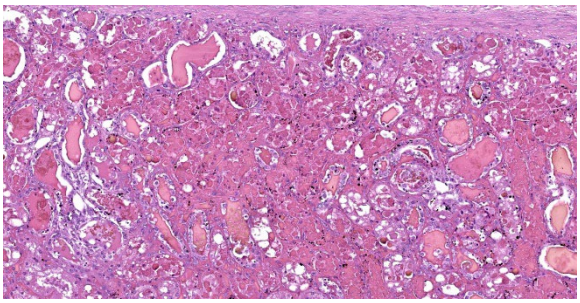

Figure 3-4. Kidney sheep. Higher magnification of affected tubular lumina, which contain variable amounts of luminal protein and hemoglobin casts. (HE, 147X)

urine is also dark red, resembling port-wine due to hemoglobinuria.[5,13]

Differential diagnoses for acute jaundice and hemoglobinuria/hemoglobinuric nephrosis in sheep include bacterial diseases such as bacillary hemoglobinuria (*Clostridium haemolyticum*) and eperythrozoonosis (*Mycoplasma ovis*), parasitic diseases such as bovine theileriosis (*Theileria lestoquardi*, *T. uilenbergior* and *T. luwenshuni*) and babesiosis (*Babesia ovis* and *B. motasi*), and plant toxicoses (*Allium cepa* and *Brassica* spp.). In lambs, leptospirosis, yellow lamb disease (*Clostridium perfringens* type A), and type D enterotoxemia (*C. perfringens* type D) should be considered as well.[3,8]

Frequent histological findings of copper poisoning include centrilobular hepatocellular necrosis accompanied by pigment laden Kupffer cells.[6,14] Rhodanine stain can be used to highlight intracellular copper. Portal mixed inflammatory infiltrates are also common.[1,6] Renal lesions usually consist of acute tubular necrosis with intratubular eosinophilic casts.[2,14] The deposition of iron-derived pigments in the cortical tubular epithelial cells, as seen in this case, has not been frequently described in the literature. However, a case presented in a previous Wednesday Slide

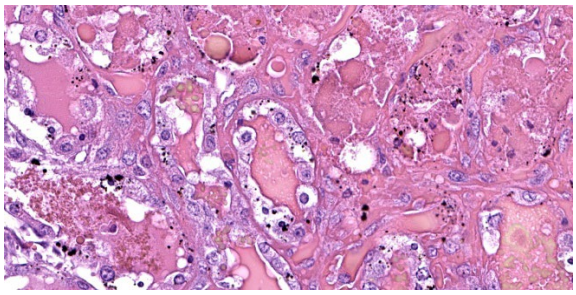

Figure 3-5. Kidney sheep. Tubular lumina contain abundant protein or hemorrhage/hemoglobin casts. Tubular epithelium is vacuolated and swollen with granular dark brown pigment or is necrotic with granular cytoplasm and sloughs into the lumen. (HE, 555X)

Conference (Case 1, Conference 14, WSC 2010-2011) also described this finding. In our case, the heavy metal screen revealed that the iron levels in the kidney were markedly elevated, with a less significant elevation in the liver. It is possible that, as intravascular hemolysis progresses, heme iron is released into the plasma, filtered through renal glomeruli and captured by proximal renal tubules eventually leading to histologically visible iron deposits (hemosiderin), which could be highlighted using special stains such as Perl's Prussian blue.

Unequivocal confirmation of copper toxicity requires determination of toxic copper levels in blood (>1.5 µg/ml), kidney (>15 ppm, wet weight) and/or liver (>250 ppm, wet weight), although it should be stressed that hepatic levels may decrease after copper is released into the bloodstream during the hemolytic crisis.[5,11]

Contributing Institution:
Plataforma de Investigación en Salud Animal, Instituto Nacional de Investigación Agropecuaria (INIA), La Estanzuela, Uruguay.

JPC Diagnosis:
1. Liver: Necrosis, centrilobular, diffuse, mild, with cholestasis and intracytoplasmic pigment.

2. Kidney: Tubular degeneration and necrosis, acute, diffuse, severe, with hemoglobin and protein casts.

JPC Comment:
The contributor provides an excellent case summary to accompany representative sections from the liver and kidney of this sheep. We agree that the changes in the kidney are severe, though the degree of necrosis within this section of liver is somewhat mild which surprised some participants. Possible explanations include slide/sampling variation as well as the notion that hepatocytes are able to extract oxygen from the portal vein with increasing efficiency during hypoxia. As such, they may be less immediately impacted by loss of erythrocytes/oxygen than the renal tubular epithelial cells supported by the vasa recta.

Conference participants discussed features of copper metabolism (or lack thereof) present within the liver. The large number of bile plugs (canalicular cholestasis) is accompanied by hepatocyte degeneration that is secondary to hypoxia and the growing anemic crisis. Together, these aspects highlight an increase in heme breakdown to biliverdin that is combined with the inability of hepatocytes to secrete bile constituents effectively. Rhodanine staining highlighted copper within hepatocytes and Kupffer cells, though iron staining was largely unremarkable despite the degree of hemolysis and elevated blood iron concentration in this case, likely attributed to intra- versus extravascular hemolysis. Masson's trichrome showed some bridging fibrosis, though this is an expected and probably

unrelated finding in an aged, grazing sheep, it is possibly indicative of the typical secondary hepatocyte injury, often plant toxicity, that initiates the cascade of hepatocyte death and copper release leading to hemolysis.

The changes in the kidney are classic in this case. We performed a Jones methenamine silver (JMS) and PAS stain to highlight the glomerular and tubular basement membrane – tubulorrhexis was not a feature of this case, however. We did not identify any copper within the kidney on rhodanine staining. Iron staining highlighted select renal tubular cells described by the contributor as containing hemosiderin; acid hematin is another differential to consider.

References:

1. Cullen JM, Stalker M. Liver and Biliary System. In: Maxie MG, ed. *Jubb, Kennedy and Palmer's Pathology of Domestic Animals*. 6th ed., Vol. 2. St. Louis, MO: Elsevier; 2016:258–352.
2. García-Fernández AJ, Motas-Guzmán M, Navas I, María-Mojica P, Romero D. Sunflower meal as cause of chronic copper poisoning in lambs in southeastern Spain. *Can Vet J*. 1999;40:799–801.
3. Giannitti F, Macias-Rioseco M, García JP, et al. Diagnostic exercise: hemolysis and sudden death in lambs. *Vet Pathol*. 2014; 51(3):624–627.
4. Gooneratne SR, Buckley WT, Christensen DA. Review of Copper Deficiency and Metabolism in Ruminants. *Can J Anim Sci*. 1989;69:819–845.
5. Gupta RK. A review of copper poisoning in animals: Sheep, goat and cattle. *Int J Vet Sci Anim Husb*. 2018;3:1–4.
6. Hovda LR. Disorders caused by toxicants. In: Smith BP, ed. *Large Animal Internal Medicine*. 5th ed. St.Louis, MO: Mosby; 2015:1578–1616.
7. López-Alonso M, Prieto F, Miranda M, Castillo C, Hernández J, Benedito JL. The role of metallothionein and zinc in hepatic copper accumulation in cattle. *Vet J*. 2005;169:262–267.
8. Maxie MG. *Jubb, Kennedy and Palmer's Pathology of Domestic Animals*. 6th ed. St. Louis, MO: Elsevier; 2016.
9. McCaughley WJ. Inorganic and Organic Poisons. In: Aitken ID, ed. *Diseases of Sheep*. 4th ed. Oxford, UK: Blackwell Science; 2007:424–439.
10. Millar M, Errington H, Hutchinson JP, Norton A. Copper poisoning in sheep associated with clover. *Vet Rec*. 2007;161:108.
11. Plumlee K. Metals and Minerals. In: *Clinical Veterinary Toxicology*. St. Louis, MO: Mosby; 2004:193–230.
12. Radostits OM, Gay CC, Hinchcliff KW, Constable PD. In: Veterinary medicine: *A textbook of the diseases of cattle, horses, sheep, pigs and goats*. 10th ed. New York, USA: Saunders Elsevier; 2007:1740-1741.
13. Roubies N, Giadinis ND, Polizopoulou Z, Argiroudis S. A retrospective study of chronic copper poisoning in 79 sheep flocks in Greece (1987-2007). *J Vet Pharmacol Ther*. 2008;31:181–183.
14. Villar D, Pallarés Martínez FJ, Fernández G. Retrospective study of chronic copper poisoning in sheep. *An Vet Murcia*. 2002;60:53–60.

CASE IV:

Signalment:
4-year-old, female, Nevisian Donkey, *Equus asinus,* equine.

History:
This animal initially presented with a 1-month history of chronic diarrhea and hyporexia. A fecal analysis returned a high

Figure 4-1. Liver, donkey. There are multifocal to coalescing, white-to-tan nodules that are often depressed and infiltrate the hepatic parenchyma. (*Photo courtesy of:* Department of Biomedical Sciences, Ross University School of Veterinary Medicine, St. Kitts, West Indies. www.veterinary.rossu.edu)

strongyle count and the animal was subsequently treated for parasites but, there was minimal clinical improvement. An abdominal ultrasound revealed significant peritoneal effusion, an abnormal appearance to the hepatic parenchyma, and an ill-defined mass caudal to the stomach that could not be distinguished as separate from the liver. Hematology, biochemistry, and abdominal fluid analysis was performed - supporting a diagnosis of hepatic disease (see section on laboratory results). Subsequent therapy involved treatment with gentamicin and ceftiofur sodium, which was eventually discontinued when peritoneal fluid analysis was inconsistent with a peritonitis. Heparin therapy was also instituted to treat presumptive hepatic lipidosis. The donkey was found collapsed in sternal recumbency three days later and was euthanized on humane grounds.

Gross Pathology:
The abdominal cavity contains approximately 9.5 L of light yellow, translucent, low-viscosity fluid. Multiple (~5 mm) pale, firm raised, nodules are present throughout the peritoneum, mesentery, serosal surfaces of the intestines and on the diaphragmatic surface of the spleen. The majority of the liver contains multifocal to coalescing, firm, white-to-tan, poorly demarcated nodules that measure 0.5-2.5 cm and occasionally have central depressions that are yellow and friable (necrosis). The remainder of the liver is pale yellow, friable, and overall, the liver is enlarged with rounded edges.

There is a large (approximately 20 cm x 10 x 6 cm) multilobulated tan mass in the region of the pancreas along the greater curvature of the stomach. Intra-abdominal lymph nodes are diffusely enlarged and prominent, with multiple nodes having multifocal to coalescing white-yellow lesions expanding the parenchyma with friable, yellow centers (necrosis).

The lungs are diffusely wet and rubbery and have mild rib impressions. Similar nodular lesions to that seen in the abdominal cavity are present in the lungs.

Laboratory Results:
Initial hematology:

Hyperproteinemia (9.0, RI:6.0-8.5g/dL), anemia (PCV 26, RI: 32-48), lymphopenia (0.5, RI: 1.5-5.0 $x10^3/\mu L$), monocytosis (0.9, RI: 0.0-0.6 1.5-5.0 $x10^3/\mu L$)

Abdominal fluid analysis:

Total protein 2.4 g/dL

Nucleated cell count: 0.15 $x10^3/\mu L$

Interpretation: Pure transudate

Abdominal fluid culture: aerobic and anaerobic culture yielded no growth.

Biochemistry on the day of euthanasia:

ALP	**2261**	50.0-170 U/L
ALT	**53**	5.0-20.0 U/L
GGT	**2125**	5.0-24.0 U/L
Bile Acids	**105**	0.0-25.0 µmol/L
TBIL	0.8	0.5-2.4 mg/dL
ALB	3.6	2.2-3.7 g/dL
BUN	9	7.0-25.0 mg/dL
CHOL	**155**	50.0-140.0 mg/dL
TRIGLYCERIDES	**>375**	11-68 mg/dL

Fungal culture of the mass yielded no growth.

Aerobic and anaerobic bacterial culture of the mass yielded rare growth of mixed bacteria. Negative for *Nocardia* sp., *Actinomyces* sp. or *Corynebacterium* sp. No anaerobes were isolated

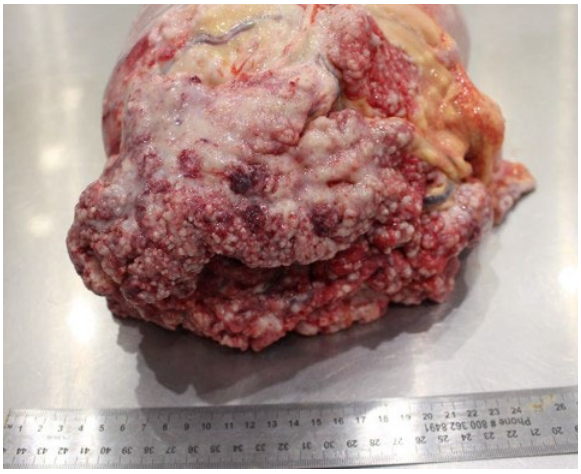

Figure 4-2. Liver, donkey. There is a multilobular mass in the region of the pancreas along the greater curvature of the stomach. (*Photo courtesy of:* Department of Biomedical Sciences, Ross University School of Veterinary Medicine, St. Kitts, West Indies. www.veterinary.rossu.edu)

Microscopic Description:
Liver: Effacing and replacing over 90% of the examined sections is a poorly demarcated, highly infiltrative, nonencapsulated neoplasm composed of islands of neoplastic epithelial cells forming cords, islands and ducts supported by moderate-to-abundant fibrocollagenous stroma. Neoplastic cells lining ductal structures are predominately columnar with a distinct brush border, variable amounts of pale eosinophilic cytoplasm, and a basilar nucleus with coarse chromatin and up to two small nucleoli. In contrast, neoplastic cells forming cords and islands are often polygonal with larger nuclei closely resembling hepatocytes. Anisocytosis and anisokaryosis are moderate and mitotic figures are rare. Rarely (and not in all sections), seemingly well-differentiated neoplastic hepatocytes appear to transition into neoplastic ductal structures. Within the neoplasm are multiple foci of coagulative necrosis and ducts are frequently filled with sloughed epithelial cells, cellular debris, and eosinophilic secretory material. Thick bands of fibrovascular tissue (scirrhous response) surround and expand the proliferating neoplastic cells and are infiltrated by low numbers of lymphocytes and plasma cells. The remaining, non-neoplastic hepatocytes have shrunken, pale eosinophilic cytoplasm and the hepatic capsule is thickened by fibrous connective tissue and lined by plump mesothelial cells.

Within sections of the pancreas, spleen, lung, and lymph node (not submitted) is a neoplastic process similar to that of the liver.

Immunohistochemistry (IHC): Sections of the mass adjacent to the pancreas and within the liver were labeled for Cytokeratin-19, and Hepar-1. The neoplastic cells forming ductal structures labeled positive with CK19 and mostly negative for Hepar-1. However, in transition zones between neoplastic cells forming cords and resembling hepatocytes

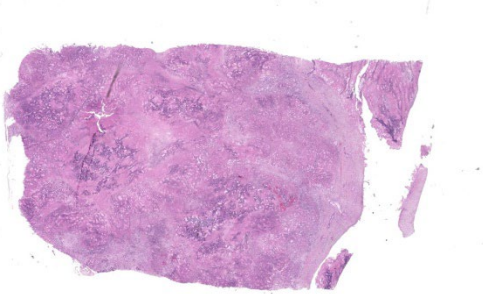

Figure 4-3. Liver, donkey. In this section of liver, normal hepatic architecture is replaced by a largely necrotic neoplasm. (HE, 5X)

and neoplastic ducts (presumably biliary) individual cells and clusters of cells in neoplastic ducts also labeled positive with Hepar-1.

Contributor's Morphologic Diagnosis:
Liver: Carcinoma (suspect cholangiolocarcinoma)

Contributor's Comment:
This case proved particularly challenging due to the extent and size of transcoelomic metastatic spread within the abdomen. The largest mass observed was in the region of the pancreas and this prompted the initial presumptive diagnosis of a pancreatic neoplasm. However, this was later disproven by microscopic examination and immunohistochemistry of the liver which demonstrated rare transitioning of hepatocytes into neoplastic biliary ducts which is more consistent with a hepatic or biliary neoplasm. In either case, both primary hepatic and pancreatic neoplasms are rare in donkeys and horses.[1,2,6]

A retrospective study of post-mortem findings in donkeys with a mean age of 30.6 years (n=1444) from the UK, found that only 4.2% of those examined (60/1444) had malignant liver neoplasms (cholangiosarcoma or bile duct carcinoma) and none had evidence of pancreatic neoplasms.[6] Similar findings were observed in a survey of donkeys diagnosed with neoplasia (n=125) in which 0.8% (1/125) were diagnosed with a primary hepatic neoplasm (biliary carcinoma) and none had pancreatic neoplasms.[2] Pancreatic adenocarcinoma in donkeys has only been reported twice in the literature with the diagnosis primary based upon location and appearance; no immunohistochemistry was performed in these cases.[3,7]

Classification schemes of primary hepatic tumors are not available for donkeys or horses but have recently been established in canines.[9] In general, primary liver neoplasms are characterized as either hepatocellular, cholangiocellular or neuroendocrine. Mature hepatocytes and cholangiocytes are the proposed origin of primary epithelial liver tumors; however cholangiolocarcinomas are believed to originate from hepatic progenitor cells and have hepatocellular, ductular and cholangiocellular characteristics.[4,9] According to the canine classification scheme, cholangiolocarcinomas differ from cholangiocellular carcinomas morphologically due to the presence of central tubular structures surrounded by solid areas with the appearance of hepatic cords or acini.[9] Furthermore, IHC patterns typical of canine tumors are distinct with tubular structures labelling positive for Keratin-19, EMA/MUC-1 and CD10 while the solid hepatocyte-like areas were positive for Keratin-19 and negative for HepPar-1, EMA/MUC-1 and CD10.

Though not a described entity in donkeys, this case most likely represents a cholangiolocarcinoma or less likely, a cholangiocellular carcinoma.

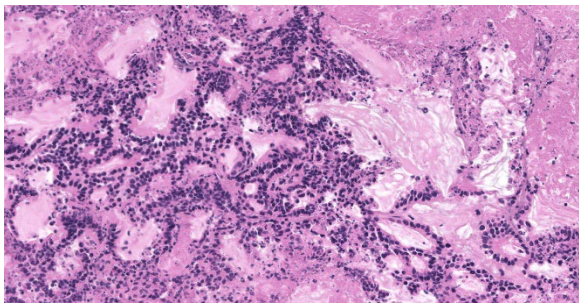

Figure 4-4. Liver, donkey. Neoplastic epithelium forms tubules within large areas of necrosis. (HE, 314X)

Contributing Institution:
Department of Biomedical Sciences

Ross University School of Veterinary

Medicine, P. O. Box 334; Basseterre, St. Kitts, West Indies

www.veterinary.rossu.edu

JPC Diagnosis:
Liver: Cholangiocellular carcinoma.

JPC Comment:
The final case of this conference is an interesting neoplasm with several great gross photos. From subgross magnification, conference participants quickly identified invasive behavior and neoplastic spread through the adjacent parenchyma, though evidence of lymphovascular invasion was less definitive. We repeated IHC for HepPar-1, CK7, and CK19 and performed PAS-Alcian Blue and Masson's trichrome stains. IHC results were similar to the contributor – special stains highlighted mucus within neoplastic bile ducts and periductular fibrosis. Based on morphology, we favored a malignant epithelial neoplasm of biliary origin (i.e. cholangiocarcinoma).

The degree of fibrosis (scirrhous response) is fairly mild in this case compared with other cholangiocarcinomas. Dr. Cullen again highlighted the relationship of biliary epithelium, mesenchyme, and myofibroblasts that was explored in Case 1. Rather than a 'disjointed conversation' leading to inappropriate proliferation of bile ducts and connective tissue as was seen in ductal plate malformation, the phenotype in neoplasia is tilted in favor of collagen fiber deposition with ductular reaction being a minor feature.

Finally, Dr. Cullen weighed in on the idea of a cholangiolocarcinoma for this case. As the contributor hints at, exact definitions of this rare neoplasm are hard to come by with few published cases – as such, readers may benefit from a quick review of Komuta et al[4] which has some excellent figures. MacSween's Pathology of the Liver (a veritable grail of hepatology) itself lacks a definition. Recently published human cases each differed in their microscopic descriptions of the tumor as well.[5,7] The use of IHC is potentially chal-

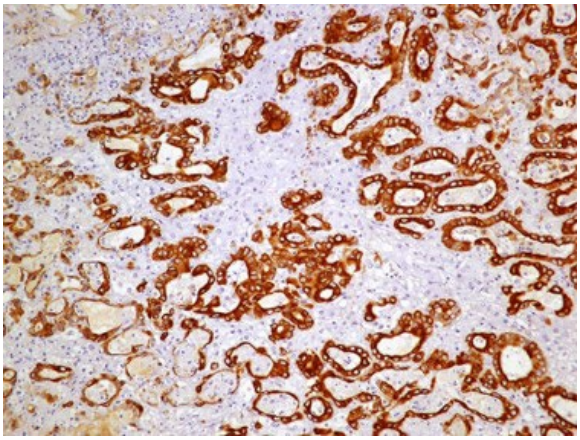

Figure 4-5. Liver, donkey. Immunohistochemical staining for CK19 demonstrates immunopositivity within the cytoplasm of neoplastic cells with ductal morphology. (anti-cytokeratin 19, 400X) (*Photo courtesy of:* Department of Biomedical Sciences, Ross University School of Veterinary Medicine, St. Kitts, West Indies. www.veterinary.rossu.edu)

lenging as ruling out metastatic adenocarcinoma may be complicated by lack of complete specificity. For example, many duct forming epithelia, as well as salivary epithelium may react with CK7 and select GI epithelial cells may be positive for HepPar-1. Hepatic progenitor cells may also variably express chromogranin A, similar to a biliary carcinoid. As such, we felt most confident that the neoplasm in this case had features supportive of a cholangiocarcinoma on H&E without IHCs to refute this interpretation.

References:

1. Beeler-Marfisi J, Arroyo L, Caswell JL, Delay J, Bienzle D. Equine primary liver tumors: A case series and review of the literature. *J Vet Diag Invest*. 2010;22:174–183.
2. Davis CR, Valentine BA, Gordon E, et al. Neoplasia in 125 donkeys (*Equus asinus*): literature review and a survey of five veterinary schools in the United States and Canada. *J Vet Diag Invest*. 2016;28:662–670.
3. Kerr OM, Pearson GR, Rice DA. Pancreatic adenocarcinoma in a donkey. *Equine Vet J*. 1982;14:338–339.
4. Komuta M, Spee B, Borght S, Vander, et al. Clinicopathological study on cholangiolocellular carcinoma suggesting hepatic progenitor cell origin. *Hepatology.* 2008;47:1544–1556.
5. Makino K, Ishii T, Takeda H, et al. Integrated analyses of the genetic and clinicopathological features of cholangiolocarcinoma: cholangiolocarcinoma may be characterized by mismatch-repair deficiency. *J Pathol*. 2024 May;263(1):32-46.
6. Morrow LD, Smith KC, Piercy RJ, et al. Retrospective Analysis of Post-Mortem Findings in 1,444 Aged Donkeys. *J Comp Pathol*. 2011;144:145–156.
7. Sato N, Yamamura K, Oda E, et al. Cholangiolocarcinoma With Multiple Recurrences Successfully Treated With Repeated Liver Resection and Radiofrequency Ablation. *Anticancer Res*. 2020 Dec;40(12):7147-7153.
8. Spanton JA, Mair TS, Krudewig C. Pancreatic adenocarcinoma in a donkey. Use of laparoscopy to aid the diagnosis. *Equine Vet Educ*. 2009;21:19–24.
9. Van Sprundel RGHM, Van den Ingh TSGAM, Guscetti F, et al. Classification of primary hepatic tumours in the dog. *Vet J*. 2013;197:596–606.

Joint Pathology Center
Veterinary Pathology Services

WEDNESDAY SLIDE CONFERENCE 2024-2025

Conference #13 04 December 2024

CASE I:

Signalment:
20-year-old, male, African lion, *Panthera leo*, Felidae.

History:
This lion had a clinical picture characterized by mild bleeding in the oral cavity, which lasted approximately for two weeks, and had been associated with an increase of the volume of the mandible. After this time, hemorrhagic episodes were observed sporadically.

Gross Pathology:
During the examination of the mandible, there was a firm, irregular mass, approximately 3.0 cm in length, with white areas interspersed with yellow foci located in the mandibula at the height of the lower left canine. Dental mobility of mandibular canines and a fracture of the mandibular bone, near to the mental protuberance were noted.

Microscopic Description:
Histopathology of the mandible revealed a non-encapsulated, expansive and infiltrative mass consisting of markedly pleomorphic keratinocytes, arranged either in mantles or in solid nests, supported by moderate to large fibrovascular stroma. In the center of some of these nests, deposition of lamellar eosinophilic material (keratin pearls) was noted and, occasionally, individual keratinocytes exhibited dyskeratosis. These cells have polygonal contours, moderate to broad cytoplasm,

Figure 1-1. Mandible, lion. Within the fractured mandible, there is a 3cm firm, irregular mass. (*Photo courtesy of:* Federal Rural University of Pernambuco, www.ufrpe.br)

slightly eosinophilic, and round to oval vesicular nuclei with loose chromatin and 1 to 2 evident nucleoli. Moderate anisocytosis, anisokaryosis, and multifocal areas of intratumoral necrosis are noted. Mitotic counts are 2-4 mitosis per higher magnification field (40X).

Contributor's Morphologic Diagnosis:
Well-differentiated squamous cell carcinoma.

Contributor's Comment:
Squamous cell carcinoma (SCC) is one of the main oral cavity tumors in domestic cats and may represent more than 60% of all oral tumors in this species.[1] In wild felids however,

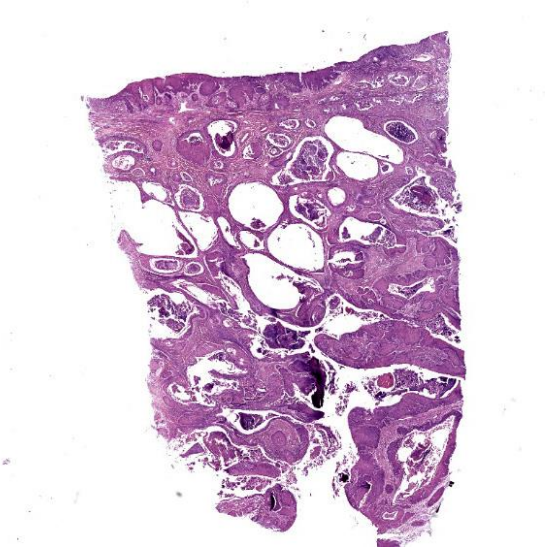

Figure 1-2. Mandible, lion. One section of mandibular mucosa is submitted for examination. Extending downward from the mucosa, there are numerous islands and trabecular of neoplastic keratinizing squamous epithelium. (HE, 5X)

its description is sporadic and current records include tumors affecting the oral cavity of lynxes and ocelots,[2-4] the ear of leopards,[5,6] the eyelid region of white tigers,[7,8] the jaw of a Siberian tiger,[9] and the leopard right hind limb.[10] In *Panthera* sp. the diagnosis of SCC is better described in the snow leopard (*P. uncia*),[11] in which cutaneous and oral SCCs can represent up to 9% of the causes of death.[12]

The high frequency of papillomas and oral SCCs associated with the isolation of papillomaviruses in *P. uncia* strengthens the hypothesis of the participation of viruses in the etiology of SCC in large felids.[12,15,16,20] Other potential factors that may be related to carcinogenesis of oral SCC in these animals include pollution of urban centers[9] as well previous dental diseases.[17,18] In large felids, the upper and lower incisors seem to show a tendency for periodontal disease[17,18] and are common sites of neoplasm growth in lions.[9,19,20] It is important to highlight that the captive environment can influence the formation of calculi and periodontal diseases in tigers and lions as compared to free-living species,[18] which can favor the formation of pre-neoplastic lesions.

The tongue and mandible seem to be important anatomical sites for SCCs in large felids, appearing as masses of rapid growth that are generally ulcerated and hemorrhagic with progressively infiltrative behavior. Microscopically, features such as the formation of keratin beads and individual keratinization of keratinocytes favored the diagnosis of SCC, considering that they are classic findings of neoplasia in well-differentiated to moderately-differentiated cases. Tumor expansiveness even favored bony lysis and cutaneous fistulation as identified in this case, whose clinical progression, degree of metastasis and evolution to death tend to be quite variable between species.

As there are few reports in the literature on wild felids, there is no definitive parameter on the survival time in cases of oral SCC in these animals. In domestic cats, neither the size of the mass nor its location in the mouth seem to be associated with survival time.[21] Important differential diagnoses in lions include potential oral cavity tumors already reported in the species, such as peripheral odontogenic fibroma, mucoepidermoid carcinoma of the salivary gland, melanomas, hemangiosarcomas and fibrosarcomas.[20,22-24]

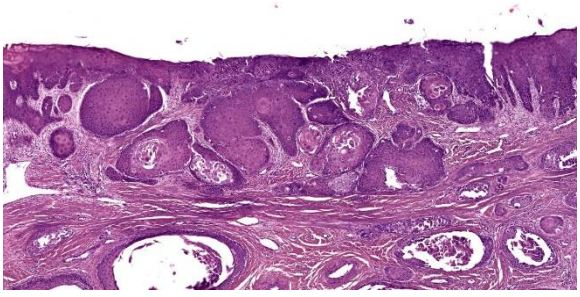

Figure 1-3. Mandible, lion. Neoplastic squamous epithelium extends downward in irregular trabeculae and islands from the oral mucosa. (HE, 57X)

Contributing Institution:
Federal Rural University of Pernambuco
Laboratory of Animal Diagnosis
Rua Dom Manoel de Medeiros
Dois Irmaos, Recife, 52171-900
Pernambuco, Brazil. www.ufrpe.br

JPC Diagnosis:
Mucosal surface (presumptive oral mucosa): Squamous cell carcinoma.

JPC Comment:
This week's moderator was Major Anna Travis, JPC Chief of Education Operations who selected an eclectic group of cases for conference participants to consider.

The contributor nicely summarizes oral SCC and oral pathology in non-domestic felids, to include a number of helpful references for those interested in reading further on this topic. Squamous cell carcinoma is the most common oral malignancy in all felids, including non-domestic ones.[20] Other notable oral predilections include FEPLOs in lions, oral papillomas in snow leopards, and eosinophilic inflammation in tigers.[20]

SCC remains a frequent WSC submission across species – the case discussion focused on associated general pathology features common across species, including keratinization. Basal cells exhibit basophilia in part due to large numbers of free ribosomes producing keratin filaments (protein; tonofilaments) that give strength to the epidermal layer. In the stratum spinosum, an even greater proportion of tonofilaments are bundled to form tonofibrils that interface with a greater number of desmosomes which further enhances tissue strength.[25] In the granular layer, keratohyalin granules containing profilaggrin serve to bind tonofibrils into larger macrofibrils. Squamous cells subsequently lose cellular organelles and nuclear contents as they transition to the stratum corneum.[25] As such, SCC represents

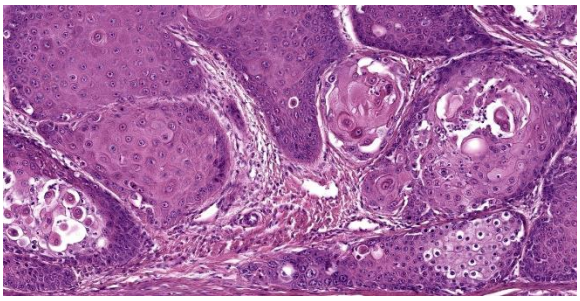

Figure 1-4. Mandible, lion. High magnification of neoplastic squamous epithelium. Within the center of nests, neoplastic cells often become individualized. (HE, 57X)

aberrancy of ordered keratinization as was evident in this case.

Conference participants discussed the exact location of this neoplasm as they lacked the terrific gross image for this case provided by the contributor. While the lack of adnexal units and presence of a non-keratinizing (lacking keratohyalin granules) epithelium were suggestive of the oral cavity, MAJ Travis reminded participants to also consider the pharynx, conjunctiva,esophagus, rectum, vulva, and even vagina as potential locations (although in felids, the oral mucosa is by far the most common location for this neoplasm).

References:

1. Murphy BG, Bell CM, Soukup JW. *Veterinary Oral and Maxillofacial Pathology*. 1st ed. Wiley-Blackwell; 2020:143.
2. Altamura G, Eleni C, Meoli R, et al. Tongue Squamous Cell Carcinoma in a European Lynx (Lynx Lynx): Papillomavirus Infection and Histologic Analysis. *Vet Sci*. 2018; 5(1):1.
3. Sladakovic I, Burnum A, Blas-Machado U, et al. Mandibular squamous cell carcinoma in a bobcat (Lynx rufus). *J Zoo Wildl Med*. 2016; 47(1): 370-373.
4. Yanai T, Noda A, Murata K, et al. Lingual squamous cell carcinoma in an ocelot (Felix pardalis). *Vet Rec*. 2003;

152(21):656-657.
5. Quintard B, Greunz EM, Lefaux B, et al. Squamous cell carcinoma in two snow leopards (Uncia uncia) with unusual auricular presentation. *J Zoo Wildl Med*. 2017; 48(2):578–580.
6. Leme MCM, Martins AMCRPF, Bodini MES, et al. Carcinoma de células escamosas em uma jaguatirica (Leopardus pardalis). *Arq Inst Biol*. 2003; 70(2):217-219.
7. Bose VSC, Nath I, Mohanty J, et al. Epidermoid carcinoma of the eyelid in a tiger (Panthera tigris). *Zoos' Print*, 2002; 17:965-966.
8. Gupta A, Jadav K, Nigam P, et al. Eyelid neoplasm in a White Tiger (Panthera tigris) - a case report. *Vet Archiv*. 2013; 83(1):115-124.
9. Oliveira AR, Carvalho T, Arenales A, et al. Mandibular squamous cell carcinoma in a captive Siberian tiger (Panthera tigris altaica). *Braz J Vet Pathol*. 2018; 11:97-101.
10. Kesdangsakonwut S, Sanannu S, Rungsipipat A, et al. Well-differentiated Squamous Cell Carcinoma in a Captive Clouded Leopard (Neofelis nebulosa). *Thai J Vet Med*. 2014; 44(1):153-157.
11. Napier JE, Lund MS, Armstrong DL, et al. A retrospective study of morbidity and mortality in the North American amur leopard (Panthera pardus orientalis) population in zoologic institutions from 1992 to 2014. *J Zoo Wildl Med*. 2018; 49(1):70–78.
12. Joslin JO, Garner M, Collins D, et al. Viral papilloma and squamous cell carcinomas in snow leopards (Uncia uncia). *American Association of Zoo Veterinarians and International Association for Aquatic Animal Medicine Joint Conference*, 2000: 155–158.
13. Bertone ER, Snyder LA, Moore AS. Environmental and Lifestyle Risk Factors for Oral Squamous Cell Carcinoma in Domestic Cats. *J Vet Intern Med*. 2003; 17(4):557-562.
14. Munday JS, Howe L, French A, et al. Detection of papillomaviral DNA sequences in a feline oral squamous cell carcinoma. *Res Vet Sci*. 2009; 86(2): 359–361.
15. Sundberg JP, Montali RJ, Bush R, et al. Papillomavirus-associated focal oral hyperplasia in wild and captive Asian lions (Panthera leo persica). *J Zoo Wildl Med*. 1996; 27(1):61–70.
16. Terio KA, McAloose D, Mitchell E. *Pathology of Wildlife and Zoo Animals*. 1st ed. Elsevier; 2018:263-285.
17. Collados J, Garcia C, Soltero-Rivera M, et al. Dental Pathology of the Iberian Lynx (Lynx pardinus), Part II: Periodontal Disease, Tooth Resorption, and Oral Neoplasia. *J Vet Dent*. 2018; 35(3):209–216.
18. Kapoor V, Antonelli T, Parkinson JA, et al. Oral health correlates of captivity. *Res Vet Sci*. 2016; 107:213-219.
19. Castro MB, Barbeitas M, Borges T, et al. Fibromatous Epulis in a Captive Lion (Panthera leo). *Braz J Vet Pathol*. 2011; 4:150-152.
20. Scott KL, Garner MM, Murphy BG, et al. Oral Lesions in Captive Nondomestic Felids With a Focus on Odontogenic Lesions. *Vet Pathol*. 2020; 57(6):880-884.
21. Northrup NC, Selting KA, Rassnick KM, et al. Outcomes of cats with oral tumors treated with mandibulectomy: 42 cases. *J Am Anim Hosp Assoc*. 2006; 42(5):350-360.
22. Junginger J, Hansmann F, Herder V, et al. Pathology in Captive Wild Felids at German Zoological Gardens. *PLoS One*. 2015; 10(6):e0130573.
23. Kloft HM, Ramsay EC, Sula MM. Neoplasia in Captive Panthera Species. *J Comp Pathol*. 2019; 166:35-44.
24. Steeil JC, Schumacher J, Baine K, et al. Diagnosis and treatment of a dermal malignant melanoma in an African lion

(Panthera leo). *J Zoo Wildl Med*. 2013; 44(3):721-727.
25. Welle MM, Linder KE. The Integument. In: Zachary JF, ed. *Pathologic Basis of Veterinary Disease*. 7th ed. St. Louis, MO: Elsevier; 2022:1095-1096.

CASE II:

Signalment:
Adult, female, Sprague-Dawley rat (*Rattus norvegicus)*

History:
An adult, female, Sprague-Dawley rat, belonging to an intentional breeding colony was presented for diagnostic investigation of hind limb paresis. This animal had been fed Certified Rodent Diet 5002 (PMI Feeds, Inc) and given municipal water *ad libitum*, and only used for intravenous administration training without any active pharmaceutical ingredient. All procedures performed on the animal were in accordance with regulations and established guidelines reviewed and approved by an Institutional Animal Care and Use Committee.

Figure 2-1. Lymph nodes, rat. Cervical and mandibular lymph nodes are enlarged and greenish. (*Photo courtesy of:* Pfizer Drug Safety Research and Development, https://www.pfizer.com/partners/research-and-development).

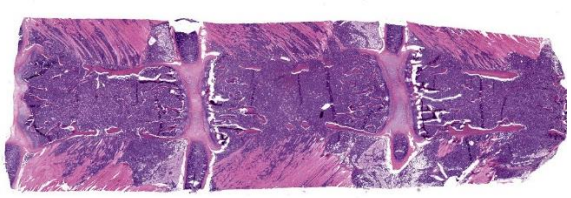

Figure 2-2. Sternum, rat. A section of sternum is submitted for examination. Neoplastic cells efface the marrow of the sternebrae and extend through the cortex into the adjacent skeletal muscle. (HE, 11X)

Gross Pathology:
A gross examination revealed enlargement and greenish discoloration of multiple lymph nodes, including iliac, inguinal, mesenteric, popliteal, and mandibular lymph nodes. The spleen was also enlarged and the femoral bone marrow appeared green. A comprehensive set of tissues were collected in 10% neutral buffered formalin. All collected tissues were routinely processed and stained with hematoxylin and eosin (H&E) for light microscopic examination.

Microscopic Description:
Sternum, bone marrow: Neoplastic cells had large, vesicular nuclei that varied in shape from round, segmented, lobulated, to ring shaped, and contained a small amount of slightly eosinophilic cytoplasm. They were noncohesive and arranged in diffuse sheets. There were approximately 5 mitotic figures per high power (400X magnification) field noted in the neoplastic cells in the bone marrow. Throughout the sheets of neoplastic cells in many of the affected tissues, there were small to moderate numbers of scattered large macrophages that contained phagocytized apoptotic cell debris.

Neoplastic cells completely replaced the normal hematopoietic elements in the medullary cavity of the sternum and had infiltrated into the surrounding bone, skeletal muscles, and joints.

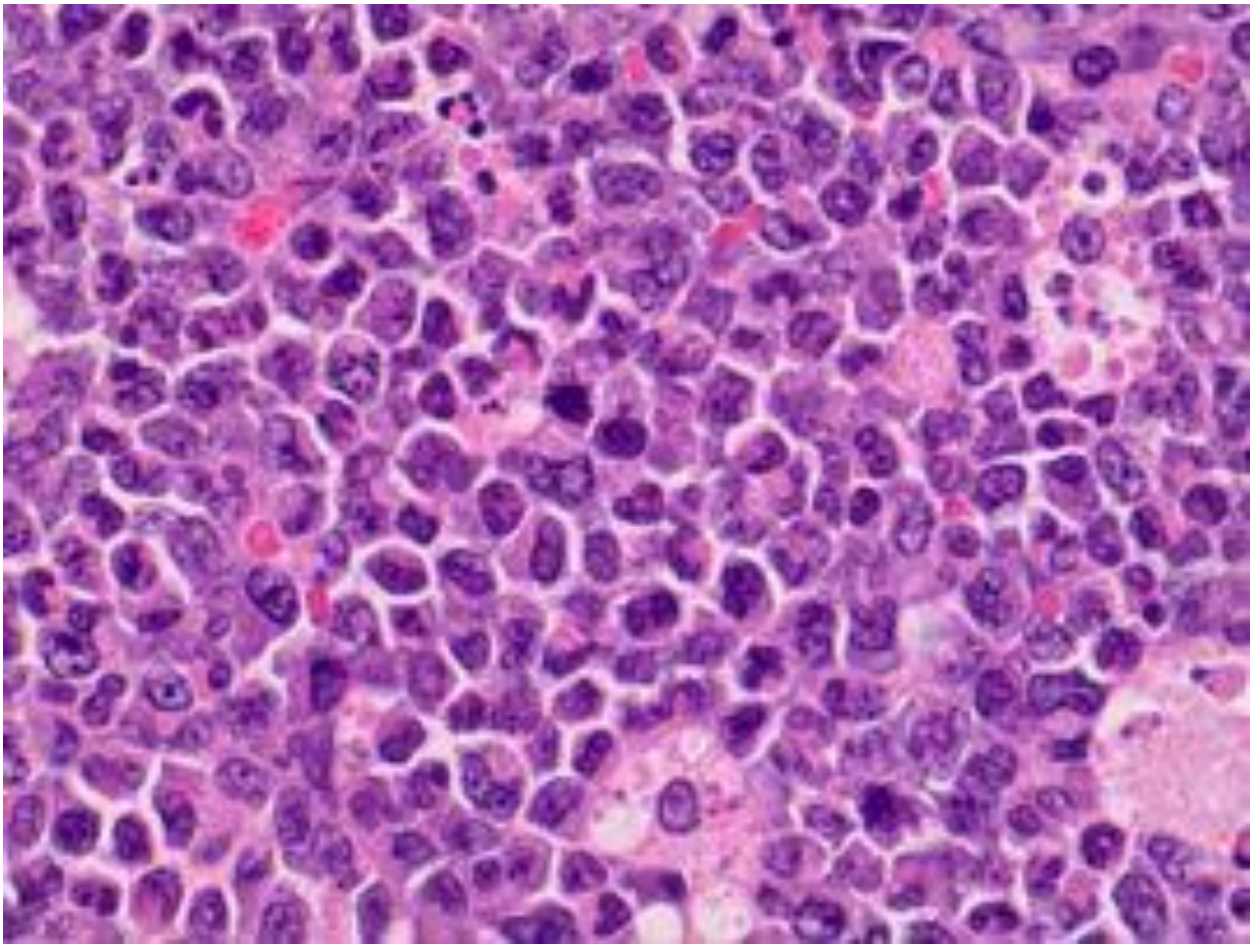

Figure 2-3. Bone marrow, rat. Neoplastic cells have large, vesicular nuclei that varied in shape from round, segmented, lobulated, to ring shaped. Note there are scattered apoptotic figures. (HE, 400X) (*Photo courtesy of:* Pfizer Drug Safety Research and Development, https://www.pfizer.com/partners/research-and-development)

Representative sections were selected for Iba-1 and MPO (myeloperoxidase) immunohistochemistry (IHC). Immunohistochemically, neoplastic cells within the bone marrow had strong cytoplasmic immunoreactivity for MPO, which is the hallmark of the myeloid lineage. Cellular debris-laden macrophages scattered throughout the sheets of neoplastic cells had strong membranous immunoreactivity for Iba-1, a macrophage marker.

Contributor's Morphologic Diagnosis:
Sternum/Bone marrow, myeloid leukemia in a Sprague-Dawley Rat

Contributor's Comment:
The current case was diagnosed as myeloid leukemia based on the characteristic cytological morphology and immunohistochemistry profile of the neoplastic cells. Various amounts of nuclear indentation noted among neoplastic cells was indicative of granulocytic differentiation and was suggestive of a more chronic leukemic process. Diffuse immunoreactivity of neoplastic cells for MPO

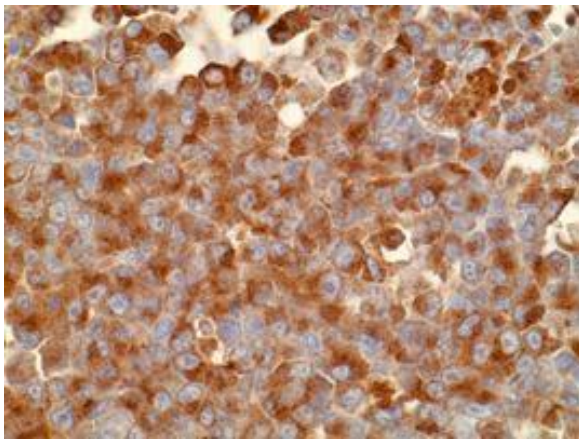

Figure 2-4. Bone marrow, rat. Neoplastic cells have strong expression of cytoplasmic myeloperoxidase. (anti-MPO, 400X) (*Photo courtesy of:* Pfizer Drug Safety Research and Development, https://www.pfizer.com/partners/research-and-development)

indicated that the cells stemmed from myeloid lineage because MPO is expressed by myeloid cells at all stages.

Massive inflammatory reactions to lesions in the skin or internal organs can stimulate compensatory myelopoiesis and result in remarkable extramedullary hematopoiesis and/or myeloid hyperplasia in the spleen and other organs as well as bone marrow, mimicking myeloid leukemia. The current case was differentiated from those compensatory reactions to inflammatory stimuli based on its invasive growth pattern, destruction of bone tissue associated with bone marrow proliferation, and the absence of inflammatory lesions.[4,6]

The macroscopic finding of green discoloration observed in the enlarged lymph nodes and bone marrow of the rat described in the current case report is associated with chloromas in humans, which has been described as a mass composed of immature granulocytic cells. This tumor occurs primarily in patients with myelogenous leukemia and typically has a green color caused by high levels of myeloperoxidase in those immature granulocytic cells.[2]

In the current case, the neoplasia was multicentric and with an invasive growth pattern. The presenting clinical finding of hind limb paresis was ascribed to extensive infiltration of neoplastic cells from the bone marrow through adjacent bones, joints, and skeletal muscles in the hind limb region. There was no evidence of tumor cell infiltration into the spinal cord or brain sections examined.

Hyaline droplets occurred in the renal proximal tubules in the current case. Hyaline droplets are known to accumulate in the identical segments of renal tubules in rats with a different neoplasm, histiocytic sarcoma. These droplets have been identified as lysozyme, which is a major secretory product of monocytes and macrophages.[3] It is important to note that IBA1 immunohistochemistry results demonstrated that apoptotic figures scattered throughout the sheets of neoplastic cells were cellular debris-laden macrophages. As with lysozyme in the case of histiocytic sarcoma, excessive production of this protein by activated macrophages is considered to be the likely cause of renal accumulation.

Contributing Institution:
Pfizer Drug Safety Research and Development
455 Eastern Point Rd.,
Groton, CT 06340
https://www.pfizer.com/partners/research-and-development

JPC Diagnosis:
Bone marrow and skeletal muscle: Myeloid leukemia.

JPC Comment:
We agree with the contributor that the tissue submitted represents a hematopoietic neoplasm for the histologic features they so nicely capture in their discussion. Conference participants honed in on infiltration of the

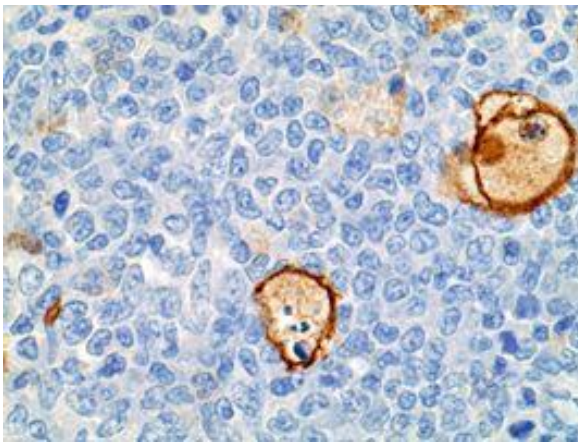

Figure 2-5. Bone marrow, rat. Scattered large macrophages that contain phagocytized apoptotic cell debris (apoptotic figures) have strong membranous expression of Iba-1 (anti-IBA1, 400X) (*Photo courtesy of:* Pfizer Drug Safety Research and Development, https://www.pfizer.com/partners/research-and-development)

surrounding adipose tissue and muscle by neoplastic cells as well as the effacement of the marrow cavity and loss of trabecular and cortical bone as major features of this case.

We performed IHCs for IBA1, myeloperoxidase, lysozyme, CD3, CD33, CD34, CD56, CD117, PAX5, as well as an EBER ISH. We confirmed the background of tumor-associated macrophages with IBA1 (while also ruling out histiocytic sarcoma), though our results for MPO, lysozyme, CD33, and CD34 were equivocal and we could not reproduce the contributor's IHC result. Curiously, we did note moderate immunoreactivity of neoplastic cells for CD3 and CD56 which suggests a potential (although we feel unlikely) potential T-lymphocyte origin for these cells, though our lab is not optimized for rodent IHCs. As such, we rendered a H&E diagnosis for the case. ISH and other IHCs for this case were unremarkable.

We previously covered hyaline droplets in rodents in a recent (WSC 24-25, Conference 6, Case 1) which featured a histiocytic sarcoma within the kidney itself. We also considered myeloid leukemia in that case – incidentally, the morphology of neoplastic cells is very similar. Ruleouts for hyaline droplets include histiocytic sarcoma,[3] lymphoma,[1] chronic progressive nephropathy, and alpha-2u globulin nephropathy.[5]

References:

1. Decker JH, Dochterman LW, Niquette AL, et al. Association of Renal Tubular Hyaline Droplets with Lymphoma in CD-1 Mice. *Toxicol Pathol*. 2012; 40: 651-655.

2. Ginsberg LE, Leeds NE. Neuroradiology of leukemia. *AJR*. 1995;165:525-534.

3. Hard GC, Snowden RT. Hyaline droplet accumulation in rodent kidney proximal tubules: An association with histiocytic sarcoma. *Toxicol Pathol*. 1991;19:88-97.

4. Long RE, Knutsen G, Robinson M. Myeloid hyperplasia in the SENCAR mouse: Differentiation from granulocytic leukemia. *Environ Health Persp*. 1986;68:117-123.

5. Swenberg JA, Short B, Borghoff S, Strasser J, Charbonneau M. The comparative pathobiology of alpha 2u-globulin nephropathy. *Toxicol Appl Pharmacol*. 1989 Jan;97(1):35-46.

6. Ward JM, Rehg JE, Morse HC. Differentiation of rodent immune and hematopoietic system reactive lesions from neoplasia. *Toxicol Pathol*. 2012;40:425-434.

CASE III:

Signalment:
Juvenile, female, giant Pacific octopus (*Enteroctopus dofleini*)

History:
This giant Pacific octopus arrived at the submitting zoo after an extended period at an outgoing airport. During the first week at the

zoo, the animal was eating well but was staying at the bottom of the enclosure. Shortly thereafter, the octopus stopped eating and was found to have several injuries consistent with self-mutilation and damage by the cohabitant anemones. Water quality was within normal limits. The octopus was found deceased a few days later.

Gross Pathology:
Macroscopic lesions included skin erosions and ulcerations and distal limb amputations. The digestive gland was uniformly soft, tan-pink, and bulging on cut section. There were no significant macroscopic lesions of the renal appendages.

Laboratory Results:
Aerobic culture of the digestive gland yielded *Carnobacterium* sp. (1+ mixed) and *Vibrio* sp. (4+ predominant).

Microscopic Description:
Renal appendage: The renal appendage is composed of folds and tubules lined by simple columnar epithelium supported by a fibrovascular stroma and separated by venous sinuses. The epithelial cells are large, with basal nuclei, mild apical vacuolation, and a brush border. Anisocytosis and anisokaryosis of the renal epithelial cells is moderate to marked. Copious globular, eosinophilic material is present within tubule lumina, and homogeneous, eosinophilic secretory product multifocally fills sinus lumina. Along the epithelial surfaces, there are innumerable cross-sectional and tangential profiles of multicellular, vermiform organisms at various stages of maturation, with no apparent associated inflammatory reaction. The organisms measure approximately 25 to 100 micrometers in diameter and consist of a central axial cell enveloped completely by a layer of ciliated peripheral cells. Several large peripheral cells with short or inapparent cilia comprise the anterior ends of the organisms (interpreted as

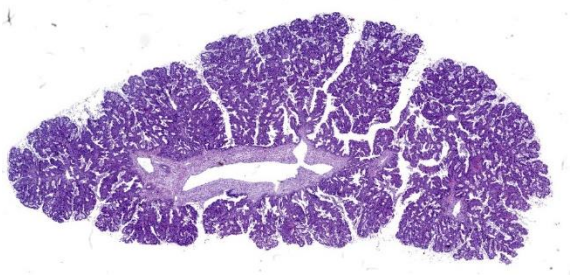

Figure 3-1. Renal appendage, octopus. One section of renal appendage is submitted for examination. (HE, 7X)

the calotte), which commonly abut the renal epithelial cells and obscure the brush border. At these sites, the epithelial cells are variably attenuated. Within the axial cell cytoplasm in a majority of the organisms, there are one or more developing embryos and single cells (agametes or fertilized eggs). The developing embryos are multicellular, often organized into an elongate structure or forming a round to oval cluster of cells (vermiform and infusoriform embryos).

Contributor's Morphologic Diagnosis:
Renal appendage: intraluminal dicyemid organisms, widespread, marked, chronic

Contributor's Comment:
The renal organs of octopuses consist of folded tissue that protrudes into the renal sac. The degree of tissue folding generally increases with the size of the organism and increases excretory capacity.[10] The folds form tubules lined by a simple columnar epithelium and separated by sinuses that originate from the vena cava. Within the tubule and renal sac lumina, one may find a variety of worm-like dicyemid organisms that are often attached to the renal epithelium without eliciting an inflammatory response.[1,3]

Dicyemids (phylum Dicyemida) are mesozoans found within the renal organs of many cephalopod species, and were an incidental finding in this giant Pacific octopus (Enter

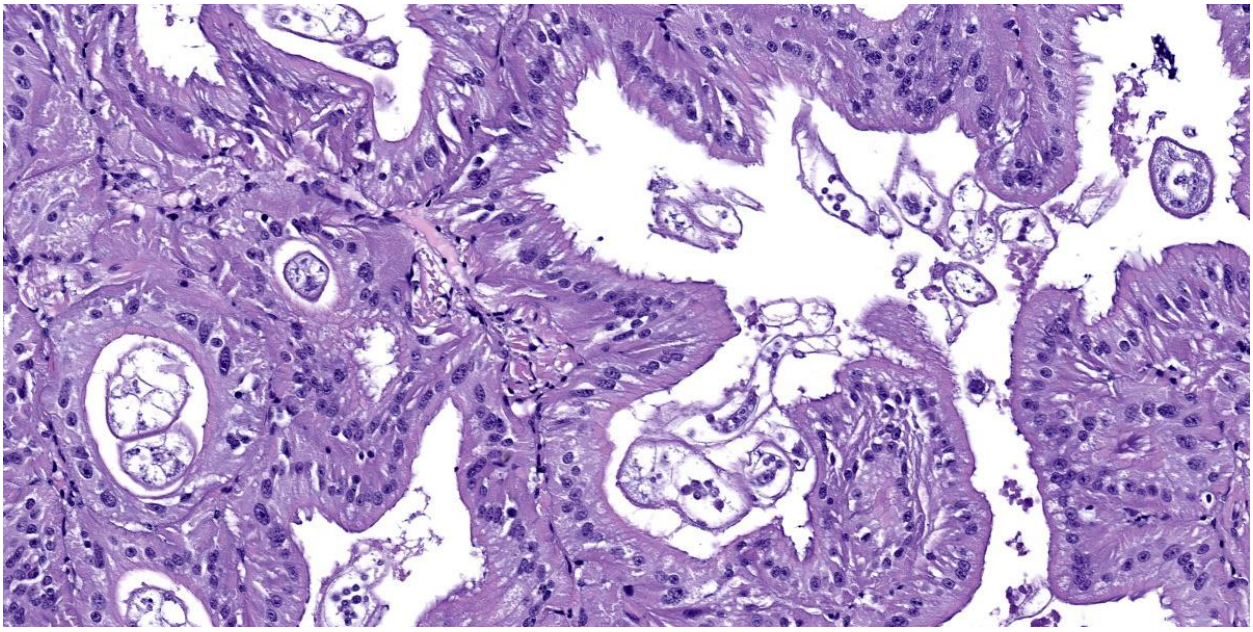

Figure 3-2. Renal appendage, octopus. Within the sinus lumina, there are numerous cross- and tangential sections of multicellular, vermiform organisms at various stages of maturation, with no apparent associated inflammatory reaction. The organisms measure approximately 25 to 100 micrometers in diameter and consist of a central axial cell enveloped completely by a layer of ciliated peripheral cells. (HE, 202X)

octopus *dofleini*). Dicyemids have been variably described as endosymbionts and as endoparasites, as they attach to the renal epithelium of the host, absorb nutrients from the urine through their peripheral cells, and can be present in large numbers. Regardless, they have not been shown to damage the renal organs or be detrimental to the host.[1] Their postulated benefits include acidification of the urine to aid excretion of ammonia and maintenance of urine flow by their ciliary movements.[1,10,14]

There are 149 documented dicyemid species to date, all of which exhibit a remarkably simple body plan that left many questions about their evolutionary origins.[15] They were initially classified as mesozoa for presumptively representing an intermediate between protozoa and metazoa. While the phylogenetic particulars of these organisms are arguably uncertain, current evidence indicates they arose from metazoan ancestors as a result of evolutionary simplification with genome reduction.[4,14]

The dicyemid life cycle consists of vermiform and infusoriform stages. Mature dicyemids are vermiform and exist within the renal organ as a nematogen, a primary rhombogen, or a secondary rhombogen.[11] These adults possess a central axial cell with intracytoplasmic agametes that is fully surrounded by 8 to 30 ciliated peripheral cells. Four to ten peripheral cells at the anterior aspect of the organism form a calotte, which interacts with the host renal epithelium.[15]

Nematogens reproduce asexually. An agamete within the axial cell cytoplasm develops into a vermiform embryo, which then exits the adult through a gap between peripheral cell membranes or by penetrating a peripheral cell.[12,13] The vermiform larva matures into either another nematogen or a primary

rhombogen and remains within the host. In contrast, primary rhombogens and secondary rhombogens, which transition from nematogens rather than mature from vermiform larvae, reproduce sexually. An agamete within the axial cell develops into an infusorigen, a hermaphroditic gonad that gives rise to oocytes and spermatocytes. Fertilization results in development of infusoriform embryos, which escape the parent organism in a manner similar to vermiform embryos.[10] While the vermiform stages are confined to the renal organs, infusoriform larvae can exit the renal organ, escape the original host, and eventually infect a new host by an unknown mechanism.[12] Many dicyemid species exhibit high host specificity, and two or three species are commonly found within a single cephalopod host.[15]

Vermiform larvae exhibit a body plan similar to the adults. Contrarily, infusoriform larvae are composed of a higher number and greater variety of cells, resulting in diverse body organizations of at least 14 different cell types.[8] The number of peripheral cells in the adults, the shape and organization of the calotte, the number of total and peripheral cells in vermiform embryos, and the number and organization of cells in infusoriform embryos are species-specific.[7-9,12] Distinguishing between dicyemid species, rhombogen and nematogen forms, and vermiform and infusoriform embryos in routine histologic sections seems quite challenging, and may be best attempted using tissue smears and particular fixation and storage techniques.

Contributing Institution:
University of Minnesota Veterinary Diagnostic Laboratory
https://vdl.umn.edu/

JPC Diagnosis:
Renal appendage: Nephritis, hemocytic, acute, multifocal, mild with vasculitis.

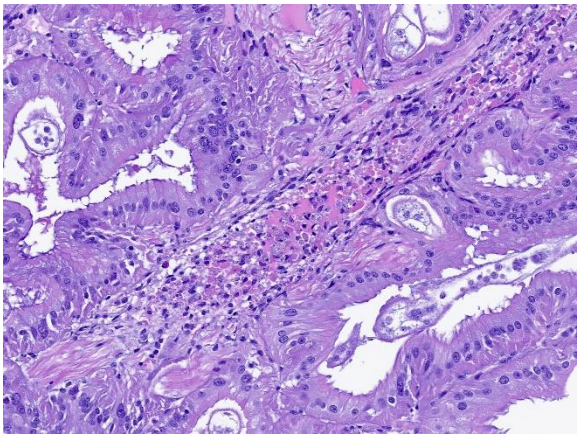

Figure 3-3. Renal appendage, octopus. There is hemocytic vasculitis within the hemolymphatic vessels. (HE, 200X)

JPC Comment:
We thank the contributor for sharing this unique tissue with us in conference. Invertebrate pathology was a recent focus of *Veterinary Pathology*[2] and the present section is an opportunity to build familiarity both with invertebrate anatomy and a common background commensal organism in octopuses. Additionally, tissue (digestive gland) from this case was also presented at the 2024 Davis-Thompson Foundation Invertebrate Histology Seminar – Dr. Elise Ladouceur was one of the moderators and weighed in similarly on this case.

The contributor provides a terrific summary of dicyemid background biology and intersection with normal octopus physiology. Although not a lesion *per se*, recognizing these as normal organisms and avoid diagnosing pathologic parasitism merits discussion among a wider audience. Conference participants hotly debated how to best capture the role of dicyemids in this case. As we typically do not create morphologic diagnoses for non-lesions, we were rescued in this case by a less prominent pathologic finding. Nonetheless, we concur with the presence of renal dicyemids, a routine finding in octopuses that should not be interpreted as a lesion. Dr. Ladouceur also noted that reduced numbers or

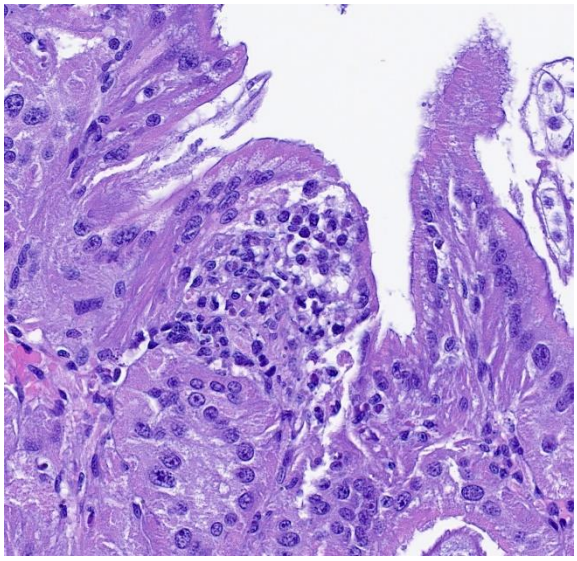

Figure 3-4. Renal appendage, octopus. There are scattered foci of hemocytic inflammation within the parenchyma of the renal appendate. (HE, 400X)

absence of renal dicyemids may represent loss of fitness, though this remains speculative.

Although somewhat subtle, there was also evidence of multifocal inflammation in the renal appendage. This was likely secondary to bacterial sepsis, consistent with the contributor's aerobic culture of the digestive gland which yielded both *Carnobacterium* and *Vibrio* species. Hemocytic inflammation effaced the walls of hemolymphatic vessels and was associated with karyorrhexis, consistent with vasculitis. Although not part of the reviewed tissues, follow up with the contributor confirmed that this animal had severe interstitial inflammation in the digestive gland centered on gram negative, curved bacilli which was consistent with *Vibrio* spp. infection. *Vibrio* spp. have been frequently isolated from skin lesions and/or organs or fluid (hemolymph) of larval, juvenile, and adult octopuses.[5,6] Additionally, other bacteria associated with mortality and sepsis in octopuses include *Pseudomonas* spp. and *Aeromonas* spp.,[5,6] though discerning the ability of these bacteria to cause primary disease, especially in mixed bacterial culture with *Vibrio*, remains uncertain. Preventative health measures such as tank cleaning and water quality management remain important considerations for captive cephalopod husbandry.[6]

References:

1. Anadón R. Functional Histology: The Tissues of Common Coleoid Cephalopods. In: Gestal C, Pascual S, Guerra Á, Fiorito G, Vieites JM, eds. *Handbook of Pathogens and Diseases in Cephalods*. Springer Open; 2019.
2. Dennis MM, LaDouceur EEB. Special focus issue on invertebrate pathology: A growing discipline requiring veterinary diagnosticians. *Veterinary Pathology*. 2023;60(5):501-502.
3. Dill-Okubo JA, Berzins IK, LaDouceur EEB, Camus AC. Mollusca: Cephalopoda. In: LaDouceur EEB, ed. *Invertebrate Histology*. John Wiley & Sons, Inc.; 2021.
4. Drábková M, et al. Different phylogenomic methods support monophyly of enigmatic 'Mesozoa' (Dicyemida + Orthonectida, Lophotrochozoa). *Proc R Soc B*. 2022;289(1978):20220683.
5. Farto R, Armada SP, Montes M, Guisande JA, Pérez MJ, Nieto TP. Vibrio lentus associated with diseased wild octopus (Octopus vulgaris). *J Invertebr Pathol*. 2003 Jun;83(2):149-56.
6. Farto R, Fichi G, Gestal C, Pascual S, Nieto TP. Bacteria-Affecting Cephalopods. In: Gestal C, Pascual S, Guerra Á, Fiorito G, Vieites J, eds. *Handbook of Pathogens and Diseases in Cephalopods*. Springer, Cham. 2019.

https://doi.org/10.1007/978-3-030-11330-8_8

7. Furuya H, Hochberg FG, Tsuneki K. Calotte morphology in the phylum Dicyemida: niche separation and convergence. *J Zool*. 2003;259:361-373.
8. Furuya H, Hochberg FG, Tsuneki K. Cell Number and Cellular Composition in Infusoriform Larvae of Dicyemid Mesozoans (Phylum Dicyemida). *Zool Sci*. 2004;21:877-889.
9. Furuya H, Hochberg FG, Tsuneki K. Cell number and cellular composition in vermiform larvae of dicyemid mesozoans. *J Zool*. 2007;272:284-298.
10. Furuya H, Ota M, Kimura R, Tsuneki K. Renal Organs of Cephalopods: A Habitat for Dicyemids and Chromidinids. *J Morphol*. 2004;262:629-643.
11. Furuya H. Progenesis in dicyemids. *Invertebr Biol*. 2024;142:e12419.
12. Furuya H, Tsuneki K. Biology of Dicyemid Mesozoans. *Zool Sci*. 2003;20:519-532.
13. Hisayama N, Furuya H. Escape Processes in Embryos of Dicyemids (Phylum Dicyemida). *J Parasitol*. 2023;109(5):496-505.
14. Lu TM, Kanda M, Furuya H, Satoh N. Dicyemid Mesozoans: A Unique Parasitic Lifestyle and a Reduced Genome. *Genome Biol Evol*. 2019;11(8):2232-2243.
15. Nakajima H, Fukui A, Suzuki K, Tirta RYK, Furuya H. Host Switching in Dicyemids (Phylum Dicyemida). *J Parasitol*. 2024;110(2):159-169.

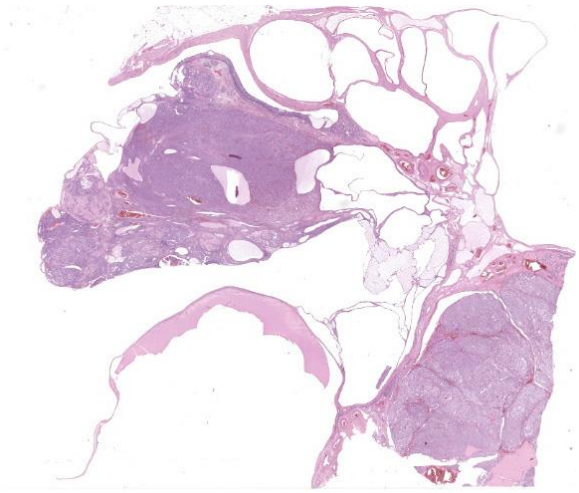

Figure 4-1. Ovary, dog. One section of ovary is submitted for examination. At subgross magnification, normal ovarian architecture is lost. There are numerous cysts measuring up to 5mm in diameter scattered throughout the section, and at least two neoplasms are visible (at upper left and lower right). (HE, 5X)

CASE IV:

Signalment:
12 years old and 3 months, female (neutered), Golden retriever, *Canis lupus familiaris*, canine

History:
The animal was surgically treated with ovariohysterectomy due to pyometra. Both ovaries and uterus were formalin-fixed and submitted for histopathological examination.

Gross Pathology:
Macroscopically, right and left ovary appeared to be increased in size. Right ovary was 3x5 cm and left ovary was 8x6 cm. In addition, both uterus and ovaries had multiple nodules and cysts, the latter containing macroscopically transparent fluid.

Laboratory Results:
Below is a table reporting the results of the immunohistochemical analysis (Tab. 1).

Table 1. Right ovary: results of immunohistochemical analysis performed by our laboratory in comparison with the positivities reported in literature for the three tumors. The positivity was cytoplasmic and diffuse in the whole tumoral population if not otherwise specified into the table.

	Present study			Literature		
Tested antigen	Epithelial tumor	Granulosa cell tumor	Dysgerminoma	Epithelial tumor	Granulosa cell tumor	Dysgerminoma
panCK	++	+	-	P[1,2,5,6,10,11,12]	P/N[1,2,5,6,10,11,12]	N[1,2,5,6,10,11,12]
Vimentin	++	++	++	P/N[1,2,3,5,6,10,11,12]	P[1,2,3,5,6,10,11,12]	P[1,2,3,5,6,10,11,12]
HER-2	+/-[§]	+/-[§]	-	N[7]	P/N[7]	N[7]
c-kit	-	-	-	P/N[11,17]	N[11,17]	P/N[11,17]
SMA	-	-	-	P/N[3]	P/N[3]	ND[3]
Desmin	++/+* (multifocal)	-	+/-** (multifocal)	P/N[2,3]	P/N[2,3]	P/N[2,3]

++ = strong positivity; + = moderate positivity; +/- = weak positivity; - = no positivity
P = positive; N = negative; P/N: some positive and some negative cases; ND: not determined
[§]HER-2 positivity was considered +/- since complete membrane staining was not observed in >10% of cells.
*Some areas were strong and some moderate in positivity. Some areas were negative.
**Perinuclear spotted positivity

Microscopic Description:
Right ovary:

Continuous with the ovarian surface epithelium, occupying 20% of the section and replacing the normal ovarian tissue, there is a moderately cellular, not well demarcated, non-encapsulated and non-infiltrative neoplastic population. The neoplasm is characterized by endophytic and esophytic tubular and tubulo-papillary structures, associated with moderate to abundant ovarian fibrovascular stroma. Tubules are occasionally ectatic and contain a moderate amount of often homogeneously eosinophilic amorphous material.

Neoplastic cells are cuboidal to columnar with indistinct cell borders, scant eosinophilic cytoplasm and round to oval (10 um) eccentrically located nuclei with finely stippled chromatin and mainly 1 distinct nucleolus. Anisocytosis and anisokaryosis are mild. Mitoses are rare (< 1 per hpf).

Close to this neoplasm, multifocally colliding, there is a second densely cellular, well-demarcated, non-encapsulated and infiltrative neoplasm occupying 40% of the section. The neoplasm is characterized by sheets of cells admixed with a very fine and scant fibrovascular stroma.

Neoplastic cells are irregularly round with distinct cell borders (up to 20 um), moderate to abundant occasionally granular slightly eosinophilic cytoplasm, occasionally showing single to multiple large empty well-defined vacuoles.

The nucleus is round to oval, rarely megalic (macrokaryosis) with finely stippled chromatin and 1 distinct nucleolus. Anisocytosis and anisokaryosis are moderate with occasional bi and multinucleation. Mitoses are on average 2-4 per high power field.

Multifocal mild hemorrhages are evident, as well as disseminated single cell necrosis/apoptosis. Entrapped in the neoplasm, there are occasional ectatic and cystic tubular structures lined by a cuboidal to flattened epithelium.

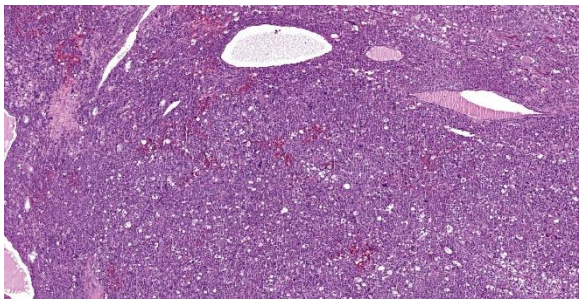

Figure 4-2. Ovary, dog. One neoplasm is composed of germ cells arranged in sheets (dysgerminoma) (HE, 60X)

At the periphery of both the neoplasms and close or involving the rete ovarii, multiple variably-sized ovarian and para-ovarian epithelial and vascular cystic spaces occasionally containing a variable amount of slightly eosinophilic amorphous material are also observed.

Close to the cystic portion, occupying 20% of the section there is a densely cellular, well demarcated, non-encapsulated and non-infiltrative neoplasm. The cells form mainly nest and tubular structures, the latter mainly with small lumens (microfollicular), separated by variably sized bands of scant fibrovascular stroma. Neoplastic cells are irregularly oval to elongated with indistinct cell borders, moderate eosinophilic fibrillar to vacuolized cytoplasm with small (5-7 um) hyperchromatic round to oval nuclei. Anisocytosis and anisockryosis are mild. Neoplastic cells focally surround microcavities containing intensely eosinophilic amorphous material (Call-Exner bodies). Mitoses are rare (<1 per hpf). Multifocal haemorragic lacunae are also present.

Contributor's Morphologic Diagnosis:
Right Ovary: papillary adenoma, dysgerminoma and granulosa cell tumor associated with multiple ovarian and para-ovarian cysts.

Left ovary (not submitted): dysgerminoma

Uterus (not submitted): cystic endometrial hyperplasia and purulent endometritis

Contributor's Comment:
This was a very unusual case of three different tumors in the same ovary of an adult female dog.

Ovarian tumors are described as a frequent condition in female dogs, but epidemiological data are incomplete. They occur more often in older animals, and usually are noted due to behavioral changes. Additionally, lactation and vaginal discharge can also be present. They also can be associated with ovarian cysts and with uterine lesions such as cystic endometrial hyperplasia and pyometra.[9,16]

Typically, ovarian tumors grow as single subtype either monolaterally, or less often, bilaterally with the latter being mainly represented by sex cord stromal tumors.[9] Only rare cases of simultaneous neoplastic lesions of different cell of origin have been described in ovaries. To our knowledge, there is only one case report of a concomitant teratoma and granulosa cell tumor growing distinctively into the two ovaries of an English Bulldog.[8]

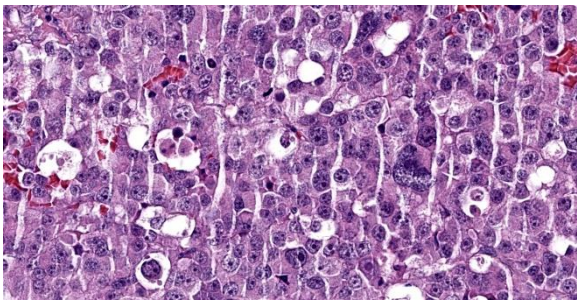

Figure 4-3. Ovary, dog. Neoplastic germ cells demonstrate moderately pleomorphic nucleoli. (HE, 585X)

Table 2. The expression of specific markers in normal human and canine epithelial, granulosa, and germ cells according to the literature.[1-3,5-7,10-12,17]

	Epithelial cells	Granulosa cells	Germ cells
Human	CKAE1/AE3, CK7 CK8 CK10 CK18 HBME-1 MUC1 VIM 17b-hydroxysteroid dehydrogenase Integrin N-cadherin	CKAE1/AE3 INH- α N-cadherin VIM	OCT3/4 SALL4 PLAP Protein VASA
Dog	CKAE1/AE3 CK7 HBME-1	CK AE1/AE3 INH- α VIM	OCT 3/4 SALL4 PLAP

CK = cytokeratin; HBME-1 = Hector Battifora mesothelial epitope-1; MUC1 = cell surface associated mucin1; VIM = vimentin; INH- α = inhibin-alfα; OCT = Octamer-binding transcription factor; SALL4 = Sal-like protein 4; PLAP = Placental alkaline phosphatase.

Papillary adenoma is a benign tumor of the surface epithelium mainly described in the bitch. Usually at the cut surface there are multiple small cysts which are a feature of this type of tumor.[5] The neoplasm can be smooth and nodular, or when arising on the surface, give the ovary a cauliflower-like appearance. There is scant connective stroma and the papillary projections are lined by small cuboidal to cylindrical cells that may have cilia. Mitotic figures are rare.[12] Papillary adenocarcinoma is the malignant counterpart of benign papillary adenomas.[5] Size is an important criterion of malignancy. Tumors that extend through the opening of the ovarian bursa are likely to be malignant and spread by implantation to the peritoneal surface. The surface of an adenocarcinoma tends to be shaggy, and it is the fronds that break off and give rise to metastatic implantations. This tumor is similar in origin and appearance to its benign counterpart, and distinguishing between them can be difficult. Additional criteria for malignancy are increased mitotic activity, invasion into the ovarian stroma, and extension into the ovarian bursa.[12] Based on features in this case, we favored a papillary adenoma.

Dysgerminoma is a tumor that develops from germ cells before differentiation. It has been recognized most often in the bitch, but is much less common in female dogs than the male testicular counterpart (i.e. seminoma). Dysgerminomas are malignant and may metastasize or spread locally, but early spread is not common. Histologically, there are no defined criteria to predict tendency to metastasize.[12] Dysgerminomas are composed of a uniform population of large round cells with clear or light-staining amphophilic cytoplasm. The nuclei are centrally located and contain abundant granular chromatin and either one or two prominent nucleoli. Mitotic figures are often numerous, and incomplete division of tumor cells may result in multinucleated giant cells. Individual tumor cells may undergo necrosis, leaving a distinctive clear space. The stroma is

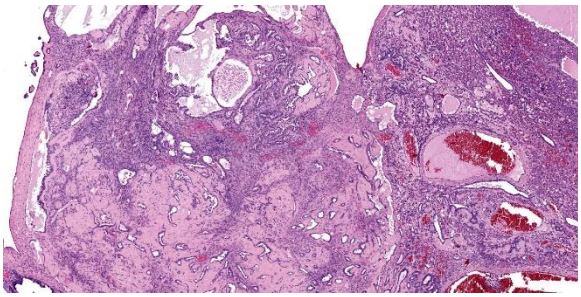

Figure 4-4. Ovary, dog. Adjacent to the dysgerminoma, there is a papillary adenoma with hyalinized stroma. (HE, 53X)

usually light and may be infiltrated with lymphocytes.[12]

Granulosa cell tumors are composed primarily of cells that resemble the granulosa cells of the ovarian follicle. They can develop from ovarian remnants and be either benign or malignant. The tumor often contains cells of the theca interna and fibroblasts. In the bitch, they are slightly less common than epithelial tumors of the ovary.[12] Steroidogenesis may be associated with granulosa cell tumors. Either estrogens or androgens can be produced, though not all granulosa cell tumors are hormonally active. Inhibin is regularly produced by granulosa cell tumors in the mare and is thought to be the cause of atrophy of the contralateral ovary.[12] Only rarely do granulosa cell tumors metastasize in cows or bitches, and such reports are even rarer in mares.[12] Neoplastic granulosa cells have spherical-to-oval, hyperchromatic nuclei, distinct nucleoli, and scant eosinophilic cytoplasm. The common patterns are follicular (microfollicular and macrofollicular), insular, trabecular, and diffuse. Often a combination of patterns exists in a single tumor. Call-Exner bodies, which are distinctive microcavities that contain watery or hyaline eosinophilic material and occasionally pyknotic nuclei are surrounded by granulosa cells in a rosette arrangement. These are seen most often in the microfollicular pattern. Some granulosa cell tumors, particularly those in the bitch, develop a tubular pattern similar to that of the Sertoli cell tumor of the testis, and like Sertoli cell tumors some of these granulosa cell tumors induce a dense fibrous stroma. Theca cells may also be present in granulosa cell tumors. Either or both cell types may be luteinized.[12]

Expression markers of different normal ovarian cell type (Table 2) can be helpful to characterize tumors of different origin particularly when less differentiated as also reported in Table 1. The tumors reported in this case presented a IHC phenotype resembling what reported into the literature for the studied markers (Table 1).

In addition to the markers performed by our laboratory, CK7, PLAP and inhibin could also be performed to further confirm the tissue origin of the identified neoplasms.[1,2,5,6,10,11,12]

Contributing Institution:

Department of Comparative Biomedicine and Food Science (Università of Padua)

Viale dell'Università, 16 (35020), Legnaro (PD), Italy

https://www.bca.unipd.it/

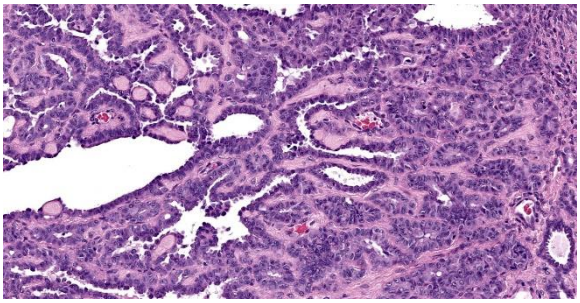

Figure 4-5. Ovary, dog. Within the adenoma, epithelial cells are cuboidal, bland, and demonstrate no definitive evidence of infiltrative growth or cellular features of malignancy. (HE, 263X)

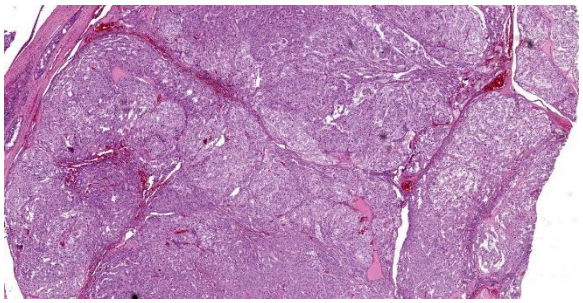

Figure 4-6. Ovary, dog. A third neoplasm featuring cuboidal to columnar cells in tubules is present (granulosa cell tumor). (HE, 55X)

JPC Diagnosis:
1. Ovary: Dysgerminoma.

2. Ovary: Papillary adenoma.

3. Ovary: Granulosa cell tumor.

4. Ovary: Cysts, multiple.

JPC Comment:
The final case of this conference features four separate entities to describe. Conference participants noted one or more neoplasms and cysts, though only a select few were tenacious enough to identify all 3 neoplastic cell populations. This is a unique slide that is a microcosm of ovarian neoplasia – it is a fine companion to the analogous testicular tumor case we reviewed in WSC 24-25 Conference 10 (Case 2 – also from a dog).

We agree with the contributor that multiple different ovarian neoplasms is not a common finding in the dog. Ovarian neoplasia itself is relatively rare in dogs, representing approximately 1-2% of all neoplasms.[14,15] Arriving at 3 separate neoplasms in a single ovary likely represents the confluence of multiple rare outcomes. That the contralateral ovary in this case (not included with this slide) also had a dysgerminoma could reflect either metastasis or a separate neoplasm arising spontaneously – the submission materials leave this aspect of the case open.

Identification of a granulosa cell tumor was straightforward in this case with recognition of Call-Exner bodies and fibrous tissue septa being helpful correlates. The intersection of the dysgerminoma and the adenoma is intriguing, but the two neoplasms are easily distinguished from each other. .We considered the possibility of a ovarian carcinoma in this case, however, definitive areas of stromal invasion are not evident in these sections.

Lastly, we agreed with the contributor that there are multiple cysts present in this case, though we did not attempt to further classify each one, especially in light of the three distinct neoplasms in the surrounding tissue. Cystic structures arising from the ovary include cysts of the rete ovarii, subsurface epithelial structures, and follicle. Paraovarian cysts are located in tissue adjacent to the ovary and include remnants of the mesonephric duct, paramesonephric duct, and mesonephric tubule.[13] Features such as the presence of ciliated epithelium, smooth muscle in the cyst wall, and a basement membrane can be used to distinguish these diagnoses.[13] Location (if known) is also helpful discriminator.

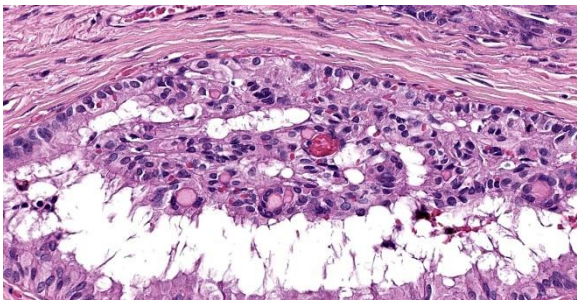

Figure 4-7. Ovary, dog. Granulosa cells are present within tubules. They often palisade along basement membranes, and in some areas, surround hyaline eosinophilic material (Call-Exner bodies). (HE, 385X)

References:

1. Auersperg N, Wong AST, Choi K-C, Kang SK, Leung PCK. Ovarian Surface Epithelium: Biology, Endocrinology, and Pathology. 2001;22(2).
2. Akihara Y, Shimoyama Y, Kawasako K, et al. Immunohistochemical Evaluation of Canine Ovarian Tumors. *J Vet Med Sci*. 2007;69(7):703–708.
3. Czernobilsky B, Shezen E, Lifschitz-Mercer B, et al. Alpha smooth muscle actin (alpha-SM actin) in normal human ovaries, in ovarian stromal hyperplasia and in ovarian neoplasms. *Virchows Arch B Cell Pathol Incl Mol Pathol*. 1989;57(1):55-61.
4. Dolenšek T, Knific T, Ramírez GA, Erles K, Mallon HE, Priestnall SL, Suárez-Bonnet A. Canine ovarian epithelial tumours: histopathological and immunohistochemical evaluation with proposed histopathological classification system. J Comp Pathol. 2024 Jul;212:42-50.
5. Kennedy PC, Cullen JM, Edwards JF, Goldschmidt MH, Larsen S, Munson L, Nielsen. *Histological classification of tumors of the genital system of domestic animals*. WHO, Washington, DC: Armed Forces Institute of Pathology; 1998.
6. MacLachlan NJ, Kennedy PC: Tumors of the genial system. In Meuten DJ: *Tumors in Domestic Animals*. 4th ed. Ames, IO: Iowa State Press;2002:547-573.
7. Matos ACHDS, Consalter A, Santos Batista BP, Fonseca ABM, Ferreira AMR, Leite JDS. Immunohistochemical expression of HER - 2 and Ki - 67 in granulosa cell tumor in bitches. *Reprod Dom Anim*. 2021;56(4):667–672
8. Oviedo-Peñata CA, Hincapie L, Riaño-Benavides C, Maldonado-Estrada JG. Concomitant Presence of Ovarian Tumors (Teratoma and Granulosa Cell Tumor), and Pyometra in an English Bulldog Female Dog: A Case Report. *Front Vet Sci*. 2020;6:500.
9. Patnaik AK, Greenlee PG. Canine Ovarian Neoplasms: A Clinicopathologic Study of 71 Cases, Including Histology of 12 Granulosa Cell Tumors. *Vet Pathol*. 1987;24(6):509–514.
10. Riccardi E, Greco V, Verganti S, Finazzi M. Immunohistochemical Diagnosis of Canine Ovarian Epithelial and Granulosa Cell Tumors. *J Vet Diagn Invest*. 2007;19(4):431–435
11. Rosa RB, Bianchi MV, Ribeiro PR, et al. Comparison of immunohistochemical profiles of ovarian germ cells in dysgerminomas of a captive maned wolf and domestic dogs. *J Ver Diagn Invest*. 2021;**33**(4):772–776.
12. Schlafer DH, Miller RB: Female genital system. In: Maxie MG, ed.. *Jubb, Kennedy, and Palmer's Pathology of Domestic Animals*. 5th ed. Philadelphia, PA: Elsevier Limited; 2007, vol 3: 450-456
13. Schlafer DH, Foster RA. Female Genital System. In: Maxie MG, ed. Jubb, Kennedy & Palmer's Pathology of Domestic Animals. Vol 3. 6th ed. St. Louis, MO: Elsevier; 2016:358-464.
14. Sforna M, Brachelente C, Lepri E, Mechelli L. Canine ovarian tumours: a retrospective study of 49 cases. Vet Res Commun. 2003;27:359–361.
15. Troisi A, Orlandi R, Vallesi E, Pastore S, Sforna M, Quartuccio M, Zappone V, Cristarella S, Polisca A. Clinical and ultrasonographic findings of ovarian tumours in bitches: A retrospective study. Theriogenology. 2023 Oct 15;210:227-233.
16. Walter B, Coelfen A, Jäger K, Reese S, Meyer-Lindenberg A, Aupperle-Lellbach H. Anti-Muellerian hormone concentration in bitches with histopathologically diagnosed ovarian tumours and cysts. *Reprod Domestic Animals*. 2018;53(3):784–792.
17. Yi C, Li L, Chen K, Lin S, Liu X. Expression of c-Kit and PDGFRα in epithelial ovarian tumors and tumor stroma. *Oncol Lett*. 2012 Feb;3(2):369-372.

Joint Pathology Center
Veterinary Pathology Services

WEDNESDAY SLIDE CONFERENCE 2024-2025

Conference #14 — 11 December 2024

CASE I:

Signalment:
Adult male limousine bull, (*Bos taurus*)

History:
Unknown.

Gross Pathology:
Post-mortem examination revealed:

- Diffuse alopecia and lichenification and multifocal erythematous nodules (Fig. 1)
- Multifocal granulomatous scleritis and conjunctivitis (Fig. 2)
- Multifocal granulomatous orchitis (Fig. 3)

No other macroscopic lesions were present.

Microscopic Description:
Epiglottis: Multifocally, in the lamina propria and within the mucous gland interstitial tissue, a moderate number of round, 400µm in diameter, protozoal cysts are visible. Cysts are composed of a multilayer wall; the following wall parts are recognizable: an external fibrillary host 'collagen layer; a thick, homogenous eosinophilic outer layer; and a thin inner layer composed host cell cytoplasm, containing multiple flattened nuclei with prominent nucleoli. The parasitophorous vacuole within the host's cell cytoplasm is 250µm in size, and contains a large number of densely packed, 3-5 µm crescentic bradyzoites (Figure 4). The inflammation around the cysts is almost absent or minimal, and mainly composed of macrophages.

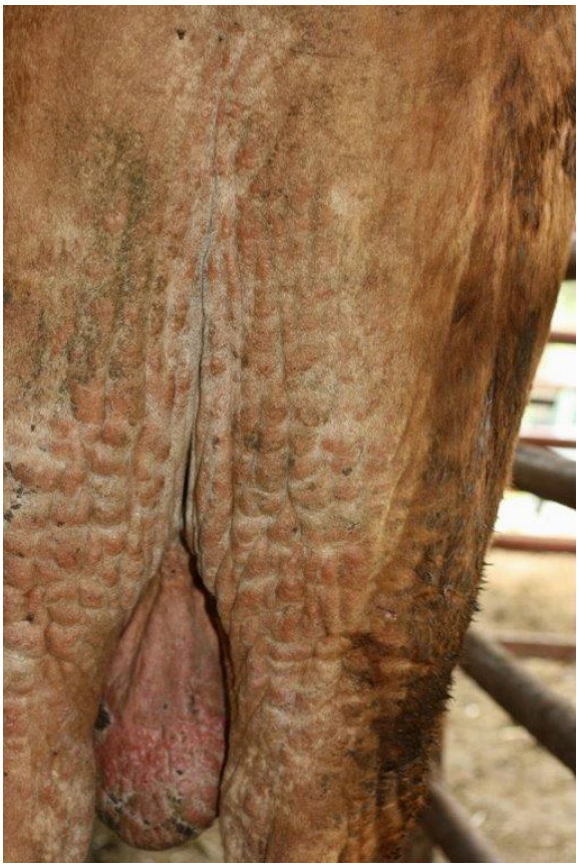

Figure 1-1. Haired skin, ox. The skin over the caudal hind legs is alopecic and markedly thickened. (*Photo courtesy of:* Laboratoire d'Histopathologie animale, Vetagro Sup, Campus vétérinaire, www.vetagro-sup.fr)

Contributor's Morphologic Diagnosis:
Epiglottis: epiglottitis, granulomatous, multifocal, minimal, with moderate number of protozoal cysts; etiology consistent with *Besnoitia besnoitii,* bovine.

Figure 1-2. Eye, ox. There are numerous protozoal cysts within the sclera (arrows). (*Photo courtesy of:* Laboratoire d'Histopathologie animale, Vetagro Sup, Campus vétérinaire, www.vetagro-sup.fr)

Contributor's Comment:
Besnoitia spp are obligatory intracellular apicomplexan protozoal parasites belonging to the *Sarcocystidae* family. Several species have been identified, affecting both wild and domestic animals. (Table 1)

Besnoitia besnoiti is the causative agent of bovine besnoitiosis. The parasite is present worldwide. Bovine besnoitiosis has an outsized economic impact because of mortality, which can reach up to 10% of clinically infected animals in Africa. Similarly, poor body condition of surviving animals may result in culling or decreased market value.[6] The disease presents seasonal variations, but this does depend on the geographical region of affected animals.[6,8] Sex predisposition is also variable;[8] young adults are more affected by the severe clinical forms than animals of less than 18 months or older than 4 years.[6]

The life cycle of *Besnoitia* is known only for 4 species, for which felidae were recognized as the definitive host.[5,8] For the other instances which include *Besnoitia besnoitii*, the definitive host, mode of transmission, and pathogenesis are not completely understood.[8] In the species for which life cycle is known, the parasite is located in the intestine and the sporulated oocysts are released with feces. The exact mode of transmission is unknown, though blood-sucking insects and direct transmission between intermediate hosts are considered possible routes.[6,8] In the first phase of intermediate host infection, tachyzoites replicate in endothelial cells, monocytes, and neutrophils. They then move into peripheral tissues where they invade fibroblasts, myofibroblasts, endothelial cells, and/or smooth muscle cells and form bradyzoite-containing cysts. This intracellular replication induces profound changes in the hosting cell with development of parasitic cysts. The definitive host is infected by ingesting cysts containing tissues.[8]

Bovine besnoitiosis has acute, subacute and chronic phases. In the acute phase, tachyzoites replicate within endothelial cells, causing vasculitis and thrombosis. Clinically, fever, anorexia, rhinitis, conjunctivitis and photophobia, subcutaneous edema and peripheral lymph node hypertrophy can be observed. In the subacute phase, tachyzoites move to peripheral tissues and invade mesenchymal cells. Small cysts can be seen in the sclera, and chronic dermatitis starts to develop. The chronic form is linked to cysts maturation and eventually associated inflammation.

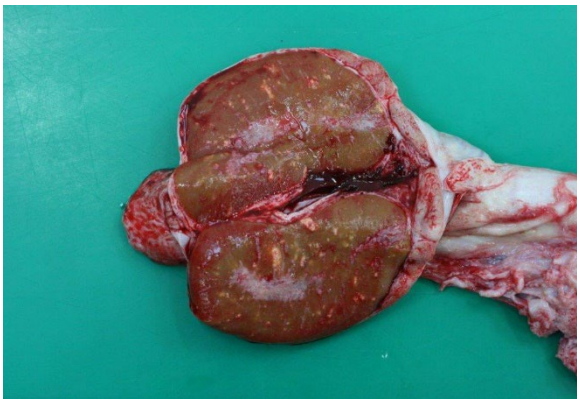

Figure 1-3. Testis, ox. There are numerous foci of granulomatous inflammation surrounding protozoal cysts within the testis. (*Photo courtesy of:* Laboratoire d'Histopathologie animale, Vetagro Sup, Campus vétérinaire, www.vetagro-sup.fr)

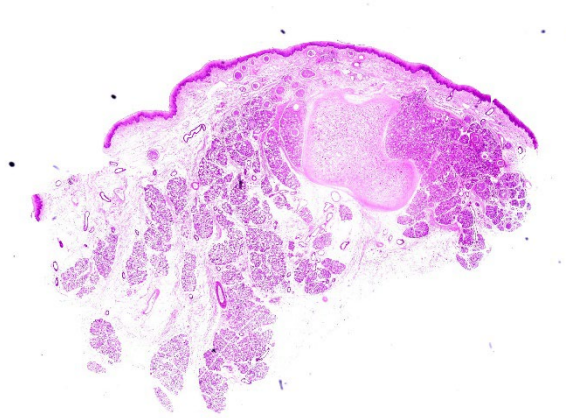

Figure 1-4. Epiglottis, ox. One section of epiglottis is submitted for examination. (HE, 5X)

Chronic dermatitis with alopecia and lichenification are often present and they can be aggravated by secondary cutaneous bacterial and fungal infections. Sterility, due to previous inflammatory reaction and vasculitis in the testis, can also be observed.[2,3,6]

Acute besnoitiosis is difficult to diagnose, while in chronic cases the histologic evidence of intra-cellular cysts is pathognomonic.[4] Today, no treatments exists.[6]

Grossly and histologically, the most affected organs are skin, upper respiratory mucosae, sclera and conjunctiva, and muscular and testicular connective.[2,6] Cysts can measure up to 0.5mm, being visible as small nodules at naked eye.[1,8]

Histologically, in the acute phase, moderate perivascular infiltrates composed of lymphocytes, plasma cells, macrophages and eosinophils are present in the dermis. Dermal edema is a consistent finding though hemorrhages are variable. Few tachyzoites can be visible in parasitophorous vacuoles within endothelial cells: they have a crescentic shape with an eosinophilic cytoplasm. Nevertheless, they can be better identified by immunohistochemistry.[4]

In the subacute and chronic phases, edema and vascular lesions regress and cysts form.

Cyst development is characterized by an increase in intracellular zoite number, host cell modifications (including increase in size, multinucleation, anisokaryosis, and prominent nucleoli) and development of a cyst wall. At the end of their maturation (34-50 days post seroconversion), cysts can be up to 400µm in size, and their size is correlated to their age.[1,4] The cyst wall is formed by 4 layers comprising an outer condensed collagen layer, an eosinophilic 30µm thick layer, a thin homogenous basophilic layer (not always visible, especially in older cysts), and a rim composed of scant cytoplasm containing multiple enlarged nuclei. The multilayer wall lines a parasitophororus vacuole containing many basophilic bradyzoites.[4] The inflammatory reaction is almost absent however. When present, especially secondary to cyst 'rupture, it is composed of macrophages, lymphocytes and plasma cells with few eosinophils. In the skin, cysts are mainly located in the papillary dermis.[1,4,8]

Table 1.

Intermediate Host	*Besnoitia spp.*	Definitive Host
Cattle	*B. besnoiti*	Unknown
Equids	*B. bennetti*	Unknown
Goats, sheep	*B. caprae*	Unknown
Reindeer, caribou	*B. tarandi*	Unknown
Rabbits	*B. oryctofelis*	Felidae
N. American opossums	*B. darlingi*	Bobcat[7]
Southern plain woodrat	*B. neotomofelis*	Felidae
Rodents	*B. wallacei*	Felidae

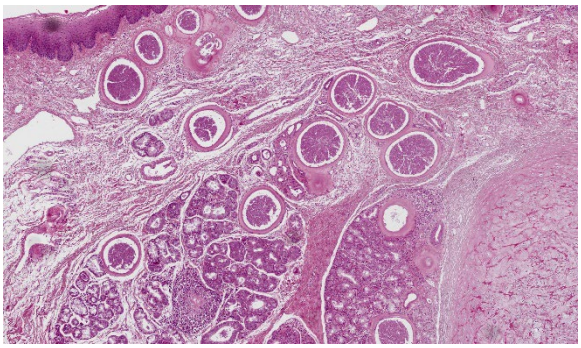

Figure 1-5. Epiglottis, ox. There are numerous apicomplexan cysts within the submucosa of the epiglottis. (HE, 146X)

Contributing Institution:
www.vetagro-sup.fr

JPC Diagnosis:
Epiglottis: Epiglottitis, granulomatous, multifocal, mild, with apicomplexan cysts.

JPC Comment:
This week's moderator was Dr. Corrie Brown from the University of Georgia who focused on infectious and transboundary diseases with conference participants. Although the Wednesday Slide Conference archives are (thankfully perhaps) not replete with Foreign Animal Disease examples, Dr. Brown nonetheless selected four cases to delve into comparative pathogenesis.

In this first case, the contributor provides several interesting gross images which are characteristic of *Besnoitia* infection. Conference participants were not entirely sure of tissue identification for the submitted histologic image, though the presence of tissue cysts, their predilection for the epiglottis, and a large wedge of cartilaginous tissue were helpful landmarks. Bradyzoites within tissue cysts were readily apparent on H&E alone, though PAS was similarly useful. In some smaller cysts, cell nuclei were still visible and peripheralized by parasitophorous vacuoles containing bradyzoites. Although not stated by the contributor, the presence of cysts within both connective tissue and glands suggests that one or more of fibroblasts, myofibroblasts, or endothelial cells were the site of tachyzoite replication in this case.

Similar to other emerging diseases, *Besnoitia* has been increasingly identified within European cattle, to include further northern locations such as Ireland.[9] As biting insects may play a role in the transmission of these protozoans, both prolonged periods of warmer temperatures and extreme temperatures due to global climate change likely aid in sustained development and dispersion of *Stomoxys* and *Tabanus*.

Dr. Brown emphasized the viewpoint of small-scale animal agriculture (i.e. 'smallholders'[10]) and the stakes at play in transboundary diseases. As each individual animal may represent significant economic value from production of meat, milk, and/or fiber, the impact of *Besnoitia* can be felt several times over. Though death is the most severe loss for smallholders of affected animals, loss of productivity (meat, milk) as well as poor quality hide in surviving animals is also a loss of income. Likewise, permanent infertility of bulls may rob smallholders of a

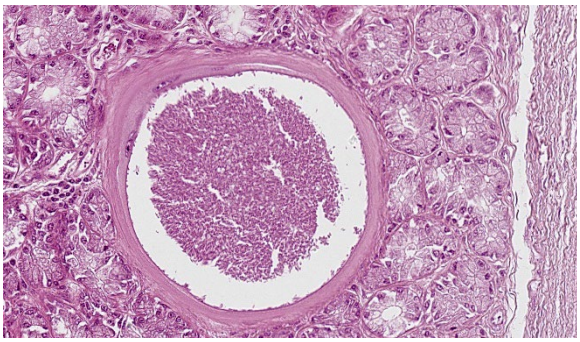

Figure 1-6. Epiglottis, ox. High magnification of a 250um apicomplexan cyst. The cyst is typical of *Besnotia* with a 5-10 um thick rim of host cell cytoplasm with multiple enlarged but flattened nuclei which in turn surround a parasitophorous vacuole containing numerous, densely packed crescentic 3-5 um bradyzoites. (HE, 560X)

prosperous future. Therefore, understanding and control of these diseases plays an important role in global food security and overall stability.

References:

1. Diezma-Díaz C, Tabanera E, Ferre I, et al. Histological findings in experimentally infected male calves with chronic besnoitiosis. *Vet Parasitol*. 2020 May 1;281:109120.
2. Gentile A, Militerno G, Schares G, et al. Evidence for bovine besnoitiosis being endemic in Italy—First in vitro isolation of Besnoitia besnoiti from cattle born in Italy. *Vet Parasitol*. 2012 Mar 23;184:108–115.
3. González-Barrio D, Diezma-Díaz C, Tabanera E, et al. Vascular wall injury and inflammation are key pathogenic mechanisms responsible for early testicular degeneration during acute besnoitiosis in bulls. *Parasit Vectors*. 2020 Mar 2;13:113.
4. Langenmayer MC, Gollnick NS, Majzoub-Altweck M, Scharr JC, Schares G, Hermanns W. Naturally Acquired Bovine Besnoitiosis: Histological and Immunohistochemical Findings in Acute, Subacute, and Chronic Disease. *Vet Pathol*. 2015 May 1;52:476–488.
5. Schares G, Joeres M, Rachel F, et al. Molecular analysis suggests that Namibian cheetahs (Acinonyx jubatus) are definitive hosts of a so far undescribed Besnoitia species. *Parasit Vectors*. 2021 Apr 14;14:201.
6. Schulz KCA. A report on naturally acquired Besnoitiosis in bovines with special reference to its pathology. :16.
7. Verma SK, Cerqueira-Cézar CK, Murata FHA, Lovallo MJ, Rosenthal BM, Dubey JP. Bobcats (Lynx rufus) are natural definitive host of Besnoitia darlingi. *Vet Parasitol*. 2017 Dec 15;248:84–89.
8. Besnoitiosis. In: Vol. 1, *Jubb, Kennedy & Palmer's Pathology of Domestic Animals*. W B Saunders Co Ltd; 2015:2456.
9. Ryan EG, Lee A, Carty C, O'Shaughnessy J, Kelly P, Cassidy JP, et al. Bovine besnoitiosis (Besnoitia besnoiti) in an Irish dairy herd. *Vet Rec*. 2016;178:608–608.
10. Lifestock International. About Us. https://lifestock.org/

CASE II:

Signalment:
Twin Oberhasli goat fetuses (kid A, kid B), *Capra aegagrus*.

History:
Received for necropsy examination in February were the bodies of twin Oberhasli goat fetuses (kid A, kid B) with placenta, reportedly stillborn/abortion. The history as stated by the submitter stated site of occurrence in San Pedro Valley River area of Arizona in the United states. Site on river, with a massive mosquito problem every year, also possible ticks; do treat to prevent but not usually effective. Unknown breeding date but doe was approximately 1-2 weeks from kidding based on ligaments starting to soften. Herd of 10, goats in good nutritional status. Put into fresh pasture 3 days prior to abortion with belly-high weeds, suspect mustard weed yellow flowers; pasture during day, hay at night, mineral supplement once weekly, dewormed twice annually, CDT immunization annually in March. Tested for Q fever, Caseous Lymphadenitis, Caprine Arthritis Encephalitis virus annually with specialty laboratory. These are the first kids born pre-term on farm in 20 years. Q fever reported in animals at another farm in area previously with one noted human testing positive from incident. Farm is a closed site, goats are inbred with only 1 buck,

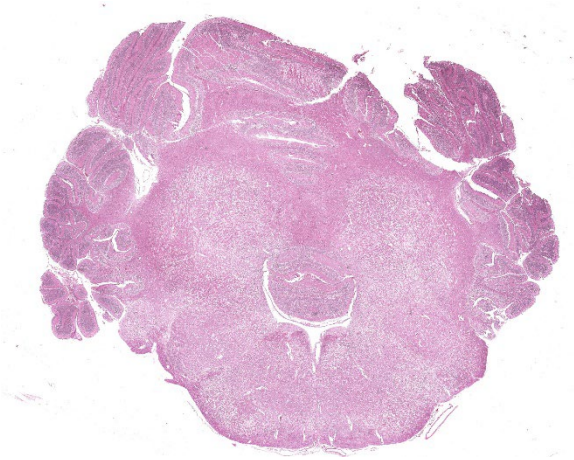

Figure 2-1. Metencephalon, kid. One section of the cerebellum and brainstem are submitted for examination. The cerebellum is mildly hypoplastic with decreased thickness of folia which collapse on themselves. There is diffuse vacuolation of the brainstem parenchyma with marked dilation of axonal sheaths. (HE, 6X)

two generations inbred; buck is sire of dam and of preterm kids. Buck has malformed head. Fetal bodies may be bruised due to doe pawing aggressively at them.

Gross Pathology:
Examined are twin goat fetuses (kid A, kid B) and placenta, all of which are in good post-mortem condition. Kid A is a 4 lb. female with a 47 cm crown to rump length that is well-haired across the body surfaces. Kid A has mild vascular congestion of the meninges but is otherwise unremarkable on external evaluation. Kid B is a 4.5 lb. male with a 37.5 cm crown to rump length that is well-haired across the body. Kid B has prominent brachygnathism (craniofacial deformity). There is widespread, moderate edema of the body wall as well as a large amount of partially clotted blood free within the peritoneal cavity (maternal or partum induced trauma vs. tissue edema & hemoperitoneum). The placenta is 0.75 lb. and appears complete, with no grossly evident lesions; environmental debris is present on surfaces.

Laboratory Results:
Bunyavirus & Cache Valley Virus gel-based PCR, Liver/Lung/Placenta (Texas Veterinary Medical Diagnostic Laboratory): Cache Valley Virus *detected*.

Coxiella burnetii Q Fever rtPCR, Pooled Liver/Lung/Placenta (Texas Veterinary Medical Diagnostic Laboratory): Not detected.

Abortion Panel Livestock Bacterial Culture, Pooled Liver/Lung/Placenta (Texas Veterinary Medical Diagnostic Laboratory): Mixed bacterial growth, negative specialized culture for *Brucella* sp. and negative specialized culture for *Campylobacter* sp.

Trace Mineral Panel, Liver (Texas Veterinary Medical Diagnostic Laboratory): cobalt 0.16 ug/g (no reference range), copper 267.42 ug/g normal (normal: 100-600), iron 324.53 ug/g normal (normal: 200-520), manganese 14.54 ug/g normal (normal: 8.0-24.0), molybdenum 0.85 ug/g below normal (normal: >1.24 ug/g), selenium 2.32 ug/g normal (normal: 1.00-4.80), zinc 252.55 ug/g normal (normal: 100-480).

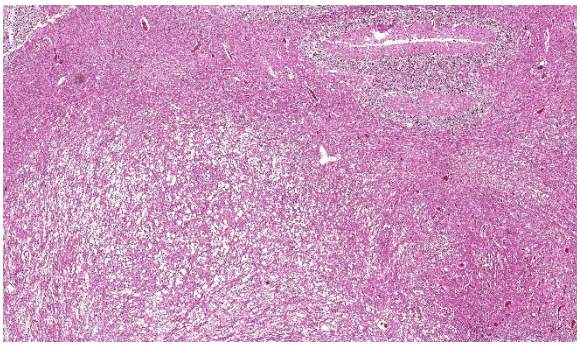

Figure 2-2. Metencephalon, kid. Higher magnification of the dilated axon sheaths within the brainstem. (HE, 44X)

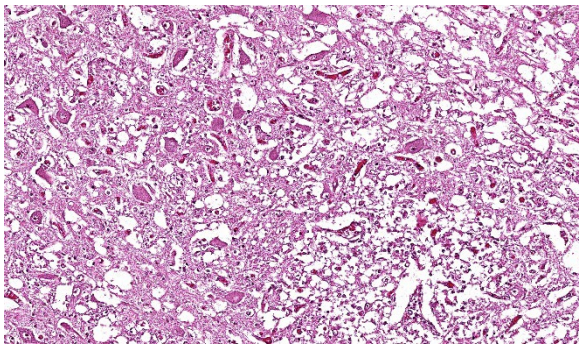

Figure 2-3. Brainstem, kid. Brainstem nuclei are hypocellular with marked loss of neurons and dilation of axon sheaths at right. (HE, 248X)

Microscopic Description:
Brain: The brainstem, and to a lesser extent the cerebellum, has variably mild to marked rarefaction of the neuropil, expanded clear Virchow Robin spaces, white matter dilated axonal tracts rarely containing swollen axons, rare random small areas with loss of cellularity with small basophilic aggregates, and variably diminished to normal nuclear density within the granular layer of the cerebellum (kid B). The grey matter of the cerebrum appears hypercellular with areas of diminished or loss layering (kid A, kid B). There is mild to moderate vascular congestion throughout the brain (kid A, kid B).

Placental meconium staining noted (not represented on JPC WSC slide submission). No significant lesions noted on histologic evaluation of major organs from kid A, kid B.

Contributor's Morphologic Diagnosis:
Brain: Rarefaction, hypoplasia, degeneration, locally extensive, grey and white matter, brainstem and cerebellum, marked (kid B)

Contributor's Comment:
Gross, microscopic, and molecular diagnostics collectively confirmed Cache Valley virus in this case. Cache Valley virus (CVV) belongs to the viral family *Bunyaviridae*, genus *Orthobunyaviridae*, serogroup Bunyamwera.[3] Cache Valley virus, Akabane virus, and Schmallenberg virus are each members of the genus *Orthobunyaviridae*. Orthobunyaviruses are usually maintained through arthropod-vertebrate-arthropod cycles.[3] These viruses have a notable tropism for fetal tissues.[3] In utero infection by these viruses causes prenatal losses and congenital deformities, including arthrogryposis and lesions in the brain ranging from hydrocephalus to hydranencephaly in certain mammalian hosts.[3,4,6]

Cache Valley virus is most frequently reported in sheep, but has been reported in other mammalian species.[3,4] Cache Valley virus has been reported as a cause of embryonic losses, fetal malformations, abortions, and stillbirths in sheep and goats.[1,3,4,6] Investigations on in utero infection of ovine fetuses show highest mortality with infection between 27-35 days gestation, highest incidence of congenital anomalies at 36-45 days gestation.[6] Typical of orthobunyaviruses, Cache Valley virus is transmitted to mammals by infected carrier arthropod vectors, with the viral identification confirmed in certain mosquitoes as well as biting midges broadly across North America.[3,4,6]

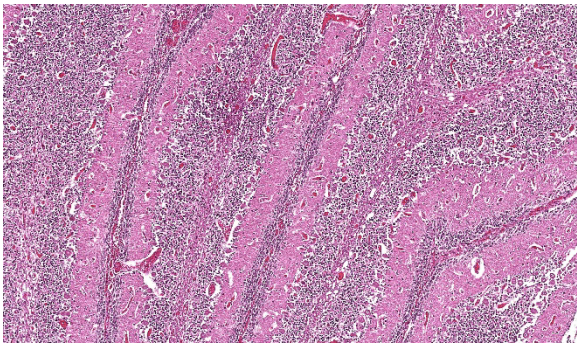

Figure 2-4. Cerebellum, kid. Cerebellar folia are markedly thinned, largely as a result of diminished nuclei within the granular layer. (HE, 146X)

Humans may potentially be infected if bitten by infected arthropod vectors, but direct mammal to mammal transmission has not been identified. Overall reported cases of Cache Valley virus causing clinical disease in humans is rare.[7]

Contributing Institution:
Arizona Veterinary Diagnostic Laboratory

https://azvdl.arizona.edu/

JPC Diagnosis:
Metencephalon: Neuronal necrosis and loss, multifocal, severe, with cerebellar hypoplasia

JPC Comment:
We thank the contributor for sharing this case with us. In particular, the long clinical history made for a good discussion of differentials and assessment of overall slide features. The group discussed ruminant abortion at length. Although Cache Valley virus was not among the group's morphologic diagnoses based on review of the slide alone, other similar agents such as border disease (pestivirus) and caprine arthritis encephalitis (lentivirus) were popular picks.

We differed from the contributor in our morphologic diagnosis concerning the matter of myelination. The asymmetry in measured crown-rump length is interesting and suggests that one twin likely died several weeks before its sibling and the accompanying abortion. Dr. Brown weighed the potential lack of myelination within the developing brain of this fetus (i.e. myelination occurs in greater proportion later in development) as another possible interpretation of the rarefaction that is evident from subgross. Additionally, the lack of spheroids (axonal degeneration correlate) is suggestive that few mature axons had yet developed in this animal. Nonetheless, we were surprised at the lack of overt autolysis in the brain given the timeline we inferred.

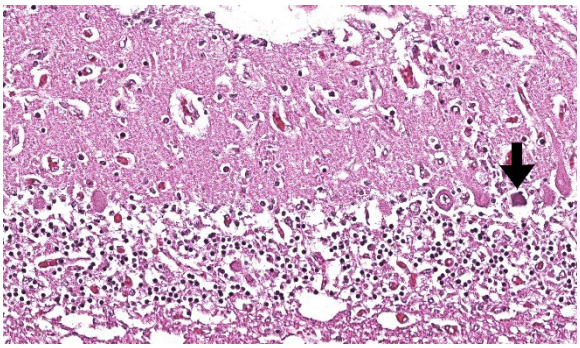

Figure 2-5. Cerebellum, kid. There are large gaps in the Purkinje cell layer and focal Purkinje cell necrosis (arrow). (HE, 477X)

We agreed with the contributor's assessment of cerebellar hypoplasia in this case. From subgross, folia were small with thin layers and increased space between folia were suggestive of this decrease in size. The accompanying necrosis, degeneration, and loss of Purkinje neurons reinforced this interpretation. Subsequently, grey matter neurons were also affected.

The pathogenesis and early lesions of CVV have been previously described.[5] Key gross findings included spinal deformity, arthrogryposis and oligohydramnios. Key microscopic findings in fetuses include necrosis in the central nervous system and skeletal muscle of 7 to 14 days postinfection, and hydrocephalus, micromyelia, and muscular loss after 21 to 28 days postinfection.[5]

The epidemiology of CVV remains incompletely understood, to include major transmission vectors and amplifying hosts across regions of North America.[2] The role of climate change in distribution of CVV across wider geography is speculative, though CVV isolation from mosquito vectors is more common later in the season (late summer and early fall).[2] Longer periods of warmer weather may also extend the breeding period for reservoir hosts and increase the number of naïve hosts to propagate the virus further.

References:

1. Cantile C, Youssef S. Nervous System. In: Maxie MG, ed. *Jubb, Kennedy, and Palmer's Pathology of Domestic Animals*. 6th edition. Elsevier; 2016.
2. Hughes HR, Kenney JL, Calvert AE. Cache Valley virus: an emerging arbovirus of public and veterinary health importance. *J Med Entomol*. 2023 Nov 14;60(6):1230-1241.
3. MacLachlan NJ. Bunyaviridae. In: MacLachlan NJ, ed. *Fenner's Veterinary Virology*. 5th edition. Elsevier; 2017.
4. OIE Terrestrial Manual 2018. Chapter 3.9.1. Bunyaviral Diseases of Animals (excluding Rift Valley fever and Crimean-Congo haemorrhagic fever). Accessed June 1, 2021. https://www.oie.int/fileadmin/Home/eng/Health_standards/tahm/3.09.01_BUNYAVIRAL_DISEASES.pdf.
5. Rodrigues Hoffmann A, Welsh CJ, Wilcox Varner P, de la Concha-Bermejillo A, Marchand Ball J, Ambrus A, Edwards JF. Identification of the target cells and sequence of infection during experimental infection of ovine fetuses with Cache Valley virus. *J Virol*. 2012 May;86(9):4793-800.
6. Schlafer DH, Foster RA. Female Genital System. In: Maxie MG, ed. *Jubb, Kennedy, and Palmer's Pathology of Domestic Animals*. 6th edition. Elsevier; 2016.
7. Centers for Disease Control and Prevention (CDC). Cache Valley Virus. Accessed June 1, 2021. https://www.cdc.gov/cache-valley/index.html

CASE III:

Signalment:
6-week-old, crossbred pig, *Sus scrofa domesticus*

Figure 3-1. Lung, pig. Gross appearance of the lungs from a pig experimentally inoculared with HPAI. The section was taken from the tip of the right cardiac lobe (arrows). (*Photo courtesy of*: USDA/ARS-National Animal Disease Center, 1920 Dayton Avenue, Ames Iowa 50010)

History:
Pig from an experimental inoculation study.

Microscopic Description:
Lung. Section of lung in which there is minimal to mild dilation of bronchi and bronchioles. These airways are empty or partially filled by fibrin, neutrophils, cell debris and macrophages. The airway epithelium is segmentally eroded in multifocal areas and small amounts of cell debris cover these regions. Other bronchi and bronchioles are lined by hypertrophied epithelial cells with large, nonbasilar nuclei and occasional mitotic figures (epithelial regeneration). In these conducting airways, there are intraepithelial lymphocytes and neutrophils. The lamina propria of some bronchi have minimal to mild infiltrates of lymphocytes and plasma cells. Some bronchi, bronchioles, small arteries, and veins have mild to moderate adventitial infiltrates of

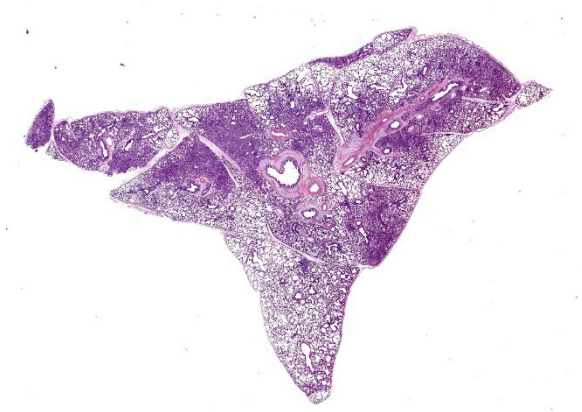

Figure 3-2. Lung, pig. There are multifocal to coalescing areas of peribronchial hypercellularity and atelectasis, as well as diffuse thickening of alveolar septa throughout the section. (HE, 7X)

lymphocytes and plasma cells that occasionally form nodular aggregates. There is multifocal minimal to moderate thickening of alveolar septae commonly around airways due to mild multifocal hyperplasia of type II cells and infiltrates of lymphocytes and macrophages. The alveolar lumens of multiple lobules contain seroproteinaceous fluid, cell debris, fibrin, occasional macrophages, and neutrophils. The interlobular septae are expanded by clear space (edema) and a mixed inflammatory infiltrate composed predominately of lymphocytes, macrophages, and plasma cells.

Contributor's Morphologic Diagnosis:
Lung: Mild to moderate multifocal acute necrotizing bronchitis and bronchiolitis with moderate to marked peribronchiolar and peribronchiolar interstitial pneumonia

Contributor's Comment:
The lung in this case featured macroscopic lesions consistent with influenza A virus infection and was from a pig experimentally inoculated with a highly pathogenic strain of avian influenza (HPAI; A/bald eagle/Florida/W22-134-OP/2022; Genotype B1.1) belonging to the goose/Guangdong 2.3.4.4b hemagglutinin phylogenetic clade. This clade has caused mass mortality events in avian and mammalian species across the globe since 2022.[2,3,5,15] The transcontinental circulation of clade 2.3.4.4b viruses within bird populations allows reassortment with low pathogenicity avian influenza (LPAI) viruses resulting in numerous genotypes of different phenotypes across species and the globe, some of which caused neurologic disease in mammals, a manifestation not observed in our study.[6,7,20] Nonetheless, the presence of NP (nucleoprotein) antigen in endothelial cells of pigs infected with A/bald eagle/FL/22 suggest this strain may spread systemically.

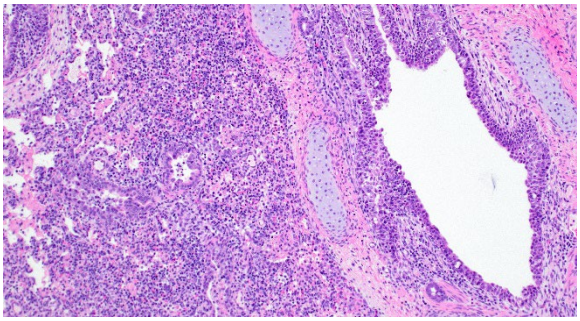

Figure 3-3. Lung, pig. Inflammation is present both within airways (the traditional target of influenza viruses) as well as the surrounding alveolar septa, which are profoundly expanded by a mixed cellular infiltrate o macrophages, lymphocytes, and fewer plasma cells, as well as type II pneumocyte hyperplasia. (HE, 400X) (*Photo courtesy of*: USDA/ARS-National Animal Disease Center, 1920 Dayton Avenue, Ames Iowa 50010)

A subset of mammalian isolates of HPAI H5N1 clade 2.3.4.4b acquired mammalian adaptation markers (E627K, D701N, or T271A) in the polymerase basic (PB) 2 protein that pose a public health risk should these viruses gain efficient transmission in mammals.[4,10] Mammalian adaption of HPAI is multigenic, and the genetic changes necessary for H5N1 strains to adapt to and transmit in swine are not well understood. Although uncommon, incursion of LPAI into commercial swine herds in North America occurs often due to unidentified sources.[8,9,11] Swine-adapted IAV (influenza A viruses) have a propensity for evolution through polymerase errors and reassortment followed by transmission through populations of densely housed commercial pigs and live pig transport. If an avian IAV strain such as H5Nx 2.3.4.4b were to infect domestic swine, there is potential for interspecies transmission, reassortment with endemic swine IAV, and/or acquisition of adaptive mutations that may allow an avian-to-mammalian switch.[10] Increased viral fitness leading to transmission of LPAI strains following reassortment with swine adapted IAV in pigs was demonstrated both in commercial swine herds and experimentally.[1,11] Furthermore, on farm transmission between pigs of a HPAI H5N1 virus and identification of a purified clone that recognizes α2,6 sialic acid receptors was reported.[14] More recently, infection of domestic pigs with clade 2.3.4.4b was demonstrated.[16]

Swine are commonly identified as a 'mixing vessel' supporting reassortment that could lead to antigenic shift.[10] Yet, at a receptor level, it has been suggested that swine are no more susceptible to infection by avian IAVs than humans.[10] The HA (hemagglutinin) of HPAI 2.3.4.4b H5N1 preferentially bind to α2,3-linked sialic acids on host cells,[7] which are at low abundance in the upper respiratory

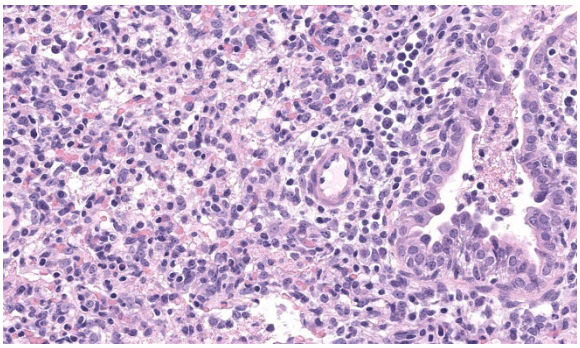

Figure 3-4. Lung, pig. High magnification of inflammatory changes within the airways and septa There is mixed inflammation, polymerized fibrin and edema within alveoli and bronchiolar lumina, and type II pneumocyte hyperplasia in these areas. (HE, 400X)

tract of swine.[12] This low abundance and historic lack of PB2 mammalian adaption mutations may explain why avian IAV does not readily transmit among swine.

The quantity of α2,3-linked sialic acids is relatively higher in the lower respiratory tract of pigs and humans and localizes to pneumocytes and non-ciliated bronchiolar cells.[13,17,19] This distribution is consistent with the extent and distribution of IAV nucleoprotein and RNA labeling in the lung of pigs inoculated with A/bald eagle/FL/22. Labeling is not commonly observed in swine-adapted IAV infection which is most commonly restricted to the conducting airway epithelium. Host-adapted IAV most consistently infect airway epithelium lining conducting airways, resulting in epithelial cell degeneration and necrosis that leads to loss of the epithelial integrity, triggering airway and alveolar inflammation that alters function and interferes with gaseous exchange. Bronchitis and bronchiolitis were a feature of this case due to replication of A/bald eagle/FL/22 in the respiratory epithelium. However, the prominent accumulation of alveolar luminal exudate because of pneumocyte infection and necrosis is not commonly observed in swine-adapted IAV

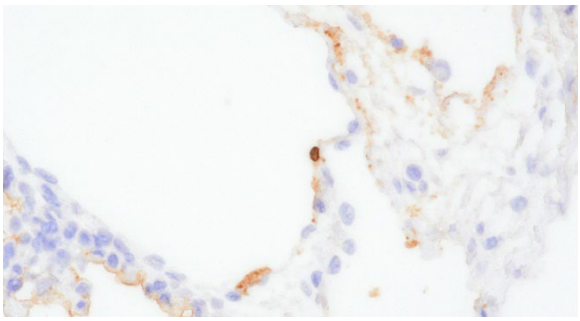

Figure 3-5. Lung, pig. Endothelial cells are immunopositive for HPAI A/bald eagle/Florida/W22-134-OP/2022; Genotype B1.1 (anti-HPAI, 400X) (*Photo courtesy of*: USDA/ARS-National Animal Disease Center, 1920 Dayton Avenue, Ames Iowa 50010)

infection and is likely in part due to the distribution of α2,3-linked sialic acids in swine and propensity of 2.3.4.4b H5N1 to bind α2,3-linked sialic acids.

There is a risk of reassortment of the HPAI H5N1 2.3.4.4b lineage with endemic swine IAV based on the susceptibility of swine to this lineage, the prevalence of IAV infection and co-morbidities in swine herds, and animal husbandry practices.[18,21] Continued phenotypic assessment of HPAI H5NX 2.3.4.4b strains will facilitate awareness and detection capabilities in the swine sector and inform risk assessments and warning systems to safeguard human health.

Contributing Institution:
Mark R. Ackermann, DVM, PhD, DACVP
Center Director
USDA/ARS-National Animal Disease Center
1920 Dayton Avenue
Ames, Iowa 5001

JPC Diagnosis:
Lung: Pneumonia, bronchointerstitial, lymphohistiocytic, subacute, multifocal to coalescing, moderate.

JPC Comment:
The contributor provides a detailed summary of HPAI that remains quite relevant to ongoing events several years after this experimental case was first sent to us. Dr. Brown discussed the current paradigm of dairy cattle-associated HPAI with the group. Recent research on the distribution of α2,3-linked sialic acids has demonstrated that the bovine mammary gland (in addition the respiratory tract) contains abundant receptors for avian influenza viruses.[22] Replication of the virus within the mammary gland epithelium is characterized by attenuation of secretory alveoli and ducts with intraluminal neutrophilic exudate, though the degree of mastitis is moderate.[22] HPAI-positive milk has been to be infectious when given orally to mice;[23] replication competent wild rodents may also play a role in the continued spread of HPAI on cattle farms.[24]

The survival and subsequent infectivity of HPAI in milk presents an important public health question.[22,23,24] Simple assays injecting virus into milk samples ('spiking') have demonstrated the hardiness of influenza A virus to heat treatment; the virus also remains infective in raw milk samples stored at refrig-

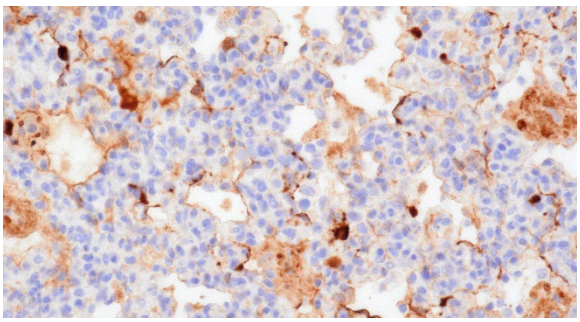

Figure 3-6. Lung, pig. HPAI A/bald eagle/Florida/W22-134-OP/2022; Genotype B1.1 (anti-HPAI, 400X) immunoprotein is distributed throughout pneumocytes and bronchiolar cells, which are high in sialic acid residues. (*Photo courtesy of*: USDA/ARS-National Animal Disease Center, 1920 Dayton Avenue, Ames Iowa 50010)

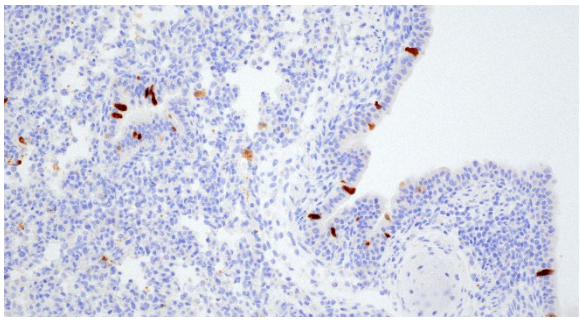

Figure 3-7. Lung, pig. HPAI A/bald eagle/Florida/W22-134-OP/2022; Genotype B1.1 (anti-HPAI, 400X) immunoprotein is within airway epithelium. (*Photo courtesy of*: USDA/ARS-National Animal Disease Center, 1920 Dayton Avenue, Ames Iowa 50010)

eration temperatures for 5 weeks.[23] Natural infection with replication in the mammary gland likely makes inactivation of the virus more difficult due to partial incorporation with fat globules and casein protein which act as an additional barrier to heat treatment.[23] That stated, the effectiveness of conventional commercial pasteurization of milk in addressing influenza A is still being characterized. In our experience (US Army Veterinary Services), many commercial facilities have adapted additional time and/or temperature controls for milk, yogurt, and other dairy products to achieve a desired product composition and provide a wide safety buffer. The recommendation to avoid raw milk nonetheless remains prudent.

We differ slightly in our interpretation of the predominant inflammatory cell type for this pneumonia and felt that the degree of necrosis was overshadowed by predominantly lymphocytes and histiocytes. Several conference participants also noted bronchial and glandular epithelial regeneration which hinted at a slightly longer time course as well. Select alveolar macrophages contained irregular eosinophilic material that some participants interpreted as botryoid inclusions (i.e. from porcine circovirus) while others interpreted necrotic macrophages as a potential correlate of PRRSV which Dr. Brown acknowledged. Absent the history provided in this case, these two viruses are important differentials in porcine granulomatous pneumonias.

References:

1. Abente EJ, Kitikoon P, Lager KM, Gauger PC, Anderson TK, Vincent AL. A highly pathogenic avian-derived influenza virus H5N1 with 2009 pandemic H1N1 internal genes demonstrates increased replication and transmission in pigs. *J Gen Virol*. 2017;98**:** 18-30.
2. Agriculture USDo: 2022-2023 Confirmations of Highly Pathogenic Avian Influenza in Commercial and Backyard Flocks. 2023.
3. Agriculture USDo: 2022-2023 Detections of Highly Pathogenic Avian Influenza in Mammals. 2023.
4. Authority EFS, Prevention ECfD, Control, et al. Avian influenza overview December 2022 – March 2023. *EFSA Journal*. 2023;21**:** e07917.
5. Bevins SN, Shriner SA, Cumbee JC, Jr., et al. Intercontinental Movement of Highly Pathogenic Avian Influenza A(H5N1) Clade 2.3.4.4 Virus to the United States, 2021. *Emerg Infect Dis*. 2022;28**:** 1006-1011.
6. Graaf A, Piesche R, Sehl-Ewert J, et al. Low Susceptibility of Pigs against Experimental Infection with HPAI Virus H5N1 Clade 2.3.4.4b. *Emerg Infect Dis*. 2023;29**:** 1492-1495.
7. Kandeil A, Patton C, Jones JC, et al. Rapid evolution of A(H5N1) influenza viruses after intercontinental spread to North America. *Nat Commun*. 2023;14**:** 3082.
8. Karasin AI, Brown IH, Carman S, Olsen CW. Isolation and characterization of H4N6 avian influenza viruses from pigs with pneumonia in Canada. *J Virol*.

2000;74**:** 9322-9327.
9. Karasin AI, West K, Carman S, Olsen CW. Characterization of avian H3N3 and H1N1 influenza A viruses isolated from pigs in Canada. *J Clin Microbiol*. 2004;42**:** 4349-4354.
10. Long JS, Mistry B, Haslam SM, Barclay WS. Host and viral determinants of influenza A virus species specificity. *Nat Rev Microbiol*. 2019;17**:** 67-81.
11. Ma W, Vincent AL, Gramer MR, et al. Identification of H2N3 influenza A viruses from swine in the United States. *Proc Natl Acad Sci U S A*. 2007;104**:** 20949-20954.
12. Neumann G. H5N1 influenza virulence, pathogenicity and transmissibility: what do we know? *Future Virol*. 2015;10**:** 971-980.
13. Nicholls JM, Chan MC, Chan WY, et al. Tropism of avian influenza A (H5N1) in the upper and lower respiratory tract. *Nat Med*. 2007;13**:** 147-149.
14. Nidom CA, Takano R, Yamada S, et al. Influenza A (H5N1) viruses from pigs, Indonesia. *Emerg Infect Dis*. 2010;16**:** 1515-1523.
15. Prevention CDCa: Technical Report: Highly Pathogenic Avian Influenza A(H5N1) Viruses. 2023
16. Rosone F, Bonfante F, Sala MG, et al. Seroconversion of a Swine Herd in a Free-Range Rural Multi-Species Farm against HPAI H5N1 2.3.4.4b Clade Virus. *Microorganisms*. 2023;11**:** 1162.
17. Shinya K, Ebina M, Yamada S, Ono M, Kasai N, Kawaoka Y. Avian flu: influenza virus receptors in the human airway. *Nature*. 2006;440**:** 435-436.
18. Trevisan G, Schwartz KJ, Burrough ER, et al. Visualization and application of disease diagnosis codes for population health management using porcine diseases as a model. *Journal of Veterinary Diagnostic Investigation*. 2021;33**:** 428-438.
19. Yao L, Korteweg C, Hsueh W, Gu J. Avian influenza receptor expression in H5N1-infected and noninfected human tissues. *Faseb j*. 2008;22**:** 733-740.
20. Youk S, Torchetti MK, Lantz K, et al. H5N1 highly pathogenic avian influenza clade 2.3.4.4b in wild and domestic birds: Introductions into the United States and reassortments, December 2021-April 2022. *Virology*. 2023;587**:** 109860.
21. Zeller MA, Anderson TK, Walia RW, Vincent AL, Gauger PC. ISU FLUture: a veterinary diagnostic laboratory web-based platform to monitor the temporal genetic patterns of Influenza A virus in swine. *BMC Bioinformatics*. 2018;19**:** 397.
22. Nelli RK, Harm TA, Siepker C, et al. Sialic Acid Receptor Specificity in Mammary Gland of Dairy Cattle Infected with Highly Pathogenic Avian Influenza A(H5N1) Virus. *Emerg Infect Dis*. 2024 Jul;30(7):1361-1373.
23. Guan L, Eisfeld AJ, Pattinson D, et al. Cow's Milk Containing Avian Influenza A(H5N1) Virus - Heat Inactivation and Infectivity in Mice. *N Engl J Med*. 2024 Jul 4;391(1):87-90.
24. Usui T, Uno Y, Tanaka K, Tanikawa T, Yamaguchi T. Susceptibility of Synanthropic Rodents (*Mus musculus*, *Rattus norvegicus* and *Rattus rattus*) to H5N1 Subtype High Pathogenicity Avian Influenza Viruses. *Pathogens*. 2024 Sep 5;13(9):764.

CASE IV:

Signalment:
Six-month-old Brangus, bovine (*Bos taurus taurus*)

History:
In the period between December 2018 and

Figure 4-1. Lung, calf. Two sections of lung are submitted for examination with varying degrees of consolidation and expansion of interlobular septa. (HE, 5X)

February 2019, a farm owner recorded the death of five six-month-old calves, including nursing and weaned calves, from a group of 117. Cattle were vaccinated against foot-and-mouth disease, rabies, and clostridiosis, and the herd was kept in native pastures. Affected calves presented similar clinical signs that included fever, apathy, severe respiratory distress, nasal discharge, and diarrhea. Clinical course lasted approximately three days, and calves died spontaneously. All calves that presented clinical signs were treated with enrofloxacin, dipyrone, imizole, and levamisole; however, no significant clinical improvement was observed. One of the deceased calves was submitted for postmortem examination.

Gross Pathology:
The calf showed good body condition. Gross findings included mild jaundice in the subcutaneous tissue, oral mucosa, and ocular conjunctiva. At the opening of the thoracic cavity, the lungs were diffusely pink-red, non-collapsed, with a rubbery texture, and presented interlobular edema on the cut surface. In the cranioventral areas of the lung and in the ventral regions of the caudal lobes, multifocal red-tan and firm areas (2-7 cm in diameter) were observed. At the inspection of the abdominal cavity, the liver was markedly enlarged, with round edges, and diffuse orange discoloration. The gallbladder was distended and filled with grumous bile. The spleen was also severely enlarged. No alterations were observed in other organs.

Laboratory Results:
Culture and isolation of *Salmonella* spp. were attempted using fresh samples of lung. These samples were added in buffered peptone water and incubated overnight (37°C). Following the pre-enrichment, they were inoculated in selective enrichment broth (Rappaport-Vassiliadis broth) and incubated at 42°C overnight. Bacterial isolates were submitted for serotyping using a slide micro-agglutination test. Fresh lung samples were tested through RT-PCR for bovine respiratory complex agents (BoHV/PI-3/BRSV) and Influenza D. Lung sections were submitted for immunohistochemistry (IHC) using a commercial polyclonal antibody against *Salmonella* spp. (Biogenesis®), as previously described by JUFFO et al. (2017).[4]

Salmonella spp. was isolated from the lungs, and the serotype identified was *Salmonella* Dublin. Mild, multifocal,cytoplasmic labeling (IHC) of the bacteria was detected in lung macrophages and freely in the pulmonary interstitial space. RT-PCR for bovine respiratory complex agents (BoHV/PI-3/BRSV) and Influenza D were negative.

Microscopic Description:
Each submitted slide presents a section of lung. Diffusely, alveolar septa are markedly thickened and expanded by severe inflammatory infiltrate of macrophages, lymphocytes, and neutrophils, as well as moderate to marked type II pneumocyte hyperplasia. Similar inflammatory infiltrate composed of large foamy macrophages, lymphocytes, neutrophils, and rare multinucleated syncytial cells, is observed filling alveolar spaces, and less

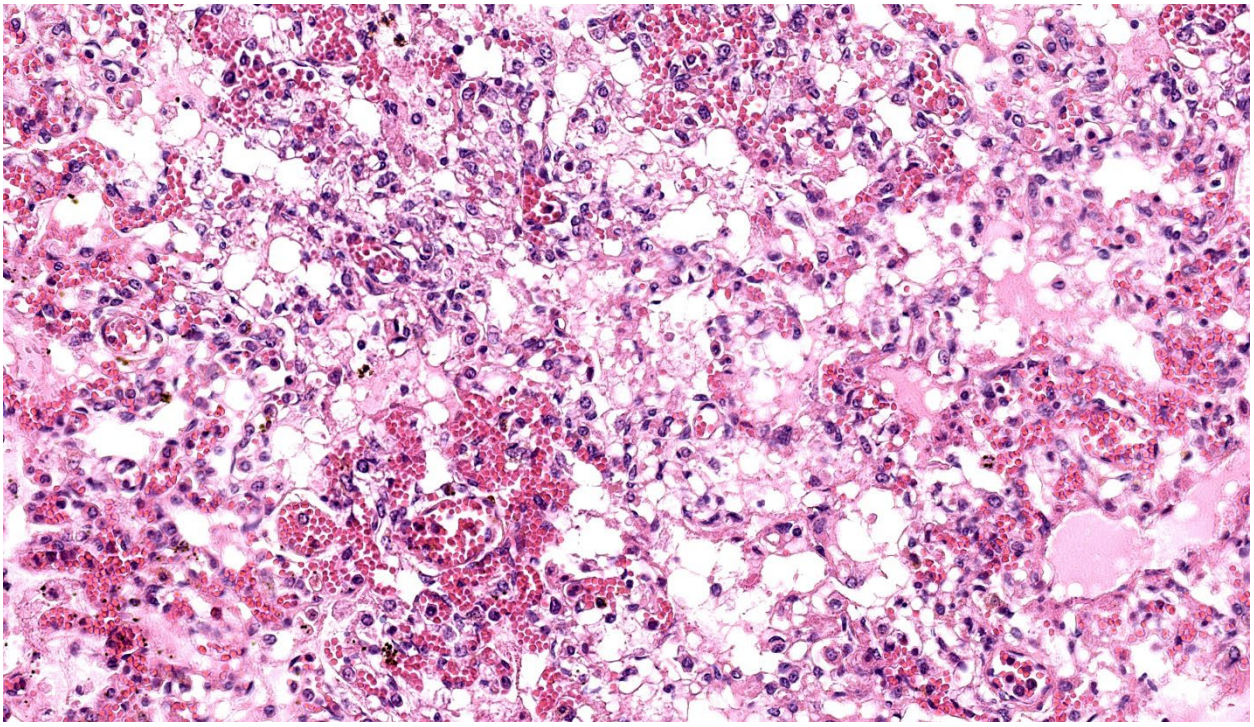

Figure 4-2. Lung, calf. Diffusely, alveolar septa are markedly congested and contain numerous macrophages and lymphocytes as well as scattered Type II pneumocyte hyperplasia. Alveolar lumina contain abundant hemorrhage, edema, polymerized fibrin, alveolar macrophages, and neutrophils. (HE, 450X)

frequently the lumen of bronchioles and bronchi. Multifocal, moderate areas of fibrin deposition, intra-alveolar hemorrhage and mild necrosis are also observed. Additionally, multifocal areas of mild thrombosis, and marked expansion of interlobular septa by eosinophilic homogenous material (edema) are observed.

Contributor's Morphologic Diagnosis:
Lung: Pneumonia, interstitial, lymphohistiocytic, and neutrophilic, multifocal to coalescing, severe, with type II pneumocyte hyperplasia, and interlobular edema, Brangus, bovine.

Contributor's Comment:
Pathological, immunohistochemical and microbiological findings supported the diagnosis of *Salmonella*-associated pneumonia in this case. In cattle, salmonellosis is predominantly caused by *Salmonella enterica* subsp. *enterica* serovar Typhimurium and *S. enterica* subsp. *enterica* serovar Dublin.[1,9,11] *Salmonella* Typhimurium may cause septicemia and is commonly detected in outbreaks of enteric disease in calves. In contrast, *S.* Dublin, a host adapted serovar in cattle, is predominantly associated with septicemia across all age groups in cattle.[11] Salmonellosis in cattle is often characterized by watery or mucoid diarrhea containing fibrin and blood, septicemia, respiratory disease, weight loss, and abortions.[8,1] Lesions include enterocolitis, pneumonia, paratyphoid nodules in the liver, necrotic foci in the kidney, and splenomegaly.[2]

In cases of *Salmonella*-associated pneumonia, the most representative changes include interstitial pneumonia, and therefore, the main differential diagnosis should include

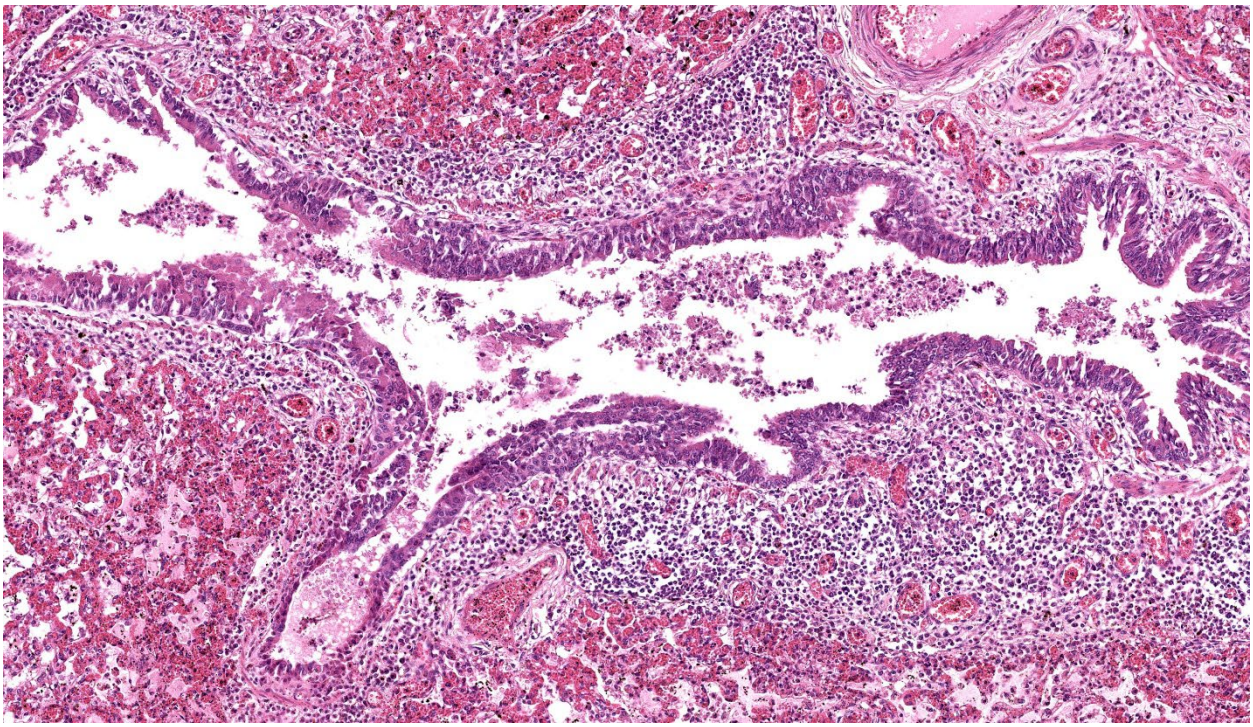

Figure 4-3. Lung, calf. Airways contain refluxed alveolar contains admixed with sloughed airway epithelium. Airway epithelium is hyperplastic, and there are numerous lymphocytes and plasma cells within the peribronchiolar tissue. Alveolar lumina contain abundant hemorrhage, edema, polymerized fibrin, alveolar macrophages, and neutrophils. (HE, 181X)

other important causes of bronchointerstitial pneumonia in calves, such as BoHV (bovine herpesvirus), PI-3 (parainfluenza virus) and BRSV (bovine respiratory syncytial virus), which were ruled out by molecular assays in this case. An outbreak of septicemic salmonellosis with lung involvement has been described in the North region of Brazil associated with serovar Dublin.[5] Salmonellosis with primary lung involvement, in the absence of enteric lesions, has been reported in the Central-West region of Brazil,[3] and in Southern Brazil, by our research group.[7] Likewise, a study conducted in the United States of America reported similar lung lesions in young cattle.[9]

The fecal-oral route represents the main route of transmission, and disease development is associated with bacterial efficiency in invading the intestinal mucosa, colonizing lymphoid tissues, and evading host immune response. Affected animals or asymptomatic carriers may spread the disease in the herd.[8] Young calves (< 6 months of age) are more vulnerable to the disease and may be infected a few hours after calving; nonetheless, adult cattle may also develop the clinical disease.[6, 8] Potential predisposing factors for the development of clinical salmonellosis include concomitant diseases, stressors and immunosuppression, which may favor the development of clinical disease or may prompt cattle to become asymptomatic carriers.[8] Infection in cattle may also be favoured by age and physiological stage.[8] In this case, we believe that weaning-associated stressors may have contributed to the development of clinical salmonellosis.

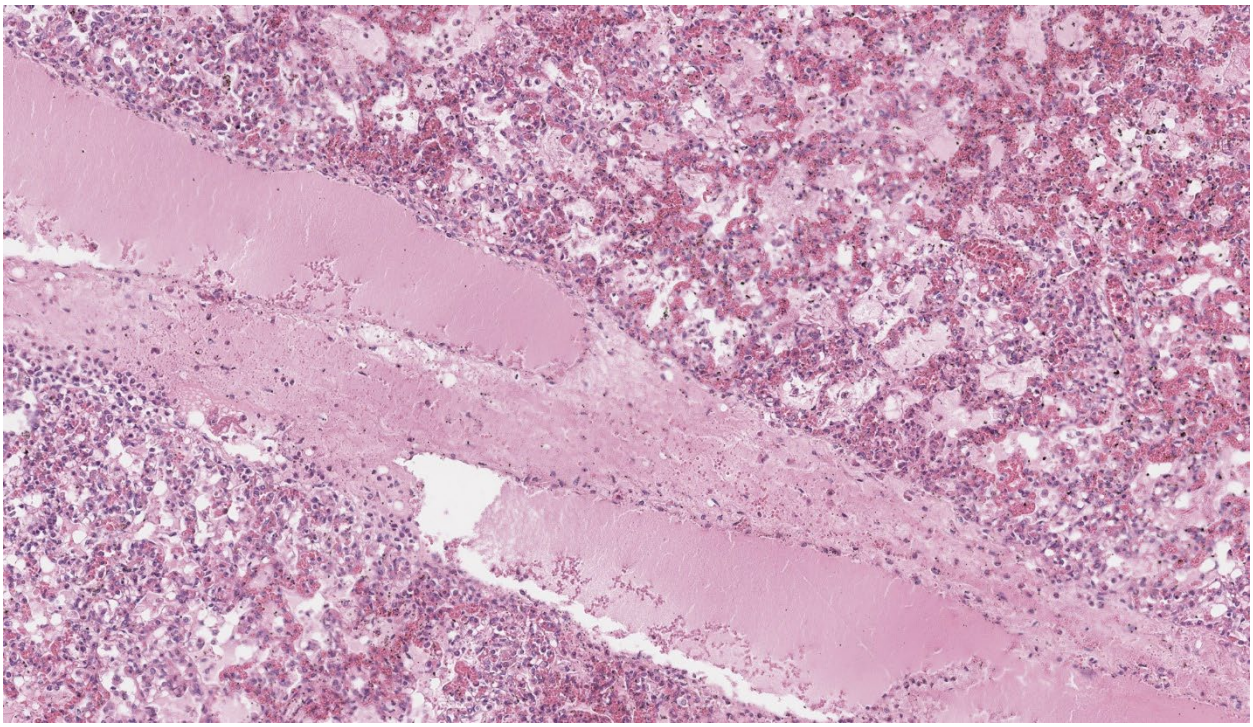

Figure 4-4. Lung, calf. Interlobular septa are markedly edematous with dilated lymphatics. (HE, 205X)

Contributing Institution:
Faculdade de Veterinária
Universidade Federal do Rio Grande do Sul
Setor de Patologia Veterinária
http://www.ufrgs.br/patologia

JPC Diagnosis:
Lung: Pneumonia, interstitial, lymphohistiocytic and neutrophilic, subacute, multifocal to coalescing, severe, with type II pneumocyte hyperplasia, thrombosis, and edema.

JPC Comment:
The final case of this conference is also a pneumonia which allows for a thoughtful comparison with Case 3. Dr. Brown emphasized several subtle aspects that hint at the underlying pathogenesis. There is hypoplasia of bronchus-associated lymphoid tissue (BALT) as well as a large thrombus in section which are suggestive of a septicemia.

The expansion of the alveolar septa is partially lymphohistiocytic like the previous case, though the distribution is very different. In the present case, alveolar septal expansion is diffuse whereas in the previous case, inflammation was multifocal and more prominent at the bronchoalveolar junction. This case fits better with a hematogenous portal of entry whereas Case 3 is more consistent with an aerogenous agent.

The conference concluded with a brief review of the role of bacteria in pneumonias. In bacterial bronchopneumonia, aerogenous entry of the agent and direct infection of the airway leads to exudation of the alveoli and bronchioles, largely with neutrophils and originating at the bronchiolar-alveolar junction. Conversely, bacterial interstitial pneumonias are the result of indirect action through cytokine effects and endotoxemia. Pulmonary intravascular macrophages (PIMs) have received increased attention for

their role in a variety of diseases.[12] In particular, these macrophages secrete proinflammatory cytokines (e.g. TNF- α) in response to both intracellular and extracellular pathogens and or related markers (e.g. LPS). These cytokines subsequently contribute to capillary dysfunction through a variety of changes such as disruption of endothelial tight junctions.[12] In concert with the action of LPS on endothelial cells (i.e. activation), the large degree of edema and fibrin in this case is hardly surprising. Macrophage activation (MAS) has also been identified as a contributor to COVID-19 related lung pathology,[13] though delineating whether cytokine-induced changes are local to the lung or systemic vasculature has spawned a related term of MAS-like immunopathology. In classic MAS, macrophages across tissue lines (e.g. Kupffer cells and alveolar macrophages) are activated concurrently, leading to hemophagocytosis and an eventual consumption coagulopathy with secondary liver dysfunction.[13] In COVID-19 however, hemophagocytosis is localized as part of a response to diffuse alveolar damage.[13] Common shared outcomes underscore similarities in molecular mechanisms of disease, particularly in the role of macrophage activation and cytokine production.

References:

1. Carrique-Mas JJ, Willmington JA, Papadopoulou C, Watson EN, Davies RH. Salmonella infection in cattle in Great Britain, 2003 to 2008. *Vet Rec* 2010(167):560-565.
2. Gelberg HB. Alimentary system and the peritoneum, omentum, mesentery, and peritoneal cavity. In: JF ZACHARY, Pathologic Basis of Veterinary Disease, 2018, 6.ed. SaintLouis, Missouri: Elsevier, 324-411.
3. Guizelini CC, Pupin RC, Leal CRB, Ramos CAN, Pavarini SP, Gomes DC, Martins TB, Lemos RAA. Salmonellosis in calves without intestinal lesions. *Pesq Vet Bras* 2019; 39(8):580-586.
4. Juffo GD, et al. Equine salmonellosis in southern Brazil. Trop Anim Heal and Prod 2017; 49: 475–482.
5. Marques ALA, Simões SVD, Garino Jr F, Maia LA, Silva TR, Riet-Correa B, Lima EF, Franklin Riet-Correa F. Salmonellosis outbreak by serovar Dublin in calves in Maranhão. *Pesq Vet Bras* 2013; 33(8):983-988.
6. Mohler VL, Izzo MM. Salmonella in calves. *Vet Clin North Am Food Anim Pract* 2009; 25:37-54.
7. Molossi FA, Cecco BS de, Henker LC, Vargas TP, Lorenzett MP, Bianchi MV, Lorenzo C, Sonne L, Driemeier D, Pavarini SP. Epidemiological and pathological aspects of salmonellosis in cattle in southern Brazil. *Cienc Rural* 2021; 51(3): e20200459.
8. Nielsen LR. Salmonella Dublin in dairy cattle: use of diagnostic tests for investigation of risk factors and infection dynamics. 219 p. PHD thesis - Department of Animal Science and Animal Health, Royal Veterinary and Agricultural University, Denmark, 2003.
9. Pecoraro HL, Thompson B, Duhamel GE. Histopathology case definition of naturally acquired Salmonella enterica serovar Dublin infection in young Holstein cattle in the northeastern United States. *J Vet Diagn Invest* 2017; 29(6):860–864.
10. Peek SF, Hartmann FA, Thomas CB, Nordlund KV. Isolation of Salmonella spp from the environment of dairies without any history of clinical salmonellosis. *Vet Med Sci* 2004; 225(4):574- 577.
11. Uzal FA, Plattner BL, Hostetter JM. Alimentary System. In: M. G Maxie. Pathology of Domestic Animals, Jubb, Kennedy & Palmer´s. 2016, 6.ed. St. Louis, Missouri: Elsevier, 2, 117-176.
12. Sun Z, Chen X, Liu J, Du Y, Duan C, Xiao

S, Zhou Y, Fang L. PRRSV-induced inflammation in pulmonary intravascular macrophages (PIMs) and pulmonary alveolar macrophages (PAMs) contributes to endothelial barrier function injury. *Vet Microbiol*. 2023 Jun;281:109730.
13. McGonagle D, O'Donnell JS, Sharif K, Emery P, Bridgewood C. Immune mechanisms of pulmonary intravascular coagulopathy in COVID-19 pneumonia. *Lancet Rheumatol*. 2020 Jul;2(7):e437-e445.

Joint Pathology Center
Veterinary Pathology Services

WEDNESDAY SLIDE CONFERENCE 2024-2025

Conference #15 28 March 2025

CASE I:

Signalment:
Table egg layers (leghorn chickens), 27-weeks old.

History:
Flock of 15000 birds. 900 new birds were added to the flock on Feb 5, 2024. A sharp drop in egg production (14%) was reported on February 15, 2024. Mortality begins on February 17 with 3+ birds dead per day until March 12, 2024. The cumulative mortality in the flock was 127 birds. The clinical signs included swollen face, eyelids, wattles, lacrimation, and mucoid nasal discharge.

Gross Pathology:
Two culled birds were submitted. The carcasses were fresh. The body condition was fair with apparent fat stores. The face, eyelids and wattles of the chickens were markedly swollen and red. The eyes were closed, and mucoid exudate expressed from the nasal sinuses. On reflecting skin, the subcutaneous tissue was markedly edematous. The cut surface of the wattles was dark red and soft in the center and surrounded by yellow-white tissue at the periphery. The thoracic and abdominal air sacs were yellowish and cloudy. There were multifocal, few, 1 mm, pale white foci in the liver parenchyma. The ovarian follicles were very small or had a few enlarging follicles (not in production). No significant gross findings in other organ systems.

Figure 1-1. Head, chicken. The face, eyelids and wattles of the chickens were markedly swollen and red. (*Photo courtesy of* Diagnostic Services Unit, Faculty of Veterinary Medicine, University of Calgary)

Laboratory Results:

Avibacterium Paragallinarum cultured from wattle and sinus swab.
Infectious Bronchitis Virus (IBV) and Mycoplasma spp. generic PCR- Low positive for IBV (CT= 32), negative for Mycoplasma spp.

Microscopic Description:
Wattle: Diffusely the center of the wattle was necrotic and hemorrhagic which is characterized by eosinophilic, cellular, and heterophilic debris mixed with pale eosinophilic fibrin, edema fluid, and hemorrhage. At the periphery was a layer of giant cells. The adjoining tissue was variably necrotic and congested and there are multifocal perivascular

Figure 1-2. Head, chicken. On reflecting the skin, the subcutaneous tissue was markedly edematous (top). The cut surface of the wattles was dark red and soft in the center and surrounded by yellow-white tissue at the periphery (bottom). (*Photo courtesy of* Diagnostic Services Unit, Faculty of Veterinary Medicine, University of Calgary)

and lymphocyte infiltrates. The infraorbital sinus was filled with pale blue homogenous mucous mixed with cellular debris, pale eosinophilic fibrin, and heterophils. The lining epithelium was multifocally sloughed and the lamina propria was multifocally congested, edematous, and infiltrated by lymphocytes, plasma cells, macrophages, and heterophils. A similar lesion is present in the lining epithelium of the nasal cavity. Lacrimal and harderian glands are moderately infiltrated by lymphocytes, plasma cells, and heterophils. The air spaces in the calvarium are filled with eosinophilic fluid, mixed with fibrin, a small number of heterophils, and sloughed lining epithelium. Other lesions included multifocal, hepatic necrosis and mild focal airsculitis, diffuse, lymphocytic and heterophilic, conjunctivitis, necro-hemorrhagic cellulitis.

Contributor's Morphologic Diagnosis:

1. Wattles: dermatitis, fibrino necrotizing and hemorrhagic, diffuse, marked, acute.
2. Infraorbital sinus and nasal cavity: Sinusitis and rhinitis, lymphoplasmacytic and heterophilic, mucoid, marked, diffuse, acute.
3. Cranial osteomyelitis, necrotizing, severe, multifocal, acute.

Contributor's Comment:

Infectious coryza (IC) is an economically important disease of intensively raised commercial chickens around the world. IC is an acute, sometimes chronic, contagious, upper respiratory tract disease that results in airsacculitis and condemnation in the broiler chickens in the processing plant and reduced egg production (up to 10-40%) in the breeders and layers.[2] The disease is spread by close contact and droplets, fomites, or the introduction of carrier chickens into a closed flock. The incubation period is about 24 hours. The affected birds in uncomplicated cases recover within 2 weeks.[1] IC is caused by *A. paragallinarum*, which is a gram-negative, fastidious organism bacterium (previously, *Hemophilus paragallinarum*). It requires factor nicotinamide dinucleotide (NAD) for invitro growth, which is often provided by striking a satellite

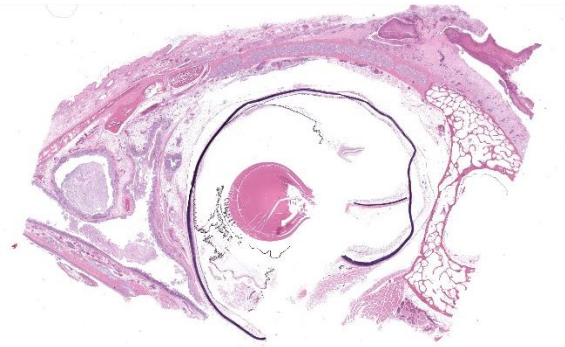

Figure 1-3. Head, chicken. A cross section of the head is submitted for examination. There is abundant exudate in the infraorbital sinus and nasal cavity at left, and a heterophilic core to the wattle at top right. (HE, 5X)

Staphylococcus aureus nurse colony on the plate. NAD- independent bacterial strains exist which sometimes pose a diagnostic challenge. In field conditions, it is often difficult to recover this bacterium, hence sending whole heads for bacterial culture is preferred if the veterinarians prefer to do necropsy in the field. *A. paragallinarum* can be categorized into 3 serovars or sub-serovars by hemagglutination inhibition tests [3,4] and/ or recently genotyping is used to categorize the bacteria with a high correlation with serovars, but the technique needs further studies.[2] The important virulence factors of *A. paragallinarum* include hemagglutinins (HAs), capsule, and RTX cytotoxin. HA is a 210 kDa protein coded by the *HMTp210* gene. The HA protein confer hemagglutination, cell adhesion, and biofilm formation. The capsule protects the bacteria from bactericidal activity of immune cells.

In this case, two whole bodies were submitted with swollen face, eyelids, wattles, lacrimation, and mucoid nasal discharge. Given the history of a sharp decline in egg production and upper respiratory signs, *Avibacterium paragallinarum, Mycoplasma gallisepticum,* and *Mycoplasma synoviae* were top differentials. An underlying Infectious bronchitis virus (IBV) was also speculated based on the history of bronchitis in the source flock from where the birds were sourced. Hemorrhagic wattles and nasal swabs were sent for bacterial culture and sensitivity, and trachea was sent for the detection of generic *Mycoplasma* and IBV PCR. The clinical signs were non-specific and can be observed with several other disease agents that can act as a primary pathogen or coexist concurrently with IC. The list includes *Mycoplasma gallisepticum, M. synoviae, Ornithobacterium rhinotracheale, Gallibacterium anatis, Pasteurella multocida,* and viral pathogens such *as* Avian Metapneumovirus virus (aMPV), IBV and infectious laryngotracheitis

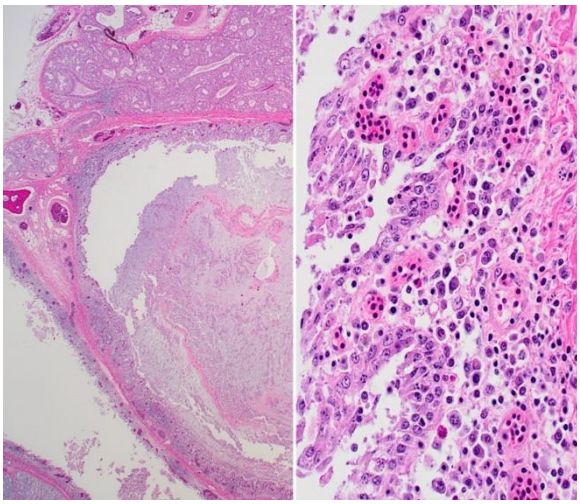

Figure 1-4. Head, chicken. The infraorbital sinus contains a mucocellular exudate within the lumen (left) and marked hyperplasia and profound mixed inflammation of the mucosal lining (right). A similar lesion is present in the nasal cavity (not pictured). (HE, 40X and 400X) (*Photo courtesy of* Diagnostic Services Unit, Faculty of Veterinary Medicine, University of Calgary)

virus (ILTV). In addition, poor management and ventilation can increase the severity of the disease.[2] No other bacteria were cultured other than *A. paragallinarum.* Low level of IBV was detected in the tracheal samples and *Mycoplasma* spp. were negative on PCR. Owing to the low level of the virus, genotyping was not possible in this case. ILT was excluded based on histopathology and the aMPV was not tested in this case as it was not in Canada at the time of the current case. The birds were not laying in this case and were not treated and culled. In general, if laying birds get infected, they can be treated, though they can become carriers following treatment and recurrence is possible. It is recommended to cull the flock as soon as it is close to the cycle completion due to biosecurity risk to commercial poultry. The affected flocks can be depopulated if the disease is not reported in the region to avoid future outbreaks. Inactivated bacterins are available to

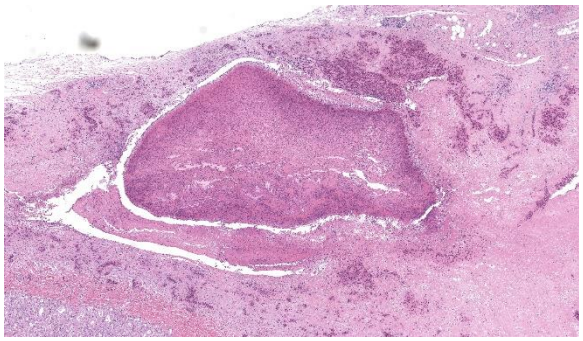

Figure 1-5. Head, chicken. The wattle is expanded by a necrotic core composed of abundant heterophilic debris and lined by a layer of epithelioid macrophages. The surrounding dermis and subcutis is effaced by a thick layer of vascularized fibrous connective tissue.

use in endemic areas to minimize the occurrence. Enhancing biosecurity and avoiding adding replacement birds to closed flocks are some of the strategies to reduce the occurrence of the disease.[1] Prior testing before movement can be done. In this case, replacement birds were introduced into the current flock without any testing which resulted in the disease outbreak. On further investigation, the source flock had a similar disease outbreak in the past. This highlights the importance of strict biosecurity, and quarantining of newly introduced birds when not raised on the same site. While the disease is very prevalent in the US and other countries, there is not much information on the occurrence of IC in Canada.

Contributing Institution:
Pathology & Diagnostic Services | Diagnostic Services Unit (DSU) | Faculty of Veterinary Medicine | University of Calgary (ucalgary.ca).
Faculty of Veterinary Medicine | University of Calgary (ucalgary.ca)

JPC Diagnosis:
1. Nasal cavity and infraorbital sinuses: Rhinitis and sinusitis, heterophilic and granulomatous, chronic, diffuse, severe, with luminal bacilli.
2. Comb: Dermatitis, necrotizing and heterophilic, chronic, diffuse, severe.
3. Harderian and conjunctival lacrimal glands: Dacryoadenitis, lymphoplasmacytic, chronic, diffuse, mild to moderate.

JPC Comment:
This conference's moderator was Dr. Tom Cecere of Virginia-Maryland CVM who led conference participants through a broad cross-section of infectious agents and production animal species. We enjoyed reviewing this first slide given that it is a microcosm of the gross pathology that the contributor nicely demonstrates, though orientation required consideration of the glands, sinuses, and unaffected epithelium accordingly. Our Gram stain confirmed gram-negative coccobacilli present within the infraorbital sinus (consistent with *Avibacterium*) along with fewer gram-positive bacilli and cocci. We interpreted the large region of necrosis and cellulitis as arising within the comb of this bird; we did not see any bacteria within this region on H&E or Gram stains. We differed from the contributor on osteomyelitis as bony changes within our section were mild (perhaps reflecting variation in submitted slides) though we did capture additional inflammation within adjacent glands as a secondary change in this case.
The contributor lays out a good differential diagnosis list for this case. Participants noted multinucleated giant cells (especially within the overlying skin) that prompted a discussion of viral syncytia (e.g. ILTV) versus granulomatous inflammation and macrophage activation. Given the likely polymicrobial infection at play in these birds, consider-

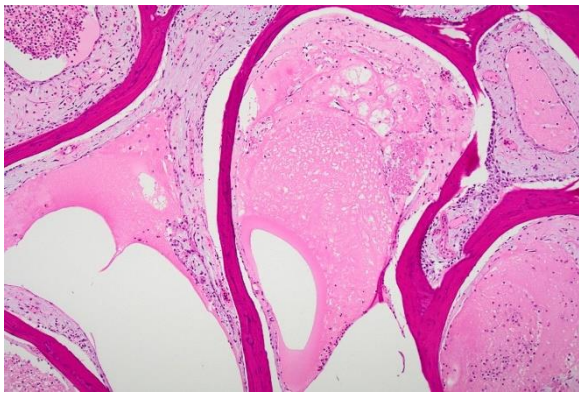

Figure 1-6. Head, chicken. The lining of the air spaces in the calvarium are markedly edematous and filled with proteinaceous fluid. (HE, 200X) (*Photo courtesy of* Diagnostic Services Unit, Faculty of Veterinary Medicine, University of Calgary)

ation of relevant histologic features and ancillary diagnostics such as culture and PCR is prudent for the supporting pathologist. Infectious coryza has also been reported on poultry farms and among smaller hobby flocks within the United States.[5,6] In contrast to this case, more acute/fulminant disease may have more fibrinous exudate and infection can extend to the abdominal air sacs and/or the pericardial sac and cause pericarditis and/or periphepatitis.[6] Complicated (polymicrobial) infections often lead to septicemia and marked flock mortality.[5,6] Flock susceptibility to IC can reflect vaccine failure (poor preparation, timing/delivery failure) as well as lack of cross-protection between different circulating serovars; use of vaccines in laying birds, meat birds, and breeder flocks varies by facilty.[6] Farm-farm transmission between poultry workers is a likely control factor as wild birds and insects have been shown to be ineffective vectors for IC.[6]

References:

1. Blackall PJ, Soriano-Vargas E. Infectious Coryza. In: Swayne DE, Boulianne M, Lounge CM, McDougald LM, Nair V, Suarez DL, eds. Vol. 2, *Diseases of Poultry*. Wiley-Blackwell 2014:890–906.
2. Gallardo RA, Da Silva AP, Egaña-Labrin S, et al. Infectious Coryza: Persistence, Genotyping, and Vaccine Testing. *Avian Dis*. 2020;64(2):157–165.
3. Kume K, Sawata A, Nakai T, Matsumoto M. Serological classification of Haemophilus paragallinarum with a hemagglutinin system. *J Clin Microbiol*. 1983;17(6):958–964.
4. Page LA. Haemophilus infections in chickens. I. Characteristics of 12 Haemophilus isolates recovered from diseased chickens. *Am J Vet Res*. 1962;23:85–95.
5. Davison S, Tracy L, Kelly DJ, Bender SJ, Pierdon MK, Mills J, Barnhart DJ, Licciardello S, Anis EAM, Wallner-Pendleton E, Dunn P, Robinson C, Ladman B, Kuchipudi SV. Infectious Coryza in Pennsylvania. Avian Dis. 2024 Sep;68(3):175-182.
6. Crispo M, Blackall P, Khan A, Shivaprasad HL, Clothier K, Sentíes-Cué CG, Cooper G, Blakey J, Pitesky M, Mountainspring G, Cutler G, Bickford A, Stoute S. Characterization of an Outbreak of Infectious Coryza (Avibacterium paragallinarum) in Commercial Chickens in Central California. Avian Dis. 2019 Sep 1;63(3):486-494.

CASE II:

Signalment:
4-week- suckling piglet, male neutered, Swiss Large White, *sus scrofa domesticus*, porcine.

History:
In March 2023, an increase in spinal deformities was detected on a Swiss breeding farm, characterized by thoracic lordosis and lumbar

kyphosis (“humpy-back syndrome”) and suckling as well as weaning piglets showed focal thickening of multiple ribs and facial oedema in an otherwise unremarkable clinical condition.

Gross Pathology:
Seven adjacent ribs show a marked focal callus formation. The longitudinal sections reveal rib fractures.

Laboratory Results:
qPCR for PCV-3 revealed high viral loads in kidney (Ct 21), mesenteric lymph node (Ct 12), rib (Ct 26) and brain (Ct 23).

Immunohistochemistry for detection of PCV-2 yielded a negative result.

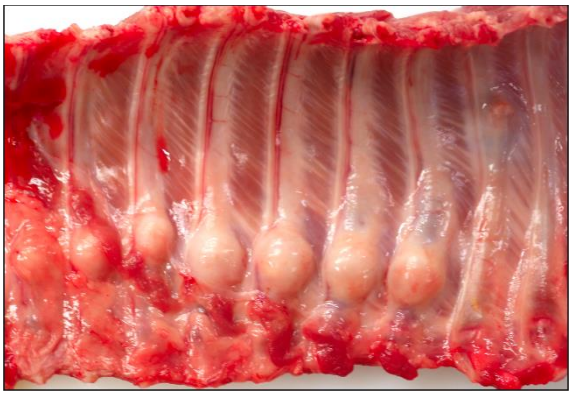

Figure 2-1. Rib, piglet. Left thoracic rib cage of a 4-week- suckling piglet showing seven adjacent rib fractures with marked callus formation. (*Photo courtesy of* Institute of Veterinary Pathology, Vetsuisse-Faculty, University of Zurich, https://www.vetpathology.uzh.ch/de.html)

Microscopic Description:
Bone, rib: In the calcification zone of the chondrocostal junction, a particularly high number of osteoblasts and osteoclasts are found (bone remodeling). Primary trabeculae vary in thickness, are fragmented and show cross-connections. The bone marrow contains all three hematopoietic cell lines with a slight increase in fibroblasts (myelofibrosis).

At the level of the macroscopically described bone distension, a blunt discontinuity of the osseous tissue is visible (fracture). The edges of the woven bone and multiple bone fragments within the fracture gap are lined by numerous multinucleated cells (osteoclasts) adjacent to scalloped, irregularly shaped bone (Howship’s lacunae). Within the fracture gap, the tissue is focally extensive replaced by irregular trabeculae of woven bone at varying stages of maturation along with granulation tissue. The immature woven bone, oriented perpendicular to the periosteum, is composed of densely organized collagen fibers and is often surrounded by numerous plump, large-nucleated mesenchymal cells (reactive osteoblasts) lying in a single layer. The granulation tissue extends into the adjacent bone marrow and is multifocally infiltrated by a moderate number of macrophages, lymphocytes, plasma cells, scattered neutrophils and few erythrocytes (acute hemorrhage).

In addition to multiple bone fragments, there are multifocal to coalescing areas of fibrous connective tissue and chondrocytes producing cartilage fragments (soft callus formation).

Furthermore, multifocal osteoid formations surrounded by osteoblasts are present. Neutrophils, fibrin and eosinophilic cellular and karyorrhectic debris (necrosis) as well as numerous multinucleated giant cells are found in the fracture gap.

Focally extending from the cortical surface and markedly elevating the periosteum, there is a periosteal proliferation of reactive, woven bone with trabeculae aligned perpendicular to the cortex (exostosis). The periosteum is diffusely highly expanded by collagenous connective tissue (periosteal fibrosis) and includes small fragments of

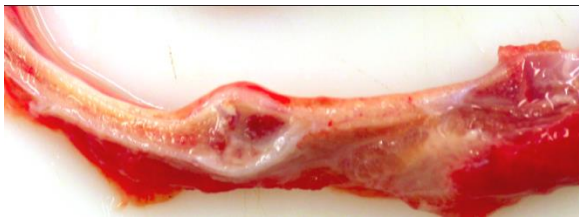

Figure 2-2. Rib, piglet. Longitudinal section of a rib with focal fracture and extensive callus formation (*Photo courtesy of* Institute of Veterinary Pathology, Vetsuisse-Faculty, University of Zurich, https://www.vetpathology.uzh.ch/de.html)

osseous tissue and abundant extravascular erythrocytes (acute hemorrhage).

The arteries in the periosteal tissue and those in the adjacent intercostal muscles and adipose tissue show infiltration of the media and the adventitia by a moderate number of small lymphocytes, plasma cells and sporadic macrophages. Similar infiltrates are found periarterially. The venous and lymphatic vessels, as well as the nerves, do not exhibit any alterations.

ISH detected abundant PCV-3 RNA in the rib (periosteal arterial walls, osteocytes and osteoblasts).

Contributor's Morphologic Diagnosis:
Bone, rib: Fracture with bone remodeling, focally extensive, marked with reactive woven bone formation (fracture callus), myelofibrosis and hemorrhage, multifocal, acute, mild to moderate as well as exostosis, periosteal, circumferential, moderate.

Arteritis and periarteritis, lymphoplasmacytic and histiocytic, multifocal, moderate to severe.

Contributor's Comment:
Circoviruses are single-stranded DNA viruses with a circular genome and one main capsid protein. They are prevalent across a variety of animals, including mammals, fish, birds, and insects. In pigs, four different porcine circoviruses (PCV) have been identified up to now: PCV-1, PCV-2, PCV-3 and PCV-4. PCVs are ubiquitous in global pig populations. While PCV-1 is accepted as non-pathogenic, PCV-2 is considered as an economically challenging pathogen on a global scale. Similarly to PCV-2, PCV-3 is widespread and detected in both healthy and diseased pigs, often in mummified and stillborn fetuses, indicating vertical and horizontal transmission of the viruses. PCV-4 has only recently been discovered and further information on this virus is required to understand its potential impact.[1]

PCV-3 infections are associated with various clinical and pathological manifestations, especially reproductive disorders, PDNS and multisystemic inflammatory diseases.[2,4] Furthermore, viral DNA has been detected in asymptomatic pigs and coinfections comprised of PCV3 with other swine pathogens have been frequently reported. This suggests that PCV-3 may act as a cofactor for some pathogens or may need other cofactors to cause clinical signs of disease.[3]

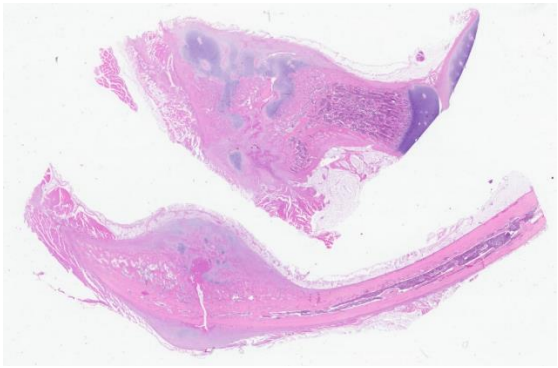

Figure 2-3. Rib, piglet. Two sections of rib with a diaphyseal fracture are submitted for examination. The physis is present in the section at top. (HE, 7X)

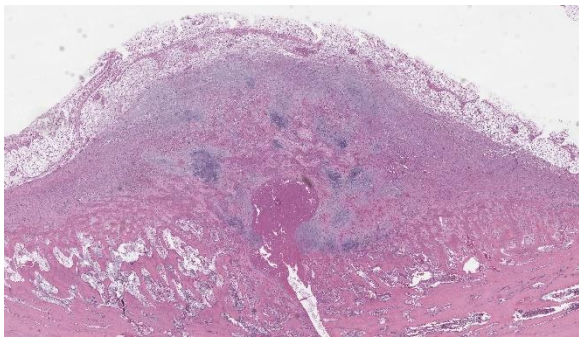

Figure 2-4. Rib, piglet. There is a large mature callus with anastomosing trabeculae of woven bone and large islands of cartilage over the fracture site (bottom center). (HE, 60X)

In situ hybridization (ISH) is used for the detection of PCV-3 in lesions. Histopathologic expertise is crucial as associated lesions may be subtle, requiring a degree of confidence to recognize these conditions. To diagnose PCV-3, a histopathologic specimen including heart, lung, spleen and lymph nodes should be submitted.[3] However, the clinical findings associated with PCV-3 are non-specific and require consideration of different pathogens. The "humpy-back-syndrome" is earliest observed in pigs of 3 weeks but most often detected at an age of 8 to 16 weeks.[4] It can arise as a secondary condition linked to multiple primary lesions within the vertebrae.[5] Primary lesions include osteomyelitis, fractures, neoplasms and metabolic diseases.[6] In addition, factors such as painful diseases of the legs and back[7], Musculo-mechanical stress on the lumbar spine[8], early onset of puberty in male pigs[9] and intrauterine viral infections[10] are contributing factors. A hereditary influence on the development of porcine kyphosis is suggested as well.[10]
The histological lesions in this case match the descriptions of PCV-3 systemic disease, but for the first time the virus has been detected by qPCR and ISH in bone lesions. In the last decade, authors reported cases of "humpy-back" pigs exhibiting histologically inflammatory vascular lesions comparable to those reported here.[4,11] Therefore, pathomorphological investigations and possible detection of PCV-3 is recommended in pigs displaying bone lesions and "humpy-back" posture.

Contributing Institution:
Institute of Veterinary Pathology
Vetsuisse-Faculty
University of Zurich
Winterthurerstrasse 268
8057 Zurich
Switzerland
https://www.vetpathology.uzh.ch/de.html

JPC Diagnosis:
Bone, rib: Diaphyseal fracture with maturing callus.

JPC Comment:
This was a case that generated a lively discussion. As Dr. Cecere did his PhD on circoviruses, he guided the group through assessing the changes present in this slide which were descriptively rewarding (and quite detailed). Ultimately, we summarized this case in a simple way and chose to focus on the H&E features before considering the ISH (and question of causation) presented in this case.

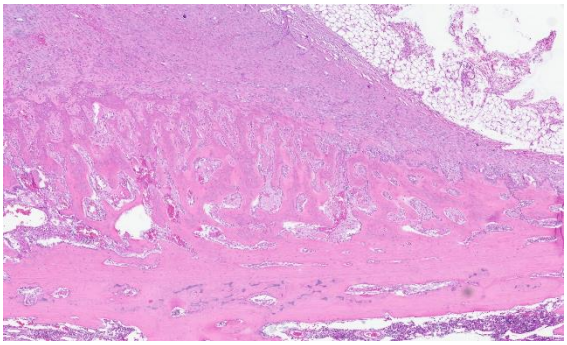

Figure 2-5. Rib, piglet. At the periphery of the callus, there is marked woven bone proliferation beneath the hypercellular periosteum. (HE, 75X)

We differed from the contributor in several

key aspects. Foremost, the section that we reviewed lacked a significant vascular component, though there is mild lymphocytic perivasculitis and lymphocytic infiltration within peripheral nerves present. There is also a lack of overt necrosis. These features make it harder to assess the role of viral-induced insult as the cause of the weakening and eventual fracture of these ribs (i.e. through disruption of blood flow to the developing bone) as there is no evidence to support this interpretation. Likewise, we reviewed the ISH image supplied by the contributor (Figure 2-6) and agree that the localization of nucleic acid within the vessel wall comports with the expected behavior of PCV-3, though the signal also extends beyond osteocytes/osteoblasts to include numerous cells within the adjacent fibrous tissue and callus. Another potential interpretation is that the non-vascular signal represents transfer of circoviral nucleic acid sto antigen-presenting cells (e.g. infiltrating histiocytes). As such, this result raises the question of "correlation or causation" i.e., changes *because of* PCV-3 or *in addition to* PCV-3. Although not included with this submission, additional information about the spleen, kidney, liver, and/or peripheral lymph nodes to confirm the presence of circoviral-associated disease (especially with corroborating ISH) was suggested by Dr. Cecere to develop this hypothesis further in future cases. Conference participants were also skeptical of myelofibrosis in this piglet and interpreted mesenchymal cells as part of the developing callus to stabilize the fracture – by convention, myelofibrosis implies a primary defect which seems less likely in this case.

It is worth briefly discussing several of the slide features in weighing differential diagnoses for this case. As this was a very young piglet, it is important to know that the

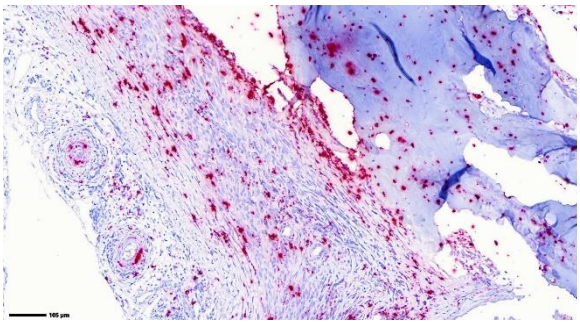

Figure 2-6. Rib, piglet. ISH detected abundant PCV-3 RNA in the rib (periosteal arterial walls, osteocytes and osteoblasts). (*Photo courtesy of* Institute of Veterinary Pathology, Vetsuisse-Faculty, University of Zurich, https://www.vetpathology.uzh.ch/de.html)

width of cortical bone closer to the physis/metaphysis (i.e., the "cut-back zone") is typically thinner for physiological reasons (this is where elongation of the bone takes place) which does not reflect osteoporosis or osteopetrosis. This animal had not yet developed a secondary center of ossification as well. Similarly, the degree of cartilage present within the primary spongiosa is appropriate for the age of this animal. Comparing the hue of physeal cartilage to cartilage within the developing callus is helpful to determine if both growth plates are in section (they are not in the slides submitted to the conference). Conference participants also discussed the 'rosary' gross appearance (Figure 2-1) which resembles a rachitic (rickets) . In the submitted sections, the physis at the costochondral junction in this animal is relatively normal histologically.

References:

1. Opriessnig T, Karuppannan AK, Castro AMMG, Xiao CT. Porcine circoviruses: current status, knowledge gaps and challenges. Virus Res. 2020 Sep;286:198044.
2. Palinski R, Piñeyro P, Shang P,et al. A Novel Porcine Circovirus Distantly Re-

lated to Known Circoviruses Is Associated with Porcine Dermatitis and Nephropathy Syndrome and Reproductive Failure. J Virol. 2016 Dec 16;91(1):e01879-16.
3. Kroeger et al. Five years of porcine circovirus 3: What have we learned about the clinical disease, immune pathogenesis, and diagnosis. Virus research, 2022, 314:198764
4. Drolet et al. Alopecia areata and humpyback syndrome in suckling piglets. The Canadian veterinary journal, 2012; 53(8):865-869.
5. Nielsen et al. Juvenile kyphosis in pigs. A spontaneous model of Scheuermann's kyphosis. Journal of pathology, microbiology and immunology - the APMIS journal, 2005, 113(10).
6. Lahrmann et al. Causes of kyphosis and lordosis with cuneiform vertebral deformation in swine. Berliner und Münchener Tierärztliche Wochenschrift, 1993, 106(4), 127-132.
7. Lahrmann et al. Deformities of the ventral column in weanling pigs caused by hemivertebrae or block vertebrae. Journal of Veterinary Medicine Series A, 1990, 38, 691-695.
8. Corradi et al. Acquired hemivertebrae in "humpy-backed" piglets. International Pig Veterinary Society Congress 2004, 1, 357.
9. Done et al. Lordosis and kyphosis ("humpy-back") in pigs. The pig journal, 1988, 41.
10. Done. Lordosis and kyphosis ("humpyback") in pigs; a second type of the condition associated with hemivertebrae. The pig journal, 1999, 43, 148-153.
11. Pallerés et al. Humpy backed pigs syndrome in spain. Anales de Veterinaria de Murcia, 2013, 29, 87-91.

Figure 3-1. Presentation, pig. The pig was presented in poor body condition, with prominent tuber ischia (pin bones) and ribs. (*Photo courtesy of*: State Veterinary Diagnostic Laboratory, Elizabeth Macarthur Agricultural Institute, Menangle, NSW, Australiahttps://www.dpi.nsw.gov.au/about-us/services/laboratory-services/veterinary)

CASE III:

Signalment:
6-12 week old, female, hybrid, *Sus scrofa domesticus*, pig.

History:
Multiple weaners on the property with poor body condition and wasting, leading to death.

Gross Pathology:
The pig was presented in poor body condition, with prominent tuber ischia (pin bones) and ribs. There was marked faecal staining around the anus. The large intestine, predominantly colon and caecum, was diffusely dilated with diffuse dark grey to red-brown discoloration of the serosa. Multifocally, the mucosa had white fibrinous lesions admixed with dark necrotic areas and areas of haemorrhage.

Laboratory Results:
Porcine circovirus type 2 real-time PCR: Positive

Salmonella enrichment culture: Positive.

Identification of *Salmonella* by serotyping: *Salmonella enterica* serovar infantis.

Brachyspira hyodysenteriae and *B. pilosicoli* multiplex PCR: Negative

Microscopic Description:
Colon or caecum (depending on the slide), H&E: Multifocally to coalescing, affecting the epithelium, lamina propria and submucosa, is marked loss of mucosa, with replacement by abundant mats of fibrillar eosinophilic material (fibrin), cellular and karyorrhectic debris, degenerate neutrophils, lymphocytes and macrophages, and colonies of basophilic bacteria with rod morphology. Small vessels in affected areas have disrupted endothelium and are often filled with thrombi. In less affected areas, crypts are markedly elongated, ectatic, with attenuated epithelium and contain amphophilic to pale basophilic fibrillar material (mucus) or filled with degenerate neutrophils and necrotic debris (crypt abscess). Multifocally, there is mild goblet cell hyperplasia. Multifocally, the lamina propria and submucosa are expanded by lymphocytes, macrophages, and plasma cells; with occasional small vessels containing thrombi. Multifocally, numerous ciliated protozoa (*Balantidium coli*) are free in the lumen or admixed with necrotic material and buried deep in the mucosa. The serosa is focally markedly expanded by neutrophils and fibroblastic proliferation, underlying a thin mat of fibrin, clear areas, and a florid perivascular infiltrate of lymphocytes and plasma cells.

Colon or caecum (depending on the slide), Warthin-Starry: Multifocally, abundant colonies of bacteria with rod morphology are highlighted within the areas of ulceration, necrosis and inflammation, previously described in H&E.

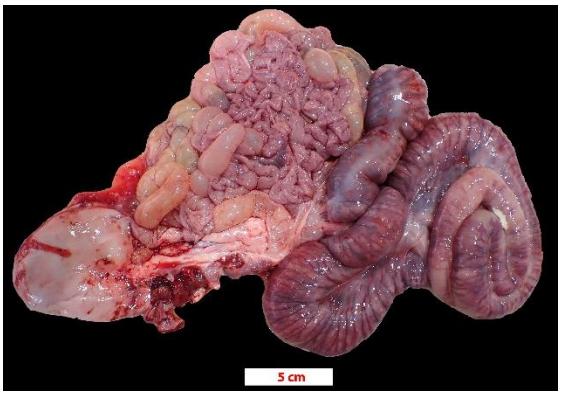

Figure 3-2. Abdominal viscera, pig. The colon and caecum are diffusely dilated with diffuse dark grey to red-brown discoloration of the serosa. (*Photo courtesy of*: State Veterinary Diagnostic Laboratory, Elizabeth Macarthur Agricultural Institute, Menangle, NSW, Australiahttps://www.dpi.nsw.gov.au/about-us/services/laboratory-services/veterinary)

Contributor's Morphologic Diagnosis:
Colon or caecum: Colitis or typhlitis, fibrinonecrotizing, multifocal to coalescing, severe, with diphtheritic membranes, goblet cell hyperplasia, thrombosis, abundant intralesional rod-shaped bacteria, and numerous intralesional protozoan ciliates, hybrid breed, *Sus scrofa*.

Contributor's Comment:
Salmonellosis is a common bacterial infection of mammals and birds, resulting in various syndromes such as septicaemia, enterocolitis, abortion and pneumonia. There are two recognized species of Salmonella*: S. enterica* and *S. bongori*, of which there are a vast number of serovars and serotypes.[5] Additionally, there are three broad groups of Salmonella serovars to consider: those that are host adapted to humans and higher primates, those that are host adapted to certain animal species and those that are not host adapted.[1] Several *Salmonella enterica* serovars, most commonly Typhimurium, Derby and Cholerasuis, have been identified

Figure 3-3. Colon, pig. Multifocally, the mucosa had white fibrinous lesions admixed with dark necrotic areas and areas of haemorrhage. (*Photo courtesy of*: State Veterinary Diagnostic Laboratory, Elizabeth Macarthur Agricultural Institute, Menangle, NSW, Australiahttps://www.dpi.nsw.gov.au/ about-us/services/laboratory-services/v eterinary)

to cause enterocolitis and septicaemia in swine;[13] Cholerasuis is host adapted to swine, while Typhimurium and Derby also commonly cause disease in ruminants and poultry.

The *Salmonella enterica* serovar isolated in this case, *Salmonella* Infantis, has been identified from both clinically normal and ill pigs, as well as in the environment and carcasses of pigs at slaughterhouses.[7] While this serotype is less commonly identified compared to Typhimurium, Cholerasuis, and Derby, prevalence of this serotype is increasing. In a number of studies across Canada, the United States and Brazil, *Salmonella* Infantis was consistently the 3rd to 4th most identified serotype in farms, slaughterhouses and in diagnostic samples at veterinary laboratories, with evidence for increasing prevalence over time.[6-8,12,15] This serotype is also of public health concern due to its zoonotic potential and antibiotic resistance.[4,7,9] *Salmonella* Infantis has been isolated in a number of food safety trials, involving both contaminated pork and poultry meat, presenting increasing risk to human health.[4,10,11] Interestingly, poultry are asymptomatic carriers of *Salmonella* Infantis.[10,14]

There are no published reports of the gross or histological changes observed with *Salmonella* Infantis infection in swine, as far as the authors are aware. Comparatively, the gross and histological changes seen in this case are most similar to infection with *Salmonella* Typhimurium in swine, where diphtheritic enterocolitis is also generally confined to the large intestine and rectum, with minimal involvement of the distal ileum.[13] Other bacterial agents that were considered in this case given the gross and histological findings included *Brachyspira hyodysenteriae* and *B. pilosicoli* as well as *Clostridium perfringens* types A and C. Both *B. hyodysenteriae* and *pilosicoli* cause fibrinonecrotic and erosive lesions limited to the colon and caecum. Diphtheritic membranes are also a common gross feature of *B. pilosicoli* infection. *Clostridium perfringens* types A and C both cause necrohaemorrhagic enterocolitis in neonatal piglets. While lesions generally involve the small intestine, severe cases also involve the large intestine.

Figure 3-4. Colon, pig. One section of colon is presented for examination. There are multifocal full-thickness mucosal ulcers. (HE, 11X)

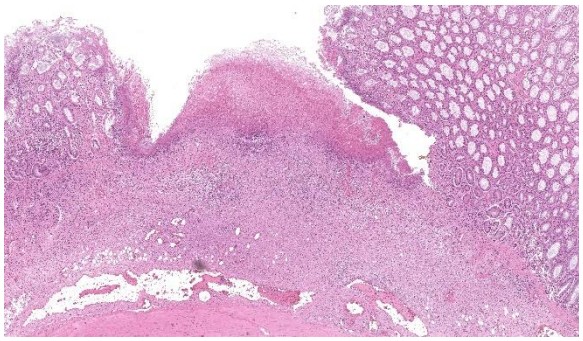

Figure 3-5. Colon, pig. Ulcers are covered by a fibrinocellular membrane and consist of abundant cellular debris admixed with infiltrating viable and necrotic neutrophils and macrophages. Inflammation and necrosis extends downward into the underlying submucosa and peripherally into the lamina propria of the adjacent mucosa. (HE, 68X)

The pathogenicity of *Salmonella* relies on a number of *Salmonella* pathogenicity islands (SPIs) and other virulence genes within the genome. The SPI-1 proteins are mainly associated with invasion of the cell, while SPI-2 proteins are involved with survival and replication within host cells; a number of virulence markers contained within SP-1 and SP-2 are present in *Salmonella* Infantis isolates, indicating the pathogenicity of this serotype.[2] Virulence associated plasmids are also vitally important for the survival and growth of *Salmonella* within macrophages.[2] Observable histological changes (reduction in villi length) can be present in the small intestine from one day post-infection with *Salmonella* Typhimurium, with severe changes such as villous atrophy and epithelial damage seen as early as two days post-infection.[3]

Contributing Institution:
State Veterinary Diagnostic Laboratory
Elizabeth Macarthur Agricultural Institute
Woodbridge Rd, Menangle
NSW, 2568
Australia

https://www.dpi.nsw.gov.au/about-us/services/laboratory-services/veterinary

JPC Diagnosis:
Colon: Colitis, ulcerative, subacute, multifocal, marked, with vasculitis, thrombosis, and diffuse lymphoid depletion.

JPC Comment:
We thank the contributor for sharing this slide with us as the ancillary diagnostics opened up a great conference discussion. Our Gram stain demonstrated gram-negative bacilli adjacent to ulcerated areas of the colon, consistent with the presence of *Salmonella* Infantis outlined above and likely the primary process in this animal though this feature was not apparent to us on H&E. Conference participants offered a number of

other possible etiologies (and/or coinfections) which had varying levels of support, including *Lawsonia* (here lacking a marked proliferative component and the degree of hemorrhage in this case is not severe), *Clostridium (Clostridioides difficile* - a good differential in a newborn animal), and African or Classical Swine fever (better supported by marked hemorrhage in additional organs). We debated the relevance of *Brachyspira* in this case despite the PCR result as we noted many spirochetes present

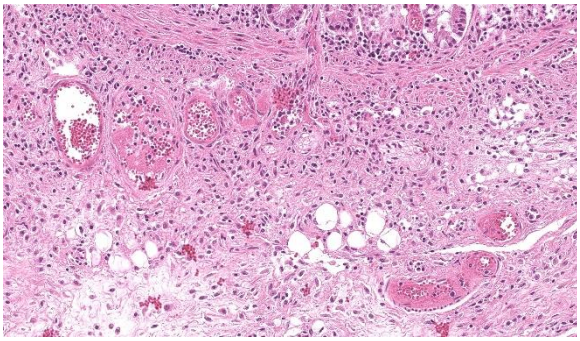

Figure 3-6. Colon, pig. Submucosal vessels often contain fibrin thrombi. (HE, 758X)

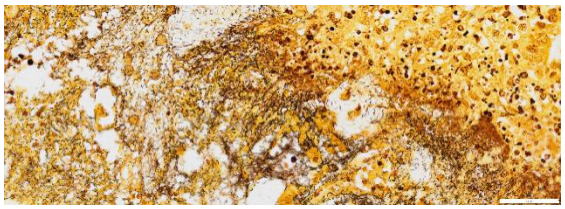

Figure 3-7. Colon, pig. A silver stain demonstrates large numbers of bacterial rods within areas of ulceration. (Warthin-Starry 3.2, 400X) (*Photo courtesy of*: State Veterinary Diagnostic Laboratory, Elizabeth Macarthur Agricultural Institute, Menangle, NSW, Australiahttps://www.dpi.nsw.gov.au /about-us/services/laboratory-services/ veterinary)

within colonic crypts on our silver stain as well (similar to Figure 3-7), though it is possible that this could reflect a normal amount to a slight overgrowth secondary to ulceration induced by *Salmonella* – the degree of mucus present on this section is not overwhelming as well. There is also a moderate number of ciliated trophozoites present within the lumen of the colon (consistent with *Balantidium coli*, a normal colonic commensal) which we did not assign any pathologic significance to.

One subtle feature of this case that should not be overlooked is the depletion in lymphoid cells within the colon. Simply put, there isn't lymphoid tissue present at all in this section which underscores the need to review tissues systemically to detect severe changes. That this animal was PCR-positive for PCV-2 is a potential explanation, though there is no corroborating evidence such as cytoplasmic botryoid viral inclusions despite the vasculitis present. *Salmonella* is another major cause of lymphoid depletion, and often accomplishes this 'task' shortly after entering aggregated lymphoid nodules (GALT; Peyer's patches) via overlying M cells. Conference participants extrapolated that the ulcers in the colon of this pig ('button-like') probably reflected this pathogenesis with accompanying infarction of the adjacent submucosal blood vessels.

References:

1. Agbaje M, Begum RH, Oyekunle MA, Ojo OE, Adenubi OT. Evolution of Salmonella nomenclature: a critical note. *Folia Microbiologica*. 2011;56**:** 497-503.
2. Almeida F, Pitondo-Silva A, Oliveira MA, Falcão JP. Molecular epidemiology and virulence markers of Salmonella Infantis isolated over 25years in São Paulo State, Brazil. *Infection, Genetics and Evolution*. 2013;19**:** 145-151.
3. Bellido-Carreras N, Argüello H, Zaldívar-López S, et al. Salmonella Typhimurium Infection Along the Porcine Gastrointestinal Tract and Associated Lymphoid Tissues. *Veterinary Pathology*. 2019;56**:** 681-690.
4. Borowiak M, Szabo I, Baumann B, et al. VIM-1-producing Salmonella Infantis isolated from swine and minced pork meat in Germany. *Journal of Antimicrobial Chemotherapy*. 2017;72**:** 2131-2133.
5. Brenner FW, Villar RG, Angulo FJ, Tauxe R, Swaminathan B. Salmonella Nomenclature. *Journal of Clinical Microbiology*. 2000;38**:** 2465-2467.
6. Clothier KA, Kinyon JM, Frana TS. Comparison of Salmonella Serovar Isolation and Antimicrobial Resistance Patterns from Porcine Samples Between 2003 and 2008. *Journal of Veterinary Diagnostic Investigation*. 2010;22**:** 578-582.
7. de Quadros CL, Manto L, Mistura E, et al. Antimicrobial and Disinfectant Susceptibility of Salmonella Serotypes Isolated from Swine Slaughterhouses. *Current Microbiology*. 2020;77**:** 1035-1042.
8. Farzan A, Friendship RM, Dewey CE, Muckle AC, Gray JT, Funk J.

Distribution of Salmonella serovars and phage types on 80 Ontario swine farms in 2004. *Canadian Journal of Veterinary Research*. 2008;72**:** 1.
9. Gal-Mor O, Valinsky L, Weinberger M, et al. Multidrug-resistant Salmonella enterica serovar Infantis, Israel. *Emerg Infect Dis*. 2010;16**:** 1754-1757.
10. Hauser E, Tietze E, Helmuth R, et al. Clonal dissemination of Salmonella enterica serovar Infantis in Germany. *Foodborne Pathog Dis*. 2012;9**:** 352-360.
11. Khalafalla F, Abdel-Atty N, Abdel-Wanis SA, Hanafy AS. Food poisoning microorganisms in chicken broiler meat. *Glob Vet*. 2015;14**:** 211-218.
12. Possebon FS, Tiba Casas MR, Nero LA, Yamatogi RS, Araújo Jr JP, Pinto JPdAN. Prevalence, antibiotic resistance, PFGE and MLST characterization of Salmonella in swine mesenteric lymph nodes. *Preventive Veterinary Medicine*. 2020;179**:** 105024
13. Uzal FA, Plattner BL, Hostetter JM. Alimentary System. *Jubb, Kennedy & Palmer's Pathology of Domestic Animals: Volume 2*. 2016**:** 1-257.e252.
14. Yokoyama E, Ando N, Ohta T, et al. A novel subpopulation of Salmonella enterica serovar Infantis strains isolated from broiler chicken organs other than the gastrointestinal tract. *Veterinary Microbiology*. 2015;175**:** 312-318.
15. Yuan C, Krull A, Wang C, et al. Changes in the prevalence of Salmonella serovars associated swine production and correlations of avian, bovine and swine-associated serovars with human-associated serovars in the United States (1997–2015). *Zoonoses and Public Health*. 2018;65**:** 648-661.

CASE IV:

Signalment:
16 weeks, male, domestic white turkey (*Meleagris gallopavo*).

History:
A flock of 7,500 domestic white male turkeys was experiencing elevated mortality as a result of both aortic rupture and culling of lame, recumbent birds. Recumbent birds had swollen intertarsal (hock) joints with bruising of the nonfeathered skin of the hock. Five affected legs were removed at the coxofemoral joint from culled carcasses and shipped to the Minnesota Veterinary Diagnostic Laboratory.

Gross Pathology:
The submitted turkey legs had skin bruising of the caudal aspect of the hock. The hocks were swollen as a result of periarticular subcutaneous edema (serosanguinous fluid) and increased volume of synovial fluid within the hock joints and sheaths of the gastrocnemius tendon and digital flexor sheaths. In two legs, the gastrocnemius tendon was partially rup-

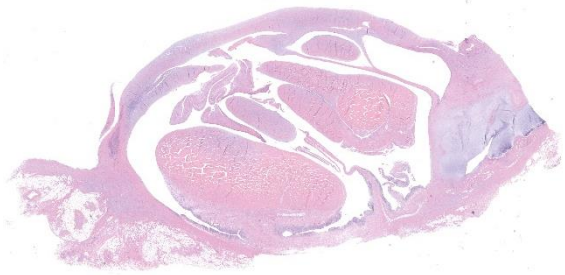

Figure 4-1. Tendons and tendon sheath, turkey. A section through the gastrocnemius and digital flexor tendons is submitted for examination. There is an adhesion between the gastrocnemius tendon and the adjacent tendon sheath (center, bottom). (HE, 10X)

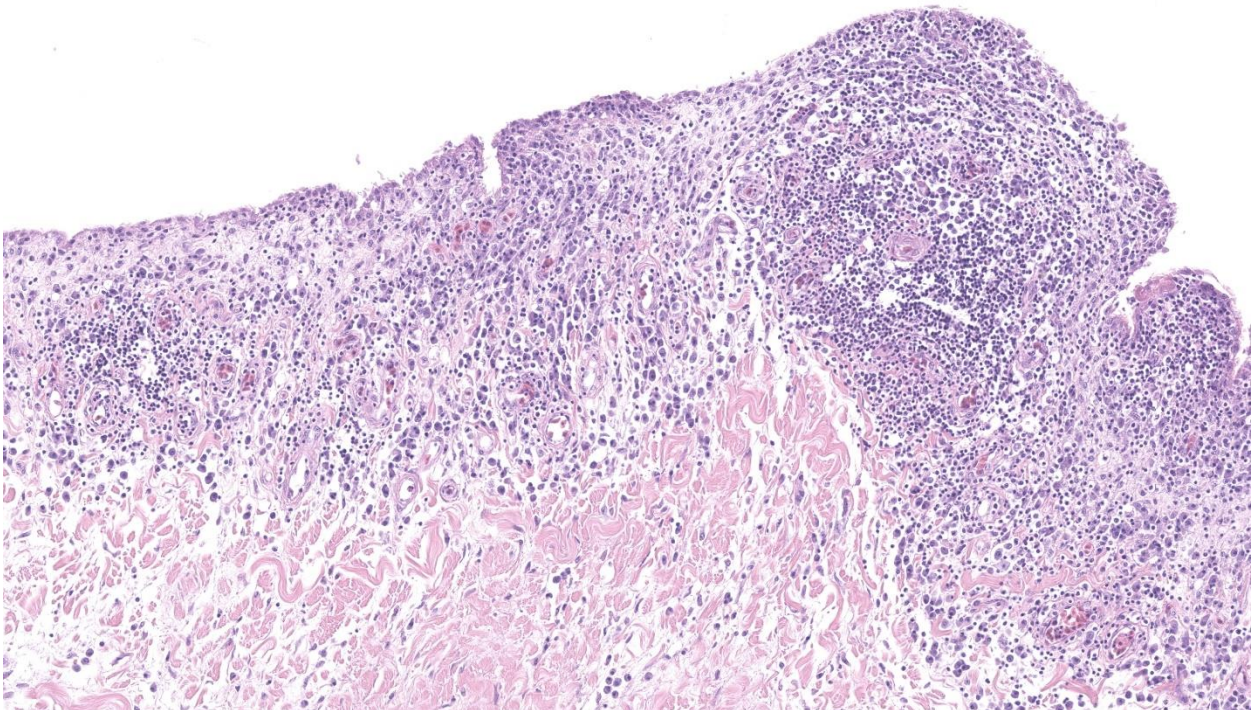

Figure 4-2. Tendon sheath, turkey. There is marked chronic inflammation of the edematous tendon sheath, with numerous lymphocytes and plasma cells, occasionally in aggregates, beneath the synovial lining. (HE, 268X)

tured proximal to the hock joint. Longitudinal sections of the femur, tibiotarsus and tarsometatarsus showed no overt lesions (no evidence of osteomyelitis or chondrodysplasia) in bone or growth plate.

Laboratory Results:
-Aerobic culture: Hock joint fluid- no significant growth

-Molecular diagnostics: Gastrocnemius tendon was positive (CT 32.5) for avian reovirus by universal avian reovirus PCR

Synovial fluid was negative for *Mycoplasma gallisepticum* and *Mycoplasma synoviae* by PCR

-Virology: Reovirus was isolated after one pass on embryonated eggs (yolk sac inoculation) and after two passes on QT-35 (quail fibroblast) cell line

Microscopic Description:
The tissue is a cross-section of gastrocnemius tendon complex, composed of the tendon and sheaths of the primary gastrocnemius tendon and multiple smaller digital flexor tendons and sheaths. Inflammation largely affects the tendon sheaths and consists of multifocal, moderate to marked infiltrates of lymphocytes and plasma cells either scattered or arranged in perivascular fashion within the edematous subsynovium. Rare heterophils are also observed. Adjacent synoviocytes are hypertrophic. No microorganisms are observed.

Contributor's Morphologic Diagnosis:
Gastrocnemius and digital flexor tendons: tenosynovitis, lymphoplasmacytic with subsynovial edema and synoviocyte hypertrophy

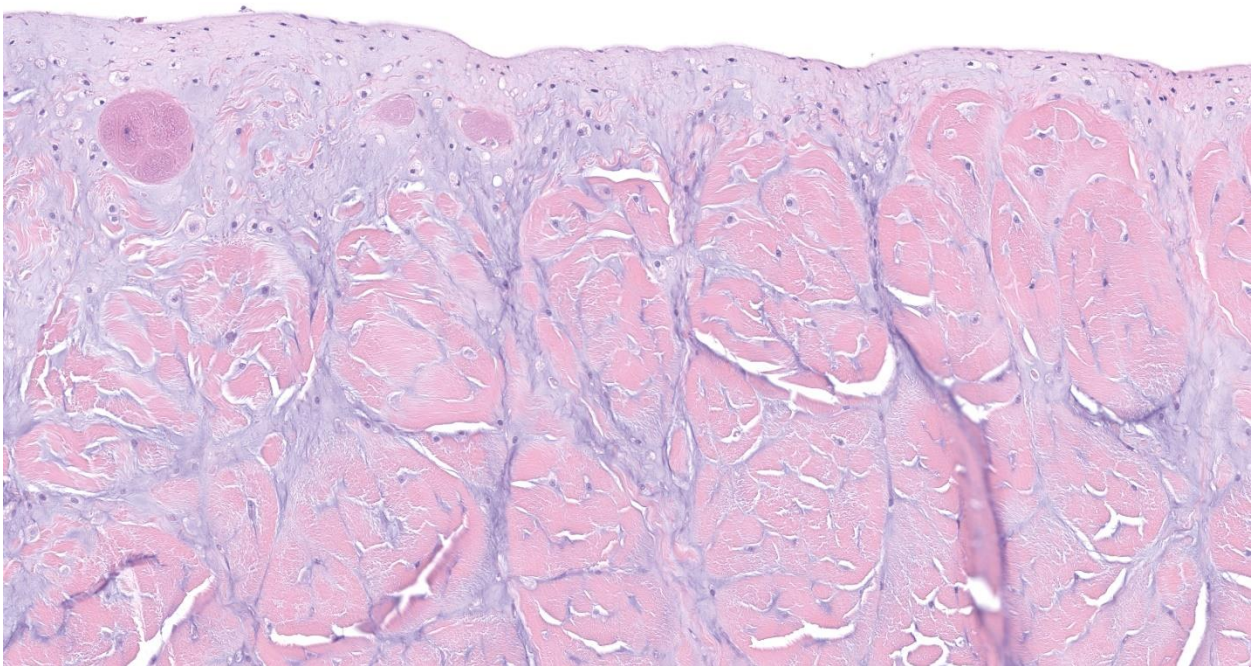

Figure 4-3. Tendon sheath, turkey. There are degenerative changes in the gastrocnemius tendon with abundant ground substance within the interstitium between collagen fibers, which is undergoing cartilaginous metaplasia. Similar, but less severe changes are seen in other tendons as well as the tendon sheath. (HE 323X)

Contributor's Comment:
Turkey arthritis reovirus (TARV) causes lameness in domestic turkeys, including both turkey breeders and meat-type turkeys, and affecting both sexes by 12-17 weeks of age. Males generally show clinical signs more often than females, likely because of the greater male body weight. In the 1980s, there were two reports of reovirus isolated from the gastrocnemius tendons of domestic turkeys affected with arthritis/tenosynovitis, but this condition was not experimentally reproduced at the time and was not observed again for nearly 25 years when it was reported in Minnesota.[2,4,5] Thereafter, there were multiple reports of TARV-associated outbreaks of lameness in market age turkeys,[3,10] resulting in substantial economic losses in the form of increased culling, mortality, poor feed efficiency, low rates of weight gain, aortic rup tures and increased condemnations at the processing plant.[3,6,10] The disease has been experimentally reproduced to confirm the involvement of reovirus and the infection has consistently been associated with uni- or bilateral lameness due to swelling of the intertarsal (hock joints), periarticular fibrosis, tenosynovitis, occasional erosion of articular cartilage of the hock joints and rupture of the gastrocnemius tendon or digital flexor tendons.[4,6,7,8] More recently, reoviruses that are genetically identical to turkey arthritis reovirus have been shown to cause or have been associated with hepatitis and meningoencephalomyelitis in turkey poults.[1] Avian reoviruses of turkeys are members of the genus *Orthoreovirus* in the family *Reoviridae* containing a double-stranded, segmented RNA genome in a double-shelled capsid. The ten genome segments are classified as L class (L1-L3), M class (M1-M3) and S class (S1-

S4) based on their electrophoretic mobility.[9] A similar condition of reoviral tenosynovitis in chickens ("viral arthritis") has been recognized for many years; however, gene segments of the chicken arthritis reoviruses bear only 80-85 % homology with the turkey arthritis reoviruses. It is likely that the turkey reoviruses represent a more recent mutation of the chicken reoviruses.

Contributing Institution:
University of Minnesota Veterinary Diagnostic Laboratory

https://vdl.umn.edu/

JPC Diagnosis:
Gastrocnemius and digital flexor tendons (presumptive): Tenosynovitis, lymphoplasmacytic, chronic, multifocal to coalescing, moderate.

JPC Comment:
The final case of this conference is a cross-section of multiple large tendons. From the H&E alone, we speculated that this likely represented the gastrocnemius and digital flexor tendons (given the approximate size/width presented) and adjusted our morphologic diagnosis accordingly. The section is nicely presented, with the distribution of lymphoplasmacytic inflammation being readily apparent even from low magnification. Conference participants also considered *Enterococcus* and *Mycoplasma synoviae* as less likely differential diagnoses for this case.

An interesting finding in this slide is the large amount of amphophilic to basophilic substance present in the affected tendon reflects notable deposition of ground substance (including proteoglycans, glycosaminoglycans;) and even cartilaginous metaplasia (Fig 4-3). We debated its origin carefully, weighing the natural progression of 'turkeydom' and rapid weight gains effect on the tendons of the legs versus virally-induced changes. The bulk of participants felt that the deposition of anastomosing ground substance was most attributable to the rapid weight gain (and increased shear and concussive force in this area.) Though it is possible that reoviral changes could weaken collagen and augment rupture of tendons, we did not have clear evidence of inflammatory cells associated with this material (i.e. tendonitis). As such, we probably could (should?) have two morphologic diagnoses for this case, but we could not agree on what to call this process with some participants unsatisfied with the vagueness of 'tendinopathy' or 'tendinosis' or if (in true WSC fashion) an expected lesion in a heavy meat bird merited an entire paragraph to explain it (it appears it does)! It is some consolation perhaps to consider a comparison to human sports-induced tendinopathies,[11] which have analogous gross and histologic appearance – something worth considering for those that enjoy running like the JPC residents do. Careful description of disorganized collagen, ground substance, the presence or absence of inflammatory cells, and changes in supporting stroma are helpful in categorizing these conditions.[11]

References:

1. Kumar R, Sharafeldin TA, Nader MS, et al. Comparative pathogenesis of turkey reoviruses. Avian Pathol. 2022;51:435-444.
2. Levisohn A, Gur-Lavie A, Weisman, J. Infectious synovitis in turkeys: Isolation of tenosynovitis virus-like agent. *Avian Pathol*. 1980;9:1-4.
3. Lu HY, Dunn PA, Wallner-Pendleton EA, et al. Isolation and molecular characterization of newly emerging avian reoviruse variants and novel strains in Pennsylvania, U.S.A., 2011-2-14. *Sci Rep*. 2015;5:14727.
4. Mor SK, Sharafeldin TA, Porter RE, et al.

Isolation and characterization of a turkey arthritis reovirus. *Avian Dis*. 2013;57:97-103.
5. Page RK, Fletcher Jr OJ, Villegas P. Infectious tenosynovitis in young turkeys. *Avian Dis*. 1982;26:924-927.
6. Porter R. Turkey Reoviral Arthritis: A Novel Condition in the United States. In: *Proceedings International Turkey Production and Science Meeting*, Chester, England. March 22, 2018. Proceedings pp. 31-35.
7. Sharafeldin TA, Mor SK, Bekele, AZ, et al. The role of avian reoviruses in turkey tenosynovitis/arthritis. *Avian Pathol*. 2014;43:371-378.
8. Sharafeldin TA, Mor SK, Bekele AZ, et al. Experimentally induced lameness in turkeys inoculated with a newly emergent turkey reovirus. *Vet Res*. 2015;46:11-16.
9. Spanididos DA, Graham AF. Physical and chemical characterization of an avian reovirus. *J Virol*. 1976;3:968-976.
10. Tang Y, Sebastian A, Yeh YT, et al. Genomic characterization of a turkey reovirus field strain by Next-Generation Sequencing. *Infect. Genetic. Evol*. 2015;32;313-321.
11. Khan KM, Cook JL, Bonar F, Harcourt P, Astrom M. Histopathology of common tendinopathies. Update and implications for clinical management. Sports Med. 1999 Jun;27(6):393-408.

Joint Pathology Center
Veterinary Pathology Services

WEDNESDAY SLIDE CONFERENCE 2024-2025

Conference #16 — 15 January 2025

CASE I:

Signalment:
12-day-old, female, collared finchbill (*Spizixos semitorques*).

History:
A parent-raised chick was found dead on the ground outside of the nest without any premonitory signs. The carcass was covered by ants. The weather conditions on the day before were reported to be very hot.

Gross Pathology:
The chick was in fair body condition with small amounts of visceral adipose tissue. No major gross changes were identified except for some loss of skin, which was presumed to be due to postmortem scavenging.

Laboratory Results:
Bacteria were identified as *Clostridium piliforme* on the basis of conventional PCR and subsequent sequencing (target bacterial 16S rRNA) utilizing formalin-fixed paraffin-embedded brain tissue.

Microscopic Description:
Scattered throughout the cerebrum and affecting approximately 30% of the neuroparenchyma are multiple poorly demarcated to coalescing areas of hypercellularity. These areas have slightly prominent vasculature and are occasionally associated with hypereosinophilia or small lakes of extravasated erythrocytes. The cells infiltrating the neuroparenchyma are with a mix of granulocytes (heterophils), macrophages, and fewer lymphocytes and plasma cells, accompanied by increased numbers of glial cells and some necrotic debris. Occasionally, neurons are hypereosinophilic with smudgy or pyknotic nuclei. Other neurons relatively frequently contain stacks of faint, long, rod-shaped bacteria. Larger blood vessels within the inflammatory foci are frequently cuffed by dense aggregates of mononuclear cells that are up to five cell layers thick. The inflammatory cells additionally involve the overlying leptomeninges.

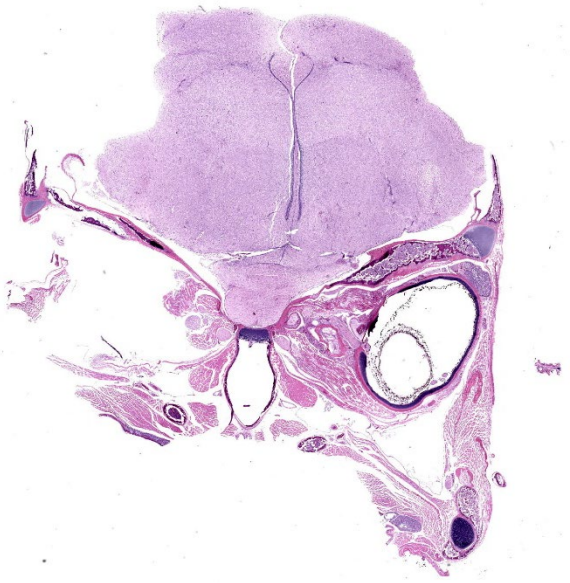

Figure 1-1. Head, collared finchbill. A slightly oblique cross section of the head is submitted for examination. (HE, 6X)

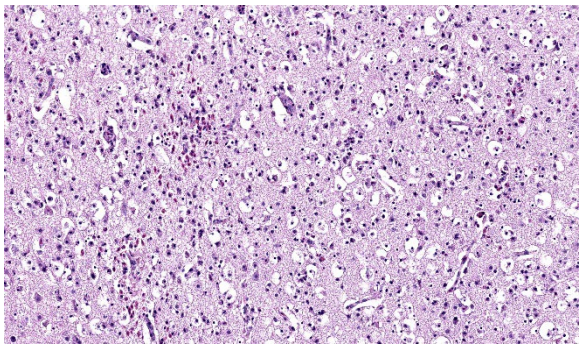

Figure 1-2. Cerebrum, collared finchbill. There are coalescing areas of hypercellularity, spongiosis, and small areas of hemorrhage within both cerebral hemispheres. (HE, 290X)

Steiner's silver and Gram stains were performed to better characterize the intracellular bacteria. Myriads of strongly argyrophilic, curvilinear to filamentous bacilli were highlighted on the silver stain, mapping to the areas of inflammation and necrosis. On the Gram stain, these bacteria were gram-negative.

Contributor's Morphologic Diagnosis:
Brain, cerebrum: moderate, multifocal to coalescing, subacute heterophilic and necrotizing meningoencephalitis with myriad intracellular argyrophilic and gram-negative filamentous bacilli, consistent with clostridial encephalitis

Contributor's Comment:
The characteristic histologic appearance of the intracellular filamentous bacilli was highly suggestive of Tyzzer's disease, caused by *Clostridium piliforme*. The etiologic diagnosis was further supported by the strongly argyrophilic and gram-negative nature of the bacteria and subsequently confirmed by molecular techniques. There were no bacteria morphologically compatible with *C. piliforme* or necrotizing inflammation in the other examined organs however.

Tyzzer's disease has been reported in a wide variety of mammalian species and is a major differential diagnosis for cases of hepatitis, myocarditis, and colitis, especially when this triad of lesions is noted concurrently.[7] While *C. piliforme* is not often thought of as a pathogen affecting birds, encephalitis in young birds is a known manifestation of Tyzzer's disease.[1,2,4,5] The condition is reported to affect both wild and captive birds from several orders, including passerines, psittacines, and piciformes. Affected birds can present with neurologic signs such as head tilt and torticollis. Histopathologic changes are often localized to the brain and characterized by multifocal to coalescing areas of mixed inflammation and necrosis.[1-2] Less commonly, birds can present with lesions in the liver, heart, and gastrointestinal tract, similar to mammals.[4]

At our institution, we have identified seven cases of avian Tyzzer's disease to date, including five metallic starlings (*Aplonis metallica*) between 11 to 25 days-old and two other collared finchbills (12 days old and 3 years, 5 months old). Six of these cases had encephalitis with no evidence of argyrophilic bacteria in the other examined tissues. The one case without brain involvement was the only adult bird in this list. This adult finchbill had multifocal random hepatitis with intracellular argyrophilic bacteria. Tyzzer's disease should be on the list of differential diagnoses in young birds with encephalitis.

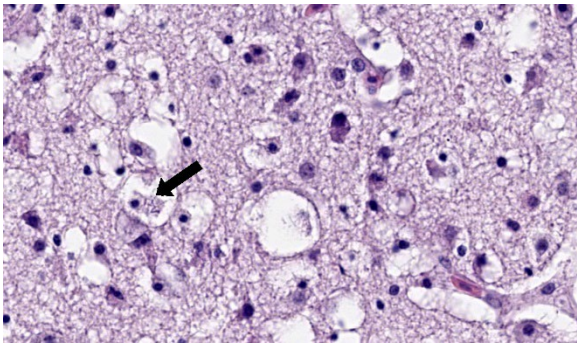

Figure 1-3. Cerebrum, collared finchbill. In areas of necrosis, glial cells occasionally contain 1x3 bacterial rods within their cytoplasm (arrow). (HE, 756X)

Contributing Institution:
San Diego Zoo Wildlife Alliance

Disease Investigations

https://science.sandiegozoo.org/disease-investigations

JPC Diagnosis:
Brain: Meningoencephalitis, heterophilic and necrotizing, subacute, multifocal, moderate with intracytoplasmic filamentous bacilli.

JPC Comment:
This week's moderator was Dr. Francisco (Paco) Uzal, Distinguished Professor of Veterinary Diagnostic Pathology at UC Davis and a in gastrointestinal and clostridial diseases.

This first case was recently shared at the Davis-Thompson Foundation's 2024 Northeast Veterinary Pathology Conference and we are pleased to share it with a wider audience. Conference participants homed in on the prominent cuffing of vessels and heterophilic inflammation within the neuroparenchyma and meninges. The increased cellularity is notable, even for an avian brain (which are typically more cellular than their mammalian counterparts.)Differential diagnoses from the group favored viral etiologies (e.g. highly pathogenic avian influenza) and avian chlamydiosis. Dr. Uzal noted that visualizing intracytoplasmic filamentous bacteria was difficult on H&E, though either a Gram or argyrophilic stains were helpful for making a definitive diagnosis.

The contributor nicely summarizes the current literature on avian cases of Tyzzer's disease and adds several observations from their own collection. We have covered *C. piliforme* many times in the WSC, most recently in a horse in Conference 4, Case 1, 2023-2024. Neurologic involvement remains rare,although there is a recent case report in a cat of systemic involvement with cutaneous

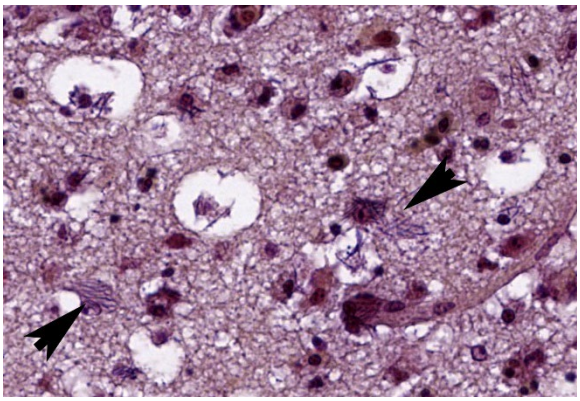

Figure 1-4. Cerebrum, collared finchbill. A tissue Gram-stain demonstrates aggregates of 1x3um rods within the cytoplasm of glial cells. (BB, 400X)

and neurologic infection.[3] In this report, immunosuppression by concurrent infection with feline panleukopenia virus and trafficking of bacteria by macrophages aided dissemination of *C. piliforme*. This is not a feature of the present case. Finally, there is a single case report (from the archives of the AFIP) of zoonotic transmission of Tyzzer's disease to a human patient infected with HIV-1 with cutaneous involvement,[6] though this lesion was benign.

References:

1. Mete A, Eigenheer A, Goodnight A, Woods L. Clostridium piliforme encephalitis in a weaver bird (Ploceus castaneiceps). *J Vet Diagn Invest*. 2011;23(6):1240–1242.
2. Mete A, Rogers KH, Woods L. Tyzzer's disease in free-ranging passerine birds in California, USA. *J Wildl Dis*. 2017;53(4):938–941.
3. Oliveira ES, Queiroz CRR, Santos DO, et al. Neurologic and cutaneous infection by Clostridium piliforme in a kitten with systemic Tyzzer disease. *J Vet Diagn Invest*. 2023 May;35(3):322-326.
4. Raymond JT, Topham K, Shirota K, Ikeda T, Garner MM. Tyzzer's disease in

a neonatal rainbow lorikeet (*Trichoglossus haematodus*). *Vet Pathol*. 2001;38(3):326–327.
5. Saunders GK, Sponenberg DP, Marx KL. Tyzzer's disease in a neonatal cockatiel. *Avian Dis*. 1993;37(3):891–894.
6. Smith KJ, Skelton HG, Hilyard EJ, et al. Bacillus piliformis infection (Tyzzer's disease) in a patient infected with HIV-1: confirmation with 16S ribosomal RNA sequence analysis. *J Am Acad Dermatol*. 1996 Feb;34(2 Pt 2):343-8.
7. Uzal FA, Plattner BL, Hostetter JM. Alimentary system. In: Maxie MG, ed. *Jubb, Kennedy & Palmer's Pathology of Domestic Animals*. 6th ed. Vol. 2. Elsevier; 2016:1-257.

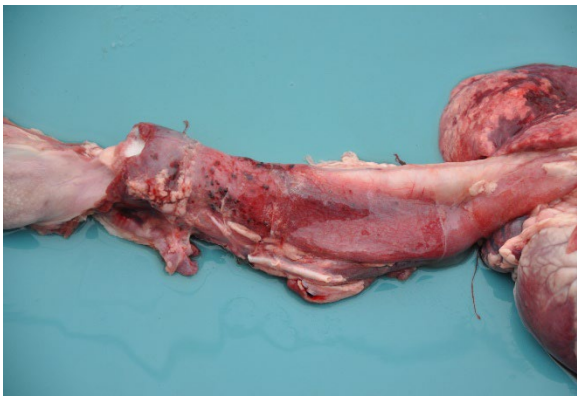

Figure 2-1. Esophagus, lamb. The cervical esophagus exhibits dilatation and sagging with congestion and petechiae on the serosa.. (*Photo courtesy of*: Setor de Patologia Veterinária, Universidade Federal do Rio Grande do Sul, Brazil (http://www.ufrgs.br/patologia/)

CASE II:

Signalment:
Less than 1 year-old female Texel ewe lamb (*Ovis aries).*

History:
Animal found dead with greenish serous nasal discharge and frothing. No previous clinical signs were reported by the owner.

Gross Pathology:

A female Texel ewe lamb was submitted to necropsy examination presenting good body condition and pale ocular mucosa. In nasal planum, a large amount of greenish serous nasal secretion was noticed. Submandibular and retropharyngeal lymph nodes presented moderate enlargement and showed diffuse dark red coloration. In the nasal cavity, moderate amount of inert plant fibers and ruminal content were seen and turbinates were diffusely hyperemic. The thoracic cavity contained a small amount of translucent liquid (hydrothorax). The lungs were not collapsed showing elastic consistency and abundant amount of foamy liquid in bronchi and trachea associated with inert plant fiber, as well as multifocal areas of consolidation found predominantly in the cranioventral region of the lungs. In the cervical segment of the esophagus moderate dilatation and sagging were noticed; the adventitia presented a moderate diffuse coloration with multifocal pinpoint hemorrhages smaller than 1 cm (petechiae). Moderate hydropericardium and multifocal areas of hemorrhage in epicardium were noted. In addition, discrete amount of hairlike parasites compatible with *Haemonchus contortus* in the abomasum

Laboratory Results:
Blood and tissue samples were tested for BTV RNA detection by RT-qPCR. Bacterial analysis was performed in lung tissue and *Mannheimia sp.* was isolated.

Microscopic Description:
A section of esophagus is examined. In muscular layer, there is severe multifocal to coalescing hyaline and flocculate degeneration and necrosis. Hyaline degeneration and necrosis are characterized by hypereosinophilic and swollen myofibers, with rounded edges

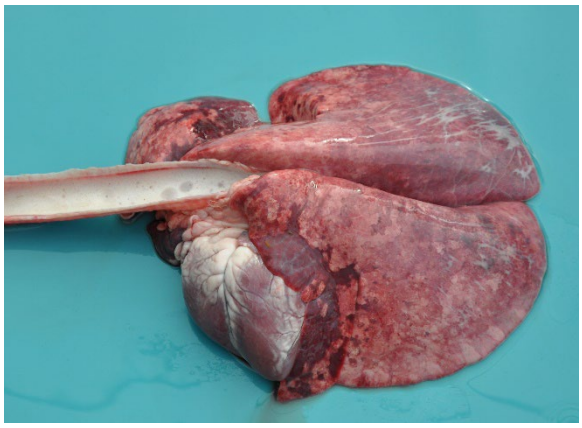

Figure 2-2. Lung, lamb. The lungs failed to collapse and there is cranioventral consolidation. (*Photo courtesy of*: Setor de Patologia Veterinária, Universidade Federal do Rio Grande do Sul, Brazil (http://www.ufrgs.br/patologia/)

in cross-section, sometimes showing hypercontracted and segmented cytoplasm with loss of striations, as well as pyknotic nuclei; eventually, myocytes display fragmented and flocculate sarcoplasm (flocculate degeneration and necrosis). Moreover, multifocally, macrophages are noted infiltrating cell sarcoplasm, as well as regenerating myofibers, which are characterized by elongated muscle cells with a row of central closely spaced nuclei containing myoblasts. In addition, moderate to severe inflammatory infiltrate of macrophages, lymphocytes, and few neutrophils, edema as well as moderate multifocal congestion were associated with necrotic areas and mild fibroblast proliferation. In some sections, marked multifocal to coalescing areas of hemorrhage are observed in tunica adventitia. Thin-walled structures consistent with *Sarcocystis sp.* were observed in some slides.

Contributor's Morphologic Diagnosis:
Esophagus: severe diffuse subacute necrotizing esophagitis.

Contributor's Comment:
The gross and microscopic findings observed in the present case were compatible with bluetongue disease, which was confirmed by detection of BTV RNA through RT-qPCR. Bluetongue virus (BTV) is a non-enveloped arbovirus, a member of the Reoviridae family, and is the prototype of the genus Orbivirus.[1] Bluetongue (BT) is a hemorrhagic disease caused by BTV, which affects domestic and wild ruminants. Among domestic species, sheep are the most susceptible and the severity of clinical signs can vary according to breed, age, and immune status of the affected flock.[2] In cattle, bluetongue is hardly noticed[6] though cattle are defined as amplifiers and reservoir hosts.[8] Virus replication in endothelial cells of small vessels results in distinct disease findings associated with vascular injury, such as tissue infarction, hemorrhage, vascular leakage, and edema.[2]

BTV is a vector-borne virus, mainly transmitted by biting midges from the genus *Culicoides*. South America has ideal climatic conditions for the survival and proliferation of *Culicoides* spp., and as reported by indirect evidence (serological investigations), BTV has spread since 1978 all over the American continent, with the exception of Uruguay.[3] BT cases are likely underreported due to the presence of very mild clinical signs, which can be mistaken for other similar endemic diseases.[3]

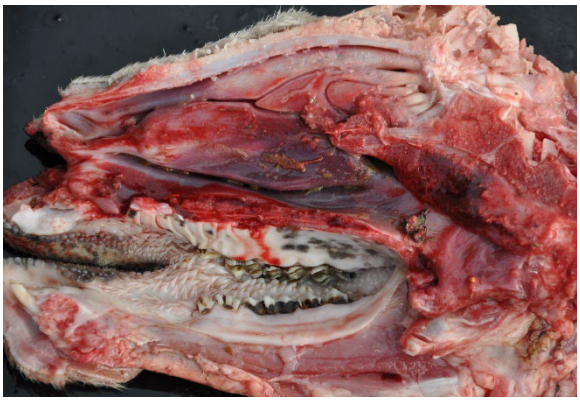

Figure 2-3. Nasal cavity, lamb. There are plant fibers and diffuse hyperemia of the turbinates within the nasal cavity. (*Photo courtesy of*: Setor de Patologia Veterinária, Universidade Federal do Rio Grande do Sul, Brazil (http://www.ufrgs.br/patologia/)

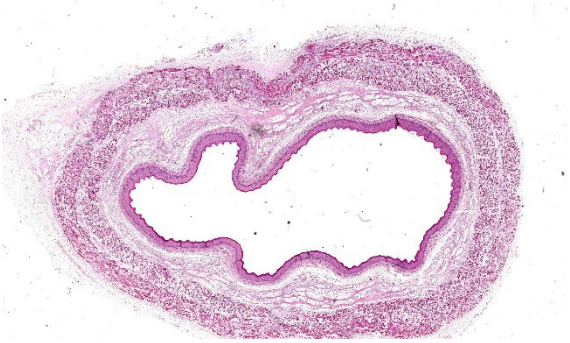

Figure 2-4. Esophagus, lamb. One section of the esophagus is submitted for examination. There is a diffuse retiform pattern of pallor within the muscularis at subgross magnification. (HE, 7X)

Typical signs in affected sheep include pyrexia, facial edema, ocular and nasal discharge, crusting of the muzzle, dyspnea, oral erosions and ulcers, coronitis, lameness and weakness.[2] The main gross findings described by Antoniassi et al[4] were esophageal dilation associated with non-collapsed enlarged lungs and foamy fluid within the trachea and bronchi, occasionally mixed with ruminal content. Hydropericardium, pale areas in the myocardium, and hemorrhagic foci scattered in the endocardium, epicardium and at the base of the pulmonary artery were also reported, as well as hyperaemia and erosions in the oral mucosa, and subcutaneous edema of the face. Aspiration pneumonia in BTV infection is related to aspiration of rumen content after reflux episodes resulting from severe injury of the esophageal muscles[4,5] which leads esophageal paralysis.[6] The disease is named bluetongue due to the fact that the tongue may become edematous, congested or cyanotic[6] though this gross lesion was not seen in the present case.

Histologically, edema, hemorrhage and microvascular thrombosis can be seen in areas with macroscopic lesions in acute presentations. These microvascular lesions are related with muscular necrosis.[6] Bianchi et al[7] described that the most common lesions found were located in lungs, esophageal striated muscle, cardiac and skeletal muscles, primarily in the neck and forelimbs.

The differential diagnosis for BTV in sheep should include foot-and-mouth disease, contagious ecthyma, sheep pox,[8] photosensitization, and peste des petits ruminants.[6] Vitamin E and selenium deficiency may be considered, once muscular necrosis associated with mineralization may resemble the changes observed in nutritional muscular dystrophy (NMD).[8] Another orbivirus to take in consideration is the Epizootic Hemorrhage Diseases Virus (EHDV), that may occasionally be responsible to mild clinical signs that resemble BTV in sheep.[6]

BTV 12,[5] BTV-1, BTV-4 and BTV-17[9] have been described in previous outbreaks in the State of Rio Grande do Sul. Until the moment, the genotyping of the virus responsible for this case has not been performed.

Contributing Institution:
Setor de PatologiaVeterinária, Universidade Federal do Rio Grande do Sul, Brazil (http://www.ufrgs.br/patologia/).

JPC Diagnosis:
Esophagus, muscularis: Degeneration and necrosis, monophasic, diffuse, moderate, with edema.

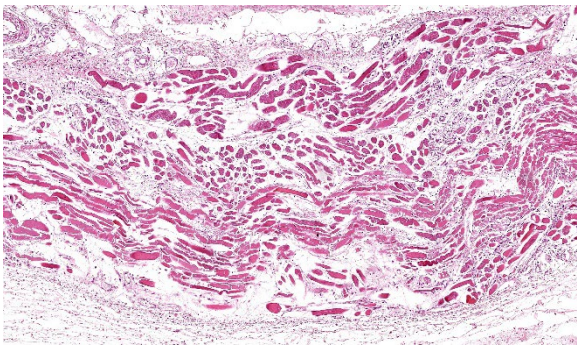

Figure 2-5. Esophagus, lamb. There is diffuse shrinkage and separation of myofibers with expansion of the interstitium. (HE, 109X)

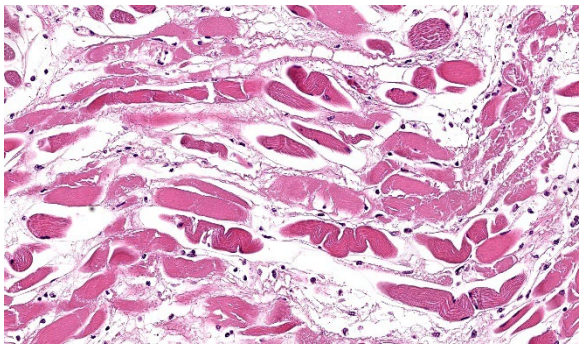

Figure 2-6. Esophagus, lamb. Myocytes exhibit one or more of the following: variation in fiber size, hypereosinophilia, loss of cross striations (degeneration), cytoplasmic granularity, fragmentation, nuclear pyknosis (necrosis.) There is edema and infiltration of the interstitium by macrophages. (HE, 475X)

JPC Comment:
This second case prompted spirited discussion among conference participants. The contributor lays out a detailed summary of bluetongue with characteristic histologic features to look for, though these are challenging to confirm in this section. Although there is notable edema and myocyte degeneration and necrosis, the cause is not apparent. We did not identify vasculitis and/or thrombosis in this particular section which would be expected in this case, as BTV is an endotheliotropic agent.

Conference participants offered ionophore toxicity as a potential etiology in this case, which is a ruleout for monophasic muscular injury in small ruminants. Vitamin E/selenium imbalance would likely result in polyphasic injury which would result in additional lesions of mineralization and fibrosis, which are lacking in this case. Early degenerative changes are present in myocytes, to include the early reversible change of hyalinization and hypereosinophilia resulting from glycogen depletion (and lack of replenishment). We covered monensin and associated muscular changes in a recent WSC in a brahman calf (Conference 5, Case 3, 2024-2025).

Our diagnosis is different from the contributor in this case. We framed this case as necrosis and degeneration (vice myositis) due to the lack of significant inflammation this section. In this case, the main driver of the lesion is the presumed vasculitis and ischemic damage – inflammation is mild at best in this lesion. Additionally, the lack of involvement of the esophageal mucosa makes the focus of the lesion more selective, and we prefer to restrict the morphologic diagnosis to the muscular tunics of the esophagus alone.

References:

1. Mertens PPC, Diprose J, Maan S, Singh KP, Attoui H, Samuel AR. Bluetongue virus replication, molecular and structural biology. *Vet Ital*. 2004; 40:426–437.
2. Maclachlan NJ, Drew CP, Darpel KE, Worwa G. The pathology and pathogenesis of bluetongue. *J Comp Pathol*. 2009; 141:1–16.
3. Lobato ZIP, Guedes MIMC, Matos ACD. Bluetongue and other orbiviruses in South America: gaps and challenges. *Vet Ital*. 2015; 51:253–262.
4. Antoniassi NAB, Pavarini SP, Ribeiro LAO, Silva MS, Flores EF, Driemeier D. Alterações clínicas e patológicas em ovinos infectados naturalmente pelo vírus da língua azul no Rio Grande do Sul. *Pesq Vet Bras*. 2010; 30: 1010–1016.
5. Antoniassi NAB, Pavarini SP, Henzel A, Flores EF, Driemeier D. Aspiration pneumonia associated with oesophagealmyonecrosis in sheep due to BTV infection in Brazil. *Vet Rec*. 2010; 166: 52–53.
6. Uzal FA, Plattner BL and Hostetter JM. Alimentary System In: Maxie MG, ed. *Jubb Kennedy and Palmer's Pathology of Domestic Animals*. Vol 2. 6th ed. Philadelphia, PA: Elsevier Saunders; 2016:1-257.
7. Bianchi RM, Panzieira W, Faccin TC, et

al. Clinical, pathological and epidemiological aspects of outbreaks of bluetongue disease in sheep in the central region of Rio Grande do Sul. *Pesq Vet Bras*. 2017; 37(2):1443-1452.
8. Radostits OM, Gay CC, Hinchcliff KW, Constable PD. *Veterinary Medicine. A Textbook of the Diseases of Cattle, Horses, Sheep, Pigs, and Goats*. 10th ed. Philadelphia, PA: Saunders Elsevier; 2007:1299-1305.
9. Guimarães LLB, Rosa JCC, Matos ACD, et al. Identification of bluetongue virus serotypes 1,4, and 17 co-infections in sheep flocks during outbreaks in Brazil. *Res Vet Sci*. 2017; 113:87-93.

CASE III:

Signalment:
11-month-old, male Doberman, *Canis lupus familiaris*, dog.

History:
The dog was presented to the referring veterinarian with a 1-month history of persisting vomiting, diarrhea, and weight loss. On abdominal ultrasound, an approximately 16 x 6 cm echogenic, heterogeneous, poorly vascularized mass was in the mesogastrium extending from the caudal aspect of the liver to the area of the urinary bladder. Peritoneal effusion and reactive intestinal serosa were also appreciated. The dog underwent laparotomy for excision of the mass, but died during surgical procedure.

Gross Pathology:
On necropsy, an 18 x 7 x 5 cm firm, poorly demarcated, tan mass was firmly adhered to the greater curvature of the gastric wall, capsule of the pancreas and serosa of the duodenum and jejunum and gastric lymph nodes. On cut surface, the mass was tan with multiple 1-4 mm yellow to green caseous areas

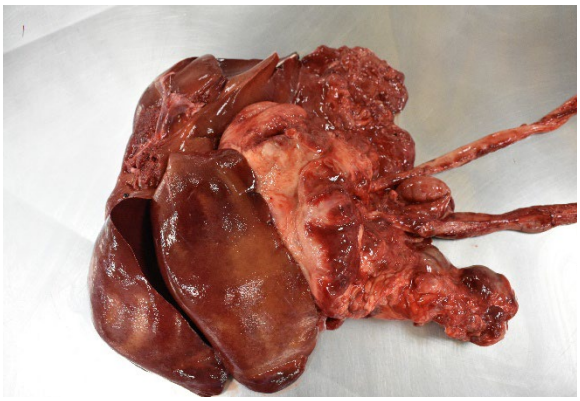

Figure 3-1. Stomach, dog. An 18 x 7 x 5 cm firm, poorly demarcated, tan mass was firmly adhered to the greater curvature of the gastric wall, capsule of the pancreas and serosa of the duodenum and jejunum and gastric lymph nodes. (*Photo courtesy of:* Setor de Patologia. Departamento de Clinica e Cirurgia Veterinárias, Escola de Veterinária, Universidade Federal de Minas Gerais, Belo Horizonte, Minas Gerais, Brazil)

and up to 8 cm cystic necrotic foci with viscous, yellow to brown exsudate. Along the serosa of the stomach, duodenum, and jejunum, there were multiple 2-4 cm in diameter nodules similar to the larger mass. The mucosa of the stomach and intestines was grossly normal, without ulcerations. The peritoneum was diffusely dark red with engorged blood vessels. The left testicle had an approximately 2 cm firm tan nodule within the parenchyma.

Laboratory Results:
The bloodwork revealed leukocytosis (23.160/mm^3) with neutrophilia (17.602/mm^3) e monocytosis (1853/mm^3). Chemistry results were normal.

Frozen fragments of the mesenteric mass were submitted to DNA extraction and panfungal PCR using internal transcribed spacer (ITS) primers. Amplified DNA product was submitted for sequencing and aligned

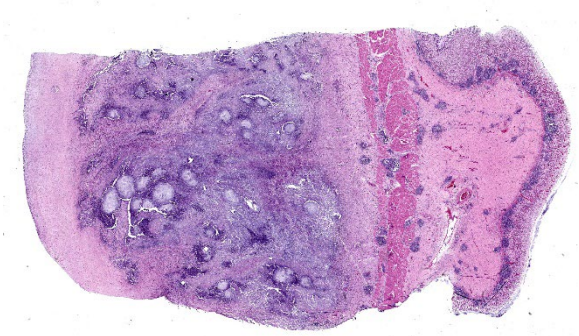

Figure 3-2. Stomach, dog. One section of stomach is submitted for examination. The serosa (left) is expanded up to 1.5cm and contains multifocal to coalescing pyogranulomas. There are numerous aggregates of lymphocytes and plasma cells within the overlying mucosa, expanded fibrotic submucosa, and muscularis. (HE, 7X)

with *Scedosporium apiospermum / Pseudoallescheria boydii* with 98.9% identity.

Microscopic Description:
Stomach: expanding the serosa and extending into the muscularis layer and submucosa is a dense inflammatory infiltrate forming multifocal to coalescing pyogranulomas. The center of the pyogranulomas contains myriads of fungal hyphae surrounded by degenerated and intact neutrophils, cellular debris, epithelioid macrophages, macrophages with foamy cytoplasm, fewer lymphocytes, eosinophils, plasma cells, and occasional Langhans multinucleated giant cells. Hyphae are 2-3 µm in diameter wide with thin non-parallel walls containing septations, irregular branching and bulbous dilations up to 9 µm in diameter. Hyphae were positive on periodic acid Schiff and Gomori methenamine silver stain. Melanine was not detected on Fontana Masson stain. The muscularis externa and serosa are expanded by reactive fibroblasts and abundant deposition of fibrous connective tissue. Lymphoid follicles in the lamina propria are hyperplastic.

Contributor's Morphologic Diagnosis:
Stomach: severe, multifocal to coalescing pyogranulomatous gastritis with numerous intralesional hyphae.

Contributor's Comment:
Fungi within the genus *Scedosporium* are saprophytes distributed worldwide in soil and fresh water, especially in environments rich in organic matter and manure.[1,11,17] *Scedosporium apiospermum* was previously known as *Scedosporium boydii*, but they are currently classified as distinct species. *Pseudoallescheria* is the teleomorph or sexual stage of *Scedosporium* spp. and usually is not present in tissue samples.[7,9]

Scedosporiosis is an emerging opportunistic fungal infection described in humans and animals.[5,17] In humans, infection with *Scedosporium apiospermum, Scedosporium boydii* and *Scedosporium aurantiacum* (collectively, the *S. apiospermum* species complex) can result in two distinct diseases: mycetoma and systemic scedosporiosis (pseudallescheriasis). Mycetoma is a chronic infection of the skin and subcutaneous tissue characterized by the production of grains.

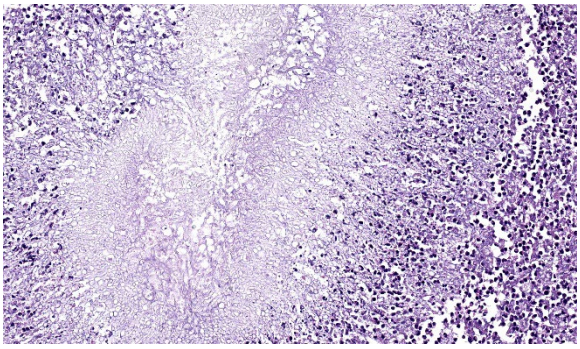

Figure 3-3. Stomach, dog. Pyogranulomas are centered on aggregates of 3-4um septate fungal hyphae with terminal conidia. (HE, 381X)

Most human patients with systemic infection are immunocompromised and common affected organs include lungs, nasal sinuses, bone, joints, and the brain[10]. Infection is usually through inhalation or traumatic inoculation through the skin. *Scedosporium*-related pneumonia is reported after near drowning in contaminated water.

In animals, few cases of cutaneous and systemic scedosporiosis are described in dogs, cats, horses, cattle, and an elephant seal.[3,4,8,14,18,21,22] In dogs, cutaneous infections are more often described in the digits, face and around the joints.[5,6,15] Infections with *Scedosporium* spp. have been reported after cutaneous traumatic injuries and surgical procedures.[6] In the present case, the distribution of the lesions suggests that the infection occurred through ingestion, although the mucosa of the affected gastrointestinal tract was intact. Gastrointestinal foreign bodies were not appreciated on gross examination and the dog had no history of previous surgical procedures. Immunosuppression and concomitant diseases are common predisposing factor for systemic infection in human patients, including infection by human immunodeficiency virus, diabetes, cystic fibrosis, neutropenia, those receiving prolonged high-dose corticosteroid therapy, or those who have undergone allogeneic bone marrow transplantation.[2,13,16,17,20] In this dog, all major organs were evaluated by histopathology and there was no evidence of concomitant diseases that could have predisposed to infection or history of previous use of immunosuppressants.

Although special stains (periodic acid-Schiff and Gomori methenamine silver) highlight characteristic morphologic features of the hyphae, these can be impossible to differentiate from *Conidiobolus* spp., *Basidiobolus* spp., *Aspergillus*, and *Fusarium* spp.[12,19] Fungal identification of *Scedosporium* spp. requires

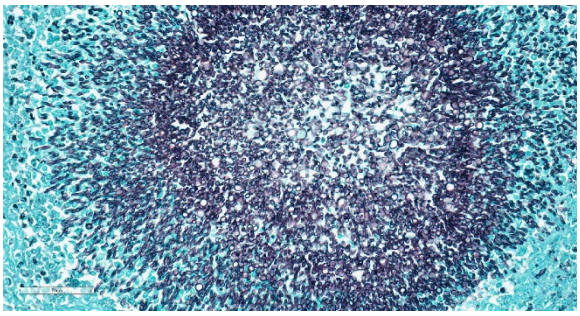

Figure 3-4. Stomach, dog. Fungal hyphae are stained well with Gomori-methenamine silver. (GMS, 200X) (*Photo courtesy of:* Setor de Patologia. Departamento de Clinica e Cirurgia Veterinárias, Escola de Veterinária, Universidade Federal de Minas Gerais, Belo Horizonte, Minas Gerais, Brazil)

culture along with DNA sequencing or matrix-assisted laser desorption/ionization time-of-flight (MALDI-TOF) mass spectrometry.[10] Scedosporiosis should be considered as a differential diagnosis for fungal pyogranulomatous gastroenteritis and peritonitis in dogs, especially when numerous fungal hyphae with bulbous dilations are observed.

Contributing Institution:
Escola de Veterinária, Universidade Federal de Minas Gerais (UFMG).

www.vet.ufmg.br

JPC Diagnosis:
Stomach: Serositis, pyogranulomatous, chronic-active, multifocal, severe, with numerous hyphae.

JPC Comment:
The contributor provides an interesting slide supported by an exhaustive background on *Scedosporium apiospermum*. The major microscopic features were readily apparent on H&E and special (fungal) stains alike. We interpreted the multifocal presence of lymphoid

aggregates as secondary to the profound serosal fibrosis and the resulting decrease in gastric motility.

We differed from the contributor's morphologic diagosis on two minor points. Similar to the discussion from Case 2, only one layer of the gastric wall is involved in the primary inflammatory process - for this reason, we describe this case as a serositis versus a gastritis. Additionally, we also noted the morphologic features of hyphae were best observed with histologic stains and not as well visualized on HE (which forms the basis of the JPC morphologic diagnosis, as special stains are not available to conference participants in advance of the conference. In this case, a silver stain best highlights the parallel walls, regular septation, irregular branching, and bulbous dilations that were generously present in section. We agree with the contributor that PCR is ideal for confirming identity of fungal agents, though morphology can help to create a prioritized list of differentials. Dr. Uzal suggested to conference participants that *Zygomyces* was unlikely in this case as hyphae have non-parallel wall hyphae and are pauciseptate[23] whereas the hyphae in this section were regularly septate and had conspicuously (and almost perfectly) parallel walls.

References:

1. Al-Yasiri MH, Normand AC, Mauffrey JF, et al. Anthropogenic impact on environmental filamentous fungi communities along the Mediterranean littoral. *Mycoses*. 2017;60(7):477-484.
2. Berenguer J, Diaz-Mediavilla J, Urra D, et al. Central nervous system infection caused by Pseudallescheria boydii: case report and review. *Rev Infect Dis*. 1989;11(6):890-6.
3. Coleman MG, Robson MC. Nasal infection with Scedosporium apiospermum in a dog. *N Z Vet J*. 2005;53(1):81-3.
4. Di Teodoro G, Averaimo D, Primavera M, et al. Disseminated Scedosporium apiospermum infection in a Maremmano-Abruzzese sheepdog. *BMC Vet Res*. 2020;2;16(1):372.
5. Elad D. Infections caused by fungi of the Scedosporium/Pseudallescheria complex in veterinary species. *Vet J*. 2011;187(1):33-41.
6. Elad D, Perl S, Yamin G, et al. Disseminated pseudallescheriosis in a dog. *Med Mycol*. 2010;48(4):635-8.
7. Guarro J, Kantarcioglu AS, Horré R, et al. Scedosporium apiospermum: changing clinical spectrum of a therapy-refractory opportunist. *Med Mycol*. 2006;44(4):295-327.
8. Gupta MK, Banerjee T, Kumar D, et al. White grain mycetoma caused by Scedosporium apiospermum in North India: a case report. *Int J Low Extrem Wounds*. 2013;12(4):286-8.
9. Haulena M, Buckles E, Gulland FM, et al. Systemic mycosis caused by Scedosporium apiospermum in a stranded northern elephant seal (Mirounga angustirostris) undergoing rehabilitation. *J Zoo Wildl Med*. 2002;33(2):166-71.
10. Hospenthal DR. Uncommon Fungi and related Species. In: *Principles and Practice of Infectious Diseases*. Part III. 9th ed. Philadelphia, PA: Elsevier; 2019: 3224-3225.
11. Kaltseis J, Rainer J, De Hoog GS. Ecology of Pseudallescheria and Scedosporium species in human-dominated and natural environments and their distribution in clinical samples. *Med Mycol*. 2009;47(4):398-405.
12. Kleinschmidt-DeMasters BK. Central nervous system aspergillosis: a 20-year retrospective series. *Hum Pathol*. 2002;33(1):116-24.
13. Kowacs PA, Soares Silvado CE, Monteiro de Almeida S, et al. Infection of the CNS by Scedosporium apiospermum after near drowning. Report of a fatal case

and analysis of its confounding factors. *J Clin Pathol*. 2004;57(2):205-7.
14. Leperlier D, Vallefuoco R, Laloy E, et al. Fungal rhinosinusitis caused by Scedosporium apiospermum in a cat. *J Feline Med Surg*. 2010;12(12):967-71.
15. Mauldin EA, Kennedy JP. Integumentary System. In: Maxie MG, ed. *Jubb, Kennedy, and Palmer's Pathology of Domestic Animals*. Vol 1. 6th ed. Philadelphia, PA: Elsevier; 2016:653- 655.
16. Montero A, Cohen JE, Fernández MA, et al. Cerebral pseudallescheriasis due to Pseudallescheria boydii as the first manifestation of AIDS. *Clin Infect Dis*. 1998;26(6):1476-7.
17. Paajanen J, Halme M, Palomäki M, et al. Disseminated Scedosporium apiospermum central nervous system infection after lung transplantation: A case report with successful recovery. *Med Mycol Case Rep*. 2019;16(24):37-40.
18. Singh K, Boileau MJ, Streeter RN, Welsh RD, Meier WA, Ritchey JW. Granulomatous and eosinophilic rhinitis in a cow caused by Pseudallescheria boydii species complex (Anamorph Scedosporium apiospermum). *Vet Pathol*. 2007;44(6):917-20.
19. Smith CG, Woolford L, Talbot JJ, et al. Canine rhinitis caused by an uncommonly-diagnosed fungus, Scedosporium apiospermum. *Med Mycol Case Rep*. 2018;8(22):38-41.
20. Suzuki Y, Oishi H, Matsuda Y, et al. Pneumonia with Scedosporium apiospermum and Lomentospora prolificans in a patient after bilateral lung transplantation for pulmonary hypertension: a case report. *Transplant Proc*. 2021;53(4):1375-78.
21. Swerczek TW, Donahue JM, Hunt RJ. Scedosporium prolificans infection associated with arthritis and osteomyelitis in a horse. *J Am Vet Med Assoc*. 2001;218(11):1800-2, 1779.
22. Tsoi MF, Kline MA, Conkling A, et al. Scedosporium apiospermum infection presenting as a mural urinary bladder mass and focal peritonitis in a Border Collie. *Med Mycol Case Rep*. 2021;15(33):9-13.
23. Rodrigues Hoffmann A, Ramos MG, Walker RT, Stranahan LW. Hyphae, pseudohyphae, yeasts, spherules, spores, and more: A review on the morphology and pathology of fungal and oomycete infections in the skin of domestic animals. *Vet Pathol*. 2023 Nov;60(6):812-828.

CASE IV:

Signalment:
5-year-old, female, Scottish blackface sheep (*Ovis aries*).

History:
Presented to the Veterinary School farm animal clinic for investigation of ill thrift. Treatment was given in response to a high faecal parasite egg count and the numbers decreased. The submitting farm has a history of ovine pulmonary adenocarcinoma.

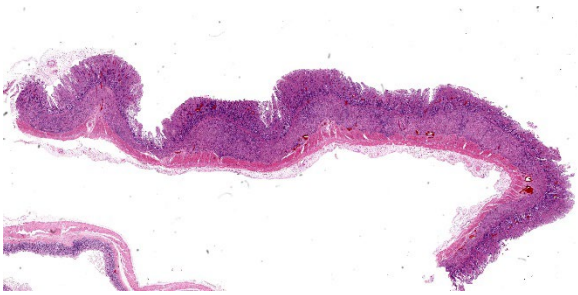

Figure 4-1. Cecum, sheep. A section of cecum is submitted for examination. (HE, 7X)

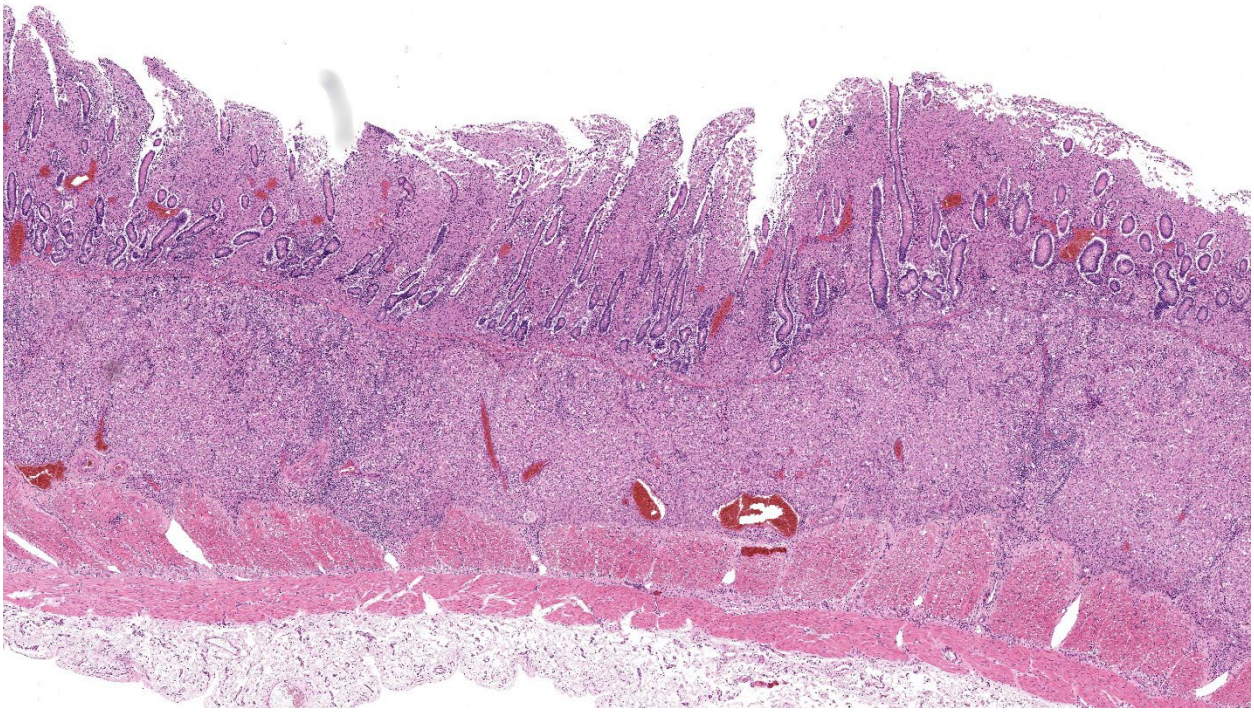

Figure 4-2. Cecum, sheep. The mucosa and submucosa are markedly expanded by a dense eosinophilic inflammatory exudate. (HE, 50X)

Gross Pathology:
Within the abdomen approximately 1 litre of yellow-tinged clear, watery fluid (hydroperitoneum) is noted.

Diffusely, the walls of the ileum and the distal third of the jejunum are moderately to markedly thickened, the mucosal surface exhibits a corrugated pattern and is bright yellow in colour. The mucosa of the caecum, diffusely, and colon, segmentally, are mildly to moderately thickened.

Multifocally, the mesenteric lymph nodes are moderately enlarged, and upon cut section show moderate multifocal expansion of the cortex by firm white-grey tissue.

Laboratory Results:
Parasitology:

- McMaster slide method: 2000 strongyle spp. eggs per gram (epg), 500 *Moniezia* spp. epg, 1100 Coccidia spp. epg, 100 *Nematodirus* spp. epg
- Baermann technique: positive for *Dictyocaulus filaria* larvae.

Serology:

- *Corynebacterium pseudotuberculosis*: Negative
- Maedi-Visna virus: Negative
- *Mycobacterium avium subsp. Paratuberculosis* (MAP): Positive

Microscopic Description:
Caecum: Separating intestinal crypts, the lamina propria and submucosa are diffusely markedly expanded by large numbers of epithelioid macrophages. Within the cytoplasm of these cells there are large numbers of 4x1µm bacilli that fail to stain with HE stain but are acid-fast positive on Ziehl-Neelsen stain. Admixed with the macrophages are small numbers of

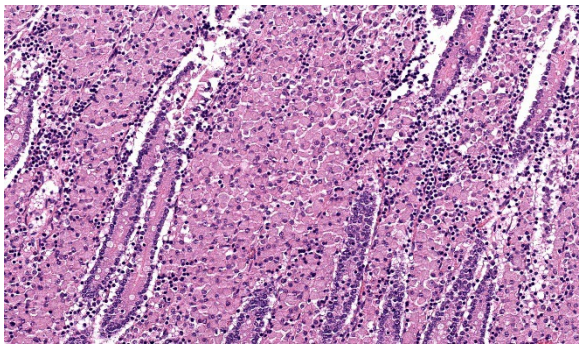

Figure 4-3. Cecum, sheep. Remaining mucosal glands are markedly separated and replaced by sheets of macrophages. (HE, 381X)

lymphocytes, plasma cells and occasional multinucleate giant cells. Similar inflammatory cell infiltrates extend, multifocally, into the inner circular and outer longitudinal muscular layers of the caecal wall. The serosa is expanded, diffusely, and the connective tissue is separated by clear, material (protein poor oedema) and contains small numbers of lymphocytes, plasma cells and macrophages, that latter containing acid-fast bacilli, which are present rarely in presumed lymphatics. Small numbers of intestinal crypts are lined by flattened enterocytes. The blood vessels are filled with moderate numbers of erythrocytes (congestion).

Contributor's Morphologic Diagnosis:
Caecum: Typhlitis, chronic, histiocytic, diffuse, marked with intra-histiocytic acid-fast bacteria.

Contributor's Comment:
The microscopic features of this enteritis are consistent with diffuse multibacillary *Mycobacterium avium subsp. paratuberculosis* (MAP) infection, also known as Johne's disease.[3,7,12]

MAP is a Gram-positive, acid-fast, aerobic, non-motile, non-spore forming bacterium of the genus *Mycobacterium*, family *Mycobacteriacea* and a member of the *Mycobacterium avium complex* which comprises *M. avium avium*, *M. avium sylvaticum*, *M. colombiense* and *M. intracellulare.*[10]

Premortem diagnosis is challenging, and the gold standard is based on faecal culture, which takes several weeks to months,[3] or other tests such as Ziehl-Neelsen stained faecal smears, ELISA, PCR, identification of MAP specific peptides, and expression of gamma interferon all of which will provide more rapid results. Liver biopsy has also been shown to have high sensitivity and specificity for identifying sheep with advanced disseminated infection.[9] On post-mortem examination, the gold standard is based on culture and isolation of the bacteria although PCR of affected intestinal tissue samples for Insertion Sequence 900 (IS900) provides faster results and is MAP specific.[3,6,11]

Infection is thought to occur in neonates and juveniles via ingestion of contaminated food, pasture, water, colostrum, and milk. MAP is thought to cross the intestinal mucosal barrier via preferential uptake by M-cells present overlying Peyer's patches and mucosal lymphoid domes. Bacteria then invade subepithe-

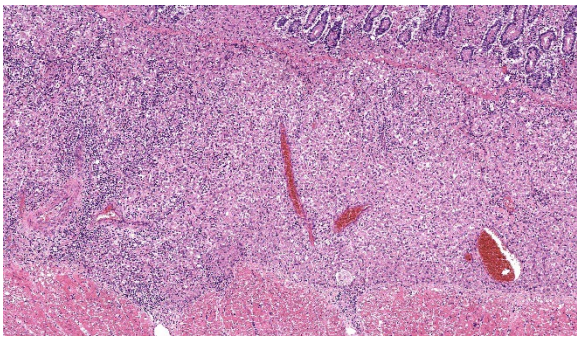

Figure 4-4. Cecum, sheep. The histiocytic infiltrate markedly expands the submucosa and extends into the superficial muscularis. (HE, 142X)

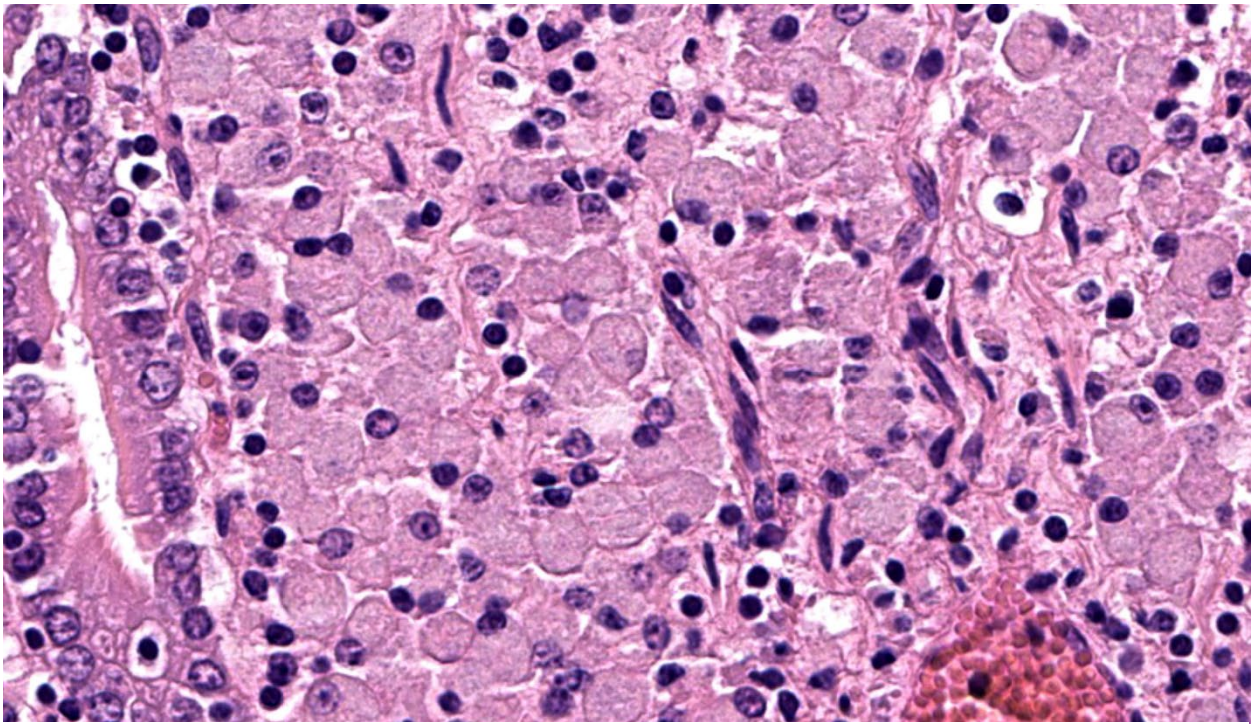

Figure 4-5. Cecum, sheep. Histiocytes have abundant grey-pink granular cytoplasm. (HE, 1250X)

lial macrophages and modulate the immune system[3,10,12] whilst concurrently inhibiting phagolysosome fusion, acidification and macrophage activation to avoid degradation.[4] Typically, the infection takes months to years before causing macroscopic lesions and clinical signs. Experimental challenge in sheep usually requires an incubation period of 4 to 8 months before the onset of clinical signs. Animals infected before 2 years of age exhibit greater pathological and clinical manifestations compared to those infected when adult.

Depending on the ensuing immune response to infection, different morphological presentations of disease develop. The paucibacillary form of the disease is driven by a Th1 cell-mediated interferon gamma response whereas the multibacillary Th2 form is a humoral response driven by IL-10. The multibacillary morphology is thought to be caused by a switch from a Th1 response towards a Th2 response or may be caused by a simultaneous Th1 and Th2 response with failure of the Th1 component of inflammation.[7] Depending on the inflammatory response, the affected macrophages display different phenotypes, either M1 iNOS (inducible nitric oxide synthase) and TNF-alpha positive activated macrophages driven by Th1 mediated inflammation or M2 CD163, IL-10 and TGF-beta positive activated macrophages mediated by a Th2 response.[2] Additionally, 3 different subsets of M2 macrophages have been described: M2a is present in allergies and helps with killing and encapsulating parasites, M2b is driven by a Th2 inflammatory response induced by IL-1 and M2c is induced by IL-10 and TGF-beta and is believed to be implicated in Johne's disease progression towards the multibacillary form.[2]

MAP is subdivided in type I/III and type II strains which affect, predominantly, sheep and cattle, respectively. Additionally, types II and III have broader host ranges.[6,11] MAP has been reported in numerous species including

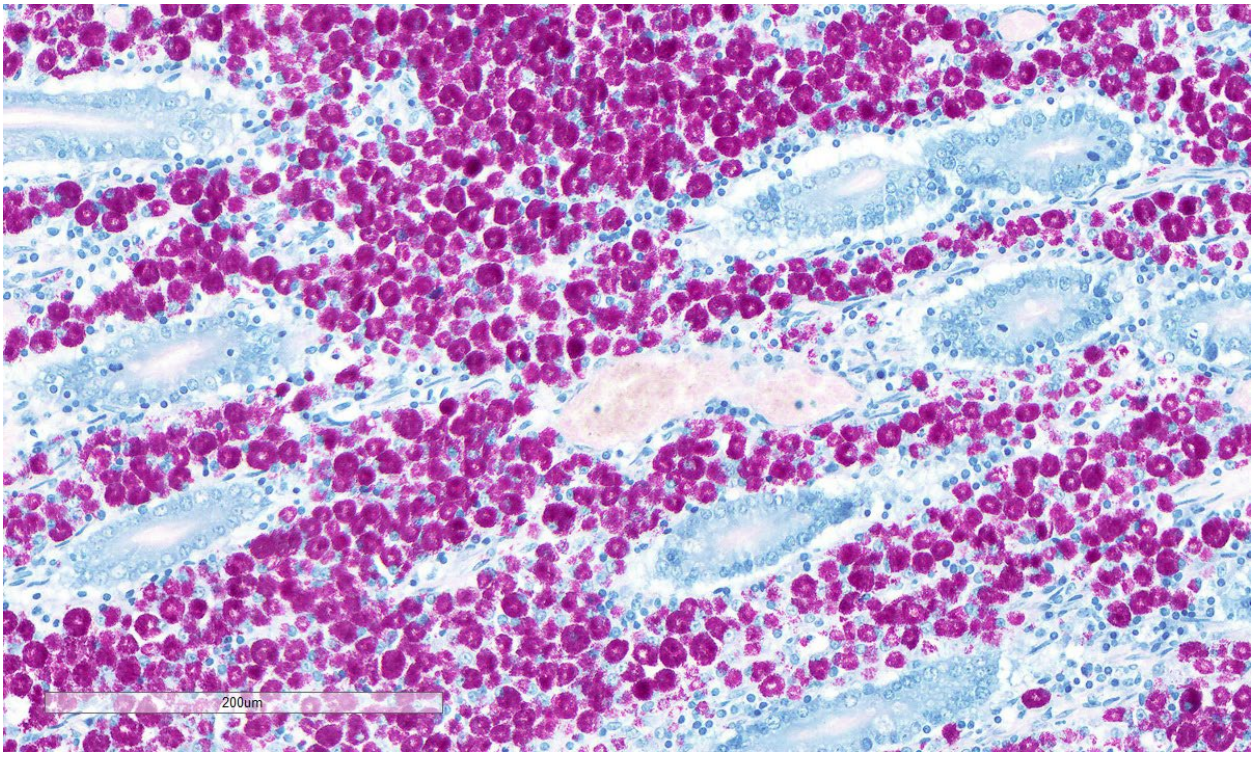

Figure 4-6. Cecum, sheep. Histiocytes contain large numbers of cytoplasmic acid-fast bacilli. (HE, 400X). (*Photo courtesy of:* Veterinary Diagnostic Services, College of Medicine, Veterinary and Life Sciences, University of Glasgow)

a wide range of captive and wild ruminants, camelids, rabbits, equids, swine, lagomorphs and primates. It has also been detected in rodents, carnivores and several species of wild birds but without evidence of disease.[11] Rabbits may play a role in the epidemiology of the disease although it is not clear if they are naturally susceptible to the disease.[1] Furthermore, MAP has been isolated from humans suffering from Crohn's disease by PCR and FISH, but in human tissues it is in a mycobacterial cell wall deficient state, so is not acid-fast.[6,11]

Contributing Institution:

Veterinary Diagnostic Services
School of Biodiversity, One Health & Veterinary Medicine
College of Medicine, Veterinary and Life Sciences
University of Glasgow
https://www.gla.ac.uk/schools/vet/cad/

JPC Diagnosis:

Intestine: Enteritis, granulomatous, chronic, diffuse, severe, with edema.

JPC Comment:
The conference concludes with a classic entity that has been a frequent submission to the WSC. There was spirited debate on tissue identification in this case as participants were divided on whether or not there were villi present (i.e. consistent with small intestine) – Dr. Uzal was unable to resolve this question definitively, so we hedged with the lessspecific "intestine" in our morphologic diagnosis.

The microscopic features of this case align

with the Th2 multibacillary pathogenesis that the contributor nicely summarizes. Sheets of macrophages expand the mucosa, lamina propria, and submucosa and ultimately result in a malabsorptive diarrhea that corresponds to the ill thrift noted clinically for this ewe. Dr. Uzal discussed that the submucosal involvement in this case was not unusual for MAP, though it may be overlooked in the description.

One feature not reported in this case is mineralization of the aorta and endocardium which is reported to occur in up to 25% of paratuberculosis cases.[8] Macrophage activation, particularly of M1 macrophages, likely drives calcification of elastic fibers via deposition of vitamin D metabolites in response to cytokines such as TNF-α, IL-1, and IL-8.[6] Plasticity of vascular smooth muscle to differentiate towards an osteoblastic phenotype under the influence of this same cytokine milieu likely also plays a role in vascular mineral deposition.[6] Conversely, M2 macrophages impair osteogenesis and/or enhance osteolysis and mineral degradation. The interplay of secreted matrix metalloproteases, available matrix constituents, and concurrent injury to the vessel via reactive oxygen species (ROS) has also been evaluated.[6] Although not as well studied as in human atherosclerosis in which these processes have been more extensively studied, an understanding of this basic process is helpful for understanding mineralization in other diseases. Important ruleouts in this case include ingestion of calcinogenic plants (e.g. *Cestrum diurnum* and *Trisetum flavescens*) and hypervitaminosis D.

References:

1. Arrazuria R, et al. Mycobacterial Infections in Rabbits: From the Wild to the Laboratory. *Transbound Emerg Dis*. 2017; 64(4):1045-1058.
2. Fernández M, et al. Macrophage Subsets Within Granulomatous Intestinal Lesions in Bovine Paratuberculosis. *Vet Pathol*. 2017; 54(1):82-93.
3. Idris SM, et al. Paratuberculosis: The Hidden Killer of Small Ruminants. *Animals (Basel).* 2021; 12(1):12.
4. Jenvey CJ, et al. Quantification of Macrophages and *Mycobacterium avium Subsp. paratuberculosis* in Bovine Intestinal Tissue During Different Stages of Johne's Disease. *Vet Pathol*. 2019; 56(5):671-680.
5. Li Y, Sun Z, Zhang L, Yan J, Shao C, Jing L, Li L, Wang Z. Role of Macrophages in the Progression and Regression of Vascular Calcification. *Front Pharmacol*. 2020 May 8;11:661.
6. Liverani E, et al. *Mycobacterium avium subspecies paratuberculosis* in the etiology of Crohn's disease, cause or epiphenomenon? *World J Gastroenterol.* 2014; 20(36):13060-13070.
7. Marquetoux N, et al. A synthesis of the patho-physiology of *Mycobacterium avium subspecies paratuberculosis* infection in sheep to inform mathematical modelling of ovine paratuberculosis. *Vet Res*. 2018; 49(1):27.
8. Rosa FB, Roussey J, Coussens PM, Langohr IM. Pathology in practice. Johne's disease. *J Am Vet Med Assoc*. 2013 Jun 15;242(12):1655-7.
9. Smith SL, et al. Liver biopsy histopathology for diagnosis of Johne's disease in sheep. *Vet Pathol*. 2014; 51(5):915-918.
10. Ssekitoleko J, et al. *Mycobacterium avium* subsp. *paratuberculosis* Virulence: A Review. *Microorganisms*. 2021; 9(12):2623.
11. Uzal FA, Plattner BL, Hostetter JM. Alimentary system. In: Maxie MG, ed. *Jubb, Kennedy, and Palmer's Pathology of Domestic Animals*. Vol 2. 6th ed. St. Louis, MO: Elsevier; 2016:194-197.
12. Windsor PA. Paratuberculosis in sheep and goats. *Vet Microbiol*. 2015; 181(1-2):161-169.

Joint Pathology Center
Veterinary Pathology Services

WEDNESDAY SLIDE CONFERENCE 2024-2025

Conference #17 22 January 2025

CASE I:

Signalment:
Seven-year-old, male rhesus macaque, *Macaca mulatta*.

History:
Euthanasia was due to chronic, progressively worsening diarrhea.

Gross Pathology:
The macaque was in very lean nutritional condition. Liver was firmer than normal, and the common bile duct was dilated and tortuous. Visceral lymph nodes of the abdomen were enlarged, soft and confluent. Large intestines had mucosal thickening.

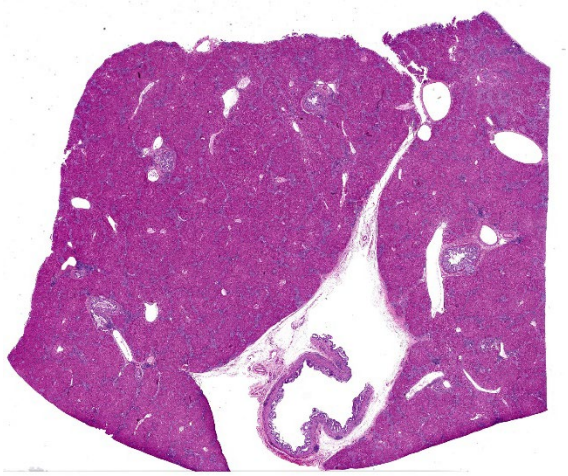

Figure 1-1. Liver, rhesus macaque. At subgross magnification, bile ducts are hyperplastic and there is bridging portal fibrosis. (HE, 7X)

Laboratory Results:
PCR: 1) Common bile duct: Enterocytozoon bieneusi positive; Cryptosporidium negative.

2) Mesenteric lymph node, spleen and ileum: Mycobacterium negative

Bacteriology: Colon: Colon: E. coli, Klebsiella pneumoniae, Proteus vulgatus, Streptococcus viridans group, & Lactobacillus spp present. Strict Anaerobes: Prevotella oris & Peptoniphilus asaccharolyticus present.

Microscopic Description:
Large intrahepatic bile ducts and the common bile duct had moderate, diffuse mucosal hyperplasia with moderate lymphocytic and plasmacytic inflammation. Portal triads were expanded by similar inflammation and bridging fibrosis is present. Gram stains revealed small colonies of 1-2 µ, gram positive organisms, typically in sloughed biliary epithelium.

The liver had numerous granulomas in all lobes. Granulomatous inflammation was also present in spleen intestines and axillary and mesenteric lymph nodes. Acid fast stain of liver sections revealed small numbers of acid-fast positive bacilli within granulomas. The ileum had sheets of epithelioid macrophages with myriad intracytoplasmic acid-fast bacteria.

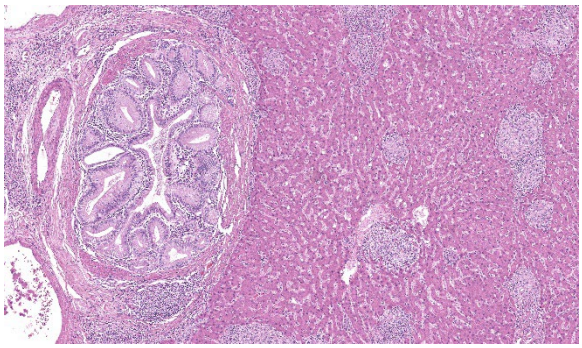

Figure 1-2. Liver, rhesus macaque. The lining of bile ducts is markedly hyperplastic and the lamina propria is infiltrated by moderate numbers of lymphocytes and plasma cells. There is biliary hyperplasia and bridging portal fibrosis. There are numerous small granulomas scattered throughout the hepatic parenchyma. (HE, 110X)

Contributor's Morphologic Diagnosis:
Liver: Cholangiohepatitis, hyperplastic, chronic. diffuse, moderate with intracellular protozoa, Enterocytozoon bieneusi.

Liver: Granulomatous hepatitis, moderate, multifocal (Mycobacterium avium complex, presumptive.)

Contributor's Comment:
Enterocytozoon bieneusi (EB) is a microsporidian parasite that is frequently associated with diarrhea and biliary disease in SHIV and SIV infected macaques. It also is a common cause of chronic diarrhea in human HIV patients. EB isolates are divided into 11 groups and numerous subgroups based on polymorphisms of *ribosomal internal transcribed scribed spacer* DNA. (ITS).[5] Most laboratory primates have organisms from Group 1, subgroup D which is the common strain that affects humans. Wild and zoo apes and monkeys have EB isolated from different groups and/or subgroups. Transmission is likely direct with organisms having been isolated in water and fresh produce. They have also been isolated from mollusks.[3,4]

EB spores have been isolated from the feces of immunocompetent animals.[6] Experimental infection of immune competent macaques by spores of human origin resulted in fecal shedding in about 8 weeks with infections persisting for months, and elevation of ALK but not ALT, GGT, or AST serum liver enzymes. Spores were isolated from bile and feces, but other developmental stages were not found and symptoms were not observed. Histology of the biliary tree of immunocompetent macaques had lymphoplasmacytic cholecystitis and choledochitis.[2]

Once infected, immunocompromised animals frequently develop symptoms concurrent with a drop in T4 (CD4) lymphocyte counts. If the T4 count remains stable, immunodeficient animals can remain asymptomatic.[2] In immune suppressed animals, infection results in hyperplastic cholecystitis and choledochitis with lymphoplasmacytic inflammatory infiltrates. Though EB is associated with diarrhea, coinfections are common so the contribution of EB to clinical signs is often uncertain. All stages of the organism can be identified by *in situ hybridization* in mucosal cells of the biliary tree, duodenum, and jejunum. Plasmodia are multinucleated; they and sporoblasts measure between 4-12 um. Spores

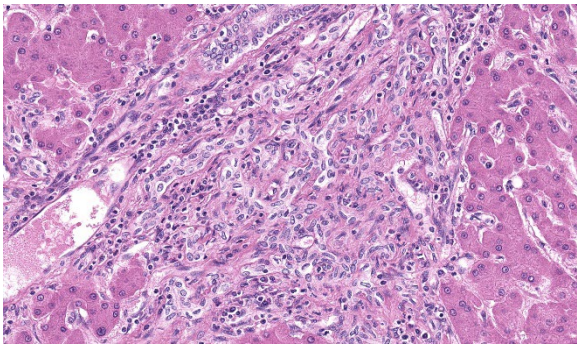

Figure 1-3. Liver, rhesus macaque. There is marked biliary hyperplasia and fibrosis expanding portal triads. (HE, 457X)

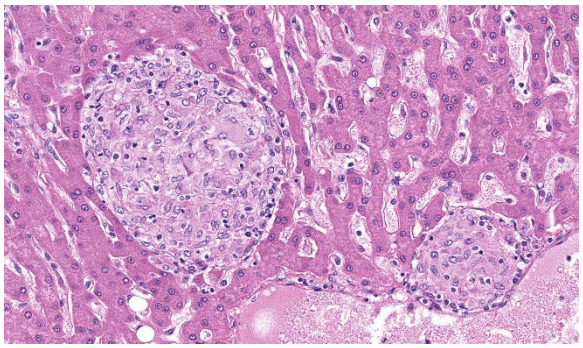

Figure 1-4. Liver, rhesus macaque. Numerous poorly formed granulomas composed of large numbers of spindled epithelioid macrophages are scattered throughout the parenchyma. (HE, 478X)

and sporoblasts measuring 0.8-1.5 um can be visualized in sloughed biliary mucosal cells by using either Ziehl-Neelson acid-fast, Brown and Hopps, Weber's modified trichrome, or methenamine silver stains. Only small numbers of organisms are found this way.[2,6,7] Differential diagnoses include another microsporidian organism, *Cryptosporidium parvum*, and ascending bacterial infections.[7]

As microsporidia rely on host cells for nucleotides and amino acids, they are considered obligate pathogens.[1] Although originally classified as protozoa, they have since been placed in a separate phylum and are thought to closely related to fungi due to protein and structural analysis, and *simple sequence repeat RNA* (SSR) gene sequencing. They are characterized by chitinous spore walls, coiled polar tubules and a radiolucent vacuole and mitochondria-like organelles that lack mitochondrial genome.[1] After ingestion, spores attach to host cell membranes using the polar tubule through which the sporoplasm enters host cell cytoplasm. It then becomes a meront which divides into plasmodia and through sporogony form sporoblasts that mature into spores.[3,4] Studies on *Encephalitozoon*, another microsporidian organism, have found that immunity is depended on CD8 lymphocytes, IFN-gamma and IL-12.[3]

A commonly associated opportunistic coinfection with EB is atypical mycobacteriosis also referred to a non-tuberculous mycobacterium (NTM). NTM are thought to be acquired from either soil or water. Species of the *Mycobacterium avium-intracellulare* species complex (MAC) are most frequently identified. Infections are characterized by diffuse granulomatous enterocolitis with large numbers of intracellular bacteria. Disseminated disease also can occur with fewer organisms present in other organs which is the is the pattern of this case. Another common NTM species is *M. kansasii* which can be present asymptomatically. *M genevense*, is a species isolated in human HIV patients causes lesions that are similar to MAC with numerous bacteria. One study found that animals were more likely to have symptoms from NTM when coinfections are present.[8,10]

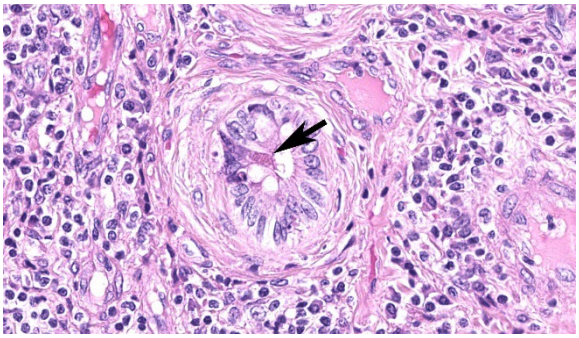

Figure 1-5. Liver, rhesus macaque. Rare biliary epithelial cells contain cytoplasmic microsporidian spores.

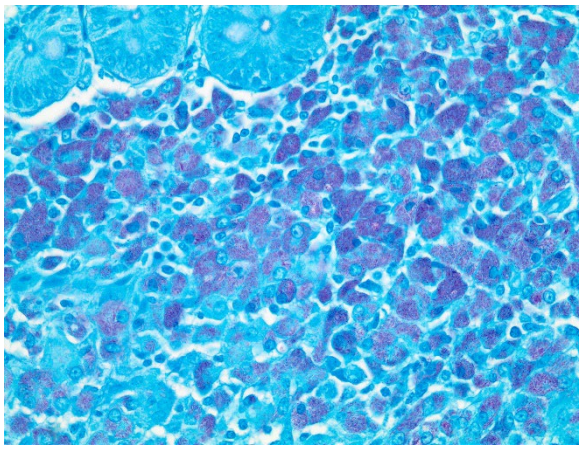

Figure 1-6. Intestine, rhesus macaque. Epithelioid macrophages within the lamina propria contain numerous cytoplasmic acid-fast bacilli. (Ziehl-Neilson, 600X) (*Photo courtesy of:* National Institutes of Health, Bethesda, MD)

The reason for the negative mycobacteria PCR results in the presence of numerous bacteria in this case is uncertain. One lab found a 45.1%% sensitivity with PCR compared to culture.[9] A source of false negative results with PCR are interfering materials such has immunoglobulin and collagen.[11]

Contributing Institution:
National Institutes of Health, ORS

JPC Diagnosis:
1. Liver: Cholangiohepatitis, proliferative and lymphoplasmacytic, chronic, diffuse, moderate, with bridging portal fibrosis and intraepithelial microsporidia.

2. Liver: Hepatitis, granulomatous, multifocal, moderate.

JPC Comment:
This week's moderator is LTC Erica Barkei, JPC's Chief of Resident Training and Education.

In this section, microsporidia are occasionally visible on H&E and special stains, particularly within sloughed biliary epithelial cells. In this section, mycobacterial "granulomas" do have epithelioid and/or multinucleate giant cell macrophages, but lack surrounding lymphocytes and fibrosis and a central core of necrosis as is typical for Th1 granulomas. As the contributor notes, macrophages containing non-tuberculous mycobacteria typically have fewer cytoplasmic organisms outside of the colon, which may reflect the relatively limited degree of granuloma development within the liver seen in this case.

There are several other important diseases of immunosuppressed macaques to consider (although not in this section.) As the contributor notes, *Cryptosporidium* may also be seen within the biliary tract, though this causes suppurative inflammation which is noticeably absent in section. Cytomegalovirus (CMV) has characteristic intranuclear viral inclusions and is also necrotizing. Other common co-infections include simian virus 40 (SV40), *Candida albicans*, *Pneumocystis carinii,* and *Toxoplasma gondii*.

References:

1. Dean P, Hirt RP, Embley TM. Microsporidia: Why make nucleotides if you can steal them? *PLOS Pathogens* 2016; 12(11): e1005870.
2. Green LC, Didier PJ, Bowers, L C. et al. Natural and experimental infection of immunocompromised rhesus macaques (*Macaca mulatta*) with the microsporidian *Enterocytozoon bieneusi* genotype D. *Microbes and Infection* 6 (2004) 996–1002
3. Han B, Weiss LM. Microsporidia: Obligate intracellular pathogens within the fungal kingdom. *Microbiol Spectr*. Author manuscript available in PMC 2017 October 1
4. Li W, Feng Y, Xiao L. Parasite of the month: *Enterocytozoon*. *Trends in Parasitology*, 2021, 20(20):1-2

5. Li W, Feng Y, Santin M. Host Specificity of Enterocytozoon bieneusi and public health implications. *Trends in Parasitology.* 2019, 35(6):436-451
6. Mansfield K, Carville A, Herbert D, et al. Localization of persistent *Enterocytozoon bieneusi* Infection in normal rhesus macaques (*Macaca mulatta*) to the hepatobiliary tree. J Clinical Microbiol. 1998, 36(8): 2336–2338
7. Mansfield K, Carville A, Shevetz D, et al. Identification of an *Enterocytozoon bieneusi*-like microsporidian parasite in Simian-Immunodeficiency-Virus-Inoculated macaques with hepatobiliary disease. *Am J of Path*.1997,150(4): 1395-1405
8. Maslow J, Brar I, Smith G, et al. Latent infection as a source of disseminated disease caused by organisms of the *Mycobacterium avium Complex* in Simian Immunodeficiency Virus–Infected Rhesus Macaques. *Journal of Infect Dis.* 2003; 187:1748–55
9. Park JS, Choi J, Lim, J, et al. The combination of real-time PCR and HPLC for the identification of non-tuberculous mycobacteria. *Ann Lab Med*. 2013, 33:349-352
10. Procop G. HIV and mycobacteria. *Seminars in Diagnostic Pathology*, 34(2017) 332-339.
11. Sidstedt M, Rådström P, Hedman J. PCR inhibition in qPCR, dPCR and MPS mechanisms and solutions. *Analytical and Bioanalytical Chem*. 2020, 412:2009–2023

CASE II:

Signalment:
Adult, male, Ezo raccoon dog (*Nyctereutes procyonoides albus*)

History:
On March 29, 2022, a crow die-off occurred in a public garden in Sapporo, Hokkaido, Japan. Based on RT–qPCR and subsequent gene sequencing analyses, carcasses collected on March 29 and May 18, 2022, were confirmed to be infected with highly pathogenic avian influenza virus (HPAIV). On the same day as the die-off, a diseased raccoon dog was also noticed by the garden workers. Three days thereafter, the raccoon dog showed severe clinical signs of depression and blindness. It was captured for treatment but was considered to be at a humane endpoint from the veterinary viewpoint; thus, it was euthanized via isoflurane inhalation. The raccoon dog was subjected to postmortem examination.

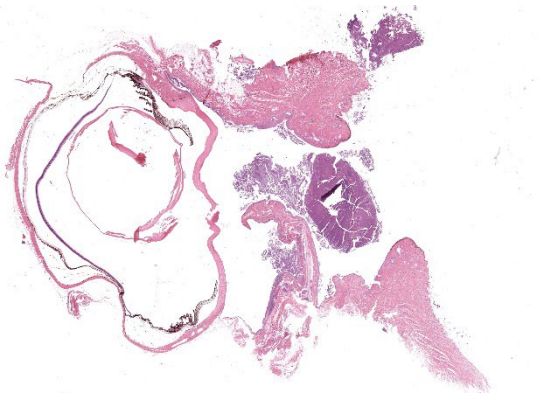

Figure 2-1. Globe and palpebra, raccoon dog. Aggregates of inflammatory debris are present within the palpebral fissure and beneath the eyelid. (HE, 7X)

Gross Pathology:
The raccoon dog was severely emaciated and moderately dehydrated. Severe bilateral conjunctivitis with eye discharge was noted, and the lenses were mildly clouded. Nematodes were detected in the stomach. The kidneys were discolored.

Laboratory Results:
HPAIV genomes of the H5 subtype were detected and the virus was isolated from the 10% homogenates of the brain, trachea, and lung of the raccoon dog.[2]

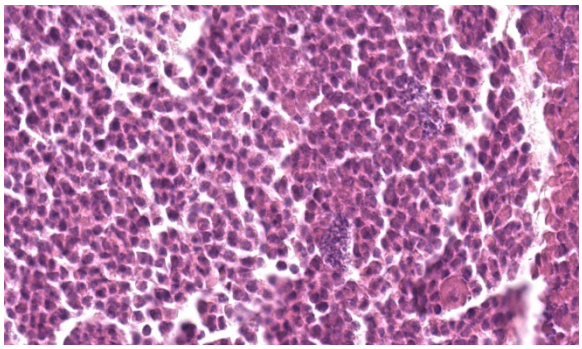

Figure 2-2. Palpebral fissure, raccoon dog. High magnification of the exudate within the palpebral fissure which is composed of viable and necrotic neutrophils, debris-laden macrophages, abundant cellular debris, and entrapped bacterial colonies. (HE, 1100X)

Microscopic Description:
Numerous degenerated and necrotic neutrophils and bacterial colonies are evident in the palpebral fissure. There is a mild infiltration of lymphocytes and neutrophils in the lamina propria of the palpebral and bulbar conjunctiva of the upper eyelid. A moderate to severe lymphoplasmacytic and mild neutrophilic infiltration with mild fibrosis is observed in the lamina propria of the third and lower eyelid. Desquamation of conjunctival epithelial cells is sometimes seen.

Contributor's Morphologic Diagnosis:
Eye (left): Conjunctivitis, diffuse, chronic, suppurative, severe

Contributor's Comment:
Immunohistochemistry using anti-influenza virus NP (nucleoprotein) monoclonal antibody (clone 183/5), detected viral antigens in columnar epithelia lining the bulbar and palpebral conjunctiva, most notably of the third eyelid.[3] Moreover, viral antigens were detected in the superficial glands under the conjunctiva of the third eyelid.[3]

This raccoon dog was found emaciated in the same park on the same day that the HPAIV-infected crow was found dead. Raccoon dogs show greater dependency on fruits, plant seeds, and insects, although they also consume animal resources during spring.[1] That stated, garden workers did not observe this animal scavenging crow carcasses. Presumably, this raccoon dog was in in close contact with crow carcasses even if it did not ingest them.

In tissues other than conjunctiva, viral antigens were detected only in the tracheal ciliated epithelium and tracheal glands.[3] Titers of infectious viruses found in the brain, lung and trachea homogenates were close to the limit of detection,[3] which is likely due to clearance of the virus by an immune response. Visual impairment is usually critical for wildlife animals. It was speculated that although the raccoon dog survived the acute phase of HPAIV infection, visual impairment caused by the secondary bacterial infection resulted in malnutrition and dehydration.

Contributing Institution:
Laboratory of Comparative Pathology
Department of Clinical Sciences
Faculty of Veterinary Medicine
Hokkaido University
Kita18, Nishi 9, Kita-ku, Sapporo 060-0818, JAPAN
https://www.vetmed.hokudai.ac.jp/organization/comp-pathol/e/index.html

JPC Diagnosis:

Conjunctiva: Conjunctivitis, neutrophilic and lymphoplasmacytic, chronic-active, diffuse, marked.

JPC Comment:
This second case has an interesting backstory that comes full circle to current events and the ongoing spread of H5N1 HPAI clade 2.3.4.4b viruses worldwide. We previously

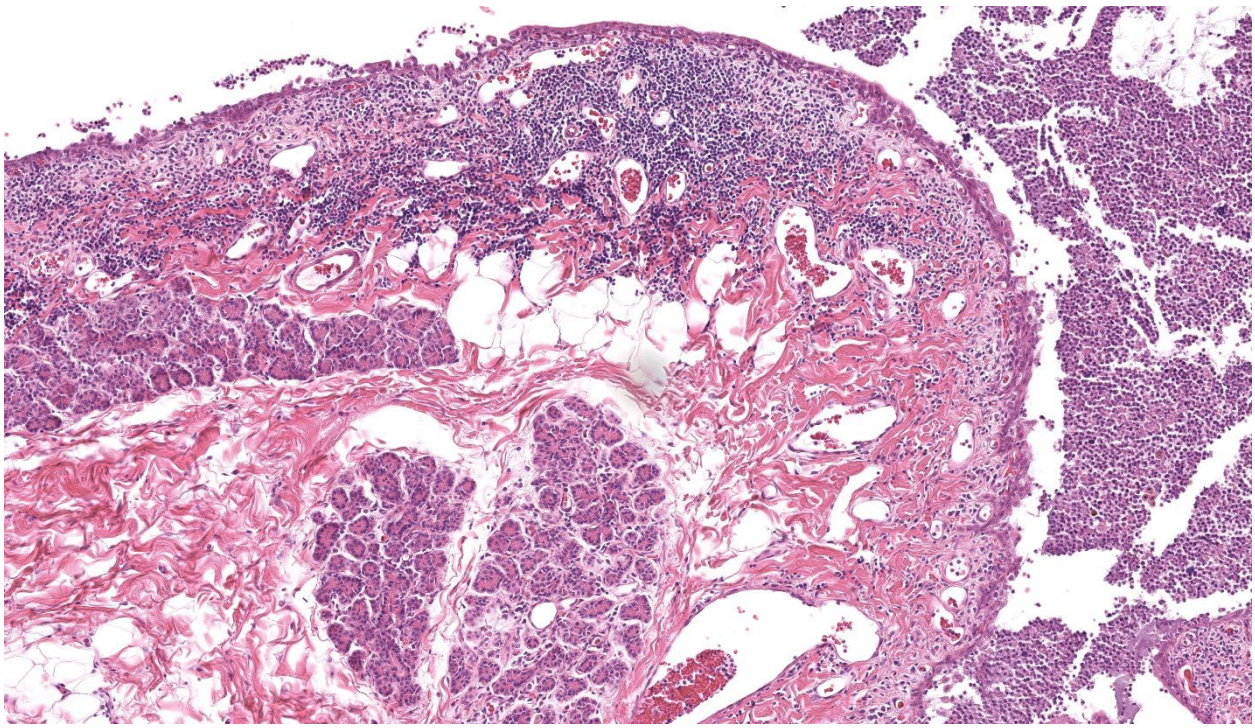

Figure 2-3. Eyelid conjunctiva. The conjunctival epithelium is hyperplastic and multifocally eroded. The subconjunctival tissue is infiltrated by large numbers of neutrophils, lymphocytes and plasma cells, which also expand the interstitial collagen between acini of the lacrimal gland. (HE, 180X)

touched on avian influenza in the context of an experimental case in a pig (Case 3, Conference 14, 2024-2025). Although we discussed the role of viral shedding into milk and zoonotic potential therein, there is still plenty more left to say on this topic.

The slide description for this case is not overly complicated, though conference participants did not immediately offer HPAI as a presumptive cause for the disruption of the conjunctival epithelium and subsequent bacterial infection in this animal. Conjunctivitis is underappreciated as a clinical sign of HPAI, though recent human cases acquired from dairy or poultry workers[2,7] have shown that this may be the only overt sign of disease. Similar to the tanuki in this case, workers exposed to HPAI may only be exposed through the conjunctiva because of mask/glove wear or occupational factors such as the proximity of the eyeline of milking parlor workers to the udders of the cows being milked. In comparison to the red fox that scavenged the carcass and developed systemic viral infection[3], this animal had evidence of chronic infection and a host adaptive immune response – this may reflect a lower viral load and impact of the route of entry. The role of α2,3 sialic acid receptors on conjunctival epithelium and zoonotic transmission of avian influenza viruses has previously been established and likely played a role in the present case.[3,4]

Similar to the fox's outcome in the present case[3], domestic cats have fallen ill or died after consumption of raw pet food diets and/or exposure to raw milk contaminated with HPAI.[5] Systemic entry of HPAIV has been associated with endothelial cell targeting and vasculitis, a feature which is noticeably absent in this tanuki. Other classic manifestations of HPAI (in cats and beyond) include

pancreatic necrosis, encephalitis, myocarditis, and adrenal necrosis.[6,8]

Finally, the contributor gave us a final puzzle to ponder for this case. As the animal was submitted as an 'Ezo' raccoon dog, we explored this aspect further. Accordingly, Ezo is borrowed from the Ainu language (an indigenous people from Northern Japan) and refers to the northern part of Meiji-era Japan, particularly Hokkaido, but also Sakhalin and the Kuril Islands.[9] In modern usage, the term has largely disappeared, but is used to refer to several species native to northern Japan such as the Ezo fox (北狐), Ezo deer (エゾシカ) and Ezo tanuki (エゾタヌキ). Additionally, there is not a consensus on the taxonomy, with *Nyctereutes procyonoides albus* and *Nyctereutes viverrinus* both being used to refer to the same species native to Japan. As the contributor of this case is from Hokkaido and refers to the animal as a tanuki,[3] we conclude that this is a native Japanese raccoon dog and not a related species that has been widely distributed across Asia and Europe.

References:

1. Akihito TS, Teduka M, Kawada S. Long-term Trends in Food Habits of the Raccoon Dog, Nyctereutes viverrinus, in the Imperial Palace, Tokyo. *Bull. Natl. Mus. Nat. Sci*., Ser. A. 2016;42(3):143–161.
2. Drehoff CC, White EB, Frutos AM, et al. Cluster of Influenza A(H5) Cases Associated with Poultry Exposure at Two Facilities - Colorado, July 2024. *MMWR Morb Mortal Wkly Rep*. 2024 Aug 29;73(34):734-739.
3. Hiono T, Kobayashi D, Kobayashi A, et al. Virological, pathological, and glycovirological investigations of an Ezo red fox and a tanuki naturally infected with H5N1 high pathogenicity avian influenza viruses in Hokkaido, Japan. *Virology*. 2023;578:35-44
4. Olofsson S, Kumlin U, Dimock K, Arnberg N. Avian influenza and sialic acid receptors: more than meets the eye? *Lancet Infect Dis*. 2005 Mar;5(3):184-8.
5. Schnirring L. H5N1 confirmed in more cats as probe into raw pet food widens. University of Minnesota Center for Infectious Disease Research and Policy (CIDRAP). 2025 Jan 14; https://www.cidrap.umn.edu/avian-influenza-bird-flu/h5n1-confirmed-more-cats-probe-raw-pet-food-widens.
6. Soda K, Tomioka Y, Usui T, et al. Susceptibility of herons (family: Ardeidae) to clade 2.3.2.1 H5N1 subtype high pathogenicity avian influenza virus. *Avian Pathol*. 2022 Apr;51(2):146-153.
7. Uyeki TM, Milton S, Abdul Hamid C, et al. Highly Pathogenic Avian Influenza A(H5N1) Virus Infection in a Dairy Farm Worker. *N Engl J Med*. 2024 Jun 6;390(21):2028-2029.
8. Wünschmann A, Franzen-Klein D, Torchetti M, Confeld M, Carstensen M, Hall V. Lesions and viral antigen distribution in bald eagles, red-tailed hawks, and great horned owls naturally infected with H5N1 clade 2.3.4.4b highly pathogenic avian influenza virus. *Vet Pathol*. 2024 May;61(3):410-420.
9. Tanoshii Japanese. Ezo. https://www.tanoshiijapanese.com/dictionary.

CASE III:

Signalment:
Juvenile, female Angus cow, bovine (*Bos taurus*)

History:
This cow was one of 45 presenting with cutaneous lumps when mustered from a herd of 95 animals. Rectal temperatures ranged from 40-41ºC and some of the affected cows appeared sick. Some cows were panting with

Figure 3-1. Haired skin, ox. Photograph from one of the affected cows in the herd. Skin nodules were raised, non-ulcerated and ranged from 10-30mm diameter and were frequently over the neck and brisket. (*Photo courtesy of:* Dr. Phillip Carter, Local Land Services, New South Wales)

increased lung sounds. The mucous membranes were pink. There was no evidence of typical photosensitization lesions in predisposed locations.

Gross Pathology:
Nodules were distributed over the neck, brisket, thorax and to a lesser extent abdomen and forelimbs. Nodules ranged from 10-30mm diameter and were not ulcerated, although the surface of some could be scratched off.

Laboratory Results:
A Pan-Herpesvirus nested PCR was performed, and the product was sent for Sanger sequencing. A BLAST query of the product sequence found it was 100% identical to Bovine alphaherpesvirus 2 [MT862164] 181 nt partial sequence. A ruminant biochemistry panel found elevation in GLDH 96 U/L (0-30 U/L), mild hyperglobulinaemia 48.4 g/L (30.0-45.0 g/L) and mild elevation in serum hemoglobin 0.25 g/dL (0.00-0.20 g/dL). A Capripoxvirus TaqMan assay on the EDTA blood and a skin scab was negative, and a Capripox double antigen multispecies ELISA performed on the serum sample was negative.

Microscopic Description:
Haired skin (x3): Within the sections of haired skin, multifocally within the epidermis, there are hypereosinophilic necrotic keratinocytes, numerous small expansions containing eosinophilic fluid (vesicles) and necrotic cell debris and degenerate neutrophils, sometimes forming small aggregates (micropustules). Multifocally, epithelial cells within the stratum basale, stratum spinosum and stratum granulosum are sloughed, replaced with clumps of multinucleated epithelial cells with hypereosinophilic cytoplasm (syncytia). Moderate numbers of epithelial cells and syncytia within the surface epithelium, and occasionally within epithelium lining hair follicles, contain 1-6µm diameter intranuclear eosinophilic inclusion bodies with margination of chromatin. Multifocally, keratinocytes are swollen with clearing of cytoplasm (ballooning degeneration). There is mild, multifocal orthokeratotic hyperkeratosis, with mild to moderate extravasated erythrocytes adjacent to the epidermal surface (hemorrhage). Throughout the superficial and

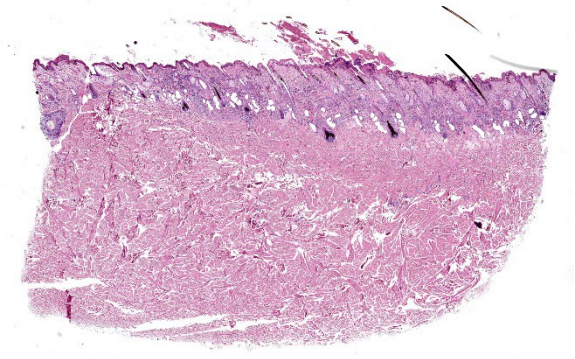

Figure 3-2. Haired skin, ox. One section of haired skin is submitted for examination. There is diffuse epidermal hyperplasia, foal hyperkeratosis and pustule formation, and a diffuse band of hypercellularity within the superficial dermis. (HE, 7X)

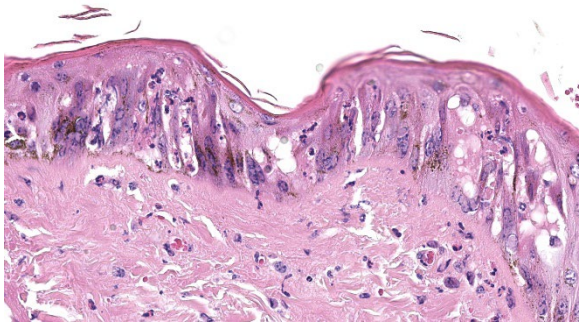

Figure 3-3. Haired skin, ox. There are numerous viral cytopathic changes within the epidermis including intra- and intercytoplasmic edema with vesicle formation, syncytia formation, and intranuclear and intracytoplasmic viral inclusions. (HE, 705X)

deep dermis, there are multifocal, moderate infiltrates of neutrophils, lymphocytes, plasma cells, eosinophils and macrophages associated with cell debris, and multifocal mild to moderate separation of dermal collagen fibres with clear space and/or eosinophilic fluid (edema). Occasionally sebaceous glands are surrounded and infiltrated by neutrophils and apocrine glands are dilated. Few lymphatic vessels in the deep dermis are dilated. Within the dermis of one section, adjacent to the cut margin, there is a focal aggregate of refractile material, surrounded by eosinophilic necrotic material, and subsequently surrounded by a moderate margin of leukocytes with squash artefact.

Contributor's Morphologic Diagnosis:
Haired skin, dermatitis, necrosuppurative and, lymphoplasmacytic multifocal to widespread, chronic-active, with edema, syncytial cells, pustules, vesicles and intranuclear epithelial eosinophilic viral inclusion bodies, *Bos taurus.*

Contributor's Comment:
Infection with Bovine Herpesvirus 2 (BoHV-2) in cattle can cause two distinct clinical conditions: one is an acute onset, mild generalized skin infection called Pseudo Lumpy Skin Disease (PLSD) which manifests as cutaneous nodules which develop a central depression; the second is Bovine Herpesvirus Mammillitis (BHM), a localized ulcerative condition affecting the teats and udder of cattle. The disease is found in many parts of the world and is likely transmitted by biting insects or mechanically by equipment used on farms. The gross appearance of the generalized skin lesions can closely resemble Lumpy Skin Disease, which has trade implications in many countries.[21]

Bovine herpesvirus 2 (BoHV-2) is an enveloped double stranded DNA virus approximately 150-200nm in size, belonging to the family Orthoherpesviridae, subfamily Alphaherpesvirinae, genus simplexvirus**.**

Bovine herpesvirus 2 infection was first identified in Southern and Eastern Africa. Since its discovery in the 1950's, it has been reported almost globally with case reports from Europe, Japan, Australia, Brazil, the United States and Israel.[2,3,8–10,13,16]

In the wild, BoHV-2 infects cattle, wild ruminants and pseudo-ruminants (hippopotamus).[13] Sheep have been experimentally infected with BoHV-2 producing clinical dis-

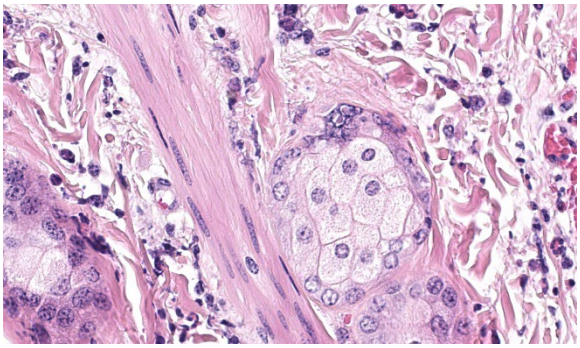

Figure 3-4. Haired skin, ox. Viral inclusions and syncytia are present within reserve cells of sebaceous glands. (HE, 847X)

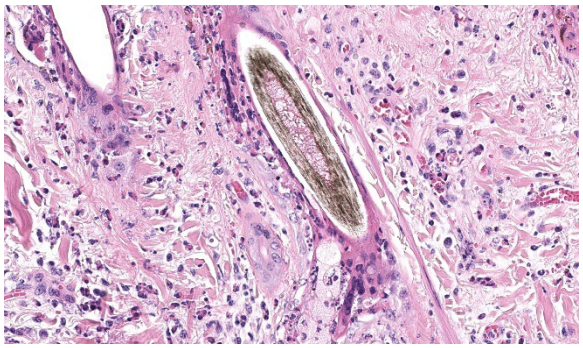

Figure 3-5. Haired skin, ox. Viral inclusions and syncytia are present within follicular epithelium. (HE, 531X)

ease similar to Bovine Herpesvirus Mammillitis.[17] Rabbits, guinea pigs and mice have also been experimentally infected with BoHV-2.[8]

Transmission of BoHV-2 most likely occurs via intradermal injection of the virus by biting insects, or via contaminated equipment coming into contact with wounds and cuts. Biting flies have been demonstrated to be able to transmit the infection between cell cultures in the lab, and the distribution and seasonality of outbreaks of Pseudo Lumpy Skin Disease are thought to be related to the distribution and peaks in biting insect activity.[6,9,12] Milking equipment is suspected of being able to transmit the virus within milking herds if clinically affected cattle are present.[5,10]

Serological surveys indicate that circulation of BoHV-2 in cattle can occur without any episodes of clinical disease suggesting most infections may be subclinical.[8,9,15]

In experiments where BoHV-2 was intradermally inoculated into the flank of cattle, a discrete raised swelling was observed at the injection site by day 3 post inoculation. Generalized discrete swellings appeared over the head, neck and dorsal body by day 6 which developed crusts which gradually lifted over the course of 3 weeks to reveal greyish-white areas of skin with reduced numbers of hairs (alopecia). Lymph node enlargement was observed by day 5 and persisted to day 10 post inoculation.[16]

In the field, the incubation period of BoHV-2 is considered to be around 1-2 weeks, with skin lesions resolving 2-4 weeks after first appearing. Neutralizing antibodies appear 7-14 days after initial exposure.[16,18] Outbreaks can occur seasonally or sporadically depending on the activity of biting insects and the presence of naive hosts.[11,19]

Post infection, like other herpesviruses, BoHV-2 becomes latent with the virus likely retreating to the neuronal tissue such as the trigeminal ganglion and possibly lymphoid tissue where it may lay dormant until infection is reactivated during periods of stress.[3,17]

Generalized infection with BoHV-2 induces Pseudo Lumpy Skin Disease, which is characterized by:[1,4,16]

- Circumscribed cutaneous nodules over the body, frequently on the head, neck, shoulders, back and perineum.
- Around 4-6 days after the appearance of gross lesions, the cutaneous lesions begin to crust over. The crusts eventually fall off leaving areas of alopecia.
- Lesions disappear when the hair regrows.
- Lymphadenitis may be observed during early stages of infection.
- Animals make a full recovery without treatment.

Localized infection with BoHV-2 of the udder and teats is called Bovine Herpesvirus Mammillitis, and is characterized by:[11,20]

- Variable sized tender edematous swellings on the udder or teats.
- Vesicles may appear on affected areas
- The overlying skin then ulcerates and becomes painful, taking 3-10 weeks to heal

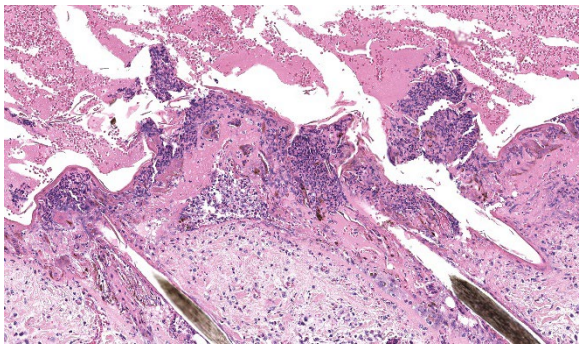

Figure 3-6. Haired skin, ox. There is multifocal full-thickness epidermal necrosis and pustule formation. (HE, 261X)

Histopathological changes of BoHV-2 infection are characterized by the formation of epithelial syncytia initially within the stratum basale and inner stratum spinosum with prominent intranuclear eosinophilic inclusion bodies.[11] Intranuclear inclusions are classified as Cowdry type A inclusions and have central eosinophilic or amphophilic deposits surrounded by a clear halo and the nuclear chromatin is pushed to the margin of the nucleus.[19] Intranuclear inclusions are most numerous after the appearance of the gross nodules but before the appearance of crusts (around 4-6 days later),[1,11] which coincides approximately with the time when virus can be isolated or detected by PCR (see below). When the lesions crust over, the epithelium becomes necrotic and infiltrated by large numbers of neutrophils. Loss of the necrotic epithelium results in an ulcer which becomes covered with haemorrhage, fibrinous exudate and numerous degenerate neutrophils. Deeper in the dermis, there is edema and a mononuclear infiltrate. As the lesion heals, there is fibrosis in the superficial dermis with perivascular infiltrates of mononuclear cells.[11]

The following assays have been reported in the literature to support the diagnosis of BoHV-2 infection.

Test	Required Samples	Notes
PCR[1,12,19]	Fresh skin lesions	Most likely to yield detectable virus DNA up to 8 days post infection or before cutaneous lesions crust over or ulcerate
Cytology[11]	Early skin lesions (<5 days after initial appearance)	Presence of syncytia with intranuclear inclusions
Serology - ELISA[15]	Serum	
Serology – Serum neutralization[9,18]	Serum	Antibodies detected as early as 10 days post inoculation or about 5-7 days after appearance of cutaneous lesions
Serology – Immunofluorescent antibody test (IFAT)[10]	Serum	
Negative staining electron microscopy[19]	Fresh skin lesions	Herpesvirus particles may be seen
Virus culture[6,9,10,16,18]	Blood, Fresh skin lesions up to around day 6-7 post infection	Vero cells Calf kidney cells Fetal bovine muscle cells Madin Darby Bovine Kidney (MDBK)

The following conditions should be considered as potential differentials for Bovine Herpesvirus-2 infection based on their clinical appearance.[4,11,20]

Disease	Clinical Presentation	Tests to diagnose/ differentiate	Key differentiating histological features
Viral			
Early-stage Lumpy Skin Disease (Capripoxvirus)	Firm circumscribed cutaneous nodules which develop central areas of necrosis and scarring	Capripox PCR, biopsy + histopathology, Electron microscopy demonstrating pox virus particles	Epidermal vacuolar swelling with intracytoplasmic inclusions. Vasculitis
Bovine Papillomavirus	Papillomas or warts of varying size on body. Mostly frequently seen in younger cattle	Biopsy + histopathology, PCR of skin lesions	Unencapsulated, proliferative cutaneous neoplasm accompanied by basal cell hyperplasia, acanthosis and hyperkeratosis
Bovine papular stomatitis (Parapoxvirus)	Raised red papules, erosions or ulcers around muzzle and nose, occasionally elsewhere on the body	Electron microscopy of tissue, virus culture, biopsy + histopathology, ELISA/Agar gel precipitation tests to look for antibodies	Epidermal vacuolar swelling with intracytoplasmic inclusions, epidermal proliferation
Pseudocowpox (Parapoxvirus)	Raised red sores, scabs or vesicles on teats, thighs or perineum	PCR on skin lesions, scabs or blood, biopsy + histopathology.	Epidermal vacuolar swelling with intracytoplasmic inclusions, epidermal proliferation
Cowpox (Orthopoxvirus)	Papules or ulcers on the teat or udder	PCR of skin lesions, electron microscopy of scabs demonstrating pox virus particles[14], biopsy + histopathology	Epidermal vacuolar swelling with intracytoplasmic inclusions, focal epidermal hyperplasia.
BVDV dermatitis	Patchy hyperkeratosis	Bovine Viral Diarrhea	

	around neck, shoulder and perineum	Virus Antigen ELISA or PCR on ear notch, blood, hair or visceral organs	
Bovine Herpesvirus 4	Vesicles, pustules and ulcers on udder. Teats are usually not involved	PCR on skin lesions, serological testing, biopsy + histopathology	Intraepithelial pustular dermatitis
Bacterial			
Dermatophilosis (*Dermatophilus congolensis*)	Papules with crusts entrapped in hair and areas of alopecia often over the dorsal aspect of head, neck and body	Bacterial cultures, cytology of crusts, biopsy + histopathology	Multiple parallel rows of cocci, trapped within alternating layers of hyperkeratosis and serous fluid and degenerate neutrophils. Purulent folliculitis
Cutaneous tuberculosis (*Mycobacterium bovis*)	Single or multiple nodules, abscesses or ulcers	PCR, mycobacterial culture, biopsy + histopathology	Pyogranulomatous dermatitis with central caseous necrosis with acid fast bacilli present.
Fungal			
Dermatophytosis (Ringworm, *Trichophyton verrucosum*)	Expanding circular hairless lesions mostly on head and neck. May appear red and moist to scaly and grey.	Dermatophyte cultures, biopsy + histopathology, PCR	Fungal hyphae clustering within hair shafts and arthrospores around the outside of hairs.
Parasites			
Mites (multiple species)	Nodules, alopecia and crusts which may be itchy	Superficial or deep skin scrapings	

Onchocercosis	Cutaneous nodules over brisket, abdomen and udder	Biopsy + histopathology	Presence of microfilaria, surrounded by eosinophilic inflammation
Besnoitiosis (*Besnoitia sp.*)	Alopecia, scaling and thickening of skin over neck ,shoulders and rump	biopsy + histopathology, PCR, serology	Presence of protozoal tissue cysts
Hypoderma sp. (warbles)	Firm raised nodules in the skin frequently along the back and shoulders	Clinical examination and presence of breathing holes Serological tests	
Neoplasia			
Cutaneous Lymphoma	Multifocal subcutaneous/intracutaneous nodules, often accompanied by alopecia, lymphadenopathy	biopsy + histopathology, haematology may reveal lymphocytosis. May arise sporadically and not necessarily be associated with bovine leukosis virus infection	Sheets of neoplastic lymphocytes.
Mast cell tumor	Mulltifocal cutaneous or subcutaneous nodules over body +/- alopecia +/- pigmented +/- ulceration	biopsy + histopathology	Sheets of neoplastic mast cells often accompanied by numerous eosinophils
Other			
Photosensitization	Alopecia, erythema and blistering of non-pigmented skin	History – exposure to toxic plants, drug administration, biochemistry – liver function, biopsy +	Coagulative necrosis of epidermis, dermal edema, vascular necrosis

		histopathology	
Skin allergies/urticaria	Haired wheals +/- crusts anywhere on the body, angioedema	History of recent drug administration, insect or plant exposure, response to glucocorticoid administration, biopsy + histopathology	Dermal edema, perivascular infiltrates of granulocytes, mast cells and lymphocytes inconsistently present in upper to mid dermis.

Contributing Institution:
Elizabeth Macarthur Agricultural Institute, Department of Primary Industries and Regional Development

JPC Diagnosis:
Haired skin: Dermatitis, necrotizing, subacute, diffuse, severe, with epithelial viral syncytia, intranuclear viral inclusions, corneal pustules, mixed dermal infiltrates, and edema.

JPC Comment:
The contributor provides an excellent section to accompany an thorough writeup on the topic. The slide has generous viral inclusions and syncytia along with raised vesicles to establish an etiological diagnosis. Conference participants did touch on the nature of intracellular and intercellular edema in this case – the lack of overt cellular swelling and intracytoplasmic inclusions lowered suspicion for a poxviral etiology.

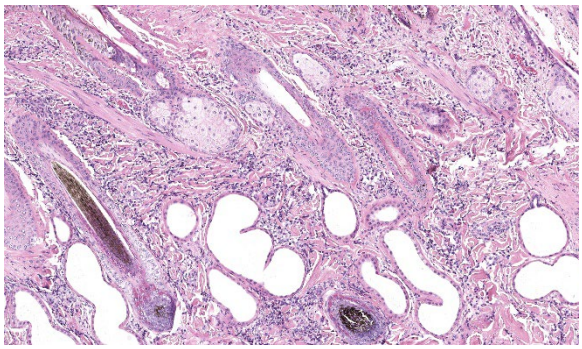

Figure 3-7. Haired skin, ox. There is marked mixed dermal inflammation, dilation of apocrine glands, and thickened and tortuous dermal arterioles. (HE, 179X)

One ancillary finding in section was a focal granuloma centered on foreign material (possibly plant material). We speculated that this might be secondary to necrosis of the overlying epithelium and entry into the dermis, though the adjacent portions of skin lack significant viral changes. This lesion is at the edge of the section and is only on one of the three sections of skin provided which limits further interpretation of this incidental observation.

References:

1. Amaral B, Dos Santos Jardim J, Cargnelutti J, Martins M, Weiblen R, Flores E. Pathogenesis of Bovine alphaherpesvirus 2 in calves following different routes of inoculation. *Pesqui Veterinária Bras*. 2020;40:360–367.
2. Brenner J, Sharir B, Yadin H, Perl S, Stram Y. Herpesvirus type 2 in biopsy of a cow with possible pseudo-lumpy-skin disease. *Vet Rec*. 2009;165(18):539–540.
3. Campos FS, Franco AC, Oliveira MT, et al. Detection of bovine herpesvirus 2 and bovine herpesvirus 4 DNA in trigeminal ganglia of naturally infected cattle by polymerase chain reaction. *Vet Microbiol*.

2014;171(1):182–188.
4. Department of Agriculture, Fisheries and Forestry. Differential diagnoses for lumpy skin disease. Australian Government 2023:
5. Gibbs EPJ, Johnson RH, Osborne AD. Experimental Studies of the Epidemiology of Bovine Herpes Mammillitis. *Res Vet Sci*. 1973;14(2):139–144.
6. Gibbs EPJ, Jonnson RH, Gatehouse AG. A Laboratory Technique for Studying the Mechanical Transmission of Bovine Herpes Mammillitis Virus by the Stable Fly (Stomoxys calcitrans L.). *Res Vet Sci*. 1973;14(2):145–149.
7. Hulo C, de Castro E, Masson P, et al. ViralZone: a knowledge resource to understand virus diversity. *Nucleic Acids Res*. 2011;39(Database issue):D576-582.
8. Huygelen C, Thienpont D, Dekeyser PJ, Vandervelden M. Allerton Virus, a Cytopathogenic Agent Associated with Lumpy Skin Disease. *Zentralblatt Für Veterinärmedizin*. 1960;7(8):754–760.
9. Imai K, Ishihara R, Nishimori T. First demonstration of bovine herpesvirus 2 infection among cattle by neutralization test in Japan. *J Vet Med Sci*. 2005;67(3):317–320.
10. Lanave G, Larocca V, Losurdo M, et al. Isolation and characterization of bovine alphaherpesvirus 2 strain from an outbreak of bovine herpetic mammillitis in a dairy farm. *BMC Vet Res*. 2020;16(1):103.
11. Mauldin EA, Peters-Kennedy J. Chapter 6 - Integumentary System. In: Maxie MG, ed. *Jubb, Kennedy & Palmer's Pathology of Domestic Animals: Volume 1 (Sixth Edition)*. W.B. Saunders 2016:509-736.e1.
12. d'Offay JM, Floyd JG, Eberle R, et al. Use of a polymerase chain reaction assay to detect bovine herpesvirus type 2 DNA in skin lesions from cattle suspected to have pseudo-lumpy skin disease. *J Am Vet Med Assoc*. 2003;222(10):1404–1407, 1366–1367.
13. Plowright W, Jessett DM. Investigations of Allerton-type herpes virus infection in East African game animals and cattle. *J Hyg (Lond)*. 2009/05/15 ed. 1971;69(2):209–222.
14. Shivanna V, Cino-Ozuna AG, Heskett C, Marthaler DG, Ganta C. Pseudocowpox virus infection in an American bison (Bison bison). *BMC Vet Res*. 2020;16(1):241.
15. Singer S, Hoffmann B, Hafner-Marx A, et al. Bovine Alphaherpesvirus 2 infections in Bavaria: an analysis of the current situation - several years after eradicating Bovine Alphaherpesvirus 1. *BMC Vet Res*. 2020;16(1):149.
16. St George TD, Uren MF, Melville LF. A generalised infection of cattle with bovine herpesvirus 2. *Aust Vet J*. 1980;56(1):47–48.
17. Torres FD, Almeida SR, Silva MS, Weiblen R, Flores EF. Distribution of latent bovine herpesvirus 2 DNA in tissues of experimentally infected sheep. *Res Vet Sci*. 2009;87(1):161–166.
18. Turner AJ, Kovesdy L, Morgan IR. Isolation and characterisation of bovine herpesvirus mammillitis virus and its pathogenicity for cattle. *Aust Vet J*. 1976;52(4):166–169.
19. Watanabe TTN, Moeller RB, Crossley BM, Blanchard PC. Outbreaks of bovine herpesvirus 2 infections in calves causing ear and facial skin lesions. *J Vet Diagn Invest*. 2017;29(5):686–690.
20. White SD, Théon AP, Angelos JA, Makhdoomi MM. Chapter 40 - Diseases of the Skin. In: Smith BP, Van Metre DC, Pusterla N, eds. *Large Animal Internal Medicine (Sixth Edition)*. Mosby 2020:1316-1351.e11.
21. World Organisation for Animal Health. Infection with lumpy skin disease virus. In: *Terrestrial Animal Health Code*.

World Organisation for Animal Health (OIE) 2024:

CASE IV:

Signalment:
8 week old, female intact, C.B-17 *scid* mouse (*Mus musculus*).

History:
This mouse was part of research project to study the role *B. burgdorferi* virulence factors in the pathogenesis of Lyme Borreliosis. The mouse was inoculated on the lumbosacral region via SQ with *Borrelia burgdorferi* B31- A3 strain and was euthanized 4 weeks post-challenge.

Gross Pathology:
Bilaterally, the tibotarsal joints were markedly thickened and swollen on the cranial aspect.

Laboratory Results:
BSK-II culture media was positive for *B. burgdorferi*. Spirochetes were isolated from a section of the tibiotarsal joint. White blood cell counts demonstrated a neutrophilia (5.57, ref 0.43 – 3.58 K/uL). Spirochetes were demonstrated in areas of tenosynovitis by immunohistochemistry and Warthin-Starry stain in the tibiotarsal joints.

Microscopic Description:
Tibiotarsal joint. Arising from antero-distal tibial metaphysis to the antero-proximal aspect of the tarsal bones is a well-demarcated, densely cellular, thickened and inflamed synovium, regionally admixed with an irregular trabecula of woven bone. The synovium is markedly hyperplastic by numerous, variably sized, spindle to spindloid synovial cells closely packed to each other and is lined by a discontinuous, single layer of plump synoviocytes. The synovium is diffusely infiltrated by large numbers of neutrophils and moderate

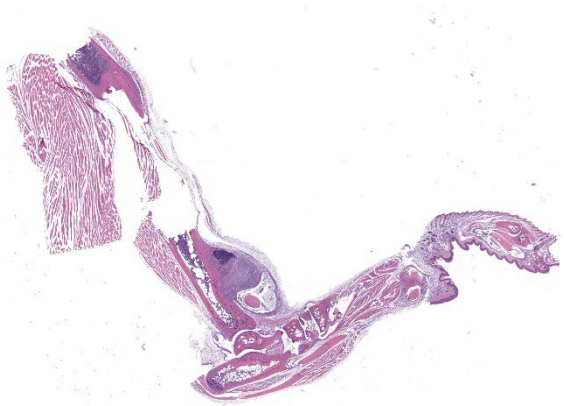

Figure 4-1. Leg, SCID mouse. A section of hind leg is submitted for examination. At subgross magnification, there is marked expansion of the tibiotarsal joint. (HE, 7X)

numbers of macrophages. The synovial space and tendon sheaths are infiltrated by moderate numbers of neutrophils and fewer macrophages mixed with eosinophilic proteinaceous fluid, fibrin, sloughed cells, necrotic cells, and karyorrhectic debris. The periosteum along antero-distal tibial metaphysis and epiphysis is expanded by an irregular intertwined trabecula of woven bone that is incompletely mineralized (periosteal remodeling) and contains numerous osteocytes. The immature trabecula is lined by osteoblasts, entraps mesenchymal stromal cells, and is regionally bounded by organized island of cartilage undergoing endochondral ossification (bone formation). The edges of the woven bone are irregular and scalloped and often lined by osteoblasts and fewer osteoclasts within Howship's lacunae (remodeling). Within the inflamed synovium a focal subperiosteal trabecula, arranged perpendicularly to zones of bone remodeling, is composed of woven bone at different stages of mineralization. The synovium and adjacent tendon sheaths in the remaining proximal tarsal bones and plantar aspect of the tibiotarsal joint is mildly hyperplastic and infiltrated by low numbers of macrophages. In these areas synovial spaces contain proteinaceous fluid mixed with individual sloughed synovial cells and rare karyorrhectic debris.

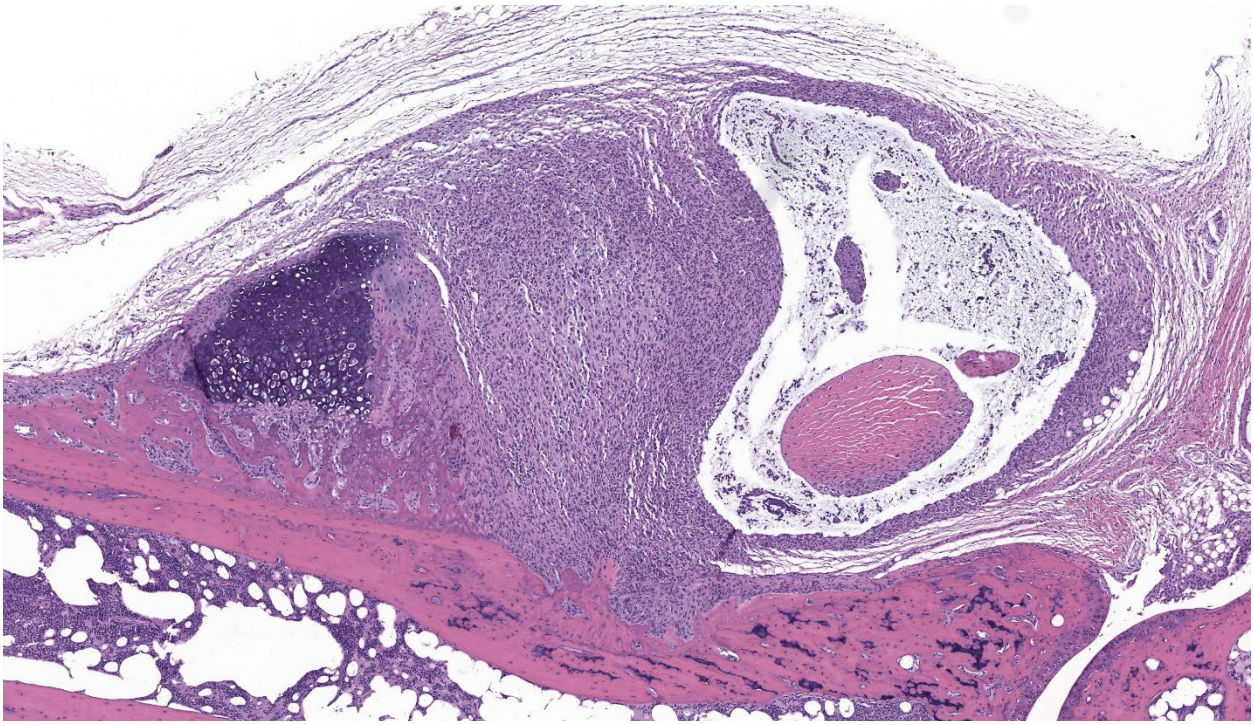

Figure 4-2. Tibiotarsal joint, SCID mouse. The tendon sheath is markedly expanded up to 1mm and the interface between it and the underlying synovium is effaced by abundant granulation tissue. Granulation tissue infiltrates the lamellar bone of the distal tibia. Dorsal to the tibiotarsal joint, there is marked periosteal new bone growth with a focal area of mature cartilage. (HE, 75X)

Contributor's Morphologic Diagnosis:
Tibiotarsal joint: Tenosynovitis**,** neutrophilic and histiocytic, with synovial hyperplasia and hypertorphy, periosteal bone formation and remodeling, regional, marked, chronic.

Contributor's Comment:
The C.B-17 *scid* (SCID) mouse presented in this submission was part of a study to determine the pathogenicity and tropism of *Borrelia burgdorferi* strains deficient in different virulence factors. The mouse was part of a control group of SCID mice that were inoculated with a high dose of *B. burgdorferi* B31-A3 (wild-type) strain. C.B-17 *scid* (SCID) mice are *homozygous* for the *Prkdc*^{scid} mutation resulting in severe combined immunodeficiency.[7] This mouse strain lacks functional lymphocytes (both T and B cells) because of impaired VDJ rearrangement.[7] SCID mice exhibited the following features: marked lymphopenia, agammaglobulinemia, and high susceptibility to opportunistic infections.[7,11]

The use of laboratory mice has provided valuable insights into the immune response and pathogenesis of Lyme arthritis and carditis. Mice infected with *Borrelia burgdorferi* (*Bb*) can also develop myositis, arteritis/vasculitis, and peripheral neuritis, which parallel with lesions seen in Lyme disease patients.[1,3,4] There are several factors that should be considered when evaluating phenotypes in this model. For example, disease severity in laboratory mice is influenced by genotype, immune status, age of the mice, *Bb* strain and passage history of the strain, infectious dose, and route of inoculation.[2,4,9] It is well-accepted that inbred mouse strains are equally

susceptible to *Bb* infection, but the susceptibility of arthritis is dependent on the mouse genotype.[3]

The C3H/HeN and C3H/HeJ mice are often used to study histopathological changes in the joints as these mouse strains develop moderate to severe subacute tenosynovitis in the tibiotarsal joints.[3,4] *Bb* reaches the tibiotarsal joint after 2 weeks of intradermal or subcutaneous inoculation of spirochetes.[4] At 4 weeks of infection, the inflammation in synovium, tendon sheaths, and periarticular connective tissue is predominantly composed by neutrophils mixed with moderate numbers of macrophages, fibrinous exudate in joint lumen, and hyperplasia and hypertrophy of the synovium surrounding the tibiotarsal joints.[4] BALB/c mice develop mild to moderate tenosynovitis and C57BL/6 mice develop mild tenosynovitis following infection with *Bb*.[4,12] In contrast, SCID mice develop more severe tenosynovitis than immunocompetent mouse strains as SCID mice exhibit higher bacterial loads in the tibiotarsal joints and develop persistent infections in tissues.[4] The lesions seen in the tibiotarsal joints of SCID mice infected with *Bb* are characterized by marked hyperplasia and hypertrophy of synoviocytes with multifocal moderate to marked neutrophilic to histiocytic inflammation in synovium, ligaments, and tendon sheaths (e.g., tibiotarsal extensor tendon), fibrin and proteinaceous exudate.[3,4] As shown in this case the lesions are commonly noted at 4 weeks of infection but can persist for 8 weeks post-inoculation when mice SCID mice are inoculated with high doses of *Bb*. Spirochetes are readily visible by silver stains and/or immunohistochemistry, which are often observed within the proliferating synovium and associated with neutrophils and macrophages. The distal tibia in SCID mice often exhibits areas of periosteal remodeling and endochondral ossification with new bone formation.[3,4] Occasionally, severe lesions in SCID mice can develop progressive pannus in joint spaces with regional inflammation and destruction of articular cartilage and subchondral bone.[4]

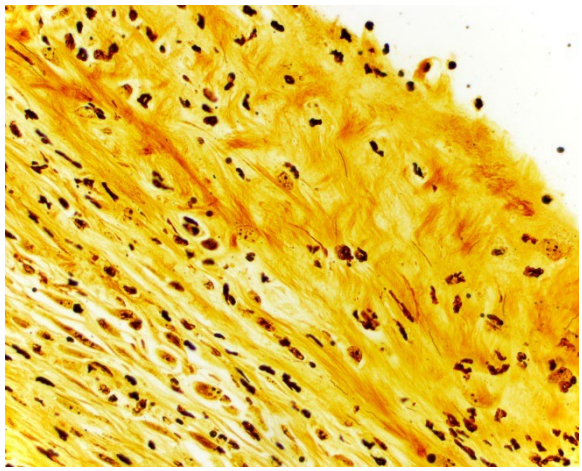

Figure 4-3. Tibiotarsal joint, mouse. Representative high magnification photomicrograph of the tibiotarsal joints from a SCID mouse in which silver impregnated spirochetes are frequently visualized in the inflamed synovium. Warthin-Starry stain. (Warthin Starry 4.0, 400X) (*Photo courtesy of:* Memorial Sloan Kettering Cancer Center, The Rockefeller University, Weill Cornell Medicine. https://www.mskcc.org/research/ski/core-facilities/comparative-medicine-pathology-0)

The use of mouse strains deficient in component of the acquired immune system have been instrumental to understand their role in host defense against *Bb* infection. Several studies have demonstrated the importance of B cell activation and immunoglobulin production in the control of *Bb* infection *in vivo*. (6, 13, 20) Mice deficient antibody production, such as $\mu MT^{-/-}$ mice (lack B cells but bear T cells) and SCID and $rag1^{-/-}$ mice (lack B and T cells) developed persistent tenosynovitis and carditis and exhibited an elevated bacterial burden in tissues. (6, 13, 20) In contrast, studies with mice lacking all T cells (TCR $\beta/\delta^{-/-}$) or only αβ TCR-expressing cells, or with mice depleted of CD4 or CD8 T

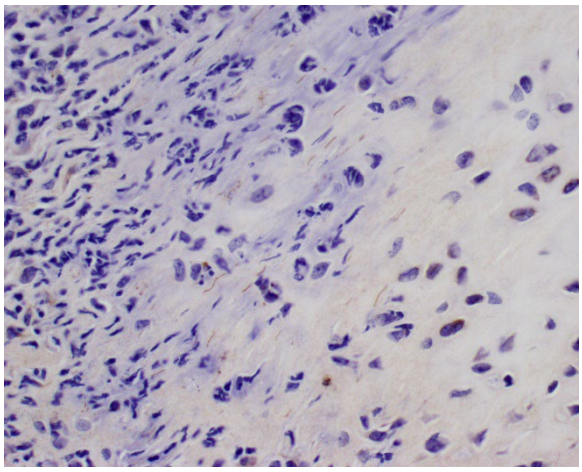

Figure 4-4. Tibiotarsal joint, mouse. Representative high magnification photomicrograph of the tibiotarsal joints from a SCID mouse in which spirochetes are detected in the inflamed synovium and periosteum. (anti-*B. burgdorferi*, 400X) (*Photo courtesy of:* Memorial Sloan Kettering Cancer Center, The Rockefeller University, Weill Cornell Medicine. https://www.mskcc.org/research/ski/core-facilities/comparative-medicine-pathology-0)

cells, have shown a minor role for T cell-deficiency during course of *Bb* infection. (20)

The signaling pathway involved for the enhanced severity of tenosynovitis in C3H mice was identified by global gene expression analysis in *Bb*-infected tibiotarsal joints. Miller et al., demonstrated that type I interferons were upregulated in the tibiotarsal joints of C3H mice at 1 week of *Bb* infection, 2-3 weeks prior the development of subacute tenosynovitis in this mouse.[14,15] The peak of type I interferons (IFN-α/β) likely occurred prior to infiltration of lymphocytes into the joints lesions of C3H mice.[14,20] The involvement of type I interferons in tenosynovitis was subsequently confirmed by either the systemic administration of a type I interferon receptor (IFNAR-1) blocking antibody or the ablation of the IFNAR1 in mice, which resulted in suppression of type 1 interferons and tenosynovitis in tibiotarsal joints of mice.[14,20] The early upregulation of IFN-responsive transcripts was absent in the joints from tenosynovitis resistant C57BL/6 mouse.[14] Instead, *Bb* infected C57BL/6 mice displayed an increased expression in genes involved in epidermal differentiation, cell adhesion, cell-cell interaction, and wound repair.[14,15] Additionally, IL10$^{-/-}$ mice on the C57BL/6 background showed several IFN-inducible transcripts were markedly upregulated in the joints at 2 weeks of infection and exhibited increased tenosynovitis severity.[18] Infected IL-10$^{-/-}$ mice also exhibited upregulation of inflammatory mediators, such as IFN-γ, CXCL9, and CXCL10 and tibiotarsal joints were infiltrated with NK cells, NKT cells, CD4^{+} T cells, and macrophages.[18]

Unlike most classical gram-negative bacterial pathogens, *Bb* does not produce LPS or toxins and lacks a specialized secretory system. Instead, the *Bb* genome encodes numerous surface lipoproteins that allow spirochetes to adapt, adhere, invade, and/or persist in tis sues.[17] These surface proteins are recognized by TLR2 receptor and induce a proinflammatory response via MyD88 signaling pathway.[8,17] In addition, CD14 is a glycosylphosphatidylinositol (GPI)-anchored membrane protein expressed on macrophages/monocytes that serves as a co-receptor for TLR2 to facilitate the activation of the innate immune response against *Bb*.[8] Previous studies have shown that the loss of either TLR2 or CD14 in mice leads to a defective innate immune response against *Bb,* and both TLR2$^{-/-}$ and CD14$^{-/-}$ mice showed an increased severity of tenosynovitis.[5,21] There are several inflammatory mediators, such as prostaglandins, leukotrienes, neutrophil recruiting chemokine (KC) among others, in which the use of targeted gene-knockout mouse strains have demonstrated their role in modulating tenosynovitis in Bb-infected mice.[6,16] In addition, classical forward ge-

netic experiments using intercross populations between C3H and B6 mice led to the identification of multiple *Bb* arthritis–associated (*Bbaa*) quantitative trait loci (QTL) on five different chromosomes of the mouse (chromosome 1, 4, 5, 11 and 12).[19]

Natural bacterial infections resulting in primary arthritis in laboratory mice are rare, but arthritis can occur as result of septicemia and/or local opportunistic bacterial infections in the joints. Septic arthritis has been described in laboratory mice infected with *Streptobacillus moniliformis* and *Corynebacterium kutscheri*.[10] Monoarticular pyogenic arthritis may occur as result of opportunistic bacterial infections due to cutaneous abrasions and lacerations infected with opportunistic bacteria.[10] Bacterial agents that can cause suppurative arthritis in laboratory mice include *Staphylococcus aureus*, Group B *Streptococcus* spp. *Rodentibacter pneumotropica*, *E. coli*, and *Klebsiella pneumoniae* spp. Experimental infections with *Mycoplasma pulmonis* can cause polyarthritis in experimentally inoculated B cell-deficient mice and SCID mice, and immunocompetent C3H/HeN mice.[10] However, arthritis is not a significant feature in natural *M. pulmonis* infections in mice.[10] *M. pulmonis* induced arthritis is characterized initially by suppurative inflammation affecting primarily the carpal and tarsal joints and associated tendon sheaths. As the process becomes chronic, lymphocytic cell infiltration and synovial hyperplasia are common histological features in the affected joints.[10]

Contributing Institution:
Laboratory of Comparative Pathology, Memorial Sloan Kettering Cancer Center, The Rockefeller University, Weill Cornell Medicine.

https://www.mskcc.org/research/ski/core-facilities/comparative-medicine-pathology-0

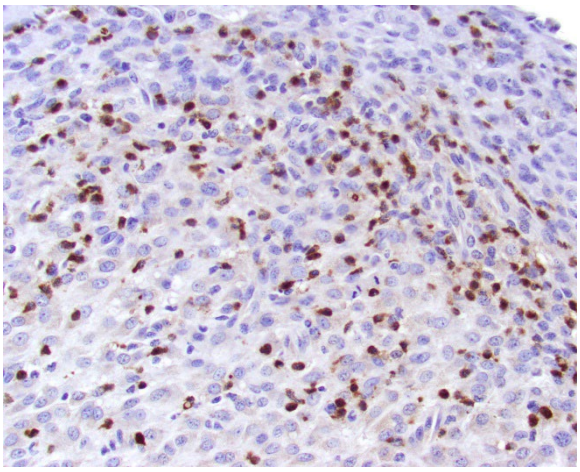

Figure 4-5. Tibiotarsal joint, mouse. Representative immunohistochemistry of the tibiotarsal joint in which moderate to large numbers of Ly6G+ neutrophils are detected in areas of synovial hyperplasia and hypertrophy. (anti-Ly6+, 400X) (*Photo courtesy of:* Memorial Sloan Kettering Cancer Center, The Rockefeller University, Weill Cornell Medicine. https://www.mskcc.org/research/ski/core-facilities/comparative-medicine-pathology-0)

JPC Diagnosis:

Tarsal joint: Tenosynovitis, proliferative and neutrophilic, chronic, diffuse, severe with focal bony lysis and periosteal new bone growth

JPC Comment:
We were excited to finally utilize this case as it has been waiting on our shelf for several years for a moderator willing to jump into the details that are so painstakingly crafted. Experimental disease cases can be difficult to read cold as JPC conference participants only get the tissue and species in advance of the conference date, and a single HE section without access to the special stains that demonstrate the presence and morphology of an infectious agent.

Many conference participants considered neoplasms such as histiocytic sarcoma and osteosarcoma as primary differentials in this case given the involvement of the cortical bone

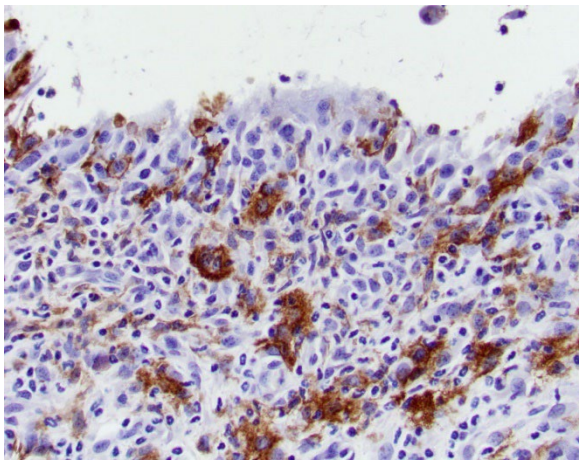

Figure 4-6. Tibiotarsal joint, mouse. Representative immunohistochemistry of the tibiotarsal joint in which moderate to large numbers of Ly6G+ neutrophils are detected in areas of synovial hyperplasia and hypertrophy. (anti-Ly6+, 400X) (*Photo courtesy of:* Memorial Sloan Kettering Cancer Center, The Rockefeller University, Weill Cornell Medicine. https://www.mskcc.org/research/ski/core-facilities/comparative-medicine-pathology-0)

and the extensor tendon. That said, the absence of mitotic figures and matrix and the presence of many neutrophils are more suggestive of granulation tissue than neoplasia. Periosteal new bone formation reflects periosteal irritation and could support either bony infection or neoplasia. Some participants considered the potential for an induced neoplasm (i.e. osteosarcoma) secondary to inflammation, though the role of *Bb* in neoplasia appears to be limited to a short description in certain human breast cancers.[22]

Conference participants also discussed "pannus" in the context of this lesion. "Pannus" describes the spread of fibrovascular or granulation tissue across multiple organs including the cornea, joint surfaces, and the endothelium. In a veterinary context, this can be confusing as chronic superficial keratitis (also referred to as "pannus") is more commonly seen in primary practice than erosive polyarthritis. Additionally, veterinary literature seldom uses the term pannus to describe thickening of the joint and/or bony/cartilaginous involvement in osteoarthritis cases. Murine tissue transplantation, particularly with SCID mice, may be one exception to this observation.[23]

References:

1. Barthold SW, Beck DS, Hansen GM, Terwilliger GA, Moody KD. Lyme borreliosis in selected strains and ages of laboratory mice. *J Infect Dis*. 1990;162: 133-138.
2. Barthold SW. Infectivity of Borrelia burgdorferi relative to route of inoculation and genotype in laboratory mice. *J Infect Dis*. 1991;163: 419-20.
3. Barthold SW, Sidman CL, Smith AL. Lyme borreliosis in genetically resistant and susceptible mice with severe combined immunodeficiency. *Am J Trop Med Hyg*. 1992;47: 605-613.
4. Barthold SW, Cadavid, D., Philipp, M. Animal Models of Borreliosis. S Samuels and J Radolph, In: *Borrelia: Molecular Biology, Host Interaction and Pathogenesis*, 1st edition, Norfolk, UK: Caister Academic Press; 2010:359-411.
5. Benhnia MR, Wroblewski D, Akhtar MN, Patel RA, Lavezzi W, Gangloff SC, Goyert SM, Caimano MJ, Radolf JD, Sellati TJ. Signaling through CD14 attenuates the inflammatory response to Borrelia burgdorferi, the agent of Lyme disease. *J Immunol*. 2005;174:1539-48.
6. Bockenstedt LK, Wooten RM, Baumgarth N. Immune Response to Borrelia: Lessons from Lyme Disease Spirochetes. *Curr Issues Mol Biol*. 2021;42: 145-190.
7. Bosma MJ, Carroll AM. The SCID mouse mutant: definition, characterization, and potential uses. *Annu Rev Immunol*. 1991; 9:323-50.
8. Cervantes JL, Hawley KL, Benjamin SJ,

Weinerman B, Luu SM, Salazar JC. Phagosomal TLR signaling upon Borrelia burgdorferi infection. *Front Cell Infect Microbiol*. 2014; 20; 4:55.
9. de Souza MS, Smith AL, Beck DS, Kim LJ, Hansen GM Jr, Barthold SW. Variant responses of mice to Borrelia burgdorferi depending on the site of intradermal inoculation. *Infect Immun*. 1993;61: 4493-7.
10. Fox J, Barthold S, Davisson M, Newcomer C, Quimby F, Smith A. Bacterial diseases. In: *The Mouse In Biomedical* Research. Vol 2, 2nd edition, San Diego, CA USA: El Sevier Inc; 2006: 325-469.
11. Franklin CL. Microbial considerations in genetically engineered mouse research. *ILAR J*. 2006; 47 :141-55.
12. Ma Y, Seiler KP, Eichwald EJ, Weis JH, Teuscher C, Weis JJ. Distinct characteristics of resistance to Borrelia burgdorferi-induced arthritis in C57BL/6N mice. *Infect Immun*. 1998;66: 161-168.
13. McKisic MD, Redmond WL, Barthold SW. Cutting edge: T cell-mediated pathology in murine Lyme borreliosis. *J Immunol*. 2000;164: 6096-6099.
14. Miller JC, Ma Y, Bian J, et al. A critical role for type I IFN in arthritis development following Borrelia burgdorferi infection of mice. *J Immunol*. 2008;181: 8492-8503.
15. Miller JC, Ma Y, Crandall H, Wang X, Weis JJ. Gene expression profiling provides insights into the pathways involved in inflammatory arthritis development: murine model of Lyme disease. *Experimental and Molecular Pathology*. 2008;85: 20-27
16. Pratt CL, Brown CR. The role of eicosanoids in experimental Lyme arthritis. *Front Cell Infect Microbiol*. 2014; 28:4:69.
17. Radolf JD, Caimano MJ, Stevenson B, Hu LT. Of ticks, mice and men: understanding the dual-host lifestyle of Lyme disease spirochaetes. *Nat Rev Micro*. 2012;10: 87-99.
18. Sonderegger FL, Ma Y, Maylor-Hagan H, et al. Localized production of IL-10 suppresses early inflammatory cell infiltration and subsequent development of IFN-gamma-mediated Lyme arthritis. *J Immunol*. 2012;188: 1381-1393.
19. Weis JJ, McCracken BA, Ma Y, et al. Identification of quantitative trait loci governing arthritis severity and humoral responses in the murine model of Lyme disease. *J Immunol*. 1999;162: 948-956
20. Weis JJ, Bockenstedt, L.K. Host Response. In: *Borrelia: Molecular Biology, Host Interaction and Pathogenesis*. 1st edition. Norfolk, UK: Caister Academic Press; 2010:413-441.
21. Wooten RM, Ma Y, Yoder RA, Brown JP, Weis JH, Zachary JF, Kirschning CJ, Weis JJ. Toll-like receptor 2 is required for innate, but not acquired, host defense to Borrelia burgdorferi. *J Immunol*. 2002; 168:348-55.
22. Gaur G, Sawant JY, Chavan AS, et al. Effect of Invasion of Borrelia burgdorferi in Normal and Neoplastic Mammary Epithelial Cells. *Antibiotics (Basel)*. 2021 Oct 24;10(11):1295.
23. Liu S. Human Xenograft Model. *Methods Mol Biol*. 2024;2766:9-15.

Joint Pathology Center
Veterinary Pathology Services

WEDNESDAY SLIDE CONFERENCE 2024-2025

Conference #22 — 29 January 2025

CASE I:

Signalment:
Young adult female wild pigeon (rock dove, *Columba livia*).

History:
The pigeon was found dead with no known history. Necropsy was performed as part of a wildlife disease screening program.

Gross Pathology:
Gross examination identified moderately thin body condition and mild pallor of the spleen.

Laboratory Results:
Immunohistochemistry for *Toxoplasma gondii* and *Sarcocystis* sp. showed strong positive immunolabeling of abundant intralesional zoites for *T. gondii* in multiple tissues (e.g., liver, lung, cloaca, brain) and no immunolabeling for *Sarcocystis* sp.

A pan-Apicomplexan PCR (18s rDNA) and sequencing of the amplicon confirmed a sequence with 100% identity to several isolates of *Toxoplasma gondii* in Genbank.

Microscopic Description:
The sections of cloaca include variable proportions of cloacal mucosa, oviduct, pericloacal skeletal muscle, subcutis, skin, and adjacent Bursa of Fabricius. There is marked, diffuse, necrotizing cloacitis and pericloacal cellulitis (panniculitis, myositis, dermatitis). Moderate numbers of inflammatory cells,

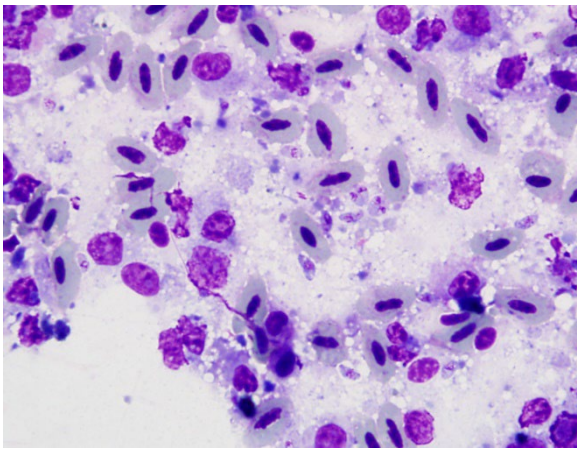

Figure 1-1. Impression smear, site unspecified, pigeon. The impression smear contains intact red blood cells, degenerate heterophils, macrophages, and free apicomplexan zoites. (*Photo courtesy of*: Wildlife Conservation Society, www.wcs.org)

abundant admixed pyknotic and karyorrhectic cell debris (necrosis), amorphous eosinophilic material (edema), and myriad protozoal zoites are present transmurally in the cloaca and throughout the pericloacal subcutis, skeletal muscle, and dermis. Inflammatory cells consist primarily of histiocytes with fewer heterophils, lymphocytes, and plasma cells. Zoites (tachyzoites) are approximately 2-3 um diameter and variably oval to crescentic (banana-shaped) with a pinpoint central nucleus and pale basophilic cytoplasm; many are individualized and extracellular, and moderate numbers are intracellular and range from individual zoites to haphazardly-arranged clustered groups (schizonts) often

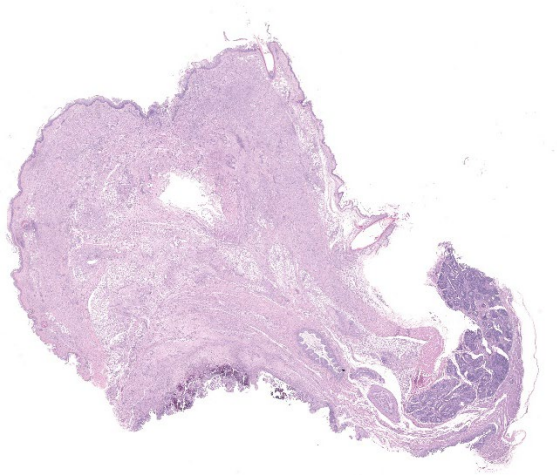

Figure 1-2. Cloaca and associated soft tissues, pigeon. A section of cloaca, associated soft tissues and bursa is submitted for examination. At subgross magnification, the cloaca (at bottom) is necrotic and the bursa (at right) is markedly atrophic and collapsed. (HE, 10X)

containing 6-16 distinct zoites. The intracellular organisms are present in endothelial cells, presumed histiocytes, fibroblasts, and myofibers. Lymphatics and blood vessels throughout the affected region are lined by hypertrophied endothelium (reactive), or are occasionally mildly thickened by intramural leukocytes or eosinophilic debris (vasculitis). The cloacal mucosa is variably moderately to markedly eroded to ulcerated, mineralized (dystrophic), and multifocally bordered by mixed bacteria along the denuded luminal surface. Skeletal myofibers are multifocally moderately fragmented, hypereosinophilic with loss of cross striations, and mineralized. The pericloacal epidermis is multifocally, variably, mildly to moderately hyperplastic, inflamed, and eroded, with intraepidermal leukocytes (heterophils, histiocytes, lymphocytes), intra- and inter-cellular swelling (edema), multifocal keratinocyte apoptosis and separation, and mild superficial dermal mineralization and pigmentary incontinence. Along the skin surface are mild segments of superficial orthokeratotic hyperkeratosis, and mild scattered loose mixed bacteria, occasional budding yeast, and debris (environmental). (A focal artefactual rent into the skin/subcutis is present in some levels).

The Bursa of Fabricius is atrophied with moderate to marked lymphocyte depletion, relative prominence of interstitial stroma, and multifocal dilated intrafollicular spaces containing basophilic fluid and occasional stippled basophilic material (mineral). Low numbers of cells (presumed histiocytes and Bursal epithelial cells) contain botryoid amphophilic intracytoplasmic inclusions (consistent with circoviral inclusions).

Contributor's Morphologic Diagnosis:
1. Cloaca and pericloacal tissue (skeletal muscle, subcutis, skin), Cloacitis and pericloacitis, necrotizing, histiocytic, diffuse, acute to subacute, moderate to marked, with abundant intralesional extra- and intra-cellular protozoal tachyzoites and schizonts, regional cloacal mucosal ulceration, multifocal vasculitis, edema, and mineralization

2. Bursa of Fabricius, Lymphoid depletion (follicle atrophy), chronic, diffuse, moderate to marked with scattered intracellular intracytoplasmic botryoid circoviral inclusions

Contributor's Comment:
Protozoal infection consistent with toxoplasmosis was initially identified by cytologic examination of organ imprints (lung, spleen, and liver) obtained during necropsy. Histologic examination confirmed disseminated protozoal infection with prominent zoite-induced necrotizing hepatitis, pneumonia, and encephalitis amongst other lesions. Infection by *Toxoplasma gondii* (toxoplasmosis) was confirmed by immunohistochemistry and PCR. The cloacal tissue section demonstrated notably florid 'cutaneous' toxoplasmosis in addition to circoviral inclusions captured

within the adjacent segment of Bursa of Fabricius, a not unexpected finding in wild pigeons and possible contributory factor for the extent of disease in this case.

Toxoplasmosis is a common obligate intracellular, apicomplexan, coccidian, protozoal infection affecting warm-blooded animals worldwide, including domestic and wild birds. Clinical toxoplasmosis has been reported in a variety of columbiformes (pigeons, doves), including individual and epizootic cases.[4] Pigeons have shown high sensitivity to natural and experimental infection with high morbidity and mortality,[3] and cases of natural infections are reported in a wide range of domestic and non-domestic pigeon species. Whereas the intermediate hosts of *T. gondii* infection are diverse, only felids are known to serve as definitive hosts for the sexual (coccidian) life stage. Major routes of intermediate and definitive host infection, respectively, are ingestion of infective oocysts, and predation of intermediate hosts by felids.

Reported clinical signs in birds include anorexia, weakness, emaciation, ocular signs (e.g., conjunctivitis, blepharitis, and exudate), dyspnea, and neurologic signs. Protozoal stages are found in many tissues, often including spleen, lung, and brain. In canaries (passeriformes) blindness has been reported as a unique but repeatable clinical presentation of natural infections, with intraocular and/or encephalitic toxoplasmosis seen histologically.[4,11]

Regardless of infected species, typical lesions of active toxoplasmosis consist of necrotizing inflammation with intralesional protozoal organisms. As in this case, the zoites and, less frequently, schizonts can be identified on cytologic tissue impression smears as individualized or clustered, extracellular or intracellular, oval to crescent-shaped pale basophilic organisms with a small nucleus and pale basophilic cytoplasm. Histology with immunohistochemistry and/or molecular testing are commonly employed for definitive diagnosis. Historically, bioassays of infected tissue homogenized and administered into mice were common.

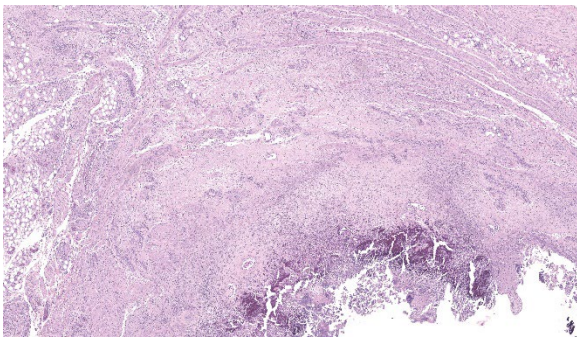

Figure 1-3. Cloaca and associated soft tissues, pigeon. Higher magnification of the necrotic cloaca and extension of inflammation and necrosis into the adjacent pericloacal soft tissues. (HE, 770X)

Another apicomplexan infection, Sarcocystosis, was considered the primarily differential diagnosis in this case, but was excluded by ancillary testing (i.e. PCR and IHC). Other differentiating features of *Toxoplasma gondii* and *Sarcocystis* sp. include: predominant forms of schizogony (endodyogeny for *T. gondii*, in which two zoites are produced, and endopolygeny for *Sarcocystis* sp., in which four or more zoites are produced and can be seen as a radial rosette arrangement); and ultrastructure (in which *Sarcocystis* sp. lack rhoptries, excretory organelles, that are present in *T. gondii*).[4] Although *Neospora caninum* is a classic differential for *T. gondii* cytologically and histologically, *N. caninum* is not known to infect birds. Systemic isosporosis (atoxoplasmosis) is another systemic coccidian infection of birds, but is morphologically distinct and was not a major differential in this case.

The heavy toxoplasmal dermatitis, panniculitis, and myositis around the cloaca in this

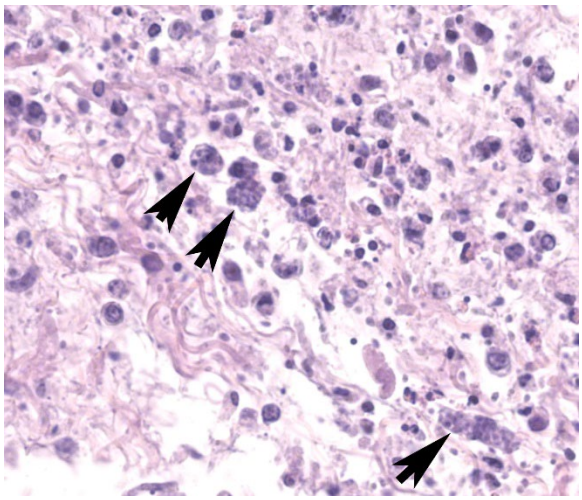

Figure 1-4. Pericloacal soft tissue, pigeon. Within the inflamed soft tissue, numerous cells (likely macrophages) contain numerous apicomplexan zoites (arrows). (HE, 457X)

case prompted a review of cutaneous toxoplasmosis which has been described in humans, few cats, and in rare cases, dogs. This infection can variably present as single localized, or up to many generalized, ulcerative, pustular, or nodular lesions, with or without pruritis. The lesions are histologically characterized by necrotizing and granulomatous or pyogranulomatous dermatitis, panniculitis, and vasculitis with extra-cellular or intra-cellular tachyzoites inhabiting a variety of cell types (e.g., macrophages, fibroblasts, glandular epithelium, and endothelium).[2,6,8] Organism numbers can vary and parasite identification is reported as histologically challenging in some cases.[6] Immunosuppression from concomitant illness and/or therapy (e.g., treatment for immune-mediate disease or transplantation) is a common predisposing factor.[6,8,10]

Basophilic botryoid cytoplasmic inclusions typical of circovirus were identified within the Bursa of Fabricius in this case. Pigeon circovirus is an incompletely described infection of young birds linked to acquired immunosuppression due to lymphocytic depletion in primary and secondary lymphoid tissues. It has been associated with propensity for a variety of secondary infections.[1,13] Circoviral infection has been linked to Young Pigeon Disease Syndrome (Young Bird Syndrome, Swollen Gut Syndrome) in racing and fancy pigeons in parts of Europe.[7] Immunosuppression was a possible contributing factor to the occurrence and severity of toxoplasmosis in this case.

Contributing Institution:
Wildlife Conservation Society

www.wcs.org

JPC Diagnosis:
1. Cloaca and pericloacal tissue (skeletal muscle, subcutis, skin): Cloacitis and pericloacitis, necrotizing, pleocellular, subacute, marked, with abundant zoites and schizonts

2. Bursa of Fabricius: Lymphoid depletion, chronic, diffuse, moderate, with cystic follicular ectasia and botryoid intracytoplasmic viral inclusions

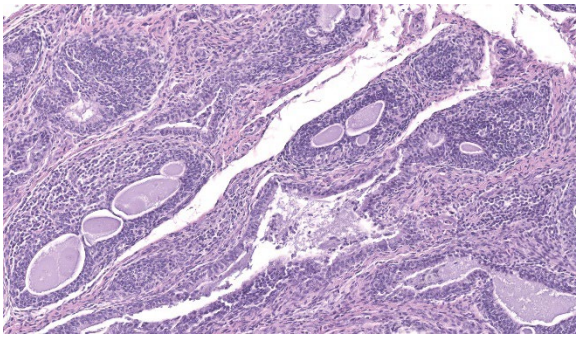

Figure 1-5. Bursa, pigeon. The bursa is markedly atrophic and depleted of B-cells. (HE, 356X)

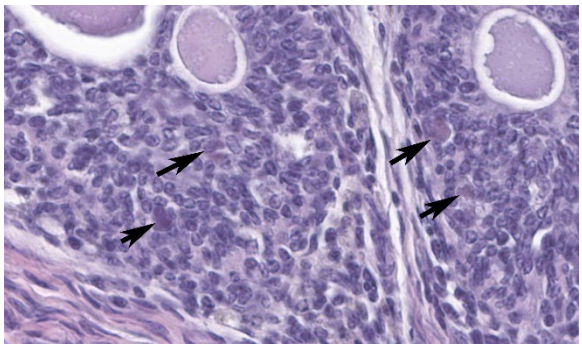

Figure 1-6. Bursa, pigeon. Macrophages adjacent to bursal follicles contain botryoid cytoplasmic inclusions (arrows). (HE 1400)

JPC Comment:
This week's moderator was Dr. Elise LaDouceur who serves as JPC's Chief of Extramural Projects and Research. Her four cases featured birds across separate classes which allowed conference participants to appreciate the role of taxonomy in formulating differential diagnoses for each case.

We thank the contributor for their submission of this neat pigeon double feature. Conference participants reviewed the anatomy of the cloaca which is composed of 3 parts – the coprodeum (continuous with the intestine), the urodeum (entry of ureters and genital ducts), and the proctodeum (terminal portion). There are two lymphoid centers within the cloaca with the larger Bursa of Fabricius overshadowing a smaller dorsal proctodeal 'lymphoglandular ridge' near the terminus proper. The section submitted represents a dorsal sagittal section that captures the bursa, dorsal proctodeum, and external portion of the vent.

We agree that the predominant slide feature was necrotizing inflammation which is characteristic of *Toxoplasma* across species and tissues. We described the cellular infiltrate as 'pleocellular' given the mixed and significant presence of histiocytes, granulocytes, lymphocytes, and plasma cells. Zoites and schizonts were generously present in section. Finding the circovirus inclusions was more difficult, particularly on the scanned slide (one benefit of reviewing glass!) – in this case they are characteristically botryoid though slightly more eosinophilic that typically seen. Dr. LaDouceur emphasized that the loss of bursal lymphocytes with concurrent prominent interstitial tissue and cystic dilatation of follicles is characteristic of lymphoid depletion, which could be caused by multiple viral infections of the bursa; however, the presence of botryoid inclusions is diagnostic for circovirus.

We conclude our case discussion with a brief review of *Isospora* and *Sarcocystis* in birds. Notably, *Isospora* (*Atoxoplasma*) most commonly infects passerine birds, not columbiform birds, such as pigeons. Histologically, it appears as coalescing nodules to sheets of histiocytes (with intracytoplasmic zoites) and lymphocytes which may be confused for lymphoma.[5,12] As the contributor mentions, *Sarcocystis* exhibits schizogony that differs from *Toxoplasma*. Tissue sarcocysts can be a helpful finding if skeletal and/or cardiac muscle is available to review. Schizogony with associated necrosis, lymphohistiocytic inflammation, and free and intracytoplasmic protozoal organisms appears similar to *Toxoplasma,* however.[7]

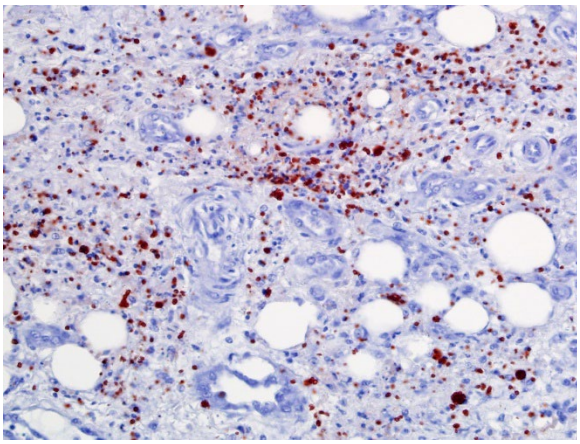

Figure 1-7. Pericloacal soft tissue, pigeon. Cytoplasmic zoites stain strongly positive for animmunomarker agains *Toxoplasma gondii*. (anti-T. gondii, 400X). (*Photo courtesy of*: Wildlife Conservation Society, www.wcs.org)

References:

1. Abadie J, Nguyen F, Groizeleau C, Amenna N, Fernandez B, Guereaud C, et al. Pigeon circovirus infection: pathological observations and suggested pathogenesis. *Avian Pathol*. 2001;30:149-158.
2. Anfray P, Bonetti C, Fabbrini F, Magnino S, Mancianti F, and Abramo F. Feline cutaneous toxoplasmosis: a case report. *Vet Dermatol*. 2005;16:131-136.
3. Biancifiori F, Rondini C, Grelloni V, and Frescura. Avian toxoplasmosis: experimental infection of chicken and pigeon. *Comp lmmun Microbiol Infect Dis*. 1986;9:337-346.
4. Dubey JP. A review of toxoplasmosis in wild birds. *Vet Parasitol*. 2002;106:121-153.
5. Flach EJ, Dodhia HS, Guthrie A, Blake DP. Systemic isosporiasis (atoxoplasmosis) in passerine birds at the Zoological Society of London, London Zoo. *J Zoo Wildl Med*. 2022 Mar;53(1):70-82.
6. Hoffmann AR, Cadieu J, Kiupel M, Lim A, Bolin SR, Mansell J. Cutaneous toxoplasmosis in two dogs. *J Vet Diag Invest*. 2012;24:636-640.
7. Mete A, Rogers KH, Wolking R, Bradway DS, Kelly T, Piazza M, Crossley B. Sarcocystis calchasi Outbreak in Feral Rock Pigeons (Columba livia) in California. *Vet Pathol*. 2019 Mar;56(2):317-321.
8. Pena HF, Moroz LR, Sozigan RKB, et al. Isolation and biological and molecular characterization of *Toxoplasma gondii* from Canine Cutaneous Toxoplasmosis in Brazil. *J Clin Microbiol*. 2014;52:4419-4420.
9. Raue R, Schmidt V, Freick M, Reinhardt B, Reimar J, Kamphausen L, et al. A disease complex associated with pigeon circovirus infection, young pigeon disease syndrome. *Avian Pathol*. 2005;34:418-425.
10. Webb JA, Keller SL, Southorn EP, et al. Cutaneous manifestations of disseminated toxoplasmosis in an immunosuppressed dog. *J Am Anim Hosp Assoc*. 2005;41:198-202.
11. Williams SM, Fulton RM, Render JW, Mansfield L, and Bouldin M. Ocular and encephalitis toxoplasmosis in canaries. *Avian Dis*. 2001;45:262-267.
12. Wong TS, Stalis IH, Witte C, Kubiski SV. Unique Isospora-associated histologic lesions in white-rumped shama (Copsychus malabaricus). *Vet Pathol*. 2022 Sep;59(5):869-872.
13. Woods LW, Latimer KS, Niagro FD, Riddell C, Crowley AM, Anderson ML, et al. A retrospective study of circovirus infection in pigeons: nine cases (1986-1993). *J Vet Diagn Invest*. 1994;6:154-164.

CASE II:

Signalment:

4-year-old, female, cockatiel (*Nymphicus hollandicus*)

History:

A 4-year-old, female cockatiel was managed by the Exotics Service over the course of one year for progressive osteolytic lesions. The patient was originally seen in the fall of 2017, for a right ulnar fracture. At that time, radiographs confirmed the ulnar fracture; in addition, mild lytic lesions were noted in multiple other bones. The animal returned in Spring of 2018. At this time, full body radiographs revealed multiple areas of bony lysis; and whole body CT confirmed wide-spread osteolysis. Her owners elected euthanasia given the poor prognosis.

Imaging:

Whole body radiographs: There are multiple radiolucent expansile lesions associated with most of the long bones, with partial destruction of the adjacent cortex. These are suspected to explain the previously observed

Figure 2-1. Whole body CT scan, cockatiel. Multiple bones exhibit a thin and moth-eaten appearance of the cortices with mild irregular expansion of the bony margins. (*Photo courtesy of: Schwarzman Animal Medical Center, Department of Anatomic Pathology. www.amcny.org*)

distal right ulna fracture, which currently appears mildly displaced, with new bone formation partially bridging it. A minimally displaced fracture of the proximal left ulna is also observed. Minimal soft-tissue swelling is associated with the punctiform lesions of the distal left metacarpophalangeal bones.

Computed tomographic images: The axial skeletal structures are normal. By contrast, multifocal lesions affect the appendicular skeleton (left proximal and distal ulna, left metacarpal bone III and proximal phalanx, right distal ulna, right metacarpal bone III and proximal phalanx, left distal femur, left distal tarsometatarsus, essentially the entire right femur, right proximal and distal tibiotarsus, right proximal and distal tarsometatarsus, questionably right pelvic limb phalanges): these are characterized by a thin and moth-eaten appearance of the cortices with mild irregular expansion of the bony margins. Irregularity of the bone margins is again present in the right distal ulna and left proximal ulna, and the site the previously described pathologic fractures. Medullary enostosis is not detected. Soft tissue swelling is minimal around these lesions.

Imaging Diagnosis:

1. Severe polyostotic aggressive osteolytic lesions of the appendicular skeleton with at least two pathological fractures

Gross Pathology:
The right femur is moderately expanded with a rough cortical surface and easily fractures with minimal manipulation. The right radius has a rough cortical surface and easily fractures with minimal manipulation. The distal aspect of the right ulna is mildly expanded with a rough cortical surface. The proximal left ulna has a rough cortical surface.

After formalin fixation and decalcification, cross sections of multiple bone reveal irregularity and thinning of the bone cortices with expansion of the medullary cavity by a soft, friable, bone tissue. The surrounding skeletal muscle and soft tissues are mottled light and dark brown.

Laboratory Results:
Touch imprint cytology, Bone, right femur, ulna, and radius: Changes varied in severity between tissue imprints and one sample is comprised of blood. There is a relative mild to moderate increase in the numbers of erythroid precursors. Touch imprints contain small to moderate numbers of osteoclasts and few macrophages.

Microscopic Description:
Long Bones (multiple sites): The medullary cavity is variably replaced and expanded by a dense inflammatory cell infiltrate, comprised

of macrophages (including epithelioid morphology) and multinucleated giant cells mixed with heterophils, necrotic cellular debris, and lesser lymphocytes and plasma cells. In some sections, this inflammatory infiltrate entirely effaces the medullary cavity. Inflammation surrounds islands of woven bone (lined by osteoblasts) or irregular, resorbing cortical bone. The cortical bone is irregular and multifocally discontinuous where it is invaded by large numbers of inflammatory cells. The endosteal surface is scalloped and are bordered by increased numbers of osteoclasts within Howship's lacunae. The bone margin is multifocally comprised of woven bone and there are multiple reversal lines. The outer cortical surface is irregular with prominent scalloping and the periosteum is predominantly expanded by a large numbers of similar inflammatory cells and small numbers of pleomorphic fibroblasts. Where present the subchondral bone is often irregular, thinned, and infiltrated by a similar inflammatory cell population and the joint capsule is variably infiltrated. The surrounding and intra-articular adipose tissue contains small hemorrhages and islands of a similar inflammatory infiltrate. Surrounding myofibers are variably degenerate and invaded by inflammation.

The overlying dermis contains small numbers of lymphocytes and plasma cells that commonly dissect between collagen fibrils. The epidermis is diffusely moderately expanded by compact orthokeratotic hyperkeratosis.

Fite-Faraco stains confirm small numbers of acid-fast positive, intrahistiocytic bacilli. In addition, the liver and small intestine have few, small granulomas.

Contributor's Morphologic Diagnosis:
Cortical bone wih joints, right and left wings and legs: Osteomyelitis, periostitis, and synovitis, granulomatous, heterophilic, chronic, multifocal to locally extensive, severe with

Figure 2-2. Long bone, cockatiel. The right femur has a roughened cortical surface (as does the right radius and left and right ulna (not shown). (*Photo courtesy of: Schwarzman Animal Medical Center, Department of Anatomic Pathology. www.amcny.org*)

few intralesional, intrahistiocytic acid-fast positive, intrahistiocytic bacilli (consistent with Mycobacterial infection), bone resorption, multifocal, severe, remodeling, mild and periosteal fibroplasia, multifocal

Skeletal muscle, right and left wings and legs:

1) Myositis, granulomatous, heterophilic, chronic, multifocal, mild to moderate
2) Myofiber degeneration, chronic, multifocal moderate with mild, multifocal myofiber regeneration and multifocal hemorrhages

Contributor's Comment:
Clinical presentation, as well as the gross and histologic findings supportive a chronic osteomyelitis with evidence of disseminated granulomatous inflammation. The presence of acid-fast positive bacilli was highly suggestive of avian mycobacteriosis, although this was not confirmed with culture or molecular testing. In birds differentials for osteomyelitis are vast and include trauma, neoplasia, lymphoproliferative disease, and infectious etiologies.[10-12] Reported neoplasms in the bones of birds include osteosarcoma,

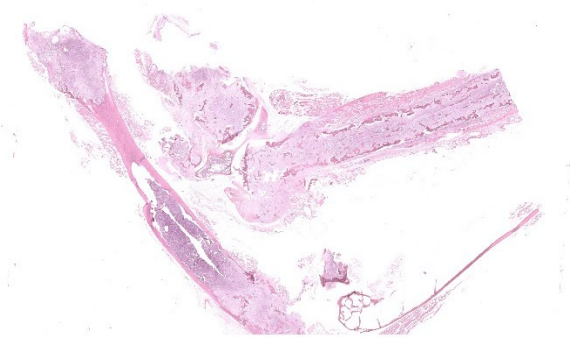

Figure 2-3. Long bone, cockatiel. Multiple long bones are submitted for examination. In each of the submitted bones, the marrow and medullary cavity is multifocally effaced by a cellular infiltrate that multifocally extends through the cortex into the adjacent soft tissue. (HE, 10X)

giant cell tumor of bone, air sac carcinoma, fibrosarcoma, and hemangiosarcoma, as well as metastatic disease.[10-12] Infectious osteomyelitis can be caused by aerobic and anaerobic bacteria (including mycobacteriosis) and fungi (e.g., aspergillosis, candidiasis cryptococcosis, and histoplasmosis).[11] In this case, the presence of few acid-fast positive, intrahistiocytic bacilli was consistent with a paucibacillary mycobacterial osteomyelitis. As in this case, skeletal mycobacteriosis commonly presents as soft tissue swelling and bone irregularity.[11] As the disease progresses, pathologic factures can occur.[11]

Mycobacterial infections are a significant cause of morbidity and mortality in numerous species, including humans.[6] This diverse group of bacteria contains organisms that range from environmental saprophytes and opportunistic pathogens to obligate pathogens.[14] Obligate pathogens include the tuberculosis group (*M. tuberculosis* and *M. bovis*) and the leprosy group (*M. lepraemurium*). Opportunistic pathogens include the saprophytes (*M. fortuitum*, *M. smegmatis*, *M. chelonae*, *M. abscessus*, and *M. thermoresistibile*) and the slow-growing (atypical)[8] organisms (*M. avium-intracellulare* complex, *M. kansasii*, and *M. ulcerans*). By convention, tuberculosis refers to infections with organisms in the tuberculosis complex, while mycobacteriosis refers to those caused by atypical or opportunistic forms.[6,15] Differentiation of mycobacterial species requires a combination of bacterial culture, biochemical tests, molecular techniques (PCR with subsequent DNA sequencing or Interferon-Gamma Release Assays (IGRAs)), and pigment production.[6,12,13]

Mycobacteria are weakly gram-positive, acid-fast positive bacilli.[1-16] Mycobacteria's lipid-rich walls make them hydrophobic, which allows them to survive in adverse environmental conditions.[10,11,14,16] In other words, it is endemic worldwide, stable in the environment, and difficult to eradicate once established.[1,4,11,16] Modes of transmission include the skin (typically at areas of skin barrier breakdown), inhalation, and ingestion.[4, 10] In birds, oral ingestion is considered the most common.[11] Infections in most species tend to be protracted and associated with a chronic wasting syndrome.[11,14-16]

Granulomatous inflammation is a distinct form of chronic inflammation, that is typically the result of a poorly degradable and persistent antigen, specific host responses (e.g., Th and macrophage responses), and the interplay of various pro- and anti-inflammatory mediators.[15] Mycobacterium species employ multiple mechanisms to ensure survival and typically do so by entering and persisting within tissue macrophages.[14,15] These include disruption of the phagosome-lysosome complex (i.e. inhibit acidification of the phagosome, phagosome-lysosome fusion), interference of cytokine synthesis and function (i.e. block injury from toxic oxygen and nitrogen intermediates), or inactivation of lysosomal enzymes.[14,15] In general mycobacterial species can suppress the ability of macrophages to be activated by cytokines, especially IFN-

gamma.[15] Complement receptors on tissue macrophages (e.g., mannose and CD14 receptors) are the major receptors responsible for mycobacterial phagocytosis.[15] Other receptors (e.g., integrin receptors, TLRs, Ig Fc receptors, CD14 receptors, scavenger receptors, etc.) are involved in the early recognition and cell signaling in response to the bacteria, which eventually leads to antimicrobial chemokine, cytokine, and metabolite synthesis.[15] Mycobacteria highjack these pathways and attenuate macrophage activation in response to IFN-gamma.[15] *Mycobacterium avium*, in particular, has a unique cell wall that prevents fusion of the phagosome to the lysosome, effectively down-regulating the killing mechanisms of macrophages.[12,15] A similar mechanism is described in *Mycobacterium tuberculosis*.[15] Migration of infected macrophages allow for discrimination of infection.[14] These infections are characterized by a strong cell mediated response, where macrophage recruitment and proliferation accelerates under the influence of cytokines produced by T-lymphocytes.[14,15] The chronic presentation of these cases and resulting tissue destruction are due to a combination of organism persistence and cell-mediated response and other host responses.[12,15]

The type of pathology and clinical disease depends on the infecting mycobacterial species, host's immune response, host's genetic susceptibility, dose of infection, mode of transmission, and infection stage.[11] Infection is typified by granulomatous inflammation.[1-16] This can manifest as diffuse visceral enlargement and/or discrete granulomas, which correlate to infiltration by a pleocellular, macrophage heavy inflammatory infiltrate.[1-15] Affected macrophages can have a large amount of amphophilic cytoplasm with a fine cytoplasmic granularity but acid-fast stains are required for confirmation of intracellular bacilli.[11] The number of bacteria can vary considerable and ranges from paucibacillary

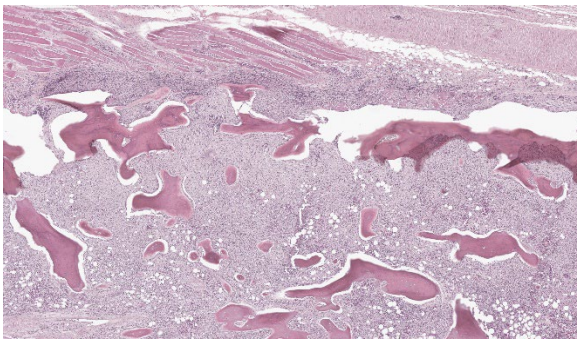

Figure 2-4. Long bone, cockatiel. The cellular infiltrate effaces bone marrow, results in lysis of hematopoetic and cortical bone, and extends into the adjacent skeletal muscle. (HE, 88X)

to abundant/florid.[11,12,15] There are two main pathologic forms of mycobacterial infection: a tubercle and lepromatous form.[11,15] The tubercle form is a Th1-biased immune response and is characterized by granuloma formation with a region of central necrosis surrounded by inflammation.[11,15] Meanwhile, the lepromatous form is a Th-2-biased immune response and is characterized by diffuse inflammation without necrosis.[11,15]

Mycobacteriosis is common in various bird species, including domestic fowl, as well as pet and exotic birds and wildlife.[12] Although all species are susceptible, captive waterfowl, collection birds, tropical and ring-necked doves, Amazon parrots, brotogerids, pionus parrots, finches, and canaries are commonly reported.[11] The disease can have severe economic impact and is associated with high levels of mortality and morbidity and reduction in egg production.[16] In one recent studying in backyard chickens, 42% of birds died from bacterial disease.[3] In this report *E. coli* and *Mycoplasma gallisepticum* or *M. synoviae* were the most common, but mycobacteriosis was reported in 6 cases.[3] Oral route appears to be the primary means of infection in birds, with lesions typically involving the gastrointestinal tract and/or liver.[11,12] Airborne and cutaneous infections can be seen to a lesser

degree.[12] *Mycobacterium avium-intracellulare* complex organism infect the intestine and due to a lack of lymph nodes, the infection subsequently disseminates easily.[12] Therefore, infection is typified by a chronic, disseminated granulomatous disease in semimature to mature birds, although localized disease can occur (i.e. dermal or intestinal mycobacteriosis).[11,12] Gallinaceous birds typically develop discrete granulomas, while psittacine and passerine species tend to develop the lepromatous form.[12] The two most common mycobacterial species to affect birds are *Mycobacterium avium-intracellulare* complex and *Mycobacterium genavense*.[9,10,11,12,16] Other reported species include *Mycobacterium tuberculosis, M. bovis, M. gordonae, M. nonchromogenicum, M. fortuitum, M. peregrinum, M. intermedium, M. celatum, M. africanum, M. simiae, M. arupense, M.* URHd0023*,* and *M. vulneris*, in addition to others.[9,12] The lesions created by these species are indistinguishable from one another and co-infection can occur; thus definitive diagnosis requires culture and/or molecular testing.[9,16]

Avian bacterial osteomyelitis can be caused by a number of ubiquitous and opportunistic bacteria, including *Mycobacterium* spp., *Staphylococcus aureus*, *E. coli*, *Salmonella* spp., *Pasteurella multocida*, *Streptococcus* spp., *Enterococcus* spp., *Pseudomonas* spp., and *Aeromonas* spp.[1] Mycobacteriosis in birds commonly involves the bone, and in one report 93% of avian mycobacteriosis cases had bone lesions.[1, 11] Infection is clinically characterized by osteolysis (as in this case), sclerosis, or bone cysts that are most commonly located in the metaphysis of long bones, ribs, and/or sternum with or without pathologic fractures.[1,12] Bacterial toxins and localized ischemia can lead to bone necrosis with sequestra formation.[1] Histologic findings include severe myeloid hyperplasia and granulomatous inflammation with eventual

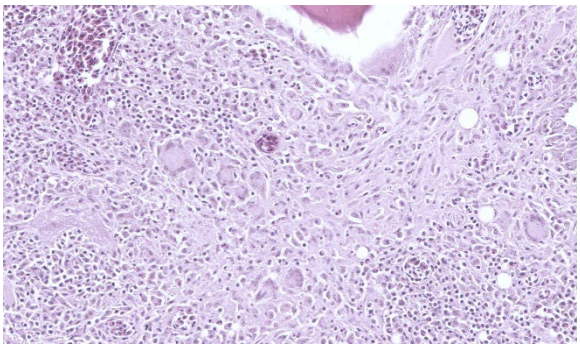

Figure 2-5. Long bone, cockatiel. The mixed cellular infiltrate is predominantly composed of epithelioid macrophages, and fewer Langhans and foreign body type giant cell macrophages, heterophils, lymphocytes and plasma cells. (HE, 556X)

bone marrow effacement and extension into the surrounding bone and soft tissues.[11, 12] Avian granulomas associated with mycobacteriosis tend not to mineralize.[1,11,12]

Mycobacterium avium-intracellulare complex organisms can cause sporadic, opportunistic disease in numerous species and is typically associated with immunosuppression.[14] Other important Mycobacteria of this complex include *M. avium paratuberculosis* (Johne's disease), *M. avium silvaticum* (wood pigeon mycobacterium), *M. avium hominissuis* (pig and human infection), and *M. intracellulare*.[10,14,16] Other important mycobacterial species in veterinary medicine include *M. tuberculosis* (human and elephants), *M. bovis* (domestic and wild animals, humans), *M. microti* (small rodents, hyraxes, llamas, pigs, and ferrets), *M. africanum* (rare in humans, cattle, and pigs), and *M. marinum, M. chelonae, M. xenopi*, and *M. liflandii* (reptile and amphibian species).[6,7,8,15] The clustering of infections in Bassett hounds, Miniature Schnauzer, Siamese cats, Somali cats, and Abyssinian cats suggest a genetic predisposition.[4,8] The cause for this predisposition is unclear but may be related to a cell-mediated immunodeficiency in either T-cells or macrophages.[4] Failure to regrow hair is a unique

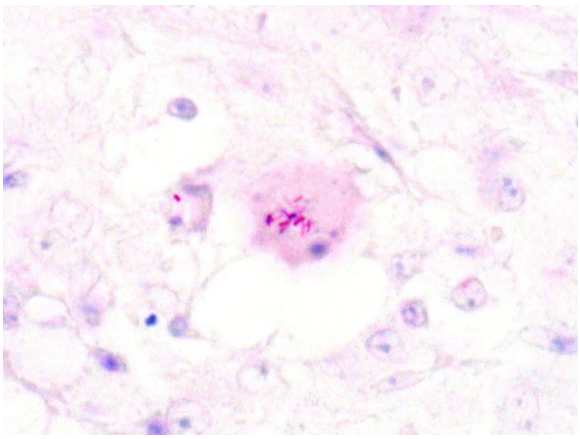

Figure 2-6. Long bone, cockatiel. Rare epithelioid macrophages contain acid-fast bacilli within their cytoplasm. (Fite-Furaco, 400X). (*Photo courtesy of: Schwarzman Animal Medical Center, Department of Anatomic Pathology. www.amcny.org*)

presentation in Abyssinian cats.[8] Important veterinary mycobacterial disease include Bovine cutaneous opportunistic mycobacteriosis (caused by atypical mycobacterial species), feline leprosy (*M. lepraemurium, M. visibilis*, and others), ulcerative dermatitis in marsupials (*M. ulcerans*), bovine tuberculosis (*M. bovis*), feline ocular mycobacteriosis (*M. bovis, M. microti, M tuberculosis, M avium-intracellulare* complex), and Johne's disease (*M. avium paratuberculosis*).[6,8,10,13,14,15] The two most common etiologic diagnoses in weedy and leafy seadragons is mycobacteriosis and scuticociliatosis, where mycobacterial infection is associated with chronic erosive and proliferative skin lesions that typically involve the snout.[2] Dissemination can occur and typically involves the liver, kidney, heart, gill, and skin.[2] The cause of canine leproid granuloma syndrome is unknown but mycobacterial infection is suspected given the presence of acid-fast bacilli in lesions.[15] Most mycobacterial infections require treatment with long course antibiotics and/or surgical excision of affected tissues.[13]

Contributing Institution:
Animal Medical Center, 510 East 62nd St.
New York, NY 10065.
http://www.amcny.org

JPC Diagnosis:
1. Hematopoietic bones and surrounding soft tissue: Osteomyelitis, synovitis, myositis, and cellulitis, granulomatous, chronic, multifocal, severe with infractions

2. Bone marrow: Granulocytic hyperplasia, chronic, diffuse, severe

JPC Comment:
The contributor provides an outstanding summary of avian mycobacteriosis to accompany an interesting case presentation. The polyostotic nature of the lesion led some to consider neoplasia or metabolic bone disease for this case. Dr. LaDouceur noted that metabolic disease such as fibrous osteodystrophy may affect multiple bones, but more importantly is not an inflammatory lesion (inflammation was abundant in this case) and would not be expected to extend into the surrounding soft tissue. Similarly, a multifocal distribution would be unusual for a primary bony neoplasia, although neoplasia is a rule out for osteolytic lesions. Metastatic carcinomas and air sac carcinomas have also been reported in the bone of birds,[17] though these are morphologically distinct from the mixed inflammatory cell population seen here.

There are a number of ancillary changes that should not be missed in this case. Although the bony changes are impressive, there are numerous small, non-displaced fractures (infractions) and degenerative changes to the joint. The adjacent joints have fibrovascular membranes that span the articular surface (pannus) that accompany villonodular proliferation of the synovium and loss of glycosaminoglycans. The hyperplastic bone marrow with marked expansion of myeloid precursors

is a common concurrent change in mycobacteriosis – we estimated a myeloid:erythroid ratio of at least 4:1 where as a normal is 0.4:1 (i.e. 10x times expanded in this case). Other rule outs for extreme myeloid hyperplasia include *Aspergillus* sp. (see Case 4 of this conference) and avian chlamydia. Additionally, we emphasize "hematopoietic bone" in our morphologic diagnosis as there is a good example of a pneumatized (and unaffected) bone on this slide as well.

References:

1. Baum RM and Hanley C. What Is Your Diagnosis. JAVMA. 2016; 248(1):51-53.
2. Bonar CJ, Garner MM, Weber ES, Keller CJ, Murray M, Adams LM, Frasca S Jr. Pathologic Findings in Weedy (*Phyllopteryx taeniolatus*) and Leafy (*Phycodurus eques*) Seadragons. *Veterinary Pathology*. 2013; 50(3) 368-376.
3. Cadmus KJ, Mete A, Harris M, et al. Causes of mortality in backyard poultry in eight states in the United States. *JVDI*. 2019; 31(3):318–326.
4. Campora L, Corazza M, Zullino C, Ebani VV, Abramo F. *Mycobacterium avium* subspecies *hominissuis* disseminated infection in a Basset Hound dog. *JVDI*. 2011; 23(5):1083–1087.
5. Chen H, Zhu D, Wang M, et al. Comparative Immunology, Microbiology and Infectious Diseases Amyloid A amyloidosis secondary to avian tuberculosis in naturally infected domestic pekin ducks (*Anas platyrhynchosdomestica*). *Comparative Immunology, Microbiology and Infectious Diseases*. 2019; 63:136–141
6. Fowler ME and Miller RE. *Zoo and Wild Animal Medicine: Current Therapy*. 6th eds. Saunders Elsevier. St Louise. 2008.
7. Fremond-Rahl JJ, Ek C, Williamson HR, Small PLC, Fox, JG, Muthupalani S. *Mycobacterium liflandii* outbreak in a Research Colony of *Xenopus* (Silurana) *tropicalis* Frogs. *Veterinary Pathology*. 2011. 48(4) 856-867.
8. Maxie M. Jubb, *Kennedy & Palmer's Pathology of Domestic Animals*. 6th eds. Saunders Elsevier. 2015.
9. Pfieffer W, Braun J, Burchell J, Witte CL, Rideout BA (2017) Whole-genome analysis of mycobacteria from birds at the San Diego Zoo. *PLoS ONE* 12(3): e0173464.
10. Quinn PJ, Markey BK, Carter ME, Donnelly WJ, Leonard FC. *Veterinary Microbiology and Microbial Disease*. Blackwell. Ames Iowa. 2006.
11. Sánchez FD, Yela IJ, Alfonseca E, Campuzano J, Morales E, Aguilar C. Respiratory tract infection caused by *Mycobacterium bovis* in a black swan (*Cygnusatratus*). *Avian Pathology*. 2016; 45(1):126-131.
12. Schmidt RE, Reavill DR, Phalen DN. *Pathology of Pet and Aviary Birds*. 2nd eds. Wiley Blackwell. Ames Iowa. 2015.
13. Shivaprasad HL and Palmieri C. Pathology of Mycobacteriosis in Birds. *Vet Clin Exot Anim*. 2012; 15:41–55.
14. Stavinohova R, O'Halloran C, Newton JR, Oliver JAC, Scurrell E, Gunn-Moore DA. Feline Ocular Mycobacteriosis: Clinical Presentation, Histopathological Features, and Outcome. *Veterinary Pathology*. 2019; 1-12.
15. Zachary JF and McGavin MD. *Pathologic Basis of Veterinary Disease*. 5th eds. Elsevier Mosby. St Louis. 2012.
16. Zhu L, Peng Y, Ye J, Wang T, Bian Z, Qin Y, Zhang H and Ding J. Isolation, Identification, and Characterization of a New Highly Pathogenic Field Isolate of *Mycobacterium avium* spp. *avium*. *Front. Vet. Sci*. 2018; 4:243.
17. Loukopoulos P, Okuni JB, Micco T, Garcia JP, Uzal FA, Diab SS. Air sac adenocarcinoma of the sternum in a Quaker parrot (Myiopsitta monachus). *J Zoo Wildl Med*. 2014 Dec;45(4):961-5.

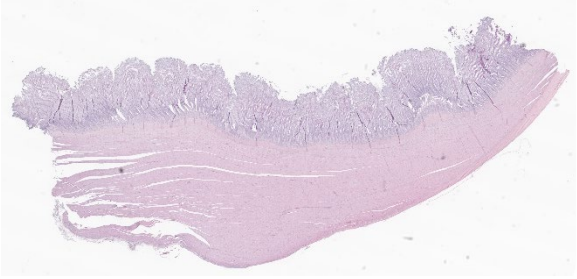

Figure 3-1. Ventriculus, tinamou. One section of ventriculus is submitted for examination. (HE, 7X)

CASE III:

Signalment:
13-year-old male elegant crested tinamou (*Eudromia elegans.*

History:
This elegant crested tinamou (*Eudromia elegans*) was housed in a zoological collection, and was euthanized due to marked weight loss and declining clinical condition. He had a history of chronic articular gout of the right third digit and mild lateral deviation of the rhinotheca resulting in malocclusion ("scissor beak").

Gross Pathology:
Gross examination confirmed beak malocclusion and a focal swelling over the proximal aspect of the right third digit that exuded white chalky to pasty material from cut surfaces. The animal was in thin body condition, with scant subcutaneous and intracavitary adipose tissue stores. The crop was moderately distended with fresh vegetables, the proventriculus was empty, and the ventriculus was filled with vegetable ingesta, small pebbles, and a small amount of green, pasty material. The intestines and ceca contained a small amount of green-brown, pasty digesta.

Laboratory Results:
Cytologic evaluation of liver, spleen, and lung impression smears was unremarkable.

Microscopic Description:
Ventriculus: Throughout the section, the koilin layer is diffusely, superficially disrupted and separated by a dense mat of elongate yeasts. The yeasts are approximately 2-3 micrometers wide and 20-40 micrometers long. They aggregate in haphazard orientations on the surface, and also stream into ventricular glands in roughly parallel-oriented, 'logjam-like' arrangements, rarely reaching the deepest portions of the glands. The lamina propria contains a scant infiltrate of granulocytes and rare lymphocytes that rarely extends into the mucosal epithelium. Small, subepithelial pools of eosinophilic to amphophilic, smudgy, acellular material are scattered throughout the lamina propria. Small-caliber blood vessels in the mucosa and tunica muscularis are multifocally surrounded by low numbers of mononuclear cells. Arterioles throughout the tunica muscularis and subtending the serosal surface are variably expanded by smudgy, eosinophilic, acellular material that partially or wholly obscures normal cellular detail in the arteriolar walls.

Contributor's Morphologic Diagnosis:
Ventriculus: Ventriculitis, heterophilic and lymphocytic, chronic, multifocal, mild, with superficial koilin disruption and myriad surface-associated yeasts

Ventriculus: Amyloidosis, arteriolar and subepithelial, chronic, multifocal, mild to moderate

Contributor's Comment:
Histopathology in this elegant crested tinamou revealed florid superficial colonization of the mucosal surface of the proventricular-ventricular isthmus and ventricular koilin by elongate yeasts. The morphology and tissue distribution of the yeasts are characteristic of *Macrorhabdus ornithogaster*. Arteriolar and

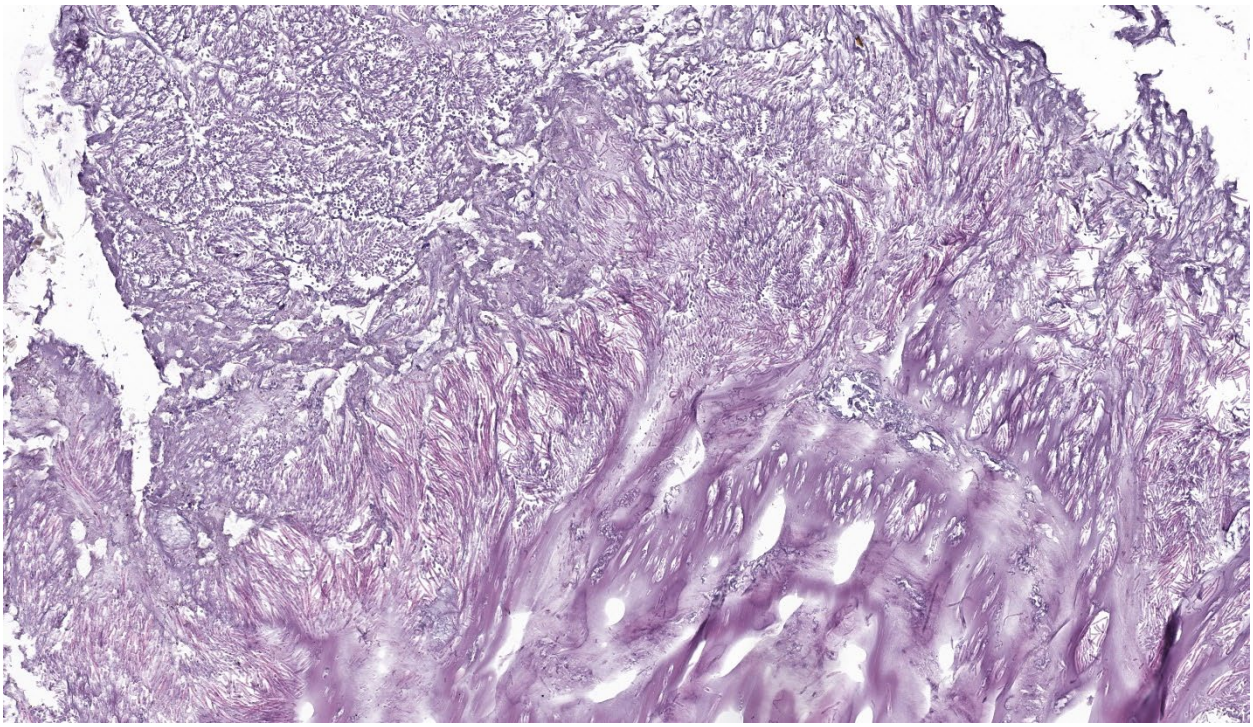

Figure 3-2. Ventriculus, tinamou. Within the superficial 2/3 of the koilin layer, there are numerous 1x2um wide, elongate filamentous yeast. (HE, 234X)

subepithelial amyloid deposition, while relatively mild in sections of the gastrointestinal tract, were manifestations of multi-organ amyloidosis that was considered to be the most important factor in this bird's clinical decline.

Macrorhabdiosis, or 'avian gastric yeast' infection, is a well-recognized condition in various avian species. The causative organism, *Macrorhabdus ornithogaster*, was famously misinterpreted to be a large bacterium ("megabacteria") after its discovery but is now recognized as an ascomycetous yeast.[9] The yeasts have a distinctive elongate morphology, measuring approximately 2-3 micrometers wide and 20-40 micrometers long, and are often arranged in densely packed clusters or streams, sometimes referred to as 'haystack,' 'matchstick,' or 'logjam' arrangements.[7,9] Infections occur at the mucosal surface of the proventricular-ventricular isthmus, with organisms sometimes penetrating into isthmus glands and extending into the koilin layer of the ventriculus. Organisms can be detected in cytologic preparations of feces or scrapings from the isthmus. Although staining characteristics can be variable, they are typically gram-positive and stain dark blue with rapid Romanowsky stains (e.g., Diff-Quik).[4] In histologic sections, the yeasts are eosinophilic and often readily identifiable with routine hematoxylin and eosin staining. They also stain positively with silver stains and Periodic acid-Schiff (PAS) stain.

Gross lesions can include emaciation, excessive proventricular mucus production, and mucosal erosions or ulcerations with hemorrhage. Histologic examination reveals variable associated inflammation and goblet cell hyperplasia in addition to the characteristic organisms. In the ventriculus, colonization can be associated with marked disruption and attenuation of the koilin layer, with variable

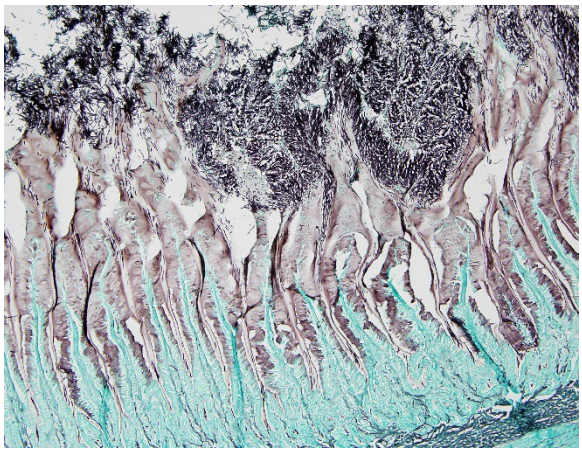

Figure 3-3. Ventriculus, tinamou. A silver stain demonstrates the morphology of these elongate yeasts. (GMS, 400X) (*Photo courtesy of:* Wildlife Conservation Society, Zoological Health Program; https://oneworldonehealth.wcs.org, www.wcs.org)

inflammation. An association with proventricular adenocarcinoma in budgerigars (*Melopsittacus undulates*) has been proposed, but the mechanism of this association is not well understood.[5]

Macrorhabdiosis can be subclinical or can be associated with a chronic, progressive, and fatal wasting syndrome.[7] Clinically significant or fatal disease associated with *Macrorhabdus ornithogaster* infection is most often diagnosed in psittacine, passerine, and gallinaceous species, but has also been reported in paleognaths such as ostriches and rheas.[1,2,3,6,8,10] While not, to our knowledge, previously reported in tinamous (also paleognaths), macrorhabdiosis has been diagnosed in one previous case from our zoological collection.

In some cases, an underlying stressor may be needed to trigger the development of clinically significant disease.[6,7] Yeasts were abundant in multiple sections of the orad ventriculus from this case, but no clear indications of chronicity, such as chronic inflammation or goblet cell hyperplasia, were observed. We suspect that the yeast overgrowth may have occurred in a relatively short period prior to death, potentially as a consequence of debilitation due to underlying disease. This tinamou's clinical decline was attributed primarily to multi-organ amyloidosis involving the liver, spleen, kidneys, myocardium, and arteries in multiple tissues, confirmed by Congo red staining of selected tissues. While suspected to be a sequela of chronic inflammation, a specific inciting cause for amyloidosis was not determined. The contribution of macrorhabdiosis to this tinamou's clinical decline is unclear.

Contributing Institution:
Wildlife Conservation Society, Zoological Health Program

https://oneworldonehealth.wcs.org

www.wcs.org

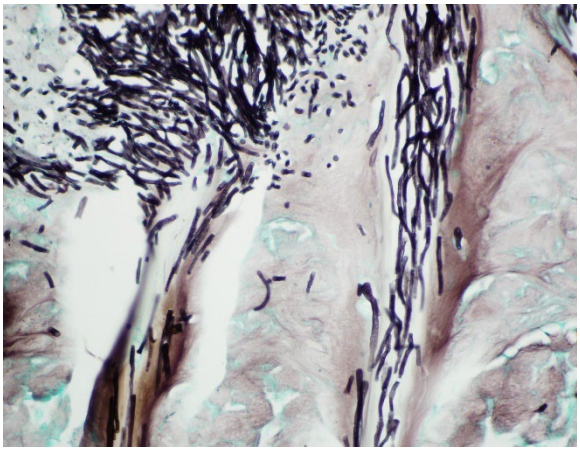

Figure 3-4. Ventriculus, tinamou. A higher magnification of the silver stain demonstrating the morphology of these elongate yeasts. (GMS, 1000X) (*Photo courtesy of:* Wildlife Conservation Society, Zoological Health Program; https://oneworldonehealth.wcs.org, www.wcs.org)

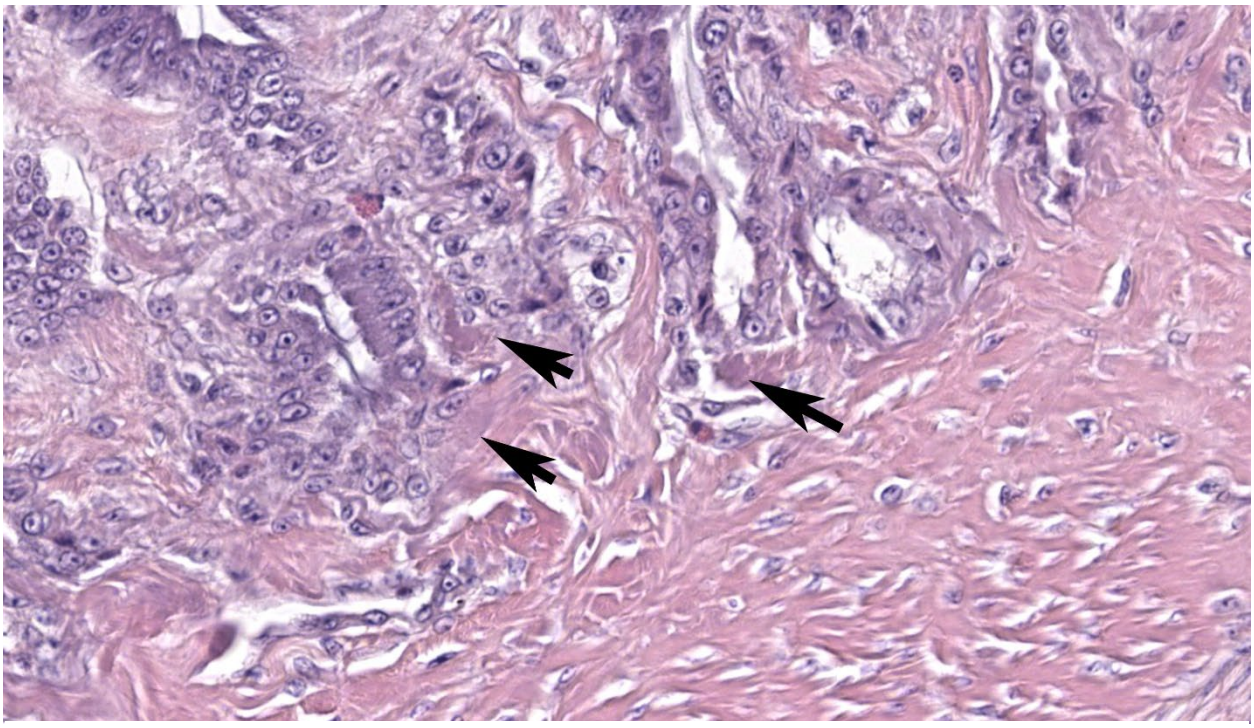

Figure 3-5. Ventriculus, tinamou. Small aggregates of amyloid are present within subepithelial areas in the lamina propria (arrows). (HE, 979X)

JPC Diagnosis:
1. Ventriculus: Koilin loss, diffuse, severe with myriad elongate yeast and mild granulocytic ventriculitis

2. Ventriculus (lamina propria and blood vessels): Amyloidosis, chronic, multifocal, mild

3. Adipose tissue: Atrophy, subacute, diffuse, mild

JPC Comment:
Case 3 offers a synopsis of classic avian lesions. We differ slightly from the contributor in identifying the primary lesion as koilin loss (which was substantial) though we agree that there is mild inflammation of the ventriculus. We added an additional morphologic diagnosis for the atrophy of fat (best observed at the serosal surface) as adipocytes are small with variably sized lipid vacuoles. Amyloid deposition in this case is subtle and easily overlooked on H&E. On this slide, amyloid is most discernable within sagittal sections of larger vessels and multifocally within the lamina propria as lightly eosinophilic to amphophilic material. In birds, common locations for amyloid deposition include the kidney (glomerulus and basement membrane), the liver (within the space of Disse), and the spleen. While we searched for a urate tophus (i.e. gout) to connect back to the clinical picture outlined by the contributor, we were unable to make this case a 'four-fer'.

The long sagittal sections of peripheral nerves (likely a nerve plexus) prompted a short group discussion. In a vacuum, this might resemble ganglioneuritis (i.e. avian bornavirus). As Dr. Ladouceur noted, avian nervous tissue is highly cellular and satellite cells could be confused for infiltrating T-lymphocytes. Once again, considering avian type is helpful as avian bornavirus affects psittacine birds (and rarely passerines) and

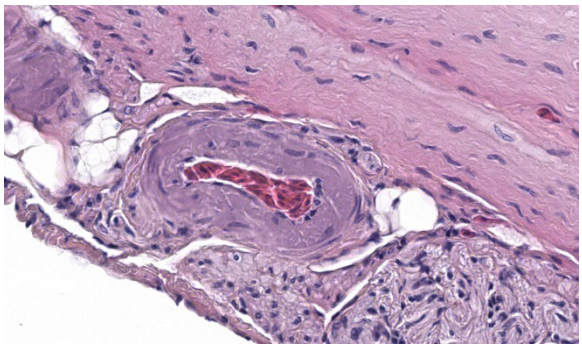

Figure 3-6. Ventriculus, tinamou. The walls of arterioles are also expanded by amyloid. (HE, 1090X)

not tinamiforms such as this tinamou. If this were a psittacine, CD3 IHC can be useful in differentiating satellite cells from infiltrating T lymphocytes in cases of suspected avian bornavirus. Screening HE sections for plasma cells is also useful (none were noted in the nerves in this case).

References:

1. Crespo R, França MS, Fenton H, Shivaprasad HL. Galliformes and Columbiformes. In: Terio KA, McAloose D, St. Leger J, eds. *Pathology of Wildlife and Zoo Animals*. Cambridge, MA: Elsevier; 2018: 747–73.
2. Huchzermeyer FW, Henton MM, Keffen RH. High mortality associated with megabacteriosis of proventriculus and gizzard in ostrich chicks. *Vet Rec*. 1993; 133: 143-144.
3. Martins NRS, Horta AC, Siqueira AM, Lopes SQ, Resende JS, et al. Macrorhabdus ornithogaster in ostrich, rhea, canary, zebra finch, free range chicken, turkey, guinea-fowl, columbina pigeon, toucan, chuckar partridge and experimental infection in chicken, japanese quail and mice. *Arq. Bras. Med. Vet. Zootec*. 2006; 58(3): 291-298.
4. Phalen DN. Update on the diagnosis and management of *Macrorhabdus ornithogaster* (formerly Megabacteria) in avian patients). *Vet Clin Exot Anim*. 2014; 17: 203-210.
5. Powers LV, Mitchell MA, Garner, MM. *Macrorhabdus ornithogaster* Infection and Spontaneous Proventricular Adenocarcinoma in Budgerigars (*Melopsittacus undulates*). *Vet Pathol.* 2019; 56(3): 486-493.
6. Reavill DR, Dorrestein G. Psittacines, Coliiformes, Musophagiformes, Cuculiformes. In: Terio KA, McAloose D, St. Leger J, eds. *Pathology of Wildlife and Zoo Animals*. Cambridge, MA: Elsevier; 2018: 775-798.
7. Schmidt RE, Reavill DR, Phalen DN. Gastrointestinal System and Pancreas. In: Schmidt RE, Reavill DR, Phalen DN. eds. *Pathology of Pet and Aviary Birds*, Second Edition. Iowa State Press. Ames, Iowa. 2015: 65, 70, 81.
8. Smith DA. Palaeognathae: Apterygiformes, Casuariiformes, Rheiformes, Struthioniformes; Tinamiformes. In: Terio KA, McAloose D, St. Leger J, eds. *Pathology of Wildlife and Zoo Animals*. Cambridge, MA: Elsevier; 2018: 633-648.
9. Tomaszewski EK, Logan KS, Snowden KF, et al. 2003. Phylogenetic analysis identifies the “megabacterium” of birds as a novel anamorphic ascomycetous yeast, *Macrorhabdus ornithogaster* nov., sp. nov. *Int J Syst Evol Microbiol.* 2003; 53(4):1201–1205.
10. Trupkiewicz J, Garner MM, Juan-Sallés C. Passeriformes, Caprimulgiformes, Coraciiformes, Piciformes, Bucerotiformes, and Apodiformes. In: Terio KA, McAloose D, St. Leger J, eds. *Pathology of Wildlife and Zoo Animals*. Cambridge, MA: Elsevier; 2018: 799-823.

CASE IV:

Signalment:
12-year-old, male, blue fronted Amazon parrot (*Amazona aestiva*).

History:
Two-week history of not acting right. One week history of acute

decline, weight loss, ataxia, increased respiratory effort/rate and loss of deep pain over 24 hours. Radiographs revealed evidence of airsacculitis, and bloodwork showed severe heterophilia. The patient's condition deteriorated despite antibiotic administration. Euthanasia was elected.

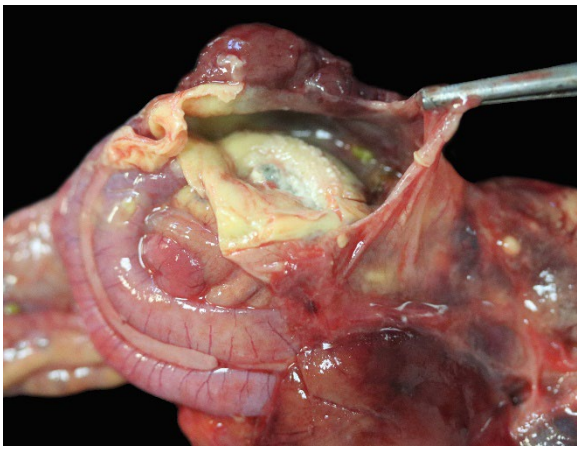

Figure 4-1. Airsac, Amazon parrot. There is yellow exudate within the airsac. (*Photo courtesy of: Schwarzman Animal Medical Center, Department of Anatomic Pathology. www.amcny.org*)

Gross Pathology:
The right and left abdominal air sacs are severely thickened and tan to yellow, with shaggy, irregular projections (airsacculitis). The coelomic cavity contains small amounts (approximately 1 mL) of tan to yellow effusion. Focal regions of yellow to tan thickening are noted over the body wall in the regions of the right and left femur. The right lung is mottled dark red, light red and pale tan. A 0.5 cm diameter, firm, tan nodule is present in the middle section of the lung lobe. Samples from this lobe sink in formalin. The left lung is also mottled light and dark red to brown and has a focal, 0.3 cm diameter tan nodule (presumed granulomatous heterophilic pneumonia). A firm region in the middle section of the lung lobe is observed. Sections from this lobe float in formalin.

The spinal cord is removed in situ, is fixed, decalcified and sectioned. In the lumbar spine, there is a focal, white, firm nodule in the bone. This nodule overlies and is just caudal to the glycogen body of the spinal cord.

Laboratory Results:
CBC: Hematocrit 38 (range 39-54%), WBC 56.5 K/µL (range 5-15 K/µL), Heterophils 44 K/µL (range 1.5-11 K/µL), Heterophil bands 5.1 K/µL (0 K/µL), Lymphocytes 2.3 K/µL (range 1-10 K/µL), Monocytes 5.1 K/µL (range 0-0.4 K/µL), Eosinophils 0 K/µL (range 0-0.3 K/µL), Basophils 0 K/µL (range 0-0.4 K/µL), thrombocytes adequate, polychromasia slight, no parasites seen.

Microscopic Description:
A section of lumbosacral vertebral column and spinal cord are examined. Within the bone of the lumbar vertebral column, a densely cellular region of inflammation is present. The cellular infiltrate comprises predominantly heterophils including degenerate heterophils and fewer macrophages, lymphocytes and plasma cells. Multinucleate giant cells and epithelioid macrophages are occasionally observed, with formation of heterophilic granulomas. Inflammatory populations result in lysis of adjacent bone, with irregular, scalloped margins of attenuated vertebral bone. Additional foci of inflammation are multifocally distributed throughout the vertebral bone

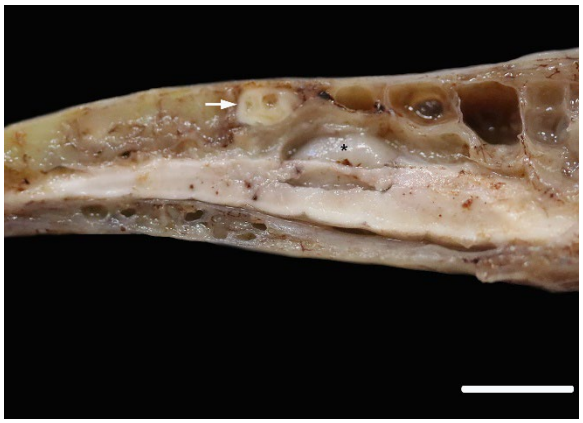

Figure 4-2. Synsacrum, Amazon parrot. There is a firm white nodule in the vertebral body dorsal to the glycogen body. (*Photo courtesy of: Schwarzman Animal Medical Center, Department of Anatomic Pathology. www.amcny.org*)

within the section. The marrow and pneumatized cavities contain lightly eosinophilic fluid (edema). The inflammation extends to the spinal cord, with heterophils and macrophages infiltrating through the meninges and into the spinal cord parenchyma. In these regions, the spinal cord exhibits myelin vacuolation with regional gliosis including Gitter cells. Axons are enlarged and homogeneously eosinophilic (spheroids). Inflammatory cells are intermixed with fungal hyphae. Hyphae occasionally surround and infiltrate vessel walls, which contain inflammatory populations, hyaline, eosinophilic, acellular material (fibrinoid change) and are surrounded by wispy, loosely arranged, eosinophilic material (edema). Fungal hyphae have parallel walls with infrequent septations, range from approximately 3 to 6 µm in width, and demonstrate acute angle, dichotomous branching, highlighted with a Gomori's methenamine silver (GMS) stain. Heterophilic, histiocytic inflammation and fungal hyphae are observed at the periphery of and minimally infiltrating into the glycogen body, which also contains small foci of hemorrhage.

Contributor's Morphologic Diagnosis:
Lumbosacral spine and spinal cord: Osteomyelitis and myelitis, heterophilic,granulomatous, lymphoplasmacytic with myriad fungal hyphae, regional myelin vacuolation with gliosis and spheroid formation, vasculitis with fibrinoid degeneration and edema.

Abdominal airsacs (not included on slide): Airsacculitis, severe, necrotizing, heterophilic, granulomatous with myriad fungal hyphae and conidiophores (morphology consistent with *Aspergillus* spp.).

Contributor's Comment:
This psittacine bird had a disseminated fungal infection, involving multiple organ systems including the lungs, air sacs, vertebral column, spinal cord, skeletal muscles, coelomic cavity, kidneys, liver, intestines, adrenal glands and thyroid glands. The most severely affected organ system was the respiratory system. Myriad fungal hyphae were present within foci of inflammation. These hyphae contained the morphologic features of

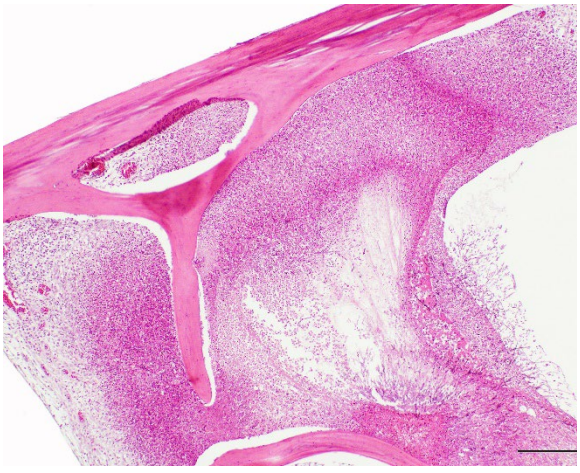

Figure 4-3. Synsacrum, Amazon parrot. There is a large focus of heterophilic inflammation within the vertebral body. Fungal hyphae extend from the inflammation at right. (HE, 200X) (*Photo courtesy of: Schwarzman Animal Medical Center, Department of Anatomic Pathology. www.amcny.org*)

Aspergillus species, including narrow width (3-6 µm), parallel walls with septation, dichotomous, acute angle branching and a tendency to be oriented in the same direction.[2,4]

In some locations, conidiophores were observed. Distinctive conidiophores (asexual fruiting bodies) occur on surfaces or cavities exposed to air, such as the air sacs.[2,7] Conidiophores consist of a stalk protruding from a mycelial foot cell, with a terminal globose, hemispherical or flask shaped vesicle. Peg-like phialides (formerly sterigmata) arise from the vesicle and may be directly connected and arranged in a single layer (uniseriate) or connected by supporting cells (metulae) and arranged in a double layer (biseriate).[2,7] Unbranched chains of conidia are formed from the distal ends of the phialides.[2,7] The conidiophores in this case appeared to be uniseriate, which is a feature of the *Aspergillus fumigatus* group, however, definitive diagnosis requires ancillary testing, as there is overlap in histomorphologic features of *Aspergillus* conidiophore morphology (see below).

A sequel to the fungal infection in this case was osteomyelitis of the lumbosacral spine with extension to the spinal cord. Frequent sites of secondary involvement in birds include the coelomic cavity, central nervous system (CNS), liver, intestines, kidney, pneumonic bone, adrenal glands and vertebral column.[8] In the submitted case, osteomyelitis was most severe in the lumbosacral portion of the spine (in the region of the corpus gelatinosum or glycogen body), but inflammation was also found in the thoracic and cervical segments. Inflammation of the lumbar vertebral column led to osteomyelitis and regional myelitis, with involvement of the glycogen body. Inflammation of the glycogen body is of uncertain significance in the context of the clinical signs. The glycogen body (corpus gelatinosum) is an ovoid, circumventricular, gelatinous structure of unknown function embedded in the lumbosacral region of the spinal cord, occupying the rhomboid sinus.[5] The corpus gelatinosum is dorsal to the spinal cord and the ventral portion encloses the central canal. Peripheral and central cellular zones have been described. Cells of this structure contain abundant, pale, vacuolated cytoplasm and peripheralized nuclei. These glycogen containing cells are hypothesized to arise from specialized, modified glial cells (astrocytes).[5] Although the function is unknown, hypotheses include an energy source for the central nervous system (CNS), transmission of hydrostatic pressure changes during movement, roles in neuron metabolism, and myelin formation.[5] Extension of the fungal infection from the abdominal airsacs to the skeletal muscle of the proximal limbs also likely contributed to the ataxia noted in the history.

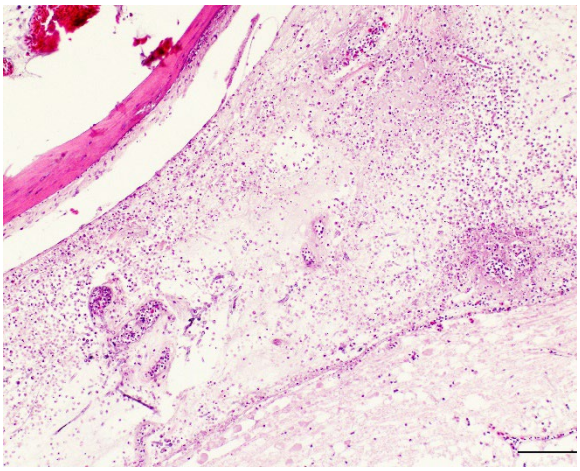

Figure 4-4. Spinal cord, Amazon parrot. Inflammation extends into the spinal cord; there are fungal hyphae and necrotic vessels at right (HE, 200X) (*Photo courtesy of: Schwarzman Animal Medical Center, Department of Anatomic Pathology. www.amcny.org*)

Aspergillosis is a non-contagious fungal disease that affects captive and wild birds.[1,3] The fungus is ubiquitous, opportunistic and saprophytic, and exposure to large

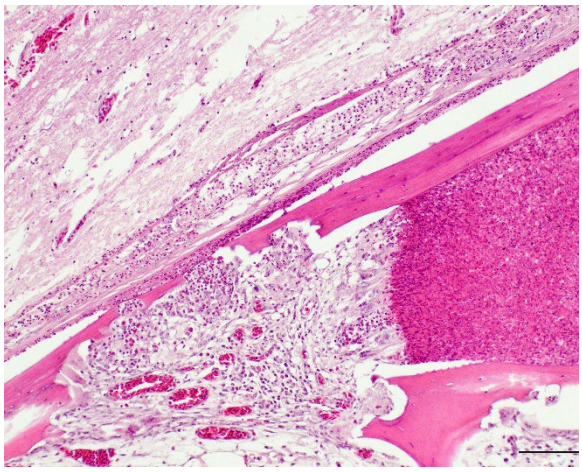

Figure 4-5. Spinal cord, Amazon parrot. Fungal hyphae are 3-4um wide, have parallel walls, sepatations, and acute angle dichotomous branching. (HE, 400X) (*Photo courtesy of: Schwarzman Animal Medical Center, Department of Anatomic Pathology. www.amcny.org*)

numbers of fungal spores can result in infection. In birds, aspergillosis is most commonly caused by *Aspergillus fumigatus*, and less commonly *Aspergillus niger*, *Aspergillus flavus*, *Aspergillus nidulans, Aspergillus glaucus, Aspergillus oryzae* and others.[1,3,7–9] A recent report detailed a case of *Aspergillus pseudoviridinutans* (a cryptic species of *Aspergillus* within section *Fumigati*) causing rhinitis in an orange winged Amazon parrot.[6] Some avian species are thought to be predisposed including *Amazona* sp., *Psittacus erithacus*, *Pionus* sp., as well as species that originate from arid environments.[6,9] Other predisposing factors include increased concentrations of environmental spores, a warm environment, improper humidity, poor ventilation, poor sanitation, and long-term storage of feed. Impaired immunity can also predispose to development of Aspergillosis, and has been reported with steroid administration, metabolic bone disease, inadequate diet, overcrowding, shipping, starvation, thermal discomfort, infections, toxins and trauma, among others.[1,3,6,8,9]

The main route of infection is thought to be inhalation. As the spores of *Aspergillus fumigatus* are smaller than spores of other *Aspergillus* spp, some may reach the lungs and air sacs.[1,6] Similar to this case, the air sacs are a common site of primary infection (inhaled air reaches caudal thoracic and abdominal air sacs before the pulmonary epithelial surfaces).[1] Leukocytosis is a common clinical feature, and is often severe (20,000 to more than 100,000 white blood cells per microliter) with a left shift, monocytosis and lymphopenia. Leukocytosis in this case was 56.5 K/µL, with heterophilia, a left shift, and monocytosis. Serological tests for aspergillus have been developed, however, false negative results can occur.[1] Serum protein electrophoresis may reflect an acute phase response, often observed with aspergillosis, which includes increased globulins with reduced albumin, increases in alpha 2 globulins and increased serum amyloid A levels.[3]

Gross lesions are variable, but generally comprise granulomas of the lungs and air sacs. In acute infections, miliary granulomas may be distributed throughout the respiratory tract.[1,8,9] White to yellow plaques (scutulae) may be seen within the respiratory tract or over serosal surfaces. Air sacs are often thickened and may contain caseous exudate or visible mycelial formation.[8,9] Nodules within the lungs may have caseous, consolidated or necrotic centers. Histologically, large numbers of degenerate heterophils are typically present, accompanied by necrosis, multinucleated giant cells, epithelioid macrophages, and variable numbers of fungal organisms.[8,9] In aerated organs, aggregates of radiating hyphae (the sunburst pattern) frequently occur.[1,2] If the infection is not eliminated in the respiratory tract, disseminated infection can occur, both by direct extension through the air sac wall and hematogenous spread.[1] More information is needed regarding virulence factors of avian aspergillosis.

Figure 4-6. Spinal cord, Amazon parrot. A silver stain demonstrates the morphology of the hyphae. (GMS, 400X) (*Photo courtesy of: Schwarzman Animal Medical Center, Department of Anatomic Pathology. www.amcny.org*)

Conidia of *Aspergillus fumigatus* may be resistant to respiratory macrophage-induced killing.[1] Invasion of blood vessels is a frequently reported sequel,[1,2] and was observed in this case.

Deposition of calcium oxalate crystals in association with *Aspergillus* spp has been documented in domestic animals and humans.[2,7] *Aspergillus* spp synthesize oxalic acid as a product of the tricarboxylic acid cycle, resulting in precipitation of calcium oxalate crystals, which may cause tissue damage.[7] The crystals are needle-like and may have wheatsheaf or rosette arrangements, are clear to pale yellow and strongly birefringent under polarized light.[2,7] In one study, cases of avian aspergillosis with oxalate crystal formation occurred commonly in respiratory tissues that interfaced with air (nasal sinus, trachea, syrinx, lung, air sac).[7] Sparse or colorless crystals can be difficult to identify without routine polarization. In the aforementioned study, calcium oxalate crystals were found in 11 of 16 avian cases after retrospective review, however, few were identified on the initial report.[7] Thus, routine polarization of slides in cases with *Aspergillus* infections in respiratory tissues is recommended.[7]

Definitive diagnosis of aspergillosis in birds is based on fungal identification and documentation of fungal organisms within the associated lesions. Hyphal morphology of *Aspergillus* is similar to that of other fungi in the hyalohyphomycosis group. Some studies found that hyphae morphologically consistent with *Aspergillus* spp were identified as other genera with culture or PCR.[4] The presence of conidiophores allows definitive diagnosis of the genus *Aspergillus*, however, there is substantial overlap in the morphologic features of the conidiophores of different Aspergillus species, including seriation, phialides arrangement and pigmentation.[7] Thus, conidia morphology cannot be relied upon for speciation of *Aspergillus*.[2,7] Fungal culture from clinical samples is considered to be the gold standard for fungal identification, however, the time frame for these cultures is often long. Additional options include use of mo-

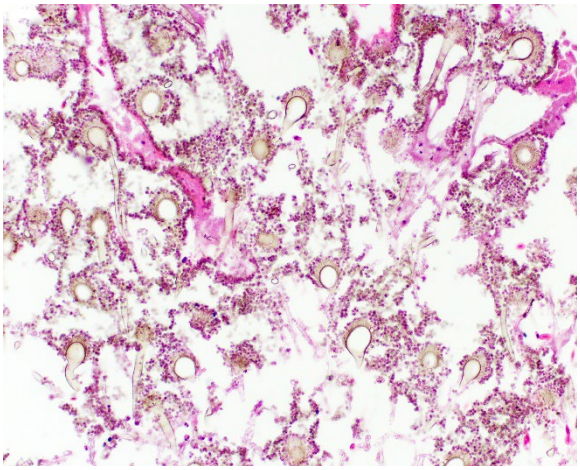

Figure 4-7. Abdominal air sacs, Amazon parrot. Conidia are present within the abdominal air sacs. (HE, 1000X) (*Photo courtesy of: Schwarzman Animal Medical Center, Department of Anatomic Pathology. www.amcny.org*)

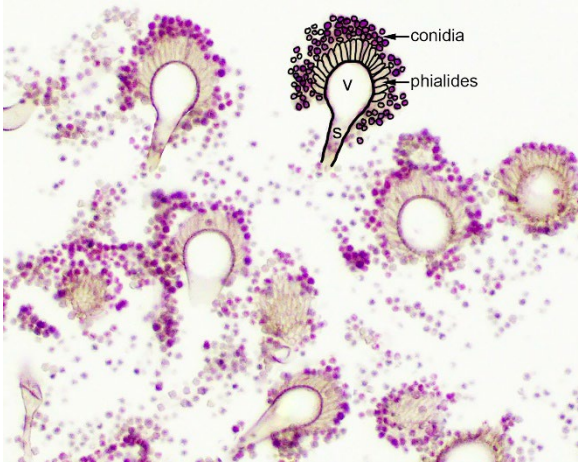

Figure 4-8. Abdominal air sacs, Amazon parrot. Diagram of diagnostic features of fungal conidia. (HE, 1000X) (*Photo courtesy of: Schwarzman Animal Medical Center, Department of Anatomic Pathology. www.amcny.org*)

lecular assays, immunohistochemistry and in-situ hybridization from formalin fixed, paraffin-embedded (FFPE) tissues and cytology slides. PCR using primers that target and amplify conserved portions of the fungal genome (internal transcribed spacers and the 5.8S rRNA gene) followed by sequencing is another potential method of identification.[3,4,6] High quality fungal DNA was able to be obtained from FFPE tissues in 70% of cases in one study, which correlated with the histological identification in 62% of cases. Matrix-assisted laser desorption ionization time-of-flight mass spectrometry (MALDI-TOF MS) is an additional potentially useful tool, however, is currently only available for some *Aspergillus fumigatus* related species.[6] Given the presence of conidiophores, additional ancillary tests for speciation were not requested in this case.

Contributing Institution:
www.amcny.org

JPC Diagnosis:
Synsacrum, lumbosacral spinal cord: Osteitis and meningomyelitis, heterophilic, necrotizing, acute, multifocal, severe with vasculitis and fungal hyphae

JPC Comment:
The contributor provides an excellent summary of the case along with many helpful figures. The framing of the entire synsacrum and glycogen body on the slide that mirrors the gross image is simply a bonus for us.

We approached our morphologic diagnosis slightly differently and emphasized (meningo)myelitis and osteitis separately. In contrast to Case 2, the bone in this section is pneumatic and lacks marrow elements. As osteomyelitis best describes inflammation of the osseus medulla (including the marrow), we made this distinction. In our review of the slides we did not observe oxalate crystals, though this may reflect a lack of free calcium to utilize in the TCA cycle (e.g. from adjacent hemorrhage and cell loss).

We covered *Aspergillus* in the guttural pouch of a horse this year in Conference 1, Case 3. Both cases feature vascular lesions, though the degree of infarction and secondary changes are much more pronounced in that horse than in this parrot. This likely reflects the route of entry via extension of the air sac versus direct hematogenous entry.

Conference participants should have been able to recognize this histologic section as "pelvis" or "synsacrum" based on either of two histologic features: the presence of the glycogen body, which is located in the lumbosacral spinal cord, or the fusion of the vertebral bodies, which represents the synsacrum.

References:

1. Beernaert LA, Pasmans F, Waeyenberghe

LV, Haesebrouck F, Martel A. Aspergillus infections in birds: a review. *Avian Pathol*. 2010;39(5):325–331.
2. Chandler FW, Kaplan W, Ajello L. *A colour atlas and textbook of the histopathology of mycotic diseases.* Wolfe Medical Publications Ltd.
3. Hauck R, Cray C, França M. Spotlight on avian pathology: aspergillosis. *Avian Pathol*. 2020;49(2):115–118.
4. Hoffmann AR, Ramos MG, Walker RT, Stranahan LW. Hyphae, pseudohyphae, yeasts, spherules, spores, and more: A review on the morphology and pathology of fungal and oomycete infections in the skin of domestic animals. *Vet Pathol*. 2023;60(6):812–828.
5. L E. Structural Insights of the Glycogen Body in Domestic Chicken. *J Cytol Histol*. 2016;2016(01).
6. Langlois I, Barrs VR, Dufresne PJ. Rhinitis due to Aspergillus pseudoviridinutans in an orange-winged Amazon parrot (Amazona amazonica). *Méd Mycol Case Rep*. 2020;30:46–50.
7. Payne CL, Dark MJ, Conway JA, Farina LL. A retrospective study of the prevalence of calcium oxalate crystals in veterinary Aspergillus cases. *J Vet Diagn Investig*. 2017;29(1):51–58.
8. Reavill DR, Dorrestein G. Psittacines, coliiformes, musophagiformes, cuculiformes. In: *Pathology of wildlife and zoo animals*. Elsevier 775–798.
9. Schmidt RE, Struthers JD, Phalen DN. *Pathology of pet and aviary birds*. John Wiley & Sons.

Joint Pathology Center
Veterinary Pathology Services

WEDNESDAY SLIDE CONFERENCE 2024-2025

Conference #19 — 29 January 2025

CASE I:

Signalment:
22 year old, female, Green anaconda (*Eunectes murinus*)

History:
This snake was humanely euthanized due to a persistent Ophidiomyces infection with clinical signs (not specified), despite over 6 months of treatment with terbinafine.

Gross Pathology:
Necropsy was performed by the clinicians, and formalin-fixed tissues were sent to our laboratory for histopathologic exam. The clinicians reported multifocal areas of brown discoloration on the ventral scales. Corneas were reported to be cloudy. There were multifocal yellow nodules in the lungs**.**

Laboratory Results:
Antemortem skin swab submitted to the Illinois Veterinary Diagnostic Laboratory was positive via qPCR for Ophidiomyces

Postmortem, panfungal PCR at the University of Florida did not detect Ophidiomyces in paraffin-embedded lung tissue.

Microscopic Description:
Randomly distributed in the lungs are multifocal to coalescing nodules composed of central areas of amorphous, eosinophilic to occasionally mineralized, necrotic debris. This central necrotic material is surrounded by moderate to high numbers of macrophages, with lymphocytes and plasma cells present at the periphery. In some granulomas, fungal hyphae that are 2-3 um wide, with parallel walls, septa, and occasional acute angle branching, stain positive with Grocott methenamine silver (GMS) and periodic-acid-Schiff (PAS) stains.

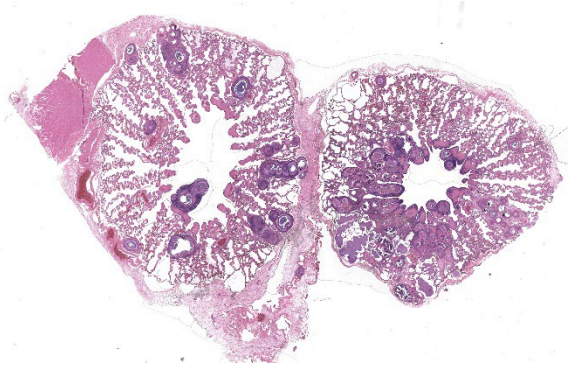

Figure 1-1. Lung, green anaconda. Scattered throughout the lung, there are numerous granulomas expanding the faveolar septa. (HE, 10X)

Contributor's Morphologic Diagnosis:
Lungs: Multifocal granulomatous pneumonia with fungi

Contributor's Comment:
This case highlights a granulomatous pneumonia caused by a fungus with histologic features consistent with *Ophidiomyces ophiodiicola*. The fungal infection is presumed to have originated from the dermal *Ophidiomyces ophiodiicola* infection detected antemortem via qPCR in dermal lesions found on this captive, green anaconda.

Figure 1-2. Lung, green anaconda. Coalescing granulomas expand the alveolar septa (HE, 111X)

Ophidiomyces ophiodiicola is the causative agent of "snake fungal disease". First described in eastern massasauga rattlesnakes in Illinois, USA, in 2011, it was originally characterized as an emerging infectious disease.[1,2] It has since been described in the eastern to mid-western United States, Canada, Europe, and in Australia.[2,3,4,5] However, recent reviews suggest that *O. ophiodiicola* may be a common, endemic disease that was previously uncharacterized, rather than an emerging infectious agent.[2,6] Retrospective testing found the earliest confirmed infection to be 1986, and there does not appear to be an increase over the last decade in the prevalence of *O. ophiodiicola* or change in its distribution, at least in North America.[2]

Originally classified within the chrysosporium anamorph of Nannizziopsis vriesii complex, it was initially unclear if *O. ophiodiicola* was a primary or opportunistic pathogen.[7] Later experimental infections of corn snakes with *O. ophiodiicola* confirmed a casual link between *O. ophiodiicola* and lesions consistent with those seen in wild snakes with snake fungal disease. In addition, they found that variation of described clinical signs in the literature may be explained by the stage of infection.[7] Increased frequency of molting, anorexia, and abnormal behaviors such as resting in conspicuous areas were also observed.[7]

The clinical presentation can vary, but typically, *O. ophiodiicola* produces a fungal dermatitis characterized by early superficial dermatitis and scale loss, and severe and chronic infections can result in extensive ulceration, facial swelling and disfiguration.[1,3,8] Histologically, lesions range from heterophilic to necrotizing epidermitis, with or without granulomatous dermatitis, granulomatous pneumonia, granulomatous endophthalmitis, and subcutaneous/intramuscular granulomas.[6] Systemic infections have been described.[9]

In addition to histopathology and histochemical stains, fungal culture and PCR are recommended for definitive diagnosis.[3] In this case antemortem dermal swabs were positive for *Ophidiomyces ophiodiicola* via qPCR. Postmortem panfungal PCR of paraffin-embedded lung tissue did not detect *Ophidiomyces ophiodiicola,* but did detect *Malassezia sp*, a presumed contaminant, given histologic features of the fungus. Given the antemortem qPCR positive, and histologic features, a presumptive diagnosis of granulomatous pneumonia due to *Ophidiomyces ophiodiicola* was made. It is likely that prolonged formalin fixation interfered with amplification of *Ophidiomyces ophiodiicola* in this case.

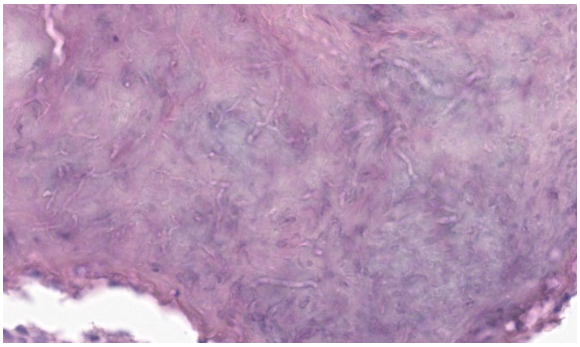

Figure 1-3. Lung, green anaconda. The outline of septate fungal hyphae may be seen within the central coagulum in several of the granulomas. (HE, 1336X)

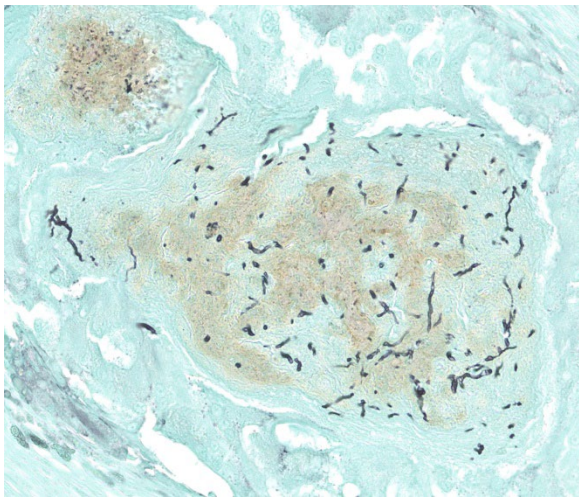

Figure 1-4. Lung, green anaconda. A GMS stain highlights the morphology of the fungal hyphae. (GMS, 637X)

Contributing Institution:
https://nmdeptag.nmsu.edu/labs/veterinary-diagnostic-services.html

JPC Diagnosis:
Lung: Pneumonia, granulomatous, chronic, multifocal, moderate, with fungal hyphae.

JPC Comment:
This week's moderator was Dr. Lauren Peiffer of Smithsonian's National Zoo and Conservation Biology Institute who explored bird and reptile cases with conference participants. This first case in a green anaconda is a rare look at a snake lung with marked ancillary changes to accompany prominent granulomas. The faveolar septa are expanded either by fibrosis and/or smooth muscle hyperplasia and contain hemosiderin-laden macrophages which reinforce the chronicity of the overall process. Fungal elements are apparent in select granulomas on H&E, but their mophology is better appreciated with GMS and PAS stains. In particular, PAS(with malachite green counterstain) was helpful for detailing septation and contour of hyphae which was consistent with *Ophidiomyces ophiodiicola*.

Dr. Peiffer discussed differentials for lung granulomas in snakes with mycobacteriosis being an important rule out. We performed modified Gram stains (Brown-Brenn, Brown-Hopps) and acid-fast stains (Fite-Faraco, Ziehl-Neelsen) which identified gram-positive bacilli with some granulomas that were highlighted with Fite-Faraco, but not Ziehl-Neelsen. These findings are consistent with *Mycobacterium* sp. and concurrent infectious agents are a common finding in granulomatous inflammation. Multiple species of mycobacteria have been reported in snakes, including *M. marinum*, *M. haemophilum*, *M. kansasii*, *M. chelonae*, and *M. leprae*.[10]

We agree with the contributor that the finding of *Malassezia* on the panfungal PCR is probably spurious and second the notion to compare the results of ancillary diagnostics in assessing their validity. *Malassezia restricta* is a common contaminant and in this case may have been preserved within the paraffin block or sampled from the operator or lab environment itself. The lack of recovery of *Ophidiomyces ophiodiicola* may reflect degradation of DNA in formalin – given the large number of hyphae present in section, we do not believe that prolonged antifungal therapy was probably not a factor.

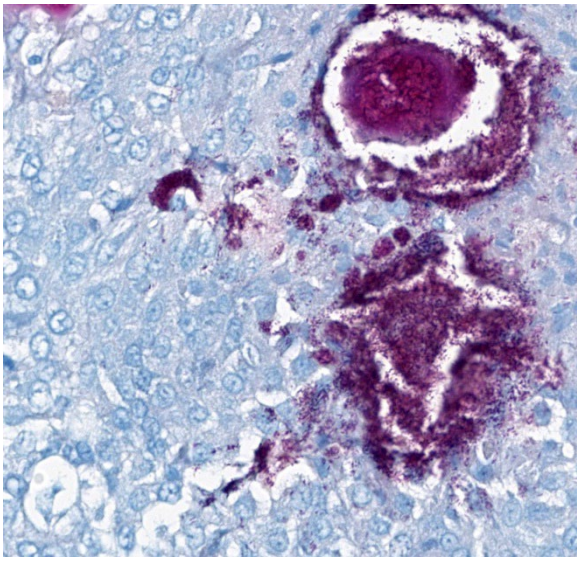

Figure 1-5. Lung, green anaconda. Some granulomas contain acid-fast bacilli. (Fite-Faraco, 858X)

References:

1. Allender MC, Dreslik M, Wylie S, Phillips C, Wylie DB, Maddox C, Delaney MA, Kinsel MJ. Chrysosporium sp. infection in eastern massasauga rattlesnakes. *Emerg Infect Dis*. 2011 Dec;17(12):2383-4.
2. Davy CM, Shirose L, Campbell D, Dillon R, McKenzie C, Nemeth N, et al. Revisiting Ophidiomycosis (Snake Fungal Disease) After a Decade of Targeted Research. *Front Vet Sci.* 2021; 8: 665805.
3. Ossiboff R. In: Pathology of Wildlife and Zoo Animals. Terio K, McAloose D, St. Leger J, eds. London, Academic Press, 2018: 912-914.
4. Franklinos LHV, Lorch JM, Bohuski E, Rodriguez-Ramos Fernandez J, Wright ON, Fitzpatrick L, Petrovan S, Durrant C, Linton C, Baláž et al. Emerging fungal pathogen Ophidiomyces ophiodiicola in wild European snakes. *Sci Rep.* 2017 Jun 19;7(1):3844
5. Sigler L, Hambleton S, Paré JA. Molecular characterization of reptile pathogens currently known as members of the chrysosporium anamorph of Nannizziopsis vriesii complex and relationship with some human-associated isolates. *J Clin Microbiol*. 2013 Oct;51(10):3338-57.
6. Anderson KB, Steeil JC, Neiffer DL, et al. Retrospective review of Ophidiomycosis (Ophidiomyces ophidiicola) at the Smithsonian's National Zoological Park (1983-2017). *Journal of Zoo and Wildlife Medicine.* 52(3), 997-1002
7. Lorch JM, Lankton J, Werner K, Falendysz EA, McCurley K, Blehert DS. Experimental Infection of Snakes with Ophidiomyces ophiodiicola Causes Pathological Changes That Typify Snake Fungal Disease. *mBio.* 2015 Nov 17;6(6):e01534-15.
8. Last LA, Fenton H, Gonyor-McGuire J, Moore M, Yabsley MJ. Snake fungal disease caused by Ophidiomyces ophiodiicola in a free-ranging mud snake (Farancia abacura). *JVDI* . 2016;28(6):709-713.
9. Dolinski AC, Allender MC, Hsiao V, Maddox CW. Systemic *Ophidiomyces ophiodiicola* Infection in a Free-Ranging Plains Garter Snake (*Thamnophis radix*). *Journal of Herpetological Medicine and Surgery* 2014; 24 (1-2): 7–10
10. Ebani VV. Domestic reptiles as source of zoonotic bacteria: A mini review. *Asian Pac J Trop Med*. 2017 Aug;10(8):723-728.

CASE II:

Signalment:
5-year-old, male, Bearded Dragon *(Pogona vitticeps)*.

History:
Three-day history of anorexia, no defecation, and dull mentation. On physical exam: poor body condition score, severe dehydration, and palpable mass in the mid-left coelomic cavity, described as mobile, firm, and ap-

Figure 2-1. Coelomic viscera, bearded dragon. The serosal surface of the stomach has multifocal, confluent, white-tan, firm, variably demarcated nodules, which extended to the adjacent fat pad, mesentery, and small inteolestine (*Photo courtesy of:* Western College of Veterinary Medicine, University of Saskatchewan, https://wcvm.usask.ca/departments/vet-pathology.php)

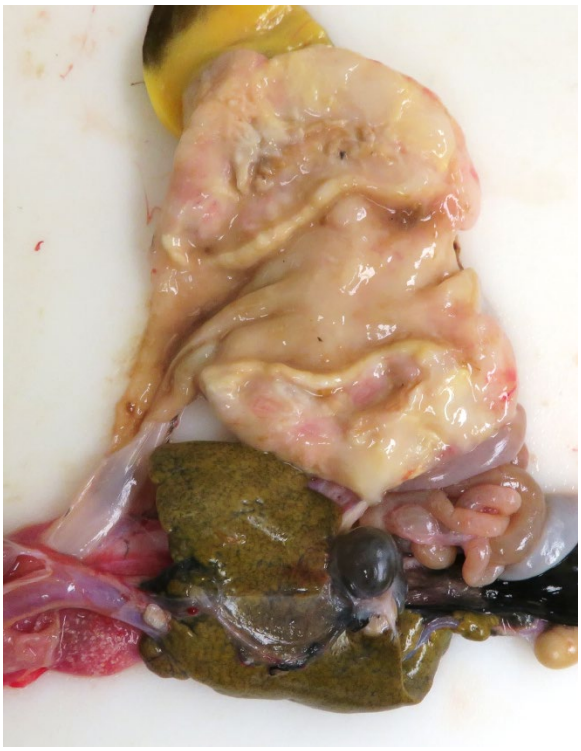

Figure 2-2. Coelomic viscera, bearded dragon. Cut surface of the gastric neoplasm. (*Photo courtesy of:* Western College of Veterinary Medicine, University of Saskatchewan, https://wcvm.usask.ca/departments/vet-pathology.php)

proximately 2 x 4 cm in size. No further diagnostics performed. Euthanasia was elected due to declining condition.

Gross Pathology:

The animal had moderate body fat stores and decreased muscle mass. The mucous membranes of the mouth were pale, and the tongue was pale yellow. The serosal surface of the stomach had multifocal, confluent, white-tan, firm, variably demarcated nodules, which extended to the adjacent fat pad, mesentery, and small intestine. On cut section, the gastric wall was diffusely thickened, white-tan, and firm.

Microscopic Description:

Gastric tumor: Expanding and effacing the gastric submucosa, tunica muscularis, and serosa, there is a well-demarcated, unencapsulated, multi-lobular, infiltrative, and densely cellular neoplasm. The growth is composed of neoplastic polygonal cells arranged in packets, sheets, and occasional pseudorosettes with nuclear palisading around blood vessels, all supported by a delicate fibrovascular stroma. The neoplastic cells have scant, poorly defined, amphophilic, finely granular cytoplasm; their nuclei are round to oval with finely stippled chromatin, and small to inconspicuous nucleoli. There is mild to moderate anisocytosis and anisokaryosis. A total of 37 mitotic figures (sometimes atypical) are counted in 10 consecutive HPF (x400). Many lymphatic vessels are occluded by neoplastic cells. There are multifocal areas of necrosis characterized by eosinophilic cellular and basophilic karyorrhectic debris and eosinophilic smooth to slightly fibrillar deposits (fibrin); sometimes intermixed with colonies of coccobacilli. There are numerous apoptotic cells and variably sized aggregates of granulo-

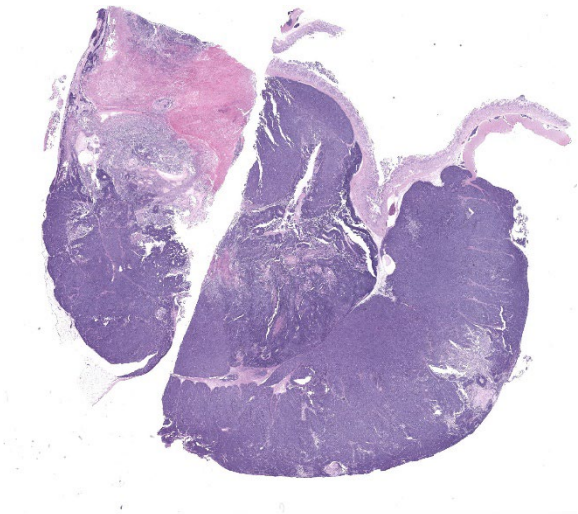

Figure 2-3. Stomach, bearded dragon. Two sections of a large partially necrotic neoplasm arising in the muscularis is submitted for examination. The gastric mucosa is present at top right. (HE, 6X).

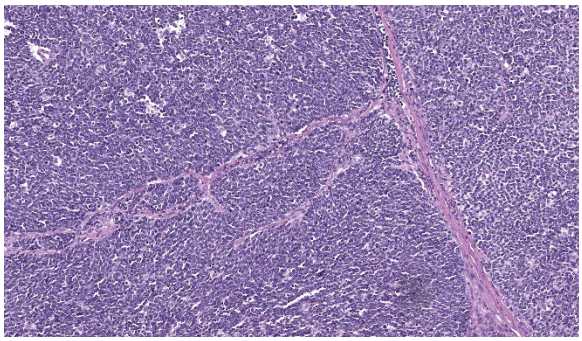

Figure 2-4. Stomach, bearded dragon. Neoplastic cells are arranged in large nests. (HE, 243X).

cytes, lymphocytes, macrophages, and plasma cells within the mass. The gastric mucosal epithelium and glands are usually spared. Approximately 10% of the neoplastic cells have argyrophilic cytoplasmic granules (confirmed with Grimelius stain).

Immunohistochemistry (IHC) for somatostatin on section of gastric tumor: cytoplasmic immunoreactivity in approximately 10% of neoplastic cells.

Contributor's Morphologic Diagnosis:
Gastric neuroendocrine carcinoma (suspected malignant somatostatinoma)

Contributor's Comment:
Neuroendocrine (NE) tumors (also called carcinoids) of the alimentary tract arise from dispersed enteroendocrine cells.[5] There are many types of enteroendocrine cells which have differences in anatomic location and hormonal mediator produced (e.g. G cells are located in the pylorus and produce gastrin), and NE tumors can be further subclassified based on these properties. NE tumors may be benign or malignant, well-differentiated or poorly differentiated, functional or non-functional, and exhibit single or multi-hormonal expression of secretory mediators.[5,9]

Gastric neuroendocrine carcinomas are a highly malignant emerging entity in young bearded dragons, and are frequently metastasized to the liver upon presentation.[9,4,7,11] Commonly observed clinical signs include anorexia, vomiting, weight loss, and lethargy.[4,7,9,11] Reported clinical pathologic abnormalities include hyperglycemia and anemia.[7,9,11] Grossly, gastric tumors are described as variable in size, multinodular but often well demarcated, pale tan to white, firm, with protrusion into the gastric lumen and ulceration of the associated gastric mucosa.[9] Occasional cases report no masses identified grossly.[9] Histopathology of these tumors are characteristic of neuroendocrine neoplasms, and they are primarily located in the gastric submucosa.[4,7,9,11] In one publication, extended IHC analysis of five cases revealed consistent immunoreactivity for somatostatin (n=5), along with varying immunoreactivity for gastrin (n=3), synaptophysin (n=2), pancreatic polypeptide (n=2), chromogranins A and B (n=1), and glucagon (n=1); and therefore further characterized the neoplasms as malignant somatostatinomas.[9]

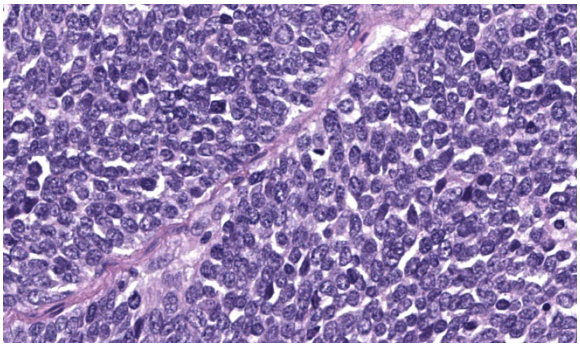

Figure 2-5. Stomach, bearded dragon. High magnification of neoplastic cells. (HE, 1168X).

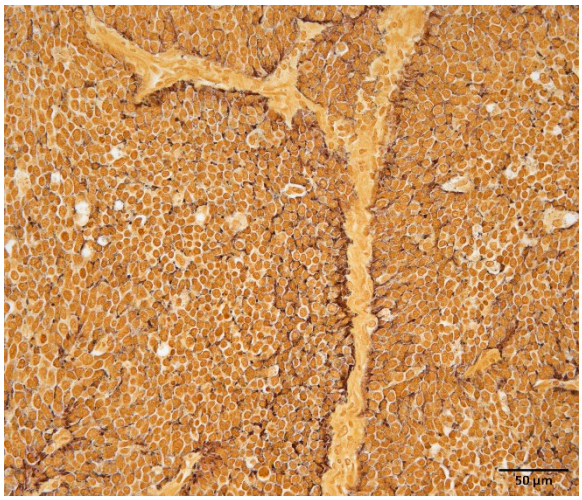

Figure 2-6. Stomach, bearded dragon. A silver stain demonstrates argyrophilic granules within neoplastic cells. (Grimelius, 400X). (*Photo courtesy of:* Western College of Veterinary Medicine, University of Saskatchewan, https://wcvm.usask.ca/departments/vet-pathology.php)

In our individual, there was widespread microscopic metastasis in the heart, lung, liver (with concurrent hepatic lipidosis), small intestine, kidney, adrenal gland, and testes. Cytoplasmic immunoreactivity for somatostatin was observed in a proportion of neoplastic cells and is similarly supportive of a more specific diagnosis of malignant somatostatinoma. However, IHC for other hormonal mediators was not pursued in our case, so the possibility of multi-hormonal expression was not assessed.

Hyperglycemia has been observed in some bearded dragons with these tumors[9,7,11] and is also noted in a proportion of people with somatostatinomas.[6] The pathogenesis of hyperglycemia is due to excessive production of somatostatin, which inhibits secretion of most pancreatic and gut hormones including insulin, leading to decreased glucose intake into cells and therefore elevation of glucose levels in the blood. In people, clinical disease due to excessive somatostatin production from NE tumors is called "somatostatin syndrome", and is characterized by diabetes mellitus, cholelithiasis, and diarrhea/steatorrhea.[6] It is possible that a similar syndrome is occurring in bearded dragons with gastric neuroendocrine carcinomas, however further investigation is needed.

In terms of comparative pathology, gastric NE tumors have been rarely reported in the dog,[3,5,8] cat,[5,10] and ferret.[1] In addition, there is a published case series of benign gastric NE tumors in three captive snow leopards.[2]

Contributing Institution:
Western College of Veterinary Medicine
University of Saskatchewan
52 Campus Dr, Saskatoon, SK, Canada S7N 5B4
https://wcvm.usask.ca/departments/vet-pathology.php

JPC Diagnosis:
Stomach: Neuroendocrine carcinoma

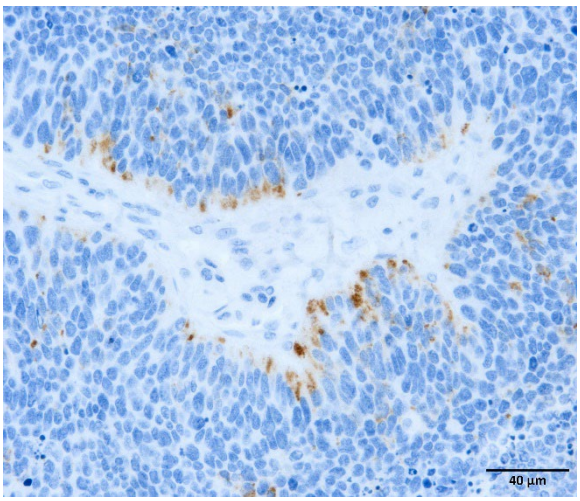

Figure 2-7. Stomach, bearded dragon. Multifocally, neoplastic cells demonstrate strong cytoplasmic immunopositivity for somatostatin. (anti-somatostatin, 400X). (*Photo courtesy of:* Western College of Veterinary Medicine, University of Saskatchewan, https://wcvm.usask.ca/departments/vet-pathology.php).

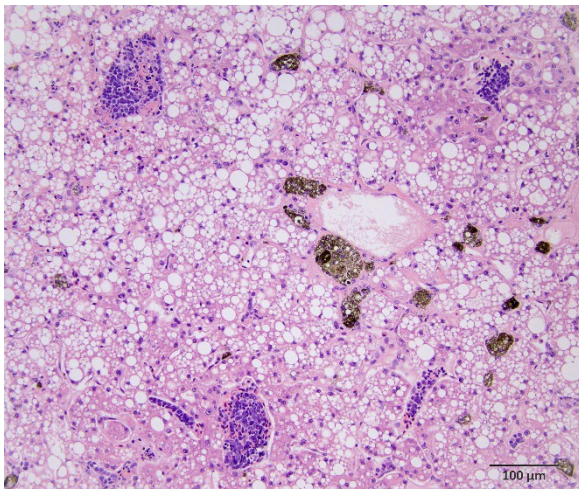

Figure 2-8. Liver, bearded dragon. There is hepatic metastasis. Hepatocytes demonstrate marked lipidosis. (HE, 400X). (*Photo courtesy of:* Western College of Veterinary Medicine, University of Saskatchewan, https://wcvm.usask.ca/departments/vet-pathology.php).

JPC Comment:
Case 2 is a classic neuroendocrine neoplasm in a bearded dragon. We attempted to characterize it further, although the JPC's IHCs (aside from a weakly reactive chromogranin) were negative or non-contributory. Dr. Peiffer emphasized the need for an antibody-specific control in addition to a species tissue control in evaluating the performance of assays that have not been validated in a particular species. This is a frequent consideration for us given that we share laboratory services with a larger human hospital, and few of our antibodies have been validated for exotic species. The Grimelius stain employed by the contributor is a creative way to assess for neuroendocrine cells producing CCK or somatostatin as these characteristically lack an argyrophil reaction.[12] That stated, it is difficult to interpret this stain without a matched control to assess stain performance. Finally, conference participants discussed the somatostatin IHC result – we considered whether the lower proportion of immunoreactive cells could reflect a different neuroendocrine neoplasm producing multiple hormones. For this reason, we settled on a neuroendocrine carcinoma as the most appropriate morphologic diagnosis for this case.

The gross images from this case are excellent and merit a short sidebar discussion. Recognizing normal anatomy is critical when interpreting lesions in zoo animals and wildlife. As the liver of reptiles contains melanomacrophages, the darkened color of the liver in this case is normal and is perhaps accentuated by the histologic finding of lipidosis reported by the contributor. Melanomacrophages are pigment-laden macrophages that contain melanin granules, though they may also contain hemosiderin and/or lipofuscin which cannot be distinguished on H&E alone. Melanomacrophages are also present in fish and amphibians. Melanomacrophage hyperplasia is a non-specific feature that can be appreciated microscopically and in some cases, grossly. Conference participants also discussed the abdominal fat pads and far caudal position of the kidneys in this species (not visible in the provided photo, unfortunately).

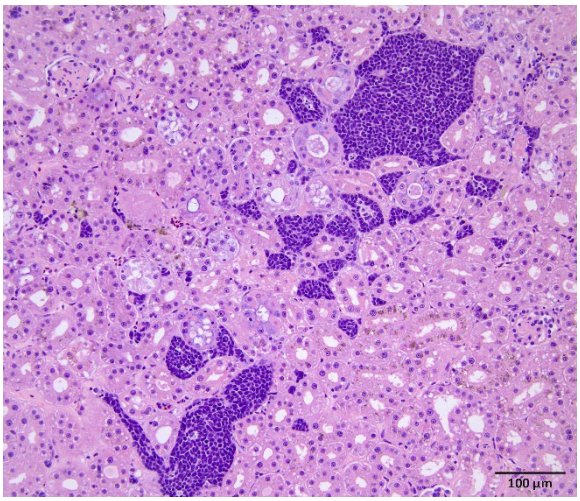

Figure 2-9. Kidney, bearded dragon. There is renal metastasis. (HE, 400X). (*Photo courtesy of:* Western College of Veterinary Medicine, University of Saskatchewan, https://wcvm.usask.ca/departments/vet-pathology.php).

References:

1. Bousquet T, Bravo-Araya M, Davies JL. Gastric neuroendocrine carcinoma (carcinoid) in a ferret *(Mustela putorius furo)*. *Can Vet J*. 2022;63(11):1109-1113.
2. Dobson EC, Naydan DK, Raphael BL et al. Benign gastric neuroendocrine tumors in three snow leopards *(Panthera uncia)*. *J Zoo Wildl Med.* 2013;44(2):441-446.
3. Herbach N, Unterer S, Hermanns W. Gastric neuroendocrine carcinoma in a dog. *Open J Pathol.* 2012;2:162-165.
4. Lyons JA, Newman SJ, Greenacre CB et al. A gastric neuroendocrine carcinoma expressing somatostatin in a bearded dragon *(Pogona vitticeps)*. *J Vet Diagn Invest.* 2010;22:316-320.
5. Munday JS, Löhr CV, Kiupel M. Tumors of the alimentary tract. In: Meuten DJ, 5th edition. *Tumors in domestic animals.* John Wiley & Sons, Inc. 2017:559.
6. Nesi G, Marcucci T, Rubio CA et al. Somatostatinoma: clinico-pathological features of three cases and literature reviewed. *J Gastroenterol Hepatol.* 2008;23(4):521-526.
7. Perpiñán D, Addante K, Driskell E. Gastrointestinal disturbances in a bearded dragon *(Pogona vitticeps)*. *J Herpetol Med Surg.* 2010;20(2-3):54-57.
8. Ovigstad G, Kolbjørnsen Ø, Skancke E et al. Gastric neuroendocrine carcinoma associated with atrophic gastritis in the norwegian lundehund. *J Comp Pathol.* 2008;139(4):194-201.
9. Ritter JM, Garner MM, JA Chilton et al. Gastric neuroendocrine carcinomas in bearded dragons *(Pogona vitticeps)*. *Vet Pathol*. 2009;46:1109-1116.
10. Rossmeisl JH Jr, Forrester SD, Robertson JL et al. Chronic vomiting associated with a gastric carcinoid in a cat. *J Am Anim Hosp Assoc.* 2002;38(1):61-66.
11. Thebeau JM, Martinson SA, Clancey NP et al. Pathology in practice. *J Am Vet Med Assoc.* 2022;259(S2):1-4.
12. Grimelius L. Methods in neuroendocrine histopathology, a methodological overview. Ups J Med Sci. 2008;113(3):243-60.

CASE III:

Signalment:
Adult great blue heron (*Ardea herodias*) of unknown sex

History:
The free-ranging heron was found dead on zoo premises. Blood was noted on the feet.

Gross Pathology:
The heron was in markedly autolyzed postmortem and mildly decreased nutritional condition. Scant dried blood coated the feet. Intracoelomic and pulmonary hemorrhage were present. Embedded in the proventricular and ventricular serosa were seven, 1 mm diameter and 6-11 cm long, tan and red nematodes with tapered tails. A gill raker fragment was firmly embedded in the proventricular mucosa. Firm, cylindrical concretions of feces filled the colon and cloaca.

Laboratory Results:
Cloacal and oropharyngeal swabs were submitted for highly pathogenic avian influenza virus (HPAIV) PCR test. HPAIV was not detected in the sample.

Microscopic Description:
Proventriculus (1 section): The serosa and adjacent adipose are focally disrupted and expanded by a 2.5 mm-diameter granuloma centered on a single, 1 mm-diameter adult nematode that has a smooth eosinophilic cuticle, polymyarian-coelomyarian musculature, hypodermal nuclei, ventral nerve cords, a pseudocoelom, a glandular esophagus with associated pseudomembranes, a reproductive tract, and an intestinal tract lined by uninucleate, columnar epithelium with a

Figure 3-1. Proventriculus and ventriculus, great blue heron. Embedded in the proventricular and ventricular serosa were seven, 1 mm diameter and 6-11 cm long, tan and red nematodes with tapered tails. (*Photo courtesy of:* University of Wisconsin CVM, Dept. of Pathology)

prominent brush border (aphasmid). The nematode is surrounded by large numbers of fragmented heterophils, epithelioid macrophages, and multinucleated giant cells. The granuloma is circumscribed by concentric layers of loose fibrous connective tissue interspersed with many plump fibroblasts and small numbers of lymphocytes. The serosal vessels are multifocally cuffed by medium numbers of lymphocytes and plasma cells. The adipose tissue is severely atrophied. A single proventricular gland is distended by an intraluminal, 0.5 x 1.5 mm adult nematode that has a smooth thin eosinophilic cuticle, indistinct musculature, a pseudocoelom filled with eosinophilic homogeneous material, a reproductive tract containing many embryonated eggs, and an intestinal tract lined by uninucleate columnar epithelium (spirurid). The eggs are 20 x 30 um and ovoid with a smooth, thick shell. Remaining glands multifocally contain eosinophilic flocculent material. The overlying lamina propria is infiltrated by small numbers of eosinophils.

Ventriculus (2 sections): The muscularis and serosa are multifocally disrupted by large, multifocal to coalescing granulomas centered on four sections of an adult aphasmid nematode similar to that previously described in the proventriculus. The granulomas are similarly circumscribed by fibrous connective tissue interspersed with medium numbers of lymphocytes, plasma cells, and eosinophils. The adjacent adipose is severely atrophied.

Contributor's Morphologic Diagnosis:
Proventriculus and ventriculus: Severe, chronic, multifocal to coalescing, granulomatous proventricular serositis and mural ventriculitis with adult aphasmid nematodes

Proventriculus: Moderate, focal glandular ectasia with intraglandular adult spirurid nematode and mild eosinophilic proventriculitis

Contributor's Comment:
Eustrongylidosis is a condition of fish-eating birds caused by infection with aphasmid nematodes in the genus *Eustrongylides*, which has 3 recognized species *E. ignotus, E. tubifex,* and *E. excisus*.[5] *Eustrongylides* spp. are found globally, except for arctic and subarctic regions, and *E. ignotus* and *E. tubifex* are the two species most often reported in the USA.[1,5] Classically, *E. ignotus* affects the ventriculus of Ciconiiformes, whereas *E. tubifex* affects the esophagus and proventriculus of mergansers, loons, and cormorants.[1,2]

For *E. ignotus*, the definitive hosts are multiple genera of herons and egrets in the family Ardeidae.[10] Intermediate hosts include a variety of fish species and oligochaete worms.[2,9] Birds shed eggs into the environment via

their feces, and eggs are consumed by the first intermediate host, an oligochaete worm.[1,5] First and second stage larvae mature within the worm.[5] The first intermediate hosts are then ingested by fish and larvae migrate through the body after penetrating the intestinal wall. Within the fish, larvae mature to the third and fourth stages and can be found in muscle, hepatopancreas, and gonads.[5] Amphibians, reptiles, and predatory fish can also serve as paratenic hosts.[1] Birds then consume parasitized fish or other paratenic hosts and infective fourth stage *Eustrongylides* larvae reach the stomach wall within 3-5 hours of ingestion.[5] Larvae mature over the next 10-15 days, and start producing eggs between 10-25 days post ingestion.[1,5] Eggs are excreted into the environment, where they can survive for several years.[5] Non-patent infections with *E. ignotus* have been reported in Pelecaniformes and non-ardeid Ciconiiforme birds, and birds of prey can also be parasitized.[1,10]

The prevalence of *Eustrongylides* spp. varies between studies and may be related to regional variation in parasite prevalence, increased prevalence in birds submitted to rehabilitation centers or for necropsy, age group studied, and affected avian species. One study in birds at a North California wildlife rehabilitation center found *Eustrongylides* sp. in 30% of necropsied herons and egrets.[6] An earlier study found only 6% of wild nestlings collected from a colony in Northern California were infected, compared to 4% of nestlings in a Rhode Island colony and 35% in a Texas colony.[3]

In affected herons and egrets, low burdens are typically subclinical whereas higher parasite burdens can contribute to individual morbidity and mortality, especially in younger birds.[6] Associated clinical signs include hypothermia, anorexia, regurgitation, weakness, and weight loss.[6,10] Multiple epizootics have been reported in wild Ardeidae, especially in nestlings in coastal rookeries.[1,9] Fatal cases are associated with severe coelomitis and sepsis when penetration of the ventriculus wall by larval eustrongylids leads to bacterial translocation.[2,9]

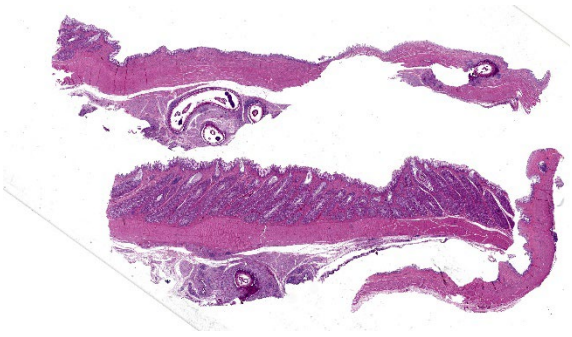

Figure 3-2. Proventriculus and ventriculus, great blue heron. Sections of ventriculus and proventriculus are submitted for examination. There are cross sections of adult aphasmid nematodes within the serosa of the proventriculus, the muscularis of the ventriculus, and an adult spirurid in a proventricular gland. (HE, 10X).

Acute lesions are found in birds as young as 2 days, as well as adults, and are most often associated with fourth-stage larvae, with rarer non-gravid adults.[9] Parasites are typically found below the serosa of the ventricle or on the ventral aspect of the serosal surface.[9] Less often, parasites and/or associated lesions can be found in the air sacs, liver, pericardium, body wall, intestine, or other caudal coelomic organs.[9] Chronic lesions occur in birds over 1 week old, and the majority involve adult parasites.[9] Tortuous, yellow-tan, tubular tunnels containing tan to red nematodes extend across the ventriculus surface, sometimes extending to the intestines and liver.[6,9] Air sacs, gallbladder, proventriculus, cloaca, body wall, and pancreas are less often involved, with esophagus, spleen, kidney and lung rarely affected.[9] More chronic and/or severe cases can have coelomitis, air sacculitis, fibrinous and fibrous adhesions, and inflammatory nodules in multiple organs.[9] For both

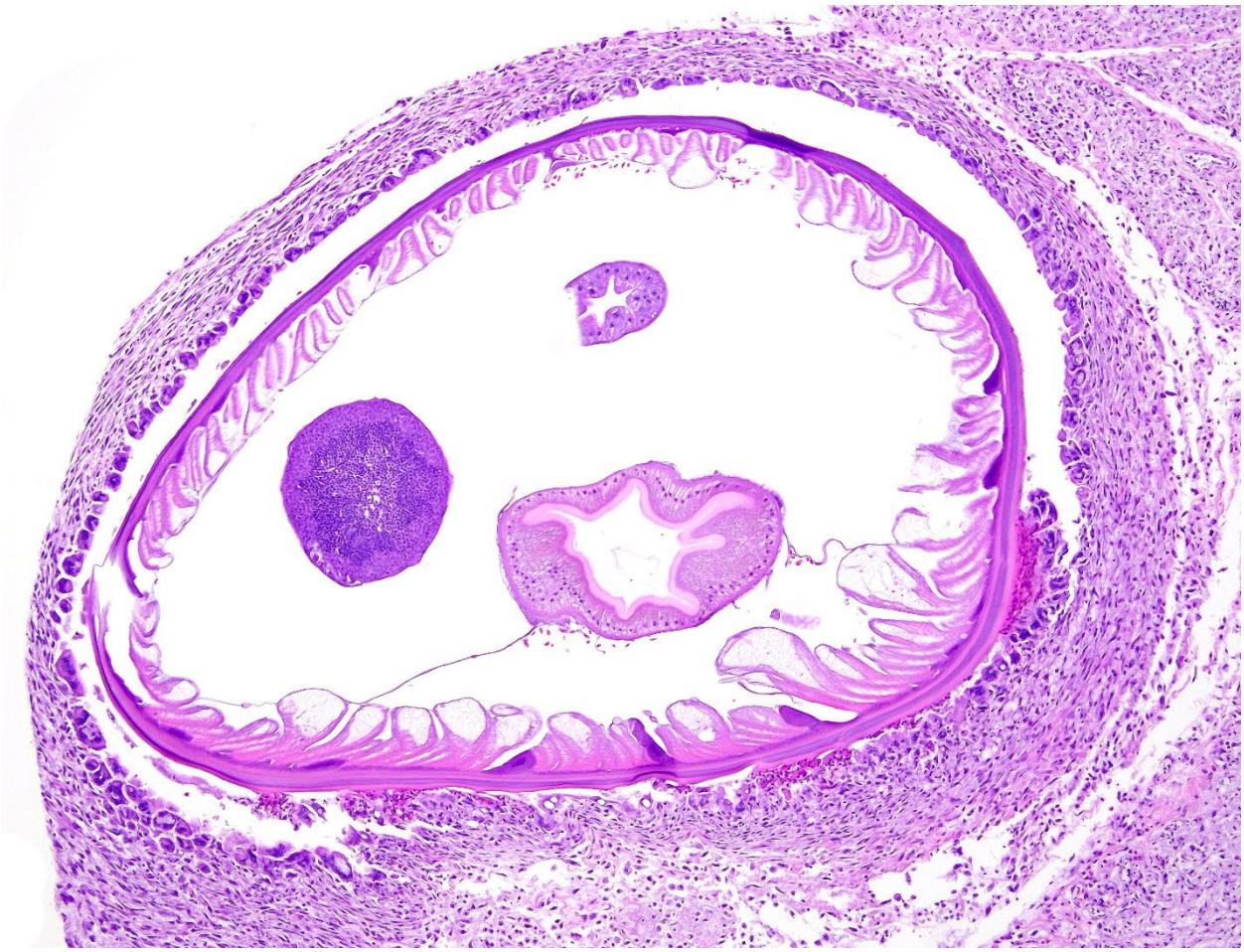

Figure 3-3. Ventriculus, great blue heron. The serosa is expanded by a granuloma centered on a cross-section of adult aphasmid nematode. Features apparent in section include a smooth, eosinophilic cuticle, a pseudocoelom, polymyarian-coelomyarian musculature, and an intestinal tract lined by uninucleate columnar epithelium with a prominent brush border. (HE, 200X) (*Photo courtesy of:* University of Wisconsin CVM, Dept. of Pathology)

acute and chronic cases, a subset are associated with subserosal hematomas.[9]

The most common microscopic findings in acute cases are parasite larvae associated with minimal hemorrhage, eosinophilic inflammation, and pyknotic cellular debris.[9] With chronicity, changes include granulomatous inflammation, necrosis, and fibrosis accompanied by bacterial colonies and eustrongylid eggs.[9] Fibrinous to fibrous tunnels connect to the ventriculus lumen and contain a single, adult parasite, with variable intramural mineralization, eosinophilic infiltrates, and bacteria.[9] Aphasmid nematodes are distinguished by bacillary bands and a single genital tract in adult females.[4] *Eustrongylides* spp. have thick-shelled, operculated eggs, a glandular esophagus, a smooth cuticle, coelomyarian musculature, and pseudomembranes.[4]

In waterbirds, a specific coelomic palpation protocol is a useful antemortem diagnostic technique, especially for more chronic cases with tunnel lesions.[8] Mineralization of parasite tunnels in the ventriculus may be visible radiographically.[10] Post-mortem diagnosis is

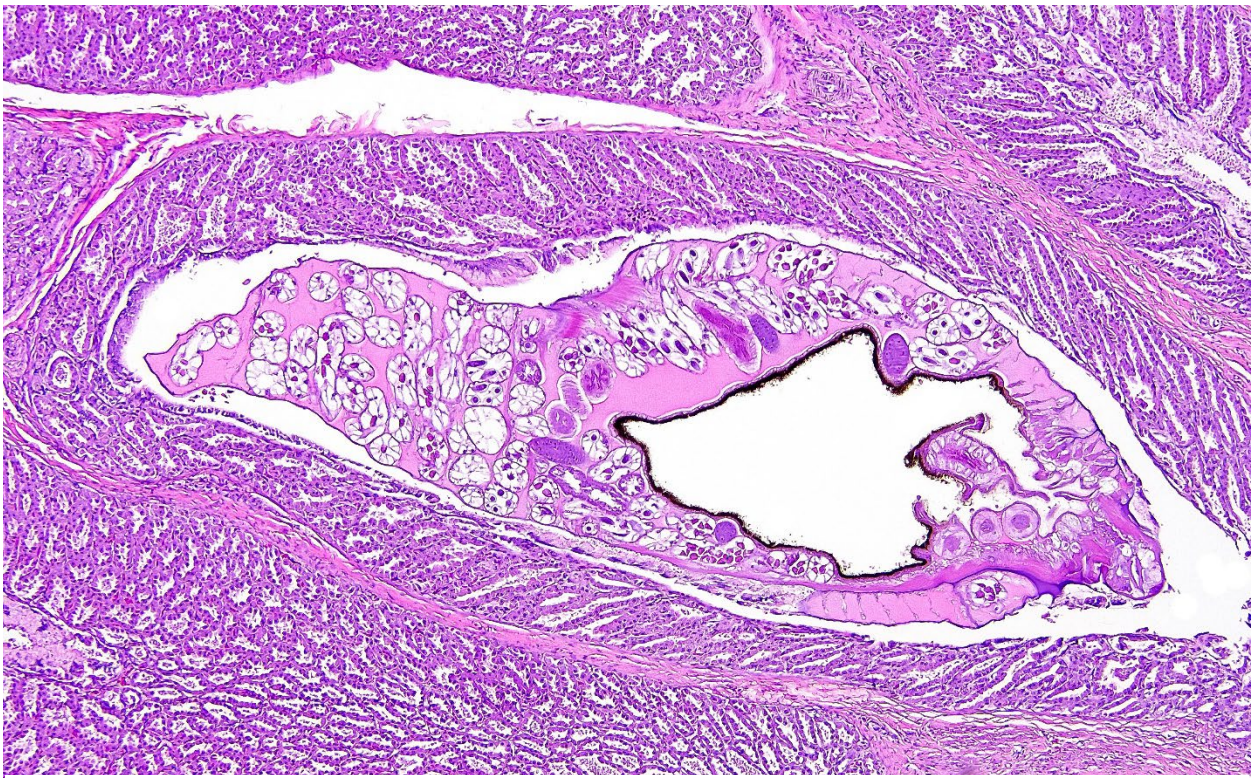

Figure 3-4 Proventriculus, great blue heron. A dilated mucosal gland contains an intraluminal, adult spiurid nematode consistent with *Tetrameres* sp. Features apparent in section include a smooth, thin, eosinophilic cuticle, indistinct musculature, a pseudocoelom filled with eosinophilic, homogeneous material, and reproductive tract with embryonated eggs. (HE, 200X) (*Photo courtesy of:* University of Wisconsin CVM, Dept. of Pathology)

typically by observation of characteristic lesions and identification of larvae or adult parasites, although molecular-genetic techniques are also reported.[5] Human eustrongylidosis is rare, reported most often in the USA in individuals with a history of ingesting live or raw fish.[5]

Tetrameres spp. are spirurid nematodes belonging to the Tetrameridae family, a group which includes three genera (Tetrameres, Microtetrameres, and Geopetitia) and dozens of species.[2,7] For *Tetrameres*, female parasites are found within proventriculus glands; males are either associated with females or within the lumen, although some species encyst within the muscular wall.[7] Sexual dimorphism is a prominent feature for Tetrameridae and females may be globular and less filiform than males due to marked uterine distention.[7] *Tetrameres* lifecycles vary based on species, but the definitive host is usually an aquatic bird and the intermediate host is usually a crustacean.[7] For parasites primarily affecting terrestrial birds, the intermediate host are typically orthopteran or coleopteran insects.[7] Prevalence varies based on species and geographic location; prevalence and intensity can also vary substantially by year and study.[7] Infection is often considered incidental, but overcrowding and high intensity infections can contribute to morbidity and/or mortality.[2] In domestic species, typical clinical signs of *Tetrameres* sp. infection include hyporexia, diarrhea, and emaciation, and

clinical signs in wild birds are less defined.[7] Aquatic birds are most often affected (e.g. Anseriformes, Ardeiformes, Gruiformes, and Charadriiformes), although Passeriformes and Galliformes can be parasitized by some species.[7] *Microtetrameres* spp. more often parasitize terrestrial birds or those feeding on land, whereas *Geopetitia* can parasitize a wide variety of wild birds globally.[7] For this case, *Microtetrameres* sp. remains a differential based on histologic features. Classic gross findings of *Tetrameres* sp. infection include red nodules in the proventricular mucosa containing red, female adult worms, which can be visible from the serosal surface, mucosal hyperplasia, necrotic material coating the proventricular mucosa, mucoid material coating the small intestinal mucosa, and green to golden-brown discoloration of small intestinal contents.[2,7] Histologically, parasites show typical features of spirurid parasites including coelomyarian musculature, large intestines lined by uninucleate cells, eosinophilic fluid within the pseudocoelom, prominent lateral chords, and small characteristic spirurid eggs within adult females.[4] Proventricular glands are distended by adult female nematodes, which can cause compressive changes in adjacent tissue, and there is variable mucosal inflammation.[7] Fecal examination may reveal ovoid, thick-shelled, larvated ova; however, these are challenging to differentiate from other spirurid eggs.[7] Typically, diagnosis is via post-mortem detection of classic lesions and worms, and speciation is primarily via examination of male worms.[7] *Tetrameres* spp. can infect both domestic and wild birds, but is not known to infect humans.[7]

Contributing Institution:
University of Wisconsin
School of Veterinary Medicine
Department of Pathobiological Sciences
2015 Linden Drive
Madison, WI 53706

JPC Diagnosis:
1. Proventriculus and ventriculus: Serositis, granulomatous, diffuse, marked with adult aphasmid nematodes

2. Proventriculus: Glandular ectasia, focal, moderate to marked, with intraglandular adult spirurid nematode

3. Adipose tissue: Atrophy, diffuse, marked

JPC Comment:
We thank the contributor for the detailed writeup and presentation of these two nematodes in section. Identifying *Eustrongylides* was not much of a diagnostic mystery as characteristic structures were easy to appreciate (and its large size helps a bit as well). The single *Tetrameres* was slightly more problematic though careful examination and comparison to *Eustrongylides* allowed conference participants to appreciate the different features. The eosinophilic fluid within the pseudocoelom was helpful as the overall shape of the nematode is not as globoid (or filled with ova) as we have seen previously which may reflect some degeneration. Incidentally, we also noticed the eosinophils the contributor describes in the adjacent portion of the proventriculus. Distinguishing granulocytes is difficult in birds, though the round granules (and adjacent metazoan parasite) are supportive. In contrast, heterophils have more elongate granules. We also added an additional morphologic diagnosis for the atrophy of fat which was quite pronounced in this case.

References:
1. Eustrongylidosis. In: Friend M, Franson JC, eds. Field Manual of Wildlife Diseases: General Field Procedures and Diseases of Birds. US Geological Survey, Biological Resources Division. 1999; 223-228.
2. Fenton H, McManamon R, Howerth EW.

Anseriformes, Ciconiiformes, Charadriiformes, and Gruiformes. In: Terio KA, McAloose D, St Leger J eds. *Pathology of Wildlife and Zoo Animals.* Associated Press; 2019.
3. Franson JC, Custer TW. Prevalence of eustrongylidosis in wading birds from colonies in California, Texas, and Rhode Island, USA. *Col Waterbirds.* 1994;17(2):168-172.
4. Gardiner CH, Poynton SL. In: An Atlas of Metazoan Parasites in Animal Tissues. Armed Forces Institute of Pathology; 1999.
5. Honcharoy SL, Soroka NM, Galat MV, Zhurenko OV, Dubovyi AI, Dzhmil VI. *Eustrongylides* (Nematoda: Dioctophymatidae): Epizootiology and special characteristics of the development biology. *Helminthologia*. 2022;59(2):127-142.
6. Horgan M, Duerr R. Gross pathology of herons and egrets (family Ardeidae) at a wildlife rehabilitation centre in Northern California. *J Wildl Rehabil.* 2021;37(1):29-41.
7. Kinsella JM, Forrester DJ. Tetrameridosis. In: Atkinson CT, Thomas NJ, Hunter DB, eds. *Parasitic Diseases of Wild Birds*. John Wiley & Sons; 2008.
8. Spalding MG. Antemortem diagnosis of eustrongylidosis in wading birds (Ciconiiformes). *Col Waterbirds*. 1990;13(1):75-77.
9. Spalding MG, Bancroft GT, Forrester DJ. The epizootiology of eustrongylidosis in wading birds (Ciconiiformes) in Florida. *J Wildl Dis*. 1993;29(2):237-249.
10. Spalding MG, Forrester DJ. Pathogenesis of *Eustrongylides ignotus* (Nematoda: Dioctophymatoidea) in Ciconiiformes. *J Wildl Dis.* 1993;29(2):250-260.

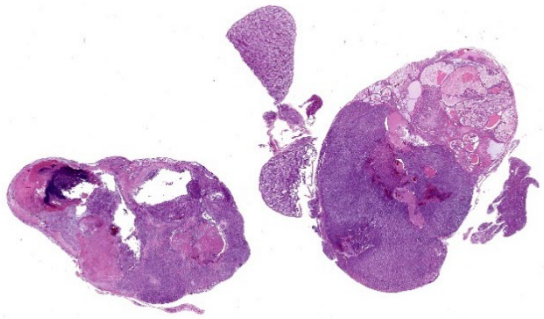

Figure 4-1. Kidney, budgerigar. Multiple sections of a kidney which is effaced by a neoplasm are submitted for examination. Normal testis is also present (center) (HE, 6X)

CASE IV:

Signalment:
Adult, male, blue and white budgerigar (*Melopsittacus undulatus*)

History:
This adult male budgerigar was housed in an indoor aviary. He had been vaccinated against West Nile virus in May, 2020. Spring of 2021, he was found dead with no reported antemortem clinical signs.

Gross Pathology:
Bilaterally effacing the kidneys is a multilobulated, poorly circumscribed, tan, soft mass. The mass moderately displaces the testes, cranially. There are scant subcutaneous and visceral adipose stores.

Laboratory Results:
Chlamydia psittaci, avian polyomavirus, and psittacine herpesvirus were not detected by real time PCR on pooled lung, liver, and kidney samples.

Microscopic Description:
Kidney, left and right: Expanding and effacing both examined sections of kidney is a large, multinodular, unencapsulated, densely cellular infiltrative neoplasm. The polygonal neoplastic cells variably form haphazardly organized tubules, papillary proliferations,

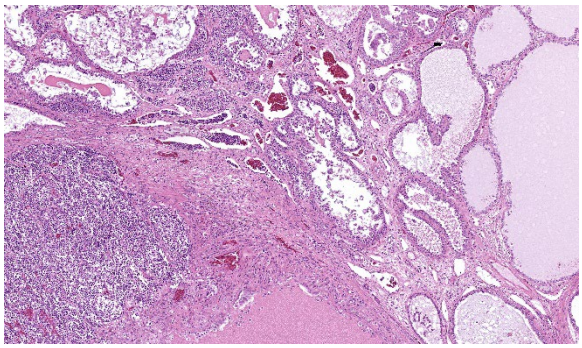

Figure 4-2 Kidney, budgerigar. The neoplasm is composed of cuboidal epithelium forming viarbly dilated tubules. A large amount of the tumor is composed of tumor cells in sheets (lower left). (HE, 154X)

and occasional cords arranged over a fine fibrovascular stroma. The neoplastic epithelial cells have distinct cell borders, scant to moderate amounts of clear to granular eosinophilic cytoplasm, and a single, basally to centrally located round nucleus with finely stippled chromatin and one variably distinct amphophilic to eosinophilic nucleolus. There is mild to moderate anisocytosis and anisokaryosis. There is approximately one mitotic figure per high power (400x) field. There are large multifocal regions of necrosis and hemorrhage with hemosiderin laden macrophages and heterophils scattered throughout the neoplasm. Mild to moderate amounts of bright homogenous eosinophilic material (proteinaceous fluid) occasionally fills neoplastic and remaining normal renal tubular lumina. The remaining normal renal parenchyma is compressed at the periphery of the mass. The remaining pre-existing renal tubules occasionally exhibit one or more of the following changes: mild to moderate ectasia, epithelial attenuation, pale vacuolated eosinophilic cytoplasm with loss of cellular detail (degeneration), and/or colorless to basophilic radiating, sharp, acicular, crystalline deposits (urate tophi), often accompanied and surrounded by heterophils and macrophages.

Contributor's Morphologic Diagnosis:
Kidney: Renal adenocarcinoma, budgerigar

Contributor's Comment:
The cellular morphology and arrangement of the mass in this case are characteristic of renal tubular epithelial origin.

Renal carcinomas and adenomas are significantly more common in budgerigars than other psittacine species, although the mechanisms for this are not completely understood.[6] Captive birds are generally understood to have a higher incidence of neoplasia than wild birds, potentially due to differences in life span, diet, and carcinogen exposure.[8] Several carcinogens, including but not limited to aflatoxins, lead, and nitrosamines, are thought to contribute to renal carcinoma development in veterinary species.[4] In addition to carcinogen exposure, several viral etiologies have been identified in renal carcinomas in some species, including induction of renal adenocarcinoma via avian erythroblastosis virus in chickens[1] and renal adenocarcinomas, also known as Lucké's tumor of leopard frogs, by ranid herpesvirus type 1 (RaHV-1).[3] Investigations into potential retroviral causes of renal neoplasms in budgerigars have not identified associated retroviruses.[7]

The most frequent presenting clinical sign of renal adenocarcinoma in birds is unilateral lameness due compression of the sciatic nerve.[8] The gross appearance of the renal adenocarcinoma in this case was very characteristic. Most renal adenocarcinomas are large, tan to reddish brown, soft to friable, and are located at the cranial pole of the kidneys (in this case, displacing the testes cranially).[8] Histologically, the variation in arrangement of tubules, papillary projections and more solid areas of tightly packed cords confirm the suspected diagnosis of renal cell adenocarcinoma. Renal adenomas have less cellular pleomorphism and are comprised of tubules lined by a single layer of epithelium with a moderate fibrovascular stroma. Avian renal carcinomas and adenocarcinomas are

reported to infrequently metastasize to the lungs and liver.[6]

A majority of the immunohistochemical characterization of renal adenocarcinomas and renal cell carcinomas has been done in canine patients. Immunohistochemistry for uromodulin and uroplakin may be useful for confirming tissue of renal origin, as these markers are commonly expressed by canine renal tumors.[2] Additionally, canine renal cell carcinomas frequently co-express cytokeratin and vimentin, and express CD10, PAX 8, and napsin A.[5] Though no immunohistochemistry was pursued in this case, it may be useful to try the above-mentioned markers in renal tumors from budgies if the diagnosis based only on morphology is in question.

In contrast to budgerigars, primary renal neoplasms are uncommon in most domestic veterinary species. The most common primary renal neoplasm in dogs, cats, cattle, and horses are renal cell carcinomas rather than adenocarcinomas. Additional differential diagnoses for a primary renal mass include renal adenoma, oncocytoma, and transitional cell papilloma and carcinoma. Renal adenomas are rare, benign epithelial neoplasms which are not commonly reported in budgerigars.[1]

Contributing Institution:
University of Wisconsin
School of Veterinary Medicine
Department of Pathobiological Sciences
2015 Linden Drive
Madison, WI 53706

JPC Diagnosis:
Kidney: Renal adenocarcinoma

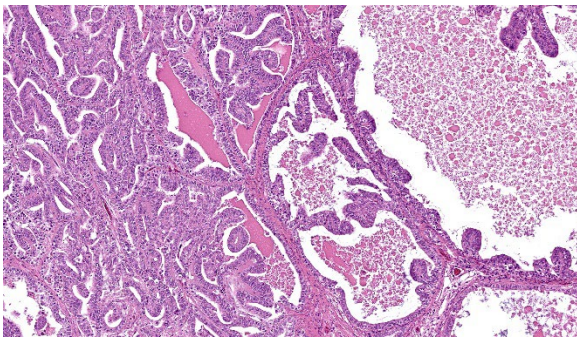

Figure 4-3. Kidney, budgerigar. In some ectatic tubules, neoplastic cells form intricate papillary projections. (HE, 154X)

JPC Comment:
The final case of this conference is another classic neoplasm, this time in a budgie. The contributor gave us several options among slides for this case. The digital section that we ultimately chose has a great assortment of ancillary features, though it might initially be misleading on tissue identification with the normal testis distracting from the relatively small portion of remaining renal cortex to evaluate. We agree that this neoplasm is a renal adenocarcinoma that has both solid and papillary-predominant regions mixed with necrotic foci. In solid regions, neoplastic cells have increased cytoplasmic clearing which has been described as a clear cell histologic subtype.

We took the contributor up on their challenge to try canine renal cell carcinoma markers for this case. Napsin A, CD10, CK7, vimentin, and uroplakin were all immunonegative. We noted moderate-to-strong nuclear immunoreactivity to PAX8 within 30% of neoplastic cells (predominately in well-differentiated cells in the papillary-predominant region), consistent with renal epithelial cell origin. This distribution also aligns with PAX8 performance in canine RCCs.[5] The remaining renal tubules served as a useful internal tissue control. That stated, there is conflicting information that the avian genome (or at least chickens) lack an orthologous *Pax8* gene[9] despite this convincing antibody performance.

Polyclonal PAX8 antibodies do cross label with PAX5 – review of lab materials indicate that we used a monoclonal mouse primary antibody (MRQ-50; Ventana) which removes this possibility. We look forward to trying this antibody with appropriate controls in future cases (see discussion in case 2 of this conference) should the opportunity arise.

References:

1. Breshears MA, Confer AW. The Urinary System. In: Zachary JF ed. *Pathologic Basis of Veterinary Disease*. 6th ed. Elsevier; 2017.
2. Cianciolo RE, Mohr FC. Urinary System. In: Maxie MG ed. *Jubb, Kennedy, and Palmer's Pathology of Domestic Animals*. 6th ed. Elsevier; 2016.
3. McKinnel RG, Carlson DL. Lucke renal adenocarcinoma, an anuran neoplasm: Studies at the interface of pathology, virology, and differentiation competence. *J Cell Physiol.* 1997;173:115-118.
4. Meuten DJ, Meuten TLK. Tumors of the Urinary System. In: Meuten DJ ed.T*umors in Domestic Animals.* 5th ed. John Wiley & Sons, Inc; 2017.
5. Peat TJ, Edmondson EF, Miller MA, DuSold DM, Ramos-Vara JA. Pax8, Napsin A, and CD10 as immunohistochemical markers of canine renal cell carcinoma. *Vet Pathol*. 2017;54:588-594.
6. Schmidt RE, Reavill DR, Phalen DN. *Pathology of Pet and Aviary Birds*. Iowa State Press; 2003.
7. Simova-Curd SA, Huder JB, Boeni J, Robert N, Hatt JM. Investigations on the diagnosis and retroviral aetiology of renal neoplasia in budgerigars (*Melopsittacus undulatus*). *Avian Pathol.* 2010;39:161-167.
8. Simova-Curd S, Nitzl D, Mayer J, Hatt JM. Clinical approach to renal neoplasia in budgerigars (*Melopsittacus undulatus*). *J Small Anim Pract*. 2006;47:504-511.
9. Freter S, Muta Y, O'Neill P, Vassilev VS, Kuraku S, Ladher RK. Pax2 modulates proliferation during specification of the otic and epibranchial placodes. Dev Dyn. 2012 Nov;241(11):1716-28.

Joint Pathology Center
Veterinary Pathology Services

WEDNESDAY SLIDE CONFERENCE 2024-2025

Conference #20 12 February 2025

CASE I:

Signalment:
Approximately 5-month-old, female, cherry shrimp (*Neocaridina davidi)*

History:
This shrimp was one of 10 ornamental dwarf shrimps housed in a 28-gallon freshwater aquarium and was found dead with no noted premonitory signs. The death of this shrimp occurred one month after a complete water change from tap water to distilled and re-mineralized water although standard water acclimation procedures were followed.

Gross Pathology:
External examination revealed numerous fine, light green to yellow, elongate to club-shaped, up to 1 mm long structures projecting outward along the interpleopodal spaces.

Figure 1-1. Presentation, shrimp. Numerous fine, light green to yellow, elongate to club-shaped, up to 1 mm long structures projecting outward along the interpleopodal spaces (*Photo courtesy of:* Department of Pathobiological Sciences and Louisiana Animal Disease Diagnostic Laboratory, School of Veterinary Medicine, Louisiana State University, Baton Rouge, LA. https://www.lsu.edu/vetmed/laddl/; https://www.lsu.edu/vetmed/pbs/index.php)

Microscopic Description:
Sagittal sections of the entire shrimp were available for histologic review. Many thalli were protruding externally within the pleopodal regions and consisted of cuticular perforating multinucleated basal cells that measured 20 µm in diameter and externally branching erect filaments that ranged from 8 to 15 µm in diameter with numerous terminal zoosporangia of varying maturational stages. Fully sporulated zoosporangia measured up to 800 µm in length and 100 µm in diameter and consisted of numerous peripherally located zoospores. The perforating basal cells were associated with a branching network of hyphal-like rhizoids that infiltrated the epidermis and subcutis, ranged from 4 to 8 µm in diameter, were uninucleated and partitioned, and occasionally contained granular material highlighted by a Grocott methenamine silver stain (GMS). The subcutaneous tissue was markedly expanded by hemolymph and heavily infiltrated by predominately granulated hemocytes. Rhizoids and associated inflammatory infiltrates extended to and surrounded the ventral nerve cord and multifocally (but minimally) invaded the ad

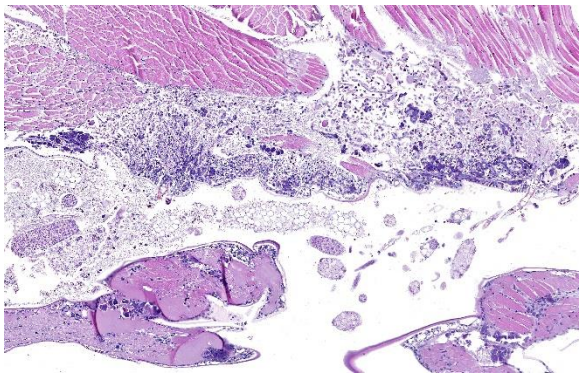

Figure 1-2. Pleopodal region. Many thalli were protruding externally within the pleopodal regions and consisted of cuticular perforating multinucleated basal cells that measured 20 µm in diameter and externally branching erect filaments that ranged from 8 to 15 µm in diameter with numerous terminal zoosporangia of varying maturational stages. (HE, 200X) (*Photo courtesy of:* Department of Pathobiological Sciences and Louisiana Animal Disease Diagnostic Laboratory, School of Veterinary Medicine, Louisiana State University, Baton Rouge, LA. https://www.lsu.edu/vetmed/laddl/)

jacent abdominal flexor musculature. All observed algae forms were strongly highlighted by a GMS stain. Similar uninucleated and partitioned, short rhizoids were also circulating within the hemolymph of the ventral cephalothorax, hepatopancreas, and around the midgut. Within these areas, pooled hemolymph contained numerous circulating hemocytes.

Contributor's Morphologic Diagnosis:
Interpleopodal subcuticular invasive and circulating rhizoids, numerous, with external zoosporangia and infiltrating granulated hemocytes

Contributor's Comment:
The external thallus portion consisting of cuticular perforating basal cells, branching erect filaments, and terminal zoospores as well as subcutaneous rhizoids within the pleopod area are morphologically consistent with *Cladogonium* sp. *Cladogonium* sp. is a parasitic epibiotic green algae of East Asian freshwater shrimp. It was first described in *Paratya improvisa* in 1950[1], then described in *Macrobranchium longipes* in 1971[2], and since then has been well characterized in *Neocaridina davidi.*[4,5] *Cladogonium* sp. is an important cause of epibiont-related morbidity and mortality in aquacultured and captive *Neocaridina davidi.* Classification of *C. ogishimae* and *C. kumaki* sp. nov. has primarily been based on morphology with limited molecular characterization grouping *Cladogonium* sp. within the order Trentepohliales although still widely accepted as belonging to the order Cladophorales and family Pithophoraceae.[1,5]

Neocaridina davidi are freshwater dwarf shrimp that are native to Taiwan and are heavily bred for the aquatic pet trade industry due to their popular small size, intense coloration, and large diversity. The lack of readily available veterinary care and scientific literature on this agent has resulted in widespread misinformation amongst shrimp hobbyists.

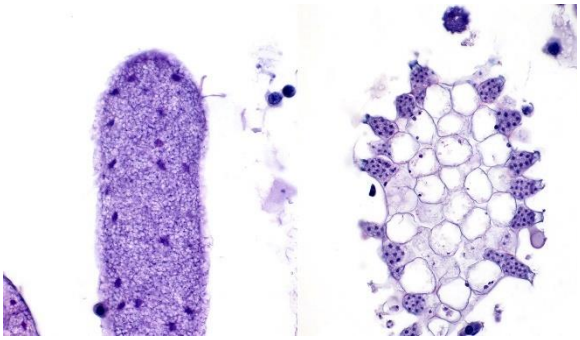

Figure 1-3. Pleopodal region. Fully sporulated zoosporangia measure up to 800 µm in length and 100 µm in diameter and consisted of numerous peripherally located zoospores. (HE, 1000X) (*Photo courtesy of:* Department of Pathobiological Sciences and Louisiana Animal Disease Diagnostic Laboratory, School of Veterinary Medicine, Louisiana State University, Baton Rouge, LA. https://www.lsu.edu/vetmed/laddl/)

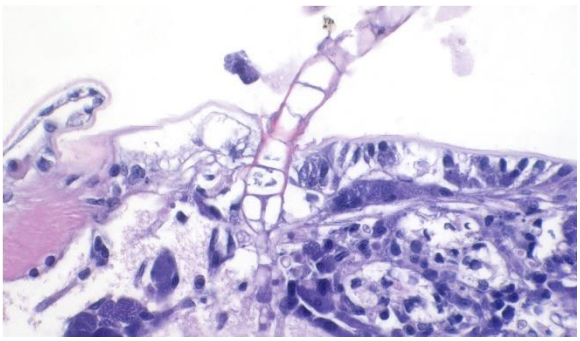

Figure 1-4. Pleopodal region. Algal basal cells perforated the cuticle, which was thin. Many granulated hemocytes infiltrated the epidermis and subcutis. (HE, 400X) (Photo courtesy of: Department of Pathobiological Sciences and Louisiana Animal Disease Diagnostic Laboratory, School of Veterinary Medicine, Louisiana State University, Baton Rouge, LA. https://www.lsu.edu/vetmed/laddl/)

The common misnomer for *Cladogonium* sp. is "green shrimp fungus" and has widely been confused with Ellobiopsidae. Ellobiopsidae is a small diverse group of protists that are closely related to dinoflagellates and are primarily ectoparasites of marine pelagic crustaceans (krill) and freshwater copepods and cladocerans (water fleas).[3] Other well recognized epibionts of *Neocaridina davidi* and their preferred anatomical location include 1) Rotifera found along the rostrum and antennas; 2) *Stentor* sp. along the rostrum and antennas; 3) *Scutariella japonica* along the rostrum, pleopods, and pereiopods; 4) *Monodiscus kumaki* sp. nov. along the rostrum, pleopods, and pereiopods; 5) *Saprolegnia* sp. along the pleopods and uropods; 6) *Holtodrilus truncates* along the rostrum, branchial chambers, pleopods, and pereiopods; and 7) *Vorticella* sp. along the chelipeds, pereiopods, pleopods, and uropods.[4,5] Of these, *Cladogonium ogishimae*, *Saprolegnia* sp., and *Scutariella japonica* are known to exhibit parasitic lifestyles.[4]

Importation of *Neocaridina davidi* and their epibionts is considered the main route of spread.[4,5] It is suspected that following rhizoid colonization of the cuticular epidermis and subcutis along the interpleopodal region, basal cells perforate the cuticle and branch externally as erect filaments with terminal zoosporangia.[1] Ciliated zoospores are then released into the environment by the mature zoosporangia. These contain chloroplasts, which impart the grossly observed green coloration and is evident in the advanced stage of infection.[6] All algal forms stain strongly with Grocott methenamine silver stain. Death is thought to be due to debilitation, potentially related to involvement of the ventral nerve cord, molting complications, and/or secondary infections.[1] Systemic infections, as was seen in this case, have not been previously described. The possibility of a systemic coinfection with *Saprolegnia parasitica* was considered; however, the circulating short rhizoid segments are morphologically identical to those within the pleopod area with branching, partitioning, and uninucleation and are morphologically distinct from *Saprolegnia* sp. filaments.

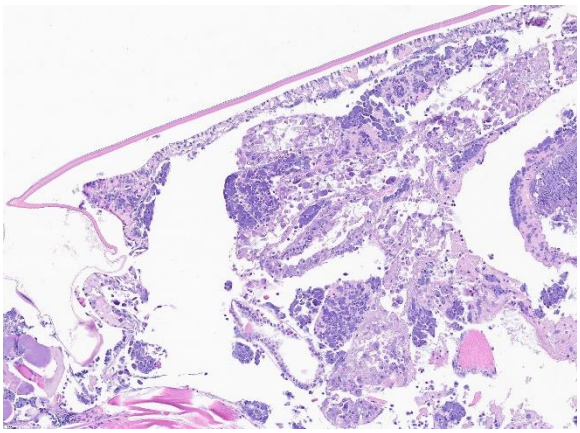

Figure 1-5. Dorsal cephalothorax, shrimp. The coelomic cavity contains numerous hemocytes, which are markedly distended by large, granular, cytoplasmic, bacterial inclusions. Similar bacterial inclusions are in the epidermis and hepatopancreatic interstitium. (HE, 100X)

Diagnosis of *Cladogonium* sp. infections is largely based on observation of the characteristic light green elongate club-shaped structures projecting outward in the pleopodal area, which are, again, evident in advanced infections as the erect filaments and immature zoosporangia largely lack chloroplasts. The prognosis is poor for heavily parasitized shrimp, which constitute the source of infection for other shrimp in the environment. While algaecides are effective at eliminating this agent by substituting copper for magnesium within chlorophyll, shrimp are exquisitely sensitive to copper toxicity and would be unlikely to survive treatment doses required to kill algae.[1] Water quality management, quarantining, and reduction of stressors such as temperature fluctuations are all important in preventing and managing outbreaks of this disease.[1] In our case, this disease manifested approximately one month after a 100% water change from tap water to distilled and re-mineralized water. During the water acclimation period, there was an ammonia spike in the temporary holding tank, which may have predisposed this shrimp to succumb to a preexisting parasitic infection. Considering that there were no additions or other changes to the tank since acquisition of the shrimp, an asymptomatic carrier state was suspected although could not be proved. No additional deaths were observed following prompt removal of the dead shrimp, and the remaining shrimps have prolifically bred under stable water and temperature parameters.

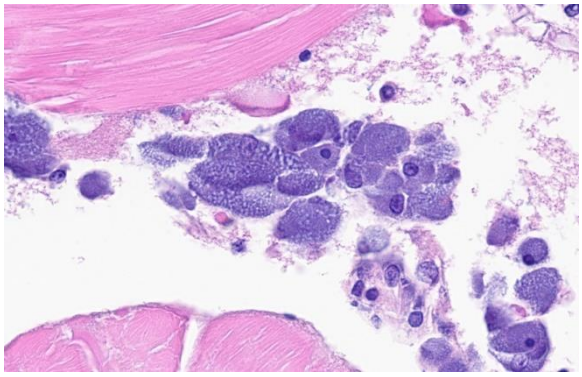

Figure 1-6. Coelom, shrimp: Hemocytes are distended up to 27 µm by granular, basophilic, cytoplasmic, bacterial inclusions, consistent with rickettsia-like organisms. (HE, 1000X)

Contributing Institution:
Department of Pathobiological Sciences and Louisiana Animal Disease Diagnostic Laboratory, School of Veterinary Medicine, Louisiana State University, Baton Rouge, LA, USA
https://www.lsu.edu/vetmed/laddl/
https://www.lsu.edu/vetmed/pbs/index.php

JPC Diagnosis:
1. Body as a whole: Hemocytosis, chronic, diffuse, severe with hemocytic and multisystemic cytoplasmic bacterial inclusions (rickettsia-like organisms)
2. Ventral carapace: dermatitis, necrotizing, acute, regionally extensive, mild with invasive algae

JPC Comment:
This week's moderator was Prof. Karen Terio from the University of Illinois who selected four exotics/wildlife cases to test conference participants on classic entities as well as several new ones. This first case features an ouotstanding, meticulously prepared sagittal section of a cherry shrimp. Preservation of major anatomic features[7] such as the eye, anterior ganglion, antenna, gills, tail fin, and pleopods facilitates slide orientation and interpretation of lesions.

We enjoyed discussing the pathogenesis of this case. The most substantial finding for mortality was likely the rickettsia-like organism (RLO) infection, which resulted in numerous bacterial inclusions within the cytoplasm of hemocytes throughout the hemolymph. Other cells (particularly the epider-

mis) also had inclusions, though less frequently. Rickettsia-like organisms are primary pathogens of invertebrates and given the severity of inflammation, RLOs were likely the main cause of the decline seen in this case. Rickettsia are obligate intracellular bacteria. Infections with RLOs are widely reported in crustaceans. Regardless of the crustacean host, disease caused by RLOs has typical histologic findings, namely bacterial inclusions in hemocytes throughout the body and less commonly in other tissues, as seen in this case.

Given the limited distribution of the algal infection, participants suspected that the algal lesion was likely secondary to generalized debilitation from RLO infection, though two separate primary pathogenic processes are possible. We did not speculate on the exact algae involved (lacking ancillary confirmation) as microhabitat and epibiont-host relationships are not entirely exact,[5] though the shape and distribution is appropriate for *Cladogonium*.

Finally, participants also discussed the nature of epibiosis. Epibiotic organisms live on the surface of another organism and this relationship can be harmless (neutral), commensalistic (both benefit), or parasitic (one benefits at the others expense). Such relationships have the potential to directly impact organismal coloration, health, and reproduction which all have significant economic impacts.[5] In the present case, this relationship bests fits with a parasitic one. It is possible that entry of thalli (direct penetration) and previous areas of carapace damage both facilitated *Cladosporium* development. That the nine other conspecifics of this shrimp were not affected points to this host-epibiont relationship being fairly muted (or at least tolerable), though *Cladogonium* should still be viewed as a pathogen nonetheless.

References:

1. Bauer J, Jung-Schroers V, Teitge F, Adamek M, Steinhagen D. Association of the alga *Cladogonium* sp. with a multifactorial disease outbreak in dwarf shrimp (*Neocaridina Davidi*). *Diseases of Aquatic Organisms*. 2021; 146:107-115.
2. Hirose H, Akiyama M. A Colorless, Filamentous Chlorophyceous Alga, *Cladogonium ogishimae* Gen. et Sp. Nov., Parasitic on Fresh-water Shrimps. *The Botanical Magazine Tokyo*. 1971; 84(993):137-140.
3. Konovalova GV. Parasitic Dinoflagellates and Ellobiopsids (Ellobiopsidae) of the Coastal Waters of the Sea of Japan. *Russian Journal of Marine Biology*. 2008;34(1):28-37.
4. Maciaszek R, Kamaszewski M, Strużyński W, Łapa P. Epibionts of ornamental freshwater shrimps bred in Taiwan. *Annals of Warsaw University of Life Sciences - SGGW - Animal Science*. 2018;57(2):133-142.
5. Maciaszek R, Swiderek W, Prati S, Huang CY, et al. Epibiont Cohabitation in Freshwater Shrimp *Neocaridina davidi* with the Description of Two Species New to Science, *Cladogonium kumaki* sp. nov. and *Monodiscus kumaki* sp. nov., and Redescription of *Scutariella japonica* and *Holtodrilus truncates*. *Animals*. 2023;13(1616):1-22.
6. Matsuyama-Serisawa K, Imai T, Nakaso M, Serisawa Y. Reconfirmation of *Cladogonium* (Chlorophyta, Cladophoraceae) being Ectoparasitic on Freshwater Shrimp. *Japanese Journal of Phycology* (Sôrui). 2014; 62:1−6.
7. Smolowitz R. Arthropoda: Decapoda. In: LaDouceur EEB, ed. Invertebrate histology. Wiley-Blackwell; 2021: 277-299.

CASE II:

Signalment:
Adult female betta fish (*Betta splendens*)

History:
This animal was wild-caught in Thailand and singly housed at the Wake Forest University Reynolda Campus for use in an experimental study evaluating differences in personality, behavior, and locomotion between wild and domestic betta fish. About 5 weeks after arrival from Thailand it appeared thin, but was observed consuming normal amounts of food. The animal hid in the tank and was found dead approximately 8 hours later. Three other female wild-caught betta fish in this cohort were also found dead. All domestically purchased male and female betta fish and male wild-caught betta fish in this cohort had no clinical signs.

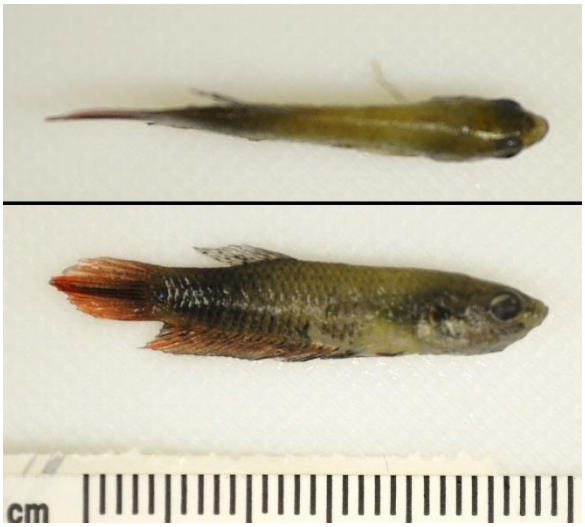

Figure 2-1. Whole body, betta. The betta was emaciated, evidenced by concavity of the middle abdomen. (*Photo courtesy of* Wake Forest Baptist Medical Center, Winston-Salem, NC 27157)

Figure 2-2. Whole body, betta. A sagittal section of the whole fish minus tail is submitted. At subgross magnification, granulomas in the liver, kidney and gills, as well as numerous cysts within skeletal muscle are evident. (HE, 9X)

Gross Pathology:
Examined was a 0.25g female betta fish (*Betta splendens*) in emaciated body condition, evidenced by concavity of the middle abdomen.

Microscopic Description:
Whole body longitudinal section: Numerous round to oval, 40-400um diameter granulomas were present in the kidneys, liver, intestine, ovary and in the gill chamber. The granulomas were composed of central cores of brightly eosinophilic material admixed with karyorrhectic debris (necrosis) surrounded by concentric layers of epithelioid macrophages. Abundant acid-fast bacterial rods were present within the cytoplasm of the macrophages and in the necrotic cores of the granulomas. The intestinal mucosa contained variably-sized, up to 200um diameter, round microsporidian xenomas**.** The xenomas had thin eosinophilic walls, contained numerous eosinophilic, 2-4 um, acid-fast oval spores, and some had central hyperplastic host nuclei. Many 0.4-0.6mm diameter round cysts with up to 3um thick eosinophilic hyaline walls were present in the skeletal musculature and body cavity that contained cross sections of trematode larvae. The larvae had 5um thick

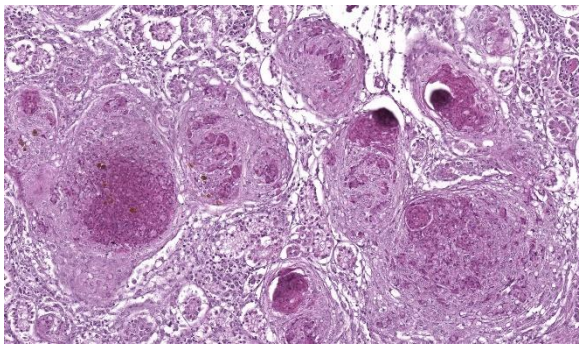

Figure 2-3. Kidney, betta. Numerous well-formed granulomas are scattered throughout the renal parenchyma (HE, 301X).

teguments, lacked body cavities, had abundant parenchymatous matrix, paired ceca, and prominent suckers. Some of the cysts contained only clear space or degenerate cells. Few aggregates of macrophages with intracytoplasmic brown granular pigment (melanomacrophages) sat adjacent to some cysts and within some granulomas.

Contributor's Morphologic Diagnosis:

1. Nephritis, hepatitis, enteritis, branchitis, and oophoritis, multifocal to coalescing, chronic, severe, granulomatous with intralesional acid-fast bacteria
2. Trematodiasis, multifocal, skeletal muscle and body cavity
3. Microsporidial xenomas, multifocal, intestinal mucosa

Contributor's Comment:
Mycobacteriosis and nocardiosis are well-recognized diseases of wild and aquacultured fishes in which actinomycetes cause severe chronic granulomatous systemic disease.[4] Mycobacteriosis is much more common in fish than nocardiosis, but both produce analogous gross and histologic lesions.[10] Bacterial morphology can help to differentiate these, as *Mycobacteria* spp. are non-filamentous, non-branching while *Nocardia* spp. are branching filamentous organisms that may resemble Chinese letters.[11] Further, the Ziehl-Neelsen acid-fast stain is useful for discrimination as *Nocardia* spp. stain poorly or not at all with this stain, and are best visualized with modified acid-fast stains, such as Fite's modified acid-fast stain[10]. Therefore, the bacteria in this case were consistent with *Mycobacteria* sp. and bacterial culture or PCR could provide species-level characterization.

Many non-tuberculous *Mycobacterium* species have been reported to cause disease in fish, although *M. marinum*, *M. chelonea* and *M. fortuitum* are the most common isolates.[6] Transmission occurs principally through ingestion of either contaminated feed, organic debris, or infected carcasses.[14] Prompt removal of dead or moribund fish within a tank is, therefore, of the utmost importance in preventing transmission. The clinical manifestations of mycobacteriosis in zebrafish are often non-specific and may include emaciation, lethargy, abdominomegaly, and changes in swimming behavior.[14] In many cases fish die without exhibiting clinical signs.[14] Chronic stress in zebrafish exacerbates the susceptibility to mycobacteriosis and increases the severity of the disease.[12] This likely played a role in this case as the fish was transported from a natural environment in Thailand to an experimental setting about 5 weeks prior to death. Notably, aquatic mycobacteria such as

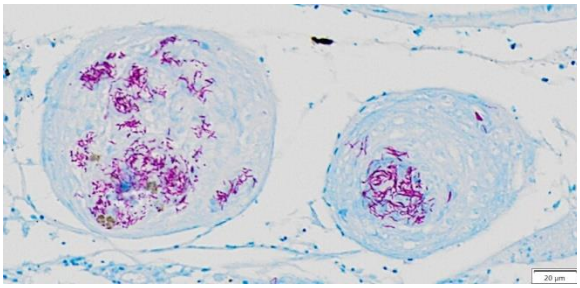

Figure 2-4. Kidney, betta. Numerous acid-fast bacterial rods are present within the granulomas (Ziehl-Nielsen, 301X). (*Photo courtesy of* Wake Forest Baptist Medical Center, Winston-Salem, NC 27157)

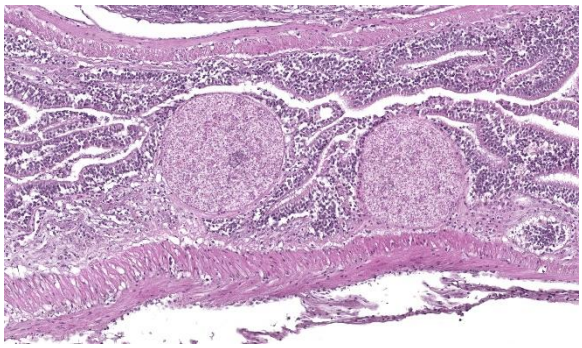

Figure 2-5. Intestine, betta. Two large microsporidial xenomas are present in the intestinal mucosa. A hypertrophied host nucleus is present within the xenoma on the left. (HE, 361X).

M. marinum pose significant zoonotic concerns including cutaneous granulomas and protracted illness, especially in immunocompromised individuals.[6]

Microsporidia are obligate intracellular eukaryotic parasites that can infect a wide range of hosts.[4] Taxonomic classification of microsporidia has shifted over time, and this group is currently considered to be most closely related to fungi based on molecular studies[4]. Fish are hosts to over 150 species of microsporidia in 14 different genera[4]. The genera can be divided according to their ability to form xenomas (*Glugea*, *Tetramicra*, *Loma*, *Ichthyosporidium*, *Jirovecia*, *Microfilum*, *Microgemma* and *Nosemoides* spp.) or not (*Nucleospora*, *Pleistophora*, *Heterosporis* and *Thelohania* spp.). Xenomas are cyst-like structures composed of hypertrophied host cells within which reside microsporidians at various life stages. The infected host cell increases in size due to the proliferating parasites and hypertrophy of the infected cell, including the host cell nucleus as seen in this case.

Coinfection of microsporidia with mycobacteria in fish is not uncommon as microsporidosis is more prevalent in immunosuppressed individuals[12] and mycobacteriosis suppresses immunity.[2] Microsporidial infestation of the gastrointestinal tract when confined to the intestinal mucosa is relatively inconsequential, as was likely in this case, as the surrounding inflammation was minimal.[3] Two microsporidians that cause significant disease in laboratory-reared zebrafish are *Pseudoloma neurophilia* and *Pleistophora hyphessobryconis.*[1] Infection with these can cause subclinical disease or overt illness and may impact experimental outcomes[1]. Extensive surveillance methods and strict biosecurity measures have been outlined to control or prevent microsporidial infection in zebrafish research facilities.[8,13] Further, zebrafish lines that are specific-pathogen free for *Pseudoloma neurophilia* have been developed.[7]

The encysted parasites were consistent with metacercariae, the larval form of digenetic trematodes.[1] The life cycle of most trematodes involves an aquatic snail intermediate host, in which asexual reproduction occurs leading to the release of cercariae into the water.[5] These penetrate the skin or gills of the fish intermediate hosts and often migrate to skeletal muscle for development into encysted metacercariae.[5] These are infective to definite hosts after consumption of the fish.[5] Natural infection is not associated with clinical disease in zebrafish and the inflammatory response is usually minimal due to the parasitic capsule, but the presence should be noted as infection may impact experimental outcomes.[1] Several species of digenean trematodes have metacercarial forms, and common species in freshwater fish in Thailand include *Haplorchis pumilo* and *Centrocestus formosanus.*[9]

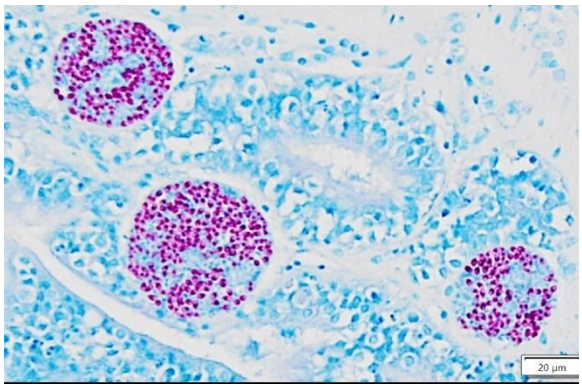

Figure 2-6. Intestine, betta. A Ziehl-Neelsen stain highlights the spores within the xenomas in the intestinal mucosa. (Ziehl-Nielsen, 400X). (*Photo courtesy of* Wake Forest Baptist Medical Center, Winston-Salem, NC 27157)

Contributing Institution:
Wake Forest School of Medicine

Department of Pathology, Section on Comparative Medicine

Medical Center Boulevard, Winston-Salem, NC 27157

www.wakehealth.edu

JPC Diagnosis:

1. Liver, heart, anterior kidney, posterior kidney, coelom, ovary: Granulomatous hepatitis, myocarditis, coelomitis, oophoritis, and nephritis, chronic, multifocal, severe
2. Skeletal muscle and coelom: Granulomas, multiple with encysted metazoans
3. Intestines: Microsporidial xenomas, multiple

JPC Comment:
This second case showcases several classic fish entities while offering some additional points for consideration. We agreed with the contributor that the multifocal granulomatous inflammation best represented mycobacteria, though we did note small numbers of filamentous, slender bacteria on Fite-Faraco that could reflect *Nocardia* spp. that could be differentiated via PCR or culture. Within affected tissues, the presence of pigmented macrophages (melanomacrophages) likely reflects sequestration of iron which is a host defense mechanism against mycobacteria. Although termed "melanomacrophages" in many texts, recent studies have demonstrated that these macrophages contain multiple pigments, to include iron and melanin, and may be more appropriately termed "pigmented macrophages."

The microsporidial xenomas within the intestine were characteristic and easy to identify in this case. Although H&E was sufficient to make the diagnosis, acid-fast stains also sharply outlined spores within affected enterocytes. With the Fite-Faraco stain, morphology was helpful to not confuse a xenoma

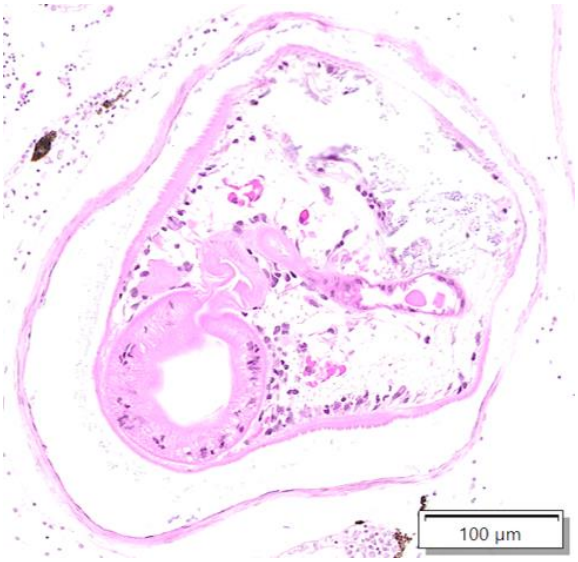

Figure 2-7. Skeletal muscle, betta. Numerous metacercariae are present within the skeletal muscle. (HE, 400X). (*Photo courtesy of* Wake Forest Baptist Medical Center, Winston-Salem, NC 27157)

with adjacent mycobacterial foci given the overlapping distribution of these lesions and staining characteristics. Conference participants also reviewed the anticipated features of non-xenoma forming microsporidial infections which characteristically have wider distribution of spores and associated inflammatory cells instead.

The metazoan parasites of this case gave conference participants pause. The encysted metazoans within skeletal muscle resemble metacercaria, though the metazoans within the coelom appear morphologically distinct and contain 10um round amphophilic to basophilic bodies (possible calcareous corpuscles), consistent with a larval cestode (i.e. a plerocercoid). Tapeworms are a common finding in both free ranging and cultured fish,[15] opening up the possibility that this case is in fact a 'four-fer'.

References:

1. Cartner S, Eisen JS, Farmer SF, Guillemin KJ, Kent ML, Sanders GE. The Zebrafish in Biomedical Research: Biology, Husbandry, Diseases, and Research Applications. 2019.
2. Fenton MJ, Vermeulen MWJI, immunity. Immunopathology of tuberculosis: roles of macrophages and monocytes. 1996;64**:** 683-690.
3. Ferguson HW. *Systemic pathology of fish. A text and atlas of comparative tissue responses in diseases of teleosts.* Iowa State University Press; 1989.
4. Frasca Jr S, Wolf JC, Kinsel MJ, Camus AC, Lombardini ED. Osteichthyes. In: *Pathology of wildlife and zoo animals*. Elsevier; 2018:953-1001.
5. Gardiner C, Poynton SLJ. An atlas of metazoan parasites in animal tissues. 1999.
6. Gauthier DT, Rhodes MWJTVJ. Mycobacteriosis in fishes: a review. 2009;180**:** 33-47.
7. Kent ML, Feist SW, Harper C, et al. Recommendations for control of pathogens and infectious diseases in fish research facilities. 2009;149**:** 240-248.
8. Kent ML, Feist SW, Harper C, et al. Recommendations for control of pathogens and infectious diseases in fish research facilities. 2009;149**:** 240-248.
9. Krailas D, Veeravechsukij N, Chuanprasit C, Boonmekam D, Namchote SJAt. Prevalence of fish-borne trematodes of the family Heterophyidae at Pasak Cholasid Reservoir, Thailand. 2016;156**:** 79-86.
10. Lewis S, Chinabut S. Mycobacteriosis and nocardiosis. In: *Fish diseases and disorders. Volume 3: viral, bacterial and fungal infections*. CABI Wallingford UK; 2011:397-423.
11. Mauldin EA, Peters-Kennedy JJJ, Kennedy, 1 PsPoDAV. Integumentary system. 2016**:** 509.
12. Ramsay J, Watral V, Schreck C, Kent MJJoFD. Husbandry stress exacerbates mycobacterial infections in adult zebrafish, Danio rerio (Hamilton). 2009;32**:** 931-941.
13. Sanders JL, Watral V, Kent MLJIJ. Microsporidiosis in zebrafish research facilities. 2012;53**:** 106-113.
14. Smith SA. *Fish diseases and medicine* CRC Press; 2019.
15. Scholz T, Kuchta R, Oros M. Tapeworms as pathogens of fish: A review. J Fish Dis. 2021 Dec;44(12):1883-1900.

CASE III:

Signalment:
11-year-old, female cockatiel (Nimphicus hollandicus).

History:
This cockatiel was first obtained by the

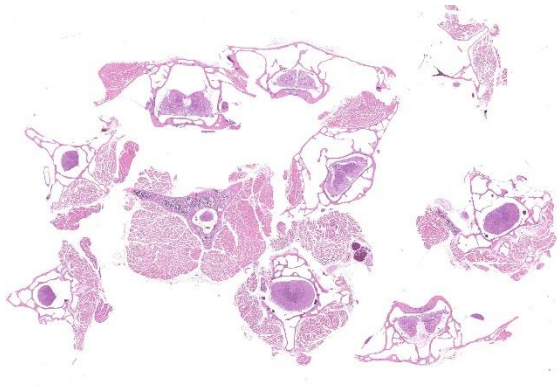

Figure 3-1. Spinal column, cockatiel. Numerous sections from all levels of the spinal column, including spinal cord and surrounding vertebral bodies consisting of pneumatic or hematopoietic bone are submitted for examination. (HE, 8X)

owner in September 2019, approximately 5 months prior to euthanasia. Initial veterinary consultation was sought with the complaint of frequent trembling and shaking. Diagnostic evaluation was initially declined, except for *Chlamydophila* testing pursued at a different clinic (unspecified), which was reported as negative. At subsequent presentation to the submitting veterinarian, the bird was thin (66 g) could barely perch, and seemed painful, with wings drooped forward. On manipulation, the wings were stiff and could not be returned to normal anatomical resting position. Euthanasia was elected.

Gross Pathology:
Examined is the body of a female, 11-month-old, 60 g, Cockatiel with a body condition score of 2 out of 5 (North Carolina Zoo Keel Score) and moderate autolysis. No significant lesions were noted.

Microscopic Description:
Examined are ten cross-sections of spinal column. Throughout all sections of the spinal cord, including cervical, thoracic, lumbar, and sacral regions, virtually all neurons within the gray matter and in the dorsal root ganglia contain large, intracytoplasmic, lamellar to globular, 5-35 µm in diameter, basophilic to eosinophilic structures. These intracytoplasmic structures often have a central, finely granular, pale center (Lafora bodies). Consistently surrounding the structures is a 2-5 µm wide band of finely granular, amphophilic cytoplasm (peripheral lysed axoplasm). Affecting approximately 20% of the axial muscles, muscle fibers are shrunken in multifocal random areas. Affected fibers have hypereosinophilic sarcoplasm with poorly defined cross striations and enlarged nuclei with open chromatin.

Period acid-Schiff staining with and without diastase applied to formalin-fixed, decalcified (formalin/formic acid solution), paraffin-embedded spinal column tissue highlights intensely PAS-positive, 5-35 µm intraneuronal cytoplasmic inclusions which are resistant to diastase digestion.

Staining of the same tissue using Luxol fast blue with cresyl violet and Acian blue (pH2.5) reveals bright violet and deep blue staining of the described inclusions, respectively.

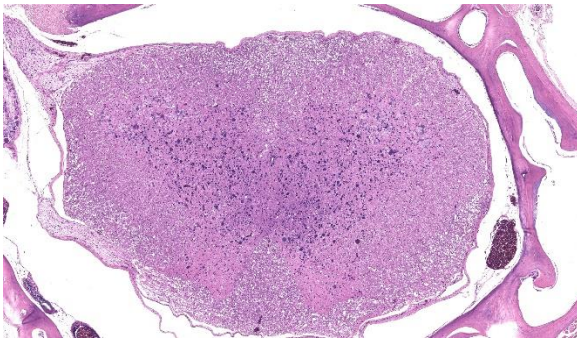

Figure 3-2. Spinal cord, cockatiel. There are numerous 10-30um deeply basophilic intracytoplasmic inclusions within neurons (which obviously results in the grey matter being disproportionately affected) (HE, 8X)

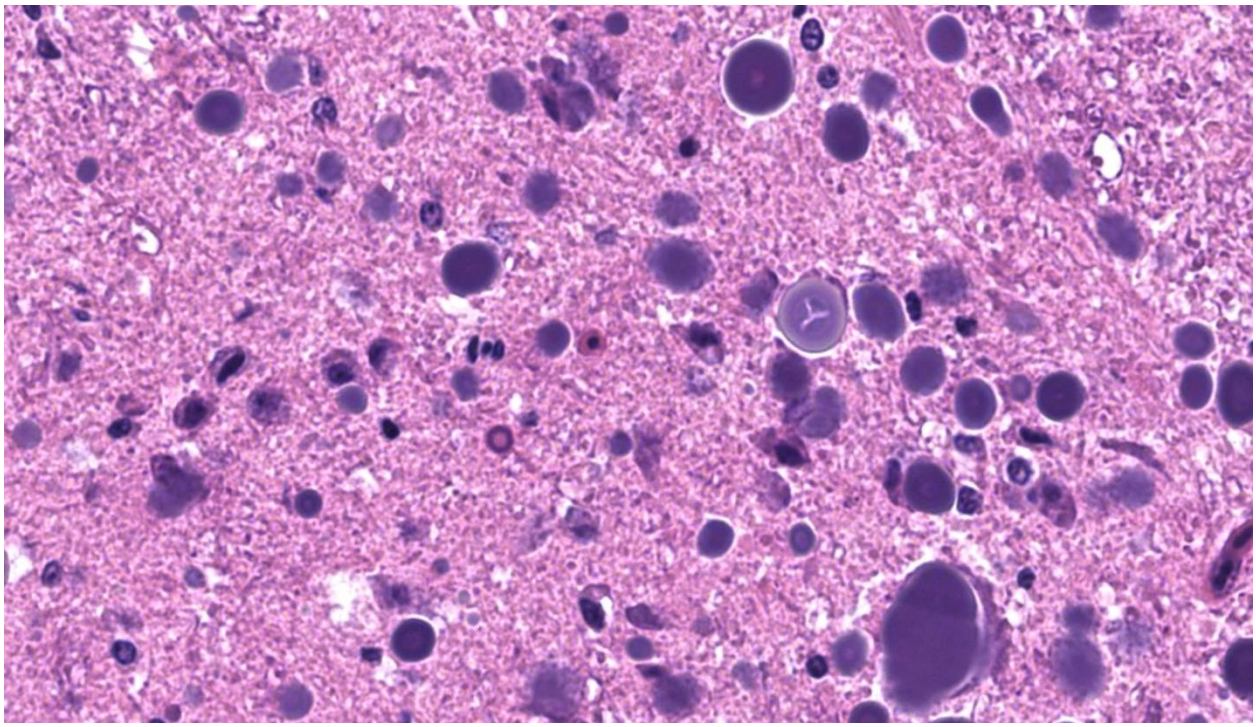

Figure 3-3. Spinal cord, cockatiel. Grey matter neurons contain numerous amphophilic to basophilic lamellated intracytoplasmic polyglucosan (Lafora) bodies. (HE, 381X)

Contributor's Morphologic Diagnosis:
Spinal cord: Numerous polyglucosan bodies consistent with Lafora disease

Contributor's Comment:
Lafora disease (neuronal glycoproteinosis) is a rare condition variably characterized by myoclonus, ataxia, weakness, behavioral abnormalities, and seizures in affected animals.[1,3-6,9,10] These clinical signs result from abnormal carbohydrate metabolism and accumulation within the perikaryon, dendrites, and axons of neurons as well as freely in the neuroparenchyma of both central and peripheral nervous tissue.[2] Inclusion bodies can also be found in other organ systems including skeletal and cardiac muscle, skin, and liver. In this case, inclusions were present in the cerebrum, spinal cord, dorsal root ganglia, perirenal ganglia, and myenteric ganglia.

These inclusion bodies, also called Lafora bodies, are spherical, basophilic, 5-35 µm, PAS-positive and diastase-resistant, and also display staining with Cresyl violet, Alcian blue pH 2.5, Bests carmine, methenamine silver, and Weils (6). Lafora bodies are composed of polyglucosan, an abnormal form of glycogen with low numbers of branches and very long glucose chains.[8] On electron microscopy, Lafora bodies are composed of radiating, branched filaments surrounding a dense central core.[9]

Disease associated with Lafora body accumulation has been described in humans, dogs, cockatiels, cattle, a fox, a cat, and a flying fox,[1,3-6,8,9] with associated genetic mutations identified in humans, miniature wirehaired dachshunds, a basset hound, and beagles.[4,7] In humans, Lafora disease is a fatal autosomal-recessive condition resulting from loss of function sequence variations in the genes *EPM2A* (encodeing laforin) or *NHLRC1* (also *EMP2B*, encodes malin),[4] encoding glycogen synthesis regulators laforin and malin, and

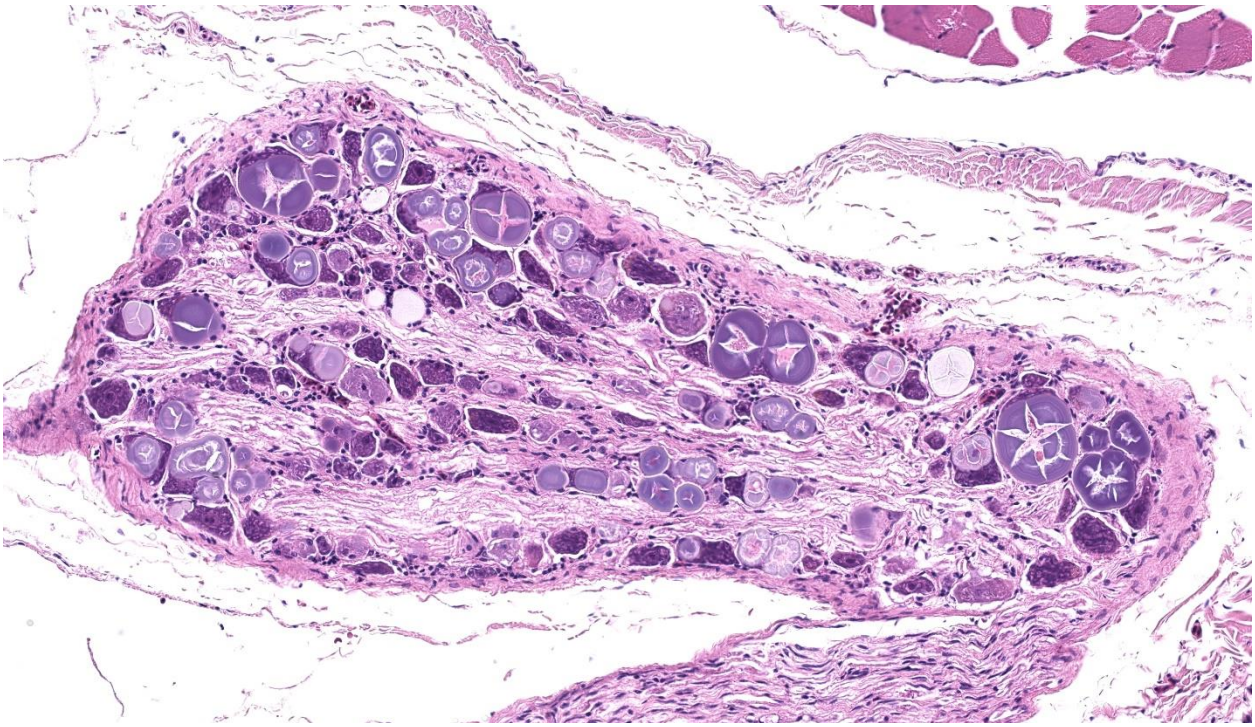

Figure 3-4. Dorsal root ganglion, cockatiel. Neurons in the dorsal root ganglion also contain prominent intracytoplasmic polyglucosan bodies.

the latter of which has also been implicated in dogs with a massive expansion of a 12 bp repeat in the gene.[4,7]

Contributing Institution:
Cornell University College of Veterinary Medicine, Department of Biomedical Sciences, Section of Anatomic Pathology

https://www.vet.cornell.edu/departments/biomedical-sciences/section-anatomic-pathology

JPC Diagnosis:

1. Spinal cord, spinal nerves, dorsal root ganglion: Intracytoplasmic polyglucosan (Lafora) bodies, numerous, with mild spongiosis
2. Spinal muscles: Atrophy, multifocal, mild

JPC Comment:
We have seen Lafora disease several times in conference, to include in an ox (WSC 2017-2018, Conference 17, Case 4) and in multiple dogs (WSC 2021-2022, Conference 7, Case 3; WSC 2012-2013, Conference 22, Case 4). The present case in a bird is interesting, though as the contributor notes this condition has previously been described in a cockatiel.[1] There is also a recent case report in a toucan from Brazil with features that mirror this case.[11]

Inclusion bodies were numerous across the provided sections of spinal cord and spinal nerves and stained readily with PAS, Alcian blue, and Luxol fast blue. We considered whether these inclusions might also be similarly present within skeletal muscle given that select myocytes also contain amphophilic globoid material. However, these myocyte inclusions did not reliably stain with PAS or Alcian blue (or at all with LFB), so

we were unable to confirm this impression. As these stains are non-specific, it is possible that inclusions in myocytes may represent an entirely different material.

We added a separate morphologic diagnosis of muscular (neurogenic) atrophy that corresponds to the decreased body condition and inability of this animal to perch. This is best observed from subgross as shrunken, condensed myofibers. Additionally, there is also medullary bone (i.e., endostosis) present which is a normal/expected finding for a mature female bird. This amphophilic to basophilic bone is deposited on the outer aspects of the medullary trabeculae and represents a dynamic calcium depot for the egg-laying cycle. Medullary bone has also been described as a premonitory sign of testicular neoplasms in male birds.[12]

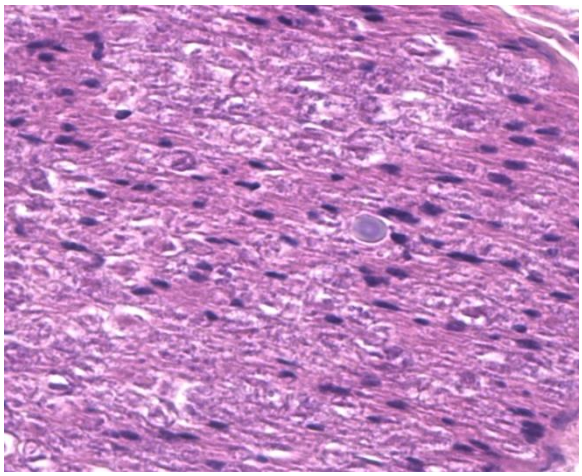

Figure 3-5. Spinal nerve, cockatiel. Rare polyglucosan bodies are present in spinal nerves. (HE, 1446X)

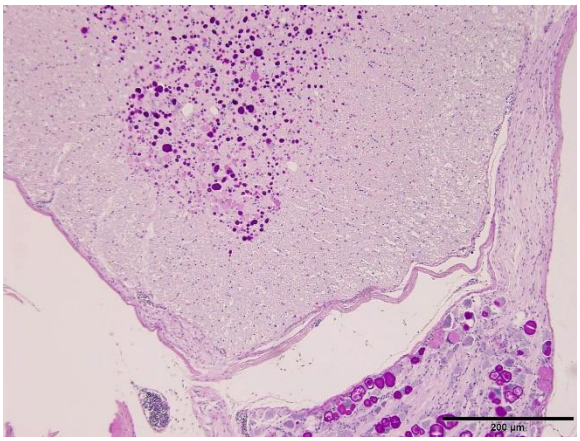

Figure 3-6. Spinal cord and dorsal root ganglia. Polyglucosan bodies stain strongly positive on periodic acid-Schiff preparations. (PAS, 100X)

References:

1. Britt JO, Paster MB, Gonzales C. Lafora Body Neuropathy in a Cockatiel. *Comp Anim Pract* 19:31–33, 1989.
2. Cantile C, Youssef S. Nervous system. In: Maxie MG, ed. *Jubb, Kennedy, and Palmer's Pathology of Domestic Animals*. 6th ed. Vol 1. St. Louis, MO: Elsevier; 2016: 255, 292.
3. Gabor LJ, Srivastava M. Polyglucosan Inclusions (Lafora Bodies) in a Gray-Headed Flying Fox (Pteropus Poliocephalus). *J Vet Diagn Invest*. 22:303–304, 2010.
4. Hajek I, Kettner F, Simerdova V, et al. NHLRC1 repeat expansion in two beagles with Lafora disease. *J Small Ani Pract* 2016; 57:650–652.
5. Hall DG, Steffens WL, Lassiter L. Lafora Bodies Associated with Neurologic Signs in a Cat. *Vet Pathol* 35:218–220, 1998.
6. Honnold SP, Schulman FY, Bauman K, Nelson K. Lafora's-Like Disease in a Fennec Fox (Vulpes zerda). *Journal of Zoo and Wildlife Medicine*. 2010; 41:530–534.
7. Lohi H, Young EJ, Fitzmaurice SN, et al. Expanded Repeat in Canine Epilepsy.

Science 307:81–81, 2005.
8. Serratosa JM, Minassian BA, Ganesh S. Progressive Myoclonus Epilepsy of Lafora. In: Noebels J, Avoli M, Rogawski M, Olsen R, Delgado-Escueta A, eds. *Jasper's Basic Mechanisms of the Epilepsies*. Oxford University Press; 2012:874–877.
9. Simmons MM. Lafora Disease in the Cow? *J Comp Path* 110:389–401, 1994.
10. Swain L, Key G, Tauro A, et al. Lafora disease in miniature Wirehaired Dachshunds. *PLOS ONE* 12:e0182024, 2017.
11. Santana CH, et al. Lafora's disease in a free-ranging toco toucan (Ramphastos toco) with neurologic disease. *Brazilian J Vet Path*. 2023; 16(2):144-147.
12. Hoggard NK, Craig LE. Medullary bone in male budgerigars (Melopsittacus undulatus) with testicular neoplasms. *Vet Pathol*. 2022 Mar;59(2):333-339.

CASE IV:

Signalment:
Juvenile, male, *Megaptera novaeangliae*, humpback whale.

History:
A juvenile male humpback whale, measuring 11 meters in length, was found stranded alive in the coast of southern Brazil. Due to its deteriorated health and unsuccessful attempts to return the animal to the ocean over two days, it was euthanized.

Gross Pathology:
At necropsy, the humpback whale was in poor body condition. Multiple marine crustaceans (*Thoracica* sp.) were adhered to the skin in the submandibular and ventral neck region. Upon internal examination, significant changes were noted in the liver. The hepatic capsula appeared opaque and whitish. The right hepatic lobe was moderately reduced in size and with multifocal and elevated areas, which upon sectioning corresponded to biliary ducts with thickened walls and dilated lumen. The lumen was filled with bile and with numerous trematodes measuring 1.5-4 cm in length, 0.3-0.4 cm in width, with flattened and leaf-shaped morphology, containing oral and ventral suckers. Morphological and molecular characterization classified these parasites as *Brachycladium goliath*. Inside the renal veins, a high number of nematodes of up to 30 cm in length, morphologically compatible with *Crassicauda* sp., were observed. Additional macroscopical findings included the multiple accessory spleens measuring from 1.5 to 5 cm in diameter. Furthermore, the small intestine showed multifocal to coalescent areas of hemorrhages (petechias and ecchymosis) and the mucosa was markedly red with cestodes measuring approximately 80 cm in length in the intestinal lumen. The gross examination of remaining organs was unremarkable.

Figure 4-1. Cerebrum, humpback whale. One section of telencephalon is submitted for examination. (HE, 6X)

Laboratory Results:
RT-Nested-PCR: positive for cetacean morbillivirus (CeMV).

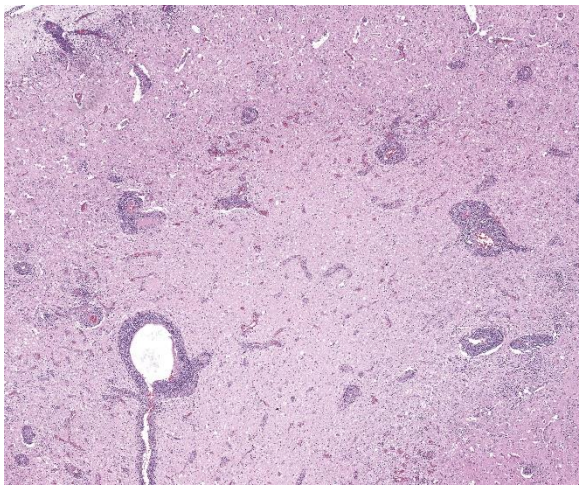

Figure 4-2. Cerebrum, humpback whale. Multifocally, there are prominent cuffs of inflammatory cells within Virchow-Robins spaces as well as gliosis and rarefaction of the adjacent neuropil. (HE, 50X)

Immunohistochemistry (IHC): IHC anti-*Morbillivirus* (anti-canine distemper virus, monoclonal) revealed moderate cytoplasmic immunolabelling in astrocytes, neuronal cell bodies, and axons).

Microscopic Description:
Brain: in the telencephalic cortex, mainly in the grey matter, there is marked and multifocal inflammatory infiltration of lymphocytes and plasma cells surrounding blood vessels (perivascular cuffings), frequently extending into the adjacent neuropil where moderate vacuolization is also frequent. Additionally, there are multifocal areas of moderate gliosis. Mild to moderate neuropil rarefaction (malacia) is evident in some areas, where there is neuronal necrosis, characterized by neurons with hypereosinophilic and retracted cytoplasm and absent or pyknotic nucleus. Moderate infiltration of Gitter cells and occasional axonal spheroids is also present. Occasional intracytoplasmic and intranuclear eosinophilic inclusion bodies are seen in neurons within affected areas. Similar lesions are also present in the brainstem and white matter of the cerebellum (slides not submitted).

Contributor's Morphologic Diagnosis:
Brain: encephalitis, lymphoplasmocitic, multifocal, marked, subacute, with mild and multifocal malacia, Gitter cell inflammatory infiltration, neuronal necrosis and occasional intracytoplasmic and intranuclear eosinophilic inclusion bodies.

Contributor's Comment:
Viruses from the genus *Morbillivirus* belong to the family Paramyxoviridae and order Mononegavirales. These are pleomorphic but frequently spherical, approximately 150 nm in diameter, RNA viruses with a nonsegmented and single-stranded linear genome.[11] Morbilliviruses can affect different species of mammals, including humans. The measles virus (MeV) is a human pathogenic *morbillivirus* that causes measles, a disease with high rates of morbidity and significant childhood mortality. Rinderpest, also known as "cattle plague", the peste des petits ruminants, and canine distemper are other notable diseases caused by morbilliviruses in mammals.[16]

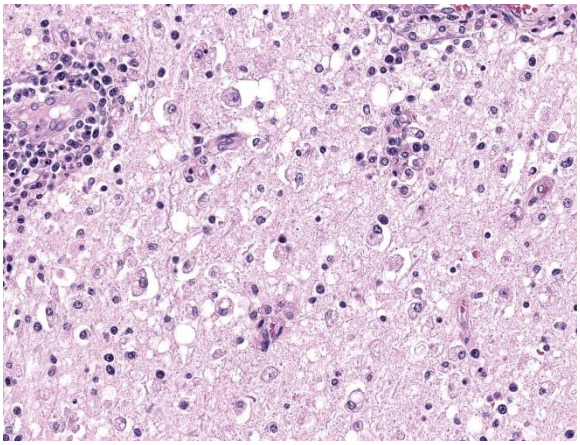

Figure 4-3. Cerebrum, humpback whale. Higher magnification of the inflammatory changes in the cerebral cortex (HE, 450X)

Morbillivirus infections resulting in massive strandings have been reported in aquatic mammals in recent decades.[3] The first description occurred in pinnipeds during 1988 and 1989 in northwest Europe, where nearly 18,000 harbor seals (*Phoca vitulina*) and hundreds of grey seals (*Halichoerus grypus*) died due to the infection by a morbillivirus identified as *Phocine Distemper Virus* (PDV).[7,9] Meanwhile, in cetaceans, the first report of a *morbillivirus* infection was described in six harbor porpoises (*Phocoena phocoena*) in Ireland in late 1988. This infection was related to the *Porpoise Morbillivirus* (PMV), a strain from the *Cetacean Morbillivirus* (CeMV). A couple of years later, infections by this virus were reported in harbor porpoises from various countries across Europe.[9,17] Since then, many strains of CeMV have been recorded causing stranding and deaths in odontocetes. However, reports in mysticetes are rare and include few cases in fin whales (*Balaenoptera physalus*)[8] and more recently, in two humpback whales in Brazil.[1]

Morbilliviruses are known to be lymphotropic and epitheliotropic, and studies have indicated that the pathogenesis associated to the CeMV infection resembles what is commonly seen in other morbillivirus infections in animals and humans.[10] When infected by CeMV, cetaceans can develop a marked interstitial pneumonia and/or non-suppurative encephalitis. Animals that survive this acute stage may acquire opportunistic infections due to the immunosuppression caused by the virus. Some animals may still have lesions of meningoencephalitis associated with demyelination. However, animals that clear out the systemic infection may develop a neurological disease with lesions restricted to the brain. In these cases, the virus is detected only in the CNS, and cytoplasmic or nuclear eosinophilic inclusion bodies are occasionally found in neurons, and astrocytes.[3] In a

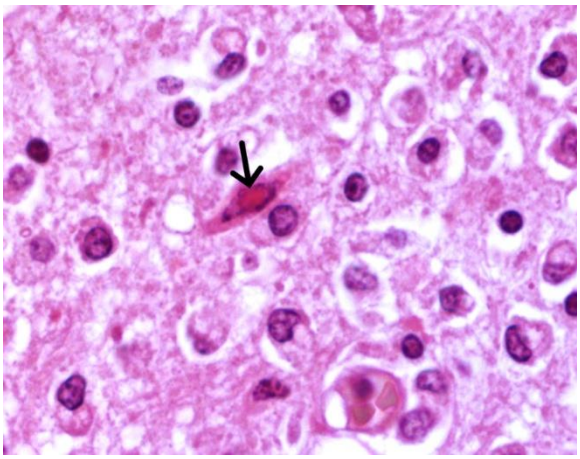

Figure 4-4. Cerebrum, humpback whale. An intranuclear eosinophilic inclusion body (arrow) is seen in a neuron. (HE, 400X) (*Photo courtesy of*: Faculdade de Veterinária, Universidade Federal do Rio Grande do Sul, http://www.ufrgs.br/patologia)

similar way, in humans with measles, the MeV infection can lead to encephalitis with inclusion bodies, particularly in immunosuppressed individuals, or to panencephalitis in persistently infected children.[5] Neurological involvement is common in carnivore morbilliviruses, as in the canine distemper, which can affect not only domestic dogs, but a broad range of domestic and wild carnivores.[4] In dogs, a strong immune response typically clears the canine distemper virus (CDV) from the tissues, resulting in fully recovery. On the other hand, with a weak immune response, the virus can penetrate epithelial tissues and the CNS, leading to clinical signs that typically appear around 20 days post-infection.[17] Neurologic signs can also develop later, due to a demyelination induced by the CDV.[14]

In this humpback whale, no macroscopic changes were seen during the evaluation of the encephalon, corroborating to previous studies on morbillivirus infections affecting the CNS of other species, such as dogs, in which neurological involvement is frequent.[15] On histological examination, CeMV infection

in cetaceans resembles the lesions described in humans and animals infected by morbilliviruses, primarily characterized by multiple mononuclear perivascular cuffings, microgliosis, neuronophagia and demyelination in the cerebral cortex. The white matter may also show areas of malacia. Intracytoplasmic and/or intranuclear eosinophilic inclusions bodies are frequently seen.[6] Furthermore, when IHC anti-*Morbillivirus* is applied, a marked immunolabelling in neurons, axons, and dendrites, as well as in astrocytes and microglial cells is described in cetaceans.[6] This is similar to what has been reported in dogs infected by CDV.[15] In the humpback whale from the present case, immunolabeling was evident in astrocytes and neurons from the telencephalon, cerebellum and brainstem, corroborating the aforementioned studies.

Differential diagnoses for mononuclear meningoencephalitis in cetaceans are limited, but they include infections caused by herpesvirus[13] and flaviviruses such as the West Nile Virus.[12] However, the Cetacean Morbillivirus remains as the most common cause of viral meningoencephalitis in cetaceans.

Contributing Institution:

Faculdade de Veterinária

Universidade Federal do Rio Grande do Sul

Setor de Patologia Veterinária

http://www.ufrgs.br/patologia

JPC Diagnosis:

Cerebrum: Meningoencephalitis, lymphoplasmacytic and necrotizing, chronic, diffuse, moderate, with neuronal necrosis, Gitter cells, and rare intracytoplasmic and intranuclear viral inclusions.

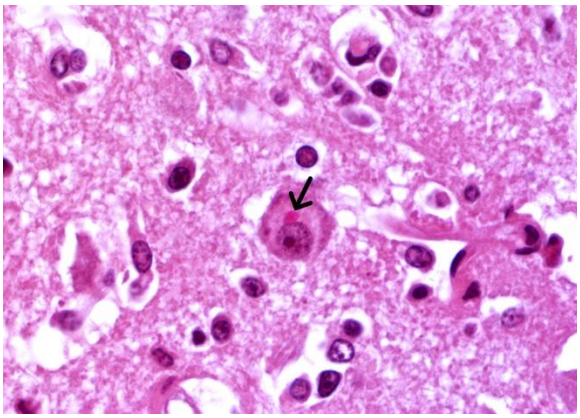

Figure 4-5. Cerebrum, humpback whale. An eosinophilic inclusion body (arrow) is evident in the cytoplasm of a neuron (HE, 400X) (*Photo courtesy of*: Faculdade de Veterinária, Universidade Federal do Rio Grande do Sul, http://www.ufrgs.br/patologia)

JPC Comment:

The final case of this conference is a (rarely seen) well-preserved whale brain. Dr. Terio noted that the brain condition in this case is very good – that this animal was euthanized and immediately necropsied is helpful for appreciating the microscopic features that the contributor nicely captures. Difficulty in accessing the brain (especially in a stranding event) combined with carcass deterioration typically confound examination in wild whales.

Microscopic features of this case mirrored morbillivirus infection in other species. Perivascular cuffing, gliosis (glial nodules), and neuronal necrosis were readily apparent, though viral inclusions within the cytoplasm and nucleus were rare which Dr. Terio confirmed is usually the case in the brain. Inclusions may be more prominent within bronchiolar epithelium in animals with respiratory changes. Viral syncytial cells were also infrequent in our section, though they too are typically more prominent in other tissues. This can be a helpful ancillary finding in cases with marked lymphoid depletion and autolysis as syncytial cells may still be discernable.

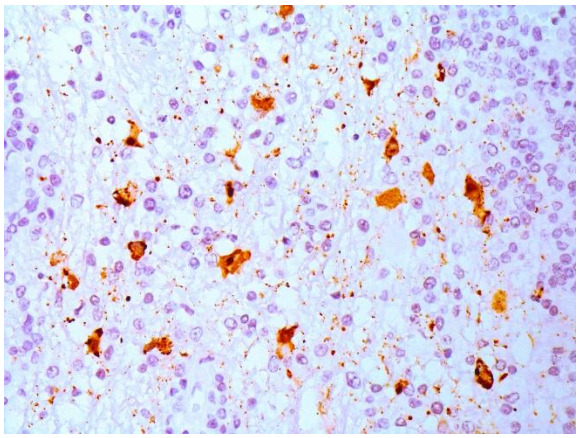

Figure 4-6. Cerebrum, humpback whale. Marked immunolabelling is seen in the cytoplasm of neurons and astrocytes in the IHC (anti-*Morbillivirus* , 400X) (HE, 400X) (*Photo courtesy of*: Faculdade de Veterinária, Universidade Federal do Rio Grande do Sul, http://www.ufrgs.br/patologia)

Conference participants discussed potential comorbidities in cetacean morbillivirus cases. Coinfection with *Brucella* (e.g. *B. ceti*) also causes neuropathology[18] and may be aided by concurrent lymphoid depletion arising from CeMV infection. Joint infection is another common sequalae of *Brucella*. Microscopically, there is marked infiltration of the meninges by lymphocytes; in acute cases, bacteria and neutrophils may be appreciated in Dr. Terio's experience. Fungal infections are also abetted by lymphoid depletion, though there were no characteristic features in this case and we did not pursue any special stains.

References:

1. Amorim DB, de Camargo LJ, Ribeiro PR, et al. Characterization of Cetacean Morbillivirus in Humpback Whales, Brazil. Emerg Infect Dis. 2024;30(6).
2. Van Bressem MF, Duignan PJ, Banyard A, et al. Cetacean morbillivirus: Current knowledge and future directions. Viruses. 2014;6(12):5145–5181.
3. Deem SL, Yates LH, Rebecca A, Montali, Richard J. Canine distemper in terrestrial carnivores: a review. J Zoo Wildl Med. 2000;31(4):441–451.
4. Fisher DL, Defres S, Solomon T. Measles-induced encephalitis. Int J Med. 2015;108(3):177–182.
5. Guardo G Di, Marruchella G, Agrimi U, Kennedy S. Morbillivirus Infections in Aquatic Mammals: A Brief Overview. J Vet Med. 2005;52:88-93.
6. Heide-Jorgensen MP, Harkonen T, Dietz R, Thompson PM. Retrospective of the 1988 European seal epizootic. Dis Aquat Organ. 1992;13(1):37–62.
7. Jo WK, Kruppa J, Habierski A, et al. Evolutionary evidence for multi-host transmission of cetacean morbillivirus. Emerg Microbes Infect. 2018;7(1):201.
8. Kennedy S. Morbillivirus Infections in Aquatic Mammals. J Comp Path. 1998;119(3):201-225.
9. Kennedy S, Smyth JA, Cush PF, Mcaliskey M, Mccullough SJ, Rima BK. Histopathologic and Immunocytochemical Studies of Distemper in Harbor Porpoises. Vet Pathol. 1991;28(1):1-7.
10. Lamb RA, Parks GD. Paramyxoviridae: the viruses and their replication. In: Fields BN, Knipe DM, Howley PM, eds. Fields Virology. 6th ed. Lippincott-Raven Press; 2013.
11. Leger J, Wu G, Anderson M, Dalton L, Nilson E, Wang D. West Nile virus infection in killer whale, Texas, USA, 2007. Emerg Infect Dis. 2011;17(8):1531–1533.
12. Sierra E, Fernández A, Fernández-Maldonado C, et al. Molecular Characterization of Herpesviral Encephalitis in Cetaceans: Correlation with Histopathological and Immunohistochemical Findings. Animals. 2022;12(9):1149.
13. Skyes JE, Vandevelde, M. Canine Distemper Virus Infection. In: Skyes JE. Greene's Infectious Diseases of the Dog and Cat. 5th ed. Elsevier; 2023.
14. Sonne L, Oliveira EC, Pescador CA, et al.

Achados patológicos e imuno-histoquímicos em cães infectados naturalmente pelo vírus da cinomose canina. Pesq Vet Bras. 2009;29(2):143–149.
15. De Vries RD, Paul Duprex W, De Swart RL. Morbillivirus infections: An introduction. Viruses. 2015;7(2):699–706.
16. Welsh MJ, Lyons C, Trudgett A, Rima BK, Mccullough SJ, Orvelp C. Characteristics of a cetacean morbillivirus isolated from a porpoise (Phocoena phocoena). Arch Virol. 1992;125(1-4):305-311.
17. Winters KA, Mathes LE, Krakowka S, Olsen RG. Immunoglobulin class response to canine distemper virus in gnotobiotic dogs. Vet Immunol Immunopathol. 1983;5(2):209–215.
18. Davison NJ, Brownlow A, Doeschate MT, Dale EJ, Foster G, Muchowski J, Perrett LL, Rocchi M, Whatmore AM, Dagleish MP. Neurobrucellosis due to Brucella ceti ST26 in Three Sowerby's Beaked Whales (Mesoplodon bidens). J Comp Pathol. 2021 Jan;182:1-8.

Joint Pathology Center
Veterinary Pathology Services

WEDNESDAY SLIDE CONFERENCE 2024-2025

Conference #21 26 March 2025

CASE I:

Signalment:
9-month-old female Sprague Dawley rat (*Rattus norvegicus*), SRG genotype (Rag2 & IL-2Rγ knockout)

History:
This rat was part of a cancer implantation study using a novel cell line. Cancer cells were implanted around 3-months-old but failed to grow. The rat was monitored for delayed growth for an additional 6 months until its presentation to clinical staff. Weekly monitoring of this rat identified a drop in weight which persisted over a 3 week span despite clinical interventions, and the rat was ultimately euthanized.

Figure 1-1. Urinary bladder, rat. The urinary bladder was markedly distended by large amounts of red-tinged fluid. (*Photo courtesy of:* University of Michigan, Unit for Laboratory Animal Medicine, Pathology Core, https://animalcare.umich.edu/busines s-services/ulam-pathology-core/)

Gross Pathology:
The urinary bladder was markedly distended by large amounts of red-tinged fluid, with blood-clots both suspended and adherent to the mucosal surface. The mucosal surface was red and roughened. Transmurally the bladder wall was red to black, and this change extended distally through the trigone and throughout the length of the urethra. At the distal end of the urethra, just proximal to the external genitalia were two large (3-5mm diameter), round, smooth, hard calculi (stones) occluding the lumen of the urethra. The stones were embedded within the mucosa and did not excise easily. Both ureters were distended with fluid (hydroureter). Both kidneys were moderately pale tan and had mildly bosselated subcapsular surfaces. There was mild to moderate dilation of the renal pelvis of both kidneys (hydronephrosis). From the renal pelvis, extending proximally through the renal papilla, medulla, and cortex is an irregular, friable, focal region of pallor.

Figure 1-2. Urinary bladder, rat. Two 3-5mm diameter, calculi are embedded in the urethral mucosa and occlude the lumen. (*Photo courtesy of:* University of Michigan, Unit for Laboratory Animal Medicine, Pathology Core, https://animalcare.umich .edu/business-services/ulam-pathology-core/)

Laboratory Results:

Bacteria Culture & Sensitivity: Tissue (kidney)

- *Staphylococcus xylosus* - Numerous
- *Enterobacter cloacae* complex - Few

Pneumocystis spp. Polymerase chain reaction (PCR): Tissue (lung)

- Negative

Microscopic Description:

Cytology (DifQuick):

Urine – Cytological preps of urine collected during necropsy showed large numbers of viable and degenerate neutrophils, streaming cellular debris, large numbers of bacterial cocci, and crystals. Bacteria are occasionally observed within neutrophils. Crystals are colorless and rhomboid (presumed struvite).

Histology (H&E):

Kidney - Extending from the renal pelvis into the medulla is a regionally extensive area of necrosis and marked suppurative inflammation with large numbers of cocci bacteria admixed throughout the cellular debris and neutrophils (pyelonephritis). The renal parenchyma in the vicinity of this lesion is characterized by interstitial edema, tubular degeneration and necrosis, with tubule lumina often containing eosinophilic proteinaceous fluid, neutrophils, cellular debris, and clusters of bacteria.

In addition to the pyelonephritis described above, there is mild bosselation of the capsular surface of the renal cortex. The cortical and medullary interstitium is expanded by extensive fibrosis with low numbers of mixed mononuclear inflammatory cells. Interstitial fibrosis often replaces tubular profiles. Remaining tubules frequently have markedly dilated lumens which range from empty to variably filled with eosinophilic proteinaceous fluid, fibrillar hyaline casts, or deeply basophilic granular material (mineralization). Tubular epithelial cells range from flattened /

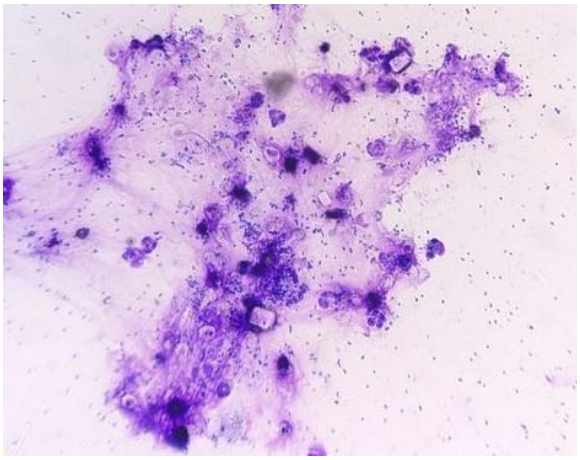

Figure 1-3. Urinary bladder, rat. Urine cytology shows large numbers of viable and degenerate neutrophils, streaming cellular debris, large numbers of bacterial cocci, and crystals. Crystals are colorless and rhomboid (presumed struvite) (*Photo courtesy of:* University of Michigan, Unit for Laboratory Animal Medicine, Pathology Core, https://animalcare.umich.edu/business-services/ulam-pathology-core/)

attenuated (atrophy) to swollen and vacuolated (degeneration) or are brightly eosinophilic, faded (lysis), and/or sloughed (necrosis). Glomeruli are frequently affected by one or more of the following changes: Dilation of the urinary space, marked global fibrosis of glomerular tufts (glomerulosclerosis), obsolescence of glomerular tufts, adherence of tufts to Bowman's capsule (synechiae), thickening of Bowman's capsule basement membrane.

Contributor's Morphologic Diagnosis:

1. Kidney: Pyelonephritis, severe, acute, necro-suppurative, with intralesional cocci bacteria (Gram positive)
2. Kidney: Nephropathy, chronic, severe, with multifocal global glomerulosclerosis, periglomerular to interstitial fibrosis, tubular degeneration/necrosis with ectasia and proteinosis, and mild interstitial lymphohistiocytic nephritis (Chronic Progressive Nephropathy)

Figure 1-4. Urinary bladder, rat. There is an area of necrosis extending from the renal pelvis to the cortex. (*Photo courtesy of:* University of Michigan, Unit for Laboratory Animal Medicine, Pathology Core, https://animal-care.umich.edu/business-services/ulam-pathology-core/)

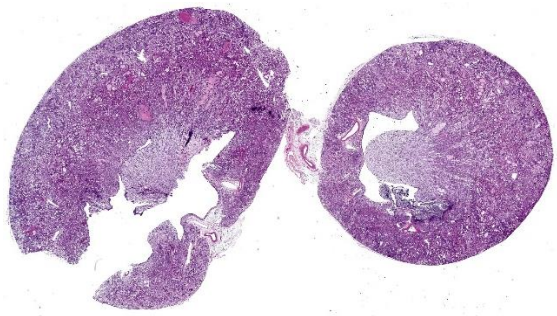

Figure 1-5. Urinary bladder, rat. Two sections of kidney are submitted for examination. Subgross lesions include tubular ectasia and interstitial fibrosis characteristic of chronic progressive nephropathy. The renal pelvis is mildly dilated and contains abundant cellular infiltrate. (HE, 8X)

Contributor's Comment:

This case highlights the importance of using a range of diagnostic techniques—including cytology, special stains, and culture—alongside standard necropsy and histology to fully understand pathological processes. It serves as a valuable reminder to students to utilize all available tools rather than relying too heavily on one method. The gross identification of pyelonephritis and uroliths led to cytological identification of crystalluria consistent with struvite (triple phosphate/magnesium phosphate) crystals, which suggests the presence of urease producing bacteria. Common urease-producing bacteria associated with struvite crystalluria include: *Proteus* spp. (gram-negative bacillus), *Klebsiella* spp. (gram-negative bacillus), *Mycoplasma* spp. (gram-equivocal, pleomorphic), *Corynebacterium urealyticum* (gram-positive bacillus), and *Staphylococcus* spp. (gram-positive cocci). Histological evaluation and Gram staining highlighted clusters of gram-positive cocci, suggesting *Staphylococcus* spp. as the most likely agent from our differential list of urease-producing bacteria. Lastly, bacterial

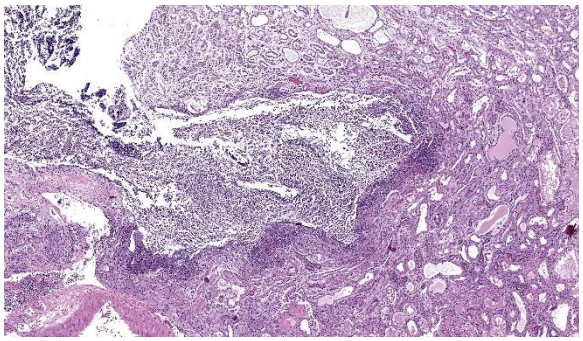

Figure 1-6. Urinary bladder, rat. There is necrosis of the renal papilla with extension into the overlying cortex. (HE, 88X)

cultures confirmed *Staphylococcus* (specifically *S. xylosus*) as the gram-positive cocci bacteria observed.

In laboratory mice and rats, pyelonephritis is most commonly caused by ascending infections from commensal or gastrointestinal bacteria.[3] Urolithiasis is generally considered uncommon, but in cases of pyelonephritis becomes more common when the bacterial culprit is one of those mentioned previously (urease-producing). *Staphylococcus xylosus*, isolated in this case, is both a common commensal organism of rodents and is urease-producing.[3,5,7]

Opportunistic infections from commensal organisms such as *S. xylosus* are likely exacerbated by immunodeficiencies/modulation. In the case of laboratory animals, cystitis and urolithiasis related to *S. xylosus* has been described in nude mice[7] and severe dermatitis has been described in Rag2 / IL-2Rγ knockout strains of mice[1] which are the same genes knocked out in the SRG strain rat utilized in this study.

The second morphological diagnosis proposed in this case is consistent with Chronic Progressive Nephropathy (CPN). This condition is one of the most well-described lesions in laboratory rats.[3,5] In particular, CPN is exceptionally common in Sprague-Dawley and Fischer 344 strains, with many rats developing clinically significant changes by 8-10 months old, and some developing histologic changes as early as 2-3 months.[5] While CPN is generally thought of as a spontaneous or age related disease, it has been recognized that high-protein diets worsen the disease severity.[3,5] Despite some persistent ambiguities in the pathogenesis of the condition, any resident or pathologist working in laboratory settings quickly becomes familiar with CPN and the spectrum of lesions it presents with, making it both a "classic" lesion as well as a practically relevant one.

Contributing Institution:
University of Michigan, Unit for Laboratory Animal Medicine, Pathology Core

https://animalcare.umich.edu/business-services/ulam-pathology-core/

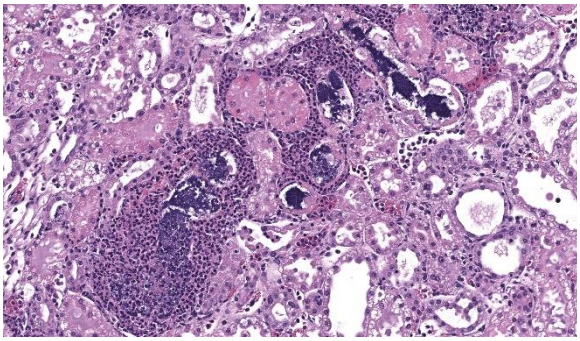

Figure 1-7. Urinary bladder, rat. Neutrophils and bacterial colonies ascend along renal tubules. (HE, 88X)

JPC Diagnosis:

1. Kidney: Tubular degeneration, necrosis, and regeneration, diffuse, moderate, with chronic interstitial lymphoplasmacytic nephritis.
2. Kidney: Pyelonephritis, necrotizing and suppurative, subacute, multifocal to coalescing, marked, with intratubular cocci, and mild hydronephrosis.

JPC Comment:

This week's moderator was Dr. Enrico Radaelli from the University of Pennsylvania's Comparative Pathology Core who led conference participants through a laboratory animal-centric conference with a few surprises. This first case is a succinct presentation with gross images and cytology that reinforce key slide interpretation. In particular, the history of urolithiasis and hydronephrosis is helpful in appreciating the irregular shape of the renal pelvis (especially in longitudinal section) and regional papillary necrosis which are discernable from the gross image. Gram-positive cocci are also numerous and consistent with the immunosuppressed state of this animal. We felt that pyelonephritis was the primary lesion in this case overall.

There was healthy debate among the group on our morphologic diagnosis. As the contributor notes, CPN is a common background lesion that inevitably encompasses changes at all levels of the nephron. We agree that these changes are present in this rat, though the severity was moderate for us compared with other conference cases we have reviewed (see Conference 23, Case 3, WSC 2012-2013 among others). We ran a Masson's trichrome stain which highlighted the multifocal and irregular distribution of fibrosis which aligns with the limited degree of capsular/contour change in this case as well. The rat in this

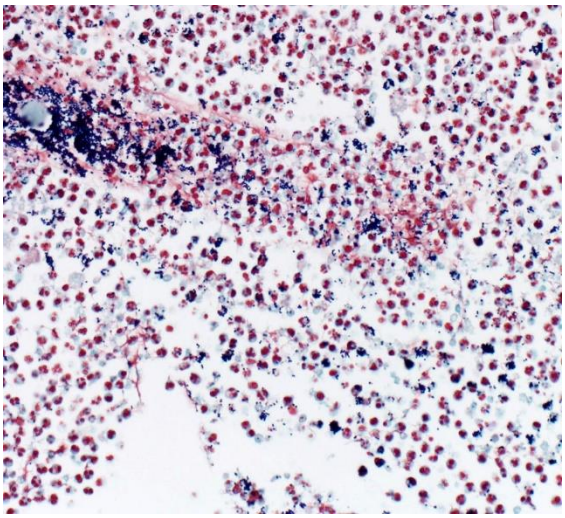

Figure 1-8. Urinary bladder, rat. A Gram stain demonstrates numerous gram-positive cocci within the renal pelvis. (*Photo courtesy of:* University of Michigan, Unit for Laboratory Animal Medicine, Pathology Core, https://animalcare.umich.edu/business-services/ulam-pathology-core/)

case was only nine months old at the time of euthanasia – for a comparison of CPN in a 2-year-old (24 months) rat and additional background literature, see Conference 12, Case 3, WSC 2019-2020.

Finally, Rag2 and IL-2Rγ warrant a brief discussion of their role in immunity. The common gamma chain (IL-2Rγ; γ_c) of the IL-2 receptor is a conserved and important component in intracellular signaling for multiple cytokines, including IL-2, IL-4, IL-7, IL-9, and IL-21.[2,4] Once ligands are bound to these receptors, γ_c forms a heterodimer and recruits Janus kinase 3 (JAK3) to further propagate these signals via STAT and induce changes in gene expression. These cytokines are vital for mature lymphoid cell proliferation (IL-2), T-helper type 2 responses (IL-4), early lymphoid/hematopoietic progenitor cell development (IL-7, IL-9), and natural killer cell development (IL-15, IL-21).[2,4] As such, knockout or mutation of IL-2Rγ (such as in X-

linked SCID) results in significant impairment of NK, T-, and B-cells.[6] Conversely, Rag2 forms one half (with RAG1) of a V(D)J recombinase that is essential for recombination of immunoglobulin and T-cell receptor variable regions that are needed for development of functional T- and B-lymphocytes.[6] Defects in Rag2 are also associated with marked immunodeficiency. The combination of Rag2 and IL-2Rγ defects is a substantial and additive deficit of both innate and adaptive immunity.

References:

1. Acuff NV, LaGatta M, Nagy T, Watford WT. Severe Dermatitis Associated with Spontaneous Staphylococcus xylosus Infection in Rag-/-Tpl2-/- Mice. Comp Med. 2017 Aug 1;67(4):344-349.
2. Felsburg PJ, Hartnett BJ, Henthorn PS, Moore PF, Krakowka S, Ochs HD. Canine X-linked severe combined immunodeficiency. Vet Immunol Immunopathol. 1999 Aug 2;69(2-4):127-35.
3. Frazier KS, Seely JC, Hard GC, Betton G, Burnett R, Nakatsuji S, et al. Proliferative and Nonproliferative Lesions of the Rat and Mouse Urinary System. Toxicologic Pathology. 2012;40-86S.
4. Noguchi M, Yi H, Rosenblatt HM, Filipovich AH, Adelstein S, Modi WS, McBride OW, Leonard WJ. Interleukin-2 receptor gamma chain mutation results in X-linked severe combined immunodeficiency in humans. Cell. 1993 Apr 9;73(1):147-57.
5. Percy DH, Barthold SW, eds. Pathology of Laboratory Rodents and Rabbits. 4th ed. Blackwell Publishing; 2016:66.
6. Perryman LE. Molecular pathology of severe combined immunodeficiency in mice, horses, and dogs. Vet Pathol. 2004 Mar;41(2):95-100.
7. Salleng KJ, Jones CP, Boyd KL, Hicks DJ, Williams MM, Cook RS. Staphylococcus xylosus Cystitis and Struvite Urolithiasis in Nude Mice Implanted with Sustained-release Estrogen Pellets. Comp Med. 2018;68(4):256-60.

CASE II:

Signalment:
An adult female Sprague Dawley rat (Rattus norvegicus)

History:
Patient presented with a multilobulated, firm facial mass on the left maxilla. Fine needle aspirate not consistent with abscessation or inflammation.

Gross Pathology:
The subcutis at the base of the left pinna is expanded by a firm, bilobed mass. The upper lobe is spherical and measures 2 cm along the widest axis; the lower lobe is spherical and measures 1 cm along the widest axis. On cut surface, the mass is well circumscribed, has a fibrous capsule, and centrally contains copious amounts of friable, tan to pink material. The central material often displays a laminar appearance.

Microscopic Description:
Haired skin: Examined are two sections of haired skin containing the grossly reported mass, skeletal muscle, and dermal adnexa. The mass is an expansile, well demarcated, and variable cellular neoplasm composed of well differentiated squamous epithelium arranged in trabeculae, islands, and papillary projections supported by pre-existing fibrovascular stroma. The neoplastic cells often exhibit sebaceous differentiation, with the

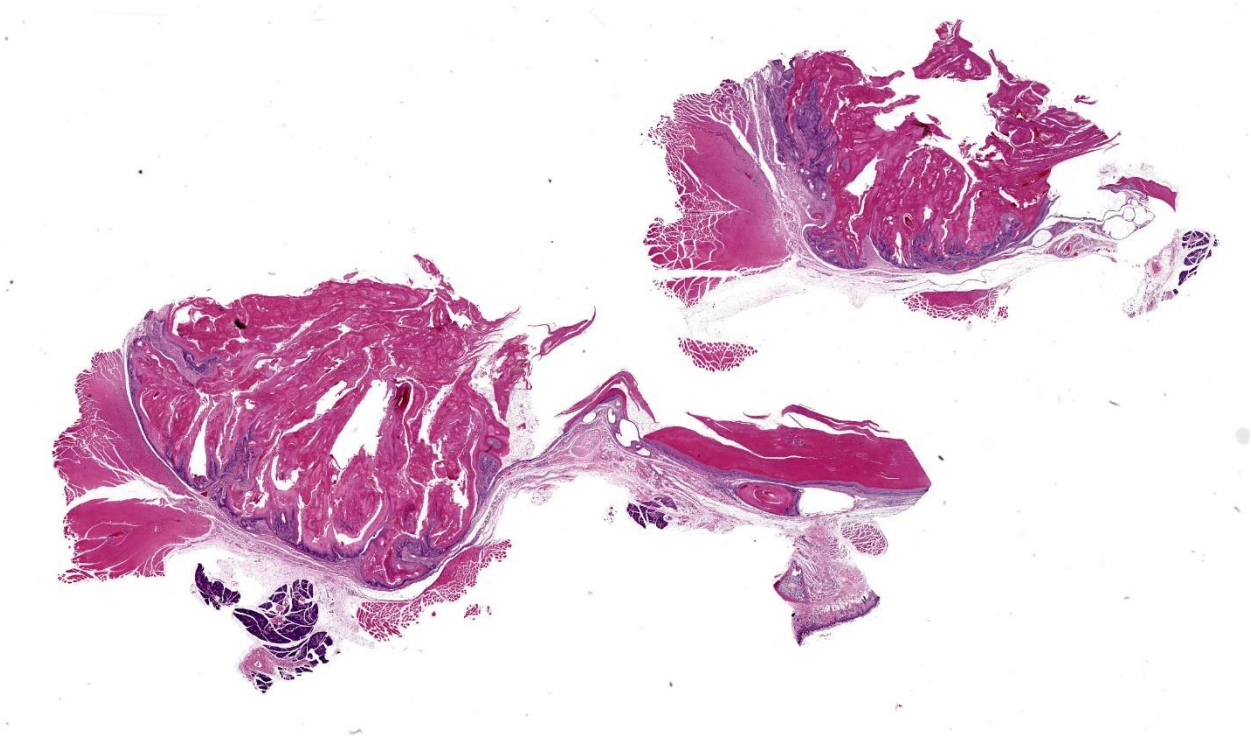

Figure 2-1. Zymbal's gland, rat. Two sections of Zymbal's gland are submitted for examination. There is marked proliferation of the squamous epithelium with large lamellae of keratin extending into the lumen.

mass centrally displaying squamous differentiation leading to abrupt keratinization organized into lamellated keratin and keratin pearls. The neoplastic cells have distinct cell borders, moderate to abundant finely vacuolated, eosinophilic cytoplasm, and round to ovoid nuclei containing finely stippled chromatin with one to two prominent nucleoli. Anisokaryosis and anisokaryosis are mild. Nine mitotic figures are observed in 10 HPF ($2.37mm^2$). Few aggregates of lymphocytes, plasma cells, eosinophils, and neutrophils infiltrate the dermis adjacent to the mass. Apocrine glands adjacent to the mass are moderately dilated and contain scant, pale eosinophilic, acellular material.

Contributor's Morphologic Diagnosis:
Zymbal's gland: Adenoma

Contributor's Comment:
Histologic evaluation of the mass is consistent with a Zymbal's gland tumor due to cellular morphology (specifically sebaceous differentiation of neoplastic cells) and anatomic location. An adenoma is diagnosed based on the lack of invasion into the underlying stroma. Zymbal's gland adenomas arise from Zymbal's holocrine glands at the base of the external ear.[1,2] These tumors often exhibit vacuolated cytoplasm, well differentiated squamous epithelium, and robust keratinization which are features in this case as well.[1,2]

Differentiation between an adenoma and a carcinoma of the Zymbal's gland can be achieved based on histomorphology and growth patterns.[1] Diagnostic features associ-

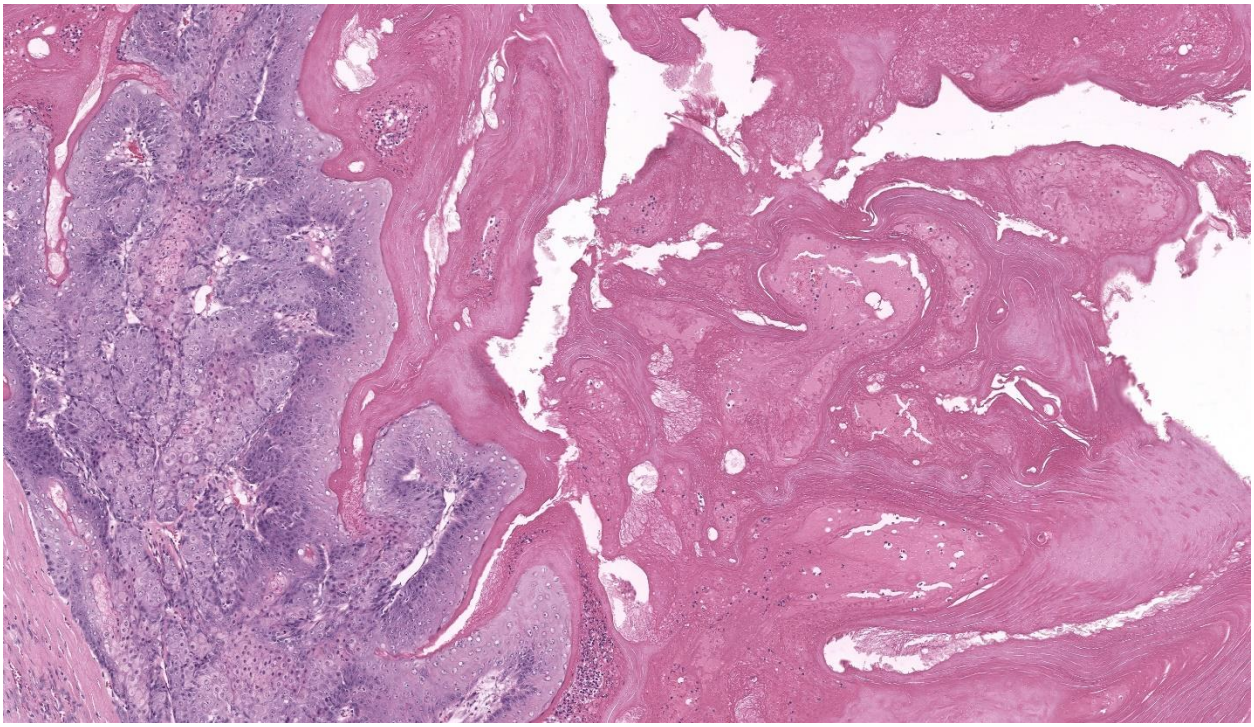

Figure 2-2. Zymbal's gland, rat. Higher magnification of the wall of the tumor with proliferating sebocytes, and more centripetally, proliferating squamous epithelium with layers of lamellated keratin and ghost cells.

ated with adenomas include well-differentiated neoplastic cells, lobulated structure, a mixture of both basaloid and mature sebaceous cells, cystic areas, and lack of nuclear atypia.[2] Diagnostic features associated with carcinomas include ulceration, irregular acini, papillary projections into cystic cavities, frequent mitoses, and increased cellular pleomorphism.[2] Differential diagnoses for an adenoma include glandular hyperplasia or a well-differentiated carcinoma while those for a carcinoma include an adenoma (for well-differentiated carcinomas) or squamous papilloma.[2]

Zymbal's glands are mostly observed and described in rats, however the structure is also present in mice.[2] Zymbal's gland typically measures approximately 3 to 5 mm in diameter, and is composed of three to four lobules.[2] While spontaneous tumors are uncommon, Zymbal's gland tumors are one of the most common tumor types in chemical associated carcinogenesis studies in laboratory rodents.[3,4,5] Specifically, Zymbal's gland tumors have been shown to be inducible by mutagenic compound 2-amino-3methylimidazo[4,5-5]quinoline among other chemical mutagens.[5]

Contributing Institution:
North Carolina State University College of Veterinary Medicine Department of Population Health and Pathobiology

https://cvm.ncsu.edu/php/

JPC Diagnosis:

Zymbal's gland: Adenoma

JPC Comment:
This second case is a WSC classic with elements such as the parotid salivary gland, auricular cartilage, and cheek muscle aiding in tissue identification. Conference participants discussed differential diagnoses including papilloma and keratoacanthoma due to the abundant keratin in section. As the contributor notes, sebaceous differentiation of neoplastic cells is a key feature to distinguish a Zymbal's gland tumor. Likewise, serial sections of this neoplasm might appear widely different (more or less sebaceous cells present) given the heterogenous distribution of these cells. We agree with the contributor that this neoplasm is an adenoma given the lack of invasion and bland cellular features. We attribute the presence of mixed inflammatory cells and edema to the inflammatory stimulus of abundant keratin. Dr. Radaelli emphasized that Zymbal's gland tumors resemble clitoral and preputial gland neoplasms given the cell of origin, though the supporting architecture is different.[2]

References:

1. Percy DH, Barthold SW, eds. Pathology of Laboratory Rodents and Rabbits. 4th ed. Blackwell Publishing; 2016.
2. Rudmann D, Cardiff R, Chouinard L, et al. Proliferative and Nonproliferative Lesions of the Rat and Mouse Mammary, Zymbal's, Preputial, and Clitoral Glands. Toxicologic Pathology. 2012;40(6_suppl):7S-39S.
3. National Toxicology Program. Toxicology and Carcinogenesis Studies of 8-Methoxypsoralen (CAS No. 298-81-7) in F344/N Rats (Gavage Studies). Natl Toxicol Program Tech Rep Ser. 1989 Jul;359:1-130.
4. Pucheu-Haston CM, Brandão J, Jones KL, et al. Zymbal gland (auditory sebaceous gland) carcinoma presenting as otitis externa in a pet rat (rattus norvegicus). Journal of Exotic Pet Medicine. 2016; 25(2):133–138.
5. Makino H, Ishizaka Y, Tsujimoto A, et al. Rat p53 gene mutations in primary Zymbal gland tumors induced by 2-amino-3-methylimidazo[4,5-f]quinoline, a food mutagen. Proc Natl Acad Sci U S A. 1992 Jun 1;89(11):4850-4.

CASE III:

Signalment:
1-year-old male intact standard fancy rat (*Rattus norvegicus domestica*)

History:
Submitted for necropsy is the body of a 1-year-old male intact pet rat adopted from a rescue a few months prior, with a reported history of waxing and waning nodular facial swelling located under the right eye, followed by diffuse facial swelling. This progressed to upper respiratory signs that resolved with enrofloxacin. The facial swelling was treated with a course of prednisolone and meloxicam. After a period of treatment, the signs worsened, characterized by a new eruption of multiple firm nodules near the nasal angle of the eyes and over the snout with increased respiratory distress. After 48h of increased respiratory rate and effort along with difficulty swallowing, the patient was euthanized due to poor prognosis.

Gross Pathology:
The lungs are entirely replaced, severely deformed, and expanded by over three dozen variably sized, up to 3.8 x 2.4 x 1.8 cm, multifocal to coalescing spherical, tan masses, rendering a bosselated appearance to the parenchyma, in particular of the right lung. On cut section, the masses extend deep within the parenchyma and exude abundant thick, opaque, light-yellow to white, malodorous pasty material (suppurative pneumonia with

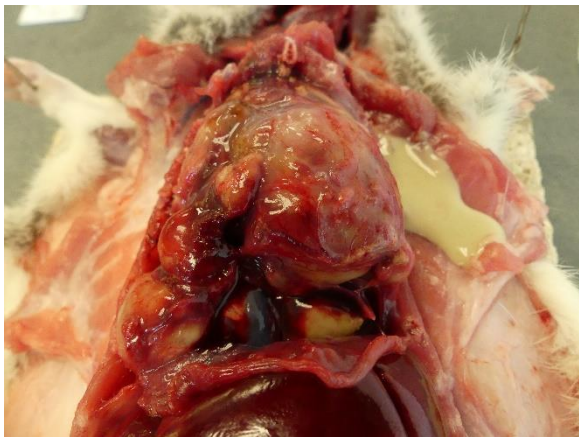

Figure 3-1. Lungs, rat. The lungs have a bosselated appearance, the right lung in particular. (Photo courtesy of: Cornell University College of Veterinary Medicine – Animal Health Diagnostic Center, Department of Biomedical Science, Section of Anatomic Pathology; https://www.vet. cornell.edu/animal-health-diagnostic-center)

bronchiectasis). Additionally, the pleura firmly adheres multifocally to the diaphragm and thoracic wall, and the heart is obscured by a pale pink mass of suppurative material and fibrosis (pericardial abscess).

Laboratory Results:
Bacterial culture was performed of the lungs, which isolated both *Mycoplasma sp.* and *Rodentibacter pneumotropicus*. Further speciation of *Mycoplasma sp.* was not conducted. Exclusion of *Filobacterium rodentium* was initially desired; unfortunately, the specific type of culture medium for this agent was not available at the testing facility.

Microscopic Description:
Lung: Up to 85% of the parenchyma in the submitted sections is effaced and replaced by variable numbers of well-delineated, coalescing spherical nodules arising within severely ectatic pre-existing bronchi (bronchiectasis), and enclosed in a thick fibrous capsule stippled with admixed lymphocytes, plasma cells, and macrophages, along with scattered stout congested capillaries. These nodules are mostly composed of central, compact amorphous eosinophilic material, vaguely imprinted with leukocytic debris, and rimmed by abundant degenerate neutrophils. The bronchial epithelium lining the areas of bronchiectasis is circumferentially replaced by an up to 10 cells-thick, keratinizing stratified squamous epithelium (squamous metaplasia). Covering this epithelium and projecting towards the lumen are mats of up to 18.0um-long and 1.0um thick, faintly amphophilic to eosinophilic filamentous bacteria.

Remnant alveoli within the surrounding parenchyma are compressed, distorted and completely filled with degenerate neutrophils, lymphocytes, plasma cells and foamy macrophages, embedded within variable quantities of light eosinophilic, proteinaceous fluid (pulmonary edema). The alveolar lining is extensively replaced by a continuous single cell-thick, low-cuboidal epithelium (pneumocytes type II hyperplasia). When appreciable, bronchial glands are prominent, mildly distorted and hyperplastic. Variably throughout the sections, bronchioles and bronchi are severely cuffed by abundant admixed lymphocytes and plasma cells, equally encircling infrequently thrombosed pulmonary arterioles.

Two additional stains, modified Steiner and Gram, were applied to a section of lung. The modified Steiner highlighted a thick mat of up to 18.0 μm-long, free filamentous argyrophilic bacteria corresponding to the organisms appreciated on hematoxylin eosin, disposed perpendicularly to the metaplastic bronchial epithelium. Thousands of identical free bacteria were distributed throughout the suppurative material filling the ectatic bronchi.

The Gram stain highlighted similar Gram-negative, filamentous bacteria throughout the

Figure 3-2. Lungs, rat. The lungs are expanded by over three dozen tan masses ranging up to up to 4cm, multifocal to coalescing spherical, tan masses. (Photo courtesy of: Cornell University College of Veterinary Medicine – Animal Health Diagnostic Center, Department of Biomedical Science, Section of Anatomic Pathology; https://www.vet.cornell.edu/animal-health-diagnostic-center)

sections, covering the metaplastic bronchial epithelium and interspersed with sparsely scattered Gram-negative, 0.3 µm-long coccobacilli. Clusters of approximately 0.2 µm in diameter, Gram-positive coccobacilli were additionally dispersed throughout the suppurative material.

Contributor's Morphologic Diagnosis:
Lung: Severe, multifocal to coalescing, chronic suppurative bronchopneumonia with bronchiectasis and myriad intralesional filamentous bacteria, lymphoplasmacytic peribronchiolitis and perivasculitis, squamous metaplasia of airways epithelium, glandular hyperplasia, type II pneumocyte hyperplasia, thrombosis and edema

Contributor's Comment:
Grossly, this case was unusually extensive with regards to the diffuse bilateral involvement of the pulmonary parenchyma, although the lesions remained more severe within the right lung, consistent with the classic unilateral, cranio-ventral lesional distribution commonly encountered with *Mycoplasma pulmonis*.

Isolation of *Mycoplasma* sp. together with bronchiectasis allowed for a diagnosis of murine respiratory mycoplasmosis, also termed chronic respiratory disease (CRD). CRD is usually considered subsequent to the combined action of *Mycoplasma pulmonis* and other respiratory pathogens such as *Filobacterium rodentium* (formerly known as CAR bacillus),[4] viral pathogens such as Sendai virus and rat coronavirus, and/or environmental causes such as high levels of ammonia.[1,3]

Mycoplasma pulmonis is directly deleterious to the respiratory epithelium, and is considered the only clinically relevant species of *Mycoplasma* in rodents.[1,3] Transmission occurs vertically or via aerosols, although the latter has experimentally proven fairly inefficient.[1,8] Colonization of the respiratory tract by *Mycoplasma sp.* results in ciliostasis and loss of cilia, subsequently reducing the efficacy of the mucociliary escalator, and caus-

Figure 3-3. Lung, rat. Bronchioles are diffusely ectatic and filled with eosinophilic cellular exudate. Adjacent alveoli are compressed. (HE, 381X)

ing mucus and inflammatory exudate accumulation within the airways. Ultimately, the ongoing buildup of lysozyme-rich inflammatory material culminates in permanent damage and dilatation of airways, resulting in bronchiectasis.[1,3] Both *Mycoplasma* microorganisms and host cell membrane fragments nonspecifically stimulate B-cell mitosis, and the resulting florid peribronchiolar lymphocytic infiltration is a salient histological feature of CRD in rats.[1] Other respiratory manifestations of mycoplasmosis in rats include rhinitis and lymphoplasmacytic tracheitis.[1,8]

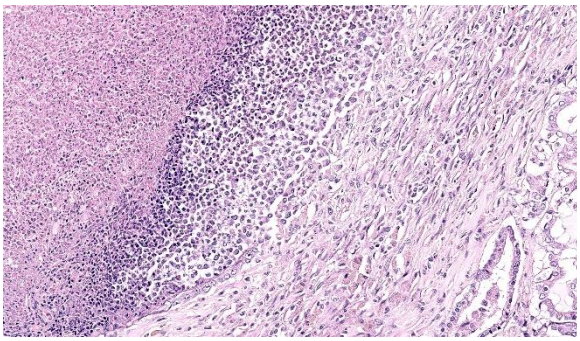

Figure 3-4. Lung, rat. Bronchiolar wall, with necrotic luminal exudate (left), a rim of viable neutrophils and fewer macrophages (center), and a fibrotic wall (right).

Given the tropism of *M. pulmonis* for ciliated epithelia, colonization and consequent inflammation of non-respiratory tissues, including the middle ear, endometrium and synovium, may also occur.[1,3] *M. pulmonis* is usually not evident on hematoxylin eosin sections, and requires ancillary tests such as culture or PCR for confirmation.

Additionally in this rat, the myriad amphophilic to light basophilic filamentous bacteria appreciated lining the inside of ectatic bronchi were considered compatible with *Filobacterium rodentium*, formerly known as Cilia-Associated Respiratory (CAR) bacillus.[4] *F. rodentium* is mostly transmitted by close contact during the neonatal period, and most strains of laboratory rats have been shown uniformly susceptible to disease.[1,3] While *M. pulmonis* and *F. rodentium* co-infection is frequent, both may individually cause illness and result in similar clinical disease and histological lesions.[1,3,8]

Histologically, *F. rodentium* is best highlighted using silver stains (such as Warthin-Starry), and characteristically forms mats of filamentous bacteria colonizing the respiratory airways, interspersed with cilia and oriented in a relatively perpendicular fashion to the epithelium.[1] *F.rodentium* has been isolated from the respiratory epithelium of other species than rat, including mice, rabbits, cattle, goats and pigs, and a recent report suggests that a particular strain of *Filobacterium sp.* could be associated with chronic bronchitis in cats.[1,5]

In the present case, these argyrophilic bacteria were emphasized using modified Steiner's stain, which additionally revealed a significant number of those microorganisms within the suppurative material filling the airways. On Gram stain, the organisms appeared faintly Gram-negative. As mentioned in the above laboratory results section, confirmation by culture was unavailable as *F.rodentium* requires specific growth media,[1,7] and this remains presumptive based on the combined histomorphological features, staining characteristics, and common reported co-involvement of *M. pulmonis* and *F.rodentium* in CRD.

Large numbers of *Rodentibacter pneumotropicus* were additionally isolated via lung culture. Formerly known as *Pasteurella pneumotropica*,[2] this Gram-negative, 0.5 to 1.2 μm-long rod to coccobacillus is a resident bacterium of the respiratory flora in rats,[1,3] and was thus considered an opportunistic co-infectious agent in the present case. Although not isolated on culture, clusters of Gram-positive bacteria were histologically appreciated;

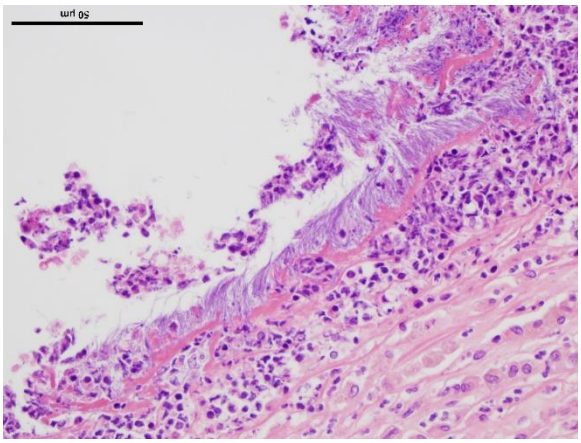

Figure 3-5. Lung, rat. Cilia are basophilic due to numerous intertwined filamentous bacilli. (Photo courtesy of: Cornell University College of Veterinary Medicine – Animal Health Diagnostic Center, Department of Biomedical Science, Section of Anatomic Pathology; https://www.vet.cornell.edu /animal-health-diagnostic-center) (HE, 400X)

Gram-positive organisms involved in respiratory disease and inducing formation of abscesses in rats include *Streptococcus pneumoniae* and *Corynebacterium kutscherii*, the latter capable of causing cutaneous abscesses.[1,3]

Additional findings, not present in the submitted slides, include the presence of nematode parasites within the renal pelvis, considered consistent with *Trichosomoides crassicauda*, a roundworm that commonly invades the murine urinary tract in individuals housed in poor hygienic conditions.[6] About five deep subcutaneous abscesses were additionally noted throughout the skin of the muzzle, with no identifiable intralesional bacteria. This was considered most probably consecutive to dissemination from the lungs in a relatively immunocompromised animal, given the absence of florid lymphoid hyperplasia in the present case, usually expected with *Mycoplasma sp.* infection.

Contributing Institution:
Cornell University College of Veterinary Medicine – Animal Health Diagnostic Center, Department of Biomedical Science, Section of Anatomic Pathology

https://www.vet.cornell.edu/animal-health-diagnostic-center

JPC Diagnosis:

Lung: Bronchopneumonia, suppurative, chronic, diffuse, severe, with bronchiectasis, fibrosis, and cilia-associated bacilli and luminal colonies of coccobacilli.

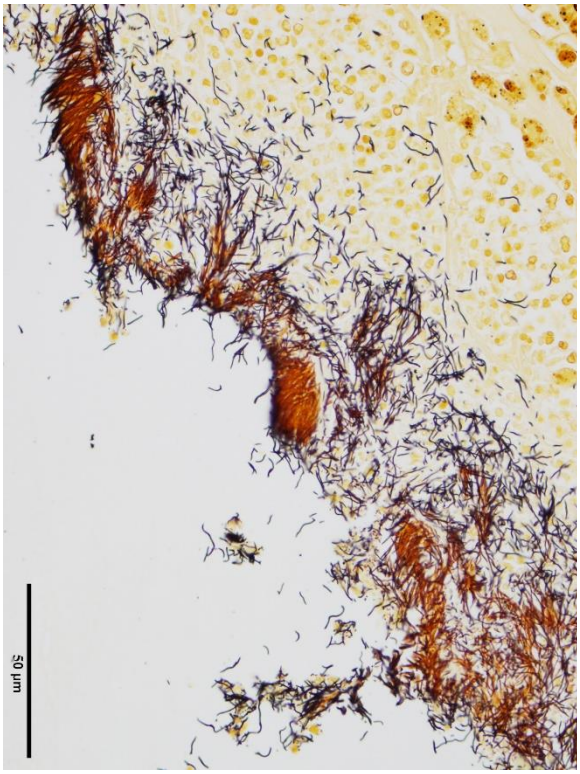

Figure 3-6. Lung, rats. A sliver stain demonstrates masts of filamentous bacilli within the cilia of the airway-epithelium. (Photo courtesy of: Cornell University College of Veterinary Medicine – Animal Health Diagnostic Center, Department of Biomedical Science, Section of Anatomic Pathology; https://www.vet.cornell.edu/ animal-health-diagnostic-center) (Steiner's, 400X)

JPC Comment:
The third case of this conference has a terrific macropscopic-microscopic correlation.. We confirm the contributor's interpretation of abundant argyrophilic filamentous bacteria with both Warthin-Starry and methenamine silver highlighting organisms within ectatic bronchioles well. We also noted a mixed population of bacteria on our Gram stain consistent with secondary opportunistic infection following ciliostasis initiated by *Mycoplasma*. Although subtle, there is also a change in appearance of ciliated epithelium with replacement of the normal eosinophilic hue towards a basophilic appearance of the cilia. Although non-specific, this is corroborating evidence of 'something added' such as *Mycoplasma*, *Bordetella*, or *Filobacterium* and can be seen even in sloughed epithelium. Although not stated by the contributor, we suspect that this animal likely had concurrent *Mycoplasma* in the ear to explain the facial signs observed.

Conference participants also discussed the presence of "oat cells" (ruptured leukocytes with streaming nuclear contents) which were a significant feature of this case. Oat cells have been described secondary to leukotoxins, a type of repeats in toxin (RTX) which is an important virulence factor for several bacterial pathogens including *Mannheimia, Pasteurella,* and *Bordetella* among others.[11] Leukotoxins can enhance both recruitment and killing of leukocytes which confers an advantage in both hampering the host immune response and extracting cellular resources for future growth. *Rodentibacter pneumotropicus* (formerly *Pasteurella pneumotropica*) is a potential source of RTX toxin in this case,[10] given the gram-negative coccobacilli we noted in section. Interestingly, lysis of leukocytes may be a double-edged sword, as extrusion of nuclear chromatin also enhances NETosis and may entrap and kill a portion of the bacteria concurrently.[9]

References:

1. Barthold SW, Griffey SM, Percy DH, eds. *Pathology of Laboratory Rodents and Rabbits.* 4th ed. Ames, IA: Wiley-Blackwell; 2016: 133-136, 140-141, 144-145.
2. Benga L, Sager M, Christensen H. From the [Pasteurella] pneumotropica complex to Rodentibacter spp.: an update on [Pasteurella] pneumotropica. Vet. Microbiol. 2018;217:121-134.
3. Fox JG, Anderson LC, Otto GM, Prtichett-Corning KR, Whary MT, eds. *Laboratory animal medicine*. 3rd ed. San Diego, CA: Elsevier; 2015:166-169, 173-175.
4. Ike F, Sakamoto M, Ohkuma M. et al. Filobacterium rodentium gen. nov., sp. nov., a member of Filobacteriaceae fam. nov. within the phylum Bacteroidetes; includes a microaerobic filamentous bacterium isolated from specimens from diseased rodent respiratory tracts Int. J. Syst. Evol. 2016; 66:150-157.
5. Načeradská M, Pekova S, Danesi P. et. A novel *Filobacterium* sp can cause chronic bronchitis in cats. PLOS ONE. 2021;16(6):e0251968.
6. Najafi F, Ghadikolai MT, Naddaf SR. et al. *Trichosomoides crassicauda* infection in laboratory rats with histopathological description in the bladder tissue. J Med Microbiol Infec Dis. 2017;5(1-2):31-34.
7. Nietfeld JC, Fickbohm BL, Rogers DG, Franklin CL, Riley LK. Isolation of cilia-associated respiratory (CAR) bacillus from pigs and calves and experimental infection of gnotobiotic pigs and rodents. J. Vet. Diagn. Invest. 1999;11:252-258.
8. Rothenburger JL, Himsworth CG,

Clifford CB, Ellis J, Treuting PM, Leighton FA. Respiratory Pathology and Pathogens in Wild Urban Rats (Rattus norvegicus and Rattus rattus). *Veterinary Pathology*. 2015;52(6):1210-1219.
9. Aulik NA, Hellenbrand KM, Klos H, Czuprynski CJ. Mannheimia haemolytica and its leukotoxin cause neutrophil extracellular trap formation by bovine neutrophils. Infect Immun. 2010 Nov;78(11):4454-66.
10. Sasaki H, Ueshiba H, Yanagisawa N, Itoh Y, Ishikawa H, Shigenaga A, Benga L, Ike F. Genomic and pathogenic characterization of RTX toxin producing Rodentibacter sp. that is closely related to Rodentibacter haemolyticus. Infect Genet Evol. 2022 Aug;102:105314.
11. Srikumaran S. Leukotoxins. Toxins (Basel). 2020 Apr 7;12(4):231.

CASE IV:

Signalment:
9-week-old, female, human-peripheral blood mononuclear cell (huPBMC)-engrafted-NOD *scid* gamma (NSG) mouse (Mus musculus)

History:
Female, human peripheral blood mononuclear cell (hPBMC)-engrafted NOD *scid* gamma (NSG) mouse purchased from an approved vendor, was submitted from an experimental cohort of mice experiencing similar clinical course of disease. One week after arrival, this cohort underwent experimental injection of MDA-MB-231 human breast cancer cells into the subcutis of the left flank (tumor xenograft model). In the 2 weeks following injection, the cohort demonstrated significant weight loss (3-5g), poor tumor engraftment, and unexpectedly high mortality. This mouse was euthanized and submitted for post-mortem examination as a representative animal.

Figure 4-1. Lungs, scid mouse. There is diffuse atelectasis of the lungs. (HE, 6X)

Gross Pathology:
The mouse weighed 16.15g and was in thin body condition (1.5/5 BCS); expected body weight for a female 9-week-old NSG mouse is 23.3 +/- 1.6g. There was diffuse pallor of the tail, ears and mucous membranes, and marked depletion of subcutaneous and visceral adipose. Scant white fascia-like tissue was noted at the tumor injection site, without evident tumor growth. The liver weighed 0.99 g (6.1% BW), was tan, and had rounded edges and a subtly irregular surface.

Microscopic Description:
All lung lobes demonstrate multifocal to coalescing consolidation and atelectasis with interstitial and alveolar septal thickening by mononuclear inflammatory cells and plump spindle cells (fibroplasia). Alveoli are multifocally lined by a continuous layer of plump, cuboidal to polygonal, epithelial cells (type II pneumocyte hyperplasia). There are dense perivascular and peribronchiolar lymphocytic cuffs up to 15 cells thick that contain low to moderate numbers of mitotic figures and

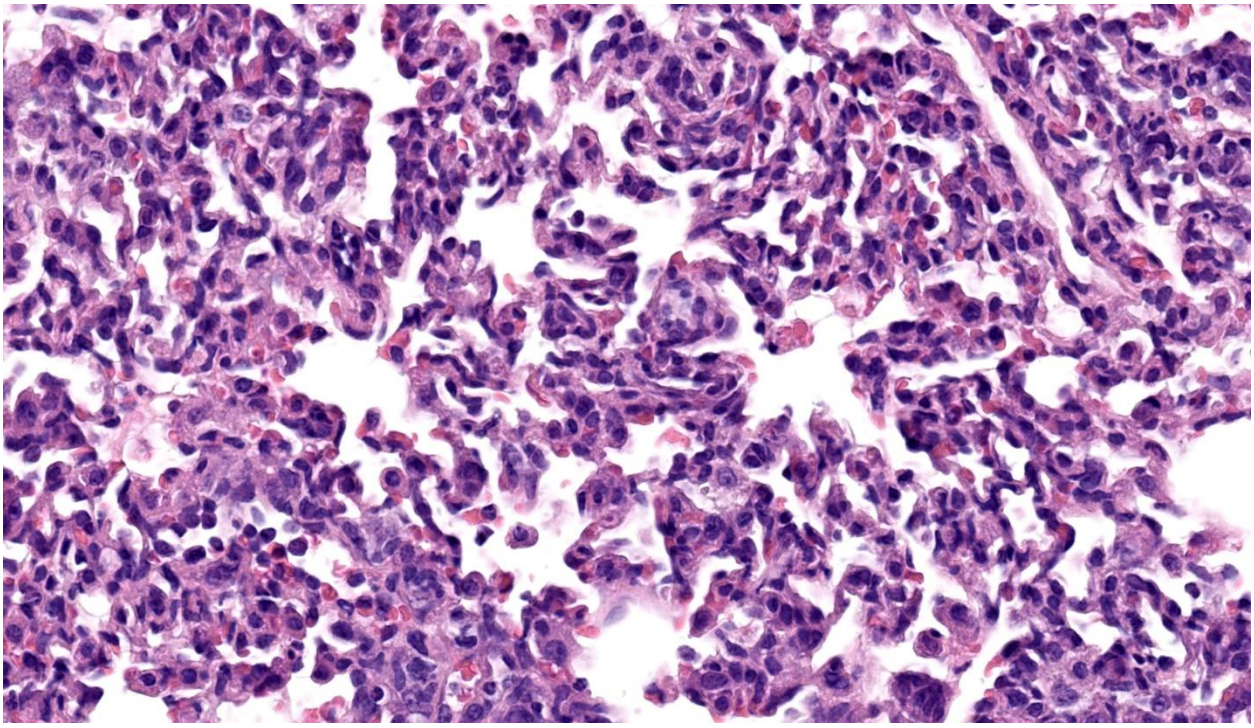

Figure 4-2. Lung, scid mouse. Diffusely, alveolar septa are hypercellular and expanded by hypertrophy of septal macrophages, circulating neutrophils, mild edema, and type II pneumocyte hyperplasia. (HE, 733X)

apoptotic bodies. Lymphocyte nuclei are subjectively slightly larger than expected (in mice).

Esophageal mucosa has multifocal vacuolar degeneration and scattered apoptosis involving basal epithelial cells, and an underlying cell-rich band of lymphocytic inflammation with fewer macrophages and scattered neutrophils along the basement membrane interface. Lymphocytic and neutrophilic inflammation extends transmurally, with severe mononuclear infiltration and aggregation in the tunica muscularis. Associated changes in skeletal muscle fibers include: 1) rounded myofibers with pale sarcoplasm lacking cross-striations and internalization of nuclei (degeneration), 2) shrunken and rounded myofibers with small hyperchromatic nuclei (atrophy), or 3) effacement and replacement of myofibers by lymphocytic inflammation (myofiber loss).

Immunohistochemistry:
Immunohistochemistry confirmed that perivascular and peribronchiolar cuffs in the lung and interface inflammation in the esophagus are primarily CD3+ cells (consistent with T lymphocytes), with low to moderate numbers of Iba-1+ leukocytes (interpreted as macrophages).

Contributor's Morphologic Diagnosis:
Lung:

Inflammation, perivascular to peribronchiolar to interstitial, lymphoproliferative and histiocytic, chronic and active, severe, with interstitial lung injury, chronic atelectasis, and type II pneumocyte hyperplasia

Esophagus:

Mucosa, basal epithelial cell vacuolization and apoptosis

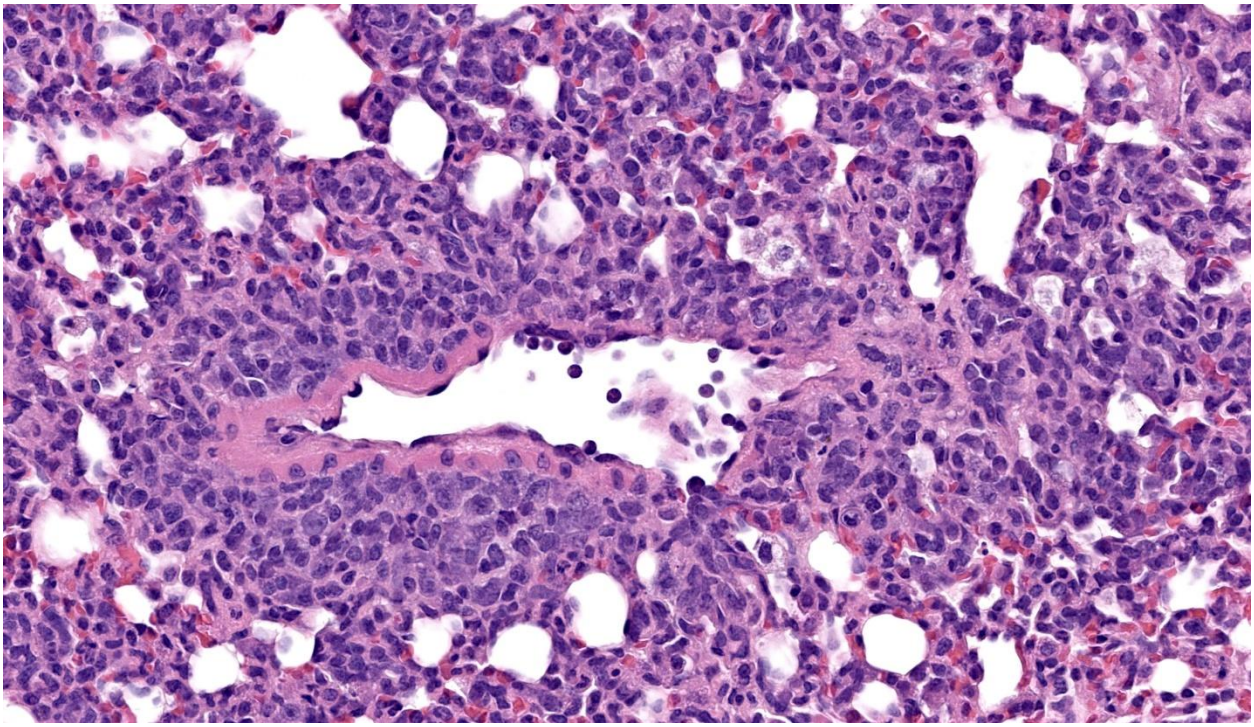

Figure 4-3. Lung, scid mouse. There are cuffs of large lymphocytes and histocytes around blood vessels throughout all lung lobes. (HE, 733X)

Esophagitis, 'interface', lymphocytic with fewer neutrophils and macrophages, multifocal to coalescing, severe, with marked submucosal and muscularis lymphocytic infiltration, and myofiber degeneration, atrophy and loss.

Condition:

Xenogeneic Graft versus Host Disease (GvHD)

Contributor's Comment:
Dense multiorgan infiltration by large lymphocytes with associated epithelial degeneration/apoptosis and a 1) a lichenoid interface pattern in skin, mucous membranes and esophagus, 2) a perivascular distribution in lung, salivary gland, and pancreas, and 3) a portal distribution in the liver are consistent with Graft-versus-Host Disease (GvHD).[10,11,14]

GvHD is a life-threatening, systemic inflammatory condition mediated by alloreactive transplanted donor lymphocytes that recognize antigenic disparities between donor (graft) and recipient (host) tissues leading to a cell-mediated adaptive immune response. The principle (but not exclusive) antigens driving GvHD are differences in Major Histocompatibility Complex (MHC) class I and II expression between donor and recipient tissues, as these molecules can be highly polymorphic between individuals.[8] MHC class I molecules are expressed on the cell surface of all nucleated cells, whereas MHC class II expression is largely limited to antigen presenting cells such as macrophages, dendritic cells, and B lymphocytes. A major component of T cell maturation in the thymus is the process of central tolerance where immature, self-reactive T cells are removed to prevent

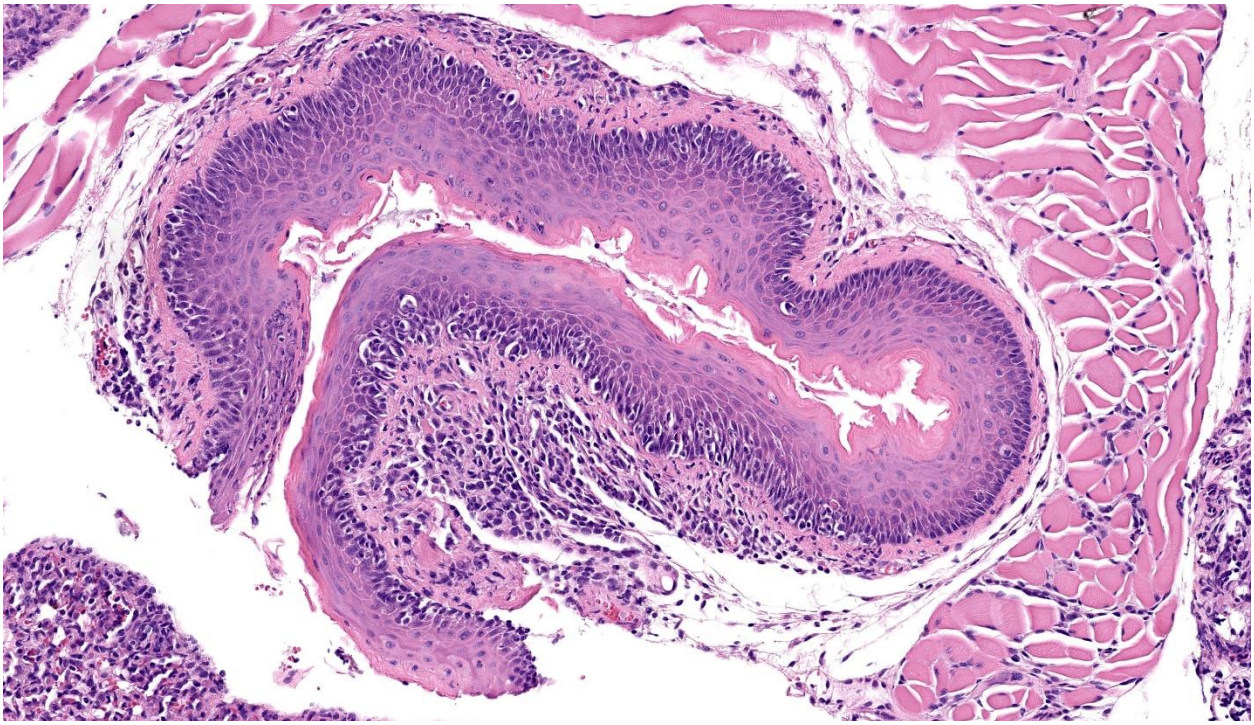

Figure 4-4. Esophagus, scid mouse. There are aggregates of lymphocytes and histiocytes within the lamina propria, which occasionally migrate into the deep layers of the mucosa. There are occasional apoptotic mucosal epithelial cells. (HE, 615X)

auto-immunity. However, in the setting of hematopoietic stem cell transplantation, the transferred immunocompetent donor T cells recognize host alloantigens as foreign, resulting in immune activation and targeting of host tissue.[3,8] The primary effector cells are donor CD8+ T lymphocytes and Natural Killer cells that recognize host MHC I molecules and induce direct cytotoxicity in these cells. Alloreactive CD4+ T cells also contribute via recognition of MHC class II molecule differences and secretion of pro-inflammatory cytokines that induce further immune activation and tissue damage.[3,8]

NSG mice are an extremely immunodeficient mouse model that lack natural killer cells, B lymphocytes and T lymphocytes.[5,12] Due to the lack of a functional adaptive immune system, these mice can be engrafted with human-derived tissues including hematopoietic stem cells, cell culture lines, and patient-derived xenografts.

Human peripheral blood mononuclear cell (hPBMC) NSG mice have become an important model in the study of GvHD, which is a major clinical problem in human hematopoietic stem cell recipients.[4,12] hPBMC NSG mice are considered an improved model of xenogenic GvHD compared to NOD/SCID and RAG2null / IL2rγnull recipients due to their earlier onset of symptoms, more pronounced weight loss, and earlier mortality.[4] Consequently, GvHD development is expected in hPBMC NSG, resulting in a shortened lifespan of approximately 3-4 months. The disease course in this case was more rapid than experienced previously by the submitting lab.

Notably, human T cells are able to recognize murine xeno-antigens presented by murine

Table 1: Histologic Criteria for GvHD[10,11,14]

	Criteria for acute GvHD	Criteria for chronic GvHD	This case:
Skin	Apoptosis in basal epithelium +/- vacuolar change; interface dermatitis; lymphocytic exocytosis and satellitosis	Acanthosis and hyperkeratosis; interface dermatitis; thickening and homogenization of dermal collagen +/- dermal and subcuticular sclerosis;	Lichenoid and peri-adnexal dermatitis with vacuolar change of basal keratinocytes
Oral cavity, oropharynx, Esophagus	Lichenoid interface inflammation; lymphocytic exocytosis; epithelial apoptosis	Lichenoid interface inflammation; lymphocytic exocytosis; epithelial apoptosis	Lichenoid interface inflammation (esophagus) with vacuolar change, epithelial apoptosis, and myofiber degeneration
Liver	Bile duct injury; lobular and portal inflammation; cholestasis	Ductopenia; progressive fibrosis; chronic cholestasis	Portal and centrilobular lymphocytic infiltration; bile duct hyperplasia and atypia
Salivary gland		Periductal lymphoplasmacytic inflammation and fibroplasia; acinar destruction and loss	Periductal lymphocytic sialadenitis with acinar loss
Intestine	Enterocyte apoptosis; crypt or basilar gland destruction; mucosal ulceration	Enterocyte apoptosis; crypt destruction, loss, distortion; mucosal ulceration; lamina propria and submucosal fibrosis	
Lung	Intrabronchiolar T cells; bronchiolar and interstitial epithelial apoptosis; perivenular cuffing; lymphocytic bronchiolitis;	Constrictive bronchiolitis obliterans; cryptogenic organizing pneumonia; chronic interstitial pneumonia	Perivascular, peribronchiolar, interstitial lymphohistiocytic inflammation with chronic atelectasis and interstitial lung injury

MHC class I and II molecules, and onset of GvHD is dependent on host expression of MHC.[2,7] hPBMC NSG MHC I/II Double Knockout mouse models demonstrate delayed onset of xenogeneic-GvHD relative to hPBMC NSG mice, and thereby may be more suitable for immuno-oncology studies and/or long-term studies requiring human T cell engraftment.[1,9]

The two major subdivisions of GvHD are acute versus chronic GvHD, which are defined by their clinicopathologic features not solely the time after transplantation.[3,13] Acute GvHD typically has rapid onset and is characterized by multiorgan lymphocytic, histiocytic, and neutrophilic inflammation with associated tissue destruction and epithelial apoptosis; the most commonly affected organs include the skin, gastrointestinal tract, and liver. In contrast, the hallmark of chronic GvHD is fibrotic/sclerotic lesions with variable leukocyte infiltration and can be observed in almost any organ.[13] While chronic GvHD classically develops >100 days post-transplantation in patients that have previously developed acute GvHD, it can also develop de novo or simultaneously with acute

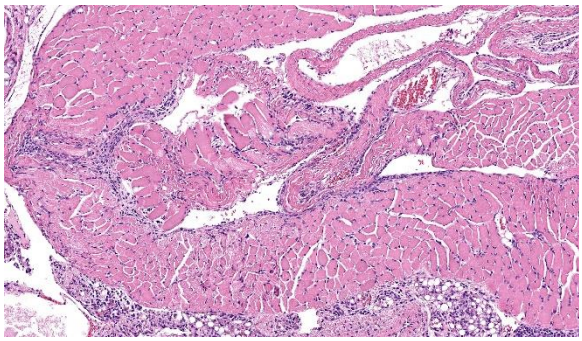

Figure 4-5. Skeletal muscle, scid mouse. Low to moderate number of lymphocyte and histiocytes infiltrate beneath the epimysium and within the perimysium of skeletal muscle. (HE, 197X)

GvHD.[3,6,13] An abbreviated summary of the histologic criteria for acute and chronic GvHD and a comparison to features supportive of a diagnosis of xenogeneic GvHD in this case are included in Table 1.

Onset and progression of GvHD in this 'humanized' mouse was likely further accelerated and exacerbated by the additional injection of non-matched, human-derived tumor cells. Failure of tumor engraftment in these mice is also consistent with a hu-PBMC-derived immune response against the tumor.[9] Given that the entire cohort of mice appeared affected, it is also possible these hPBMCs were unusually reactive resulting in accelerated onset of GvHD.

Expected lung changes in GvHD are characterized by intrabronchiolar T cells, apoptosis, and perivenulitis, which can progress acutely to respiratory distress and death, or to constrictive bronchiolitis obliterans (CBO) in chronic GvHD.[11,14] Fibrosis was not prominent in these lung sections, which is attributed to the relatively short course of disease. Lung changes are more extensive than in similar cases here, and may suggest a role for opportunistic infection as a contributor to mortality in this cohort (e.g., *Chlamydia* spp. infection). *Mycoplasma pulmonis* and *Filobacterium rodentium* are excluded from rodent areas at this site. As bacteria were not identified with Gram stain and the clinical concern resolved after that cohort, further diagnostics were not pursued.

Contributing Institution:

Johns Hopkins University, School of Medicine
Department of Molecular and Comparative Pathobiology
https://mcp.bs.jhmi.edu/

JPC Diagnosis:

1. Lung: Pneumonia, interstitial and lymphohistiocytic, subacute, diffuse, marked, with perivascular and peribronchiolar lymphoid proliferation.
2. Esophagus: Esophagitis, interface and lymphocytic, subacute, multifocal, moderate.
3. Skeletal muscle: Myositis, lymphocytic, subacute, multifocal, moderate.
4. Thyroid gland: Thyroiditis, lymphocytic, subacute, multifocal, mild.
5. Adipose tissue: Steatitis, lymphocytic, subacute, multifocal, mild.

JPC Comment:
The final case of this conference provided a healthy challenge for participants, with the knowledge of hematopoietic stem cell involvement in this humanized mouse being essential for understanding the underlying pathogenesis that the contributor nicely summarizes. We opted for multiple morphologic diagnoses to capture the distribution of inflammatory cells, though the underlying changes were similar across the lung, esophagus, skeletal muscle, thyroid, and adjacent adipose tissue. We did note a very mild acidophilic macrophage pneumonia in this mouse, though this is a non-specific finding and

likely follows from the marked inflammation of the lung.

The contributor IHC results help to describe the distribution of inflammatory cells in this case. With the assistance of Dr. Radaelli, we further characterized these cells with the aid of a mouse-specific CD86 (B7; marker of antigen presenting cell), CD4/CD8 (T-cell markers), and CD79 (B-cell). CD86-positive cells were widely distributed in tissue while B-cells were sparse in the lung with none in esophagus or muscle. CD4+ T-helper cells were present in moderate numbers in the lung, muscle, and esophagus while CD8+ cytotoxic T-cells were notable in the lung, esophagus, and the thyroid with the latter not being as obvious on the H&E section. One limitation is that we did not have a human macrophage marker available (e.g. CD45) to fully demonstrate the xenogeneic attack inherent in this case however.

Finally, Dr. Radaelli discussed humanized mice as well as several of the undesired consequences of this exploratory model during his pre-conference lecture which we abridge here.[9] Humanized mice are interspecies chimeras that offer a potential avenue to explore tumor oncogenic signatures (biomarkers), test therapeutic interventions, and assess relative toxicity therein through a stable line that supports continued/stable tumor growth. Because these mice are severely immunosuppressed and bathed in a veritable shower of cytokines to enhance human hematopoietic stem cell line proliferation, there is also the possibility of myeloid cell hyperactivation,[15] excessive lymphoproliferation, and even oncogenic activation of latent viruses (e.g. Epstein-Barr virus) in human tissue grafts.[16] Opportunistic infection, as seen in Case 1 of this conference, is yet another consideration. While the potential benefits of this model are significant, pathologists also play an important role in advocating for the welfare of these mice and identifying issues or limitations of a given mouse type.[17]

References:

1. Brehm MA, Kenney LL, Wiles MV, et al. Lack of acute xenogeneic graft- versus-host disease, but retention of T-cell function following engraftment of human peripheral blood mononuclear cells in NSG mice deficient in MHC class I and II expression. *FASEB J*. 2019;33(3):3137-3151.
2. Ehx G, Somja J, Warnatz HJ, et al. Xenogeneic Graft-Versus-Host Disease in Humanized NSG and NSG-HLA-A2/HHD Mice. *Front Immunol*. 2018;9:1943.
3. Ghimire S, Weber D, Mavin E, Wang XN, Dickinson AM, Holler E. Pathophysiology of GvHD and Other HSCT-Related Major Complications. *Front Immunol*. 2017;8:79.
4. Ito R, Katano I, Kawai K, et al. Highly sensitive model for xenogenic GVHD using severe immunodeficient NOG mice. *Transplantation*. 2009;87(11):1654-1658.
5. The Jackson Laboratory. Strain 005557 NOD.Cg-Prkdcscid Il2rgtm1Wjl/SzJ. Accessed June 28, 2023. https://www.jax.org/strain/005557.
6. Jagasia MH, Greinix HT, Arora M, et al. National Institutes of Health Consensus Development Project on Criteria for Clinical Trials in Chronic Graft-versus-Host Disease: I. The 2014 Diagnosis and Staging Working Group report. *Biol Blood Marrow Transplant*. 2015;21(3):389-401.e1.
7. King MA, Covassin L, Brehm MA, et al. Human peripheral blood leucocyte non-obese diabetic-severe combined immunodeficiency interleukin-2 receptor gamma

chain gene mouse model of xenogeneic graft-versus-host-like disease and the role of host major histocompatibility complex. *Clin Exp Immunol*. 2009;157(1):104-118.
8. Kumar V, Abbas AK, Aster JC. Diseases of the immune system. *In:* Robbins and Cotran Pathologic Basis of Disease, 10th ed. Philadelphia, PA, Elsevier Saunders; 2021.
9. Radaelli E, Hermans E, Omodho L, et al. Spontaneous Post-Transplant Disorders in NOD.Cg- Prkdcscid Il2rgtm1Sug/JicTac (NOG) Mice Engrafted with Patient-Derived Metastatic Melanomas. *PLoS One*. 2015;10(5):e0124974.
10. Salomao M, Dorritie K, Mapara MY, Sepulveda A. Histopathology of Graft-vs-Host Disease of Gastrointestinal Tract and Liver: An Update. *Am J Clin Pathol*. 2016;145(5):591-603.
11. Shulman HM, Cardona DM, Greenson JK, et al. NIH Consensus development project on criteria for clinical trials in chronic graft-versus-host disease: II. The 2014 Pathology Working Group Report. *Biol Blood Marrow Transplant*. 2015;21(4):589-603.
12. Shultz LD, Brehm MA, Garcia-Martinez JV, Greiner DL. Humanized mice for immune system investigation: progress, promise and challenges. *Nat Rev Immunol*. 2012;12(11):786-798.
13. Vigorito AC, Campregher PV, Storer BE, et al. Evaluation of NIH consensus criteria for classification of late acute and chronic GVHD. *Blood*. 2009;114(3):702-708.
14. Xu L, Drachenberg C, Tavora F, Burke A. Histologic findings in lung biopsies in patients with suspected graft-versus-host disease. *Hum Pathol*. 2013;44(7):1233-1240.
15. Tarrant JC, Binder ZA, Bugatti M,et al. Pathology of macrophage activation syndrome in humanized NSGS mice. *Res Vet Sci*. 2021 Jan;134:137-146.
16. Tillman H, Vogel P, Rogers T, Akers W, Rehg JE. Spectrum of Posttransplant Lymphoproliferations in NSG Mice and Their Association With EBV Infection After Engraftment of Pediatric Solid Tumors. *Vet Pathol*. 2020 May;57(3):445-456.
17. Willis E, Verrelle J, Banerjee E,et al. Humanization with CD34-positive hematopoietic stem cells in NOG-EXL mice results in improved long-term survival and less severe myeloid cell hyperactivation phenotype relative to NSG-SGM3 mice. *Vet Pathol*. 2024 Jul;61(4):664-674.

Joint Pathology Center
Veterinary Pathology Services

WEDNESDAY SLIDE CONFERENCE 2024-2025

Conference #22 — 2 April 2025

CASE I:

Signalment:
Late-term aborted, female lamb from lowland sheep (*Ovis aries*).

History:
Eight aborted lambs from six abortions were submitted for necropsy. Twenty-two late-term abortions had occurred in a group of 230 lowland ewe lambs (1-year-old) over an 8-day period. The ewe lambs were due to start lambing approximately 1 week later. Twin pregnancies had been particularly affected and occasionally one twin was born alive and survived. The ewe lambs had been kept outdoors on grass only, with no access to silage or concentrates, appeared in good body condition and had been vaccinated against toxoplasmosis and ovine campylobacteriosis, but not against ovine enzootic abortion (syn. enzootic abortion of ewes (EAE)).

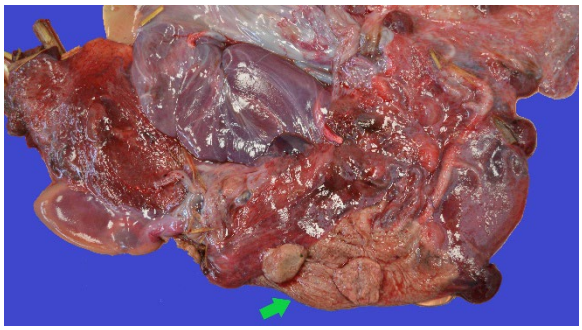

Placenta, sheep: There is a focally extensive area of moderately thickened, non-translucent, slightly dry and brown intercotyledonary tissue and similarly dry and brown cotyledons (Photo courtesy of: Department of Pathobiology and Population Sciences, Royal Veterinary College, Hawkshead Lane, North Mymms, Hertfordshire, United Kingdom, AL9 7TA. The website address is www.rvc.ac.uk)

Gross Pathology:
Six out of the eight submitted aborted lambs were received with all or part of their placentas. Three placentas were grossly unremarkable. In the other three placentas, there was a focally extensive area of moderately thickened, non-translucent, slightly dry and brown intercotyledonary tissue and similarly dry and brown cotyledons. Large adjacent areas were moderately edematous with injected blood vessels. The aborted lambs were well-preserved with no evidence of maceration or mummification. Some aborted lambs had small amounts of serosanguinous fluid in the abdominal cavity and occasional subcutaneous or perirenal bruising.

Laboratory Results:
Laboratory testing was carried out on four of the six abortions. Culture of fetal stomach contents from three cases revealed a very heavy pure growth of hemolytic Gram-positive rods that were identified as *Listeria ivanovii*. Enriched culture was negative for *Campylobacter* spp. Placental smears stained with modified Ziehl-Neelsen were negative for *Brucella* spp., *Chlamydia* spp. and *Coxiella*

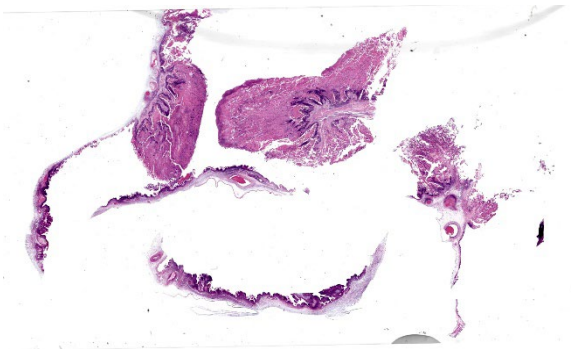

Placenta, sheep: Sections of cotyledon and intercotylendonary placenta are submitted for examination. (HE, 6X)

spp. PCR for *Toxoplasma gondii* and border disease virus were both negative.

Microscopic Description:
Chorioallantois, cotyledons and intercotyledonary tissue: The cotyledons and intercotyledonary tissue are extensively necrotic, expanded by edema and multifocal fibrin deposits and infiltrated by high numbers of viable and degenerate neutrophils, fewer macrophages and several prominent colonies of short, Gram-positive, rod-shaped bacteria (bacilli), measuring 0.5–2 µm in length (*Figure 2*). Multifocally, there are degenerate and necrotic trophoblasts, some of which contain intracytoplasmic Gram-positive bacilli. Several blood vessel walls, mainly arteries, contain intraluminal fibrin thrombi and the blood vessel walls are moderately to markedly infiltrated and expanded by high numbers of viable and degenerate neutrophils and fibrin.

Contributor's Morphologic Diagnosis:
Chorioallantois, cotyledons and intercotyledonary tissue; acute, focally extensive, marked, necro-suppurative placentitis with large numbers of intralesional Gram-positive bacilli and multifocal, marked, necrotizing and neutrophilic vasculitis with acute intraluminal fibrin thrombi

Contributor's Comment:
The microscopic findings in the chorioallantois and the pure growth of *Listeria ivanovii* from fetal stomach contents support this abortion outbreak to be the result of listerial infection.

L. ivanovii, formerly known as *L. monocytogenes*, serotype 5 [8] is a recognized cause of ovine,[1,6,9] caprine[5] and bovine[3] abortions, but rarely causes other conditions. It appears to be especially pathogenic for sheep but is less commonly isolated than *L. monocytogenes*.[7]

The most common lesions in abortions caused by *L. monocytogenes* are necro-suppurative cotyledonary and intercotyledonary placentitis, autolysis of aborted fetuses, miliary foci of necrosis in the liver and spleen, and marked necrotizing enteritis,[4,7] whereas less is known about typical lesions in abortions caused by *L. ivanovii*.

The present case had necro-suppurative placentitis and fibrino-suppurative vasculitis, which has not been previously described in cases of ovine abortions due to *L. ivanovii*,[1,6,9] but has been described in a case of caprine abortion.[5] Interestingly, only rare, microscopically evident, necrotic foci in the liver were identified in this case, even though grossly apparent necrotic hepatitis is commonly described in ovine and bovine abortions due to

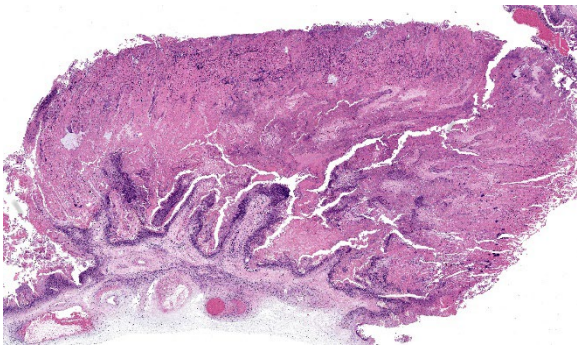

Placenta, sheep: There is diffuse coagulative and lytic necrosis of the cotyledon. (HE, 33X)

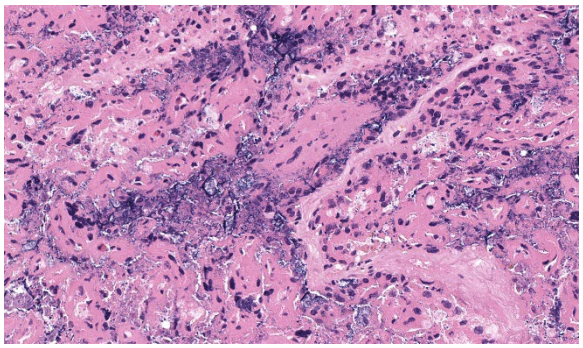

Placenta, sheep: There are innumerable bacteria within the necrotic cotyledon. (HE, 608X)

L. monocytogenes [7] and also in previous cases of ovine abortions due to *L. ivanovii*.[1,6,9] Also, the lungs had moderate neutrophilic bronchopneumonia which was likely the result of inhaled amniotic fluid with admixed listerial bacteria. Similarly, bronchopneumonia has been described in an ovine,[6] caprine[5] and bovine[3] abortion case caused by *L. ivanovii*.

In abortion outbreaks caused by *L. monocytogenes,* infection most often spreads by ingestion of food or water contaminated by feces, urine, placenta or vaginal discharge from affected ewes. Also, consumption of contaminated poor-quality silage is a well-known and important source of infection with *L. monocytogenes*.[7] Previously reported ovine abortion outbreaks caused by *L. ivanovii* often coincided with periods of cold and wet weather[1,6,9] and feeding of spoiled hay[9] or moldy hay and barley.[6] In the herein described abortion outbreak, the ewe lambs had only been on grass, suggesting that *L. ivanovii* infection may have been directly acquired from the pasture environment. This route of exposure has been proposed in a case series of weaned lambs in the United Kingdom with visceral *L. ivanovii* infections.[2] Interestingly, in this submission, the farmer reported that some abortions consisted of one dead lamb and one live unremarkable lamb including one of those submitted from which *L. ivanovii* was isolated. This is in contrast to previous reports.[1,6,9]

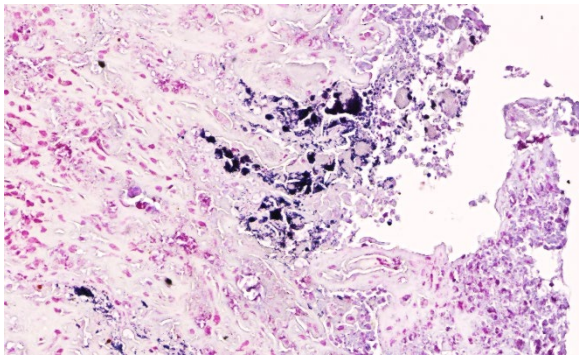

Placenta, sheep: The bacilli within the necrotic cotyledon are gram-positive. (Gram, 400X) (Photo courtesy of: Department of Pathobiology and Population Sciences, Royal Veterinary College, Hawkshead Lane, North Mymms, Hertfordshire, United Kingdom, AL9 7TA.)

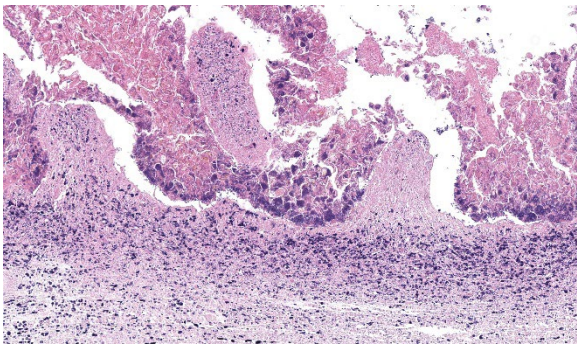

Placenta, sheep: There is necrosis of the intercotyledonary epithelium and the trophoblasts are swollen with intracytoplasmic bacilli. (HE, 308X).

The present case highlights the importance of testing for common as well as less common abortion pathogens and sampling of several tissues for histology to confirm isolated pathogens microscopically.

Contributing Institution:
Department of Pathobiology and Population Sciences, Royal Veterinary College, Hawkshead Lane, North Mymms, Hertfordshire, United Kingdom, AL9 7TA. The website address is www.rvc.ac.uk: https://vet.purdue.edu/cpb/

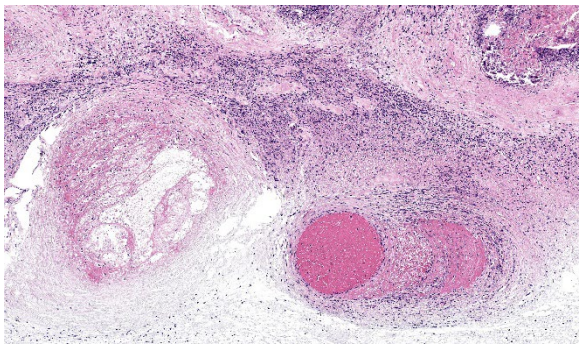

Placenta, sheep: There is necrotizing vasculitis and thrombosis of the endometrial vessels. (HE, 308X).

JPC Diagnosis:
Placenta: Placentitis, necrosuppurative, subacute, diffuse, severe, with vasculitis, thrombosis, and numerous extracellular and intratrophoblastic bacilli.

JPC Comment:
This week's moderator was Dr. Maggie Highland from the University of Wisconsin Veterinary Diagnostic Laboratory. Dr. Highland emphasized the diagnostic workup of small ruminant abortion in her pre-conference lecture and revisited these concepts in this first case which we excerpt again here.

From subgross magnification, tissue identification of the placenta in this case is facilitated by recognition of ruminant cotyledonary structure. Although there is marked coagulative (and subsequently lytic necrosis) present in this tissue, the state of tissue preservation is representative of typical abortion cases. The major diagnostic features present include vasculitis and innumerable intratrophoblastic cytoplasmic bacilli which provide a clear mechanism for abortion (interruption of blood flow and placental insufficiency). Conference participants considered several possible etiological agents including *Chlamydia* (which would also have vasculitis and intracytoplasmic bacteria) as well as *Brucella* (vasculitis) and *Coxiella* (lacks vasculitis, but centered on trophoblasts).[7] Other potential rule outs for small ruminant abortion include Border disease virus (and BVDV) as well as toxoplasmosis, though the latter is associated with cotyledonary necrosis without vasculitis.[7]

Our Gram stain was helpful for resolving *Listeria* as the probable agent given the size and slight curvilinear shape – we noted large numbers of gram-positive bacteria both free and within trophoblasts. Conference participants wondered if the large number of organisms present on this slide represented a particular tropism/niche (and corresponding fitness) of *L. ivanovii* for placenta. Likewise, we speculate that *Listeria* hitting twins harder than singleton lambs reflects a decreased placental reserve for twins over singletons. Although not performed at the JPC, Giemsa and/or Gimenez stains to enhance visualization of trophoblastic organisms is a helpful part of the diagnostic workup.[7] Culture of fetal abomasal contents may prove vital in instances where the placenta lacks diagnostic information. Dr. Highland emphasized reporting PCR/culture results as "not detected" or cultures as "no growth: rather than 'negative' in both instances– this distinction carries some weight in animals previously treated with antibiotics and precludes potential client misinterpretation of "negative" results.

References:

1. Chand P, Sadana JR. Outbreak of *Listeria ivanovii* abortion in sheep in India. *Vet Rec*. 1999;145(3):83-84.
2. Dunnett E, Florea L, Thurston L, Floyd T, Collins R, Otter A. Deaths of weaned lambs with visceral *Listeria ivanovii* infections. *Vet Rec Case Rep*. 2020;8: e001254.

3. Gill PA, Boulton JG, Fraser GC, Stevenson AE, Reddacliff LA. Bovine abortion caused by *Listeria ivanovii*. *Aust Vet J*. 1997;75(3):214.
4. Low JC, Donachie W. A review of *Listeria monocytogenes* and listeriosis. *Vet J*. 1997;153(1):9-29.
5. Moeller RB. Causes of caprine abortion: diagnostic assessment of 211 cases (1991-1998). *J Vet Diagn Invest*. 2001;13:265-270.
6. Sahin M, Beytut E. Abortions in sheep due to *Listeria ivanovii* in the Kars Region. *Turk J Vet Anim Sci*. 2006;30:503-506.
7. Schlafer DH, Foster RA. Listeriosis. Female Genital System. In: Maxie MG, ed. *Jubb, Kennedy, and Palmer's Pathology of Domestic Animals*. Vol 3. 6th ed. St. Louis, MO: Elsevier; 2016:398-402, 402-406, 408-409,414-416, 420-421.
8. Seeliger HPR, Rocourt J, Schrettenbrunner A, Grimont PAD, Jones D. *Listeria ivanovii* sp. nov. *Int. J. Syst. Bacteriol*. 1984;34(3):336-337.
9. Sergeant ESG, Love SCJ, McInnes A. Abortions in sheep due to *Listeria ivanovii*. Aust Vet J. 1991;68(1):39.

CASE II:

Signalment:
<30-day-old (neonate), female, Texel lamb, *Ovis aries*

History:
Death of 20, <30-day-old lambs was reported in a flock of 450 nonvaccinated Texel sheep in a farm in the department of Rivera, Uruguay, in October 2023 (spring season in the Southern Hemisphere). The flock was grazing natural grassland on a low terrain that used to be used for the cultivation of rice, and following a severe flooding event, the affected lambs exhibited severe apathy and hemoglobinuria, progressing to death within 24-48 hours.

Liver, lamb: There is diffuse dark red discoloration of the right kidney and dark red urine (hemoglobinuric nephrosis). The adipose and subcutaneous tissues are yellow (jaundice), and the skeletal muscles are pale pink (consistent with anemia). (Photo courtesy of Instituto Nacional de Investigación Agropecuaria (INIA), La Estanzuela, Colonia 70006, Uruguay. www.inia.uy)

Gross Pathology:
The main gross findings included yellowish discoloration of the subcutaneous and adipose tissues (jaundice), diffuse bilateral dark-red discoloration of the kidneys with dark-red urine filling the urinary bladder (hemoglobinuria), pale skeletal muscles (anemia) (Figure 1), dark pink to red mottled lungs with rubbery/meaty texture and intraluminal bronchial and tracheal froth (pulmonary edema).

Laboratory Results:

	Tissues	
Tests for detecting *Leptospira*	**Liver**	**Kidney**
Immunohistochemistry*	Positive	Negative
qPCR for pathogenic	Positive	Positive

Leptospira spp. (targeting the *lipL32* gene)		
PCR targeting the 16S rDNA gene followed by sequencing for species identification	*L. kirschneri*	*L. kirschneri*

*Using *Leptospira* multivalent fluorescent antibody conjugate (LEP-FAC) as primary antibody.

Microscopic Description:
Liver: diffusely there is disruption of the histoarchitecture of hepatic cords in the centrilobular (periacinar) areas with a bridging pattern. Within these regions hepatocytes are frequently dissociated and individualized from the hepatic cords and are either swollen with vesicular nucleus (hydropic degeneration) or shrunken with angular cell borders and hypereosinophilic cytoplasm and nuclear pyknosis or karyorrhexis (necrosis) (Figure 2). In these areas there is multifocal infiltration of neutrophils, lymphocytes and histiocytes, occasionally grouping around necrotic hepatocytes, although similar inflammatory infiltrates are present in the sinusoids of the midzonal and periportal regions where hepatocytes are preserved. Portal tracts are moderately and multifocally expanded by inflammatory cells, notably histiocytes, lymphocytes and rare neutrophils, and/or fibroblasts embedded in a loose extracellular collagenous matrix (fibrosis/fibroplasia).

Contributor's Morphologic Diagnosis:
1. Liver: multifocal random neutrophilic and lymphohistiocytic hepatitis with severe diffuse acute periacinar hepatocellular necrosis, lamb.

2. Liver: hepatitis, portal, lymphocytic and histiocytic, with fibrosis, lamb

Contributor's Comment:
The clinical signs and gross pathological findings in this lamb were highly suggestive of acute (likely intravascular) hemolysis. Differential diagnoses include "yellow lamb disease" (a poorly characterized enterotoxemia presumably caused by *Clostridium perfringens* alpha toxin), *Mycoplasma ovis* infection, and toxic plants causing hemolysis (i.e. *Allium* spp., *Brassica* spp., *Indigofera* spp., *Urochloa arrecta*).[2,3,8,9] In older sheep, chronic copper toxicity is characterized by similar clinical and pathological findings.[2] In this case, an etiologic diagnosis of leptospirosis was established based on intralesional identification of *Leptospira* spp. antigen by immunohistochemistry in the liver (Figure 3), and molecular identification of *Leptospira kirschneri* in the liver and kidney (see laboratory results section).

The nature and distribution of the microscopic lesions in the liver of the lamb, notably diffuse acute periacinar hepatocellular degeneration/necrosis, suggest that they probably resulted, at least in part, from hypoxia perhaps secondary to hemolytic anemia. However, a direct action of leptospiral invasion and multiplication in the liver, as high-

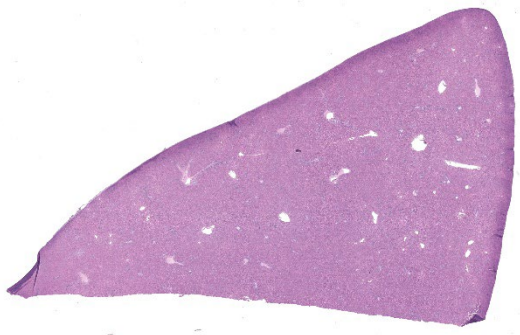

Liver, lamb: One section of liver is submitted for examination with no obvious changes at subgross magnification. (HE, 7X)

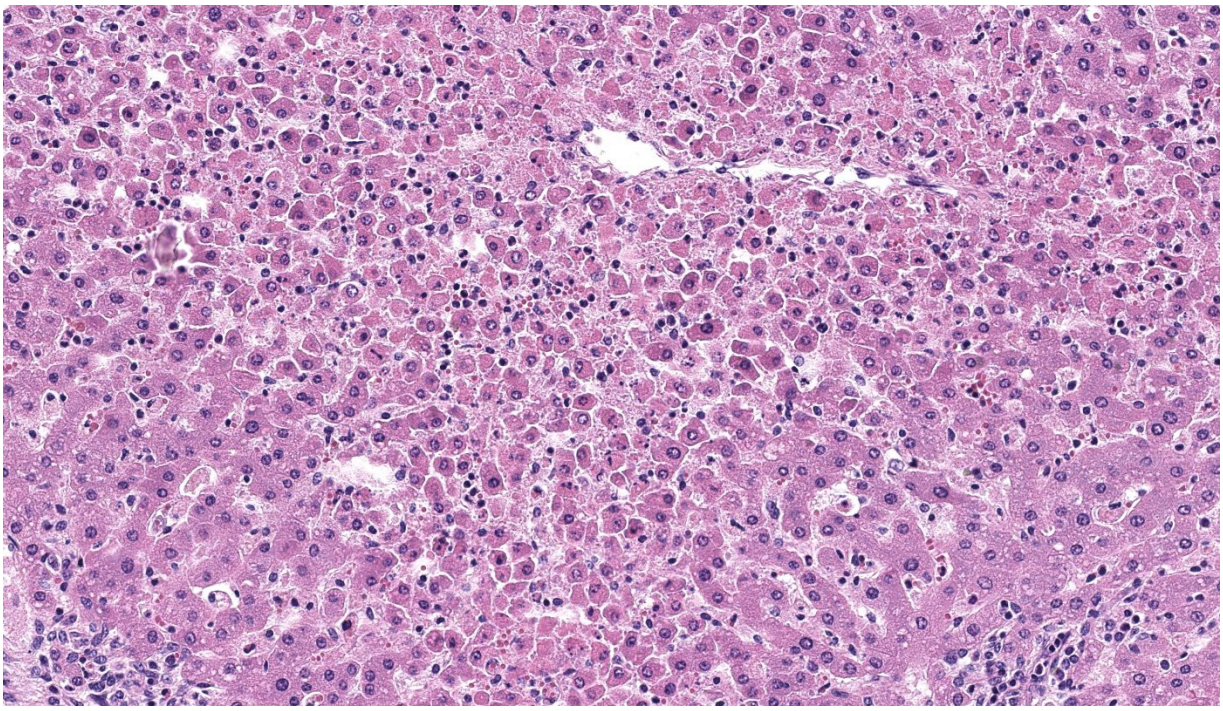

Liver, lamb: Within centrilobular and midzonal areas, there is disassociation of hepatic plates with individualization and rounding up of hepatocytes. (HE, 381X)

lighted immunohistochemically, probably contributed to the inflammatory and necrotizing lesions seen in the hepatic parenchyma. It was not clear whether the portal lesions in this case were due to *Leptospira* infection or a pre-existing incidental finding. No *Leptospira* antigen could be clearly identified in the portal tracts or bile ducts. Notably, despite the jaundice seen grossly, no significant bile stasis was observed histologically in the liver, suggesting pre-hepatic jaundice probably resulting from hemolysis.

Leptospirosis is a zoonotic disease of worldwide distribution caused by spirochetes in the genus *Leptospira*. The taxonomy of the genus has evolved enormously in recent years, and now contains several pathogenic species such as *L. interrogans*, *L. borgpetersenii*, *L. noguchii*, and *L. kirschneri*, within which more than 350 serovars have been identified.[4] While a wide range of wild and domestic animal species can be infected by a wide range of serovars, some serovars are adapted to a given animal species (maintenance hosts) and cause disease in another species (incidental hosts).[1] The major host-adapted serovars are Hardjo in cattle and sheep, Icterohaemorrhagiae and Copenhageni in rats, Ballum in mice, Canicola in dogs, and Pomona and Bratislava in pigs. Dogs, cattle, pigs, and horses are the main incidental domestic animal hosts and suffer from the disease in diverse degrees from asymptomatic to lethal.[4]

The natural niche of pathogenic *Leptospira* spp. are the proximal renal tubules and the genital tract in certain maintenance hosts. Transmission might be direct through contact with urine, lochia, milk, genital mucosa (venereal transmission), or transplacental. Infection of incidental hosts is usually indirect, via environmental contamination by urine of carrier animals. Under ideal wet, warm, and neutral to slightly alkaline conditions leptospires may survive for weeks or months in water-logged soil or water. Thus, in temperate climates leptospirosis occurs especially in the wet season and the risk of exposure and infection is increased by heavy

rainfall, agricultural irrigation and/or flooding. In tropical and subtropical areas, the disease can occur year-round.[1,4]

In incidental hosts, infection may cause severe acute or subacute systemic disease during bacteremia (leptospiremic phase), particularly in young animals. After leptospiremia has ceased, chronic disease can manifest as abortion, stillbirth, infertility, or recurrent uveitis. The acute/subacute systemic disease is clinically characterized by fever, jaundice, hemolytic anemia, hemoglobinuria, pulmonary congestion, and occasional meningitis.[1]

Leptospira genomes encode many proteins of unknown or poorly defined function and the molecular bases for virulence are poorly understood. Adhesion to host cells and components of the extracellular matrix likely plays a role in virulence. Flagellar motility, notably controlled by chemotaxis, is key to *Leptospira* virulence, as are several mechanisms allowing the bacteria to escape or resist the host immune response. How the lipopolysaccharide (LPS) contributes to virulence is still poorly known, but mutations that alter the LPS structure attenuate virulence. Pathogenic *Leptospira* spp. also produce sphingomyelinase-like enzymes with phospholipase C, hemolytic, and apoptotic activities. As these are absent in the saprophytic *Leptospira* spp. they are thought to contribute to virulence.[4]

Leptospirosis is a complex disease; its pathogenesis has not been fully elucidated and varies for different serovars in different animal species.[1] Leptospires entry to the body through mucous membranes (conjunctival, oral, genital) or via damaged or compromised skin, without inducing notable lesions at the point of entry.[4] The mechanisms used to enter the bloodstream through endothelial cells are not well understood; however, motility seems to be essential for pathogenic *Leptospira* spp. to cross tissue barriers, which is thought to occur through intracellular

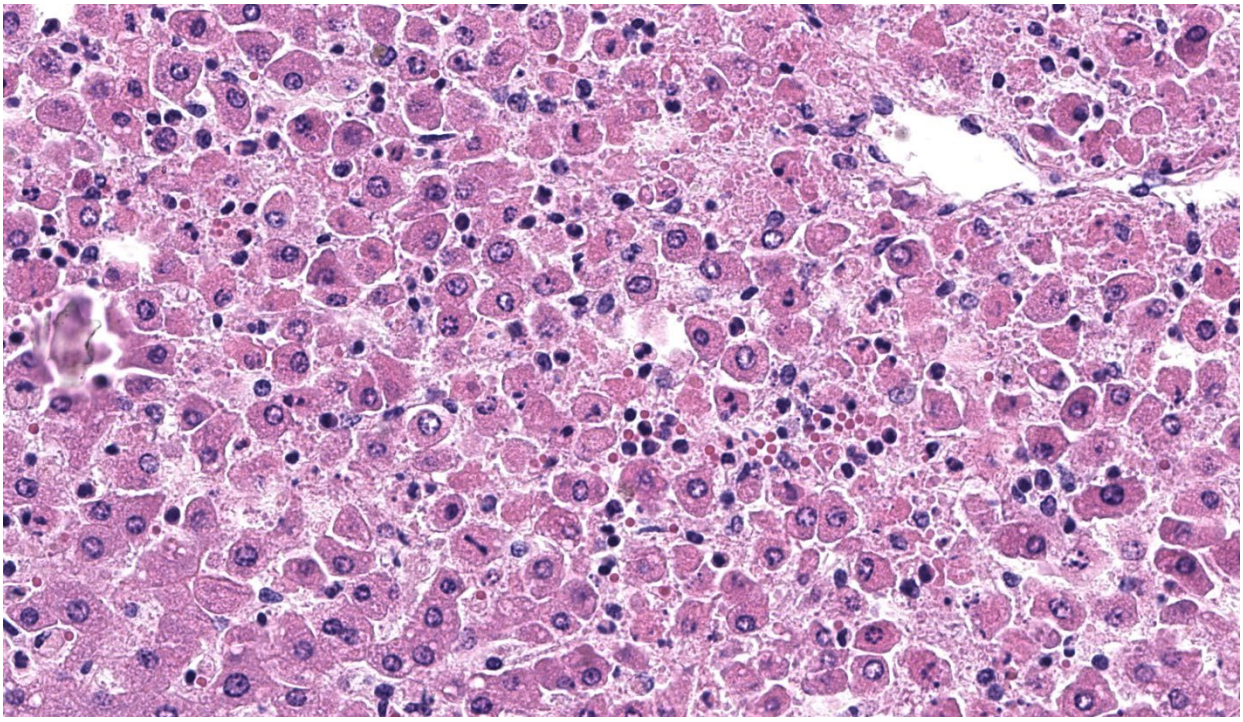

Liver, lamb: Individualized hepatocytes demonstrate granular eosinophilic cytoplasm with variable pyknosis and karyorrhexis. Hepatocytes are surrounded by abundant granular eosinophilic debris which fills sinusoids; there are few intact hepatocytes. (HE, 721X).

translocation. During the leptospiremic phase (hematogenous dissemination), which can last up to 7 days, the main symptom is fever, while clinicopathological findings frequently include leukocytosis and thrombocytopenia. Hemorrhages in the liver, kidneys, and/or lungs can develop in the acute phase of the disease, at which stage inflammation is usually absent.

After rapid hematogenous spread, leptospires interact through adhesins with a range of host tissue proteins in different organs.[4] The pathogen multiplies especially well in the liver, kidney, lungs, placenta, mammary gland, and cerebrospinal fluid (CSF).[1] *Leptospira* have developed strategies to evade host defenses and resist the complement system. Although generally considered an extracellular pathogen, it is also able to penetrate host cells and survive inside macrophages and other phagocytes involved in the innate immune response. Leptospires have also developed strategies to escape recognition by pattern-recognition receptors of the innate immune system that recognize microbe-associated molecular patterns (i.e. Nod-like and Toll-like receptors). However, the innate immune system can detect *Leptospira* and activate an immune response and the expression of cytokines.[4] After tissue colonization, hepatitis, and hepatocellular death (apoptosis/necrosis) can be seen early in the disease associated with leptospiral invasion. In the kidneys, interstitial nephritis is seen, but can be quite discrete, whereas hemoglobinuria can occur in ruminants.[4] Development of agglutinating and opsonizing antibodies after approximately 6-7 days clears the agent from most organs except from immunoprivileged sites such as the proximal tubules of the kidneys, the CSF, and the vitreous humor of the eyes. Certain serovars can also survive and establish chronic infection in the genital tract of maintenance hosts.[1]

In sheep, *Leptospira* infection is usually asymptomatic, although severe disease

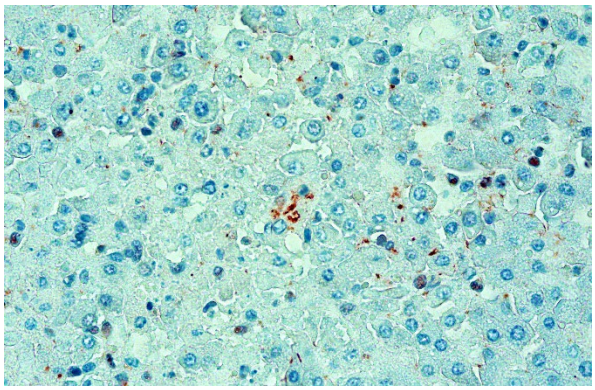

Liver, lamb. There is scattered strong granular to linear immunoreactivity for leptospiral antigen within Kupffer cells. (anti-Leptospira spp., 400X) (Photo courtesy of Instituto Nacional de Investigación Agropecuaria (INIA), La Estanzuela, Colonia 70006

occurs sporadically in young animals. In neonate lambs, leptospirosis is usually characterized by leptospiremia with hemolysis, anemia, and death. There is little information on the species and serovars involved in fatal cases of leptospirosis in sheep. In Uruguay, sporadic outbreaks of acute fatal leptospirosis in lambs associated have been associated with *L. interrogans* serogroup Pomona serovar Kennewicki.[5] *L. kirschneri*, the species detected in the case described herein, has been identified as one of the dominant *Leptospira* species (along with *L. interrogans*) associated with human leptospirosis in central Malaysia.[7]

Regardless of the acting species, it is important to determine the serovars involved in outbreaks of leptospirosis and/or infecting animals and humans in different geographic regions, so that circulating serovars can be included in vaccines, considering that immunity is serovar specific. Unfortunately, the serovar involved in the ovine case presented here could not be identified as attempts to culture and isolate this labile and fastidious organism were unsuccessful. Of note, the serovar Kennewicki which has been isolated from sheep,[5] cattle[10] and humans[6] in Uruguay is not included in the locally available commercial vaccines for livestock.

Contributing Institution:
Instituto Nacional de Investigación Agropecuaria (INIA), Route 50, Kilometer 11, La Estanzuela, Colonia 70006, Uruguay.
www.inia.uy

JPC Diagnosis:
Liver: Hepatitis, necrotizing, acute, diffuse and centrilobular, moderate, with hepatocellular disassociation.

JPC Comment:
The contributor provides an excellent summary of leptospirosis that weaves in some of the salient features of this case. Histologic changes were apparent even from low-magnification and we agree with the contributor that the underlying pathogenesis is acute centrilobular hepatitis that is probably augmented by hypoxic effects. Although anemia is more of a clinical diagnosis than a histologic one, we could not help but notice the paucity of erythrocytes within sinusoids that corresponds to the intravascular hemolysis characteristic of this agent. Dissociation (individualization) of hepatocytes was another important feature of this case which has been attributed to hepatic infectious with several species of *Leptospira*.[11] These bacteria can infiltrate the space of Disse and cause dissociation of hepatocytes through physical disruption and breakdown of intracellular tight junctions. A second consequence of the loss of tight conjunctions is leakage of bile from the canaliculus – this is a form of intrahepatic cholestasis that lacks dilatation of bile canaliculi.[11] In this case, the lack of bile plugs despite systemic icterus fits with this interpretation.

We also ran a Masson's trichrome stain to evaluate liver structure and concurrent pathology. We differed from the contributor in that we did not observe hepatic fibrosis, to include within centrilobular regions with hepatocyte loss. This argues against a prolonged event, to include secondary hypoxic changes and/or sinusoidal outflow obstruction (see Conference 12, Case 2 of this year for a relevant example). Finally, we debated the relevance of periportal cellular infiltrates. While some participants considered oval cell hyperplasia, the group consensus was for extramedullary hematopoiesis given the age of this animal and concurrent loss of erythrocytes necessitating demand.

The lack of histologic renal changes in this young lamb likely reflected a very acute course of disease and an insufficient time course for bacteremia to bring the agent to the lumina of renal tubules via the renal vasculature. That stated, the positive qPCR result in the kidney is intriguing, and we wonder whether the detection of nucleic acid therein could reflect cross-contamination.

References:

1. Cianciolo RE, Mohr CF. Urinary system. In: Maxie MG, ed. Jubb, Kennedy, and Palmer's Pathology of Domestic Animals. 6th ed. Vol 2. Amsterdam, The Netherlands: Elsevier; 2016:433–439.
2. Cullen JM, Stalker MJ. Liver and Biliary system. In: Maxie MG, ed. Jubb, Kennedy, and Palmer's Pathology of Domestic Animals. 6th ed. Vol 2. Amsterdam, The Netherlands: Elsevier; 2016:258–352.
3. Giannitti F, Macias Rioseco M, García JP, et al. Diagnostic exercise: hemolysis and sudden death in lambs. Vet Pathol. 2014;51(3):624–627.
4. Goarant C, Adler B, de la Peña Moctezuma A. *Leptospira*. In: Prescott JF, MacInnes JI, Van Immerseel FV, Boyce JD, Rycroft AN, Vázquez-Boland JA, eds. Pathogenesis of Bacterial Infections in

Animals. 5th ed. Hoboken, NJ, USA: Wiley Blackwell; 2023: 502–527.
5. Hamond C, Silveira CS, Buroni F, et al. *Leptospira interrogans* serogroup Pomona serovar Kennewicki infection in two sheep flocks with acute leptospirosis in Uruguay. Transbound Emerg Dis. 2019; 66(3):1186–1194.
6. Meny P, Menéndez C, Quintero J, et al. Characterization of *Leptospira* isolates from humans and the environment in Uruguay. Rev Inst Med Trop Sao Paulo. 2017; 59:e79.
7. Philip N, Affendy NB, Ramli SNA, et al. *Leptospira interrogans* and *Leptospira kirschneri* are the dominant *Leptospira* species causing human leptospirosis in Central Malaysia. PLoS Negl Trop Dis. 2020;14(3): e0008197.
8. Uzal FA, Giannitti F, Asin J. Yellow lamb disease (*Clostridium perfringens* Type A enterotoxemia of sheep): A review. Animals (Basel). 2022; 12(12): 1590.
9. Windsor PA. Anaemia in lambs caused by *Mycoplasma ovis*: Global and Australian perspectives. Animals (Basel). 2022; 12(11): 1372.
10. Zarantonelli L, Suanes A, Meny P, et al. Isolation of pathogenic *Leptospira* strains from naturally infected cattle in Uruguay reveals high serovar diversity, and uncovers a relevant risk for human leptospirosis. PLoS Negl Trop Dis. 2018; 12(9):e0006694.
11. Miyahara S, Saito M, Kanemaru T, Villanueva SY, Gloriani NG, Yoshida S. Destruction of the hepatocyte junction by intercellular invasion of Leptospira causes jaundice in a hamster model of Weil's disease. Int J Exp Pathol. 2014 Aug;95(4):271-81.

CASE III:

Signalment:
3-year-old, male, Merino X, *Ovis aries*, ovine

History:
Animal found dead two weeks after moved onto a paddock with a predominance of soursobs (*Oxalis cernua*) in pasture.

Gross Pathology:
Post-mortem performed by referring veterinarian. Post mortem findings included heart petechial haemorrhages, leathery appearance of renal capsules and mild hepatomegaly.

Microscopic Description:
There is moderate multifocal predominantly cortical and less often medullary tubular loss, interstitial fibrosis and mild multifocal interstitial infiltrates of lymphocytes and plasma cells. Remnant tubules are often lined by degenerate, necrotic or attenuated epithelium. Bowman's capsules and glomerular mesangium are thickened by fibrosis, with frequent synechia and scattered obsolescent glomerular tufts. Tubules are frequently ectatic, expanded up to 6 times normal diameter and filled with amorphous translucent eosinophilic material (protein), occasional sloughed epithelial cells and clear-yellow to lightly basophilic refractile crystals. Crystals are com

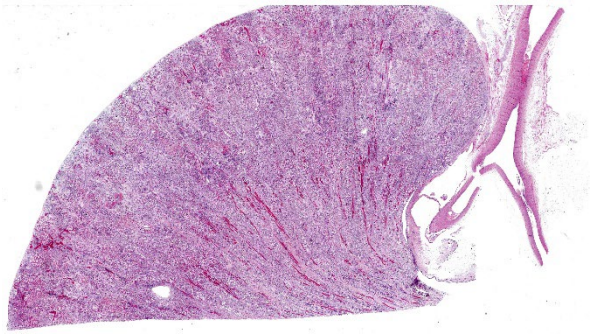

Kidney, sheep: A section of kidney is submitted for examination. (HE, 8X)

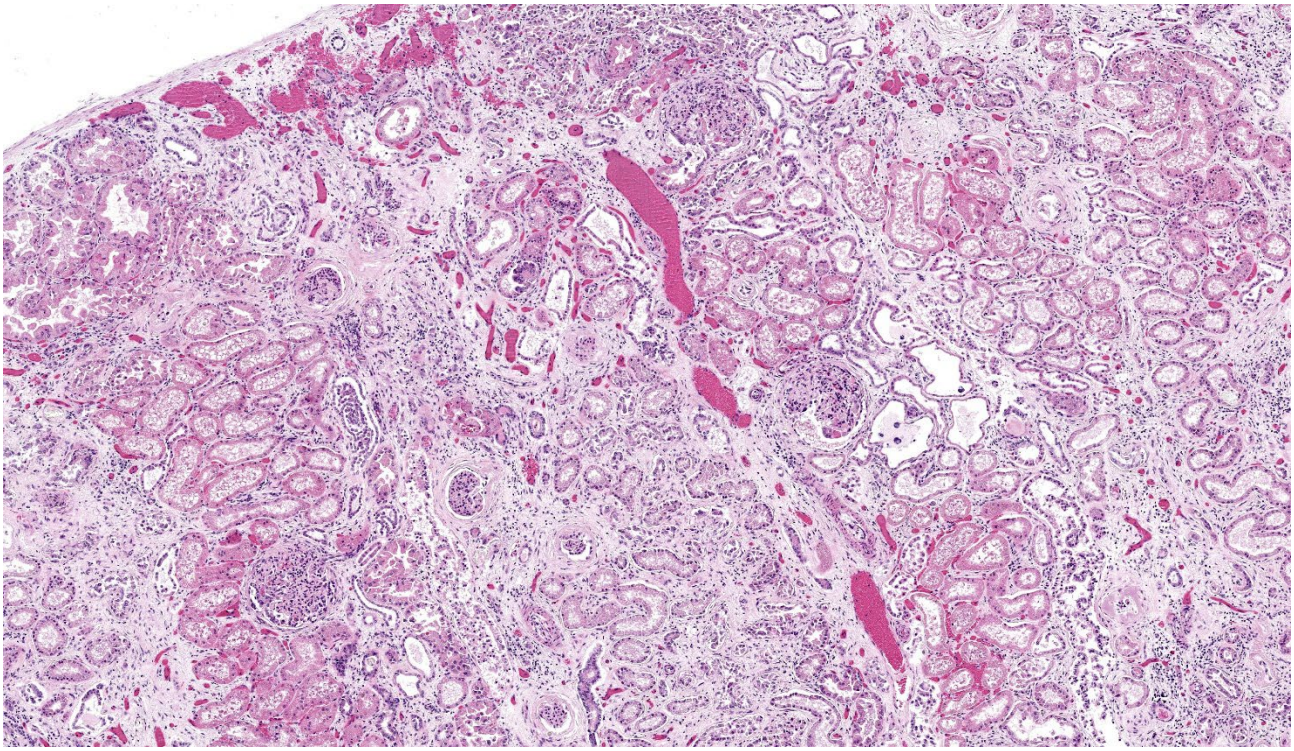

Kidney, sheep: Within the cortex, there is loss of tubules, marked interstitial fibrosis, mild lymphoplasmacytic inflammation, and various glomerular changes including variation in size, hypercellularity, and periglomerular fibrosis. (HE, 71X)

posed of radiating angular shards of variable size and shape and are birefringent under polarised light (calcium oxalate).

Contributor's Morphologic Diagnosis:
Lymph nodes, spleen and liver: T-cell lymphoid hyperplasia, severe, diffuse
Liver: Pericholangitis and perivasculitis, mild, multifocal, lymphoplasmacytic with erythrophagocytosis and extramedullary hematopoiesis

Contributor's Comment:
Oxalate nephrosis is the outcome of excessive calcium oxalate accumulation within renal tubules, forming insoluble crystals and resulting in tubular obstruction and acute renal failure.[5] Tubular epithelial injury may also result from inflammation-mediated free-radical damage and interference with oxidative phosphorylation; however there is conjecture over the concentrations required to elicit these changes.[5,12] Oxalate is the ionic form of oxalic acid and is derived from a number of sources.[4] Endogenous production occurs in the liver via oxidation of glycolate to form glyoxalate or via the metabolism of hydroxyproline, a component of collagen. This is followed by conversion to oxalate by the action of lactate dehydrogenase.[4] Primary hyperoxaluria (PH) is the predominant cause of oxalate toxicity in humans, caused by increased endogenous production due to defective enzyme activity.[4] This may involve defects in alanine glyoxalate aminotransferase (PH1), glyoxalate/hydroxypyruvate reductase (PH2), or mitochondrial 4-hydroxy 2-oxoglutarate adolase (PH3).[4] Primary hyperoxaluria is rare in domestic species, but has been reported in cats, dogs, and Beefmaster cattle, and is suspected in Australian wildlife species Gilbert's potoroo (*Potorous gilbertii*) and koalas (*Phascolarctos cinereus*).[1,5,6,13]

Secondary oxaluria predominates in domestic and non-domestic species, caused by increased intestinal absorption or increased intake of oxalates or oxalate precursors such as ethylene glycol or ascorbic acid (vitamin C).[1,4] In ruminants, oxalate toxicity is most commonly caused by ingestion of plants containing soluble oxalates, usually in the form of sodium or potassium oxalate. [3,5,10] This includes a vast range of plant species but is most commonly reported following ingestion of *Halogeton glomeratus* (halogeton), *Sarcobatus vermiculatus* (greasewood), *Rheum rhaponticum* (rhubarb), *Oxalis* spp. (soursobs) and *Rumex* spp. (sorrel, dock), *Portulaca oleracea* (purslane), *Chenopodium album* (lamb's quarter), *Bassia hyssopifolia* (bassia), *Amaranthus* spp. (pigweed), *Salsola tragus* (Russian thistle) and *Beta vulgaris* (sugar beets).[3,5,10] Oxalate concentration in these plants is dependent on a number of factors and varies between species. Higher concentrations are found in leaves rather than stems and seeds, and young plants commonly have higher concentrations than aged plants.[5,10] Concentration is also known to decrease as the plant dries; however, plants with extremely high concentrations may be potent enough to cause intoxication even after a dry summer.[5,10]

After ingestion, soluble oxalates are rapidly absorbed from the gastrointestinal tract, resulting in acute disease as soon as 2 hours post-ingestion.[9] In plasma, oxalates complex with calcium, causing hypocalcemia and precipitation of calcium oxalate within renal tubules and the vascular lumens of various tissues, resulting in vascular necrosis, haemorrhage and acute renal failure.[5,10] The kidneys are the most severely affected due to their primary role in oxalate excretion.[9] Ruminants are more tolerant of ingested oxalates than monogastrics due to the action of ruminal microbes such as *Oxalobacter formigenes,* which degrade oxalate to produce carbon dioxide and formate.[5,11]

Clinical signs of acute toxicity are caused largely by hypocalcemia and include ruminal stasis and subsequent bloat; twitching and

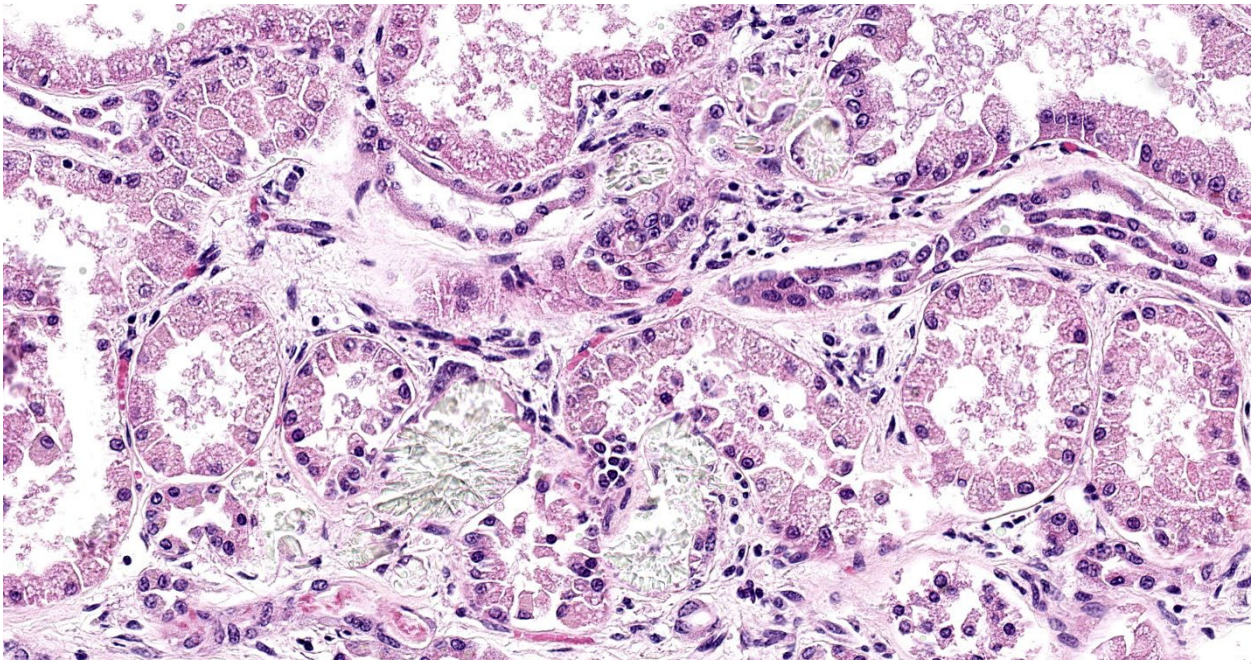

Kidney, sheep: Within the cortex, there is loss of tubules, marked interstitial fibrosis, mild lymphoplasmacytic inflammation, and various glomerular changes including variation in size, hypercellularity, and periglomerular fibrosis. (HE, 71X)

tetany which may progress to seizures; and weakness and bradycardia.[9] Animals that survive acute hypocalcemia may succumb within a number of days to acute renal failure, characterised by anorexia, depression, weight loss and diarrhoea.[9] Sheep are more commonly affected than cattle, however both species are equally susceptible under experimental conditions, suggesting that differing grazing patterns may contribute to differences in natural susceptibility.[5] The characteristic clinical and pathological findings of acute oxalate intoxication in sheep include hypocalcemia, azotemia, and nephrosis associated with precipitation of birefringent calcium oxalate crystals in renal tubules.[3,7,8]

Ruminal oxalate-degrading bacteria increase with gradual exposure to higher concentrations of oxalate, allowing adapted animals to consume greater quantities.[2,3,11] The development of acute toxicity also varies depending on rate of consumption, the availability of water and other feed and the total amount consumed.[10] Therefore, management relies on limiting availability of oxalate-containing plants and providing access to other feed sources.[9]

Contributing Institution:
Veterinary Diagnostic Laboratory, School of Animal and Veterinary Sciences, University of Adelaide Roseworthy Campus, Mudla Wirra Rd, Roseworthy SA, 5371, Australia
https://www.adelaide.edu.au/vet/about-us/pathology

JPC Diagnosis:
1. Kidney: Tubular degeneration, necrosis, and loss, diffuse, with proteinosis, tubulorrhexis, and numerous oxalate crystals.
2. Kidney: Nephritis, interstitial, lymphoplasmacytic, chronic, diffuse, moderate, with glomerular synechiae and periglomerular and interstitial fibrosis

JPC Comment:
This third case prompted intense discussion among participants. The contributor provides a outstanding histologic section to accompany a quality summary of oxalate toxicosis. We homed in on the disparity between acute and chronic changes on the slide, aided by Masson's trichrome, Jones methenamine silver, and PAS stains. We agree that the tubular changes, tubulorrhexis and leakage of the urinary filtrate into the interstitium, where it mimics edema fluid) reflect a primary process of a subacute time course, though we could not agree that the chronic interstitial nephritis followed from this same tubular obstruction. Masson's trichrome showed marked interstitial and periglomerular fibrosis that does not fit with the relatively short time course between introduction to pasture and death of this animal. To satisfy these concepts for this case, we created two separate morphologic diagnoses and interpreted this case as superimposed acute renal failure on a background of chronic subclinical renal insult.

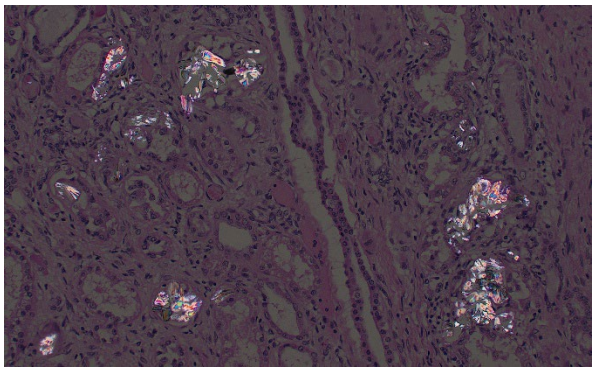

Kidney, sheep: Oxalate crystals are birefringent with polarized light. (HE 400X)

Some participants also commented on the possibility of calcium carbonate uroliths given that the morphology of some crystals did not completely fit with oxalates. Calcium carbonate uroliths are also common in ruminants, particularly when calcium availability is high. Habituation of *Oxalobacter* in the rumen to oxalate-containing forage presents one such opportunity as breakdown of calcium oxalate increases free calcium significantly.[11] It is also worth noting that oxalate crystals can also be a normal finding in the urine of ruminants, especially when concentrated.[11] In the present case, there is clear association with tubular changes to include tubulorrhexis that is outlined clearly with JMS and PAS stains.

There are other considerations for this case that were briefly entertained by the contributor already. Primary hyperoxaluria has been described in sheep breeds, to include the Zwartbles (a Dutch breed).[14] The condition is autosomal recessive and involves a loss of function missense mutation in the gene encoding for alanine-glyoxylate aminotransferase (Type 1 hyperoxaluria). The associated nephropathy is severe and heterozygous sheep may still develop histologic changes within the kidney.[14] That this animal was cross bred raises the possibility of a similar gene interaction. Finally, production of oxalates by fungi such as *Aspergillus* remain an uncommon possibility. Nephrosis following ingestion of contaminated feed has been previously described.[15] It is possible that this case reflects a multifactorial pathogenesis that leaves conference participants satisfied not matter their prevailing theory of the case.

References:

1. Diseases of the Urinary System. *In*: Veterinary Medicine, eds. Constable PD, Hinchcliff KW, Done SH, Grünberg W, 11 ed., pp. 1095-1154. Elsevier Ltd., 2017
2. Allison M, Littledike E, James L: Changes in ruminal oxalate degradation rates associated with adaptation to oxalate ingestion. Journal of animal science 45: 1173-1179, 1977.
3. Aslani MR, Movassaghi AR, Najarnezhad V, Pirouz HJ, Bami MH: Acute oxalate intoxication associated to ingestion of eshnan (Seidlitzia rosmarinus) in sheep. Trop Anim Health Prod 43: 1065-1068, 2011.
4. Bhasin B, Urekli HM, Atta MG: Primary and secondary hyperoxaluria: Understanding the enigma. World J Nephrol 4: 235-244, 2015.
5. Cianciolo RE, Mohr FC: Urinary System. *In*: Jubb, Kennedy & Palmer's Pathology of Domestic Animals: Volume 2, pp. 376-464.e371. 2016
6. Forshaw D, Horwitz AM, Ellard K, Friend JA, Greed L, Metz M: Hyperoxaluria, hyperglycoluria and renal oxalosis in Gilbert's potoroos (Potorous gilbertii). Aust Vet J 95: 250-258, 2017.
7. Jacob RH, Peet RL: Acute oxalate toxicity of sheep associated with slender iceplant (Mesembryanthemum nodiflorum). Australian Veterinary Journal 66: 91-92, 1989.
8. McKenzie RA, Bell AM, Storie GJ, Keenan FJ, Cornack KM, Grant SG: Acute oxalate poisoning of sheep by buffel grass (*Cenchrus ciliaris*). Australian Veterinary Journal 65: 26, 1988.
9. Means C: Insoluble Oxalates. *In*: Clinical Veterinary Toxicology, ed. Plumlee KH, pp. 340-341. Mosby, Inc. , Saint Louis, 2004.
10. Pickrell JA, Oehme F: Soluble Oxalates. *In*: Clinical Veterinary

Toxicology, ed. Plumlee KH, pp. 345-346. Mosby, Inc., Saint Louis, 2004.
11. Rahman MM, Abdullah RB, Wan Khadijah WE: A review of oxalate poisoning in domestic animals: tolerance and performance aspects. J Anim Physiol Anim Nutr (Berl) 97: 605-614, 2013.
12. Schepers MSJ, van Ballegooijen ES, Bangma CH, Verkoelen CF: Oxalate is toxic to renal tubular cells only at supraphysiologic concentrations. Kidney Int 68: 1660-1669, 2005.
13. Speight KN, Boardman W, Breed WG, Taggart DA, Woolford L, Haynes JI: Pathological features of oxalate nephrosis in a population of koalas (Phascolarctos cinereus) in South Australia. Vet Pathol 50: 299-307, 2013.
14. Letko A, Dijkman R, Strugnell B, Häfliger IM, Paris JM, Henderson K, Geraghty T, Orr H, Scholes S, Drögemüller C. Deleterious AGXT Missense Variant Associated with Type 1 Primary Hyperoxaluria (PH1) in Zwartbles Sheep. Genes (Basel). 2020 Sep 29;11(10):1147.
15. Botha CJ, Truter M, Bredell T, Lange L, Mülders MS. Putative Aspergillus niger-induced oxalate nephrosis in sheep. J S Afr Vet Assoc. 2009 Mar;80(1):50-3.

CASE IV:

Signalment:
2-month-old, female, Toggenburg goat (*Capra aegagrus hircus*)

History:
Presented with clinical complaints of vomiting and lethargy. Huge amount of fluid in peritoneal cavity (ascites). No abnormalities found on echocardiac examination and blood examination. Laparascopy performed: suspicion of encapsulating peritoneal sclerosis. Died at night.

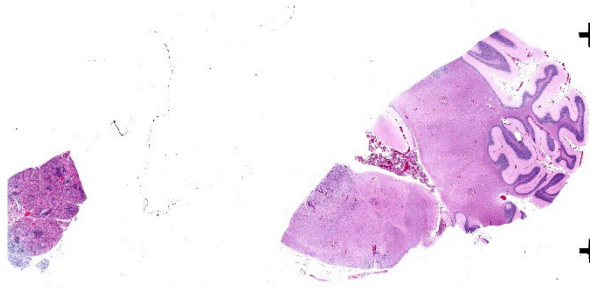

Lung and brainstem/cerebellum, goat: There is diffuse atelectasis and foci of hypercellularity in the lung at subgross magnification. (HE, 8X)

Gross Pathology:
A 2-month-old female Toggenburg goat kid presented for nystagmus, incoordination, and inability to ambulate. Several days prior, this kid's sibling was euthanized for similar severe neurologic signs.

Laboratory Results:
Immunohistochemical staining for Caprine Arthritis and Encephalitis Virus was positive on brainstem and lung tissue (Michigan State University, Veterinary Diagnostic Laboratory).

Aerobic culture grew few colonies *Streptococcus infantarius, Streptococcus equinus,* and coagulase negative *Staphylococcus* spp. *Mycoplasma spp.* PCR was negative.

(Ohio Department of Agriculture, Animal Disease Diagnostic Laboratory).

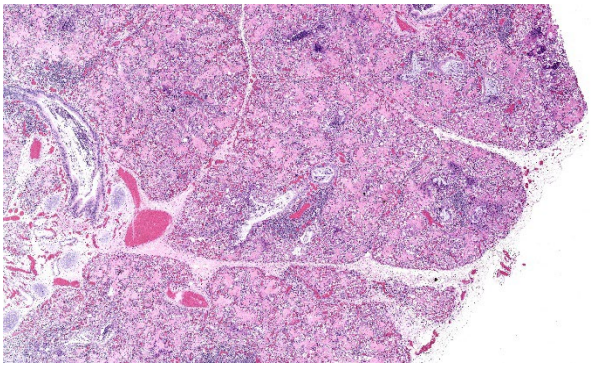

Lung, goat. There is marked BALT hyperplasia, and airway lumina contain a cellular infiltrate with abundant mucus. Alveoli are filled with brightly eosinophilic edema fluid and fibrin and a cellular exudate. (HE, 43X)

Microscopic Description:
Brainstem and cerebellum: Regionally affecting the brainstem white matter along the midline is an area of neuropil loss and replacement by numerous macrophages with foamy eosinophilic cytoplasm with eccentrically placed nuclei (gitter cells) and mild to moderate numbers of reactive astrocytes, microglia, and admixed lymphocytes and fewer plasma cells. Myelin sheaths are frequently replaced by gitter cells and are rarely dilated with either swollen hypereosinophilic axons (spheroids) or macrophages (digestion chambers). Scattered throughout the affected region is abundant eosinophilic cellular debris. Virchow Robin's spaces are multifocally expanded by numerous lymphocytes, histiocytes, and fewer plasma cells (perivascular cuffs).

Lungs: Diffusely alveoli are filled with large amounts of eosinophilic amorphous proteina-

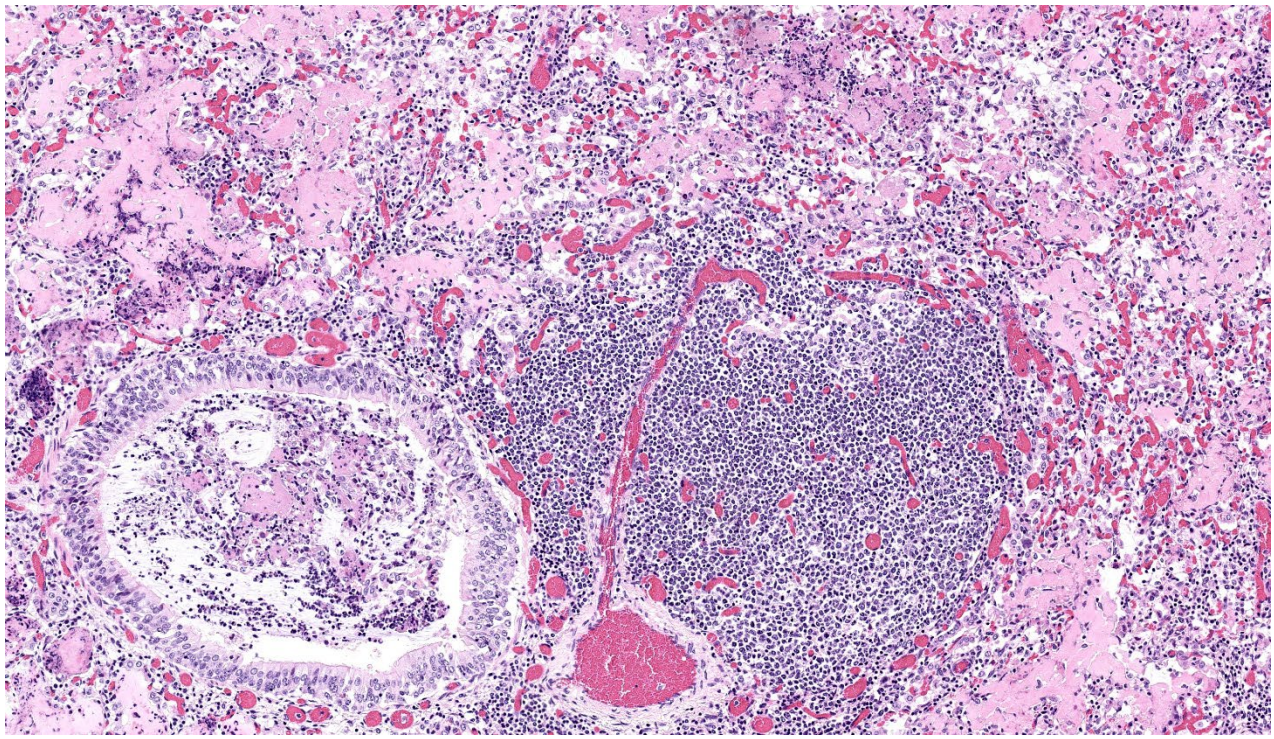

Lung, goat. There is marked BALT hyperplasia, and airway lumina contain a cellular infiltrate with abundant mucus. Alveoli are filled with brightly eosinophilic edema fluid and fibrin and a cellular exudate. (HE, 43X)

ceous fluid (alveolar proteinosis) and multifocal admixed foci of necrotic cellular and

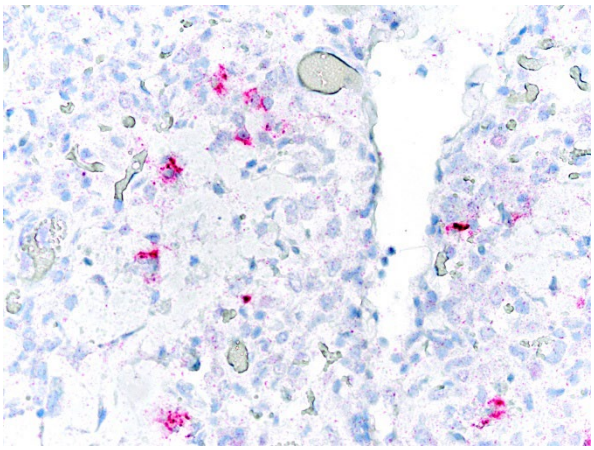

Lung, goat. Multifocally, mononuclear cells demonstrate strong cytoplasmic immunolabeling for CAEV. (anti-CAEV, 400X) (Photo courtesy of The Ohio State University College of Veterinary Medicine, Department of Veterinary Biosciences, https://vet.osu.edu

nuclear karhyorrhectic debris. Multifocally, alveoli are lined by plump type II pneumocytes (type II pneumocyte hyperplasia). Vari ably, alveolar septa are expanded by moderate numbers of lymphocytes, histiocytes and

fewer plasma cells. Bronchi and large bron chioles contain abundant degenerate neutrophils admixed with eosinophilic cellular and karyorrhectic debris and moderate amounts of basophilic mucin. Lymphoid tissue surrounding bronchi and bronchioles is moderately hyperplastic, with frequent prominent germinal centers.

Contributor's Morphologic Diagnosis:
Brainstem: Severe, focally extensive, lymphohistiocytic leukoencephalitis with axonal degeneration and neuropil necrosis

Lungs:

a. Marked, diffuse, chronic, lymphohistiocytic interstitial pneumonia with type II pneumocyte hyperplasia and alveolar proteinosis

b. Moderate, multifocal, acute, suppurative bronchopneumonia

Contributor's Comment:
Brainstem lesions, interstitial pneumonia, and immunohistochemistry results in this case are consistent with small ruminant lentivirus infection (SRLV), or Caprine Arthritis and Encephalitis Virus (CAEV).

CAEV is a lentivirus within the Retrovirus family. CAEV and Maedi-Visna virus (MV), also called Ovine Progressive Pneumonia, are together referred to as the small ruminant lentiviruses (SRLV).[4] Previously CAE and MV were considered species-specific, with CAEV affecting goats and MV affecting sheep; however, several studies have documented cross-species and co-infections demonstrating both species are susceptible to each virus.[1, 7]

Other prominent lentiviruses include Equine Infectious Anemia Virus, Bovine Immunodeficiency Virus, and Feline Immunodeficiency Virus in domestic species and Human Immunodeficiency Virus in humans. In contrast to these other lentiviruses, SRLVs are unique in

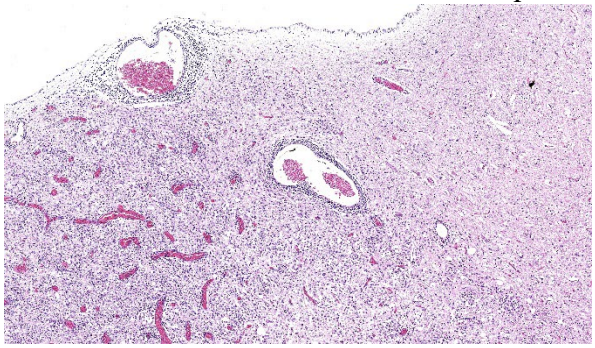

Brainstem, goat: There are multifocal areas of profound inflammation and parenchymal necrosis within the brainstem along the midline subjacent to the 4th ventricle. Vessels in these areas are cuffed by lymphocytes and plasma cells. (HE, 131X)

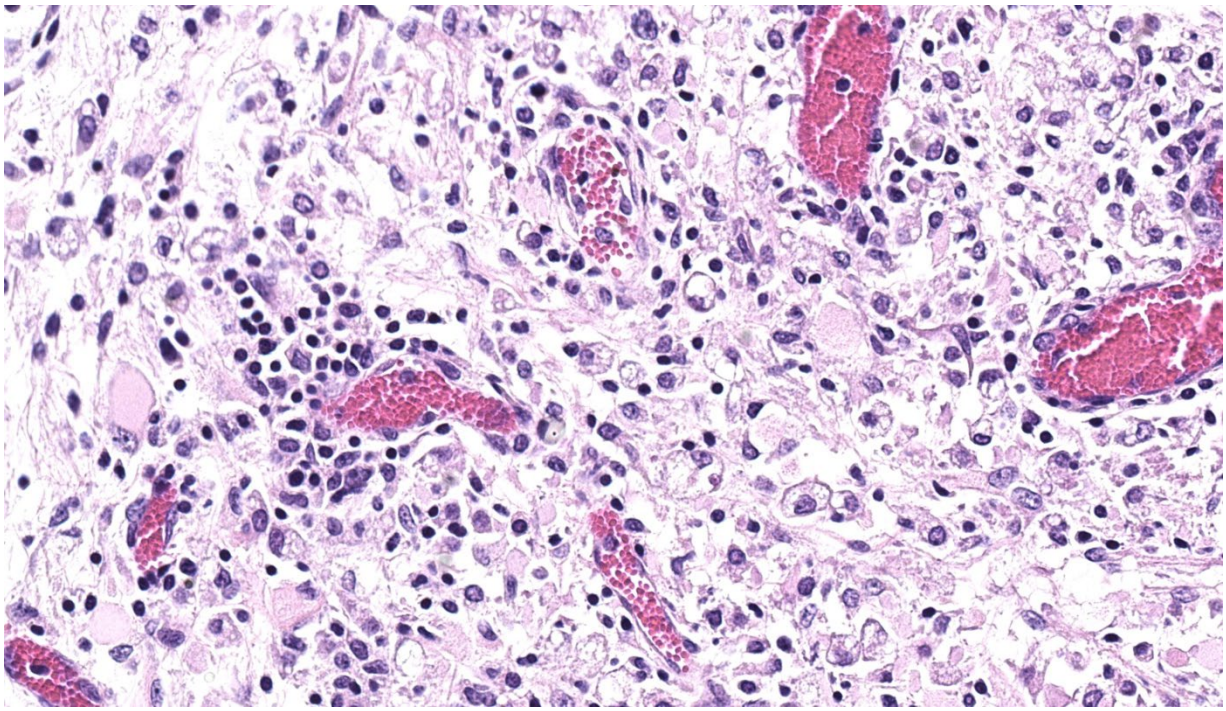

Brainstem, goat. Higher magnification of inflamed areas with chromatolytic swollen neurons, numerous Gitter cells and other glia, and cuffs of lymhocytes around vessels. (HE, 713X)

that they do not cause immunodeficiency in infected animals.[3, 6] The mechanism by which SRLVs are able to evade the host immune system despite an appropriate immune response is not fully understood. One proposed mechanism is that tropism of SRLVs for monocytes, macrophages, and dendritic cells allows the virus to evade the host immune system and disseminate systemically.[6] Once in target tissues, the virus can infect other cell types including microglia, endothelial cells, fibroblasts, and epithelial cells, though replication is restricted in these cells.[1, 3, 5] These additional tissue targets, particularly mammary epithelium, likely serve as important reservoirs of infection.[1, 5]

Transmission primarily occurs through ingestion of milk/colostrum or inhalation of nasal secretions.[3, 5] In utero transmission can occur infrequently in sheep and SRLVs have been detected in semen, though transmission via this route has not been documented.[2, 3] In the present case, the dam of the affected goat kid tested positive for CAEV prior to pregnancy and the kid likely became infected following ingestion of colostrum and milk. This is further supported by the reported similar clinical signs in the sibling of the present animal.

Infection with SRLVs leads to slowly progressing, often subclinical, inflammatory disease.[3] When clinical, four pathologic presentations, either alone or in combination, are recognized: encephalomyelitis, interstitial pneumonia, arthritis, indurative mastitis. Which form is present is variable and depends on various factors including species affected and age of the animal. Adult sheep typically present with pneumonia and/or encephalomyelitis while adult goats present with the arthritic form and goat kids present with the neurologic form.[4, 5, 8]

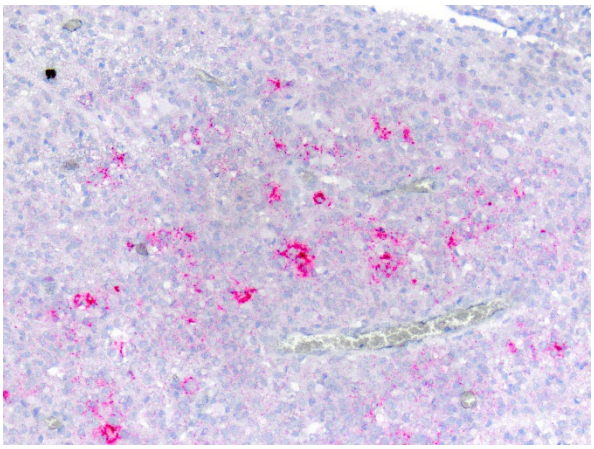

Brainstem, goat. Multifocally mononuclear cells demonstrate strong cytoplasmic immunolabeling for CAEV. (anti-CAEV, 400X) (Photo courtesy of The Ohio State University College of Veterinary Medicine, Department of Veterinary Biosciences, https://vet.osu.edu

As in the present case, the neurologic form in both sheep and goat kids is histologically characterized by lymphocytic and/or histiocytic demyelinating leukoencephalomyelitis frequently resulting clinically in progressive ataxia beginning in the hindlimbs.[3] The respiratory form is histologically characterized by lymphohistiocytic interstitial pneumonia, lymphoid follicle proliferation, and alveolar septa that are thickened by interstitial fibrosis and smooth muscle hypertrophy.[3, 8] In sheep, type II pneumocyte hyperplasia is uncommon, while in goats it is frequently present.[3] Additionally alveoli can be filled with abundant dense eosinophilic proteinaceous material.[3, 8] Electron micrographs of this fluid reveal numerous myelin figures consistent with surfactant.[9] In human medical literature, this accumulation of surfactant is termed alveolar proteinosis and is considered secondary to functional disruptions of alveolar macrophages.[10] There are a variety of documented causes of alveolar proteinosis in humans while in goats it has been described with CAEV as well as pulmonary adenomatosis.[9, 10] Therefore, alveolar proteinosis does not appear to be specific to CAEV but likely manifests secondary to alveolar macrophage dysfunction during infection.

The arthritic form, common in adult goats, is characterized by synovial villous hyperplasia with necrosis, mineralization, and fibrosis of the synovium with chronic infection.[3] Finally, the mastitis form is frequently subclinical and is a significant source of economic losses. It is frequently non-painful and involves infiltration of the mammary interstitium by lymphocytes, plasma cells, and macrophages that with time progresses to fibrosis.[3,5]

The concurrent suppurative bronchopneumonia in this case is not typical for reported SRLV respiratory lesions. We suspect that this may represents a separate bacterial infection; multiple bacterial agents were cultured from the lung to support this hypothesis, but the weak growth of mixed bacteria makes it difficult to interpret whether this reflect true infection or contaminants. *Mycoplasma* spp. infection was also considered as an additional contributor, but PCR for this agent was negative.

Contributing Institution:
The Ohio State University College of Veterinary Medicine
Department of Veterinary Biosciences
Anatomic Pathology Service
1925 Coffey Road
Columbus, OH 43210
https://vet.osu.edu/departments-offices/biosciences

JPC Diagnosis:
1. Lung: Pneumonia, interstitial, lymphohistiocytic, chronic, diffuse, marked, with peribronchiolar and perivascular lymphoid

hyperplasia, type II pneumocyte hyperplasia, and alveolar proteinosis.
2. Lung: Bronchopneumonia, suppurative, subacute, multifocal, moderate.
3. Brainstem: Rhombencephalitis, necrotizing and lymphohistiocytic, subacute, focally extensive, severe, with gliosis.

JPC Comment:
The final case of this conference was descriptively rewarding for participants. The presence of brain and lung on the same slide from a young animal prompted many to immediately favor small ruminant lentiviruses, though there were several features of this case that were perplexing given the age of this animal. Foremost, the degree of alveolar proteinosis is marked, reflecting significant dysfunction of pulmonary macrophages. Given that these viruses utilize monocyte precursors both as a reservoir and means of trafficking virus to naïve tissue macrophages,[11] we considered whether this might reflect coinfection (CAEV and OPP) and/or a distinct viral subtype that is more virulent. In theory, only few monocyte precursors retain lentivirus (i.e. susceptible but not permissive to viral replication) and it should take time to develop histiocytic interstitial pneumonia.

As the contributor notes, pneumonia is a more common finding in older animals (reflecting this notion) and is rarer in goats. It is likely that the goat kids in this case were secondarily infected with another agent that augmented monocyte recruitment and subsequent tissue macrophage activation and cytokine production that hampered surfactant handling.[11] Notably, there is BALT hyperplasia present which is suggestive of *Mycoplasma* infection (or at least marked antigen presentation) which aligns with bacterial culture results and the airway-specific histological changes. For his reason, we separated this secondary bronchopneumonia out as a distinct morphologic diagnosis.

Dr. Highland concluded the conference discussion reminding participants about challenges in testing for small ruminant lentiviruses and emphasized that young animals with few infected monocytes may be seronegative or below detection limits of given assays. In larger goat herds and sheep flocks, the cost of serial testing presents a significant economic roadblock for controlling or eradicating these diseases.

References:

1. Blacklaws BA. Small ruminant lentiviruses: immunopathogenesis of visna-maedi and caprine arthritis and encephalitis virus. *Comp Immunol Microbiol Infect Dis.* 2012 May;35(3):259-69.
2. Blacklaws BA, Berriatua E, Torsteinsdottir S, et al. Transmission of small ruminant lentiviruses. *Vet Microbiol.* 2004 Jul 14;101(3):199-208.
3. Caswell JL, Williams KJ. Respiratory system. In: Jubb, Kennedy and Palmer's Pathology of domestic animals, vol. 2. Sixth Edition. Elsevier. St.Louis, Mo, 2016:465-591.
4. Cantile C, Youssef S. Maxie MG, Youssef S. Nervous system. In: Maxie MG, ed. Jubb, Kennedy, Palmer's Pathology of Domestic Animals. Vol.1. 6th ed. Philadelphia, PA: Elsevier; 2016:378-379.
5. Gomez-Lucia E, Barquero N, Domenech A. Maedi-Visna virus: current perspectives. *Vet Med (Auckl)*. 2018 May 21;9:11-21.
6. Larruskain A, Jugo BM. Retroviral infections in sheep and goats: small ruminant lentiviruses and host interaction. *Viruses*. 2013 Aug 19;5(8):2043-61.

7. Leroux C, Cruz JC, Mornex JF. SRLVs: a genetic continuum of lentiviral species in sheep and goats with cumulative evidence of cross species transmission. *Curr HIV Res.* 2010 Jan;8(1):94-100.
8. Moroz A, Czopowicz M, Sobczak-Filipiak M, et al. The prevalence of histopathological features of pneumonia in goats with symptomatic caprine arthritis-encephalitis. *Pathogens*. 2022;11(6):629.
9. Sims LD, Hale CJ, McCormick BM. Progressive interstitial pneumonia in goats. *Australian Veterinary Journal*. 1983;60:368-371.
10. Trapnell BC, Nakata K, Bonella F, et al. Pulmonary alveolar proteinosis. *Nature Reviews Disease Primers*. 2019;5(1):16.
11. Stanton JB, Zachary JF. Mechanisms of Microbial Infections. In: Zachary JF, ed. Pathologic Basis of Veterinary Disease. 7th ed. St. Louis, MO: Elsevier; 2022:254-255.
1.

Joint Pathology Center
Veterinary Pathology Services

WEDNESDAY SLIDE CONFERENCE 2024-2025

Conference #23 — 9 April 2025

CASE I:

Signalment:
2-year-old male white-faced saki monkey (*Pithecia pithecia*)

History:
A privately owned 2-year-old male white-faced saki monkey (*Pithecia pithecia*) was brought to the University of Tennessee College of Veterinary Medicine's zoo medicine service for hindlimb lameness. Radiographs identified generalized osteopenia and a folding fracture of the right tibia. The monkey had been housed exclusively indoors since birth.

Hindlimb, monkey: There is a midshaft fracture of the tibia. (Photo courtesy of: University of Tennessee College of Veterinary Medicine, https://vetmed.tennessee.edu/)

Gross Pathology:
Midway along the tibial diaphysis of the right hindlimb, approximately 5.5 cm distal to the stifle, was a 3 cm in diameter, circumferential, white, firm, boney proliferation (callus). The tibia and fibula immediately distal to the callus were bent and directed approximately 70 degrees caudally.

On cut section, there was a 2 cm diameter rim of periosteum, skeletal muscle, and subcutis immediately surrounding the callus which was dark red to black (hemorrhage) and had a translucent yellow wet gelatinous appearance (edema). Bone marrow was dark red, soft, and floated in 10% neutral buffered formalin.

Laboratory Results:
A serum chemistry panel identified severely elevated alkaline phosphatase (ALP) at 4167 u/L and mild hypocalcemia with 0.9 mmol/L ionized calcium.

Microscopic Description:
Right tibia: The cortical bone is thin, discontinuous, and replaced by loose fibrovascular tissue (fibroplasia). Fragments of cortical bone are surrounded by fibrovascular tissue and segmentally lined by a single layer of osteoblasts or increased numbers of osteoclasts within Howship's lacunae (resorption). There

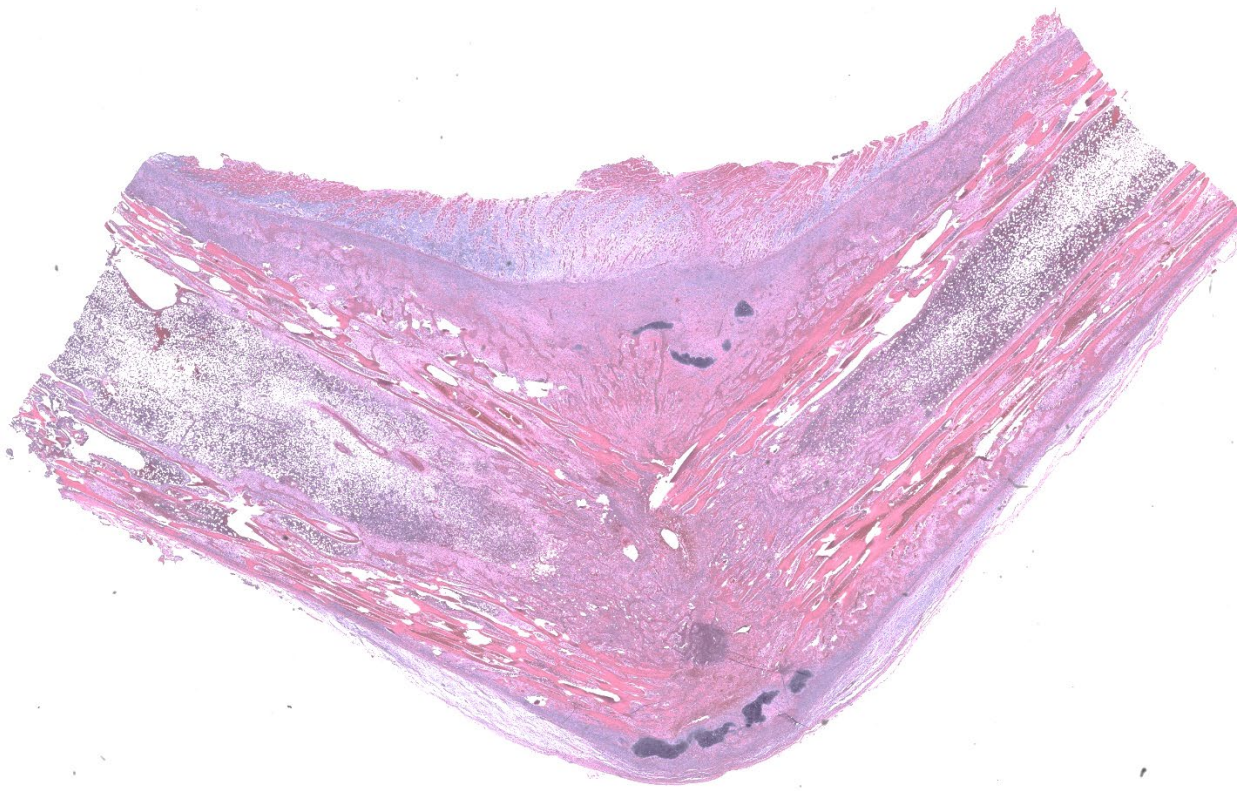

Tibia, monkey. There is a midshaft diaphyseal fracture with callus formation. The two ends of the bone are thicker than normal, and there is atrophy of the overlying skeletal muscle. (HE, 8X)

are bands of thick fibrovascular tissue expanding the periosteal and endosteal margins with frequent islands and irregular trabeculae of immature woven bone lined by osteoblasts. There is a focal complete cortical defect and the long axes of bone are positioned at approximately 90 degrees (fracture). At the fracture site, cortical bone is surrounded and separated by the previously described fibrovascular connective tissue mixed with erythrocytes transitioning to basophilic cartilaginous matrix with chondrocytes and irregular trabeculae of woven bone. The marrow cavity has approximately 50% cellularity with megakaryocytes, and erythroid and myeloid precursors of various developmental stages. A lightly basophilic myxomatous matrix extends into and surrounds adjacent skeletal muscle bundles which are frequently small and rounded (atrophy).

Contributor's Morphologic Diagnosis:

Right tibia: Severe chronic diffuse fibrous osteodystrophy with a diaphyseal fracture and callus

Contributor's Comment:

Contributing Institution:
University of Tennessee College of Veterinary Medicine
2407 River Drive
Knoxville, TN 37996
https://vetmed.tennessee.edu/

This white-faced saki monkey (*Pithecia pithecia*) had nutritional secondary hyperparathyroidism with fibrous osteodystrophy and a

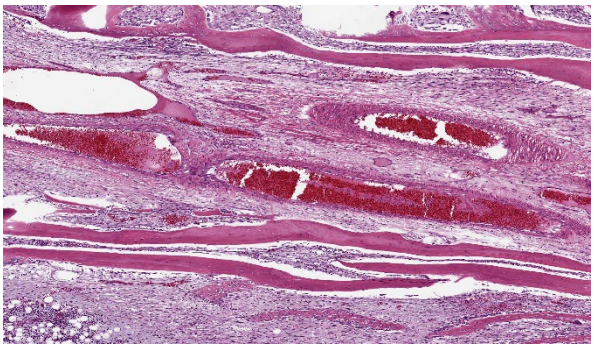

Tibia, monkey. The cortical bone is no longer compacted, resorbed, and is infiltrate by abundant densely cellular fibrous connective tissue. (HE, 95X)

pathologic tibial fracture. In this case, radiographs also showed a generalized diffuse decrease in radiodensity of all bones, indicating osteopenia.

Metabolic bone disease includes multiple morphologic entities which can occur in combination in the same individual. These include rickets, osteomalacia, osteoporosis, and fibrous osteodystrophy, all caused by deficiencies or imbalances in vitamin D, calcium, and/or phosphorous.[1]

Fibrous osteodystrophy is characterized by extensive bone resorption, proliferation of fibrous tissue, and the formation of poorly mineralized immature bone.[1] The pathogenesis includes an elevation of parathyroid hormone (PTH) which may be caused by primary hyperparathyroidism, secondary hyperparathyroidism, or hypercalcemia of malignancy. Primary hyperparathyroidism may be caused by a functional parathyroid neoplasm (adenoma or adenocarcinoma) and secondary hyperparathyroidism may be caused by either renal disease or nutritional imbalances of calcium, phosphorous, and/or vitamin D.

Vitamin D may be obtained from the diet and radiation of the skin with ultraviolet light. Metabolic bone disease is not uncommon in privately owned non-human primates, as their diets may be inadequately balanced, they often receive insufficient exposure to ultraviolet light, and lack supplementation of their diet with vitamin D3 (cholecalciferol).[3] New World monkeys have specific vitamin D requirements to maintain serum calcium levels and are thus exquisitely sensitive to calcium and vitamin D deficiencies.[5] A lack of exposure to ultraviolet light impedes the conversion of 7-dehydrocholesterol in the skin to pre-vitamin D3.[4] Pre-vitamin D3 is then isomerized to vitamin D3 (cholecalciferol). Forms of vitamin D from the diet and skin undergo hydroxylation in the liver, forming 25-hydroxycholecalciferol or 25-hydroxyvitamin D [25(OH)D], which is the form of vitamin D in the circulation. This is then hydroxylated in the kidney by 1α-hydroxylase to form calcitriol (1, 25-dihydroxyvitamin D), the metabolically active form of vitamin D.[2]

Although the diet is unknown, the history of being housed exclusively indoors likely led to vitamin D deficiency and nutritional hyperparathyroidism in this monkey. The parathyroids had diffuse chief cell hyperplasia consistent with secondary hyperparathyroidism. There was no clinical, gross, or histologic evidence of renal disease.

JPC Morphologic Diagnosis: 1. Long bone: Osteoclast-mediated bone resorption,

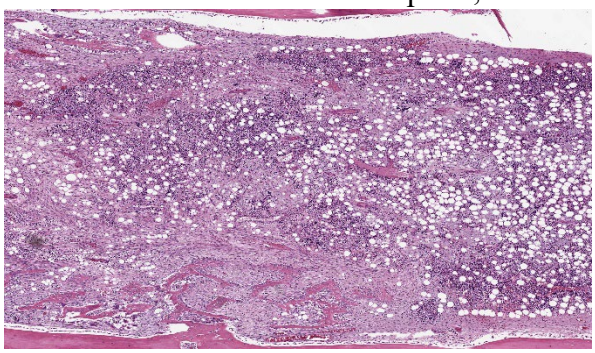

Tibia, monkey. The cortical bone is no longer compacted, resorbed, and is infiltrate by abundant densely cellular fibrous connective tissue. (HE, 95X)

marked, with cortical fibrosis, pathologic fracture, and callus.

2. Skeletal muscle: Atrophy, multifocal, marked.

JPC Comment: This week's moderator was Dr. Brian Murphy from the University of California at Davis, who selected four bone and oral pathology-centered cases to dazzle conference participants. This first case is beautifully sectioned with a characteristic gross photo that drew an audible reaction from the group. Participants discussed metabolic bone disease at length with Dr. Murphy and used slide features to draw inferences which we faithfully attempt to capture below.

Foremost, evaluation of bone should start first from subgross magnification. While we approach all of our descriptions in this manner, Dr. Murphy emphasized the importance of a careful survey of the cortex, periosteum, endosteum, marrow elements, and surrounding tissue before jumping to higher magnifications. Likewise, evaluation of bone ALWAYS requires radiographs and a detailed clinical history to support interpretation. In this case, the presence of a large, well-developed callus is helpfully centered by the contributor and provides a clue for the apparent right-angle turn in the direction of the bone. That said, the callus is the *effect* and not the *cause* of the lesion in this saki monkey (although it is impressive). Evaluation of adjacent cortical bone reveals the answer, in that it is both wide and lytic with the presence of numerous osteoclasts and fibrous tissue – these features together yield the diagnosis of fibrous osteodystrophy. Dr. Murphy noted that in chronic cases, the presence of osteoclasts may be minimal or absent, though the diagnosis can still be made. The atrophy of skeletal muscle in this case is also distinctive and is itself another effect – we considered the possibility of both disuse and abnormal weight-bearing as contributory factors.

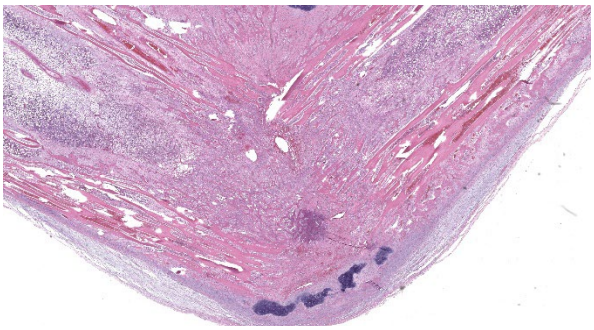

Tibia, monkey. There is a folding fracture of the tibial diaphysis, with periosteal new bone trabeculae oriented perpendicular to the surface of the bone, callus formation with abundant fibrous connective tissue and islands of cartilage, and fibrosis an and atrophy of the overlying skeletal muscle. (HE, 22X)

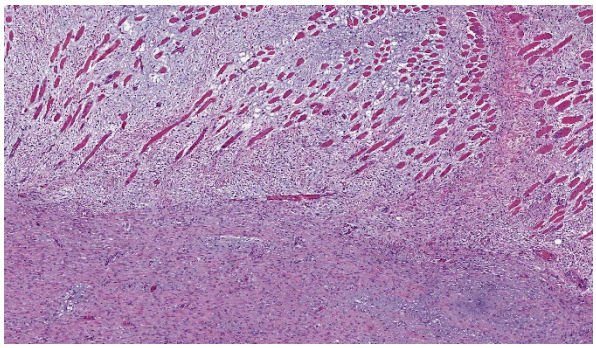

Tibia, monkey. Above the fracture site, the periosteum is markedly thickened and hypercellular and the skeletal muscle is atrophic and infiltrated by abundant cellular fibrous connective tissue. (HE, 87X)

In addition, evaluation of metabolic bone disease can reveal multiple concurrent processes with overlapping histologic features which the pathologist should expect. In young animals, fibrous osteodystrophy can co-exist with rickets, which warrants consideration of the physis for disorganization and expansion of the zone of hypertrophy as well as evaluation of the metaphysis for unmineralized osteoid.[1] The cortex is generally thickened with unmineralized osteoid along the periosteum. In adult animals, osteomalacia also reflects inability to mineralize osteoid, but there is no

open physis to consider. There may be decreased numbers of thin bony trabeculae and/or cortical thinning.[1] Osteoporosis (a *clinical* syndrome reflecting pain, lameness, and/or bony deformation) may also be superimposed on cases of metabolic bone disease due to microfracture and infraction (fracture without cortical displacement) of bone. Before rendering a final diagnosis, it is helpful to summarize all associated slide features and weigh whether one or more processes is occurring that could explain the constellation of histologic signs.

References:

1. Craig LE, Dittmer KE, Thompson KG. Bones and joints. In: Maxie, MG ed. *Jubb, Kennedy, and Palmer's Pathology of Domestic Animals.* 6th Vol. 1. St. Louis, MO: Elsevier; 2016:60-80.
2. Dittmer KE, Thompson KG. Vitamin D Metabolism and Rickets in Domestic Animals: A Review. *Veterinary Pathol*. 2011;48(2):389-407.
3. Hatt JM, Sainsbury AW. Unusual case of metabolic bone disease in a common marmoset (Callithrix jacchus). *Veterinary Rec*. 1998;143(3):78-80.
4. Minich DJ, Henry BA, Levens GP. Metabolic bone disease in a white-faced saki (Pithecia pithecia). *Vet Rec Case Rep*. 2022;10:e393
5. Olson EJ, Shaw GC, Hutchinson EK, et al. Bone Disease in the Common Marmoset: Radiographic and Histological Findings. *Veterinary Pathol*. 2015;52(5):883-893.

CASE II:

Signalment:

A 7-year-old spayed male domestic shorthair cat (*Felis silvestris catus*)

Humerus, cat: Radiographs reveal a focally expansile lesion and bone lysis in the right third proximal humerus with evident thinning of the cortical bone extending towards the diaphysis. (Photo courtesy of Department of Comparative Biomedicine and Food Science, Viale dell'Università 15, 35020, Legnaro (PD), Italy; https://www.bca.unipd.it/)

History:

A 7-year-old, spayed male domestic shorthair cat, weighing 4.65 kg (body condition score: 5/9), regularly vaccinated and living indoor, was presented to the Veterinary Clinic for evaluation of grade III lameness in the right forelimb. The owner reported that the lameness was observed for a few days following a trauma. Upon presentation, the cat was bright and alert, but exhibited an aggressive behaviour. Physical examination revealed no abnormalities, muscular asymmetry or atrophy were not observed in the forelimbs. The orthopaedic examination indicated moderate pain reaction

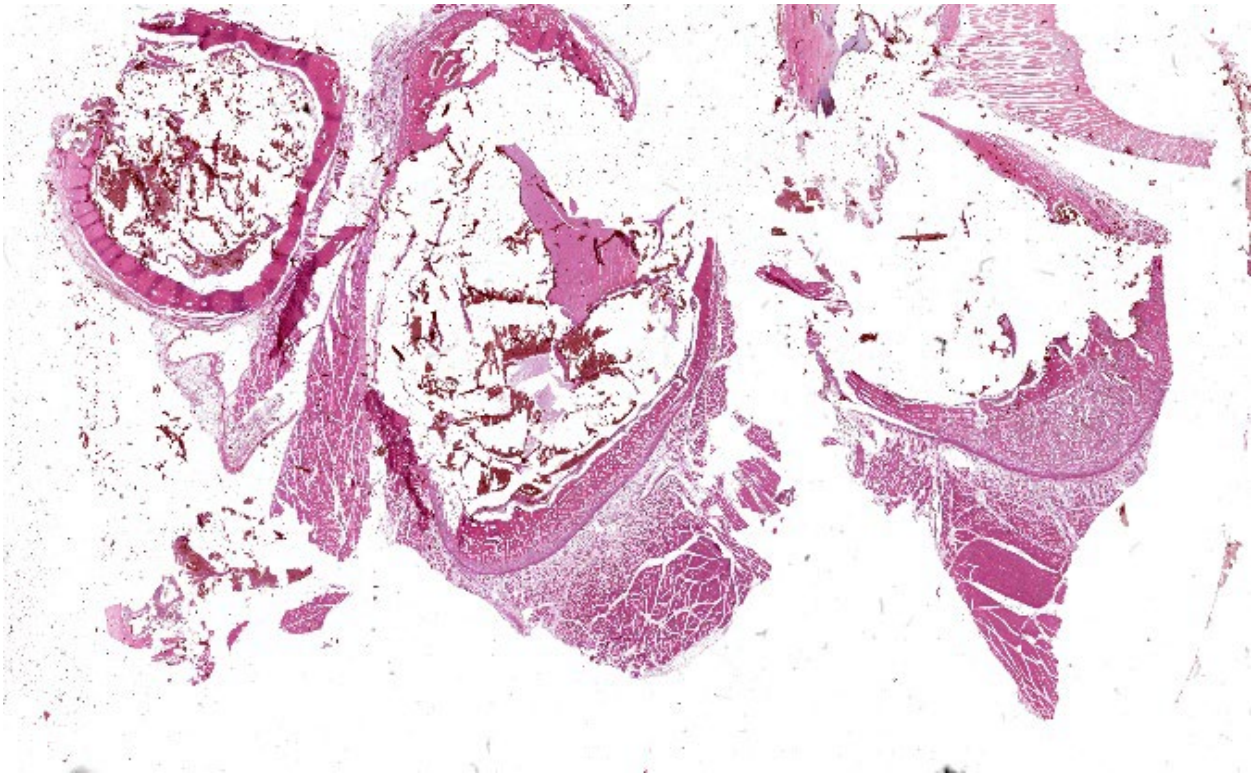

Humerus, cat: Three transverse sections of the humerus are submitted for examination. In each section, the medulla is effaced by large blood filled spaces. There is marked periosteal new bone growth in 2/3 sections. (HE, 6X)

upon palpation of the proximal humeral epiphysis and scapulo-humeral joint. The neurological examination was unremarkable. Under anaesthesia, radiography revealed a focally expansile lesion and bone lysis in the right third proximal humerus with evident thinning of the cortical bone extending towards the diaphysis. There was mild focal periosteal reactivity. The lesion was compartmentalized by trabeculae traversing an area of radiolucency, resulting in a mild "soap bubble" appearance. Soft tissue swelling was also observed overlying the region adjacent to the humeral lesion.

Chest and contralateral limbs X-rays were within normal limits. Ultrasound study of adjacent axillary and superficial cervical lymph nodes was also within normal limits.

Fine-needle aspiration (FNA) was performed on the bone lesion. The needle easily penetrated the cortical bone into the medullary canal. Cytologic evaluation of FNA revealed hemo-diluted cytological samples with mild cellularity, primarily consisting of haematopoietic elements, small lymphocytes and occasional small aggregates of round to spindle cells with indistinct cells borders and abundant, basophilic cytoplasm, with oval nuclei, reticular chromatin and prominent nucleoli (figures 3 and 4). The anisocytosis and anisokaryosis were moderate. Finally, rare foamy macrophages were observed.

The cytological diagnosis indicated bone marrow contamination due to the sampling procedure. The presence of occasional mesenchymal elements with moderate atypia could suggest a sarcomatous origin of the lesion, for which histopathological confirmation was recommended.

The owner declined the biopsy procedure and provided informed consent for the amputation with scapulectomy and axillary lymph node dissection.

Gross Pathology:

Grossly, an expansile, raised, round nodular lesion measuring about 18 x 12 x 10 mm was present on the third lateral superior proximal humerus. On the cut surface, a cavity full of blood was found within the centre of the bone, expanding the cortex, and internally septated, creating multiple hematic lacunae of variable sizes and cyst-like appearance. A mild periostal thickening, above the cystic lesion was observed. The joints were unremarkable, and no masses were present in the surrounding soft tissue.

Microscopic Description:

Bone and soft tissue from the periphery of the right proximal humerus. Affecting 70% of the sections and located eccentrically in the bone cavity, involving the medullary cavity, and extending into the cortex, a round, well-demarcated, non-infiltrative, non-capsulated mass composed of multiple blood-filled spaces of variable sizes is observed, measuring about 15 x 10 x 8 mm. These spaces contain numerous extravasated red blood cells admixed with eosinophilic, fibrillar, material (fibrin), eosinophilic amorphous material (serous) and are well delimited by septa of variable thickness leaning on spicules of bone (fig. 5). The septa are composed of moderately cellular proliferation characterized by spindle cells with minimal atypia (possible fibrovascular proliferation), multifocally arranged in solid areas (fig. 6). Admixed, mild to moderate proliferation of

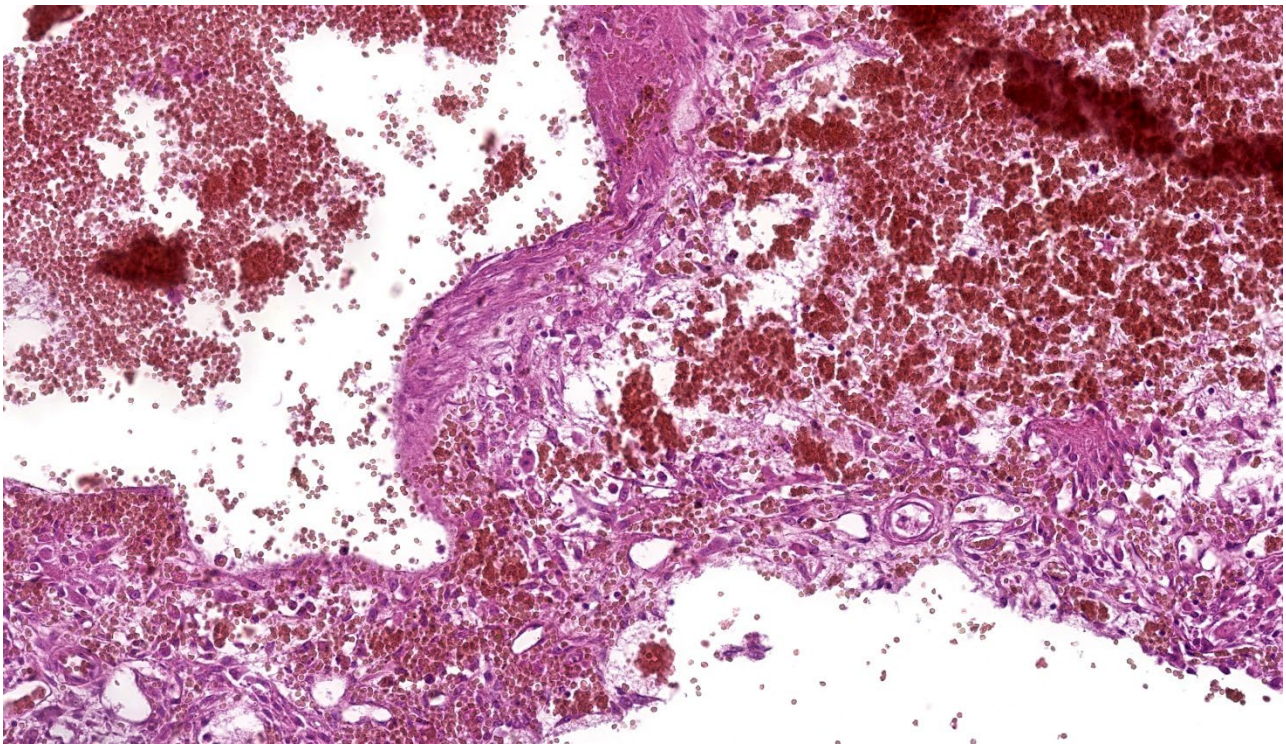

Humerus, cat: Blood-filled spaces are separated by fibrous septa which contains variable combinations and concentrations of hemorrhage, siderophages, mixed inflammation, fibroblasts and dense collagen (HE, 381X).

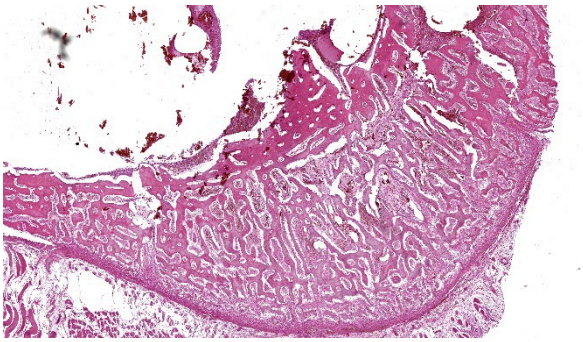

Humerus, cat: In 2/3 sections, the cortical bone is thinned, and there are anastomosing trabeculae of periosteal new bone arising from the hypercellular periosteum. (HE, 381X)

round to oval cells with moderate, eosinophilic, cytoplasm and an eccentric, round, nucleus (possibly osteoblasts, fig. 7) was noticed. Scattered osteoclasts and foamy macrophages with abundant, pink to yellow-brown cytoplasm (hemosiderophages) are observed. The trabecular bone affected by the cystic mass shows, multifocally, irregular margins with shallow pits (Howship's lacunae) occasionally associated with osteoclasts (bone resorption). The rest of bone shows tinctorial alterations, from intense to pale eosinophilic matrix, in which randomly scalloped lines could be observed (new bone deposition). The periosteum appears highly cellular (reactive) while, multifocally, a mild inflammatory infiltrate composed of lymphocytes, plasma cells and rare hemosiderophages is evident. The surrounding skeletal myofibers are separated by optically empty material (edema) and occasionally show a decreased diameter (mild atrophy).

Contributor's Morphologic Diagnosis: Humerus: Focal, monolateral, aneurysmal bone cyst with bone remodelling

Contributor's Comment: Aneurysmal bone cysts (ABCs) are benign, locally expanding bone masses, containing numerous blood-filled or serosanguineous fluid-filled spaces, not usually lined by endothelium, located between bone trabeculae.[8,11] Adjacent tissue to the spaces can vary from well-differentiated fibrous or fibro-osseous tissue to pronounced proliferation of undifferentiated mesenchymal cells admixed with osteoclast-like multinucleated giant cells. ABCs are often locally aggressive, tending to cause lytic bone lesions[12] and destruction of the inner cortical bone layers during expansion.[8] Haemorrhages and hemosiderosis are frequent.[8]

The causes and pathogenesis of ABCs remain unknown;[8] however, they could be consequences of ischemic necrosis, haemorrhage, disruption or shunting of intramedullary blood vessels, or congenital/acquired vascular malformations.[8,11] Local alteration in blood flow has also been thought to play a role.[3] Increased venous pressure may occur secondary to trauma or a tumor, resulting in dilation of the vascular bed and subsequent erosion of bone.[3]

ABCs have been reported rarely in dogs, cats, horses, and cattle,[3] predominantly occurring in the flat bones of the axial[11] and appendicular skeleton.[3] Limited cases are reported in animals to establish age or site prevalence.[3] In cats, ABCs have been described in the scapula,[1,5] pelvis, [9,12] metatarsal bone,[7] humerus,[4] and rib.[2] Radiographically, ABCs appear as expansile, osteolytic lesions contained by a thin, "ballooned" periosteum with an internal "soap-bubble" appearance caused by internal septa. Grossly, ABCs resemble benign bone cysts, telangiectatic osteosarcoma, and hemangiosarcoma.[3] ABCs typically exude blood from the cut surface, and may contain solid areas in addition to multiple blood-filled cysts (multiloculated[3]). Pathologic fracture may be present.[3] Complete resection is the treatment of choice when possible, and carries a favourable prognosis.[12] Other treatment options include surgical curettage with bone grafting, and radiation therapy.[11] Recurrence after complete surgical excision of the aneurysmal bone

cyst (ABC) has not been reported in animals. However, malignant transformation of an aneurysmal bone cyst to a chondrosarcoma has been reported in a dog.[3] In humans, ABC is now considered as a benign locally destructive bone neoplasm.[6]

ABCs must be differentiated from both benign and malignant lesions,[10] such as unicameral bone cyst (UBC),[12] osteosarcoma, hemangiosarcoma, fibrosarcoma, and plasma cell myeloma.[3] One of the major histologic differential diagnosis is telangiectatic osteosarcoma.[1,10] However, we excluded it because nuclear pleomorphism and a high mitotic rate were not features of mesenchymal/associated cells in our case. For the same reason, we have excluded fibrosarcoma, plasma cell myeloma, and hemangiosarcoma. Moreover, we have excluded UBC because it is unicameral, while ABCs are multiloculated[3] as in our case. Finally, fungal infection and osteomyelitis were ruled out due to negative Periodic acid–Schiff (PAS) staining and the very mild inflammatory infiltration. Indeed, acute osteomyelitis are characterized by the presence of fibrin and a dense population of neutrophils and necrotic cells in the primary spongiosa while the presence of neutrophils and plasma cells within the reactive bone and connective tissue supports a diagnosis of chronic osteomyelitis,[3] all features not detected in our case.

Contributing Institution:
Department of Comparative Biomedicine and Food Science, Viale dell'Università 15, 35020, Legnaro (PD), Italy;
https://www.bca.unipd.it/

JPC Morphologic Diagnosis: Long bone: Simple bone cyst (pseudocyst).

JPC Comment: We greatly appreciate that the contributor of this second case included radiographs and accompanying cytology to support case discussion. Although anatomic pathologists may feel some discomfort in interpretating radiographs, the group (and Dr. Murphy) felt it was important to maintain basic competency in recognizing and describing bony changes and using this information to enhance slide evaluation. We agree with the radiologic assessment of bony lysis with at best a mild periosteal reaction in this case, and not an aggressive lesion, which typically combines both bony proliferation and lysis.

Evaluation of this slide provides some challenge due to processing artifact, due to the large blood-filled spaces. The composition and arrangement of spindle cells led some participants to promote the idea that this process resembled a seroma forming within bone (i.e. a response to trauma). It is clear from the current literature that the genesis remains nebulous however.

Lastly, it wouldn't be Wednesday Slide Conference without a good semantic argument and this case offered a perfect minor quibble to occupy at least 5 minutes. While the term "aneurysmal bone cyst" is well established in the veterinary literature, it is also worth mentioning that this is itself a misnomer as there is no lining epithelium present. As such, aneurysmal bone *pseudocyst* probably is more appropriate to the lesion, but we hate making the associated literature even harder to read/categorize. Dr. Murphy muddied the waters further by observing that human literature partially reserves aneurysmal bone cyst for cases with a known genetic component[13] – it is unclear if similar circumstances might apply to the cat in this case. We liked the safety of "simple bone cyst" as an umbrella term and the parallels to human nomenclature, and ultimately combined the two in our

morphologic diagnosis (and eschewed "aneurysm bone cyst" entirely.

References:

1. Benamou J, Lussier B, Alexander K, Gains MJ, Savard C. Use of magnetic resonance imaging and histopathologic findings for diagnosis of an aneurysmal bone cyst in the scapula of a cat. *J Am Vet Med Assoc*. 2012;240(1):69–74.
2. Biller DS, Johnson GC, Birchard SJ, Fingland RB. Aneurysmal bone cyst in a rib of a cat. *J Am Vet Med Assoc*. 1987;190(9):1193–1195. (PDF not available)
3. Craig LE, Dittmer KE, Thompson KG. Chapter 2 - Bones and Joints. In: Maxie MG, ed. *Jubb, Kennedy & Palmer's Pathology of Domestic Animals: Volume 1 (Sixth Edition)*. W.B. Saunders 2016:16-163.e1.
4. Kim K, Kim H, Kim H, et al. Humeral Aneurysmal Bone Cyst in a Cat with Sequential Computed Tomographic Findings. 2022;9(11):594.
5. Manca S, Mate de Haro L, Civello A, Martí J. Aneurysmal bone cyst in the scapula of a young cat. 2022;10(4):e459.
6. Nasri E, Reith JD. Aneurysmal bone cyst: a review. *J Pathol Transl Med*. 2023;57(2):81–87.
7. Nicetto T, Coltro A, Massari F. Tarsometatarsal stabilization after metatarsal bone amputation for treatment of an aneurysmal bone cyst in a cat. 2021.
8. Olson EJ, Carlson CS. Bones, Joints, Tendons, and Ligaments1. In: Zachary JF, ed. *Pathologic Basis of Veterinary Disease (Sixth Edition)*. Mosby 2017:954-1008.e2.
9. Saunders JH, Heimann M, Taeymans O, Snaps FR. Aneurysmal bone cyst in the pelvis of a cat. 2003;72(6).
10. Stewart HL. Aneurysmal bone cysts as a diagnostic consideration in juvenile patients: Considerations from humans and animals. 2023;35(4):189–193.
11. Voss K. 4 - Diseases of bone. In: Montavon PM, Voss K, Langley-Hobbs SJ, eds. *Feline Orthopedic Surgery and Musculoskeletal Disease*. W.B. Saunders 2009:55–62.
12. Winbladh K, Fransson BA, Svensson G, Karlstam E, Uhlhorn M. Aneurysmal bone cyst in the pelvis of a cat: successful outcome of partial iliectomy with limb preservation. 2020;6(2):2055116920974984.
13. Ye, Pringle LM, Lau AW, et al. TRE17/USP6 oncogene translocated in aneurysmal bone cyst induces matrix metalloproteinase production via activation of NF-kappaB. Oncogene. 2010;29(25):3619–29.

CASE III:

7 years old, female, domestic rabbit (*Oryctolagus cuniculus*)

History: The animal presented with a swelling of the left buccal region, and a firm nodular mass was identified, described as being in

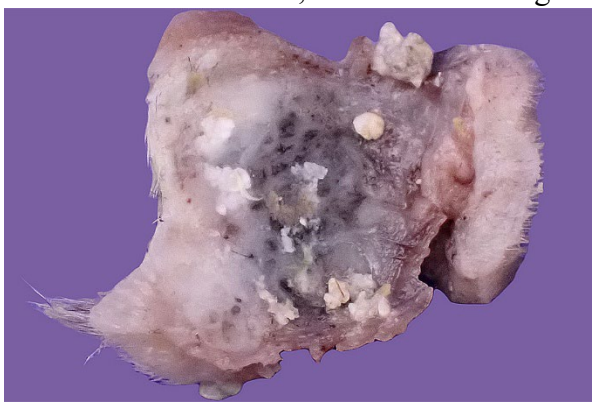

Cheek, rabbit: Buccal/labial skin with embedded approximately ovoid neoplastic nodule. (Photo courtesy of: International Zoo Veterinary Group Pathology, https://www.izvg.co.uk/pathology/pabout.htm)

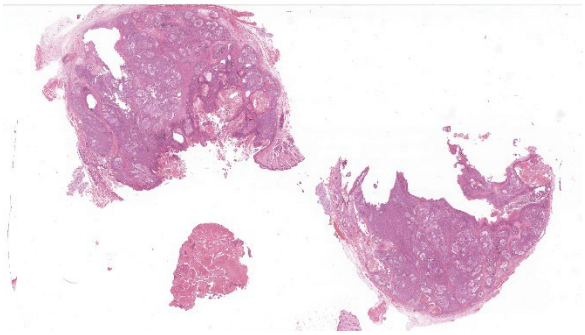

Cheek, rabbit: Multiple sections of a neoplasm are submitted for examination. (HE, 8X)

the lip (not obviously attached to the gingiva/bone). The submitting veterinary surgeon performed an incisional biopsy and a single piece of tissue was submitted for histopathologic examination. Following initial diagnosis, further surgery was undertaken to remove the lesion in its entirety, attached to a small areas of surrounding buccal/labial skin.

Gross Pathology: The resection specimen was an irregularly ovoid firm nodule (approximately 30 x 25 x 18 mm greatest dimensions) attached to a piece of haired skin (Fig. 1). Incision revealed a relatively well-circumscribed non-encapsulated nodule, with firm to hard, slightly gritty to chalky, grey, cream, and tan mottled cut surfaces (Fig. 2). The lesion required overnight decalcification prior to histological processing.

Laboratory Results:
N/A

Microscopic Description:
Buccal skin: The lesion comprises a relatively well circumscribed non-encapsulated nodular neoplasm expanding within haired skin which forms the lateral margins. The neoplasm is composed of interconnecting is-

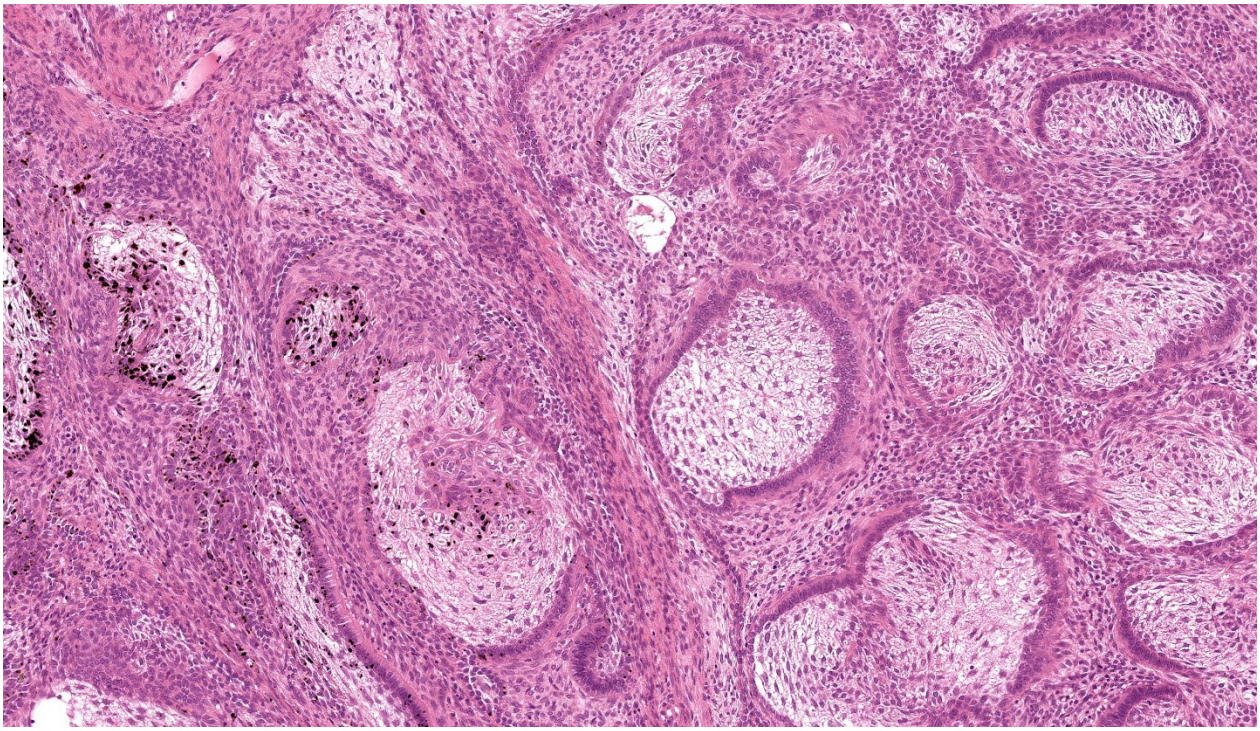

1Cheek, rabbit: The neoplasm is composed of thick anastomosing trabeculae of palisading epithelium resembling odontogenic epithelium surrounding loosely arrange mesenchyme reminiscent of dental pulp. (HE, 181X)

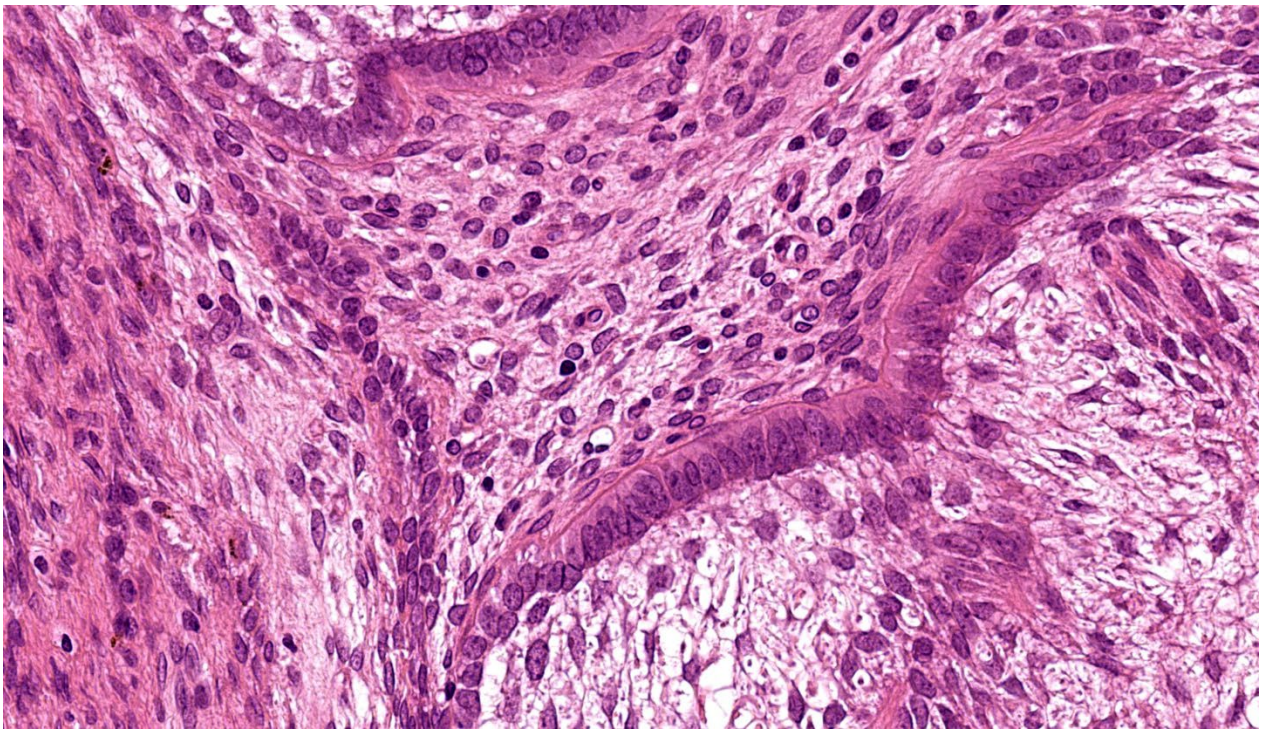

2Cheek, rabbit: High magnification of neoplastic epithelium. (HE, 750X)

lands and cords of odontogenic epithelium. Odontogenic epithelium is characterized by peripheral palisading of epithelial cells which have apical nuclei and basal cytoplasmic clearing and central cells which are separated by prominent stellate bridges (Fig. 3). Intracytoplasmic melanin granules are a variable feature within this cellular population, multifocally throughout the lesion. Cellular pleomorphism is moderate. Mitoses range from 0-1 per HPF (per 40x objective), with moderate anisocytosis and anisokaryosis. Odontogenic epithelia frequently form concentric nodules (somewhat reminiscent of Pacinian corpuscles, Fig. 3 arrow) and there are areas of slender anastomosing ribbons. Multifocally, there are cystic structures partially or predominantly lined by palisading odontogenic epithelium which contain dyskeratotic hyperkeratotic debris (Fig. 4). Stratified squamous epithelium with para- and orthokeratotic hyperkeratosis lines further cystic structures, forming an extensive central area of invagination within the neoplasm with coalescent columns of squamous epithelial cells and cystic accumulations of orthokeratotic and parakeratotic debris (Fig. 5). Some of these cystic areas have substantial amounts of heterophilic inflammation with epithelial erosion and ulceration and inflammation extending into the subjacent neoplastic populations. Fragments of mucinous salivary gland are present in the deeper connective tissues (consistent with minor salivary gland/buccal origin). The basal margin of resection comprises compressed striated muscle fibers, including atrophic and regenerative fibers, adipocytes, and varying amounts of fibrosis.

Contributor's Morphologic Diagnosis: Keratoameloblastoma (keratinizing acanthomatous epulis), with focal squamous differentiation, buccal skin.

Contributor's Comment: Histological features are consistent with ameloblastoma, a rare neoplastic entity in rabbits, which has only been described in recent years (since

2009). In total only twelve cases have been described in the literature.[1-7] According to one recent study of odontogenic neoplasms the prevalence of ameloblastoma in rabbits is around 0.24%.[3] As in other domestic species, these are locally aggressive neoplasms and although they are not considered to carry a metastatic risk, they often invade underlying tissues (including alveolar bone) resulting in loss of teeth. Maxillary and mandibular origin have both been described. However, not all typical cases are apparently associated with the cutaneous or mucosal epithelium on clinical inspection, and subcutaneous origin (external to the buccal musculature) has also been described. This may be pertinent to buccal/labial location in this case. Although evidence suggests that these odontogenic-like tumors of the rabbit cheek may be derived from ectopic rests of transformed tooth germ, the histogenesis of these lesions remains unresolved.[2]

If ameloblastomas are therapeutically irradiated, other malignancies including squamous cell carcinoma, fibrosarcoma and osteosarcoma have been reported to occur, in some cases several months to years following treatment, in other domestic species.[8]

Keratoameloblastoma is an uncommon histologic subtype (n=2) amongst the twelve ameloblastoma-like lesions recorded in rabbits to date. This subtype is characterized by keratin formation by ameloblastic epithelium and has also been identified as a rare entity in the human literature.[9] Squamous differentiation (differentiation of neoplastic epithelium towards a keratinizing squamous epithelial phenotype, rather than keratinization arising from ameloblastic cells) has also been recorded in ameloblastoma in rabbit. Whether this has any prognostic significance has not yet been evaluated.

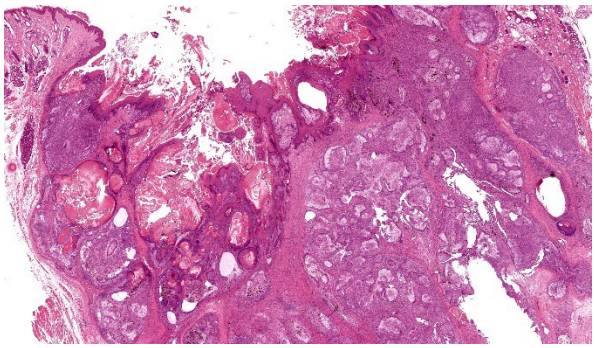

/Cheek, rabbit: The overlying epithelium is markedly hyperplastic and hyperkeratotic. (HE, 28X)

Contributing Institution:
International Zoo Veterinary Group Pathology
Station House, Parkwood Street
Keighley
West Yorkshire
United Kingdom
BD21 4NQ
https://www.izvg.co.uk/pathology/pabout.htm

JPC Morphologic Diagnosis: Haired skin: Ameloblastoma.

JPC Comment: This third case presented a bit of a conundrum for the group. While the neoplasm description is straightforward, placing an ameloblastoma in the cheek and/or lip without an apparent source of dental germinal epithelium led us to further explore the idea of an ectopic ameloblastoma (see reference #2 below) or back off this interpretation and use the qualifier of "ameloblastoma-like" to allow for the possibility of another cell of origin. Other similar neoplasms that could mimic ameloblastoma due to overlapping features include trichoblastoma (to include "adamantanoid" trichoblastoma) and basal cell adenoma.[2] The presence of pigment within neoplastic cells is also not typical of ameloblastoma but is a common finding in follicular tumors which gives some credence to the latter theory of this case.

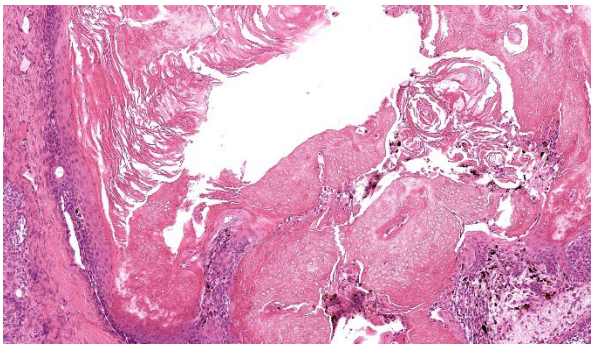

Cheek, rabbit: Higher magnification of keratinizing epithelium with lamellar keratin and ghost cells. (HE, 205X)

Dr. Murphy reviewed the Vickers-Gorlin criteria[10] for diagnosis of ameloblastoma which include hyperchromatic basal cell nuclei, basilar cell palisading and antibasilar nuclear location, and cytoplasmic vacuolation. We also note the prominent, thickened rim (subepithelial band) of hyalinized collagen that blends with the basement membrane (colloquially the Vickers-Gorlin change or Vickers-Gorlin effect[2]) though whether this is a consistent or useful feature of rabbit ameloblastomas was not determined by our discussion.

We also discussed the architectural contrast between the deeper portion of this neoplasm necrotic, ulcerated surface and the multifocal keratinization present at the surface. The contributor lays the case nicely for considering keratoameloblastoma. The most recent WHO classification of benign odontogenic tumors makes no mention of this entity however,[9] which reflects the need to learn more. One aspect of the slide that conforms to keratoameloblastoma that might be overlooked is the abundant dystrophic mineralization of keratin – this is also noted radiographically in more advanced/pronounced human cases.[9]

References:

1. Rätsep E, Ludwig L, Dobromylskyj M. Orofacial masses in domestic rabbits: a retrospective review of 120 cases from 2 institutions, 2000-2023. J Vet Diagn Invest. 2024 Feb 22:10406387241234326.
2. Murphy BG, Swan E, Affolter VK, et al. Odontogenic-like neoplasms of the rabbit cheek: pathological features and comparison to cutaneous trichoblastoma and jaw-associated ameloblastoma. Vet Pathol. 2023 Mar;60(2):178-184.
3. Baum B. Not just uterine adenocarcinoma-neoplastic and non-neoplastic masses in domestic pet rabbits (*Oryctolagus cuniculus*): a review. Vet Pathol. 2021 Sep;58(5):890-900.
4. Miwa Y, Nakata M, Takimoto H, et al. Spontaneous oral tumours in 18 rabbits (2005-2015). J Small Anim Pract. 2021 Feb;62(2):156-160.
5. Völker I, Kammeyer P, Hinzmann B, Lüerssen D, et al. Peripheres keratinisierendes Ameloblastom bei einem Zwergkaninchen (Oryctolagus cuniculus f. dom.) [Peripheral keratinizing ameloblastoma in a dwarf rabbit (Oryctolagus cuniculus f. dom.)]. Tierarztl Prax Ausg K Kleintiere Heimtiere. 2014;42(5):331-5.
6. Loukopoulos P, Komnenou A, Papadimitriou S, et al. Follicular ameloblastoma in a dwarf rabbit (Oryctolagus cuniculus). Proceedings of the European Society of Veterinary Clinical Pathology (ESVCP) and European College of Veterinary Clinical Pathology (ECVCP) 11th Annual Congress. October 7-9, 2009. Thessaloniki, Greece, p. 167
7. Madarame H, Enaga S. Peripheral acanthomatous ameloblastoma in a rabbit with review of previous submissions of the Armed Forces Institute of Pathology Wednesday Slide Conference. J Vet Med Sci. 2009 Jul;71(7):987-9.
8. Mayer MN, Anthony JM. Radiation therapy for oral tumors: canine acanthomatous ameloblastoma. Can Vet J. 2007 Jan;48(1):99-101.

9. Robinson L, Smit C, Fonseca FP, et al. Keratoameloblastoma: A report of seven new cases and review of literature. Head Neck Pathol. 2022 Dec;16(4):1103-1113.
10. Vickers RA, Gorlin RJ. Ameloblastoma: Delineation of early histopathologic features of neoplasia. Cancer. 1970 Sep;26(3):699-710.

CASE IV:

Signalment: 7 year, spayed female, giant schnauzer, *Canis familiaris*

History: This dog presented to the University of Wisconsin-Madison Veterinary Care for evaluation of an oral mass that was first noted 2 months prior to presentation. Physical exam revealed a pink, irregular mass at the gingiva between teeth 101-102. Computed tomography revealed marked osteolysis of the maxilla associated with the mass and enlarged mandibular and cervical lymph nodes, with no other signs of metastatic disease. A partial maxillectomy was performed and the maxilla was submitted for histologic examination.

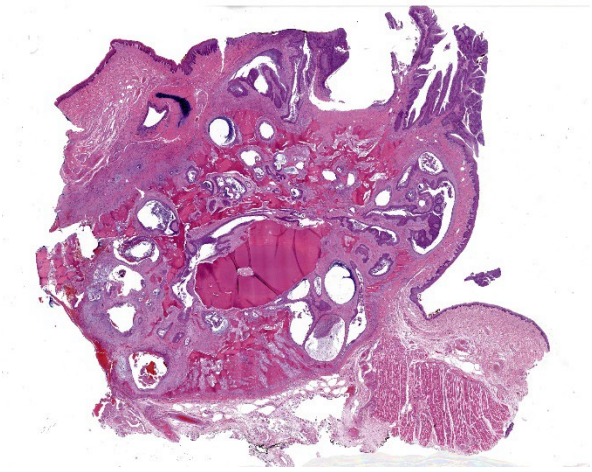

Gingiva, dog: A section of gingiva with an infiltrative cystic and proliferative neoplasm is submitted for examination. The neoplasm forms papillary fronds extending from the gingiva (HE, 8X)

Gross Pathology: The tissue sample submitted for histologic examination consisted of a section of right maxilla including teeth 101-104 and 201. A 0.4 x 1.2 x 1.8 cm pink, soft, exophytic mass expanded the gingiva dorsal to teeth 101-103 and extended to the rostral hard palate. The specimen was decalcified prior to sectioning.

Laboratory Results: A fine needle aspirate and cytology of the enlarged lymph nodes was diagnosed as consistent with lymphoid hyperplasia. A complete blood count was unremarkable. Serum biochemical abnormalities included globulins 3.9 g/dL (2.2-3.5), AST 82 U/L (21-53), ALT 227 U/L (4-87), cholesterol 487 mg/dL (149-319), and triglycerides 261 mg/dL (32-190).

Microscopic Description: Gingiva. Arising from and markedly expanding the hyperplastic gingival epithelium and infiltrating the subepithelial stroma and alveolar bone is an unencapsulated, poorly demarcated, densely cellular exophytic and invasive mass. The mass is composed of neoplastic epithelial cells forming papilliferous projections into the oral cavity supported by a fibrovascular stalk and extending deep to the basement membrane to form nests and trabeculae supported by a moderate amount of fibrovascular stroma. Neoplastic cells are polygonal with distinct cell borders and often prominent intercellular bridges, abundant pale to brightly

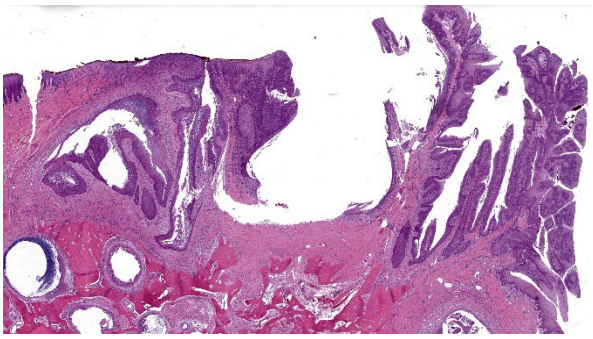

Gingiva, dog: The neoplasm extends outward from the gingival surface, forming both a wide based front (left) or long papillary fronds. (HE, 22X)

eosinophilic cytoplasm, a round to oval nucleus, finely stippled chromatin, and up to six prominent magenta nucleoli. Anisocytosis and anisokaryosis are marked, there is occasional binucleation, and mitoses range from 2-4 per high-powered field (0.237 mm^2). There is frequent individual cell necrosis and larger foci of central necrosis and vacuolation containing eosinophilic and karyorrhectic debris and neutrophils. The superficial stroma supporting the exophytic mass and its stalk are moderately expanded by clear space (edema) that contains small numbers of neutrophils and macrophages, and the deeper stroma is expanded by multifocal and coalescing regions of hemorrhage and small to moderate numbers of neutrophils that encircle and infiltrate the lobules of neoplastic cells. In regions of alveolar bone invasion, the margins of remaining bone are scalloped and occasionally lined by osteoclasts within Howship's lacunae, and the affected bone contains multiple resting and reversal lines. In more severely affected regions, irregular trabeculae of pale woven bone are deposited on the pre-existing bone and are lined by plump osteoblasts.

Contributor's Morphologic Diagnosis:

Gingiva: Papillary squamous cell carcinoma

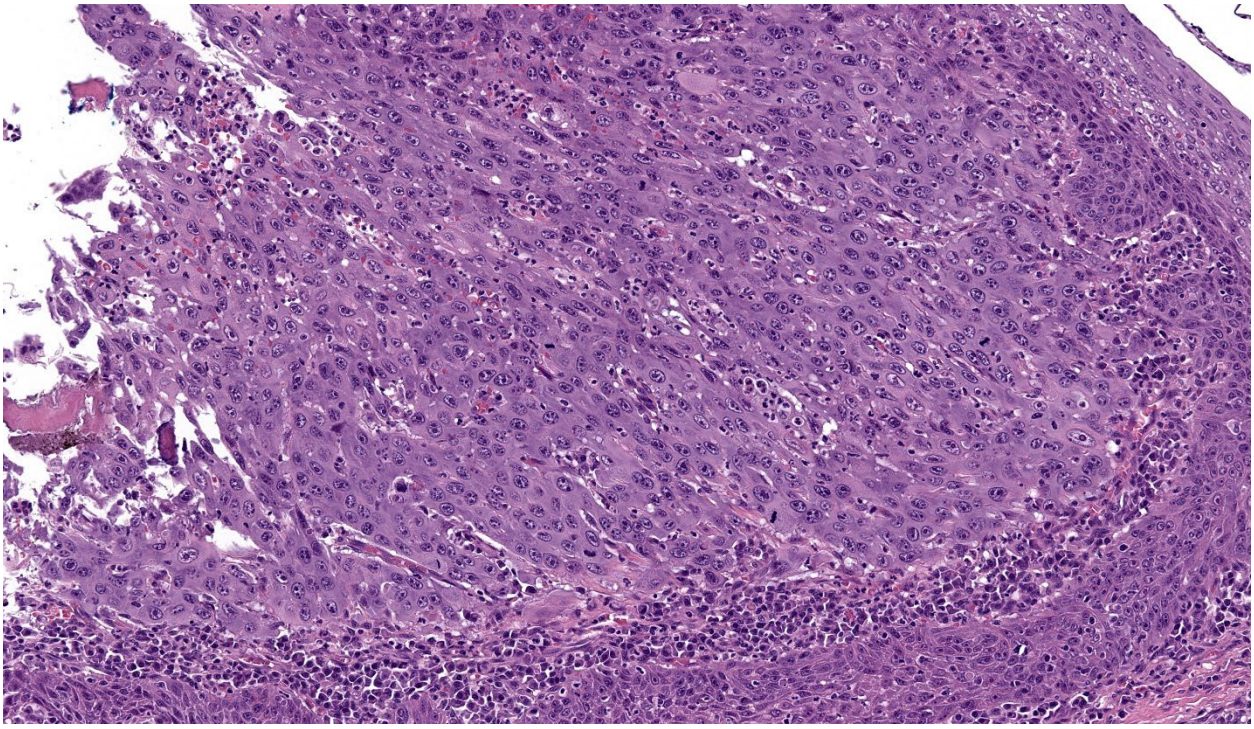

3Gingiva, dog: Neoplastic squamous epithelium demonstrates a wide base with an intact basement membrane, a lack of maturation, as well as large nuclei with prominent (HE, 181X)

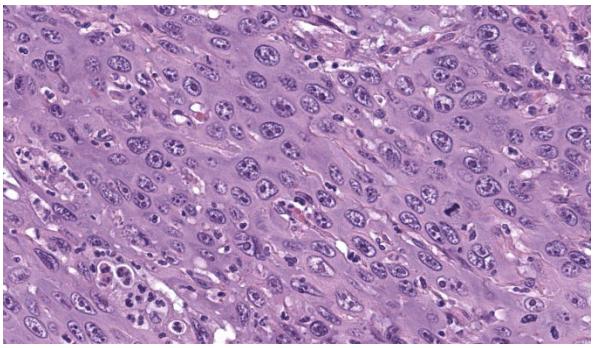

Gingiva, dog: High magnification of neoplastic squamous epithelial cells. (HE, 965X)

Contributor's Comment: This case was diagnosed as a papillary squamous cell carcinoma (PSCC) arising from the gingival epithelium. PSCC is a subtype of oral SCC based on a classification scheme defined by the World Health Organization.[1] In one retrospective study on canine oral SCC, PSCC comprised 6% of cases, compared to the more common conventional subtype which represented 82% of cases.[9] Other subtypes of oral SCC that have been defined in dogs include basaloid, verrucous, adenosquamous, and spindle cell.[1,9] At this time, subtyping is not routinely performed and it is unclear if there is an association between subtype and biologic behavior. In humans, PSCC tends to demonstrate local confinement and more feasible excision, and thus is associated with a more favorable prognosis.[1]

PSCC is differentiated from conventional SCC by the presence of neoplastic epithelial cells forming papillary fronds into the oral cavity, in addition to infiltrating the basement membrane into the subjacent stroma. Invasion beyond the basement membrane and keratinization can be minimal with this subtype, thus complicating the diagnosis in some cases.[7,8] Other histologic features that may be seen with PSCCs include degeneration of apical neoplastic cells and abundant intraepithelial neutrophils.[7] PSCCs can also occur as an intraosseous cavitated cyst within the bone (cavitating pattern), as opposed to the non-cavitating pattern featured in this case.[7,8] Similar to this case, PSCCs appear to have a predilection for the gingiva of the dentate jaws, with the majority occurring on the rostral aspect.[9,10]

Risk factors for development of oral PSCC are not well-defined. This neoplasm has been primarily documented in young dogs,[2,11] however multiple reports have shown that this subtype additionally affects adult and aged dogs, similar to this case.[9,10] While papillomavirus infection has been associated with oral SCC in humans and cutaneous SCC in dogs, studies exploring the association between canine oral SCC and papillomavirus infection have not demonstrated a similar relationship.[1, 3-5] Further, there is no evidence at this time that canine PSCC represents progression of an oral squamous papilloma.

Differential diagnoses in this anatomic location in dogs include canine acanthomatous ameloblastoma (CAA), oral squamous papilloma, and viral papillomas. CAA is differentiated from PSCC by the lack of characteristic papillary formations and by the presence of neoplastic odontogenic epithelium and stroma resembling periodontal ligament. While PSCC can macroscopically resemble oral squamous papilloma or viral papilloma,

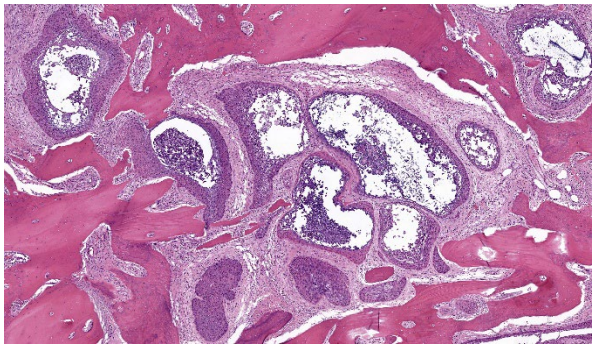

4Gingiva, dog: Nests of neoplastic cells infiltrate the underlying alveolar bone. There is central necrosis within some of the larger nests. (HE, 72X)

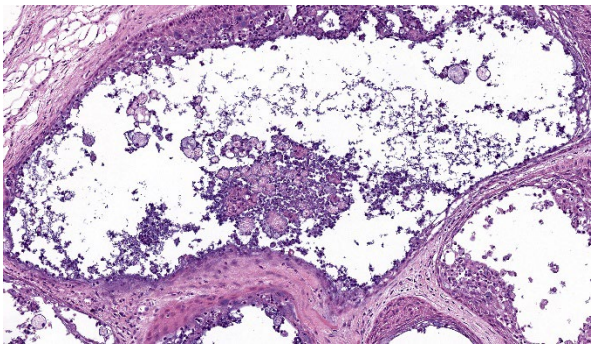

5Gingiva, dog: There is infiltration of the nests of neoplastic cells with neutrophils, loss of desmosomal attachment, vacuolation and individualization of neoplastic squamous epithelial cells, and central necrosis with abundant bluish cellular material.

both entities can be histologically differentiated from PSCC by the confinement of neoplastic epithelial cells to the basement membrane and lack of cytopathic effects (for viral papillomas).[6]

Contributing Institution:
University of Wisconsin
School of Veterinary Medicine
Department of Pathobiological Sciences
2015 Linden Drive
Madison, WI 53706

JPC Morphologic Diagnosis: Gingiva, incisive bone, and incisor: Papillary squamous cell carcinoma.

JPC Comment: The final case of this conference presents an interesting slide with a few subtle features to discover. Localization of this section to first or second incisor tooth is possible as the nasopalatine canal (incisive canal) is neatly outlined with a sickle of cartilage (lower right corner). Likewise, changes to the incisor tooth merit description as there is apparent lysis of dentin and repair as well as hypercementosis – we interpret the irregular shape and attachment of the tooth as a direct reaction to the neoplasm. We appreciated having a full thickness cross-sectional view to discuss these changes as typical biopsy specimens of this neoplasm are largely superficial.

Conference participants agreed with the contributor's diagnosis of papillary SCC, though discussion of ancillary features and overlap with differential diagnoses still produced a fruitful discussion. The basic structure of this neoplasm is epithelial and we add salivary gland neoplasms as a consideration to the contributor's differential list. CAA and papillary SCC are the most similar, though comedonecrosis (if present) is not consistent with CAA. We also noted several islands of epithelial cells outlined by ribbons of eosinophilic material that lacked osteocytes (dentin-like) which prompted consideration of an odontoma. Other portions of the neoplasm contain woven bone and osteoidal matrix induced by the neoplasm which could be confused with osteosarcoma or osteoinductive squamous cell carcinoma in a more limited biopsy sample. Once again, the value of lesion location, radiographs, and a biopsy sampling that includes the underlying invaded bone is critical for an accurate diagnosis.

References:

1. Barnes L, Everson JW, Reichart P, Sidransky D. Tumours of the oral cavity and oropharynx. In: World Health Organization classification of tumors – pathology and genetics of head and neck tumors. Lyon: *IARC Press*. 2005;163-208.
2. Furuta K, Nishi K, Park C, et al. A case of papillary squamous cell carcinoma in the mandible of a young

French bulldog. *Can Vet J*. 2021;62(11):1181-1184.
3. Luff J, Rowland P, Mader M, Orr C, Yuan H. Two Canine Papillomaviruses Associated With Metastatic Squamous Cell Carcinoma in Two Related Basenji Dogs. *Vet Pathol*. 2016;53(6):1160-1163.
4. Mauldin EA and Peters-Kennedy J. Integumentary system. In: Maxie MG, ed. *Jubb, Kennedy, and Palmer's Pathology of Domestic Animals*. Vol 1. 6th ed. St. Louis, MO: Elsevier; 2016:711.
5. Munday JS, French A, Harvey CJ. Molecular and immunohistochemical studies do not support a role for papillomaviruses in canine oral squamous cell carcinoma development. *Vet J*. 2015;204(2):223-225.
6. Munday JS, Lohr CV, Kiupel M. Tumors of the alimentary tract. In: Meuten DJ, ed. *Tumors in Domestic Animals.* 5th ed. Ames, IA: John Wiley & Sons; 2017:503-507,524.
7. Murphy BG, Bell CM, Soukup JW. Tumors Arising from the Soft Tissues. In: *Veterinary Oral and Maxillofacial Pathology*. 1st ed. John Wiley & Sons, Inc: 2020: 139-143.
8. Nemec A, Murphy BG, Jordan RC, Kass PH, Verstraete FJ. Oral papillary squamous cell carcinoma in twelve dogs. *J Comp Pathol*. 2014;150(2-3):155-161.
9. Nemec A, Murphy BG, Kass PH, Verstraete FJ. Histological subtypes of oral non-tonsillar squamous cell carcinoma in dogs. *J Comp Pathol*. 2012;147(2-3):111-120.
10. Soukup JW, Snyder CJ, Simmons BT, Pinkerton ME, Chun R. Clinical, histologic, and computed tomographic features of oral papillary squamous cell carcinoma in dogs: 9 cases (2008-2011). *J Vet Dent*. 2013;30(1):18-24.
11. Stapleton BL, Barrus JM. Papillary squamous cell carcinoma in a young dog. *J Vet Dent.* 1996;13(2):65-68.

1.

Joint Pathology Center
Veterinary Pathology Services

WEDNESDAY SLIDE CONFERENCE 2024-2025

Conference #24 — 23 April 2025

CASE I:

Signalment:
120-day-old, male, commercial swine (*Sus scrofa domesticus)*

History:
Two growing-finishing farms in the Midwest region of Brazil experienced outbreaks of sudden death among pigs aged between 120 and 130 days. The mortality rate ranged between 9% and 10% in the affected batches. Upon clinical examination, some pigs exhibited nonspecific signs such as trembling, dyspnea, and squealing sounds shortly before death. Pigs from multiple pens of both sexes, especially the largest animals in the batch, were affected. The antimicrobial and antipyretic treatment used did not yield any response. Additionally, large numbers of black rats (*Rattus rattus*) were observed inhabiting the facilities during farm visits. The rodent control measures implemented on the farm were ineffective.

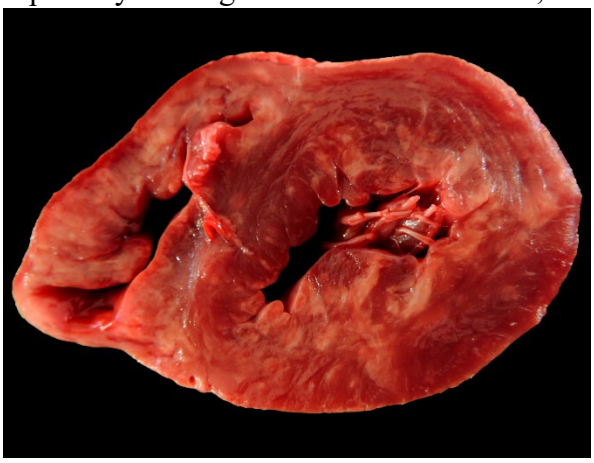

Heart, pig: On the cut surface of the myocardium, there were areas of pale tan discoloration ranging from 0.5-1 cm in diameter, sometimes coalescing, and more pronounced in the right and left ventricles. (Photo courtesy of Faculdade de Veterinária, Universidade Federal do Rio Grande do Sul, Setor de Patologia Veterinária, http://www.ufrgs.br/patologia).

Gross Pathology:
At necropsy, major lesions were observed in the heart, which was enlarged and showed on the epicardial surface multifocal pale to slightly white areas, ranging from 0.5-1 cm in diameter, which extended through the myocardium on the cut surface. These pale areas were more pronounced in the right and left ventricles, occasionally presenting a gritty texture. Mild hydropericardium and pulmonary edema were also observed.

Laboratory Results:
RT-PCR: samples of liver, lymph node, and heart tested positive for Encephalomyocarditis virus. Brain sample tested negative.

Microscopic Description:
Heart, left ventricle: in the myocardium, multifocally, there are areas of necrosis of the cardiomyocytes, characterized by hypereosinophilia, loss of cellular detail, nuclear karyolysis and pyknosis, associated with non-

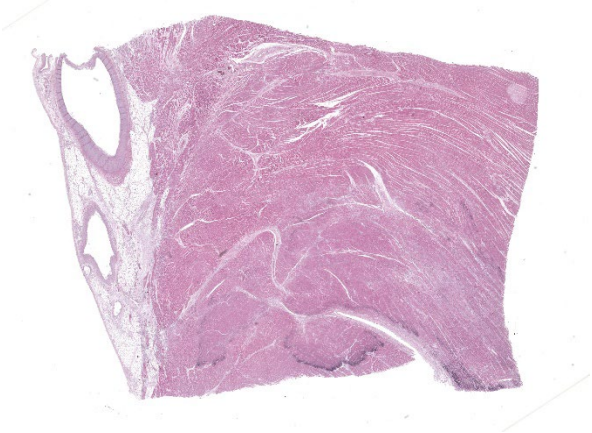

Heart, pig: One section of ventricle is submitted for examination. Serpiginous areas of mineralization are evident at subgross magnification. (HE, 10X)

suppurative inflammation, composed of macrophages, lymphocytes and plasma cells. This inflammatory infiltrate frequently replaces the necrotic cardiomyocytes and infiltrates the myocardial interstitium. In some areas, there is deposition of intracytoplasmic basophilic granular material in necrotic cardiomyocytes (highlighted by Von Kossa histochemistry - mineralization). Additionally, mild fibrous connective tissue proliferation is also present in the myocardial interstitium.

Contributor's Morphologic Diagnosis:

Myocarditis, necrotizing and lymphoplasmohistiocytic, multifocal, moderate, with dystrophic mineralization.

Contributor's Comment: The *Picornaviridae* family consists of small, non-enveloped, single-stranded RNA viruses, which include the *Cardiovirus* genus. Encephalomyocarditis virus (EMCV) is classified within the genus *Cardiovirus*, specifically as *Cardiovirus* A (the genus *Cardiovirus* comprises six species named A to F).[5,9]

EMCV is cause of myocarditis in several wildlife species, including non-human primates, as well as domestic animals, particularly swine, and humans.[1,3,4,6,11] Although the name 'encephalomyocarditis' originates from the initial association of the virus with brain and cardiac lesions, encephalitis is not consistently observed in natural EMCV infections in pigs.[8,12] Encephalitis mainly occurs in experimental infections in mice and swine fetuses, whereas myocarditis is a frequent lesion in both natural and experimental infections.[1,8,12]

Rats and mice serve as reservoir species for EMCV, spreading the virus and causing outbreaks in susceptible animals.[3,7,8] Several dead black rats (*Rattus rattus*) from the reported farms were subjected to necropsy, revealing positive RT-PCR results for EMCV in fecal samples. Accordingly, the presence of rodent infestation at the farms where the outbreak occurred indicates a failure of the control system and suggests rodents as potential reservoir and disseminator of EMCV in this report. On the other hand, EMCV infection is usually subclinical and may demonstrate that recovered pigs play an important

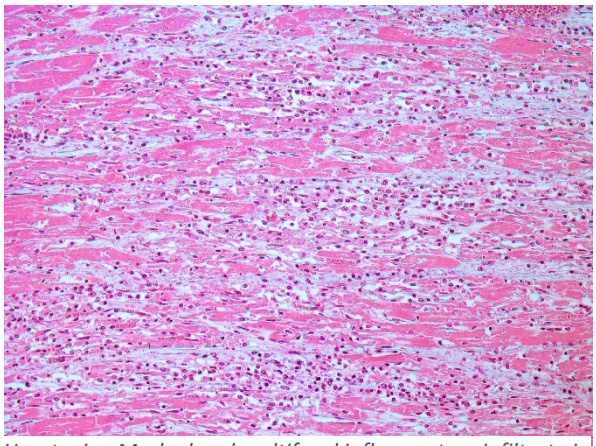

Heart, pig. Marked and multifocal inflammatory infiltrate is observed in the interstitium and dissecting cardiac fibers. (HE, 200X) (Photo courtesy of Faculdade de Veterinária, Universidade Federal do Rio Grande do Sul, Setor de Patologia Veterinária, Universidade Federal do Rio Grande do Sul, Setor de Patologia Veterinária, http://www.ufrgs.br/patologia).

role in the dissemination of EMCV. Therefore, in addition to controlling rodents, it is crucial to identify subclinical animals for more effective disease control.[2]

EMCV infection can result in characteristic myocardial lesions, with a pattern of viral myocarditis (non-suppurative inflammation), myocardial necrosis, and marked dystrophic mineralization which are clues for histopathological diagnosis.[8,12] However, some differential diagnoses should be considerate such as *Aphthovirus* infection, *Parvovirus* infection, and vitamin E/selenium (VitE/Sel) deficiency.[12,14] VitE/Sel deficiency is the most important differential diagnosis for commercial pigs and can also lead to cardiac mineralization patterns similar to those seen in EMCV infection. However, VitE/Sel deficiency is more common in nursery pigs compared to finishing pigs, and other lesions such as cardiac hemorrhages, hepatic necrosis, and muscular necrosis may be present in this condition, which are useful for pathological differentiation.[10,12] Additionally, RT-PCR detection of EMCV is crucial to confirm the diagnosis.[8]

In Brazil, the first occurrence of EMCV in pigs was reported in 1985 on a farrowing

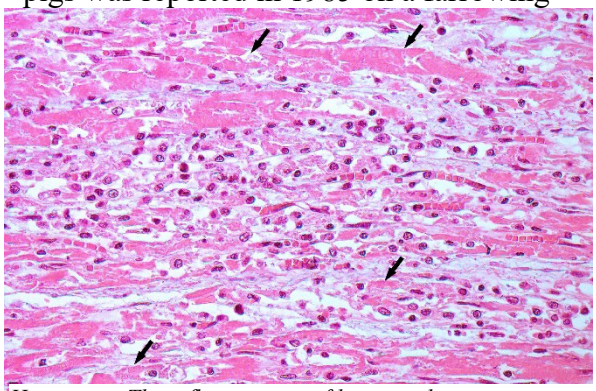

Heart, pig. The inflammatory infiltrate replaces necrotic cardiomyocytes and is composed of lymphocytes, plasma cells, and macrophages. Note necrotic cardiomyocytes (black arrows), characterized by loss of cellular details and cross striations, nuclear karyolysis and pyknosis.(HE, 400X) (Photo courtesy of Faculdade de Veterinária, Universidade Federal do Rio Grande do Sul, Setor de Patologia Veterinária, http://www.ufrgs.br/patologia).

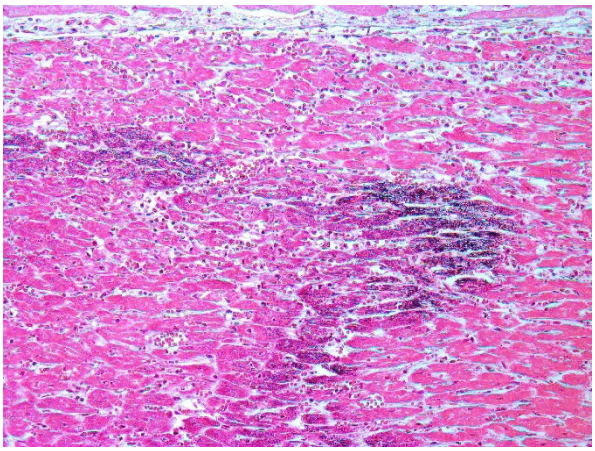

Heart, pig. Necrotic cardiomyocytes showing deposition of intracytoplasmic basophilic granular material (dystrophic mineralization). (HE, 200X) (Photo courtesy of Faculdade de Veterinária, Universidade Federal do Rio Grande do Sul, Setor de Patologia Veterinária, http://www.ufrgs.br/patologia).

farm in the southern region, affecting one sow and resulting in the death of 9 out of 10 piglets.[13] After a 38-year gap with no further documented cases, an outbreak in growing-finishing pigs occurred in 2023.[8] The phylogenetic analysis of the VP1 gene from the EMCV identified in this outbreak, showed that the samples contained similar strains that had their closest relatives identified in humans in Peru.[6,8] However, epidemiological, serological, and field studies on the distribution of EMCV in Brazil are limited, and more research is needed to understand the real impact of EMCV.

Contributing Institution:

Faculdade de Veterinária
Universidade Federal do Rio Grande do Sul
Setor de Patologia Veterinária
http://www.ufrgs.br/patologia

JPC Morphologic Diagnosis: Heart, ventricle: Pancarditis, necrotizing and lymphohistiocytic, monophasic, subacute, multifocal, marked.

JPC Comment: This week's moderator was Dr. Patty Pesavento from the University of

California-Davis, who explored viral and vascular pathology with conference participants. We enjoyed discussing this first case as its descriptive features reinforced the underlying pathogenesis of EMCV. Dr. Pesavento's first question to the group challenged them to consider the target cell for the virus – is it the myocyte or something else?

The answer in this case is probably both. Prior research has shown that vascular cell adhesion molecule 1 (VCAM1) is the necessary receptor for EMCV infection,[16] though other sialylated surface glycoproteins may play a role depending on EMCV strain. Supporting this interpretation of endothelial cells within capillaries being a target is the distribution of changes across all layers of the heart (i.e. pancardial) and regionally distinctive areas of necrosis and mineralization that are suggestive of damage to small-caliber blood vessels. A Movat's pentachrome stain highlights that much of the increased clear space in section reflects edema versus fibrosis.

We appreciate the contributors' morphologic diagnosis and added a single modifier to qualify the necrosis as monophasic in this case. The dystrophic mineralization in this case is remarkable and we speculate that the punctate basophilic foci may represent mineralization of organelles (mitochondria) secondary to ATP depletion and calcium dysregulation.

The contributor provides several good differential diagnoses for this case. Other important rule outs for porcine myocarditis (pancarditis) include porcine circovirus 2, porcine parvovirus, and toxin ingestion such as cottonseed (gossypol).[12] Dr. Pesavento also noted two other important scenarios re-

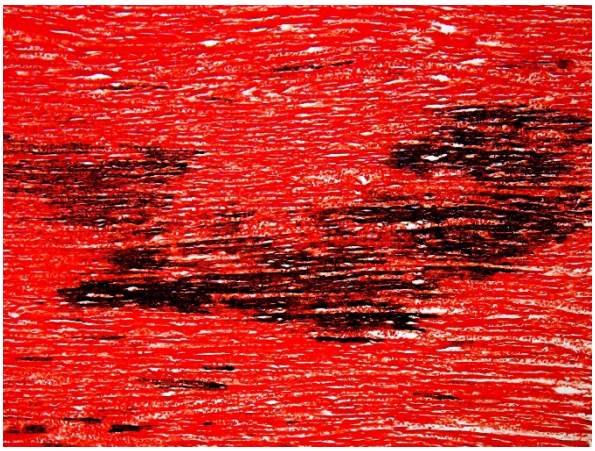

Heart, pig. Von Kossa-positive intracytoplasmic basophilic granular material (mineralization - calcium). (Von Kossa, 200X) (Photo courtesy of Faculdade de Veterinária, Universidade Federal do Rio Grande do Sul, Setor de Patologia Veterinária, http://www.ufrgs.br/patologia).

lated to transmission of EMCV for participants to be aware of. As rodents are a common nuisance in zoological parks, they may contaminate feed and water with virus, or in select cases, be ingested directly by primates or other species.[3] Finally, EMCV has been shown to persist within the porcine myocardium, which presents an unusual hazard for xenotransplantation of hearts to cardiac patients.[15] As recipients are highly immunosuppressed, the potential for subsequent permissive replication and spread to the CNS leading to severe encephalitis should not be overlooked.

References:

1. Alexandersen S, Knowles NJ, Belsham GJ, et al. Picornaviruses. In: *Diseases of Swine*. John Wiley & Sons, Ltd 2019:641–684.

2. Billinis C, Paschaleri-Papadopoulou E, Psychas V, et al. Persistence of encephalomyocarditis virus (EMCV) infection in piglets. *Vet Microbiol*. 1999;70(3-4):171-177.

3. Canelli E, Luppi A, Lavazza A, et al. Encephalomyocarditis virus infection in an Italian zoo. *Virol J*. 2010;7(1):64.

4. Cardeti G, Mariano V, Eleni C, et al. Encephalomyocarditis virus infection in Macaca sylvanus and Hystrix cristata from an Italian rescue centre for wild and exotic animals. *Virol J*. 2016;13(1):193.

5. Carocci M, Bakkali-Kassimi L. The encephalomyocarditis virus. *Virulence*. 2012;3(4):351–367.

6. Czechowicz J, Huaman JL, Forshey BM, et al., Prevalence and risk factors for encephalomyocarditis virus infection in Peru. *Vector Borne Zoonotic Dis*. 2011;11(4):367–374.

7. Foglia EA, Pezzoni G, Bonilauri P, Torri D, Grazioli S, Brocchi E. A recent view about encephalomyocarditis virus circulating in compartmentalised animal population in Northern Italy. *Sci Rep*. 2023;13(1):592.

8. Gris AH, Alves RS, Camargo LJ, et al. Reemerging of Encephalomyocarditis Virus in Pigs in Brazil: Pathological and Viral Characterization. *Transbound Emerg Dis*. 2023;2023:1–6.

9. Lefkowitz EJ, Dempsey DM, Hendrickson RC, Orton RJ, Siddell SG, Smith DB. Virus taxonomy: the database of the International Committee on Taxonomy of Viruses (ICTV). *Nucleic Acids Res*. 2018;46(D1):D708–D717.

10. Menegatt JCO, Perosa FF, Gris AH, et al. Main Causes of Death in Piglets from Different Brazilian Nursery Farms Based on Clinical, Microbiological, and Pathological Aspects. *Animals*. 2023;13(24):3819.

11. Oberste MS, Gotuzzo E, Blair P, et al. Human Febrile Illness Caused by Encephalomyocarditis Virus Infection, Peru. *Emerg Infect Dis*. 2009;15(4):640–646.

12. Robinson WF, Robinson NA. Chapter 1 - Cardiovascular System. In: Maxie MG, ed. *Jubb, Kennedy & Palmer's Pathology of Domestic Animals*: Volume 3 (Sixth Edition). W.B. Saunders 2016:1-101.e1.

13. Roehe PM, Rodrigues NC, Oliveira SJ de, et al. Encephalomyocarditis virus (EMCV) in swine in the state of Rio Grande do Sul, Brazil. *Rev Argent Microbiol*. 1985;16(2):117–120.

14. Scollo A, Mazzoni C, Luppi A. Management of encephalomyocarditis virus infection in Italian pig farms: a case report. *BMC Vet Res*. 2023;19(1):54.

15. Brewer LA, Lwamba HC, Murtaugh MP, Palmenberg AC, Brown C, Njenga MK. Porcine encephalomyocarditis virus persists in pig myocardium and infects human myocardial cells. *J Virol*. 2001 Dec;75(23):11621-9.

16. Huber SA. VCAM-1 is a receptor for encephalomyocarditis virus on murine vascular endothelial cells. *J Virol*. 1994 Jun;68(6):3453-8.

CASE II:

Signalment:
3-week-old male Bulldog (*Canis familiaris*)

History:
The puppy was born by caesarean section and was from a litter of eight. At 18 days old it was found shaking, anorexic and lethargic and was

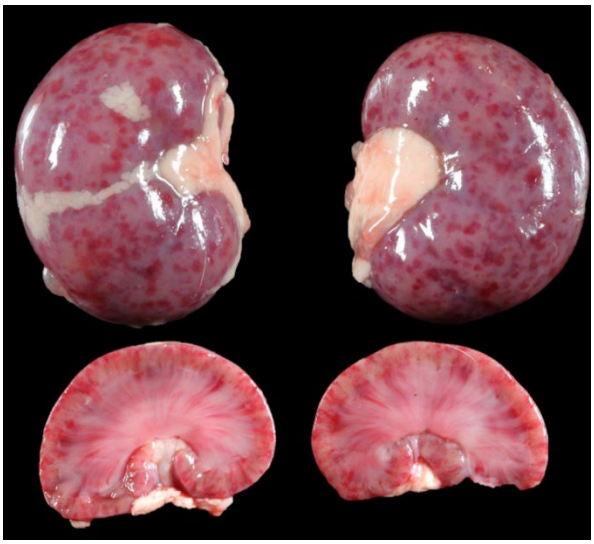

Kidney, puppy: There were multifocal to coalescing petechial to ecchymotic hemorrhages in the renal cortex that on cut surface extended into the renal parenchyma. (Photo courtesy of: Massey University School of Veterinary Science)

treated empirically with amoxicillin and dexamethasone. The puppy deteriorated and within 48 hours was hospitalized and placed in an oxygen tent. A serosanguinous nasal discharge and regurgitation of milk from the nose and mouth were present. The puppy was the second of the litter to die; a third puppy was unwell at the time this puppy was presented for postmortem examination.

Gross Pathology:

The 3-week-old male Bulldog puppy was in only adequate body condition (total body weight 735g). On external examination, a moderate amount of white fluid (milk) was present in the nasal passages. On internal examination, there were multifocal to coalescing petechial to ecchymotic hemorrhages throughout the renal cortex that on cut surface extended into the renal parenchyma. The liver was diffusely pale and had multifocal petechial hemorrhages, and multifocal 1 mm pitted areas on the capsular surface. No other gross lesions were present elsewhere.

Microscopic Description:

Kidney: Affecting approximately 30% of the renal parenchyma, with lesions predominantly localized in the cortex, are multifocal randomly distributed foci of coagulative necrosis characterized by tinctorial aberrations and retention of cellular architecture, with accumulations of cellular and karyorrhectic debris admixed with haemorrhage, fibrin and edema. Renal tubular epithelial cells within these areas are degenerate with swollen, pale and vacuolated cytoplasm, or necrotic with hypereosinophilic cytoplasm and nuclear pyknosis and occasional sloughing into luminal spaces. Rare 2-4 um eosinophilic, intranuclear viral inclusions are present within renal tubular epithelial cells. Multifocally, glomeruli rarely display segmental necrosis, characterized by hypereosinophilia, loss of cellular detail and the presence of karyorrhectic debris. Visceral and parietal epithelium are hypertrophied in affected glomeruli.

Liver: Within the liver, there is multifocal random hepatocellular necrosis, characterized by loss of normal architecture and replacement by cellular and karyorrhectic debris, hemorrhage and low numbers of neutrophils and macrophages. Rarely, hepatocytes adjacent to

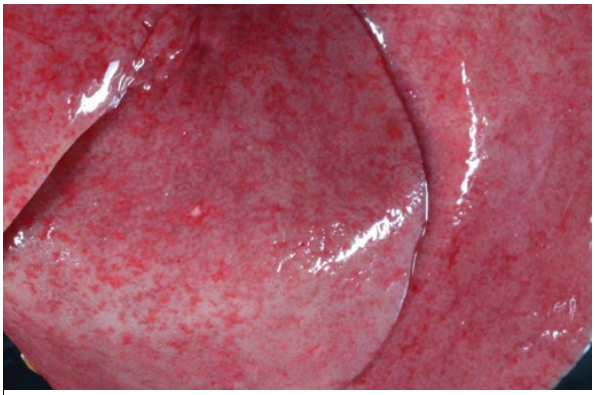

Liver, puppy. The liver was diffusely pale and had multifocal petechial hemorrhages, and multifocal 1 mm pitted areas on the capsular surface. (Photo courtesy of: Massey University School of Veterinary Science)

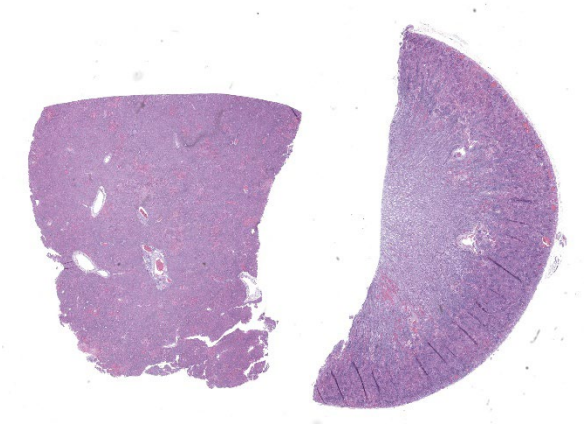

Liver, kidney, puppy: One section of liver and one of kidney are submitted for examination. Areas of hepatic necrosis and renal hemorrhage are evidence at subgross magnification. (HE, 11X)

areas of necrosis have 2-4 um, eosinophilic intranuclear viral inclusion bodies, which are surrounded by a clear halo and peripheralize nuclear chromatin. Periportal areas are mildly expanded by edema and low numbers of neutrophils and macrophages. Diffusely, small and medium arteriolar walls are moderately expanded by edema, with endothelial cells showing a spectrum of cell degeneration and necrosis including nuclear and cytoplasmic swelling, pyknosis, karyorrhexis and karyolysis.

Contributor's Morphologic Diagnosis:
Kidney: Severe, acute, multifocal, necrohemorrhagic nephritis with rare epithelial intranuclear viral inclusions.

Liver: Severe, acute, multifocal random, necrohemorrhagic hepatitis with rare epithelial intranuclear viral inclusions and multifocal arteriolar endothelial necrosis.

Contributor's Comment: The lesions in this case are consistent with acute infection with canine herpesvirus-1 (CaHV-1). CaHV-1 is an Alphaherpesvirus which infects both domestic and wild canids and was first described as a cause of neonatal puppy mortality in the 1960s.[2] It has a worldwide distribution and is antigenically similar to other Alphaherpesviruses of veterinary significance including feline herpesvirus-1, phocid herpesvirus-1 and equine herpesvirus-1 and 4.[2,4]

CaHV-1 is inactivated in temperatures over 40ºC (104ºF) and is readily broken down in the environment. Neonatal puppies aged less than 3 weeks of age become infected through direct contact and inhalation or ingestion of infected oronasal or genital secretions during passage through the birth canal, postnatal grooming by the dam or through contact with other shedding hosts including littermates.[2,3,8] Following exposure, it is thought that CaHV-1 infects epithelial cells of the oropharynx and lymphocytes in the tonsils. Leukocyte trafficking in lymphocytes spreads the virus systemically, where it targets endothelial cells indiscriminately and epithelial cells of several organ systems including the kidney, spleen, lung and liver.[8] Gross lesions in neonates are considered diagnostic and include miliary necrosis and petechial hemorrhages in multiple organs, particularly the kidneys.[1,8] This is further confirmed by demonstration of intranuclear viral inclusion bodies, though other relevant diagnostic tests include virus isolation, immunofluorescence, and polymerase chain reaction.[1] There may be pleural or peritoneal effusions, splenomegaly, lymphadenomegaly,

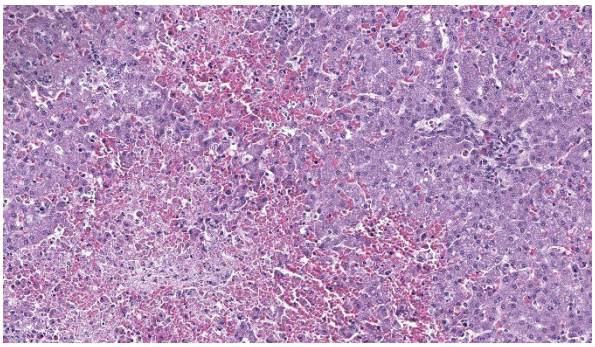

Liver, puppy. There are large areas of coagulative necrosis scattered randomly throughout the hepatic parenchyma. (HE, 301X)

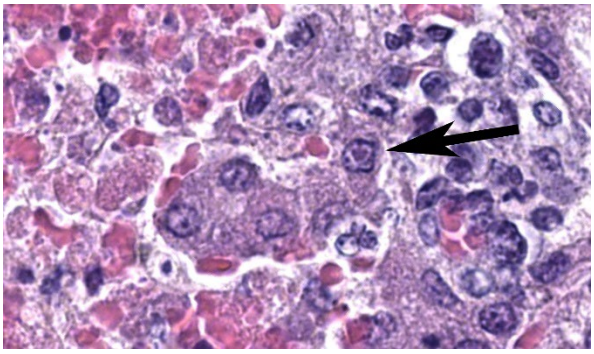

Liver, puppy: At the periphery of necrotic foci, rare hepatocellular nuclei contain a single rhomboidal 2-4um intranuclear inclusion. (HE, 850X)

and wet lungs with froth in the airways.[7] This puppy also had a severe necrotizing bronchopneumonia with intranuclear inclusion bodies in the bronchiolar epithelial cells.

Ocular lesions may not always be obvious if the affected puppy's eyelids are not yet open (after 10-14 days) and include panuveitis, retinitis and optic neuritis. Puppies that survive infection may have blindness, cataracts, optic nerve atrophy, and retinal degeneration or dysplasia.[3] Meningoencephalitis may also be seen, with lesions including multifocal glial nodules and cerebellar cortical necrosis without significant inflammation.[5]

An incubation period of 3-10 days is followed by 1-3 days of nonspecific clinical signs including vomiting, inappetence and abdominal pain.[2,7] The mortality rate can be up to 100% in some litters, with neonatal susceptibility thought to be due to a combination of immune naivety and a lower body temperature which improves the ability of CaHV-1 to enter cells, replicate and spread.[2,8] Infected puppies may shed virus within respiratory and ocular secretions, saliva, urine and on mucosal surfaces, and thus serve as a source of virus for other littermates. Puppies that are infected after 3 weeks of age or those that have been exposed to maternally derived antibody are generally resistant to disease.[3]

Infection of adult dogs and older puppies is associated with mild upper respiratory tract disease; CaHV-1 is yet to be shown to be a primary pathogen in canine infectious tracheobronchitis.[1,7] Severe fibrinonecrotic or hemorrhagic bronchopneumonia leading to respiratory distress and death has been occasionally reported in adult dogs.[6] Infection of a naïve dam during pregnancy can result in placental necrosis with mid-gestational abortion and stillbirths or weak puppies that die soon thereafter. Development of maternal antibody prevents disease in subsequent litters. Adult animals may also show lymphoid hyperplasia and hyperemia of the genital mucous membranes.[2]

CaHV-1 can establish latency within canids, existing within the trigeminal ganglia, lumbosacral ganglia, tonsils and parotid salivary glands. Recrudescence of infection can occur at times of physiological stress or treatment with immunosuppressive doses of corticosteroids. These animals may serve as a source of infection within breeding colonies,[2,3] and can shed virus from mucosal surfaces including those not involved in producing clinical disease.[3]. Serological studies may be of use in determining prevalence in kennels and at-risk breeding stock.[1]

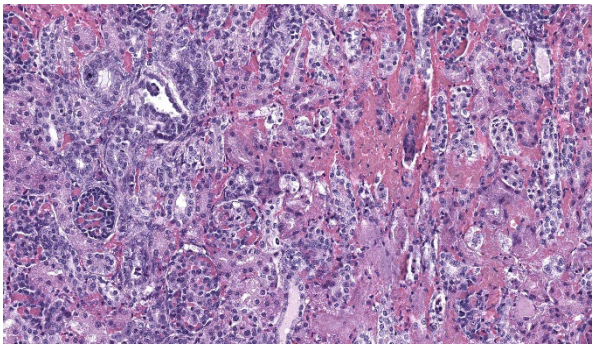

Kidney, puppy: There are areas of hemorrhage and tubular necrosis scattered throughout the cortex. (HE, 252X)

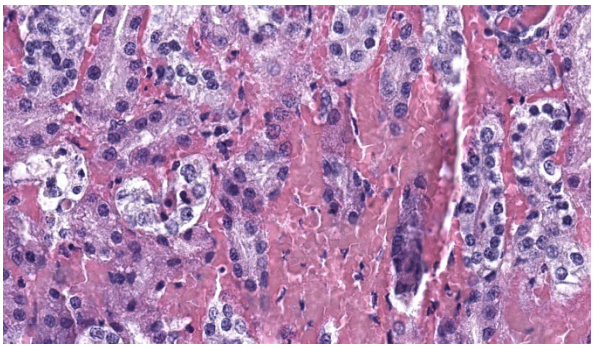

Kidney, puppy. Higher magnification of an area of interstitial hemorrhage and tubular necrosis. (HE, 350X)

Contributing Institution:
Massey University
School of Veterinary Science
Private Bag 11 222
Palmerston North 4442
New Zealand

JPC Morphologic Diagnosis: 1. Liver: Hepatitis, necrotizing, multifocal to coalescing and random, moderate, with rare hepatocellular intranuclear viral inclusions.

2. Kidney: Nephritis, necrotizing, tubular and glomerular, multifocal, moderate.

JPC Comment: This second case is a double feature, with the contributor kindly sharing features of CaHV-1 in two separate tissues with us. Microscopic features of the virus were classic for alphaherpesviruses, with Dr. Pesavento remarking that changing the signalment of the animal to another (e.g. horse, cow) would still bring conference participants to consider their respective alphaherpesvirus (EHV-1, BHV1) accordingly. Canine adenovirus and sepsis are other important rule outs for this case. Adenovirus would also have intranuclear inclusions and centrilobular hepatic necrosis (due to ischemia and endotheliotropism) while CaHV-1 is more hepatotropic – animal age is therefore helpful in weighting these differentials. Bacterial sepsis should reflect a greater number of neutrophils which can be confirmed via a simple touch impression on the necropsy floor. Dr. Pesavento emphasized this point in her preconference lecture to participants and urged anatomic pathologists to develop basic familiarity with cytology and incorporate it to drive case management decisions during case prosection.

This case has overlap with Case 4 of this conference and both are best reviewed together. Here, intranuclear inclusions were sparse (especially in the kidney) though the constellation of microscopic features were nonetheless suggestive of CaHV-1. The gross image of the kidney reinforces this differential – we debated whether the subcapsular hemorrhage correlated with the expansion of the renal interstitium microscopically, though distinguishing between simple congestion versus hemorrhage was characteristically difficult.

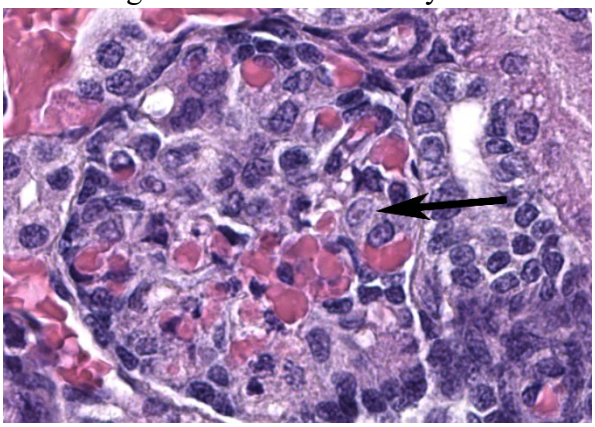

Kidney, puppy: Rare podocyte nuclei contain intranuclear viral inclusions. (HE, 1405X).

Dr. Pesavento highlighted several subtle slide features that pointed to this animal being very young, including fetal glomeruli with cuboidal epithelium, thinned renal cortex (decreased corticomedullary ratio) and decreased space between glomeruli, and smaller overall size of hepatocytes. From low magnification, the increased basophilia (colloquially, 'blueness') reflects these developing

cells and the active transcription of nucleic acids therein.

References:

1. Decaro N, Carmichael LE, Buonavoglia C. Viral reproductive pathogens of dogs and cats. Vet Clin Small Anim. 2012;42:583-598.

2. Decaro N, Martella V, Buonavoglia C. Canine adenoviruses and herpesvirus. Vet Clin Small Anim. 2008;38:799-814.

3. Evermann JF, Ledbetter EC, Maes RK. Canine reproductive, respiratory and ocular diseases due to canine herpesvirus. Vet Clin Small Anim. 2011;41:1097-1120.

4. Gaskell R, Willoughby K. Herpesviruses of carnivores. Vet Micro. 1999;69:73-88.

5. Jager MC, Sloma EA, Shelton M, Miller AD. Naturally acquired canine herpesvirus-associated meningoencephalitis. Vet Path. 2017;54(5):820-827.

6. Kumar S, Driskell EA, Cooley AJ, et al. Fatal canid herpesvirus 1 respiratory infections in 4 clinically healthy adult dogs. Vet Path. 2015;52(4):681-687.

7. Schlafer DH, Foster RA. Female genital system. In: Maxie MG, ed. Jubb, Kennedy, and Palmer's Pathology of Domestic Animals Volume 3. 6th ed. Missouri, USA: Elsevier; 2016:358-464.

8. Zachary JF. Mechanisms of microbial infections. In: Zachary JF, ed. Pathologic basis of veterinary disease. 6th ed. Missouri, USA: Elsevier, 2017:132-241.

CASE III:

Signalment:
14-day-old, Angus calf, Bovine, *Bos taurus*. Male.

History:
Six out of fifty 2–3-week-old, Angus calves were found dead with other calves presenting with lethargy, tachypnea, hypersalivation, circling, tremors, and seizures, with rapid deterioration preceding to death. Calves were otherwise in good body condition. No abnormalities of calves were observed at birth. These calves originated from artificially inseminated heifers.

Laboratory Results:
Bovine herpesvirus real time PCR positive on fresh brain

Bovine herpesvirus-5 real time PCR positive on fresh brain

Listeria spp. selective culture on fresh brain negative

Chlamydia pecorum real time PCR on brain dry swab negative

Aqueous humor urea, glucose, β-hydroxybutyrate, calcium, magnesium, nitrate, nitrite

Cerebrum, calf: One section of cerebrum is submitted for examination. Prominent perivascular cuffs are present at subgross magnification. (HE, 8X)

analytes within normal limits. Aqueous humor potassium is elevated (likely due to delayed post-mortem sampling or vitreous contamination).

Contributor's Microscopic Description: Brain; rostral cerebrum:

Multifocally, the meninges contain small numbers of lymphocytes, occasional macrophages and extravasated erythrocytes (hemorrhage), and rare neutrophils. Frequently, blood vessels in the white and to a lesser extent the gray matter are cuffed by up to 4-5 layers of lymphocytes, macrophages, and rare plasma cells. Occasional scattered neurons are shrunken, angular, hypereosinophilic, and have pyknotic or karyorrhectic nuclei (neuronal necrosis), rarely surrounded by up to 5 glial cells (satellitosis) and karyorrhectic nuclear debris. Multifocal patches in the gray matter have moderate numbers of neurons and rare astrocytes contain large, basophilic to amphophilic, intranuclear viral inclusions which peripheralise the chromatin (. Multifocally in the gray and white matter, there are abundant glial cells (gliosis), with astrocytes with vesiculated nuclei, which are often paired or clustered, frequently with karyorrhectic nuclei (glial cell necrosis) with large amounts of karyorrhectic nuclear debris scattered throughout the neuropil. Extensively within the gray matter and extending into the white matter, blood vessels, neurons, and glial cells are surrounded by clear spaces (edema) with frequent small, irregular clear spaces expanding the neuropil (spongiosis).

Contributor's Morphologic Diagnosis: Brain, rostral cerebrum: Meningoencephalitis, lymphohistiocytic, subacute, multifocal, severe with multifocal neuronal and glial cell

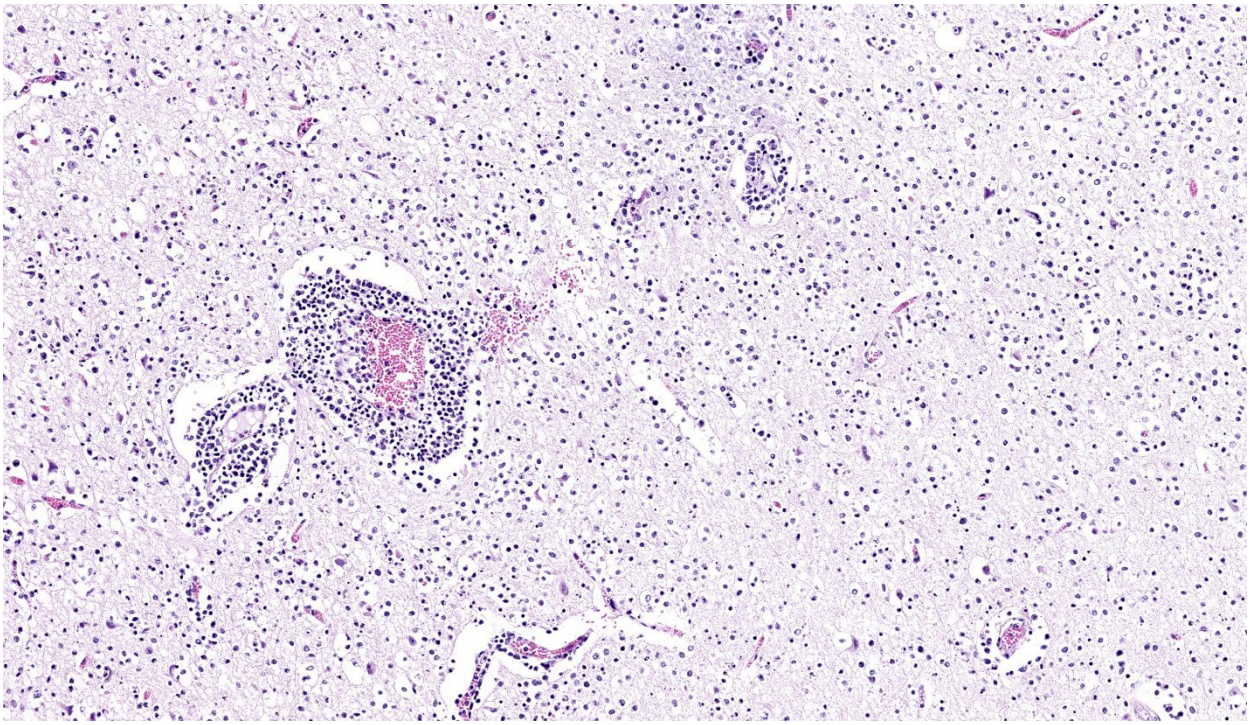

Cerebrum, calf: There are prominent cuffs of lymphocytes, macrophages, and fewer neutrophils, which infiltrate the adjacent parenchyma. There is also edema and gliosis, with prominent astrocytes and numerous microglia. (HE, 178X)

Contributor's Comment: Bovine herpesvirus-5 (BoHV-5) is an alphaherpesvirus known to cause meningoencephalitis in young cattle. BoHV-5 is closely related to BoHV-1 (the causative agent of bovine infectious rhinotracheitis) and was originally considered to be a "neurogenic variant of BoHV-1" or "BoHV-1.3".[4] After further comparative studies with different strains of BoHV-1, it was determined that this virus had distinct and differing genomic and antigenic properties and was reclassified as BoHV-5 by the International Committee on Taxonomy of Viruses in 1992.[4,10] BoHV-5 encephalitis outbreaks have been reported mostly in South American countries such as Brazil and Argentina, but also sporadically in other countries including Australia, and within North America and Europe.[4,9] BoHV-5 is part of a group of herpesviruses known to cause specific disease syndromes in bovines summarized in table 1 below.

BoHV-5 associated encephalitis is a typically a sporadic disease, but occasional outbreaks can occur in groups of calves and yearlings.[7] Morbidity can reach up to 50% and few symptomatic individuals survive.[7] The incubation period is approximately 1-2 weeks followed by presentation of clinical signs including depression, anorexia, weakness, proceeding to neurological signs such as circling, head pressing, incoordination, blindness, muscular tremors, convulsions, paddling, and death.[4,7] Nasal and ocular discharges have also been reported in some outbreaks of BoHV-5 associated disease, mimicking the classical clinical presentation of BoHV-1.[7]

Both BoHV-1 and -5 have many commonalities in their pathogenesis including the ability

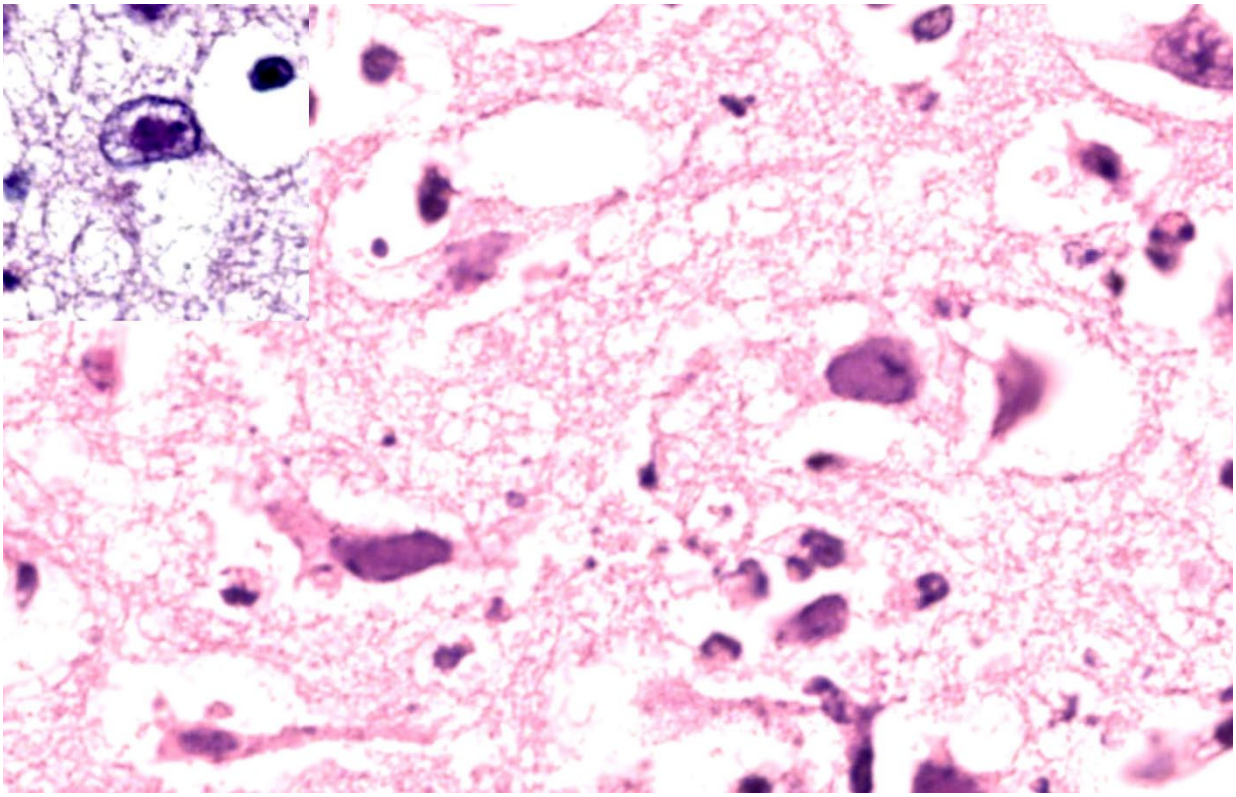

Cerebrum, calf: Herpesviral inclusions peripheralize the chromatin with neurons and an astrocytes (inset, top left) contains a viral inclusion surrounded by a clear halo (HE, 800X)

to infect epithelial cells at the portal of entry, establish latency in the trigeminal ganglia, and can be reactivated by natural or experimental stressors.[4,7] BoHV-5 associated disease differs from that of BoHV-1 as they have different neuroinvasion and neurovirulence capabilities with BoHV-1 rarely causing encephalitis.[7] The exact pathogenesis of BoHV-5 is unknown. Transmission occurs via direct contact, aerosolization, or indirect spread through contaminated feed and water, or semen.[4,7] Following inoculation, BoHV-5 infects and replicates within epithelial cells at the portal of entry (e.g., nasal or vaginal mucosa).[4] Several possibilities for BoHV-5 neural invasion are being investigated including local spread from infected nasal epithelial cells with intra-axonal transport via the trigeminal or olfactory pathways, or by hematogenous viremic spread.[4,6] Once BoHV-5 has gained entry to the central nervous system, it can cause acute meningoencephalitis or become latent within the sensory ganglia, with possible reactivation and clinical recrudescence induced at times of stress.[11]

The characteristic histopathological changes associated with BoHV-5 are non-suppurative meningoencephalitis with mononuclear perivascular cuffing, gliosis, satellitosis, neuronophagia, trigeminal ganglioneuritis, and neuronal necrosis and degeneration.[7] Malacia is reported variably across literature, can take a laminar cortical necrosis pattern of polioencephalomalacia (PEM), and is proposed to occur dependent on strain neurovirulence or individual susceptibility.[1,3] Intranuclear alphaherpesviral inclusion bodies are occasionally present in degenerate neurons and astrocytes.[7] Histopathological changes are most severe within the frontal cortex, with milder changes described variably within the diencephalon, parietal and occipital cortices, cerebellum, basal nuclei, and brain stem.[2] In our case, milder changes were observed within the dorsal cerebrum, thalamus, and brainstem.

Possible histological differential diagnoses of BoHV-5 meningoencephalitis in calves include BoHV-1 infection, rabies, or malignant catarrhal fever, listeriosis, sporadic bovine encephalomyelitis (caused by *Chlamydia pecorum*), or less likely PEM causes such as lead or sulfur toxicity, thiamine deficiency, or salt poisoning.[5]

Table 1: Outline of bovine diseases associated with bovine herpes viral infections.

Bovine herpesvirus type	**Subfamily**	**Disease associations**
BoHV-1[6-8]	Alpha	• Infectious bovine rhinotracheitis (IBR) • Infectious pustular vulvovaginitis (IPV) and balanoposthitis (IPB) • Meningoencephalomyelitis • Systemic disease in neonates • Abortion • Bronchopneumonia
BoHV-2[6,7]	Alpha	• Pseudolumpy skin disease Ulcerative mammillitis
BoHV-4 ("Bovine cy-	Gamma	• Metritis • Abortion • "Epivag" syndrome in-

tomegalovirus")[8]		cluding: vaginitis, salpingitis, oophoritis or epididymitis • Mammillitis • Pneumonia • Enteritis
BoHV-5[6,7]	Alpha	• Meningoencephalitis

Contributing Institution:
NSW Animal and Plant Health Laboratories
Elizabeth Macarthur Agricultural Institute
Woodbridge Rd, Menangle
NSW, Australia, 2568
https://www.dpi.nsw.gov.au/about-us/services/laboratory-services/veterinary

JPC Morphologic Diagnosis: Cerebrum: Meningoencephalitis, lymphohistiocytic, subacute, diffuse, moderate, with neuronal necrosis and glial and neuronal intranuclear viral inclusions.

JPC Comment: The third case of this conference is yet another alphaherpesvirus and does not disappoint. Recent (and quite timely) publication[12] reviewing bovine herpesviral meningoencephalitis was a welcome addition to our discussion. Gross images from that publication nicely highlight the predominant frontal lobe distribution of BoHV-5, to include the sometimes dramatic malacia that the contributor notes above. We considered many of the same differential diagnoses that the contributor helpfully notes, but would also add rabies (though 5 animals is a bit of a stretch), bovine astrovirus, West Nile virus, and listeriosis as other broader differentials for bovine meningoencephalitis. Dr. Pesavento emphasized low power evaluation of any brain section for symmetry, position of the midline, distribution of features (to include portion of the brain examined), and loss of parenchyma to help sort (or rule out) these possibilities. Intranuclear viral inclusions were fairly generous in this case which aided in recognition of the etiological agent.

Mild neutrophilic inflammation was an unexpected finding in this calf's brain given the primary viral etiology. We considered a secondary process such as sepsis, though there is little lymphoid necrosis present within perivascular lymphoid cuffs and neutrophils are well within the parenchyma itself. One potential explanation is the young age (14 days) of this animal and insufficient time course to develop and deploy other innate/adaptive immune cells in large numbers akin to some of the NOD/Rag1/ILrg2 fully immunodeficient mice we have considered in conference this year (see Conference 11, Case 3 for one such example). We anticipate that in a slightly older animal histopathologic features would reflect non-suppurative meningoencephalitis alone.

Conference discussion of this case concluded with review of vascular features. In comparison to Case 4, this brain lacked changes in major blood vessels, though there was capillary damage coincident with eosinophilic fluid which we interpreted as true edema to accompany the spongiosis noted (versus processing artifact alone). Dr. Pesavento reminded conference goers that Factor VIII IHC is a potentially useful IHC marker for vascular damage as it also labels platelets, with the resulting perivascular aggregate serving as a reliable label when other markers (e.g. CD31) might be difficult to interpret alone.

References:

1. Belknap EB, Collins JK, Ayers VK, Schultheiss PC. Experimental-Infection of Neonatal Calves with Neurovirulent Bovine Herpesvirus Type-1.3. *Veterinary Pathology*. 1994;31**:** 358-365.

2. Cagnini DQ, Cunha PHJ, Pantoja JCF, et al. Histopathological, immunohistochemical, and molecular study of BHV-5 infection in the central nervous system of experimentally infected calves. *Pesqui Vet Brasil*. 2015;35**:** 337-343.

3. David N, Huebner SO, Riet-Correa F, Halfen D, Lemos RA. Reactivation of latent bovine herpesvirus type 5 in cattle with polioencephalomalacia induced by ammonium sulphate. *Pesqui Vet Brasil*. 2007;27**:** 435-441.

4. Del Medico Zajac MP, Ladelfa MF, Kotsias F, et al. Biology of bovine herpesvirus 5. *Vet J*. 2010;184**:** 138-145.

5. Dore V, Smith G. Cerebral Disorders of Calves. *Vet Clin North Am Food Anim Pract*. 2017;33**:** 27-41.

6. Engels M, Ackermann M. Pathogenesis of ruminant herpesvirus infections. *Vet Microbiol*. 1996;53**:** 3-15.

7. Jubb KVF, Kennedy PC, Palmer N. *Pathology of domestic animals*, 6th ed., vol. 1. St. Louis: Elsevier; 2016.

8. Jubb KVF, Kennedy PC, Palmer N. *Pathology of domestic animals*, 6th ed., vol. 3. St. Louis: Elsevier; 2016.

9. Kessell A, Finnie J, Windsor P. Neurological diseases of ruminant livestock in Australia. IV: viral infections. *Aust Vet J*. 2011;89**:** 331-337.

10. Roizmann B, Desrosiers RC, Fleckenstein B, Lopez C, Minson AC, Studdert MJ. The family Herpesviridae: an update. The Herpesvirus Study Group of the International Committee on Taxonomy of Viruses. *Arch Virol*. 1992;123**:** 425-449.

11. Vogel FS, Caron L, Flores EF, et al. Distribution of bovine herpesvirus type 5 DNA in the central nervous systems of latently, experimentally infected calves. *J Clin Microbiol*. 2003;41**:** 4512-4520.

12. Santos BS, Lemos RAA, Rech RR, Barros CSL, Rissi DR. Bovine herpesviral meningoencephalitis: large case study and literature review. *Journal of Veterinary Diagnostic Investigation*. 2025;37(3):417-428.

CASE IV:

Signalment:
10 day-old, female, Standardbred horse, *Equus caballus,* equine

History:
In the late spring of 2023, five, 3-4 day old foals in a Standardbred breeding farm developed clinical signs of pneumonia over a period of several weeks. Four of these foals did not respond to antibiotic treatment and died

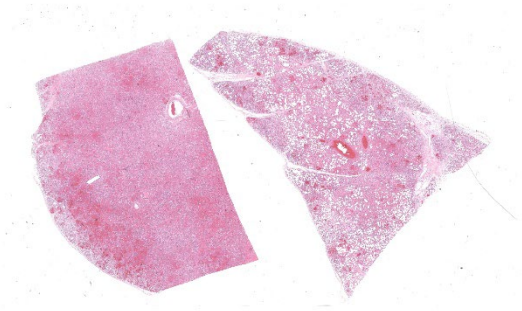

Lung, foal: Two sections of lung, varying in lesion severity, are submitted for examination. At this magnification, there is abundant hemorrhage and edema within both sections. (HE, 6X)

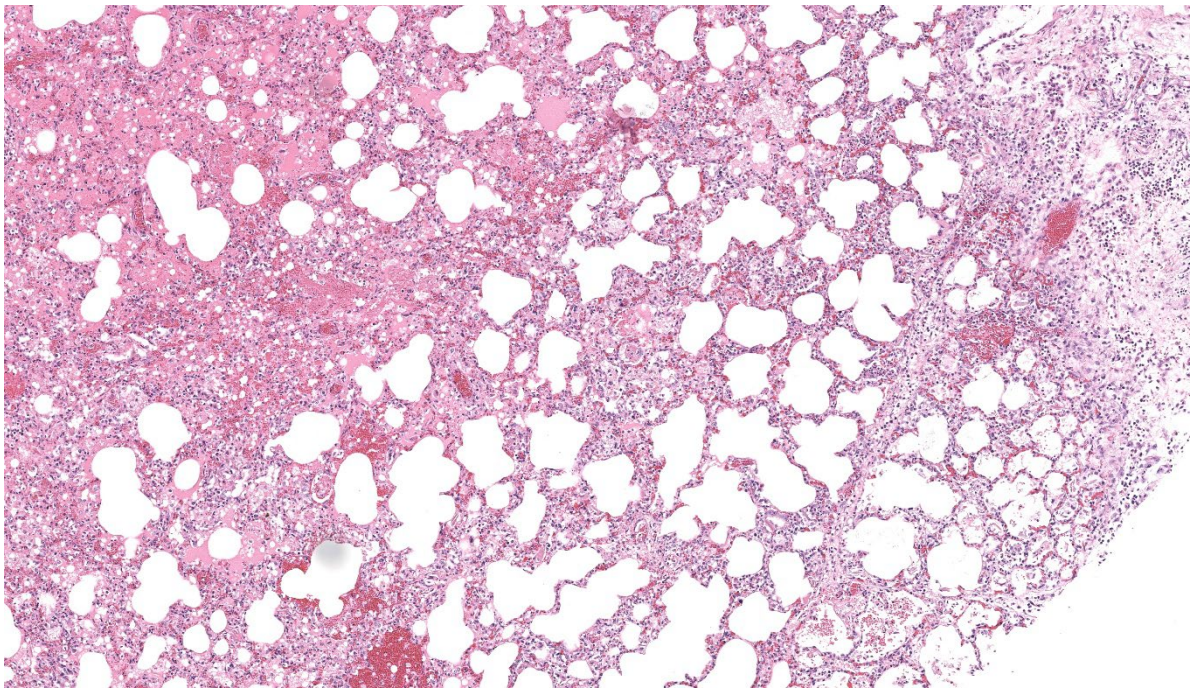

Lung, foal: There is diffuse interstitial pneumonia with thickening of alveolar septa and abundant alveolar edema and hemorrhage. (HE, 171X)

at approximately 8-10 days of age. Two of these foals were necropsied and both exhibited severe acute interstitial pneumonia and severe edema, with microscopic features most consistent with acute diffuse alveolar damage. Equine herpesviruses 1 and 4, and equine influenza type A were not detected in PCR testing of lungs samples from both foals. No clinical abnormalities were noted in the dams of these foals, or in any other horses on the farm.

The last of these foals (the 5th one reported) was noted to be lethargic and tachypneic at 4 days of age. This filly was treated with ceftiofur sodium, gentamicin, flunixin meglumine, dexamethasone, furosemide, and oxygen therapy. Radiographs of the thorax revealed abnormalities consistent with interstitial pneumonia. Despite treatment, the foal's condition progressively worsened until she suddenly decompensated and began agonal breathing early morning, 6 days after clinical signs were first noted. The filly was humanely euthanized with IV Euthanyl and submitted for necropsy.

Gross Pathology:

The filly was thin. The lungs were moderately expanded, diffusely dark pink to red, rubbery in texture, and failed to collapse. Large amounts of white froth were noted in the trachea. Small amounts of clear yellow tinged fluid were present in the pericardial sac. The remaining carcass was grossly unremarkable.

Laboratory Results:

Aerobic culture of the lung yielded no microbial growth. Samples of lung from this foal, and from both previously necropsied foals from this farm, were submitted for the equine respiratory pathogen PCR panel offered by the Cornell University Animal Health Diagnostic Centre. Equine adenoviruses 1 and 2,

Equine herpesviruses 1 and 4, Equine rhinitis viruses A and B, and influenza virus matrix, were not detected. Streptococcus equi was also not detected. Equine arteritis virus (EAV) was detected in lung samples from all three foals. Virus isolation from lung samples from each of these foals using cloned monkey cell lines was performed and EAV isolates were recovered from all three samples. Preliminary genomic sequencing of these isolates reveals that this virus has 97% homology with American Type Culture Collection (ATCC) reference strains of EAV isolated in North America approximately 30 years ago. Additional genomic sequencing and phylogenetic analysis of these isolates are ongoing.

Microscopic Description:
The most significant microscopic abnormalities were present in sections of lung which exhibited diffuse filling of most alveoli with dark pink, proteinaceous fluid admixed with occasional small deposits of amorphous fibrinoid debris, small bits of pyknotic cell debris, few degenerate neutrophils, small numbers of macrophages, and frequent erythrocytes. In a few areas, a thin layer of fibrinoid debris lines alveoli (hyaline membranes). In areas, scattered keratin squames are also noted in alveoli (attributed to terminal aspiration). Inter-alveolar septa are often mildly thickened and moderately congested. In areas where alveolar fibrin deposits are more prominent, plump polygonal cells with pale vesicular nuclei partially line alveoli (early type II pneumocyte hyperplasia). The epithelium lining of bronchi and bronchioles is generally intact. In a few scattered small and medium caliber arteries, there are foci where sparse cell debris, sometimes accompanied by small amounts of dense, hyalinized fibrinoid material, and occasional pyknotic nuclei partially effaces the tunica media.

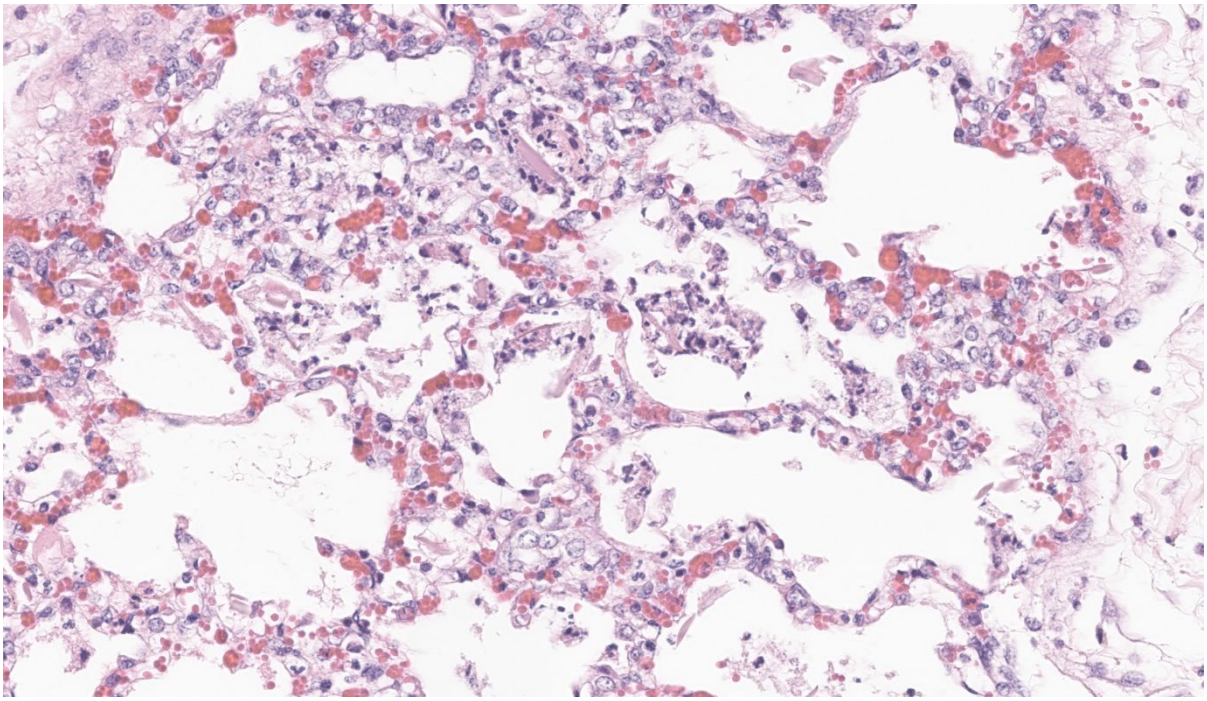

Lung, foal: High magnification of alveolar septa which are expanded by varying combinations and concentrations of congestion, edema, fibrin, septal macrophage hypertrophy. Neutrophils, cellular debris, and scattered type II pneumocyte hyperplasia. (HE,554X)

No significant microscopic abnormalities are noted in sections of kidney, liver, brain, adrenal gland, spleen, heart, or intestine.

Contributor's Morphologic Diagnosis:
Lung:

1. Severe, acute, fibrinous, interstitial pneumonia with marked pulmonary edema, multifocal type II pneumocyte hypertrophy and hyperplasia, and few scattered foci of mild, peracute, vascular, fibrinoid necrosis
2. Multifocal, intra-alveolar keratin squames (attributed to terminal or agonal aspiration)

Contributor's Comment: The clinical signs described in this foal are attributed to respiratory failure resulting from severe acute interstitial pneumonia and pulmonary edema. The microscopic appearance of these lung lesions were consistent with diffuse alveolar damage due to diffuse injury to type I pneumocytes and/or endothelial cells in alveolar septa. In acute stages of diffuse alveolar damage, pulmonary edema, exudation of fibrin into alveoli, and the formation of hyaline membranes (aggregates of fibrin, other serum proteins and cell debris) that line alveoli lumina are the first lesions typically apparent, rapidly followed by type II pneumocyte hyperplasia. If the affected individual survives long enough, interstitial fibrosis may be seen. These lesions often clinically manifest as acute respiratory distress syndrome (ARDS) in humans and animals. This clinical condition presents as acute onset pulmonary edema resulting in hypoxemia that does not respond to oxygen supplementation, with no evidence of concurrent left atrial enlargement (or primary left heart failure).[1]

Diffuse alveolar damage has been associated with a wide range of etiologies in animals.[1]

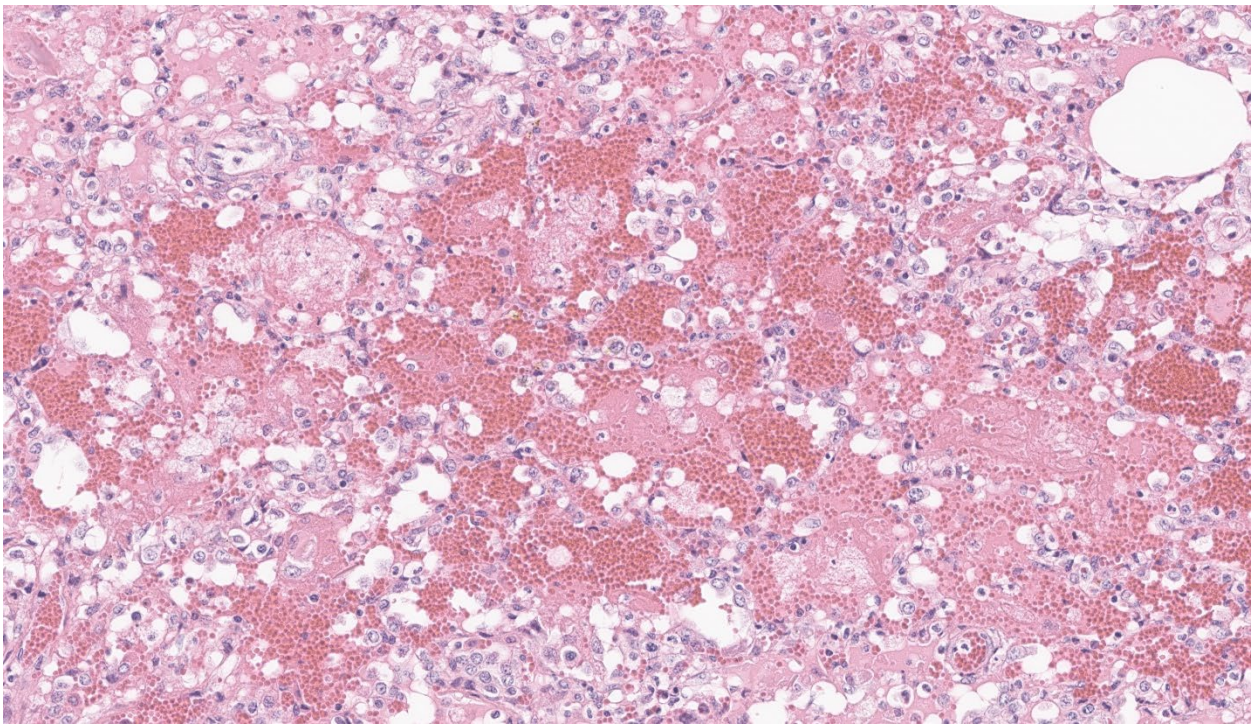

Lung, foal: There are large areas in which alveoli are flooded with hemorrhage and edema (HE, 381X)

In this case, given the microscopic appearance of lesions, the clinical history, and involvement of multiple animals, an infectious etiology (most likely a viral infection) was highly suspected. Initial PCR testing of lung samples from this foal and the two other necropsied horses for equine herpesvirus 1 and 4 and equine influenza virus were negative which prompted additional PCR testing for a wider range of respiratory pathogens including equine adenoviruses, equine rhinitis viruses and equine arteritis virus (EAV). Only EAV was detected in each of the examined samples and this outbreak of acute interstitial pneumonia in foals was attributed to infection with this pathogen.

Equine arteritis virus (EAV) is a small enveloped, RNA, non-arthropod-borne virus in the family Arteriviridae, and the order Nidovirales and causes a condition termed equine viral arteritis. EAV was first isolated from an outbreak of respiratory disease and abortion in a Standardbred breeding farm in Bucyrus, Iowa in 1953.[8] Since then, serologic studies have revealed a worldwide distribution of EAV, although several counties including Iceland, Singapore, Japan, and New Zealand may be free of the virus.[5] The virus is highly species specific and infection is limited to equids such as horses, donkeys, mules and zebra. In the United States, a very high percentage of Standardbreds have been found to be seropositive (70-90%), compared to other breeds (such as Thoroughbreds), while in some European countries, the seroprevalence of EAV in some Warmblood stallions is very high. Most infections in adult horses are inapparent or cause mild clinical signs and are rarely fatal.[8] Most infections involve mares bred to a persistently infected stallion. Very young, old, or debilitated and immunosuppressed horses may develop more severe clinical signs, and rarely develop fatal disease. Clinical signs in adult infected horses most commonly consist of pyrexia, depression, anorexia, dependent edema, conjunctivitis, periorbital and supraorbital edema, respiratory distress and leukopenia.[8] After infection and a period of viremia, the virus is

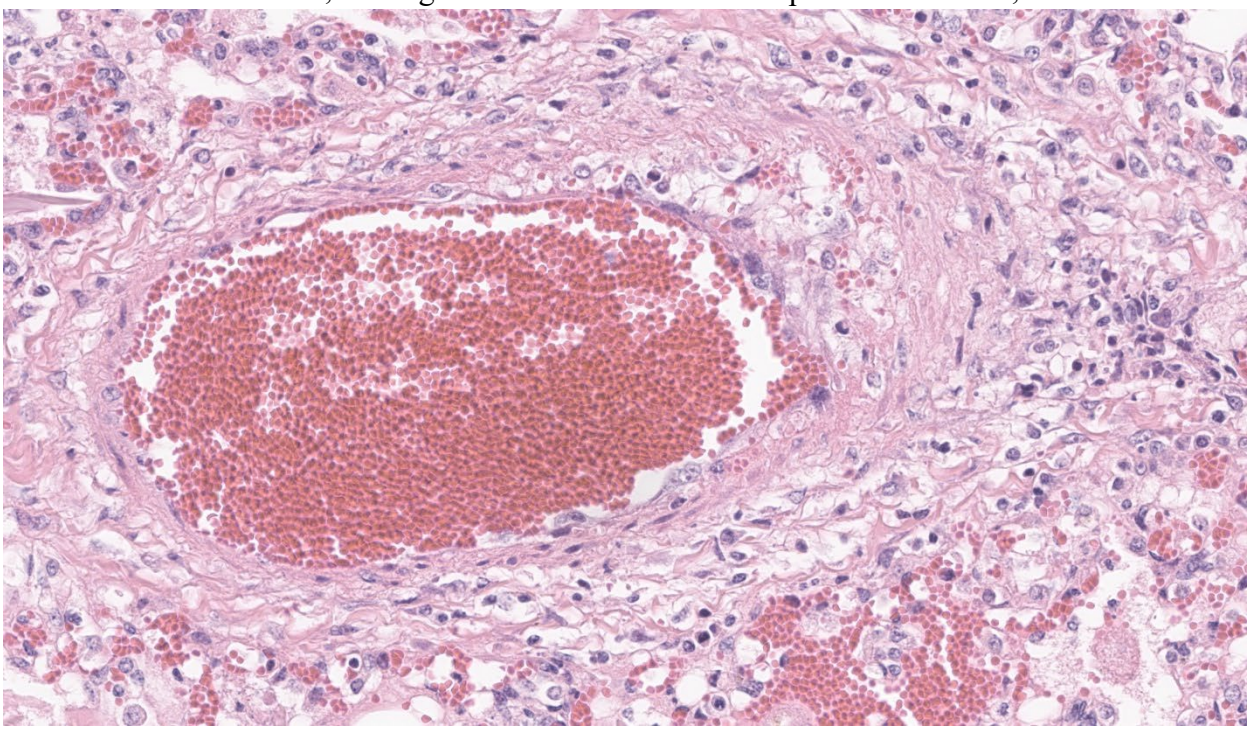

Lung, foal: There is segmental necrosis of the wall of an arteriole with necrosis of smooth muscle cells, infiltrations of neutrophils, cell debris, mural hemorrhage and edema, and adventitial edema. (HE, 571X)

widely disseminated and is replicating in macrophages and endothelial cells within 3 days. Clinical signs of EAV infection are the result of endothelial injury and increased vascular permeability resulting in edema, congestion and hemorrhage in subcutaneous tissues, lymph node and viscera.[3,8]

Abortion is another common manifestation of EAV infections in horses. In natural outbreaks, abortion rates of less than 10% to 71% of infected mares have been reported. Mares are typically between 3 and 10 months of gestation when abortion occurs. In these cases, the fetus and placenta are often expelled without premonitory signs and may be autolyzed or well preserved. Lesions in the fetus are often not seen, and when present, may consist of mild interstitial pneumonia, mild perivascular lymphoplasmacytic infiltrates, and fetal membranes may appear edematous. Rarely, vasculitis may be seen in the allantochorion and in fetal visceral sites.[3] In most cases of EAV infection, abortion is likely largely due to acute vasculitis, edema and hemorrhage within the uterus resulting in impaired placental perfusion and hypoxia. Hypoxic injury may also cause decreased placental progesterone production and local release of prostaglandins that would also promote premature placental separation and fetal death.[3] Interestingly, abortions were not noted during this outbreak, possibly due to the late stage of gestation when the mares were infected. Alternatively, it is also possible that the strain of EAV virus in this outbreak had a low abortigenic potential.[7]

Equine arteritis virus infection resulting in severe, fulminating, interstitial pneumonia has been reported in neonatal foals and was the primary presentation of affected horses on this farm.[3,7,8] The prognosis for affected foals despite aggressive treatment, is poor and most infections in neonatal foals are fatal. This cluster of cases would suggest that the dams were infected just days prior to parturition or that foals were exposed to the virus in the first few days of life. Intestinal lesions have also been reported in affected foals but no such lesions were noted in our cases.

Transmission of the majority of EAV infections is via venereal and respiratory routes. Transmission of EAV through indirect contact with contaminated fomites may occur, but is generally not considered a major contributor to the spread of disease. However, the latter was implicated as a contributing factor in the spread of EAV infection in an outbreak in a veterinary teaching hospital.[2] Persistently infected carrier stallions are the reservoir responsible for maintenance of EAV in equine populations. Once infected, stallions harbor the virus in the ampulla of the vas deferens, other accessary sex glands, and in portions of the lower genitourinary tract, from where they shed virus in semen for weeks to months to years. Some stallions may shed virus in semen for the rest of their lives. Maintenance of the carrier state in stallions appears to be testosterone dependent and currently, the only effective means of eliminating infection in these horses is via surgical castration[8]. Carrier stallions may infect mares via natural breeding and via artificial insemination of infected semen. Once infected, a recently bred mare (or a recently infected stallion) may develop clinical signs and shed virus in respiratory secretions within 7-10 days[7]. Horizontal transmission of the virus via aerosolized respiratory secretions to other close contacts is a common cause of spread within the herd.[7,8] In cases where mares have aborted due to EAV infection, exposure to the fetus, placenta and placental fluids is another potential source of infection.[7] Infected mares, geldings and foals less than 6 months of age, clear the virus 28 days post-infection.[7,8]

Although several reports of outbreaks of EAV infection can be found in the literature, those primarily involving significant disease only in neonates are rare. One such case report[4] has features similar to that described in our cases. Affected foals also presented with severe, acute, fatal interstitial pneumonia with no obvious clinical signs were noticed in the mares. In the mentioned reference, each of the affected foals were thought to be immunocompromised to some degree, due to colostrum deprivation, death of the dam, or prematurity, which may have contributed to the severity of disease noted. Interestingly, in our cases, no such factors appeared to be at play, but each of the three affected foals necropsied were deficient in selenium. All had liver levels of less than 0.20 ppm wet weight (0.20 ppm is the lowest amount of selenium our assay can accurately quantify): adequate reference range of selenium in equine liver is 0.30-1.00 ppm. There were no lesions of white muscle disease (or nutritional myopathy) in any of the necropsied foals. However, selenium is an important essential trace element involved with a wide variety of physiologic processes in animals, including normal immune system function, regulation of growth and development, protection against oxidative stress and has antimicrobial (including antiviral) effects.[6] It is interesting to speculate that selenium deficiency in the dams and affected foals may have played a role in the severity of disease seen in the foals in this outbreak of equine viral arteritis.

Contributing Institution:
Department of Pathology and Microbiology
University of Prince Edward Island
www.upei.ca

JPC Morphologic Diagnosis: Cerebrum: Meningoencephalitis, lymphohistiocytic, subacute, diffuse, moderate, with neuronal necrosis and glial and neuronal intranuclear viral inclusions.

JPC Comment: The contributor provides a spectacular slide to accompany a thorough summary of EVA and a putative cause for the changes observed in this case. Dr. Pesavento was excited to review this case as equine viral arteritis is a rare submission to the WSC and the microscopic features gave us much to discuss. The inclusion of squamous epithelial cells is an unexpected secondary feature to explore – we considered the contributor's interpretation of agonal inspiration and also wondered about perinatal fetal stress (and inhalation of amniotic contents) as several participants pointed out possible meconium as well. Within this section, we also note segmental fibrinoid necrosis of larger arterioles that highlight the route of entry of EAV and subsequent genesis of the abundant edema present.

Differential diagnoses for this case included other viruses such as Hendra virus (paramyxovirus), equine herpesvirus 1, African horse sickness (orbivirus), and equine infectious anemia virus (lentivirus) which share overlapping gross and microscopic features, to include the prolific pulmonary edema seen in this case. Discriminating features include time course of the disease and geography (i.e. current transboundary diseases). Syncytial cells within the bronchiolar epithelium did resemble viral syncytia of paramyxoviruses, though we attributed this change to increased turnover of lung epithelial cells due to viral effects versus direct infection as bronchiolar epithelial cells lacked direct cytopathic changes. For this reason, we differed from the contributor and did not label this pneumonia as 'bronchointerstitial'. Other potential

vasculocentric ruleouts include leptospirosis, purpura hemorrhagica, and plant toxicity such as hoary alyssum (*Berteroa incana*).

Finally, we briefly revisited the concepts of diffuse alveolar damage and interstitial pneumonia which we previously debated in Conference 9, Case 2 of the current conference year (in a dog). That case also featured large balls of fibrin filling alveoli, allowing us to introduce the term 'fibrinous and organizing pneumonia'. The present case is decidedly more acute, with few cells embedded within the fibrin meshwork and little evidence of reorganization. Dr. Pesavento also drew the distinction between diffuse alveolar damage (a histologic finding) and interstitial pneumonia (interstitial lung disease) itself which is used more broadly (and sometimes, confusingly) between veterinary pathologists. For a more complete review of this topic, we direct the reader to an excellent and recent publication.[9]

References:

1. Caswell JL, Williams KJ. Respiratory System; *In: Jubb, Kennedy's and Palmers Pathology of Domestic Animals*. Vol 2, 6th ed. Elsevier; 2016;509-511.
2. Collins JK, Kari S, Ralston SL, Bennett DG, et al. Equine viral arteritis at a veterinary teaching hospital. *Preventive Veterinary Medicine.* 1987;4:389-397.
3. Del Piero F. Equine viral arteritis. *Veterinary Pathology.* 2000; 37:287-296.
4. Del Piero F, Wilkins PA, Lopez JW, et al. Equine viral arteritis in newborn foals: clinical, pathological, serological, microbiological, and immunohistochemical observations. *Equine Veterinary Journal.* 1997;29(3):178-185.
5. Gilkerson JR, Bailey KE, Diaz-Mendez A, et al. Update on viral disease of the equine respiratory tract. *Vet Clin Equine.* 2015; 31:91-104.
6. Hosnedlova B, Kepinska M, Skalickova S, et al. A summary of new findings on the biological effects of selenium in selected animal species – A critical review. *International Journal of Molecular Sciences*. 2017; 18:2209.
7. Timoney PJ, McCollum WH. Equine viral arteritis. *Veterinary Clinics of North America: Equine Practice*. 1993;9(2):295-309.
8. Balasuriya UBR. Equine viral arteritis. *Vet Clin Equine*. 2014;30:543-560.
9. Carvallo FR, Stevenson VB. Interstitial pneumonia and diffuse alveolar damage in domestic animals. *Veterinary Pathology*. 2022;59(4):586-601.

Joint Pathology Center
Veterinary Pathology Services

WEDNESDAY SLIDE CONFERENCE 2024-2025

Conference #25 30 April 2025

CASE I:

Signalment:
3-year-old, 9-month pregnant, female, Jersey *(Bos taurus taurus*).

History:
The cow was dried off on June 28, 2022. She had been doing well until August 17, 2022, when she was found recumbent and was diagnosed with possible pink eye. She was treated with aspirin, penicillin, and dexamethasone subconjunctivally. On August 18, 2022, she remained recumbent, began convulsing, and died at 9:30 am. She was submitted for postmortem examination by 11:00 am on the same day.

Gross Pathology:
Fair body condition with mild muscle mass, minimal external adipose stores, and moderate internal adipose stores in all expected locations. Avulsion of the lateral right hind limb dew claw; multifocal 2 to 15 cm diameter area abrasions on the right hip and on the lateral aspect of the right fore limb; and, a 15 x 11 cm area of subcutaneous edema and a 35 x 20 cm area of subcutaneous hemorrhage on the right thorax over the ribs and right shoulder.

Thoracic negative pressure and mild, serosanguineous pleural effusion. Multifocal thoracic cranioventral fibrous adhesions that span between lung, pericardial sac, diaphragm, and body wall. Mild ventrocranial laryngeal edema. Severe, diffuse, frothy, white foam extending from the larynx to the secondary bronchi. Mild to moderate, white frothy fluid oozes from the lungs on the cut section. Multifocal epicardial and left ventricular endocardial petechiae. A focal, 5.5 x 3 cm hemorrhage at the base of the right atrium overlaying adipose tissue.

A focal well-demarcated, 4 x 1 cm subacute healing ulcer on the right lateral aspect of the tongue. Rumen has decreased dry ingesta (dehydrated) with admixed birdshot and rocks. No magnet. There is expected postmortem rumen mucosal sloughing.

The abomasum contains rocks admixed with green organic material and the mucosa has multifocal occasional subacute ulcers. The biliary tract is patent with normal bile. There is a fibrous adhesion of the right liver lobe to the omentum. The liver is moderately congested.

The right caudal mammary quarter has a thick, viscous, white-to-tan discharge without flocculent material, and on section, the mammary gland is pale tan and oozes a cloudy white thick fluid. The supramammary lymph nodes are enlarged and wet.

The subdural space of the brain and the cervical spinal cord has viscous, translucent to yellow serous meningeal fluid and multifocal

hemorrhage. The right ventrocranial aspect of the cerebral frontal lobe and olfactory lobe and bulb are regionally tan to yellow, soft, and friable (encephalomalacia). The area's meninges are thickened by fibrin, edema, and hemorrhage.

The left eye has a regional soft expansion of the conjunctiva (iatrogenic) and is overlaid by at least 3 thin white linear nematodes (favor *Thelazia gulosa*).

FETUS: The left uterine horn has a single female fetus. The fetus is well muscled with abundant adipose stores. The maternal aspect of the chorioallantois is overlaid by multifocal brown, mucoid material. There are multiple (< 5) small (< 0.5 cm), white, discrete, firm, and focal nodules on the amniotic sac. The fetus is 18.4 kg, 72.5 cm from crown to rump, has erupted incisors, and is fully haired with eyelashes (9 month, near term). No thoracic negative pressure and lung sections sink in formalin. The thoracic cavity has mild, serosanguineous fluid. The right lateral and cranial aspect of the liver has a large 10 x 6 cm cyst. When cut, the cyst oozes red-tinged serous fluid with scant fibrin. There is focal hemorrhage of the ruminal serosa and regional suffusive hemorrhage on the right ventricle epicardium.

Laboratory Results:

1) A multiplex real-time PCR performed by the USA CDC on fresh brain from the right frontal/olfactory lobe was positive for *Naegleria fowleri* and negative for *Acanthamoeba* spp. and *Balamuthia mandrillaris.*

2) Immunohistochemistry performed by the USA CDC on formalin-fixed paraffin-embedded right frontal/olfactory lobe was immunoreactive for free-living amoeba and *Naegleria*-specific antibodies.

3) Three environment water samples were submitted to Biological Consulting Services of North Florida Inc. for *N. fowleri* analysis. Water from the concrete pond and from the drinking trough of an adjacent pen did not detect *N. fowleri*. Water from the drinking trough of the pen that housed the affected cow was positive for *N. fowleri*.

Microscopic Description:

Brain, right frontal lobe/olfactory lobe: Involving 40% of the section and extending to the leptomeninges, there is locally extensive encephalomalacia with fibrin thrombi, vasculitis, vascular fibrinoid degeneration, neutrophils, cellular debris, hemorrhage, and fibrin. Within these areas, often perivascular admixed with neutrophils, are ovoid to polygonal 8-10 um diameter organisms that have small 1-2 um nuclei that contain a single central nucleolus (karyosome) with a granular amphophilic vacuolated cytoplasm (amoeba trophozoites). Bordering the area of malacia are streams of degenerate neutrophils and fibrin, and within the adjacent intact neuropa

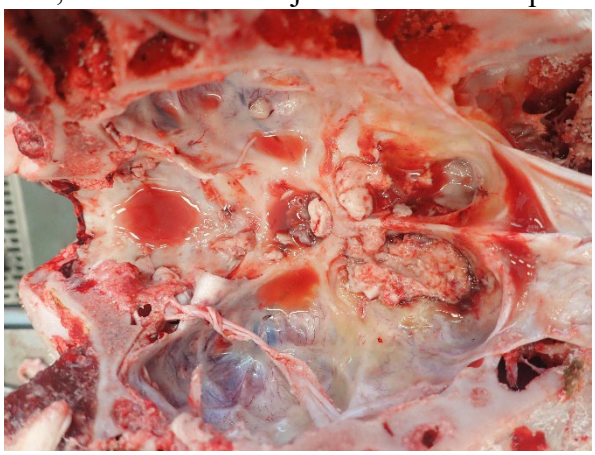

Cranium, ox: The remnant neuroparenchyma of the right frontal/olfactory lobe is soft, friable, tan to light yellow, and has multifocal hemorrhage (encephalomalacia). The adjacent subdura is thickened by fibrin and edema. (Photo courtesy of: Midwestern University, College of Veterinary Medicine, Diagnostic Pathology Center. *https://www.mwuanimalhealth.com/diagnostic-pathology-center.)*

The cow's drinking water trough that tested positive for N. fowleri was heavily fouled by organic debris (Photo courtesy of: Midwestern University, College of Veterinary Medicine, Diagnostic Pathology Center. *https://www.mwuanimalhealth.com/diagnostic-pathology-center.)*

renchyma and leptomeninges, are frequent dense perivascular cuffs of lymphocytes, plasma cells, and histiocytes with variable spongy change, fibrin, vascular fibrinoid degeneration, reactive vascular endothelium, and hemorrhage.

Contributor's Morphologic Diagnosis:

Brain, frontal right lobe/olfactory bulb: Meningoencephalitis, necrotizing, suppurative, mononuclear, multifocal, severe, acute to subacute, with intralesional amoeba trophozoites

Contributor's Comment: The cow's morbidity and mortality were due to necrotizing encephalitis caused by *Naegleria fowleri*, a eukaryotic, amphizoic, thermophilic, and free-living amoeba that is ubiquitous in the environment. Multiplex PCR performed on fresh brain from the right frontal and olfactory lobe confirmed *N. fowleri.* Immunohistochemistry performed on a formalin-fixed paraffin-embedded section of the affected brain detected intralesional *N. fowleri*. Analysis of the cow's drinking water visually detected amoeba trophozoites, and PCR confirmed *N. fowleri*, thereby determining the probable environmental source. Although the necrotizing inflammation was most severe in the right frontal and olfactory lobes, histopathology recognized similar lesions with fewer amoeba in the ventral periventricular cerebellum, brainstem, fourth ventricle choroid plexus, and cervical spinal cord. The distribution of these secondary inflammatory nidi suggests the amoebae spread via the cerebrospinal fluid following primary invasion of the right olfactory bulb.

Naegleria fowleri, *Balamuthia mandrillaris, Acanthamoeba* spp., and *Sappinia pedata* are pathogenic free-living amoebae that naturally cause central nervous system (CNS) disease in mammals.[3,6] These ubiquitous amoebae are opportunistic, target immunocompetent and immunosuppressed hosts, and may occupy soil, air, and water.[3,6] Infections occur in humans and animals; however, *S. pedata* has

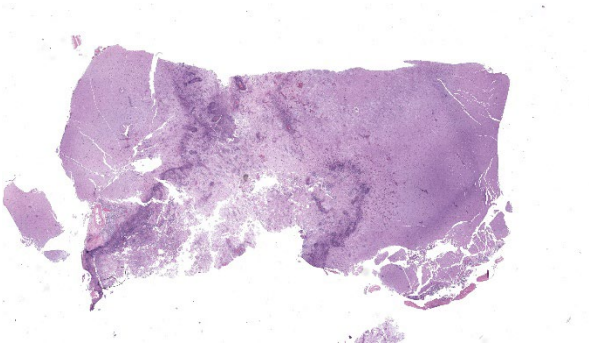

Cerebrum, ox: A large area of necrosis is partially bounded by a dense band of infiltrating neutrophils and cellular debris. (HE, 8X)

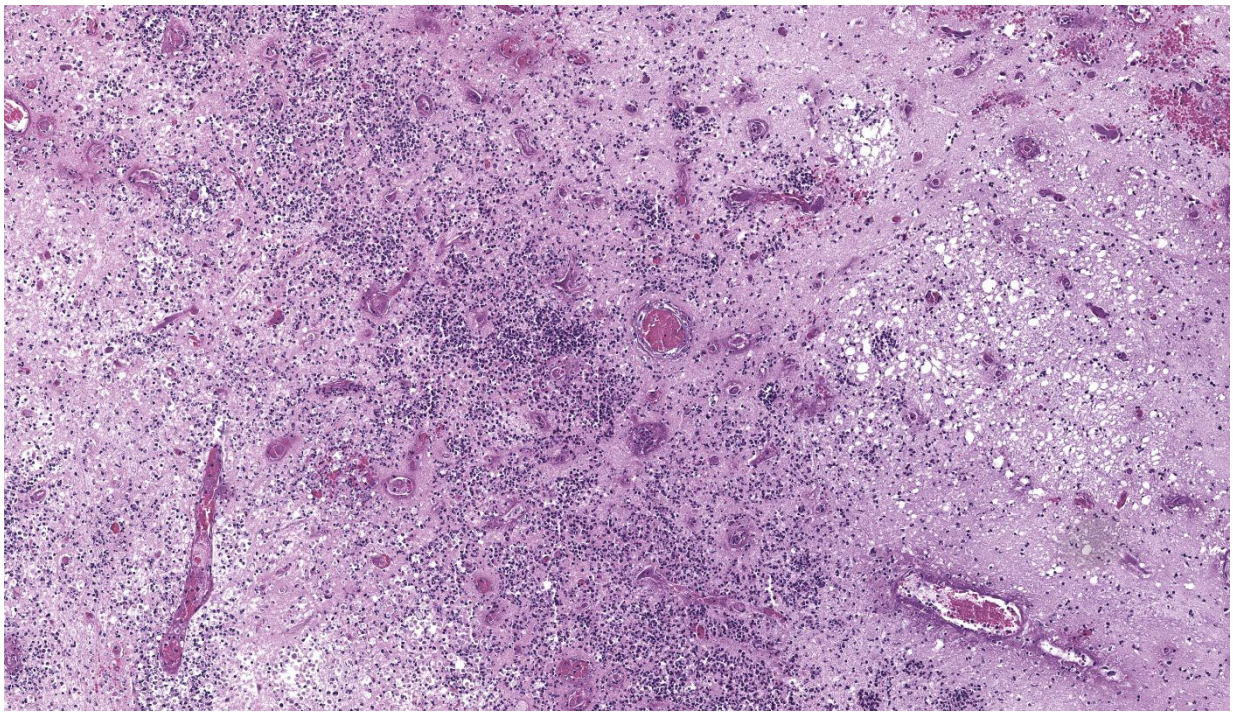

Cerebrum, ox: There is necrosis of the neuroparenchyma with abundant perivascular inflammation. (HE, 135X)

occurred in only one human case of encephalitis.[4,6] Unlike other amoeba, *N. fowleri*, the cause of fulminating primary amoebic meningoencephalitis, causes encephalitis following a direct entry into the CNS via the olfactory neuroepithelium, and the resulting lesions lack intralesional cysts.[6]

Naegleria fowleri naturally subsists on phagocytosed bacteria and thrives in unchlorinated warm bodies of water (upwards of 45ºC), including freshwater pools, puddles, lakes, rivers, hot springs, aquaria, sewage, irrigation canals, ponds, irrigation ditches, and thermally polluted effluents of power plants.[1,6] Resistant cysts form during adverse environmental conditions; otherwise, the protozoa is in a transitory flagellate stage or, more frequently, is an infectious amoeboid trophozoite equipped with a vesicular nucleus that has a single central nucleolus (karyosome).[6] Trophozoites reproduce by binary fission and will become cysts if food is lacking or the environment impairs growth.[6] Human and animal infections develop when nasal passages are inadvertently (e.g., during aquatic activities) or purposefully (e.g., nasal flush) exposed to warm unchlorinated or inadequately chlorinated water harboring infectious trophozoites. Trophozoites are first phagocytosed by the sustentacular cells of the olfactory neuroepithelium, then migrate through the cribriform plate, invade the leptomeninges, and finally, access the rostral neuroparenchyma where they can proliferate and potentially spread to other neuroanatomical locations.[6] Generally, onset of disease is rapid, as soon as 24 hours, and death usually occurs within a week.[6] This cow was likely exposed to *N. fowleri* during drinking activities and perhaps inadvertently snorted contaminated water or transferred amoeba to the nostrils during licking, which allowed trophozoites to reach and invade the right cribriform plate and subsequently cause malacia of the right frontal/olfactory lobe. Although the cow's drinking water was purported to be chlorinated, the trough contained warm stagnant water, there was surface scum, and a

thick layer of organic debris lined the bottom-collectively, these factors probably inhibited efficient chloramination and facilitated the survival of *N. fowleri* trophozoites.

Meningoencephalitis due to *N. fowleri* is reported in cattle from Costa Rica, the state of Paraiba, Brazil, California, USA, and now Arizona, USA.[2,4,5] As in this case, the incidence of *N. fowleri* in California cows correlated with warm summer temperatures, acute CNS clinical signs, olfactory and cerebellar necrosuppurative lesions, and the probable exposure to trophozoites in drinking water.[2]

Although uncommon in cattle, amoebic meningoencephalitis caused by *N. fowleri* is an important differential diagnosis of an acutely neurologic cow that is most likely during the summer in a geographic area with high ambient temperatures. Other important and more common differential diagnoses for neurologic disease in cattle include rabies virus, polioencephalomalacia, lead toxicosis, salt toxicity, thrombotic meningoencephalitis, cerebral abscess, and bacterial meningitis.[2]

Contributing Institution:
Midwestern University, College of Veterinary Medicine, Diagnostic Pathology Center

https://www.mwuanimalhealth.com/diagnostic-pathology-center

JPC Morphologic Diagnosis: Cerebrum: Meningoencephalitis, necrotizing and suppurative, focally extensive, subacute, severe, with vasculitis, thrombosis, and numerous amoebic trophozoites.

JPC Comment: This week's moderator was Dr. Jey Koehler from Auburn University who selected an array of neuropathology cases to

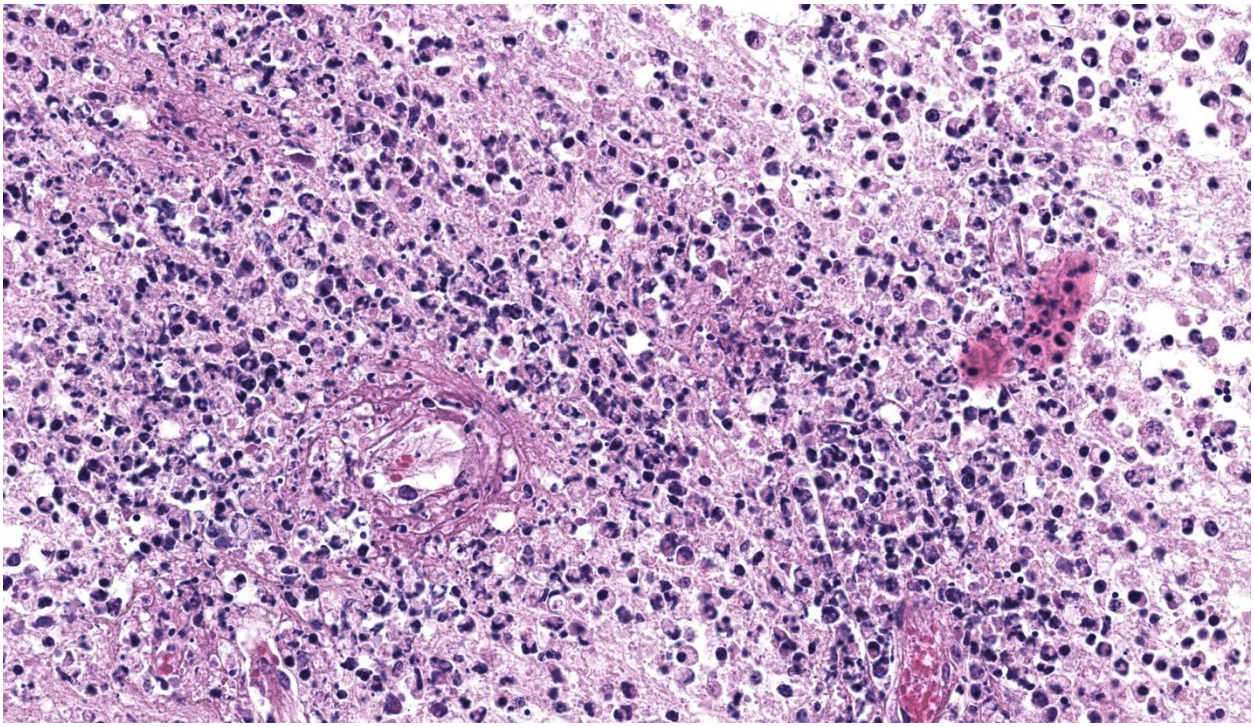

Cerebrum, ox: Necrotic and thrombosed vessels are surrounded by large numbers of necroitic and few viable neutrophils and abundant cellular debris. There is necrosis of the neuroparenchyma with abundant perivascular inflammation. (HE, 578X)

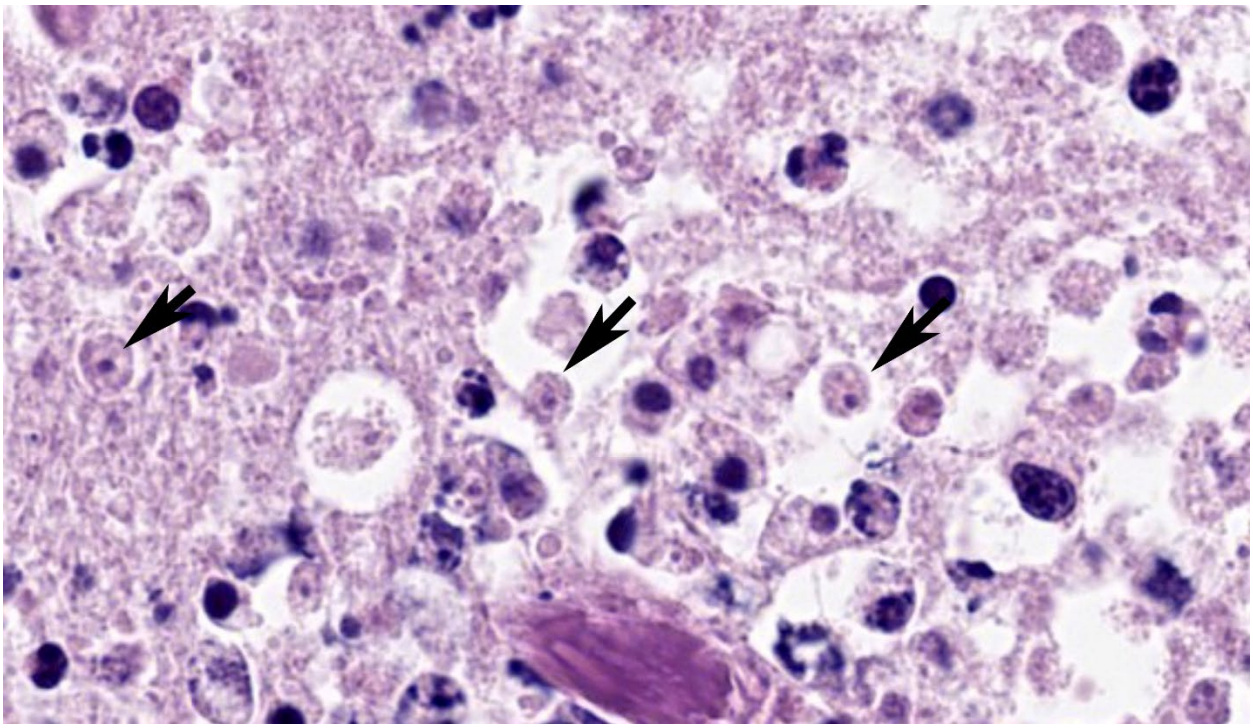

Cerebrum, ox: Numerous amoebae with prominent karyosomes are scattered throughout the necrotic and inflamed neuropa-renchyma. (HE, 870X)

discuss with conference participants. Her pre-conference lecture on evaluation of the nervous system proved helpful in refining descriptive elements and recognizing important artifacts within the brain and spinal cord – herein we capture some of these pearls of wisdom in our discussion.

This first case leaves little doubt from subgross where the lesion is on the slide, though there are several descriptive features not to miss on higher magnification. The cause of the abundant necrotizing inflammation is characteristic with amoeba having distinct, round central nuclei and round karyosomes that were best appreciated with the iris diaphragm closed down. In comparison to *Balamuthia* and *Acanthamoeba*, we did not note any tissue cysts, though Dr. Koehler posited that *Naegleria* infection is rapidly fatal to most (all?) animals, leaving little time for these to develop.[8] The marked fibrinoid vasculitis and many fibrin thrombi reflect both direct damage to vessels from secreted amoebic proteases and trogocytosis of neural tissue (literally, nibbling of host cells to gain nutrients!)[7] in addition to the indirect ischemic effects. The large presence of neutrophils reflects both amoebic recruitment and response to cellular injury. Dr. Koehler emphasized that remembering the number of neutrophils (granulocytes) within the neuroparenchyma was easy – that number should be zero (or else prompt you to look further for why they are there). For another example of amoebic disease (*Entamoeba*) with necrotizing inflammation in a colobus monkey, see Conference 9, Case 1 from this year.

The contributor provides an interesting take on *Naegleria* that is cemented by a solid gross photo of the waterer for this animal. Absent this highly suggestive image, conference participants also discussed other causes of focal encephalitis which included dehorning injury/trauma, abscessation (e.g. from a

nose ring), bovine herpesviruses, *Histophilus*, and angioinvasive fungi (*Aspergillus)*. We did not identify any other agents present in section, however.

Finally, conference participants enjoyed an enlightening discourse on the nature of necrosis within the brain, encephalitis, and true malacia. We differed from the contributor's interpretation of this case slightly in that we feel that the separation of the neuroparenchyma is largely artifactual (i.e. the process of cutting a soft brain) versus true cavitation due to necrosis. Dr. Koehler emphasized that thin gliovascular strands extending between adjacent vessels within increased clear space histologically are consistent with malacia (see Conference 5, Case 4 of the current year for an excellent example in a SV40-infected macaque) which was not observed here and not consistent with the mechanism of injury expected for *Naegleria*. We briefly debated whether this case represents an encephalitis versus meningoencephalitis given the minimal involvement of the overlying meninges and the notion that observed changes may simply extend outward towards the meninges. We ultimately accepted the contributor's note that this lesion was distributed multifocally and features may have differed in other sections.

References:

1. Blair B, Sarkar P, Bright KR, Marciano-Cabral F, Gerba CP. *Naegleria fowleri* in Well Water. *Emerg Infect Dis.* 2008;14(9):1499-1501.

2. Daft BM, Visvesvara GS, Read DH, Kinde H, Uzal FA, Manzer MD. Seasonal meningoencephalitis in Holstein cattle caused by Naegleria fowleri. *J Vet Diagn Invest*. 2005;17:605-609.

3. Hawkins SJ, Struthers JD, Phair K, et al. Diagnostic evaluation of fatal Balamuthia mandrillaris meningoencephalitis in a captive Bornean orangutan (*Pongo pygmaeus*) with identification of potential environmental source and evidence of chronic exposure. *Primates*. 2021;62(1):51-61.

4. 4. Pimentel LA, Dantas AF, Uzal F, Riet-Correa F. Meningoencephalitis caused *by Naegleria fowleri* in cattle of northeast Brazil. *Res Vet Sci.* 2012;93(2):811-812.

5. 5.Visvesvara GS, De Jonckheere JF, Sriram R, Daft B. Isolation and Molecular Typing of *Naegleria fowleri* from the Brain of a Cow That Died of Primary Amebic Meningoencephalitis. *J Clin Microbiol.* 2005;43(8):4203-4204.

6. 6. Visvesvara G, Moura H, Schuster F. Pathogenic and opportunistic free-living amoebae: Acanthamoeba spp., Balamuthia mandrillaris, Naegleria fowleri, and Sappinia diploidea. *FEMS Immunol Med Microbiol.* 2007;50:1–26.

7. 7. Herman EK, Greninger A, van der Giezen M, et al. Genomics and transcriptomics yields a system-level view of the biology of the pathogen Naegleria fowleri. BMC Biol. 2021 Jul 22;19(1):142.

8. 8. Fouque E, et al. Cellular, biochemical, and molecular changes during encystment of free-living amoebae. Eukaryot Cell. 2012 Apr;11(4):382-7.

CASE II:

Signalment:
1 year, 2 months old male sitatunga

History:
This sitatunga (*Tragelaphus spekii*) was born at a zoological institution in the mid-Atlantic region. He was apparently healthy at birth, nursed well, and had normal baseline bloodwork. He received routine vaccinations for tetanus at 8 and 12 weeks of age and rabies at 16 weeks. At 3 months of age, he was first reported to have mild, intermittent ataxia in the rear limbs, which continued over the next several months, along with occasional rear limb lameness. There were periods when the ataxia became more severe and the animal became lethargic; at times signs progressed to leg crossing, circling and falling. He was somewhat responsive to treatment with NSAIDs and antibiotics, but intermittent ataxia persisted. Bloodwork was always within normal limits and spinal radiographs were unremarkable. Vitamin E serum levels were slightly low but similar to other animals in the collection that did not have clinical signs. He was treated with injectable vitamin E/Selenium weekly with some improvement in ataxia. At 11 months of age the animal presented with acute worsening of ataxia, with a right head tilt, right circling and collapsing, horizontal nystagmus, and crossing of legs in front and back. Over the next two months he was treated with NSAIDs, vitamin E/selenium and showed mild improvement. On the day prior to necropsy, he acutely became severely ataxic, with crossing of front and rear legs, right head tilt, severe right circling leading to falling, and decreased awareness of surroundings. Euthanasia was elected.

Cerebrum, sitatunga: One section of cerebrum is submitted for examination. At subgross magnification, an area of hemorrhage is present in the meninges (upper left). (HE, 8X)

Gross Pathology:
Post-fixation, on cut section there was an area of hemorrhage within the parenchyma at the level of the right basal ganglia, and multiple dark brown areas within the meninges and extending into the superficial cortex

Laboratory Results:
PCR targeting a portion of the rRNA ITS-2 region of *Parelaphostrongylus spp* was performed on DNA isolated from formalin-fixed brain tissue from this case. The resulting PCR product showed 100% sequence identity to *P. tenuis*

Microscopic Description:
Cerebrum at the level of the basal ganglia: Beneath the meninges and extending into the outer layers of the cerebral cortex is a focally extensive area of hemorrhage, with rarefaction of the neuropil and abundant eosinophils, lymphocytes, histiocytes, and plasma cells. Throughout the parenchyma, there are multiple smaller tracts of hemorrhage, necrosis and loss of neuropil. Within some of these lesions are several, 100-250 um in diameter cross sections of adult nematodes characterized by a thin smooth cuticle, coelomyarian musculature, accessory hypodermal chords, a large intestinal tract with few multinucleate

cells, and a reproductive tract. There is moderate to severe periventricular edema and gliosis, and multifocal lymphoplasmacytic perivascular cuffing.

Contributor's Morphologic Diagnosis:
Brain: meningoencephalitis, lymphohistiocytic and eosinophilic, multifocal, chronic active, severe, with reactive gliosis, hemorrhage, necrosis, and intralesional nematodes

Contributor's Comment: The necrotizing tracts in the brain caused by migrating nematodes are consistent with the clinical signs of progressive ataxia, circling, head tilt, and loss of awareness of surroundings. Histological characteristics of the organism including a thin smooth cuticle, coelomyarian musculature, accessory hypodermal chords, and a large intestinal tract with few multinucleate cells, are consistent with a metastrongyle nematode.[4] PCR and DNA sequencing confirmed identification of *Parelaphostrongylus tenuis*.

P. tenuis, also known as the meningeal worm, is a nematode most commonly found in white-tailed deer which is the definitive host. In this species, adult worms are found within the cranial venous sinuses and the subdural space. Here, adults lay eggs that travel through the venous blood and into the lungs. In the lungs, eggs embryonate into larvae which move into the respiratory tract, then are swallowed and eliminated into the feces. Larvae then penetrate into the foot of terrestrial molluscs. Deer or aberrant hosts become infected by ingesting gastropods which contain infective larvae. After ingestion, larvae migrate to the spinal cord and develop into adults in the dorsal horn of the gray matter. They migrate into the spinal subdural space and into the cranium, through the dura mater and into the venous sinuses.[1]

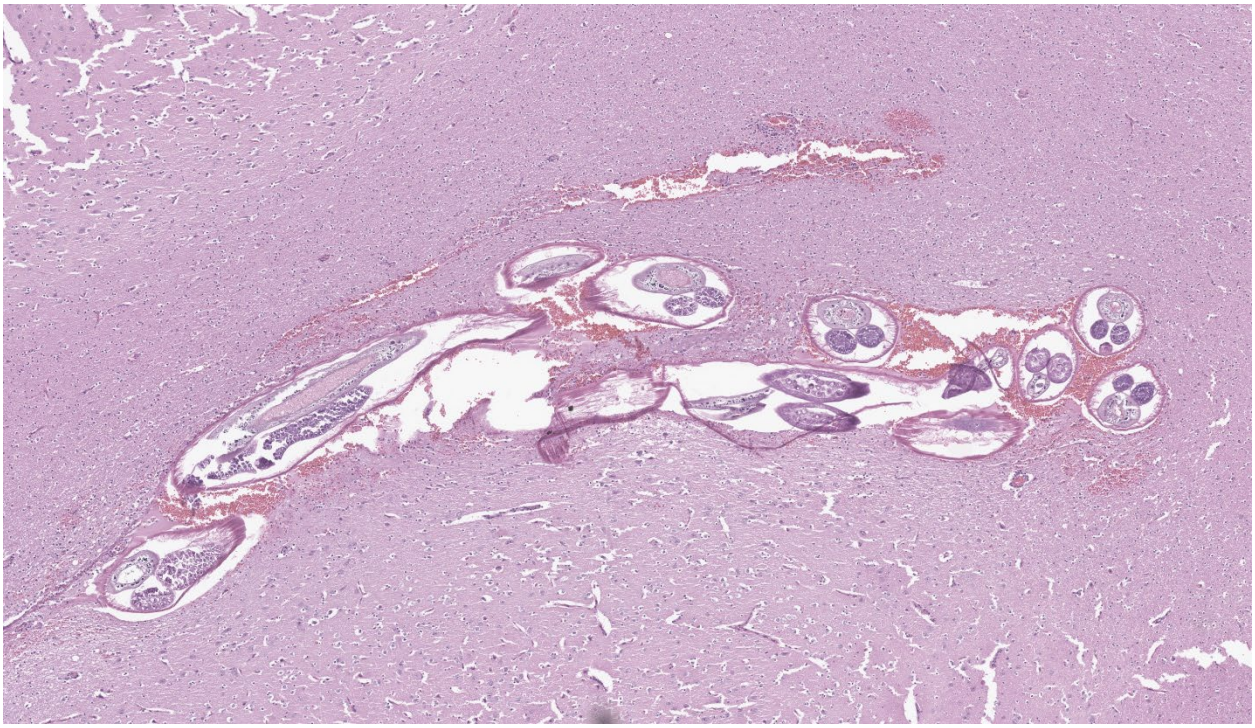

Cerebrum, sitatunga: At the junction of the white and gray matter, multiple cross- and tangential sections of an adult female metastrongyle are evident within a hemorrhagic migration tract. (HE, 73X)

White-tailed deer commonly harbor meningeal worms, particularly in areas of deciduous forest regions where the habitat is suitable for gastropods. Prevalence in white-tailed deer populations is highly variable and has been reported to be up to 94% in certain areas.[6]

P. tenuis causes little damage to the definitive host, but can cause severe neurologic disease in other animals such as moose, caribou, wapiti, mule deer, fallow deer, elk, llamas, alpacas, wolves, horses, antelope, sika deer, sheep, calves, goat, and guinea pigs.[1-3,5-10] Clinical signs can include ataxia, hypermetria, paresis, paralysis, head tilt, circling, blindness, weight loss, depression, seizures, and death. Treatment of mildly affected animals has been successful with anthelminthics such as ivermectin, steroids, and supportive care. However, prognosis is guarded in animals with severe neurological signs.[6] To our knowledge, this is the first report of *P. tenuis* infection in a sitatunga.

Contributing Institution:
Johns Hopkins University, School of Medicine
Department of Molecular and Comparative Pathobiology
Broadway Research Building, #811
733 N. Broadway
Baltimore, MD 21205
Phone: 443-287-2953
Fax: 443-287-5628
http://mcp.bs.jhmi.edu/

JPC Morphologic Diagnosis: Cerebrum: Meningoencephalitis, necrohemorrhagic, focally extensive, subacute, moderate, with adult metastrongyle nematode.

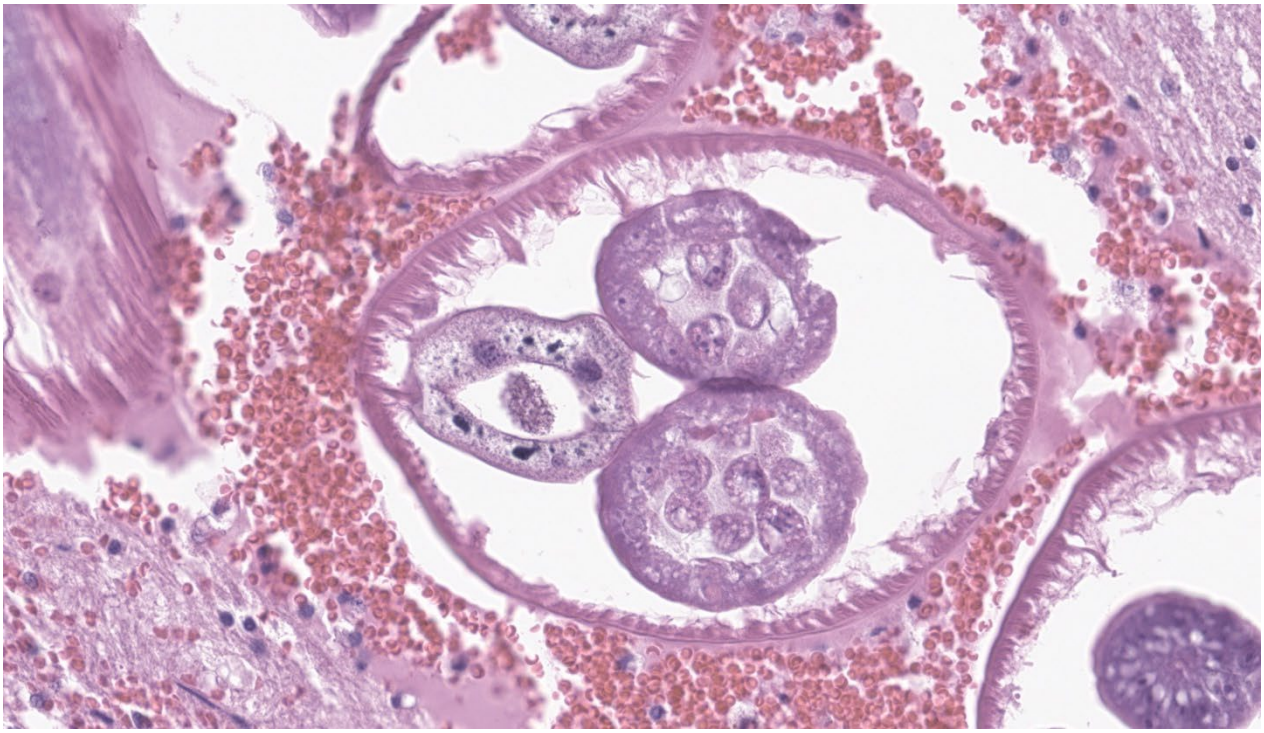

Cerebrum, sitatunga: A cross section of the nematode exhibits the following: a think cuticle, pseudocoelom, polymyarian, coelomyarian musculature, a large intestine with multiple uninucleate cells, and two ross sections of uterus with luminal ova. (HE, 626X)

JPC Comment: The contributor provides a lovely section of *P. tenuis* that illustrates the characteristic features of this nematode in histologic section. While PCR is an important tool in diagnostic and research settings, it is important to recognize these features and generate a putative 'culprit' as recovery of nucleic acids, particularly from formalin-fixed tissue can present issues with organism identification. In contrast to the first case, the thickening of the meninges is more pronounced here and is accompanied by both rarefaction (small/fine-sized vacuolar change of the parenchyma) and spongiosis (appreciably larger vacuoles) in the immediate vicinity. The linear tract of necrosis and hemorrhage functions almost as a signpost towards the profiles of these nematodes, though absent these arriving at a specific diagnosis would be difficult and we would also have to consider migrating foreign material (e.g. grass awn) as an outside possibility. Dr. Koehler noted that after the animal's death, nematodes may continue to actively traverse the CNS and therefore be missed in histologic section. One interesting feature of this case was that the pigmented intestinal epithelial cells of *P. tenuis* were highlighted with Prussian blue, suggesting that these nematodes accumulate iron through ingestion of tissue and red blood cells. We differed from the contributor's morphologic diagnosis only in severity, though admittedly, this is separate and distinct from clinical effect whereby even mild processes within the brain can have marked effects.

While the periphery of this section does not have many significant changes, it does provide an opportunity to discuss some of the challenges of processing nervous tissues for histologic section as discussed by Dr. Koehler in her preconference. In some cases, autolysis will soften the brain and chattering or tearing of tissue is inevitable. One quick test for autolysis is to examine glial cells in the parenchyma – well-preserved/fixed tissue should have small, round glial cells. The submitted tissue in this case is fixed appropriately, but possibly had minor deviations in temperature, reagent mixture, and/or workflow that led to artifactual separation – the difference may be as small as a few seconds or a few degrees Fahrenheit! We say all of this to emphasize that the production of quality slides is a laborious process and histology technicians all around the world work minor miracles every day to allow us to do the work that we do. We appreciate what the contributor provides here and provide this note as a reference to those starting out on their neuropathology journey.

References:

1. Anderson RC. The ecological relationships of meningeal worm and native cervids in North America. *J. Wildl. Dis.* 1972; 8**:**304–310.

2. Dobey CL, Grunenwald C, Newman SJ, Muller L, Gerhold RW. Retrospective study of central nervous system lesions and association with Parelaphostrongylus species by histology and specific nested polymerase chain reaction in domestic camelids and wild ungulates. J Vet Diagn Invest. 2014 Nov;26(6):748-54.

3. Bak EJ, Jean YH, Woo GH. Eosinophilic encephalomyelitis in horses caused by protostrongylid parasites. J Vet Sci. 2017 Dec 31;18(4):551-554.

4. Gardiner, CH, Poynton, SL. *An Atlas of Metazoan Parasites in Animal Tissues*. (1999).

5. Gerhold RW, Keel MK, Arnold K, Hotton D, Beckstead RB. Parelaphostrongylus tenuis-associated meningoencephalitis in a sika deer (Cervus nippon). J Wildl Dis. 2010 Jan;46(1):287-90.

6. Lankester, MW. Extrapulmonary lungworms of cervids. In: Samuel, W, Pybus, M, Kocam, A, eds. *Parasitic diseases of Wild Mammals*. Iowa State University Press, 2001: 228-246.

7. Mitchell, KJ, *et al.* Diagnosis of Parelaphostrongylus spp . infection as a cause of meningomyelitis in calves. *J. Vet. Diagnostic Investig.* 2011; 23:1097–1103.

8. Southard T, Bender H, Wade SE, Grunenwald C, Gerhold RW. Naturally occurring Parelaphostrongylus tenuis-associated choriomeningitis in a guinea pig with neurologic signs. Vet Pathol. 2013 May;50(3):560-2.

9. Tanabe M, Gerhold RW, Beckstead RB, de Lahunta A, Wade SE. Molecular confirmation of Parelaphostrongylus tenuis Infection in a horse with verminous encephalitis. Vet Pathol. 2010 Jul;47(4):759.

10. Wünschmann A, Armien AG, Butler E, Schrage M, Stromberg B, Bender JB, Firshman AM, Carstensen M. Necropsy findings in 62 opportunistically collected free-ranging moose (Alces alces) from Minnesota, USA (2003-13). J Wildl Dis. 2015 Jan;51(1):157-65.

CASE III:

Signalment:
8-year-old spayed female domestic shorthair cat (*Felis catus).*

History:
The patient presented for an approximately 72-hour progressive history of seizures manifesting as lip twitching, masticatory movements, excessive vocalization, blindness, and ptyalism. Interictal behavioral changes of restlessness, loss of environmental awareness and elevated pain as perceived by the owner were also reported. At first presentation (48 hours), a focal, full thickness ulcer was observed on the right cranial tongue. Physical examination was otherwise unremarkable. Complete blood cell count and blood chemistry were also unremarkable and the patient was sent home with robenacoxib and buprenorphine for pain control. At the final presentation (72 hours), the patient was reported to be hyperthermic and extremely agitated. While attempting to place an IV catheter for treatment, the patient underwent acute cardiac arrest.

Gross Pathology:
There were no remarkable gross findings within the formalin fixed brain. The right rostral tongue had a focal, linear, well-demarcated, purple to dark purple ulceration that measured 9 mm x 5 mm x 2 mm. The left lateral aspect of the tongue had a linear, red to dark red focus that measured 5 mm x 2 mm.

Laboratory Results:
Feline Herpes Virus - 1 PCR: Negative.
Snap FeLV/FIV Combo Test: Negative.

Microscopic Description:
Cerebrum, hippocampus: Confined to the hippocampus and most prominent within CA1, scattered neurons are characterized by swelling, vacuolation, prominent nissl substance or are shrunken and angular with hypereosinophilic cytoplasm and fading or pyknotic nuclei. Glial cells are increased in number with frequent reactive astrocytes. Microglial cells frequently flank neuronal debris

A section of diencephalon and anterior cerebellum is submitted for examination. At this magnification, the prominent neurons of the hippocampus are difficult to see (with the exception of those of the dentate gyrus). (HE, 8X)

and are occasionally within degenerate and necrotic neurons (neuronophagia). There is proliferation of small caliber blood vessels lined by hypertrophic endothelium with rare perivascular aggregates of small numbers of mononuclear cells and edema. Neurons occasionally have basophilic glassy, nuclei.

Contributor's Morphologic Diagnosis:
Cerebrum, hippocampus: Neuronal degeneration and necrosis, moderate to marked, regionally extensive and bilateral, acute with neuronophagia, astrocytosis, gliosis, microvascular proliferation, perivascular inflammation.

Other significant histological findings (slides not submitted):
Tongue: Full thickness ulceration, marked, multifocal, acute with necrosuppurative glossitis, muscular necrosis, neuritis and abundant intralesional bacterial colonies.

Condition: Feline hippocampal and piriform lobe necrosis (FHN)

Contributor's Comment: A diagnosis of feline hippocampal and piriform necrosis (FHN) was given based on clinical presentation and histopathologic lesions consistent with those described in the literature and previous case reports. FHN is an acute onset neurologic disorder characterized clinically by rapidly progressive, often refractory focal, complex-partial and/or generalized tonic-clonic seizures. Interictal behavioral changes reflective of limbic dysfunction are common: loss of environmental awareness, agitation/aggression, hyperesthesia, ptyalism, pyrexia, urinary retention and hyperexcitability are described.[5,7,8,15] FHN has been reported in several countries: Australia, Austria, England, Finland, Italy, Switzerland, and the

United States.[4,7,9,15,17,19,22] No sex, breed nor age disposition has been identified.

Neurologic examination and laboratory findings are non-specific. Therefore, clinical diagnosis is often by exclusion, coupling clinical presentation with Magnetic Resonance Imaging (MRI) findings (the hippocampus and piriform lobes are T2 and FLAIR hyperintense, T1 hypointense, +/- contrast enhancement).[4,7,9,15,17,19,22] Gross examination of the brain is regularly unremarkable, however, accentuated vascular structures or mild malacic changes in the piriform lobe and hippocampus have been described.[1,7] Definitive diagnosis of FHN is made via histopathology. Microscopically, FHN is characterized by varying degrees of acidophilic neuronal necrosis confined to the hippocampus and piriform lobe structures. The distribution of lesions is bilateral and symmetric, and tend to be most prominent within CA1. Microvascular proliferation, microgliosis/neuronophagia and astrocytosis are also common features. Lymphohistiocytic perivascular inflammation, and central chromatolysis may also be present, though less frequently.[5,7]

Aforementioned, the exact pathogenesis of FHN is yet to be elucidated. Epileptogenic, immune-mediated, infectious, toxic, vascular, structural, degenerative and paraneoplastic processes have all been proposed.[3,4,7,9,10,15,19,20,22] Given the shared clinical presentation and histologic findings of FHN across a potpourri of suggested etiologies, some authors hypothesize that FHN is more suggestive of a pathogenic neurolocalization as opposed to a specific entity.[19] Hippocampal pyramidal neurons are particularly susceptible to endogenous excitotoxicity, so it seems conceivable that alterations in metabolism, function and/or architecture of this neuroanatomical region could uncouple the regulatory mechanisms of neurotransmitter metabolism (hypothesized to be glutamate

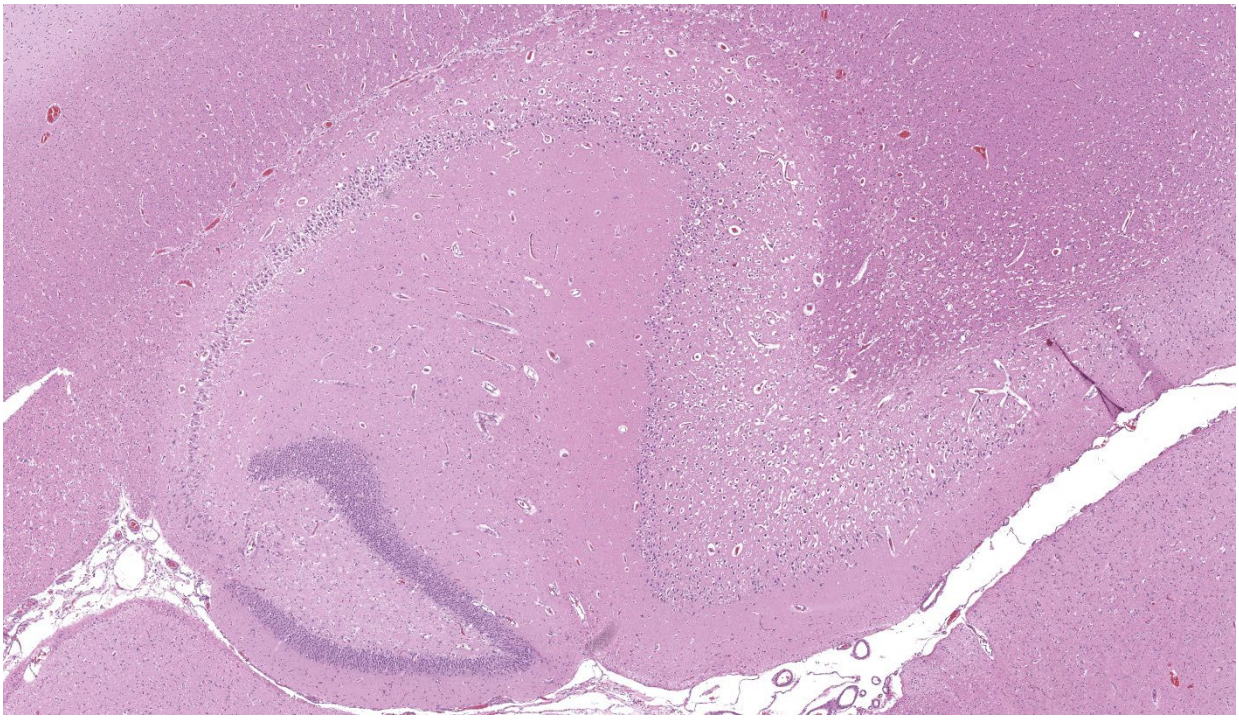

Hippocampus, cat. Neurons of the hippocampal regions CA1-CA3 lack significant differential staining, but those of the dentate gyrus stain normally. (HE, 37X)

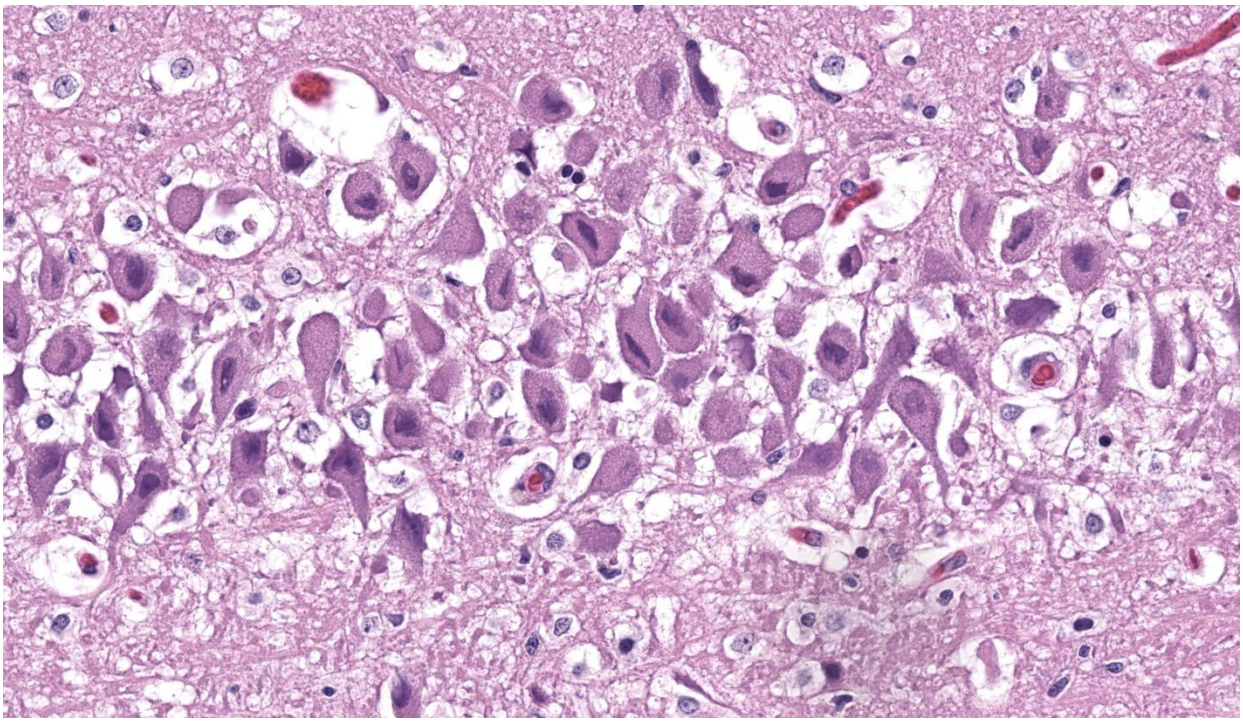

Hippocampus, cat. Neurons of the hippocampal regions CA1-CA3 are degenerating (with marked cytoplasmic vacuolation and condense nuclei) and few overtly necrotic (hyperchromatic cells with pyknotic nuclei) are present. (HE, 750X)

and/or aspartate),[2,5] leading to regionally extensive edema, ischemia and necrosis.

The scope of comparative pathology of the FHN phenotype is relatively narrow. Bilateral ischemic changes have been reported in dogs with refractory epilepsy and/or prolonged seizures.[11,12] However, the topic represents an exciting area of immunology and neuropathology research. The clinical presentation and histologic findings described in FHN are similar to those described in human Autoimmune Limbic Encephalitis (ALE).[3,10,13,20] Many cases of ALE are defined by aberrant production of antibodies against the neuronal cell membrane antigens.[3,10,13,16,20,21] Antibodies against voltage-gated potassium channel complex (VGKC) extracellular domains of leucine-rich glioma-inactivated 1 (LGI1) and contactin-associated protein-like 2 (CASPR2) are some of the most prevalently isolated, which together have been defined as LG1 encephalitis. Voltage-gated potassium channels (VGKCs) represent a group of signaling proteins capable of modulating a wide variety of synaptic functions, most prominently neuronal excitability and neurotransmitter release. Dysfunction or damage to the VGKC complex carries the potential of hyperexcitability, seizure and resulting excitotoxicity. In veterinary literature, recent studies have demonstrated the presence of anti-LGI1 antibodies in cats with clinical presentations, MRI findings and histologic hippocampal necrosis/sclerosis that parallel human LG1 encephalitis. Clinically, this constellation of findings has been termed feline complex partial seizures with orofacial involvement (FEPSO). FEPSO may represent an immune-mediated etiology of FHN, and carries the potential to serve as a spontaneously occurring animal model of human LG1 encephalitis.[3,10,19]

Unfortunately, feline epilepsy is often enigmatic as many epileptic cats have atypical seizures, genetic markers for feline epilepsy

are poorly described, and a complete neurologic work up is often not performed.[17] Therefore, these challenges hinder a more thorough depiction of the processes underlying the FHN phenotype, resulting in ambiguous diagnoses which muddle antemortem characterization and histopathologic correlation (when available). Fortunately, growing awareness of FHN as a component in feline epilepsy will hopefully chaperone further exploration and clarification on the likely heterogeneous FHN phenotype.

In the presented case, several neurons had smudgy to glassy, basophilic appearance prompting PCR for feline herpesvirus-1, which was negative. Thus, the histogenesis remains unclear. FeLV/FIV status for this animal was negative and the cat was up to date on vaccinations and was housed solely indoors, decreasing suspicions for rabies and/or *Toxoplasma* spp. The ulceration observed on the tongue was attributed as a sequelae to an unobserved seizure.

Contributing Institution:
Colorado State University Veterinary Diagnostic Laboratory
Fort Collins, CO
https://vetmedbiosci.colostate.edu/vdl/

JPC Morphologic Diagnosis: Hippocampus: Neuronal degeneration and necrosis, segmental, with reactive astrocytosis and spongiosis.

JPC Comment: Although the lesion in this case is somewhat understated relative to the other slides in this conference, the contributor's summary is anything but, and wonderfully summarizes the current literature on this entity (and we appreciate the callback to previous WSC!). The sagittal sectioning of this brain provides another opportunity to check for autolytic change, using the granular and molecular layer interface as a good anchoring point – these layers should be in apposition

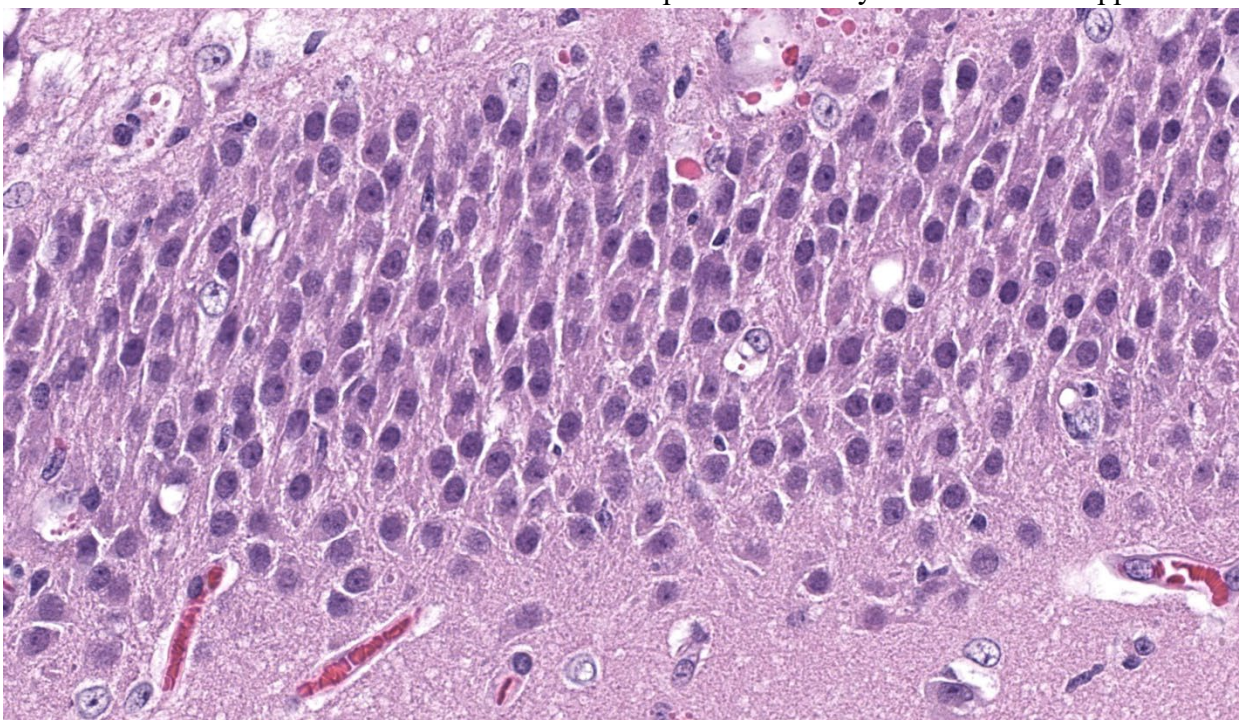

Diencephalon, cat. Neurons of the dentate gyrus for comparison. (HE, 750X)

with little vacuolation and condition of cerebellar neurons should also be evaluated.[23] The slide is well-preserved with little artifact present.

The hippocampal changes in this case are better appreciated with a matched animal control, or at least, review of pertinent veterinary literature[24] to brush up on the various subfields of the cornu ammonis (CA). Neuronal necrosis within CA1 was appreciable as shrunken, eosinophilic cells with pyknotic nuclei, though Dr. Koehler reminded conference participants that the ventral hippocampus can also have darker neurons as an artifact secondary to tissue manipulation and excessive pressure, and that these should be carefully distinguished. Other corroborating evidence such as reactive astrocytes (with increased cytoplasm, peripheralized chromatin, and occasional doublets representing division) also confirmed that changes observed were real. We captured this distinction of 'reactive' in our morphologic diagnosis as we feel that it emphasizes not only the cellular changes of astrocytes, but the increased cell number elicited by this process.

This case also had good examples of simultaneous cytotoxic and vasogenic edema. This is possibly attributed to seizure episodes, though glutamate effects are more localized to CA3 and changes in this cat were attenuated. Likewise, seizure episodes might also generate lesions in other portions of the brain (e.g. head trauma and hemorrhage) which are absent in this section, though the effects of global hypoxia and cytokine generation might explain vascular-centered edema in this brain. We also briefly discussed the smudgy inclusions within neurons noted by the contributor – these likely reflect clumped protein aggregates and cellular dysfunction (unfolded protein response and integrated stress response)) and should not be confused with viral inclusion bodies, to include Negri bodies from rabies virus.[18]

References:

1. The Joint Pathology Center. Feline hippocampal necrosis. JPC Wednesday Slide Conference; 2013-2014, Conference 22, Case 2. https://www.askjpc.org/wsco/wsc_showcase2.php?id=MjRJVGMxMm9vVFR1clh1Zm4yeTRWZz09.

2. Barker-Haliski M, White HS. Glutamatergic Mechanisms Associated with Seizures and Epilepsy. Cold Spring Harb Perspect Med. 2015 Jun 22;5(8):a022863.

3. Binks S, Lamquet S, Crawford AH, Meurs A, Irani SR, Pakozdy A. Parallel roles of neuroinflammation in feline and human epilepsies. Vet J. 2022 Dec;290:105912.

4. Brini E, Gandini G, Crescio I, Fatzer R, Casalone C. Necrosis of hippocampus and piriform lobe: clinical and neuropathological findings in two Italian cats. J Feline Med Surg. 2004 Dec;6(6):377-81.

5. Cantile C., Youssef S. Nervous System. (2016). In: Jubb, Kennedy, and Palmer's Pathology of Domestic Animals, ed. Maxie M.G. 6th edition. Philadelphia: Elsevier, vol 1, p 398-400.

6. Dow, S. W., Poss, M. L. and Hoover, E. A. (1990): Feline immunodeficiency virus: a neurotropic lentivirus. J. Acquir. Immune Defic. Syndr. 3, 658–668.

7. Fatzer R, Gandini G, Jaggy A, Doherr M, Vandevelde M. Necrosis of hippocampus and piriform lobe in 38 domestic cats with seizures: a retrospective study on clinical and pathologic findings. J Vet Intern Med. 2000 Jan-Feb;14(1):100-4.

8. Fletcher NF, Meeker RB, Hudson LC, Callanan JJ. The neuropathogenesis of feline immunodeficiency virus infection: barriers to overcome. Vet J. 2011 Jun;188(3):260-9.

9. Fors S, Van Meervenne S, Jeserevics J, Rakauskas M, Cizinauskas S. Feline hippocampal and piriform lobe necrosis as a consequence of severe cluster seizures in two cats in Finland. Acta Vet Scand. 2015 Jul 28;57(1):41.

10. Glantschnigg-Eisl U, Klang A, Kneissl S, Lang B, Waters P, Irani SR, Binks SNM, Pakozdy A. A feline model of spontaneously occurring autoimmune limbic encephalitis. Vet J. 2023 Jun-Jul;296-297:105974.

11. Hasegawa D, Fujita M, Nakamura S, Takahashi K, Orima H (2002) Electrocorticographic and histological findings in a shetland sheepdog with intractable epilepsy. J Vet Med Sci 64:277–279.

12. Hasegawa D, Nakamura S, Fujita M, Takahashi K, Orima H (2005) A dog showing Klüver–Bucy syndome-like behavior and bilateral limbic necrosis after status epilepticus. Vet Neurol Neurosurg J 7:1–14.

13. Hasegawa D, Ohnishi Y, Koyama E, Matsunaga S, Ohtani S, Nakanishi A, Shiga T, Chambers JK, Uchida K, Yokoi N, Fukata Y, Fukata M. Deleted in colorectal cancer (netrin-1 receptor) antibodies and limbic encephalitis in a cat with hippocampal necrosis. J Vet Intern Med. 2019 May;33(3):1440-1445.

14. Hora AS, Tonietti PO, Guerra JM, Leme MC, Pena HF, Maiorka PC, Brandão PE. Felid herpesvirus 1 as a causative agent of severe nonsuppurative meningoencephalitis in a domestic cat. J Clin Microbiol. 2013 Feb;51(2):676-9.

15. Klang A, Högler S, Nedorost N, Weissenbacher-Lang C, Pákozdy Á, Lang B, Weissenböck H. Hippocampal necrosis and sclerosis in cats: A retrospective study of 35 cases. Acta Vet Hung. 2018 Jun;66(2):269-280.

16. Montojo MT, Petit-Pedrol M, Graus F, Dalmau J. Clinical spectrum and diagnostic value of antibodies against the potassium channel related protein complex. Neurologia. 2015 Jun;30(5):295-301.

17. Moore SA. Seizures and epilepsy in cats. Vet Med (Auckl). 2014 Jul 30;5:41-47. doi: 10.2147/VMRR.S62077. PMID: 32670845; PMCID: PMC7337200.

18. Nietfeld JC, Rakich PM, Tyler DE, Bauer RW. Rabies-like inclusions in dogs. *J Vet Diagn Invest.* 1989;1(4):333-338.

19. Pakozdy A, Gruber A, Kneissl S, Leschnik M, Halasz P, Thalhammer JG. Complex partial cluster seizures in cats with orofacial involvement. J Feline Med Surg (2011) 13:687–93. 10.1016/j.jfms.2011.05.014

20. Pakozdy A, Halasz P, Klang A, Bauer J, Leschnik M, Tichy A, Thalhammer JG, Lang B, Vincent A. Suspected limbic encephalitis and seizure in cats associated with voltage-gated potassium channel (VGKC) complex antibody. J Vet Intern Med. 2013 Jan-Feb;27(1):212-4. doi: 10.1111/jvim.12026. Epub 2012 Dec 28. PMID: 23278981.

21. Plantone D, Renna R, Koudriavtseva T. Neurological diseases associated with autoantibodies targeting the voltage-gated potassium channel complex: immunobiology and clinical characteristics. *Neuroimmunology and Neuroinflammation*. 2016; 3: 69-78.

22. Scalia B, Caine A, Pittaway R, Cherubini GB. Feline temporal lobe epilepsy: seven

cases of hippocampal and piriform lobe necrosis in England and literature review. J Feline Med Surg. 2022 Jun;24(6):596-608.

23. Wohlsein P, Deschl U, Baumgärtner W. Nonlesions, unusual cell types, and postmortem artifacts in the central nervous system of domestic animals. Vet Pathol. 2013 Jan;50(1):122-43.

24. Zilli J, Schänzer A, Büttner K, Kressin M, Schmidt MJ (2022) Quantitative and qualitative evaluation of the hippocampal cytoarchitecture in adult cats with regard to the pathological diagnosis of hippocampal sclerosis. PLOS ONE 17(5): e0268010.

CASE IV:

Signalment:
Adult, female intact, North American beaver (*Castor canadensis*)

History:
The beaver was found in a creek bed and animal control found the beaver lethargic and unresponsive. Following capture, the animal was reported to be "rolling in the crate". The beaver was brought to a local wildlife rehabilitation center where she was reported to be neurologic and ataxic while walking with impaired vision. Euthanasia was elected and the animal submitted for necropsy exam.

Brain, beaver: One hemisection of diencephalon and one of brainstem and pituitary gland are submitted for examination. At low magnification, perivascular cuffs and areas of pallor are seen in the cerebrum and thalamus. (HE, 6X)

Gross Pathology:
A 7.14 kg intact female beaver (*Castor canadensis*) was submitted for necropsy, 3 days postmortem and in fair postmortem condition. The nutritional state was fair based on small amounts of visceral and subcutaneous adipose tissue, and muscling was adequate. The lungs, heart, liver, kidneys, spleen, and gastrointestinal tract were unremarkable. The stomach contained a moderate amount of pale tan and fibrous digesta. The small intestine contains a moderate amount of tan to grey, mucoid digesta. The large intestine and rectum contain an abundant amount of well-formed feces.

Laboratory Results:
Rabies antigen and highly pathogenic avian influenza PCR of fresh brain was negative. Canine Distemper IHC had variable immunoreactivity in the nucleus of neurons and astrocytes in the brain (interpreted as artifact) and negative by PCR on formalin fixed, paraffin embedded brain and lung.

Microscopic Description:
Brain, cerebrum: Examined are sections of cerebrum, hippocampus, and mid-brain. Predominately affecting the left hemisphere of the cerebrum, numerous eosinophils, macrophages, lymphocytes and plasma cells expand the perivascular and meningeal space. Abundant eosinophils and fewer plasma cells, and increased glial cells are scattered throughout the neuropil of affected areas. Embedded within the neuropil of the white matter are cross and tangential sections of

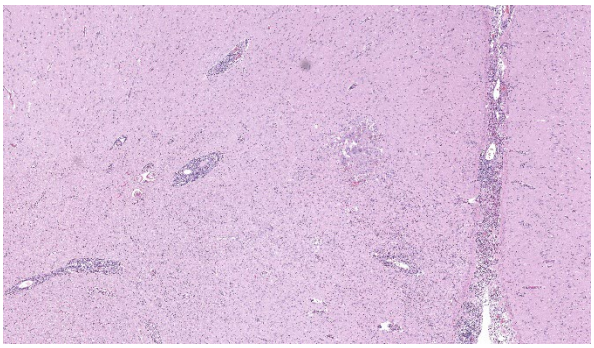

Cerebrum, beaver: The meninges and Virchow-Robins spaces are expanded by large number of lymphocytes, macrophages and eosinophils, and multifocal migration tracts are present within the parenchyma. (HE, 56X)

larval nematodes. The nematodes are approximately 70 µm in diameter with a 2.5 um thick cuticle and prominent lateral chords and lateral alae. The pseudocoelom contains coelomyarian musculature and digestive tract composed of uninucleate columnar cells. Scant inflammatory cells surround the nematodes. Multifocally within the grey and white matter are foci of necrosis characterized by disruption, loss and vacuolation of the neuropil and presence of macrophages and Langerhans type multinucleated giant cells with fewer lymphocytes and glial cells, and scant plasma cells. Throughout the cerebrum, there are rare necrotic neurons and neurons surrounded by glial cells (satellitosis). The white matter of the midbrain is rarified with bands of eosinophilic, fibrillar material, increased clear space, glial cells and astrocytes. Rare neurons within the adjacent gray matter are variably replaced by homogenous to coarsely stippled basophilic mineral.

Brain, brain stem: Section contains histologically unremarkable brain stem.

Brain, pituitary, pars distalis: Section contains histologically unremarkable pars distalis.

Contributor's Morphologic Diagnosis: Brain, cerebrum: Eosinophilic and necrogranulomatous meningoencephalitis, chronic, severe, with gliosis and nematode larvae

Brain, midbrain: White matter degeneration, chronic, moderate, with astrogliosis and astrocytosis (glial scar)

Contributor's Comment: *Baylisascaris* species are nematodes that share the order Ascaridia with *Toxocara canis* and *Toxocara cati*. The most widespread and ubiquitous *Baylisascaris* is *B. procyonis*. Raccoons (*Procyon lotor*) and dogs (*Canis familiaris*) are the definitive hosts of *B. procyonis,* although numerous species of mammals and birds have been identified as intermediate hosts,[3] including a report in two American beavers (*Castor canadensis*).[2] In raccoons, *B. procyonis* is confined to the intestines and rarely causes disease.[3] In definitive hosts, eggs hatch and develop into adults in the intestine and subsequently females lay eggs that are passed into the environment with feces, continuing the cycle. Consumption of contaminated feces or an infected host may cause reinfection in the definitive host or infection in intermediate hosts. In intermediate hosts, larvae do not develop into adults, but

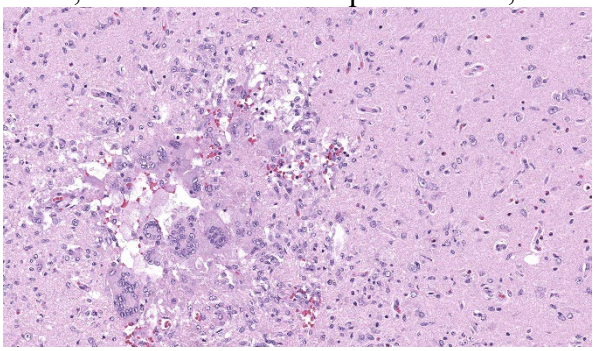

Cerebrum, beaver: The meninges and Virchow-Robins spaces are expanded by large number of lymphocytes, macrophages and eosinophils, and multifocal migration tracts are present within the parenchyma. (HE, 56X)

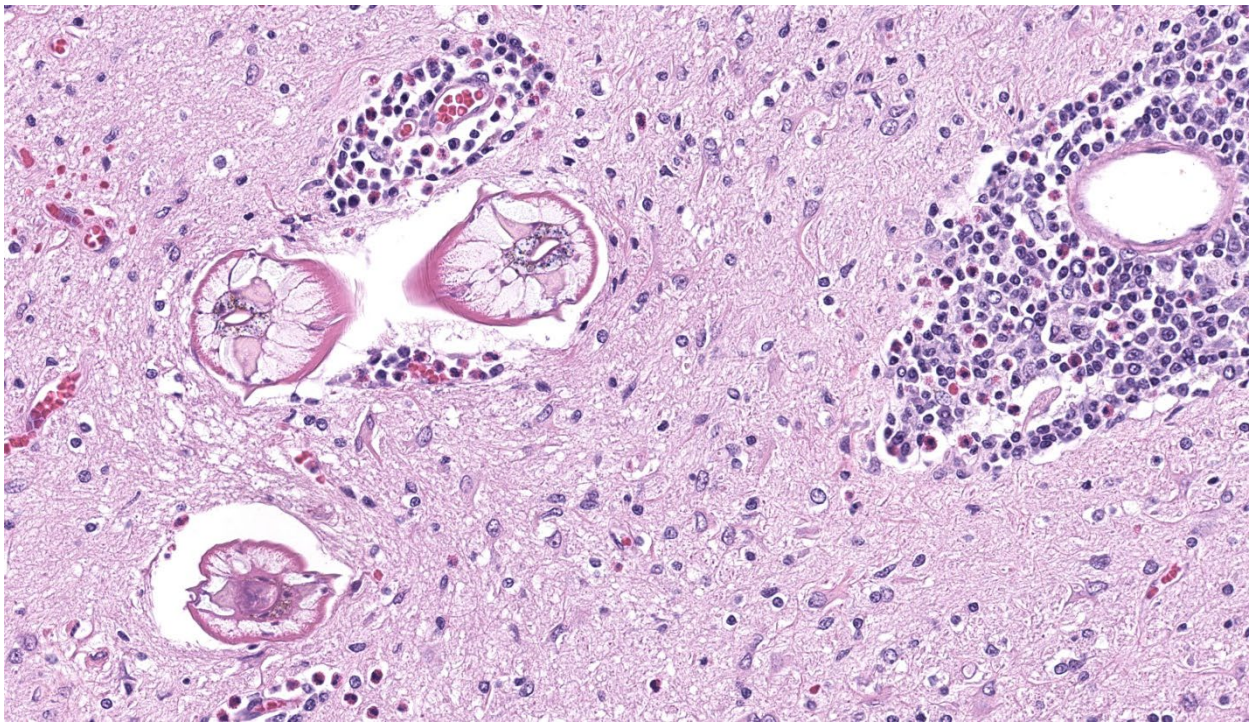

Cerebrum, beaver: Adjacent to a vessel cuffed by large number of lymphocyte, macrophages and eosinophils, there are three cross sections of a larval ascarid nematode with a thin cuticle with lateral alae, a pseudocoelom, polymyarian-coelomyarian musculature, prominent lateral chords, and a small intestine lined by multinucleated cells. (HE, 480X)

can migrate to numerous tissues such as the brain (neural larval migrans, NLM), eye (ocular larval migrans, OLM), and viscera (visceral larval migrans, VLM) where they may cause substantial disease and death.[3] The precise pathogenesis of larval migrans is unclear, however, migration through the intestinal epithelium into the portal vasculature or lungs has been proposed.[7]

Compared to *Toxocara* spp., *B. procyonis* is particularly pathogenic due to aggressive tissue migration,[6,9] continued growth and development of larval migrans,[6,9] and release of tissue damaging proteins and host eosinophilic toxins.[4,6,8]. Most often, lesions are nodular foci consisting of larvae encased in granulomas with substantial eosinophilic inflammation. In this case, there was substantial meningoencephalitis and there were granulomas, but larvae were not observed encased in a granuloma (perhaps as a function of cut).It has been reported that encapsulation of larva takes longer in the central nervous system.[7]

B. procyonis is reported to be widespread in raccoons in North America with a prevalence between 37 and 82% of raccoons affected.[6,11] *B. procyonis* has also spread through Europe with the introduction of American raccoons.[12] *B. procyonis* is recognized as zoonotic and it can cause fatal visceral and neural larval migrans in children, though ocular migrans is more common in adults.[3] In a survey of 150 adults from California, as many as 7% of non-symptomatic adults tested seropositive, suggesting that the prevalence in human populations may be higher than previously thought.[13]

At least nine species of *Baylisascaris* have been described (Table 1), with the most notable being *Baylisascaris procyonis* due to its destructive larval migration. It is also the only known species of *Baylisascaris* to infect humans. While reports of larval migrans in

Baylisascaris procyonis are common, in other species confirmed disease in naturally infected paratenic hosts are rare (Table 1). However, all species of *Baylisascaris* are potentially pathogenic, as most species have been shown to experimentally infect and cause disease in rodents.[10]

In this case, the only other histologic findings were a mild eosinophilic and lymphoplasmacytic enterocolitis with a single, intraluminal, unidentified nematode egg in cross section and a focal lymphoplasmacytic interstitial nephritis with minimal eosinophils. Parasites are common in wildlife species, and the eosinophilic enterocolitis and intraluminal parasitic egg is consistent with a parasitic enteropathy. The clinical significance of these findings is unknown.

Table 1. *Baylisascaris* species and definitive hosts with reported larval migrans in natural infected paratenic hosts.

Baylisascaris spp.	**Definitive host(s)**	**Natural Paratenic Host**
Baylisascaris columnaris	Skunks	Primates[15]
Baylisascaris devosi	Fishers, martens, wolverines	No reports
Baylisascaris laevis	Marmots, ground squirrels	No reports
Baylisascaris melis	Badgers	No reports
Baylisascaris potosis	Kinkajou	No reports
Baylisascaris procyonis	Raccoon, dogs	Humans,[14] mammals, and birds[1]
Baylisascaris schroederi	Giant Panda	No reports
Baylisascaris transfuga	Bears	Moose[5]
Baylisascaris venezuelensis	Spectacled bear	No reports

Contributing Institution:
Colorado State University
Department of Microbiology, Immunology, and Pathology
https://vetmedbiosci.colostate.edu/vdl/

JPC Morphologic Diagnosis: Transverse cerebrum at the level of the thalamus: Meningoencephalitis, necrotizing, eosinophilic, and granulomatous, subacute, multifocal and asymmetric, marked, with gliosis and larval ascarids.

JPC Comment: The final case of this conference provides both overlapping and differing features in comparison to the *P. tenuis* meningoencephalitis observed in Case 2 in a sitatunga. Cross-sections of larval *Baylisascaris* were focal in the sections we reviewed, though the expansion of the leptomeninges and reactive astrocytes with distinct processes are a solid indication of a more clinically severe process that led to the decline of this animal. While both cases were necrotizing, there is a sizable eosinophil contingent as well as the presence of multinucleated giant cell macrophages which are conspicuous here. We considered the chronicity of this case at length – did the presence of multinucleated giant cells not indicate a transition to chronic inflammation? The presence of inflammatory cells within the neuroparenchyma (reminder from Case 1 discussion: the number of eosinophils in the brain is should still be zero) is an indicator of the breach of the blood-brain barrier, and the entry of large histiocytes should theoretically take longer given their size and circulating number. Dr.

Koehler stood fast on subacute chronicity, noting that the large numbers of eosinophils and macrophages can appear relatively quickly within the brain (within 72 hours) and that meningeal fibrosis was a better arbiter of the actual transition to chronic inflammation – this was not a feature of this case at all. Conversely, the large numbers of intact eosinophils argued against a longer time course as lifespan within tissue is several days on average and overall numbers should decline with time. Accordingly, the features of this case certainly straddle the line of acute and chronic, though the clinical history of 'Justin Beaver' (this animal's actual given name) leaves much information to our imagination and allows both camps to feel vindicated in their interpretation. Finally, we extend a special thank you to the contributor for their excellent summary (Table 1) of *Baylisascaris* across species and hope others will find it useful.

References:

1. Bauer C. Baylisascariosis--infections of animals and humans with 'unusual' roundworms. *Vet Parasitol*. 2013;193**:** 404-412.

2. Desprez I, Yabsley MJ, Fogelson SB, et al. Baylisascaris procyonis larva migrans in two captive north american beavers (Castor canadensis). *J Zoo Wildl Med*. 2017;48**:** 232-236.

3. Gavin PJ, Kazacos KR, Shulman ST. Baylisascariasis. *Clin Microbiol Rev*. 2005;18**:** 703-718.

4. Hamann KJ, Kephart GM, Kazacos KR, Gleich GJ. Immunofluorescent localization of eosinophil granule major basic protein in fatal human cases of Baylisascaris procyonis infection. *Am J Trop Med Hyg*. 1989;40**:** 291-297.

5. Hoberg EP, Burek-Huntington K, Beckmen K, Camp LE, Nadler SA. Transuterine infection by Baylisascaris transfuga: Neurological migration and fatal debilitation in sibling moose calves (Alces alces gigas) from Alaska. *Int J Parasitol Parasites Wildl*. 2018;7**:** 280-288.

6. Kazacos KR. Baylisascaris procyonis and related species. In: W. M. Samuel MJP, and A. A. Kocan, eds. *Parasitic diseases of wild mammals*. 2 ed. Ames, IA: Iowa State University Press; 2001:301-341.

7. Kazacos KR. Visceral, ocular, and neural larva migrans. In: Connor DH, Chandler FW, Schwartz DA, Manz HJ, Lack EE, eds. *Pathology of infectious diseases*. Stamford, CT: Appleton and Lange; 1997:1459-1473.

8. Moertel CL, Kazacos KR, Butterfield JH, Kita H, Watterson J, Gleich GJ. Eosinophil-associated inflammation and elaboration of eosinophil-derived proteins in 2 children with raccoon roundworm (Baylisascaris procyonis) encephalitis. *Pediatrics*. 2001;108**:** E93.

9. Richardson D, Krause P. *North American Parasitic Zoonoses*, vol. 6. Norwell, MA: Kluwer Academic Publishers; 2003.

10. Sapp SGH, Gupta P, Martin MK, et al. Beyond the raccoon roundworm: The natural history of non-raccoon Baylisascaris species in the New World. *Int J Parasitol Parasites Wildl*. 2017;6**:** 85-99.

11. Straif-Bourgeois S, Cloherty E, Balsamo G, Gee L, Riegel C. Prevalence of Baylisascaris procyonis in Raccoons Trapped in New Orleans, Louisiana, 2014-2017.

Vector Borne Zoonotic Dis. 2020;20**:** 22-26.

12. Umhang G, Frantz AC, Ferté H, et al. Surveys on Baylisascaris procyonis in two of the three French wild raccoon populations. *Int J Parasitol Parasites Wildl*. 2024;23**:** 100928.

13. Weinstein SB, Lake CM, Chastain HM, et al. Seroprevalence of Baylisascaris procyonis Infection among Humans, Santa Barbara County, California, USA, 2014-2016. *Emerg Infect Dis*. 2017;23**:** 1397-1399.

14. Wise ME, Sorvillo FJ, Shafir SC, Ash LR, Berlin OG. Severe and fatal central nervous system disease in humans caused by Baylisascaris procyonis, the common roundworm of raccoons: a review of current literature. *Microbes and Infection*. 2005;7**:** 317-323.

15. Zimmerman D, Dangoudoubiyam S, Kazacos K. Serological diagnosis of Baylisascaris procyonis in primates using a human ELISA test. *Journal of Wildlife Medicine*. 2019;50**:** 414-420.